DECEMBER 1977

analytical chemistry

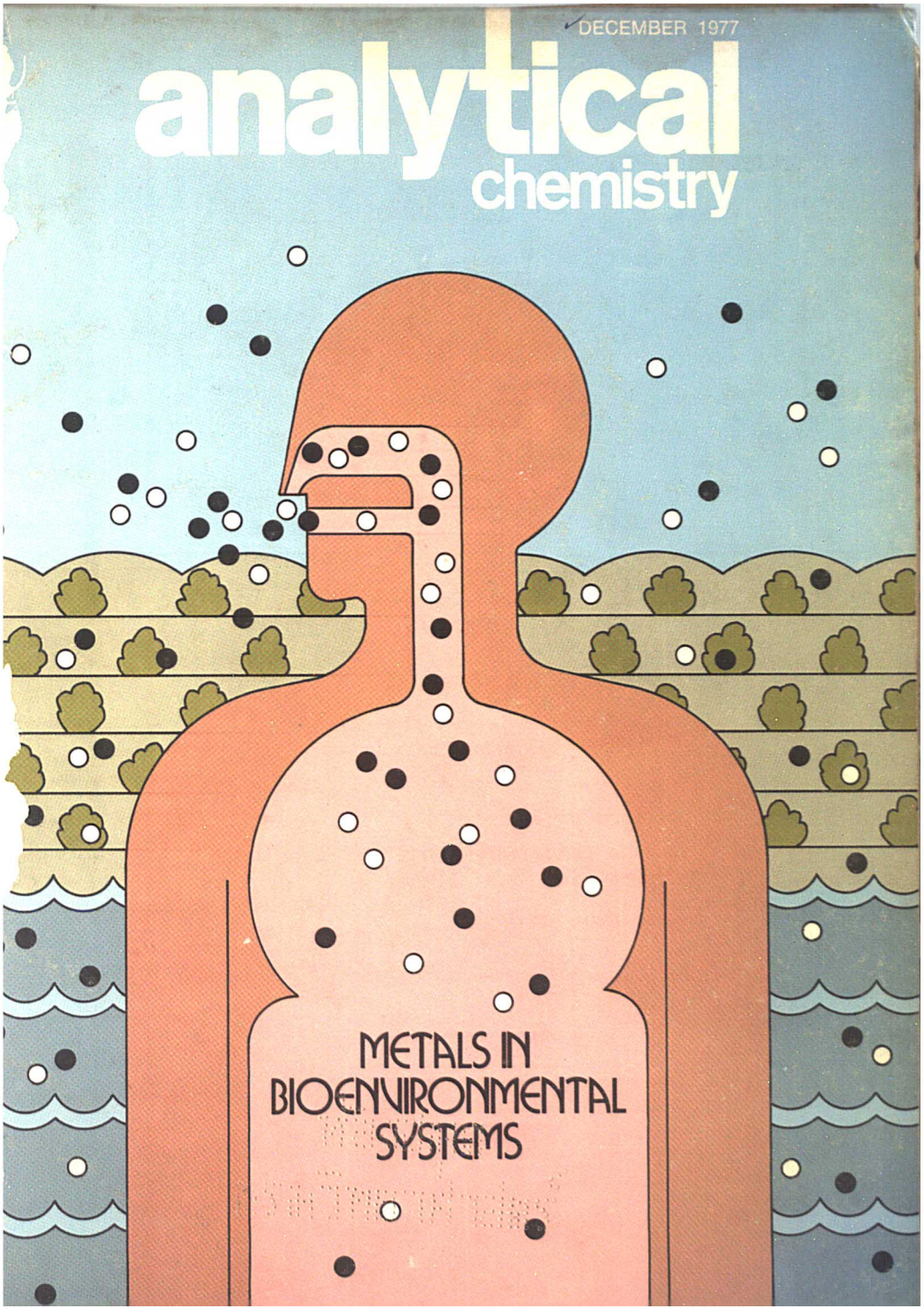

METALS IN BIOENVIRONMENTAL SYSTEMS

NANOpure.

The New Standard for Reagent Grade Water.

Standard purity meter with dual-range scale provides accurate purity verification at a glance; satisfies quantitative record keeping requirements.

Delivers up to three liters per minute of Type I water (CAP, ASTM) at exceptionally low cost.

Optional pump provides pure water instantly; features continuous or 30 second push button rinse-up.

Pressurized pure water can be piped to remote outlets

Compatible with a range of pretreatment systems including ROpure reverse osmosis.

Compact, lightweight and attractive for convenient wall mounting right in the laboratory.

Pleated-membrane submicron filter removes microorganisms and particulates; useful life far exceeds that of the flat-disc type

Convenient screw-in cannisters contain cartridges with twice the ion-exchange capacity of other popular systems. Four-module system with Organic Removal also available.

NANOpure and NANOpure cartridges are available for immediate delivery from your laboratory supply distributor.

The Barnstead Guide to Reagent Grade Water - everything you need know about reagent grade water. Helps you make an informed decision when evaluating pure water systems. Write for your free copy.

SYBRON | Barnstead

Barnstead Company
Division of Sybron Corporation
225 Rivermoor Street
Boston, Massachusetts 02132
(617) 327-1600

CIRCLE 22 ON READER SERVICE CARD

Don't miss the boat!

(it's ready to analyze your sample for S, N, or X).

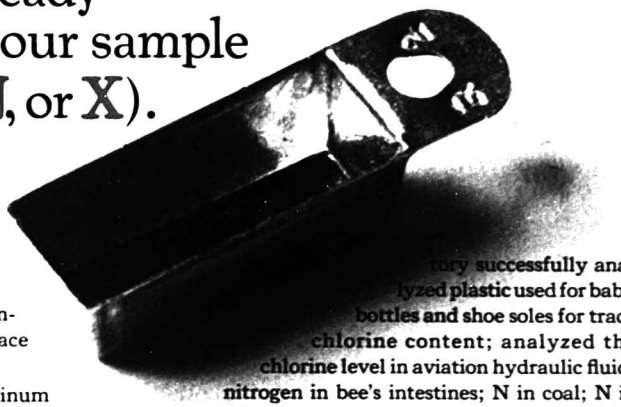

Can the Dohrmann Microcoulometric Titrating System successfully analyze your sample—solid or liquid—for trace amounts of S, N, or X?

Yes, thanks to this tiny platinum sample-handling boat, the MCTS probably can.

The boat is one of several introduction devices that allow the MCTS to analyze an enormous range of samples, including solids, brines, catalysts, and many other difficult materials.

Recently the Dohrmann Applications Laboratory successfully analyzed plastic used for baby bottles and shoe soles for trace chlorine content; analyzed the chlorine level in aviation hydraulic fluid; nitrogen in bee's intestines; N in coal; N in sterile disposable paper products used in operating rooms, and sulfur in gasoline, oil, water, and pure toluene diisocyanate.

Our Applications Lab will be happy to discuss a free feasibility study on *your* sample, whether we need to use a boat or not. Give Mel Carter, Bob Booth, or Madeline Moore a call.

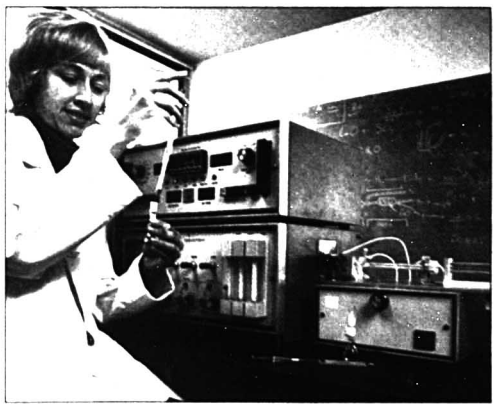

Madeline Moore begins the analysis of a sample sent into the Dohrmann Applications Lab. Five minutes later, the precise amount of the element being analyzed (S, N, or X) will be displayed on the digital readout.

ENVIROTECH

DOHRMANN

3240 Scott Boulevard
Santa Clara, California 95050
Telephone (408) 249-6000
Telex 346 395

CIRCLE 54 ON READER SERVICE CARD

There are lots of good reasons to use Whatman Advanced Ion Exchange Celluloses for separations of nucleic acids, proteins, enzymes. Here are ten of them:

- **Faster Kinetics of Exchange.** Whatman microgranular AIEC's absorb 6.5 times more bovine serum albumin in 5 minutes than conventional DEAE cellulose. Desorb rapidly, thoroughly.
- **Higher Polyelectrolyte Capacity.** For example, Grade DE 52 absorbs approximately 500 mg of bovine serum albumin in 20 minutes.
- **Greater Accessibility of Exchange Sites.** With no loss of dimensional stability. Hence superior protein capacity and kinetics of adsorption.
- **Greater Uniformity of Substitution.** Greater than conventional ion exchange celluloses. Excellent reproducibility of results.
- **Uniform Charge Density.** Thus, greater protein loadings, sharper elution bonds, better selectivity.
- **Easier Handling, High Dimensional Stability.** Available wet (pre-swollen) or dry. Rigorous control of physical form.
- **Optimized Range.** DEAE (anion) or CM (cation). Both wet or dry, microgranular or fibrous. Select best form for the particular application.
- **Narrow Particle Size Range.** For easier column packing, better packed-column reproducibility, higher packing densities, more predictable flow rates.
- **Dependable Reproducibility.** Whatman AIEC's are always the same, batch-to-batch, so performance is predictable, reproducible.
- **Whatman Quality.** Painstaking, meticulous manufacture, rigorous quality control.

Whatman Advanced Ion Exchange Celluloses. At your laboratory supply dealer or from **Whatman Inc.** ■ 9 Bridewell Place, Clifton, New Jersey 07014 ■ (201) 777-4825

CIRCLE 234 ON READER SERVICE CARD

Whatman

Volume 49, No. 14, December 1977
ANCHAM
49(14) 1193A-1282A/2129-2420 (1977)
ISSN 0003-2700

analytical chemistry

© Copyright 1977
by the American Chemical Society

No part of this publication may be reproduced in any form without written permission from the American Chemical Society

Published monthly with review issue added in April and Laboratory Guide in August by the American Chemical Society, from 20th and Northampton Sts., Easton, Pa. 18042. Executive and Editorial headquarters, American Chemical Society, 1155 16th St., N.W., Washington, D.C. 20036 (202) 872-4600. Second class postage paid at Washington, D.C., and at additional mailing offices.

1977 Subscription rates—including surface postage

	1 yr	2 yr	3 yr
MEMBERS			
Domestic	$ 9.00	$16.00	$22.00
PUAS	17.00	32.00	46.00
Canada, Foreign	18.00	34.00	49.00
NONMEMBERS			
Domestic	12.00	21.00	29.00
Canada	21.00	39.00	56.00
PUAS	23.00	43.50	64.00
Foreign	24.00	45.50	67.00

Airmail and air freight rates are available from Membership & Subscription Services, ACS, P.O. 3337, Columbus, Ohio 43210, (614) 421-7230.

New and renewal subscriptions should be sent with payment to the Office of the Controller at the ACS Washington address.

Subscription service inquiries and changes of address (include both old and new addresses with ZIP code and *recent mailing label*) should be directed to the ACS Columbus address noted above. Please allow six weeks for change of address to become effective.

Claims for missing numbers will not be allowed if loss was due to failure of notice of change of address to be received in the specified time; if claim is dated (a) North America: more than 90 days beyond issue date, (b) all other: more than one year beyond issue date; or if the reason given is "missing from files".

Microfiche subscriptions, one year only, are available at the same rates but are mailed first class domestic and airmail foreign.

	Write or call
Microfiche subscriptions, for inquiries and payments	Special Issues Sales American Chemical Society 1155 16th St., N.W. Washington, D.C. 20036 202-872-4364
Single issues, current year, $2.50 except review issue, $4.00	
Back issues and volumes	
Microfilm editions from Vol. 1 to present	

Advertising Management: Centcom, Ltd., 25 Sylvan Road South, Westport, Conn. 06880 (203) 226-7131

CONTENTS

REPORT

G. B. Morgan and E. W. Bretthauer discuss future analytical requirements for determination of trace and ultratrace levels of metals in bioenvironmental systems **1210 A**

REPORT

Results from a survey of ANALYTICAL CHEMISTRY authors on publication practices are presented **1217 A**

INSTRUMENTATION

R. E. Sturgeon considers the factors affecting atomization and measurement in graphite furnace atomic absorption spectrometry **1255 A**

INSTRUMENTATION

S. D. Brown examines the theory and reviews experimental procedures for Zeeman effect-based background correction in atomic absorption spectrometry **1269 A**

NEWS

E. sz. Kovats, J. H. Purnell, and A. A. Zhukhovitskii receive the M. S. Tswett Chromatography Medals. The Analytical Chemistry Division invites applications for the Graduate Fellowship Program. NSF announces the Small Business Innovation Applied to National Needs program and the Science Faculty Professional Development grants **1223 A**

BOOKS

An audio course on ORD and CD and books on gas analysis by GC and AA are reviewed by Robert Woody, G. G. Esposito, and G. F. Kirkbright **1247 A**

EDITORS' COLUMN

"A History of Analytical Chemistry" and the 50th anniversary of ANALYTICAL CHEMISTRY symposium are covered. The JOURNAL moves toward SI **1253 A**

EDITORIAL

The Analytical Division fellowship program continues to be outstandingly successful **2129**

Technical Contents/Briefs	**1196 A**
Letters	**1208 A**
Author Index	**IBC**
Future Articles	**IBC**
Call for Papers	**1225 A**
Meetings	**1226 A**
Short Courses	**1226 A**
New Products	**1236 A**
Chemicals	**1239 A**
Manufacturers' Literature	**1240 A**

Our cover is based on the REPORT: exposure of trace metals from all pathways in the environment impacts on health and welfare

ห้องสมุด กรมวิทยาศาสตร์
31 มี.ค. 2521

Briefs

Quantitative Analysis of Mixtures by Carbon-13 Nuclear Magnetic Resonance Spectrometry 2130

Results, without nuclear Overhauser enhancement suppression, are presented. Mixtures, which are not simply isomeric, are quantified at varying concentrations with an average RMS error of 1.6%.

Thomas H. Mareci* and Katherine Násfay Scott, Veterans Administration Hospital, and Department of Radiology, University of Florida, Gainesville, Fla. 32610
Anal. Chem., 49 (1977)

Classification of Binary Carbon-13 Nuclear Magnetic Resonance Spectra 2136

Bayes, Maximum Likelihood, and Simplex Learning Machine classifiers are used to predict the presence of 24 organic structural features by examination of ^{13}C NMR spectra.

Charles L. Wilkins* and Thomas R. Brunner, Department of Chemistry, University of Nebraska—Lincoln, Lincoln, Neb. 68588
Anal. Chem., 49 (1977)

Combined Retrieval System for Infrared, Mass, and Carbon-13 Nuclear Magnetic Resonance Spectra 2141

A combined retrieval system based on three different spectrometric data as well as the corresponding data file structures are described. The identification of the compounds depends entirely upon their spectra.

Jure Zupan* and Matej Penca, Chemical Institute Boris Kidrič, Ljubljana, Yugoslavia, and **Dušan Hadži,** Faculty of Natural Sciences and Technology, University of Ljubljana, Yugoslavia, and **Jože Marsel,** Institute Josef Stefan, University of Ljubljana, Ljubljana, Yugoslavia
Anal. Chem., 49 (1977)

Positional and Geometric Characterization of Olefinic Double Bonds by Fluorine Magnetic Resonance Spectrometry 2146

Hexafluoroacetone ketal derivatives of linear olefins are used to determine both double bond position and geometry of the original olefin using spectral parameters obtained from ^{19}F NMR.

Michelle V. Buchanan, David F. Hillenbrand, and James W. Taylor,* Department of Chemistry, University of Wisconsin, Madison, Wis. 53706
Anal. Chem., 49 (1977)

Deconvolution and Background Subtraction by Least-Squares Fitting with Prefiltering of Spectra 2149

The statistical accuracy is only slightly sub-optimal when a suitable digital filter is used, yet the influence of fairly curved backgrounds can be removed without recourse to explicit calculation and scaling.

Peter J. Statham, Department of Electrical Engineering and Computer Sciences, University of California, Berkeley, Calif. 94720
Anal. Chem., 49 (1977)

* Corresponding author

Quantitative Analyses of Multicomponent Fluorescence Data by the Methods of Least Squares and Non-Negative Least Sum of Errors 2155

Quantitative information is obtained from fluorescent mixtures, even in cases of severe overlap and poor signal/noise ratios.

I. M. Warner, E. R. Davidson,* and G. D. Christian, Chemistry Department BG-10, University of Washington Seattle, Wash. 98195
Anal. Chem., 49 (1977)

Comparison of Experimental and Theoretical Calibration Curves in Solid-Surface Fluorescence Analysis 2160

Experimental and theoretical reflected and transmitted fluorescence calibration curves for thin-layer chromatoplates are compared to give support for a new theory on fluorescence densitometry.

R. J. Hurtubise, Department of Chemistry, University of Wyoming, Laramie, Wyo. 82071
Anal. Chem., 49 (1977)

Room-Temperature Phosphorescence of Compounds Adsorbed on Sodium Acetate 2164

The interactions of *p*-aminobenzoic acid with a sodium acetate surface are considered in detail and a mechanism for the adsorption is postulated.

R. M. A. von Wandruszka and R. J. Hurtubise,* Department of Chemistry, University of Wyoming, Laramie, Wyo. 82071
Anal. Chem., 49 (1977)

Theoretical Assessment of Precision in Dual Wavelength Spectrophotometric Measurement 2170

Equations describing the contributions of different sources of noise to the imprecision of dual wavelength spectrophotometric measurement are developed and evaluated.

K. L. Ratzlaff and D. F. S. Natusch,* School of Chemical Sciences, University of Illinois, Urbana, Ill. 61801
Anal. Chem., 49 (1977)

Supply and Removal of Sample Vapor in Graphite Thermal Atomizers 2176

Sample introduction from the graphite wall is determined by the wall temperature, whereas the removal of vapor from the cell is dominated by either diffusion in static systems or convection in flow-through systems.

Wim M. G. T. van den Broek and Leo de Galan,* Laboratorium voor Analytische Scheikunde, Technische Hogeschool, P.B. 5029, Delft, The Netherlands
Anal. Chem., 49 (1977)

Background Correction for the Analysis of High-Solids Samples by Graphite Furnace Atomic Absorption 2187

An atomic absorption system composed of a continuum source and a wavelength modulated echelle monochromator is used for the direct analysis of Cd, Pb, and Cu in 3% NaCl, serum, and urine by graphite furnace atomization.

J. M. Harnly and T. C. O'Haver,* Department of Chemistry, University of Maryland, College Park, Md. 20742
Anal. Chem., 49 (1977)

LOOKS LIKE *A* pH METER.

WORKS LIKE *A* COMPUTER.

a digital specific ion meter

ORION has developed the Model 901 to further simplify all analyses made using pH, specific ion, and gas-sensing electrodes. A series of operating modes covers the full range of analytical methods used for performing electrode analyses:

direct reading concentration	
incremental methods:	**known (standard) addition**
	known subtraction
	analate (sample) addition
	analate subtraction
absolute and relative millivolts:	**Gran's plots and titrations**
pH	

Results are calculated in real time with an accuracy that will satisfy the most demanding research applications – yet the 901 is simple enough to be used in all routine quality control applications.

Analytical parameters are entered on the digital switches on the control panel, with standardization and blank correction accomplished at the push of a button. Results are read directly from the LED display in the unit system of your choice. The 901 completely eliminates the use of calibration curves, tables, or calculations.

how the 901 works

The Model 901 has a high input impedance analog amplifier and analog-to-digital converter similar to that used in digital pH/mv meters. The output of the converter is fed to a microprocessor which is pre-programmed with equations for calculating pH's and concentrations. Parameters needed to solve the electrode equations are supplied to the microprocessor from the switches and pushbuttons on the front panel.

Twice each second the electrode's potential is digitalized and fed to the microprocessor, and the analytical result is calculated using the pre-programmed equations. A concentration result ranging between .000 and 999. is shown on the LED display in a three-digit floating decimal point format. Calculated pH results between 0.000 and 13.999 are displayed.

pushbutton blank correction

The 901 has a blank correction feature that is especially useful in overcoming two problems frequently encountered in making low-level measurements: slow time response of the electrode and deviation of the electrode response from theoretical.

In the first case a background level of the species measured is added to all samples and standards to bring the concentration up to the region of fast time response. The blank correction feature is used to automatically subtract this background level from the result.

In the second case the electrode potential in the blank solution is entered into the microprocessor's memory by pushbutton so that the results are automatically corrected over the region of nontheoretical response.

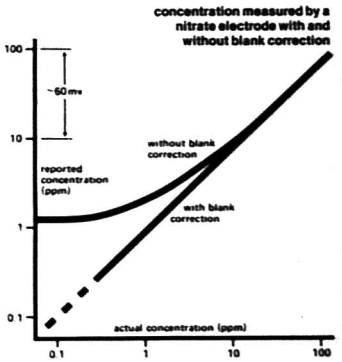

volume correction

When analyses are carried out by one of the incremental methods, the volume change that takes place when the standard is added to the sample (or vice versa) should be taken into consideration if a correct result is to be calculated. The various incremental modes include a volume correction factor that the microprocessor uses in calculating the result.

call us

Can we discuss applications for the 901 – or arrange a demonstration in your laboratory? Call us toll-free at 800-225-1480 (except Mass.) and ask for one of our Technical Service Representatives. In Canada call 800-363-9270.

ORION RESEARCH

380 Putnam Ave., Cambridge, MA 02139

CIRCLE 156 ON READER SERVICE CARD

Briefs

Cumulative Sum Charts for Monitoring of Radioactivity Background Count Rates 2193

The value of a quality control technique of general applicability is illustrated by the improved accuracy obtained in the measurement of radioactivity background.

Roger A. G. Marshall, School of Chemistry, Thames Polytechnic, Woolwich, London SE18 6PF, United Kingdom

Anal. Chem., 49 (1977)

Particle Size Effects in the Determination of Respirable α-Quartz by X-ray Diffraction 2196

The detection limit and accuracy are shown to be highly dependent on the particle size and preferred orientation of available reference standards.

J. W. Edmonds,* The Dow Chemical Company, Analytical Laboratories, Midland, Mich. 48640, and **W. W. Henslee and R. E. Guerra,** The Dow Chemical Company, Central Laboratory, Freeport, Tex. 77541

Anal. Chem., 49 (1977)

Proton Induced X-ray Emission Analysis of L-Cells Grown in Vitro 2203

Trace element concentrations in L-cells are determined by proton induced x-ray emission analysis.

R. R. Zombola,* P. A. Kitos, and R. C. Bearse, University of Kansas, Lawrence, Kan. 96045

Anal. Chem., 49 (1977)

Pulse-Counting Techniques in Organic Mass Spectrometry 2205

With pulse-counting techniques in GC/MS, accurate mass measurements and quantitations of small amounts of sample are possible.

Jedidja Freudenthal* and L. G. Gramberg, National Institure of Public Health, Laboratory of Toxicology, P.O. Box 1, Bilthoven, The Netherlands

Anal. Chem., 49 (1977)

Analysis of Triglycerides by Gas Chromatography/Chemical Ionization Mass Spectrometry 2209

Triglycerides with ≤62 C atoms are analyzed and odd carbon number triglycerides are determined by CI(NH_3) mass spectrometry.

Takeshi Murata, Analytical Application Laboratory, Kyoto Laboratory, Shimadzu Seisakusho Ltd., Nakagyo-ku, Kyoto, Japan

Anal. Chem., 49 (1977)

Gas Chromatographic Determination of β-Hydroxyethylhydrazine in the Presence of Its Synthesis By-products 2213

An assay procedure is presented for β-hydroxyethylhydrazine with a precision of ±1.3%. The other synthesis by-products are also quantitated.

Phillip J. Palermo, Norwich Pharmacal Company, Division of Morton-Norwich Products, Inc., Norwich, N.Y. 13815

Anal. Chem., 49 (1977)

Spectroscopic Element Detector for Gas Chromatography 2215

An improved helium glow discharge is used to selectively detect individual elements in GC effluents. A background corrector with variable reference wavelength is used to improve the selectivity of the system.

Cyrus Feldman* and Daniel A. Batistoni, Analytical Chemistry Division, Oak Ridge National Laboratory, Oak Ridge, Tenn. 37830

Anal. Chem., 49 (1977)

Unrecognized Systematic Errors in Quantitative Analysis by Gas–Liquid Chromatography 2222

In addition to the usual parameters affecting the measurements (such as temperature and gas flow), it is necessary to consider the volume of liquid injected, and the concentration of the standards.

Adam Shatkay* and Solange Flavian, Israel Institute for Biological Research, Ness-Ziona, Israel

Anal. Chem., 49 (1977)

Determination of Sulfobetaine Amphoteric Surfactants by Reverse Phase High Performance Liquid Chromatography 2228

A method is developed for the direct analysis of sulfobetaine amphoteric surfactants by reverse phase HPLC using methanol/water 80/20 (v/v) as the mobile phase with an accuracy of 3%.

Nicholas Parris, Warner M. Linfield, and Robert A. Barford,* Eastern Regional Research Center, Agricultural Research Service, U.S. Department of Agriculture, 600 East Mermaid Lane, Philadelphia, Pa. 19118

Anal. Chem., 49 (1977)

Reversed Phase High Performance Liquid Chromatographic Separations of Nucleotides in the Presence of Solvophobic Ions 2231

When tetra-*n*-butylammonium ion is used in the mobile phase to produce an in situ ion-exchange column, relative retentions of nucleotides are different from those previously reported.

Norman E. Hoffman* and John C. Liao, Todd Wehr Chemistry Building, Marquette University, Milwaukee, Wis. 53233

Anal. Chem., 49 (1977)

Simultaneous Determination of Chlordiazepoxide and Its *N*-Demethyl Metabolite in 50-μL Blood Samples by High Pressure Liquid Chromatography 2235

The simple and accurate method allows for the determination in individual mice of the concentration curves of the drug and one of its metabolites.

Hebe B. Greizerstein* and Caryn Wojtowicz, Research Institute on Alcoholism, New York State Department of Mental Hygiene, 1021 Main St., Buffalo, N.Y. 14203

Anal. Chem., 49 (1977)

Really Good Gas Calibration Standards Take 25 Years

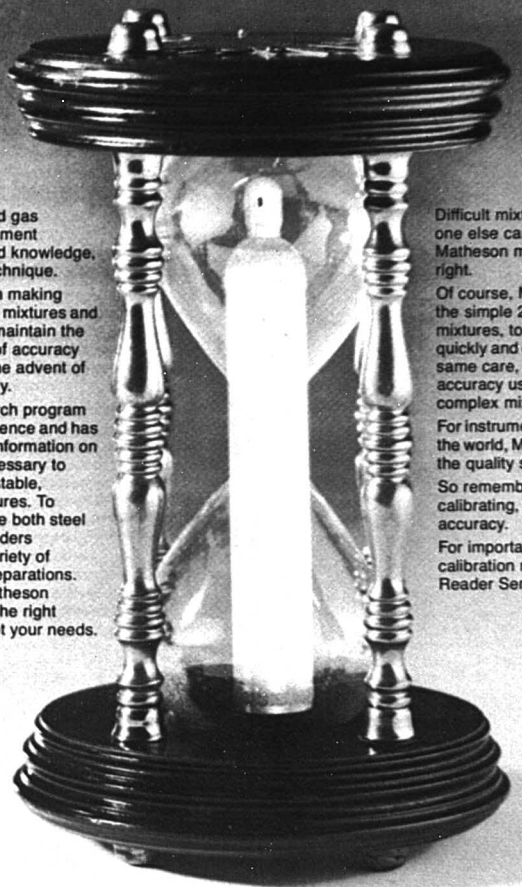

To make really good gas standards for instrument calibration you need knowledge, experience, and technique.

Matheson has been making accurate calibration mixtures and analyzing them to maintain the highest standards of accuracy since long before the advent of gas chromatography.

A continuing research program supports this experience and has provided valuable information on the techniques necessary to prepare accurate, stable, economic gas mixtures. To achieve this, we use both steel and aluminum cylinders combined with a variety of internal cylinder preparations. You can rely on Matheson technology to pick the right combination to meet your needs.

Difficult mixtures...the kind no one else can make...take time. Matheson makes sure they're right.

Of course, Matheson can supply the simple 2- and 3-component mixtures, too. We supply them quickly and economically with the same care, precision, and accuracy used to make the more complex mixtures.

For instrument calibration around the world, Matheson mixtures are the quality standard.

So remember, if it's worth calibrating, it's worth Matheson accuracy.

For important information on calibration mixtures, use the Reader Service No.

Matheson has what it takes to deliver accurate gas mixtures on time.

Matheson
Lyndhurst, N.J. 07071

East Rutherford, N.J. 07073/Morrow, Georgia 30260
Gloucester, Massachusetts 01930/Joliet, Illinois 60434
La Porte, Texas 77571/Cucamonga, California 91730
Newark, California 94560/Bridgeport, N.J. 08014
Dorsey, Maryland 21227/Whitby, Ontario, Canada L1N 5R9
Edmonton, Alberta, Canada T5B 4K6/B 2431 Oevel, Belgium
6056 Heusenstamm, West Germany

CIRCLE 142 ON READER SERVICE CARD

Briefs

Identification of Nucleosides and Bases in Serum and Plasma Samples by Reverse-Phase High Performance Liquid Chromatography 2237

Absorbance ratios, enzymatic peak shifts, and fluorescence detection are used together with retention times to identify nucleosides and bases in HPLC chromatograms of serum and plasma samples.

Anté M. Krstulovic, Phyllis R. Brown,* and Douglas M. Rosie, Department of Chemistry, University of Rhode Island, Kingston, R.I. 02881
Anal. Chem., 49 (1977)

Separation and Determination of Copper(II) and Iron(II) as Their Monothiothenoyltrifluoroacetone Complexes with Pyridine by Extraction Spectrophotometry and Reversed-Phase Thin-Layer Chromatography 2241

The separation and determination of copper(II)(0–12 μg/mL) and iron(II) (0–100 μg/mL) with monothiothenoyltrifluoroacetone in cyclohexane with or without pyridine by extraction spectrophotometry is established.

Takaharu Honjo,* Yoshinori Fujioka, Hitoshi Itoh, and Toshiyasu Kiba, Department of Chemistry, Faculty of Science, Kanazawa University, Kanazawa, Ishikawa, 920, Japan
Anal. Chem., 49 (1977)

Solvent Effect on the Liquid–Liquid Distribution of Monothiothenoyltrifluoroacetone and Its Metal Chelates of Copper(II), Cobalt(II), and Zinc(II) 2246

The solvent effect is examined with the use of equations derived from regular solution theory. Data for thenoyltrifluoroacetone are also presented for comparison.

Takaharu Honjo,* Ryumon Honda, and Toshiyasu Kiba, Department of Chemistry, Faculty of Science, Kanazawa University, Marunouchi, Kanazawa, Ishikawa 920, Japan
Anal. Chem., 49 (1977)

Determination of Trace Levels of Nitrates by an Extraction-Photometric Method 2249

Trace levels of nitrates are extracted as an ion pair with crystal violet using chlorobenzene. The results in the range of 60–720 ppb agree within a standard deviation of 28 ppb.

Philip Baca and Henry Freiser,* Department of Chemistry, University of Arizona, Tucson, Ariz. 85721
Anal. Chem., 49 (1977)

Detection of Trinitrotoluene in Water by Fluorescent Ion-Exchange Resins 2251

A semi-quantitative method for monitoring the wastewater from ammunition plants for TNT on a continuous bases is described.

Carl A. Heller,* Robert R. McBride, and Matthew A. Ronning, Chemistry Division (Code 385), Naval Weapons Center, China Lake, Calif. 93555
Anal. Chem., 49 (1977)

Separation of Hydroaromatics and Polycyclic Aromatic Hydrocarbons and Determination of Tetralin and Naphthalene in Coal-Derived Solvents 2253

The standard deviation for tetralin is 0.024% and for naphthalene is 0.035%. An empirical structure-retention correlation for reversed-phase HPLC is developed.

J. F. Schabron and R. J. Hurtubise,* Department of Chemistry, University of Wyoming, Laramie, Wyo. 82701, and **H. F. Silver,** Mineral Engineering Department, University of Wyoming, Laramie, Wyo. 82701
Anal. Chem., 49 (1977)

Open-Pore Polyurethane Columns for Collection and Preconcentration of Polynuclear Aromatic Hydrocarbons from Water 2260

A method for removing and concentrating aromatic hydrocarbons from water on in-situ prepared high capacity open pore polyurethane sorbents is described.

James D. Navratil, Rockwell International, Rocky Flats Plant, Golden, Colo. 80401, and **Robert E. Sievers* and Harold F. Walton,** Department of Chemistry, University of Colorado, Boulder, Colo. 80309
Anal. Chem., 49 (1977)

Selection and Cleaning of Plastic Containers for Storage of Trace Element Samples 2264

Twelve different plastics are examined by gravimetry, isotope dilution mass spectrometry, and neutron activation analysis for levels of impurities present.

John R. Moody* and Richard M. Lindstrom, National Bureau of Standards, Institute for Materials Research, Analytical Chemistry Division, Washington, D.C. 20234
Anal. Chem., 49 (1977)

Principles of Nephelometric Titrations and Application to Titration of Dilute Solutions of Bromide 2268

Exact theoretical calculations for nephelometric titrations demonstrate the optimum scattering angle and particle size.

E. J. Meehan* and S. Yamaguchi, Department of Chemistry, University of Minnesota, Minneapolis, Minn. 55455
Anal. Chem., 49 (1977)

Determination of Nitrite Ion Using Differential Pulse Polarography 2272

Nitrite ion is determined at the ppb level by differential pulse polarography using the reaction between nitrite ion and diphenylamine to form diphenylnitrosamine.

Shaw-Kong Chang, Raymond Kozeniauskas, and George W. Harrington,* Department of Chemistry, Temple University, Philadelphia, Pa. 19122
Anal. Chem., 49 (1977)

Fourier Transform Infrared Analysis below the One-Nanogram Level 2275

The preparation of samples with microscopic techniques results in identifiable Fourier transform infrared spectra on ng amounts of material.

R. Cournoyer,* J. C. Shearer, and D. H. Anderson, Industrial Laboratory, Eastman Kodak Company, Rochester, N.Y. 14650
Anal. Chem., 49 (1977)

Turn your back on Aquatest II...

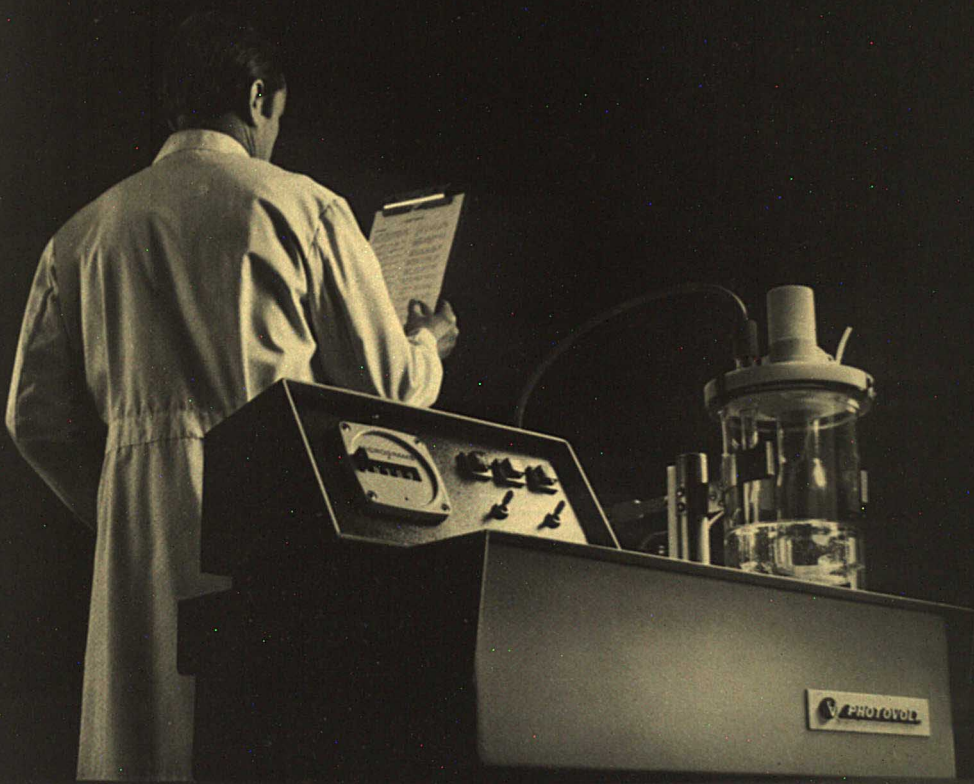

It measures moisture without you.

There's no standardizing, no measuring, no computations, no burettes, no drying of glassware. In fact, we've eliminated everything but just 2 simple steps: **1** Insert sample. **2** Flip switch.

Result: digital readout in micrograms of water.

Aquatest II, the only truly automatic titrator, measures water in either liquids or solids by the *electrolytic generation* of Karl Fischer reagent.

Call now for free demonstration
in your lab and without obligation.
Call toll-free **(800) 221-5182.**
In New York State, call collect **(212) 989-0484.**

Photovolt Corporation
1115 BROADWAY, NEW YORK, N.Y. 10010
CIRCLE 177 ON READER SERVICE CARD

Briefs

Spectrophotometric Determination of Acrylonitrile 2277

The method is based on the absorbance of the pyridine–acrylonitrile complex at 411 nm. The precision is ±3.18% in the 5–30 ppm range.

Maynard E. Hall* and John W. Stevens, Jr., University of Arkansas, Graduate Institute of Technology, Post Office Box 3017, Little Rock, Ark. 72203 *Anal. Chem., 49 (1977)*

Determination of Optimum Compromise Flame Conditions in Simultaneous Multielement Flame Spectrometry 2280

A response parameter, P_J, is described which permits the mathematically simple selection of optimum compromise excitation conditions in simultaneous multielement flame spectrometry.

D. F. Brost, B. Malloy, and K. W. Busch,* Department of Chemistry, Baylor University, Waco, Texas 76703 *Anal. Chem., 49 (1977)*

Categorization of Papers by Trace Metal Content Using Atomic Absorption Spectrometric and Pattern Recognition Techniques 2285

Trace metal concentrations determined by nonflame atomic absorption are used as the data set for identification of 19 bond papers by pattern recognition techniques.

P. J. Simon, B. C. Giessen, and T. R. Copeland,* Department of Chemistry and The Institute for Chemical Analysis, Applications, and Forensic Science, Northeastern University, Boston, Mass. 02115 *Anal. Chem., 49 (1977)*

Flameless Atomic Absorption Spectrometric Determination of Ultratrace Elements in Silicon Tetrachloride 2289

Nanogram per gram levels of transition metals are determined in $SiCl_4$ by AAS using a carbon rod atomizer. Precisions and accuracies obtained on a silica standard range from ±1.4 to ±13% and ±4.5 to ±18%, respectively.

T. Y. Kometani, Bell Laboratories, 600 Mountain Avenue, Murray Hill, N.J. 07974 *Anal. Chem., 49 (1977)*

Nitrogen Compounds in Coal Derived Liquids 2292

Five liquid products from different pilot plant scale coal liquefaction processes are examined by column chromatography, GC/MS, low voltage MS, and high resolution MS.

Joseph E. Schiller, Grand Forks Energy Research Center, Energy Research and Development Administration, Box 8213, University Station, Grand Forks, N.D. 58202 *Anal. Chem., 49 (1977)*

Enhancement of Retention by Ion-Pair Formation in Liquid Chromatography with Nonpolar Stationary Phases 2295

The mechanism of ion-pair reversed-phase chromatography is investigated both theoretically and experimentally. Retention of catecholamines with alkyl sulfates proceeds via ion-pair formation in the mobile phase.

Csaba Horvath,* Wayne Melander, Imre Molnar, and Petra Molnar, Chemical Engineering Group, Department of Engineering and Applied Science, Yale University, New Haven, Conn. 06520 *Anal. Chem., 49 (1977)*

Chemically-Bonded Aminosilane Stationary Phase for the High-Performance Liquid Chromatographic Separation of Polynuclear Aromatic Compounds 2306

A commercially available packing material, μBondpak NH_2, is used as a substitute for silica or alumina for normal-phase HPLC separations of aliphatic hydrocarbons and polynuclear aromatic compounds.

S. A. Wise,* S. N. Chesler, H. S. Hertz, L. R. Hilpert, and W. E. May, Institute for Materials Research, Analytical Chemistry Division, National Bureau of Standards, Washington, D.C. 20234 *Anal. Chem., 49 (1977)*

Determination of Some Thiourea-Containing Pesticides by Pulse Voltammetric Methods of Analysis 2310

The polarographic behavior of thiourea, phenylthiourea, α-naphthylthiourea and benzyl(iso)thiourea is investigated in Britton–Robinson buffer and sodium hydroxide solutions.

Malcolm R. Smyth* and Janet G. Osteryoung, Department of Microbiology, Colorado State University, Fort Collins, Colo. 80523 *Anal. Chem., 49 (1977)*

Field Effect Potentiometric Sensors 2315

Potentiometric responses of blocked, capacitively-coupled sensors of the form $AgBr/SiO_2/Si$ are presented. Theory and applications to chemically sensitive field effect transistors are described.

Richard P. Buck* and David E. Hackleman, William R. Kenan, Jr., Laboratories of Chemistry, The University of North Carolina, Chapel Hill, N.C. 27514 *Anal. Chem., 49 (1977)*

Quantitation of Secondary Ion Mass Spectrometric Images by Microphotodensitometry and Digital Image Processing 2322

A technique using both the chemical and spatial information in the elemental images produced by an ion microscope is described and evaluated.

J. D. Fassett, J. R. Roth, and G. H. Morrison,* Department of Chemistry, Cornell University, Ithaca, N.Y. 14853 *Anal. Chem., 49 (1977)*

Top Notch.

Of all the precision balances made by Ohaus, the Triple Beam is most-used overall in the classroom, lab, plant, clinic and hospital.

Small wonder; its three notched and center-reading tiered beams are as easy to read as this. This tough top-loader has a tare beam and poise that makes repetitive weighings and chemical formulations fast and sure.

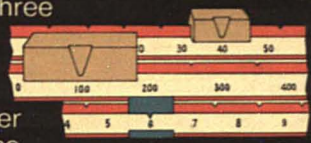

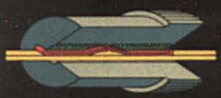

Low-cost, portable and maintenance-free, the Triple Beam is also versatile; accessories include footed scoop and counterweight in either stainless steel or polypropylene. There's also a zero-adjust compensator and other numerous features.

If you'd like these Triple Beam features along with the convenience of a direct reading dial, find out about the Ohaus Dial-O-Gram 1600 series. Write the Ohaus Scale Corporation, 29 Hanover Road, Florham Park, New Jersey 07932.

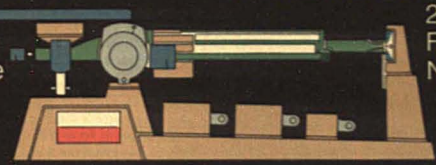

OHAUS

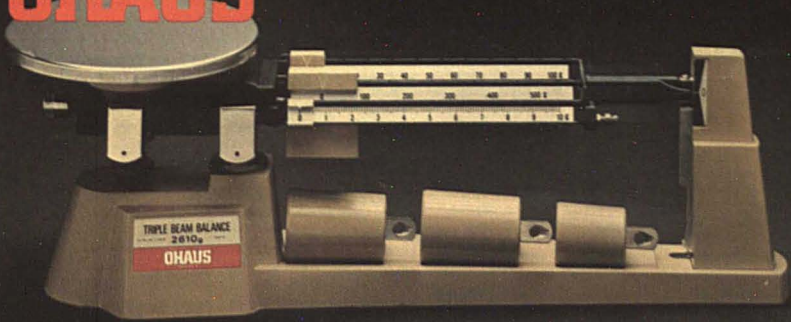

Measuring up since 1907

CIRCLE 157 ON READER SERVICE CARD

Briefs

Quantitative Elemental Analysis of Substituted Hydrocarbon Monolayers on Platinum by Auger Electron Spectroscopy with Electrochemical Calibration 2330

Hydrocarbon coverage is determined by thin-layer coulometry, from which proportionality constants relating Auger electron intensity to coverage are obtained.

James A. Schoeffel, Varian Associates, Vacuum Division, 25 Route 22, Springfield, N.J. 07081, and **Arthur T. Hubbard,*** Department of Chemistry, University of California, Santa Barbara, Calif. 93106 *Anal. Chem., 49 (1977)*

Determination of Carboxylic Esters by Acid Fusion Reaction Gas Chromatography 2337

A procedure for the determination of the combined acid content of nonvolatile carboxylic esters by gas chromatographic analysis of the acidic hydrolysis products is described.

Richard J. Williams and Sidney Siggia,* Department of Chemistry, University of Massachusetts, Amherst, Mass. 01003 *Anal. Chem., 49 (1977)*

Analysis of Polysiloxanes by Alkali Fusion Reaction Gas Chromatography 2343

A variety of alkyl and aryl substituents are determined in polysiloxane fluids, gums, and resins by alkali fusion reaction GC with good precision (±1.0% relative) and accuracy (±0.5% absolute).

David D. Schlueter and Sidney Siggia,* Department of Chemistry, University of Massachusetts, Amherst, Mass. 01003 *Anal. Chem., 49 (1977)*

Determination of Imides, Aromatic Polyimides, Polyamides, and Poly(Amide–Imides) by Alkali Fusion Reaction Gas Chromatography 2349

The amine and/or diamine reaction products are recovered with good precision (±1.0% relative) and accuracy.

David D. Schlueter and Sidney Siggia,* Department of Chemistry, University of Massachusetts, Amherst, Mass. 01003 *Anal. Chem., 49 (1977)*

Determination of Metapramine in Plasma by Gas Chromatography with Nitrogen-Selective and Electron-Capture Detection 2354

The detection limits for underivatized compounds and *N*-heptafluorobutyric derivatives are 15 ng/mL and 35 ng/mL plasma, respectively, and the relative standard deviations are 3.85% and 6.64%.

Alain R. Viala,* Jean-Paul Cano, and Alain G. Durand, Laboratoire de Toxicologie Générale et Biotoxicologie, Faculté de Pharmacie, 27 Boulevard Jean Moulin, 13005 Marseille, France, and **Theo Erlenmaier,** Hewlett-Packard GmbH, Böblingen, West Germany, and **Roger M. Garreau,** Hewlett-Packard France, Lyon, France *Anal. Chem., 49 (1977)*

Critical Evaluation of the Copper(II) Solubilization Method for the Determination of the Complexation Capacity of Natural Waters 2358

Thermodynamic calculations indicate that for realistic ligand concentrations ($\leq 10^{15}$ M), the copper(II) solubilization method is insensitive to most monomeric biogenic ligands and underestimates the true complexation capacity of natural waters.

P. G. C. Campbell,* Marc Bisson, Robert Gagné, and André Tessier, Université du Québec, INRS-Eau, C.P. 7500, Ste-Foy, Québec, Canada G1V 4C7 *Anal. Chem., 49 (1977)*

Correspondence

Molecular Weight and Association of Coal-Derived Asphaltenes 2363

I. Schwager, W. C. Lee and T. F. Yen,* University of Southern California, Chemical Engineering Department, University Park, Los Angeles, Calif. 90007 *Anal. Chem., 49 (1977)*

Interference of 1-Chloro-2-propanol in the Determination of Bis(chloromethyl) Ether in Air by Gas Chromatography–Mass Spectrometry 2365

Frans L. Schulting* and Eric R. J. Wils, Chemical Laboratory TNO, Rijswijk (ZH), The Netherlands *Anal. Chem., 49 (1977)*

Exchange of Comments: Repetitive Determination of Isonicotinic Acid Hydrazide in Flow-Through Systems by Series Reactions 2367

J. F. Fitzloff, Department of Medicinal Chemistry, and **M. I. Blake,*** Department of Pharmacy, University of Illinois at the Medical Center, Chicago, Ill. 60612, and **V. V. S. Eswara Dutt,** Department of Health and Human Ecology, California State College, San Bernardino, Calif. 92407, and **Horacio A. Mottola,*** Department of Chemistry, Oklahoma State University, Stillwater, Okla. 74074 *Anal. Chem., 49 (1977)*

Aids for Analytical Chemists

Analyzer for Determining Fuel Vaporization Pressure Curves of Gasoline and Gasoline–Alcohol Fuels 2368

John H. Baudino, Frank J. Chloupek, and Arthur W. Crowley,* Atlantic Richfield Company, Harvey Technical Center, Harvey, Ill. 60426 *Anal. Chem., 49 (1977)*

Modified Microwave-Induced Plasma Discharge Chamber 2372

Andrew T. Zander, Rod K. Williams, and Gary M. Hieftje,* Department of Chemistry, Indiana University, Bloomington, Ind. 47401 *Anal. Chem., 49 (1977)*

If you're in the market for a mass spectrometer, talk to Du Pont, the first company in mass spectrometry worldwide.

If you have a sample identification problem that might be solved by mass spectrometry, DuPont will be happy to consult with you. You will profit from a depth of international experience that goes all the way back to the beginning—the development of the first commercial mass spectrometer in 1941. Some of the scientists who had roles in the early achievements are still with us.

Over the years we have designed GC/MS hardware to meet growing needs in environmental science, biomedical and industrial research and other applied areas. We've pioneered such technological innovations in GC/MS as: High speed differential pumping. Commercial capillary column GC/MS. Dual CI/EI source. Digitally controlled push-button operation. And we're still pioneering.

In experience and technology, DuPont is the first company in mass spectrometry worldwide. DuPont Mass Spectrometers have solved a wide range of research and measurement problems around the globe. To find out how the latest GC/MS technology can be applied to your needs, write to DuPont Instruments, Room 36074, Wilmington, DE 19898. Or call our hotline: (302) 772-5429.

Mass Spectrometers
Scientific & Process Instruments Division

DUPONT

CIRCLE 53 ON READER SERVICE CARD

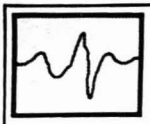

Chemometrics: Theory and Application

ACS Symposium Series No. 52

Bruce R. Kowalski, *Editor*
University of Washington

A symposium sponsored by the Division of Computers in Chemistry of the American Chemical Society.

Order from:
SIS/American Chemical Society
1155 16th St., N.W.
Wash., D.C. 20036

This new collection constitutes an invaluable aid for every analytical chemist, instrument designer, and builder interested in the search for better measurement system control as well as up-to-date optimization and measurement analysis methods.

Increased use of chemical measurements, combined with the proliferation of computers in chemical laboratories, has prompted a drive for new and improved methods to design and control experiments and to analyze the wealth of data that can be generated.

The results of this research effort are discussed in 12 chapters covering the development and application of new mathematical and statistical analysis methods to extract useful chemical information from chemical measurements.

CONTENTS

Optimization Methodology in Chemistry • ARTHUR and Experimental Data Analysis • Abstract Factor Analysis • Target-Transformation Factor Analysis • Application of Factor Analysis to the Study of Rain Chemistry • Electron Spin Resonance of Spin Labels • Stirred-Pool Controlled-Potential Chronocoulometry • Application of Nonlinear Regression Analysis to Chemical Data • Structure–Activity Studies • Enthalpy–Entropy Compensation • How to Avoid Lying with Statistics • SIMCA: A Method for Analyzing Chemical Data in Terms of Similarity and Analogy

288 pages (1977) $21.00 clothbound
LC 77-9088 ISBN 0-8412-0379-2

Archaeological Chemistry

ADVANCES IN CHEMISTRY SERIES No. 138

A symposium sponsored by the Division of the History of Chemistry of the American Chemical Society. Edited by Curt W. Beck.

Order from:
Special Issues Sales
American Chemical Society
1155 Sixteenth St., N.W.
Washington, D.C. 20036

An invaluable sourcebook and working tool describing methods and case histories in which archaeological objects are analyzed using both established and new sophisticated techniques.

Thirteen papers highlight: (1) new methods applied to old archaeological problems, and (2) new types of artifacts studied by traditional methods.

Nondestructive techniques covered: Mössbauer effect spectroscopy, electron microprobe, x-ray fluorescence spectrometry, and whole object neutron activation analysis.

Objects surveyed: Laurion lead ores, Sasanian silver, Egyptian pottery, medieval stained glass, Luristan bronze, Mexican silver and pottery, Near Eastern clays and ivory, Chinese ink, Umayyad and Byzantine coins, Chinese bronze, artists' pigments, and more.

254 pages. 16 color plates. (1974) $26.50 Clothbound. (ISBN 0-8412-0211-7). Postpaid in U.S. and Canada, plus 40 cents elsewhere.

Briefs

Monitoring and Identification of Nonvolatile Organic Deposits in Used Catalysts 2374

Jacob Shen* and J. L. O'Kane, The Standard Oil Company (Ohio), 4440 Warrensville Center Road, Warrensville Heights, Ohio 44128 *Anal. Chem., 49 (1977)*

Removal of Europium Shift Reagents from Nuclear Magnetic Resonance Samples 2375

Gary P. Juneau, Department of Chemistry, Louisiana State University, Baton Rouge, La. 70803 *Anal. Chem., 49 (1977)*

Borohydride-Flame Determination of Arsenic in Phosphoric Acid 2376

Irvin May* and L. Paul Greenland, U.S. Geological Survey, Reston, Va. 22092 *Anal. Chem., 49 (1977)*

Calibration Procedure to Minimize Errors in Continuous Analysis by Ion Selective Electrodes 2377

Lorenzo Liberti* and Antonio Pinto, Istituto di Ricerca Sulle Acque-Consiglio Nazionale delle Ricerche, via De Blasio 5, Zona Industriale, 70122 Bari, Italy *Anal. Chem., 49 (1977)*

Demountable Temperature Jump Cell 2378

John R. Sutter,* Chemistry Department, Howard University, Washington, D.C. 20059, and **Richard M. Reich,** American Instrument Company, Silver Spring, Md. 20910 *Anal. Chem., 49 (1977)*

Low Volume Reference Electrode for Electrochemical Detection and Fraction Collection in High Performance Liquid Chromatography 2379

Curt R. Freed* and Paul A. Asmus, University of Colorado Medical Center, Division of Clinical Pharmacology:C237, 4200 East Ninth Ave., Denver, Colo. 80262 *Anal. Chem., 49 (1977)*

Correction. Steady-State Kinetic Treatment of the Emission from Reduced Pressure Microwave Induced Discharges in Helium 2380
F. W. Lampe, T. H. Risby, and F. A. Serravallo

Correction. Removal of Water in the Distillation of Hydrocarbon Mixtures 2380
T. H. Gouw

Author Index 2383

Keyword Index 2401

"A"-Page Index 2417

THE LECO® EC-12 CARBON DETERMINATOR

AUTOMATIC DIRECT READING AND AFFORDABLE

Contact LECO® for information or a demonstration.

LECO™

LECO CORPORATION 3000 Lakeview Ave. St. Joseph, MI 49085, U.S.A. Phone: (616) 983-5531

CIRCLE 127 ON READER SERVICE CARD

TRACE ORGANIC ANALYSIS BY LCEC!

Our business is helping you with the determination of trace organics in the environment, foodstuffs, body fluids, tissue homogenates, plant material, pharmaceuticals, and bulk industrial chemicals. Complete high performance liquid chromatographs with electrochemical (amperometric) detection are available for your application.

If you have an electroactive molecule on your mind, you should consider liquid chromatography with electrochemical detection. LCEC methods have already been developed for a number of important natural products and drug metabolites. Application notes are available. If you already work in HPLC, we can supply you with several detectors ranging in price from $300 to $1,500 depending on your application.

Send for details . . .

BIOANALYTICAL SYSTEMS, INC.

P. O. Box 2206

West Lafayette, Ind. 47906

(317) 463-1414

CIRCLE 24 ON READER SERVICE CARD

Letters

Citation Error and One Scientist

Sir: Citation analysis, earlier the prerogative of the historian and sociologist of science, has been proposed for measuring the quality of research (for example, J. R. Cole and S. Cole, "Social Stratification in Science", University of Chicago Press, Chicago, 1973). Just as for new instruments and techniques that are often oversold initially, enthusiasm for counting of citations in the *Science Citation Index* (*SCI*) should not normally be extended to an attempt at objective measurement of the quality of an *individual* scientist. Its use should certainly be tempered by an understanding of the more obvious methodological pitfalls such as first author, homonym (homograph), excessive self-citation, and plagiarism of references. To elucidate some of the less evident problems, we made a study of the citations received by Professor I. M. Kolthoff, fairly described as the dean of analytical chemists. Since several hundred citations are attributed to him annually, it was felt that a substantial as well as systematic sampling of these secondary citation problems could be obtained by a study of this one scientist. The two most serious sources of citation error were avoided. The homonym problem, as anticipated for this case, was negligible, and the first-author problem was circumvented by the use of a comprehensive and accurate bibliography for Kolthoff.

Even in the virtual absence of a homonym problem, serious questions as to identification were encountered. As we became more familiar with *SCI* entries, we increasingly realized the extent to which there were entries with incorrect spelling of the surname, interspersion among surnames spelled incorrectly as Kolthoff, incorrect initials, and inaccurate references such as incorrect title and year, volume, or page numbers. (Detailed data can be obtained by writing to W.E.H.) Once an error has been perpetrated, it is often copied in the bibliographies of other authors. When an incorrect reference is combined with a false heading, the results can be confusing for the would-be citation analyst and cause serious distortion in a citation count.

If citation counts are used in an evaluation process for individuals, it is surely essential that all citations intended for the subject of the study be included, and that citations intended for others be excluded. In our opinion, such a goal would be almost impossible to achieve because of errors arising from the homonym problem, the first-author problem (or alternatively, the difficulty in obtaining an accurate bibliography), and errors introduced by authors and by the *SCI* itself.

This letter in no way is intended to denigrate the use of the *SCI* in the assessment of *aggregates* of scientists or as a powerful literature aid to research. We intend to submit other findings not discussed here to a nonchemical journal.

D. Edmonds
W. E. Harris
Department of Chemistry
University of Alberta
Edmonton, Alta., Canada T6G 2G2

Publisher's Note

To conform to provisions of U.S. copyright law effective January 1, 1978, the American Chemical Society is instituting new procedures.

Contributors and readers will notice two changes:

1) Authors will be required to transfer copyright to ACS by means of a simple form. The relationship between the Society and the author will remain unchanged, however, since under prior copyright law ACS has in fact been the copyright owner of individual articles.

2) Issues published after 1/1/78 will have a multiple-digit code at the foot of the first page of most articles. This code signifies ACS participation in the not-for-profit Copyright Clearance Center. Operation of the Center will permit libraries and other institutions to reproduce legally and without delay journal articles beyond "fair use" as described in the new law and accompanying guidelines.

Questions on the new copyright law or ACS procedures may be addressed to the Office of the Director, Books and Journals Division, American Chemical Society, 1155 16th Street, N.W., Washington, D.C. 20036. Or call (202) 872-4556 or 4367.

If you are responsible for any of these types of analytical analysis . . .

PHYSICAL PROPERTIES
- Thickness
- Crystallinity
- Polymerization
- Vulcanization
- Phase Change
- Hydrogen Bonding

KINETICS—REACTIONS
- Time Resolved Spectroscopy
- Continuous Flow Analysis
- Degradation Studies
- Flammability
- Photochemistry

THEORETICAL
- Molecular Orientation
- Molecular Interactions
- Pure Rotation

NEW METHODS
- GC-IR
- HPLC-IR

LOW ENERGY
- ATR
- Emittance
- Highly Scattering
- Strongly Absorbing
- TLC Samples
- In Situ Paint, Ink, Paper, etc.
- Minerals and Soils
- Chemiluminescence
- Matrix Isolation

SMALL QUANTITY
- Micro Samples
- Trace Gasses
- Nanograms

GAS ANALYSIS
- OSHA/EPA Compliance
- Toxic Emissions

SPEED AUTOMATION
- Automated Quality Control
- FDA/OSHA/EPA Compliance Analysis
- Ease of Use
- Replace Several Dispersive IR's
- Any Data Format

NON-CHEMICAL SEPARATIONS
- Surface Coatings
- Solvent Subtract (Aqueous Solutions)
- Major Component Subtract
- Contaminant Analysis
- Additive Analysis
- Coupling Agents, Binders
- Plasticizers
- Residues
- Multiple Films
- Emulsions
- In Vivo
- TLC
- Surfactants

Check the benefits of using the Nicolet 7199 FT-IR System:

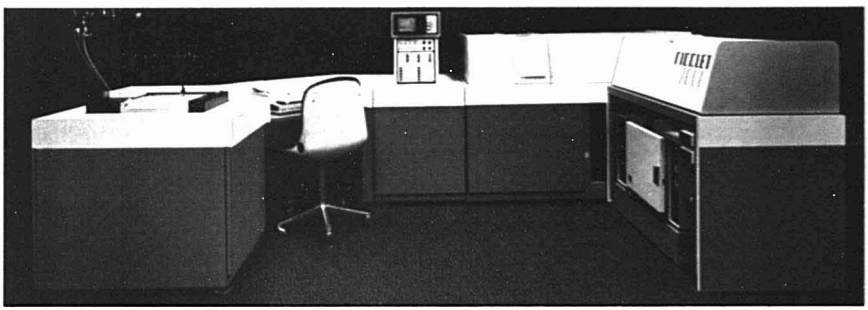

☐ Ease of use through convenient Master Control Station with Display Oscilloscope, system status indicators, automatic display control with roll and zoom capability, automatic experiment control for repetitive experiments at the push of a button and alphanumeric display of frequency and intensity information.

☐ Alignment stability through use of dual air bearings, and laser fringe reference interferometer provide absolute long-term wavenumber accuracy of .01 cm^{-1}.

☐ Subtraction—Automatic absorbance subtraction or interactive spectral display subtraction for detection of trace contaminants, QC testing and many other different spectroscopic techniques.

☐ High resolution of 0.06 cm^{-1} throughout spectral range is a measure of instrument quality and may be used for gas analysis or air pollution monitoring.

☐ Emission—Accessories and software are available for qualitative sample emission measurements.

☐ ATR—The 7199 System's sensitivity and a 3 mm IR focus at the sample make ATR measurements fast and routine for studying opaque IR samples and greatly reducing sample preparation time.

☐ Simultaneous data acquisition, processing and plotting due to NIC-1180 Data System's vectored priority interrupts and direct memory access and time-share capabilities.

For the rest of the details on the 7199 FT-IR or to discuss your analytical application, please telephone or write Nicolet.

NICOLET INSTRUMENT CORPORATION

5225 Verona Road
Madison, Wisconsin 53711
Telephone: 608/271-3333

CIRCLE 151 ON READER SERVICE CARD

ห้องสมุด กรมวิทยาศาสตร์

G. B. Morgan and E. W. Bretthauer
Environmental Monitoring and Support Laboratory
U.S. Environmental Protection Agency
Las Vegas, Nev. 89114

METALS IN BIOENVIRONMENTAL SYSTEMS

Public concern for the protection and enhancement of health and welfare has grown steadily over the past two decades. There is every indication that this concern will persist and that the public will increase its demand for correction of the problems arising from toxic pollutants as the pollutants transcend the environmental media—air, land, water, and food. The chronic exposure of man to increasing amounts of environmental trace metals is one of the problems of immediate concern and poses the following questions:

- What is the limiting burden?
- Can the increased exposure to abnormal amounts of trace metal pollutants continue without measurable alteration of the normal biochemical functions of man and the rest of the ecological system?
- Are adverse subtle effects already beginning to appear?

To answer these questions it is convenient to develop a model (providing adequate biological input information is available), relating the effects or biochemical changes to long-term, low-level exposure to both trace and ultratrace levels of toxic metals. To obtain such input information, it is necessary to look at the total exposure from all pathways, including air, food, water, and dust. We must determine the total absorption and residual concentration in the various parts of the body and then determine the biochemical reactions taking place in the body at the potential binding sites, i.e., metalloenzymes and nucleic acids.

A pollutant-oriented integrated monitoring system is the only way that definitive data can be obtained to determine the total exposure to the critical receptor from the various sources and to determine the chemical and physical forms of the pollutants reaching the receptor from each pathway. This system defines the complex relationship between sources, pollutants, and pathways.

To provide the needed experimental and environmental data associated with the above requirements, the chemist is required to measure trace elements at extremely low concentrations—nanogram or subnanogram levels. In other words, he must be able to measure the low levels likely to be encountered in the environment, in biological organisms, and even their accumulation in a single cell. A great deal of data on long-term, low-level exposure to trace levels of metallic and metalloid elements in the environment is needed before the effects on humans can be definitively established. We presently lack such information even on the more toxic metallic and metalloid pollutants present in trace concentrations, let alone the information for those metals present in the ultratrace concentrations. To date, environmental surveillance with reference to trace metallic and metalloid pollutants has been largely after the fact. For before-the-fact surveillance for epidemiological studies, analytical data must be available virtually on a real-time basis. Accurate measurements of trace metals as they move through the environment are useful for determining the exposure/dose of the critical receptor. To obtain accurate measurements, many questions must be asked relative to the source and transport of the pollutants, exposure/dose relationships, and the biological effects. Some of these questions are as follows:

What is the objective or the goal of the measurement program?

What pollutants are of primary importance?

Who or what is the critical receptor?

What are the pathways of the pollutant through the environment and what physical and chemical changes will occur as it passes through the various media?

How is a representative and accurate measurement of the pollutant obtained?

How is the measurement of the exposure related to the dose?

What are the observed or expected effects?

The analytical chemist has a primary responsibility to assist in developing answers to all of these questions. Many of the past epidemiological studies have been planned and carried out without the participation of the analytical chemist, and such action has resulted in some of the problems that we now face. On the other hand, many chemists in the past were not particularly comfortable in assisting in the development of these answers, but preferred sitting back and analyzing samples delivered to the laboratory. The chemist's input into the program design should include providing detailed recommendations

Exposure of man to increasing amounts of trace and ultratrace metals and metalloid pollutants is a problem of immediate concern. An integrated multimedia monitoring system is necessary to determine accurately the sources and pathways of these pollutants as well as total exposure to the receptor. The analytical chemist's input into such a system includes recommendations on sampling procedures and methods of analysis. Sensitivity, accuracy, selectivity, and cost-effectiveness of the various available methods must be considered. Interpretation of the data and adequate quality assurance are prime responsibilities of the analytical chemist.

on the type and size of sample to be obtained, methods of sample preservation and preparation, and the method of analysis. In recommending the method of analysis, he must consider the various available methods in terms of sensitivity, accuracy, selectivity, and cost effectiveness. Finally, it is the prime responsibility of the analytical chemist to interpret the analytical data, provide qualifications with certain data if necessary, and to implement a quality assurance program to assess the validity of the data being provided.

Pollutant Pathways Studies

Studies of pollutant flows through the environment are essential to the development of advanced monitoring systems in a number of ways. For example, the inter- and intramovements of a pollutant are necessary for the design of a pollutant-oriented integrated monitoring system for the determination of pollutant levels in the various environmental compartments as well as for the determination of the total exposure of the critical receptor. Through such studies, pollutant levels at any given point in the environment can be estimated. Based on these estimated levels, the optimum sampling site or sites for making definitive measurements can be identified. These studies are also extremely useful in determining or estimating the effects of industrial or urban areas on surrounding regions. This is of particular importance for land use or water use planning. Another use of these studies is to determine the fate of toxic metallic and metalloid pollutants, particularly those conserved in the environment.

The California Institute of Technology (Cal Tech), through work partially sponsored by EPA, has developed a method for constructing mass balances for pollutants that move in a connected manner through the air, land, food, and water in an urban industrial region (*1*). The principle upon which this method is based is a conservation of mass for a given chemical element. The method employs chemical element balances for flow diagrams depicting the movement of pollutants through the environment; rates of flow and accumulation for a particular metal can be estimated and then measured for the separate environmental compartments. This method has been tested for lead, zinc, cadmium, and arsenic.

Three basic types of information are needed to construct a mass balance. The development of a mass balance should be initiated by developing a flow diagram for each species of interest. The data necessary to prepare such a diagram are divided into three categories: source or input data, receptor site data, and regional or area output data. The output data refer to the flow of pollutants from an urban or industrial area into the outlying regions. The primary criterion of success for constructing a mass balance is that the sum of the input flows should equal the sum of the output flows plus the pollutant or metal conserved in the area. One problem that has been encountered is obtaining accurate source emission rates. The lack of an accurate emission inventory may result in the failure to identify an important environmental pathway. The most accurate trace metal mass balance constructed to date has been for lead, which is emitted primarily from automotive exhaust. Not only has lead been measured as a pollutant itself, but it has also been correlated to carbon monoxide, which is emitted from the same source. By measuring carbon monoxide at selected sites, verification of the predicted lead level at a given point has been achieved.

The Cal Tech scientists have developed a method to verify the relationship between airborne concentration and deposition of trace metals from the atmosphere. These researchers have shown that for the Los Angeles basin, the airborne size distributions of lead, zinc, and cadmium are bimodal with the upper mode occurring at greater than 10 μm equivalent diameter. Sedimentation of large particles dominates mass deposition near the source. However, this is not the case far from sources. Once the larger particles have settled out, the small particles may remain airborne for considerable periods of time and may be transported over long distances. Most probably these smaller particles are deposited by diffusional deposition. Deposition velocities on rough natural surfaces are likely to be large.

In the Los Angeles basin study, estimates were made of the daily emissions of lead from automobiles (Figure 1) and from lead smelters to the atmosphere. These emissions were then re-

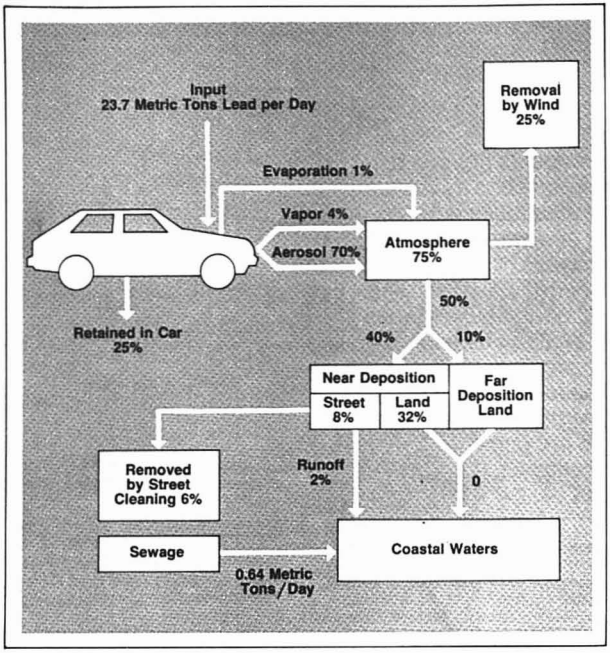

Figure 1. Fate of lead contributed from automotive fleet

lated to the amounts deposited on lands and roadways, and the quantity advected from the basin. Some 24 metric tons of lead as a gasoline additive are consumed each day in the basin. Of this, approximately 18 tons per day are emitted from the exhaust to the atmosphere, and some 6 tons per day are retained in the automobile exhaust system. Of the lead emitted into the atmosphere, approximately two-thirds is deposited in the Los Angeles basin with the remainder advected out of the basin. The one-third advected out of the Los Angeles basin is a major source of atmospheric lead for regions downwind. In addition, more than half of the anthropogenetic lead in the Los Angeles coastal waters comes from automobile exhaust.

The pollutant balance-flow pathway approach is general and can be applied to all environmental pollutants. Although the method does not reveal the details of pollutant dispersion in the environment, the requirements of the mass balance demand that all important environmental pathways, chemical and physical transformations, and sinks be identified and quantified. This is potentially a very powerful method in assessing the environmental impact of a pollutant. There are problems, however, in that large uncertainties exist for both input and output terms for most pollutant species due to a very meager data base. Refinement of this method will require much more detail, better source characterizations, and a better theoretical and experimental understanding of the pollutant pathways and removal processes in the environment, from the source to the receptor. Some of the pathways that must be quantitated are shown in Figure 2.

The integrated monitoring systems approach takes into account not only the pathways of pollutants through the environment to the critical receptor, but the pathways of the pollutant within the critical receptor so that some measurement can be obtained concerning the dose. It is important to realize that effects are based upon dose, not exposure. Figure 3 shows the possible pathways of trace metals in a critical receptor and also the tissues of the body, such as blood, soft tissue, and bone, where the pollutant may be monitored. Information of this type can indicate the dose of the pollutant to the receptor and also indicate some of the changes in biochemical functions that may take place. For many toxic trace metals, the blood level is presently the most important factor in determining effects.

Analytical Requirements for Assessment of Human Exposure

Over the past two decades, analytical chemistry has been elevated to a sophisticated automated state. Unfortunately, however, there has been a lag in applying these more sophisticated methods to the routine measurement of environmental pollutants. This has been due to the high cost associated with automation as well as a lack of understanding the applications and the limitations of these more sophisticated methods. The lower limits of detection for a large number of trace metals are already adequate for situations where large or composite samples can be collected. Conversely, however, we do not have adequate methods, in most cases, for measuring trace and ultratrace levels of metals in cellular and subcellular components.

In spite of the enormous amount of literature dealing with metallobiochemistry of living organisms, very few attempts have been made to understand the metabolism of trace and ultratrace metals at typical environmental levels. Again, the paucity of data is because of the lack of proper analytical techniques. Perhaps more use should be made of neutron and/or proton activation analysis for in vivo tracer studies of ultratrace metals as well as for the study and identification of metal biocomplexes in human tissue. As has been identified many times, the weakest link in pollution health effects studies is inadequate knowledge of individual exposure.

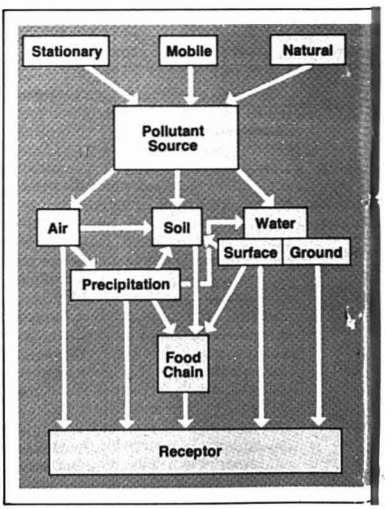

Figure 2. Environmental pathways of pollutants from source to receptor

Analytical Requirements for Measurement of Trace and Ultratrace Metals

There are no widely accepted definitions of trace and ultratrace elements. In the following discussion trace elements will be defined as those elements found at the parts per million (ppm) concentration, and ultratrace elements will be defined as elements occurring below the ppm level. Obviously, almost all of the radionuclides are determined at the ultratrace levels. The exceptions would be a few of the naturally occurring radionuclides such as uranium and thorium, which are determined at trace concentrations.

Generally, the concentration determines whether an element is toxic, benign, or essential. Frequently, however, knowledge of the chemical species (ion or compound form) is equally important. This situation is further complicated by the synergistic effects of groups of elements in both metabolism and toxicity. Due to the considerable difference in the analytical techniques between stable and unstable elements, separate sections in this manuscript will be devoted to each of these elemental types.

Stable Elements

Existing analytical techniques are capable of detecting practically all stable elements of current and future interest. The analytical procedures that appear to have greatest capabilities for trace and ultratrace level stable elemental analysis at the present time are spark source mass spectrometry, neutron activation analysis, optical emission spectrometry, and, at the trace level, x-ray emission spectrometry. At ultratrace concentrations the methods may not be very accurate. However, a semiquantitative survey is frequently useful at these levels.

Gas chromatography (GC), GC–mass spectrometry (GC–MS), gas chromatography–microwave emission spectrometry (GC–MES), and infrared Fourier transform spectrometry are routinely used for metallo-organic compound speciation determination.

Proper sampling procedures are of the utmost importance for trace and ultratrace analysis. For solid samples a homogeneous and representative sample must be obtained. Contamination of the sample must be prevented. In the case of soils, plant tissue, or animal tissue, this may not be an easy task. In the case of liquids, the samples must be adequately preserved to prevent precipitation, chemical transformation, and/or adsorption of the elements of interest. The sample container itself must not contribute to the analysis result. Since any sample handling may easily introduce contaminants, methods that require minimal sample treatment should be employed. The arc or spark optical emission, neutron or proton activation, spark source mass spectrometry, and x-ray emission techniques meet this requirement for solids. Furthermore, all of these techniques are very sensitive and are rapid multielement procedures. For aqueous solutions the plasma excitation optical emission and the other techniques mentioned above may be used. In the case of spark source mass spectrometry and x-ray emission, the solutions that may introduce contaminants must be evaporated. Atomic absorption (AA) does not have the sensitivity for many of the elements required and is not a multielement technique. Furthermore, AA is most easily adapted to liquid solutions.

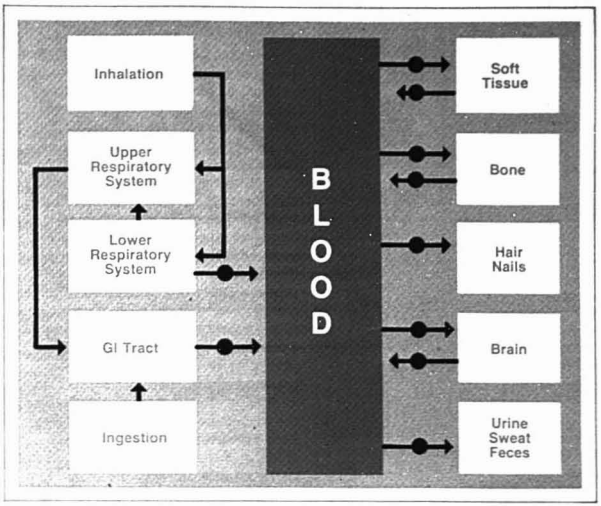

Figure 3. Pathways of metals in critical receptor
● Rates variable, depending on many factors

A critical problem in analyzing samples at the trace and ultratrace levels is the calibration of the analytical instrumentation. Normally, highly diluted aqueous solutions are used to calibrate most instruments. At trace and ultratrace levels the calibration standards are not very stable and are easily contaminated. Therefore, it is very important to have independent accuracy standards that have certified values of a wide range of trace elements at low concentrations. At the present time the National Bureau of Standards has only a few Standard Reference Materials (SRM) available for plant, animal, or soil analysis. None of these has an adequate range of trace or ultratrace elements certified. Clearly, more SRM's are needed for trace and ultratrace elements in animal and soil samples. The existing plant SRM's should also have more trace and ultratrace elements certified.

If ultratrace analyses of metals are to be performed accurately, the analytical laboratory must be extremely clean. This necessitates the use of a carefully filtered air supply. All reagents must be ultrapure, certified, and maintained in an ultrapure state. The deionized water supply must be carefully monitored to ensure that trace element contamination is absent. Careful attention must be given to the personal hygiene of all technicians because hair, skin, cosmetics, excretions, and exhaled air can possibly lead to contamination.

In the case of trace and ultratrace analysis, very strict quality assurance procedures must be instituted and enforced. Only careful, experienced personnel are qualified to perform these types of analyses. Very close monitoring of reagent blanks, standards accuracy, and sample preservation must be maintained to perform analyses at these low concentration levels. Blank levels may easily obscure natural levels of trace or ultratrace elements.

Radioactive Elements and Isotopes

The area of radionuclide analysis offering the greatest challenge is the measurement of the naturally occur-

Hot Box

Tem-Pres Internally Heated Pressure Vessels

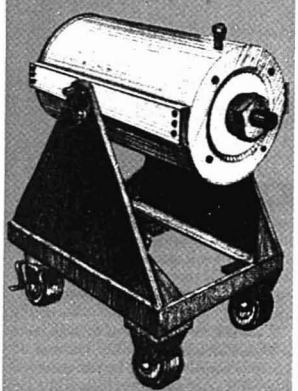

For subjecting samples to pure hydrostatic pressures up to 10 kilobars and temperatures up to 1400°C simultaneously, Tem-Pres offers a variety of pressure vessels with a furnace located inside the vessel housing. Easily replaceable, cartridge-type furnaces, with dual control zones, allow complete control of hot-zone location.

The units operate horizontally or vertically, and open at either end for easy access to the furnace and sample-holding assembly.

specialists in high pressure/high temperature research systems

contact R. M Shoff
Leco Corporation
Tem-Pres Division
1401 South Atherton Street
State College, Pennsylvania 16801
Phone: 814-237-7631

LECO®

CIRCLE 126 ON READER SERVICE CARD

ring alpha emitters and the artificially produced transuranium actinides. Procedures for these elements require time-consuming separations (precipitations, solvent extraction or extraction chromatography, ion-exchange chromatography, electrodeposition) and extremely long measurement times (hours to days).

In this area of analysis many invalid results are now caused by processing high-level samples in moderate- or low-level laboratories or moderate-level samples in low-level laboratories. The lack of knowledge of the appropriate activity of unknown samples is due primarily to the lack of techniques to adequately screen the samples prior to analysis. The erroneous results are caused by cross-contamination between samples, contamination of one or more of the many reagents used in the sample decomposition or analytical separations, mismatching the amount of tracer to the amount of activity actually in the sample, and contamination of counting systems.

A large percentage of actinide analyses currently conducted in the United States is done by contract, under some form of contractual arrangement, where a certain number of analyses are performed for a given amount of money. This fact has probably contributed "directly" or "indirectly" to some of the more serious errors in assessments of actinides in the environment. It has been our experience over the past 10 years that there are many samples that are expected to be accommodated by a "routine" procedure but in reality are quite unusual or nonroutine. For example, soils collected in the same geographic areas may vary considerably, both in their ability to be completely solubilized in a given dissolution procedure, and in the types and levels of chemical interferences with the measurement process. Similar situations exist in the analysis of animal or plant tissue samples. Over the past few years we have recognized that as many as 40% of the samples encountered cannot be considered "routine" and that as much as 10 times the effort may be required to analyze these unusual sample types and produce results comparable to those obtained from the analysis of a "routine" sample.

There is also an urgent requirement for additional standard reference materials containing the naturally occurring alpha emitters and the actinides. The most critical materials would include radium, polonium, thorium, uranium, and plutonium in soil, air filters, water, animal tissue and vegetation. At least two levels of these SRM's should be prepared. One level should be slightly above background levels, and the second SRM should contain moderately higher levels. The only materials available at present are a National Bureau of Standards sediment sample certified for plutonium and several soil samples containing known levels of uranium and thorium produced by the International Atomic Energy Agency and the Energy Research and Development Administration.

References

(1) S. K. Friedlander et al., W. M. Kick Laboratories, California Institution of Technology, "Mass Balances for Pollutants in Urban Regions", Special Report to U.S. Environmental Protection Agency, November 1976.
(2) G. L. Fisher, *Sci. Total Environ.*, **4**, 373 (1975).
(3) E. Sabbioni and F. Sirardi, *ibid.*, **5**, 145 (1977).
(4) E. Schuck and G. Morgan, "Design of Pollutant Oriented Integrated Monitoring System", International Conference on Environmental Sensing and Assessment, IEEE, September 1975.

Presented at the Division of Analytical Chemistry, 174th Meeting, ACS, Chicago, Ill., August 28–September 2, 1977.

George B. Morgan is director of the U.S. Environmental Protection Agency's Environmental Monitoring and Support Laboratory at Las Vegas, Nev. He directs a multidisciplinary staff of nearly 400 people in the development of systems and techniques to monitor environmental quality.

Erich W. Bretthauer is chief of the U.S. Environmental Protection Agency's Methods Development and Analytical Support Branch, Environmental Monitoring and Support Laboratory, Las Vegas, Nev. His interests include the development of analytical methods for the measurement of both radioactive and stable pollutants.

Anyone interested in MICROANALYSIS who doesn't get in touch with us, is missing the boat...

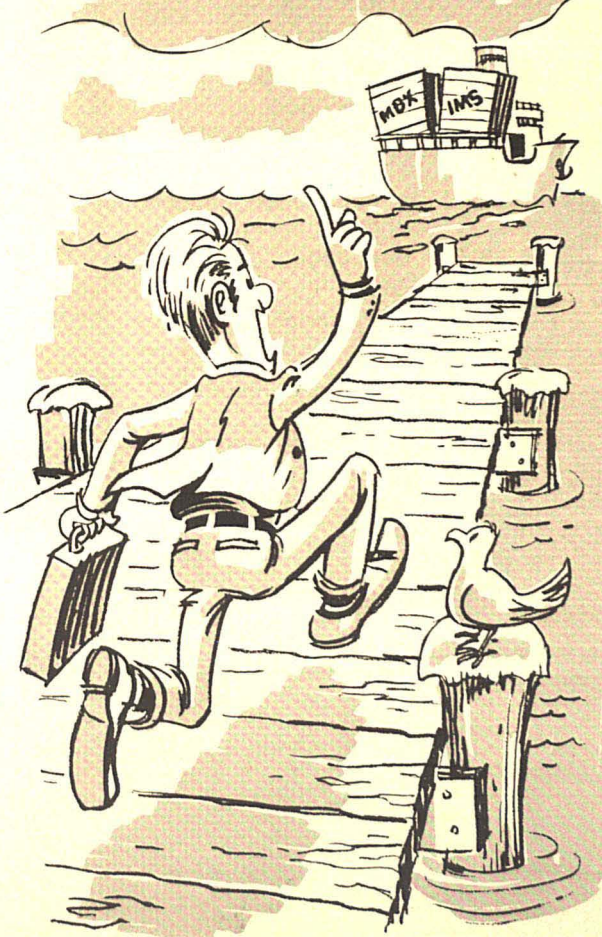

We have the finest Analytical instruments in the world.

Since our introduction of the world's first electron microprobe, no other company has been able to offer as fine a product line of instruments for microanalysis as we do now. Whether your problems are qualitative, quantitative, elemental distribution or trace element identification, our MBX and IMS-3f are the tools you need for quick, accurate solutions. In addition to our outstanding performances, our modularity will allow us to make a configuration to meet your needs and your budget. If you would like to know more, please circle reader service card number below.

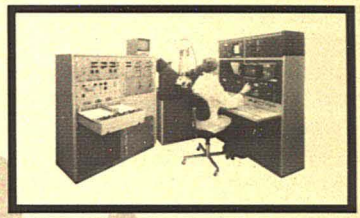

MBX A modular, versatile combination SEM and electron microprobe. A choice of accessories, useful for metallurgy, biology, geology, materials studies and quantitative analysis.

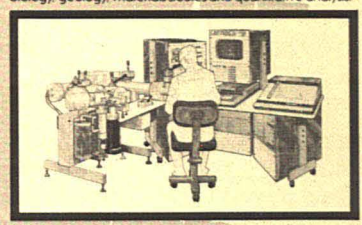

IMS-3f The only second generation ion microanalyzer available today. The analyzer design offers high mass resolution and optimum sensitivity along with direct ion imaging.

CAMECA

Cameca Instruments Inc.
37 Brownhouse Road
Stamford, Connecticut 06902. USA
Phone (203) 348-5252
Telex 710 474 33 46
Cameca
103 Boulevard Saint-Denis
B.P. No. 6, 92403 Courbevoie. France
Phone (1) 333 23 65
Telex 620 348+
Representatives Worldwide
Cameca is a Subsidiary of Thomson-CSF

CIRCLE 33 ON READER SERVICE CARD

HERE'S HOW TO HANDLE PLUNGER PROBLEMS.

This syringe was designed to solve the problem of bending plungers. If you've been having that problem, this Hamilton 800 Syringe is your answer. It has a strong metal stem which travels through the handle and acts as a sturdy guide for the smaller plunger. The stem threads onto the plunger, stablizing it and helping to prevent the plunger from bending.

It is really comfortable to hold and convenient to use a syringe with a handle. The weight balances nicely in your hand and allows you to hold the syringe without the heat of your body affecting the sample.

The flange in the handle contains a friction ring that gives you an adjustable drag on the stem-plunger, providing resistance against high pressure.

These syringes are essentially the tried and true Hamilton 700 Series Syringes, with accurate delivery to $\pm 1\%$. We've just added the handle to make them more convenient and versatile.

If you damage the glass, needle or plunger, you don't have to throw the whole syringe away. Just replace the syringe assembly.

The glass barrel threads into the handle to give you a solid connection. It's easy to make replacements.

The syringe with a handle. It comes in 5 μl and 10 μl capacities. (801N illustrated)

For more information and literature on our 800 Series Syringes, write to John Nadolny, Hamilton Co., P.O. Box 10030, Reno, Nevada 89510.

HAMILTON

CIRCLE 95 ON READER SERVICE CARD

ANALYTICAL CHEMISTRY's Authors:

Publication Practices

Josephine M. Petruzzi,
ANALYTICAL CHEMISTRY

The authors of articles in ANALYTICAL CHEMISTRY, an international broad-based journal, represent a wide variety of interests and specialties. Since the publication of research results is a key element in the research process, it is important to understand the many factors involved in journal/author relationships. Information from our authors on these facets of analytical publication is likely of wide interest because of the unique role the JOURNAL plays in its discipline.

Where do the authors of papers in ANALYTICAL CHEMISTRY work? What are they trying to accomplish in their reported work? Where do they publish and why? What journals are important to them? To answer these and other questions we sent a survey questionnaire to a group of ANALYTICAL CHEMISTRY's authors.

There were 282 papers published from January through June 1977. We sent a total of 253 questionnaires to all unduplicated corresponding authors of these articles. By our cutoff date for returns, we had received 210 replies for a response of 83%. After the cutoff date, we received nine more responses for an overall response rate of 87%. The data given in this survey report are based on the 210 replies received before the cutoff date.

Demographic data on the respondent authors are shown in Table I. The percentage of non-U.S. authors who publish in ANALYTICAL CHEMISTRY doubled in the last eight years. Foreign authorship increased overall from 13% in 1969 to 19% in 1974, and to 26% for the current respondent sample. This sample, which includes 54 foreign authors, nearly duplicates the percentage of foreign authors (27%) found in a survey of 220 authors conducted in 1975 (*1*). It is interesting to note from Table I the relatively low number of authors from foreign industry and the contrasting larger percentage from foreign governmental institutions. Table II presents data on institutions represented by the respondent authors in the current survey along with data collected earlier (*1*).

Reasons for Work

We asked the authors to give the single most important reason for undertaking the specific work published in ANALYTICAL CHEMISTRY. All of the authors responded, and 16 gave mixed reasons. The responses are summarized in Table III. Nearly a third of all authors undertook the reported work "to expand the capabilities of a particular analytical technique". More authors from universities, 18%, were seeking "basic information on some part of an analytical operation", contrasted with 8 and 4%, respectively, from authors in government or industry. In addition, three academic authors indicated in the "other" column that they were doing "theoretical" work and/or basic research of more "fundamental interest". In contrast, university authors were less likely to be developing a specific analytical determination than their counterparts in government or industry. Not surprisingly, only industrial authors were interested in "product quality".

Other reasons given included a "safety investigation" (government), defending a previous publication (in-

Table I. Institutional Affiliations and Foreign/Domestic Distribution

Type of Institution	No. of respondents			% Foreign
	Domestic	Foreign	Total	
University	90	34	124	27
Government	25	14	39	36
Industry	39	6	45	13
Nonprofit/mixed[a]	2	0	2	0
Total	156	54	210	26

[a] Combinations, such as one university author and another industry.

Table II. Institutional Affiliations of Authors of Papers Published in ANALYTICAL CHEMISTRY

Type of Institution	%	
	1975	1977
University	62	59
Government	12	19
Industry	19	21
Nonprofit/mixed[a]	7	1
Total	100	100

[a] Combinations, such as one university author and another industry.

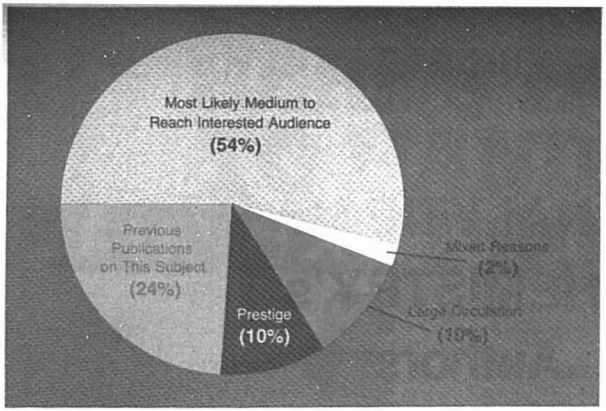

Figure 1. Reasons for publishing in ANALYTICAL CHEMISTRY
Two out of 210 authors did not answer this question

Table III. Reasons for Doing Reported Work

Reason	% University [a]	Government [b]	Industry [c]
Solve a methodology problem	17	18	18
Obtain basic information on some part of an analytical operation	18	8	4
Expand the capabilities of a particular analytical technique	34	31	31
Develop a specific analytical determination	12	28	22
Ascertain instrument capability	2	3	4
Develop an instrument design	5	0	2
Meet Federal, state, or local regulations	2	0	2
Determine product quality	0	0	11
Other, please explain	5	5	2
Mixed reasons [d]	6	8	2
Total	101 [e]	101 [e]	98 [e]

[a] 124 Respondents. [b] 39 Respondents. [c] 45 Respondents. [d] Authors who indicated more than one reason. [e] Figures do not add to 100 because of rounding.

Table IV. Manuscript Review Prior to Submission to ANALYTICAL CHEMISTRY?

Answer	% University [a]	Government [b]	Industry [c]
No	67	18	11
Yes			
Informal review only	25	18	33
Formal internal review	6	64	56
Other, please explain [d]	2	0	0
Total	100	100	100

[a] 123 Respondents. One did not answer. [b] 39 Respondents. [c] 45 Respondents. [d] Other: "I don't know how it was reviewed." "Widely reviewed by users here and abroad as part of a field test program."

dustry), answering a previous author (university), and evaluating a previously proposed analytical method (university). One academic author performed his work "to explore the analytical utility and develop any promising aspects" of a new class of reagents. Another university author was working "to develop a tutorial program by which metallurgy students could simulate and study the effects of changes in steel properties".

Journal Selection and Presubmission Review

A majority (54%) of the authors said they submitted their work to ANALYTICAL CHEMISTRY because it was the most likely medium to reach an interested audience (Figure 1). Twenty-three percent chose the JOURNAL for its "prestige". Ten percent were attracted because of previous publications in their subject matter in the JOURNAL, and 10% because of its large circulation.

Impressive differences between the three groups are manifest in answers about manuscript review prior to submission to ANALYTICAL CHEMISTRY (Table IV). These data certainly support the concept of academic freedom since two-thirds of university authors submitted papers to the JOURNAL without review. Only 6% of the papers from academic institutions had gone through a formal review process, contrasted with 64% of authors from government and 56% from industry. Fifty-six percent for industry does not seem overly large considering the concern with proprietary information and general secrecy in many commercial companies.

Benefits of Publication

In analyzing the responses to the chief benefits of publication, it was necessary to weight the answers and normalize for sample size. The data were analyzed according to authors' affiliations. We also analyzed the data for domestic vs. foreign authorship, but did not find any significant differences based on this.

The most important single benefit of publication was to communicate information. Nearly as important was the self-satisfaction gained from having accomplished recognized work of significance. University authors showed a slightly more pronounced wish to communicate information. Government authors were significant-

ly more aware of the need to meet job requirements than authors from industry or universities.

Enhancement of the reputation and visibility of the author placed third. However, government authors attached significantly more importance to this. Following closely in fourth place and given about equal importance by all is the view that publication is a professional obligation.

Some particularly interesting answers about the benefits of publication included: "keeps our country from being buried by the progress of other countries" (U.S. author); "organizes one's work into a coherent whole as it is completed"; "stimulates more work in this field in the chemical community"; "helps to influence the direction of research and views on the reported topic"; "completes the fundamental trinity of research: work, write, publish" (university author). A government author volunteered that meeting job requirements and securing a promotion or advancement in work activities were virtually synonymous—"these motivations are not insignificant in view of our 'publish or perish' attitude in most government and university organizations, and this attitude leads to excessively fragmented publications". Two authors indicated that the self-satisfaction was derived from doing the work, not from publication.

Important Journals

The authors were asked to list the five most important journals in which they publish and/or which publish material most useful in their work. We analyzed only the first three listed journals by weighting data according to rank in order of the authors' responses. Table V lists the journals in order of decreasing importance. Ten journals are listed from the university-affiliated authors since this group was more than twice as large as the industry and government groups.

Expectably, ANALYTICAL CHEMISTRY was named first by a comfortable majority of the three groups. However, in each group the next journal most frequently cited for first place received relatively few mentions. For academic authors, *J. Am. Chem. Soc.* received seven listings for first place. No other journal received more than one mention for first place from government authors. The industrial group gave three mentions to *J. Am. Chem. Soc.* for first place.

Most striking was the very large number of journals important to authors, especially notable with those in industry and government when the number of respondents was compared with the number of different journals included among the first three in importance. This suggests the wide variety in interests of ANALYTICAL CHEMISTRY's contributors and the key role the discipline and JOURNAL play in other disciplines.

Other data showing journal links are regularly compiled by the Institute for Scientific Information and published in their annual "Journal Citation Reports". Some of this information relating to analytical journals was presented in an abbreviated form in ANALYTICAL CHEMISTRY (2).

Table V. Most Important Journals

University [a]	Government [b]	Industry [c]
ANAL. CHEM.	ANAL. CHEM.	ANAL. CHEM.
J. Am. Chem. Soc.	*J. Chromatogr.*	*J. Chromatogr.*
Anal. Chim. Acta	*Environ. Sci. Technol.*	*J. Am. Chem. Soc.*
J. Phys. Chem.	*J. Am. Chem. Soc.*	*Anal. Chim. Acta*
J. Chromatogr.	*J. Phys. Chem.*	*J. Chromatogr. Sci.*
J. Chem. Phys.		
Appl. Spectrosc.		
Inorg. Chem.		
Clin. Chem.		
Talanta		

[a] 120 Respondents, 102 different journals. [b] 35 Respondents, 52 different journals. [c] 43 Respondents, 50 different journals.

Table VI. Number of Articles Published (Excepting Reported Article in ANAL. CHEM.) Since January 1974

No. of articles	% Respondents		
	University	Government	Industry
0	7	18	20
1–2	8	8	25
3–5	17	24	25
6–10	25	24	20
More than 10	43	26	9
Total	100	100	99 [a]

[a] Figure does not equal to 100 because of rounding.

Numbers of Publications

Our authors were asked to indicate the number of articles (other than the one in ANALYTICAL CHEMISTRY) that they had published since January 1974. These data show marked differences according to the employing institutions of the authors (Table VI). Over 40% of the university authors had 10 or more publications in this period, in contrast to 26% in government and fewer than 10% in industry. Nearly three-quarters in government had more than three publications in this time period, compared to a little over half in industry. Apparently, there is a greater drive for government and university authors to publish.

The idea of more publications from university authors was reinforced by the answers given to the question of whether a future publication was planned and the journal to which the manuscript would be sent. One university author had seven manuscripts in various stages of preparation. Another had three under review at ANALYTICAL CHEMISTRY.

Six New HPLC Columns

Two ion exchange columns
Now you can purchase high efficiency, high capacity, 10 micron ion exchange columns. They're Brownlee Labs packed columns and they're available now from Rheodyne. Look at the chromatogram below!

Are you in Reverse Phase?
Choose RP-2, RP-8, or RP-18 (new). To help you decide which one to use, we have a little note for you.

It is Technical Note #910 and it compares the three reverse phase packings and gives a useful insight into their application.

Fully specified and doubly guaranteed
Brownlee Labs guarantees each column with respect to plates per meter and peak symmetry. Each column is shipped with its own test chromatogram which shows completely specified test conditions and results.

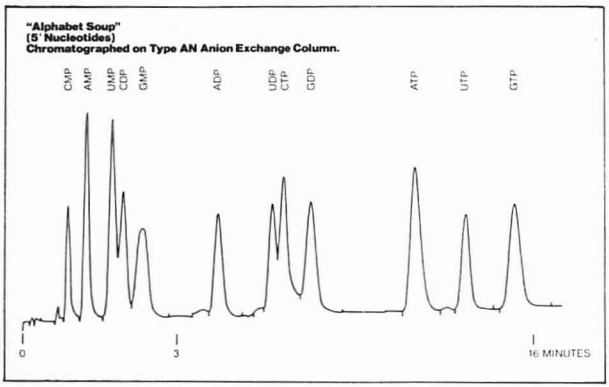

Brownlee HPLC columns* available through Rheodyne

Guaranteed Minimum Specifications		Plates per meter	Symmetry
Reverse Phases			
RP-2 (new)	10 micron	12,000	1.8
RP-8	10 micron	18,000	1.6
RP-8	5 micron	36,000	1.6
RP-18 (new)	10 micron	12,000	1.8
RP-18 (new)	5 micron	24,000	1.8
Adsorption Phases			
Si 100	10 micron	20,000	1.6
Si 100	5 micron	36,000	1.6
Alox T (new)	10 micron	14,000	1.6
Polar Bonded Phases			
NH2	10 micron	18,000	1.6
DIOL	10 micron	16,000	1.6
Ion Exchangers			
AN (new)	10 micron	10,000	2.0
KAT (new)	10 micron	16,000	2.0

*Column packings are LiChrosorb (a trademark of E. Merck, Darmstadt, Germany).
All columns are 4.6 mm I.D. x 25 cm long.

Write for price list and Technical Note #910. Please address Rheodyne, Inc., 2809 Tenth Street, Berkeley, Calif. 94710. For even faster service, phone (415) 548-5374.

RHEODYNE
THE LC CONNECTION COMPANY
CIRCLE 186 ON READER SERVICE CARD

Our authors were also asked where they had last published an article other than in ANALYTICAL CHEMISTRY. Interestingly, responses to this question and the one discussed in the preceding paragraph on future publications elicited somewhat contradictory information. Fifty-nine (30%) respondents answered one or both questions with names of journals they had not listed among the five most important journals in which they publish and/or which publish material useful to their work.

In the contradictory cases, the journals listed as important were more apt to be large, well-known, and widely distributed journals, whereas those listed as last published in and under consideration for future articles were smaller, less widely circulated, and lesser-known journals.

Conclusions

The data collected in this survey offer concrete evidence that some commonly held ideas about publication practices of authors are valid. For example, our data on ANALYTICAL CHEMISTRY show that academic authors outnumber governmental and industrial authors by three to one, publish more papers, and are less apt to have their manuscripts reviewed before submission. The percentage of foreign authors has doubled in the last eight years. Three-quarters publish in ANALYTICAL CHEMISTRY to reach its audience and because of its prestige. Half are working at solving methodology problems or expanding the capabilities of analytical techniques. Although the desire to communicate information and the satisfaction gained from publication of recognized work are seen as major benefits, our authors are aware of the increased visibility and enhanced reputation that come from publication. The authors of papers in ANALYTICAL CHEMISTRY have a diversity of interests as reflected in the variety of journals that are important to them.

Acknowledgment

The author is indebted to Lorrin R. Garson of the Research and Development Department, Books and Journals Division of the American Chemical Society for his aid in preparing the questionnaire and especially for his help in the data analyses. The author is also indebted to the ANALYTICAL CHEMISTRY authors who answered the survey questionnaire promptly and carefully.

References

(1) Petruzzi, J., *Anal. Chem.*, **47** (14), 1277A (1975).
(2) Petruzzi, J., *ibid.*, **49** (8), 741A (1977).

ADD TO THE SCOPE OF YOUR 'SCOPE WITH A 3M SIMS/SEM SYSTEM

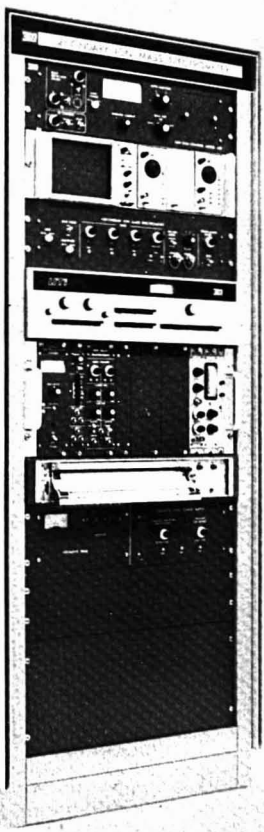

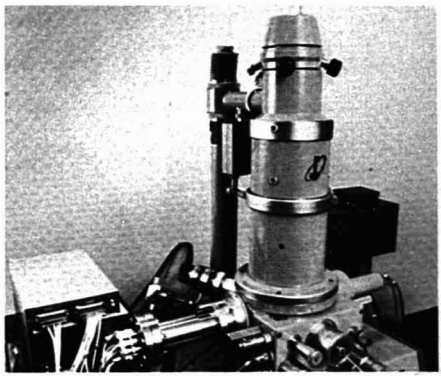

Low Z detection, depth profiling and a surface sensitivity measured in Angstroms are only three benefits offered by a 3M SIMS System. There are more...

Our extensive experience in the chemical analysis of surfaces with SIMS and our history of providing this capability as an attachment to existing instruments have resulted in a 3M SIMS System optimally designed for your SEM. That's why 3M Analytical Systems takes "turnkey" responsibility for the installation. When we say it's ready to go, you can be sure it's *really* ready to go.

And we've barely scratched the surface of our SIMS System here. The full scope of its capabilities must be seen to be appreciated. If you'd like a few more reasons for seeing a demonstration, call 612/733-3909, or write: Analytical Systems, 3M Company, 3M Center, Building 209, St. Paul, MN 55101 and ask for our latest SIMS/SEM brochure. In Europe: Cambridge Instruments, GmbH, Dortmund, Germany.

3M COMPANY

CIRCLE 138 ON READER SERVICE CARD

X-ray analytical equipment is a big investment. Don't you deserve a look at the best investment?

Whether it be spectrometers or diffractometers, Siemens analytical x-ray units are the best investment.

Siemens SRS 200 is a sequential spectrometer that uses x-ray fluorescence methods to non-destructively analyze solid, powder, and liquid samples for all elements from fluorine to uranium. Sample changers are available to accommodate up to 80 specimens. That's flexibility.

For process control applications demanding speed and accuracy, the MRS 400 spectrometer provides up to 28 simultaneous analyses in less than one minute. That's speed.

Siemens D 500 diffractometer provides for material examination; including structure and layer determination, texture and stress measurement, and phase analysis.

The D 500 is available with 1, 30, or 80 specimen magazines, with sample rotation capabilities... perfect for the routine analysis of a large number of samples.

All three units are designed and built to be either automatic or manual. So when you invest in an automatic unit, you get an automatic unit, not just a retrofitted manual instrument.

For more information on your best x-ray analytical investment and a free x-ray periodic table chart, write or call: Mr. Pedro Arredondo, Siemens Corporation, Analytical Systems Division, 1 Computer Drive, Cherry Hill, N.J. 08002, (609) 424-9212.

SIEMENS

CIRCLE 193 ON READER SERVICE CARD

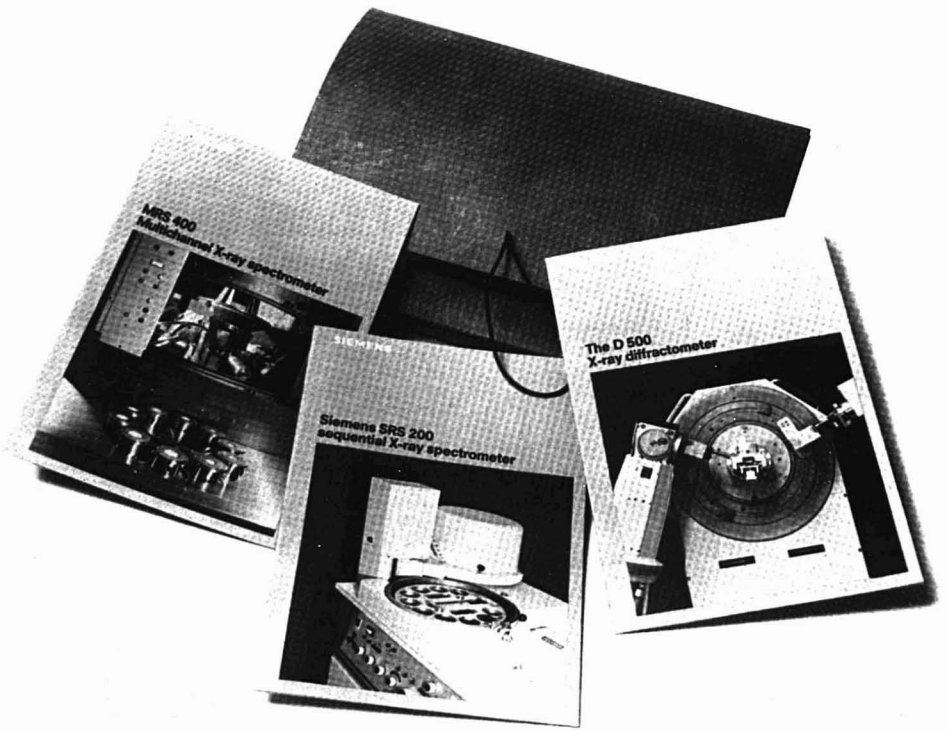

Chromatography Awards

Erwin sz. Kováts

John H. Purnell

Alexander A. Zhukhovitskii

The M. S. Tswett Chromatography Medals were awarded to Erwin sz. Kováts, John Howard Purnell, and Alexander Abramowich Zhukhovitskii at the 12th International Symposium on Advances in Chromatography held in Amsterdam, The Netherlands, November 7–10, 1977.

Erwin sz. Kováts, professor of chemistry at Ecole Polytechnique Fédérale, Lausanne, Switzerland, is honored for the development of the retention index system for the gas chromatographic identification of individual compounds. He showed the correlation of this system with various chemical and physical characteristics of the substances and the possibility of using this system for the characterization of the polarity of stationary phases. Professor Kováts is a native of Budapest, Hungary. Soon after he was graduated from the Technical University Budapest in 1949, he moved to Switzerland and has been living there since. He is the author and coauthor of over 50 scientific publications. In 1969 he served as the chairman of the scientific committee organizing the Symposium on Column Chromatography held in Lausanne, October 7–10.

John Howard Purnell, professor at University College, Swansea, Wales, UK, is cited for his studies on the thermodynamics of chromatography and the separation process. Professor Purnell's interests are divided between gas kinetics and chromatography. His involvement in gas chromatography began in 1955. He was one of the first physical chemists to recognize the analytical power of gas chromatography and the first to apply the technique to the study of gas-phase kinetics. His wide-ranging contributions include studies of the thermodynamics of retention and selectivity, understanding the separation in the column and the relationship of the efficiencies of various column types, and improvements in stationary phase systems and gas chromatographic instrumentation. Dr. Purnell is the author and coauthor of over 100 scientific papers. His book "Gas Chromatography" published in 1962 represents one of the most popular texts in the field.

Alexander Abramowich Zhukhovitskii, professor at Steel and Alloys Institute, Moscow, USSR, is cited for his lifelong work in chromatography, particularly for development of a number of novel approaches such as vacancy chromatography, chromatography without carrier gas, and differential chromatography. His research activities over almost half a century range from quantum chemistry, the theory of liquid and solid state, and the theory of solutions to surface phenomena. Dr. Zhukhovitskii is the author and coauthor of more than 300 scientific articles, five monographs and textbooks, and more than 50 certificates of inventions and patents in various fields of engineering.

Graduate Fellowships

The Fellowship Committee of the American Chemical Society Division of Analytical Chemistry announces its Graduate Fellowship Program for 1978. These fellowships, awarded annually on a competitive basis, provide funds for graduate study and research in analytical chemistry at any accredited ACS institution of the appointee's choice (see page 2129). Research directors at these institutions must be members of the Analytical Chemistry Division. Two types of fellowships are available: full year, $5000 stipend, and summer, $1000 stipend. Last year three full-year and seven summer fellowships were awarded. Funds were provided by Perkin-Elmer Corp., Procter & Gamble, The Upjohn Co., Carle Instruments Inc., Olin Corp. Charitable Trust, Society for Analytical Chemists of Pittsburgh, and the Division of Analytical Chemistry.

Application blanks and detailed information are available from T. R. Williams, Chairman, Fellowship Committee, c/o Dept. of Chemistry, The College of Wooster, Wooster, Ohio 44691. Final award announcements will be made in April.

Ajay Bose (left) and his coworker H. Fujiwara are shown with the chemical ionization mass spectrometer manufactured by Scientific Research Instruments, Inc., of Baltimore, Md.

Positive and Negative CIMS for Biological Studies

In the short span of a decade, chemical ionization mass spectrometry (CIMS) has become one of the most promising analytical tools for the study of natural products, drug metabolism, and some aspects of biomedical research. Ajay K. Bose of Stevens Institute of Technology, Hoboken, N.J., is among many in the field currently investigating the application of this technique to biomedical studies. At the recent International Congress of Pure and Applied Chemists, held in Tokyo during the week of September 4–10, 1977, Dr. Bose and his research associates presented a report on the negative and positive CIMS techniques as clinical diagnostic tools.

The use of negative CIMS enables Dr. Bose and his colleagues to analyze blood plasma directly without the extensive purification and derivatization processes that are usually necessary. They have had particular success in monitoring changes in bile acid patterns. Bile acids are believed to be produced by the body to help digest food and to remove excess cholesterol. Because of these and other biological implications, bile acids are currently of great medical interest. Compounds containing chlorine are also analyzed by the negative CIMS method with very high sensitivity. Dr. Bose suggests use of the technique to search for products in the body derived from highly toxic polychlorinated compounds. One reagent gas extensively used by the group is CF_2Cl_2 (Freon 12). Highly satisfactory chloride adduct mass spectra ($M + Cl^-$) have been obtained for prostaglandins, oligopeptides, bile acid conjugates, oligosaccharides, etc.

Of the various compounds reported to be suitable as the reagent gas for positive CIMS, Dr. Bose and his research associates have found ammonia to be most convenient for the study of compounds such as steroid hormones, bile acids, prostaglandins, phospholipids, penicillin and related antibiotics, oligopeptides, alkaloids, and glycosides. In most cases, an intense pseudomolecular ion corresponding to ($M + NH_4^+$) or ($M + 18$) is observed. As the source of ammonia in the reagent gas, they have used $^{15}NH_4Cl$ in the direct probe to distinguish between NH_4^+ and H_2O and to establish whether an ion is truly an ammonia adduct ion.

Through combined use of negative and positive CIMS, it is possible, starting with a single drop of blood, to obtain a very detailed picture of the individual components present in less than an hour.

Easy Access to Air Pollution Literature

Pertinent articles about almost any subject can be readily found through computerized searches of a large number of bibliographic files of the literature. These files are searched by use of computer terminals connected online to massive storage and retrieval systems. The terminals located in many libraries and other facilities are in instant communication with the bibliographic files through services made available by Lockheed Information Systems, System Development Corp., and Bibliographic Retrieval Services, Inc. (addresses below). The files consist of indexed literature citations, many with abstracts. Among the files on-line with Lockheed is the U.S. Environmental Protection Agency's (EPA) APTIC file of more than 80 000 air pollution citations. (APTIC is an acronym for the former Air Pollution Technical Information Center.)

In addition to access through the commercial sources, EPA provides free literature searches on air pollution to the following category of requesters: state and local air pollution control, transportation, and planning agencies; environmental citizens groups; national government agencies of other countries; along with requesters holding verified EPA contracts or grants for air pollution control work. Requests on letterhead stationery are honored. Qualified organizations should apply to EPA Library (MD-35), Research Triangle Park, N.C. 27711 (919-541-2794 or 629-2779, Federal Telephone System). Below are the service company names and addresses:

Lockheed Information Systems
3251 Hanover Street
Palo Alto, Calif. 94303
800-227-1960 (toll free)

System Development Corp.
2500 Colorado Ave.
Santa Monica, Calif. 90406
800-421-7229 (toll free)

Bibliographic Retrieval Services
1462 Erie Blvd.
Schenectady, N.Y. 12305
518-374-5011

Small Business Receives NSF Innovation Awards

The National Science Foundation (NSF) has announced a total of 42 awards totaling $1 028 000 to small business firms under the program, Small Business Innovation Applied to National Needs. The program is designed to utilize the unique innovative capabilities of small firms to bring new research approaches to important problems in the areas of resources, the environment, and productivity. Projects awarded cover many topics, including hydrometallurgy used in solution mining, chemical threats to man and the environment, earthquake engineering, and ways to improve the Nation's productivity. Phase I awards (a two-phase program) are designed for feasibility research efforts and range from $17 500 to $25 000. Those projects showing most promise after the feasibility study may be funded for the principal research efforts in Phase II. For Phase I, 42 awardees were chosen from 329 proposals submitted by companies having 1–195 employees. Among the awardees are several firms receiving awards for their work in the topical areas of interest to analytical chemists:

Fein-Marquart Association, Inc., Baltimore, Md. ($24 874), for "Approaches for the Acquisition of Mass Spectral Data for Inclusion in the NIH/EPA Mass Spectral Data Base"

International Diagnostic Technology, Santa Clara, Calif. ($25 000), for "Improved Methods for the Rapid Detection of Microbial Contaminants"

Ionomet Co., Waban, Mass. ($25 000), for "Mass Spectrometry Photoplate for Environmental Trace Element Research"

The use of infrared spectrophotometers interfaced with a high-speed laboratory computer system enables researchers at Furman University in Greenville, S.C., to examine the conformational structures of both simple and complex organic molecules. The heart of the instrument system is the computer, which has revolutionized the way in which spectrometric data are analyzed. For instance, the computer assists the conformational experiments by expanding weak signals automatically. And in the subtraction spectrometry the computer instantaneously subtracts spectral bands of one sample from those of another. In the photo a Perkin-Elmer infrared spectrophotometer linked with a Perkin-Elmer Interdata 6/16 computer system is demonstrated by graduate student James Holtzclaw

IRT Corp., San Diego, Calif. ($24 854), for "Immunochemical Assay for Asbestos in the Environment"

Moleculon Research Corp., Cambridge, Mass. ($24 805), for "Reactive Tapes for Automatic Environmental Analysis"

Science Faculty Professional Development Program

The National Science Foundation invites applications for the Science Faculty Professional Development Program grants. The program is designed to help experienced, full-time, two- and four-year college and university science teachers involved primarily in undergraduate science instruction improve their teaching ability to better prepare students for current employment requirements.

In implementing this aim, grants will be awarded to U.S. science teachers to pursue research or study at academic or industrial laboratories. Approximately 130 grants will be made in 1978, and the awards will be announced by mid-April. An applicant must clearly state the specific gains anticipated and the contributions the applicant hopes to make toward the objectives of the program. Awards are made for study or work in the mathematical, physical, medical, biological, engineering, and social sciences, and the history and philosophy of science. Interdisciplinary work is also encouraged. Interested persons should contact Science Faculty Professional Development Program, Division of Scientific Personnel Improvement, National Science Foundation, Washington, D.C. 20550. The closing date for submission of applications is December 16, 1977.

Call for Papers

20th Annual Rocky Mountain Conference on Analytical Chemistry Denver, Colo. August 7–9, 1978. The conference is sponsored jointly by the Rocky Mountain Section of the Society for Applied Spectroscopy and the Rocky Mountain Chromatography Discussion Group. Papers in all fields of analytical chemistry are invited. Submit abstracts of not more than 200 words by April 15, 1978, to Daniel A. Netzel, Conference Chairman, Laramie Energy Research Center, Box 3395, University Station, Laramie, Wyo. 82071 (307-721-2370).

Required Reading

from Waters the Liquid Chromatography People

New!

Analysis of Pharmaceutical Products

Describes rapid, economical assay & quantitation methods for many drug products. LC separations of cough preparations, antibiotics, vitamins, and tranquilizers are detailed as well as various specialized LC techniques.

CIRCLE 230 ON READER SERVICE CARD

New!

Paired-Ion Chromatography

The technique of Paired-Ion Chromatography, an alternative to ion exchange is described. PIC™ allows simultaneous analysis of acids, bases, and neutral compounds.

CIRCLE 231 ON READER SERVICE CARD

New!

Detectors Brochure

Discusses choosing a LC detection system for specific applications. The merits of Model 440 UV/Visible Absorbance Detector and 400 Series Differential Refractometers are cited.

CIRCLE 232 ON READER SERVICE CARD

free from

WATERS ASSOCIATES

215 Maple Street, Milford, MA 01757
Telephone (617) 478-2000

OUR SMALL-SPACE METERING PUMP IS BIG ON ACCURACY.

Our Series 20 Chem/Meter hydraulic diaphragm metering pump will give you repetitive accuracy within ± 1% or better.

Measuring only 9¾" x 4⅛" x 3 7/16", it's designed for steady, continuous feeding of clear fluids. How? The programmed cam drive produces a constant velocity discharge—when the full displacement of two plungers working 180° apart are combined in a common manifold, a steady flow is established. And it provides capacities to 4.9 and 16.0 ML/min—with pressures to 1000 psig.

The series 20 Chem/Meter's wetted parts are made of corrosive resistant stainless steel with sapphire ball-seats and teflon diaphragms. With its totally enclosed, no-seal leakproof design and remote capacity control, its features make it ideal for applications such as chromatography columns, laboratory apparatus and industrial wet process analytical equipment.

To get all the details on why our little Chem/Meter is a big performer, write Chempump Division, Crane Co., Warrington, Pa. 18976.

CRANE **CHEMPUMP**

CIRCLE 35 ON READER SERVICE CARD

photoionization detector for gas chromatography

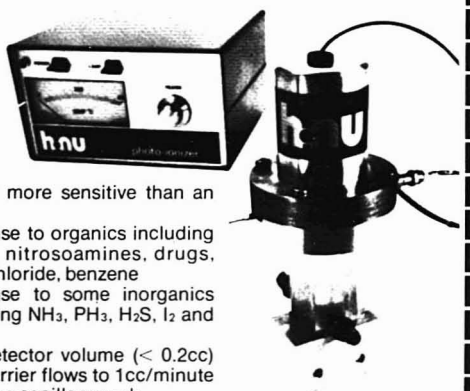

- 10-50x more sensitive than an FID
- response to organics including PAHs, nitrosoamines, drugs, vinyl chloride, benzene
- response to some inorganics including NH_3, PH_3, H_2S, I_2 and Br_2
- low detector volume (< 0.2cc) and carrier flows to 1cc/minute optimize capillary work

h nu

hnu systems 30 ossipee rd.
newton, ma. 02164

(617) 964-6690

CIRCLE 98 ON READER SERVICE CARD

News

Meetings

The following meetings are newly listed in ANALYTICAL CHEMISTRY. *The 1977 and 1978 meetings listed earlier appear in the September, October, and November issues*

- **ASTM Symposium on Use of Ultrasonic Arrays for Imaging in the Industrial and Medical Fields.** Jan. 24–28, 1978. Ft. Lauderdale. *Contact: L. E. Burgess, ASTM, 1916 Race St., Philadelphia, Pa. 19103. 215-299-5505*
- **25th Annual Conference of the Western Spectroscopy Association.** Jan. 25–27, 1978. Asilomar Grounds, Pacific Grove, Calif. *Contact: A. Abu-Shumays, Varian Associates, Palo Alto, Calif. 94303*
- **Symposium on Microprocessors in Measurement and Control.** Feb. 28–March 1, 1978. Cutlers Hall, Sheffield, England. *Contact: R. G. Keiller, Sira Institute Ltd., South Hill, Chislehurst, Kent BR7 5EH, England*
- **10th Annual Symposium on Advanced Analytical Concepts for the Clinical Laboratory.** Mar. 16–17, 1978. Oak Ridge National Laboratory. *Contact: Charles D. Scott, Associate Director, Chemical Technology Div., Oak Ridge National Laboratory, P.O. Box X, Oak Ridge, Tenn. 37830. Page 1136 A, Nov.*
- **International Conference on Computers and Optimization in Analytical Chemistry.** Apr. 5–8, 1978. Amsterdam. *Contact: Secretary, Computers and Optimization in Analytical Chemistry, Laboratory for Analytical Chemistry, Nieuwe Achtergracht 166, Amsterdam, The Netherlands*
- **ISA's Analysis Instrumentation Division Meeting.** May 23–25, 1978. Stouffer's Greenway Plaza Motel, Houston, Tex. *Contact: Thomas Puzniak, Gulf Science & Technology Co., P.O. Box 2038, Pittsburgh, Pa. 15230. 412-362-1600. Page 1136 A, Nov.*

Short Courses

ACS Courses. For more information, contact: Department of Educational Activities, American Chemical Society, 1155 Sixteenth St., N.W., Washington, D.C. 20036. 202-872-4508

Modern Techniques in Gas Chromatography
New York City. Dec. 2–3. Harold

The 204 Chromatograph expansion plan

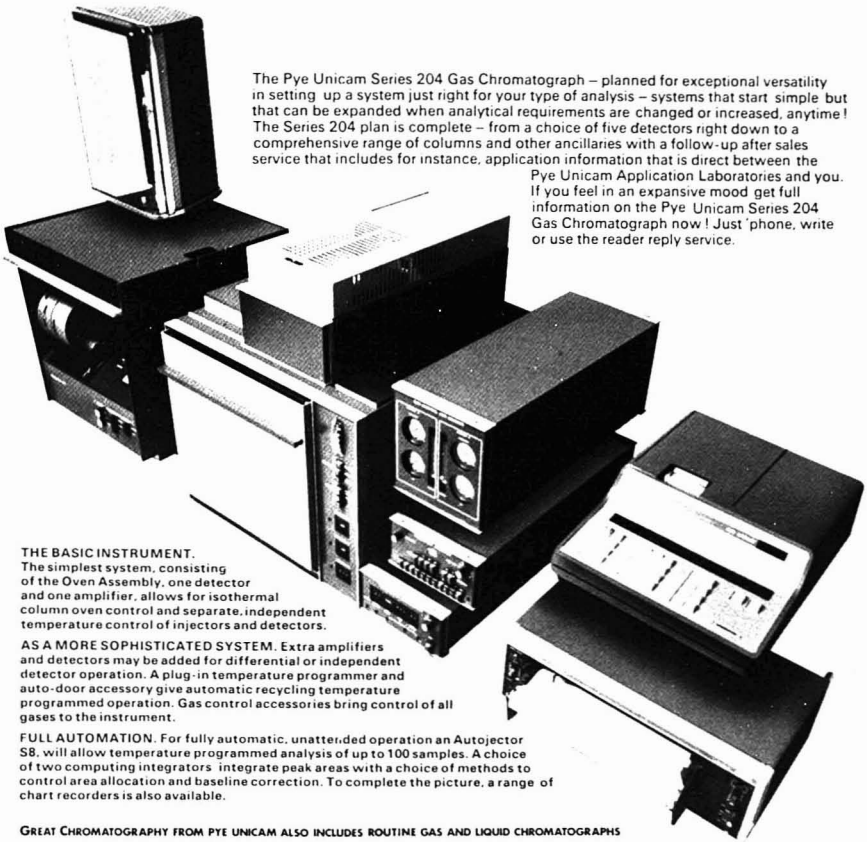

The Pye Unicam Series 204 Gas Chromatograph – planned for exceptional versatility in setting up a system just right for your type of analysis – systems that start simple but that can be expanded when analytical requirements are changed or increased, anytime! The Series 204 plan is complete – from a choice of five detectors right down to a comprehensive range of columns and other ancillaries with a follow-up after sales service that includes for instance, application information that is direct between the Pye Unicam Application Laboratories and you. If you feel in an expansive mood get full information on the Pye Unicam Series 204 Gas Chromatograph now! Just 'phone, write or use the reader reply service.

THE BASIC INSTRUMENT. The simplest system, consisting of the Oven Assembly, one detector and one amplifier, allows for isothermal column oven control and separate, independent temperature control of injectors and detectors.

AS A MORE SOPHISTICATED SYSTEM. Extra amplifiers and detectors may be added for differential or independent detector operation. A plug-in temperature programmer and auto-door accessory give automatic recycling temperature programmed operation. Gas control accessories bring control of all gases to the instrument.

FULL AUTOMATION. For fully automatic, unattended operation an Autoject or S8, will allow temperature programmed analysis of up to 100 samples. A choice of two computing integrators integrate peak areas with a choice of methods to control area allocation and baseline correction. To complete the picture, a range of chart recorders is also available.

GREAT CHROMATOGRAPHY FROM PYE UNICAM ALSO INCLUDES ROUTINE GAS AND LIQUID CHROMATOGRAPHS

Pye Unicam Ltd
York Street, Cambridge, England CB1 2PX
Cambridge (0223) 58866. Telex: 817331

A member of the Pye of Cambridge Group

CIRCLE 173 ON READER SERVICE CARD

SPECTRASPAN IV

plasma spectrometry at atomic absorption prices

Spectraspan IV computer-aided plasma-emission spectrometers offer far more capabilities than atomic absorption units, yet are competitively **priced.**

Think about it. For about the cost of an atomic absorption unit, you can have a simple totally-integrated system that performs all common atomic absorption analyses **plus** analysis of:

- **Boron and phosphorus**
- **Elements which form refractory compounds**
- **Complex solutions having dissolved-solids contents as high as 20 per cent**
- **High acid concentrations**
- **Trace to major element concentrations**
- **Difficult elements including some non-metals**

All Spectraspan IV systems are compact bench-top units designed for sequential quantitative analysis of most elements automatically. Rapid comprehensive qualitative analysis is also available. Conversion from one mode of operation to the other can be accomplished in seconds.

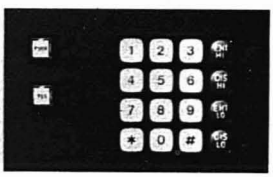

These low-cost systems feature unique Echelle Grating Spectrometers that provide high dispersion of all wavelengths from 190 to 800nm, and powerful dedicated INTEL microprocessors that improve operating efficiency by providing overall control, calibration, monitoring, and reporting with minimum operator attention. In addition, Spectraspan IV systems consume little power, and operate on safe, inert argon which eliminates the need for lamps and explosive gases.

If you want to increase your capabilities to meet today's analytical requirements without increasing costs, invest in Spectraspan IV. Call SMI now for details. SMI is an acknowledged leader, and the company that has more plasma-emission spectrometers in use by satisfied customers throughout the world than any other manufacturer.

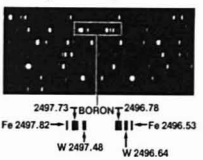

SMI

SPECTRAMETRICS INCORPORATED
204 ANDOVER STREET, ANDOVER, MA 01810
(617) 475-7015

CIRCLE 194 ON READER SERVICE CARD

Choosing your Graduate School?
Find out which schools are concentrating in your area.

Involved in Research?
Learn what papers your colleagues are writing in your field.

The Directory of Graduate Research 1977

Comprehensive listing of U. S. and Canadian Universities offering doctoral programs in chemistry, chemical engineering, biochemistry and pharmaceutical/medicinal chemistry including detailed information on research professors and their publications.

Whether you are a recognized authority in your field, just about to start your graduate study, or concerned with research in chemical science, it is vital for you to know who is working in your area, what they are doing, and where they are doing it.

The Directory of Graduate Research lists complete information on universities—details on professors, the papers they have published, their areas of specialization. For added convenience, individual researchers are also listed alphabetically and individual telephone numbers are included in most cases.

Researcher or graduate student, you will find this comprehensive, 868-page, 8½ × 11 volume one of the best investments you can make. The cost is just $25.00.

To order your new 1977 copy, call: (202) 872-4364, write or mail the coupon below.

Dept. 101
American Chemical Society
1155 16th Street, N.W.
Washington, D. C. 20036

Please send me _____ copies of the Directory of Graduate Research, 1977 Edition @ $25.00 a copy.

Name _____

Affiliation (if any) _____

Address ☐ Home ☐ Organization

_____

City _____ State _____

Zip _____ Phone _____

McNair and Stuart Cram. Given in conjunction with the Eastern Analytical Symposium. $195, ACS members; $235, nonmembers

Solving Problems with Modern Liquid Chromatography
New York City. Dec. 3–4. J. J. Kirkland and Lloyd Snyder. Given in conjunction with the Eastern Analytical Symposium. $220, ACS members; $260, nonmembers

Liquid Chromatography: Theory and Practice
Blacksburg, Va. Dec. 6–9. Harold McNair, James Miller, and William Baitinger. $425, ACS members; $485, nonmembers

Laboratory Safety: Recognition and Management of Hazards
San Francisco. Dec. 7–9. Norman Steere and Maurice Golden. $255, ACS members; $305, nonmembers

Thin-Layer Chromatography
San Francisco. Dec. 8–9. Victor Rodwell and Donald McNamara. $195, ACS members; $235, nonmembers

Microprocessors and Minicomputers
Blacksburg, Va. Dec. 11–16. Raymond Dessy and the Chemistry Department Instrument and Design Group from VPI&SU. $425, ACS members; $485, nonmembers

Column Selection in Gas Chromatography
Cleveland. Feb. 25–26, 1978. Given in conjunction with the Pittsburgh Conference. Harold M. McNair and Walter R. Supina. $165, ACS members; $205, nonmembers

Thermal Methods of Analysis
Cleveland. Feb. 25–26, 1978. Given in conjunction with the Pittsburgh Conference. Wesley W. Wendlandt and Ilya M. Sarasohn. $195, ACS members; $235, nonmembers

Statistics for Experimental Design
Cleveland. Feb. 25–26, 1978. Given in conjunction with the Pittsburgh Conference. John Hromi. $195, ACS members; $235, nonmembers

Thin-Layer Chromatography
Cleveland. Mar. 3–4, 1978. Given in conjunction with the Pittsburgh Conference. Victor W. Rodwell and Donald J. McNamara. $195, ACS members; $235, nonmembers

In Fraction Collecting, there are probably three names to know.

Buchler is one of them.

Buchler's Fractomette® Alpha 200 gives you more features as standard. Its low base price includes: automatic shutdown after preset number of tubes—up to a full 200; automatic flow interruption upon tube shift; heavy, rigid plastic dust cover; and much more . . . including Buchler's exclusive lift-off platform and patented overflow shutoff system. Reliability is enhanced by solid-state pull-out electronics and a dependable, easy-to-read L.E.D. digital display.

The Alpha 200 is big in value but small in size: it takes only 1¼ square feet of space and was designed with cold-room use in mind. We have other circular and linear Fraction Collectors up to 400 tubes, as well as the Fracto-Scan™ for reliable UV monitoring. All are available through leading laboratory supply houses.

SEARLE **Buchler Instruments**
Division of Searle Diagnostics Inc.
1327 Sixteenth Street
Fort Lee, New Jersey 07024 U.S.A.
201-224-3333

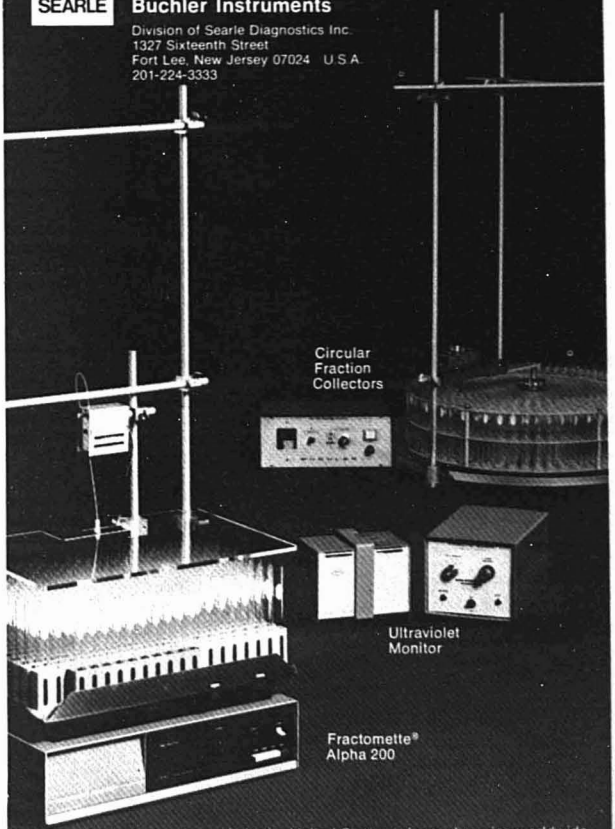

Buchler Instruments: made in the United States, sales and service worldwide.

CIRCLE 27 ON READER SERVICE CARD

Solving Problems with Modern Liquid Chromatography
Cleveland. Mar. 3–5, 1978. Given in conjunction with the Pittsburgh Conference. J. J. Kirkland and Lloyd R. Snyder. $220, ACS members; $260, nonmembers

Laser Technology: Fundamentals and Applications
Atlanta, Feb. 13–14, 1978; Los Angeles, Apr. 10–11, 1978; Chicago, June 12–13, 1978; New York, Dec. 5–6, 1978. Benjamin J. Pernick and Kenneth G. Leib. Sponsored by New York University, School of Continuing Education. *Contact:* Heidi E. Kaplan, Dept. 14NR, New York Management Center, 360 Lexington Ave., New York, N.Y. 10017. 212-953-7262

Gas Chromatography
Occidental College, Los Angeles. Mar. 20–22, 1978. $200. *Contact:* C. D. West, Department of Chemistry, Occidental College, Los Angeles, Calif. 90041. 213-259-2762

16th Annual Introductory Course in Gas Chromatography
College of Pharmacy, U. of Illinois. Mar. 21–24, 1978. Sponsored by the Chicago Chromatography Discussion Group. $135 (includes lunches, text, and laboratory manual). Registration will be limited to the first 60 students. *Contact:* J. B. Himes, The Richardson Co., 2701 W. Lake St., Melrose Park, Ill. 60160

For Your Information

An article entitled **"C/N Ratios in Source Rock Studies"** by Douglas W. Waples of the Colorado School of Mines is published in the school's *Mineral Industries Bulletin.* The article examines the use of carbon-to-nitrogen ratio data in the understanding of the types of material, known as kerogens, that generate oil and gas. As the kerogens break down and yield oil or gas, the residue becomes depleted in hydrogen and nitrogen. Geochemists can analyze the kerogens to determine how far along the oil generation process is, as well as the nature of the original organic material when the process began. *Mineral Industries Bulletin,* Vol. 20, No. 5, September 1977, is available for $2.00 from the Colorado School of Mines, Publications Office, Golden, Colo. 80401.

The ninth annual report on patterns of graduate enrollment and postdoctoral support in science and engineering fields was released by the National Science Foundation (NSF). The report entitled **"Graduate Science Education Student Support and Postdoctorals, Fall 1975"** (NSF 77-313) provides a detailed analysis of statistics supplied annually by graduate science department chairmen in PhD granting institutions in the U.S. through the survey of Graduate Science Student Support and Postdoctorals. The report examines patterns of student and postdoctoral support in terms of major sources of funds and types of major support, level of study, citizenship, and sex of students in science and engineering disciplines. Copies of the report are available from the Superintendent of Documents, U.S. Government Printing Office, Washington, D.C. 20402 for $2.20 per copy, Stock Number 038-000-00-33-0.

The International Union of Pure and Applied Chemistry (IUPAC) announces the publication of two reports entitled **"Polarographic Half-Wave Potentials of Inorganic Substances in *N,N'*-Dimethylformamide"** and **"Dimethylformamide: Purification, Tests for Purity and Physical Properties".** The reports were prepared by IUPAC Analytical Chemistry Division's Commission on Electroanalytical Chemistry and published in the IUPAC journal *Pure and Applied Chemistry,* Vol. 49, No. 6 (1977).

Gardner Laboratory (P.O. Box 5728, 5521 Landy Lane, Bethesda, Md. 20014), manufacturer of appearance measurement and quality control instruments, **announces the appointment of the Wm. B. Tabler Co. as their technical representative** in the Midwest. The Tabler Co. has represented Gardner in Tennessee, Kentucky, southern Indiana, and the greater Cincinnati area for the past decade. The territory to be served by the new agreement includes Illinois, Wisconsin, Minnesota, eastern Iowa, Michigan, Indiana, southwest Ohio, Kentucky, and Tennessee. Corporate offices of Tabler are located at 3004 S. Preston St., Louisville, Ky. Regional offices are located at 525 N. Quentin Rd., #507, Palatine, Ill.

Hellma—the largest assortment of highest precision glass and quartz cells.
Standard · Flow-through · Constant-temperature
Anaerobic · Special Designs
Also available—ULTRAVIOLET LIGHT SOURCES
Deuterium Lamps · Mercury Vapor Lamps
Hollow Cathode Lamps · Power Supplies
HELLMA CELLS, INC.
Write for literature
Box 544
Borough Hall Station
Jamaica, New York 11424
Phone (212) 544-9534
CIRCLE 94 ON READER SERVICE CARD

INDEX TO ADVERTISERS IN THIS ISSUE

CIRCLE INQUIRY NO.	ADVERTISERS	PAGE NO.
2	* Academic Press Flamm Advertising	1245A
1	* Anderson Laboratories, Inc. Worrell-Ericson Advertising Agency	1245A
18, 19	J. T. Baker Chemical Company Naimark & Barba	1242A, 1245A
26	Barnes Engineering Company Jarman, Spitzer & Felix, Inc.	1249A
22	Barnstead Company Marketing Dimensions, Inc.	IFC
28	Berghof Tubinger Satzatelier	1248A
24	* Bioanalytical Systems, Inc.	1208A
23	Bodman Chemicals J L Advertising	1246A
21	* Brinkmann Instruments, Inc. Blatt Advertising, Inc.	OBC
20	* Bruker Instruments Schwietzer Advertising	1282A
27	Buchler Instruments Fletcher-Walker-Gesell, Inc.	1229A
25	* Burdick & Jackson Laboratories, Inc. Studio 5 Advertising	1242A
33	* Cameca Instruments SSS Art Service	1215A
34	Chemtrix, Inc. Fred Schott & Associates	1264A
35	Crane Company Doremus Uptown	1226A
54	* Dohrmann Fred Schott & Associates	1193A
53	* E.I. DuPont de Nemours & Co., Inc. N W Ayer ABH International	1205A
85	GCA/Precision Scientific Winterkorn, Hammond and Lillis, Inc.	1267A
82, 83	* Gilson Medical Electronics, Inc. Towell, Inc. Advertising	1259A
95	* Hamilton Company Mealer & Emerson, Inc.	1216A
94	* Heilma International, Inc. Miller Advertising Agency, Inc.	1230A
97	* Hewlett-Packard Dancer Fitzgerald Sample, Inc.	1261A
98	HNU Systems Demon Advertising Agency	1226A
106	ICN Pharmaceuticals, Inc. Silverman, Inc.	1237A
126, 127	LECO Corporation F Y I	1207A, 1214A
138, 143	3M New Business Ventures Division Kerker & Associates	1221A, 1257A
142, 144	* Matheson Kenyon Hoag Associates	1199A, 1239A
140	MC/B Manufacturing Chemists, Inc. Langeler/Mason, Inc. Advertising	1235A
141	* Mettler Harris D. McKinney, Inc.	1273A

LABORATORY SERVICE CENTER

URANIUM

FLUORIMETRIC ANALYSIS

Sample Fusion Rotary Burner

Reproducible uranium fusions of NaF pellets ~24 fusions in 2-4 min

SASKATCHEWAN RESEARCH COUNCIL
Instrument Laboratory
30 Campus Drive
Saskatoon, Sask.
Canada, S7N 0X1

L-Aspartic Acid • p-Bromophenacyl Bromide • tert-Butyl Chloride
p-Chlorophenoxyacetic Acid • 1,2-Cyclohexanedione • Diacetyl Monoxime
3,5-Dihydroxybenzoic Acid • Dimethyl Adipate • N,N′-Diphenylbenzidine
s-Diphenyl Urea • p-Fluorobenzoic Acid • Glutaric Acid & Anhydride
N-Methylacetamide • Methylene Iodide • Mono, Di, & Trimethylamine HCl
Methyl Furoate • Methyltriphenylphosphonium Bromide • Neocuproine & HCl
Protocatechuic Acid • Saligenin • Silver Diethyldithiocarbamate
Tetraiodoethylene • Tripalmitin • Uracil • Xanthine • Xylitol • Xylose

Write for our Products List of over 3000 chemicals

Tel: 516-273-0900 TWX: 510-227-6230

EASTERN CHEMICAL
Division of GUARDIAN CHEMICAL CORP.
BOX 2500 K
HAUPPAUGE, N. Y. 11787

LAB SAFETY

Send for 1977 Catalog

LAB SAFETY SUPPLY CO.
P.O.Box 1422, Janesville, WI 53545

Microparticle Standards

Large assortment of well-characterized microspheres and micropowders for analytical, research, and testing applications. Range of diameters from .05 to 500 microns (μm). Size and other physical properties are listed for each product. Materials include polystyrene, glass, pollens, minerals, many others. Write or telephone for Data File 45.

Duke Scientific Corporation
445 Sherman Avenue
Palo Alto, CA 94306
Phone (415) 328-2400

Laboratory Service Center (Equipment, Materials, Services, Instruments for Leasing), Maximum space — 4 inches per advertisement. Column width, 2-3/16"; two-column width, 4-9/16". Artwork accepted. No combination of directory rates with ROP advertising. Rates based on number of inches used within 12 months from date of first insertion. Per inch: **1" — $58; 12" — $57; 24" — $56; 36" — $55; 48" — $54.**

CALL OR WRITE BARBARA AUFDERHEIDE

ANALYTICAL CHEMISTRY
25 Sylvan Road, So.
Westport, Ct. 06880
203-226-7131

INDEX TO ADVERTISERS IN THIS ISSUE

CIRCLE INQUIRY NO.	ADVERTISERS	PAGE NO.
139	**Microelectrodes, Inc.** Aries Graphics	1240A
137	* **Mitsubishi Chemical Industries Ltd.** Global Advertising Company, Ltd.	1253A
151	**Nicolet Instrument Corp.** Technical Communications	1209A
150	* **Nissei Sangyo Instruments, Inc.** Kaneko-Murakami, Inc.	1271A
149	* **Norton** Northlich, Stolley of Akron, Inc.	1277A
157	* **Ohaus Scale Corporation** Michel-Cather, Inc.	1203A
156	* **Orion Research, Inc.** OBC Advertising	1197A
169	**Parr Instrument Company** F. Willard Hills Advertising Agency	1240A
178–182	* **Perkin-Elmer Corporation** Marquardt & Roche, Inc. Advertising	1274A–1275A, 1278A–1279A, 1280A–1281A
170, 171	* **Philips Electronic Instruments, Inc.**	1224B, 1224C
167, 168	* **Philips Electronic Instruments, Inc.** Dobbs Advertising Company, Inc.	1268A
177	**Photovolt Corporation** Michel-Cather, Inc.	1201A
175, 176	* **Princeton Applied Research Corporation** The Message Center	1249A
173	** **Pye Unicam, Ltd.**	1227A
186	* **Rheodyne** Bonfield Associates, Inc.	1220A
201	* **Sargent-Welch Scientific Company** Polytech Advertising	1254A
187	* **August Sauter** Planen & Werben	1251A
190	* **Scientific Glass Engineering, Inc.** Arden Advertising Agency	1244A
188	* **Scientific Products** Mitchel Suttner McPhilliamy Inc. Advertising	1265A
193	* **Siemens** Hanson, Fassler, Kolody, Inc.	1222A
189	* **G. Frederick Smith Chemical Company** Andrew Show Advertising	1246A
194	**Spectrametrics** S. Gunnar Myrbeck & Company, Inc.	1228A
192	**SPEX Industries, Inc.** Seymour Nussenbaum	1233A
195–196, 198	* **Varian** Moran, Lanig & Duncan Advertising	1241A, 1243A
230–232	* **Waters Associates** Edward W. Fischer & Associates	1225A
234	* **Whatman, Inc.** J. S. Lanza & Associates	1194A
233	* **Wilks Scientific Corporation** WILSCI Advertising	1263A

* *See ad in ACS Laboratory Guide*

** *Company so marked has advertisement in the foreign regional edition only*

Advertising Management for the American Chemical Society Publications

CENTCOM, LTD.

Thomas N. J. Koerwer, President; James A. Byrne, Vice President; Clay S. Holden, Vice President; Benjamin W. Jones, Vice President; Robert L. Voepel, Vice President; C. Douglas Wallach, Vice President, 25 Sylvan Rd. South, Westport, Connecticut 08880 (Area Code 203) 226-7131

ADVERTISING SALES MANAGER
James A. Byrne

SALES REPRESENTATIVES

Atlanta, GA . . . Robert E. Kelchner, CENTCOM, Ltd. Telephone: 203-226-7131

Boston, MA . . . Don Davis, CENTCOM, LTD. Telephone 203-226-7131

Chicago . . . Thomas Hanley, CENTCOM, LTD., 540 Frontage Rd., Northfield, Ill. 60093. 312-441-6383.

Cleveland . . . James Pecoy, CENTCOM, LTD., Suite 205, 18615 Detroit Ave., Lakewood, Ohio 44107. 216 228-8050.

Houston . . . Robert LaPointe, CENTCOM, LTD., 415-692-0949.

Denver . . . Clay S. Holden, CENTCOM LTD., 213-776-0552.

Los Angeles 90045 . . . Clay S. Holden, CENTCOM, LTD., Newton Pacific Center, 3142 Pacific Coast Highway, Suite 200, Torrance, CA 90505, 213-325-1903

New York 10017 . . . Don Davis, Richard L. Going, CENTCOM LTD., 60 East 42nd St., 212-972-9660

Philadelphia . . . Richard L. Going, CENTCOM LTD., GSB Building, Suite 510 1 Belmont Avenue Bala Cynwyd, Pa. 19004. Telephone: 215-667-9666

San Francisco, CA . . . Robert LaPointe, CENTCOM, LTD., Room 235, 1499 Bayshore Highway, Burlingame, CA 94010. Telephone: (415) 692-0949

Westport 06880 . . . Don Davis, CENTCOM, LTD., 25 Sylvan Rd. So., 203-226-7131.

Manchester, England . . . Jill E. Loney, Technomedia Ltd., 216, Longhurst Lane, Mellor, Stockport, SK6 5PW, Telephone: 061-427-5660

Reading, England . . . Malcolm Thiele, Technomedia Ltd., Wood Cottage, Shurlock Row, Reading, RG10 OOE. Telephone 073-581-302

Paris, France . . . Patric B. Hale, Technomedia Ltd., 18 Rue Gounod, 92 Saint-Cloud, Paris. Telephone: 602-24-79

Tokyo, Japan . . . Haruo Moribayashi, International Media Representatives Ltd., 1, Shibe-Kotohiracho, Minato-ku Tokyo. Telephone: 502-0656

PRODUCTION DEPARTMENT

Production Director
Joseph P. Stenza

Advertising Production Assistant
Barbara Aufderheide

PRODUCT CAPSULES

Scan this list for products of interest. Then, circle the indicated numbers on the adjacent reply card and selected literature from advertisers in the previous issue will be sent to you.

No.	Product Capsules
301	Balances
302	Baths; Circulators
303	Biological Analyzers
304	Books; Periodicals; Catalogs
305	Centrifuge Equipment
306	Chemicals; Reagents; Gases
307	Chromatography, Gas
308	Chromatography, Liquid
309	Chromatography, Thin Layer
310	Computers; Calculators
311	Coolers; Freezers
312	Densitometers
313	Electrical Equip: Amplifiers; Power Supplies; Voltmeters; etc.
314	Electrochemical: pH Meters; Ion Meters; Titrators; Electrodes
315	Electrophoresis
316	Elemental Analyzers
317	Environmental Analyzers
318	Fourier Transform Data Systems
319	Furniture; Fume Hoods
320	Gas Chrom/Mass Spec Systems
321	Labware: Glass; Plastic; Metal
322	Lasers
323	Mechanical Equip: Presses; Mills; etc.
324	Microscopes
325	Mixers; Stirrers; Blenders; Shakers
326	Nuclear Instruments
327	Oscilloscopic Instruments
328	Ovens; Furnaces; Heaters
329	Photometers; Colorimeters
330	Pipets; Samplers; Dispensers
331	Pumps; Flowmeters
332	Recorders; Integrators
333	Services, Analytical; Consultants
334	Signal Averagers
335	Spectro, AA
336	Spectro, Fluorescence
337	Spectro, Infrared
338	Spectro, Mass
339	Spectro, NMR
340	Spectro, UV/Vis
341	Spectro, X-Ray
342	Stills; Demineralizers
343	Supplies: Lubricants; Detergents; etc.
344	Thermal Analyzers
345	Valves; Fittings; Tubing
346	Vacuum Equipment

MULTIELEMENT SOLUTION STANDARDS

SPEX has the SOLUTIONS for your problems . . .

prepared from assayed SPEX HiPure Materials. The concentration of each element is certified on the label. You specify the elements, we provide solutions in various matrices chosen to prevent precipitation and hydrolysis.

MULTIELEMENT SOLUTION STANDARDS
for multielement instrumental analyses (ICP, DCP, AA)

SINGLE-ELEMENT AA StAndArds FOR 68 ELEMENTS (in choice of matrices)

SPEX INDUSTRIES, INC.
P.O. BOX 798 METUCHEN, N.J. 08840 (201) 549-7144

SOLUTION STANDARDS

CIRCLE 192 ON READER SERVICE CARD

FIRST CLASS
Permit No. 25682
Philadelphia, Pa.
19101

BUSINESS REPLY CARD
No postage stamp necessary if mailed in the United States

POSTAGE WILL BE PAID BY

ANALYTICAL CHEMISTRY
P. O. Box #8660
Philadelphia, Pennsylvania 19101

Analytical Chemistry — DECEMBER 1977 — Valid through April 1978

NEW PRODUCTS, CHEMICALS, LITERATURE: 401 402 403 404 405 406 407 408 409 410 411 412 413 414 415
416 417 418 419 420 421 422 423 424 425 426 427 428 429 430 431 432 433 434 435 436 437 438 439 440 441 442
443 444 445 446 447 448 449 450 451 452 453 454 455 456 457 458 459 460 461 462 463 464 465 466 467 468 469
470 471 472 473 474 475 476 477 478 479 480 481 482 483 484 485 486 487 488 489 490 491 492 493 494 495 496

ADVERTISED PRODUCTS: 1 2 3 4 5 6 7 8 9 10 11 12 13 14 15 16 17 18 19
20 21 22 23 24 25 26 27 28 29 30 31 32 33 34 35 36 37 38 39 40 41 42 43 44 45 46
47 48 49 50 51 52 53 54 55 56 57 58 59 60 61 62 63 64 65 66 67 68 69 70 71 72 73
74 75 76 77 78 79 80 81 82 83 84 85 86 87 88 89 90 91 92 93 94 95 96 97 98 99 100
101 102 103 104 105 106 107 108 109 110 111 112 113 114 115 116 117 118 119 120 121 122 123 124 125 126 127
128 129 130 131 132 133 134 135 136 137 138 139 140 141 142 143 144 145 146 147 148 149 150 151 152 153 154
155 156 157 158 159 160 161 162 163 164 165 166 167 168 169 170 171 172 173 174 175 176 177 178 179 180 181
182 183 184 185 186 187 188 189 190 191 192 193 194 195 196 197 198 199 200 201 202 203 204 205 206 207 208
209 210 211 212 213 214 215 216 217 218 219 220 221 222 223 224 225 226 227 228 229 230 231 232 233 234 235
236 237 238 239 240 241 242 243 244 245 246 247 248 249 250 251 252 253 254 255 256 257 258 259 260 261 262

PRODUCT CAPSULES: 301 302 303 304 305 306 307 308 309 310 311 312 313 314 315 316 317 318 319 320 321 322 323
324 325 326 327 328 329 330 331 332 333 334 335 336 337 338 339 340 341 342 343 344 345 346

Name_____ Position_____

Company_____

Street_____ City_____

State_____ Zip_____ Telephone_____

USE . . .

these postage paid reply cards for free data

on all products advertised in this issue.

Analytical Chemistry — DECEMBER 1977 — Valid through April 1978

NEW PRODUCTS, CHEMICALS, LITERATURE: 401 402 403 404 405 406 407 408 409 410 411 412 413 414 415
416 417 418 419 420 421 422 423 424 425 426 427 428 429 430 431 432 433 434 435 436 437 438 439 440 441 442
443 444 445 446 447 448 449 450 451 452 453 454 455 456 457 458 459 460 461 462 463 464 465 466 467 468 469
470 471 472 473 474 475 476 477 478 479 480 481 482 483 484 485 486 487 488 489 490 491 492 493 494 495 496

ADVERTISED PRODUCTS: 1 2 3 4 5 6 7 8 9 10 11 12 13 14 15 16 17 18 19
20 21 22 23 24 25 26 27 28 29 30 31 32 33 34 35 36 37 38 39 40 41 42 43 44 45 46
47 48 49 50 51 52 53 54 55 56 57 58 59 60 61 62 63 64 65 66 67 68 69 70 71 72 73
74 75 76 77 78 79 80 81 82 83 84 85 86 87 88 89 90 91 92 93 94 95 96 97 98 99 100
101 102 103 104 105 106 107 108 109 110 111 112 113 114 115 116 117 118 119 120 121 122 123 124 125 126 127
128 129 130 131 132 133 134 135 136 137 138 139 140 141 142 143 144 145 146 147 148 149 150 151 152 153 154
155 156 157 158 159 160 161 162 163 164 165 166 167 168 169 170 171 172 173 174 175 176 177 178 179 180 181
182 183 184 185 186 187 188 189 190 191 192 193 194 195 196 197 198 199 200 201 202 203 204 205 206 207 208
209 210 211 212 213 214 215 216 217 218 219 220 221 222 223 224 225 226 227 228 229 230 231 232 233 234 235
236 237 238 239 240 241 242 243 244 245 246 247 248 249 250 251 252 253 254 255 256 257 258 259 260 261 262

PRODUCT CAPSULES: 301 302 303 304 305 306 307 308 309 310 311 312 313 314 315 316 317 318 319 320 321 322 323 324 325 326 327 328 329 330 331 332 333 334 335 336 337 338 339 340 341 342 343 344 345 346

Name_____ Position_____

Company_____

Street_____ City_____

State_____ Telephone_____

FIRST CLASS
Permit No. 25682
Philadelphia, Pa.
19101

BUSINESS REPLY CARD
No postage stamp necessary if mailed in the United States

POSTAGE WILL BE PAID BY

ANALYTICAL CHEMISTRY
P. O. Box #8660
Philadelphia, Pennsylvania 19101

PRODUCT CAPSULES

Scan this list for products of interest. Then, circle the indicated numbers on the adjacent reply card and selected literature from advertisers in the previous issue will be sent to you.

No.	Product Capsules
301	Balances
302	Baths; Circulators
303	Biological Analyzers
304	Books; Periodicals; Catalogs
305	Centrifuge Equipment
306	Chemicals; Reagents; Gases
307	Chromatography, Gas
308	Chromatography, Liquid
309	Chromatography, Thin Layer
310	Computers; Calculators
311	Coolers; Freezers
312	Densitometers
313	Electrical Equip: Amplifiers; Power Supplies; Voltmeters; etc.
314	Electrochemical: pH Meters; Ion Meters; Titrators; Electrodes
315	Electrophoresis
316	Elemental Analyzers
317	Environmental Analyzers
318	Fourier Transform Data Systems
319	Furniture; Fume Hoods
320	Gas Chrom/Mass Spec Systems
321	Labware: Glass; Plastic; Metal
322	Lasers
323	Mechanical Equip: Presses; Mills; etc.
324	Microscopes
325	Mixers; Stirrers; Blenders; Shakers
326	Nuclear Instruments
327	Oscilloscopic Instruments
328	Ovens; Furnaces; Heaters
329	Photometers; Colorimeters
330	Pipets; Samplers; Dispensers
331	Pumps; Flowmeters
332	Recorders; Integrators
333	Services, Analytical; Consultants
334	Signal Averagers
335	Spectro, AA
336	Spectro, Fluorescence
337	Spectro, Infrared
338	Spectro, Mass
339	Spectro, NMR
340	Spectro, UV/Vis
341	Spectro, X-Ray
342	Stills; Demineralizers
343	Supplies: Lubricants; Detergents; etc.
344	Thermal Analyzers
345	Valves; Fittings; Tubing
346	Vacuum Equipment

The best of both worlds.

MC/B and EM, associates of E. Merck, Darmstadt, Germany, offer a comprehensive line of laboratory reagents and specialties for research. They are available from conveniently located distributors across the United States. MC/B is the new authority for laboratory analysis and technical service.

Call on us for:

Inorganic reagents and acids
Sorbents, plates and columns for chromatography
Solvents, solutions, stains and dyes
Organics for synthesis and biosciences
Indicators and instrumentation chemicals

Write today or circle the reader service card to receive our product listings and technical information.

CIRCLE 140 ON READER SERVICE CARD

MC/B® **MANUFACTURING CHEMISTS, INC.** EM®

Associate of **E. Merck, Darmstadt, Germany**

2909 Highland Avenue, Cincinnati, Ohio 45212
Telephone (513) 631-0445

REGIONAL SALES OFFICES

East	Central	West
Suite #16	Suite #404	P.O. Box 7203
4 Cornwall Drive	9575 West Higgins Rd	2121 S. Leo Ave
East Brunswick, N.J. 08816	Rosemont, Ill. 60018	Los Angeles, Ca. 90022
(201) 257-7900	(312) 823-1778	(213) 685-5280

New Products

Portable Oscilloscopes

Model OS 3300B is a 50 Hz dual-trace, dual-timebase oscilloscope for analyzing high-speed transients in general-purpose laboratory and servicing applications. High sensitivity, fast time-base speeds, high accelerating potential, and comprehensive triggering abilities match this unit to the most difficult traces. Priced at $1630 including probes. Model OS 4000/4002 combines all the features of the OS 4000 digital storage oscilloscope with automatic trigger-initiated analog and digital outputs. The OS 4000/4002 is ideal for displaying, recording, and analyzing transient waveforms. $4900. Gould Inc., Instrument Systems Div. **417**

Chromatography Data Processor

Model 308 features continuous display of run progress using a unique front-panel visual display. Other standard features include memory storage capacity for 80 peak areas, peak normalization, internal reference, edit of unwanted peaks, recalculation facilities, five automatic baseline handling features, and a built-in diagnostic center with self-test and debug programs in permanent memory. The compact, vertical design saves bench space and allows easy interface. Laboratory Data Control **416**

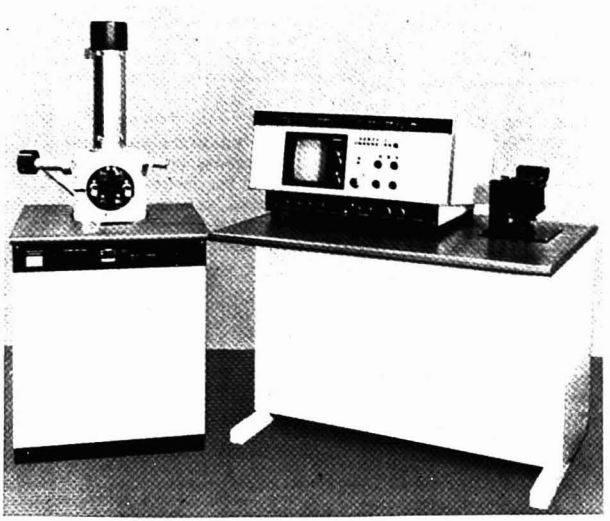

The S-400 Series scanning electron microscope line consists of three models: the S-450 with 60 Å guaranteed resolution, 2–30-kV accelerating voltage, and 20–200 000× magnification; the S-430 with 70 Å guaranteed resolution, 2–25-kV accelerating voltage, and 30–200 000× magnification; and the S-410 with 70 Å guaranteed resolution, 2–25-kV accelerating voltage, and 30–150 000× magnification. Included in all three S-400 Series SEM's are automatic magnification correction for working distance change; automatic brightness control; pushbutton activated, full-frame viewing mode; low magnification (100×) mode; stigmator monitor; focus monitor; and a completely automatic evacuation system. Options available include dual magnification, energy-dispersive x-ray analyzers, and automatic data display. Perkin-Elmer Corp. **403**

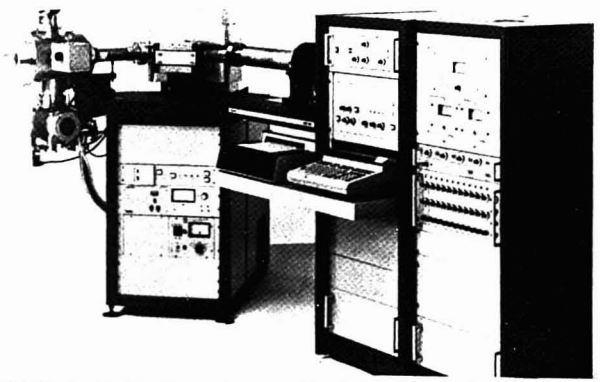

MAT 260 mass spectrometer provides precise determination of isotope ratios in solid samples such as uranium, plutonium, strontium, lead, rubidium, and lithium. This is made possible by einzel lens focusing and a stigmatic focusing analyzer system featuring nearly 100% transmission. The dispersion of the system corresponds to that of a conventional system with a 46-cm ion beam radius. Other features include computer-controlled analysis and highly stable and ultralinear ion-current amplifiers. Varian MAT **401**

Sequential Timer/Programmer for GC and LC

The digital valve sequence programmer is designed for sample selection and injection, controlling switching valves, starting and stopping computer and data system, and other precision timing applications in gas and liquid chromatography. The DVSP is available with two, three, and four intervals, each having a pair of digital time switches, a three-position toggle switch, a LED, and an output relay. Additional features include crystal time base for freedom from power line frequency variation, CMOS logic for high noise immunity, and no moving parts other than output relays. Valco Instruments Co. **413**

For more information on listed items, circle the appropriate numbers on one of our Readers' Service Cards

Have You Read A Good Book Lately?

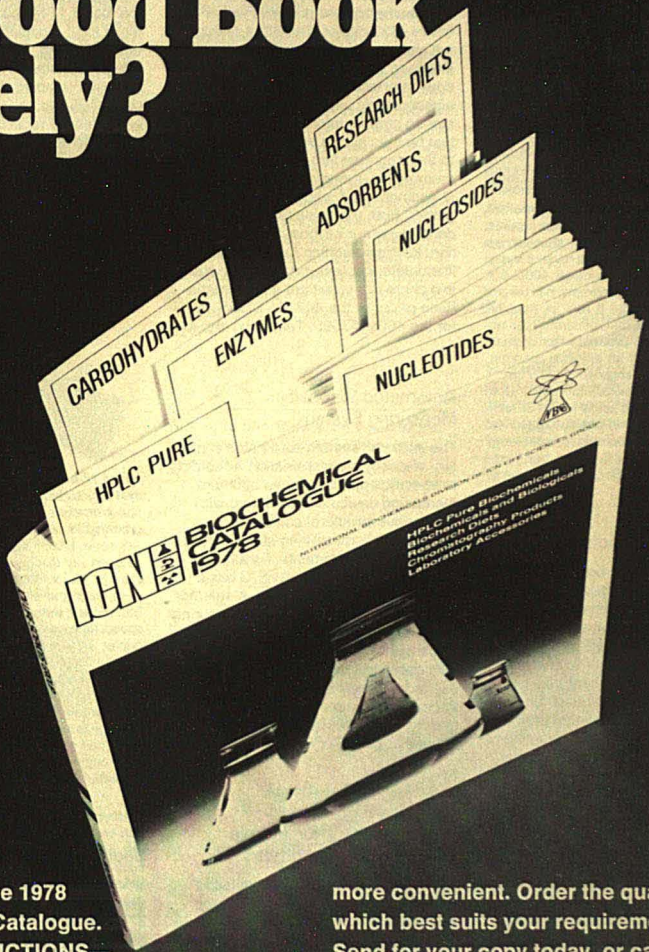

Introducing the 1978 Biochemical Catalogue.

- **PRICE REDUCTIONS—savings on hundreds of items.**
- **NEW PRODUCTS—HPLC Pure Biochemicals. The highest commercial purity available.**
- **NEW SELECTION OF PACKAGE SIZES—Make purchasing and specifying easier, more convenient. Order the quantity which best suits your requirements. Send for your copy today, or call 216-831-3000.**

ICN Pharmaceuticals, Inc.
Life Sciences Group
26201 Miles Road
Cleveland, Ohio 44128

Agenda for 1978 ICN-UCLA SYMPOSIA ENCLOSED!!!

CIRCLE 106 ON READER SERVICE CARD

AccuLab Infrared spectrophotometers, high-performance, low-cost instruments, feature pushbutton controls for abscissa expansion, scanning speeds, and reverse mode. Models 7 and 8 cover the range 4000–600 cm^{-1} and offer two slit programs, narrow and wide. In addition, Model 8 has an AccuSet meter that simplifies fast, accurate gain adjustments. It also has provisions for ordinate scale expansion with an external recorder. Model 9 covers the range 4000–375 cm^{-1}, and Model 10 covers 4000–250 cm^{-1}. Both have the same features as the Model 8. Additional features of all four include rugged and durable design, center-focusing for low-energy application, stepper-drive motors, and nonhygroscopic optics. Beckman Instruments **402**

UV–VIS Spectrophotometer

Model HS 870 accepts both microliter and milliliter type cuvettes to enable the researcher the option of using the instrument as a continuously variable wavelength monitor for HPLC or to do standard spectrophotometric analysis. The double-beam instrument features a digital data display as well as three switchable modes of operation permitting measurement of transmission, absorbance, and concentration. Automatic gain control and zero suppression are standard. A BCD output for computer interfacing is optionally available. The continuously variable monochromator has a wavelength range of 190–700 nm. $5666–$6307. Schoeffel Instrument Corp. **407**

Fraction Collector

Model 2070 UltroRac II features three collection modes: timed-flow, drop-count, and a new pulse control mode that gives precise-volume fractions. The instrument is also equipped with a 12-h memory and synchronized event marking. The drive mechanism is powered by two motors to give precise tube positioning and a tube change time of only 1 s. Solid state electronics are used for control and display. LKB Instruments **409**

Computer Display Terminals

Models 4024 and 4025 allow scrolling of both alphanumerics and graphics. They are the only faster scan terminals available that can copy up to 53 lines of alphanumerics and graphics with a Tektronix 4632 copier. The 4024 features full alphanumeric capability and a copy interface while the 4025 features the copy interface and combined graphic-alphanumeric capability. A method of storing graphic information called a virtual bit map allows the graphic memory to be integrated into the alphanumeric memory list, thereby scrolling the alphanumeric and graphic information together. Both terminals feature a standard typewriter keyboard layout. Standard keyboard editing functions such as line delete, character delete, line insert, and character insert are all automatic. Base price for the 4024 is $2995 and for the 4025, $3595. Tektronix, Inc. **414**

Automated Viscosity Measuring System

The AVS unit system automates capillary viscosity measurements. According to specific applications, an optimum measuring device can be set up with the various structural components. AVS/N with a measuring stand is suited for single measurements. Results are displayed digitally. The AVS/G basic unit provides a tape printout. A selector module is designed for serial measuring sequences with application of up to six viscometers. The automated sampler successively measures the liquids, rinses the viscometer, and changes the samples. A common feature of the AVS system is the precision guaranteed by the use of quartz-crystal clocks. Schott **410**

Data Processor for Atomic Absorption Spectrometry

The system consists of a modified HP 97 printing programmable calculator linked to an Atomspek interface unit and can be used with the Atomspek Series H1550 atomic absorption spectrophotometers. The unit will interpret data received from the instrument, perform the necessary calculations, and then print out the results in percentage concentration for either the absorption or emission modes. Programs are provided on magnetic cards for curvature correction, automatic calibration and recalibration, standard addition techniques, and sample numbering. Rank Hilger, Westwood, Margate, Kent CT94JL, England **412**

Polarographic Analyzer

Model 364 polarographic analyzer is designed to serve the needs of the educational market. It retains the same operating modes and high sensitivity of the Model 174A, but has fixed values of clock rate, modulation amplitude, and output filtering. The 364 may be connected to a standard 174/70 drop timer and uses standard PARC 174A accessories. Data can be displayed on any available recorder. The Model 364 is easy to operate with minimal controls, making it ideal for routine analyses. $1195. Princeton Applied Research Corp. **408**

Midas IV mass spectrometer data analysis system interfaces with most quadrupole mass spectrometers. It is a complete user-programmable system and incorporates the Tektronix Model 4051 graphic system with cathode ray display and magnetic tape data storage. Major features include the capability of operating in either full spectrum Scan or Sim modes, automatic self-calibration, high-speed data buffering, integral alphanumeric printer, and full graphic data presentation. The Midas IV interface has all analog and digital inputs and outputs and control logic necessary to control and acquire data from the mass spectrometer. A general-purpose software package is included with the system; however, users can easily modify programs or develop new ones to meet specific requirements. Scientific Software & Instrument Co. **404**

Sedimentation Balance

Model 4610 incorporates the welghing system and electronics of the Series 3700 balances. Its weighing system can be used for sedimentation analyses as well as for regular weighing up to 50 g, at 1-mg readability. A specially adapted flat recorder provides continuous recording of the sedimentation process. A commercially available thermostat is sufficient to maintain the temperature of the sedimentation jar. Automatic recording of the sediment in relationship to time produces, after several derivations, the particle-size distribution curve. Sartorius-Werke GmbH, P.O. Box 19, D-3400 Goettingen, West Germany **411**

Liquid Chromatography Precolumns

The prepacked precolumns are designed for use as "guard columns" with the expensive microparticulate analytical columns. The columns are all 3.2 mm i.d. and 42 mm long and are available packed with five different types of microparticulate materials. The precolumn to be used with any particular analytical column should be selected on the basis of similarity between the packing materials. Altex Scientific Inc. **415**

High-Pressure Flow Cell

The 7000 psi flow cell is similar in construction to the standard Model 153 cell and is interchangeable with the cells that mount in the Model 150, 151, 152, and 153 detectors. To withstand the pressure the cell is constructed with a stainless steel body. It comes in two diameters that give either 8- or 20-μL cell volume and 10 mm pathlength. The cells can be used in either gradient elution or column recycle liquid chromatography systems to significantly improve detector performance. Altex Scientific Inc. **418**

Chemicals

High-Purity Platinum Thermoelement

Standard Reference Material 1967, platinum wire, is designed for calibration of base-metal and noble-metal thermocouple materials from −197 to 1767 °C. This material, designated Pt-67, replaces the former thermoelectric standard, Pt-27 and is a selected, highly homogeneous portion of the earlier standard. Extensive characterization and homogeneity tests have been performed. SRM 1967 is available as 0.51-mm-diameter wire (24 AWG) priced at $143 per meter. Office of Standard Reference Materials, Room B311, Chemistry Building, National Bureau of Standards, Washington, D.C. 20234

For more information on listed items, circle the appropriate numbers on one of our Readers' Service Cards

Support for Reverse Phase Chromatography

LC-4 is a monomolecular layer of octadecyltrichlorosilane chemically bonded to high efficiency pellicular packing Chromosorb LC-2. The organic phase is permanently bonded with a relatively stable Si-C-type bond, presenting an aliphatic alkyl group on the surface which provides an excellent reverse phase separation. Properties of LC-4 include chemical and hydrolytic stability, stability at high flow rates and varying solvent compositions, narrow particle size distribution, easy dry packing, nonpolar surface, spherical particle shape, no column bleeding, and fast mass transfer and high column efficiency. Johns-Manville **423**

N',N'-Bis(*p*-phenylbenzylidene)-α,α'-bi-*p*-toluidine

With BPhBT liquid crystal high-temperature separations can be achieved for polynuclear aromatic hydrocarbons of higher molecular weight than chrysene. The compound is available as a prepared GC packing or column. Analabs, Inc. **421**

TN-2000 x-ray elemental analysis system consists of a high-resolution interactive display, backlighted control keypad, and the mainframe console housing the powerful LSI-11 microcomputer, x-ray processing electronics, and data storage memory. The control keypad and large screen display are lightweight modules that can be conveniently located remotely from the mainframe for best operation within a laboratory. With its dedicated microprocessor, the display provides comprehensive graphic information, including elemental identification lines and unique elemental symbol peak labels. Operation is simple and efficient since all measurement parameters are selected from labeled functions on the keypad, which is coupled with the interactive display for straightforward analysis setup. The system is directly expandable to accommodate extended x-ray elemental analysis capabilities, including software packages for automated quantitative analysis. Tracor Northern, Inc. **405**

Atomic Absorption Users, Matheson Flash Arrestors Can Protect You, Your Instrument, and Your Lab.

Acetylene is an extremely flammable gas. Many welding accidents have been caused by acetylene flashback—the reversing of the torch flame such that it travels through the hose back into the pressure regulator and /or cylinder. When this happens, the result can be disastrous. Atomic absorption users also experience flashbacks at the instrument burner heads. The same hazard potential, as experienced in welding, exists.

Now AA users can minimize the hazards to themselves, their instruments, and their laboratories by installing a Matheson 6103L Flash Arrestor in their acetylene line.

Easy to install, the model 6103L can be connected in minutes on the outlet of your present acetylene regulator.

We also have a 6103R to protect your N_2O line.

Matheson
Lyndhurst, N.J. 07071

CIRCLE 144 ON READER SERVICE CARD

Manufacturers' Literature

"What Can Liquid Chromatography Do for You?" Presents a comprehensive view of the many aspects of liquid chromatography. Included are descriptive examples of the ways in which LC has been used in many areas. 15 pp. Waters Associates **426**

Leak Detection Systems. Provides information on complete line of leak detectors, including the many uses and advantages for each system. 8 pp. Du Pont Instruments **427**

Electronic Balances. Describes full line of the PL series of compact, precision top-loading balances. 8 pp. Mettler Instrument Corp. **428**

Liquid Chromatography Application Notes. Three new "LC at Work" application notes are available. They are No. 30 on separation of peroxides and hydroperoxides, No. 31 on analysis of Nitrosan, and No. 32 on fluorescence detection of LSD. Varian Instrument Div. **429**

Chemical Services. Describes the company's analytical, testing, and research capabilities including services covering metals, soaps and detergents, paints and coatings, waxes and polishes, pharmaceuticals and drugs, petrochemicals, foods, cosmetics, and chemical specialties. 4 pp. United States Testing Co., Inc. **430**

Instrumentation Modules. Describes McKee-Pederson Instruments' instrument modules that can be used in a variety of electrochemical experiments and may be grouped functionally to form precision test and control systems. Includes operational amplifier, log ratio amplifier, multiplier, digital voltameter, counter/timer, and sample/hold amplifier. 7 pp. Pacific Photometric Instruments **431**

Hydrogen. Features the thermophysical properties of hydrogen and its applications, as well as production, supply and delivery methods, and general safety precautions for handling both gaseous and liquid forms. 12 pp. Airco Industrial Gases **439**

Oxygen Bomb Calorimeters. Describes the complete line for measuring the heat of combustion of any solid or liquid fuel. 24 pp. Parr Instrument Co. **438**

Infrared Spectrophotometers. Features the Series 4200 designed for use in a variety of applications in the biochemical, industrial, and educational fields. Specifications, ordering information, and a complete line of accessories are included. 18 pp. Beckman Instruments, Inc. **432**

Amino Acid Analysis of Collagen. Describes the development of a single-column collagen analysis with the Model D-500 amino acid analyzer. Details of sample preparation, operating conditions, analytical procedure, and results of typical analyses are given. Durrum Instrument Corp. **433**

X-ray Fluorescence Determination of Sulfur in Water. Report outlines sample preparation, experimental conditions, and results and discusses tube-excited fluorescence analysis and its applicability in view of the results of the study. 5 pp. Ortec Inc. **434**

Laboratory Services. Details services available including routine instrumental and wet chemical analyses and microbiological testing, as well as environmental services, bench scale studies, applied research, methods development, and consulting. Arro Laboratories, Inc. **440**

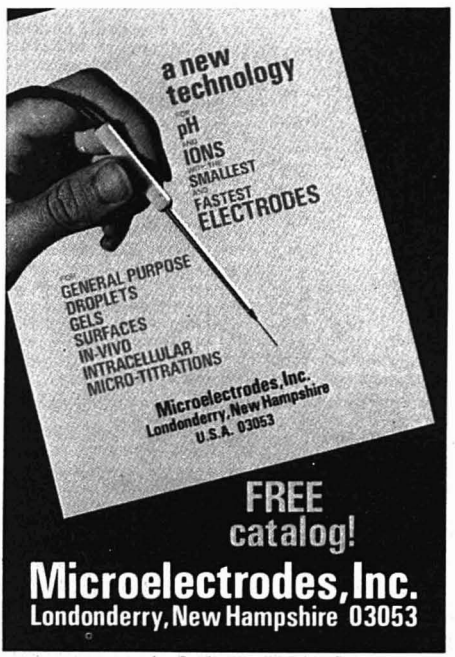

CIRCLE 139 ON READER SERVICE CARD

PARR® BOMBS

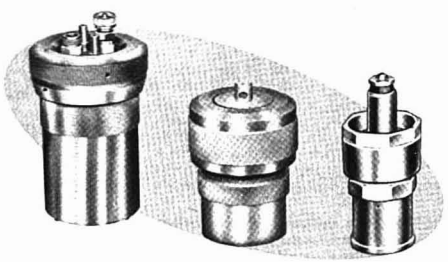

For Oxygen Combustion
For Acid Digestion
For Alkaline Fusion

Standard procedures for sulfur and halogens depend upon Parr oxygen or peroxide combustion bombs for oxidizing solid or liquid samples rapidly with complete recovery of all combustion products; while Parr digestion and fusion bombs give the analyst several effective systems for dissolving silicates, ores and other difficult materials in strong acids or alkalis without losing trace constituents. For details, write or phone: Parr Instrument Company, Moline, Illinois 61265. 309/762-7716

CIRCLE 169 ON READER SERVICE CARD

AND NOW THE VARIAN AA-575... NEVER BEFORE HAS AA BEEN SO EASY, SO PRECISE, SO PRODUCTIVE.

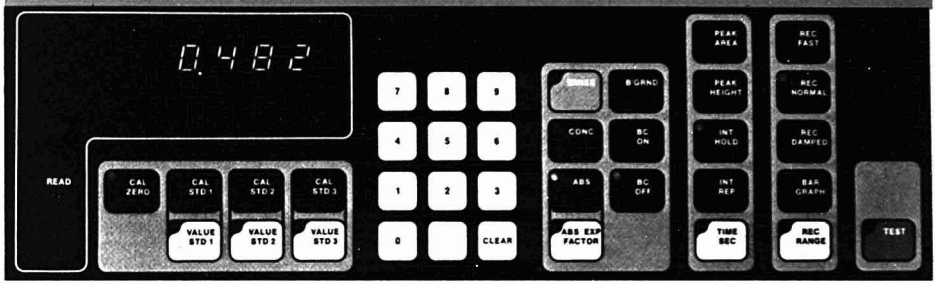

With full microprocessor intelligence, the Varian AA-575 dramatically reduces the time and skill required to get precise answers by atomic absorption analysis.

The AA-575, a unique combination of simplicity and flexibility, allows inexperienced lab technicians to produce answers quickly and reliably, while researching chemists have available the specialized capability to crack the most demanding analytical problems. Capability from push-button double-beam background correction, four chart recording modes, instant recall of peak height and peak area, full compatibility with CRA-90 carbon rod atomizer, ASD-53 sampling dispenser, and the open ended flexibility of the HP9815A programmable calculator.

And yet with all this capability it is the easiest instrument to use. The powerful computer (8 bit microprocessor, 8K memory) controls all signal processing and performs all result processing. The operator is given easy set-up and fast answers. The finger touch control panels, an automatic flame management system, four lamp turret and energy

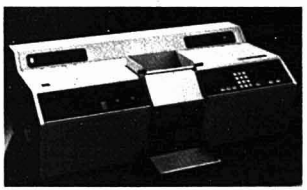

meter all contribute to fast, simple operation. The AA-575 communicates clearly with the operator if inadvertent errors have been made during calibration or operation.

Varian is determined to help solve your analytical problems with a wide range of versatile, high performing spectrophotometers or complete AA analytical systems.

For information write Varian Instrument Division, 611 Hansen Way, Box D-070, Palo Alto, CA 94303.

Circle 198 for product literature.

For immediate response with complete product information on the new AA-575 microprocessor equipped AAS, phone one of Varian's AA field chemists:

EAST
Jim Steensrud - Florham Park, NJ 07932
(201) 822-3700

MIDWEST
Doug Shrader/Jerry Shkolnik
Park Ridge, IL 60068 (312) 825-7772

WASHINGTON DC, SOUTHEAST & MIDSOUTH
Fred Delles/John Morrow
Houston, TX 77036 (713) 783-1800

WEST
Robert Cunico - Los Altos, CA 94022
(415) 968-8141

varian

Manufacturers' Literature

Hard-Layer TLC Plates. GHL Series abrasion-resistant TLC plates feature aninorganic binder that eliminates problems due to solvent-binder interaction. 3 pp. Analtech, Inc. **435**

Laboratory Filtration. Includes details of filter paper classification system, comparison information, sizing chart, and important properties of filter papers. Eaton-Dikeman **436**

Laboratory Tubing. Describes and illustrates tubing, glass tubing connectors, corrugated tubing, pressure-sensitive Teflon TFE tape, metering pumps, and other products. Penntube Plastics Co. **437**

Determination of Theophylline in Serum. The method discussed requires only 50 μL of serum and involves a simple protein precipitation step followed by separation and quantitation with HPLC. 6 pp. Hewlett-Packard Co. **441**

UV Spectroscopy. Four application studies are available on the Model 57 scattered transmission accessory, SiO_2 thickness measurements, derivative spectroscopy, and second derivative spectroscopy. Perkin-Elmer Corp. **444**

Organometallics for Electronics. Comprehensive listing of organometallic chemicals created for electronics applications. 8 pp. Alfa Div., Ventron Corp. **442**

Gas Encyclopedia. Presents comprehensive data on gases, their properties, uses, and safe handling. 1160 pp. Lif-O-Gen, P.O. Box 149, Woods Rd., Cambridge, Md. 21613

Hot Plates. Features the PC-101 hot plate/stirrer with a 100 sq in. surface. 4 pp. Corning Glass Works **443**

Limits for Gases and Vapors. Wall chart lists the maximum allowable limits set by OSHA for more than 400 gases and vapors. Wilks Scientific Corp. **445**

Measurement and Control System. Macsym One is a minicomputer-based measurement and control system designed to automate laboratory research experiments by performing data acquisition, data storage, data-base management, data processing, timing and control of experiments, and reporting of results in printout or graphical form. 4 pp. Analog Devices **451**

Desiccant Selector Chart. Lists eight drying agents ranging from aluminum oxide to zinc chloride and gives information on suitability for drying, residual water, grams of water per gram of desiccant, cost per 10 g of water, regeneration, and reaction mechanism. J. T. Baker Chemical Co. **446**

Trace Metal Standards. Describes aqueous and oil matrix trace metal reference standards for use with atomic absorption, atomic emission, atomic fluorescence, and emission spectroscopy instrumentation. Arro Laboratories, Inc. **447**

UV–VIS Spectrophotometers. Describes the complete line of Coleman Junior Series spectrophotometers for routine work in clinical and educational laboratories. 16 pp. Perkin-Elmer Corp. **448**

Liquid Chromatography for the Coatings Industry. Details are given on how one coating vehicle manufacturer uses LC/GPC for everything from quality control of incoming materials through plant-to-plant quality assurance to competitive product analysis. Waters Associates Inc. **449**

ULTREX® Ultrapures

When you simply can't tolerate impurities or uncertainties in your starting materials.

Over 100 of the purest reagents and chemicals available anywhere in the world. Every product is accompanied by a detailed Certificate of Analysis of the actual lot supplied. In terms of spectrochemically detectable impurities, ULTREX products are typically 99.995% to 99.99995% pure. And the extremely low content of all impurities (often at the parts per billion level) satisfies the most rigid use requirements.

Whenever your requirements for purity and product definition are stringent, ULTREX ultrapures can indeed insure against loss of time, effort, and other expenses.

Consider ULTREX when you just can't afford to gamble with impurities or uncertainties.

Write for new ULTREX ultrapure Reagent brochure

J. T. Baker Chemical Co.
Phillipsburg, N.J. 08865
201 859-5411

J.T.Baker® CHEMICALS

CIRCLE 19 ON READER SERVICE CARD

Our SOLVENTS leave you NOTHING to remember us by... residue-free

"DISTILLED-IN-GLASS" SOLVENTS

from

BURDICK & JACKSON LABORATORIES

Ask for Data Sheet BJ-25 "Distilled-in-Glass" Solvents
BJ-21 Liquid Scintillation Counting

BURDICK & JACKSON LABORATORIES, INC.
MUSKEGON, MICHIGAN 49442 (616) 726-3171

CIRCLE 25 ON READER SERVICE CARD

Model 3700, the greatest gas chromatograph, gets greater all the time.

Varian announces the first capillary system that is easy to use and the first dual-flame FPD for high selectivity

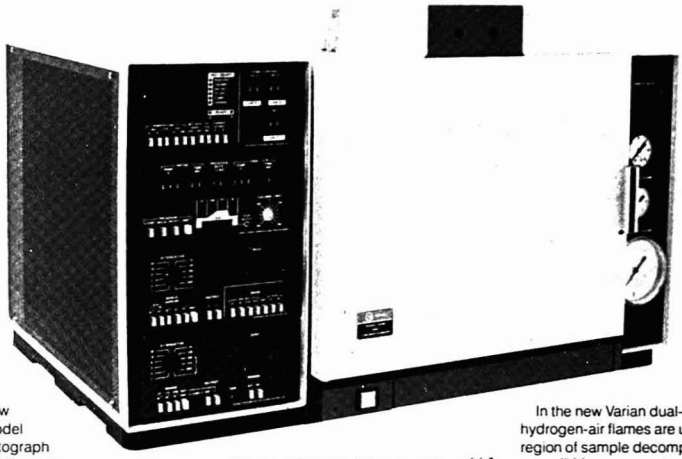

Both advances are now available on Varian Model 3700, the gas chromatograph that brings together all the major chromatographic breakthroughs and offers new applications capabilities in every component.

NEW CAPILLARY SYSTEM

The entire Model 3700 Chromatograph is optimized for capillary column chromatography: the all-glass injector-splitter; extra large 1350 cubic inch column oven; simple column installation; special thermostatted pneumatics; and full automation capability including the only single channel data system that can handle 0.5 sec peak widths.

The new all-glass capillary injector-splitter provides four sample-injection modes. It features a unique positive septum purge to prevent septum bleed problems and a buffer volume for more reproducible splits.

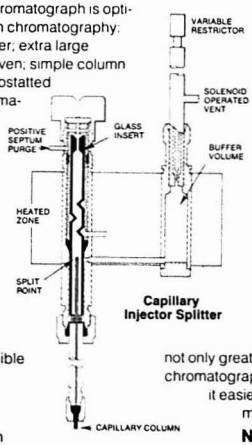

Capillary Injector Splitter

Easy capillary column installation. In the past, only those with super dexterity and patience could install capillary columns. Now, the 3700 capillary system changes all that. Columns can be installed in a few minutes without straightening the ends and without using a costly cage. Column ends slip directly into the fittings at the glass lined injector and detector inserts. All types of capillary columns can be used: WCOT, SCOT, PLOT, and others. This new column installation design saves at least three hours everytime you install a new column.

Capillary and packed column chromatography in one instrument. The 3700's large column oven, and widely separated and independently heated injectors, make it possible to do both capillary and dual packed column chromatography in the same chromatograph. This not only greatly increases the utility of the chromatograph for many labs; it also makes it easier to relate packed column methods to capillary methods.

NEW DUAL-FLAME FPD

The new flame photometric detector for the 3700 features a proprietary dual-flame design that overcomes many of the limitations of single-flame FPD's such as quenching and compound dependency, and provides high selectivity, linearity and detectivity.

In the new Varian dual-flame design, two hydrogen-air flames are used to separate the region of sample decomposition from the region of emission. Since Flame 1 provides the energy to break down the large molecules in the effluent, Flame 2 can use all of its energy for S and P emission. Consequently, there is no quenching and much less compound dependency. An important benefit of the new design is the greatly improved selectivity of S and P with respect to hydrocarbons and with respect to each other.

P/C* > 10^5;
S/C: 10^3 to 10^6.
*C in n-hexadecane

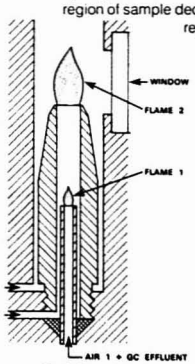

Dual-Flame FPD

Other major 3700 performance features include: New ESP* monitor. New non-contaminating FID. New highest sensitivity TCD. New ^{63}Ni ECD with a *linear* dynamic range > 10^4 and an MDQ < 0.1 pg of lindane. And new carrier gas flow stability because all critical flow control elements are isolated in an independently heated oven.

*Electro Sensor Panel

For full information on the greatest gas chromatograph ever made, circle Reader Service No. 195. To have a Varian representative call, circle Reader Service No. 196.

varian

Varian Instrument Division, 611 Hansen Way, Box D-070, Palo Alto, California 94303

Catalogs

pH Electrodes. Over 30 types of electrodes are described including combination electrodes, separate reference and measuring electrodes, metallic electrodes, ion electrodes, and temperature electrodes. 7 pp. Pope Scientific Inc. **453**

Needle Valves. Describes the complete line of needle valves for use in instrument air lines, panel boards, sampling systems, corrosives, metering service, pilot plants, and research laboratories. 24 pp. Hoke Inc. **454**

Spectrophotometer Cells. Features standard cells as well as anaerobic, micro, water-jacketed, and self-masking cells. Most cells available in optical glass, UV quartz, IR quartz, ES quartz, or Quarasil. 16 pp. Precision Cells Inc. **455**

Laboratory Supplies. Contains information on the complete line of products available for the laboratory. 196 pp. Lab-Line Instruments, Inc. **456**

Laboratory Supplies. Features sterile sampling systems, centrifuges, glass stills, reference books, microscopes, and many more products for the laboratory. 40 pp. Ace Scientific Supply Co. **457**

Chromatographic Accessories. Details the complete line of micro syringes, micropipetters, valves, fittings, Teflon tubing, pressure sample injectors, rotary valves, pneumatic actuators, miniature tubing fittings, plus other accessories. 40 pp. Unimetrics Corp. **458**

Inorganic and Organic Laboratory Reagents. Price List 771C lists more than 3000 reagents including new "instrument-matched" solvents designed to excel at specific methods of instrumental analysis. 117 pp. J. T. Baker Chemical Co. **459**

For more information on listed items, circle the appropriate numbers on one of our Readers' Service Cards

Microliter Syringes. Features full line of syringes including fixed needle, removable needle, guided plunger, gas-tight, and HPLC syringes plus repair kits and accessories. 15 pp. Scientific Glass Engineering, Inc. **460**

Scientific Apparatus. Includes laboratory vibratory analytical mill, Micro-Mesh/Micro-Sort sieves, new time-temperature controller, glass/Teflon homogenizers, gas leak detector, hand-held pyrometer, and information on sample concentration, tissue homogenization, and particle sizing. 32 pp. Tekmar Co. **461**

Laboratory Products. *Update* features many items of general interest to the laboratory scientist, as well as items specifically related to the use and handling of compressed gases. 32 pp. Matheson Update **462**

Laboratory Clamps. Describes the full line of laboratory clamps, lab frames, and lab frame components. 8 pp. GCA/Precision Scientific Group **463**

S.G.E.

gas chromatography mass spectrometry

accessories

Capillary Columns and Support Cages

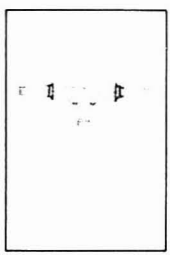

Molecular Jet Separator

Syringes

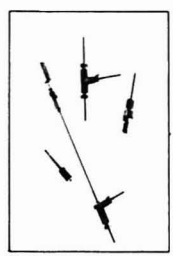

Valves and Low Hold-Up Unions

Glass Lined Tubing and Graphite Ferrules

Head Office
Scientific Glass Engineering Pty. Ltd.,
111 Arden Street
North Melbourne, Australia 3051
Tel: 329 6633

U.S. Office
Scientific Glass Engineering, Inc.
2800 Longhorn Blvd., Suite 104
Austin, Texas 78759
Tel: 512/837-7190

European Office
Scientific Glass Engineering (U.K.) Ltd.,
657 North Circular Road,
London NW2 7AY, Great Britain
Tel: 01-452-6244

CIRCLE 190 ON READER SERVICE CARD

CIRCLE 1 ON READER SERVICE CARD

HPLC Solvents by J.T. Baker

Maximum consistency lot-to-lot, bottle-to-bottle, lot-to-lot, bottle-to-bottle, lot-to-lot, bottle-to-bottle, lot-to-lot, bottle-to-bottle, lot-

Extremely tight specifications and superior product definition minimize the most frequent HPLC problems. 17 Baker HPLC solvents provide maximum reproducibility... total predictability... exceptional consistency. And actual lot analysis lets you verify this.

Write:
HPLC Dept. 7
J.T. Baker Chemical Company
Phillipsburg, N.J. 08865
(201/859-5411)

J.T.Baker CHEMICALS

CIRCLE 18 ON READER SERVICE CARD

Environmental Analysis

Edited by GALEN W. EWING

This book contains the papers presented at the 1976 meeting of FACSS–The Federation of Analytical Chemistry and Spectroscopy Societies–held in Philadelphia, November 15-19, 1976. These papers were selected from the 400 total presentations, because they cover the analysis of air and water and other areas of the environment. All methods of such analysis are represented, including chromatography, atomic absorption and emission, electrochemical methods, and other pertinent areas. Some of the papers represent a review of the state of the art with respect to a particular technique, others describe a special application; a few describe new techniques.

1977, 368 pp., $18.50/£13.15 ISBN: 0-12-245250-X

Inelastic Ion-Surface Collisions

Edited by N. H. TOLK, J. C. TULLY, W. HEILAND, and C. W. WHITE

FROM THE PREFACE:

Inelastic outershell processes occurring in collisions of fast atomic and molecular particles with surfaces have received an extraordinary amount of recent attention.

With the exception of Chapter 6 . . . this book is a compilation of major presentations given at the International Workshop on Inelastic Ion-Surface Collisions held July 1976 at Bell Laboratories, Murray Hill, New Jersey. The major emphasis throughout the book is on identifying and studying the underlying physical mechanisms associated with ionization, neutralization, and excitation responsible for the observed sputtering and particle backscattering outershell inelastic collision phenomena.

In addition to the excellent treatments on the role of the bulk, the surface and the near surface interaction regions on the degree of ionization, neutralization, and excitation, there are a number of contributions on newly observed and in some instances controversial phenomena. These new topics include oscillations in the energy dependence of backscattered ions, wake riding states, and optical polarization effects from beam transmission through tilted foils and from beam particle bombardment of surfaces at grazing incidence.

1977, 368 pp., $19.00/£13.50 ISBN: 0-12-703550-8

The Determination of Sulphur Containing Groups

Volume 3/**ANALYTICAL METHODS FOR SULPHIDES AND DISULPHIDES**

By M. R. F. ASHWORTH

Number 3 in The Analysis of Organic Materials:

An International series of Monographs
Series editors: R. Belcher and D. M. W. Anderson

This volume, the third on the determination of sulphur-containing groups, presents the methods which are available to detect, identify, separate and to determine compounds containing sulphide or disulphide groups. The compounds considered are those in which the –S–S groups are attached to carbon atoms linked otherwise only to hydrogen or to other carbon atoms, which covers thia and dithiaalkanes, cycloalkanes, and arenes.

1977, 220 pp., $21.50/£11.00 ISBN: 0-12-065003-7

Send payment with order and save postage plus 50¢ handling charge.

Prices are subject to change without notice.

ACADEMIC PRESS, INC.
A Subsidiary of Harcourt Brace Jovanovich, Publishers
111 FIFTH AVENUE, NEW YORK, N.Y. 10003
24-28 OVAL ROAD, LONDON NW1 7DX

CIRCLE 2 ON READER SERVICE CARD

Many a meticulous analyst has discovered to his delight that BURDICK & JACKSON Distilled-in-Glass™ Solvents are uncommonly trouble-free.

Recommended by more equipment manufacturers (HPLC) than any other solvent, because they are:

- residue-free
- the ultimate in UV transparency, and
- of uniformly high purity

Bodman's super service cuts time and freight costs. Order from:

BODMAN Chemicals

P.O. Box 500, Media, PA 19063
Phone: (215) 459-5600 — Telex: 834223
and
300-D Piedmont Court
P.O. Box 48184, Doraville, GA 30362
Phone: (404) 447-8550

CIRCLE 23 ON READER SERVICE CARD

GFS CHEMICALS

WE ARE

MANUFACTURERS

PRODUCING MOST OF THE

ANALYTICAL CHEMICALS

WE SUPPLY
AND YOU CAN STILL BUY

DIRECTLY

GFS

ANALYTICAL CHEMICALS SINCE 1928

G. FREDERICK SMITH CHEMICAL COMPANY

867 McKinley Ave.
Columbus, Ohio 43223

FOR PROMPT SHIPMENT
614 224-5343

CIRCLE 189 ON READER SERVICE CARD

REPRINTS
REPRINTS
REPRINTS

to aid you in your work.

☐ 1973 (ChemTech)
Visual Aids for Technical Presentations
Garret R. Hyde $2.00

☐ 1973 (Chemical Reviews)
Intramolecular Hydrogen Transfer in Mass Spectra. I. Rearrangements in Aliphatic Hydrocarbons and Aromatic Compounds
Joan T. Bursey, Maurice M. Bursey, David G. I. Kingston
..... $5.00

☐ 1973 (Chemical Reviews)
Lanthanide Shift Reagents for Nuclear Magnetic Resonance Spectroscopy
Anthony F. Cockerill, Geoffrey L. O. Davies, Raymond C. Harden, David M. Rackham
..... $4.00

☐ 1973–1975 (ChemTech)
Enzyme Engineering
W. R. Vieth, K. Venkatasubramanian
Part I through IV $5.00
Combined I through IV .. $6.50
Part V alone $2.00

☐ 1975 (Accounts of Chemical Research)
Special Issue on the Chemistry of Vision
Edited by Eva L. Menger—($1.50 each on ten or more)
..... $3.00

☐ 1973 (Accounts of Chemical Research)
The Chemical Composition of the Lunar Surface
Anthony L. Turkevich..... $2.00

☐ 1975 (Analytical Chemistry)
Pharmaceuticals and Related Drugs
Richard E. Huettemann, Mary L. Cotter and Charles J. Shaw
..... $3.50

☐ 1969 (Journal of Agricultural & Food Chemistry)
Symposium on Natural Food Toxicants
19 papers from the Atlantic City Symposium in 1968. 128 pages.
Paper $3.00

☐ 1971 (Journal of Agricultural & Food Chemistry)
Symposium on Characterization of Proteins
18 papers from the Chicago meeting in 1970. 125 pages.
Paper $3.50

Prepayment is required. Make check or money order payable to the American Chemical Society
Send to: **Business Operations, Books and Journals Division**, ACS
1155 16th Street, N.W., Washington, D.C. 20036

Name _____

Address _____

City _____ State _____ Zip _____

Introduction to Chiroptical Spectroscopy

Optical Rotatory Dispersion and Circular Dichroism in Organic and Biological Chemistry. Lawrence Verbit. 153-page manual + 4 cassettes (3.8 hours). Department of Educational Activities, American Chemical Society, 1155 Sixteenth St., N.W., Washington, D.C. 20036. 1977. $145. Additional manuals, 1–9 copies, $12.50 each; 10–49 copies, $12.50 each; 50 or more, $10.50 each

Reviewed by Robert Woody, Department of Biochemistry, Colorado State University, Fort Collins, Colo. 80523

Chiroptical spectroscopy (circular dichroism and optical rotatory dispersion) is a technique of wide utility in organic and inorganic chemistry and in biochemistry. Despite this, the average undergraduate majoring in chemistry or biochemistry encounters only brief mention (if that) of circular dichroism in formal course work. Even graduate students rarely receive a systematic exposition of chiroptical techniques.

Lawrence Verbit has prepared an audio course designed to provide an introduction to the practice and applications of CD and ORD. The course consists of lectures contained on four tape cassettes and an accompanying manual containing figures, tabular material, and references. The introduction describes the physical nature of the phenomena, methods of measuring CD and ORD, and molecular symmetry and chirality. This is followed by examples of applications to conformational and configurational problems in organic and biochemistry. The Faraday effect and MCD are then discussed. The concluding section deals with practical aspects of obtaining CD and ORD spectra, such as sample preparation, care of cells, and calibration. Several commonly encountered pitfalls are discussed, together with ways of avoiding them.

Advanced undergraduates and beginning graduate students in organic and biochemistry will find this audio course a useful introduction to the methods of CD and ORD. It could also benefit teachers, research workers, and technicians with no prior experience in this area. An audio course of this type is an *introduction*, not a complete exposition of the subject. Those using CD and ORD in their research must consult more detailed reviews and the recent literature.

This brings me to my only substantial criticism of the course. The applications cited are largely from the earlier literature, with hardly any more recent than 1970. This can be defended from the pedagogical standpoint, but references to recent monographs and reviews are needed to guide the further studies of graduates of this course. Such a bibliography of recent reviews is provided for magnetic CD, but not for natural CD and ORD, the main topics.

The expert will find some statements that are recognizably oversimplified, but overall, both the spoken and written parts are generally free of errors. I would recommend this course to students and any others who have no prior experience with CD and ORD and who wish to become acquainted with these important spectroscopic techniques.

Fundamentals of Gas Analysis by Gas Chromatography. Brian Thompson. 132 pages. Paperbound. Varian Instrument Division, 670 East Arques St., Sunnyvale, Calif. 94086. 1977. $15

Reviewed by George G. Esposito, U.S. Army Environmental Hygiene Agency, Aberdeen Proving Ground, Md. 21010

This is a concise, clearly written, practical book intended to acquaint the reader with basic information that will assist in the selection of columns, valving, and various column-valve configurations. In the introduction the author states, "The emphasis here is on general principles of gas separation and chromatograph operation, not on specific applications".

The first chapter contains a detailed account of columns used in gas analysis. The composition of various column packings is described, and mechanisms responsible for the separation of gases are elucidated. Molecular sieves and porous polymers are described in great detail because of their wide application in gas analysis. Considerably less attention is given to silica gel and alumina; other adsorbents such as spherical carbon molecular sieves, treated silica gels, bonded liquid phases, and Florisil are scarcely mentioned. Unfortunately, there is no discussion of column tubing materials and adsorbent particle size and their effect on column efficiency. Furthermore, mesh size is not specified for most chromatograms. An outstanding part of the chapter is the large amount of retention data used to rank the porous polymers in order of polarity. Accordingly, the summary and general conclusions concerning porous polymer performance provide an excellent introduction to their utility in gas separation.

In Chapters II and V on carrier gas control and sample introduction, the basic concepts involved are clearly set forth in complete detail, including the limitations and advantages of different flow control techniques and sampling devices.

Chapter VII covers quantitative and calibration techniques in gas analysis. For the most part, this section is informative and interesting; however, the part dealing with the comparison of peak height and area measurements is somewhat ambiguous. The author states, "Peak height is not directly proportional to quantity, . . .", and he provides a calibration curve (Figure 7-1) to support his hypothesis. However, in Figure 7-4, concerned with surface adsorption effects in exponential dilution, peak height responses to vinyl chloride are shown to be linear over the 1–1000 ppm concentration range. In the reviewer's experience, peak height measurements are generally in proportion to concentration if sample quantities tested are within the linear range of the detector.

Chapters III, IV, VIII, and X deal with multicolumn systems and switching valves, balancing columns, column selection and valving configuration, and valving configurations. The information contained in these sections is worth the price of the book. The author's skillful presentation of these topics demonstrates his extensive knowledge of the field. Through judicious column selection, column positioning, and valve manipulation, the author shows the complete separation of complex gas mixtures. He summarizes principles, provides detailed description of equipment, and shows at least one example to illustrate the use of each specific system.

Chapters VI and IX are devoted entirely to specific applications. Apparently, the author considers hydrogen analysis (Chapter VI) of sufficient import to merit special emphasis. Some applications presented in Chapter IX

Autoclaves
50 ml to 750 ml
PTFE lined

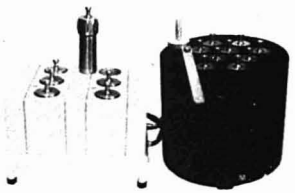

Digestion Bombs
with PTFE-vessel 10 ml and 250 ml

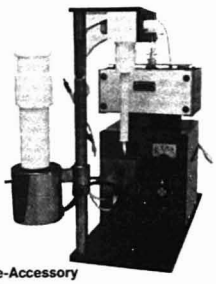

Hg-, As-, Se-Accessory
for Atomics

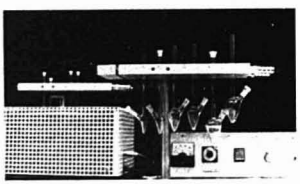

Micro-Refluxer for GC + HPLC

Fractioner for UZ · UF-Membranes
PTFE-Labware · SiC-Fibers
Customer-Research · Electronic Business

BERGHOF
West Germany
P.O.Box 1523
D-7400 Tübingen 1

CIRCLE 28 ON READER SERVICE CARD

Books

demonstrate principles described earlier in the book. Conversely, other applications make use of columns, namely, graphatized carbon and bonded liquid phases, that have not been discussed in any other chapter.

The total number of references is small: 18. The reviewer would like to have seen a more extensive bibliography.

In spite of the few criticisms, the book is well organized, essentially free from errors, and replete with chromatograms and schematics illustrating apparatus and results. Readers should find the text interesting and conducive to problem solving in the ever-expanding field of gas analysis.

Atomic Absorption Spectroscopy. 1st English Edition. Bernhard Welz. xii + 267 pages. Verlag Chemie International Inc., 175 Fifth Ave., New York, N.Y. 10010. 1976. $30.30

Reviewed by G. F. Kirkbright, Department of Chemistry, Imperial College of Science & Technology, South Kensington, London SW7 2AY, England

Atomic absorption spectroscopy (AAS) is practiced by analytical chemists and analysts engaged in a wide variety of disciplines ranging from biochemistry and medicine, foodstuffs and agricultural chemistry, general inorganic chemistry, environmental chemistry, geochemistry and mining, prospecting and petrochemistry to metallurgy. Despite the current widespread acceptance of AAS and the improved general understanding of its capabilities and limitations, information reviews and texts on the fundamental principles of AAS and its applications are needed. The practicing analyst must be provided with up-to-date information on recent advances in instrumentation and methodology.

This book was first published in German in 1972. Fortunately, it was translated into English while the author was completing the second German edition. Consequently, all of the most recent developments in the technique and methodology of AAS included in the second German edition have been incorporated into the English edition. This is particularly important in the consideration of electrothermal atomization techniques applied to AAS. The present state-of-the-art for these important devices, which have radically changed the role of AAS in practice and extended its range of application dramatically, is dealt with thoroughly in this text. Extensive treatment is given to these de-

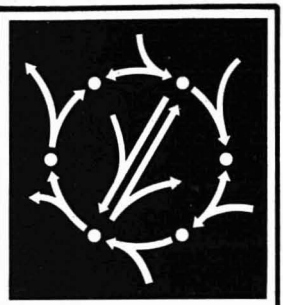

Drug Metabolism Concepts

ACS Symposium Series No. 44

Donald M. Jerina, *Editor*
The National Institutes of Health

A symposium co-sponsored by the Division of Medicinal Chemistry and the Division of Analytical Chemistry of the American Chemical Society.

Eight chapters present in-depth research reports on the role of enzyme systems, especially cytochrome P-450, in drug activation and detoxification. This timely study on drug metabolic pathways is vital because of the possibilities of toxic or carcinogenic intermediates caused by the action of enzymes on drugs and anesthetics.

CONTENTS

Cytochrome P-450 in Oxygen Activation for Drug Metabolism • Synthetic Models for the Reaction Stages of Cytochrome P-450 • Isolation of Mutliple Forms of Liver Microsomal Cytochrome P-450 • Resolution of Multiple Forms of Rabbit Liver Cytochrome P-450 • Enantiomeric Selectivity and Perturbation of Product Ratios as Methods for Studying the Multiplicity of Microsomal Enzymes • Purified Cytochrome P-448 and Epoxide Hydrase in the Activation and Detoxification of Benzo[a]pyrene • In vitro Reactions of the Diastereomeric 9,10-Epoxides of (+) and (−)-*trans*-7,8-Dihydroxy-7,8-dihydrobenzo[a]pyrene with Polyguanylic Acid • Metabolic Activation in Chemical-Induced Tissue Injury

196 pages (1977) clothbound $15.50
LC 77-2279 ISBN 0-8412-0370-9

SIS/American Chemical Society
1155 16th St., N.W./Wash., D.C. 20036

Please send _____ copies of *SS 44 Drug Metabolism Concepts* at $15.50 per copy.

☐ Check enclosed for $ _____ . ☐ Bill me. Postpaid in U.S. and Canada, plus 40 cents elsewhere.

Name _____

Address _____

City _____ State _____ Zip _____

Spectrophotometers are their business. Accessories are ours.

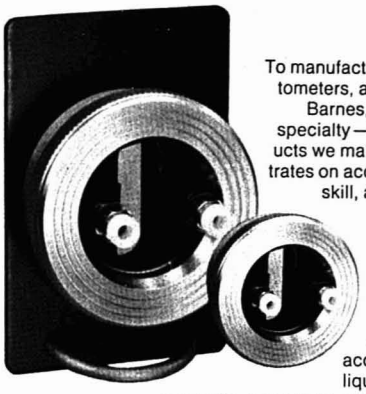

To manufacturers of infrared spectrophotometers, accessories are a sideline. To Barnes, analytical accessories are a specialty—the only spectroscopy products we make. Because Barnes concentrates on accessories, all of our attention, skill, and experience is invested in quality and instrument compatibility at low prices. And for quick, personal service, we offer a toll-free number outside Connecticut (800) 243-3498.

Ask for the Barnes analytical accessories catalog—windows, liquid and solid sampling items, gas cells, reflectance units, and much more. What's an afterthought for most manufacturers is Barnes' first thought.

Barnes Engineering Company, 30 Commerce Road, Stamford, Ct. 06904, (203) 348-5381.

BARNES **Your IR spectroscopy source**

CIRCLE 26 ON READER SERVICE CARD

Topics in . . .

Chemical Instrumentation—II

An ACS Reprint Collection

A volume of reprints from the *Journal of Chemical Education*

Galen W. Ewing, *Editor*

This new collection of selected reprint articles from the "Topics in Chemical Instrumentation" column in the JOURNAL OF CHEMICAL EDUCATION provides excellent coverage of the field from January, 1970 through November 1975.

In order to furnish the most complete, up-to-date information on the subject, many of the authors have added supplemental material to their papers. The 36 reprints are listed according to subject matter rather than by chronological order.

This useful collection will be of particular interest to analytical chemists, college chemistry faculties, research chemists, librarians, and those seeking an introduction to the state of the art.

CONTENTS

A Review of Wavelength Calibration Methods for Visible-Range Photoelectric Spectrophotometers • Instrumentation for Fluorescence and Phosphorescence • Optical Rotatory Dispersion and Circular Dichroism • Atomic Spectroscopy Atomization Systems • Multiplex Spectrophotometry • Nuclear Magnetic Resonance Spectrometers • X-Rays and Electrons in Analytical Chemistry, with Emphasis on Instrumentation • Infrared Detectors • Nuclear Quadrupole Resonance Spectroscopy • Electron Spectroscopy Instrumentation • Step Perturbation Relaxation Techniques • Scanning Electron Microscopy • Reference Electrodes • Anodic Stripping Voltammetry • The Measurement of Electrolytic Conductance • Thermal Analysis Techniques • Analytical Applications of High Resolution Mass Spectrometry • Liquid Chromatography Detectors • Recent Developments in Instrumentation for Liquid Chromatography • Current Trends in Gel Permeation Chromatography • Instrumentation for Thin Layer Chromatography • Centrifugal Analyzers—A New concept in Automation for the Clinical Chemistry Laboratory • Continuous Flow Measurement of Beta Radiation Using Suspended Scintillators • Nuclear Radiation Detectors • Laboratory Automation—A Case History • Laboratory Integrators • Lock-in Amplifiers • Signal Averagers • Home-Built Equipment in the Teaching Laboratory • Sir Charles' Bridge • An Introduction to Microelectronics • Inert Atmosphere Enclosures • Analytical Instrumentation: 1940–41 Vintage • Calculators for the Chemist • Analysis of Gases in Metals: Fusion and Extraction Methods • Specialized Instruments for the Determination of Sulfur by the Combustion Method

310 pages (1977) hardback $12.00
ISBN 0-8412-0367-9 LC 73-153064

Order from:
SIS/American Chemical Society
1155 16th St., N.W./Wash., D.C. 20036

Chemists, Spectroscopists can now simplify Signal Pulse Measurements

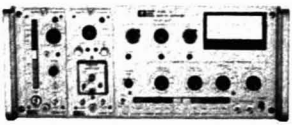

PARC's most exciting Boxcar Averager ever—the Model 162 brings you incredible functional versatility, wide dynamic range, and ease of operation—all at an affordable price.

Whether you work in CARS*, Atomic Fluorescence, Pulsed NMR or some other application requiring the measurement of weak pulsed signals—you should consider the Model 162's unique attributes.

+Flexible dual channel operation for baseline subtraction and reference signal normalization.

+Sampling gate apertures from 100 picoseconds to 5 milliseconds—selectable to accommodate your signal.

+Digital storage plug-in option** automatically compensates for already low memory leakage currents to accommodate signals appearing at extremely low repetition rates.

*Coherent Anti-Stokes Raman Spectroscopy
**Model 162/99

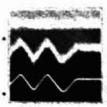

Send for your free Signal Averager Catalog.

For more details, write or call today. Princeton Applied Research Corporation, P. O. Box 2565, Princeton, New Jersey 08540; phone: 609/452-2111.

PRINCETON APPLIED RESEARCH
AN EG&G COMPANY
405

FOR ADDITIONAL INFORMATION CIRCLE 175
TO HAVE A SALESMAN CALL CIRCLE 176

vices in the chapter that reviews both the types of systems commonly encountered in practice and the current interpretation of the nature of the atomization processes which occur in these. Flameless atomic absorption techniques are also taken into consideration in all of the other chapters, including those devoted to technique, the individual elements, and specific applications. A particularly useful feature of the book, seen from the viewpoint of the reader who might have a general interest in the applicability of the technique, is the final chapter concerned with its application in specific disciplines. This chapter is well documented with references that allow more detailed information on specific applications to be readily obtained.

The format is most satisfactory. The important information is easily found and is presented in lucid style. The book is well produced and illustrated, and few errors were noticed by this reviewer. It can be given unqualified recommendation both as a tutorial text in the technique and an up-to-date review of its present status.

New Books

Radiotracer Techniques and Applications, Vols. 1 and 2. E. Anthony Evans and Mitsuo Muramatsu, Eds. Vol. 1, xiii + 687 pages. Vol. 2, xiii + 1211 pages. Marcel Dekker, Inc., 270 Madison Ave., New York, N.Y. 10017. 1977. Vol. 1, $65; Vol. 2, $49.75

A total of 23 chapters on radiotracer techniques contributed by 37 international experts is presented in this two-volume series. The fundamental techniques in the design of tracer experiments are discussed in chapters 1–7 of the first volume. These include the selection of radionuclides, safety aspects of radiotracer experiments, measurements of radioactivity with special emphasis on biological samples, the preparation and analysis of radioactive compounds, and the problems associated with the natural decay process in storage. Also in volume 1 are chapters 8–14 which deal with basic chemical problems such as the special behavior of radionuclides at maximum isotopic abundance, isotope effects, exchange processes, solution properties, and diffusion and interfacial phenomena. Chapters 15–20 in volume 2 describe many applications of radiotracer techniques to biological research. These include applications to studies of biosynthesis, drug metabolism, cytology, enzyme assays, metabolism of chemicals used in agriculture, and marine biology. The final three chapters are of special interest to clinical investigators. These chapters deal with the assay of drugs and hormones by competitive protein binding (including radioimmunoassay), diagnostic applications of radionuclides, and a discussion on development of radioactive drugs in the treatment of cancer. Both volumes are reproduced from typewritten text.

Dithizone. H.M.N.H. Irving. iv + 106 pages. The Chemical Society, Burlington House, London, W1V 0BN, England. 1977. $14.50

This short monograph published as volume 5 of a series of topics of interest to analytical chemists is concerned with the organic reagent, dithizone. The monograph reviews in great detail the chemistry of dithizone from its initial introduction by Hellmuth Fischer in 1925 to the status of the reagent in the contemporary analytical practice. The review concentrates on theoretical aspects at the expense of practical details, which can be best obtained from the original literature. The contents include the introduction, the properties of dithizone, metal–dithizone complexes and their formulae, the photochemistry of metal dithizonates, the extraction of metal dithizonates, the less familiar dithizone complexes, organometallic dithizonates, practical considerations, some additional applications of dithizone, and some unresolved problems.

Computer-Assisted Structure Elucidation (ACS Symposium Series 54). Dennis H. Smith, Ed. viii + 151 pages. American Chemical Society, 1155 Sixteenth St., N.W., Washington, D.C. 20036. 1977. $15.50

The papers collected in this volume illustrate the ways in which computers can be used in the elucidation of unknown molecular structures. The papers were originally presented at a symposium sponsored by the Division of Chemical Information at the 173rd National Meeting of the American Chemical Society, New Orleans, 23 March 1977. Methodologies discussed include library search techniques, automated interpretation of data, pattern recognition, structure generation, and ranking of candidate structures based on prediction of spectroscopic or chemical behavior. The book is reproduced from author-furnished typewritten text.

Pyrolysis–Gas Chromatography. R. W. May, E. F. Pearson, and D. Scothern. vii + 109 pages. The Chemical Society, Burlington House, London W1V 0BN, England. 1977. $14.40

As is evident from the total pages, the text is a short monograph intended for the practicing analyst. Chapter 1 serves as an introduction to gas chromatography and will be of interest only to those unfamiliar with the technique. The several different types of pyrolyzers are described in chapter 2, and the major analytical uses of pyrolysis–GC are presented in chapter 3. Chapter 4 deals with the identification of the pyrolysis products eluted from the chromatograph column. The necessity for standardization in pyrolysis–GC is discussed in chapter 5.

Continuing Series

The Determination of Sulphur-containing Groups, Vol. 3: Analytical Methods for Sulphides and Disulphides. M.R.F. Ashworth. xi + 220 pages. Academic Press Inc., 111 Fifth Ave., New York, N.Y. 10003. 1977. $21.50

This monograph belongs to the long-standing series, "The Analysis of Organic Materials", edited by R. Belcher and D.M.W. Anderson. This volume, the third on the determination of sulfur-containing groups, presents various analytical methods for sulfide and disulfide compounds in which the sulfur group is carried primarily by a carbon atom joined either to hydrogen or to another carbon atom. These compounds include thia- and dithia-alkanes, cycloalkanes, and arenes. Of the many heterocyclic structures theoretically eligible for treatment, only the important thiophenes and biotin have been included. Methods for amino acids such as cysteine, and homocysteine, methionine, and lantionine are presented only where they are clearly dependent on the disulfide or sulfide group. In the compilation of analytical methods, the author has chosen to limit the description of each method to only a brief discussion to allow for the introduction of a large number of methods for which the reader can consult the original literature for full details. The space is equally divided into Part I (sulfides) and Part II (disulfides). Each part is further divided according to the type of reaction, reagents, bond cleavage, and the types of analytical methods used. The literature references include some as recent as 1975.

ASTM Publications

The following are available from the American Society for Testing and Materials, 1916 Race St., Philadelphia, Pa. 19103 (USA, Canada, and Mexico add 3% shipping charges. Other countries add 5%)

Part 41 of 1977 Annual Book of ASTM Standards. 936 pages. 1977. $28

Part 41 contains 120 ASTM standard methods of which 35 are new, revised, or changed in status since the 1976 edition. Contents include ASTM test methods for conditioning and weathering, density testing, thermal analysis, thermal expansion; apparatus for testing laboratory balances, filtration materials, glassware laboratory apparatus, hydrometers, metalware laboratory apparatus, microchemical apparatus; statistical methods; space simulation and applications of space technology; mechanical testing; particle size measurement; durability of nonmetallic materials; pipeline coatings; hazard potential of chemicals; occupational health and safety aspects of materials; evaluation of testing and/or inspection agencies; and metric practice.

Part 42 of 1977 Annual Book of ASTM Standards. 544 pages. 1977. $17

Part 42 on emission, molecular and mass spectrometry, chromatography, resinography, and microscopy contains 66 ASTM standard methods. Among the new standards are x-ray emission spectrometric analysis of stainless steel, recommended practices for internal reflectance spectrometry; testing for linearity of fluorescence measuring systems, test for minimum detectable fluorescence of quinine sulfate and cyclohexane, and recommended practice for testing flame ionization detectors used in gas chromatography.

Compare Balances . . .

Sauter has a broader range of electronic and mechanical balances; far heavier, sturdier construction; and better prices.

Electronic Precision Balance Typ RS 25

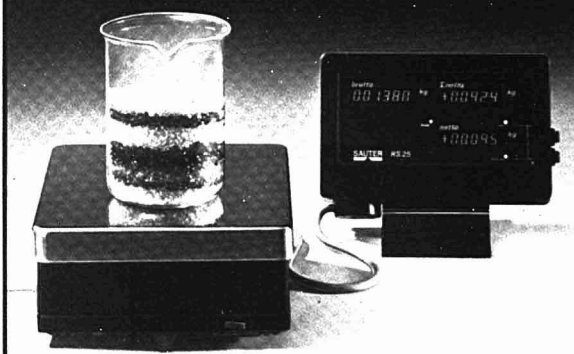

Electronics
12 Capacities
Dual ranges. Automatic Tare. Analog and Digital outputs. Readings to 10 mg. Capacities from 80 g to 1200 kg.

Analyticals
18 Models
Readability to 1 microgram, capacities from 2 mg to 200 grams. Tare, pre-weigh, hydraulic release, high weighing chambers, etc.

Top Loaders
20 Models
Digital and „hands-off" Analog models with capacities from 160 g to 20 kg. Readability to 1 mg. Interchangeable pans. Tare. Auto-Levelling, etc.

Compounding? Batching? Be sure with Sauter!

Three digital readouts give an overview of the whole operation. Read the weight of each ingredient as you add it. And also read the total weight of all the ingredients previously added. All electronic, 1 gram precision, 25 kg capacity.

For a catalog describing the extensive Sauter Lab Balance line, write or call:

SAUTER

August Sauter of America, Inc.
80 Fifth Avenue
New York, N. Y. 10011
Phone (212) 685-6659
Telex 421790

CIRCLE 187 ON READER SERVICE CARD

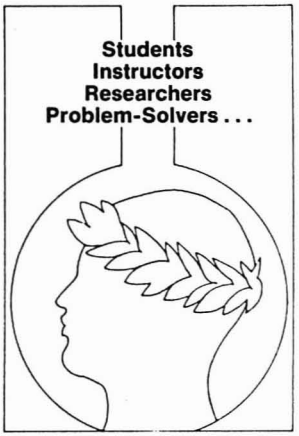

keep on top of recent advances in analytical chemistry with the latest edition of

MODERN CLASSICS IN ANALYTICAL CHEMISTRY

Volume II

Edited by Alvin L. Beilby, Seaver Chemistry Laboratory, Pomona College, Claremont, California

A selection from the best feature articles that appeared in issues of ANALYTICAL CHEMISTRY from 1970 through 1975.

Particularly suitable as supplementary reading for the advanced student of analytical chemistry and for those who must keep up with the latest developments in analytical chemistry and instrumentation, this convenient collection of source material contains valuable information presented only in outline form in many modern textbooks.

Volume II 314 pages (1976) $8.50 paperbound
Volume I 268 pages (1970) $5.75 paperbound

Postpaid in U.S. and Canada, plus 40 cents elsewhere.

CONTENTS (Volume II)

Development of Analytical Chemistry As a Science
Izaak M. Kolthoff

Spectroscopy

Carbon-13 Nuclear Magnetic Resonance Spectroscopy
George A. Gray

Atomic Absorption Spectroscopy—Stagnant or Pregnant?
Alan Walsh

Multielement Flame Spectroscopy
Kenneth W. Busch and George H. Morrison

Atomic Fluorescence Spectrometry
J. D. Winefordner and R. C. Elser

Fourier and Hadamard Transform Methods in Spectroscopy
Alan G. Marshall and Melvin B. Comisarow

Atomic Spectrochemical Measurements with a Fourier Transform Spectrometer
Gary Horlick and W. K. Yuen

X-Ray Energy Spectrometry
David E. Porter and Rolf Woldseth

X-Ray Photoelectron Spectroscopy
William E. Swartz, Jr.

Tunable Lasers in Analytical Spectroscopy
James R. Allkins

Surface and Thin Film Compositional Analysis: Description and Comparison of Techniques
Charles A. Evans, Jr.

Surface and Thin Film Analysis
Charles A. Evans, Jr.

Electrochemistry

The Renaissance in Polarographic and Voltammetric Analysis
Jud B. Flato

Anodic Stripping Voltammetry
T. R. Copeland and R. K. Skogerboe

Chromatography

Foundations of Modern Liquid Chromatography
L. S. Ettre and C. Horvath

The Development of Chromatography
Leslie S. Ettre

Process Gas Chromatography
R. Villalobos

Automation and Instrumentation

GC/MS/Computers
Francis W. Karasek

Computerized Signal Processing
Gerald Dulaney

Microprocessors. Part I: Bridging the Gap
Raymond E. Dessy, Peter Janse-Van Vuuren, and Jonathan A. Titus

Microprocessors. Part II: Applications
Raymond E. Dessy, Jonathan A. Titus, and Peter Janse-Van Vuuren

Automated Reaction-Rate Methods of Analysis
Howard V. Malmstadt, Emil A. Cordes, and Collene J. DeLaney

Instruments for Rate Determinations
Howard V. Malmstadt, Collene J. Delaney, and Emil A. Cordes

Measurement Techniques

Applications of Chemiluminescent Reactions to the Measurement of Air Pollutants
Robert K. Stevens and J. A. Hodgeson

Chemiluminescence and Bioluminescence in Analytical Chemistry
W. Rudolf Seitz and Michael P. Neary

Immobilized Enzymes: Analytical Applications
Howard H. Weetall

Ultrapurity in Trace Analysis
James W. Mitchell

The Other Face of the Measurement Base
Richard W. Roberts

Measurement Analysis by Pattern Recognition
Bruce R. Kowalski

Comparison of Analytical Techniques for Inorganic Pollutants
R. F. Coleman

The Analytical Approach

Urgent Production Problem Solved by Unique Capabilities of Analytical Chemists
Claude A. Lucchesi

Effects of Raw Material Change in Manufacturing Process Resolved
John Mitchell, Jr.

Analytical Chemists Vital in Commercialization of New Food Packaging Material
V. F. Gaylor

Multitechnique Approach Solves Construction Materials Failure Problems
William G. Hime

Analytical Chemists in the U.S. Customs Service
Daniel W. Vomhof

Recognition and Solution of Production Problems in Vitamin Manufacture
E. MacMullan, R. Hagel, and R. Gomez

Finding the Flavor Component: A Job for the Analytical Chemist
W. Noel Einolf

The Forensic Chemist. An "Analytical Detective"
Larry S. Eichmeier and Michael E. Caplis

Industrial Analytical Chemists and OSHA Regulations for Vinyl Chloride
S. P. Levine, K. G. Hebel, J. Bolton, Jr., and R. E. Kugel

Art Conservation

Art Conservation: Culture Under Analysis. Part I
Ben B. Johnson and Thomas Cairns

Art Conservation: Culture Under Analysis. Part II
Ben B. Johnson and Thomas Cairns

Index Listing of "Report for Analytical Chemists" Articles in ANALYTICAL CHEMISTRY, 1970–1975.

Index Listing of "Instrumentation" Articles in ANALYTICAL CHEMISTRY, 1970–1975.

SIS/American Chemical Society
1155 16th St., N.W./Wash., D.C. 20036

Please send the following books:

Modern Classics in Analytical Chemistry

_____ (**Vol. II** $8.50 paperbound)
_____ (**Vol. I** $5.75 paperbound)

☐ My check for $_____ is enclosed. ☐ Bill me. Postpaid in U.S. and Canada, plus 40 cents elsewhere. (Prices subject to change without notice.)

Name _____

Address _____

City _____ State _____ Zip _____

SI Units

Starting with the January 1978 issue, ANALYTICAL CHEMISTRY will begin its move toward SI units. This move toward the usage of the International System of Units (SI) had been agreed to by ACS editors as general policy for all ACS publications. It was also decided that although in principle the change to strict SI usage is desirable, each editor should have the option to make any necessary adjustments dictated by practical reality. [See Dr. Laitinen's editorial, "Moving Towards SI Units", *Anal. Chem.*, **48**, 633 (1976).] As a consequence of the ACS editors' action, the question of SI usage was discussed at the 1976 and 1977 ANALYTICAL CHEMISTRY Advisory Board meetings. The consensus was that the adoption of SI usage should be initiated by the leading analytical chemistry journal.

Of course, it is impractical, if not impossible, to completely convert the January and subsequent issues. Because many non-SI units are in common use and because many units will not be readily given up, exceptions to the rules will have to be allowed. Conversion to SI usage will be slow since the conversion is a learning process. Not until all analytical chemists accept and use SI will the JOURNAL be able to convert exclusively to SI.

Some simple and convenient conversions will be made. Units that are convertible by multiples of ten will be changed; for example, millimicrons are already being changed to nanometers. Also, in certain cases the SI equivalent of units from other systems will be parenthetically included. The ease with which any changes can be made will depend on the continuing cooperation of our authors and reviewers.

The January issue of ANALYTICAL CHEMISTRY will provide a list of SI units as well as those exceptions acceptable. Obviously, the list of worthwhile exceptions cannot be complete, and we welcome any serious suggestions for candidates to add or delete from this list. The revised ACS "Handbook for Authors", which will be available in the near future, will give the general policy on SI for ACS publications. The availability of this handbook will be announced.

Historical Notes

"A History of Analytical Chemistry", coedited by H. A. Laitinen and G. A. Ewing, is in print in hard cover. The book, 358 pages including both subject and name indexes, has been published by the ACS Analytical Chemistry Division. In two editorials [*Anal. Chem.*, **48**, 1 (1976); **49**, 689 (1977)] Professor Laitinen discussed the plans and goals of the project resulting in the publication of this book. Although we will have a formal review of the book in a future issue of ANALYTICAL CHEMISTRY, at this time we want to call special attention to its availability for two reasons. First, we think it's appropriate to recognize the efforts of the two editors, four topical editors of major chapters, and 51 contributors from the profession. All of these dedicated people contributed their time and effort without remuneration of any kind. Any profits accruing to the Division will serve to support divisional activities, especially the graduate research fellowship program.

Second, the introduction to the book, pages 1–7, traces the evolution of ANALYTICAL CHEMISTRY as indicative of the evolution of the field it represents. ANALYTICAL CHEMISTRY enters its 50th volume year in 1978. It is gratifying to have in one place, details of the JOURNAL's growth, both in scope and importance, since its beginnings in 1929 as a spin-off from *Industrial and Engineering Chemistry*.

At the 1978 fall ACS meeting in Miami Beach, Professor Laitinen will chair a symposium on "50 Years of Analytical Chemistry—the Journal and the Science" in honor of Lawrence T. Hallett, editor emeritus of ANALYTICAL CHEMISTRY. The symposium will cover the years by decades, stressing the relationship between the JOURNAL and the science. These presentations will appear in the A pages of ANALYTICAL CHEMISTRY in the November and December issues, 1978.

Copies of "A History of Analytical Chemistry" are available from Frank Guthrie, Department of Chemistry, Rose-Hulman Institute of Technology, Terre Haute, Ind. 47803. Cost to ACS Analytical Division members is $7.00; nonmembers, $10; add $1.00 for foreign postage. Checks or money orders should be made payable to the ACS Division of Analytical Chemistry.

CIRCLE 137 ON READER SERVICE CARD

Schott—the glass makers for Abbe and Zeiss—bring you...

the THALAMID® combination electrode

A superior electrode exemplifying not only the expertise in scientific glassmaking originated at Schott & Gen. in the days of Ernst Abbe and Carl Zeiss, but, as well, the innovative approach to all details of a product which has characterized Schott's contributions to the laboratory.

In this combination electrode, scientifically designed pH-sensitive glasses are combined with a unique, high-performance electrochemical system, a superior reference junction and sound, time-tested construction to provide accuracy, stability, durability and reliability.

The outstanding features of this electrode are detailed below; and we'll be happy to send you a bulletin on the entire Schott electrode line, available exclusively from Sargent-Welch.

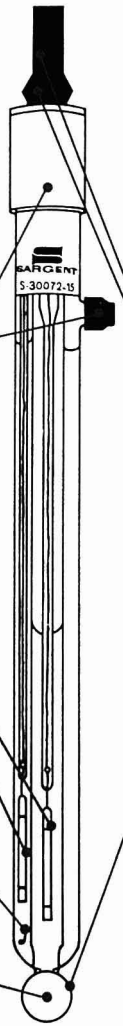

Stainless steel (18-8-2) cap resists corrosion and provides mechanical strength for secure clamping.

Refill aperture for reference electrode has a rubber cap to provide a tight seal against electrolyte leakage or creepage and a side tube for connection to a remote reservoir.

THALAMID® (thallium amalgam) cartridge form internal elements are characterized by stability, absence of thermal decomposition and low hysteresis at temperatures up to 135°C, by freedom from complex formation with sample components (including cyanide), by indifference to the KCl electrolyte and polarization currents and by a long service life. In these respects the THALAMID system is superior to one or both of the calomel and silver-silver chloride systems. Identical elements in glass and reference electrodes provide thermal and electrical symmetry to speed temperature equilibrium and reduce asymmetry potential.

Liquid junction comprises a platinum filament sealed through the glass wall of the reference electrode. This junction provides low resistance, a low electrolyte leak rate, a constant junction potential, good performance in samples with very high and very low salt contents, and resistance to clogging by slurries or viscous solutions. It is located just above the pH-sensitive bulb to minimize sample volume demand. For difficult samples requiring large electrolyte flow and frequent purging, a combination electrode with ground junction is available.

Internal buffer is specially compounded for stability with temperature change and with time, and for compatibility with the glass surface. Nominal pH is 7, suited to all common pH meters.

Special coaxial cable shields the glass electrode conductor from electromagnetic and capacitive interference and has a tough, waterproof cover. It is non-microphonic and does not affect the meter reading when moved.

Hermetic seal between cap and cable is made by vulcanizing to exclude moisture and relieve mechanical strain on the internal elements of the electrode.

Only two membrane glasses cover all applications. Type N (general purpose) and Type H (high temperature-high alkalinity). **Type N**—Suitable for all uses except those involving high temperature and/or high sodium ion concentrations (high alkalinity). Response is very close to Nernstian and linear even in highly acid solutions. Na^+ ion response is very low (insignificant below pH 12.5 at 25°C) and, even more important, it is stable where significant. Type N glass electrodes can be used continuously from 0° to 80°C, intermittently to 100°C. Low specific resistance allows a 0.5 mm wall with a total resistance of only 100 megohms (10 mm bulb) at room temperature. The heavy wall, high inherent glass strength and careful fabrication result in a strong, shock resistant construction. **Type H**—In contrast with Type N glass, Type H has a lower sodium ion error, improved chemical resistance, and a longer life expectancy at high pH and/or elevated temperature, and a higher electrical resistance. It is the glass of choice for measurements at a pH above 1 in solutions with high alkali metal content and for use in photographic developers and nonaqueous systems. With Type H glass, can be used at temperatures up to about 110°C, the boiling point of the reference electrolyte, or, with suitable pressurizing, to 135°C.

SARGENT-WELCH SCIENTIFIC COMPANY

7300 NORTH LINDER AVENUE • SKOKIE, ILLINOIS 60076 • (312) 677-0600

Anaheim/Birmingham/Chicago/Cincinnati/Cleveland/Dallas/Denver/Detroit/Springfield, N.J./Toronto/Montreal

CIRCLE 201 ON READER SERVICE CARD

R. E. Sturgeon[1]
Metal Ions Group
Department of Chemistry
Carleton University
Ottawa, Ont., Canada K1S 5B6

Factors Affecting Atomization and Measurement in Graphite Furnace Atomic Absorption Spectrometry

Atomic absorption spectrometry (AAS) is a highly specific means of elemental analysis based on the selective absorption of line radiation by atomic species in the vapor phase. To observe AA signals it is necessary to generate a population of free, neutral atoms of the element of interest. Although combustion flames are the most widely used media for the atomization of samples (conversion of the sample into atomic vapor) in AAS, the demand for better sensitivity and limits of detection, the necessity for more economical use of the sample, and the fundamental limitations of flame techniques have led to the development of a variety of electrothermal (flameless) atomizers as an alternative atomization medium (*1–3*). The advantages inherent in the application of electrothermal (ET) atomization to AAS are well recognized: the possibility of determining a large number of elements with high sensitivity, selectivity, accuracy, and speed, coupled with the simplicity and relatively low cost of apparatus, makes AAS with ET atomization potentially ideal for trace and ultratrace analysis. It is therefore not surprising that the technique has been shown to be of considerable value for the detection and quantitative determination of trace amounts of metals and metalloids in a variety of matrices (*1–5*).

Despite widespread use, however, the basic principles of operation of ET atomizers remain largely unclear. The purpose of this article is to focus attention on some fundamental aspects of electrothermal atomization and methods of recording AA signals generated by these devices. Discussion will be limited to tube-type graphite furnaces of the Massmann design (*6*), shown in Figure 1, since these are currently the most popular models commercially available. In most cases, however, the principles covered will also apply to ET atomizers of less familiar design. An understanding of their fundamental operation will identify those factors important in the design of more effective ET atomizers as well as provide a useful theoretical framework from which interpretation of analytical data may be drawn.

Principles of Operation

Commercial ET atomizers are resistively heated devices that generally employ a three-stage heating program to dry, char, and atomize the sample. Power is supplied from a low-voltage ($\simeq$10 V), high-current source capable of delivering up to 500 A. The temperature of the atomizer is a complicated function of time and various other factors such as the input power, the mass of the atomizer, and its heat losses by convection, conduction, and radiation. Figure 2 shows the time-dependent central temperature of the interior surface of a Perkin-Elmer HGA-2100 atomizer (a popular commercial atomizer of the Massmann design) at various levels of input power. The time axis commences with the initiation of the atomization stage of the heating program. The 500 K intercept common to each heating curve is the temperature of the atomizer at the completion of the charring stage. In all cases, the temperature asymptotically approaches an upper steady-state value that reflects the balance between the input power and the heat losses. The initial rate of heating of the atomizer as well as its steady-state temperature is proportional to the input power. The general shape of these heating curves applies to all commercial atomizers employing a three-stage heating program.

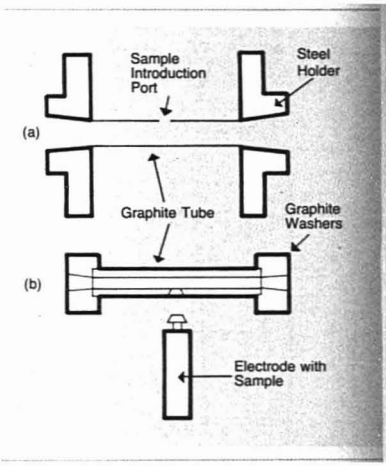

Figure 1. Massmann furnace for (a) AAS; (b) L'vov graphite cuvette

Figure 3 shows the relationship between the temperature of the surface of the atomizer and the absorbance-time characteristics of the signals from a number of elements atomized in the HGA-2100 (the magnitudes of the signal peaks are not drawn to scale as the relative peak heights for the elements vary approximately in the ratio 250:5:3:1 for Cd:Cu:Cr:Mo). In contrast to the steady-state signals obtained with the flame AA technique, analytical signals generated by ET atomizers are transient pulses of, at most, a few seconds duration, their exact shape for a given element being determined by the physical and chem-

[1] Present address, Division of Chemistry, National Research Council of Canada, Montreal Road, Ottawa, Ont., Canada K1A 0R6.

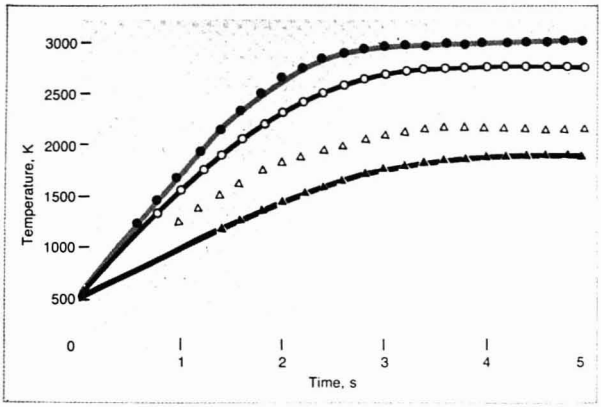

Figure 2. Temperature-time characteristics of interior surface of Perkin-Elmer HGA-2100 at various power outputs of atomization stage
● 3.2 kW O 2.6 kW △ 1.8 kW ▲ 1.3 kW

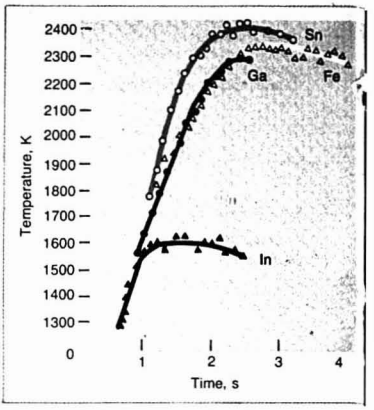

Figure 4. Excitation temperature-time profiles of atomic vapor in HGA-2100 with heating rate of 1.23 K ms^{-1} of atomizer

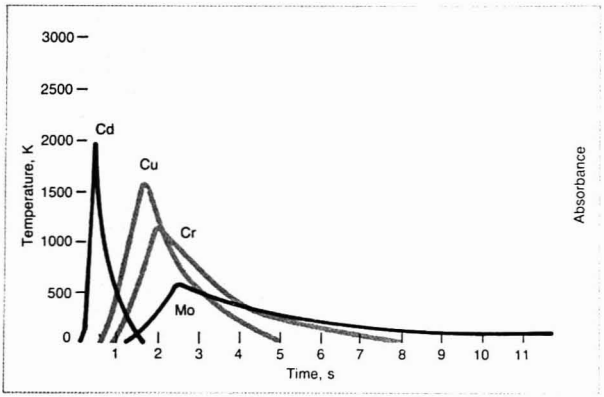

Figure 3. Absorbance-time profiles of a number of elements superimposed on temperature-time profile of surface of HGA-2100. Input power = 3.2 kW

ical properties of the sample matrix, by the properties of the atomizer (geometry, construction material), its rate of heating, and by the distortion of the signal caused by the finite response time of the amplifier-recorder system. The signal shapes are similar to those observed for consecutive first-order chemical reactions, i.e., the concentration of free atoms (product) is kinetically controlled by the rates of two opposing processes: the rate of introduction of atoms into the analytical volume of the atomizer (the analytical volume being defined by the geometry of the beam of source radiation that is within the viewing field of the spectrometer) and their rate of loss from it, the signal maximum marking the point of balance between the two rates. The temperature at which rapid atomization commences (appearance temperature) is uniquely determined by the physicochemical properties of each element and is a constant, independent of the rate of heating of the atomizer, its geometry, and surface characteristics (*7–10*). Unlike the flame and the L'vov graphite cuvette technique (to be discussed), sample atoms produced by commercial ET atomizers are released at specific minimum temperatures into a nonisothermal environment, and the signal is recorded during a time period over which the temperature of both the atomization medium and the atomic vapor is rapidly changing.

Figure 4 shows the spectroscopically measured excitation temperature (two-line absorption method) of In, Ga, Fe, and Sn vapor produced in the HGA-2100 (*11*).

The measurement of vapor temperature by spectroscopic methods is equivalent to the measurement of the population ratio of the absorbing species included within the viewing field of the spectrometer, and to the determination of an effective temperature that corresponds to this ratio according to a Boltzmann distribution:

$$\frac{g_2}{g_1}\exp\left|-(E_2-E_1)/kT_{\text{eff}}\right| = \int_0^l n_2(x)dx \Big/ \int_0^l n_1(x)dx \quad (1)$$

where $n_1(x)$ and $n_2(x)$ are the densities of the thermometric species in the lower and upper quantum states of the transition, and l is the optical path length. Consequently, an average or weighted average temperature is not measured (*12*); rather, the effective temperature is applicable only to the population ratio of states 1 and 2.

Although the steady-state temperature of the atomizer was 3000 K, the measured excitation temperature varied with the element atomized. Maximum excitation temperatures attained by the vapor are lower than the temperatures of the atomizer surface and do not coincide with the peaks of the absorption pulses of the elements. The gradient in the surface temperature along the optical axis of the atomizer (spatial nonisothermality) is of primary importance in determining the temperature-time characteristics of

SURFACE ANALYSIS SPOKEN HERE

3M ISS and SIMS attachment systems can augment your AES and ESCA data to give you more complete surface analysis capability.

Growing numbers of AES and ESCA users have come to the realization that their present capabilities can't solve all their everyday, real-world problems. Their companies need and expect more complete surface analysis data from them.

As a result, more and more of these users are turning to 3M Analytical Systems. That's because only 3M offers complete, fully compatible ISS and SIMS Attachment Systems for their existing AES or ESCA equipment. Complete, operational systems—not just bits and pieces. Systems for which 3M assumes "turnkey" responsibility.

If your present surface analysis equipment isn't telling you the whole surface story, talk to us. We can help translate your problems into solutions. Call 612/733-3909, or write: Analytical Systems, 3M Company, 3M Center, Building 209, St. Paul, MN 55101. In Europe: Cambridge Instruments, GmbH, Dortmund, Germany.

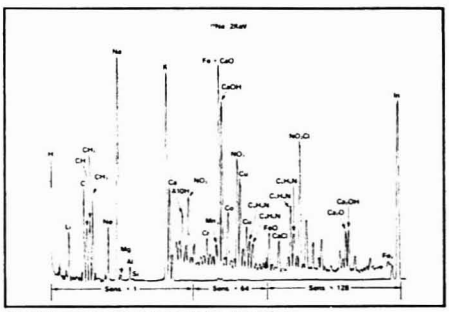

SIMS Spectra: Contaminated Indium Foil

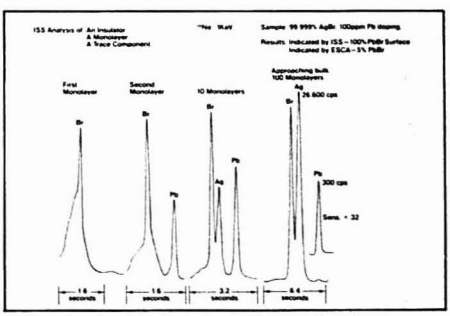

ISS spectra showing: Analysis of insulators; Monolayer sensitivity; Trace detection

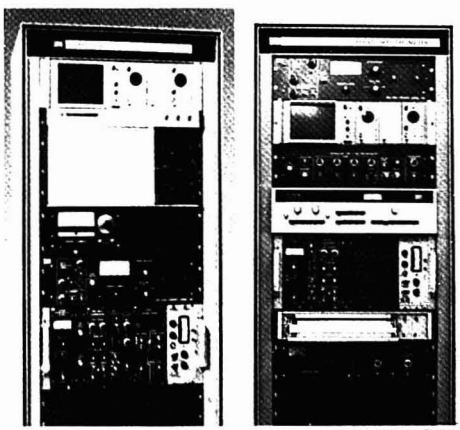

We speak your language

3M COMPANY

CIRCLE 143 ON READER SERVICE CARD

the atomic vapor. The magnitude of the thermal gradient is dependent on the geometry of the atomizer, its material of construction, and the arrangement by which the electrical contacts supply power to the atomizer. The thermal gradient is also time dependent since it is proportional to the instantaneous temperature of the center of the atomizer [thermal gradients in excess of 1000 K cm^{-1} exist in the HGA-2100 when the central temperature is 3000 K (*11*)]. During atomization, atomic vapor is distributed throughout the volume of the atomizer by a process of accelerated diffusion of vapor from the center to the cooler extremities of the atomizer (*13*). The rate of diffusion across any imaginary plane within the atomizer is affected by the instantaneous gradient in the temperature of the atomizer across the plane. The atomic vapor is in thermal equilibrium with the wall of the atomizer at each point throughout its length; hence, the flux of atoms across the thermal gradient quenches the population of the excited electronic state, lowering the measured excitation temperature. As a result, the excitation temperature-time characteristics of the atomic vapor are dependent on the physicochemical properties of the thermometric species (atomic weight and size, reactivity, appearance temperature) and reflect the temporal and spatial nonisothermality of the atomizer.

Signal Measurement

The most widely used method of measuring signals given by ET atomizers is the measurement of the maximum or peak absorbance attained. An alternative method is to record the integrated absorbance, obtained by measuring the area under the signal pulse over the period of time during which free atoms reside within the analytical volume of the atomizer. L'vov and coworkers (*14–16*) have assessed the relative merits of both methods of signal measurement from a theoretical viewpoint. By considering only the kinetics of mass transfer of sample vapor through the analytical volume of an isothermal cuvette (Figure 1), with the assumptions that the element to be determined is completely atomized and that removal of atomic vapor from the analytical volume is determined solely by diffusion under a concentration gradient, expressions were derived relating the peak and integrated absorbance to analyte mass. The peak absorbance is, as expected, a complex function of both the time taken to atomize the sample and the residence time of the atomic vapor within the analytical volume, i.e.,

$$A_p = k_A\, 2\, N_o \frac{\tau_2^2}{\tau_1^2} \times \left[\frac{\tau_1}{\tau_2} - 1 + \exp\left(-\tau_1/\tau_2\right)\right] \quad (2)$$

whereas the integrated absorbance is dependent solely on the residence time, i.e.,

$$\int_0^\infty A_t dt = k_A N_o \tau_2 = A_o \tau_2 \quad (3)$$

where A_p is the peak absorbance, k_A is a constant relating absorbance to atom concentration, N_o is the number of atoms of the element to be determined in the sample, τ_1 is the atomization time—the time duration of transfer of atoms into the analytical volume, τ_2 is the residence time of the atomic vapor—the mean length of time spent by an atom within the analytical volume, and A_o is the absorbance that would result if all of the analyte atoms were confined within the analytical volume at a single instant of time. If a sample can be completely atomized within a time $\ll \tau_2$, then from Equation 2

$$A_p \approx k_A N_o = A_o \quad (4)$$

in which case the peak absorbance corresponds to a measure of the total number of atoms in the sample. Provided $\tau_1/\tau_2 \ll 1$, small variations in the value of τ_1 and/or τ_2 that may take place during measurements have only a minor effect on the relationship expressed by Equation 4. If, however, $\tau_1 \geq \tau_2$ the peak absorbance depends on both τ_1 and τ_2 so that a simple relationship between A_p and N_o is possible only if τ_1/τ_2 = constant. The integrated absorbance is neither dependent on the rate nor on the time, τ_1, of entry of sample vapor into the analytical volume. This is extremely significant since measurement of $\int_0^\infty A_t dt$ permits one to prevent varying sample composition from affecting the analytical results. The avoidance of peak height measurement also allows for less demanding power requirements for atomization and consequent lower operating temperatures of the atomizer. Additionally, the possibility of measuring the absorption given by low volatility metals arises, such as tungsten, whose peak sensitivity is extremely poor.

L'vov and coworkers (*5, 15, 17*) have successfully used the integration method of measurement for the analysis of trace metals in a variety of matrices. With the use of an isothermal graphite cuvette employing separate heating to vaporize and atomize the sample, as shown in Figure 1, the integrated absorbance is constant, independent of the rate of sample atomization (*15*) and also of the sample composition (*17*). Table I presents results obtained by L'vov et al. (*15*) for the atomization of 2.5×10^{-10} g Tl in a graphite cuvette at various levels of additional heating of the electrode and without additional heating (to vary the rate of sample atomization). The integrated absorbance remains practically constant despite the considerable differences in rates of atomization that are reflected, indirectly, in the magnitude of the peak absorbance. Thus, with a properly designed cell, the integration method of measurement is not influenced by the kinetics of sample entry into the analytical volume. Table II presents the results obtained for the determination of copper in various powdered materials (*17*). The copper content was calculated using a calibration curve prepared from an aqueous solution of pure copper. Agreement between the certified and measured contents is confirmation of the advantages of the integration method of measurement because the analytical results were independent of the sample composition.

The principles of operation of commercial ET atomizers are similar to those of the graphite cuvette; however, the environment into which the atom-

Table I. Integrated Absorbance by 2.5×10^{10} g Tl for Various Rates of Sample Atomization[a]

Peak absorbance	Integrated absorbance
0.72	1.7
0.66	1.7
0.51	1.8
0.32	2.0
0.24	1.7
0.16	1.7
0.13	1.9
0.09	1.7

[a] Reproduced from ref. *15*; cuvette: length 40 mm, diameter 2.5 mm, T = 1670 K, pressure = 4 atm Ar.

Table II. Determination of Copper in Solid Materials[a]

Sample	Copper, % Certified	Copper, % Found[b]
MgO	0.003	0.0027
Fe_2O_3	0.003	0.0028
Cr_2O_3	0.003	0.0027
Al_2O_3	0.003	0.0028
ZnO	0.003	0.0027
Al–Mg ferrite	0.003	0.0034
Ni–Zn ferrite	0.003	0.0030
$BaCO_3$	0.003	0.0029
$BaCO_3$	0.01	0.0088

[a] Reproduced from ref. *17*. [b] Calibration carried out using aqueous standards and measured by integration.

Gilson presents a masterwork of precision and performance for **liquid column chromatography...** The Model HM Holochrome

VARIABLE WAVELENGTH DETECTOR

- **UV-VIS • DUAL BEAM**
- **HOLOGRAPHIC MONOCHROMATOR— 190 to 600 nm.**
- **INTERCHANGEABLE FLOW CELLS— INCLUDES AN 8 μl VOLUME 10 mm LIGHT PATH CELL FOR HPLC APPLICATIONS**

This Model HM uses a stabilized Deuterium light source and the newest precision Holographic grating monochromator to provide continuous digital wavelength adjustment from 190 to 600 nanometers, without changing light sources.

Holographic Monochromator Reduces Light Dispersion

A monochromator provides greater flexibility, narrower bandwidth, and longer life than interference filters. The use of a holographically constructed concave grating simplifies the optics. This eliminates some lenses and mirrors that would normally be required with a conventional flat plane grating monochromator, thus reducing light dispersion.

High Sensitivity. Low Noise

Full-scale sensitivity can be set from .01 to 2 AU. The combination of high sensitivity and narrow bandwidth results in superior peak resolution as well as wide sensitivity range. Gilson UV/VIS Holochrome monitor utilizes integrated circuit electronics and light intensity sufficient to maintain low noise levels with long light path. Noise is less than .0002 AU.

Flow Cells for HPLC and Gravity Systems

Pressure limit 35 kg/cm² (500 psi)

KEL-F FOR HPLC
10 mm light path—8 μl volume
BLOWN QUARTZ FOR BUBBLE-FREE OPERATION
10 mm light path—70 μl volume
2.5 mm light path—32 μl volume
Gilson HM flow cells optimize bubble-free operation, long light path, small cell volume, and minimum peak broadening.

Two Recorder Outputs For Tall and Short Peaks

Two recorder outputs can be set at different sensitivity levels (for example .01 and 2 AU). In this way, both tall and short peaks can be recorded simultaneously with optimum resolution.

GILSON COLUMN MONITORS ARE CONSTRUCTED FOR COLD ROOM OPERATION

CALL OR WRITE:

Gilson Medical Electronics, Inc.
Serving research laboratories for more than a quarter of a century

U.S.A. MANUFACTURING PLANT
P.O. Box 27, Middleton, Wisconsin 53562
Telephone 608/836-1551 Telex No. 26-5478

EUROPEAN MANUFACTURING PLANT
Gilson Medical Electronics, Inc. (FRANCE) S.A.
Boite Postale 45, 95400 Villiers-le-bel
Arnouville-LesGonesse, FRANCE
Telephone 990 54-41 Telex No. 69-1182F

HPLC

Circle #82 for informational literature
Circle #83 for demonstration

Table III. Effect of Atomization Power on Peak and Integrated Absorbance[a]

Element	Power, W	A_p	$\int A_t dt$
Cd	3150	0.144	0.066
	2580	0.155	0.091
	1800	0.171	0.137
	1320	0.142	0.178
	1000	0.108	0.195
	600	0.048	0.220
	460	0.022	0.198
Zn	3150	0.257	0.145
	2580	0.298	0.214
	1440	0.273	0.263
	830	0.141	0.332
	680	0.135	0.273
Cu	3150	0.220	0.430
	2800	0.215	0.450
	2370	0.140	0.420
Al	3150	0.236	0.436
	2580	0.196	0.380
	1950	0.040	0.186
Sn	3150	0.312	0.482
	2580	0.214	0.442
	1950	0.128	0.404

[a] HGA-2100; Ar sheath gas, internal purge gas interrupt.

ic vapor is passed is distinctly different. In view of this, it remains to compare the analytical performance of commercial ET atomizers with that of the graphite cuvette, as well as to consider the applicability of signal integration to these devices.

Analytical Results

L'vov's model for signal measurement is based on the pulsed atomization of samples, the atomic vapor subsequently passing into an isothermal cuvette. It is evident from earlier discussion that, with commercial ET atomizers, introduction of the sample into the analytical volume takes place over a comparatively long period of time (Figure 3) and into an environment of rapidly rising temperature, complicated by the presence of temperature-dependent thermal gradients. Additionally, loss of atomic vapor from the analytical volume is not by a process of simple diffusion.

The primary factors that influence the signal-time characteristics of all elements are the rate of heating of the atomizer and its geometry. Both parameters play a significant role in determining the sensitivity of a measurement and will be briefly considered in assessing the analytical performance of commercial ET atomizers. A third parameter that can also alter the kinetics of atom formation is the physicochemical nature of the graphite surface (porosity, reactivity, density, permeability). This aspect will not be considered in this discussion since its effects are most pronounced with refractory analytes, there being little effect on medium and high volatility analytes (*10*).

The effect of the atomization power on the peak and integrated absorbance by a number of elements in the HGA-2100 is shown in Table III. The peak absorbance is highly dependent on the kinetics of formation and loss of atoms, as predicted by Equation 2. Numerous authors have studied the effects of the rate of heating of the atomizer (atomization power) on the peak absorbance, the reported relationships varying from linear-to-exponential increases in the signal peak to a decrease in the signal peak as the rate of heating is increased. Because the rate at which a sample evaporates (and also the rate of molecular dissociation) depends on the rate of increase of temperature, at temperatures at which the analyte has a significant vapor pressure, it is important that the atomizer attain a sufficiently high temperature before a sizable fraction of the element is lost from the analytical volume. On the other hand, the temperature of the atomizer should not be increased more than is necessary to completely vaporize (and dissociate) the analyte, since the rate of loss of atomic vapor becomes too large. Table IV shows the effect of the atomization power on the measured atomization and residence times for a number of elements in the HGA-2100. Although the measured τ_1 and τ_2 values only approximate the true magnitudes of these parameters, because of the difficulty in experimentally measuring these variables (*18*), the data are useful for the trends which they show. In all cases, the τ_1 and τ_2 values decrease with increasing atomization power: τ_1 because the rate of atomization increases, τ_2 because the upper temperature of the atomizer increases; hence, the rate of loss of atomic vapor increases. It is the inseparability of the rate of heating of the atomizer and the maximum temperature which it attains that presents a major problem with commercial ET atomizers employing three-stage heating programs. The advantages of using the maximum rate of heating (minimum τ_1) cannot be fully realized because of this effect. The ratio τ_1/τ_2 for most elements, measured under optimum conditions of atomization, is close to unity (*18*). The low rates of heating (large τ_1) and unfavorable rate of loss of atomic vapor (small τ_2) result in a peak absorbance less than the maximum potentially attainable (cf. Equation 4).

Table IV. Effect of Atomization Power on Ratio τ_1/τ_2 with HGA-2100

Element	Power, W	τ_1, ms	τ_2, ms	τ_1/τ_2
Cd	3150	220	220	1.0
	2580	240	260	0.9
	2200	270	270	1.0
	1800	320	310	1.0
	1440	390	360	1.1
Zn	3150	230	260	0.9
	2580	250	280	0.9
	2200	290	380	0.8
	1440	430	640	0.7
	1240	500	880	0.6
Cu	3150	930	1140	0.8
	2580	1060	1360	0.8
	2200	1190	1520	0.8
Al	3150	760	1180	0.7
	2580	1010	1690	0.6
	2200	1470	3420	0.4
Sn	3150	820	700	1.2
	2580	1190	1110	1.1
	2200	1450	1360	1.1

In contrast to the predictions of Equation 3, the integrated absorbance is also highly dependent on the kinetics of atom formation and loss in commercial ET atomizers (*7, 8, 18*). This is largely the result of the variation of τ_2 with atomization power, as shown in Table IV.

In addition to its thermal characteristics, the geometry of the atomizer also exerts a large effect on the peak and integrated absorbance. Absorbance is proportional not to the total number of atoms present within the atomizer, but to the effective length of the absorbing volume, $\int_0^l N(x)dx$, where $N(x)$ is the concentration of atoms at point x in an absorbing volume of total length l. L'vov (*5*) has shown that the effective length of the absorbing volume at the peak of the absorbance pulse is given by:

$$\left[\int_0^l N(x)dx\right]_{\text{peak}} = N_o/S \qquad (5)$$

where S is the cross-sectional area of the atomizer. The integral value of the effective length of the absorbing volume, Q_{Nl}, is given by:

$$Q_{Nl} = \tau_2 N_o/S = l^2 N_o/8\,DS \qquad (6)$$

where D is the diffusion coefficient characterizing the loss of atomic vapor. Equations 5 and 6 have been derived with the assumptions that (a) atomic vapor is uniformly distributed over the cross section of the atomizer; (b) $\tau_1/\tau_2 \ll 1$, hence, the number of atoms within the atomizer at the peak of the absorbance pulse is N_o (Equation 4); (c) Equation 3 is valid; and (d) the loss of atomic vapor is by diffusion from the center to the extremities of the atomizer. For comparison of the performance of different atomizers the ratio of the effective length of the absorbing volume to the total number of atoms of an element is important (*19*).

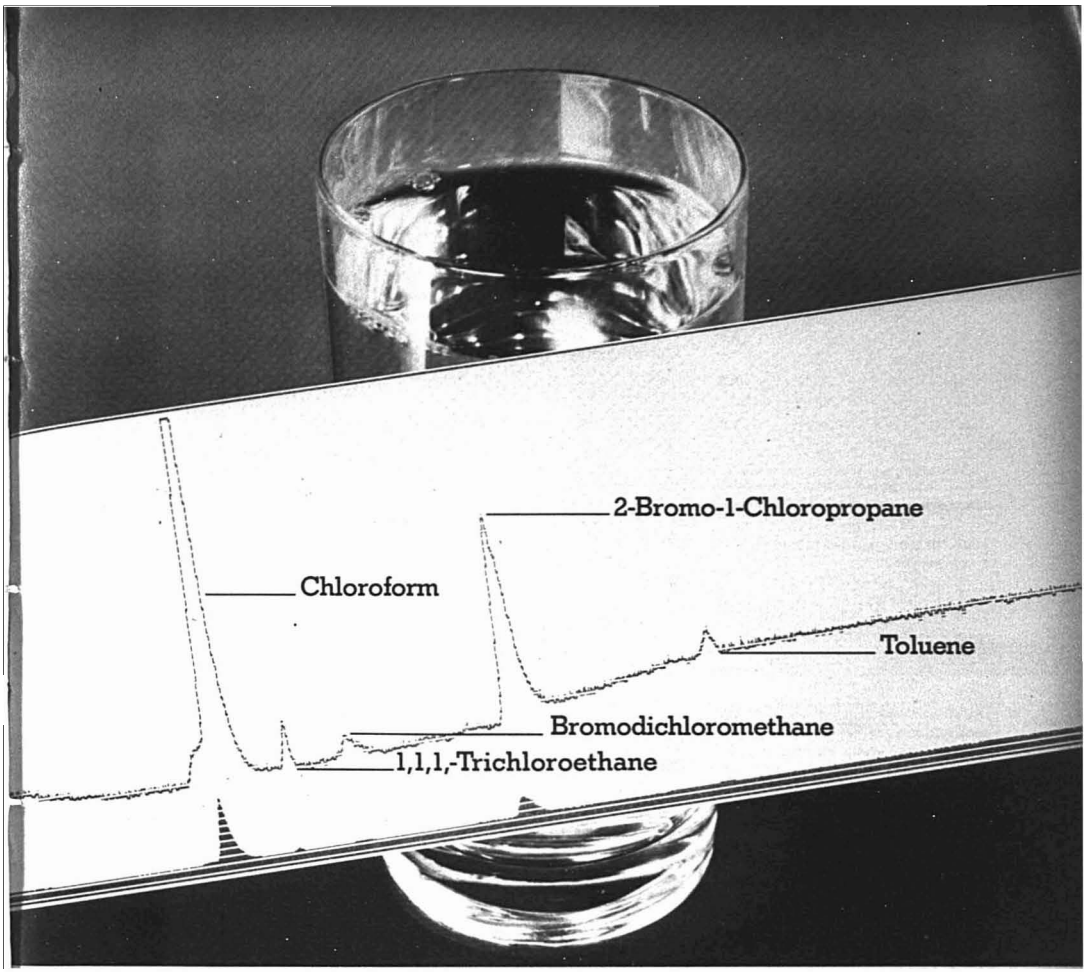

Low-cost GC/MS identifies sub-ppb pollutants in drinking water.

Talk about price/performance! Our HP 5992A GC/MS positively identifies and quantitates exceedingly low levels of chloroform, 1,1,1-trichloroethane, bromodichloromethane, 2-bromo-1-chloropropane (internal standard) and toluene in ordinary drinking water.

Moral: if you're struggling to meet TSCA or other Federal standards (air, water or solid), an HP 5992A can make your job a lot easier. And it can do it for about half the cost of any other GC/MS with data system.

The HP 5992A is easy to use (desktop computer-controlled), fits on your lab bench and comes with powerful software—a pollutant library, selected ion monitoring and an AUTOTUNE program, for example.

For detailed specs on this surprisingly sensitive and affordable answer to increasingly stringent government requirements, call your local HP office or write to the address below.

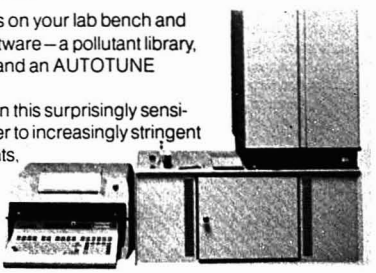

HEWLETT hp PACKARD

For assistance call: Washington (301) 948-6370; Chicago (312) 255-9800; Atlanta (404) 955-1500; Los Angeles (213) 877-1282.

1507 Page Mill Road, Palo Alto, California 94304

23705

CIRCLE 97 ON READER SERVICE CARD

Table V. Experimental Sensitivity Ratios Between HGA-2100 and CRA-63 [a]

Element	Peak method, g HGA	Peak method, g CRA	HGA/CRA ratio	Integration method, g HGA	Integration method, g CRA	CRA/HGA ratio
Cd	5.4×10^{-13}	9.5×10^{-14}	5.7	3.3×10^{-13}	5.2×10^{-13}	1.6
Zn	2.2×10^{-13}	8.4×10^{-14}	2.6	4.1×10^{-13}	6.3×10^{-13}	1.5
Sn	2.9×10^{-11}	9.1×10^{-12}	3.2	1.9×10^{-11}	4.8×10^{-11}	2.5
Cu	8.7×10^{-12}	2.7×10^{-12}	3.2	1.1×10^{-11}	6.7×10^{-12}	0.6
Al	1.1×10^{-11}	1.3×10^{-11}	0.9	2.7×10^{-11}	4.8×10^{-11}	1.8
Mo	1.1×10^{-11}	7.5×10^{-12}	1.5	6.3×10^{-12}	7.7×10^{-12}	1.2
V	4.6×10^{-11}	3.1×10^{-11}	1.5	2.7×10^{-11}	5.5×10^{-11}	2.0

[a] Obtained using pyrolytic-graphite-coated tubes. Sensitivity defined as the mass of element in grams which gives a peak absorbance of 0.0044 or an integrated absorbance of 0.0044 absorbance × second.

With the peak method of measurement one gets:

$$\left[\int_0^l N(x)dx\right]_{\text{peak}} \Big/ N_o = 1/S \quad (7)$$

and for the integration method of measurement:

$$Q_{NI}/N_o = l^2/8\,DS \quad (8)$$

Differences in sensitivity between the peak and integration methods of measurement for various electrothermal atomizers may be compared with the use of Equations 7 and 8. Table V compares the ratio of the peak and integrated sensitivity for a number of elements using the HGA-2100 and a Varian Techtron CRA-63. A diffusion coefficient of 5 $cm^2\ s^{-1}$ was selected as a reasonable value of D in an argon atmosphere at 2000 K (*5*, page 288). From the geometry of the two atomizers, Equations 7 and 8 predict that the HGA-2100 will give a 2.5-fold increase in the integration method of measurement over that given by the CRA-63, and that the peak height method of measurement with the CRA-63 offers a fourfold increase in sensitivity over that given by the HGA-2100. Table V shows that the differences in sensitivities between the atomizers are roughly as predicted for Cd, Zn, and Sn. Agreement between theoretical and experimental values for other medium and low volatility elements is poor because of the nonisothermality of the HGA-2100 atomizer along its length as compared to the uniformly heated CRA-63 (*11*). With high volatility elements this problem is not severe since with constant heating the subsequent temperature increases as the extremities of the atomizer reevaporate the condensed analyte into the analytical volume. With low volatility elements the final temperature at the extremities of the atomizer is not sufficient for rapid reevaporation of the condensate. As a result, the effective residence time of atomic vapor is decreased, i.e., the characteristic value of l for the HGA-2100 is not the geometric length of the atomizer but the length of its hot "working zone".

An additional factor that can influence the peak height and integrated absorbance is the nature of the analyte matrix. Depending on its composition, the matrix may accelerate or delay the release of atomic vapor from the sample (*20*, *21*), thereby varying the thermal characteristics of the environment into which the analyte atoms are released (Figure 3). Such an effect will alter the kinetics of formation and loss of atomic vapor (since both processes are temperature dependent) and hence the measured peak height and integrated absorbance.

In addition to the kinetics of atomization and sample matrix composition affecting the integrated absorbance, signal integration with commercial ET atomizers offers little improvement over the peak height method of measurement with respect to sensitivity (Table V), limit of detection, precision, and linear dynamic range of working curves (*7*, *8*). The advantages of signal integration predicted by theory cannot be realized with existing commercial ET atomizers. It is evident that these atomizers do not meet the requirements of correct use of the integration method of measurement, primarily because of their temporal and spatial nonisothermality as well as the inseparability of the rate of heating from the maximum temperature attained by these devices. Table VI summarizes the assumptions made in applying the peak height and integration methods of signal measurement, and the suitability of commercial ET atomizers in meeting them.

Despite numerous shortcomings, commercial ET atomizers remain excellent analytical tools for trace metal

Table VI. Applicability of Peak Height and Integration Methods of Signal Measurement with Commercial ET Atomizers

	Assumption	Condition	Applicability to commercial ET atomizers
a.	All sample atoms enter analytical volume	$\int_0^\infty N_t dt = N_o$	Many elements form stable carbides and are not vaporized from surface of atomizer
b.	Diffusional loss of atomic vapor under a concentration gradient	τ_2 = constant	Temporal and spatial nonisothermality of atomizer causes τ_2 to be sensitive to atomization conditions and sample matrix
c.	$A_{\text{peak}} = A_o$	$\tau_1 \ll \tau_2$ (Equation 4)	Generally, $\tau_1 \approx \tau_2$ with tube-type atomizers; hence, maximum peak sensitivity is not realized
d.	$\int_0^\infty A_t dt = A_o \tau_2$	Assumptions a and b above	Integrated absorbance is highly sensitive to atomization conditions
e.	$A_t = k_A N_o$	Suitable τ_{RC} for detector system	Response time of read-out system may be too slow to record signals without distortion

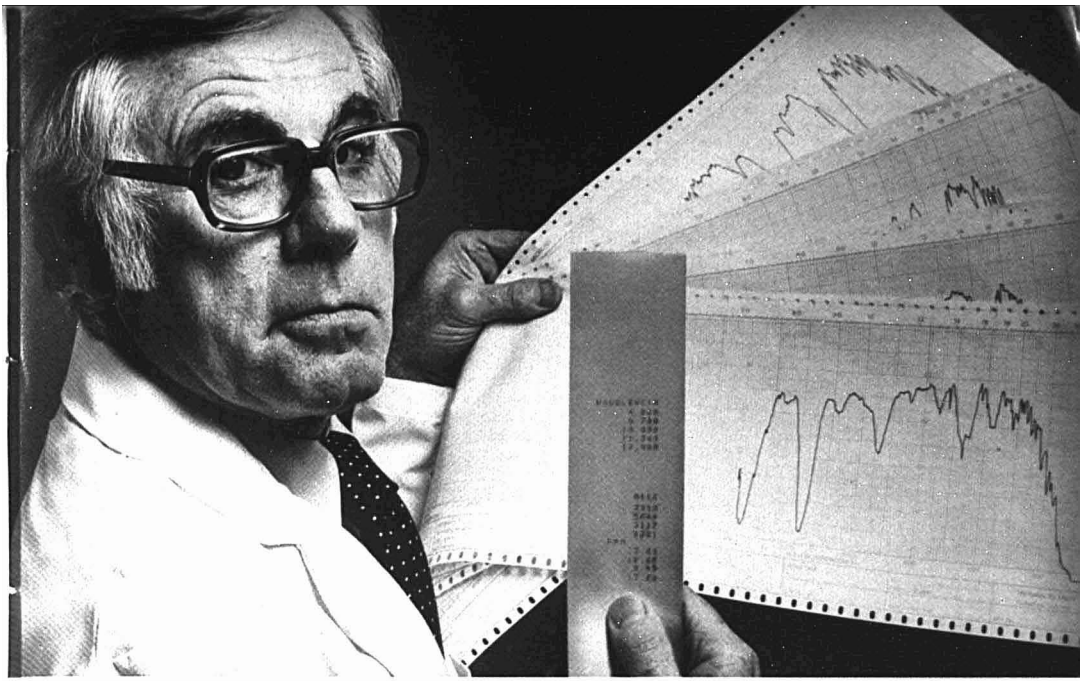

Who said IR can't do routine quantitative measurements?

The MIRAN* 80 combines a high-performance, single-beam infrared spectrometer with a programmable microcomputer. There's no data reduction for you to do. Once programmed, the MIRAN 80's built-in computer, after one keystroke, will carry out a complete analysis, subtract out interferences, make the traditional time-consuming calculations, and print out the concentrations of up to 11 components, all in less than two minutes!

The MIRAN 80 also gets off to a fast start. It accepts solid, liquid or gas samples directly without need for elaborate sample preparation. No dissolving, vaporizing or separating. Simply fill a cell with liquid, drop a film sample in the cell slide, or draw a gas sample into the analyzer's 20-meter gas cell. Then, press a button on the keyboard and concentrations (parts per million or percent) are printed out on a convenient paper tape.

All this and accuracy that's typically 1% relative . . . and a typical repeatability of one part per thousand.

When you're faced with a multitude of multi-component analyses, let the speed, accuracy and economy of the MIRAN 80 work for you.

Send today for our new MIRAN 80 literature. Or contact us for a demonstration. Foxboro/Wilks, Inc., P.O. Box 449, South Norwalk, CT 06856. Telephone (203) 853-1616

The MIRAN 80 can! It gives you direct readout of concentrations in under 2 minutes per sample.

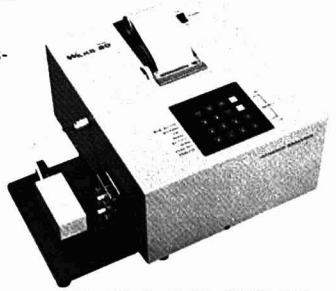

*Registered trademark

WILKS
Foxboro/Wilks, Inc.

CIRCLE 233 ON READER SERVICE CARD

analyses. Although many analyses are routinely accomplished under nonoptimal conditions, the peak height method of recording has proved to be a reliable and valuable measurement technique, provided its limitations are realized and the proper precautions are taken during its use. It is becoming increasingly evident, however, that ET atomization is subject to severe matrix interference effects as a result of variations in matrix composition influencing the kinetics of formation and loss of atomic vapor. In such circumstances, peak height measurement is not practicable. Superior analyses would be obtained if the integration method of measurement could be successfully applied.

Conclusions

The unsuitable thermal characteristics of present atomizers are not conducive to the correct use of the integration method of signal measurement. In this respect, a number of factors are considered important in the design and operation of more efficient ET atomizers.

- The atomizer should be tubular in design to contain the atomic and molecular vapor. This improves vapor-tube wall thermal equilibration and increases the vapor temperature (as opposed to atomizers of the open design, i.e., filament devices), thus promoting molecular dissociation.
- The atomizer should be constructed of pyrolytic graphite. This material has the desirable properties of low permeability to gases, low porosity, high purity, a high sublimation temperature, a high resistance to oxidation, and a high thermal conductivity. Additionally, incandescent graphite provides a highly reducing environment that aids in the reduction of thermally stable oxides to metals.
- The atomizer should be capable of achieving high rates of heating. This maximizes the rate of analyte evaporation and the rate of molecular dissociation, thereby increasing the instantaneous atom population within the analytical volume, minimizing the amount of analyte lost by diffusion both as atoms and molecules, reducing the extent of penetration of the analyte into the pores of the surface of the graphite tube, and minimizing the extent of fractional atomization of elements from samples with different volatilities.
- The maximum temperature attained by the atomizer must be made to be independent of its rate of heating. Separation of the rate of heating from the maximum temperature to be attained by the atomizer allows an optimum steady-state temperature to be set for each element which should be high enough to prevent vapor condensation but low enough to prevent excessive diffusional loss from the analytical volume.
- Temporal and spatial nonisothermality of the atomizer must be minimized, both to generate higher atomic vapor temperatures (promoting molecular dissociation) and to reduce the concentration gradient within the atomizer (hence, loss of vapor). Nonisothermality may be eliminated or reduced through proper design of the atomizer, use of suitable construction material, and by the use of high rates of heating.
- The atomizer should be as long as possible, its upper length being limited by the requirements of higher power consumption, of achieving rapid heating, of maintaining a condition of isothermality along the length of the tube and a reasonable throughput of the emission source radiation. The integral value of the effective length of the absorbing volume is proportional to the square of the length of the hot working zone of the atomizer.
- The atomizer tube should be of minimum cross-sectional area to maximize both the effective length of the

Chemtrix digital pH-plon meter

$319.

Proof that quality need not be high-priced.

How to measure pH

1. Always store electrode in de-ionized water when not in use.
2. Be sure pH bulb is full. Swing cable around to force fluid into bulb.
3. Use fresh buffers.
4. Rinse thoroughly between sample measurements.
5. For proteins and organics always use a calomel reference (order our H205).

Special programs for OEM's. Ask us.

Up here in Oregon we keep our overhead low and our standards high. For example, our Type 60A pH-plon Meter uses the best quality components available...yet it costs $306 less than a competing unit. You can pay more, but you won't get more performance than Type 60A gives you.

We have considerable applications data to support our claims for Type 60A (which is also great for specific-ions). Furthermore, Chemtrix guarantees satisfaction. If Type 60A disappoints you in any way, we'll gladly take it back.

Specifications

Accuracy: 0.01 pH • pH range: 0–14 • Millivolt range: ±1999 • Temp compensation: 0–100°C • Readout: 7-segment LED • Power: 110–220 VAC

Features

Auto-polarity • Slope adjustment • Recorder output • Auto calibration-no buffer • Tilt-up handle • BNC and U.S. connectors

CHEMTRIX INC.

163 S.W. Freeman Avenue, Hillsboro, Oregon 97123 Telephone (503) 648-0762

CIRCLE 34 ON READER SERVICE CARD

When you choose EM Laboratories you get something extra... S/P

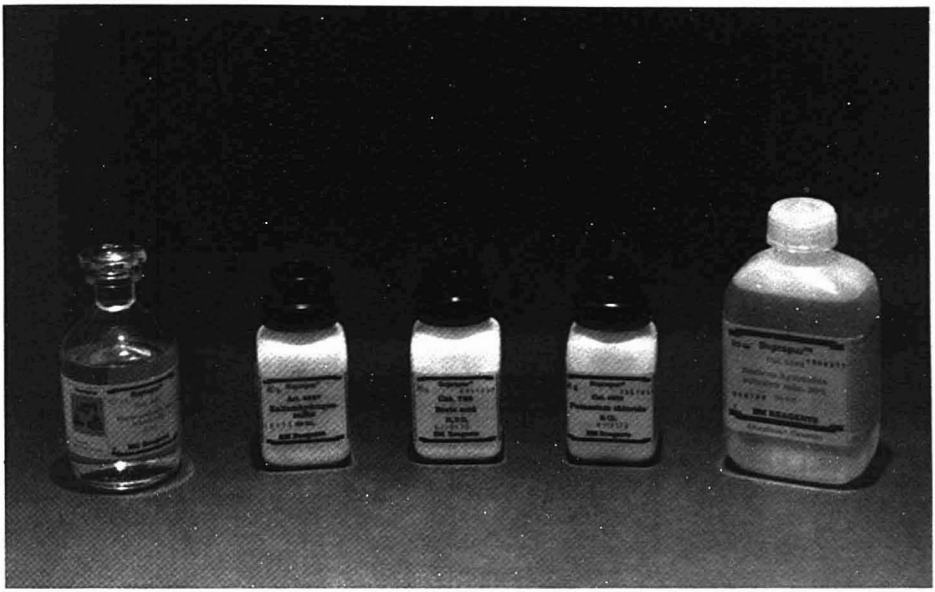

Finally, there's a line of ultrapure reagents which won't cost you a fortune. They're Suprapur® reagents. EM Laboratories' ideal combination of price and purity.

Suprapur® reagents are manufactured by and are a trademark of E. Merck, Darmstadt, Germany. Each container carries a guaranteed minimum assay of impurities—often in the range of 10^{-6}%... and less.

For a variety of analytical and research techniques. Atomic Absorption instrumental analysis. Emission Spectrography. X-Ray Fluorescence analysis of particulate matter. Materials Research. Think Suprapur® reagents.

EM Laboratories, Inc.
associate of
E. Merck, Darmstadt, Germany

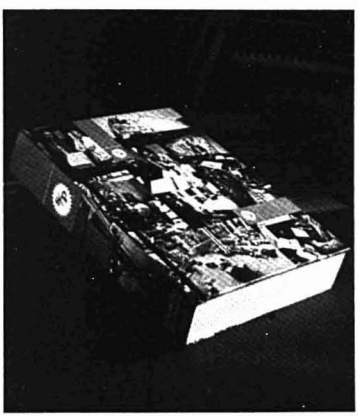

Something extra... S/P

S/P carries a lot of laboratory items. But, then, S/P is a leading distributor for more than 550 top manufacturers. To handle this huge inventory smoothly, we have 25.4 million cubic feet of warehousing space, 1.9 million cubic feet of chemical vaults, and 25 strategically located stocking centers. You benefit with a wider choice in all grades and price ranges. And we're flexible enough to stock any laboratory supply items and chemicals used in research, quality control or production specifically for you. It's all part of the S/P Responsive System of service for professionals like you. Call your S/P Representative and take stock of him.

S/P

scientific products

distributor of chemicals, laboratory supplies and scientific instruments

Division of American Hospital Supply Corporation
1430 Waukegan Road, McGaw Park, IL 60085

CIRCLE 188 ON READER SERVICE CARD

Are you a secret copy-clipper?

Do you yearn to keep your very own copy?

Do you have to wait while others read your copy?

Order your own subscription to Analytical Chemistry

all for a dollar a copy . . . or less!

You're working on a problem . . . and in that filing system of your mind, you recall that Analytical Chemistry covered the subject a few months ago. The company copy is long gone — but if you keep your own issues . . . you can be a hero!

Analytical Chemistry includes so much important timely (and timeless) information, it can be used again and again.

That's why a stack of back issues can be your personal, private library of often-needed information — and at-your-elbow reference facility — a great way to prove a point, and settle arguments.

THE FOURTEEN ISSUE YEAR

Analytical Chemistry is a monthly — but we observe 14 months a year! That is because every subscription includes two extra bonus issues:

THE ANNUAL LABORATORY GUIDE TO INSTRUMENTS, EQUIPMENT AND CHEMICALS
and
THE APRIL ANNUAL REVIEWS

That must make Analytical Chemistry one of the great bargains in chemical literature available today!

Look through this copy and notice the features you get every month: THE REPORT, INSTRUMENTATION, NEWS, NEW PRODUCTS, BOOKS, and the ANALYTICAL APPROACH (which appears periodically).

Every regular monthly issue also brings you articles written by the leaders in the field, detailing innovations in the field, and clarifying the basics.

A DOLLAR A COPY DOES IT!

A one-year subscription includes twelve regular monthly issues and two bonus issues . . . all fourteen copies for just $10.00 if you are an ACS member . . . or $14.00 if you're not! In all other countries, the cost is $19.00 for members, $23.00 for nonmembers . . . and still a great buy at less than $1.25 a copy. Available in hard copy or microfiche.

THE RISK IS ALL OURS

If you are not happy with your subscription to Analytical Chemistry, we will send you a refund — promptly — for the unused portion of your payment.

Don't be a secret copy clipper . . . use the coupon below to enter your personal subscription now!

American Chemical Society **1978**
1155 Sixteenth Street, N.W., Washington, D.C. 20036

Please enter my subscription to Analytical Chemistry as follows:

		U.S.	Canada	All Other Countries
ACS Members*	1 Yr.	☐ $10.00	☐ $19.00	☐ $19.00
	3 Yrs.	☐ $25.00	☐ $52.00	☐ $52.00
Nonmembers — Personal	1 Yr.	☐ $14.00	☐ $23.00	☐ $23.00
	3 Yrs.	☐ $38.00	☐ $65.00	☐ $65.00
Nonmember — Institutional	1 Yr.	☐ $14.00	☐ $23.00	☐ $29.00
	3 Yrs.	☐ $38.00	☐ $65.00	☐ $77.00

☐ Payment enclosed (payable to American Chemical Society).
☐ Bill me ☐ Bill company ☐ Hard Copy ☐ Microfiche

Name _____

Position _____

Address _____

City _____ State _____ ZIP _____

Allow 60 days for your first copy to be put in the mail.

absorbing volume at the peak of the absorbance pulse and the integral value of the effective length of the absorbing volume. The minimum cross-sectional area will be determined by the throughput of the emission source radiation.

- The atomizer tube should be of minimum mass to maximize its rate of heating.

References

(1) G. F. Kirkbright, *Analyst (London)*, **96**, 609 (1971).
(2) A. Syty, *Crit. Rev. Anal. Chem.*, **4**, 155 (1974).
(3) R. Woodriff, *Appl. Spectrosc.*, **28**, 413 (1974).
(4) G. M. Hieftje, T. R. Copeland, and D. R. deOlivares, *Anal. Chem.*, **48**, 142R (1976).
(5) B. V. L'vov, "Atomic Absorption Spectrochemical Methods of Analysis", Adam Hilger, London, England, 1970.
(6) H. Massmann, *Spectrochim. Acta*, **23B**, 215 (1968).
(7) R. E. Sturgeon, C. L. Chakrabarti, I. S. Maines, and P. C. Bertels, *Anal. Chem.*, **47**, 1240 (1975).
(8) R. E. Sturgeon, C. L. Chakrabarti, and P. C. Bertels, *ibid.*, p 1250.
(9) R. E. Sturgeon, C. L. Chakrabarti, and C. H. Langford, *ibid.*, **48**, 1792 (1976).
(10) R. E. Sturgeon and C. L. Chakrabarti, *ibid.*, **49**, 90 (1977).
(11) R. E. Sturgeon and C. L. Chakrabarti, *Spectrochim. Acta*, **32B**, 231 (1977).
(12) I. Reif, V. A. Fassel, and R. N. Kniseley, *ibid.*, **31B**, 377 (1976).
(13) R. E. Sturgeon and C. L. Chakrabarti, *Anal. Chem.*, **49**, 1100 (1977).
(14) B. V. L'vov, *Zh. Prikl. Spektrosk.*, **8**, 517 (1968).
(15) B. V. L'vov, D. A. Katskov, and G. G. Lebedev, *ibid.*, **9**, 558 (1968).
(16) D. A. Katskov and B. V. L'vov, *ibid.*, **15**, 783 (1971).
(17) V. P. Borzov, B. V. L'vov, and G. V. Plyushch, *ibid.*, **11**, 217 (1969).
(18) R. E. Sturgeon, PhD thesis, Carleton University, Ottawa, Ont., Canada, 1977.
(19) B. V. L'vov, "Electrothermal Atomization—The Way Towards Absolute Methods of Atomic Absorption Analysis", presented at the 3rd Federation of Analytical Chemistry and Spectroscopy Societies Conference and the 6th International Conference on Atomic Spectroscopy, Philadelphia, Pa., Nov. 15–19, 1976.
(20) K. Ohta and M. Suzuki, *Talanta*, **23**, 560 (1976).
(21) J.G.T. Regan and J. Warren, *Analyst (London)*, **101**, 220 (1976).

Ralph Sturgeon is a research associate with the Division of Chemistry of the National Research Council of Canada (Ottawa). His current research interests focus on the development of suitable standards to be used in the analysis of marine samples for a variety of trace metals.

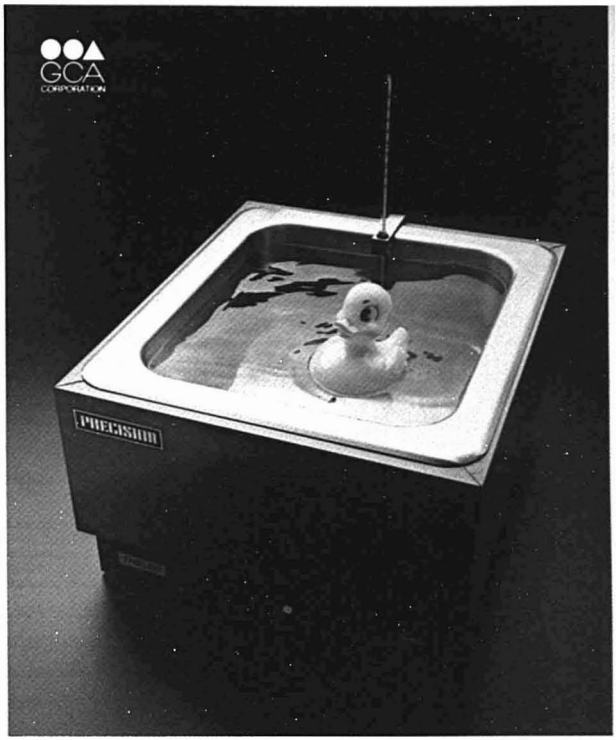

37°C ± 0.15°C AND A FREE DUCK

Buy a bath for your lab the way you buy a bath for your rubber duck.
Buy it to last 20 years.
Precision baths are constructed of one-piece, deep-drawn stainless steel chambers, with no welds or seams to wear or weaken.
Buy guaranteed temperature.
The model 184, shown here, is measured in five places for ±.15°C uniformity at 37°C and at 56°C.
Buy a name you can trust.
Precision. We've built more baths than anyone else . . . for forty years.
Free Duck. Just for sending for the world's most complete catalog of laboratory baths, we'll send you a free duck. Write Precision Scientific Group, 3737 West Cortland Street, Chicago, Illinois 60647.

CONSTANT TEMPERATURE TAKES
PRECISION™

CIRCLE 85 ON READER SERVICE CARD

*Extra Precision, Extra Performance in Liquid Chromatography

EXTRA PRECISION
Philips NEW XP Digital Programmer is microprocessor controlled for extra precision, so that resolution of % B in A is controlled to ± 0.5% to give the highest repeatability of retention times. The Gradient Programmer requires only one pump for simplicity and economy, provides 9 segments each up to 99 minutes and each capable of being programmed with a choice of 99 curve shapes plus a step function. This XP series flexibility always assures the proper program for your problem rather than a compromise.

EXTRA PERFORMANCE
The XP Digital Solvent Delivery System gives smooth, pulse-free operation up to 10,000 PSI with flow rates up to 10 ML. This high pressure capability shortens analysis time and pulse-free operation allows operation at higher sensitivity for higher performance.

To complete the total LC System Philips offers a wide range of XP Detectors to assure the highest level of performance in liquid chromatography. You have a choice of four detectors to let you select the correct one for the job:

1. Fixed Wavelength UV Detector
Operates at 254 NM;

2. Variable Wavelength UV Detector
Operates to 190 NM;

3. Unique Electron Capture Detector
Is available for those compounds with electron affinity. (It's selective response allows detection of electron capturing compounds down to 25 picograms while ignoring non electron capturing species.);

4. Universal Flame Ionization Detector
Is available when little is known about the sample. It gives a universal and linear response for all organic compounds.

The NEW Philips XP Series brings together microprocessor controlled Gradient System, a high performance Solvent Delivery System, and the widest available range of Detectors to provide the best solution to your LC problems. For more information call or write today to: Philips Electronic Instruments, 85 McKee Drive, Mahwah, N.J. 07430 • (201) 529-3800.

INTRODUCING THE PHILIPS XP*-LC

PHILIPS

Circle #167 for literature requests

PHILIPS®

Circle #168 for demonstration requests

Steven D. Brown
Laboratory for Chemometrics
Department of Chemistry
University of Washington
Seattle, Wash. 98195

Zeeman Effect-Based Background Correction in Atomic Absorption Spectrometry

During the last seven years, the development of flameless atomization techniques has made it possible to directly analyze for a variety of elements in many matrices by atomic absorption spectrometry (AAS). Direct analysis is desirable because each addition of reagent and each manipulation of the sample add contaminants (*1, 2*). However, direct analysis by AAS, especially flameless AAS, requires efficient background correction to compensate for the strong absorption of the matrix. Procedures such as nonresonant line correction (*3*), continuum-arc source correction (*4*), and continuum-source, wavelength-modulated echelle monochromator (*5*) techniques have been used previously in attempts to remove background absorption. Recently, a pair of new methods based on the Zeeman effect have been used to perform background correction. The older of the two, Zeeman source-shifted background correction, is similar to the older nonresonant line technique, in that it generates a pair of nonresonant lines very near the resonance line, while the newer of the two, Zeeman analyte-shifted background correction, utilizes the polarization characteristics of the analyte resonance line to perform background correction. This paper examines the theoretical basis for these techniques and reviews the experimental procedures utilizing the Zeeman effect to perform background correction.

Principles of Zeeman Effect

The quantum states of an atom undergo drastic changes when that atom is placed in a magnetic field; states that were degenerate may separate, and spectral lines may split into three or more components. The separation of states that arises from the interaction of the magnetic field with the magnetic moment of the electronic system of the atom can be fairly easily shown (*6, 7*) to generate the new energy states E, so that:

$$E = E^0 + \mu_B B M_J g \qquad (1)$$

where μ_B is the Bohr magnetron ($e\hbar/2m_e$), B is the magnetic induction in gauss, M_J is the magnetic quantum number, and g is the Landé g factor, $g = 1 + |[J(J+1) + S(S+1) - L(L+1)]/[2J(J+1)]|$ and where E^0 is the original energy of the state, in cm^{-1} with L, S, and J being the usual orbital, spin, and total angular momentum quantum numbers, respectively. Transitions between these new states are given by the usual selection rule

$$\Delta M_J = 0, \pm 1 \qquad (2)$$

which holds for both emission and absorption (*7*). The $\Delta M_J = 0$ components (called the π components) have their electric vectors linearly polarized parallel to the magnetic field, while the $\Delta M_J = \pm 1$ components (called the $\sigma\pm$ components for *senkrecht*, or perpendicular) have their electric vectors linearly polarized perpendicular to the magnetic field. The $\sigma\pm$ components are circularly polarized about the lines of force, also, with the $\sigma+$ and $\sigma-$ component vectors rotating in opposite directions. Figure 1 illustrates the spatial distributions for π and $\sigma\pm$ components of a typical Zeeman-shifted line. There is no π transition along a line of force in the field, since the $\Delta M_J = 0$ transition is forbidden there.

Intensities for lines viewed perpen-

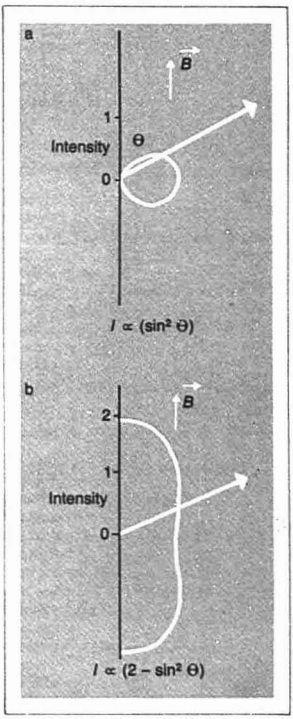

Figure 1. Spatial distribution of intensities of π (a) and $\sigma\pm$ (b) components for Zeeman-shifted line
$\vec{B}$ is direction of magnetic field, and θ is angle of observation for intensity I

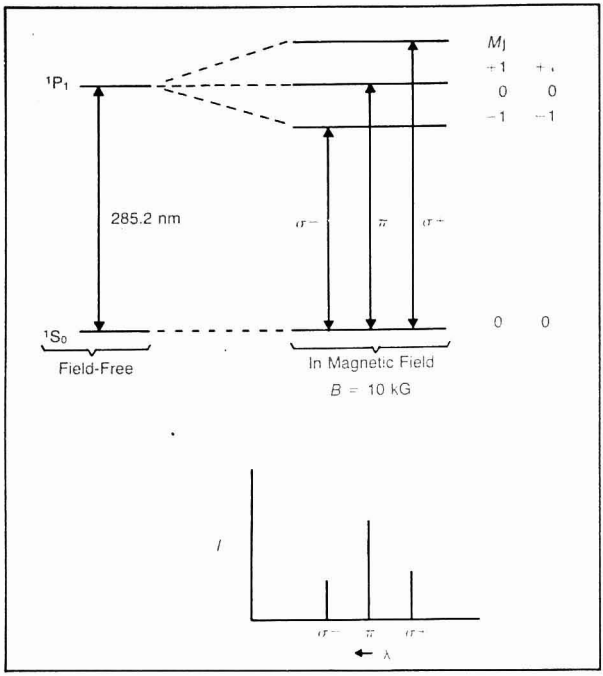

Figure 2. Normal Zeeman effect in magnesium

dicular to the magnetic field can be shown to be (*7, 8*):

$\Delta J = 0$ π component:

$$I_{\Delta M=0} = AM^2$$

$\sigma \pm$ components:

$$I_{\Delta M=\pm1} = \frac{A}{4}(J \pm M)(J \mp M + 1)$$

$\Delta J = +1$ π component:

$$I_{\Delta M=0} = B[(J+1)^2 - M^2]$$

$\sigma \pm$ components:

$$I_{\Delta M=\pm1} = \frac{B}{4}(J \mp M + 1)(J \mp M + 2)$$

$\Delta J = -1$ π component:

$$I_{\Delta M=0} = C(J^2 - M^2)$$

$\sigma \pm$ components:

$$I_{\Delta M=\pm1} = \frac{C}{4}(J \pm M)(J \pm M - 1)$$

where A, B, and C are constants. The number and the intensity of Zeeman-shifted spectral lines will depend strongly upon the initial and final terms of a given spectral transition, as well as the strength of the applied field.

The discussion above applies equally to absorption or emission of radiation by atoms in a magnetic field, the only difference being whether the absorbed or the emitted light is polarized. The splitting of spectral lines produced by the magnetic field, as well as the polarization of those lines, forms the basis of backgound correction by the Zeeman effect.

Normal Zeeman Effect. The "normal" Zeeman effect (called normal because it was explicable by classical physics) arises either when both terms involved in the transition are singlets, or when the g values for both terms are identical. An example is given in Figure 2. Here, the 285.2-nm line for magnesium is shown. At a magnetic field strength of 10 kG, the $\sigma\pm$ components are separated from the π component by 3.8×10^{-3} nm while the π component is not shifted form the field-free line position, as $E_\pi = E^0$. In general, "normal" Zeeman-shifted lines form a triplet of intensity ratio 1:2:1 that is symmetric about the field-free line.

Anomalous Zeeman Effect. When the terms are not singlets and where $g_i \neq g_f$, more splittings occur, because $J \neq L$. Now, a variety of transitions obeying the selection rule become possible, because electronic spin angular momentum is also involved in the energy of any given state. Since classical physics could not treat electron spin, it cannot explain the new energies and their corresponding transitions, and they are grouped under the heading "anomalous" Zeeman effect. The anomalous splitting of the sodium D lines provides a familiar example; this is illustrated in Figure 3. When sodium atoms are placed in a magnetic field, the D_1 line is split into four lines, corresponding to two $\Delta M_J = 0$ transitions (π) and two $\Delta M_J = \pm1$ transitions ($\sigma\pm$). The sodium D_2 line is split into six lines, two of which are π transitions. In general, anomalous Zeeman patterns are symmetric about the field-free line, with the π components shifted somewhat less than the $\sigma\pm$ components. A few special cases exist, however, where lines either show no splitting (e.g., the Ti 571.3-nm line, a $^5D_0 \leftarrow {}^5F_1$ transition) or show the "normal" Zeeman triplet but with anomalous separations (e.g., the Hg 253.6-nm line, a $^1S_0 \leftarrow {}^2P_1$ transition). Table I gives the Zeeman shifts for the sodium D line example above. As can be seen from Table I and Figures 2 and 3, Zeeman shifts are very small ($\sim 10^{-3}$ nm), making the lines quite close together in moderate magnetic fields.

Table I. Zeeman Shifts[a] for Sodium D Lines (in nm)

Field-free wavelength	Polarization	Zeeman shift, in 10 kG field
D_1: 589.59	$\sigma-$	-5.07×10^{-3}
	π	-2.53×10^{-3}
	π	$+2.53 \times 10^{-3}$
	$\sigma+$	$+5.07 \times 10^{-3}$
D_2: 589.00	$\sigma-$	-6.31×10^{-3}
	$\sigma-$	-3.79×10^{-3}
	π	-1.27×10^{-3}
	π	$+1.27 \times 10^{-3}$
	$\sigma+$	$+3.79 \times 10^{-3}$
	$\sigma+$	$+6.31 \times 10^{-3}$

[a] Calculated from data in ref. 6.

Isotope and Hyperfine Zeeman Splittings. In addition to the complications introduced by a nonzero electronic spin angular momentum value, another complication exists in that

Hitachi Polarized Zeeman Atomic Absorption Spectrophotometer

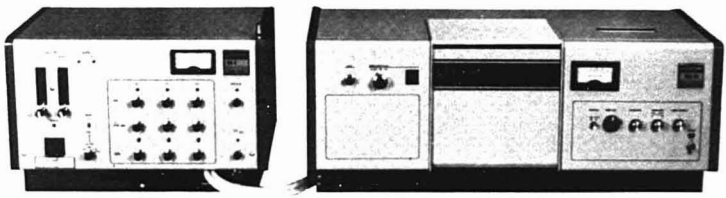

Why let precision and accuracy go up in smoke?

This is exactly what can happen if you're using a conventional graphite atomizer system. Eliminating background is a necessity for obtaining precision and accuracy. This can mean many hours of sample preparation.

Hitachi has solved this problem. Our Polarized Zeeman Atomic Absorption Spectrophotometer eliminates most, if not all, sample preparation while greatly increasing both precision and accuracy.

- Precise background correction to 1.7A—up to 5 times better than conventional deuterium lamp techniques.
- Direct analysis of most samples including blood, urine, organic material, sea water, acids, etc.
- 10 times better accuracy and precision.
- Simple, easy operation—few controls, no alignment.

Don't let your samples get lost in the smoke. Contact your Hitachi Distributor for more information, specifications and notes on your particular requirements.

NSI HITACHI SCIENTIFIC INSTRUMENTS
Nissei Sangyo Instruments, Inc.
392 Potrero Avenue • Sunnyvale, California 94086 • (408) 737-2522

CIRCLE 150 ON READER SERVICE CARD

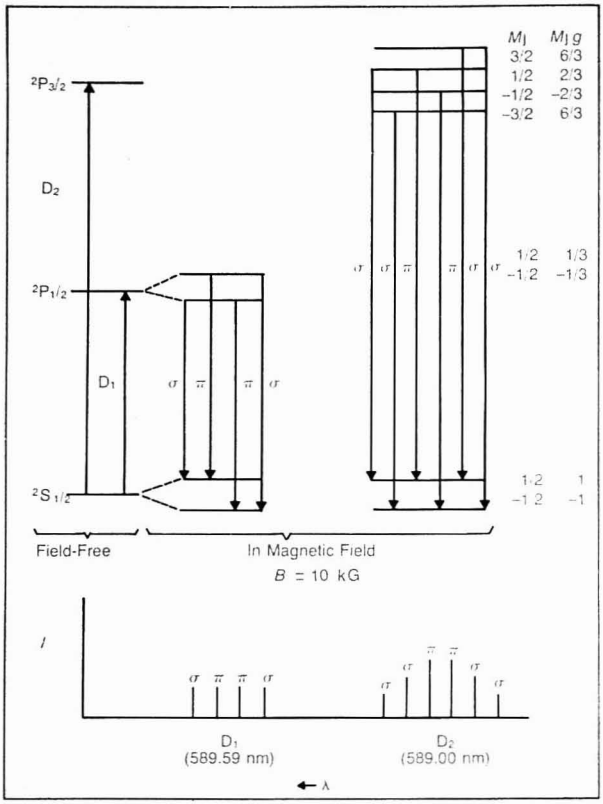

Figure 3. Anomalous Zeeman effect in sodium

some elements consist of a variety of relatively abundant isotopes. In these cases, isotope Zeeman splitting, caused by differences in the atomic masses of the atoms in the field, will occur. The contribution of isotopic Zeeman splittings to the total Zeeman splittings can be small or large, depending upon the atomic mass differences and abundance of the various isotopes. Further hyperfine Zeeman splitting, caused by the interaction of the atom's nuclear magnetic moment (when it is nonzero) with both the atom's electronic total angular momentum and the external magnetic field can also occur, but is usually very small. The Zeeman pattern for mercury, illustrated in Figure 4, provides a good example of both isotope and hyperfine effects (*9, 10*). Cadmium and zinc also show these splittings, but to a much lesser extent, so much so that isotopic and hyperfine Zeeman splittings are neglected in the analytical applications discussed below (*11*).

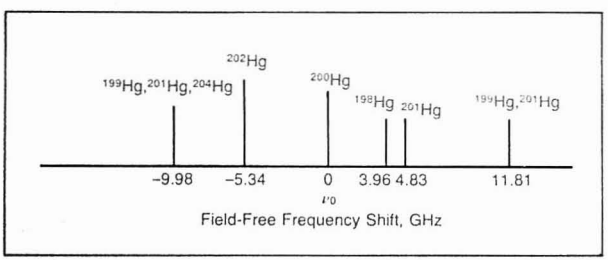

Figure 4. Zeeman effect in mercury

Effects of Temperature and Pressure on Zeeman-Shifted Lines

Along with the natural width of a line, due to the finite lifetime of the excited state, Doppler broadening (due to motion of the atom relative to the detector) and collision broadening (due to collisions with like or foreign atoms or molecules) will contribute to the overall linewidth. In a hollow cathode lamp, Doppler effects dominate because of the low pressure, but in a furnace, where both temperatures and pressures are higher, both Doppler and collision broadening are important in determining linewidths (*12*). In both cases, natural linewidth is relatively insignificant. Collision broadening also introduces a shift, called the Lorentz shift, into the wavelength of the resonance line, which is always shifted to lower wavelength (*13*). These factors broaden and slightly shift further all of the π and $\sigma\pm$ components of a Zeeman-shifted line. Table II gives calculated Zeeman shifts for the Ca 422.7-nm line and includes the approximate contributions of the Doppler broadening, the collision broadening, and the Lorentz

Table II. Calculated[a] Broadening and Shift Parameters for Calcium

Doppler halfwidths	
Source, at 550 K	5.10×10^{-4} nm
Atomized sample, at 2310 K	1.046×10^{-3} nm
Collision halfwidths	
Source, at 550 K, 5 torr	$\sim 10^{-11}$ nm
Atomized sample, at 2310 K, 760 torr	9.67×10^{-4} nm
Total halfwidths	
Source	5.10×10^{-4} nm
Atomized sample	1.634×10^{-4} nm
Zeeman shift	
10 kG field	3.79×10^{-3} nm
Lorentz shift	
Source	$\sim 10^{-11}$ nm
Atomized sample	2.63×10^{-4} nm

[a] Calculated using formulas 3, 5, and 11 from ref. *11*, with data taken from ref. *14*, assuming a collision cross section $\sigma^2 = 10 \times 10^{-16}$ cm^{-2}.

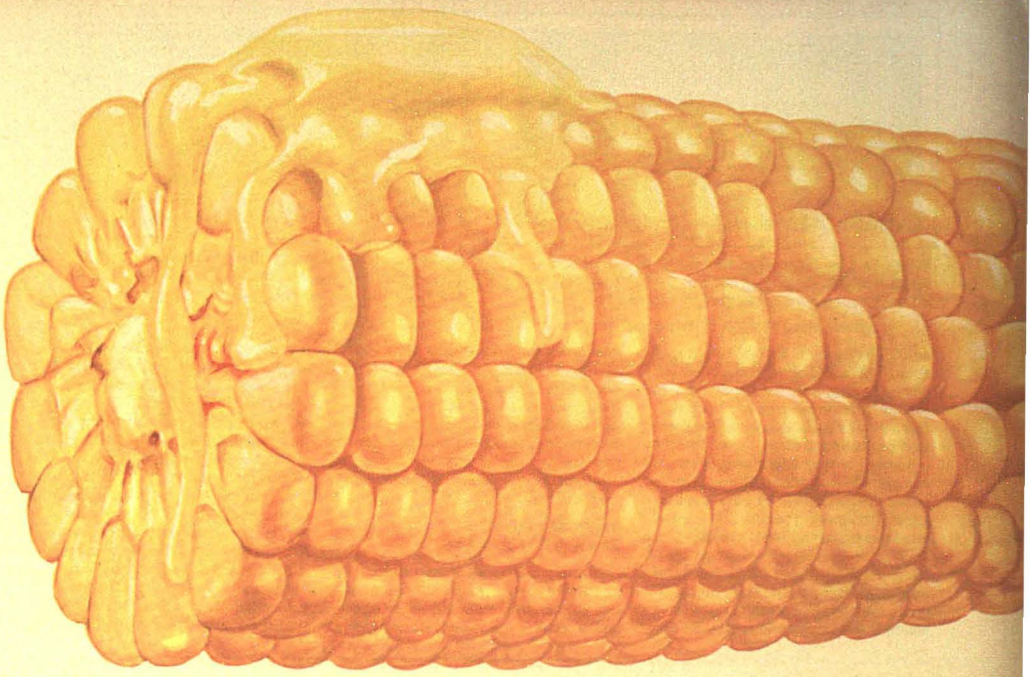

Will the vegetable shortening in the product melt before you want it to?

The Mettler FP61 will give you an accurate, objective answer. This instrument specializes in determining melting points. It can help you make a better food product, check the purity of substances, or help in identifying them. Once set, the FP61 does not have to be watched. It will digitally display the melting point until the sample is changed. The entire melting process can be recorded graphically if you connect the FP61 to a recorder. Mettler helps solve problems in analytical laboratories and on the production floors of industry. We market a great variety of weighing and measuring instruments. All of them made with the world-renowned Mettler craftsmanship. And all of them backed by a worldwide team of service specialists who can be there whenever you need them. Mettler – instruments and people you can depend on.

Depend on Mettler for the answer.

Mettler

Electronic balances and weighing systems · Thermoanalytical instruments · Automatic titration systems · Laboratory automation

Mettler Instrumente AG, CH-8606 Greifensee-Zürich, Switzerland · Mettler-Waagen GmbH, D-63 Giessen 2, Postfach 2840, BRD
Mettler Instrumenten B. V., Postbus 68, Arnhem, Holland · Mettler Instrument Corporation, Box 100, Princeton, N. J. 08540, USA

CIRCLE 141 ON READER SERVICE CARD

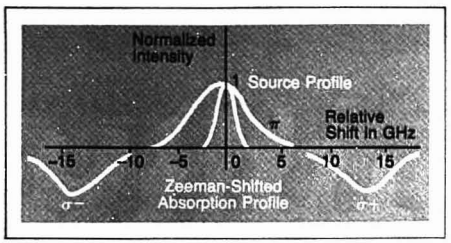

Figure 5a. Line broadening effects—lamp in magnetic field, T_{LAMP} = 550 K, T_{SAMPLE} = 2310 K, Ca 422.7-nm line in 10 kG field, both curves normalized to 1 for clarity

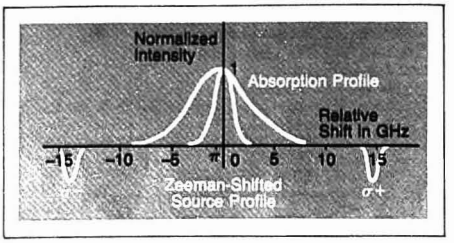

Figure 5b. Line broadening effects—atomized sample in magnetic field, T_{LAMP} = 550 K, T_{SAMPLE} = 2310 K, Ca 422.7-nm line in 10 kG field, both curves normalized to 1

shift. The Zeeman shift dominates, although broadening is pronounced, when the field either is applied to a Ca hollow cathode lamp or to a heated cell containing Ca atoms, as is shown in Figures 5a and 5b.

In both of the cases above, the π component coincides with the resonance line, while the $\sigma\pm$ components are shifted away from the line. The same general trend occurs in the anomalous Zeeman effect, but since the π-π and σ-σ separations are not as pronounced, the individual components are broadened to the point where they merge to form π and $\sigma\pm$ *envelopes* that, depending upon the applied field, the element, and the transition, separate to a greater or lesser extent (*10, 15*). The small hyperfine effects are obscured by the broadenings, and even isotope shifts can vanish; usually only very heavy atoms show observable isotope Zeeman shifts (*13*).

Experimental Implementation of Zeeman Effect in AAS

Source-Shifted Zeeman Background Correction. Of the two methods now available using Zeeman effect shifts to accomplish background correction, source-shifted Zeeman background correction is the older, having first been used by Hadeishi and coworkers (*10, 16–19*) in 1971, and later adapted by Koizumi and Yasuda for furnaces (*11, 20, 21*) and by Stephens and coworkers for flames (*22–25*). It is based on the premise that background absorption is largely broadband molecular scattering and absorption (*4, 26*), one which is now firmly established (*11, 27, 28*). Since these molecules and particles responsible for the background absorption have small g values (*29*), it is reasonable to expect that their absorption is unaffected by

NEW AUTOTHINKING AA AUTOSAMPLER

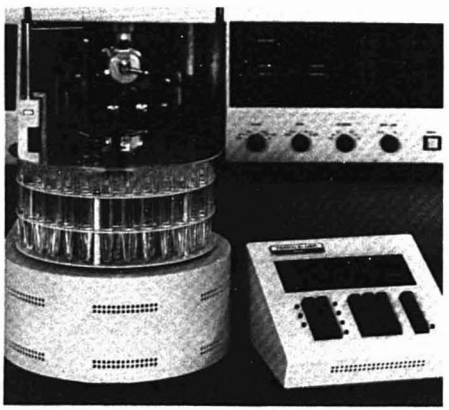

The new Perkin-Elmer Flame Autosampler, the AS-50, helps you to analyze up to 50 samples automatically in as little as 15 minutes. The AS-50 with microcomputer control virtually thinks for itself. After the last sample is analyzed, the table reindexes to its initial position and a buzzer sounds to tell you that work has been completed on this series of samples.

With the Model 460 and 603, the AS-50 will even trigger the calibration functions automatically. For the utmost in accuracy, you can even recalibrate in the middle of a run automatically, and naturally you may select a sample aspiration time most appropriate for the element being measured. Precision is excellent and carryover is minimal.

Find out how the AS-50 can help you to get more results from your AA faster, more easily, and with the excellent precision and accuracy you have come to expect from a well-designed AA. Ask your Perkin-Elmer representative for literature and a demonstration. Or write Perkin-Elmer Corporation, Main Avenue, MS-12, Norwalk, CT 06856. Phone (203) 762-6681.

PERKIN-ELMER

CIRCLE 178 ON READER SERVICE CARD

the presence of the magnetic field, since ΔE is small. In this method, the spectral lines from the hollow cathode (or other) lamp in a magnetic field are separated into π and $\sigma\pm$ components, and these new lines are passed through the atomized sample. The π component is absorbed by both the sample and background species, as π components are largely unshifted, but the Zeeman-shifted $\sigma\pm$ components are absorbed by only the background species. Conversion of the π and $\sigma\pm$ signals to logarithms, and finally subtraction of the latter from the former, yield the true sample absorbance.

The basic experimental arrangement for this method is diagrammed in Figure 6. The compensator is needed to ensure that the initial intensities $I_{0\pi}$ and $I_{0\sigma\pm}$ are equal, while the rotating prism allows alternate detection of I_π and $I_{\sigma\pm}$. Nontime-shared systems (*11, 23*) also have been used by removing the rotating polarizer and substituting Wollaston prisms (*30*) along with two photomultiplier tube (PMT) units, one for the π component and the other for one of the $\sigma\pm$ components. A variable phase retardation plate coupled with a linear polarizer (*31*) can also be used in place of the rotating polarizer.

This technique has been used successfully in correcting as much as 1.7 absorbance units of background absorption in the analysis of the "normal" Zeeman elements Pb (*18, 21, 23*), Ag (*23*), Mg (*23*), and Cd (*21, 23*). Detection limits varied from near that of a conventional hollow cathode limit (Mg) to about two to four orders of magnitude poorer. The anomalous Zeeman elements Cr (*23*), Fe (*23*), Cu (*23*), and Ni (*23*) could also be analyzed using Zeeman background correction, but detection limits (*11*) and sensitivities (*23*) were poorer, due to the broadening of the π envelope as well as the shifting of some π components outside of the absorption line. Mercury (*10, 20*), an element with hyperfine Zeeman and anomalous Zeeman effects, also has been analyzed using the above arrangement.

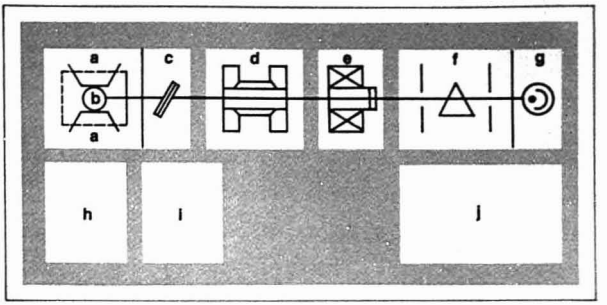

Figure 6. Experimental arrangement for source-shifted Zeeman background correction (*21*)

a) Magnet (10 kG), b) lamp (Pb, Cd, Zn), c) compensator, d) graphite furnace, e) polarizer, f) monochromator, g) photomultiplier, h) oscillator, i) power supply (3 kVA), j) signal processing unit

Zeeman-Analyte-Shifted Background Correction. The second method using Zeeman shifts to correct

THE BEST IN EDLs FOR AA NOW GOES DOUBLE

Electrodeless Discharge Lamps have many advantages... they are bright, stable, sensitive, and long-lived.

However, they also take a few minutes to warm up. This inconvenience is now removed with the new Perkin-Elmer dual-lamp EDL Power Supply containing two separate and independent EDL power supplies. Now when you're running As and you want to change to Se, the lamp is warmed up and ready to go. Just change the lamp in the holder, adjust the instrument wavelength and five seconds later you're measuring Se (or any of the other thirteen elements for which EDLs are available). The patented* Perkin-Elmer EDLs with lamp, cavity and antenna all pre-adjusted are as easy to use as our famous Intensitron® hollow cathode lamps.

EDLs are currently available for As, Bi, Cd, Cs, Ge, Hg, P, Pb, Rb, Sb, Se, Sn, Te, Tl, and Zn.

Ask your Perkin-Elmer representative for all the facts on EDLs and the new dual-lamp EDL Power Supply. Or write Perkin-Elmer Corporation, Main Ave., MS-12, Norwalk, CT 06856. Phone (203) 762-6681.

*U.S. Patent No. 3,873,884

PERKIN-ELMER

CIRCLE 179 ON READER SERVICE CARD

for background absorption involves more directly the polarization of the π components (*15, 32–35*). Here, the sample cell containing the atomized sample is placed in the magnetic field, and a conventional hollow cathode lamp is used as the source. By alternately polarizing the incident light parallel and perpendicular to the magnetic field, one sees first background absorption and then background and sample absorption, because the $\sigma\pm$ components have been shifted away from the sample atom's resonance line and the remaining π components of the resonance line absorb *only* parallel polarized light, while the background equally absorbs both polarizations of light (*35*). The experimental arrangement for this method is shown in Figure 7. The unit diagramed there is also equipped with a modulated light source and phase-sensitive detection to minimize the effects due to emission of the furnace. This unit, unlike the one shown in Figure 6, is a true double-beam spectrometer, with both beams traveling the same path length at the *same* wavelength. In this method, correction is performed *at* the resonance line, not at a slightly different wavelength, an important advantage.

A variety of elements has been analyzed using this newer Zeeman method for background correction. In cases where a selection of lines is available, the line with the smallest π shift frequently gives the best sensitivity even when its transition probability is smaller, because one obtains a larger differential absorption. This is especially true for Ag and Cr (*35*). Here, the anomalous Zeeman effect splittings of the π components cause little problem, as the *absorption* line is being broadened, not, as in the previous method, the source line. This keeps the source line profile inside the absorption line profile and provides a wider dynamic range, better sensitivity, and less dependence upon fluctuations in the light source (*15, 35*). This method is limited in correcting for background absorption only in that a minimum signal must be observable by the detector. Hence, brighter sources would enable a larger correction range (*35*).

Background Correction by Zeeman Effect: How Well Does It Work?

The brief descriptions given above for the two methods of implementing the Zeeman effect in analytical atomic absorption spectrometry have given some idea of the relative merits of the two, but further comparisons are interesting. Table III lists the detection limits for a variety of elements by nonflame AAS using the two background correction methods above, as well as data obtained without background correction. The data indicate that the analyte-shifted Zeeman correction technique is more sensitive than the source-shifted Zeeman correction method and approaches the sensitivity of noncorrected measurements. Sensitivities using the most common form of background correction, the deuterium arc, are frequently decreased by factors of five to fifty (*35*) because of under- or over-compensation of background absorption (*37*), so that the sensitivity of the analyte-shifted Zeeman correction method must be considered as comparable, or even superior, to arc correction systems. The background correction range of both Zeeman shift-based methods is wider than either the deuterium arc or even the more intense xenon-mercury arc (*38*), a significant advantage when less cooperative sample matrices are encountered.

In addition to their wide background correction range, Zeeman-shifted correction techniques also have a wide range of wavelengths where they can perform useful correction, limited only by the availability of suitable lamps. Spectral lines below 190 or above 600 nm lie outside the more intense region of arc continua, and it is necessary either to reduce hollow cathode intensity to match the continuum intensity, or to increase the slit width when one uses an arc as the background corrector in these regions. Reduction of hollow cathode intensity can decrease the signal-to-noise ratio of a system where photomultiplier shot noise or electronic noise is the major source of noise, while increased slit width can result in nonlinear calibration curves and increased shot noise from furnace emission. Zeeman-shifted correction techniques neither suffer from these problems nor from the exacting optical axis alignment restrictions imposed on a continuum arc correction system because of the use of two lamps.

Source-shifted Zeeman correction methods require special, magnetically stable lamps, however, and this requirement has been the source of some problems because these sources are more noisy, as well as far less stable, then commercial hollow cathode lamps (*22*). Signal-to-noise ratios and detection limits suffer. There is also a report (*39*) that resonance line self-absorption, leading to wavelength shifts and intensity variations, can occur in these lamps. Various designs

(*Continued on page 1280 A*)

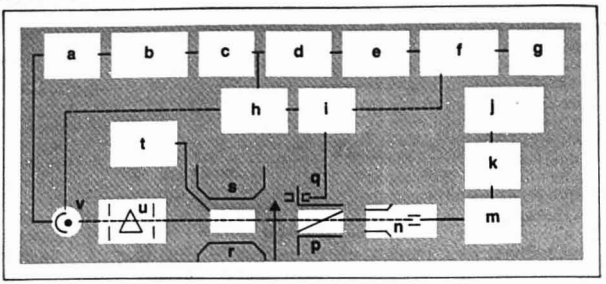

Figure 7. Experimental arrangement for analyte-shifted Zeeman background correction (*35*)

a) Preamp, b) mechanical filter (1.5$^{\pm 0.11}$ kHz), c) detector, d) log converter, e) line pass filter (100 Hz), f) synchronous rectifier, g) recorder, h) high-voltage generator, i) gate circuit, j) mechanical oscillator (1.5 kHz), k) direct current superimposing voltage, m) hollow cathode lamp power source, n) hollow cathode lamp, p) senarmon prism (rotating), q) phase monitor, r) permanent magnet (11 kG), s) graphite atomizer, t) SCR power supply, u) monochromator, v) photomultiplier

Table III. Detection Limits by Flameless AAS (in pg)

Element	Wavelength, nm	Transition	With correction SSZ[a]	With correction ASZ[b]	No correction, HGA-2000[c]
Pb	288.3	$^3P_0 \leftarrow {}^3P_1$	100 50[d]	4	6
Cd	228.8	$^1S_0 \leftarrow {}^1P_1$	5	0.3	0.1
Zn	213.8	$^1S_0 \leftarrow {}^1P_1$		1	0.06
Mg	285.2	$^1S_0 \leftarrow {}^1P_1$		0.1	. . .
Ni	232.0	$^3F_4 \leftarrow {}^2G_5$		30	10
Fe	248.3	$^5D_4 \leftarrow {}^5F_5$		4	3
Cu	324.7	$^2S_{1/2} \leftarrow {}^2P_{3/2}$		10	1
Ag	328.0	$^2S_{1/2} \leftarrow {}^2P_{3/2}$		0.9	0.25

[a] Source-shifted Zeeman correction. Data from ref. *21*, except where noted. [b] Analyte-shifted Zeeman correction. Data from ref. *35*. [c] Data from ref. *36*. [d] Data from ref. *18*.

FREE GUIDE to the selection of lab tubing.

Our new information-packed bulletin for Tygon® laboratory tubing, Tygon vacuum tubing and Tygon micro-bore tubing gives complete product operating criteria, chemical resistance properties, selection data and more. Everything you need to know to choose the right tubing for your needs.

Tygon R-3603 tubing is standard in laboratories across the country. Tygon is crystal-clear. Flexible as rubber. Non-aging and non-oxidizing. Doesn't affect the solutions or gases it carries. And it complies with Federal Specification L-T-790A Type II.

Let Tygon tubing perform for you. Write now for bulletin LT-300, or call toll-free 800-321-9634 (except Ohio).

NORTON PLASTICS AND SYNTHETICS DIVISION
PO BOX 350 AKRON, OHIO 44309 TEL: (216) 633-3224

34-201

CIRCLE 149 ON READER SERVICE CARD

Forensic Science

ACS Symposium Series No. 13

Geoffrey Davies, *Editor*

A symposium sponsored by the Divisions of Analytical Chemistry and Chemical Education of the American Chemical Society.

A fascinating volume that reflects the growing public interest in forensic science as a key analytical tool in establishing criminal guilt or innocence.

Nineteen chapters give an up-to-date status report on educational preparation as well as new applications and refinements of research techniques.

This wide-appeal book will be of special interest to the analytical chemist, police officer, law enforcement program head, college instructor, and general reader alike, with its comprehensive coverage of the latest developments in:

- forensic science education and research; LEAA's research program
- materials science methods; SEM analysis; bullet search systems; firearm residue detection; arson debris analysis; differential scanning calorimetry
- ink, bloodstain, and physiological fluid analysis; forensic toxicology; heroin sample comparison; photoluminescence techniques

204 pages (May 1975) $17.95 clothbound

SIS/American Chemical Society
1155 16th St., N.W./Washington, D.C. 20036

Please send _____ copies of *No. 13 Forensic Science* at $17.95 per book.

☐ Check enclosed for $_____. ☐ Bill me.
Postpaid in U.S. and Canada, plus 40 cents elsewhere.

Name

Address

City State Zip

TWO GIANT

Perkin-Elmer introduces two new groups of liquid chromatographs – Series 2 and Series 3. They give you the most advanced LC for your money.

All at once you have unprecedented alternatives in liquid chromatography. These instruments are all state-of-the-art, significant additions to the Perkin-Elmer line. They're not cost-burdened with features that should be options. Instead, they're an innovative concept in matching price to performance.

Series 2. Five modular units.

For economy and efficiency, any LC system you buy should be closely tailored to the work it must do. This is the main advantage of the Series 2 modular design. Begin with the simplest practical unit — add more modules and accessories later.

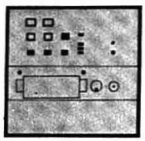

The Series 2/1, with a single pump, is the basic unit. It's compatible with all commercial LC detectors. The pumping system has only three moving parts, so it's dependable and exceptionally easy to maintain. Series

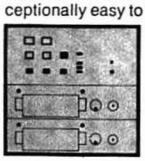

2/2 adds a second pump for more efficiency and output. Its basic linear gradient capability can quickly approximate solvent conditions necessary for isocratic separation.

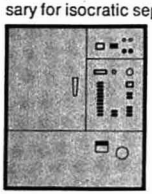

In the LC-65T Detector/Oven, superior UV/Visible detection is combined with temperature control. Series 2/1, combined with the LC-65T, joins the reliable, convenient solvent delivery of the one to the spectrophotometric detection and temperature control of

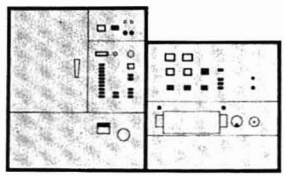

the other. You get better quality separations with improved column efficiency, along with more readily optimized separation time. Series 2/2, combined with the LC-65T, has the additional pump that provides gradi-

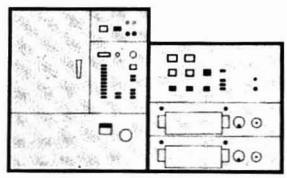

ent and flow-programming capability, and the Detector/Oven for temperature control and UV/Visible detection.

Series 3. Two units with microprocessor control.

Everything you need for highly precise qualitative and quantitative analyses is designed into these instruments. At the same time, they have all the convenience you need for routine problem solving. Both have their solvent delivery systems under microprocessor control. And both include high pressure capability and a wide flow rate range for analytical and preparative separations.

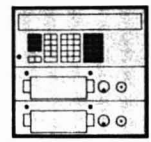

Series 3 adds the precision and convenience of microprocessor control to the dual-pump solvent delivery system of Series 2/2. It's also compatible with all commercially available LC detectors. Series 3 with the

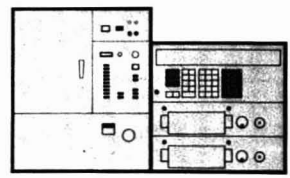

LC-65T adds up to the top of the line. It has the full solvent delivery capability of the Series 3 along with two other features for reliable problem solving: (1) temperature control and (2) UV/Visible spectrophotometric detection. The first results in excellent reproducibility. The second lets you check each step with confidence in developing a separation.

A wide choice of Perkin-Elmer accessories is available for all these instruments. Find out how efficiently Series 2 and Series 3 can fit all your liquid chromatography needs. Contact your Perkin-Elmer representative, or write Perkin-Elmer Corporation, Main Avenue, Norwalk, CT 06856.

PERKIN-ELMER

CIRCLE 180 ON READER SERVICE CARD

STEPS IN LC

Series 2/2 with LC-65T

Series 3 with the LC-65T

for lamps suitable for use in magnetic fields have been used, including electrodeless discharge lamps (*40*), RF-powered vapor discharge lamps (*25*), and dc generated plasma lamps (*22*), along with special hollow cathode lamps (*11*). The limited number of elements used, the stability, and the longevity of these lamps are problems still to be resolved. Analyte-shifted Zeeman correction techniques use conventional hollow cathode lamps, and thus avoid the magnetically stable lamp problem, but encounter another problem in that the magnet restricts the kind and the dimensions of the atomizer used, because it is necessary to expose the atomized sample to a uniform magnetic field. Graphite tube (*35*), tantalum strip (*15*), and carbon rod (*34*) furnaces have been used without difficulty, and even flames have also been tried (*32, 33*). Special magnet designs are also desirable to avoid changes in the magnetic field caused by the effects of cell thermal radiation on the magnet material (*35*).

Because both source-shifted and analyte-shifted Zeeman correction techniques generate the correction within the atom and are therefore not subject to limitations of spectral range, a width range of elements can be analyzed using background correction, with detection limits very near non-correction values. The one restriction is only that the element must possess a resonance line that shows a suitable Zeeman effect, either normal or anomalous, in a reasonable (10–15 kG) magnetic field. This requirement is the most severe disadvantage, since many of the stronger resonance lines show strong anomalous Zeeman effects and spread the π envelope to such a large extent that a weaker resonance line showing a more tightly grouped π envelope gives greater sensitivity. Chromium analysis by analyte-shifted Zeeman background correction is a good example (*35*). The π shift of the $^7S_3 \leftarrow {}^3P_3$ (357.9 nm) transition is smaller than that for the $^7S_3 \leftarrow {}^3P_4$ (359.4 nm) transition, a line normally used in AAS because of its larger transition probability; here the 357.9-nm line is more sensitive because of its larger $P_\perp/P_\parallel$ ratio, a consequence of a tightly grouped π envelope. A similar, but less severe problem exists for sodium (Figure 3). In source-shifted Zeeman correction techniques, the large π spread leads to nonlinear calibration curves and higher detection limits, since the π spread here broadens the source line.

The main disadvantage of these new techniques when compared to arc correction techniques used to be availability, but this is no longer true. One manufacturer has placed a spectrometer using Zeeman analyte-shifted correction on the market, and others may be expected to follow suit soon. Commercial availability of the Zeeman effect-based correction systems will certainly benefit all of analytical atomic absorption spectrometry. These systems greatly ease the problems involved in direct analysis (*35*) and will be of great help there, but they also provide an impetus for a re-examination of the existing techniques to see how they can benefit from efficient and simple background correction. Research into better detectors and more intense light sources is given new urgency as well. Zeeman-shifted background correction is clearly one of the major advances in atomic absorption spectrometry.

Acknowledgment

The author thanks B. R. Kowalski and G. D. Christian of this department for helpful criticisms and comments, and H. Koizumi of Hitachi, Ltd., for providing two of the figures.

References

(1) M. Zief and J. W. Mitchell, "Contami-

TMA MADE PDQ

Thermomechanical analysis is the most sensitive way to measure a material's temperature-dependent properties. It's also simple, fast, and precise when you use the Perkin-Elmer TMS-2 Analyzer.

With the TMS-2 to gauge dimensional or viscoelastic changes, you can determine properties like expansion coefficient, heat distortion temperature, softening point, and heat shrink behavior. TMA measurements correlate well with many ASTM tests. What's more, the TMS-2 routinely performs them with much greater speed and precision.

Perkin-Elmer's unique *modular design* saves you money. The TMS-2 can be programmed simultaneously with the DSC-2 Differential Scanning Calorimeter or as an independent system with the UU-1 Temperature Program Control. In addition, the TMS-2 uses the same heater control unit and First Derivative Computer Accessory as the TGS-2 Thermogravimetric Analyzer. Hence, the TMS-2 can be added to or purchased with a TGS-2 at minimum cost.

Find out more about the TMS-2 from Perkin-Elmer, the leader in modern Thermal Analysis instrumentation. Write today to Perkin-Elmer Corporation, Main Avenue, Norwalk, CT 06856, or phone 203-762-6915.

PERKIN-ELMER

CIRCLE 181 ON READER SERVICE CARD

nation Control in Trace Metal Analysis", Wiley, New York, N.Y., 1976.
(2) R. W. Dabeka, A. Mykytiuk, S. S. Berman, and D. S. Russell, *Anal. Chem.*, **48**, 1203 (1976).
(3) J. B. Willis, "Methods of Biochemical Analysis", in "Advances in Analytical Chemistry and Instrumentation", J. D. Winefordner, Ed., Vol 9, Chap. 3, Wiley-Interscience, New York, N.Y., 1971.
(4) S. R. Koirtyohann and E. E. Pickett, *Anal. Chem.*, **38**, 585 (1966).
(5) A. T. Zander, T. C. O'Haver, and P. N. Keliher, *ibid.*, **48**, 1166 (1976).
(6) F. K. Richtmeyer, E. H. Kennard, and J. N. Cooper, "Introduction to Modern Physics", 6th ed., McGraw-Hill, New York, N.Y., 1969.
(7) E. U. Condon and G. H. Shortley, "The Theory of Atomic Spectra", Cambridge Univ. Press, Cambridge, 1951.
(8) F. F. Feofilov, "The Physical Basis of Polarized Emission", English transl., State Physio-Mathematical Press, Moscow, USSR, 1959.
(9) H. Schüler and J. E. Keyston, *Z. Phys.*, **72**, 423 (1931).
(10) T. Hadeishi and R. D. McLaughlin, *Science*, **174**, 404 (1971).
(11) H. Koizumi and K. Yasuda, *Spectrochim. Acta*, **31B**, 237 (1976).
(12) A.C.G. Mitchell and M. W. Zemansky, "Resonance Radiation and Excited Atoms", Cambridge Univ. Press, Cambridge, 1962.
(13) H. G. Kuhn, "Atomic Spectra", Longmans, Green, London, England, 1962.
(14) H. C. Wagenaar and L. De Galan, *Spectrochim. Acta*, **28B**, 157 (1973).
(15) H. Koizumi and K. Yasuda, *ibid.*, **31B**, 523 (1977).
(16) T. Hadeishi, D. A. Church, R. D. McLaughlin, B. D. Zak, M. Nakamura, and B. Chang, *Science*, **187**, 348 (1975).
(17) T. Hadeishi, *Appl. Phys. Lett.*, **21**, 438 (1972).
(18) T. Hadeishi and R. D. McLaughlin, *Anal. Chem.*, **48**, 1009 (1976).
(19) T. Hadeishi and R. D. McLaughlin, *Am. Lab.*, **7** (8), 57 (1975).
(20) H. Koizumi and K. Yasuda, *Anal. Chem.*, **47**, 1679 (1975).
(21) H. Koizumi and K. Yasuda, *ibid.*, **48**, 1178 (1976).
(22) R. Stephens and D. E. Ryan, *Talanta*, **22**, 655 (1975).
(23) R. Stephens and D. E. Ryan, *ibid.*, p 659.
(24) D. E. Veinot and R. Stephens, *ibid.*, **23**, 849 (1976).
(25) R. Stephens, *ibid.*, **24**, 233 (1977).
(26) S. R. Koirtyohann and E. E. Pickett, *Anal. Chem.*, **38**, 1087 (1966).
(27) J. W. Robinson, G. D. Hindman, and P. J. Slevin, *Anal. Chim. Acta*, **66**, 165 (1970).
(28) H. L. Kahn and D. C. Manning, *Am. Lab.*, **4** (8), 51 (1972).
(29) G. Hertzberg, "Molecular Spectra and Molecular Structure", Van Nostrand-Reinhold, New York, N.Y., 1950.
(30) R. S. Longhurst, "Geometric and Physical Optics", Longmans, Green, London, England, 1957.
(31) B. D. Zak, B. Chang, and T. Hadeishi, *Appl. Opt.*, **14**, 1217 (1975).
(32) C. Parker and A. Pearl, British Patent 1,385,791 (January 5, 1972).
(33) Y. Uchida and S. Hattori, *Oyo Butsuri*, **44**, 852 (1975); *Chem. Abstr.*, **84**, 11953y.
(34) J. B. Dawson, E. Grassam, D. J. Ellis, and M. J. Keir, *Analyst*, **101**, 315 (1976).
(35) H. Koizumi, K. Yasuda, and H. Katayama, *Anal. Chem.*, **49**, 1106 (1977).
(36) S. Slavin, W. B. Barnett, and H. L. Kahu, *At. Absorp. Newslett.*, **11** (2), 37 (1972).
(37) B. V. L'vov, *Spectrochim. Acta*, **24B**, 53 (1969).
(38) M. S. Epstein and T. C. Rains, *Anal. Chem.*, **48**, 528 (1976).
(39) H. Koizumi and M. Katayama, unpublished work quoted in ref. *35*.
(40) Tj. Hollander and H. P. Broida, *J. Quant. Spectrosc. Radiat. Transfer*, **7**, 965 (1967).

Paper written while author was supported by the Office of Naval Research as a research assistant. Financial support provided by an American Chemical Society, Division of Analytical Chemistry Fellowship, sponsored by the Perkin-Elmer Corp.

Steven Brown is a graduate student in analytical chemistry at the University of Washington. His research interests include the application of lasers to optical and vibrational spectroscopy, new methods of data reduction, and electrochemical methods for trace metal speciation.

TGA EASY AS A-B-C-D

Your thermogravimetric analyses hit a new level of simplicity and precision with the Perkin-Elmer TGS-2.

(A) **The analyzer unit** combines a thermobalance with a patented internal microfurnace that heats and cools as fast as 320°C/min. It controls isothermal temperature to a few tenths of a degree. Equilibration times are less than a minute.

(B) **The recording microbalance** has ultimate sensitivity of 0.1 μg and a 5-gram capacity. Its calibrated weight supression control has three full-scale ranges of 10, 100, and 1000 mg, so that almost any sample weight or fractional weight can be displayed as full scale on the recorder.

(C) **The heater control** simplifies temperature calibration—its range and zero controls are calibrated directly in degrees C.

And (D) **the first derivative computer** accessory provides 42 full-scale sensitivities precalibrated directly in mg/min.

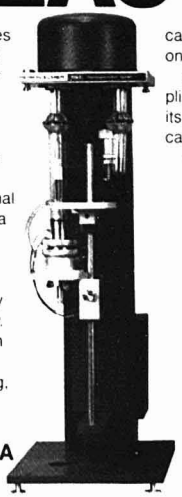

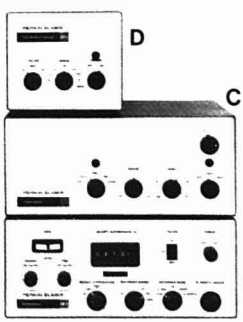

Finally, we made this analyzer part of a modular system for complete thermal analysis, including the Differential Scanning Calorimeter and thermomechanical analyzers, so you can get just what you need for the performance you want. Learn about all the features of this up-to-the-minute thermogravimetric analyzer from Perkin-Elmer, leader in instrumentation for materials research and quality control. Write Perkin-Elmer Corp., Main Ave., Norwalk, CT 06856. Or phone (203) 762-6915.

PERKIN-ELMER

CIRCLE 182 ON READER SERVICE CARD

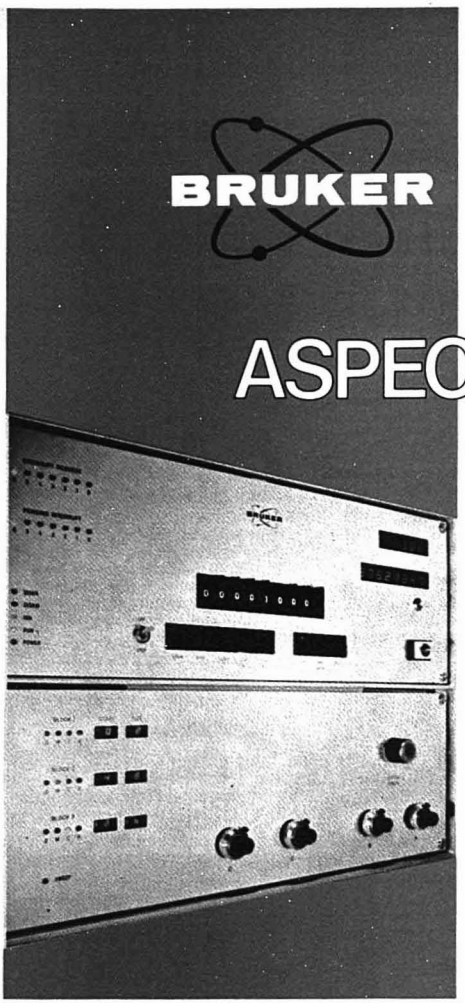

The ASPECT 2000 is a complete data acquisition and processing system which can be used efficiently wherever the time dependence of physical observables must be stored and analyzed. It is a high performance minicomputer with dual-input A/D converter, D/A converters and numerous interfaces. Together with its comprehensive software, the ASPECT 2000 offers unmatched capabilities for data-collection, calculation, analysis and output.

- 24-bit word length
- Fast A/D converter: 250 KHz @ 12-bits
- 2 programmable real-time clocks
- 2 direct-memory-access channels
- 3 arithmetic registers
- 4 index registers for addressing
- 7 vectored interrupt levels
- Fast MOS solid-state memory capacity of up to 80 K
- Hardware multiply-divide
- ROM binary tape loader and disk bootstrap

The ASPECT 2000 is included as the superior data system in all Bruker high resolution NMR, pulsed NMR, EPR and FT/Infrared spectrometers.

Also available for your special data acquisition-processing needs.

Call or Write for Details or a Demonstration

BRUKER INSTRUMENTS, INC.

Manning Park
Billerica, Mass. 01821
Phone (617) 272-9250

539 Beall Avenue
Rockville, Maryland 20850
Phone (301) 762-4440

1801 Page Mill Rd., Suite 212
Palo Alto, Calif. 94304
Phone (415) 493-3173

2410 Dunwin Drive, Unit 4
Mississauga, Ontario, Canada, L5L 1J9
Phone (416) 625-2374

CIRCLE 20 ON READER SERVICE CARD

analytical chemistry

Editor: **Herbert A. Laitinen**

EDITORIAL HEADQUARTERS
1155 Sixteenth St., N.W.
Washington, D.C. 20036
Phone: 202-872-4570 Teletype: 710-8220151

Managing Editor: Josephine M. Petruzzi
Associate Editor: Andrew A. Husovsky
Associate Editor, Easton: Elizabeth R. Rufe
Assistant Editors: Barbara Cassatt, Nancy J. Oddenino, Deborah C. Stewart
Production Manager: Leroy L. Corcoran
Art Director: John V. Sinnett
Designer: Alan Kahan
Artist: Diane Reich

Advisory Board: Donald H. Anderson, Richard P. Buck, Velmer Fassel, David Firestone, Robert A. Hofstader, Marjorie G. Horning, Philip F. Kane, Barry L. Karger, J. Jack Kirkland, Lynn L. Lewis, Harry B. Mark, Jr., Walter C. McCrone, Harry L. Pardue, Eugene A. Sawicki, W. D. Shults

Instrumentation Advisory Panel: Gary D. Christian, Nathan Gochman, Robert W. Hannah, Gary Horlick, Peter J. Kissinger, James N. Little, Sidney L. Phillips, R. K. Skogerboe, Donald E. Smith

Contributing Editor: Claude A. Lucchesi
Department of Chemistry, Northwestern University, Evanston, Ill. 60201

Published by the
AMERICAN CHEMICAL SOCIETY
1155 16th Street, N.W.
Washington, D.C. 20036

Books and Journals Division
Director: D. H. Michael Bowen
Editorial: Charles R. Bertsch
Magazine and Production: Bacil Guiley
Research and Development: Seldon W. Terrant
Circulation Development: Marion Gurfein

Manuscript requirements are published in the April 1977 issue, page 686. Manuscripts for publication (4 copies) should be submitted to ANALYTICAL CHEMISTRY at the ACS Washington address.

The American Chemical Society and its editors assume no responsibility for the statements and opinions advanced by contributors. Views expressed in the editorials are those of the editors and do not necessarily represent the official position of the American Chemical Society.

The Analytical Division Fellowship Program

Over ten years have passed since the last editorial mention of the ACS Analytical Division fellowships [*Anal. Chem.*, **39**, 697 (1967)]. It is not entirely coincidental that the program was initiated in 1966, the same year that the editorship changed hands.

From a modest beginning of two summer fellowships in the first year, the program has grown to three full-year and seven summer fellowships in 1977. It is particularly gratifying that industrial sponsorship has been gradually strengthened, because one of the initial objectives of the program was to replace the Merck Analytical Fellowships which were awarded on a nationally competitive basis from 1949 to 1957.

The Fellowship Committee of the Division, which consists of industrial as well as academic scientists, is charged with the responsibility of receiving applications and judging their merit. Although an impressive group of applications is received each year, more students should be encouraged to apply, and to re-apply if still eligible and unsuccessful in the first attempt. For details, see page 1223A, this issue. This is particularly true because of the prospects of increasing available funds from industrial sponsors as well as through the sale of the book "A History of Analytical Chemistry" which was recently published by the Division.

Although the benefits of the fellowship program to the profession and the student recipients are apparent, the benefits to industrial sponsors should also be emphasized. Each recipient of a full-year fellowship is required to visit the firm that sponsored the fellowship. There is no commitment on the part of donor or recipient to future employment, but the visitations have in fact led to such a result.

The Analytical Division is the only ACS Division sponsoring fellowships on a national scale, and it can be proud of an outstandingly successful program.

Quantitative Analysis of Mixtures by Carbon-13 Nuclear Magnetic Resonance Spectrometry

Thomas H. Mareci[1] and Katherine Násfay Scott

Veterans Administration Hospital, and Department of Radiology, University of Florida, Gainesville, Florida 32610

Results for quantitative analysis of mixtures by carbon-13 magnetic resonance, without nuclear Overhauser enhancement suppression, are presented. Two systems which are not simple isomeric mixtures are considered. Mixtures of two steroids, 3β-acetoxy- and 3β-chlorocholesterol, and mixtures of two aromatic acids, 3,4-dihydroxyphenylpropionic and 3,4-dimethoxyphenylacetic acid, were quantified in varying concentrations from 2 to 98 mol% with an average RMS error of 1.6%. Spin-lattice relaxation times, effective transverse relaxation times, and nuclear Overhauser enhancements for these systems were determined. Based on these values, criteria were developed for the selection of resonances to be compared to yield accurate results.

With the advent of commercially available Fourier transform nuclear magnetic resonance, carbon-13 spectroscopy has become a practical tool in many laboratories. However, carbon-13 magnetic resonance (CMR) has several inherent problems that make quantitation difficult. The low natural abundance of carbon-13 nuclei and low sensitivity to observation relative to protons require signal averaging for observation. The length of the carbon relaxation times (0.1 to 100 s) increases the time required for observation, because it is necessary to allow the carbon spin system to recover between sampling pulses to avoid saturating the system. Hence, a delay is usually inserted after the acquisition of data and before the next sampling pulse. Thus for samples with moderate to low concentration, the time required to obtain adequate signal to noise may be many hours. The proton decoupled carbon-13 spectrum provides the simplicity which makes CMR such a useful tool but introduces an additional intensity variation due to the nuclear Overhauser enhancement (NOE). Since the amount of enhancement is dependent on the dipole relaxation of the carbon spin through carbon–hydrogen coupling, carbons which are not directly bonded to hydrogen and far removed from any surrounding hydrogens will have little or no enhancement. Thus the variation in observed carbon resonance intensities due to NOE can be as great as a factor of 2.988.

Two methods have been used to suppress NOE, yet these methods introduce additional problems. The first method involves gating the proton decoupler such that it is on only during data acquisition, collapsing the spin multiplets, and suppressing the Overhauser enhancement. This pulse technique requires a delay between data acquisition and the next sampling pulse. The delay required can vary from 5 to 10 times the spin lattice relaxation times for the observed carbon resonances (*1*). This technique reduces signal to noise because of the suppression of NOE and lengthens experimental time by the amount of the additional delay required; therefore when sample size or concentration problems require extensive signal averaging, the experimental time can become extremely long, thus prohibiting the use of this method.

[1]Address correspondence to the Department of Radiology, University of Florida.

Secondly, NOE can be suppressed by the addition of paramagnetic materials to the sample solution. These paramagnetic species provide an additional mechanism for spin–lattice relaxation which, at the proper concentration of paramagnetic species, will predominate over dipole–dipole relaxation between ^{13}C–^{1}H and thus no NOE will be observed. However, use of paramagnetic species presents several problems (*2*). When the dipole–dipole interaction is efficient enough to relax the carbons quickly ($\gtrsim 0.3$ s), it will be impossible to suppress NOE effectively with relaxation agents without introducing considerable line broadening. This situation occurs with steroids in moderately concentrated solutions because the dipole–dipole interaction dominates relaxation and rotational motion is such that relaxation times are very short (~ 0.3 s). Also the reagent can complex with particular substrate functional groups (e.g., OH, NH_2), thus preferentially suppressing some NOE's over others. Both of the above techniques of NOE suppression reduce signal to noise and the gated decoupler method greatly increases experimental time. The reduced spin–lattice relaxation by the addition of paramagnetic materials shortens experimental time; yet when the sample is to be recovered after analysis, the paramagnetic species must be separated from the sample. From the above considerations, it is apparent that both techniques for NOE suppression must be used with careful consideration, and in some cases neither technique would produce useful quantitative results.

O'Neill and Pringuer (*3*) have found they could quantify a mixture of toluene diisocynate isomers by comparing the resonances of the methyl carbons of each isomer without suppressing the NOE. Thus the problems inherent to the techniques for NOE suppression can be avoided. However, they assumed the relaxation times and NOE's to be very similar. Hence, this technique is difficult to generalize to other isomeric mixtures or to mixtures of compounds which are not simply related through isomerism.

To determine the conditions necessary for accurate results of quantifying mixtures by CMR, mixtures for two types of systems were prepared at known concentrations. Neither technique for NOE suppression was employed; therefore NOE measurements were carried out and the results considered to determine the validity of assumptions made from knowledge of molecular structure. Since the quantity of sample available in our work is limited, we measured spin–lattice relaxation times to determine the most efficient pulse method for accurate results. The conditions of computer definition of resonances were considered and the most accurate means of quantitation determined.

EXPERIMENTAL

Materials. 3,4-Dimethoxyphenylacetic acid (98% pure), 3,4-dihydroxyphenylpropionic acid (98% pure), and 3β-acetoxycholesterol (97% pure) were obtained from Aldrich Chemical Company. 3β-Chlorocholesterol was prepared from cholesterol and thionyl chloride using the method of Winstein and Kosower (*4*). A white solid, mp 96–8 °C (lit. mp 96–7 °C), 86% yield resulted.

The aromatic acids, 3,4-dimethoxyphenylacetic acid and 3,4-dihydroxyphenylpropionic acid were combined in solution at

varying relative molar concentrations of 50%–50%, 30%–70%, 10%–90%, 5%–95%, and 2%–98% with 3,4-dihydroxyphenylpropionic acid the lesser component. The steroids, 3β-acetoxycholesterol and 3β-chlorocholesterol, were combined in solution at the same varying concentrations as the aromatic acids with 3β-acetoxycholesterol the lesser component.

Solutions of mixtures with a total molarity of 2.0 were made with a stock solution of deuteriochloroform which contained 5% (v/v) hexafluorobenzene as the field-frequency lock material and 10% (v/v) tetramethylsilane as a chemical shift reference. Spectra were obtained in 10-mm diameter sample tubes fitted with Teflon vortex plugs.

Instrumentation. A Bruker HX-90 spectrometer in the single coil configuration, equipped with a Nicolet 1083 computer, was used to obtain carbon-13 spectra at 22.628 MHz in the Fourier transform mode with complete carbon–hydrogen decoupling.

For the mixtures of aromatic acids, free induction decays (FID's) for a spectral width of 4000 Hz were collected in 8192 data points at a repetition rate of 60 s. A tip angle of 30° was used (90° tip angle corresponds to a pulse length of 21 μs). Signal averaging was performed for 1024 scans, requiring a total time of 17.1 h. Fourier analysis was performed on the accumulated FID giving a computer resolution of 0.98 Hz per data point. Line broadening was performed on each spectrum to give 4 to 5 computer data points above half maximum intensity for each resonance line. For the mixture of steroids, FID's for a spectral width of 5000 Hz were collected in 8192 data points at a repetition rate of 5 s. A tip angle of 40° was used and signal averaging was performed for 16 384 scans, requiring a total time of 22.8 h for all the mixtures except 2%–98%. A total of 32 768 scans were accumulated for the 2%–98% mixture, requiring 45.6 h. Fourier analysis gave a computer resolution of 1.22 Hz per data point. Line broadening was also performed to give the same 4 to 5 computer data points above half maximum intensity as was used as a criterion for linewidths for the aromatic acids.

Spectrometer stability was determined by accumulating 10 spectra of 1024 scans each over a 14-h period. The standard deviation of the resonance intensity determination varied from 1.8 to 3.1% with an average deviation of 2.5%.

Quantitation. To quantify the concentration of each mixture, comparisons were made between four resonances from each molecule. The resultant percentages were averaged and the standard deviation of the four percentages was calculated.

Relaxation Time Measurements. Longitudinal relaxation times, T_1's, were measured using the inversion–recovery technique (5) and calculated by a least square curve fit to the log of intensity ratios as a function of τ values. Effective transverse relaxation times, T_2^*'s, were determined from line widths. The line broadened spectra were measured, then the line broadening parameter subtracted to give natural line widths.

Nuclear Overhauser Enhancement Measurements. NOE's were determined for each carbon resonance under consideration. Gated decoupling suppresses NOE (6) and the ratio of the peak areas with and without NOE suppression can be used to determine the enhancement factor. The peak area for carbon resonances completely decoupled from hydrogen by continuous broad-band decoupling was compared with the peak area for the same carbon resonance decoupled from hydrogen by gated decoupling of a single hydrogen resonance during the time of the sampling pulse and data acquisition. Gated single frequency decoupling was used because gated broad-band decoupling over a modulation sweep width necessary to cover the hydrogen spectrum did not provide complete decoupling. The modulation rate of our broad-band decoupler is 10 c/s, and during the gated decoupling sequence the decoupler is on for only 1.0 s. Hence, the decoupling rate is insufficient to cover the necessary hydrogen sweep width of 400 Hz. Incomplete decoupling reduces the observed peak area by an amount proportional to the amount of residual coupling. Therefore, gated broad-band decoupling will introduce an error into the value of the observed NOE. Using the gated single frequency method, the error in our NOE measurements was determined to be ±0.3 or approximately 10%.

RESULTS AND DISCUSSION

Pulse Technique, Relaxation Times, and NOE. In order to obtain quantitative results for pulsed Fourier transform nuclear magnetic resonance, several factors must be considered. First, the strength and duration of the excitation pulse must be optimized to provide sufficient frequency range to cover the observed spectrum. Secondly, the pulse strength and repetition rate of the pulse sequence must also be optimized to provide efficient excitation of the spin system without the introduction of phase or intensity anomalies. Finally, careful consideration must be given to NOE which can vary from carbon to carbon within a given spin system.

Consider the usual case of the spin system in a stationary magnetic field of strength, H_0, subjected to a sequence of rectangular rf pulses oriented perpendicular to H_0 with frequency ω, magnetic field strength $2H_1$, duration τ, and period T.

By examining the frequency spectrum of the rf pulse obtained by Fourier transformation (7), the condition for a deviation of less than 2% in applied rf power across an observed frequency range of 5000 Hz requires the pulse length, τ, to be less than 25 μs. To minimize the pulse length, the output voltage of the rf amplifier should be increased with the practical limitation that the waveform retain a rectangular shape. This limit is approximately 4 μs for our system.

To optimize the pulse parameters H_1 and τ, consider the spin system in a frame of reference rotating about H_0 with angular frequency, $-\omega$. For the duration, τ, of the pulse, the spins precess about an effective magnetic field of strength, H_{eff}. The steady-state response of the spin magnetization to a sequence of rf pulses is obtained in the Block formalism (8) and two cases of H_1 field strength have been treated previously.

Ernst and Anderson (7) examined the situation where H_1 is very large, thus $H_{eff} \simeq H_1$, and the spins precess about H_1 with precession or "tip" angle, α, given by

$$\alpha = \gamma H_1 \tau \tag{1}$$

They optimized H_1 and τ by determining the optimum α for maximum observed magnetization in the plane perpendicular to H_0. This value is dependent on the time between pulses, T, and the longitudinal and transverse relaxation times, T_1 and T_2^*, respectively. By averaging over the precession angle of the spin about the stationary field in the rotating frame, they determined the optimum value of the tip angle to be given by the condition

$$\cos \alpha_{opt} = E_1 \tag{2}$$

provided $T >> T_2^*$, such that $(E_2^*)^2 << 1$. The terms E_1 and E_2^* are abbreviations for the exponential factors $\exp(-T/T_1)$ and $\exp(-T/T_2^*)$, respectively.

Jones and Sternlicht (9) considered the more general case of spin precession about the effective field, H_{eff}, with the tip angle, δ, given by

$$\delta = \gamma H_{eff} \tau = \gamma H_1 \tau \sec \beta \tag{3}$$

where β is the angle between the effective field, H_{eff}, and the rf field, H_1, and is dependent on the offset, $(\omega_0 - \omega)$, of the pulse frequency from the spin resonance frequency. They determined the optimum tip angle for this situation to be given by the condition

$$\cos \delta_{opt} = \begin{cases} E_1 \sec^2 \beta - \tan^2 \beta \\ \quad \text{For } |\beta| \leq {}^1/_2 \arccos(-E_1) \\ -1 \\ \quad \text{For } {}^1/_2 \arccos(-E_1) \leq |\beta| < \dfrac{\pi}{2} \end{cases} \tag{4}$$

provided $T >> T_2^*$, such that $E_2^* << 1$. Note that when $\beta \to 0$, this reduces to the above result, Equation 2, of Ernst and Anderson.

Jones and Sternlicht have also shown that for a given field strength, H_1, spins with equivalent T_1's will have the same optimum τ values to within 5% for β between 0° and 30°. Therefore, relative intensities will be insensitive to β for $\beta \leq 30°$.

The above considerations indicate that the rf field strength, H_1, should be maximized, then the pulse length, τ, adjusted to fulfill the optimum tip angle condition for efficient excitation of the spin system. In the case of adequate rf field strength, $\beta < 30°$, the condition of Equation 2 for optimum tip angle can be assumed to hold and can be applied to the spin system under consideration. For the offsets used in our experiments and the output parameters of our spectrometer, β had a maximum value between 18° and 30°, therefore, Equation 2 could be applied.

Maximum signal to noise in a given experimental time is achieved by increasing the pulse repetition rate. Several factors limit the repetition rate, hence the interval between pulses, T, used to determine the optimum tip angle. There is the obvious instrumental limitation that T must be long enough to allow sampling of the FID between pulses. However, phase and intensity anomalies can be introduced into the observed spectrum if T is not long enough to allow sufficient relaxation. Phase distortion can come from two sources. First, if transverse relaxation is not complete between pulses, phase distortion will be introduced into the observed spectrum (*10*). Second, if the observed FID has not decayed sufficiently at the end of the observation time, a phase distortion will be introduced in the Fourier transformed spectrum. We applied an exponential multiplication factor to the FID to introduce line broadening. This increases the decay rate in the observed spectrum; therefore, this source of phase distortion did not present a problem. The final consideration in the choice of the pulse interval, T, is to avoid intensity anomalies due to differences in T_1's. Intensity anomalies due to instrumental techniques can be introduced into the observed spectrum from two sources. The first is insufficient longitudinal relaxation between pulses. If the longest T_1 in the spin system is used in the condition for optimum tip angle, Equation 2, the intensity variation for all spins will be less than 5% if T is chosen to be three times the longest T_1 of the spin system. Hence, anomalies due to differences in T_1's will be minimized with this choice of T. If the resonances compared have very similar chemical shifts and relaxation times, T can be set equal to the minimum required for resolution, thus giving the maximum signal to noise per unit time. The resonances with the longest T_1's will be the most saturated but the comparison of resonances with similar T_1's will still produce quantitative results. Even with incomplete knowledge of relaxation times for a particular system, an estimate can be made of the longest T_1 and this can be used to determine pulse conditions. The second source of intensity anomalies is a possible frequency dependent attenuation of observed intensity due to filtering of the input signal at the computer analog to digital converter. The exact nature of this attenuation is dependent on the type of filters used and the choice of the frequency range filtered. Our computer uses low pass 4-pole Butterworth filters which attenuation −3 dB at the high end of the chosen frequency range. To avoid a frequency dependent attenuation across the observed frequency range, the input filter setting must be chosen greater than the observed frequency range. For a 5000-Hz sweep width, we chose a filter setting of 7500 Hz which gave the desired response across the frequency range without introducing additional noise.

Finally, relative intensity variations due to differences of NOE must be considered. The mechanism for the development of the NOE is dipole–dipole relaxation between the observed carbon-13 nucleus and neighboring hydrogen nuclei when the hydrogen nuclei are decoupled from the carbon-13 nuclei by saturation of the hydrogen resonances. When carbon-13 relaxation is dominated by the dipolar mechanisms, NOE attains its maximum value of 2.988. As the contribution from mechanisms other than dipole–dipole interaction becomes significant (*11*), the NOE is decreased with the limit that no NOE is observed when these mechanisms dominate relaxation. When neither the dipole–dipole interaction nor any other mechanism dominates the relaxation, care must be taken in comparing carbon resonance intensities for quantitation.

Table I. Spin–Lattice Relaxation Times, Effective Transverse Relaxation Times, and Nuclear Overhauser Enhancements for Selected Carbons of the Steroids

3β-Acetoxycholesterol

Carbons[a]	T_1, s	T_2*, s	NOE[c]
C_3	0.26 ± 0.20[b]	0.12	2.9
C_4	0.23 ± 0.13	0.080	2.9
C_5	2.75 ± 0.21	0.18	3.0

3β-Chlorocholesterol

Carbons[a]	T_1, s	T_2*, s	NOE[c]
C_2	0.27 ± 0.10[b]	0.099	2.5
C_3	0.33 ± 0.04	0.12	2.6
C_4	0.26 ± 0.10	0.086	2.4
C_5	2.70 ± 0.05	0.18	3.1

[a] Carbon numbering as in Figure 2. [b] Standard deviation. [c] Values accurate to ±0.3.

The dipolar contribution to relaxation rate (*12*) is dependent on the correlation time for the rotational motion of the carbon–hydrogen system and the distance from the carbon to the hydrogens. For molecules undergoing isotropic motion, the relative magnitude of the dipolar contribution for a particular carbon depends only on the number and distance of separation of the hydrogen nuclei that contribute to relaxation. For anisotropic molecular motion, the dipolar contribution also depends on the location of the carbon nucleus in the molecular structure.

For moderate to large size molecules, the dipolar mechanism is expected to dominate relaxation (*13*). Therefore, molecular systems, such as steroids, should exhibit full NOE for the backbone carbons where motion is approximately isotropic and the correlation times are such that spin rotation makes a negligible contribution (*12*). Table I shows the values of T_1, T_2*, and NOE for selected carbons in the steroids considered here. The values of T_1 for 3β-chlorocholesterol are very similar to those reported previously (*12*). Within experimental error, all the carbons considered attain the maximum value of NOE indicating that relaxation is dominated by the dipolar mechanism.

For small molecules, the dipolar mechanism may not dominate; therefore, care must be taken in resonance comparison. Table II contains T_1, T_2*, and NOE values for the carbons of the aromatic acids considered here. The large values of T_1 and small values of NOE for the substituted ring carbons indicate a small contribution from the dipolar mechanism and a significant contribution from other mechanisms, which reduce the observed NOE.

Therefore, for large molecules where the dipolar mechanism is expected to dominate or for small molecules where other mechanisms make a significant contribution, differences in observed NOE can be minimized by comparing carbons at similar locations in the molecular structures and with the same number and separation of hydrogen nuclei contributing to relaxation.

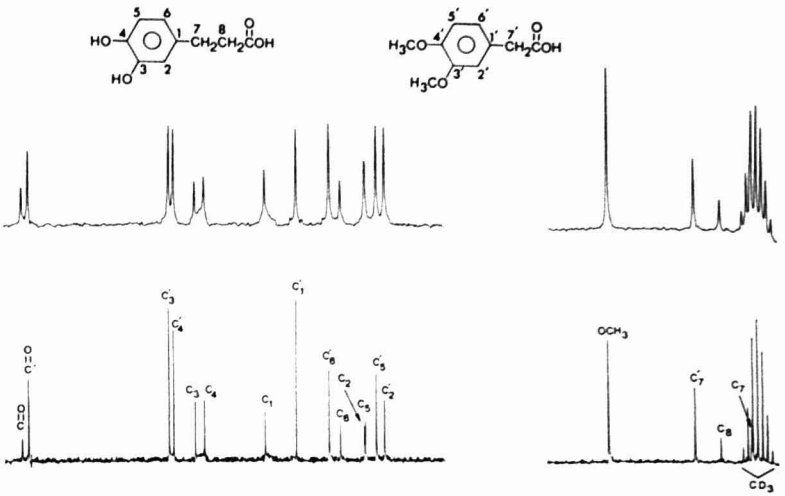

Figure 1. CMR spectra of 30% 3,4-dihydroxyphenylpropionic acid and 70% 3,4-dimethoxyphenylacetic acid. 1062 scans. Lower spectrum: without line broadening. Upper spectrum: exponential multiplication with 4.0-Hz line broadening. The CD_3 resonance of the solvent is shown at extreme right

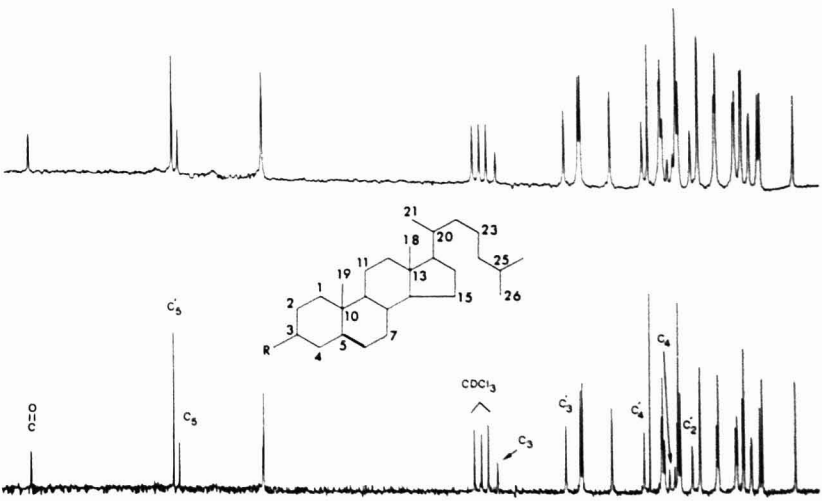

Figure 2. CMR spectra of 30% 3β-acetoxycholesterol (R = $OCOCH_3$) and 70% 3β-chlorocholesterol (R = Cl). Carbons of 3β-chlorocholesterol are designated by prime numbering. 11.5-K scans. Lower spectrum: without line broadening. Upper spectrum: exponential multiplication with 2.5-Hz line broadening

Quantitation. In order to evaluate CMR as a technique for quantitation of mixtures, we prepared mixtures of known component concentrations for two types of systems. The systems were chosen to provide a range of relaxation times and NOE's (see Tables I and II) and to relate to molecules of biological importance. The first type of system prepared was a mixture of the aromatic acids, 3,4-dihydroxyphenylpropionic acid and 3,4-dimethoxyphenylacetic acid. The substituent positions on the aromatic ring for the two acids are the same (see Figure 1) but the substituents are quite different. Comparisons were made between carbons 3 and 6 of the aromatic ring, between carbonyl carbons and between methylene carbon 8 adjacent to the carbonyl carbon of 3,4-dihydroxyphenylpropionic acid, and methylene carbon 7 adjacent to the carbonyl carbon of 3,4-dimethoxyphenylacetic acid. These aromatic acids model the catecholamine neurotransmitters and related metabolic compounds studied in our laboratory. The second type of system was a mixture of

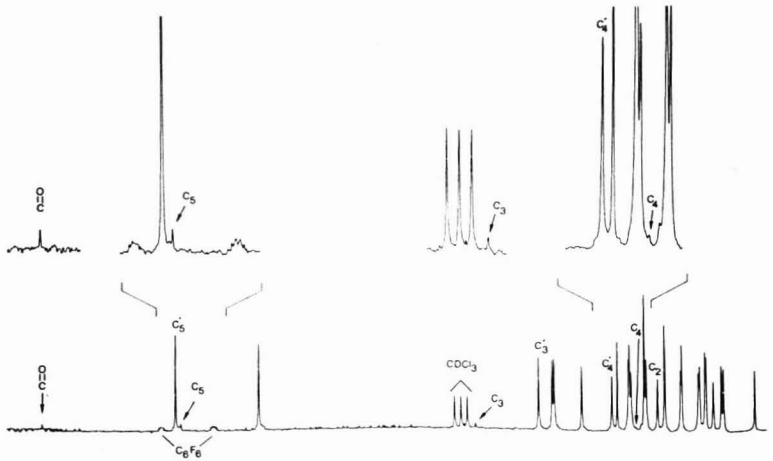

Figure 3. CMR spectrum of 5% 3β-acetoxycholesterol and 95% 3β-chlorocholesterol. 16-K scans, exponential multiplication with 2.5-Hz line broadening. Insets are shown at twofold horizontal expansion and fourfold vertical expansion

Table II. Spin–Lattice Relaxation Times, Effective Transverse Relaxation Times, and Nuclear Overhauser Enhancements for the Aromatic Acid Carbons

3,4-Dihydroxyphenylpropionic acid

Carbons[a]	T_1, s	T_2*, s[d]	NOE[e]
C=O	9.7 ± 0.15[c]	0.20	1.7
C_1	15.9 ± 0.15		2.0
C_2[b]	1.2 ± 0.02		2.7
C_3	11.2 ± 0.11	0.32	1.6
C_4	10.7 ± 0.05		1.2
C_5[b]	1.2 ± 0.02		2.7
C_6	1.2 ± 0.04	0.15	3.0
C_8	1.7 ± 0.28	0.19	3.0

3,4-Dimethoxyphenylacetic acid

Carbons[a]	T_1, s	T_2*, s[d]	NOE[e]
C'=O	8.2 ± 0.05[c]	0.27	1.6
C_1'	12.4 ± 0.04		2.3
C_2'	1.5 ± 0.03		2.4
C_3'	24.7 ± 0.02	0.24	1.9
C_4'	21.9 ± 0.04		2.0
C_5'	2.1 ± 0.14		2.6
C_6'	1.6 ± 0.03	0.16	3.1
C_7'	1.7 ± 0.27	0.14	2.5
$OC'H_3$	3.85 ± 0.35		

[a] Carbon numbering as in Figure 1. [b] Carbons with same chemical shift. [c] Standard deviation. [d] Values reported for carbons considered in quantitation. [e] Values accurate to ±0.3.

steroids, 3β-acetoxycholesterol and 3β-chlorocholesterol. They differ only in the functional group at the 3β position but gave a large enough chemical shift difference in the resonances adjacent to the 3β position (see Figure 2) to provide for comparison between nonequivalent carbon resonances at the 2, 3, 4, and 5 positions. This system provides a good model for our work on the radiopharmaceutical ^{131}I-19-iodocholest-5-en-3β-ol (*14*).

The carbon resonances compared for quantitation were chosen for similarity in molecular environment and sufficient chemical shift nonequivalence such that no distortion is caused by resonance overlap. Assignments were made using chemical shifts and coupling constants; then resonances of carbons at similar locations in molecular structure and the same number and separation of hydrogens were compared to quantify the component concentrations.

These criteria for choice of resonances for comparison do not limit the application of this method to simple isomeric mixtures. But they do require that compounds compared have the same general size and structure, such as the examples examined here. This is required to minimize the effect that differences in rotational motion would have on relaxation and, hence, the observed NOE. In the previous section it was pointed out that if dipole–dipole interactions dominate carbon-13 relaxation, then the observed NOE is independent of molecular motion and the number and separation of hydrogen nuclei surrounding the carbon-13 nucleus. However, if there is a contribution to relaxation from any mechanism other than dipole–dipole interaction, then there is also a dependence on the number and separation of hydrogens surrounding the carbon-13 nucleus. Therefore, it is necessary to compare carbon resonances which have the same number and separation of hydrogens to minimize possible differences in the dipolar contribution to NOE.

To quantify the component concentrations in a mixture, comparison can be made between relative peak heights or areas for a number of resonances, then the ratios averaged to determine the concentration of each component. These parameters can be determined in a number of ways. The peak heights and areas are generated as numerical results by our computer program (*15*). We found these results to depend critically on the signal to noise ratio and the baseline. Figures 2 and 3 exhibit a slight roll in the baseline which is perceived by the computer as additional noise causing inaccuracies in the results. The resonances of the 5% component in Figure 3 were not detected by the computer program; therefore no results were generated for these resonances. This is because the program was unable to distinguish these resonances from the background noise level. To obtain accurate results from our program, it would have been necessary to have a noise level approaching zero which is impractical with samples of limited concentrations. For peak height determinations, we relied on measurements of maximum peak height above average baseline from the plotted spectra. The minimum we could

detect was a height above average baseline equal to the peak to peak noise. Using this criterion, we were able to detect the 2% component in the 2%–98% mixture of steroids. But we could not detect the 2% component in the 2%–98% mixture of aromatic acids in a reasonable length of time (24 h) because of the length of the spin–lattice relaxation times of the nonprotonated carbons of the aromatic rings. The areas were determined by planimetry or measurement of integrated intensity from an integral subroutine in our computer program.

All of these methods of quantitation are critically dependent on the line shape for accurate results. An integral Fourier transform of the FID gives a spectrum which is a continuous function of frequency. The resulting line shape is equivalent to the slow passage continuous wave line shape if the value of $E_2^* << 1$ (*10*). However, the computer calculated Fourier transform of a FID defined by a discrete number of data points provides a spectrum which is a function of discrete frequencies. The definition of the resonance is determined by the number of data points used during the Fourier transform. Therefore, the resulting line shape is dependent on the memory block size used as well as the resonance line width.

Carbon-13 line widths can be quite narrow, for example the substituted ring carbons of the aromatic acids. These resonances have line widths of approximately 1.0 Hz which are defined by only 1 or 2 data points in a transformed spectrum of a 5000-Hz sweep width in 4096 data points. The resonance height and area will be distorted at this definition. This can be seen clearly by comparing the upper and lower spectra of Figure 1. Quantitation by comparing peak heights or areas at this definition will give inaccurate results.

The resonance definition can be improved in a number of ways. The number of data points used in the transformation can be increased by the technique of zerofill (*16*). This is limited to twice the initial block size, thus doubling the number of data points defining a resonance. Also the number of data points used to acquire the FID can be increased. This is limited only by the amount of memory available and the desired repetition rate. The final way of improving line-shape definition is the mathematical process of broadening a resonance by exponential multiplication of the FID before transformation.

A multiplication by an exponential function with a negative time constant broadens the resonances in the transformed spectrum, thus effectively improving definition. Since our system is limited to 8192 data points for observing the FID, it was necessary to exponentially weigh the observed FID to improve definition upon transformation. There are practical limits to the amount of line broadening applied. As line broadening increases, resolution decreases which can cause overlap of close lying resonances as can be seen in Figure 2. Here the resonance of carbon 4 is very close to the multiple resonances of the other methylene carbons of the steroid backbone. In the upper spectrum, line broadening has been applied which obscures the baseline around carbon 4. If too much line broadening is applied, the resonance would become distorted and the intensity would not be accurate. Also small resonances can be reduced in intensity such that they are not visible above the noise. We found the minimum definition for accurate results to be approximately 2 data points above half maximum intensity for area determination and 3 data points above half maximum intensity for peak height determination. We chose a definition of 4 to 5 data points above half maximum intensity as a criterion for broadening.

The results for quantitation by this procedure are shown in Table III and IV. Both systems were quantified by peak heights giving good agreement with the actual composition. If peak heights are to be used for quantitation, comparison must be made between resonances with similar T_1's, NOE's, and T_2^*'s. The values reported in Tables I and II for these systems vary over a wide range, yet the values for the resonances that were compared are very similar. The aromatic acid peak areas were determined by the integral subroutine and the steroid peak areas by planimetry, also giving good agreement with the actual composition. Quantitation by peak areas requires only that resonances with similar T_1's and NOE's be compared.

Table III. Results for Quantitation of Mixtures of 3,4-Dihydroxyphenylpropionic Acid and 3,4-Dimethoxyphenylacetic Acid

Composition[a]	Relative peak heights	Relative peak areas[b]
50% 50%	49.9 (±1.9) 50.1	50.1 (±1.2) 49.9
30% 70%	30.2 (±2.1) 69.8	31.0 (±2.2) 69.0
10% 90%	10.1 (±2.1) 89.9	9.7 (±1.5) 90.3
5% 95%	5.4 (±2.0) 94.6	4.8 (±2.7) 95.2
2% 98%	Not observed above noise level	

[a] Known compositions; 3,4-dihydroxyphenylpropionic acid listed first then 3,4-dimethoxyphenylacetic acid. [b] Peak areas as determined by the integral subroutine. Value in parentheses is the relative standard deviation.

Table IV. Results for Quantitation of Mixtures of 3β-Acetoxycholesterol and 3β-Chlorocholesterol

Composition[a]	Relative peak heights	Relative peak areas[b]
50% 50%	51.2 (±1.1) 48.2	48.3 (±3.7) 51.7
30% 70%	30.4 (±2.5) 69.6	27.1 (±1.5) 72.9
10% 90%	10.6 (±1.7) 89.4	7.7 (±0.8) 92.3
5% 95%	6.0 (±1.5) 94.0	5.6 (±2.0) 94.4
2% 98%	3.3 (±1.8) 96.7	1.6 (±0.2) 98.4

[a] Known compositions; 3β-acetoxycholesterol listed first then 3β-chlorocholesterol. [b] Peak areas as determined by planimetry. Value in parentheses is the relative standard deviation.

If resonances are compared with similar chemical shifts, T_1's and NOE's, the experimental time can be reduced even further by decreasing the delay between pulses. To test this, two experiments were performed on the 50%–50% mixture of steroids. In the first experiment, the delay was set equal to the longest T_1 in the system, 2.75 s. Quantitation by peak heights and areas both gave quantitative results. The values by peak heights are 50.5 (± 2.15), 49.5 (± 2.15) and by areas are 51.7 (± 3.74), 48.3 (± 3.74). In the second experiment, the delay was set equal to the minimum required for resolution, 0.8192 s. This also gave quantitative results. The values by peak heights are 50.9 (± 2.38), 49.1 (± 2.38) and by areas are 50.6 (± 4.28), 49.4 (± 4.28). The values in parentheses are the standard deviations of the measurement.

The resonances compared were chosen because they are similarly located in molecular structures of the same general size, and have the same number and separation of hydrogens.

This ensures similarity in relaxation rates and, hence, observed NOE. This allows the procedure to be applied not only to isomers but also to many systems where other methods would be impractical. In large systems, such as steroids, proton magnetic resonance can prove too complex to yield quantitative results; yet this is when CMR becomes most useful. For, in general, as the size of the molecule increases, the relaxation times decrease and the CMR experimental time decreases making it a practical analytic tool.

In summary, this method overcomes problems present in previous methods of quantitation by CMR which required either very long experimental times or sacrificing resolution. Our technique affords a method of quantifying mixtures which are not simply isomers in a reasonable length of time without expensive instrumentation or contamination of the sample by relaxation reagents.

LITERATURE CITED

(1) D. Canet, *J. Magn. Reson.*, **23**, 361–364 (1976).
(2) G. C. Levy and U. Edlund, *J. Am. Chem. Soc.*, **97**, 4482–4485 (1975).
(3) I. K. O'Neill and M. A. Pringuer, *Org. Magn. Res.*, **6**, 398–399 (1974).
(4) S. Winstein and E. M. Kosower, *J. Am. Chem. Soc.*, **81**, 4399–4408 (1959).
(5) R. L. Vold, J. A. Waugh, M. P. Klein, and D. E. Phelps, *J. Chem. Phys.*, **48**, 3831–3832 (1968).
(6) R. Freeman, H. D. W. Hill, and R. Kaptein, *J. Magn. Reson.*, **7**, 327–329 (1972).
(7) R. R. Ernst and W. A. Anderson, *Rev. Sci. Instrum.*, **37**, 93–102 (1966).
(8) F. Block, *Phys. Rev.*, **70**, 460–527 (1946).
(9) D. E. Jones and H. Sternlicht, *J. Magn. Reson.*, **6**, 167–182 (1972).
(10) R. Freeman and H. D. W. Hill, *J. Magn. Reson.*, **4**, 366–383 (1971).
(11) K. F. Kuhlmann, D. M. Grant, and R. K. Harris, *J. Chem. Phys.*, **52**, 3439–3448 (1970).
(12) A. Allerhand, D. Doddrell, and R. Komaroski, *J. Chem. Phys.*, **55**, 189–198 (1971).
(13) S. Berger, F. R. Kreissl, D. M. Grant, and J. D. Roberts, *J. Am. Chem. Soc.*, **97**, 1805–1808 (1975).
(14) M. W. Couch, K. N. Scott, T. H. Mareci, and C. M. Williams, *Steroids*, **27**, 451–458 (1976).
(15) J. W. Cooper, "An Introduction to Fourier Transform NMR and the Nicolet NIC-80 Data System", Nicolet Instrument Corp., Madison, Wis., 1974.
(16) T. C. Farrar and E. D. Becker, "Pulse and Fourier Transform NMR", Academic Press, New York, N.Y., 1971, p 75.

RECEIVED for review May 12, 1977. Accepted September 1, 1977. Financial support was provided by the Medical Research Service of the Veterans Administration.

Classification of Binary Carbon-13 Nuclear Magnetic Resonance Spectra

Charles L. Wilkins* and Thomas R. Brunner

Department of Chemistry, University of Nebraska—Lincoln, Lincoln, Nebraska 68588

A data base of 3782 binary coded proton noise-decoupled ^{13}C nuclear magnetic resonance spectra has been used to develop Bayes, Maximum Likelihood, and Simplex Learning machine classifiers for the computer-assisted interpretation of such spectra. Comparison of the results of applying these classifiers to prediction of presence or absence of 24 structural features using over 3400 test spectra revealed that the Bayes classifier yielded best classification performance. Both the ease of development of Bayes classifiers for new categories and the levels of categorization reliability obtained recommend this method as an attractive component of an on-line spectrum interpretation system.

In previous papers, investigations of a number of heuristic pattern recognition strategies for the computer-assisted interpretation of ^{13}C nuclear magnetic resonance spectra were reported (*1–5*). The impetus for this work was our belief that the sensitivity of ^{13}C chemical shifts to structure variation and the widespread availability of instrumentation for routine natural abundance ^{13}C spectral measurements made this structure elucidation technique an imperative target of pattern recognition research. One of the attractive features of empirical approaches to data interpretation is the lack of a need for complete theoretical understanding of the phenomena which produce them, prior to interpretation of the data. Indeed, the computational methods employed here and previously have the potential for highlighting unrecognized patterns in the data (hence, pattern recognition) and directing the investigator's attention toward relationships which may enhance theoretical understanding. Our most ambitious research efforts involved the use of a set of 1767 spectra which comprised the largest such data set yet to be used as a test of pattern recognition interpretation of carbon NMR data (*5*). Earlier work had relied, for training of categorizers, exclusively on a set of 500 spectra drawn from the Johnson and Jankowski collection (*6*) and was primarily devoted to studies of the merits of various data preprocessing techniques (*1–3*). In this paper, results made possible by the use of a new and larger carbon-13 NMR data base containing close to four thousand ^{13}C NMR spectra are reported. Two similarity measures, the maximum likelihood (*7, 8*) and a Bayes discriminant procedure (*9*), are compared in their performance with that of weight vectors derived using the simplex method (*5, 10*) for the detection of presence or absence of 24 structural features.

We have found that Bayes discriminant functions, based upon the a priori peak occurrence probabilities derived from a set of 3782 binary coded spectra, perform at a satisfactorily high level to make them usable as primary components of a structure interpretation system. The computational ease of developing such decision functions and their overall performance levels appear, at this time, to make this new approach an excellent method for computer-assisted NMR data interpretation. Previously, a simplex optimization training procedure (*10*) was used to develop classifiers and resultant prediction performance was compared with that found for linear learning machine classifiers. As a result of examining close to 2000 unknown spectra for prediction of three common structural properties, we concluded that the simplex method, when used with binary coded data, showed promise as a superior route to the requisite high-reliability classifiers desirable for an on-line interpretation system (*5*). Subsequently, a report of pattern recognition analysis of ^{13}C nuclear magnetic resonance spectra of a set of 43 norbornanes and another set of 12 polychlorinated diphenyl ethers has appeared (*11*). More recently, Munk and co-workers have completed a study of five different types of pattern classifiers for classification of nucleosides, carbohydrates, and steroids, using a data set of 2471 binary coded spectra drawn from the lit-

Table I. Structural Feature Frequency for 3782 ^{13}C Nuclear Magnetic Resonance Spectra

Feature	Number
Mono-substituted benzene	343
Any 6-membered carbon aromatic system	1152
Methoxy	385
Any COOH	374
R-ethyl	394
Any methyl	2506
Allylic carbon	368
Any carbon-carbon double bond	2147
Carbon α to a carbonyl	314
Any carbonyl	1353
Acetyl	295
Methylene alpha to hydroxy	251
HO—C—	541
C(=O)—C=	476
$H_2C-CH_2-CH_2$	752
$R_2C-C=$(R = any alkyl group)	550
Me—C=	564
Fused cyclic (aliphatic)	300
Tertiary butyl	216
Isopropyl	257
Ethyl	699
Cyclic carbon aromatic system	1239
Cyclic carbon and nitrogen aromatic system	359
Fused cyclic aromatic system	239
Any NMe_2	149
$H_2C-CH_2-C=O$	46
Any C ≡ N	96
$X-CH_2-CH_2$ (X = halogen)	89
Any C ≡ C	60
R—(−Cl)C=O	24
C(−X)—C(X = halogen)	70
C(−OH)—CH_2—CH_2	178
O=C—O—Me	98
HO—C=	144
$H_2N-C=$	157
H_2N-C-H	119
$O_2N-C=$	122
Cl—C=	148
Br—C=	56
I—C=	25
F—C=	71
MeO—C=	114
N≡C—C=	40
$H_2N-C-COOH$	148
Cyclic aromatic oxygen and carbon containing system	65
Cyclic aromatic sulfur and carbon containing system	56

erature (242 spectra) and the ^{13}C NMR data base (2229 spectra, see below), with very encouraging results (*12*).

EXPERIMENTAL

Data Base. As a data base for the present study, we have used a set of 4405 ^{13}C NMR spectra which have been compiled by the Environmental Protection Agency and are being placed in computer-readable form by us. In this research, 3782 of these spectra were coded in binary form (peak–no peak) using 256 1-ppm resolution elements. Chemical shifts were referenced to internal tetramethylsilane. Thus a "1" for an interval indicates the presence of a peak with a chemical shift in that range and a "0" indicates the absence of a peak. Figure 1 is a histogram of the peak occurrence frequencies over the range 0–220 ppm at 0.1-ppm resolution for the 3782 spectrum set. Table I contains information regarding structural feature frequency for the compounds whose spectra are included.

Computation Methods. Pattern classification using simplex pattern recognition (*5*, *10*) with initialization conditions determined by a preliminary linear learning machine analysis (*1*, *5*) was carried out using between 290 and 300 member training sets composed of equal numbers of class and non-class spectra. For simplex computations, the Fisher ratio feature selection method was used (*5*), selecting those features possessing the 128 largest Fisher ratios for each category. Alternately, features visually selected from histograms (vide infra) were used. Prediction performance was determined using most of the remaining 3482 spectra, in each case, as unknowns. For predictions, those spectra possessing no peaks in the resolution intervals represented in the weight vectors were excluded. This procedure resulted in a minimum of 3402 predictions and an average of 3435 predictions for the 24 structure questions involved. Maximum likelihood (*8*) and Bayes (*9*) classifiers were derived from the entire 3782 spectrum set. Classifier performance was evaluated by considering both the figure of merit (M) and a posteriori class membership probabilities (*13*).

RESULTS AND DISCUSSION

The most accurate and complete analysis of ^{13}C nuclear magnetic resonance spectra would result from a thorough and detailed theoretical study of the data. For a number of reasons, including the present lack of complete theoretical understanding of the problem, such a method is simply not practical as a routine means of interpreting spectra for structure analysis purposes. It is abundantly clear that, as Surprenant and Reilley have recently observed, "... The wide chemical shift range and narrow line width combine to yield what at first appears to be a limitless number of possible spectra ..." and that "... an unassisted human cannot consider effectively the enormous number of possibilities ..." (*14*). These facts strongly suggest that empirical computer-assisted analysis should be pursued. As a result, a number of such techniques have been the subject of recent investigation by both ourselves and others. These methods fall into the three broad categories of: parametric methods (which, in general, have relied on the development of linear additivity parameters) (*14–19*); heuristic methods (*1–4*, *20*); and the use of similarity measures (of which, we consider spectral search systems to be one example) (*12*, *14*, *21*). The present results bear on the relative efficacy of learning machine (heuristic) interpretation of spectra as opposed to use of empirical peak occurrence probabilities for structural characterization via either Bayes or maximum likelihood classifiers.

Spectra Representation. Before discussing the results, it is necessary to briefly consider how binary coded spectra are represented for computational purposes. As explained earlier, each spectrum is divided into a fixed number of resolution elements, each of which is assigned a binary value of "1" or "0", depending upon whether a peak is found within the resolution element. Thus, the spectra can be conveniently stored as either 256 bit binary numbers (because 256 resolution elements are used), with the bit position specifying the resolution elements, or as bit strings in vectors which can readily be used to form dot products with various weight vectors for categorization. For similarity comparison, identical spectra would be those with identical bit patterns (binary number representations). When these data are used with either a linear learning machine (*22*) or simplex pattern recognition (*10*) classifier, any particular spectrum may be viewed as a point in n-dimensional hyperspace, with the values of the binary digits in its 256 bit representation specifying the coordinates. A computational consequence of representing spectra in binary form is that only additions need be performed to obtain dot products, greatly reducing the computational time required for the prediction process.

Figure of Merit. For comparison of classifier performance, we have used the a posteriori classification probabilities and the figure of merit (*13*), or relative information gain, of the classifiers. The information gain $I(A, B)$ is the difference between the a priori uncertainty $H(A)$ regarding class membership and the residual uncertainty $H(A|B)$ following application of the clasifier. That is,

$$I(A,B) = H(A) - H(A|B) \quad (1)$$

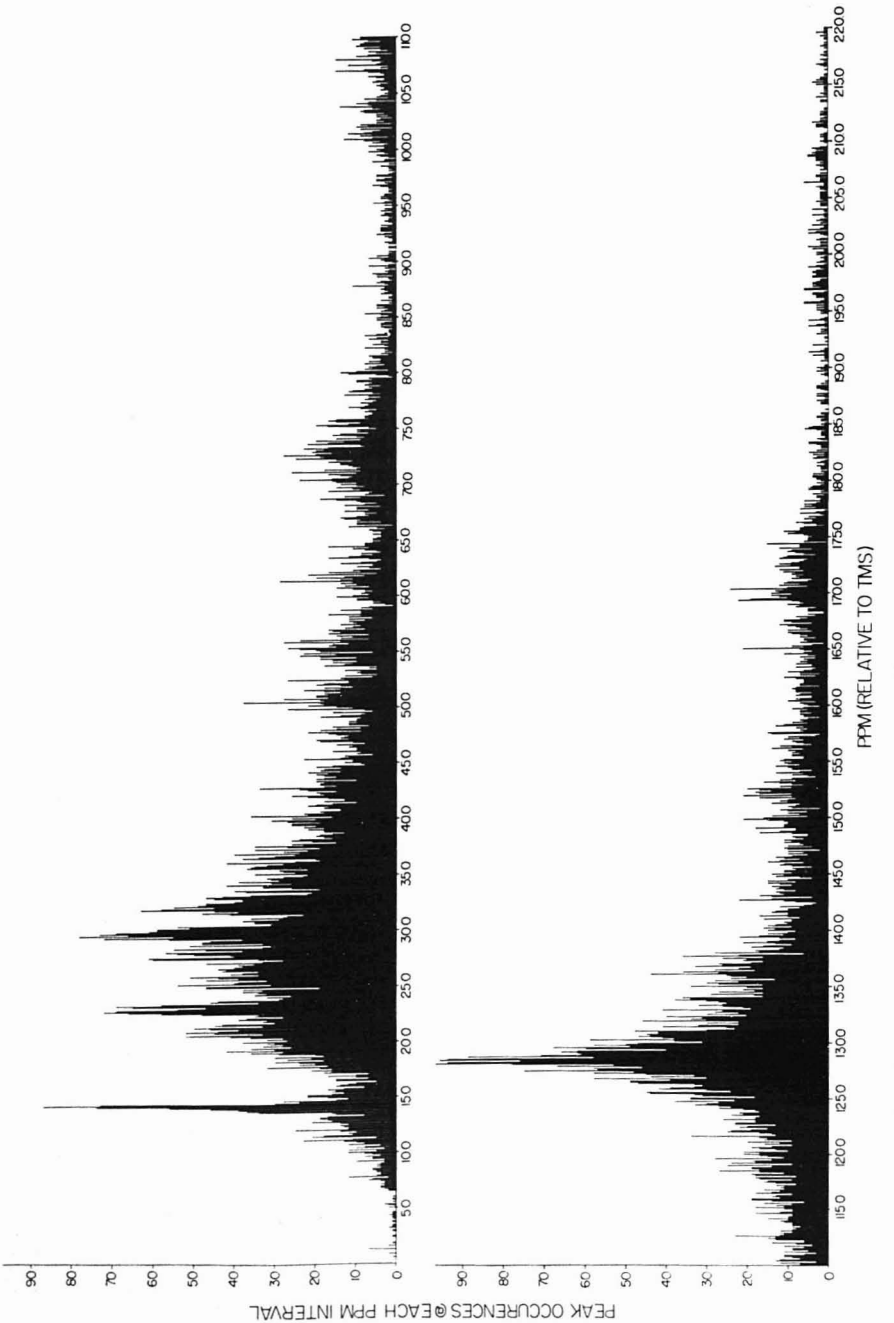

Figure 1. Histogram of ^{13}C NMR peak occurrence at 0.1-ppm resolution for 3782 proton noise-decoupled spectra

where, for the two class case,

$$H(\mathrm{A}) = -p(i)\log_2 p(i) - p(k)\log_2 p(k) \quad (2)$$

and

$$H(\mathrm{A}|\mathrm{B}) = -p(i|j)\log_2 p(i|j) - p(k|n)\log_2 p(k|n) \quad (3)$$

with j being prediction of class i and n prediction of class k.

Because the minimum *residual* uncertainty $H(\mathrm{A}|\mathrm{B})$ is zero bits, the maximum information gain $I(\mathrm{A},\mathrm{B})_{max}$ is

$$I(\mathrm{A},\mathrm{B})_{max} = H(\mathrm{A}) \quad (4)$$

The figure of merit, M, is defined as the ratio

$$M = I(\mathrm{A},\mathrm{B})/H(\mathrm{A}) \quad (5)$$

Simplex Pattern Recognition Predictions. As a result of our earlier work in which we applied the modified sequential simplex optimization procedure to the generation of weight vectors for the prediction of presence or absence of three common structural features, we concluded that the method showed promise for use in the elaboration of an on-line structure interpretation system for ^{13}C NMR spectra (*5*). In that study, the resulting classifiers were tested using approximately 2000 unknown spectra with each of the categorizers. For the questions examined, the simplex procedure (described in detail in Ref. 5 and 10) resulted in generally higher prediction performance than the linear learning machine classifiers, regardless of the number of spectral resolution elements included. Accordingly, at the outset of the present research, we used simplex pattern recognition to generate weight vectors for 24 structure feature categories, chosen both because of adequate representation of the categories in the data base (see Table I) and because of their possible utility in the on-line interpretation system we are developing. Initial results, using Fisher ratio feature selection, were discouraging; in general, the performance of the resulting classifiers was abysmal. This was clearly apparent from the low figures of merit (M) obtained (for 14 of the 24 classifiers, $M \leq 0.10$) and from consideration of the various prediction probabilities. It seemed possible that, with the larger number of both spectra and categorizers involved, the categories were simply inseparable at the level of spectral resolution we had chosen. With that in mind, we plotted histograms of peak occurrence, both for the entire data set (3782 spectra, Figure 1) and for a number of the class and non-class pairs (in these cases, the non-class was simply the entire set minus the class members). In order to make visual comparison easier, the histogram of the less populous member of each pair was normalized by multiplying it by the ratio of more populous to less populous class membership. When the histograms were examined, it did appear that visual selection of regions of non-overlap might improve performance. This was done for several of the categorization questions and the resulting improvement achieved made it clear that a major source of the poor performance initially observed was the particular method of feature selection used. Although this observation was informative, we sought a method of categorizer development which was relatively automatic, reproducible, and which would make the best use of the information available. Visual comparison of histograms is certainly useful for qualitative comparisons which can be helpful to the spectroscopist in spectral interpretation or in deciding whether a highly accurate categorizer might be possible to develop. On the other hand, this approach cannot, by its nature, be either automatic or reproducible, relying as it does on subjective judgment. We therefore decided to examine maximum likelihood classification (*8*) and a binary Bayes classifier method (*9*). Both of these make use of peak presence and absence probabilities to develop categorizers and are, in essence, similarity measures.

Maximum Likelihood and Bayes Classifiers. Because the size and composition of the present spectral data seem sufficiently large and representative of actual ^{13}C spectra which might be the subject of application of the on-line interpretation system, it was considered worthwhile to use the statistics of these data as a first approximation to actual peak occurrence statistics. Whenever such statistics are known, or can be estimated, then it becomes possible to employ Bayes classification procedures. This is advantageous because it can be shown that the chance of being wrong when a classification is made is then the *minimum* overall risk (called the Bayes risk) and is the best performance that can be achieved. Of course, for virtually all real-world problems, including the present one, the actual statistics can never be known, since that would require that all possible measurements had been performed. Thus, to the degree the data are not representative and, hence, present inadequate statistical information, less than optimum classification performance will be achieved. Accordingly, the criteria for usefulness of such procedures must remain empirical. For the present, those criteria are assessments of performance of resulting classifiers based on the use of a large well-characterized test set.

Both the maximum likelihood and the Bayes classification methods examined in the present work rely on use of class conditional probabilities for both peak presence and absence to develop weight vectors which serve as predictors. Isenhour and co-workers have used the maximum likelihood procedure with some success in the interpretation of binary coded infrared spectra (*7, 8*) and, more recently, Munk and his students (*14*) applied the technique, with similar results, to ^{13}C NMR analysis. The maximum likelihood estimate $G_i(\mathbf{X})$, is a simple function of the probabilities for peak presence (R_i) and peak absence (Q_i) for the class i.

$$T_i = R_i Q_i = \prod_{j=1}^{256} p_{ji}^{x_j}(1 - p_{ji})^{1-x_j} \quad (6)$$

Taking the log of T_i and expanding, $G_i(\mathbf{X})$ is obtained:

$$G_i(\mathbf{X}) = \sum_{j=1}^{256} x_j \log\left[\frac{p_{ji}}{1 - p_{ji}}\right] + \sum_{j=1}^{256} \log(1 - p_{ji}) \quad (7)$$

Note that this function is linear in x_j and represents a discriminant function which is simply the dot product of the spectrum and a weight vector

$$G_i(\mathbf{X}) = \sum_{j=1}^{256} x_j w_{ji} + w_{0i} \quad (8)$$

where

$$x_j = 0 \text{ or } 1$$

$$w_{ji} = \log\left[\frac{p_{ji}}{1 - p_{ji}}\right] \quad (9)$$

$$w_{0i} = \sum_{j=1}^{256} \log(1 - p_{ji}) \quad (10)$$

For the chemistry applications cited, this method was used as a multicategory classifier, with the unknowns being assigned to that class for which $G_i(\mathbf{X})$ was a maximum. In our application, the maximum likelihood estimator has been used as a binary discriminant function, with unknowns being assigned to the category for which $G_i(\mathbf{X})$ is larger. This has been done by dividing the 3782 spectrum data set into class and non-class groups for each of the 24 structural features and developing weight vectors for each of the two groups in every case. This procedure is equivalent to examining the value of an alternate likelihood ratio discriminant for the two-class case where $G(\mathbf{X})$ is defined as

$$G(\mathbf{X}) = \log [G_i(\mathbf{X})/G_k(\mathbf{X})] \quad (11)$$

Here, the unknown is assigned to class i for $G(\mathbf{X}) > 0$ and class k otherwise. Neither of these discriminants considers directly the a priori class membership probabilities, but rather makes class assignments on the basis of closest similarity. For the Bayes classifier, the likelihood ratio is used directly in deriving the discriminant function. Thus, a likelihood ratio for the class (i) and non-class (k) spectra is defined as T_i/T_k.

$$\frac{P(x_i)}{P(x_k)} \prod_{j=1}^{256} \left[\frac{p_{ji}}{p_{jk}}\right]^{x_j} \left[\frac{1-p_{ji}}{1-p_{jk}}\right]^{1-x_j} \quad (12)$$

This gives the discriminant function

$$G(\mathbf{X}) = \sum_{j=1}^{256} x_j \log \left[\frac{p_{ji}}{p_{jk}}\right] + (1 - x_j) \log \left[\frac{1-p_{ji}}{1-p_{jk}}\right] + \log \frac{P(i)}{P(k)} \quad (13)$$

where $P(i)$ is the a priori probability of class membership and $P(k)$ is the a priori probability of non-class membership. This discriminant is also linear in x_j and can be written

$$G(\mathbf{X}) = \sum_{j=1}^{256} x_j w_j + w_0 \quad (14)$$

where

$$x_j = 0 \text{ or } 1$$

$$w_j = \log \frac{p_{ji}(1-p_{jk})}{p_{jk}(1-p_{ji})} \quad (15)$$

$$w_0 = \sum_{j=1}^{256} \log \left[\frac{1-p_{ji}}{1-p_{jk}}\right] + \log \frac{P(i)}{P(k)} \quad (16)$$

As before the function is simply the dot product of the spectrum and a weight vector. For $G > 0$ the unknown is assigned to class i, otherwise to the non-class, k.

For the two-class case, therefore, the Bayes discriminant simply adjusts the decision threshold in accord with the a priori class and non-class probabilities to maximize classifier performance. Both the maximum likelihood and Bayes classification methods are based on the certainly incorrect assumption of statistical independence of each peak probability from all others. As stated earlier, an assumption of sufficient sample statistics is also implicit in the methods. As a result, one's interpretation of results obtained with these classifiers must be tempered with the understanding that only empirical, and not theoretical, arguments must be made with regard to their meaning. In spite of the faulty assumptions forced upon us by the demands of mathematical tractibility, both classification procedures are encouragingly reliable in their recognition of both the presence and absence of structural features from examination of spectra. Table II summarizes the figure of merit values obtained for 24 structural features with two of the three classification procedures (maximum likelihood and Bayes). The values for these are reflective of *recognition* of the various features, since the statistics were derived from the entire 3782 spectrum data set which was then used to test performance. The simplex values, which in all cases were significantly lower, were the results of *predictions* for the ca. 3482 spectra not used in training the classifier in each case. Examination of this table shows that in all but one category (acetyl) the Bayes classifier performed as well (and often substantially better) than the other methods. In order to assess the possible usefulness of categorizers which are indicated by the figure of merit to be superior, it is helpful to consider the a posteriori probabilities $P(i|j)$ and $P(k|n)$ (i.e., given that a prediction of class (i) membership (j) or non-class (k) membership (n) has been made, what is the probability that prediction is correct?). Table III presents those data for

Table II. Figures of Merit for Recognition of Structural Features

Structural question	No. of class members	Figures of Merit: Maximum likelihood	Figures of Merit: Bayes
Mono-substituted benzene	343	0.24	0.27
Any 6-membered carbon aromatic	1152	0.46	0.49
Methoxy	385	0.19	0.26
Any COOH	374	0.12	0.25
R-ethyl	394	0.14	0.38
Any methyl	2506	0.13	0.14
Allylic carbon	368	0.06	0.09
Any carbon-carbon	2147	0.50	0.52
Carbon α to carbonyl	314	0.10	0.21
Any carbonyl	1353	0.22	0.38
Acetyl	295	0.19	0.15
Methylene α to hydroxyl	251	0.14	0.17
Alcohol	541	0.25	0.33
Conjugated carbonyl	476	0.15	0.26
$-(CH_2)_3-$	752	0.24	0.26
$R_1C-C=(R\equiv alkyl)$	550	0.07	0.07
Me—C=	564	0.12	0.15
Alicyclic	300	0.22	0.30
tert-Butyl	216	0.10	0.12
Isopropyl	257	0.03	0.10
Ethyl	699	0.18	0.25
Carbon aromatic	1239	0.42	0.45
Carbon and nitrogen aromatic	359	0.14	0.19
Fused carbon aromatic	239	0.17	0.31

Table III. A Posteriori Classification Probabilities[a]

Structural question	Maximum likelihood $P(i\|j)$	Maximum likelihood $P(k\|n)$	Bayes $P(i\|j)$	Bayes $P(k\|n)$
Mono-substituted benzene	24.2	98.8	47.2	96.4
Any 6-membered carbon aromatic	69.1	97.2	73.4	96.8
Methoxy	27.3	97.1	55.8	95.2
Any COOH	19.2	97.2	67.2	94.6
R-ethyl	20.8	97.5	61.0	96.9
Any methyl	84.6	52.9	82.4	58.7
Allylic carbon	18.3	94.7	37.4	93.1
Any carbon-carbon double bond	93.1	86.7	93.2	85.5
Carbon α to carbonyl	16.7	97.1	42.8	96.0
Any carbonyl	73.6	81.6	84.0	86.8
Acetyl	21.5	98.2	62.6	94.4
Methylene α to hydroxyl	14.8	98.6	36.4	96.3
Alcohol	41.3	96.2	69.1	94.1
Conjugated carbonyl	25.9	96.7	47.6	95.3
$-(CH_2)_3-$	44.9	95.2	54.9	92.9
$R_1C-C=(R\equiv alkyl)$	26.9	91.8	50.4	88.4
Me—C=	26.5	95.7	43.0	92.1
Alicyclic	29.0	97.5	57.2	96.6
tert-Butyl	11.5	98.4	52.2	95.7
Isopropyl	10.0	96.5	31.2	95.4
Ethyl	39.7	94.1	58.1	92.2
Carbon aromatic	70.7	95.4	73.8	95.0
Carbon and nitrogen aromatic	18.1	98.3	35.8	95.8
Fused carbon aromatic	13.8	99.3	36.6	98.3
Average	35.1	93.1	56.4	92.6

[a] All numbers are percent.

the maximum likelihood and Bayes classifiers.

When the data in Table III are considered, it is apparent that the Bayes classifier achieves far more balanced behavior than the maximum likelihood method. Non-class categorizations ($P(k|n)$) are made with approximately the same high reliability, averaging 92.6% and 93.9% correct, respectively. However, class categorizations are far more reliable for the Bayes method, averaging 56.4% correct, instead of 35.1%, which is the value for the other method. It is possible that class categorization reliability could be improved by using a higher spectral resolution encoding of the data (e.g., 0.1-ppm intervals, rather than 1 ppm) or by use of a feature selection preprocessing step. Our visual examination of class/non-class histogram pairs suggests that the level of performance attained may be near the maximum possible using linear discriminants. In any case, the present results strongly suggest that the Bayes classifier performs in precisely the manner most desirable for on-line interpretation system intended to help guide the spectroscopist in spectral interpretation. In the absence of the prediction of membership in a structural feature class, there is a high probability that the compound whose spectrum is examined does not possess that feature. On the other hand, when a structural classification is made, there is a reasonably high possibility that the compound may possess that structure. Thus, a system using such categorizers should be easily capable of directing the spectroscopist's attention toward those structural features most probably present and, at the same time, minimize the expenditure of time spent on less likely alternatives.

LITERATURE CITED

(1) C. L. Wilkins, R. C. Williams, T. R. Brunner, and P. J. McCombie, *J. Am. Chem. Soc.*, **96**, 4182 (1974).
(2) T. R. Brunner, R. C. Williams, C. L. Wilkins, and P. J. McCombie, *Anal. Chem.*, **46**, 1798 (1974).
(3) T. R. Brunner, C. L. Wilkins, R. C. Williams, and P. J. McCombie, *Anal. Chem.*, **47**, 662 (1975).
(4) C. L. Wilkins and T. L. Isenhour, *Anal. Chem.*, **47**, 1849 (1975).
(5) T. R. Brunner, C. L. Wilkins, T. F. Lam, L. J. Soltzberg, and S. L. Kaberline, *Anal. Chem.*, **48**, 1146 (1976).
(6) L. F. Johnson and W. C. Jankowski, "Carbon-13 NMR Spectra", Wiley, New York, N.Y., 1972.
(7) S. R. Lowry, H. B. Woodruff, G. L. Ritter, and T. L. Isenhour, *Anal. Chem.*, **47**, 1126 (1975).
(8) H. B. Woodruff, G. L. Ritter, S. R. Lowry, and T. L. Isenhour, *Appl. Spectrosc.*, **30**, 213 (1976).
(9) R. L. Duda and P. E. Hart, "Pattern Classification and Scene Analysis", Wiley-Interscience, New York, N.Y., 1973, pp 32–34.
(10) G. L. Ritter, S. R. Lowry, C. L. Wilkins, and T. L. Isenhour, *Anal. Chem.*, **47**, 1951 (1975).
(11) M. Sjostrom and U. Edlund, *J. Magn. Reson.*, **25**, 285 (1977).
(12) H. Woodruff, private communication; H. B. Woodruff, C. R. Snelling, Jr., C. A. Shelley, and M. M. Munk, manuscript submitted for publication.
(13) L. J. Soltzberg, C. L. Wilkins, S. L. Kaberline, T. F. Lam, and T. R. Brunner, *J. Am. Chem. Soc.*, **98**, 7139 (1976).
(14) H. L. Suprenant and C. N. Reilley, *Anal. Chem.*, **49**, 1134 (1977).
(15) D. M. Grant and E. G. Paul, *J. Am. Chem. Soc.*, **86**, 2984 (1964).
(16) G. B. Savitsky and K. Namikawa, *J. Am. Chem. Soc.*, **86**, 1956 (1964).
(17) L. P. Lindeman and J. Q. Adams, *Anal. Chem.*, **43**, 1245 (1971).
(18) J. E. Sarneski, H. L. Surprenant, F. K. Molen, and C. N. Reilley, *Anal. Chem.*, **47**, 2116 (1975).
(19) A. L. Burlingame, R. V. McPherson, and D. M. Wilson, *Proc. Natl. Acad. Sci. U.S.A.*, **70**, 3419 (1973).
(20) R. E. Carhart and C. Djerassi, *J. Chem. Soc., Perkin Trans. 2*, 1753 (1973).
(21) B. A. Jezl and D. L. Dalrymple, *Anal. Chem.*, **47**, 203 (1975).
(22) N. J. Nilsson, "Learning Machines", McGraw-Hill, New York, N.Y., 1965.

RECEIVED for review July 18, 1977. Accepted September 22, 1977. Support of this research by the National Science Foundation under Grants MPS-74-01249 and CHE-76-21295 is gratefully acknowledged. The computer-readable ^{13}C NMR data base is being compiled under United States Environmental Protection Agency Contract No. 68-01-3344 with the University of Nebraska—Lincoln.

Combined Retrieval System for Infrared, Mass, and Carbon-13 Nuclear Magnetic Resonance Spectra

Jure Zupan* and Matej Penca

Chemical Institute Boris Kidrič, Ljubljana, Yugoslavia

Dušan Hadži

Faculty of Natural Sciences and Technology, University of Ljubljana, Yugoslavia

Jože Marsel

Institute Josef Stefan, University of Ljubljana, Ljubljana, Yugoslavia

A combined retrieval system based on three different spectrometric data: infrared, mass, and ^{13}C NMR, as well as the corresponding data file structures are described. The identification of the compounds depends entirely upon their spectra. The retrieval system may be used either for searching all three types of spectra, two, or one only. The results of 300 test searches are presented and the accuracy, precision, performance, and similarity coefficients for all three search types are evaluated. The performances of infrared, mass, and ^{13}C NMR spectra searches are 0.77, 0.91, and 0.95, respectively. The similarity coefficients for compound pairs are calculated with an algorithm based on WLNs of both compounds.

The utility of several spectrometric methods for fast and reliable identification of chemical compounds has been vastly augmented by the use of computers in searching collections of spectral data. A number of search systems have been developed (*1–36*) and besides spectra they may retrieve other information such as fragments, molecular formula, chemical name, or the complete structure. Most of the search systems are designed for a single type of spectra or even for one sort of data base (*1–29*). The evaluation algorithms and also the experience show that though the reliability of searching may be quite high, it is never absolute. Very often the fault is in the quality of the data base, but the incompleteness of transforming the whole information contained in the original spectra into the coded form may also cause misses in the search. One possibility for improvement is to combine the searching for several types of spectra (*30–36*). This should be advantageous also in the development of methods that will allow ultimately the construction of the molecular structure

Table I. Record Structure and Data Available in the Present Data Bases of the COSMOSS System

		IR	MS	^{13}C NMR
No. of bits per feature	Position	240	540	240
	Intensity	120	180	120[b]
	Third feature	120	One word (60)	120
	Structure	420	420	420
	Identification No.	One word (60)	One word (60)	One word (60)
Total		960	1860	960
Structure description	WLN	Yes[a]	No	Yes
	Chemical name	Yes[a]	Yes	Yes
	Molecular formula	Yes[a]	Yes	Yes
Total number of records		92000	16000	1600

[a] For 2000 compounds only. [b] For 650 compounds only.

Table II. Classification of Intensity Values and Third Rated Features for Different Types of Spectra

		Third feature		
Code	Intensity, %	IR $(100\cdot\sigma)/\bar{x}$		^{13}C NMR multiplicity
000	less than 5.0	undefined		not known
001	5.0-16.9	less than 0.5	sharp	singlet
010	17.0-33.9	0.5-0.9	sharp	doublet
011	34.0-50.9	1.0-1.9	normal	triplet
100	51.0-67.9	2.0-4.9	normal	quartet or higher
101	68.0-84.9	5.0-6.9	normal	odd
110	85.0-99.9	7.0-10.0	broad	even
111	100.0	more than 10.0	broad	not detectable

starting with spectral data and possible auxiliary information.

In comparison with other combined systems dealing with different spectrometric data, our intentions in constructing a new one were: (1) it should work as a black box: using only the spectra as input data. No protocols should be needed to describe the problem. In this respect, this system clearly differs: from those of Gray (*35*) and Gribov (33), partially from Koptjug (*34*), but is related to those of Clerc (*30–32*) and Heller (*23,36*); (2) all data files should be uniform (*32*) so that no difficulties would arise adding new spectra collections; (3) the search strategy should be carried out in two parts: the first one is very fast and rather loose yielding roughly 1% of data on goodfile and the second, performed only on the goodfile, should sort the spectra using rating algorithms that are normally slower by an order of magnitude than the search algorithms.

As the result of these premises and on the basis of our previous work on the search systems (*8, 13, 15*), the system COSMOSS (COmbined Spectral and MOlecular Structure Search) was developed. At the moment three types of data files can be used simultaneously or separately, i.e., infrared, mass, and ^{13}C NMR. The system is, of course, at the moment far from perfect but with more practical experience we hope to improve the system.

DATA BASE

The recorded structure in the data files should be chosen so that it may be easily applied to different types of spectrometric information. In general terms, each spectrum can be regarded as a group of signals plotted in some kind of "energy" or "time" scale vs. absolute or relative intensity. Each peak or signal has, of course, some other properties relevant to the structure of the compound that could be stored and used for identification (e.g., half intensity width, asymmetry, shape, multiplicity, etc.) but the most important ones are certainly the position and intensity. Thus the guideline of our data base organization is to code the position and the intensity of each peak separately and to provide an additional place for the so-called "third feature" that might be useful for some special identification purposes.

The "energy" scale is divided for each type of spectra into the appropriate number of intervals, represented by bits initially set to zero and turned after to 1 if some peak occurs in the particular interval. This part of the record is called the position section. As shown in Table I the infrared, mass, and ^{13}C NMR full spectral ranges are coded with 240, 540, and 240 bits, respectively. The digitation step for mass and ^{13}C NMR spectrometric data is the same over the whole spectral range, i.e., 1 m/e and 1 ppm from 1–540 m/e and from 1–240 ppm, respectively, while for the infrared spectra this is not so. The digitation interval in the ASTM-WYANDOTTE collection (*37*) of infrared spectra is based on the mμ scale from 1.0–15.9 mμ. This description ceases to be adequate or efficient in the regions somewhere above 12.5 mμ or below 800 cm^{-1}. Most of the modern infrared spectrophotometers have the operating interval up to 50 mμ or 200 cm^{-1}, requiring the linear scaling in cm^{-1}. This transformation will cause the same kind of trouble in the other part of the spectrum, though smaller. Therefore we decided to form two digitation steps: the first is 33.3 cm^{-1} wide in the region 2000–4000 cm^{-1} and the second of 10 cm^{-1} in the region 200–2000 cm^{-1}, amounting together to 240 bits.

In the order of peaks in the position section, a three-bit place is provided for each one in the next, called intensity, section. Infrared and ^{13}C NMR spectra are assumed to have a maximum of 40 peaks (120 bits) while for mass spectra this limit is extended to 60 (180 bits). If the spectrum has more than the allowed number of peaks, those with the lowest intensity are rejected and only 40 or 60 are coded. The full intensity range is divided into eight intervals (Table II) each coded with three bits (000–111). The intensities in mass and ^{13}C NMR spectra are coded relatively to the highest peak, while the infrared spectra are coded in the transmission scale.

As mentioned before a special "third feature" for infrared and ^{13}C NMR spectra is chosen to be the relative half width of the peak and multiplicity, respectively.

The third part of the record provides a three-bit place for coding eight different values (000–111) of the third feature of each peak. For low resolution mass spectra where the peaks are very uniform, the molecular weight of the compound has been chosen as the third representative feature of the whole spectrum. This choice has another advantage: it enables one to organize the molecular weight search for mass spectra very easily.

The fourth part of the record contains the information about the structure of the compound and is thus called the information part. It has 420 bits which is sufficient for 70 hollerith characters of the 6-bit character set. The complete structure information should be composed from the Wiswesser line formula chemical notation (WLN) (*38*), chemical name (CN) and molecular formula (MF). Each item is separated from the preceding one by two blanks. If some part of the structure information is not available or not known, it is omitted. If the information is longer than 70 characters, the rest is cut off. However, with more than 75% of data which contain the full information, there is still some place left over. In this order the structural information is entered into the information section of the record. There is no doubt that WLN is the most valuable information since the complete structure, molecular formula, and molecular weight can be obtained straightforward. Unfortunately, with the exception of the ^{13}C NMR collection (*39*) and a small part of the infrared file (*40*), no other data have the complete WLN–CN–MF information.

The last 60-bit-long part ensures the relationship of the particular record information with the other information sources. Normally the corresponding catalog number is stored here.

The weakest point in the present data organization scheme are the 420-bit-long information parts in each file that occupy more than 35% of all space on drums or tapes. This immense waste of space carrying the same information three or more times (if further spectrometric data would be included) can be reduced by creating a new random access file containing only the structure and catalog number information. Thus the complete 420-bit-long information part in each file could be skipped and the relationship to the structure information should be provided via the last number in the record: the address of the beginning of the particular record in the random access file. Such a solution requires, of course, larger computer facilities with direct memory access routines that are not always available to the users. It is a very time consuming procedure to create such a file and get proper connectivity addresses to each record in the data files but, fortunately, this has to be done only once.

Finally, the data sources should be mentioned. The large majority of 92 000 IR spectra is based on the ASTM-WYANDOTTE collection (*37*), and only very few, about 2000 of them (*40*) have the full intensity, shape, and WLN–CN–MF information. In practice the search very seldom runs over the whole collection. For laboratory use, smaller files (polymers, surface active agents, etc.) were created for standard or special use. The most frequently used files are Sadtler (*41*) and DMS (*42*) collections, marked with CA and FA and containing about 35 000 and 13 000 spectra, respectively. For mass spectra, the Aldermaston collection (*43*) with about 16 000 spectra is used. It has the complete intensity information, chemical name and molecular formula, but lacks completely the WLN. According to some tests in our and other laboratories (*44*), the collection has many doubles and a surprisingly large amount of wrongly coded spectra. The smallest collection, but in all other respects the best, is the ^{13}C NMR data file containing, only about 1600 spectra. It has in a large part the complete intensity, multiplicity, and WLN–CN–MF information.

THE SYSTEM

The retrieval strategy of the search system COSMOSS is tightly bound to this data base structure. The complete process of one search is done in three clearly separated parts. First, the input data are read in the free format and the corresponding masks of peak positions and no peak regions are formed. Second, the search through the position part only of each record over the entire file is performed and the records that pass the logic .AND. operations with all masks are saved on a goodfile. Third, the rating algorithm sorts the spectra from the goodfile according to the discrepancies in the intensity, position, and presence or absence of each peak in comparison with the corresponding peaks in the input spectrum. After this sorting, the spectra with the five highest scores are output. It should be mentioned that the masks for the peak positions (with the exception of the mass spectra search) are set up in a way that allows finding the peak with the tolerance of ±1 digitation step.

Table III. Default Values and Range Limits for Different Spectrometries if Not Specified together with the Band Position

	IR	MS	^{13}C NMR
Units of band position	cm^{-1} mμ if specified	*m/e*	ppm
Range limits set when exceeded (message)	200–4000	1–540	1–240
Intensity	50%	10%	50%
Band shape	2% normal	...	...
Multiplicity	...	...	1 (singlet)
Obligate presence if not requested	never	if intensity is greater than 33%	always

The system COSMOSS is supposed to assist the analyst who has either infrared, mass, ^{13}C NMR, or any combination of these spectra to find out if the identical or very similar spectra were stored in the data files. We trust that the system is able to provide, using the rating algorithms, some valuable hints about the structure of the unknown compounds even if the requested spectra are not in the files.

As input, only the spectral data are requested. These data are input in the form of groups. Each group separated with slashes describes one peak or no peak region in the particular spectrum. The two very first groups are reserved for the search identification (IR, MS, or ^{13}C NMR) and heading. If some group of data is input incomplete, the default values are set on the place of the missing or incorrect one. The default values are collected in Table III.

After each search the rank or top list of the five (even if there are more of them on the goodfile) most probable compounds is issued. The rating criteria depends on the respective spectra. They are subject to our greatest concern and are being continously developed. The example output lists are shown in Figure 1. In one run, any number of spectra can be input.

TEST OF THE RETRIEVAL ABILITY

A test for the retrieval system should be made keeping in mind the fact that such a system is almost always used as a black box, and that it is only the best hit that counts. If for example the correct compound is retrieved and placed on the second position of the top list, this achievement is very good from the computational point of view but is of very limited value for the user, if the top rated compound is completely different from the correct one (*45*). This is the reason why the COSMOSS system outputs only the first five top rated compounds.

As a test, 300 spectra (100 for each spectrometry IR, MS, and ^{13}C NMR, respectively) were randomly chosen from the compounds whose spectra were known to be in the three data files, and coded by hand. The retrieval strategies and the rating algorithms which differ for each spectrometry were then checked, according to Erley's suggestions (*46*) for accuracy, precision, and performance. The results of the test are shown in Table IV. It can be readily seen that the performance gap

```
COMBINED SPECTRAL AND MOLECULAR SEARCH SYSTEM C O S M U S S
DEVELOPED BY THE SPECTROSCOPY GROUP AT K.I.B.K.. LJUBLJANA

IR/ TEST SEARCH  3-METHYL INDOLE /

INFRARED SPECTRAL SEARCH - INPUT DATA

   1   3448.  CM    50. INT.  M SHAPE   1. OBLIGATORY PEAK
   2   2941.  CM    50. INT.  M SHAPE   1. OBLIGATORY PEAK
   3  (2778. - 2000.)  NO PEAK REGION  -  CM-1
   4   1449.  CM    50. INT.  M SHAPE   1. OBLIGATORY PEAK
   5   1389.  CM    50. INT.  M SHAPE   0. OBLIGATORY PEAK
   6   1351.  CM    50. INT.  M SHAPE   0. OBLIGATORY PEAK
   7   1087.  CM    50. INT.  M SHAPE   1. OBLIGATORY PEAK
   8   1075.  CM    50. INT.  M SHAPE   1. OBLIGATORY PEAK
   9   1010.  CM    50. INT.  M SHAPE   1. OBLIGATORY PEAK
  10    971.  CM    50. INT.  W SHAPE   1. OBLIGATORY PEAK
  11    926.  CM    50. INT.  M SHAPE   1. OBLIGATORY PEAK
  12    880.  CM    50. INT.  M SHAPE   0. OBLIGATORY PEAK
  13    741.  CM    50. INT.  M SHAPE   1. OBLIGATORY PEAK

TOP LIST OF THE MOST PROBABLE COMPOUNDS

          PTC.     WLN-CN-MF INFORMATION

   1     66.67    CYCLODECANONE-1-, 6-HYDROXY-          1850FA
   2     54.55    PHOSPHONIUM, /2-PHENACYCLIDENE        1287+FA
   3     52.17    INDOLE, 3-METHYL-                     1232FA
   4     50.50    BICYCLO/2,2,1/HEPTANE ENDO-2-C        5475FA
   5     48.00    1+4-REN/OQUINONEIMINE, M-PHENY        10039FA

// RETRIEVAL TIME 10.391 SEC.

MS/ TEST SEARCH  3-METHYL INDOLE /

MASS SPECTRAL SEARCH - INPUT DATA

   1   (  1. -  35.)  NO PEAK REGION  -  M/E
   2     51. M/E  10. INT.    0. OBLIGATORY PEAK
   3     63. M/E  10. INT.    0. OBLIGATORY PEAK
   4     65. M/E  10. INT.    0. OBLIGATORY PEAK
   5     77. M/E  10. INT.    0. OBLIGATORY PEAK
   6   (  80. -  88.)  NO PEAK REGION  -  M/E
   7   (  90. - 100.)  NO PEAK REGION  -  M/E
   8    103. M/E  10. INT.    0. OBLIGATORY PEAK
   9   (105. - 125.)  NO PEAK REGION  -  M/E
  10    129. M/E  10. INT.    0. OBLIGATORY PEAK
  11    130. M/E 100. INT.    1. OBLIGATORY PEAK
  12    131. M/E  50. INT.    1. OBLIGATORY PEAK
  13   (140. - 540.)  NO PEAK REGION --  M/E

TOP LIST OF THE MOST PROBABLE COMPOUNDS

          PTC.     WLN-CN-MF INFORMATION

   1     79.67    3-METHYLINDOLE C9,H9,N              API 0627
   2     72.52    5-METHYL INDOLE  C9,H9,N            AST 1509
   3     72.27    6-METHYL INDOLE  C9,H9,N            AST 1508

// RETRIEVAL TIME 6.329 SEC.

CNMR/ TEST SEARCH  3-METHYL INDOLE /

C NMR SPECTRAL SEARCH - INPUT DATA

   1     9. PPM  50. INT.   0. MULT.  1. OBLIGATORY PEAK
   2   111. PPM  50. INT.   0. MULT.  1. OBLIGATORY PEAK
   3   119. PPM  50. INT.   0. MULT.  1. OBLIGATORY PEAK
   4   122. PPM  50. INT.   0. MULT.  1. OBLIGATORY PEAK
   5   128. PPM  50. INT.   0. MULT.  1. OBLIGATORY PEAK
   6   136. PPM  50. INT.   0. MULT.  1. OBLIGATORY PEAK

TOP LIST OF THE MOST PROBABLE COMPOUNDS

          PTC.     WLN-CN-MF INFORMATION

   1     79.16    T56 BMJ D  3-METHYLINDOLE  C9H9N1     942C

// RETRIEVAL TIME  1.306 SEC.
```

Figure 1. Output examples of all three search types. A low similarity between the input and retrieved spectra indicates either errors in the coding or that there is no counterpart of the input spectrum in the file

between the infrared and the other two types of spectra is very impressive. It is believed that there are two main sources of this large discrepancy:

The spectrum description (in digitized form) is for ^{13}C NMR and especially for MS spectra very clear and precise in comparison with those of infrared spectra. The position and

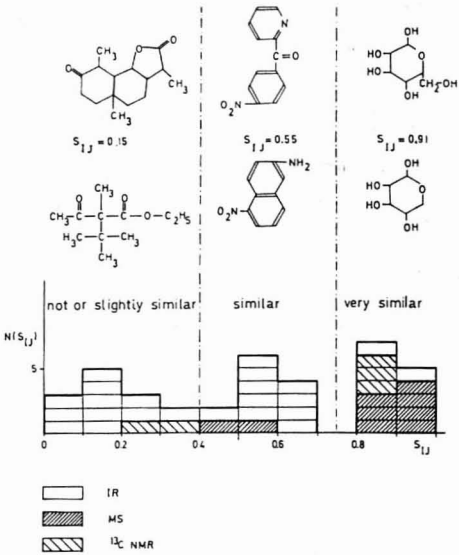

Figure 2. The similarity between the structures of the top rated and requested compounds for all unsuccessful searches. To get a visual impression of the meaning of the terms very similar, similar, and slightly similar, for each one an example with the corresponding similarity coefficient $s_{I,J}$ is drawn

peak shapes are for MS and ^{13}C NMR spectra much better fixed and sharp, thus the shifts in positions could be detected and classified very easily: either the spectrum is coded wrong or it does not belong to the requested compound. On the contrary, the peaks in the infrared spectra are normally much broader and hence the coding is much more difficult and subject to some arbitrariness (*40*).

The data collection for infrared spectra has besides the known shortcomings in intensity information, which make the rating algorithms rather inefficient, a relatively high number of completely miscoded spectra. The latter is true, though to a lower extent, for the Aldermaston collection as well. However, in the case of mass spectra, this shortcoming is balanced by the extensive intensity information.

In order to obtain for the user the more interesting information about the practical efficiency of the system, we have compared the structure of the top rated compounds of all unsuccessful searches with those of the requested ones. The comparison was made on the basis of the similarity coefficient calculated from both WLNs: the top and the requested compounds. The similarity coefficient $s_{I,J}$, between two structures I and J expressed with WLN(I) and WLN(J) is obtained from the following formula:

$$s_{I,J} = p_{I,J} - k_{I,J}d_{I,J} \qquad (1)$$

where $p_{I,J}$ is the percent of common elements and symbols and $d_{I,J}$ is the average displacement for all common symbols in both WLN(I) and WLN(J) notations, $k_{I,J}$ is the weight factor describing the influence of the displacement on the similarity coefficient. In the present calculation $k_{I,J}$ was taken to be 0.5 for comparing the acyclic parts of the notations and zero for others. The detailed explanation of the $s_{I,J}$ calculation can be found in (*47*). The distribution of the similarity coefficients calculated for all the unsuccessful searches is shown in Figure 2. It is apparent that a very easy distinction

Table IV. Test Results for 300 Searches

		IR	MS	^{13}C NMR
Number of test compounds (N_{tot})		100	100	100
Number of correct answers in the ith place of the top list $N(i)$	i			
	1	77	91	95
	2	3	2	2
	3	0	2	0
	4	1	1	0
	5	0	0	1
Total compounds found (NT)		81	96	98
Compounds not found (NF)		19	4	2
$A = NT/N_{tot}$	Accuracy	0.81	0.96	0.98
$P = 1/NT \sum_{i=1}^{5} N(i)/i$	Precision	0.97	0.97	0.98
$Q = A \cdot P$	Performance	0.79	0.93	0.96
$N(1)/N_{tot}$		0.77	0.91	0.95

between the satisfactory and unsatisfactory searches can be made on this basis. As expected from the reasoning in the preceding paragraph, the mass and ^{13}C NMR searches yield much better results if they fail to retrieve the correct spectrum than does the infrared search.

It should be stressed that neither the accuracy, precision, or performance nor the similarity coefficients depend exclusively on the quality of the search and rating algorithms but reflect rather the accommodation of these algorithms to the particular data base. If the data file has too many errors or is deficient in information (this may be seen in the case of infrared collection) or is too small (the case of ^{13}C NMR file), none of the retrieval systems is able to provide the user with a compound very similar to the correct one if it does not exist in the file or is wrongly coded.

It is also interesting to mention the adaptation period of an untrained user on the retrieval responses of the system. While there were no difficulties with the ^{13}C NMR and very little with mass searches (only in indicating the intensities), at least 40–50 searches were necessary for the user to learn how to input infrared spectra to obtain better results than at the beginning, in spite of the fact that the coding rules for the formation of the data base are very well known (*37*) and provide that all peaks with the intensities above 30% to be coded.

ABOUT THE IMPLEMENTATION

The program COSMOSS is written completely in FORTRAN IV language using strictly the ANSII approved statements. All machine dependent constants are stored in common blocks and all calculations using them (i.e., finding the proper word address from the bit position in a bit string, shifts for different word lengths and so on) are made as separate routines which can be very easily exchanged. The program is now operating on a CDC-Cyber 172 computer using the 60-bit-long word and requires 55000_8 words of central memory. The average search speed, including the encoding of free format input, calculating and outputting the top list is about 1100 spectra per second. In the present stage, the system is used in batch processing via terminals but the implementation for interactive work is under development.

CONCLUSION

In such an ambitious project as is the construction of an analytical black box system based on different spectra, there is present at each stage of development the question—What next? Besides the standard maintenance of the system such as filtering and updating of the data files, making more virtuous rating algorithms, or reprogramming some I/O routines in a more efficient way, some essential improvements have to be made. In our opinion two main goals for the future work are of first importance:

To develop the preprocessing program that should identify the structure fragments of the unknown compound on the basis of the input spectra before the actual search runs are performed. This can be achieved either by the hierarchical tree decisions based on average vectors (*48*) or using some standard method of artificial intelligence (*49*).

To evaluate the top lists obtained by different searches for each spectrometry relative to each other, forming a final multispectrometry top list including of course all classifying hints obtained from the preprocessing routine. The evaluation of this part of the problem is bound to the full structure information in all files. We wish to emphasize that it is the WLN description which is most important for this routine, and that it is the one that makes possible (*47*) a quantitative computation of the similarity between two structures.

LITERATURE CITED

(1) R. A. Sparks, Storage and Retrieval of WYANDOTTE–ASTM Infrared Spectral Data Using an IBM 1401 Computer, American Society for Testing Materials, Philadelphia, Pa., 1964.
(2) D. H. Anderson, and G. L. Covert, *Anal. Chem.*, **39**, 1288 (1967).
(3) D. S. Erley, *Anal. Chem.*, **40**, 894 (1968).
(4) F. E. Lytle and T. L. Brazie, *Anal. Chem.*, **42**, 1532 (1970).
(5) G. A. Massios, *Am. Lab.*, **3**, 55 (1971).
(6) R. W. Sebasta and G. G. Johnson, Jr., *Anal. Chem.*, **44**, 260 (1972).
(7) C. S. Rann, *Anal. Chem.*, **44**, 1669 (1972).
(8) J. Zupan, D. Hadži, and M. Penca, *Kem. Ind.*, **23**, 275 (1974).
(9) E. C. Penski, D. A. Padowski, and J. B. Bouck, *Anal. Chem.*, **46**, 955 (1974).
(10) K. Schaarschmidt, R. Riemer, and E. Steger, *Z. Chem.*, **14**, 374 (1974).
(11) H. B. Woodruff, S. R. Lowry, and T. L. Isenhour, *J. Chem. Inf. Comput. Sci.*, **15**, 207 (1975).
(12) R. C. Fox, *Anal. Chem.*, **48**, 717 (1976).
(13) J. Zupan, D. Hadži, and M. Penca, *Comput. Chem.*, **1**, 71 (1976).
(14) E. M. Kirby, R. N. Jones and D. G. Cameron, *CODATA Bull.*, **21**, 18 (1976).
(15) J. Zupan, J. T. Clerc, and D. Hadži, *Vestn. Slov. Kem. Drus.*, **23**, 73 (1976).
(16) B. Pettersson and R. Ryhage, *Ark. Kemi.*, **26**, 293 (1967).
(17) L. R. Crawford and J. D. Morisson, *Anal. Chem.*, **40**, 1464 (1968).
(18) S. L. Grotch, *Anal. Chem.*, **42**, 1214 (1970).
(19) B. A. Knock, I. C. Smith, D. E. Wright, R. G. Ridley, and W. Kelly, *Anal. Chem.*, **42**, 1526 (1970).
(20) H. S. Hertz, R. A. Hites, and K. Beiemann, *Anal. Chem.*, **43**, 681 (1971).
(21) S. L. Grotch, *Anal. Chem.*, **43**, 1362 (1971).
(22) L. E. Wangen, W. S. Woodward, and T. L. Isenhour, *Anal. Chem.*, **43**, 1605 (1971).
(23) S. R. Heller, DCRT/CIS, MSSS User's Manual, Division of Computer Research and Technology, Bethesda, Md, (1972).
(24) S. R. Heller, *Anal. Chem.*, **44**, 1951 (1972).
(25) S. R. Heller, H. M. Fales, and G. W. A. Milne, *Org. Mass. Spectrom.*, **7**, 107 (1973).
(26) S. L. Grotch, *Anal. Chem.*, **45**, 2 (1973).
(27) P. R. Naegeli and J. T. Clerc, *Anal. Chem.*, **45**, 739A (1974).
(28) R. Schwarzenbach, J. Meili, H. Könitzer, and J. T. Clerc, *Org. Magn. Res.*, **8**, 11 (1976).
(29) R. J. Feldman, S. R. Heller, K. P. Shapiro, and R. S. Heller, *J. Chem. Doc.*, **12**, 41 (1972).
(30) J. T. Clerc, C. Jost, T. Meier, and R. Schwarzenbach, *Chimia*, **27**, (12) 665 (1973).
(31) J. T. Clerc and F. Erni, *Top. Curr. Chem.*, **39**, 91 (1973).
(32) J. T. Clerc, Computers in Chemical Research and Education, Proceedings, D. Hadži, Ed., Elsevier Publishing Co., Amsterdam, 1973, Vol. 2, p 3/109.
(33) L. A. Gribov, V. A. Dementyev, M. E. Elyashberg, and E. Z. Yakupov, *J. Mol. Struct.*, **22**, 161 (1974).
(34) V. A. Koptjug, *Z. Chem.*, **15**, 41 (1975).
(35) N. A. Gray, *Anal. Chem.*, **47**, 2426 (1975).
(36) The NIH-EPA Chemical Information Systems, Status Report No. 4, Dec. 1976.
(37) "Codes and Instructions for WYANDOTTE-ASTM", American Society for Testing Materials, 1916 Race St., Philadelphia, Pa., (1964).

(38) E. G. Smith and P. A. Baker, The Wiswesser Line-Formula Chemical Notation, 3rd ed., CIMI, Cherry Hill, N. J., 1975.
(39) OCETH ^{13}C NMR Data Collection, Laboratorium für Organische Chemie, ETH, Zürich
(40) J. T. Clerc, R. Knutti, H. Koenitzer, and J. Zupan, *Fresenius' Z. Anal. Chem.*, **283**, 177 (1977).
(41) Sadtler Standard Spectra, Sadtler Research Laboratories, Philadelphia, Pa.
(42) DMS, Documentation of Molecular Spectroscopy, Weinheim, Verlag Chemie, and London:Butterworth.
(43) Aldermaston Mass Spectrometry Data Collection, Reading, U.K.
(44) J. T. Clerc, private communication.
(45) J. T. Clerc and J. Zupan, Proceedings of the IUPAC, International Symposium on Technique for the Retrieval of Chemical Information, London, Nov. 1976.
(46) D. S. Erley, *Appl. Spectrosc.*, **25**, 200 (1971).
(47) J. Zupan and D. Hadži, "Computers in Chemical Research Education and Technology", E. V. Ludena and F. Brito, Ed., Advances Studies Center IVIC, Caracas, Appartado 1827 (1977).
(48) M. Penca, J. Zupan, and D. Hadži, *Anal. Chim. Acta*, in press.
(49) T. L. Isenhour and P. C. Jurs, *Anal. Chem.*, **43** (10), 20A, (1971) and references cited therein.

RECEIVED for review May 9, 1977. Accepted June 29, 1977. Financial support of the Research Community of Slovenia is gratefully acknowledged. The work was supported in part also by the Pharmaceutical Factory KRKA.

Positional and Geometric Characterization of Olefinic Double Bonds by Fluorine Magnetic Resonance Spectrometry

Michelle V. Buchanan, David F. Hillenbrand, and James W. Taylor*

Department of Chemistry, University of Wisconsin, Madison, Wisconsin 53706

Conversion of *n*-alkenes to hexafluoroacetone ketals has allowed the characterization of the double bond position and geometry using ^{19}F NMR. Geometry can be determined by the chemical shift, with a 0.775 ppm separation between the cis and trans isomers. Double bond position can be determined by the value of $\Delta\nu_{AB}$ for the A_2B_2 pattern, which decreases as the bond moves to the center of the molecule. A method by which $\Delta\nu_{AB}$ may be estimated without the use of computer simulation is discussed. Application of these findings to the quantitative determination of geometric mixtures of linear alkenes is examined. Prior separation is required for analysis of positional mixtures but not for geometric mixtures.

The determination of both the geometry and the position of the double bond in large alkenes has proven to be a difficult problem because of the minor differences in physical properties of isomeric alkenes. One approach to characterizing these compounds is an analytical technique which provides a derivative wherein the differences between the isomers are maximized. For efficiency, the chemical preparation of the sample derivative needs to be simple, and the analysis should yield both the geometry and the position of the double bond without the use of standards.

The derivatives which were first used to give information on both geometry and position of the double bond were cyclic esters. The first of these were cycloboronate esters (I) which were prepared from 1,2- and 1,3-diols (*1–3*). In another

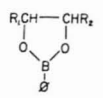

I

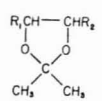

II

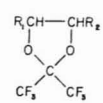

III

approach, a cyclic acetone ketal (II) was prepared by stereospecific conversion of the alkene to its diol using OsO_4, followed by condensation of the diol with acetone to form the corresponding cyclic ketal (*4, 5*). Mass spectral examination of the electron impact induced fragmentation gave ions which could be related to both the geometry and position of the original double bond. These isomers could be separated by gas–liquid chromatography to provide geometric identity between isomers of the same olefin, but positional isomers could not be distinguished if the original double bond were near the center of a long chain. Furthermore, this derivative was quite easily hydrolyzed so all handling procedures had to exclude moisture.

The hexafluoroacetone (HFA) analogue of the acetone ketal (III) was synthesized to give more easily interpreted mass spectra because it would allow for the distinction between fragments originating in the ring as opposed to those from the hydrocarbon chain (*6, 7*). This derivative was successful in determining the bond position and was easily handled, but it could not be used to distinguish between geometric isomers without reliance on gas chromatographic retention times and standards.

Because the HFA ketal has two sets of three equivalent fluorine atoms in the ring, it was thought that these fluorines might provide a sensitive probe into both the geometry and position of the double bond. The purpose of the present paper is to examine the use of HFA and ^{19}F NMR as a tool for the characterization of *both* the geometry and the position of double bonds in linear alkenes.

EXPERIMENTAL

The 2,2-bis(trifluoromethyl)-1,3-dioxolanes were prepared by first stereospecifically converting the olefin into the corresponding bromohydrin (IV). Then the bromohydrin was condensed with HFA to form the ketal (V). All olefins were used as received from

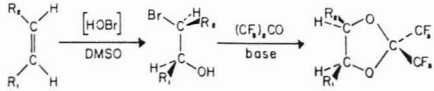

IV V

Chem Samples Co., Columbus, Ohio, and hexafluoroacetone was obtained from PCR, Inc., Gainesville, Florida. A detailed account of the experimental process for the preparation of the derivatives may be found in the literature (*7*).

Preparative gas chromatography was performed using a Varian-Aerograph Model 705 gas chromatograph with a 0.95 mm o.d. × 6.1 m aluminum column packed with 10% OV-1 on 60/80 mesh Gas Chrom Q. Normal operating conditions were: injector, 200 °C; flame ionization detector, 200 °C; detector split ratio, 10:1;

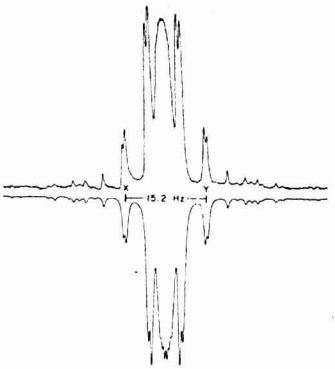

Figure 1. Proton-decoupled ^{19}F NMR spectrum of HFA derivatized *cis*-4-octene ($\Delta\nu_{AB}$ = 10.5 Hz) with computer simulated spectrum below

column, 150 °C; flow rates: air, 400 mL/min; hydrogen, 22 mL/min; helium (carrier), 200 mL/min. Injections of 50–100 μL were made and the heart cut material was collected at room temperature.

The proton-decoupled ^{19}F NMR spectra were obtained at 94.176 MHz at an ambient probe temperature of 28 °C and deuterium lock using a Varian XL-100/15 NMR spectrometer with the Varian FT Accessory and Varian 620-L computer. The spectra were run with 50 μL of the compound and 10 μL of hexafluorobenzene (HFB) dissolved in 300 μL of acetone-d_6. The chemical shifts of the compounds were referenced to the sharp singlet of HFB (136 Hz downfield from a hexafluorobenzene standard sealed in a capillary). HFB was used as the internal reference because it was found that the chemical shifts of the olefin derivatives could be quite sensitive to changes in concentration. When referenced to internal $CFCl_3$, this concentration effect is large (0.43 Hz upfield shift for each 1-μL increment of $CFCl_3$ added, up to 30 μL), and would necessitate careful control of the concentrations of all species in solution to ensure reproducible chemical shifts. However, when the chemical shifts of the derivatives are referenced to internal HFB, the dependence of chemical shifts on concentration is negligible (0.05 Hz upfield shift for each 1-μL increment of HFB added, up to 30 μL) compared to the 73 Hz separation between cis and trans isomers. Sample preparation and handling are also simplified using HFB. The problem of chemical shift changes due to concentration and solvent variation will be discussed in a subsequent paper (8). Quantitative determinations of mixtures of cis and trans olefins were made either by using an internal integral standard to calibrate the spectral integral, or by using standard addition techniques. Ethyl trifluoroacetate (Aldrich Chemical Co., Milwaukee, Wis.) was found to be a suitable internal integral standard because its chemical shift is close to, but does not interfere with, the derivatized olefin signals.

Fourier transform NMR was used because the enhanced signal-to-noise ratio allowed accurate determination of the peak positions of the small side peaks of the spectra (Figure 1). The positions of these small peaks were greatly affected by small changes in $\Delta\nu_{AB}$ and J_{AB} whereas the positions of the more intense central peaks changed very slightly. Thus, knowing the positions of the small peaks, it is possible to determine $\Delta\nu_{AB}$ and J_{AB} more precisely. Confirmation of the values of $\Delta\nu_{AB}$ and J_{AB} was obtained by simulated spectra. These spectra were obtained on the University of Wisconsin Chemistry Department's IBM 7094 using Bothner-By and Castellano's LAOCN3 self-iterative program (9). This program was easily modified to accept the nine equivalent coupling constants of the A_3B_3 pattern in one parameter set. Only six parameters were allowed in one set in the original program. The spectra were simulated by first inputting values of $\Delta\nu_{AB}$ and J_{AB} and allowing the computer to generate a table of frequencies and intensities of the lines expected in the spectrum. The calculated frequencies were then matched with the observed

Table I. Chemical Shifts of Hexafluoroacetone Derivatives vs. C_6F_6

	cis-2	cis-3	cis-4	cis-5
Octene	7912.6	7913.6	7916.4	
Decene	7912.1	7912.4	7918.6	7917.2
Dodecene		7915.1		
	trans-2	trans-3	trans-4	trans-5
Octene	7836.9	7843.8	7841.2	
Nonene		7842.8		
Decene	7836.7	7842.7	7844.4	7845.4
Dodecene		7841.4		

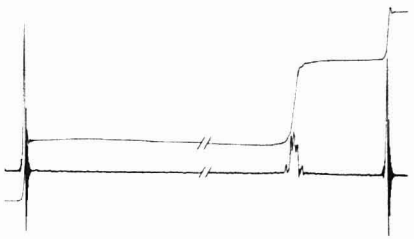

Figure 2. Proton-decoupled ^{19}F NMR spectrum of a mixture of 90 μL of *cis*-4-decene (7918.6 Hz) and 50 μL of *trans*-4-decene (7844.4 Hz) with 50 μL of ethyl trifluoroacetate (8328.3 Hz) added as an integral standard

experimental frequencies and input to the computer. All calculated frequencies not observed in the experimental spectrum due to either low intensity or line overlap were not used. The computer then iteratively calculated, by a least-squares criterion, the chemical shifts and coupling constants which yielded the best fit. The best fit values for $\Delta\nu_{AB}$ and J_{AB} were used to plot the resulting spectra using a Bruker WH 270 (BNC 12 computer) and the ITRCAL six spin self-iterative program. The ITRCAL program had been modified to operate with 32 K of display by Jeff Luce of Nicolet, Inc., Madison, Wis.

For derivatives with values of $\Delta\nu_{AB}$ less than 5 Hz, the self-iterative LAOCN3 program was not used because the small side peaks (Figure 1) were not visible. Without the small side peaks, not enough frequencies were available to obtain unique values of $\Delta\nu_{AB}$ and J_{AB} in the simulations. In these cases, the ITRCAL program was used to generate a matrix of spectra with different values of $\Delta\nu_{AB}$ and J_{AB}. The experimental spectra were then compared with these simulated spectra and fit using line width and intensities as criteria for a match.

RESULTS AND DISCUSSION

The ^{19}F NMR of the HFA derivatives produce spectra with an A_3B_3 pattern, such as displayed in Figure 1. The ^{19}F spectra yield three parameters: chemical shift; J_{AB}, the coupling constant; and $\Delta\nu_{AB}$, the difference in chemical shift between the two sets of equivalent nuclei. The success of the analysis of the derivatized olefins using ^{19}F NMR rests, therefore, on changes in these three spectral parameters with double bond position and geometry.

The chemical shifts of the derivatives, taken as the center of the A_3B_3 pattern, are shown in Table I. As can be seen from these data, the chemical shifts of the derivatives are constant with bond position but vary systematically with the original geometry about the double bond. The cis isomers exhibited an average chemical shift of 7915 Hz with the trans isomers showing 7842 Hz. These values are 84.04 and 83.27 ppm, respectively, from HFB, and represent a separation of 73 Hz at the 94.176 MHz ^{19}F Larmour frequency.

The separation of 73 Hz was found to be sufficient for identifying which geometric cis or trans linear alkene was present as shown in Figure 2. The amounts of cis and trans

Table II. Quantitative Measurement of Olefin Geometric Mixtures

Volumes of compounds added (μL) cis/trans	Integral intensity ratios		Error, %
	Theoretical	Experimental	
10/50	0.20	0.21	5.0
30/50	0.60	0.60	0.0
40/50	0.80	0.80	0.0
50/50	1.00	1.03	3.0
60/50	1.20	1.23	2.5
70/50	1.40	1.38	1.4
80/50	1.60	1.58	1.3
90/50	1.80	1.85	2.8
100/50	2.00	2.06	3.0

isomers in a mixture were determined by integration, using ethyl trifluoroacetate to calibrate the spectral integral. As shown in Table II, the amounts could be determined within ±5% regardless of the particular linear olefin pairs employed.

Computer simulation yielded both the $\Delta\nu_{AB}$ values and the coupling constants, J_{AB}, between the two sets of nuclei, A and B. These are shown in Table III. The calculated values of the coupling constants for each series of geometric isomers are identical within experimental error (±0.1 Hz) with the average value of J_{AB} cis = 9.1 Hz and J_{AB} trans = 8.4 Hz. Because these $^4J_{FF}$ (four bond) couplings arise from through-space interactions (*10, 11*), they are sensitive to changes in distance between the two trifluoromethyl groups. The lower J_{AB} value for the trans case suggests a possible increase in the angle between the two trifluoromethyl groups. This could occur if the steric interaction of the alkyl groups causes the ring to assume a slightly different conformation for the two geometric isomers.

Except for the cis-2 case, within each geometric series, $\Delta\nu_{AB}$ decreases as the double bond moves to the center of the molecule, as can be seen from the data in Table III. This allows the original double bond position to be determined by the value of $\Delta\nu_{AB}$. Because of the unique symmetry when $R_1 = R_2$, both *trans*-5-decene and *trans*-4-octene yield values of $\Delta\nu_{AB} = 0$. As the alkyl groups become more dissimilar, the value of $\Delta\nu_{AB}$ increases until it finally reaches a maximum at the trans-2 case. The $\Delta\nu_{AB}$ cis values are larger overall than $\Delta\nu_{AB}$ trans, since both alkyl groups are adjacent to one trifluoromethyl group in the cis case, making the environments of the two trifluoromethyl groups even more dissimilar. However, just as in the trans case, $\Delta\nu_{AB}$ cis increases as the difference in the alkyl groups increases. The only exception is when the original molecule is *cis*-2-decene or *cis*-2-octene. In these cases, the values of $\Delta\nu_{AB}$ are anomalously small.

The 1-octene derivative (7860.0 Hz vs. HFB), like the cis-2 olefin derivatives, has a small value of $\Delta\nu_{AB}$. The data in Table III show that for the cis case, small $\Delta\nu_{AB}$ values occur only when one alkyl chain has fewer than two carbons. From molecular models, it may be seen that an alkyl group with two or more carbons can interact more strongly with its adjacent trifluoromethyl group than can the smaller groups (R = H or CH_3). It is possible that without this interaction, the two trifluoromethyl groups become more equivalent, yielding small $\Delta\nu_{AB}$ values. Further, when R_1 = H, the molecule is less symmetric than when $R_1 = CH_3$, giving 1-octene a larger $\Delta\nu_{AB}$ value (4 Hz) than the cis-2 derivative.

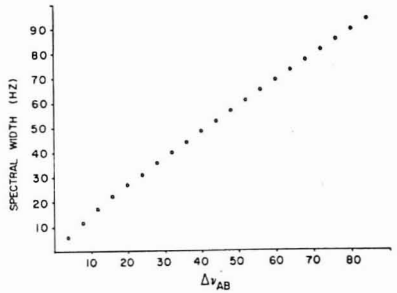

Figure 3. Spectral width as a function of $\Delta\nu_{AB}$ for an A_3B_3 pattern

Computer simulations showed that as $\Delta\nu_{AB}$ increased (J_{AB} remaining constant), the spectral width of the main portion of the spectrum, between points *X* and *Y* in Figure 1, increased as shown in Figure 3. All of the olefin derivatives in this study have $\Delta\nu_{AB}$ values between 0 and 15 Hz. In this region, a straight line relationship with spectral width may be assumed with a slope of 1.45. By dividing the spectral width in hertz between points *X* and *Y* by 1.45, the value of $\Delta\nu_{AB}$ for the olefin derivatives may be estimated within a few tenths of a hertz (Table III). Below $\Delta\nu_{AB}$ = 1 Hz, the spectrum assumes the appearance of a singlet and the spectral width becomes complicated by line width. Above $\Delta\nu_{AB}$ = 15 Hz, the slope becomes unity. Although any line position in the main part of the spectrum could have been monitored for a relationship with $\Delta\nu_{AB}$, points *X* and *Y* were chosen because these two features remain distinct as $\Delta\nu_{AB}$ decreases to 1 Hz. The only overlap appears with *trans*-4-decene and *trans*-5-decene, which cannot be distinguished using this estimation technique because both have $\Delta\nu_{AB}$ values less than 1 Hz and thus, points *X* and *Y* are not distinct. However, if the linewidths of these two compounds are compared with that of the internal reference, HFB, they can be distinguished. Since both HFB and *trans*-5-decene are singlets, they have the same linewidth, whereas *trans*-4-decene is not a true singlet and has a linewidth broader than that of HFB.

In an analytical application, therefore, it is necessary only to determine the values of the points *X* and *Y* in hertz to determine the actual bond position. The geometry is determined by the location of the center of resonance. Thus the double bond position and geometry of an unknown linear olefin can be determined using the values of $\Delta\nu_{AB}$ and the

Table III. Computer Simulated Values of $\Delta\nu_{AB}$ and J_{AB}[a]

	Octene			Nonene			Decene			Dodecene		
	J_{AB}	$\Delta\nu_{AB}$	$\Delta\nu_{AB}$[c]	J_{AB}	$\Delta\nu_{AB}$	$\Delta\nu_{AB}$[c]	J_{AB}	$\Delta\nu_{AB}$	$\Delta\nu_{AB}$[c]	J_{AB}	$\Delta\nu_{AB}$	$\Delta\nu_{AB}$[c]
trans-2	8.41	7.44	7.5				8.44	7.78	7.9			
trans-3	8.4	1.9	1.9	8.4	1.8	1.9	8.4	1.7	1.7	8.4	1.5	1.6
trans-4	8.4	0.0	...				8.4	0.2	>0[b]			
trans-5							8.4	0.0	0[b]			
cis-2	9.1	0.2					9.1	0.2	...			
cis-3	9.14	14.17	13.9				9.11	14.22	14.0	9.01	13.85	13.6
cis-4	9.14	10.53	10.5				9.09	9.57	9.6			
cis-5							9.16	7.96	8.0			

[a] Values for non-iterative simulations are given with fewer significant figures. See text. [b] See text for explanation. [c] Values obtained from spectrum and Figure 3.

chemical shifts from ^{19}F NMR spectra of the hexafluoroacetone derivatized olefins. The proton decoupled spectra are obtained using the acetone-d_6 solvent as a lock signal and are referenced to the singlet of internal hexafluorobenzene. Values of $\Delta\nu_{AB}$ for the A_3B_3 pattern may be obtained directly from the spectral width, eliminating the need for computer analysis and simulation of the spectra. Because of the employment of ^{19}F, the NMR technique is sensitive only to the derivative of the olefin and the derivatives need not be purified as done in this study before being subjected to NMR analysis. Mixtures of geometric isomers and isomers of different bond positions could be determined by this technique coupled with GC/MS.

The HFA derivatization technique has been shown to be useful for linear olefins and, more recently, we have also applied it to long chain ($>C_{16}$) linear fatty acids. Work is currently in progress to expand the application of this analysis to cyclic olefins and steroids.

LITERATURE CITED

(1) C. J. W. Brooks and J. Watson, *J. Chem. Soc., Chem. Commun.*, 952 (1967).
(2) C. J. W. Brooks and I. Maclean, *J. Chromatogr. Sci.*, **9**, 18 (1971).
(3) W. Blum and W. J. Richter, *Helv. Chim. Acta*, **57**, 1744 (1974).
(4) R. E. Wolff, G. Wolff, and J. A. McCloskey, *Tetrahedron*, **22**, 3093 (1966).
(5) J. A. McCloskey and M. J. McClelland, *J. Am. Chem. Soc.*, **87**, 5090 (1965).
(6) B. M. Johnson and J. W. Taylor, *Org. Mass Spectrom.*, **7**, 259 (1973).
(7) B. M. Johnson and J. W. Taylor, *Anal. Chem.*, **44**, 1438 (1972).
(8) M. V. Buchanan, D. F. Hillenbrand and J. W. Taylor, in preparation for submission to *J. Magn. Reson.*
(9) A. A. Bothner-By and S. M. Castellano, in "Computer Programs for Chemistry", Vol. I, D. F. Detar, Ed., W. A. Benjamin, Reading, Mass., 1968, pp 10–53.
(10) L. Petrakis and C. H. Sederholm, *J. Chem. Phys.*, **35**, 1243 (1961).
(11) S. Ng and C. H. Sederholm, *J. Chem. Phys.*, **40**, 2090 (1964).

RECEIVED for review July 12,, 1977. Accepted September 15, 1977. This research has been supported by the National Science Foundation under grants MPS-74-23569 and MPS-75-21059.

Deconvolution and Background Subtraction by Least-Squares Fitting with Prefiltering of Spectra

Peter J. Statham[1]

Department of Electrical Engineering and Computer Sciences, University of California, Berkeley, California 94720

Deconvolution of overlapped peaks in a spectrum is complicated by the presence of a high background component. A method of background subtraction, which involves suppressing the background in both the specimen data and peak models with a digital filter before proceeding to a conventional least-squares fit, is analyzed. The dimensions of a "top-hat" filter are found which give a suitable compromise with regard to statistical accuracy and sensitivity to both background curvature and possible errors in the peak models. The major advantages over conventional techniques are that the shape of the background need not be known explicitly, there is no need to find suitable points away from peaks for background scaling, and any background that is approximately linear over the range covered by a single peak will be effectively removed.

This paper addresses itself primarily to the problem of finding peak areas in a digitized x-ray energy spectrum obtained with a solid-state detector, although the problem is essentially one of deconvolving overlapped peaks in the presence of a high background component. In the usual linear least-squares procedure, the sum of a number of functions is fitted to the specimen data to find the contribution from each peak. Each function must exactly model the peak, or series of peaks (for example, the Kα and Kβ peaks for a given chemical element) it is meant to represent, and the procedure is only applicable when the specimen data can be represented by a linear sum of the model functions plus statistical "noise". In the special case of x-ray spectra excited by electron bombardment of a flat polished specimen, the background shape can be predicted quite accurately (*1*, *2*) and the background can therefore be subtracted away provided that suitable points, away from peaks, can be found for scaling, or if the shape function is calculated at every point, the background can be included as an additional function in the fitting procedure. However, when electron-beam-excited specimens are not perfectly flat (for example, particles), or if we are dealing with x-ray fluorescence or γ-ray spectra, the background shape is not so predictable and one has to exploit any features which distinguish background from peaks. In this respect, the most obvious feature is the slow variation of the background with energy compared with the faster variation of structure in the peaks. This suggests methods such as interpolating the background beneath the peaks using smooth analytical functions but this may be inaccurate when carried out over the large range required when several peaks overlap (*3*). To get around this problem, coefficients for a polynomial function can be included as undetermined parameters in the least-squares analysis, thus removing the need for an explicit fit to available background points. However, the function used must accurately represent the background over the whole fitting range and while regions of high curvature, such as absorption steps, can be accommodated by including higher terms in the polynomial, this may make the technique unstable with regard to small errors in the peak model functions.

An earlier study (*3*) discussed further methods of background correction where the background is implicitly taken into account in the peak deconvolution process. In the "iterative stripping" approach (*3*), peaks are removed in stages using a symmetric, zero-area weighting function at each stage to estimate the area of each peak above local background. This method is quick and very easy to program but is limited to resolving peaks which are greater than 0.66 fwhm (full width half maximum) apart. The iterative process demands a

[1] Present address, Link Systems, Halifax Road, High Wycombe, Bucks, England HP12 3SE.

solution which, apart from "noise", has a smooth residual and can in fact be shown to be closely equivalent to a special case of a least-squares approach (*4*). Thus, a development to overcome the resolution limit involves preconditioning both the measured data and the peak model functions with a digital filter before proceeding to a conventional least-squares fit. Digital filtering is a linear operation so if the background is completely suppressed, peak structure in the specimen data can be represented by a linear sum of the filtered model functions and the least-squares approach is justified.

Brouwer and Jansen (*5*) suggested fitting the first derivative of a Gaussian function to the first derivative of the specimen data, but this only removes the influence of a constant background component. A background which is linear over the range of each peak can be suppressed by convolution with a "top-hat" weighting function since this produces a result similar to the negative of the smoothed second derivative; Schamber (*6*) has used this form of digital filter and demonstrated its successful application in an analysis system for x-ray and γ-ray spectra. Since the basic technique is described clearly in (*6*), the present paper will focus on details of the theory and will examine the effects of using different digital filters prior to a least-squares analysis.

DETAILS OF THE METHOD

If y_i represents the count accumulated in channel i of the histogram representing the x-ray spectrum from the specimen and h_i represents a weighting function then, after filtering,

$$y_i' = \sum_{k=-s}^{k=+s} h_k y_{i+k} \tag{1}$$

s indicates the extent of non-zero values of h_i so that $W = 2s + 1$ is the "support" of the filter and it is assumed that the integer subscripts denote contiguous channels separated by equal increments of energy. If $p_{m,i}$ represents the count in channel i that would correspond to the mth peak model, then the model for the filtered peak is

$$p_{m,i}' = \sum_{k=-s}^{k=+s} h_k p_{m,i+k} \tag{2}$$

Each count y_i is distributed statistically according to a Poisson distribution and for practical purposes the variance can be approximated by y_i. Since y_i' is a linear sum of independent random variables, the variance is

$$\sigma_{ii}'^2 \simeq \sum_{k=-s}^{k=+s} h_k^2 y_{i+k} \tag{3}$$

However, whereas the statistical contribution is uncorrelated between different channels in the original data set y_i, the covariance, $\sigma_{ij}'^2$, between y_i' and y_j' is non-zero whenever $|i - j| < 2s + 1$ because the filtering operation introduces a channel-to-channel correlation in the statistical noise. In the least-squares procedure, suitable coefficients c_m would be chosen to minimize

$$\epsilon^2 = \sum_{i=i_1}^{i=i_2} (y_i' - \sum_{m=1}^{m=NP} c_m p_{m,i}')^2 W_i' \tag{4}$$

where NP is the number of peak model functions, the fitting range extends from channel i_1 to i_2 and W_i' is a weight which in the simplest case would be set to unity. However, when the statistical deviations are correlated from channel-to-channel, as they are for the filtered data y_i', minimization of Equation 4 is an oversimplification. In this case, if $n = i_2 - i_1 + 1$, an $n \times n$ matrix $\mathbf{W}'$ can be defined as the inverse of the $n \times n$ matrix $\mathbf{S}'$ whose ijth element is $\sigma_{ij}'^2$. If matrices $\mathbf{Y}'$ $(n \times 1)$, $\mathbf{C}$ $(NP \times 1)$ and $\mathbf{P}'$ $(NP \times n)$ have elements y_i', c_m and $p_{m,i}'$ respectively, $i_1 \le i \le i_2$, $1 \le m \le NP$, then minimization of

$$[\mathbf{Y}' - \mathbf{P}'^{\mathrm{T}}\mathbf{C}]^{\mathrm{T}}\mathbf{W}'[\mathbf{Y}' - \mathbf{P}'^{\mathrm{T}}\mathbf{C}] \tag{5}$$

where "T" denotes the transpose of a matrix, results in the normal equations

$$[\mathbf{P}'\mathbf{W}'\mathbf{P}'^{\mathrm{T}}]\mathbf{C} = \mathbf{P}'\mathbf{W}'\mathbf{Y}' \tag{6}$$

which can be solved for $\mathbf{C}$. This procedure results in estimates, c_m, which have the minimum variance (*7*) and is therefore the "correct" solution to the present problem. However, from a practical point-of-view, the determination and subsequent inversion of the matrix $\mathbf{S}'$ is not to be taken lightly, since n may typically exceed 100. As a practical compromise, $\mathbf{W}_i'$ can be set to $1/\sigma_{ii}'^2$ (Equation 3) and ϵ^2 is minimized. Differentiating Equation 4 with respect to each c_m and equating the results to zero to define a minimum results in the normal equations in matrix form as

$$\mathbf{AC} = \mathbf{B} \tag{7}$$

where

$$a_{mn} = \sum_{i=i_1}^{i=i_2} p_{m,i}' p_{n,i}' W_i'$$

$$b_m = \sum_{i=i_1}^{i=i_2} p_{m,i}' y_i' W_i'$$

and

$$W_i' = 1/\sum_{k=-s}^{k=+s} h_k^2 y_{i+k}$$

with the solution

$$\mathbf{C} = \mathbf{A}^{-1}\mathbf{B} \tag{8}$$

ERROR ANALYSIS

The error analysis is complicated by the fact that the weighting coefficients, W_i', depend on the input data so that each c_m is not simply a linear sum of independent random variables. The following treatment overlooks the statistical nature of W_i' so the implicit assumption is that small changes in the weighting scheme do not alter the results. Although this assumption seems reasonable when W_i' varies fairly smoothly over a limited range of values, it is less likely to hold when y_i approaches zero in some regions so that W_i' becomes very large. It should therefore be understood that although the variance estimates are useful for characterizing the method, some caution should be exercised when using them to determine the experimental error in a practical analysis, particularly when the background is very low or statistical noise is great.

The statistical fluctuations in y_i are uncorrelated from channel to channel and if c_m is regarded as a linear sum of y_i, then the variance in c_m

$$\sigma_{c_m}^2 \simeq \sum_{i=i_1-s}^{i=i_2+s} \left(\frac{\partial c_m}{\partial y_i}\right)^2 y_i \tag{9}$$

where the variance in channel i has been approximated by y_i. Now,

$$\frac{\partial c_m}{\partial y_i} = \sum_{j=i_1}^{j=i_2} \left[\frac{\partial c_m}{\partial y_j'} \cdot \frac{\partial y_j'}{\partial y_i}\right] \tag{10}$$

From Equation 1 we have

$$\frac{\partial y_j'}{\partial y_i} = h_{i-j} \tag{11}$$

and from Equations 7 and 8,

$$\frac{\partial c_m}{\partial y_j'} = \sum_{n=1}^{n=NP} a_{mn}^{-1} p_{n,j}' W_j' \tag{12}$$

so that

$$\frac{\partial c_m}{\partial y_l} = \sum_{j=i_1}^{j=i_2} \left(\sum_{n=1}^{NP} a_{mn}^{-1} p_{n,l}' W_l' \right) h_{i-j} \tag{13}$$

If we let

$$p_{n,l}'' = \sum_{j=i_1}^{j=i_2} p_{n,j}' W_j' h_{i-j}$$

then, rearranging the summations and substituting into Equation 9 gives

$$\sigma_{c_m}^2 \simeq \sum_{i=i_1-s}^{i=i_2+s} \left(\sum_{n=1}^{NP} a_{mn}^{-1} p_{n,l}'' \right)^2 y_l \tag{14}$$

The evaluation of this formula can be costly in terms of both additional memory storage and computation time when several peaks are involved but it can be used to examine the suitability of various filters, and a useful approximation for practical use is discussed below.

CHOICE OF FILTER

Digital filters have been used successfully by a number of investigators (*8–10*) for peak detection in the presence of background and noise; the data are weighted according to Equation 1 and if the filtered result, y_i', exceeds some multiple of σ_{ii}' (Equation 3) then it is assumed that a peak is present in the vicinity of channel i. Given the constraint that the filter must completely suppress background, the best filter will be one that allows detection of the smallest peaks while remaining insensitive to statistical fluctuations in regions of the spectrum where there are no peaks. There does not seem to be any closed-form analytical solution for the optimal filter but Hnatowicz (*10*) has shown that a symmetric, zero-area weighting function, consisting of the sum of a positive Gaussian peak and a negative constant, represents the best of the linear filters so far suggested for detecting Gaussian peaks on a linear background.

When the linear filtering is to be followed by a least-squares fit, it is even less obvious how to decide on an optimal filter. Intuitively, one might expect the filter to emphasize spatial frequencies typical of peaks, at the expense of the slow-varying background and rapidly-varying statistical fluctuations. However, the least-squares fitting of an essentially smooth filtered peak profile to the filtered data might also be expected to reduce the sensitivity to statistical fluctuations. With the added complication of a data-dependent weighting scheme, a closed-form solution for the optimum filter seems unattainable, even in rather specialized cases. Furthermore, there are practical considerations to optimize in addition to statistical accuracy so the approach I have taken is one of numerical simulation. Perhaps the simplest of the background-suppressing filters is the "top-hat" defined by the relationship

$$y_i' = \frac{1}{2M+1} \sum_{j=i-M}^{j=i+M} y_j - \frac{1}{2N} \left[\sum_{j=i-M-N}^{j=i-M-1} y_j + \sum_{j=i+M+1}^{j=i+M+N} y_j \right] \tag{15}$$

which corresponds to the definition,

$$h_i = \frac{1}{2M+1} \qquad \text{for } |i| \leq M$$

$$h_i = -\frac{1}{2N} \qquad \text{for } M < |i| \leq M+N$$

$$h_i = 0 \qquad \text{otherwise} \tag{16}$$

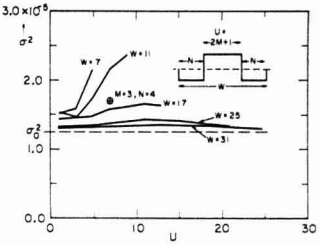

Figure 1. Statistical variance for fitted peak when P/B = 1000. Specimen data consist of peak, fwhm = 7.5, height = 10 000 counts on uniform background of 10 counts/channel and is fitted with a single peak, fwhm = 7.5, height = 10 000 counts, thus giving a mean result of 1. σ_0^2 is the variance when background is zero and prefiltering is not used

Since this has already been used with success (*3, 6, 9*) and its behavior is similar to that of the Gaussian-plus-negative-constant filter (*9*), the simulations have been designed to find the optimum parameters for a "top-hat" filter. To facilitate discussion, it should be noted that the "top-hat" filter essentially corresponds to taking the average over $U = 2M + 1$ channels about the channel of interest and subtracting the mean of averages over N channels on either side of this central region; the total "support" of the filter is thus $W = 2M + 1 + 2N$. The filter produces a result similar to the negative of the smoothed second derivative of the data so a single peak is transformed into a central positive lobe with negative lobes on either side and a background which is linear is completely suppressed.

The effects of using a particular filter depend to some extent on the form of the specimen data. Therefore, the simulations have been designed to represent extremes which encompass the range of situations which would normally be encountered. The specimen data directly affect the weighting coefficients, W_i', so if these are all set to unity, one can regard the simulation as either not favoring any particular form of the data or else corresponding to a situation where the background is much larger than the peaks.

Statistical Accuracy. The statistical accuracy of each fitted peak height can be computed using Equation 14, and Figure 1 shows how the variance depends on filter dimensions when the specimen data consist of a single peak superimposed on a low background; for a given support, W, it is apparent that U should be as small as possible. When the peak-to-background ratio is very low, the variance in the fitted result directly determines the detection limit for a small peak; Figure 2 shows that for a given support, a large U for the central average is favored in contrast to the situation in Figure 1 where the background is almost negligible. In either situation, it is apparent that increasing W much beyond 17 produces only a marginal reduction in the variance and this figure varies in direct proportion to the fwhm of the peak, which in all the present examples is 7.5 channels.

It is interesting to see how the statistical accuracy compares with that of the ideal case where the background level is known exactly and is subtracted from the data before proceeding to a conventional least-squares fit. Although, when the background is very low (Figure 1), the variance with prefiltering can be only marginally greater than the theoretical minimum, σ_0^2, the variance for a peak on a high background (Figure 2) is still about a factor of two greater than σ_0^2 even with a broad filter support. However, in practice the background is not known exactly and to σ_0^2 we must add a term which is roughly inversely proportional to the number of peak-free points that are available for estimating the background. Thus, for ex-

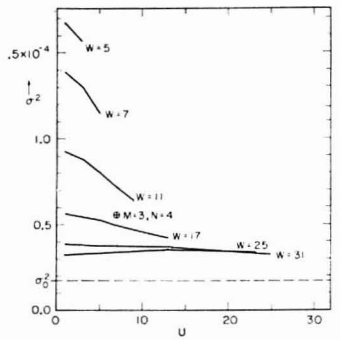

Figure 2. Statistical variance for fitted peak when $P/B = 0$. Specimen data: a uniform background of 10 000 counts/channel, is fitted with a peak, fwhm = 7.5, height = 10 000 counts, so the mean result is zero. σ_0^2 is the theoretical limit in accuracy, obtained by fitting a peak to the background-subtracted data, assuming the background is known exactly

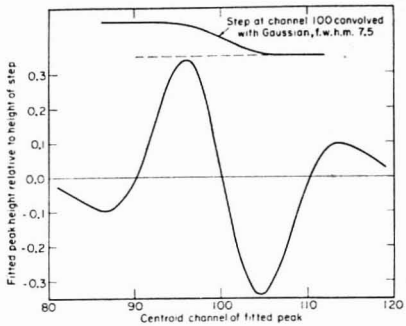

Figure 3. Results of fitting a single peak, fwhm = 7.5 channels, to a smoothed step using prefiltering with $M = 3$, $N = 4$ and uniform weighting

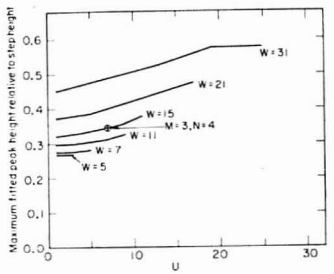

Figure 4. Sensitivity to curvature. Specimen data consist of a step function convolved with a Gaussian function, fwhm = 7.5 channels and is fitted with a single Gaussian peak, fwhm = 7.5 channels. For various filters, plots show maximum fitted height that can occur for any centroid position when uniform weighting is used

ample, if the average of 5 channels is used to determine the background which is to be subtracted, then the variance for a conventional least-squares fit in Figure 2 is 5.8×10^{-5} which is bettered by the prefiltering technique provided W is greater than 17.

Sensitivity to Curvature. Usually, the background can be regarded as linear only over a restricted range and any curvature will not be suppressed by the filter. In the case of x-ray energy spectra produced by electron-excitation of a thick, flat sample, severe departures from linearity occur near absorption steps and for energies below 2 keV where x-ray absorption is great. It is difficult to make any general predictions about curvature at low energies because so many experimental factors are involved, but absorption steps can be modeled quite well by a step function,

$$S_i = H \quad \text{for } i \leqslant i_c$$
$$S_i = 0 \quad \text{for } i > i_c$$

provided it is convolved with a unit area Gaussian with the same fwhm as the peaks. H thus represents the height of the step which occurs at channel i_c. In an x-ray spectrum, a step produced by differential absorption of the continuum occurs near every major peak. Since these steps are not removed by the filter, they are a significant source of error when we are trying to determine whether a trace amount of another element is present in the vicinity of a major element peak. Since the relative positions of the step and the suspected peak are dependent on the atomic numbers of the chemical elements involved, simulations were designed to find the maximum error that could occur. A step of height $H = 10\,000$ counts was convolved with a unit area Gaussian with fwhm = 7.5 channels and the result used as the specimen data. A single Gaussian peak of height 10 000 counts, fwhm 7.5 was fitted to the data for different values of its centroid position using the prefiltering technique with uniform weighting ($W_i' = 1$ in Equation 7). The step would normally be superimposed on the sum of a smooth background and a series of peaks or may represent the residual component in the fitting of several large peaks so a uniform weighting scheme seemed a less-biased choice than one which favored a particular form of the data. The results for a particular filter ($M = 3$, $N = 4$) are shown for illustration in Figure 3 where it is apparent that the largest errors occur when the centroid of the suspected peak is about 0.5 fwhm away from the step. The maximum absolute value which occurs for various filter choices is plotted in Figure 4. As the support, W, is increased, the maximum error also increases, a behavior one might expect because a filter with a broad support cannot suppress curvature as well as a narrow one. As W is reduced, the "top-hat" filter produces a result closer to the negative second derivative of the data and eventually, the maximum error which can occur amounts to a peak height less than $^1/_3$ of the height of the step.

Sensitivity to Errors in the Peak Model. Systematic errors arise in the least-squares technique whenever the functions chosen to model the peaks do not truly represent the peak shapes constituting the data. In an x-ray energy spectrometer, this can occur because of drift or count-rate-dependent effects in the pulse-measuring electronics. Furthermore, incomplete charge collection in the solid-state x-ray detector results in low-energy tailing and a consequent departure from a Gaussian peak model. Many of these problems can be circumvented by frequent calibration of the spectrometer and by using experimentally-measured peak profiles instead of analytical approximations such as the Gaussian function. However, there are statistical limitations to the accuracy of any calibration procedure, and chemical wavelength shifts can cause the peak centroid for a given chemical element in the specimen to differ from that of the corresponding peak model (*11*). Therefore, when prefiltering is introduced into the least-squares technique, it is desirable for small errors in the peak models to only have a marginal influence on the results. The fitted result for a solitary peak is fairly insensitive to small errors in the peak model (for

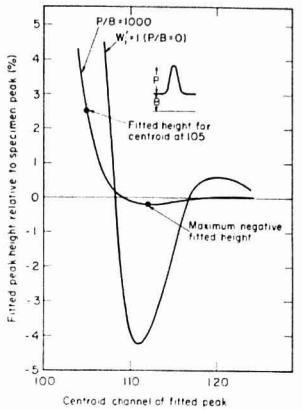

Figure 5. Fitted peak height as a function of centroid position for second peak when a single peak centred at 100.25 plus a uniform background is fitted with two peaks, fwhm = 7.5, and the first is centered at channel 100. Prefiltering is used with $M = 3$, $N = 4$ and two weighting schemes are employed

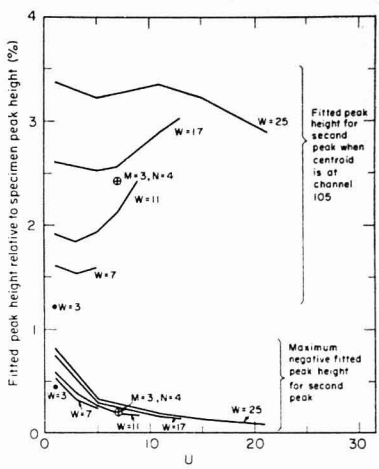

Figure 6. Sensitivity to peak shift. Specimen data consist of a peak, fwhm = 7.5 channels, centered at 100.25 channels, superimposed on a uniform background of 10 counts. Two peaks of fwhm 7.5 are fitted to the data; the first is centered at 100 but the centroid of the second is varied and the fitted peak height is observed

example, see plots in (*6*)) but this is not the case when multiple peak overlaps are to be resolved. A particularly bad case occurs when a very small peak is overlapped by a large one. The range of systematic errors which can occur for the small peak in effect defines a detection limit as a function of both separation from the large peak and the likely errors in the peak model (*3*). In the present case, simulations were designed to examine the influence of the filter function on the errors which could be produced by a slight error in peak position. The specimen data consisted of a single Gaussian peak, fwhm = 7.5 channels centered at a position corresponding to 100.25 channels and superimposed on a uniform background. Two peaks with fwhm = 7.5 were fitted to the data, one with centroid at 100 and the other with centroid at a series of positions throughout the range of the data. The fitted heights for the second peak thus give a measure of the sensitivity to a relative shift of 0.25 channel in the specimen spectrum. When the second peak is centered at channel 101, the fitted peak heights relative to that of the specimen peak are close to 0.75 and 0.25 as might be expected from the ratio of distances from each peak centroid to the true peak position. This result is insensitive to changes in both the peak-to-background ratio in the specimen data and changes in the filter parameters. As the second peak centroid is shifted to higher channel numbers, the fitted height decreases, goes negative, and eventually reaches a negative maximum whose absolute value is never again exceeded for any further shift to higher channels. This behavior is illustrated by Figure 5 for two extremes of the peak-to-background ratio. When the background is high or the general level of the specimen data is roughly uniform because several peaks overlap ($W'_i = 1$ in Figure 5) then there is relatively little difference between the performance with various filters; although the positions of the extrema are altered by changes in U and W, the magnitude of the maximum negative error varies only from 5.6% to 4.2% as W is increased from 3 to 17 and changes in U have a virtually negligible effect. However, with a specimen peak of height 10 000 superimposed on a background of 10 counts ($P/B = 1000$) differences are apparent as a consequence of the nonuniform weighting. Since, in practice, peak separations of several channels are commonly encountered, I chose to look at the fitted height for the second peak when centered at channel 105 together with the maximum negative fitted height in order to evaluate each filter. The results are shown in Figure 6. As U is increased, the central positive lobe of the filtered peak becomes broader so one might expect the effects of residual errors to extend further. This behavior is seen in the plots for the fitted height for a centroid at channel 105 where, in most cases, the values increase for high values of U. The maximum negative peak height decreases with increasing U presumably because the weights, W'_i, play a greater role as the negative lobes of the filtered peak are forced outwards.

Optimal Filter. In the figures, the greatest variations are seen in the statistical variance for a zero peak-to-background ratio and in the errors due to peak shift but other effects are fairly insensitive to the choice of filter; from the results I suggest that $W = 15$, $U = 7$, ($M = 3$, $N = 4$) is a suitable compromise with regard to the various effects. Representative points for this filter are shown with a cross on each graph and Figures 3 and 5 give a detailed account of the errors which can arise from a residual absorption step or peak shift. Since the parameters will depend directly on the peak fwhm, suitable values in general would be integers which are close to satisfying U = fwhm, $W = 2 \times$ (fwhm). The examples chosen are representative of an x-ray energy spectrum recorded at 20 eV/channel where peak fwhm = 150 eV and 0.25 channel corresponds to a shift of 5 eV.

It is obvious to question whether there is a better filter than the "top-hat". Zero-area functions based on higher derivatives would suppress more curving backgrounds but with a sacrifice in terms of statistical accuracy. Since the shape of the optimal "top-hat" appears to be closely matched to that of the peak, it is quite possible that a slight improvement in statistical accuracy could be obtained by using a positive Gaussian plus negative constant instead. However, it is not clear why any of the other effects should be markedly reduced and one of the strong arguments in favor of the "top-hat" is that the convolution does not involve a series of multiplications, and sums can be obtained very rapidly using integer arithmetic in a computer.

PRACTICAL APPLICATION

If the intensity ratios are not significantly altered by differential absorption (*3*), the model function, $p_{m,i}$, can consist of the full series of peaks in correct proportion (e.g. $K\alpha_1$, $K\alpha_2$, $K\beta_1$, etc.) which correspond to ionization of one shell of a particular chemical element. In this way, good results can be obtained for severe overlap situations in x-ray spectra which would be impossible to resolve accurately using a single peak for each model. As emphasized above, it is very important that the peak models be accurate in any least-squares fitting procedure. Although peaks can be modeled with suitable analytical functions, it can be much simpler to use experimentally-obtained peak profiles directly for each peak model (*12*). In electron microprobe analysis, this is accomplished by storing reference spectra from standards which contain sufficiently few elements so that the series of peaks for an element of interest can be isolated from the rest of the spectrum. There is an added benefit because absorption steps, while they are not exactly proportional to peak heights, do depend on them so the influence of steps will be canceled out to a large extent when stored standard spectra are used for models.

Despite the many possible causes of error, it is still desirable to have some estimate of the statistical error in each result but the evaluation of Equation 14 can be extravagant in terms of both memory storage and computer time when several peaks are involved. If $p_{n,i}'$ is approximated by $p_{n,i}'W_i'$, and σ_{ii}^2 is approximated by $y_i \Sigma h_k^2$ (Equation 3), then Equation 14 can be reduced (F. H. Schamber, personal communication) to give

$$\sigma_{c_m}^2 \simeq a_{mm}^{-1} \cdot \frac{(2M+1)\cdot(2N)}{(2M+1+2N)} \qquad (17)$$

which is easy to compute when the inverse matrix A^{-1} is available. This approximation has been tested for a two-peak deconvolution (fwhm = 7.5) over a range of peak separations from 1 to 24 channels using the filter suggested above ($M = 3, N = 4$). The variance estimate was always within a range of +67% to −40% of the correct value and thus appears to be a useful approximation.

DISCUSSION

The author's program has been used for electron microprobe analysis at the Department of Mineralogy and Petrology, Cambridge University, and difficult overlap situations such as that involving the titanium K series and barium L series peaks have been successfully resolved (N. Charnley, personal communication). Furthermore, Schamber (*6*) summarizes published literature which quotes results of x-ray analyses that have been performed using the prefiltering technique. Since the dimensions of the optimal "top-hat" fortuitously turn out to be close to those suggested on empirical grounds in (*3*) and (*6*), the above evidence can be included as experimental verification of the technique.

The prefiltering technique is as effective as subtracting a piece-wise linear approximation of the background from the spectrum and, just as in the iterative-stripping approach, one can expect to see systematic errors of the order of 0.3% concentration by weight in electron microprobe analysis for elements with peaks at low energies where background curvature is severe. Methods based on theoretical prediction are potentially capable of higher accuracy but the form of the continuum at low energies (<2 keV) is not yet fully understood and great care must be taken to eliminate all spurious instrumental contributions to the observed background (*1, 2*). Since the prefiltering method does not make any assumptions about the exact nature of the background shape, it is insensitive to any smooth spectral artifact such as pile-up continuum or the spectrum from backscattered electrons which penetrate the detector window, and can be applied to a wide variety of spectra.

LITERATURE CITED

(1) P. J. Statham, *X-Ray Spectrom.*, **5**, 154–168 (1976).
(2) P. J. Statham, Proc. 11th Ann. Conf. Microbeam Analysis Society, Miami Beach, Fla., 1976, 10A–10I.
(3) P. J. Statham, *X-Ray Spectrom.*, **5**, 16–28 (1976).
(4) P. J. Statham, Ph.D. Thesis, University of Cambridge, England, 1975.
(5) G. Brouwer and J. A. J. Jansen, *Anal. Chem.*, **45**, 2239–2247 (1973).
(6) F. H. Schamber, Proc. Symposium on "X-Ray Fluorescence Analysis of Environmental Samples", Chapel Hill, N.C., 1976, T. Dzubay, Ed., Ann Arbor Science Publications, Ann Arbor, Mich., 1977, pp 241–257.
(7) P. G. Guest, "Numerical Methods of Curve Fitting", Cambridge University Press, 1961, pp 253–263.
(8) A. L. Connelly and W. W. Black, *Nucl. Instrum. Methods*, **82**, 141–148 (1970).
(9) A. Robertson, W. V. Prestwich and T. J. Kennett, *Nucl. Instrum. Methods*, 100, 317–324 (1972).
(10) V. Hnatowicz, *Nucl. Instrum. Methods*, **133**, 137–141 (1976).
(11) T. R. Sweatman and J. V. P. Long, *J. Pet.*, **10**, 332 (1969).
(12) F. H. Schamber, Proc. 8th Nat. Conf. of Electron Probe Analysis Society of America, New Orleans, La., 1973, paper 85.

RECEIVED for review June 20, 1977. Accepted September 19, 1977. The author is financed by a N.A.T.O. postdoctoral fellowship provided by the Science Research Council, London, England. Further support was provided by National Institutes of Health Grant GM 17523-05 and E.R.D.A. at Donner Laboratory, Berkeley, Calif.

Quantitative Analyses of Multicomponent Fluorescence Data by the Methods of Least Squares and Non-Negative Least Sum of Errors

I. M. Warner,[1] E. R. Davidson,* and G. D. Christian

Chemistry Department BG-10, University of Washington Seattle, Washington 98195

Quantitative information can be obtained from fluorescent mixtures using the methods of least squares or linear programming, based on previously determined calibrated excitation–emission matrices (EEM) of known components, even in cases of severe overlap and poor signal/noise ratio. The least squares fitting technique was found satisfactory for analysis of a three-component mixture if all components were known. Linear programming, used to minimize the total error with individual errors constrained to be positive, is preferred when not all components are known. Instrument stability is a major limitation of accuracy if slow scanning instruments are used.

In recent years, the trend in analytical spectroscopy has been toward the development of new multicomponent techniques. These techniques have taken form through a parallel growth of new instrumentation designs (*1, 2*) and new data reduction strategies (*3*). The rapid growth and developments in solid-state circuitry indicate that the design of new instrumentation is probably in an embryonic stage at this time and even greater advances are to be expected.

In the area of spectroscopic data reduction, two major types of strategies have been explored: 1) techniques for qualitatively analyzing the data to determine the identity of unknown constituents and 2) techniques for quantitative analysis of known constituents in a mixture. For qualitative data interpretation, many methods such as factor analysis (*4*) and pattern recognition (*5*) have evolved. For quantitative data analyses of multicomponent mixtures, a brief search through the literature indicates that least squares is the usual method of choice. The least-squares method is one of the many "curve fitting techniques" and can vary in usage from simple statistical analysis of data (*6, 7*) to more sophisticated schemes for the analysis of multicomponent systems (*8, 9*). Recently, Leggett (*10*) has discussed the application of non-negative linear least squares to the analysis of multicomponent spectral data. Related topics such as linear and nonlinear least squares (*11*), multiparameter curve fitting (*12*), and weighting factors (*13*) in least-squares analyses have also been discussed.

For the improved analysis of multicomponent fluorescence data, instrumentation (*14*) has been described recently which is capable of rapidly acquiring the emission–excitation matrix (EEM), **M**, whose elements M_{kl} are the relative numbers of photons emitted at wavelengths λ_l by a solution illuminated with light of wavelengths λ_k. For a single emitting species, M is given approximately by

$$M_{kl} = \alpha x_k y_l \tag{1}$$

In this equation, x_k is a scalar proportional to the relative fraction of photons absorbed at λ_k and y_l is a scalar proportional to the relative fraction of photons emitted at λ_l. The constant, α, contains all of the concentration dependent terms of the matrix, **M**.

If we assume that the absorbance is small (≤0.01) at all monitored wavelengths, then for a mixture of "r" components, **M** has the form

$$\mathbf{M} = \sum_{i=1}^{r} \alpha_i \mathbf{x}^i \mathbf{y}^i \tag{2}$$

where the i's serve to denote the various components of the mixture.

Recent studies (*15*) have shown that analysis of the emission–excitation matrix through the eigenvalues and eigenvectors of $\mathbf{MM}^T$ and $\mathbf{M}^T\mathbf{M}$ produces distinct advantages for qualitative analysis which cannot be realized via single wavelength measurements. Other studies (*14*) have shown through simulated data that quantitative analysis of multicomponent mixtures using the emission–excitation matrix should provide useful results.

This paper provides two systematic approaches to the quantitative analysis of a multicomponent emission–excitation matrix using as a basis the previously determined calibrated EEM of known components. In the case where all of the components are known, it is reasonable to use a least-squares fitting technique to derive the concentration of each component. An alternative approach is explored using linear programming to impose linear constraints to obtain the concentration of each component.

Least Squares Analysis. Since in routine quantitative analyses in the chemical laboratory the components are all specified but the amounts are unknown, Equation 2 can be represented as

$$\mathbf{M} = \sum_i c_i (\mathbf{M})_i \tag{3}$$

where $(\mathbf{M})_i$ is the standard matrix produced by species i and c_i is its concentration divided by its standard concentration. Then the best approximation to **M**, in the least-squares sense, requires that the weighted sum of the squares of the elements of the error matrix, **E**, be a minimum. That is if

$$E_{kl} = M_{kl} - \sum_i c_i (M_{kl})_i$$

then

$$\sum E_{kl}^2 T_{kl} = \min \tag{4}$$

where the T_{kl} values represent weighting factors. Differentiation of Equation 4 gives the least squares condition

$$\sum_j \left[\sum_{kl} T_{kl} (M_{kl})_i (M_{kl})_j\right] c_j = \sum_{kl} T_{kl} (M_{kl})_i M_{kl} \tag{5}$$

where M_{kl} is a matrix element of the observed EEM, and $(M_{kl})_i$ and $(M_{kl})_j$ are matrix elements of the standard EEM's for the ith and jth components.

[1] Present address, Department of Chemistry, Texas A&M University, College Station, Texas 77840.

Non-Negative Least Sum of Errors. If not all of the components are known, the analysis is more difficult. Suppose, for example, that the rank of **M** is large but only the standard spectrum $(\mathbf{M})_1$ is known. Then the most one can say is

$$M_{kl} - c_1(M_{kl})_1 \geq 0 \text{ for all } kl$$

or

$$0 \leq c_1 \leq \min_{kl} [M_{kl}/(M_{kl})_1] \tag{6}$$

If there is any frequency at which this molecular species is the only emitter, then $\min_{kl}[M_{kl}/(M_{kl})_1]$ will actually equal c_1. Similarly, if two components' spectra are known and r is large,

$$M_{kl} - c_1(M_{kl})_1 - c_2(M_{kl})_2 \geq 0 \tag{7}$$

or

$$0 \leq c_1 \leq \min_{kl} \{[M_{kl} - c_2(M_{kl})_2]/(M_{kl})_1\} \leq \min_{kl} [M_{kl}/(M_{kl})_1]$$

and

$$0 \leq c_2 \leq \min_{kl} \{[M_{kl} - c_1(M_{kl})_1]/(M_{kl})_2\} \leq \min_{kl} [M_{kl}/(M_{kl})_2] \tag{8}$$

Again, under favorable conditions, these relations may actually give the values of c_1 and c_2.

Linear programming is a well-established method for optimization in the presence of such linear inequalities, and any one of many excellent monographs (*16*) can be consulted on the general theory of the technique. The simplex tableau (*16*) is one algorithm for locating the maximum of a linear combination of unknown variables, subject to linear constraints (equalities or inequalities) that restrict the permissible values of the variables. Suppose, for instance, that we have a mixture of "R" components of unknown concentrations and that we know the standard EEM of only "r" of them ($r \leq R$). Then as in Equations 6 and 7 we can write a set of constraining equations to express the fact that the residual error should be non-negative as

$$E_{kl} = M_{kl} - \sum_i c_i(M_{kl})_i \geq 0 \tag{9}$$

where the symbols are as defined for Equation 4. An inequality constraint of this form can be written for each value of k and l. Thus, for a K by L matrix, "K times L" equations can be written. Then the problem is to maximize the expression

$$\Gamma = \sum_{i=1}^{r} A_i c_i \tag{10}$$

subject to the constraints of Equation 9 and the additional constraint that $c_i \geq 0$. The A_i coefficients of the c_i's must be a set of positive weights such that Γ is maximum for the "correct" choice of the c_i. The procedure used here has been to sum the elements of the constraining equations so that

$$A_i = \sum_{kl} (M_{kl})_i T_{kl} \tag{11}$$

Then $\sum E_{kl}T_{kl} = \sum M_{kl}T_{kl} - \Gamma \geq 0$ so a maximum Γ corresponds to minimum total error.

There are two serious difficulties with this approach. The first is that, in practice, it is not practical to apply linear programming methods to very large sets of inequalities. A "50 by 50" matrix would generate 2500 inequalities, which is computationally impractical as a routine analysis procedure. Hence, the set of inequalities must be truncated somehow.

The second difficulty is shared with non-negative least squares, which minimizes the objective function $\sum_{kl}E_{kl}^2T_{kl}$ rather than $\sum_{kl}E_{kl}T_{kl}$, subject to the same inequalities given above. Because the minimum, in either case, will often occur at the same vertex of the convex polytope defined by the linear inequalities, non-negative least total error and least-square error should give comparable results, although the work involved in finding the solution may be different. As illustrated by Equation 6 or 8, the concentration is quite likely, in practice, to be determined by a single ratio $M_{kl}/(M_{kl})_1$. In the region of low signal, this ratio is essentially a random number so the minimum ratio is likely to be produced by a low random fluctuation. Thus, it is essential in any non-negative error approach to use only regions of the matrices with good signal/noise ratios. As will be discussed in the Experimental section, this was accomplished by using only regions of maximum signal to generate inequalities.

Errors in the Least-Squares Calculated Concentrations. Since the data to be analyzed by Equation 5 will contain experimental error, there will be some error associated with the calculated c_i's. It is therefore desirable to calculate the degree of reliability of the least squares calculated c_i's. Techniques have been previously described (*17*) for calculation of the variance of each c_i assuming no error in the standard spectra and only error in the mixture spectra. Since this assumption is clearly incorrect for most analytical data, it is desirable to derive new formulas for calculating the variance of the c_i's. For "r" number of components, Equation 5 can be expressed in matrix notation as

$$\mathbf{WC} = \mathbf{P} \tag{12}$$

where **W** is an $r \times r$ matrix and **C** and **P** are $r \times 1$ matrices. Then the unique variance of c_i, contributed by the uncertainty in the experimentally determined mixture matrix is given by

$$\sigma^2_{\text{mix}}(c_i) = \sum \left(\frac{\partial c_i}{\partial M_{kl}}\right)^2 \sigma^2(M_{kl})$$

or

$$\sigma^2_{\text{mix}}(c_i) = \sum_{kl} T^2_{kl}(V_{kl})_i^2 \sigma^2(M_{kl}) \tag{13}$$

$$(V_{kl})_i = \sum_r W^{-1}_{ir}(M_{kl})_r$$

where $\mathbf{W}^{-1}$ is the inverse of **W** in Equation 12 and $\sigma^2(M_{kl})$ is the estimated variance of the klth element of the mixture matrix. The other terms are as defined previously for Equation 5. The unique variance contributed by the uncertainty in the standard matrices can be shown to be given by

$$\sigma^2_{\text{std}}(c_i) = \sum \left(\frac{\partial c_i}{\partial (M_{kl})_j}\right)^2 \sigma^2(M_{kl})_j$$

or

$$\sigma^2_{\text{std}}(c_i) = \sum_{kl} T^2_{kl} \sum_j [E_{kl}W^{-1}_{ij} - (V_{kl})_i c_j]^2 \sigma^2(M_{kl})_j \tag{14}$$

where $\sigma^2(M_{kl})_j$ is the estimated variance of the klth element of the jth standard and the other terms are as defined previously. The total variance of the calculated c_i's is then given by

$$\sigma^2_{\text{total}}(c_i) = \sigma^2_{\text{mix}}(c_i) + \sigma^2_{\text{std}}(c_i) \tag{15}$$

Data Weighting. Frequently in analytical measurements, the degree of uncertainty varies with the magnitude of the datum. In those cases, it is often found advantageous to give certain data a higher degree of importance than others in determining the least-squares fit to the data set. This is termed "weighting" the data. It is important to correctly

determine the weighting factors since different weights will give different answers. For photon limited noise, the weights are usually the inverse of the magnitude of the signal (*13*). In the results presented in this paper, weight factors of unity were used since comparable results were obtained with all weighting schemes.

EXPERIMENTAL

Apparatus. For the study of the various porphyrin mixtures, the computerized fluorometer previously described (*15*) was used. The data were acquired using an RCA 8852 photomultiplier detector in the photon counting mode. Standard EEM's were obtained from prepared samples of known concentrations in 6-nm intervals over a wavelength range in excitation of 470 to 644 and 550 to 724 nm in emission unless otherwise stated. Mixture EEM's were run under conditions as close to those of the standard samples as possible. The total absorbance at all wavelengths of interest was kept below 0.01.

Data Analysis. The quantitative data reduction part of a Fortran IV coded program written for the CDC-6400 and based on the least-squares and simplex tableau algorithms presented in this paper was used for data analysis.

The raw data from the fluorometer include scattered light and dark current, and so are not in the form assumed in Equation 3 since these additional sources of signal are independent of concentration. Hence, a blank sample was run and subtracted in order to obtain the EEM. Because the major source of noise in the above apparatus comes from photon statistics, the EEM has its largest random errors in the stray light region. Since drift in the photomultiplier tube was suspected, the blank was multiplied by a constant to give a best fit to the regions of the EEM containing only dark current and scattered light.

It is anticipated that in the future it will be possible to build a data bank of standard spectra. This will require considerable data compression. For one component solutions, the factorization shown in Equation 1 offers a convenient means to reduce the data from a square array to two vectors. Consequently, for most of our analyses the standard matrices were eigenanalyzed to give the best rank one approximation of the form 1, as described in reference *15*. This rank one matrix was treated as the standard matrix of the pure component.

The linear programming calculation was accomplished using a standard simplex tableau algorithm package from the Boeing Mathematical Library at the University of Washington computer center. Rather than use the entire 900 data points, various regions of the matrices were selected (five from each standard spectrum) to define the constraining equations of Equation 9. Thus, for the one-, two-, and three-component systems, five, ten and fifteen constraining equations were used, respectively. In this case where only a small number of constraining equations are used, noise in the data could produce results which are more in error than the least-squares results. To minimize this effect, each constraining equation was obtained by a summation of 25 neighboring points. This was achieved by dividing each standard matrix into 5 × 5 submatrices. The twenty-five points in each submatrix were summed to produce a total of 36 possible coefficients in Equation 9 for a 30 × 30 matrix (100 for a 50 × 50 matrix). The five most intense regions from each standard were used to obtain the desired number of constraining equations. This procedure selected regions of maximum signal/noise and reduced the wild fluctuations which would be produced by applying Equation 9 in a region where **M** was entirely determined by noise.

Reagents. The porphyrin compounds used for sample preparation were provided by the research group of Martin Gouterman, Department of Chemistry, University of Washington. Stock solutions were prepared using spectral grade pyridine as solvent. All samples were prepared by dilution from the same stock solutions.

DISCUSSION

Least-Squares Analysis. Three sets of experiments were run corresponding to mixtures of one-, two-, and three-component systems. The first experiment was designed to show the linearity of the fluorescence intensity. Five solutions of free base octaethylporphin (H_2OEP) were prepared at various concentrations. Figure 1(a) shows an isometric projection of the EEM for a typical concentration before subtraction of the blank. The matrices were obtained over the intervals shown in 6-nm increments giving a total of 900 data points in each matrix. The rank one spectrum reconstructed by Equation 1 with dark current and scattered light removed is shown in Figure 1(b) and was chosen to be the standard sample and was fitted to the other matrices. Results are shown in Table I along with the input concentrations. The correlation coefficient of calculated concentration vs. volumetrically determined concentration was 0.9997. These results indicate that the fluorescence is linear and reabsorption and quenching processes are negligible.

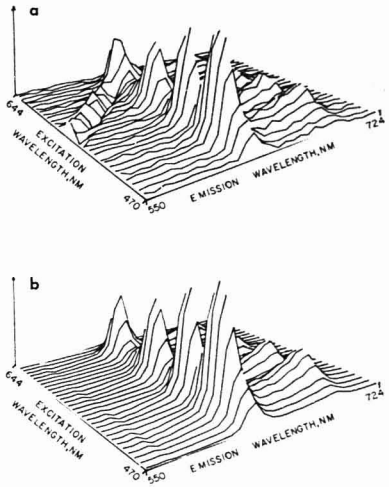

Figure 1. (a) EEM for a 5.52 × 10^{-7} M solution of H_2OEP. (b) Rank one EEM with scattered light and dark current removed

Table I. Least-Squares and Linear Programming Analysis of Experimentally Acquired Single Component (H_2OEP)

True concn, 10^{-7} M	Least-squares concn, 10^{-7} M[a]	Estimated std dev	Simplex concn, 10^{-7} M[a]
1.51	1.43	0.04	1.30
2.76	2.79	0.18	2.58
5.52	5.52	0.10	5.40
11.00	11.10	0.60	10.58

[a] Calculated using the spectrum of a 5.52 × 10^{-7} M solution as standard.

The second system analyzed was a mixture of free base octaethylporphin (H_2OEP) and free base tetraphenylporphin (H_2TPP). There is significant overlap between these two components in both excitation and emission. This mixture is clearly an excellent test for the least squares algorithm. Figures 2(a)–(b) show the standard matrices for H_2TPP and the mixture matrix with the dark current and most of the scattered light subtracted. There clearly remains a large photon noise component in the scattered light section of the mixture matrix. Least-squares fitting the standard matrices to the mixture sample gave the results shown in Table II. Comparison to the known concentrations of H_2OEP and H_2TPP shows the errors are 0.8% and 7%, respectively. These results are clearly satisfactory when one considers that each matrix required 20 minutes to acquire. Dark current drift

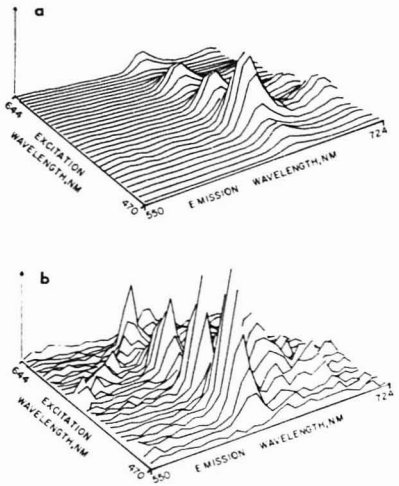

Figure 2. (a) Rank one H_2TPP standard EEM. (b) Mixture matrix (H_2OEP plus H_2TPP) with scattered light subtracted (data collected at 6-nm increments)

Table II. Least-Squares and Linear Programming Analysis of Experimentally Acquired Binary Mixture of H_2OEP and H_2TPP

Component	True concn, 10^{-7} M	Least-squares concn, 10^{-7} M[a]	Estimated std dev	Simplex concn, 10^{-7} M[a]
H_2OEP	6.21	6.26	0.19	5.96
H_2TPP	5.76	6.16	0.24	5.72

[a] Calculated using the spectrum of a 6.21×10^{-7} M H_2OEP solution and of a 5.76×10^{-7} M H_2TPP solution as standards.

Table III. Least-Squares and Linear Programming Analysis of Experimentally Acquired Ternary Mixture of H_2OEP, $SnCl_2OEP$, and ZnOEP

Component	True concn, 10^{-7} M	Least-squares concn, 10^{-7} M[a]	Estimated std dev	Simplex concn, 10^{-7} M[a]
H_2OEP	2.42	2.46	0.02	2.38
ZnOEP	21.4	21.6	0.5	21.0
$SnCl_2OEP$	3.04	3.44	0.23	3.22

[a] Calculated using the spectrum of a 4.83×10^{-7} M H_2OEP solution, a 2.14×10^{-6} M ZnOEP solution, and a 6.07×10^{-7} M $SnCl_2OEP$ solution as standards.

and lamp fluctuations would be expected to affect the results obtained over such a time period. The video fluorometer described in reference 2 could acquire the same data in 16.7 ms, thus negating the effects of dark current drift and lamp fluctuations.

A three-component system of zinc octaethylporphin (ZnOEP), tin(IV) dichlorooctaethylporphin ($SnCl_2OEP$) and H_2OEP was analyzed. Isometric projections of the rank one standard matrices are shown in Figure 3(a)–(c). A similar projection of the mixture matrix with scattered light and dark current removed is shown in Figure 3(d). These matrices were analyzed over the wavelength ranges of 450 to 646 nm in excitation and 550 to 746 nm in emission. Data were obtained in 4-nm increments, producing a 50 × 50 matrix of 2500 data

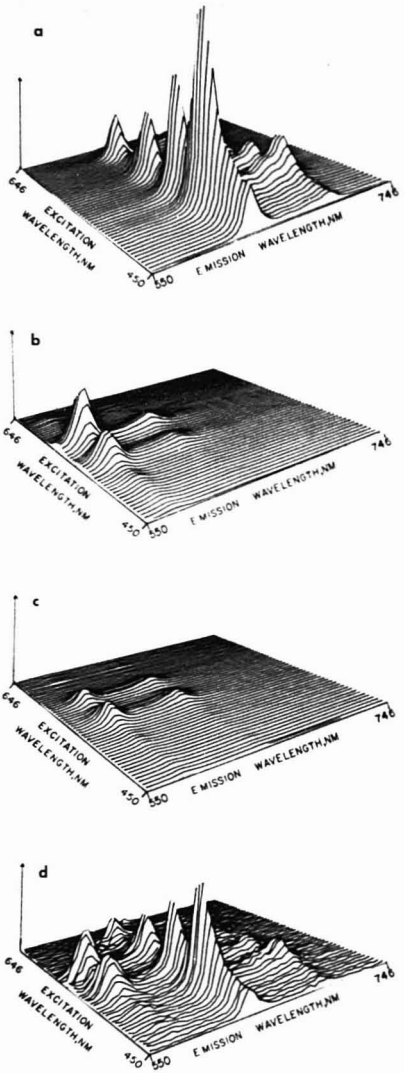

Figure 3. (a) Rank one H_2OEP standard EEM. (b) Rank one ZnOEP standard EEM. (c) Rank one $SnCl_2$ OEP standard EEM. (d) Mixture with scattered light removed (data collected at 4-nm increments

points. Results of the least squares analysis of this mixture are given in Table III. The calculated concentrations for ZnOEP and H_2OEP were satisfactory, but the $SnCl_2OEP$ concentration was 13% in error.

It might be thought that the 13% error in the three-component system described above could be attributed to the overlap between ZnOEP and $SnCl_2OEP$. These components differ by only 3 or 4 nm in excitation. When one considers that the resolution of the data is only 4 nm, this is a significant

Table IV. Least-Squares and Linear Programming Analysis of Experimentally Acquired Ternary Mixture of H_2OEP, H_2TPP, and ZnOEP

Component	True concn, 10^{-7} M	Least-squares concn, 10^{-7} M[a]	Estimated std dev	Simplex concn, 10^{-7} M
H_2OEP	6.21	6.55	0.25	6.35
H_2TPP	5.76	7.35	0.31	6.22
ZnOEP	3.00	4.26	0.21	3.91

[a] Calculated using the spectrum of a 6.21×10^{-7} M H_2OEP solution, a 5.76×10^{-7} M H_2TPP solution, and a 3.00×10^{-7} M ZnOEP solution as standards.

overlap. Consequently, another three-component system with significantly less overlap was analyzed over the same wavelength range and resolution as the one- and two-component systems described above. The ternary system analyzed was a mixture of H_2TPP, ZnOEP, and H_2OEP. The results of the least-squares fit and the estimated error are shown in Table IV. In spite of reduced spectral overlap, this system gave worse results than the previous one.

The effect of the reduction of the standard matrices to rank one was examined by using the original data (with blank subtracted) in the analysis. The results were somewhat worse, because of the larger noise in the raw data, but did show that the factorization of the standard matrices was not a significant source of error.

It was also conceivable that the problem in the mixture samples was energy transfer or reabsorption. However, one noticeable conclusion from the least-squares analyses was that the three-component results were always high. If energy transfer was a serious problem, one would expect that one component would be lower than expected while another would be high. Similarly, for reabsorption, one would expect lower results. Therefore, the deviations of the apparent concentrations from the true concentrations cannot be readily explained through non-ideality of the fluorescence process. Rather, the deviations can be better explained by some systematic fluctuation in the instrumentation, such as dark current drift. Use of the algorithms with a video fluorometer have produced improved accuracy (*18*). Since a video fluorometer is subject to less instrumental drift over the time period of the analysis, this lends further support to the conclusion that the deviations encountered above are primarily a function of instrumental fluctuations.

Linear Programming Analysis. The one-, two-, and three-component systems described above were also analyzed by the linear programming techniques described by Equations 9 and 10. Results of the analyses are shown in Table I, II, III and IV. For the one- and two-component examples, the simplex method gave larger errors than the least-square result and was systematically low. For the three-component systems where the least squares worked less well, the simplex procedure appears to be better. If, however, because of the bad data the least-squares results were assumed to represent the best possible analysis (i.e., the data do not obey Equation 3), then the linear programming results would be low in this case as well.

We found that, in the cases where all components are not specified, this selection of inequalities along with the simplex tableau technique usually gave better results than the least squares. To illustrate, we report results for the two-component system of H_2OEP and H_2TPP assuming only a single component. Then, since there is overlap between the two components, the results of the least-squares analyses assuming only one component are expected to be high. Table V gives the results of this experiment. The least-squares method gave results 11% high while the linear programming method produced results only 3% low. A non-negative residual method is better than least squares in this example when all components are not known.

Table V. Least-Squares and Linear Programming Analysis of Experimentally Acquired Binary Mixture of H_2OEP and H_2TPP, Assuming Only H_2OEP Present

Component	True concn, 10^{-7} M	Least-squares concn, 10^{-7} M[a]	Estimated std dev	Simplex concn, 10^{-7} M
H_2OEP	6.21	6.89	0.32	6.02

[a] Standard is the same as in Table II.

CONCLUSIONS

The experimental results show that it is feasible to analyze the emission–excitation matrix quantitatively and determine the concentrations of known components both by the method of least squares and by linear programming. It was demonstrated that quantification is possible even in cases of severe overlap and poor signal/noise ratio. The major limitation on the reliability of the results appears to be the reproducibility of the instrumentation. Missing information regarding some of the components present also strongly affects the least-squares analysis of the other components.

ACKNOWLEDGMENT

The authors gratefully acknowledge the technical assistance of F. Kampas and M. Gouterman in the use of their computerized fluorometer which allowed the acquisition of experimental data for analysis. The porphyrin compounds were kindly provided by M. Gouterman. Finally, we thank J. VanZee for his invaluable assistance in transmitting data to the larger computer and writing the UW/FOCAL language.

LITERATURE CITED

(1) T. C. O'Haver and W. M. Parks, *Anal. Chem.*, **46**, 1886 (1974).
(2) I. M. Warner, J. B. Callis, E. R. Davidson, M. Gouterman, and G. D. Christian, *Anal. Lett.*, **8**, 665 (1975).
(3) T. Hirschfeld, *Res./Dev.*, **27**, 20 (1976).
(4) E. R. Malinowski and M. McCue, *Anal. Chem.*, **49**, 284 (1977).
(5) B. R. Kowalski, *Anal. Chem.*, **47**, 1152A (1975).
(6) P. N. Rowe, *Chemtech.*, **4**, 9 (1974).
(7) G. R. Cornish, *Chem. Ind. (London)*, **7**, 317 (1973).
(8) J. C. Sternberg, H. S. Stillo, and R. H. Schwendeman, *Anal. Chem.*, **32**, 84 (1960).
(9) L. Meites, *Anal. Chim. Acta*, **74**, 177 (1975).
(10) D. J. Leggett, *Anal. Chem.*, **49**, 276 (1977).
(11) B. Musulin, *J. Chem. Educ.*, **50**, 79 (1973).
(12) T. Meites and L. Meites, *Talanta*, **19**, 1131 (1972).
(13) D. E. Sands, *J. Chem. Educ.*, **51**, 473 (1974).
(14) I. M. Warner, J. B. Callis, E. R. Davidson, and G. D. Christian, *Clin. Chem. (Winston-Salem, N.C.)*, **228** 1485 (1976).
(15) I. M. Warner, J. B. Callis, G. D. Christian, and E. R. Davidson, *Anal Chem.*, **49**, 564 (1977).
(16) B. Noble, "Applied Linear Algebra", Prentice-Hall, Englewood Cliffs, N.J., 1969.
(17) A. Ralston, "A First Course in Numerical Analysis", McGraw-Hill Book Company, New York, N.Y., 1965, p 247.
(18) D. W. Johnson, personal communication, 1977.

RECEIVED for review June 28, 1977. Accepted September 6, 1977. This work was supported in part by NIH grant 1R016M22311-01.

Comparison of Experimental and Theoretical Calibration Curves in Solid-Surface Fluorescence Analysis

R. J. Hurtubise

Department of Chemistry, University of Wyoming, Laramie, Wyoming 82071

Scattering coefficient-layer thickness product terms and absorption coefficient-layer thickness product terms were obtained experimentally from aluminum oxide and silica gel chromatoplates using fluoranthene as a model compound. The terms were employed to obtain theoretical fluorescence calibration curves from simplified equations derived from a recent theory on fluorescence densitometry. Experimental fluorescence calibration curves were also obtained and compared to the theoretical calibration curves for ranges of linearity, approximate points of first slope change, and relative fluorescence response in the reflected and transmitted modes. The results indicate that the theory should have applicability in fluorescence thin-layer densitometry.

Solution luminescence analysis is used extensively for the analysis of a variety of samples (*1*). Solid surface luminescence, whereby luminescence is measured as radiation transmitted or reflected from a solid surface, has been used as a precise and accurate analytical technique in areas such as pharmacy, biochemistry, medicine, and pollution studies (*2–7*).

Little work has been done on the theoretical analytical aspects of luminescence reflected or transmitted from solid surfaces. Pollak and Boulton (*8*) used the Kubelka and Munk theory (*9*, *10*) of radiation transfer in scattering media to develop a theory of fluorescence from thin-layer chromatoplates. Pollak (*11*, *12*) further discussed this theory and its potential application to thin-layer chromatography. Goldman (*13*) also used the Kubelka and Munk theory of radiative transfer in scattering media to develop a theory of fluorescence for thin-layer chromatoplates. Neither Pollak and Boulton, nor Goldman gave any experimental data to support their theoretical conclusions.

There is a definite need in solid surface luminescence analysis for a theory that has been substantiated by experimental data. Presently, experimental conditions are determined by trial and error, and empirical calibration curves are used without sound theoretical basis. In this work experimental data were obtained from thin-layer chromatoplates using fluoranthene as a model compound. The data were employed to offer experimental support for the Goldman theory. The Goldman theory was investigated because it is more directly related to the Kubelka and Munk theory. Pollak and Boulton (*8*) and Pollak (*11*) used the Kubelka and Munk theory and an electrical transmission line with resistive parameters as a model simulating the optical behavior of chromatographic media. The data reported are not sufficient to substantiate or refute either theory because much more experimental data will be needed to fully develop a useful theory in solid surface luminescence analysis. However, the data do lend support to the Goldman theory.

EXPERIMENTAL

Apparatus. A Schoeffel SD3000 spectrodensitometer equipped with a SDC 300 density computer (Schoeffel Instruments, Westwood, N.J.) was used in all measurements with a Fisher Recordall series 5000 recorder. The spectrodensitometer contained a high pressure xenon lamp and a miniature quartz-type monochromator that was set at 370 nm for fluorescence excitation or transmission–absorption modes. Ultraviolet cut-off filters were used in both transmission and reflection modes. Wedge monochromators set at 470 nm were employed in the fluorescence reflection and transmission single beam modes. For reflectance measurements the Schoeffel reflectance assembly was adjusted to a constant height above the stage of the instrument. For transmission–absorption measurements, the instrument was zeroed in the double beam mode with the chromatoplate and 7-60 filters (Esco Products, Oak Ridge, N.J.) in the substage filter holder. The filters were used to eliminate fluorescence interference from fluoranthene in absorption measurements. The filters were not used in the measurements with no absorbing component on the chromatoplates (A_0 values). The inlet and exit slits for all fluorescence and transmission–absorption readings were set at 2.0 mm and 3.0 mm, respectively. For two aluminum oxide chromatoplates developed in *n*-hexane, the inlet slit was set at 1.0 mm to obtain A_0 readings.

Reagents. Fluoranthene was purchased from Aldrich Chemical Co., Milwaukee, Wis., and recrystallized from ethanol. Ethanol was distilled before use. Aluminum oxide (Al_2O_3) chromatoplates and silica gel (SiO_2) chromatoplates were obtained from Brinkmann, Westbury, N.Y.

Procedures. For the undeveloped and developed SiO_2 and Al_2O_3 chromatoplates, 5 μL of ethanol standard solutions of fluoranthene were spotted for every spot. Each sample was spotted in duplicate and absorbance and fluorescence values for a given amount of fluoranthene were averaged. The amounts of fluoroanthene spotted are given below. For undeveloped chromatoplates the samples were spotted in two rows. The developed chromatoplates were allowed to develop until the *n*-hexane solvent front reached 10.0 ± 1.0 cm.

Plates 1, 2, 5, 6	0.05 μg, 0.10 μg, 0.15 μg, 0.20 μg, 0.25 μg
Plate 3	0.05 μg, 0.10 μg, 0.15 μg, 0.20 μg, 0.25 μg, 0.30 μg, 0.40 μg, 0.50 μg, 1.0 μg, 2.0 μg
Plates 4, 7, 8	0.025 μg, 0.05 μg, 0.10 μg, 0.12 μg, 0.15 μg, 0.20 μg, 0.25 μg, 0.30 μg, 0.40 μg, 0.50 μg

For some chromatoplates, reliable absorbance values could not be obtained at 0.025 μg; thus these points were not used in the calculations. Fewer spots were used for Plates 1, 2, 5, 6 because these plates were developed with *n*-hexane. The fewer spots ensured that there would not be overlap of spots.

Transmission–absorption data from SiO_2 or Al_2O_3 chromatoplates with fluoranthene adsorbed on them were obtained by zeroing the instrument with the chromatoplate and then obtaining the resulting absorbance from recorder tracings. Average A_0 values were obtained by averaging several A_0 values determined across the chromatoplate. For these measurements the instrument was zeroed initially with a clean chromatographic glass plate with the chromatographic material removed. Fluorescence data in the reflection and transmission modes were obtained by zeroing the instrument initially with the chromatoplate and then measuring peak heights corresponding to fluorescence from recorder tracings.

RESULTS AND DISCUSSION

General Comments. Goldman and Goodall (*14–16*) have described the densitometric application of the absorptiometry

theory of Kubelka and Munk. They based the theory on a one-dimensional approximation to transfer of radiation in scattering media for components on thin-layer chromatoplates that absorb radiation. For fluorescence densitometry Goldman (*13*) took into consideration both excitation and fluorescent radiation in scattering media and obtained two pairs of differential equations. One pair corresponded to absorption of exciting radiation in the transmitted and reflected directions and the other pair corresponded to fluorescent radiation emitted in the transmitted and reflected directions. After further mathematical treatment of the two pairs of differential equations, Goldman arrived at two general equations that encompassed a wide range of fluorescer concentrations. One equation represented fluorescence transmitted through a thin-layer chromatoplate and the other equation fluorescence reflected from the surface of a thin-layer chromatoplate. The complexity of these equations almost necessitates the use of a computer to process experimental data. Goldman presented two simplified equations for very low concentrations of fluorescer at relatively large values of scattering coefficients for exciting and fluorescent radiation. The simplified equations should be of use in chemical analysis because under certain conditions they show a linear relationship between fluorescence and amount of fluorescer adsorbed on a scattering material. The equations are given below and are the ones investigated in this work.

$$I^+/i_0\alpha = {}^1/_3\ kX(1\text{-}7/30\ sX\cdot kX) \quad (1)$$

$$J^+/i_0\alpha = {}^2/_3\ kX(1\text{-}4/30\ sX\cdot kX) \quad (2)$$

Where I^+ = transmitted fluorescence, i_0 = initial exciting intensity, α = the proportion of absorbed radiation converted into fluorescence, k = absorption coefficient of exciting radiation, s = scattering coefficient of exciting radiation, X = thickness of the scattering medium, and J^+ = reflected fluorescence.

In Equations 1 and 2, the scattering coefficient for fluorescent radiation does not appear because of mathematical approximations. For Goldman's more complex equations, he assumed the scattering coefficient of exciting radiation was equal to the scattering coefficient of fluorescent radiation for graphs of both I^+ and J^+ vs. kX. The term kX is proportional to the amount of absorbing compound in the exciting beam (*15*).

Several assumptions that were made in deriving the equations in the Goldman theory follow: (a) the exciting light beam is parallel and normal to the absorbing component on the thin-layer chromatoplate; (b) the reflections and absorptions occur at infinitesimal distances and are constant over the frequency range of exciting radiation, the area illuminated by the exciting radiation, and the depth of the absorbing component; (c) the exciting and fluorescent radiation travel in the chromatoplate only in the directions perpendicular to the surfaces of the chromatoplate; (d) the chromatographic material does not absorb the exciting radiation.

Experimental Values of kX and sX. Because X always appears in either kX or sX in Equations 1 and 2, it was not necessary to determine X in this work but only sX and kX. The factor sX was calculated with the following equation (*9*), $T_0 = 1/(sX + 1)$ where T_0 is the transmission of the chromatoplate when kX is zero. T_0 was calculated from the equation, $A_0 = \log 1/T_0$ and A_0 was determined experimentally. The A_0 values for the two developed Al_2O_3 chromatoplates were obtained at an inlet slit setting of 1.0 mm. The A_0 values were somewhat dependent on the inlet slit setting. For example, for Al_2O_3 plate 2, average A_0 values of 0.98 and 1.07 were obtained at inlet slit settings of 1.0 mm and 1.5 mm, respectively. However, the A_0 values obtained across the chromatoplates generally varied at least this much especially with Al_2O_3 chromatoplates. All but two A_0 values were determined at a constant inlet setting of 2.0 mm. The variation of A_0 across the chromatoplates is considered a fundamental limitation of the systems studied. One of the main purposes of this study was to use a commercial instrument and chromatoplates to establish their capability to obtain acceptable data. More homogenous chromatoplates and possibly more sophisticated instrumentation would be needed to obtain highly accurate data.

The kX values for fluoranthene were calculated by successive approximations with a programmable calculator using the general Kubelka and Munk equation for transmission in scattering media (*9*, *15*), which is given below.

$$T = \frac{b}{a \sinh (bsX) + b \cosh (bsX)}$$

T = transmittance of a chromatoplate with an absorbing material in the scattering medium

$$a = \frac{s + k}{s} = \frac{sX + kX}{sX}$$

$$b = (a^2 - 1)^{1/2}$$

It would be ideal to express kX simply in terms of T and sX; however, this is quite complicated theoretically. In this work T was calculated from the equation, $A = \log 1/T$, where A is equal to A_0 plus the experimental absorbance for fluoranthene. The term sX was calculated as described above. Using successive approximations to obtain kX was a relatively simple operation.

It was assumed that the chromatographic material did not absorb exciting radiation. Goodall (*17*) showed that chromatographic material such as silica gel and aluminum oxide absorb very weakly at 340 nm. The excitation wavelength used in this work was at 370 nm. For the situation where chromatographic material would absorb exciting radiation, the absorption would have to be taken into consideration. Polycyclic aromatic hydrocarbons and nitrogen heterocycles are two classes of compounds that generally absorb at wavelengths greater than 340 nm and are fluorescent. The results in this work should be applicable to these two important classes of compounds and other classes.

Calculation of $I^+/i_0\alpha$ and $J^+/i_0\alpha$. Once sX and kX were obtained, it was possible to calculate $I^+/i_0\alpha$ and $J^+/i_0\alpha$ from Equations 1 and 2. With these values and the corresponding kX values, theoretical calibration curves were plotted for reflected and transmitted fluorescence. Experimental fluorescence calibration curves were obtained for fluoranthene in the transmission and reflection modes and several comparisons were made with the theoretical curves. One comparison was the microgram values at which the theoretical curves and experimental curves approximately first changed slope. These values were obtained at the point of intersection of two extrapolated straight lines that were tangent to the two major portions of the calibration curves (Figures 1 and 2). The kX values from the theoretical calibration curves were converted to microgram values and the comparisons are shown in Table I. The data were obtained for fluoranthene on developed and undeveloped aluminum oxide and silica gel chromatoplates. This was done to see if the chromatographic conditions had any influence on the reflected or transmitted fluorescence. The data show fairly good comparison between theoretical and experimental values for both developed and undeveloped chromatoplates whether the fluorescence was measured in the transmitted or reflected modes. The results indicate with the conditions employed in this work that Goldman's simplified equations can be used to predict approximately when a calibration curve first changes slope in

Table I. Comparison of Theoretical and Experimental Approximate Points of First Slope Change in Terms of Microgram of Fluoranthene

					Transmitted fluorescence						
	Developed Al_2O_3			Undeveloped Al_2O_3			Developed SiO_2			Undeveloped SiO_2	
Plate	Theor.	Exptl.	Plate	Theor.	Exptl.	Plate	Theor.	Exptl.	Plate	Theor.	Exptl.
1	0.12	0.17	3	0.15	0.17	5	0.16	0.18	7	0.15	0.18
2	0.12	0.18	4	0.11	0.15	6	0.16	0.20	8	0.18	0.18
					Reflected fluorescence						
1	0.12	0.14	3	0.21	0.15	5	0.16	0.22	7	0.19	0.13
2	0.13	0.15	4	0.16	0.14	6	0.14	0.15	8	0.18	0.16

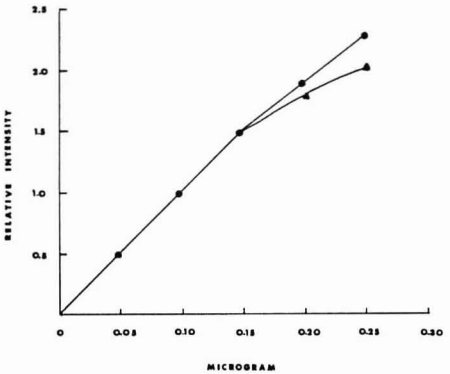

Figure 1. Comparison of experimental (●) and theoretical (▲) calibration curves from developed Al_2O_3 plate 1 in the fluorescence transmission mode

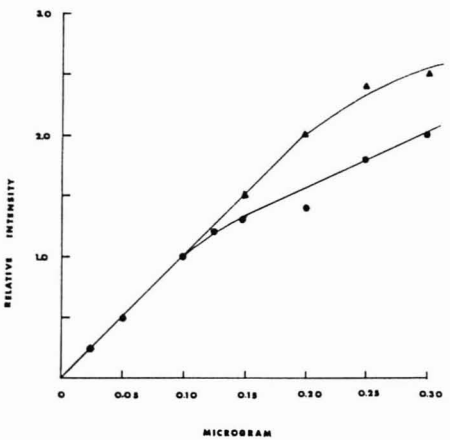

Figure 2. Comparison of experimental (●) and theoretical (▲) calibration curves from undeveloped SiO_2 plate 7 in the fluorescence reflection mode

reflected or transmitted modes with acceptable accuracy. Goldman (*13*), using unsimplified equations for reflected and transmitted fluorescence, made rough graphs of theoretical calibration curves at low fluorescer concentration. He predicted the range of linearity of reflected fluorescence should be approximately twice that obtained by transmission in terms of kX. The data in Table I do not support this conclusion. The simplified Goldman equations used in this work to obtain theoretical calibration curves show that the range of linearity of reflected and transmitted fluorescence in terms of kX are relatively close to one another. The experimental values in Table I support this and show that the range of linearity of reflected and transmitted fluorescence are relatively close.

Table II. Experimental Ratios of Slopes of Calibration Curves of Transmitted Fluorescence to Reflected Fluorescence

Plate	Deveioped Al_2O_3	Plate	Undeveloped Al_2O_3
1	0.39	3	0.26
2	0.36	4	0.51
	Developed SiO_2		Undeveloped SiO_2
5	0.62	7	0.91
6	0.58	8	0.89

Figures 1 and 2 compare two sets of theoretical and experimental calibration curves with their relative intensity values normalized. Normalization was accomplished for the experimental curves by dividing the relative intensity values by the relative intensity value obtained for 0.10 μg fluoranthene. For the theoretical curves the calculated relative intensity values were divided by the calculated relative intensity value for 0.10 μg fluoranthene. The relative intensity values at 0.10 μg were chosen because they were on the linear part of the calibration curves and were considered more accurate than values at lower amounts of fluoranthene. As seen in Figure 1 for an Al_2O_3 chromatoplate the theoretical and experimental curves are superimposable to about 0.15 μg and beyond that they diverge with the experimental curve showing larger relative intensity values per microgram of fluoranthene. Figure 2 shows the theoretical and experimental curves for a SiO_2 chromatoplate. As indicated the two curves are superimposable to about 0.10 μg and then they diverge with the theoretical curve showing larger relative intensity values per microgram of fluoranthene. Both experimental curves change slope and then appear to become linear at higher amounts of fluoranthene. Most of the experimental curves were linear and then changed slope and gradually curved downward. Experimental calibration curves for fluoranthene from 0–2 and 0–4 μg on undeveloped Al_2O_3 chromatoplates showed that the curves became almost parallel with the abscissa at about 1 μg. One important contribution of the Goldman theory, considering the conditions employed in this work, is the capability of predicting approximately when the calibration curve first changes slope. Further work is needed to explain the nonsuperimposability of the curves.

According to Goldman's simplified equations, the theoretical ratio of the slopes of a linear transmitted fluorescence calibration curve to a linear reflected fluorescence calibration curve is 0.50, namely $^1/_3kX/^2/_3kX$. Table II compares the

Table III. kX[a] and sX Values

Plate	Transmission, kX	Reflection, kX	sX	Transmission, 7/30 $sX \cdot kX$	Reflection, 4/30 $sX \cdot kX$
1	0.080	0.066	8.1	0.15	0.071
2	0.086	0.071	8.6	0.17	0.081
3	0.058	0.047	16	0.22	0.10
4	0.0014	0.0013	43	0.14	0.073
5	0.047	0.058	2.9	0.032	0.022
6	0.041	0.031	6.6	0.063	0.027
7	0.048	0.034	4.9	0.055	0.022
8	0.056	0.050	4.4	0.058	0.029

[a] The kX values correspond to the microgram values in Table I.

slopes of the experimental calibration curves obtained in this work. The ratio of slopes for calibration curves obtained for the developed Al_2O_3 and SiO_2 chromatoplates compare favorably with the theoretical ratio. As indicated the experimental ratios for the developed Al_2O_3 are lower than the theoretical ratio of 0.50. The experimental ratios for the developed SiO_2 chromatoplates are higher than the theoretical ratio. This shows that the reflected fluorescence from the Al_2O_3 chromatoplates is relatively greater than the reflected fluorescence from the SiO_2 chromatoplates. The experimental ratio for the undeveloped Al_2O_3 plate 3 was only 0.26. The low value may indicate that the fluoranthene did not penetrate the aluminum oxide chromatoplate to any great extent because with a ratio of 0.26 the reflected fluorescence is substantially greater than the transmitted fluorescence. The ratios for the undeveloped SiO_2 chromatoplates are close to 1. This indicates that the fluorescent signals measured in the reflected and transmitted modes were approximately the same. With the undeveloped SiO_2 chromatoplates, it was observed that the fluorescence of fluoranthene at a given amount was much greater than its fluorescence on the developed SiO_2 chromatoplates. For example, a typical ratio of the slopes of the calibration curves for the undeveloped chromatoplate to developed chromatoplate was 2.27 and 3.51 for reflected fluorescence and transmitted fluorescence, respectively. This suggests that the fluorescence quantum efficiency of fluoranthene is enhanced greatly on undeveloped SiO_2 chromatoplate by an adsorption mechanism, or other mechanisms, different from the one for fluoranthene when it is developed chromatographically and is also worthy of further investigation. Fluorescence emission spectra for fluoranthene on developed and undeveloped SiO_2 chromatoplates showed essentially no change in the shape or fluorescence maxima. Thus, the change in quantum efficiency is not related to spectral shifts. Apparently the fluorescence intensity of fluoranthene is so great and the layer thickness of the chromatoplates is such that signals in the reflection or transmission modes do not show a substantial difference in fluorescence intensity. The thicknesses of the Al_2O_3 and SiO_2 layers were both 0.25 mm. The data suggest that the fluorescence intensity in the reflection and transmission modes is independent over a range of layer thicknesses for strongly fluorescent components. Goldman did not consider these aspects in the development of his theoretical equations and they were not investigated in this work. The simplified equations apparently cannot be used to predict the ratio of relative fluorescence intensities in the transmitted and reflected modes for highly fluorescent components over a certain range of layer thicknesses. More work is necessary to establish the layer thickness dependency of the fluorescent signals.

Table III lists the experimental kX values of fluoranthene when the calibration curves approximately first changed slopes and the experimental sX values for all the chromatoplates. Also, 7/30 $sX \cdot kX$ and 4/30 $sX \cdot kX$ products were calculated using the experimental kX and sX values and appear in Table III. As Equations 1 and 2 indicate, the terms 7/30 $sX \cdot kX$ and 4/30 $sX \cdot kX$ are important in determining the points at which fluorescence transmission and reflection calibration curves become nonlinear and the relative response in the nonlinear region. As discussed earlier the theoretical and experimental calibration curves for a given chromatoplate became nonlinear at approximately the same microgram (or kX) value whether fluorescence is measured in the transmission or reflection modes. Equations 1 and 2 and the data in Table III show that the product 7/30 $sX \cdot kX$ is approximately twice the product 4/30 $sX \cdot kX$. This information in conjunction with Equations 1 and 2 suggests that the relative change in reflected fluorescence intensity after a calibration curve becomes nonlinear should be greater than the relative change in transmitted fluorescence intensity. This was found to be true experimentally; however, it is doubtful whether this region will be useful analytically compared to linear calibration curves and it was not investigated further in this work.

The data in Table III indicate the 7/30 $sX \cdot kX$ and 4/30 $sX \cdot kX$ products for SiO_2 chromatoplates are smaller than the corresponding products for Al_2O_3 chromatoplates. This indicates that the linear range for SiO_2 chromatoplates in terms of microgram (or kX) should be greater than the linear range for Al_2O_3 chromatoplates. Generally, the experimental results in Table I support this whether fluorescence is measured in the transmitted or reflected modes. However, the greater linear range for SiO_2 is not substantial. Exceptions are the experimental value for plate 7 in the reflected fluorescence mode and the theoretical value for plate 3 in the reflected fluorescence mode in Table I. The Kubelka and Munk theory and thus the Goldman theory assume uniform particle size of the scattering medium. The commercial chromatoplates employed probably have a range of particle sizes and more work is needed to determine the magnitude of the effect of particle size as related to the Goldman theory. Kortüm (9) has discussed the dependence of scattering coefficient on particle size and states it is nearly inversely proportional to the average particle size. Table III shows that the sX values for Al_2O_3 plates 1–4 are greater than the sX values for SiO_2 plates 5–9. This suggests that the average particle size for the SiO_2 chromatoplates is larger than the average particle size for the Al_2O_3 chromatoplates. Particle size appears to be a major factor contributing to the smaller 7/30 $sX \cdot kX$ and 4/30 $sX \cdot kX$ products for SiO_2 chromatoplates (Table III).

CONCLUSIONS

More work under a variety of experimental and instrumental conditions is needed to establish the validity of Goldman's equations. However, the results of this work indicate that under certain conditions Goldman's simplified equations can be applied to solid surface fluorescence analysis to predict approximately at what point a calibration curve will become nonlinear and the approximate range of linearity of a calibration curve.

Also the results show that it is more advantageous to measure reflected fluorescence because of the greater relative fluorescence response except in those cases where the fluorescence quantum efficiency and layer thickness are such that reflected fluorescence and transmitted fluorescence give approximately the same response.

LITERATURE CITED

(1) G. G. Guilbault, "Practical Fluorescence: Theory, Methods, and Techniques", Marcel Dekker, New York, N.Y., 1973.
(2) A. P. Shroff and C. J. Shaw, *J. Chromatogr. Sci.*, **10**, 509 (1972).
(3) J. C. Touchstone, "Quantitative Thin-Layer Chromatography", Wiley-Interscience, New York, N.Y., 1973.
(4) E. Sawicki, T. W. Stanley, and W. C. Elbert, *J. Chromatogr.*, **20**, 348 (1965).

(5) G. G. Guilbault, "New Fluorometric Methods of Analysis of Biologically Important Compounds", in *Natl. Bur. Stand. (U.S.), Spec. Publ.*, **378**, Accuracy in Spectrophotometry and Luminescence Measurements, Proceedings of a Conference held at NBS Gaithersburg, Md., March 22-24, 1972.
(6) R. A. Puynter, S. L. Wellons, and J. D. Winefordner, *Anal. Chem.*, **46**, 736 (1974).
(7) R. M. A. von Wandruszka and R. J. Hurtubise, *Anal. Chem.*, **48**, 1784 (1976).
(8) V. Pollak and A. A. Boulton, *J. Chromatogr.*, **72**, 231 (1972).
(9) G. Kortüm, "Reflectance Spectroscopy", Springer-Verlag, New York, N.Y., 1969.
(10) W. W. Wendlandt and H. G. Hecht, "Reflectance Spectroscopy", Interscience Publishers, New York, N.Y., 1966.
(11) V. Pollak, *Opt. Acta*, **21**, 51 (1974).
(12) V. Pollak, *J. Chromatogr.*, **133**, 49 (1977).
(13) J. Goldman, *J. Chromatogr.*, **78**, 7 (1973).
(14) J. Goldman and R. R. Goodall, *J. Chromatogr.*, **40**, 345 (1969).
(15) J. Goldman and R. R. Goodall, *J. Chromatogr.*, **32**, 24 (1968).
(16) J. Goldman and R. R. Goodall, *J. Chromatogr.*, **47**, 386 (1970).
(17) R. R. Goodall, *J. Chromatogr.*, **78**, 153 (1973).

RECEIVED for review July 8, 1977. Accepted October 4, 1977.

Room-Temperature Phosphorescence of Compounds Adsorbed on Sodium Acetate

R. M. A. von Wandruszka and R. J. Hurtubise*

Department of Chemistry, University of Wyoming, Laramie, Wyoming 82071

The room temperature phosphorescence behavior of a number of compounds adsorbed on sodium acetate was investigated. Comparisons of molecular structures and consideration of reflectance, fluorescence, and infrared spectra allowed the postulation of certain molecular criteria for room temperature phosphorescence. The interactions of *p*-aminobenzoic acid with a sodium acetate surface were considered in detail. The adsorption was found to involve the formation of the sodium salt of *p*-aminobenzoic acid on the sodium acetate surface, as well as hydrogen-bonding. Only protic solvents could be used. Room temperature phosphorescence measurements of chemisorbed compounds on sodium acetate provided a novel way of surface area determination. It was also shown that the phosphorescent compounds are adsorbed flatly on sodium acetate. Analytical findings for several compounds are reported.

Room temperature phosphorescence of adsorbed ionic organic molecules was first reported by Roth (*1*) and later by Schulman and Walling (*2*, *3*). Paynter et al. (*4*) put the phenomenon to its first analytical use. The use of a sodium acetate adsorbent in room temperature phosphorimetry was introduced by von Wandruszka and Hurtubise (*5*). They employed it for the determination of *p*-aminobenzoic acid (PABA) in vitamin tablets. The phosphorescence signal of the adsorbed compound was found to be insensitive to moisture, and quantitation was achieved with a spectrodensitometer. The same approach was later applied to folic acid, *p*-hydroxybenzoic acid, and benzocaine (*6*).

In this paper, the use of sodium acetate in room temperature phosphorimetry is extended to yet other compounds. Consideration is also given to the theoretical aspects of the adsorption process. The phosphorescence properties of a variety of compounds adsorbed on sodium acetate were studied. Other surfaces were also investigated. Infrared, reflectance, and fluorescence spectra of adsorbed species, and surface area data for adsorbent and adsorbates were obtained. From the information gathered, generalizations could be made about the molecular requirements of the adsorbed species. A hypothesis for the adsorption process is presented.

EXPERIMENTAL

Apparatus. Phosphorescence measurements were made with a Perkin-Elmer MPF-2A Fluorescence Spectrophotometer and with a Schoeffel SD 3000 Spectrodensitometer as described previously (*5*). Fluorescence spectra were obtained in the same fashion.

Reflectance spectra were obtained with the Schoeffel spectrodensitometer in the double beam mode with a blank adsorbent sample in the reference beam.

The IR spectra were obtained with a Perkin-Elmer 621 Grating Infrared Spectrophotometer.

Reagents. Ethanol was purified by distillation as described by Winefordner and Tin (*7*). Other solvents were reagent grade and used without further purification. PABA was reagent grade and purified by recrystallization from ethanol. *p*-Aminohippuric acid was purified by recrystallization from water and folic acid by recrystallization from benzene. *p*-Aminophenol was purified by washing with ethanol, and terephthalic acid was recrystallized from ethanol. Other compounds were reagent grade and used without further purification.

Procedures. The samples for the reflectance measurements were prepared by addition of ethanolic solutions of the compounds to the adsorbent and subsequent evaporation, as described previously (*5*). The amount of adsorbate used for reflectance spectra was 500 ng on 10 mg adsorbent. The spectra were obtained with the spectrodensitometer and taken point-by-point at 5-nm intervals. For the determination of phosphorescence and fluorescence maxima, 200 ng adsorbate was used on 10 mg adsorbent.

KBr pellets were used for the IR spectra. They were prepared with a Wilks Mini-press. For the spectra of pure compounds, 200 mg KBr was mixed with 8 mg of the compound. For the spectra of adsorbed compounds, 15 mg of the adsorbed system (sodium acetate plus compound) was used with 200 mg KBr. Of these mixtures, 60 mg was used to prepare each pellet. No more than the indicated amount of sodium acetate-adsorbed compound system could be used in a pellet because larger amounts of sodium acetate gave opaque pellets that could not be cleanly separated from the die. The amount of adsorbed compound on the sodium acetate had to be sufficient to be detected in the IR spectra. However, the systems of interest were those that showed room temperature phosphorescence, so too much adsorbate could not be used because the phosphorescence would be quenched. It was found that an amount of adsorbed compound that was 1.0%, by weight, of the sodium acetate adsorbent, satisfied both criteria.

The surface area determination of anhydrous sodium acetate powder was carried out by Quantachrome Corporation, 69 Glen

Table I. Room Temperature Phosphorescence of Compounds Adsorbed on Sodium Acetate

Compounds giving room temperature phosphorescence

Compound	Excitation, nm	Emission, nm	Strength of signal
p-Aminobenzoic acid (PABA)	290	426	very strong
p-Aminobenzoic acid, sodium salt	290	426	very strong
p-Aminohippuric acid	328	448	strong
p-Hydroxybenzoic acid	285	420	moderate
Folic acid	320	465	moderate
5-Hydroxyindoleacetic acid (5-HIAA)	312	510	moderate
5-Hydroxytryptophan (5-HTP)	355	500	moderate
Benzamide of PABA	300	430	weak
3-Methyl-4-aminobenzoic acid	290	430	weak
N,N-Dimethyl-4-aminobenzoic acid	290	430	weak
m-Aminobenzoic acid	290	430	weak
Hydroquinone	285	430	very weak
p-Hydroxymandelic acid	290	420	very weak

Compounds not giving room temperature phosphorescence

Sulfanilic acid	*p*-Aminophenylacetic acid	Isonicotinic acid
Terephthalic acid	*p*-Hydroxycinnamic acid	Gallic acid
p-Aminophenol	*m*-Hydroxybenzoic acid	*p*-Aminophthalic acid
o-Aminobenzoic acid	Aspirin	4-Hydroxy-3-methoxybenzoic acid
Benzoic acid	*p*-Chlorobenzoic acid	3-Hydroxytyramine
Aniline	*p*-Bromobenzoic acid	7-Aminocephalosporanic acid
Benzocaine	*p*-Nitrobenzoic acid	1-Amino-2-naphthol-4-sulfonic acid
N,N-Dimethyl-4-aminobenzaldehyde	Halazone	Isocinchomeronic acid
Sulfanilamide	Phthalic acid	*p*-Aminosalicylic acid
3-(*p*-Hydroxyphenyl)-propionic acid	Potassium acid phthalate	Serotonin
p-Hydroxyphenylacetic acid	Isophthalic acid	Tryptophan
p-Aminobenzyl alcohol	*p*-Toluic acid	Luminol

Cove Road, Greenvale, N.Y., using the BET method.

RESULTS AND DISCUSSION

Low Temperature and Room Temperature Phosphorescence. The room temperature phosphorescence behavior of a number of compounds adsorbed on sodium acetate was investigated (Table I). PABA gave the strongest signal at room temperature, but at 77 K adsorbed samples of *p*-aminohippuric acid and *p*-hydroxybenzoic acid phosphoresced more strongly. A comparison of phosphorescence intensities at room temperature and at liquid nitrogen temperature is given in Table II. The data imply that differences in room temperature phosphorescence intensities are not due to inherent molecular effects, but rather to differences in rigidity of the adsorbed species. PABA appears to be adsorbed most strongly, since it retained relatively the greatest fraction of phosphorescence at room temperature.

Table II. Phosphorescence Intensities of Compounds Adsorbed on Sodium Acetate[a]

Compound	77 K	Room temp.	Room temp/77 K
p-Aminobenzoic acid	1000	333	0.333
p-Hydroxybenzoic acid	1040	48	0.046
3-Methyl-4-aminobenzoic acid	232	29	0.125
N,N-Dimethyl-4-aminobenzoic acid	260	42	0.16
Benzocaine	146	...	...
Terephthalic acid	238	0.9	0.0038
Hydroquinone	38	6.8	0.18
Folic acid	132	43	0.32
p-Hydroxymandelic acid	56	6.5	0.116
p-Aminohippuric acid	1200	262	0.218
5-Hydroxyindoleacetic acid	200	32	0.160
5-Hydroxytryptophan	210	39	0.186

[a] 77 K phosphorescence of PABA arbitrarily set at 1000 units. All compounds 500 ng/10 mg NaOAc.

Molecular Requirements and Experimental Conditions. Consideration of molecular structures in Table I shows that additional ring substituents on PABA negatively affect room temperature phosphorescence. Examples include 3-methyl-4-aminobenzoic acid, where the methyl group attached to the 3 position led to a 11.5-fold reduction in room temperature phosphorescence intensity compared to PABA. It also caused the phosphorescence to be more sensitive to moisture. Prolonged exposure to the atmosphere gave a 2-fold reduction in room temperature phosphorescence of 3-methyl-4-aminobenzoic acid, while the PABA signal was not affected. Compounds in which the substituents led to a total absence of room temperature phosphorescence included *p*-aminosalicylic acid, 4-aminophthalic acid, and 3-methoxy-4-aminobenzoic acid. Benzocaine (ethyl-4-aminobenzoate) gave no room temperature phosphorescence when adsorbed on sodium acetate. The signal for *N,N*-dimethyl-4-aminobenzoic acid was reduced 7.9-fold as compared to PABA (Table II).

These considerations suggest a number of structural requirements for strong adsorption and room temperature phosphorescence of compounds similar to PABA. The presence of the carboxyl group attached to the 1 position appeared to be one requirement for compounds with the benzene nucleus. Compounds lacking this requirement are aniline, sulfanilic acid, and derivatives of benzaldehyde and benzyl alcohol (Table I). They did not show room temperature phosphorescence on sodium acetate. The same was true for most compounds in which the carboxyl group was displaced one or more carbon atoms from the ring. However, *p*-aminohippuric acid was an exception, showing a strong phosphorescence signal. Attached to the 4 position on the ring, an electron-donating, hydrogen-bonding substituent appeared to be necessary. Table I shows several compounds lacking this requirement. The only suitable groups found were amino and hydroxyl groups. Interestingly, isonicotinic acid with nitrogen in the 4 position in the ring system gave no room

Table III. Surfaces Tested for Terephthalic Acid Room Temperature Phosphorescence

Sodium acetate	Sodium adipate
Sodium propionate	Sodium pimelate
Sodium butyrate	Magnesium hydroxide
Sodium valerate	Barium hydroxide
Sodium oxalate	Calcium hydroxide
Sodium tartrate	Lithium acetate
Sodium formate	Quaternary ammonium ion exchange resin (AG 50W-X8, Bio-Rad)

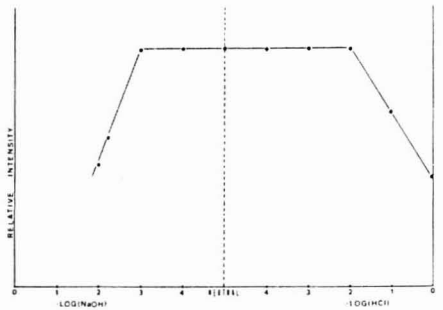

Figure 1. Room temperature phosphorescence intensity of PABA evaporated onto sodium acetate from ethanolic solutions of different acid and base strengths

temperature phosphorescence. All molecules investigated showed low temperature phosphorescence when adsorbed on sodium acetate.

Terephthalic acid, with two carboxyl groups para to each other, was investigated on a number of surfaces (Table III). In no case could more than extremely weak room temperature phosphorescence be detected. Dissolving the compound in an alkaline solution and then evaporating onto the surfaces gave no improvement.

Two compounds with the indole nucleus showed room temperature phosphorescence on sodium acetate, 5-hydroxyindoleacetic acid (5-HIAA) and 5-hydroxytryptophan (5-HTP). The signals were observed only when alkaline ethanolic solutions of these compounds were evaporated on sodium acetate. Both 5-HIAA and 5-HTP were unstable in alkaline solutions and formed green and brown decomposition products, respectively, when left for more than 20 minutes (*8*). These products did not give room temperature phosphorescence. To avoid decomposition, aqueous stock solutions of pH 2 were prepared. Small amounts of these solutions were added to an excess 0.04 N ethanolic NaOH less than a minute before evaporation. No decomposition products were observed in this short period and the systems showed analytically useful room temperature phosphorescence. Tryptophan and serotonin (5-hydroxytryptamine) were treated similarly but did not give room temperature phosphorescence.

The effect of pH on the phosphorescence of PABA adsorbed on sodium acetate was investigated. PABA was dissolved in a series of ethanolic NaOH and HCl solutions and each was evaporated onto sodium acetate. The room temperature phosphorescence intensities obtained are shown in Figure 1. The decrease of the signal in more strongly acid solutions was probably due to protonation of the carboxyl and possibly the amino groups, preventing strong interaction with the sodium acetate surface. In the alkaline solutions, the reduced intensities could be due to precipitation of NaOH upon evaporation. A similar effect was noted when PABA was evaporated onto sodium acetate mixed with sodium hydroxide.

Table IV. Room-Temperature Phosphorescence Characteristics of Ionic Organic Molecules Adsorbed on Sodium Acetate

Compound	Excitation peak, nm	Emission peak, nm	Limit of detection, ng	Linear range of calibration curve, ng
p-Aminohippuric acid	318	448	5	0-140
5-Hydroxyindoleacetic acid	312	510	50	0-200
5-Hydroxytryptophan	320	500	50	0-150

The determination of PABA, using room temperature phosphorescence on sodium acetate has been described in detail (*5*). Analytical results for *p*-hydroxybenzoic acid, folic acid, and benzocaine were reported (*6*). Analytically useful results have now been obtained for *p*-aminohippuric acid, 5-HIAA, and 5-HTP (Table IV). There was some overlap between the fluorescence emission and the phosphorescence emission spectra for 5-HIAA and 5-HTP. However, the signal measured at 510 nm was 92% phosphorescence for 5-HIAA and at 500 nm was 98% phosphorescence for 5-HTP.

Solvents. Ethanol was the solvent routinely used for room temperature phosphorescent compounds. Water could be used as a solvent for PABA, although it dissolved the sodium acetate adsorbent. After evaporation of the water, the crystalline residue showed room temperature phosphorescence. The intensity of the signal was reduced 3-fold compared to a similar ethanolic sample. This was probably due to the formation of the trihydrate of sodium acetate, a less suitable adsorbent. The same reduction in intensity was observed when an ethanolic PABA solution was evaporated onto the trihydrate instead of onto anhydrous sodium acetate.

n-Propanol could be used as a solvent in room temperature phosphorescence work, but this was not commonly done because of the longer time required for its evaporation. Other solvents that could be used were isopropanol and isobutanol. Aprotic solvents such as ether, acetone, dimethylformamide (DMF), and cyclohexane gave no room temperature phosphorescence of PABA on sodium acetate.

Adsorption Mechanism. Adsorption of PABA on sodium acetate is preceded by partial neutralization with dissolved sodium acetate in alcoholic solutions. The PABA anion formed has a strong tendency to adsorb on the surface, forming the sodium salt. This is supported by the strong room temperature phorphorescence of the sodium salt of PABA (Na-PABA) when it adsorbs on sodium acetate suspended in an ethanolic solution of Na-PABA. No signal was observed for PABA and Na-PABA dissolved in acetone or DMF. This is probably due to ion pairing and the formation of conjugated species in these solvents (*9*). It may be hypothesized that the formation and adsorption of the anion also occurs in other compounds that phosphoresce on sodium acetate. In 5-HIAA and 5-HTP solutions, the dissolved acetate does not give the required neutralization of the solute. Addition of a stronger base such as NaOH is therefore necessary. This is in agreement with the generally much smaller acid dissociation constant of molecules with an indole nucleus (*10*).

After evaporation of the solvent, ethanol, samples of Na-PABA and K-PABA gave phosphorescence signals that were 16% stronger than the signal of a similar PABA sample. When the PABA and Na-PABA samples were cooled down to 77 K, their phosphorescence intensities were equal. The data strongly suggest that the PABA is not completely ionized on sodium acetate. It was calculated from the phosphorescent data that 84% of PABA is converted to the sodium salt on the sodium acetate surface. Further evidence for ionization

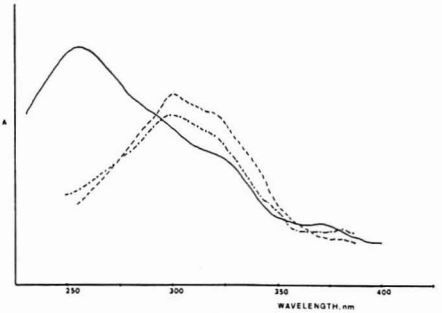

Figure 2. Reflectance spectra of PABA adsorbed on sodium acetate (——), starch (- - -) and talc (- · - · -)

was provided by reflectance data discussed below. An important consequence of the ionized adsorbate strongly adsorbing on sodium acetate is the previously noted relative insensitivity of the phosphorescence signals to moisture. Apparently, the chemisorption interactions between adsorbent and adsorbate are so favorable that the adsorbate effectively displaces adsorbed water from the surface and the predominant interactions are directly between adsorbent and adsorbate. Water thus cannot effectively compete for occupied sites on the adsorbent.

Reflectance Spectra. The mode of adsorption of PABA and other compounds was studied with the aid of reflectance spectroscopy. The surfaces chosen were sodium acetate, talc, and starch (Figure 2). Sodium acetate is a polar surface which interacts strongly with many of the compounds investigated. It was the only surface found that gave room temperature phosphorescence of adsorbed molecules. Talc and starch are relatively less polar (*11*) and the compounds studied did not give room temperature phosphorescence when adsorbed on them. The reflectance spectra of PABA on lithium acetate and potassium acetate were found to be the same as the PABA spectrum on sodium acetate. This is in contrast to Zeitlin's and Van Lieu's results with mononitrophenols adsorbed on alkali metal carbonates (*12*). They found a hypsochromic shift in the reflectance spectra with increasing effective nuclear charge of the adsorbent cation, i.e., $Li^+ > Na^+ > K^+$. Their interpretation of the results was that the smaller cations polarized the adsorbate more effectively, thus causing a hypsochromic shift. PABA probably formed the carboxylate anion on all three acetate surfaces, resulting in the same reflectance spectra.

There was a hypsochromic shift of 35 nm in the reflectance maximum of PABA on sodium acetate as compared to PABA on talc or starch (Figure 2). This indicated strong interactions between sodium acetate and adsorbed PABA, suggesting the formation of the sodium salt of PABA upon adsorption. This was supported by the reflectance spectra of the sodium salt of PABA evaporated onto sodium acetate and starch. The same reflectance maximum was obtained on the two surfaces and this maximum was the same as that of PABA adsorbed on sodium acetate. When PABA was evaporated onto sodium acetate from an acetone solution, no room temperature phosphorescence resulted. The reflectance spectrum of this sample had a 282 nm maximum, indicating that the PABA molecule was the adsorbed species. Phosphorescence did appear when a little moisture was introduced to the sample. This was probably due to the ionization of the adsorbed species and consequently its strong chemisorption to the surface. Subsequent extensive drying did not reduce the phosphorescence intensity.

Table V. Reflectance Maxima of Compounds Adsorbed on Sodium Acetate, Starch, and Talc

Compound	Maximum on NaOAC, nm	Maximum on starch or talc, nm
Aniline	250, 290	250, 290
Benzoic acid	240, 270	240, 275
N,N-Dimethyl-4-aminobenzoic acid	275	325
3-Methyl-4-aminobenzoic acid	270	300
m-Aminobenzoic acid	320	330
o-Aminobenzoic acid	330	350
p-Hydroxybenzoic acid	250	275
Sodium salt of PABA	255	255
PABA	260	295

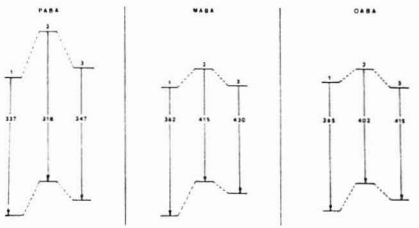

Figure 3. Relative energy levels of PABA, *m*-aminobenzoic acid (MABA), and *o*-aminobenzoic acid (OABA) on sodium acetate (1), in cyclohexane (2), and on starch (3). Fluorescence wavelengths are shown in nanometers

The reflectance maxima of other compounds adsorbed on sodium acetate, talc and starch are listed in Table V. It can be seen that the compounds expected to interact strongly with the surface, by forming the sodium salt, had hypsochromic shifts when adsorbed on sodium acetate. The table includes the compounds that exhibited room temperature phosphorescence.

The para arrangement of the substituents in PABA enhances the electron-withdrawing character of the carboxyl group and the electron-donating character of the amino group (*13*). The radiation-absorbing process can be represented by an intramolecular charge transfer from the amino group to the carboxyl group (*13, 14*):

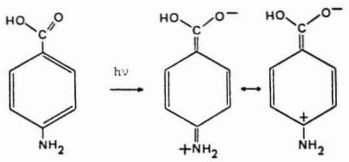

The species adsorbed on sodium acetate is the PABA anion. This makes the charge transfer a more energetic process, leading to the observed blue shift in the reflectance spectrum (Figure 2). Similar arguments can be invoked for other compounds showing hypsochromic reflectance shifts on sodium acetate. The shift for *m*-aminobenzoic acid was rather small, only 10 nm. It is interesting to note that the charge transfer mechanism cannot be applied to this molecule, because of its meta configuration.

The fluorescence spectra of PABA, *m*-aminobenzoic acid, and *o*-aminobenzoic acid, dissolved in cyclohexane, adsorbed on sodium acetate and on starch were obtained. It was assumed that the solvent–solute interactions in cyclohexane were

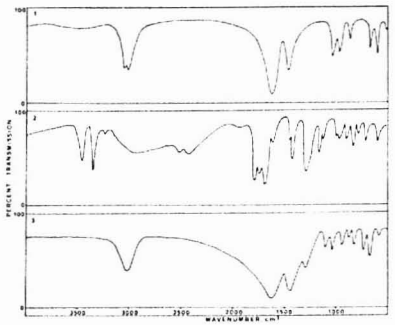

Figure 4. IR spectra of sodium acetate (1), PABA (2), and PABA adsorbed on sodium acetate (3). KBr pellets were used

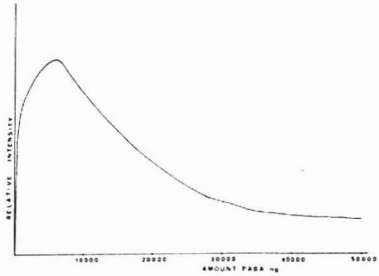

Figure 5. Room temperature phosphorescence intensity of PABA on 10 mg sodium acetate

minimal, so that there was relatively little disturbance of the molecular energy levels of the solute. When adsorbed on sodium acetate and starch, the energy levels of the molecules were altered to varying degrees. This led to different maximum fluorescence emission wavelengths (Figure 3). The molecular energy levels of PABA will be lower in the ground state and the excited singlet state compared to PABA in cyclohexane when PABA forms the sodium salt on sodium acetate because of greater interaction of the PABA anion with sodium acetate (Figure 3). A 19-nm bathochromic shift in the fluorescence maximum was observed for the sodium acetate adsorbed species compared to the molecular species in cyclohexane. This indicates that the interaction between PABA and sodium acetate is greater in the excited singlet state than in the ground state. Strong excited triplet state interactions are supported by the room temperature phosphorescence of the PABA–sodium acetate system. The fluorescence maximum of PABA on starch was at a longer wavelength than the emission of the cyclohexane solution. However, on starch the adsorbed species will be the PABA molecule, rather than the anion. Thus, the relative lowering of energy levels in the ground and excited singlet states will not be as great compared to lowering of energy levels with the anion. This is indicated in Figure 3. Adsorption probably involves hydrogen-bonding between adsorbent and adsorbate, but this does not lead to room temperature phosphorescence. *m*-Aminobenzoic acid and *o*-aminobenzoic acid show little or no room temperature phosphorescence and their fluorescence emissions on sodium acetate were at shorter wavelengths relative to their cyclohexane solutions. These compounds probably form the sodium salts on the surface, but it appears the positions of the amino and carboxyl groups in the molecule prevent them from adsorbing as strongly and rigidly as PABA. Especially excited singlet state adsorption is weaker leading to the hypsochromic fluorescence shift on sodium acetate (Figure 3). The fluorescence maxima on starch show a bathochromic shift and the interactions should be similar to those of PABA on starch. However, the interactions are weaker as indicated by the smaller bathochromic shift compared to PABA on starch.

Infrared Spectra. The mode of adsorption of PABA on sodium acetate was further investigated by infrared spectroscopy. The spectra of PABA, of sodium acetate and of PABA adsorbed on sodium acetate are shown in Figure 4. Strong sodium acetate bands obscured much of the adsorbate spectra, but a number of observations and conclusions could be made. The N–H stretching vibrations of PABA at 3350–3450 cm^{-1} disappeared for PABA adsorbed on sodium acetate. They were probably shifted to longer wavelengths and broadened, due to hydrogen-bonding between the amino group and the carboxyl groups of the surface sodium acetate. The peaks possibly disappeared under the strong methyl stretch band of sodium acetate at 3000 cm^{-1}. The spectrum of a similarly prepared *o*-aminobenzoic acid sample retained its N–H peaks when adsorbed on sodium acetate. Because there is an intramolecular hydrogen bond between the amino group and carboxyl group in *o*-aminobenzoic acid, this compound apparently is not held to the surface by strong intermolecular hydrogen-bonding. *o*-Aminobenzoic acid does not show room temperature phosphorescence. *p*-Hydroxybenzoic acid on sodium acetate gives room temperature phosphorescence. Its infrared spectrum lacks the phenolic O–H stretching frequency at 3300 cm^{-1}. Again, this is probably due to hydrogen-bonding between the hydroxyl group and carboxyl group of the surface. The O–H stretching frequency of *m*-hydroxybenzoic acid, which does not show room temperature phosphorescence, remained in the infrared spectrum of the adsorbed system.

The C–N stretching frequency of PABA at 1280 cm^{-1} still appeared in the adsorbed system, as did a number of peaks in the finger-print region. The formation of the sodium salt of PABA upon adsorption on sodium acetate should lead to the disappearance of any carboxyl–OH frequencies. This cannot be seen in the spectra because of broad adsorbent infrared bands in the regions of interest.

Surface areas. Kortüm and Oelkrug (*15*) and Kortüm (*16*) have described a method of determining surface areas of adsorbents by reflectance measurements of the adsorbate. Their systems consisted of sodium chloride adsorbent and an adsorbed lactone dye. The color of the dye was different in the primary adsorbed layer, as compared to further adsorbed layers. No such color change occurred in the PABA–sodium acetate system. The reflectance values decreased with increasing amounts of adsorbed PABA. A plot of the Kubelka–Munk function vs. amount of PABA adsorbed gave a curve that was not well defined and the point at which monolayer coverage occurred could not be determined. However, chemisorbed PABA molecules on the sodium acetate surface are distinguished from physically adsorbed molecules on top of the primary layer by their room temperature phosphorescence behavior. Only molecules that strongly and directly interact with the sodium acetate surface are held rigidly enough to show room temperature phosphorescence. PABA molecules in the second and subsequent adsorbed layers will not phosphoresce but rather decrease the signal by absorbing exciting radiation as well as emitted phosphorescence from the chemisorbed layer. A series of room temperature phosphorescence measurements of PABA on sodium acetate were taken (Figure 5). The maximum signal was obtained for 6100 ng PABA on 10 mg sodium acetate.

The surface area occupied by a flatly adsorbed PABA molecule was calculated to be 68.8 $Å^2$ by Snyder's method (*17*),

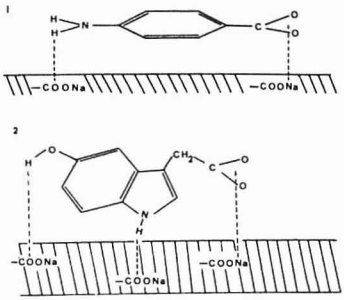

Figure 6. Adsorption of PABA (1) and 5-HIAA (2) on a sodium acetate surface

which has been proven to give reliable results in adsorption chromatography. If it was assumed that the PABA molecule was adsorbed flatly and that the maximum phosphorescence signal corresponded to completion of the monolayer, then the calculated surface area value for the sodium acetate adsorbent was 1.8 m^2/g. This value was identical with the value obtained by the BET method (see Experimental). This indicates that the above mentioned assumptions were correct.

Snyder's method was also used to calculate the flat surface area of one sodium acetate molecule and it was found to be 34.1 $Å^2$. So the molecular surface area ratio between adsorbate and adsorbent was 68.8 $Å^2$/34.1 $Å^2$ or 2.02/1. At the point of maximum room temperature phosphorescence, the molar surface ratio was 1.97/1. This shows that 1 mol of PABA would adsorb on two surface moles of sodium acetate. Such an arrangement can lead to good overlap between the carboxyl group on sodium acetate and the functional groups of PABA (Figure 6). This overlap allowed for the strong interactions necessary for room temperature phosphorescence. When the same geometric model was used for *m*-aminobenzoic acid, a far less favorable overlap of the groups resulted.

A similar study was done with *p*-aminohippuric acid and with 5-HIAA, both of which give room temperature phosphorescence on sodium acetate. In both cases, it was found that the molecular surface area ratio of the flatly adsorbed molecule with sodium acetate corresponded to the molar surface area ratio at the point of maximum phosphorescence. As mentioned earlier, a small part of the signal measured for 5-HIAA was due to fluorescence. This may introduce a slight error, but it would not significantly affect the correspondence between the surface area ratios. So it is again indicated that the molecules are adsorbed flatly. Good overlap of functional groups was also possible with these compounds. For instance, the molecular surface area of a flatly adsorbed 5-HIAA molecule was calculated to be 105.4 $Å^2$. The molecular surface area ratio between adsorbate and adsorbent was 105.4 $Å^2$/34.1 $Å^2$ or 3.09/1, indicating the adsorption of one 5-HIAA molecule on three sodium acetate species (Figure 6). A possible reason for the absence of room temperature phosphorescence of PABA adsorbed on potassium acetate and lithium acetate surfaces is the different molecular sizes of these adsorbents. The surface area of a potassium acetate unit is 37.7 $Å^2$ and of a lithium acetate unit 31.5 $Å^2$, compared to 34.1 $Å^2$ for sodium acetate. This could lead to less favorable overlaps of the functional groups of adsorbate and adsorbent and hence a less rigid adsorption on the potassium and lithium salts.

Surface adsorption data could not be obtained from fluorescence measurements because both chemisorbed and physically adsorbed species can fluoresce. The fluorescence of 4-aminosalicylic acid samples adsorbed on sodium acetate was measured. The intensity was found to increase beyond 40 μg *p*-aminosalicylic acid on 10 mg sodium acetate. There was no break in the curve to indicate monolayer coverage.

CONCLUSIONS

Room temperature phosphorimetry of compounds adsorbed on sodium acetate has the analytical advantages of selectivity and insensitivity to moisture. Sensitivity is good and low limits of detection have been achieved. Certain molecular requirements for room temperature phosphorescence have been established. They may be used as a guideline for investigation of other molecules and surfaces in order to give the technique a still broader analytical scope.

LITERATURE CITED

(1) M. Roth, *J. Chromatogr.*, **30**, 276 (1967).
(2) E. M. Schulman and C. Walling, *Science*, **178**, 53 (1972).
(3) E. M. Schulman and C. Walling, *J. Phys. Chem.*, **77**, 902 (1973).
(4) R. A. Paynter, S. L. Wellons, and J. D. Winefordner, *Anal. Chem.*, **46**, 736 (1974).
(5) R. M. A. von Wandruszka and R. J. Hurtubise, *Anal. Chem.*, **48**, 1784 (1976).
(6) R. M. A. von Wandruszka and R. J. Hurtubise, *Anal. Chim. Acta*, in press.
(7) J. D. Winefordner and M. Tin, *Anal. Chim. Acta*, **31**, 239 (1964).
(8) Shaw and Morris, *Biochem. Prep.*, **9**, 92 (1962).
(9) S. Patai, "The Chemistry of Carboxylic Acids and Esters", Interscience, New York, N.Y., 1969, p 236.
(10) W. J. Houlihan, Ed., "Indoles", Part One, Wiley-Interscience, New York, N.Y., 1972, p 11.
(11) H. Zeitlin, N. Kondo and W. Jordan, *J. Phys. Chem. Solids*, **25**, 641 (1964).
(12) H. Zeitlin and Van Lieu, *J. Catal.*, **4**, 546 (1965).
(13) H. H. Jaffé and M. Orchin, "Theory and Applications of Ultraviolet Spectroscopy", John Wiley and Sons, New York, N.Y., 1965, p 260.
(14) N. Mataga, *Bull. Chem. Soc. Jpn.*, **36**, 654 (1963).
(15) G. Kortüm and D. Oelkrug, *Z. Phys. Chem. (Frankfurt am Main)*, **34**, 58 (1962).
(16) G. Kortüm, "Reflectance Spectroscopy", Springer-Verlag, New York, N.Y., 1969, p 270.
(17) L. R. Snyder, "Principles of Adsorption Chromatography", Marcel Dekker, New York, N.Y., 1968, p 199.

RECEIVED for review August 3, 1977. Accepted September 19, 1977.

Theoretical Assessment of Precision in Dual Wavelength Spectrophotometric Measurement

K. L. Ratzlaff[1] and D. F. S. Natusch*[2]

School of Chemical Sciences, University of Illinois, Urbana, Illinois 61801

Equations are presented which describe the contributions of several sources of independent, square root, proportional, and constant error to dual wavelength spectrophotometric (DWS) measurement. In the absence of interfering species in solution, the principal sources of imprecision are usually photon shot noise, source flicker, and readout noise and DWS measurement may be more precise than conventional single wavelength spectrophotometric measurement because of reduction of sample presentation errors. In the presence of interferents, independent and square root errors increase markedly but proportional error is unaffected. For high precision measurement, it is generally desirable to employ a high intensity light source in conjunction with suitable modulation.

The technique of dual wavelength spectrometry (*1, 2*) represents a fundamental departure from conventional ratiometric single wavelength spectrophotometry. In single wavelength spectrophotometry (SWS), a light beam consisting of a single narrow wavelength band passes through separate sample and reference cells and the transmitted intensities are processed as separate sample and reference signal channels. In dual wavelength spectrometry (DWS), however, two light beams having distinct narrow wavelength bands pass through a single sample cell and the transmitted intensities at each wavelength are processed as separate signals (*3*).

The main advantages claimed for DWS over SWS are the improved selectivity, sensitivity, and accuracy of analyte absorption measurement in the presence of severe spectral overlap from interferents which absorb or scatter light at the analytical wavelengths (*3–8*). In addition, claims of improved precision have been made (*4*) although these claims have not been substantiated quantitatively.

It is the object of this paper, therefore, to present equations describing the contributions of each source of error in DWS to the overall precision of measurement. Assessment of the magnitude of each contributed error is then used to establish measurement precision under different operating conditions, and criteria are presented for the design and operation of high precision DWS instrumentation. Similar assessments have already been published for SWS (*9–13*) and these are used as a basis for comparing the two types of measurement.

BASIS OF THE DWS MEASUREMENT

DWS measurement involves determination of the absorbance difference, ΔA, between absorbances A_1 and A_2 measured at two different wavelengths, λ_1 and λ_2. Since Beer's law holds,

$$\Delta A = A_1 - A_2 = (\epsilon_1 - \epsilon_2)bc \tag{1}$$

where ϵ_1, ϵ_2, b, and c are molar absorptivities, path length, and analyte concentration. The absorbances A_1 and A_2 can be expressed in terms of incident and transmitted light intensities such that

$$\Delta A = -\log\frac{I_1}{I_2} + \log\frac{I_{01}}{I_{02}} \tag{2}$$

where I_1, I_2, are transmitted intensities and I_{01}, I_{02} are incident intensities at wavelengths λ_1 and λ_2, respectively.

Equations 1 and 2 are thus the DWS equivalents of the Beer's law expression and the definition of absorbance in conventional SWS. The second term in Equation 2 takes account of any differences in measured incident light intensity due to differences in source output, wavelength discrimination, detector response, or instrumental gain between wavelengths λ_1 and λ_2. For most conventional spectrometers employing continuous, nonpulsed, light sources and stable detectors this second term is essentially constant for given λ_1 and λ_2 and is close to zero. Since Equation 2 has the log ratio form of SWS absorbance, it is apparent that the advantage of instrumental drift rejection is retained in DWS.

For applications of DWS to equilibrium methods of analysis, two wavelengths are normally chosen at which the absorbance or scattering of the interferent is equal but the absorbances of the analyte are different. In this situation the measured absorbances, A_1', A_2', at wavelengths λ_1 and λ_2 are related to the analyte absorbances, A_1, A_2, by the relations

$$A_1' = A_1 + D \tag{3}$$

$$A_2' = A_2 + D \tag{4}$$

where D is the optical density (absorbance or scattering) due to the interferent. Since the measured value of ΔA is independent of D, Equation 1 can be applied directly to calculate the analyte concentration.

CALCULATION OF PRECISION

Equations describing the percent relative standard deviation (RSD) of the DWS measurement contributed by each source of noise or uncertainty are presented below. Many of these are straightforward extensions of equations already developed for SWS measurement (*12*) and differ only in the fact that consideration of error contributions to signals at two distinct wavelengths is necessary.

Since most significant errors are associated with the optical components of a spectrometer we have, in conformity with precision studies for SWS (*12*), considered error contributions to the photoanodic signal. For this purpose the DWS absorbance, ΔA, is expressed as

$$\Delta A = -\log\left[\frac{E_{01}\ 10^{-(D+A_1)}}{KE_{01}\ 10^{-(D+\beta A_1)}}\right] \tag{5}$$

where E_{01} is the photoanodic signal voltage produced by the incident radiation intensity, I_{01}, at wavelength λ_1, and

$$\beta = \epsilon_2/\epsilon_1 \tag{6}$$

$$K = I_{01}/I_{02} \tag{7}$$

E_{01} is related to the photoanodic current, i_{01}, produced by I_{01} and the associated resistance, R_f, of the OA current-to-voltage

[1]Present address, Department of Chemistry, Northern Illinois University, DeKalb, Ill. 60115.
[2]Present address, Department of Chemistry, Colorado State University, Fort Collins, Colo. 80523.

converter by $E_{01} = -i_{01} R_f$. Equation 5 can be obtained by combination of Equations 2–4, 6, 7.

Application of propagation of error mathematics to Equation 5 leads to a generalized expression for the percent relative standard deviation, % $\sigma_{\Delta A}$, in ΔA due to any source of random noise. Thus

$$\% \sigma_{\Delta A} = \frac{10^D}{2.303\,(1-\beta)A_1}\left[\left(\frac{\sigma_1 10^{A_1}}{E_{01}}\right)^2 + \left(\frac{\sigma_2 10^{\beta A_1}}{KE_{01}}\right)^2\right]^{1/2} \times 100\% \quad (8)$$

where σ_1 and σ_2 are the standard deviations associated with the signals at each wavelength. The total percent RSD from all sources of noise can be obtained by taking the square root of the sum of the squares of % $\sigma_{\Delta A}$ contributed by each source.

For the purpose of the following discussion we assume that the determination of K, which actually "zeroes" the instrument, is performed with significantly higher precision than any individual measurement of ΔA. Even if K were to be determined each time I_1 and I_2 are measured, it can be shown that the overall precision would never be changed by more than a factor of 2. Therefore, we have chosen to consider the uncertainty in K to be negligible.

In practice, different types of noise give rise to only four functional forms of Equation 8 so that the overall precision is effectively determined only by those sources which predominate for each functional category. These categories are determined by the dependence of the standard deviations σ_1, σ_2 (Equation 8) on photomultiplier signal intensity. In considering the various sources of noise, it is useful to distinguish between those whose energy spectra are frequency dependent (black noise) and those which are frequency independent (white noise). This is because frequency dependent noise can be more effectively reduced by modulation techniques than is the case for white noise. Similarly, pattern noise can often be effectively reduced insofar as it is often highly correlated within the signal time frame.

Independent Error. When the standard deviation of the signal intensity is independent of the magnitude of the signal, the associated error is called Type I (*9–12*) or Independent (*13*) error. Sources of independent error include dark current shot and excess noise, digitization noise, thermal or Johnson noise, and noise associated with readout devices reading in units of ΔA. This last source of noise, although signal independent, gives rise to a different functional form of Equation 8, due to the fact that it is not introduced until after logarithmic conversion; it will be considered separately in a later section.

The standard deviation, σ_I, associated with signal independent noise is the same at both wavelengths so Equation 8 can be written

$$(\% \sigma_{\Delta A})_I = \frac{\sigma_I 10^D}{2.303\,E_{01}(1-\beta)A_1}\left[10^{2A_1} + K^{-1}10^{2\beta A_1}\right]^{1/2} \times 100\% \quad (9)$$

Figure 1 shows a plot of $(\% \sigma_{\Delta A})_I$ vs. A_1 from Equation 9 for several representative values of the molar absorptivity ratio, β, in the absence of absorbing or scattering interferents (i.e., $D = 0$). A representative value of the ratio σ_I/E_{01} of 1×10^{-5} has been chosen for illustration of independent error; however, choice of other values merely moves the precision curves along the Y axis without changing their shape.

Curve A in Figure 1, for which $\beta = 0$ and $K = 1$, also represents the SWS situation under the same conditions and can be obtained by replotting figures presented in previous work (*9, 10, 12*) on logarithmic axes. It is apparent that

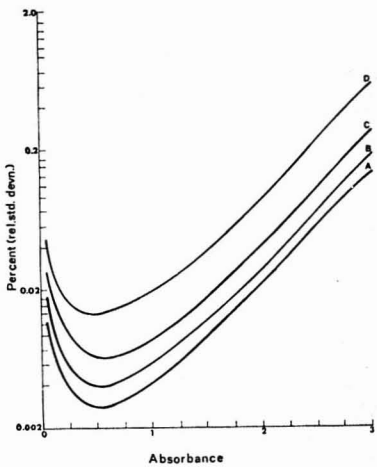

Figure 1. Independent error. Curves A, B, C, and D are for values of β of 0.0, 0.25, 0.50, and 0.75, respectively, where $K = 1$. These curves are computed for $\sigma_I/E_{01} = 1 \times 10^{-5}$ (Equation 9)

independent errors will always be of greater magnitude in DWS than in SWS. This is also true in the presence of an interferent ($D > 0$) which increases independent error by a factor of 10^D. It should be noted, however, that A_1 cannot be separated from D in the SWS experiment so determination of its associated precision is rather meaningless. Although not immediately obvious from Equation 9, Figure 1 shows that $(\% \sigma_{\Delta A})_I$ is essentially proportional to $(1-\beta)^{-1}$.

The absorbance corresponding to minimum independent error is obtained by numerical evaluation of the transcendental equation

$$2.303\,A_1(10^{2A_1} + \beta K^{-1}10^{2\beta A_1}) = 10^{2A_1} + K^{-1}10^{2\beta A_1}$$

which is the derivative with respect to A_1 of Equation 9 with $D = 0$. For $K = 1$ and $0 \le \beta \le 0.9$, $(\% \sigma_{\Delta A})_I$ is a minimum between values of A_1 of 0.44 and 0.49. This variation is barely perceptible in Figure 1.

Evaluation of the signal independent standard deviation, σ_I, in Equation 9 enables assessment of the parameters controlling and the relative magnitudes of each source of independent error mentioned above.

Dark Current Noise. The combined contribution of photomultiplier dark current shot and excess noise to σ_I is given (*12*) by

$$\sigma_I = [\sigma_{ex}^2 + 2meR_f^2 \Delta f i_d(1+\alpha)]^{1/2} \quad (10)$$

where e is the electron charge and i_d, m, and α are, respectively, the photomultiplier dark current, average gain, and relative variance of the gain. Δf is the noise equivalent bandwidth of the signal amplifier-readout system and R_f the resistance of the OA current-to-voltage converter. σ_{ex} is the standard deviation due to excess dark current noise.

Dark current noise, which is primarily frequency independent excess noise, is usually the predominant source of independent error in spectrophotometric measurement. Rothman et al. (*12*) report a standard deviation of 10^{-12} A, which corresponds to σ_I/E_{01} in the range 10^{-5}–10^{-6}, for dark current noise. Generally, the higher value is realized only when narrow slit widths, weak sources, or poor detection response

at the wavelength of interest are encountered.

Digitization Noise. Where photomultiplier signals are processed in the digital domain, conversion can introduce an uncertainty (or pattern noise) of plus or minus the quantization level whose magnitude depends upon the resolution of the analog-to-digital converter. In this situation, the uncorrelated standard deviation due to digitization noise is $\sigma_1 = q/\sqrt{12}$ (*14–16*). Unless low resolution analog-to-digital conversion is employed, the resulting independent error is generally small compared to that due to dark current.

Johnson Noise. This consists of so-called "white" thermal noise in amplifier resistances. The standard deviation, σ_1, due to Johnson noise is $(4kTR_f\Delta f)^{1/2}$ where R_f and Δf are as defined for Equation 10 and k and T are Boltzmann's constant and the absolute temperature, respectively (*10, 17*). Under most normal operating conditions, Johnson noise makes a negligible contribution to independent error; however, it may become comparable with dark current noise where very broad bandwidths (Δf) are employed. This condition is rarely encountered.

Square Root Error. When the standard deviation of the signal intensity is proportional to the square root of the magnitude of the signal the associated error has been termed Type II (*9–12*) or Square Root (*13*) error. This error is due only to the shot effect which is the result of frequency independent statistical fluctuations in the photoelectron pulse rate (*9–13, 18–20*). The standard deviation in signal intensity, σ_s, due to shot noise is equal to $[2meR_f^2\Delta f i_{01}(1+\alpha)]^{1/2}$ where the variables are as defined for Equation 10. In terms of the photomultiplier reference voltage, E_{01}, the standard deviations due to shot noise in signals derived from wavelengths λ_1 and λ_2 are thus

$$\sigma_1 = (2meR_f\Delta f E_{01}10^{-(D+A_1)})^{1/2}$$

$$\sigma_2 = (2meR_f\Delta f K E_{01}10^{-(D+\beta A_1)})^{1/2}$$

Inserting these standard deviations into Equation 8 gives the percent RSD due to shot noise square root error as

$$(\%\,\sigma_{\Delta A})_S = \frac{10^{D/2}}{2.303(1-\beta)A_1}\left[\frac{2meR_f\Delta f}{E_{01}}(10^{A_1} + K^{-1}10^{\beta A_1})\right]^{1/2} \times 100\% \qquad (11)$$

Figure 2 shows a plot of $(\%\,\sigma_{\Delta A})_S$ vs. A_1 from Equation 11 for several representative values of β and values of $D = 0$, $m = 2 \times 10^4$, $R_f = 10$ MΩ, $\Delta f = 10$ Hz, and $E_{01} = 1$ V. This last value corresponds to the production of 1.5×10^6 photoelectrons during the period of measurement of λ_1. Such a value is considered to be representative of modern DWS and SWS spectrometers since photoelectron pulse rates generally lie in the range 1×10^6 to 1×10^9 s^{-1} and measurement intervals range from 1×10^{-3} to 5×10^{-1} s.

Curve A in Figure 2, for which $\beta = 0$ and $K = 1$, represents the SWS situation (*9–13*). As in the case of independent error, it can be seen that $(\%\,\sigma_{\Delta A})_S$ is essentially proportional to $(1-\beta)^{-1}$; however the influence of an interfering species (i.e. $D > 0$) is significantly smaller than for independent error.

The absorbance corresponding to minimum square root error is obtained by numerical evaluation of the transcendental equation

$$1.152\,A_1(10^{A_1} + \beta K^{-1}10^{\beta A_1}) = 10^{A_1} + K^{-1}10^{\beta A_1}$$

which is the derivative with respect to A_1 of Equation 12. For $K = 1$ and $0 \le \beta \le 0.9$, $(\%\,\sigma_{\Delta A})_S$ is a minimum between values of A_1 of 0.86 and 0.99 which is approximately twice the corresponding absorbance for independent error as expected from consideration of Equations 9 and 11.

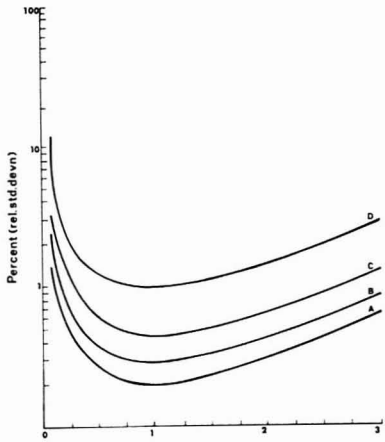

Figure 2. Square root error. Curves A, B, C, and D are for values of β of 0.0, 0.25, 0.50, and 0.75, respectively, where $K = 1$. These curves are computed for E_{01}^{-1} ($2\,meR_f\Delta f$) $= 5 \times 10^5$ (Equation 11)

Proportional Error. When the standard deviation of the signal intensity is directly proportional to the magnitude of the signal, the associated error has been termed Type III (*9–12*) or Proportional (*13*) error. Such noise, which includes light source flicker, beam modulation noise, and noise resulting from variations in sample presentation, can have substantially different contributions to DWS and SWS. Uncertainty introduced by the finite resolution of absorbance readout devices has the same functional form as proportional error and is included in this section even though the actual noise is independent of signal intensity.

The standard deviation of signal intensity due to proportional noise is equal to $\xi i_p R_f$ (*10*) where i_p is the photoanodic current, R_f the OA circuit resistance, and ξ is the so-called "flicker" factor. ξ is thus the standard deviation per volt and depends on bandwidth for most sources. Writing the product i_pR_f as a voltage gives the standard deviations in signals at wavelengths λ_1 and λ_2 as

$$\sigma_1 = \xi_1 E_{01}10^{-(D+A_1)}$$

$$\sigma_2 = \xi_2 K E_{01}10^{-(D+\beta A_1)}$$

Inserting these standard deviations into Equation 8 then gives the percent RSD for proportional error as

$$(\%\,\sigma_{\Delta A})_P = \frac{(\xi_1^2 + \xi_2^2)^{1/2}}{2.303(1-\beta)A_1} \times 100\% \qquad (12)$$

It can be seen from Equation 12 that $(\%\,\sigma_{\Delta A})_P$ is exactly proportional to $(1-\beta)^{-1}$ and inversely proportional to A_1 so that no minima occur. Also, by contrast with independent and square root errors, proportional error is independent of the presence of an interfering species. Figure 3 shows a plot of $(\%\,\sigma_{\Delta A})_P$ vs. A_1 from Equation 12 for several values of β and a value of $\xi_1 = \xi_2 = 4 \times 10^{-4}$. The flicker factor value chosen for illustration is representative of that due to light source flicker (*10, 12*). Individual sources of proportional error are considered below.

Light Source Flicker. Proportional errors in DWS are usually dominated by that due to light source flicker which is a type of "1/*f*" noise, so-called because of the inverse

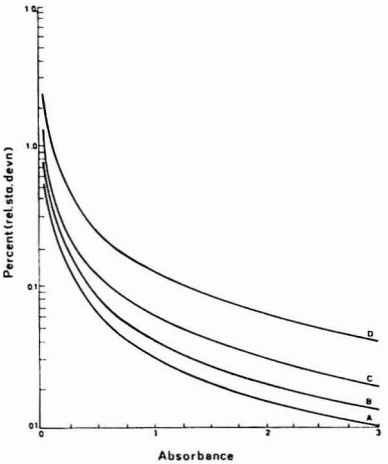

Figure 3. Proportional error. Curves A, B, C, and D are for values of β of 0.0, 0.25, 0.50, and 0.75, respectively, where $K = 1$. These curves are computed for $\xi_1 = \xi_2 = 4 \times 10^{-4}$ (Equation 12)

frequency dependence of its power spectrum (*21*). The contribution of source flicker to the percent RSD is obtained simply by writing $\xi_s = \xi_1 = \xi_2$ in Equation 12 where ξ_s is the flicker factor for the light source. Since $\xi_s = 4 \times 10^{-4}$ is representative of flicker factors reported (*10*, *12*) for a conventional tungsten lamp, the curves in Figure 3 reasonably describe the theoretical light source flicker in DWS when a tungsten lamp is employed. In practice, however, it is advantageous to use higher intensity light sources such as a tungsten iodide lamp, a xenon arc, or a CW laser. Such high intensity sources are generally more difficult to regulate than weak sources so that larger light source flicker factors may be encountered. Nevertheless, the effective reduction of source flicker noise by modulation and of shot noise by increased E_{01} can result in improved precision.

Beam Modulation Noise. The technique of modulation is often used specifically to combat $1/f$ noise in SWS. In the case of DWS, however, modulation is intrinsic to instrumental operation. Where a single DWS detector is employed, the transmitted beams are alternately monitored and any $1/f$ noise or drift which is correlated within the time frame of the modulation cycle is rejected. Where separate detectors are used to monitor each wavelength continuously $1/f$ noise is completely correlated and rejected although differential drift between detectors may become significant.

While modulation may reduce the influence of correlated $1/f$ noise (e.g., light source flicker) it can also contribute pattern noise at the modulation frequency. In terms of the classification used herein, the contribution of this noise depends upon the way in which modulation is achieved. Two alternative methods can be distinguished. The first, or *beam modulation*, employs two distinct wavelength isolation devices whose fixed wavelength outputs are alternately sampled. The second, or *wavelength modulation*, employs a single wavelength isolation device whose output is wavelength modulated. Noise generated by beam modulation contributes to proportional error but that generated by wavelength modulation contributes to constant error which is discussed in a later section.

Beam modulation error is given by Equation 12 in which the flicker factors ξ_1 and ξ_2 now refer to the uncertainties associated with beam modulation at each wavelength. These are determined by the way in which modulation is achieved, the quality of the multiplexing optics, and the mode of signal processing employed. Experimental measurements of flicker factors due to beam modulation are not available; however, they would need to be comparable to or greater than about 4×10^{-4} for beam modulation noise to exceed that due to conventional light source flicker.

Beam modulation in DWS is generally accomplished mechanically by means of a rotating sector or a rotating or vibrating mirror (*3*). If one assumes that modulation flicker factors are determined primarily by the uncertainty associated with mechanical movement, it seems unlikely that their magnitude will exceed 4×10^{-4} for low frequency ($\lesssim$100 Hz) operation. Higher frequency ($\sim$1 kHz) operation may, however, give rise to larger flicker factors as a result of vibration.

Sample Presentation. Variations in sample presentation also give rise to proportional error. Such variations originate from vibration and from irreproducibility of the sample cell position in the cell holder and of the cell holder itself (*12*). Signal imprecision then results from (i) variations in sample and cell transmission characteristics, (ii) variations in path length, and (iii) variations in photocurrent which occur when the refracted light beam strikes regions of the photocathode surface having different quantum efficiences. Mechanisms (i) and (iii) both produce proportional errors but mechanism (ii) gives rise to a constant error discussed in a later section.

Since, in DWS measurement, both beams pass through the same sample cell and are detected by the same photomultiplier, sample presentation errors will be correlated, and thus rejected, to the extent that they are independent of wavelength. Variations in cell transmission are due to reflection, which is essentially independent of wavelength, and to refraction and scattering which, although wavelength dependent (*22*, *23*), are relatively constant over the short wavelength interval normally employed in DWS. Furthermore, under most operational circumstances, the photocathode response is relatively constant at the two wavelengths. Consequently, the uncorrelated fractions of the flicker factors ξ_1, ξ_2 in Equation 12 will be small so that proportional error due to sample presentation is negligible in DWS.

By contrast, Rothman et al. (*12*) have shown that flicker factors due to sample presentation in SWS are commonly as large as (and often larger than) $\xi_1 = 6 \times 10^{-3}$ ($\xi_2 = 0$) which results in percent RSD values approximately an order of magnitude greater than those depicted by curve A ($\beta = 0$, $K = 1$) in Figure 3. It is apparent, therefore, that sample presentation errors, which are frequently the limiting proportional error in SWS, are unlikely to be limiting in DWS.

Readout Resolution. The finite resolution of absorbance readout devices such as analog meters, digital displays, and recorders can introduce considerable uncertainty into spectrophotometric measurement (*12*). Although the associated standard deviation, σ_{ar}, is independent of signal intensity the percent RSD, given by

$$(\%\,\sigma_{\Delta A})_R = \frac{\sigma_{ar}}{(1-\beta)A_1} \qquad (13)$$

has the same functional form as proportional error. This is because uncertainty is contributed in the final electronic stage of the spectrophotometer after logarithmic conversion.

Readout resolution error has been discussed for transmittance measurements by Rothman et al. (*12*) who have shown that it can severely limit the precision of SWS measurement. Thus, an analog meter can contribute errors which are 10 to 70 times greater than those depicted in Figure 3. Errors contributed by $3^1/_2$ and $4^1/_2$ digital panel meters,

respectively, were shown (*12*) to be 3 to 14 and 0.3 to 1.4 times as great as those in Figure 3. Although not considered by Rothman et al. (*12*), most analog recorders would also be expected to contribute substantial readout error. This error can, of course, be minimized by employing scale expansion and by reading the recorder trace only after several time constant periods have elapsed.

It can be concluded, therefore, that readout errors will constitute the limiting error having proportional form in both SWS and DWS unless a high resolution readout device or scale expansion is employed. It will be noted that, for readout errors, exactly the same considerations apply to DWS as to SWS except that the percent RSD is increased by a factor of $(1 - \beta)^{-1}$ in DWS for a given value of A_1.

Constant Error. Where the noise or uncertainty associated with a signal is proportional to molar absorptivity or path length, the resulting error will be termed Constant error. Such errors are due to noise associated with wavelength modulation and with variations in sample path length and are described by separate error functions.

Wavelength Modulation Noise. Where the output of a single wavelength isolation device is modulated to produce alternate beams of wavelength λ_1 and λ_2, the standard deviation of the absorbance, A, at each wavelength is given by μM_A where μ is the uncertainty in wavelength determination and M_A and M_D are the slopes of the absorbance and interferent curves at the wavelength in question. Assuming that μ is the same at both wavelengths the total standard deviation of ΔA is

$$(\sigma_{\Delta A w}) = \mu[(M_{A1}A_1 + M_{D1}D)^2 + (M_{A2}\beta A_1 + M_{D2}D)^2]^{1/2}$$

where the subscripts refer to wavelengths λ_1 and λ_2. The percent RSD in ΔA due to wavelength modulation noise is then

$$(\%\ \sigma_{\Delta A})_{Cw} = \frac{\mu[(M_{A1}A_1 + M_{D1}D)^2 + (M_{A2}\beta A_1 + M_{D2}D)^2]^{1/2}}{(1 - \beta)A_1} \times 100\% \quad (14)$$

Equation 14 shows that when interfering species are absent ($D = 0$), or when the values of M_{D1} and M_{D2} are small, the percent RSD due to wavelength modulation noise is independent of A_1 but may be strongly dependent on the absorptivity ratio β. When interferents are present and the values of M_{A1} and M_{A2} are substantially less than those of M_{D1} and M_{D2}, however, the form of Equation 14 approaches that for proportional error at small A_1 and tends towards a constant value at large A_1.

Wavelength modulation can be achieved by means of an oscillating grating, mirror, or slit in the wavelength isolation device. The last of these methods is commonly employed in differential UV-visible spectrometers which constitute a sub-set of DWS instruments. The maximum value of μ in Equation 14 will then be the measured standard deviation of either wavelength. These have been determined (*16*, *24*) for the cases of an oscillating slit ($\mu = 0.01$ nm at 546.1 nm), an oscillating refractor plate ($\mu = 0.001$ nm at 253.7 nm), and an oscillating grating ($\mu = 0.0004$ nm at 283.3 nm). Values of the slopes M_{A1}, M_{A2} in Equation 14 range from 0.15 to 0.004 nm^{-1} and are most commonly around 0.05 nm^{-1}. Using this value for both M_{A1} and M_{A2} and choosing $\mu = 0.01$ nm, $\beta = 0.5$, and $D = 0$, Equation 14 gives a maximum constant error of 0.12%. By comparison with proportional and square root errors in DWS, a constant error of this magnitude is only marginally significant. It appears reasonable, therefore, to assume that wavelength modulation error is usually insignificant except, perhaps, where a noisy modulation technique is employed in conjunction with narrow absorption peaks and small $\Delta\lambda$. Such conditions are most likely to occur in differential spectrometers.

Path Length Variation. Variations in the length of the light path passing through different samples can occur when a cell is tilted so that the angle of incidence is $\pi/2 \pm \theta$ rather than $\pi/2$ (*12*). The measured DWS absorbance from Equation 1 is thus

$$\Delta A = (\epsilon_1 - \epsilon_2)\ bc \sec \theta$$

Since all values of θ lead to a positive error, random path length variations give rise to a systematic error which contributes to the accuracy rather than the precision of measurement.

Summation of Errors. The precision of the overall DWS measurement can be closely approximated by considering only those errors which predominate in each functional category. For most conventional DWS spectrometers, these will be dark current noise, photon shot noise, source flicker, and wavelength modulation noise. For SWS spectrometers, however, it has been shown that sample presentation uncertainty normally replaces source flicker as the limiting proportional error(*12*). It must be stressed, however, that individual spectrometer components and operating conditions differ so that the relative magnitudes of different noise contributions may vary considerably. For example, readout uncertainty or beam modulation noise may predominate in the proportional category where a readout device of limited resolution or a noisy modulation technique is employed.

In order to illustrate how the predominant sources of error in each functional category contribute to the overall DWS measurement precision, each is evaluated as a function of absorbance in Table I, both in the presence and absence of an interferent. The limiting contributions to SWS measurement are presented for comparison. The data in Table I are calculated for $\beta = 0$ and $K = 1$. For dark current noise, $\sigma_1/E_{01} = 10^{-5}$, and 10^6 photoelectrons are assumed to arrive during the measurement interval for the purpose of calculating shot noise error. A sample presentation flicker factor of $\xi_1 = 6 \times 10^{-3}$ is employed for SWS and a source flicker factor of $\xi_1 = \xi_2 = 4 \times 10^{-4}$ is used for DWS. Consideration of constant errors and proportional error due to limited readout resolution is omitted since the former are small and independent of absorbance and the latter can be made negligible by scale expansion or choice of a high resolution readout device. It should be noted, however, that constant wavelength modulation error may become significant near the absorbance minimum (Table I) when no interfering species are present.

DISCUSSION

Examination of the data presented in Table I and in Figures 1–3 shows that the relative contributions of the different types of noise vary considerably as a function of absorbance in both DWS and SWS. This variation is particularly apparent for DWS measurement in the presence of the interferents due to the fact that independent and square root errors are increased by factors of 10^D and $10^{D/2}$ respectively, while proportional error is unaltered. Thus, although independent dark current noise normally makes only a minor contribution to the overall DWS precision it can become a significant error when an interferent is present.

As pointed out previously, the intrinsic precision of SWS is usually superior to that of DWS under comparable conditions due to the fact that the effective absorptivity $(\epsilon_1 - \epsilon_2)$ is usually smaller in DWS. Nevertheless, the advantage gained by using a single sample cell, and thereby reducing sample presentation errors, can result in DWS having greater overall

Table I.

Relative Percentage Error, % σ_A, for SWS

Source	D	A_1 = 0.01	0.05	0.1	0.2	0.5	1.0	1.5	2.0	2.5	3.0
Dark current	0	0.06	0.01	0.007	0.004	0.003	0.004	0.009	0.02	0.06	0.15
Photon shot	0	6.2	1.3	0.65	0.35	1.8	0.14	0.17	0.22	0.31	0.46
Sample presentation	-	26.1	5.2	2.6	1.3	0.52	0.26	0.17	0.13	0.10	0.09
$(\Sigma(\%\sigma_A)^2)^{1/2}$	0	26.8	5.4	2.7	1.4	0.55	0.30	0.24	0.26	0.33	0.50

Relative Percentage Error, % σ_A, for DWS

Source	D	A_1 = 0.01	0.05	0.1	0.2	0.5	1.0	1.5	2.0	2.5	3.0
Dark current	0	0.06	0.01	0.007	0.004	0.003	0.004	0.009	0.02	0.06	0.15
Photon shot	0	6.2	1.3	0.65	0.35	1.8	0.14	0.17	0.22	0.31	0.46
Source flicker	-	2.5	0.49	0.25	0.12	0.05	0.02	0.02	0.01	0.01	0.008
	0	6.7	1.4	0.70	0.37	0.18	0.14	0.17	0.22	0.31	0.48
	0.5	11.3	2.3	1.2	0.63	0.32	0.25	0.30	0.39	0.60	0.93
	1.0	19.7	4.0	2.1	1.1	0.56	0.46	0.53	0.72	1.12	2.04
$(\Sigma(\%\sigma_A)^2)^{1/2}$	1.5	35.0	7.1	3.7	2.0	1.0	0.82	0.97	1.4	2.5	5.3
	2.0	62	12.7	6.6	3.5	1.8	1.5	1.9	3.08	6.3	15.2
	2.5	111	22.8	11.8	6.3	3.3	2.9	4.1	7.9	18.2	46.5
	3.0	204	42.1	21.8	11.8	6.3	6.3	10.6	22.8	55.8	146

precision that SWS. It should be stressed, however, that this precision advantage is manifest only in situations where the absorptivity ratio, β, can be made close to zero without resorting to large $\Delta\lambda$. In such situations DWS may be the method of choice for performing high precision measurements at low absorbances.

The main advantage of DWS is, however, its ability to discriminate against interferents. In this situation the precision attainable is highly dependent on the relative magnitudes of A_1 and D as illustrated in Table I. While a rather high relative dark current noise level has been chosen for the purpose of illustration in Table I, it is apparent that high precision operation over a wide absorbance range is limited to samples for which D is quite small (0.5–1.0). Furthermore, operation at even moderate precision is likely to be impractical for $D > 2.0$ except in cases where a limited intermediate absorbance range is acceptable.

The precision data presented in Table I point out those sources of error which must be minimized in order to improve DWS measurement precision under different conditions. They also suggest several operational and instrumental parameters which can be optimized.

Operationally, the only parameters which are readily adjustable are the absorbances of the analyte and interferent and the wavelengths employed. Thus, dilution or concentration of the sample (which maintain the ratio A_1/D constant) can result in a small but significant improvement in precision. A much greater effect may be achieved by variation of the wavelength difference, $\Delta\lambda$, so as to minimize the absorptivity ratio, β. In this regard there is considerable flexibility in the choice of wavelengths when the interferent is a scattering material; however, for an absorbing species, this choice is largely determined by spectral constraints (*23*).

While it is desirable to employ a wavelength difference which achieves $\beta \sim 0$, it should be stressed that large $\Delta\lambda$ may result in there being a significant uncorrelated fraction of the wavelength uncertainty in each beam. In such circumstances, the proportional sample presentation error increases substantially and is enhanced where thermal gradients, mechanical instabilities, or flow cell cavitation effects occur. Consequently, it is not always justifiable to assume that sample presentation errors are negligible in DWS.

It is noteworthy that differential spectrometers, which operate with a very small wavelength difference, maintain β very close to unity. Consideration of Equation 8 shows that the precision of such instruments must generally be poor, being greatest at the point(s) of maximum slope of the absorbance curve and lowest at the absorbance peak. Furthermore, some of the wavelength modulation methods employed may contribute substantial wavelength modulation noise which is also maximized at the absorbance peak. Such considerations raise serious questions about the advisability of using differential UV-visible spectrometers for quantitative determinations. This is particularly pertinent to their current use for measuring gaseous air pollutants.

A second approach to improvement of DWS precision involves modification of those spectrometer components which contribute the limiting sources of noise in each category. In this regard it is important to emphasize that reduction of independent and square root errors (which depend on D) is generally preferable to reduction of proportional error in situations where interferent levels are substantial. It is equally important to consider the frequency spectra of the limiting noise contributions since frequency dependent noise can often be significantly reduced by suitable modulation whereas frequency independent white noise cannot. It is generally desirable, therefore, to increase frequency dependent noise relative to white noise.

The foregoing considerations dictate that high light source intensity should be actively sought in improving DWS measurement precision. Thus, the greatly enhanced signal voltage, E_{01}, reduces the contribution of dark current noise (and to some extent shot noise) to the signal while additional source flicker noise (which is $1/f$ noise) can be effectively reduced by modulation. Also, since source flicker contributes a proportional error, its contribution does not increase with D.

Probably the most obvious, though most frequently neglected, source of error in both DWS and SWS is the resolution of the readout device. Since this error may often limit the overall measurement precision, it is necessary to employ either a $4^1/_2$ digital panel meter or scale expansion where high precision measurements are required.

CONCLUSIONS

The following general conclusions can be drawn regarding the precision of dual wavelength spectrophotometric measurement:

1. The principal sources of imprecision in DWS are usually photon shot noise, source flicker, and readout noise when sample interferents are absent.

2. The use of intense light sources in conjunction with suitable high frequency modulation (100–1000 Hz) is generally desirable for high precision DWS measurement.

3. In the absence of interferents, the precision and detection limits of SWS and DWS are normally comparable. DWS may, however, be more precise than SWS where the latter measurement has substantial associated sample presentation error.

4. In the presence of interferents, DWS precision is markedly reduced because of increase of independent and square root errors. In particular, dark current noise may become significant under these conditions.

5. The use of very small wavelength differences, as in differential spectroscopy, results in poor measurement precision.

While the above conclusions are generally valid, it must be stressed that the different functional dependences of errors of different types on A_1 and D lead to a complex overall dependence which will vary with individual instruments and measurements. To some extent, therefore, it is appropriate to consider each instrument and each type of measurement as a special case.

LITERATURE CITED

(1) B. Chance, *Rev. Sci. Instrum.*, **22**, 634 (1951).
(2) B. Chance, *Methods Enzymol.*, **24**, 322 (1972).
(3) T. J. Porro, *Anal. Chem.*, **44** (4), 93A (1974).
(4) S. Shibata, M. Furukawa, and K. Goto, *Anal. Chim. Acta*, **46**, 271 (1969).
(5) S Shibata, M. Furukawa, and K. Goto, *Anal Chim. Acta*, **53**, 369 (1971).
(6) S. Shibata, K. Goto, and Y. Ishiguro, *Anal. Chim. Acta*, **62**, 305 (1972).
(7) R. L. Sellers, G. W. Lowry, and R. W. Kane, *Am. Lab*, March (1973).
(8) S. M. Gerchakov, *Spectrosc. Lett.*, **4**, 403 (1971).
(9) J. D. Ingle, Jr., and S. R. Crouch, *Anal Chem.*, **44**, 1375 (1972).
(10) J. D. Ingle, Jr., and S. R. Crouch, *Anal Chem.*, **44**, 785 (1972).
(11) J. D. Ingle, Jr., *Anal. Chem.*, **45**, 861 (1973).
(12) C. D. Rothman, S. R. Crouch, and J. D. Ingle, Jr., *Anal. Chem.*, **47**, 1226 (1975).
(13) H. L. Pardue, T. E. Hewitt, and M. J. Milano, *Clin. Chem. (Winston-Salem, N.C.)*, **24**, 1028 (1974).
(14) P. C. Kelly and G. Horlick, *Anal Chem.*, **45**, 518 (1973).
(15) K. Steiglitz, "An Introduction to Discrete Systems", Wiley, New York, N.Y., 1974.
(16) K. L. Ratzlaff, K. R. O'Keefe, and D. F. S. Natusch, manuscript in preparation.
(17) W. J. McCarthy, in "Spectrochemical Methods of Analysis", J. D. Winefordner, Ed., Wiley, New York, N.Y., 1971, pp 493–518.
(18) RCA Photomultiplier Manual, RCA Electronic Components, Harrison, N.J., 1970.
(19) H. V. Malmstadt, M. L. Franklin, and G. Horlick, *Anal. Chem.*, **44** (8), 63A (1972).
(20) M. L. Franklin, G. Horlick, and H. V. Malmstadt, *Anal. Chem.*, **41**, 2 (1969).
(21) H. V. Malmstadt, C. G. Enke, S. R. Crouch, and G. Horlick, "Optimization of Electronic Measurements", W. A. Benjamin, Menlo Park, Calif., 1973.
(22) W. Heller, H. L. Bhatnager, and M. Nakagaki, *J. Chem. Phys.*, **36**, 1163 (1962).
(23) K. L. Ratzlaff and D.F.S. Natusch, submitted to Anal. *Chem.*
(24) J. D. Defreese, Ph.D. Thesis, University of Illinois, Urbana, Ill., 1975.

RECEIVED for review January 19, 1976. Resubmitted December 20, 1976. Accepted August 22, 1977. This work was supported by the National Institute of Environmental Health Sciences, NIH, under Grant No. 7-R01 ES 01472- 01.

Supply and Removal of Sample Vapor in Graphite Thermal Atomizers

Wim M. G. T. van den Broek and Leo de Galan*

Laboratorium voor Analytische Scheikunde, Technische Hogeschool, P.O. Box 5029, Delft, The Netherlands

The time-dependent supply and removal of sample atoms have been measured separately for two commercial graphite thermal atomizers. In either type the release of the atoms from the graphite wall is determined by the wall temperature and described by an Arrhenius-type rate constant. With common heating rates, the equivalent time constant is about 1 s. The removal of the atoms from the cell depends on the type of atomizer used. In the Varian Techtron minifurnace, diffusion is the dominating process and the equivalent time constant is less than 70 ms. In the larger Perkin-Elmer furnace operated under flow conditions, convection leads to equally small time constants. If, however, the argon flow is stopped completely, diffusion and, to some extent, expansion raise the time constant to about 1 s. Theoretical analysis and experimental measurement show that only in the latter case some 25% of the sample can be contained in the cell. Under common operating conditions, this efficiency is less than 10%.

The great sensitivity and the correspondingly low limits of detection of the thermal atomizers in atomic absorption spectrometry stem from the ability to contain a substantial amount of the analyte in the observation zone for a finite period of time. The basic condition towards the realization of this goal has first been formulated by L'vov (*1*): the rate of supply of the analyte into the observation region must at least be equal to its rate of removal from this zone. There is no doubt that constricted, furnace-type atomizers fulfil this condition better than open filament-type atomizers. This advantage partly explains the waning interest in the latter type atomizers in favor of the enclosed cylindrical graphite cuvettes. Of the different designs described in the literature or commercially available, two extremes have become popular and typical: a Varian Techtron minifurnace with a length/diameter ratio of 3 and a Perkin-Elmer furnace with a length/diameter ratio of 6.

However, at present very little is known about the time-dependence of the analyte supply into and its removal from either type of furnace. Henceforth, their efficiency in containing the analyte inside the graphite enclosure is equally unknown. It is true that the mechanism of sample release from the graphite wall has received increased attention in the past few years (*2–4*), but the time-dependence and the shape of the transient signal has been considered in only a few papers. Fuller (*5*) assumes a very simple model consisting of two exponentials to describe the release and removal of copper in a Perkin-Elmer HGA-70 graphite furnace. He concludes from curve fitting his transient absorbance signal that the rate of removal exceeds the supply rate 3–20 times, depending on the atomization temperature. A much more thorough study has been described by Tessari, Torsi, and Paveri-Fontana (*6–8*), who describe the supply of the analyte by an Arrhenius-type rate constant and relate the removal of the analyte to diffusion and convection. Unfortunately, these investigations refer to a home-made open graphite rod atomizer and their data cannot be used for the enclosed commercial furnaces. Recently, Sturgeon and Chakrabarti

(9) studied the removal of analyte vapor from an enclosed furnace, but it will be shown that their data on removal rates may be subject to a serious systematic error.

The major object of the present study is the accurate and independent measurement of the supply and the removal of analyte vapor under typical analytical conditions in two commercial atomizers. The actual mechanisms of sample supply and removal need not be known to obtain quantitative data from which conclusions can be drawn about the efficiency of sample containment of either furnace. However, it appears that the results can be interpreted in terms of relatively simple expressions and vapor loss mechanisms.

THEORY

Relation between Absorbance and Number of Atoms inside the Furnace. Experimental information about the number of analyte atoms inside the cylindrical furnace is obtained by measuring the absorbance of a characteristic spectral line. At any moment, t, the relation between these two quantities can be expressed through Beer's law as

$$A(t) = \frac{0.43\ 2\sqrt{4\pi \ln 2}\, e^2\lambda^2 f g_0}{mc^2\, Z} \int_0^L \frac{H(t,x)\mathrm{d}N(t,x,\Delta y,\Delta z)}{\Delta\lambda_D(t,x)\Delta y \Delta z} \tag{1}$$

where e and m are the charge and the mass of the electron, c is the velocity of light, λ and f are the wavelength and the oscillator strength of the resonance line considered and g_0 and Z are the statistical weight of the ground state and the partition function of the element in concern. All these factors are independent of the time, t, and the position, x, along the line of observation, but the same is not necessarily true of the terms under the integral sign. Here $\Delta\lambda_D$ is the Doppler width of the atomic absorption line inside the furnace and H allows for the shift and collision width of this absorption line in relation to the width of the hollow-cathode primary source line (*10, 11*). Finally $\mathrm{d}N(t,x,\Delta y,\Delta z)$ is the number of analyte atoms inside a small volume $\mathrm{d}x\Delta y\Delta z$ and the integration extends over the length, L, of the furnace.

The awkward integral in Equation 1 is easily solved by introducing the following approximations.

(i) The Doppler width, $\Delta\lambda_D$, and the line shape factor, H, both increase with the gas temperature, $T(t,x)$, inside the furnace and, hence, depend upon the time, t, and the position, x, of observation. Fortunately, the ratio is much less temperature-dependent than either factor and its variation over the tube length is less than 10% at any time. This will allow us to place this ratio before the integral sign. In a second approximation we shall also ignore the time-dependence of this ratio, so that we can equate the variation of the atom number with that of the absorbance. This is not entirely valid during the initial rapid heating of the furnace, as will be discussed below.

(ii) Narrow beam observations across the furnace revealed that the variation of the absorbance over the diameter of the furnace is less than 10% for the minifurnace and less than 25% for the larger furnace. This allows us to assume a homogeneous distribution of the atoms over the cross section of the furnace, s. The ensuing uncertainty in the proportionality between absorbance, A, and atom number, N, is less than 10% in all cases.

It should be noted that the atoms need not be distributed homogeneously over the tube length, because the measured absorbance always reflects the integral of the number density along the line of observation. Insofar, however, as the atoms persist in front of the furnace, the effective tube length may be larger than the geometrical length, L. This will also be discussed below.

With these approximations, Equation 1 becomes

$$A(t) = \frac{0.43\ 2\sqrt{4\pi \ln 2}\, e^2\lambda^2 g_0 f H}{mc^2\Delta\lambda_D Zs} N(t) \tag{2}$$

where $N(t)$ is the time-dependent total number of analyte atoms in the furnace.

The uncertainty in the proportionality factor between absorbance and atom number arises mainly from the oscillator strength, f, and the line shape factor, H. The latter was estimated from the studies by Wagenaar and de Galan in flames (*12*). Note, however, that this uncertainty only impairs the absolute application of Equation 2 in estimating the furnace efficiencies. It is unimportant for the analysis of the time-dependence of the transient signal, which is the major object of the present investigation.

Time-Dependence of the Atom Number. Two approaches have been proposed in the literature to describe the variation of the number of analyte atoms in the furnace. The first originates from L'vov (*1*) and has also been utilized by Fuller (*5*)

$$\frac{\mathrm{d}N(t)}{\mathrm{d}t} = \left(\frac{\mathrm{d}N}{\mathrm{d}t}\right)_{in} - \left(\frac{\mathrm{d}N}{\mathrm{d}t}\right)_{out} \tag{3}$$

where the two terms on the righthandside express the rate of supply and the rate of removal of the atoms. In the maximum of the transient absorbance signal, the rates are equal. It is tempting to assume that the rising slope of the transient signal is equal to the rate of supply (*4*) and that the falling portion of this signal is determined entirely by the rate of removal (*9*). However, Equation 3 shows that this is true only if the smaller term in the difference is negligible in comparison with the larger one. If this condition is not fullfilled, a systematic error is made. Although Equation 3 is quite general, it can only be solved for special cases. Indeed, it is generally assumed that $(\mathrm{d}N/\mathrm{d}t)_{out}$ is proportional to $N(t)$. This is equivalent to an exponentially decaying removal of the atoms. However, this is not always observed in practice. Also, the formulation of $N(t)$ in terms of a differential equation does not lend itself easily for experimental analysis. To this end, a second approach formulated by Tessari et al. (*6*) is more useful. Here, the rate of supply is retained, but the time-dependent variation of $N(t)$ is expressed as a convolution

$$N(t) = \int_0^t S(t')R(t-t')\mathrm{d}t' \tag{4}$$

where $S(t) = (\mathrm{d}N/\mathrm{d}t)_{in}$ is the supply rate of the atoms and $R(t)$ is the normalized response of the system ($R_{max} = 1$) upon the supply of an infinitely rapid pulse of atoms. This formulation is equally general as Equation 3 but it is much more amenable to experimental verification. To this end we shall review a few properties of the convolution integral.

(i) If the removal function $R(t)$ is very rapid in comparison to the supply function, then

$$N(t) = S(t)\int_0^\infty R(t)\mathrm{d}t = S(t)\cdot\tau_R \tag{5}$$

where τ_R is defined as the equivalent time constant of the removal function. Thus the shape of $N(t)$ or $A(t)$ in this case reflects the time-dependence of the supply function. Conversely, if the supply of the analyte vapor is very rapid in comparison with the removal function, then

$$N(t) = R(t)\int_0^\infty S(t)\mathrm{d}t = R(t)\cdot N_0 \tag{6}$$

where N_0 is the total number of analyte atoms introduced into the graphite furnace. Hence, the shape of the experimental $A(t)$ curve is now equivalent to the shape of $R(t)$. The convolution integral thus expresses much more clearly than

the differential Equation 3 the conditions that must be fulfilled in order to measure the supply and removal function independently. Experimental realization of both alternatives will be described in the next section.

(ii) The integral of the time-dependent number of atoms is given by

$$\int_0^\infty N(t)\mathrm{d}t = [\int_0^\infty S(t)\mathrm{d}t][\int_0^\infty R(t)\mathrm{d}t] = N_0 \cdot \tau_R \qquad (7)$$

so that in combination with Equation 2 the total area of the measured absorbance curve is also proportional to $N_0\tau_R$ provided that all analyte elements are completely atomized, i.e. no molecules or ions are formed in the vapor phase.

(iii) Just as was done for the removal function in Equation 5, it is possible to define an equivalent time constant for the supply function as

$$\tau_S = \frac{\int_0^\infty S(t)\mathrm{d}t}{S_{max}} = \frac{N_0}{S_{max}} \qquad (8)$$

Now, the efficiency of the graphite furnace in containing the analyte atoms is directly related to the ratio τ_R/τ_S (*1*). If this ratio is very small, it means that the atoms are slowly released and rapidly removed, so that Equation 5 applies and the maximum number of atoms in the furnace is given with Equation 8 as

$$N_{max} = S_{max}\tau_R = \frac{N_0\tau_R}{\tau_S} \qquad (9a)$$

If, on the other hand, τ_R/τ_S becomes very large, the atoms are rapidly supplied and slowly removed, so that Equation 6 applies and the maximum of analyte atoms is given by

$$N_{max} = R_{max} \cdot N_0 = N_0 \qquad (9b)$$

This means that with increasing value of τ_R/τ_S the efficiency $\eta = N_{max}/N_0$ is first equal to τ_R/τ_S and ultimately approaches unity. The exact correlation between N_{max}/N_0 and τ_R/τ_S depends, of course, upon the relative shapes of the supply function, $S(t)$, and the removal function, $R(t)$.

Physical Description of the Supply Function. One of the objects of the present investigation is to relate the measured transient signals to physical parameters of the analyte and the atomizer. For the supply of the sample we can use the extensive studies that have been published in the past few years. It is generally assumed that after evaporation of the solvent (during drying) and the matrix (during ashing), the analyte is retained as a mono-atomic layer on the graphite surface. Indeed, 1 ng of analyte atoms then covers an area of about 1 mm^2, which is much less than the cross section of the droplet introduced on the furnace wall.

For the release of the analyte atoms, L'vov first assumed that the rate of evaporation is constant (*1*) and in a later publication took it to increase linearly with time (*13*). Fuller (*5*) assumed that the rate of supply is proportional to the number of analyte atoms still retained at the graphite wall. This assumption greatly facilitated the solution of the differential Equation 3. Tessari et al. (*6*) utilized the same model, but also accounted for a variation of the rate constant during atomization. This is necessary, because in most atomizers the release of the analyte takes place during and as a consequence of the warming up of the graphite wall. In other words, the heating of the tube is the rate-determining step and Tessari et al. showed that their data could be well described by an Arrhenius-type expression for the rate constant

$$S(t) = \left(\frac{\mathrm{d}N}{\mathrm{d}t}\right)_{in} = -\frac{\mathrm{d}N_w}{\mathrm{d}t} = Be^{-E/RT_w}N_w \qquad (10)$$

where T_w is the temperature and N_w is the number of analyte atoms at the graphite wall. Realizing that $\int S(t)dt = N_0 = N_w$ ($t = 0$), we obtain for the rate of supply of the analyte atoms

$$S(t) = N_0 Be^{-E/RT_w(t)} \exp[-\int_0^t Be^{-E/RT_w(t')}\,\mathrm{d}t'] \qquad (11)$$

During the first moments of analyte release, the integral in Equation 11 is practically zero and a semilogarithmic plot of $S(t)$ vs. $1/T_w(t)$ will yield the values for the activation energy, E, and the frequency factor, B. Provided $S(t)$ is slow in comparison with $R(t)$ (Equation 5), the initial portion of the normal absorbance signal measured in commercial atomizers yields the same information. This procedure has been successfully utilized by Sturgeon et al. (*4*) in order to clarify the processes and reactions responsible for analyte release. The present derivation demonstrates the validity of this approach more clearly than their analysis, where at one point of the derivation it was necessary to assume steady-state conditions ($dN/dt = 0$). Obviously, this is only valid in the maximum of the absorbance curve, whereas in fact the initial part of this curve must be used, as has been done by Sturgeon et al. (*4*). They were able to assign the experimentally observed activation energies to those of distinct chemical and physical processes, such as vaporization, dissociation, carbide formation. The exponential term in the Arrhenius expression thus appears to be well validated.

Much less is known about the frequency factor, B. The experimental determination as described above is very imprecise. Indeed from curve-fitted supply functions, Tessari et al. derived values of B between 10^{11} s^{-1} and 10^{17} s^{-1} (*8*, *14*) in agreement with estimates calculated by Cordes (*15*).

In summary it appears that at present Equation 11 offers the best description of the analyte introduction process. Of the two parameters, the activation energy is readily measured and well correlated with actual processes at the graphite surface, but the frequency factor is only roughly known and still impredictable.

Physical Description of the Removal Function. In comparison to the supply of the analyte atoms into the graphite cell, the removal of the vapor from the furnace has received much less attention. After L'vov (*1*) most authors (*5*, *9*, *16*) simply state that the rate of analyte loss is proportional to the number of analyte atoms present in the furnace. This is equivalent to an exponentially decaying removal function. This behavior would be expected from a purely diffusion controlled transport process and the rate constant would then be proportional to D/L^2, where D is the mass diffusivity. Indeed, Fuller observed a slight increase of his rate constant for sample removal with temperature.

In real furnaces, several factors disturb this simple picture.

(i) In the first place the sample is introduced onto and released from the center of the furnace wall only. Consequently, even for a pure diffusion process, the analyte vapor requires some time to reach the open furnace ends and disappear gradually into the ambient space. This means that the response function will be constant for an initial period of time and then decrease exponentially. The mathematical description of this process is presented in the appendix and yields that $R(t)$ is stationary for a period of time equal to $0.024\ L^2/D$ and decays exponentially with a time constant equal to $0.101\ L^2/D$. Hence the total equivalent time constant due to diffusion is equal to

$$\tau_d = \frac{0.125L^2}{D} \qquad (12)$$

which agrees with the expression of L'vov (*1*).

The diffusivity depends, of course, upon the vapor temperature inside the furnace. For tube lengths of about 1 cm and a diffusivity of 3 cm^2/s, this time constant is of the order of 40 ms.

(ii) As remarked earlier, the analyte is supplied into and removed from the furnace during a period of time, when the wall temperature and hence the gas temperature is still increasing. Consequently, the vapor inside the furnace is expanding and this will expel the analyte from the furnace. The equivalent time constant for this process is approximately given by

$$\tau_e = \frac{T(t_0)}{\left(\frac{dT}{dt}\right)_{t_0}} \tag{13}$$

where $T(t_0)$ and $(dT/dt)t_0$ are the temperature and the heating rate of the vapor at the moment, t_0, of introduction of a particular analyte atom. For ordinary heating rates, this time constant generally exceeds the diffusive time constant by far, except in rare cases of long tubes and small diffusivities.

(iii) In the larger commercial graphite furnaces, a constant flow of protecting gas is employed that partly enters the furnace through holes drilled in the wall. This induces a convective transport of the vapor from the furnace. The time constant of this process will be related to the ratio of the cell volume, V, and the cold gas flow rate through the furnace, F. In addition the cold gas is heated after its introduction into the furnace and this enhances the effective flow rate through expansion, i.e.

$$\tau_c = K \cdot \frac{V}{F} \cdot \frac{300}{T} \tag{14}$$

However, the proportionality factor, K, is difficult to predict, because it depends upon the flow pattern through the furnace. Still, it is obvious that for a typical cell volume of a few cm^3, a flow rate of 1 L/min at 300 K and a furnace temperature, T, of 1000 K, the time constant can easily become as small as 50–100 ms, which is much smaller than either expansive or diffusive time constants in large furnaces.

(iv) So far we have only considered transport processes in the gas phase that can be described in general terms. In real furnaces, element-specific removal processes may also occur. For example, element recombination in the gas phase (2), diffusion through the porous graphite wall (*4*, *16*), condensation at and possibly redesorption from the cooler furnace ends (*9*, *14*) have all been suggested as possible sample loss processes. These will not be considered, because they can, in principle, be prevented by appropriate furnace design. In the present study, the elements were selected in such a way that these disturbing effects are minimal, but the reader is warned that our results need not necessarily apply to the conditions prevailing in a particular analysis.

In general then, the removal function of a graphite furnace is the complex result of at least three different transport processes: diffusion, expansion, and convection. The integration into one analytical expression is a formidable problem that surpasses the object of this investigation. If, however, all three processes can be approximated by an exponential decay, then the overall response function will also be a decreasing exponential. This is true because an exponentially decaying response function is equivalent to a rate of analyte loss proportional to the number of atoms in the furnace, hence

$$\left(\frac{dN}{dt}\right)_{out} = -\left[\frac{N}{\tau_d} + \frac{N}{\tau_e} + \frac{N}{\tau_c}\right] = -N\sum_i \frac{1}{\tau_i}$$

with the solution

$$N(t) = N(t_0)\exp\left[-t\sum_i \frac{1}{\tau_i}\right] = N(t_0)\cdot R(t) = N(t_0)e^{-t/\tau_R}$$

Therefore the time constant of the overall removal function is equal to

$$\frac{1}{\tau_R} = \frac{1}{\tau_d} + \frac{1}{\tau_e} + \frac{1}{\tau_c} \tag{15}$$

This will at least be approximately true for the systems presently investigated.

Equality of Wall Temperature and Vapor Temperature. Whereas the surface temperature, T_w, of the graphite wall, which is responsible for the release of the analyte (Equation 11), is readily measured, this is not true for the vapor temperature, T, which appears in all removal time constants (Equations 12, 13, 14). The equality of these two temperatures has long been taken for granted, but has been shown to be incorrect for larger furnaces in two recent publications (*17*, *18*). With some simplifying but realistic assumptions, this problem is readily treated in terms of heat transfer coefficients. The full results will be presented elsewhere (*19*), but the conclusions of these calculations can be stated as follows.

(i) In static systems, without convection, the time lag between wall temperature and gas kinetic temperature is no more than 5 ms and the difference between those two temperatures depends upon the heating rate and the furnace diameter, but at any cross section never exceeds 5 K in the system presently investigated. Naturally, there will be a gradient of both the wall temperature and the vapor temperature along the furnace, but this does not impair the conclusion for each infinitesmal cross section.

(ii) With forced convection this situation is markedly different, because at any moment during the atomization the cold inert gas needs time to reach the wall temperature. This time can be converted into an equivalent distance travelled by the inert gas. Obviously, the distance needed for the inert gas to reach the wall temperature depends upon the furnace diameter, the wall temperature, and the flow rate of the inert gas. For the larger furnace considered in this study it may take 1.5 cm before the centrally introduced argon has been heated to 90% of the wall temperature. Consequently, towards the end of the atomization step the wall temperature of the graphite can exceed the average gas temperature inside the furnace by several hundred degrees. This agrees with the experimental evidence (*17*, *18*).

EXPERIMENTAL

Two different atomizers have been investigated. One a Varian Techtron Carbon Rod Atomizer model 63 and the other a home-made copy of the Perking-Elmer HGA-72. In the latter case the commercial model could not be used as such, because it did not permit the measurement of the temperature distribution along the furnace wall. To this end a narrow slit was engraved in the housing, allowing a variable observation position through a sliding window. The wall temperatures were measured with a pyrometer utilizing a silicon photo element (Siemens BPY 11) with a response time less than 1 ms. The voltage across a 100 kΩ output impedance was recorded on an ordinary strip-chart recorder (0.6 s full scale deflection). Control measurements on a rapid UV-recorder showed this observation system to be ten times more rapid than the fastest temperature variation recorded. The pyrometer was calibrated against a commercial optical pyrometer and against the melting points of small metallic particles introduced in the furnace. The pyrometer selects an area of about 4 mm^2 from the outer furnace wall, but the calibration procedure ensures that the reading reflects the inner wall temperature.

The furnaces are heated with a constant voltage derived from a 5-kW variable transformer. Maximum temperatures up to 3000

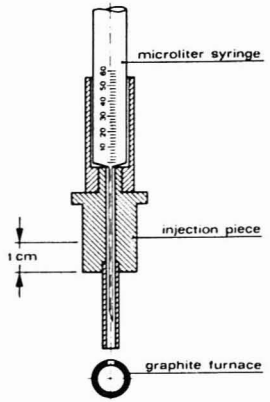

Figure 1. Injection piece for the rapid introduction of mercury vapor into the heated graphite furnace

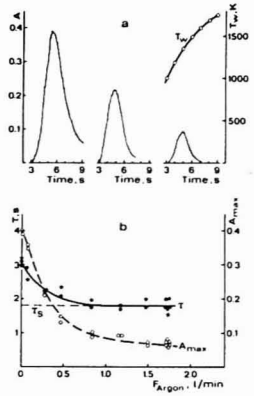

Figure 2. Experimental measurement of the supply function. (a) Transient signals measured for silver in the HGA-72 furnace for a constant heating program (extreme right drawing) and increasing forced-convection flow rates. (b) Peak absorbance (o) and normalized peak area τ (☆) as a function of convective argon flow rate. With increasing flow rate, the latter parameter approaches the time constant, τ_S, of the supply function

K are possible with either furnace.

The absorbance is measured in the usual way. Primary radiation from commercial hollow-cathode lamps is mechanically chopped at 400 Hz, dispersed by a 0.25-m monochromator and phase-sensitively detected by a photomultiplier and a lock-in amplifier. Because the absorbance varies much more rapidly than the furnace temperature, this cannot be recorded accurately on an ordinary recorder. Instead, a rapid two-pen recorder is used to record the atomizing voltage of the furnace on one channel and the transmittance on the other channel. The frequency bandwidth of 125 Hz was verified to be sufficient to record the fastest signals undistorted.

As stated in the preceding section, the absorbance signal reflects either the supply function or the removal function of the graphite furnace if the alternative process is made very rapid. A comparatively rapid removal function was realized by forcing a high flow of inert gas through the furnace. With increasing flow rate the peak absorbance continuously decreases, but the signal shape ultimately becomes unvariable. At this point the supply function is obtained.

A rapid, pulse-like introduction of metal was realized in the following manner. An injection syringe is filled with 10 μL (for the smaller furnace) or 50 μL (for the larger furnace) of air saturated with mercury vapor. The syringe is placed in an injection piece provided with a ceramic guiding tube, as illustrated in Figure 1. The distance between the end of the tube and the introduction orifice of the furnace is about 2 mm, whereas the distance between the orifice and the end of the injection needle is about 12 mm. In this way the injection needle is protected against the furnace heat.

At any moment during the atomization cycle, the mercury vapor could be manually injected into the furnace, so that the variation of the removal function with the furnace temperature could be studied. Using a suitable injection syringe, the mercury vapor could be introduced in less than 10 ms, which is three times more rapid than the fastest removal function recorded.

All chemicals were reagent grade or better.

RESULTS AND DISCUSSION

The Supply Function. Figure 2a presents the absorbance signals obtained for a constant amount of silver and a particular atomizing voltage applied to the larger furnace with increasing argon flow through the furnace. As expected, the signal first becomes narrower with increased forced convection, but at an argon flow rate of 0.8 L/min a constant shape is reached which describes the supply function at this particular heating program. Simultaneously, the maximum absorbance continues to decrease (Figure 2b), but the equivalent time constant obtained from the normalized signal is constant within the experimental error of about 10%. It was verified that these results are independent of the amount of silver introduced as long as we stay within the linear portion of the analytical curve (<100 ng).

Similar experiments were carried out for the smaller furnace and for two other elements, lead and manganese. The examples in Figure 3 are selected from a large amount of data to illustrate the conclusions to be drawn from these experiments. The first and most important conclusion agrees with that of others (*4*, *8*, *14*): the supply function is determined entirely by the furnace temperature. Over the range of operating conditions studied (atomizing temperatures between 1000 and 2000 K, heating rates between 100 and 1000 K/s. The entire absorbance signal always falls within the rising portion of the temp. profile (compare Figure 2a). For slow heating to low maximum temperatures, the supply of analyte vapor can easily persist for more than 5 s, but for heating rates and atomizing temperatures normally employed in practical analysis, it lasts typically about 1 s in either furnace for all three elements studied.

Given this strong temperature dependence, it is important to check if the supply function can be adequately described by first-order kinetics, as suggested in the theory section. To this order the experimentally measured supply functions are compared with theoretical curves calculated from Equation 11 with known heating curves, $T_w(t)$. In all cases the initial portions of the experimental curves were used to obtain the pertinent activation energy and frequency factor (required for Equation 11) from a semilogarithmic plot of $A(t)$ vs. $1/T_w(t)$ (*4*). In addition, the theoretical curves are normalized to the same area as the experimental curves, both areas being proportional to N_0, the amount of analyte introduced into the furnace.

With these adaptations it is not surprising that the initial portions of the curves coincide completely. Also, the positions of the absorbance maximum agree very well. Obviously, however, the theoretical supply function falls off much more sharply than the experimental curve. Accordingly, the experimentally observed maximum absorbance is lower than the theoretically predicted value. This means that the supply of

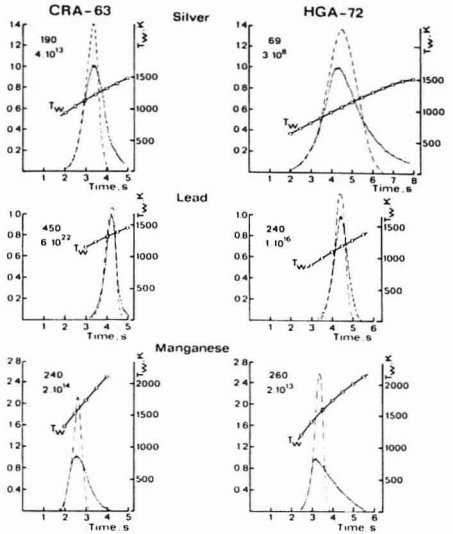

Figure 3. Experimental (—) and theoretical (- - -) supply functions for silver, lead, and manganese in two commercial atomizers. Experimental curves are normalized to unit peak height. The numbers in each drawing designate the activation energy (in kJ/mol) and the frequency factor (in s^{-1}) derived from the initial portion of the experimental curves. These data are used to calculate the theoretical supply curves after Equation 11 with the area normalized to that under the corresponding experimental curve

analyte vapor cannot be fully described by a first-order rate constant with an Arrhenius-type temperature dependence. This conclusion agrees with the limited success of Torsi and Tessari to describe the supply function of lead by a single set of values for the activation energy and the frequency factor (*14*). Actually, Figure 3 shows that lead is a favorable example in comparison with the larger disagreement observed for silver and manganese in either furnace.

Two reasons can be advanced to explain these differences. In the first place the experimental supply function may be stretched by gas phase phenomena occurring after the initial volatilization of analyte vapor from the furnace wall (Note that the supply function refers to the total mass of analyte vapor in the furnace, integrated along its length). Thus adsorption and redesorption of vaporized analyte atoms as well as dissociation of dimers formed in the gas phase both account for a secondary atom supply that would elongate the overall supply function. The fact that the curves in Figure 3 agree somewhat better for the smaller CRA-63 furnace than for the larger HGA-72 furnace lends support to this argument. However, it should be realized that the supply functions are measured under rapid forced convection that makes the period spent by an individual atom in the gas phase very brief. Also, the agreement for silver and manganese in the smaller furnace is still only moderate.

Therefore, we are inclined to believe that the discrepancies observed in Figure 3 are not due to gas phase reactions but indicate that the parameters E and B in the Arrhenius expression (Equation 10) are not equal for all analyte atoms of one particular element. This might be due to the fact that the adsorption sites at the graphite surface are not completely equivalent: some carbon atoms release the adsorbed analyte more readily than others. The activation energies presented in Figure 3 thus represent a lower limit valid for the most easily released analyte atoms, because they are derived from the initial portion of the supply function. The same conclusion would apply to the data of Sturgeon et al. obtained in a similar way (*4*).

Several arguments support this conclusion, at least qualitatively. Despite the limited accuracy of the stated activation energies (±20 kJ), the values for silver and lead show significant differences between either furnace. These may be related to difference in electrical and heat conductivity or in surface texture between the pyrolytically coated CRA-63 and the normal graphite HGA-72 (*20*). It was also observed that the supply function, and hence the values for E and B, changes gradually with prolonged usage of a particular furnace tube. And finally, the activation energies found in this study disagree with those found by others. Sturgeon et al. (*4*) measured an activation energy of 385 kJ for manganese in contrast to our value of about 250 kJ and only 193 kJ for lead, which is lower than both our values (240 and 450 kJ) and the value of 315 kJ reported by Torsi and Tessari (*4*).

In summary we conclude that the release of atoms from the graphite surface in commercial atomizers is controlled entirely by the heating program applied. Under ordinary conditions it may be characterized by an equivalent time constant of about 1 s. Appreciable reduction of this time constant requires a much more rapid heating than provided in present instruments.

Secondly, it has been shown that the shape of the supply function depends strongly upon the physicochemical properties of the graphite surface and can only be approximately described in terms of a single first-order Arrhenius-type rate constant. The prolonged supply of analyte vapor observed is probably due to variable reactivity of the surface atoms and to a lesser extent to gas-phase reactions.

Removal Function in a Small Furnace. The Varian Techtron CRA 63 furnace system is characterized by the following data. It is a small furnace (length 9 mm, diameter 3 mm); it is uniformly heated (at 2000 K, the temperature difference measured up to 1 mm from the edges is 100 K) with heating rates up to 1000 K/s, there is no convective flow inside the furnace, but outside the furnace the vapor is swept away by an upward flow of inert gas. Consequently, we expect diffusion to be the dominant removal process and, according to Equation 12, the equivalent time constant should depend on the vapor temperature inside the furnace through the diffusivity.

The following experiment was carried out to evaluate this hypothesis. For atomization voltages between 3.6 and 8.3 V supplied to the furnace, 10 μL mercury vapor was rapidly injected onto the furnace at various moments after the application of the power. The absorbance of the mercury line at 254 nm was recorded. The general shape of the signal is illustrated in Figure 4a. It was verified that this shape is independent of the amount of mercury vapor introduced (up to 50 μL). The initial rise of the signal is due to the finite time of 10 ms needed for the vapor introduction, but the rapid decrease of the signal very closely follows an exponential decay. The time constant is thus found as the slope of a semilogarithmic plot of absorbance vs. time.

The time constant can be plotted against the moment of mercury injection and in this way a separate hyperbolical curve was obtained for each atomization voltage: the time constant decreases with increasing moment of injection. However, if the measured wall temperatures are used to convert each curve into a plot of time constant vs. the furnace temperature at the moment of injection, all curves coincide into the one general curve presented in Figure 5. Indeed, it can be seen that within the experimental error, all time constants mea-

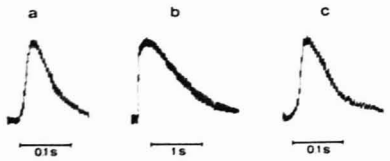

Figure 4. Experimentally determined response functions using the mercury injection technique. (a) CRA-63 furnace. (b) HGA-72 furnace without convective argon flow. (c) HGA-72 furnace with forced convection of 1.6 L/min. Note difference in time scales

Table I. Diffusivity Values, Calculated after Ref. 18

	Diffusivities (cm^2/s)				
Element	Pb	Ag	Ag	Hg	Mn
Ambient gas	Ar	Ar	N_2	Ar	Ar
Temperature, K					
500	0.23	0.27	0.31	0.33	0.33
1000	0.90	1.0	1.2	1.1	1.3
1500	1.8	2.2	2.5	2.3	2.7
2000	3.0	3.6	4.0	3.7	4.4
2500	4.4	5.3	5.9	5.4	6.5

sured for different atomization voltages and different moments of injection can be related to one parameter, the wall temperature of the graphite which for this small, static system is practically equal to the vapor temperature. With increasing temperature, the time constant decreases from 200 to 30 ms which is appreciably smaller than the time constant of the supply function (Figure 3).

The dashed curve in Figure 5 represents the theoretical diffusive time constant, expressed by Equation 12. Data for the diffusivity calculated from the Chapman–Enskog theory (*21*) are given in Table I and are estimated to be accurate within 10%. The curves in Figure 5 agree well for the lower temperature range, but for higher furnace temperatures the experimental values are two times larger than the theoretical predictions. One possible explanation of this discrepancy is an incorrect temperature dependence of the calculated diffusivities. The data entered in Table I for mercury show that D is proportional to $T^{1.8}$. However, in order to reconcile the theory with experiment, this dependence must be taken as $D \sim T^{1.2}$, which is outside the margin of uncertainty. Therefore, another explanation appears more plausible.

In calculating the time constant with Equation 12, the length, L, is taken to be equal to the geometrical length of the furnace. However, for rapid removal, the mercury atoms leave the furnace with appreciable momentum and may not be directly carried away with the upward stream of lighter argon atoms outside the furnace. A simple momentum calculation shows that, indeed, the mercury atoms may persist for another 2 mm outside the graphite furnace before they leave the region of observation. This would increase the effective length by 50% and L^2 by a factor of two. This effect thus easily explains the difference between the experimental values and the straightforward theoretical calculation.

We conclude, therefore, that the removal of analyte atoms from the small Varian Techtron furnace is due to diffusion, leading to time constants between 100 and 30 ms for mercury. For other elements, the time constants will be smaller or larger according to differences in the diffusivities. The examples given in Table I show, however, that the variation of the diffusivity is relatively small. For example, at 1500 K, the values vary between 1.8 and 3 cm^2/s, so that the range of τ_R will not differ greatly from that estimated above for mercury, for which D (1500 K) is equal to 2.3 cm^2/s.

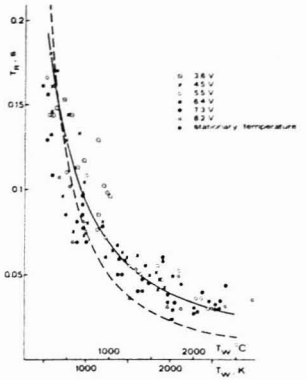

Figure 5. Time constant for the response function in the CRA-63 furnace as a function of the wall temperature. Different symbols correspond to different heating programs. The solid line represents a weighted average through the data points, whereas the dashed curve represents a theoretical estimate based on diffusion as the sole removal process (Equation 12)

Removal Function in a Static Larger Furnace. Similar experiments as described above for the larger Perkin-Elmer furnace operated without forced convection yield, of course, much larger time constants. The geometrical length of this furnace is 53 mm and its diameter is 8.5 mm. The general shape of the removal function is shown in Figure 4b. Again the shape is independent of the amount of mercury vapor introduced (50 μL in this case) and the time constant is typically of the order of 1.5 s. However, the shape of the removal function is different from the one obtained with the smaller furnace. After rapid injection of the mercury vapor within 10 ms, the absorbance signal is seen to first increase slightly and then decrease rather slowly. The initial increase is probably due to an increase of the absorption coëfficient with the increasing temperature through the factor $H/\Delta\lambda_D$ in Equations 1 and 2. Thus, it does not reflect an increase in the number of mercury atoms inside the furnace. This number stays constant for the small period of time needed for the atoms to diffuse away from the center of the furnace towards the end of the tube. At this point in time, we expect an exponential decay, if the dominant process is diffusion. However, it was observed that various data collected for different atomization voltages and different moments of mercury injection cannot be described by a single temperature dependence (as in Figure 5), but depend also upon the heating rate applied (Figure 6a). This is not due to the variation of the temperature along the furnace. Indeed, this longitudinal variation increases with increasing heating rate and hence the average temperature inside the furnace becomes lower. In turn, at each particular central wall temperature, the effective diffusivity is smaller for faster heating rates so that the time constant would be increased. Actually, the reverse is observed: faster heating reduces the time constant. The correct explanation is that in a static furnace of this size, expansion contributes significantly to the removal of analyte atoms. According to Equation 13, the equivalent time constant of this process does not only depend upon the temperature at the moment of injection, but also decreases with increasing heating rate. Insofar as different atomizing voltages correspond with different heating rates, the curves in Figure 6a do not coincide.

Another consequence of the expansive contribution is that the tail of the removal function in Figure 4b does not follow an exponential decay. Therefore, the overall time constant,

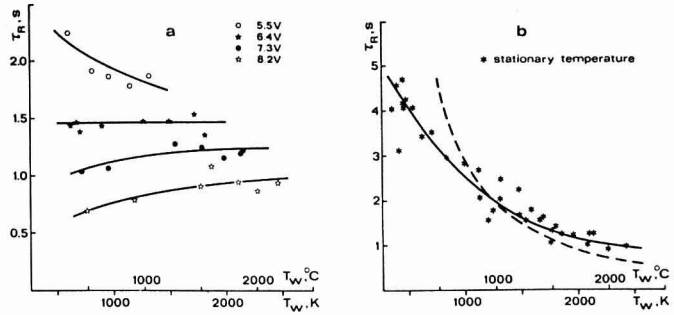

Figure 6. Time constant for the response function in the HGA-72 under static conditions (no convective argon flow). (a) Nonstationary temperatures arising from different heating programs illustrating the influence of thermal expansion. (b) Stationary temperatures reached at the end of different heating programs. The solid curve connects the data points. The dashed curve represents the theoretical estimate based on Equation 12. Note the difference in time scale between *a* and *b*

Table II. Relative Importance of Expansion in Comparison to Diffusional Removal of Atoms in the HGA-72 Furnace

Injection conditions		Experimental time constants, s		Expansion time constants, s	
Temperature, K	Heating rate, K/s	τ_R (Fig. 5a)	τ_d (Fig. 5b)	τ_e (Eq. 15)	τ_e (Eq. 13)
800	190	1.45	2.9	2.9	4.1
800	115	1.96	2.9	6.0	6.7
1300	250	1.20	2.0	3.0	5.1
1300	160	1.47	2.0	5.7	8.0
1800	260	0.95	1.34	3.2	6.8
1800	140	1.24	1.34	16	13
2300	125	1.00	1.03	35	18

τ_R, is determined in this case as the area under the experimental curve (Equation 5). The results presented in Figure 6a show that the time constant varies between 0.7 and 2 s depending upon the furnace temperature and its heating rate, characterized by the atomizing voltage.

If the furnace is allowed to reach a stable temperature before the mercury vapor is injected, then expansion is no longer operative and a single temperature-dependent curve is again observed for all atomizing voltages. This is shown in Figure 6b, which may be compared with Figure 5. The dashed curve again represents the theoretical estimate of the diffusive time constant calculated from Equation 12. In contrast to Figure 5 the lower temperature portion of this curve does not agree very well with experiment. The reason is that it is extremely difficult to realize a truly static system and prevent all draft through the long open tube. This effect should be more pronounced in even longer furnaces (*16*). Because atomization temperatures below 700 K are not realistic anyhow, this portion of the curve will not be considered further.

At higher temperatures the theoretically predicted time constant is 30% smaller than the experimentally observed one. Again, this is partly due to the elongation of the effective tube length by outward diffusion of the atoms discussed in connection with Figure 5. In addition, a second reason for the observed difference is a significant variation of the diffusivity along the tube. The dashed curve in Figure 6b is calculated on the basis of the wall temperature in the center of the tube. In contrast to the smaller furnace, however, the longer furnace exhibits an appreciable decrease of the temperature towards the ends, that are clamped into water-cooled electrodes. Measurements indicate a temperature drop of 100 K over 1.5 cm from the center and, no doubt, the temperature decreases even more towards the tube endings. The inherent decrease of the diffusivity can easily account for the discrepancy observed between the experimental and theoretical curves in Figure 6b.

Returning now to Figure 6a we can estimate the relative contributions of diffusion and expansion in a long furnace that is being heated up to its final temperature. Using Equation 15 we can derive the expansive time constant, τ_e, from the measured τ_R value and the measured diffusive time constant τ_d (Figure 6b). Alternatively, we can also calculate values for τ_e from Equation 13. The results are presented in Table II. In view of the highly approximate nature of both estimates, the agreement between the data in the final two columns of this table is considered to be satisfactory. It shows that for elements vaporized at relatively low temperatures and ordinary heating rates, expansion contributes significantly to the removal process and its equivalent time constant is quite comparable to the diffusive time constant. At higher furnace temperatures, the heating rate is usually also higher, but the inherent reduction of the expansive time constant is outweighed by an even larger acceleration of the diffusion process. Consequently, involatile elements requiring a high vaporization temperature are removed from a static furnace almost entirely by diffusion. At temperatures over 1500 K, this is by far the dominant removal process.

This conclusion is based entirely on experiments with mercury, because this is the only element that could be introduced rapidly enough to warrant accurate measurement of the pure removal function. It need not be valid for other elements. Indeed, Sturgeon and Chakrabarti recently suggested that specific interactions with the graphite wall account for major analyte losses (*9*). However, quantitative data presented in their paper indicate that this conclusion may have been based on erroneous measurements. For example, the authors report for a smaller furnace than the one presently studied, a removal time constant at 2500 K of 3 s (compare Figure 6b). Accordingly, the derived diffusivity of 1 $cm^2 s^{-1}$

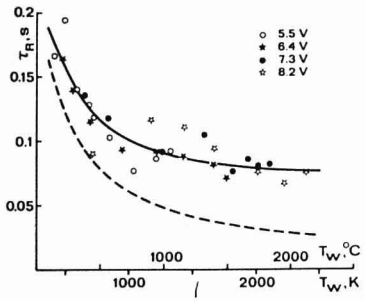

Figure 7. Time constant for the response function in the HGA-72 under forced convection (1.6 L/min). The solid curve connects the data points. The dashed curve represents the theoretical estimate based on convective flow as the sole removal process (Equation 14). Further discussion in the text

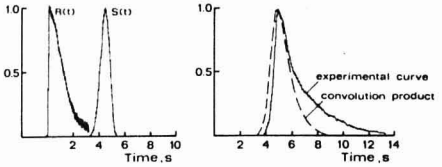

Figure 8. Comparison between experimental transient signal for lead (solid line in right drawing) and theoretical prediction (dashed line in right drawing) under static conditions in the HGA-72. The latter curve is calculated as the convolution integral from the supply function for lead and the removal function for mercury (left drawing) determined experimentally under identical conditions

is five times smaller than the accepted values (Ref. 1, Table 1) as recognized by the authors. Also their removal rate is not inversely proportional to the pressure as would be suspected for a diffusion-controlled process. This cannot be convincingly explained. In the introduction of the paper, Sturgeon and Chakrabarti recognize that their procedure to derive the removal rate constant from the tail of the transient absorbance curve may be in error. Indeed, the discussion of Equations 3 and 6 has shown that it is essential that the introduction be much more rapid than the removal in order to measure the latter correctly. In view of the slow supply of analyte vapor in commercial atomizers, it appears that the transient curves obtained by Sturgeon and Chakrabarti without such precautions actually reflect the supply function only.

Removal Function in a Larger Furnace with Forced Convection. In analytical practice the Perkin-Elmer furnace is usually not operated under completely static conditions, because this unacceptably shortens the life-time of the furnace. Under normal operating conditions the protective argon flow rate is 1.6 L/min. An appreciable though unknown fraction of this actually enters the furnace through holes drilled in the wall, the central one serving to introduce the sample. It is not surprising then that the removal function is now significantly shortened (Figure 4c) and the equivalent time constant is again a function of the temperature at the moment of injection only (Figure 7). This is expected, because forced convection is now the dominant removal process and the equivalent time constant is inversely proportional to the gas temperature inside the furnace.

Again, however, the experimental time constants appreciably exceed the theoretical τ_c values calculated from Equation 14 (dashed curve in Figure 7). Several arguments can be advanced to account for this difference. In the first place, there is a significant difference between the vapor temperature in the dynamic furnace and the central wall temperature (*20*). This difference depends upon the flow rate of the argon and is proportional to the wall temperature itself. At 1500 K, it can easily amount to 500 K near the injection port where the cold argon is introduced. The actual vapor temperature is thus lower than the wall temperature and this raises the convective time constant according to Equation 14.

A second process may be even more important. If the total argon flow were introduced into the injection port and would flow laminarly through the furnace, the convective time constant at room temperature is easily calculated from the furnace volume as 110 ms (Equation 14). The extrapolated experimental curve yields a twofold higher value of about 220 ms at room temperature (Figure 7). Consequently, only 50% of the argon enters the furnace centrally, whereas the other 50% is distributed over smaller holes drilled towards the ends of the graphite tube. This is the situation at room temperature, but at higher temperatures this distribution may well be different, due to differences in gas viscosity.

These considerations are not only offered here to account for differences between theory and experiment, but also to indicate how complex the phenomena are in a dynamic furnace operated under forced convection.

The much lower time constants shown in Figure 7 as compared to the results in Figure 6 demonstrate the preponderance of forced convection over diffusion. In technological literature this would be expressed as the Péclet number (i.e. $vL/2D$, where v is the linear velocity of the argon) being much larger than unity. Indeed, the calculated Péclet number turns out to be 10 or more, dependent on the gas temperature.

Efficiency of Commercial Furnaces. The previous results have made it clear that under normal operating conditions the removal function of commercial graphite atomizers is much more rapid then the supply function. In the static Varian Techtron minifurnace and in the larger Perkin-Elmer furnace operated under forced convection, the analyte atoms are removed within 0.1 s (Figures 5 and 7), whereas they are released from the graphite surface over about 1 s. Consequently, the transient signal observed in practical analyses very closely agrees with the supply function.

Only in larger furnaces operated under static conditions, the removal function becomes comparably slow to the supply function, both having time constants of about 1 s. As an example, Figure 8 shows the removal function for mercury and the supply function for lead and the calculated convolution integral (Equation 4). Indeed, the total transient signal is significantly broader than either function separately. The directly measured transient absorbance signal for lead under these conditions is even broader. This was also observed for other elements and must be attributed to adsorption and redesorption of initially vaporized analyte. This effect would be more pronounced under completely static conditions, where the vapor spends a comparatively long time inside the furnace.

When the removal function is much more rapid than the introduction function, its influence cannot be detected from the shape of the convolution product. In that case Equation 7 offers another possibility to check the validity of our measurements from ordinary absorbance signals. Because the integral of the transient atom number is equal to $N_0\tau_R$, the area of the transient absorbance curve should also be directly proportional to the time constant of the response function. Such an analysis is presented in Table III for four elements.

The first column of this table gives experimental values for the ratio of the absorbance areas measured under different conditions and corrected for differences in furnace cross section (Equation 3) and for differences in the amount of analyte introduced. These ratios should be equal to the ratios

Table III. Correspondence between Peak Area of the Transient Signal and Time Constant of the Response Function

Element	Systems compared	Corrected ratio of peak areas	Ratio of τ_R
Ag	HGA-72 stop/HGA-72 flow	9.7	15
	CRA-63/HGA-72 flow	0.73	0.81
Pb	HGA-72 stop/HGA-72 flow	15	16
	CRA-63/HGA-72 flow	0.98	0.70
Mn	HGA-72 stop/HGA-72 flow	11	12
	CRA-63/HGA-72 flow	0.90	0.62
Cd	HGA-72 stop/HGA-72 flow	5.7	6.3
	CRA-63/HGA-72 flow	0.48	0.72

of the corresponding τ_R values, which are presented in the next column. Here the τ_R values are taken from the Figures 4, 5, and 6 for the average temperatures during the atomization peak. Good to fair agreement is found in nearly all cases.

We now turn to the important aspect of the efficiency of the graphite furnace to maintain the analyte vapor within the observation region. In the theory section we have related this efficiency, N_{max}/N_0, to the ratio of the time constants τ_R/τ_S. For small values both ratios are numerically equal. For larger values of τ_R/τ_S the efficiency increases more slowly and the exact relationship depends upon the relative shape of the supply function and the response function. However, a few examples shown in Figure 9 show that for an exponentially decaying response function, different supply functions yield only minor variations in predicted efficiencies. Consequently, for known time constants it is possible to estimate the efficiency from Figure 9 at least in first approximation.

Now, the efficiency can also be calculated from the known amount of analyte introduced into the furnace, N_0, and the maximum number, N_{max}, derived from the measured peak absorbance with Equation 2. Here it must be assumed that all vaporized analyte is completely atomized. This yields an experimental value for the efficiency. These data are entered in Table IV for four elements and three different furnace conditions.

The first and perhaps most important conclusion to be drawn from Table IV is the observation that for ordinary analytical conditions, the efficiencies of both commercial furnaces are rather low. The agreement between predictions based on measured time constants and values derived from peak absorbances is surprisingly good in view of the uncertainties connected with the oscillator strength and the line shape factors of the transitions considered. It must be concluded that only 5 to 10% of the analyte atoms introduced are contained in the furnace at the moment of maximum absorbance. The smaller Varian Techtron furnace does not perform much better than the larger Perkin-Elmer furnace.

If, however, in the latter furnace the convective argon flow is stopped completely, the ratio of the time constants, τ_R/τ_S, increases by an order of magnitude and the predicted efficiencies are raised to 50% or better. Except for cadmium this is not completely realized in practice, but the improvement is significant. Naturally, this gain in analytical sensitivity is obtained at the cost of a severely reduced life time of the furnace tube under these conditions.

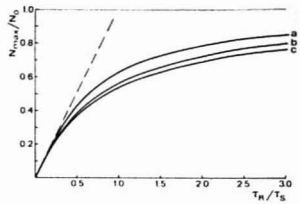

Figure 9. Theoretical efficiency curves (N_{max}/N_0) as a function of τ_R/τ_S calculated for an exponentially decaying removal function and three different supply functions, shaped as a square wave (a), a parabola (b), and a cosine (c), respectively

The present considerations allow the formulation of an ideal furnace design, by which we mean a furnace which is practical to operate and yields efficiencies of 50%. Assuming that with controlled heating we can reach a heating rate of 1000 K/s, it should be possible to reduce the time constant of the supply function to 0.4 s. Figure 9 shows that an efficiency of 50% is reached when $\tau_R = \tau_S$ is also 0.4 s. In a static furnace, Equation 12 then gives the effective length as $L = 1.8\sqrt{D}$ or about 3 cm for a diffusivity of 2.5 cm^2/s at 1500 K. The diameter of this furnace can be 4 mm to accommodate an acceptable aperture of the optical beam and allow the introduction of 20 μL of sample solution. The total duration of the signal is still long enough (0.6 s) to be manageable by ordinary registration units.

CONCLUSION

The present study has shown that the transient number of analyte atoms in commercial graphite thermal atomizers can be described as the convolution integral of two functions: a supply function and a removal function. It appeared possible to relate the shape and the duration of these functions in first approximation to simple chemical, physical, and geometrical parameters of the system. The supply function is determined by the heating of the furnace and by the frequency factor and activation energy of the dominant analyte release process. The time constant of the removal function is determined by either convection (in flow-through systems) or diffusion (in static systems). It is thus related to the convective flow rate and the furnace volume or to the diffusivity and the furnace length.

Theoretical predictions based on these simple physical processess already overestimate the actually observed removal rates, so that there appears to be no need to consider specific loss processes due to chemical interactions of the analyte with the furnace wall (9). In better approximations of the complete analytical signal, such processes as the adsorption/redesorption of the volatilized atoms, the flow pattern of the inert shielding gas, a possible variation of the activation energy, and the extension of the atoms outside the furnace must be taken into account. Nevertheless, the developed model agrees rather well with experimental evidence obtained from actual absorbance curves.

Table IV. Experimental and Theoretical Values of Efficiencies ($\eta = N_{max}/N_0$) in Three Different Furnace Conditions

	Data for elements			CRA-63			HGA-72 flow			HGA-72 stop		
Element	λ, nm	f	$H/\Delta\lambda_D$ 10^{12} m^{-1}	τ_R/τ_S	$\eta_{theor.}$	η_{exptl}	τ_R/τ_S	$\eta_{theor.}$	η_{exptl}	τ_R/τ_S	$\eta_{theor.}$	η_{exptl}
Silver	328.1	0.506	0.24	0.11	0.11	0.11	0.04	0.04	0.05	0.68	0.45	0.20
Lead	283.3	0.21	0.28	0.16	0.15	0.11	0.13	0.12	0.07	2.0	0.70	0.28
Manganese	279.5	0.16	0.36	0.05	0.05	0.08	0.06	0.06	0.06	0.68	0.45	0.25
Cadmium	228.8	1.25	0.48	0.17	0.16	0.19	0.15	0.14	0.27	0.95	0.53	0.86

Especially, the prediction that commercial atomizers do not at any moment contain more than about 10% of the analyte atoms introduced is confirmed by the measured maximum absorbances of easily atomized elements. A further increase of the sensitivity and corresponding decrease of the limits of detection by a factor of five thus appears possible.

APPENDIX

Response Function Due to Diffusion from a Cylindrical Furnace in Terms of Planar Sources. We consider a cylindrical tube of length L. At $t = 0$ an infinitely narrow pulse of unit mass is introduced homogeneously over the cross section at the center of the tube, where $x = 0$. For times $t > 0$ this planar source of atoms gives rise to the following distribution due to diffusion (*18*, *19*)

$$\frac{dM}{dx}(t,x) = (4\pi Dt)^{-1/2} \exp\left(-\frac{x^2}{4Dt}\right) \tag{A1}$$

Initially the total mass of atoms, inside the furnace, which is given as the integral of dM/dx over the tube length, remains unity. After a certain time the diffusing cloud reaches the ends of the tube, where we must impose the boundary condition $(dM/dt)\ (t, \pm L/2) = 0$. This is realized by introducing two virtual *negative* sources (*22*) of unit mass at $x = \pm L$, so that

$$\frac{dM}{dx}(t,x) = (4\pi Dt)^{-1/2} \left\{ \exp\left(-\frac{x^2}{4Dt}\right) - \exp\left[-\frac{(x-L)^2}{4Dt}\right] - \exp\left[-\frac{(x+L)^2}{4Dt}\right] \right. \tag{A2}$$

When, after another period of time, the virtual source at $x = L$ starts to influence the number of atoms at $x = L/2$, two more virtual *positive* sources must be introduced at $x = \pm 2L$. The number of planar sources considered thus depends on the period of time considered and the desired accuracy of the atomic distribution inside the furnace. The general expression is then

$$\frac{dM}{dx}(t,x) = (4\pi Dt)^{-1/2} \sum_{n=-k}^{+k} (-1)^n \exp\left[-\frac{(x-nL)^2}{4Dt}\right] \tag{A3}$$

The total mass inside the furnace is then obtained by integrating this expression from $x = -L/2$ to $x = +L/2$. Since the original mass source was normalized, this is also the response function due to diffusion, or

$$R_d(t) = (4\pi Dt)^{-1/2} \int_{-L/2}^{+L/2} \sum_{n=-k}^{+k} (-1)^n \exp\left[-\frac{(x-nL)^2}{4Dt}\right] dx = (4\pi Dt)^{-1/2} \sum_{n=-k}^{+k} (-1)^n \int_{-L/2}^{+L/2} \exp\left[-\frac{(x-nL)^2}{4Dt}\right] dx \tag{A4}$$

The integrals are easily found in terms of error functions; we obtain

for one source, $k = 0$ $\quad R_d(t) = \text{erf}\ (L/4\sqrt{Dt})$

for three sources, $k = 1$ $\quad R_d(t) = 2\ \text{erf}\ (L/4\sqrt{Dt}) - \text{erf}\ (3L/4\sqrt{Dt})$

for five sources, $k = 2$ $\quad R_d(t) = 2\ \text{erf}\ (L/4\sqrt{Dt}) - 2\ \text{erf}\ (3L/4\sqrt{Dt}) + \text{erf}\ (5L/4\sqrt{Dt})$

etc.

With increasing time, t, the error functions take on smaller values and the number of sources must be taken so large that the contribution of the final term is equal to one (argument greater than three). If we plot $R_d(t)$ vs t, we obtain a curve that can be approximated quite closely as

$$R_d\left(t < \tau_1 = 0.024\frac{L^2}{D}\right) = 1$$

$$R_d(t > \tau_1) = \exp\left[-\frac{16D(t-\tau_1)}{1.62L^2}\right] = \exp\left[-\frac{\pi^2 D(t-\tau_1)}{L^2}\right] \tag{A5}$$

The last expression is similar to the one given by L'vov (*1*) and by Woodriff et al. (*16*), although the latter authors did not account for the initial period $\tau_1 = 0.024\ L^2/D$ during which the atoms remain inside the furnace. Hence $R_d = 0.010$ for $t = 0.5\ L^2/D$ and the summation in Equation A4 must be extended to $k = 4$ to make the argument of the final error function larger than 3.

It is also seen that the equivalent time constant of the diffusive response function is equal to

$$\tau_d = \frac{0.024L^2}{D} + \frac{L^2}{\pi^2 D} = 0.125\frac{L^2}{D} \tag{A6}$$

This value has been proposed by L'vov (*1*) and is used by Sturgeon and Chakrabarti (*9*).

Finally, the assumption of an infinitely narrow real source cannot be realized in practice. The finite width of the experimentally introduced atomic vapor will reduce the initial period τ_1 somewhat.

LITERATURE CITED

(1) B. V. L'vov, "Atomic Absorption Spectrochemical Anaysis," Adam Hilger, London, 1970.
(2) J. Aggett and A. J. Sprott, *Anal. Chim. Acta*, **72**, 49 (1974).
(3) W. C. Campbell and J. M. Ottaway, *Talanta*, **21**, 837 (1974).
(4) R. E. Sturgeon, C. L. Chakrabarti, and C. H. Langford, *Anal. Chem.*, **48**, 1792 (1976).
(5) C. W. Fuller, *Analyst (London)*, **99**, 739 (1974).
(6) S. L. Paveri-Fontana, G. Tessari, and G. Torsi, *Anal. Chem.*, **46**, 1032 (1974).
(7) G. Torsi and G. Tessari, *Anal. Chem.*, **47**, 839 (1975).
(8) G. Tessari and G. Torsi, *Anal. Chem.*, **47**, 842 (1975).
(9) R. E. Sturgeon and C. L. Chakrabarti, *Anal. Chem.*, **49**, 1100 (1977).
(10) H. C. Wagenaar, I. Novotny, and L. de Galan, *Spectrochim. Acta, Part B*, **29**, 301 (1974).
(11) H. C. Wagenaar and L. de Galan, Spectrochim. Acta, *Part B*, **30**, 361 (1975).
(12) H. C. Wagenaar, C. J. Pickford, and L. de Galan, *Spectrochim. Acta, Part B*, **29**, 211 (1974).
(13) B. V. L'vov, *Zh. Prikl. Spektrosk.*, **15**, 783 (1971).
(14) G. Torsi and G. Tessari, *Anal. Chem.*, **48**, 1318 (1976).
(15) H. F. Cordes, *J. Phys. Chem.*, **72**, 2185 (1968).
(16) R. Woodriff, M. Marinkovic, and R. A. Howald, *Anal. Chem.*, **49**, 2008 (1977).
(17) M. J. Adams and G. F. Kirkbright, *Anal. Chim. Acta*, **84**, 79 (1976).
(18) R. E. Sturgeon, and C. L. Chakrabarti, *Spectrochim. Acta, Part B*, **32**, 231 (1977).
(19) Internal report, to be published.
(20) R. E. Sturgeon and C. L. Chakrabarti, *Anal. Chem.*, **49**, 90 (1977).
(21) R. B. Bird, W. E. Stewart, and E. N. Lightfoot, "Transport Phenomena", John Wiley & Sons, New York, N.Y., 1960.
(22) H. S. Carslaw and J. C. Jaeger, "Conduction of Heat in Solids", Oxford University Press, London, 1959.

RECEIVED for review June 23, 1977. Accepted September 7, 1977.

Background Correction for the Analysis of High-Solids Samples by Graphite Furnace Atomic Absorption

J. M. Harnly and T. C. O'Haver*

Department of Chemistry, University of Maryland, College Park, Maryland 20742

A direct absorbance read-out circuit has been built for use with an AA system consisting of a continuum source and an echelle monochromator modified for wavelength modulation (CEWM-AA). The system is shot noise limited and capable of correcting for 3.0 absorbance units of nonspecific source attenuation. Cd, Pb, and Cu are analyzed directly in 3% NaCl, serum, and urine. CEWM-AA detection limits in 3% NaCl were equivalent to or better than those for conventional background-corrected line source AA and Zeeman effect AA.

The most commonly-used background correction technique for conventional line source AA employs a continuum source in addition to the primary elemental source. This dual source technique was first described by Koirtyohann and Pickett (*1*) and has subsequently been adopted by almost all manufacturers of AA instruments. Difficulty in characterizing background corrected line source AA (AAL-BC) arises from the necessity of exactly aligning the beams from two sources (*2–5*) and of selecting the appropriate spectral bandpass (*5*) and electronic gain (*6*). Morganthaler (*7*) and Hendrikx-Jongerius and De Galan (*4*) have stated that 1.0 absorbance unit represents the maximum allowable source attenuation for AAL-BC systems. Most AAS manufacturers recommend modification of the sample or of the method of preparation if attenuation approaches this level (*8, 9*). Recently the dependence of the accuracy of background correction on the optimization of the various optical and electronic parameters was again stressed by Morris and Newstead (*10*). They reported a source attenuation limit of 1.7 absorbance units for the Pye Unicam SP2900 AAS (*11*) which features improved control for these parameters.

The central assumption upon which the operation of AAL-BC is based is that the average absorption measured over the monochromator spectral bandpass (typically 0.1-1 nm) is equal to the background absorption under the (much narrower) analyte atomic absorption line. This assumption is generally valid for light losses due to scattering which is smoothly wavelength dependent. However, it has been shown that AAL-BC may give inaccurate background correction (*4, 12, 13*) when the fine structure of the molecular background absorption or atomic absorption of the matrix falls within the spectral bandpass of the monochromator. Inaccurate results will, of course, also arise fron the rarer occurrence of direct spectral overlap of atomic lines (*14, 15*).

The only commercially-available alternative to AAL-BC is the Hitachi Zeeman effect AA (ZAA) (*16–20*). Since only a single source is employed, the problem of exact beam alignment does not arise. Furthermore, the background readings are taken much closer (≈0.01 nm) to the analyte line. Accurate correction for attenuation of 1.7 absorbance units has been reported. With the magnetic field around the source, the selection of spectral lines is limited somewhat by the magnetically induced fine structure of the source line (*18*). This problem appears to have been solved by placing the magnetic field around the atomization source (*19, 20*). However, a new uncertainty arises concerning the magnetically induced fine structure in the absorption spectrum of metallic components of the sample.

Conceptually, the simplest means of correcting for background spectral interferences in atomic absorption is the use of wavelength modulation in conjunction with a continuum primary source. Such a system, employing a medium resolution monochromator, was first described by Snelleman (*21*). The modulation process sweeps the absorption profile repeatedly across the exit slit, resulting in a ripple in the photo-signal which is proportional to the intensity absorbed and is independent of broad band additive interferences (*22*). Zander et al. (*23*) combined a high intensity continuum source and a wavelength modulated high resolution echelle monochromator (*24*). This system, dubbed CEWM-AA, has both of the essential advantages of ZAA: a single source is used and only the narrow spectral region near the analyte line is examined. Moreover, the single source suffices for all elements. A useful feature of this system is that the photomultiplier output and the wavelength modulation waveform may be combined to give a real-time x–y oscilloscope display of the absorption spectrum near the analyte line. Nonspecific source attenuation and spectral line overlap can be visually detected.

In the simplest sense the background correction capabilities of wavelength modulation with a continuum source (WM-AAC) assumes an unstructured background over the modulation interval. However, the technique has also been used to correct for more complex spectral interferences. Koirtyohann et al. (*25*), using square wave modulation, have measured emission peaks in highly structured background. Epstein and O'Haver (*26*) and Sydor and Hieftje (*27*) used wavelength modulation to compensate for spectral overlap interferences in atomic emission. Zander er al. (*15*) demonstrated that CEWM-AA is capable of correcting for all major types of spectral interferences in atomic absorption, including direct spectral overlaps with separation as little as 0.003 nm.

The calculation of absorbance for WM-AAC is not straightforward. Snelleman (*21*) used the log of the ac component as an approximation of absorbance. This convention has been employed by more recent researchers investigating a variety of WM-AAC systems (*28–30*). The approximation is valid provided that the analyte absorption is small and that the source attenuation is sufficiently small that I_0 and $I_0 - I$ do not decrease by more than a few percent. These criteria tend to exclude most real-world samples.

Zander et al. (*23*) were the first to attempt to calculate true absorbance values usng the CEWM-AA system. These calculations were based on separate measurements of I_0 and $I_0 - I$. Absorbances for samples causing significant source attenuation could not be calculated as there was no means of determining I_0 during atomization. Hager (*22*) has shown that a ratioing of the ac component (proportional to $I_0 - I$) to the dc component (proportional to I_0) will produce a signal which is dependent only on the analyte concentration and is independent of the source intensity.

This paper will describe an electronic circuit for the real-time ratioing of the ac signal to I_0. This circuit, used with the CEWM-AA system, results in an instrument which: (1)

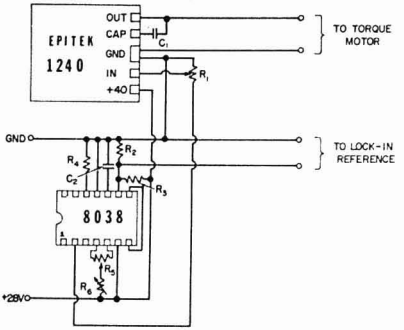

Figure 1. Waveform generator circuit. C_1 = 1000 μF; C_2 = 0.15 μF; R_1 = 0–100 kΩ; R_2 and R_3 = 100 kΩ; R_4 = 82 kΩ; R_5 and R_6 = 0–10 kΩ

gives a real-time absorbance read-out, continuously corrected for source attenuation; (2) using only a single source, gives capabilities exceeding those of a double beam system; and (3) has reduced the overall system noise level to the shot noise limit.

The source attenuation limits for the CEWM-AA system will be defined and the operating characteristics will be described. To demonstrate the system's capability to handle real samples, Cd, Pb, and Cu are analyzed in 3% NaCl, blood serum, and urine. These matrices have been selected because of their well documented spectral interferences (*31–37*). The background correction capabilities of the CEWM-AA system will be compared to those of existing commercial AA systems whenever possible.

EXPERIMENTAL

The CEWM-AA system has been described (*15*). For these studies, an Eimac 300-W Xe "VIX-UV" continuum lamp (PS. 300-1 Eimac Power Supply, Varian Eimac Div., San Carlos, Calif.) was substituted for the 150-W Eimac lamp used previously. The lamp was run at 15 A in the continuous mode. An improved Model 102 echelle monochromator (Spectrametrics, Inc., Andover, Mass.) was used. The newer model provided greater order separating dispersion resulting in less stray light due to order overlap.

The monochromator was modified for wavelength modulation by placing a quartz refractor plate (1 inch × 1 inch × $^1/_8$ inch) mounted on a torque motor (Model S4-075B, MFE, Salem, N.H.) approximately 10 cm behind the entrance slit. The refractor plate was modulated sinusoidally at 80 Hz using an integrated circuit waveform generator and a modular audio amplifier (Model 1240, Epitek Electronics, Ltd., Ottawa, Canada). This circuit is shown in Figure 1. Entrance and exit slits 25 μm wide and 300 μm high were used at all times, except where noted.

The atomization source was either a Perkin-Elmer HGA 2000 or the burner assembly from a Varian Techtron AA-4. For the flame configuration, an air–acetylene flame was used with a Techtron AB-41 (10-cm slot) burner head and a Techtron GCU-2 gas control unit (Varian Techtron, Melbourne, Australia).

Direct Absorbance Read-Out Circuit. In a conventional double-beam atomic absorption spectrophotometer, absorbance is derived from measurements of the incident and transmitted intensities, I_0 and I, respectively. Both I_0 and I are assumed to be measured at the same wavelength, the difference being that the I_0 measurement is made by utilizing optical components (mirrors, etc.) which bypass the primary beam around the atomizer. In the CEWM-AA system described here, on the other hand, I_0 is defined as the *intensity of the primary beam transmitted through the atomizer at a wavelength just off the analyte absorption line*, while I is defined as before. This definition of I_0 is identical to the conventional one if the analyte does not absorb at the wavelength where I_0 is measured, if the source–monochromator–detector response changes insignificantly over the wavelength modulation interval and if there is no nonspecific source attenuation. The first two conditions are easily ensured by the proper choice of modulation interval (typically about 0.01 nm). The particular advantage of this new definition of I_0, however, is that nonspecific source attenuation has no effect on the ratio of I_0 to I, since both I_0 and I are transmitted through the atomizer and are attenuated by the same factor. The only requirement is that the source attenuation be the same at the wavelengths where I and I_0 are measured, which is generally the case since the modulation interval is only about 0.01 nm. Thus, by defining I_0 in this way, we obtain all the benefits of double-beam *and* background corrected operation with a much simpler optical system.

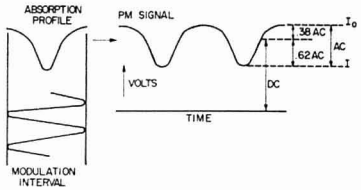

Figure 2. Photomultiplier output signal for the CEWM-AA system showing analyte absorption

Sinusoidal wavelength modulation across an isolated atomic absorption line produces a ripple or ac component in the photosignal as shown in Figure 2. This waveform represents a convolution of the modulation waveform, the atomic absorption profile, and the monochromator slit function as has been described mathematically by O'Haver et al. (*38*). The photomultiplier signal consists of an ac signal superimposed on a dc signal. With a sufficiently large modulation interval, the upper limit of the ac component corresponds to I_0 and the lower limit to I, as shown in Figure 2. In this manner, the average I_0 value actually represents the average of source intensities measured just off both sides of the analyte line. Using these values, absorbance can be calculated in the normal manner.

The easiest way to accomplish the absorbance computation electronically is to measure the ac and dc component independently. Let us consider the case of sinusoidal modulation of a Gaussian profile at the optimum modulation interval. Using a numerical integration procedure similar to that described by O'Haver et al. (*38*), it can be shown that I_0 equals the dc component plus 38% of the peak-to-peak ac component and I equals the dc component minus 62% of the ac component (Figure 2). The absorbance is:

$$ABS = \log\left(\frac{I_0}{I}\right) = \log\left(\frac{DC + 0.38\,AC}{DC - 0.62\,AC}\right) \quad (1)$$

where AC and DC are the peak-to-peak ac component and dc component, respectively.

The measurement of DC is straight-forward using a low pass filter. The value of AC is determined using a lock-in amplifier. It can be shown (Equation 18 of reference 38) that the lock-in output, E_L, is 0.274 of the peak-to-peak voltage of the input signal:

$$E_L = 0.274\,AC \quad (2)$$

Moreover, the lock-in will amplify the signal by some factor M depending on which sensitivity range is used. Thus we can write:

$$AC = \frac{E_L}{0.274\,M} \quad (3)$$

In order to prevent overload of the lock-in input circuit, it is necessary to attenuate the input signal by a factor, R. Taking this factor into account:

$$AC = \frac{RE_L}{0.274\,M} \quad (4)$$

Combining Equations 1 and 4 gives:

$$ABS = \log\left(\frac{DC + \left[\frac{0.38\,R}{0.274\,M}\right]E_L}{DC - \left[\frac{0.62\,R}{0.274\,M}\right]E_L}\right) = \log\left(\frac{DC + K_1E_L}{DC - K_2E_L}\right) \quad (5)$$

where the K's represent the terms in brackets.

Figure 3 shows a block diagram of the electronic circuit which solves Equation 5. All op amps are National Semiconductor type LM 316H. The log ratio module is an Infotronics LR 101. The lock-in amplifier is a Princeton Applied Research Model 128.

A 1 MΩ resistor (R_1) serves as the photomultiplier load. Op amp No. 1 is used as a pre-amp to increase the signal voltage to close to 10 V (maximum voltage rating of op amp output). The signal is then applied through a voltage divider to the lock-in amplifier and to the low pass filter (op amp No. 2). A lock-in output time constant of 0.3 s was selected (0.1 s proved too small to adequately filter the ac component at the low pass filter, op amp No. 2). This time constant was closely matched at the low pass filter (op amp No. 2) in order to avoid transient signals which can arise from a mismatch of the numerator and denominator time constants in a ratio system (*10*).

The lock-in amplifier is tuned to twice the wavelength modulation frequency. The reference signal is provided by the 8038 waveform generator (Figure 1). The lock-in's front-end high pass filter is used in the "50 Hz" position to avoid "OVERLOAD" situations from occurring with sudden changes in I_0 caused by source attenuation during the ash or atomization cycle. Even using the least sensitive scale, "250 mV", the lock-in input is overloaded for samples with no background attenuation and high atomic absorption. With I_0 adjusted to 10 V, the maximum possible value for AC is 10 V. The lock-in is capable of handling only 0.9 V peak-to-peak (0.250 V/0.274). Consequently, a voltage divider must be used to decrease AC by a factor of 11 (R = 11). In this least sensitive scale, 0–250 mV on the front meter is amplified by a factor of 4 (M = 4) at the output connector. Thus E_L will vary from 0 to 1 V.

Op amp No. 3, 4, and 5, combine DC and E_L as shown in Equation 5. Op amp No. 4 performs the numerator addition while No. 3 and 5 perform the denominator subtraction. With R = 11 and M = 4, K_1 and K_2 are 3.81 and 6.22, respectively. These factors define the ratio of the resistor values at op amp No. 4 and 3 (100 kΩ/26.2 kΩ = 3.81, 100 kΩ/16.05 kΩ = 6.23). Absorbances computed by this circuit were found to agree with those calculated from direct measurements of I and I_0 estimated from the oscilloscope display of the photosignal.

The log ratio module computes absorbance based on the input I_0 and I values. This module enters a failure mode if its input voltages drop below 6 mV. The limits of analyte atomic absorption are therefore given by the equation:

$$ABS = \log\left(\frac{I_0}{0.006}\right) \quad (6)$$

Assuming I_0 has been adjusted to 10 V initially the attenuation would be:

$$SOURCE\ ATTENUATION = \log\left(\frac{10}{I_0}\right) \quad (7)$$

Combining the two gives:

$$ABS + ATTENUATION = \log\left(\frac{10}{0.006}\right) = 3.22 \quad (8)$$

We would therefore predict that we could tolerate a background absorbance of about 3 absorbance units at low analyte atomic absorbances. Higher analyte absorbances limit the source attenuation that can be tolerated; however dilution of the sample would then become feasible. If the light beam is totally blocked,

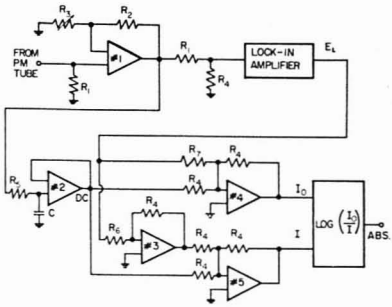

Figure 3. Circuit for direct absorbance read-out for CEWM-AA. R_1 = 1 MΩ; R_2 = 470 kΩ; R_3 = 23.5 or 470 kΩ; R4 = 100 kΩ; R_5 = 2 MΩ; R_6 = 16.0 kΩ; R_7 = 26.2 kΩ; C = 0.15 μF. E_L, DC, I_0, and I are defined in the text

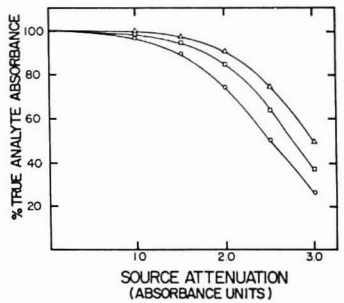

Figure 4. The effect of a 10-mV bias voltage on the accuracy of the computed analyte absorbance as a function of source attenuation. (Δ) 0.05 absorbance. (□) 0.1 absorbance. (○) 1.0 absorbance

of course, the ratio operation will fail and the output goes to a 10-V limit.

The failure mode can be averted by applying a negative bias to op amp No. 2. Thus, even if the photomultiplier signal goes to zero, the same small positive voltage is seen at the I_0 and I inputs to the log ratio module, and the module will continue to output zero absorbance but with a much larger noise component. Equation 5 can be rewritten:

$$ABS = \log\frac{DC + K_1E_L + V_B}{DC - K_2E_L + V_B} \quad (9)$$

where V_B is the bias voltage (typically 10 mV). Erroneously low absorbances will result when V_B becomes significant with respect to I. Assuming I_0 to be initially adjusted to 10 V and the bias voltage to be 10 mV, Figure 4 shows the effect of source attenuation on the computed analyte absorbance. The induced error depends greatly on both analyte absorbance and source attenuation. In practice, it was found that the use of this bias voltage resulted in no practical advantage.

Characterization of the Electronics. To test the source attenuation tolerance of the direct absorbance read-out circuit, a steady state atomization source (air–acetylene flame) and artificially induced source attenuation were used. I_0 was adjusted to approximately 10 V with the slits 25 μm wide and 500 μm high. Attenuation was achieved by combining the use of appropriate filters and reduction of the slit height. Analyte absorbance was introduced by aspiration of appropriate standards.

This experimental configuration did not reproduce the rapid changes in absorbance which are observed for real samples using a flameless atomization device. However, the time constants for

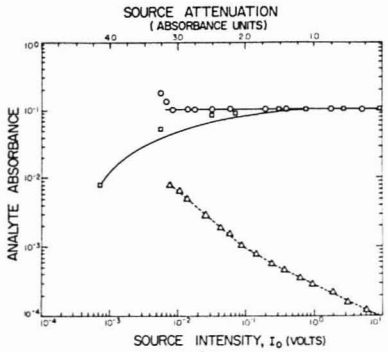

Figure 5. Analyte absorbance and absorbance noise as a function of source attenuation. (O) analyte absorbance, no bias voltage. (□) analyte absorbance, 10-mV bias. (Δ) absorbance noise, rms. (—) predicted analyte absorbance, with and without bias voltage. (- - - -) straight lines fitted to absorbance noise

both branches of the circuit (*AC* and *DC*) were carefully matched as explained earlier. No transient signals were observed even when source attenuation went quickly from 0.0 to 4.0 absorbance units (the worst case).

Analysis of High Attenuation Samples. Cd, Pb, and Cu were analyzed in rat blood serum, fresh human urine, and 3% NaCl (reagent grade). Standards for all three elements were prepared in deionized water and in 3% NaCl solution.

Furnace temperatures for the ashing and atomizing cycle were taken from Perkin-Elmer's "Analytical Methods Using the HGA Graphite Furnace" (*39*). A drying temperature of 125 °C was used. The length of the drying, ashing, and atomizing cycles was 10, 30, and 8 s, respectively, for all standards and samples for all three elements.

RESULTS AND DISCUSSION

Characterization of the Electronics. The ability of the electronics to handle high source attenuation was tested as described in the Experimental section. Figure 5 shows the observed (points) and predicted (solid lines) absorbance signals and the absorbance noise levels as a function of source attenuation.

With a bias of 10 mV applied to both I and I_0, a longer working range is realized. However, a 5% deviation of the electronically computed absorbance from the true absorbance is observed with a source attenuation of 2.0 absorbance units. Reasonable experimental agreement with the predicted absorbance was obtained for attenuation as high as 4.0 absorbance units. The use of the method of standard additions would permit analysis of samples with source attenuation this severe, provided the increased noise levels could be tolerated. Without the bias voltage, the source attenuation limit is approximately 3.0 absorbance units for samples with analyte absorbance of 0.2 or less. Unlike the bias voltage case, the correct absorbance is computed for source attenuation from 0 to 3.0 absorbance units.

The decision whether or not to employ bias would depend on the nature of the analyte and the matrix. For samples where matrix effects cause a change in slope (multiplicative interference), the method of standard additions would be used anyway. Deviation of the computed absorbance from the true absorbance because of the electronics would have no effect on the analysis since all the method of additions samples would be expected to give the same degree of attenuation. If calibration standards were employed, no bias would be used unless it was known the source attenuation didn't exceed 2.0 absorbance units. The circuit has been built so the bias may be turned on or off from a switch on the front panel. In both modes, the limits of attenuation are dictated by the electronics.

Figure 5 also shows that for background absorbances up to 2.0, the signal-to-noise ratio decrease with the square root of the decrease in I_0 (increase in source attenuation). This is as expected for a short noise limited system. A log–log plot of absorbance noise vs. I_0 gives a slope of −0.48 at higher intensities. The slope of −0.89 at lower intensities occurs as a result of the increased significance of the electronic noise as the I and I_0 inputs get closer to zero volts.

As for any shot noise limited system, the signal-to-noise ratio decreases with the square root of the decrease of the source intensity. A source attenuation of 2.0 absorbance units will be accompanied by a degradation of the detection limit by a factor of 10, regardless whether the source is attenuated by the sample matrix at a given wavelength or results from the selection of another wavelength where the Eimac source is less intense. The pre-amp or photomultiplier gain can always be increased to bring I_0 back to its original value (preserving the 3.0 source attenuation limit) but the loss in the signal-to-noise ratio cannot be reclaimed. Thus, if the rms noise at a given wavelength is known, the noise at any other wavelength is predictable from the source spectrum, and the noise during the analysis of any sample is predictable from the background attenuation. Additionally, the detection limit of any element can be calculated if the sensitivity is known.

Analysis of High Background Samples. To demonstrate the background correction capabilities of the CEWM-AA spectrometer using real samples, Cd, Cu, and Pb were analyzed in 3% NaCl, rat blood serum, and human urine using the Perkin-Elmer HGA 2000 graphite furnace. For each element, the furnace temperature programs recommended by the Perkin-Elmer methods manual (*39*) were used. Other than this, no special efforts were made to optimize sensitivity or to minimize the source attenuation. The drying and ashing stages were kept as short as possible. A 30-s ash cycle was necessary to prevent spattering of the complex matrix samples. In several cases, larger than normal sample sizes were employed to test the ability of the system to handle source attenuations much higher than normal.

Data for the analysis of Cd and Cu in the various matrices is shown in Figures 6 and 7, respectively. The upper trace in each figure shows the transmitted source intensity, I_0, the middle trace shows the analyte absorbance signal, and the lower trace shows the background noise signal obtained for each matrix measured just off the analyte line.

The source intensity trace shows the I_0 value that is used in the analyte absorbance computation at each point in the analysis. Any decrease in the source intensity is a result of attenuation of the source by the matrix. As can be seen for the Cd data in Figure 6, even though only 20 μL sample sizes were used, considerable attenuation of the source occurred. The peak source attenuation is approximately 1.8, 2.0, and 2.0 absorbance units for 3% NaCl, serum, and urine, respectively. This degree of attenuation is greater than that observed for similar sample sizes at longer wavelengths (e.g., for Cu in Figure 7) and undoubtedly reflects the increased scatter and molecular absorption expected in the UV.

Despite the large attenuation of the source, clearly defined Cd absorbance peaks are readily seen in 3% NaCl and urine (there is no detectable Cd in rat blood serum). No difference in the analyte absorbance was noted for either the 3% NaCl or urine matrix when a 10-mV electronic bias voltage was applied. Since the source attenuation is close to 2.0 absorbance units, this indicates the analyte peak didn't occur at the point of maximum attenuation. A close comparison of the position of the absorbance peaks to the source attenuation reveals the Cd is volatilized a short time before the main background

Table I. Detection Limits for Cd in Complex Matrices

Matrix	Concn, ppb	Abs.	mAbs/pg[a]	Noise, p-p, Abs.	Det. limit ppb	Det. limit pg[a]
H_2O	1	0.018	0.90	0.008	0.2	4
3% NaCl	10	0.140	0.70	0.070	2.0	40
Serum	...[b]	...	...	0.062	...	...
Urine	9.2[c]	0.155	0.82	0.046	1.1	22
Beam blocked	...	...	...	0.105	...	...

[a] Based on 20-μL sample size. [b] No Cd detectable in rat blood serum. [c] Determined by method of standard additions.

Table II. Detection Limits for Cu in Complex Matrices

Matrix	Sample size, μL	Concn, ppb	Abs.	mAbs/pg	Noise p-p, Abs	Det. limit ppb	Det. limit pg
H_2O	20	10	0.012	0.060	0.001	0.3	6.7
	100	10	0.047	0.047	0.001	0.1	8.5
3% NaCl	20	10	0.005	0.025	0.003	2.4	48
	100	10	0.013	0.013	0.0072	2.2	222
Serum	20	1640[a]	0.569	0.017	0.001	1.2	20
	100	1640	1.22	0.007	0.006	3.2	323
Urine	20	19.5[a]	0.023	0.059	0.002	0.7	14
	100	19.5	0.054	0.028	0.0035	0.5	51

[a] Determined by method of standard additions.

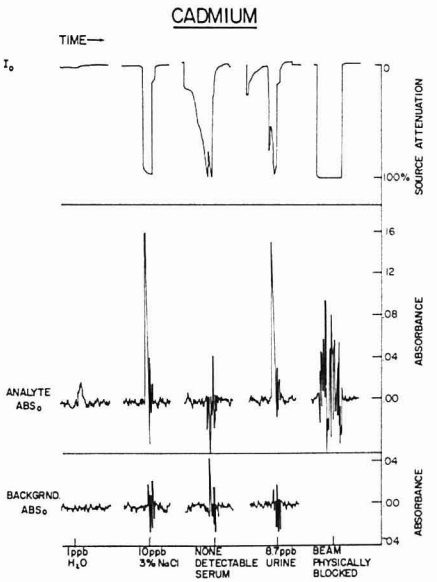

Figure 6. Traces of I_0, analyte absorbance, and background absorbance noise (off the line) for the analysis of Cd in H_2O, 3% NaCl, serum, and urine (20-μL sample size)

component. The method of standard additions was used to determine the Cd concentration in urine (9.2 ppb) and to verify that the suppression of 1.0 ppb Cd in 3% NaCl was a matrix effect.

The background noise trace (bottom of Figures 6 and 7) is obtained by tuning the monochromator 0.01 to 0.02 nm to one side of the analytical line and repeating the analysis. This is meaningful because of the use of the continuum primary source. At this offset wavelength, there can be no analyte

Table III. Detection Limits for Pb in Complex Matrices

Matrix	Concn, ppb	Abs.	mAbs/pg[a]	Noise p-p, Abs	Det. limit ppb	Det. limit pg
H_2O	50	0.052	0.052	0.0028	1.0	22
3% NaCl	50	0.049	0.049	0.0123	5.0	100
Serum	...[b]	...	...	0.0103	...	...
Urine	...[b]	...	...	0.0092	...	...

[a] Based on 20-μL sample size. [b] No Pb detectable.

absorbance; however, the source attenuation of the matrix remains very nearly the same. In fact, from the scope display of the spectrum, it was clear that there was no resolvable fine structure within the 0.01-nm modulation interval. The background signals shown in Figure 6 result from the increased noise levels as the source intensity is attenuated by the sample.

The applicability of the concept of "detection limits" to flameless atomization devices has been questioned because of the "baseline upset" encountered whenever a blank is analyzed (2). This baseline upset has been attributed to deformation of the graphite furnace at high temperatures, residual analyte, and imperfect alignment of the background corrector. With the CEWM-AA system, detection limit measurements can be made without these problems. Since I_0 is defined as the source intensity on both sides of the analyte line, the reference and the analyte wavelengths are both present in the single beam which passes through the furnace. Graphite deformation will affect I_0 and I in an identical manner. Residual analyte, which may exist on the graphite tube or end cones, can no longer make a contribution when the monochromator is tuned off the analyte line. Finally, since a single source is used, there can be no such thing as an imperfectly aligned background corrector. As a result, using off-the-line background noise levels, a valid detection limit can be calculated for standards and samples, regardless of the matrix, as shown in Table I.

The background noise levels for Cd in aqueous and complex matrices constitutes a near "worst case" situation for CEWM-AA. This is mostly due to the comparatively low intensity of the Eimac source at this wavelength (228.8 nm). The Eimac source gives a photocathode current 100 times larger at its most intense wavelength (~480.0 nm) (23). As

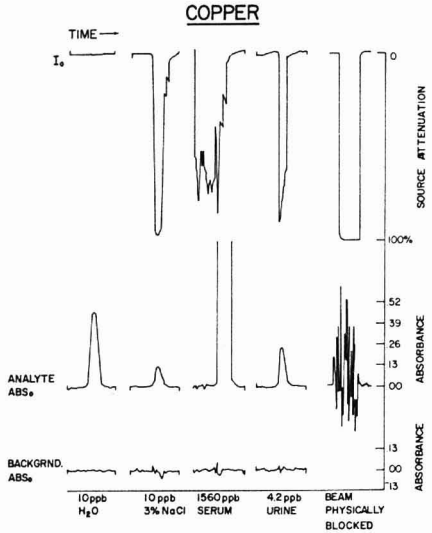

Figure 7. Traces of I_0, analyte absorbance, and background absorbance noise (off the line) for the analysis of Cu in H_2O, 3% NaCl, serum, and urine (100-μL sample size)

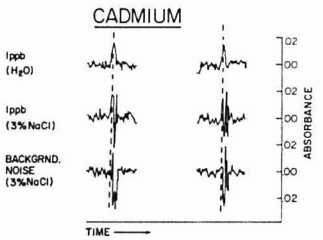

Figure 8. Traces of analyte absorbance and background absorbance noise (off the line) for duplicate analyses of Cd in H_2O and 3% NaCl

a result, elements at higher wavelengths show lower background noise levels. This can be seen readily upon comparing Cd to Cu (324.7 nm, Figure 7 and Table II) or Pb (283.3 nm, Table III).

Particular care must be taken in the measurement of the background noise levels. First, the accuracy of the determination of the peak-to-peak noise levels is very poor when based on a single analysis. The values listed in this paper represent an average of five determinations. In addition, as was pointed out earlier for Cd, the analyte absorbance peak may precede or trail the major noise component. Consequently detection limits, as reported in this paper, are conservative because they are based on the maximum background noise levels. This can be seen for 1 ppb Cd in 3% NaCl in Figure 8. Based on the maximum background noise levels, the detection limit is 2 ppb. However, 1 ppb is readily distinguished as the peak which precedes the noise component. With a little care, an effective detection limit below 1 ppb could be realized.

More accurate detection limits could be determined if the noise levels were known at the moment of peak analyte absorbance. Alternatively, if I_0 were known at the peak absorbance, the noise levels could be calculated with reasonable accuracy (Figure 5).

Table IV. Background Corrected Detection Limits (pg): Aqueous Matrices

	Conventional (*6*)	ZAA (*20*)	CEWM-AA[a]
Cd (2288)	0.1	0.3	4
Pb (2170)	5	...	...
(2833)	...	4	22
Cu (3247)	5	10	7
Atomizer	CRA-63	Zeeman Furnace	HGA-2000

[a] This work.

Tables I, II, and III show the results obtained for the analysis of Cd, Pb, and Cu in H_2O, 3% NaCl, serum, and urine. For Cu, a 100-μl sample size was also used in addition to the 20-μL samples in order to determine whether or not the improved background correction capability would allow larger samples to be used to reduce concentration detection limits. As expected, all elements show a degradation of the detection limits in the complex matrices, as a result of the increased background noise levels and matrix suppression interferences. The slope of the analytical curve was calculated for each solution in terms of milliabsorbance/pg and can be used as an indicator of the severity of the matrix suppression effect. The data for the 100-μL Cu samples show that the atomization efficiency of the atomizer is reduced with such large samples, with the result that the expected improvement in the concentration detection limit with larger sample size is not observed.

Comparison of Background Correction Systems. It is difficult to compare the CEWM-AA system directly to commercially available background corrected AA instruments because of the dearth of published information. The data that are available must be considered carefully because of the different atomization sources and sample matrices used.

The parameter most frequently considered is the maximum source attenuation by the matrix that an instrument can tolerate. Pye Unicam (*10*) and Hitachi (*17*) both quote a limit of 1.7 absorbance units for their instruments. CEWM-AA, as discussed earlier can tolerate 3.0 absorbance units of attenuation. Attenuation limits for other commercial instruments are not available. It would be informative to compare detection limits for aqueous solutions analyzed in the background corrected mode. However, with the exception of the Hitachi ZAA instrument, for which background correction is an inherent feature, no detection limits of this nature have been published by any manufacturers of AA instruments. For conventional background corrected line source instruments (AAL-BC), the data reported by Donnelly et al. (*6*) represents the only information that could be found. The comparative data are shown in Table IV. CEWM-AA is approximately an order of magnitude worse for Cd and a factor of 3 to 4 worse for Pb when detection limits are compared to those for ZAA and AAL-BC. This comparison reflects the relatively low intensity of the Eimac VIX-UV lamp in the UV region. For Cu, CEWM-AA has detection limits only a factor of 2 worse than those for AAL-BC and fractionally better than ZAA detection limits. It must be remembered, however, that a different atomization source was used with each of the three systems.

Detection limits in a high salt matrix provide a more realistic comparison of the background correction capabilities of the instruments. Unfortunately, no data of this nature are available from any of the manufacturers of AA instruments. Detection limits for a Perkin-Elmer 303 equipped with a D_2 lamp and an HGA 2000 graphite furnace have been reported by Cruz and Van Loon (*34*). Detection limits for a ZAA system

Table V. Background Corrected Detection Limits (pg): High Salt Matrices

Matrix	Conventional (34) Varied	ZAA (40) 3% NaCl	CEWM-AA[a] 3% NaCl
Cd (2288)	40	···	40
Pb (2170)	200	···	···
(2833)	···	350	100
Cu (3247)	240	50	50
Atomizer	HGA-2000	···[b]	HGA-2000

[a] This work. [b] Self-built furnace.

employing the magnetic field around the light source were calculated from analytical traces published by Hadeishi and McLaughlin (40). These detection limits are compared to the detection limits for CEWM-AA in Table V. CEWM-AA is comparable to or better than ZAA and AAL-BC for every element. Unfortunately, Gruz and Van Loon (34) employed different salt matrices. Close examination of their data shows that they encountered less source attenuation but a slightly greater matrix suppression effect. Consequently, a rough comparison of the data for all three systems appears justifiable.

LITERATURE CITED

(1) S. R. Koirtyohann and E. E. Pickett, Anal. Chem., **28**, 585 (1966).
(2) H. L. Kahn, M. Bancroft, and R. H. Emmel, *Res/Dev.*, **27**, 30 (1976).
(3) D. C. Manning, *At. Absorp., Newsl.*, **11**, 112 (1972).
(4) C. Hendrikx-Jongerius and L. De Galan, *Anal. Chim. Acta*, **87**, 259 (1976).
(5) A. T. Zander, *Am. Lab.*, **8**, 11 (1976).
(6) T. H. Donnelly, J. Ferguson, and A. J. Eccleston, *Appl. Spectrosc.*, **29**, 158 (1975).
(7) L. Morganthaler, *Am. Lab.*, **4**, 41 (1975).
(8) "Atomic Absorption Methods Manual, Volume II, Flameless Operations", Instrumentation Laboratory (1976).
(9) "Instructions, Model 603, Atomic Absorption Spectrophotometer" (993-9208) March 1976.
(10) L. R. Morris and R. A. Newstead, "Improved Background Correction for AAS", Paper No. 97, Pittsburgh Conference on Analytical Chemistry and Applied Spectroscopy, Cleveland, Ohio, 1977.
(11) L. R. Morris and R. A. Newstead, "A Compact Double Beam AAS", Paper No. 102, Pittsburgh Conference on Analytical Chemistry and Applied Spectroscopy, Cleveland, Ohio, 1977.
(12) K. C. Thompson and R. G. Godden, *Analyst (London)*, **101**, 96 (1976).
(13) J. Y. Marks, R. J. Spellman, and G. Wysocki, *Anal. Chem.*, **48**, 1474 (1976).
(14) J. Y. Marks and G. G. Welcher, Paper No. 176, 3rd Annual Meeting of FACSS, Philadelphia, Pa., 1976.
(15) A. T. Zander, T. C. O'Haver, and P. N. Keliher, *Anal. Chem.*, **49**, 838 (1977).
(16) H. Koizumi and K. Yasuda, *Anal. Chem.*, **47**, 1679 (1975).
(17) H. Koizumi and K. Yasuda, *Anal. Chem.*, **48**, 1178 (1976).
(18) H. Koizumi and K. Yasuda, *Spectrochim. Acta, Part B*, **31**, 237 (1976).
(19) H. Koizumi and K. Yasuda, *Spectrochim. Acta, Part B*, **31**, 523 (1976).
(20) H. Koizumi, K. Yasuda, and M. Katayama, *Anal. Chem.*, **49**, 1106 (1977).
(21) W. Snelleman, *Spectrochim. Acta, Part B*, 403 (1968).
(22) R. N. Hager, Jr., *Anal. Chem.*, **45**, 1131A (1973).
(23) A. T. Zander, T. C. O'Haver, and P. N. Keliher, *Anal Chem.*, **48**, 1166 (1976).
(24) P. N. Kelliher and C. C. Wohlers, *Anal Chem.*, **48**, 140 (1976).
(25) S. R. Koirtyohann, E. D. Glass, D. A. Yates, E. J. Hinderberger, and F. E. Lichte, *Anal Chem.*, **49**, 1121 (1977).
(26) M. S. Epstein and T. C. O'Haver, *Spectrochim. Acta, Part B*, **30**, 135 (1975).
(27) R. Sydor and G. M. Hieftje, *Anal. Chem.*, **48**, 2030 (1976).
(28) R. C. Elser and J. D. Winefordner, *Spectrochim. Acta, Part B*, **23**, 403 (1968).
(29) G. J. Nitis, .V. Svoboda, and J. D. Winefordner, *Spectrochim. Acta, Part B*, **27**, 345 (1972).
(30) C. Veillon and P. Merchant, Jr., *Appl. Spectrosc.*, **27**, 361 (1973).
(31) M. D. Amos, P. A. Bennet, K. G. Brodie, P. W. Y. Lung, and J. P. Matoušek, *Anal. Chem.*, **43**, 211 (1971).
(32) J. Y. Hwang, P. A. Ullucci, S. B. Smith, Jr., and A. L. Malenfant, *Anal. Chem*, **43**, 1319 (1971).
(33) D. A. Segar and J. G. Gonzalez, *Anal Chim. Acta*, **58**, 7 (1972).
(34) R. B. Cruz and J. C. Van Loon, *Anal. Chim. Acta*, **72**, 231 (1974).
(35) R. D. Ediger and J. D. Keiber, *At. Absorp. Newsl.*, **13**, 61 (1974).
(36) F. Perry, S. R. Koirtyohann, and M. Perry, Jr., *Clin. Chem. (Winston-Salem, N.C.)*, **21**, 626 (1975).
(37) F. J. Fernandez, *Clin. Chem. (Winston-Salem, N.C.)*, **21**, 558 (1975).
(38) T. C. O'Haver, M. S. Epstein, and A. T. Zander, *Anal. Chem.*, **49**, 458 (1977).
(39) "Analytical Methods for AAS Using the HGA Graphite Furnace", Perkin-Elmer (990-9972), March 1973.
(40) T. Hadeishi and R. D. McLaughlin, *Science*, **187**, 348 (1975).

RECEIVED for review July 27, 1977. Accepted August 29, 1977. Presented in part at the 28th Pittsburgh Conference, Cleveland, Ohio, 1977. From a Dissertation to be submitted to the Graduate School, University of Maryland, by J. M. Harnly, in partial fulfillment of the requirements for the Ph.D. Degree in Chemistry. Financial support provided by USDA, Agricultural Research Service, Nutrient Composition Laboratory.

Cumulative Sum Charts for Monitoring of Radioactivity Background Count Rates

Roger A. G. Marshall

School of Chemistry, Thames Polytechnic, Woolwich, London SE18 6PF, United Kingdom

Cumulative summation is a simple statistical technique which could be applied more widely in analytical chemistry. The background count rate of a radiochemical counter has been examined as an illustration of its use. The variation in the level of the background can contribute significantly to the error of radioactive measurements. However, when a number of samples of low activity have to be counted, the error may be minimized by initially estimating the background very accurately and thereafter assuming it to be constant. It is recommended that the constancy of the background count rate be then monitored using a cumulative sum chart. This will indicate comparatively rapidly when abrupt changes in the count rate of the order of one standard deviation of the measurement have occurred. The precise point at which the change occurred can also often be deduced and, if necessary, the results can be corrected retrospectively.

It is impossible to measure the activity of a radioactive source without simultaneously recording the background radiation and counter noise. An estimate of the background count rate (R_b) is made in the absence of the source and subtracted from the total source plus background count rate (R_t) to obtain that for the source alone (R_s), i.e.,

$$R_s = R_t - R_b \tag{1}$$

Thus the error in the estimate of the background (σ_b) must be added to that of the total source plus background (σ_t) to obtain the sample error (σ_s) according to the standard equation for the propagation of independent error (*1*):

$$\sigma_s = \sqrt{(\sigma_t^2 + \sigma_b^2)} \tag{2}$$

There are many sources of error in counting such as self-absorption, backscatter, and geometric effects, which are

specific to the source being measured. If these are assumed to be negligible, the error will arise solely from the statistical nature of the decay process. This will obey a Poisson distribution which will approximate to a Gaussian distribution if the number of counts in the reading is greater than approximately 10 (2). In addition, for a reading of N_i counts the standard deviation will approximate to $\sqrt{Ni}$ (3). Therefore, if the counting period had been T_i, then the standard deviation of the count rate will be given by:

$$\sigma_i = \frac{\sqrt{N_i}}{T_i} = \sqrt{\frac{R_i}{T_i}} \tag{3}$$

Thus substituting in Equation 2 the source error becomes:

$$\sigma_s = \sqrt{\left(\frac{R_t}{T_t} + \frac{R_b}{T_b}\right)} \tag{4}$$

Thus the contribution of the background to the source error will increase as the source count rate decreases, i.e., as R_t approaches R_b, although it can clearly be reduced by increasing the time spent on measuring the background.

If one has only a fixed period available for counting a single sample, the most efficient distribution of the time to minimize the source error is such that the ratio of the counting times of the source, T_t, and background, T_b, is equal to the square root of the ratio of the count rates of the sample and background (3, 4), i.e.

$$\frac{T_t}{T_b} = \sqrt{\left(\frac{R_t}{R_b}\right)} \tag{5}$$

Thus it would be possible to spend up to half the counting period on measuring the background count rate for a very weak source. However, for counting a series of samples in a fixed time period, the proportion of the total time spent on the background can be reduced depending on the square root of the number of samples (5).

NEW APPROACH

An alternative more efficient approach, when the number of low activity samples is large as for instance in environmental monitoring or in biochemical or agricultural tracer studies, is to assume that the background is constant. Its level can then be estimated at the beginning of the work with a very long counting period giving great accuracy. Its error will then be negligible compared to that of the source count rate and Equation 2 reduces to:

$$\sigma_s = \sigma_t \tag{6}$$

Clearly there must be some history of work with the detector before such an assumption can be made and additional care may have to be taken in the laboratory. For instance, active γ sources should not be moved unnecessarily and the containment of samples to be counted should be doubly checked.

Naturally the constancy of the background will have to be checked regularly and the results of the checking may be occasionally added to the total sum of background counts giving an increasingly accurate estimate of the background. For instance, at the start of the series of measurements, the background could be counted for 10 000 s and thereafter monitored twice daily for 1000-s periods. Then at the end of 5 days, provided there had been no significant change in the background (see below), a new even more accurate estimate of the background averaged over the total 20 000 s can be calculated. Clearly the time periods chosen and the frequency of monitoring will depend principally upon the activity of the samples, the confidence placed in the counter,

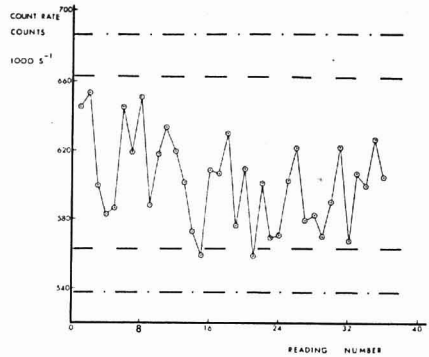

Figure 1. Shewart chart with warning limits (– –) and action limits (•–•–•)

and the ease with which samples could be recounted if necessary.

The procedure for monitoring the background should, of course, be as sensitive to real change as possible. If a large change of background level (>3 σ_b) occurs, there should be no problem in detecting it immediately and investigating the cause. However, when the change in the background count rate is of the same order as the standard deviation of the count obtained in the routine monitoring, careful analysis is required. For instance, if the background is known to be 1000 counts per counting period, is a monitoring reading of 1064 counts due to statistical variation or is it an indication of a real 6.4% or 2 σ_b change in the background level? Problems of this type are best handled by standard graphical quality control methods.

CUMULATIVE SUMMATION

Simple control charts of the Shewart type have been recommended for monitoring counter efficiency (6). This involves plotting the observed values in sequence against a series of horizontal lines representing control limits. Inner control (warning) limits are usually at approximately two standard deviations and outer control (action) limits at three standard deviations from the target value (7). Figure 1 shows 30 consecutive 1000-s readings of the background of a Geiger-Müller counter in this form. Various rules then operate to indicate when the mean value has changed; for instance, one reading outside the outer limit or two consecutively outside the inner limit. A slightly more complicated procedure has been recommended in which groups of consecutive readings are taken and the mean and range of the group plotted as above (8).

An alternative approach to the same data is to plot the cumulative sum, or cusum, of the differences between the reading and a target value against the number of the reading (9). Thus if R is the target count rate and $R_1, R_2 \ldots R_r$ the successive readings, then the cumulative sum is given by:

$$S_r = (R_1 - R) + (R_2 - R) \ldots (R_r - R) \tag{7}$$

$$S_r = \Sigma_{i=1}^{r} (R_i - R) \tag{8}$$

In this case the target value would be the background count rate obtained over the long initial period of time and the cumulative sum would be better called the cumulative deviation. If there has been no change in background, the monitoring readings will be scattered about R giving some positive and some negative values and essentially a zero cusum. However, if the background increases abruptly to a new

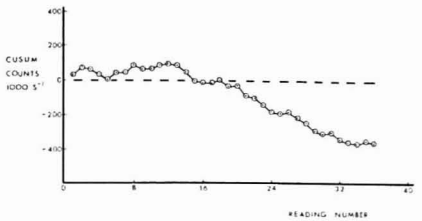

Figure 2. Cumulative sum chart

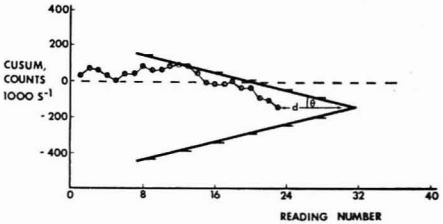

Figure 3. Use of V-mask with $d = 8$ and $\tan\theta = 0.25$

constant value, there will be more positive than negative values so that the cusum will increase. The cusum control chart will then show a line sloping upwards—while if the background has decreased the line would be sloping downwards. Figure 2 shows the same data as in the previous figure presented in cusum form. The target value has here been set equal to the initial background level so that an approximately horizontal line is produced. When the line starts to slope downward, i.e., after the thirteenth or eighteenth reading, a decrease in the background is indicated. As the counter was in fact not in use for a week after the eighteenth point, it is assumed that the change occurred then.

Cusum charts are normally presented with the reading number plotted on the abscissa at 1-unit intervals and with the same ordinate distance equivalent to approximately 2σ units. With this scale, random variations appear quite small and a change in the mean of the series of 2σ from the target value will produce a line of 45° slope from the horizontal. If the cusum line is a curve with increasing slope, then there has been a steady increase in the background level rather than a single fixed change.

The mean of the readings after the point of change can easily be calculated from the change in cusum:

$$\text{New count rate} = R + \frac{\text{change in cusum}}{\text{change in number of readings}} \quad (9)$$

Thus in Figure 2, the mean of the first eighteen results is 613 counts 1000 s^{-1} and that of the latter eighteen 593 counts 1000 s^{-1}, so that the change represents 0.8 standard deviation ($\sigma_b = \sqrt{613}$).

When one has obtained a set of data such as that above, one is obviously presented with the problem of whether the change at point 18 is a real change or an apparent change caused by statistical variation. Two principal procedures exist for making objective assessments of a point of change: one depends on a decision interval (*10*) and the other upon the use of a V-mask (*11*). This latter technique involves the horizontal superimposition of a V-shaped mask on the cusum control chart with its vertex a distance d units ahead of the most recent point. When the cusum line cuts either of the arms of the mask, a real change in the series mean is deemed to have occurred. The simple visual nature of this test technique makes it particularly easy for unskilled personnel to use. Figure 3 shows the V-mask in position and testing the cusum line after the twenty-third reading; as the cusum line crosses the V-mask, a real change of background is indicated.

The value of d and the angle made by the arm of the V to the horizontal, namely θ, will determine how rapidly a change in the mean will be spotted. A mask using $d = 8$ and $\tan\theta = 0.25$ has been found satisfactory. With this mask a $2\sigma_b$ change in the background level will be detected on average after four readings, a $1\sigma_b$ change after 8 readings, and a $0.5\sigma_b$ change after 18 readings (*9, 12*). A normal control chart of the Shewart type would run for approximately twice as long with deviations of this magnitude before action was indicated (*13*).

This increase in rapidity of action signals is the principal advantage of the cusum chart, but a second advantage is the ease with which the point of change can be detected. Thus even with small alterations of level (ca. $\pm\ \sigma_b$), the point of change can be located within two or three readings. Therefore in certain laboratories it should be possible to correct the background retrospectively if the difference is deemed important, as well as to assign a cause to the disturbance. It is in addition worth noting that very occasionally spurious results which are outside the Shewart 3σ action limits have been recorded without there being any subsequent change in the cusum line from the horizontal. It is considered that such odd results are best ignored and the background assumed to be still constant.

RESULTS

Over two hundred 1000-s readings were taken of the background of a halogen-quenched end-window Geiger-Müller tube shielded by 4 cm lead over an eight-week period. Changes in the level of the background occurred three times and corresponded to 0.37, 0.59, and 1.1 σ_b. These represented shifts of 1.5, 2.4, and 4.5% in the mean value of the background. A V-mask with $\tan\theta = 0.25$ and $d = 8$ indicated these changes after 18, 8, and 4 readings, respectively, which is by chance quicker than expected on average (*14*).

A 4.5-cm diameter well-type NaI(Tl) crystal shielded by 4 cm lead was monitored for over one hundred 1000-s counting periods and showed changes of background equivalent to 1.3, 1.8, and $2.6\sigma_b$ (2.5, 3.4, and 5.0% of background count rate) which were detected after 5, 3, and 3 readings, respectively. A second scintillation detector of the same type with an additional 5 cm lead brick wall on four sides to reduce ambient radiation was monitored for 4000-s counting periods over a six-month span. The longer counting period was expected to show up more minor changes, but in fact none were observed. Only two changes occurred: the first of $4.1\sigma_b$ (3.5%) and the second of $2.7\sigma_b$ (2.3%). These changes were of course immediately apparent and would have been obvious even without the cusum chart. However, if 1000-s counting periods had been used instead, the changes would have been equivalent to $2.0\sigma_b$ and $1.3\sigma_b$ when a cusum chart would have been useful for identifying them.

DISCUSSION

It has been shown here how cumulative summation has been of value in reducing the time spent in monitoring the background count rate. All the changes observed were abrupt and there were no cyclic or, more surprisingly, no gradual changes. The cumulative sum technique is thus well suited to this type of control. Its major advantage is that small changes of the same order of magnitude as the standard deviation can be more rapidly detected than by other techniques such as that of Shewart. If the change in mean is less

than approximately 0.5σ, the Shewart chart will indicate the change more rapidly, but of course changes of this magnitude are in many cases less important. Changes greater than 2σ are usually apparent rapidly even to the nonstatistically minded.

The technique has also been applied to the monitoring of the efficiency of a Geiger-Müller tube. This was measured initially for a long period and then daily for shorter periods using the same radioactive source. Small abrupt changes in the efficiency of the tube were observed occasionally. Other quantities, such as the variance or the range of a set of readings, could also be treated by the cumulative sum technique.

This method has proved of value in two areas of radiochemistry but it is considered that the technique could be of benefit in other related fields such as x-ray fluorescence analysis or in thickness and density gauging. In addition it could be usefully applied to the routine observation of noise or background levels and instrumental efficiency of many analytical operations where large numbers of readings must be taken. Examples could be the measurement of residual current in polarography or the peak area in GC standard additions. The only fundamental difference between these applications and radioactivity measurements is that in the former cases the standard deviations must be obtained from a series of measurements at the start of the exercise.

ACKNOWLEDGMENT

The author thanks S. Dawson for painstakingly recording so many readings.

LITERATURE CITED

(1) D. A. Pantony, "Statistics, Theory of Error and Design of Experiment", R.I.C., Lecture Series No 2, London, 1961, p 24.
(2) A. A. Jarrett, "Statistical Methods used in the Measurement of Radioactivity with some useful Graphs and Nomographs", AECU – 262, 1946, p 11.
(3) G. Friedlander, J. W. Kennedy, and J. M. Miller, "Nuclear and Radiochemistry", John Wiley & Sons, New York, N.Y., 1964, p 176.
(4) G. D. Chase and J. D. Rabinowitz, "Principles of Radioisotope Methodology", Burgess Publishing Co., Minneapolis, Minn., 1962, p 84.
(5) R. Loevinger and M. Berman, *Nucleonics*, **9** (1), 26–39 (1951).
(6) R. T. Overman and H. M. Clark, "Radioisotope Techniques", McGraw-Hill Book Co., Inc., New York, N.Y., 1960, p 129.
(7) M. J. Moroney, "Facts from Figures", Penguin Books, New York, N.Y., 1956, Chap. 11.
(8) R. A. Faires and B. H. Parks, "Radioisotope Laboratory Techniques", George Newnes Ltd., London, 1960, p 160.
(9) R. H. Woodward and P. L. Goldsmith, "Cumulative Sum Techniques", Oliver and Boyd, London, I.C.I. Ltd., Monograph No. 3., 1964.
(10) W. D. Ewan and K. W. Kemp, *Biometrika*, **47**, 363–80 (1960).
(11) G. A. Barnard, *J. R. Stat. Soc., Ser. B*, **21**, 239–71 (1959).
(12) P. L. Goldsmith and H. Whitfield, *Technometrics*, **3**, 11–20 (1961).
(13) W. D. Ewan, *Technometrics*, **5**, 1–22 (1963).
(14) N. L. Johnson, *J. Am. Stat. Assoc.*, **56**, 835–40 (1961).

RECEIVED for review September 21, 1976. Resubmitted July 29, 1977. Accepted July 29, 1977.

Particle Size Effects in the Determination of Respirable α-Quartz by X-ray Diffraction

J. W. Edmonds*

The Dow Chemical Company, Analytical Laboratories, Midland, Michigan 48640

W. W. Henslee and R. E. Guerra

The Dow Chemical Company, Central Laboratory, Freeport, Texas 77541

Thin layers ($\lesssim$200 $\mu g/cm^2$) of α-quartz particles on silver and poly(vinyl chloride) membranes are shown to exhibit preferred orientation enhancing the ($10\bar{1}1$) diffraction line (3.34 Å) for particles in the normally accepted size range for x-ray diffraction standards (<15 μm). Respirable silica (<5 μm) analyses performed by x-ray diffraction using α-quartz standards whose particle size distribution does not match the field sample distribution exhibit errors up to 300% of the amount of α-quartz present. Sample concentration in the personal samplers is shown to be an effective means of increasing sensitivity and establishing a nondestructive analysis, but particle size determination of field samples is necessary to aid selection of an appropriately sized standard. Observed threshold sensitivity for α-quartz at the 95% confidence level (2σ above background) is 11 $\mu g/cm^2$.

Recognition of the health hazard due to prolonged exposure to airborne respirable silica has prompted the development of many analytical methods for silica based upon spectrophotometric (*1*, *2*), infrared (*3–5*), and x-ray diffraction (*6–22*) techniques. For the most part, sampling procedures have developed independently from the analytical methods, with the exception of modified membrane cassettes for personal samplers (*10*, *18*). Attempts to implement one analytical method for all Dow Laboratories (*23*) have emphasized the desirability of a direct nondestructive technique which would permit reproducible sensitivity during interlaboratory cross-checks. X-ray diffraction was selected because of its ability to distinguish among polymorphs and its sensitivity in reported methods. The difficulties experienced in devising a suitable direct x-ray diffraction method have identified a number of problem areas which were previously unknown or inadequately investigated. Particle size distributions of field samples and quartz standards, quality of quartz standards, surface effects of sampling membranes, and modified sampling techniques are some of the critical areas to be discussed.

While these results are concerned primarily with sandblasting and therefore only with α-quartz at threshold limit values (TLV) of 100 $\mu g/m^3$ of air or lower, the results should be generally applicable or identify critical problems for further investigation in other industries.

EXPERIMENTAL

Many of the experiments were run independently in the Midland and Freeport laboratories but led to similar conclusions.

Therefore, the experiments will be described in general terms for clarity, and differences discussed only where significant.

Standards of α-quartz examined were Minusil 5 (three lots), Minusil 15, and three standards prepared by suspending silica flour or ball milled rock quartz in ethyl alcohol or water and collecting sedimentation fractions. Relative particle size distributions were obtained using a Coulter Counter Model TAII and ammonium thiocyanate in dimethylformamide (DMF) as the electrolyte. DMF was found to adequately dissolve the poly(vinyl chloride) (PVC) membranes used for sample collection.

Membranes studied included silver (25-mm diameter, 0.45 μm, Selas Flowtronics FM-25), and poly(vinyl chloride) (Mine Safety Appliances FWS-B, 5 μm, and Millipore BDWP, 0.6 μm). Membranes were mounted in the diffractometer using a brass cylinder with a concentric ring hold down. This permitted the PVC membranes to be suspended at the diffractometer center and drawn taut with no extraneous grease or other adhesive. Silver membranes were set flat on an aluminum block when possible. Many of the silver membranes exhibited a noticeable concavity which made the placement of the sample at the instrument center difficult. All membranes were rotated in the beam in an attempt to average the effects of particle orientation and nonuniform distribution. Lack of rotation can cause intensity variations for all types of membranes and deposition methods.

Membranes with known amounts of deposited α-quartz were prepared by filtration of stock suspensions or by air collection in a dust chamber. Stock suspensions were prepared by placing 0.100 g of a dried α-quartz standard in a 1-L volumetric flask and filling with deionized water which had been filtered through a 0.22-μm Millipore Duratube filter cartridge. An aliquot of this suspension (100 μg/mL) was diluted to 1 L to form a second stock suspension (2–4 μg/mL). It is critical that the suspensions be vigorously agitated for at least 30 s before any aliquot is removed, since concentration gradients set up very quickly. All aliquots were withdrawn from the center of the suspension. A Millipore filtering apparatus was used with approximately a 16-mm effective filter diameter in the filter chimney (the exact chimney diameters were found to vary slightly).

Microbalance weights (Cahn Instruments Model G or Perkin-Elmer AM-2 ratioing electrobalance) and apparent weights calculated from volume were plotted vs. x-ray intensity for a series of *liquid* filtered membranes. A straight line relationship was observed for x-ray intensity vs. apparent weight calculated from aliquot volume, but slightly scattered data points with occasional large discrepancies resulted when the microbalance weights were used (*21*). For this reason, it appears to be more valuable for liquid filtered standards to invest time in multiple determinations based solely on dilution data.

A Wright dust feed mechanism (*24*) was used to generate a dust atmosphere in a 160-L air chamber. Membranes were placed in the filter holder cassette of a personal sampler (*25*) with the cyclone separator removed. Membranes were dried at 60 °C, weighed on a microbalance, collected, dried, and reweighed.

The x-ray diffractometer used was a Norelco Philips vertical goniometer fitted with a closed sample chamber, θ compensating slit, graphite monochromator, scintillation counter, and long fine focus copper target tube. The membranes on the sample holder were mounted in the radiation chamber in a rotating sample mount. Midland scans were made at $^1/_2$° 2θ/minute from 30° to 22° 2θ with the copper tube operated at 35 kV and 25 mA. Freeport scans were made at 50 kV and 35 mA with a helium purge of the sample chamber. A standard membrane was scanned before and after the samples to correct for instrument variations, including power (kV and mA) and monochromator alignment. Increasing power to the tube does not increase the signal to noise ratio. Purging the sealed radiation chamber with helium offers about a 20% increase in signal to noise and is therefore a recommended procedure.

The α-quartz 3.34-Å diffraction peak ($10\bar{1}1$) appears at 26.71° ± 0.05° 2θ because of variations in membrane surface smoothness created by the sample holder. For diffraction scans, the background line is drawn midway between the peak-to-peak noise from 27.5° to 25.5° 2θ (Figure 1). Root mean square (*rms*) noise ($2\tilde{\sigma}$) is estimated as 0.67 of peak-to-peak noise. The height of the 3.34-Å line is measured above the mean background and corrected for *rms* noise, ($I_c = I - rms/2$). I_c must be greater than the measured

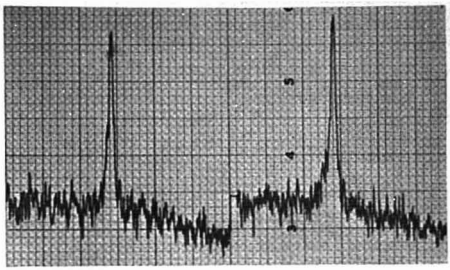

Figure 1. (Left) $^1/_2$° min^{-1} scan of an open faced membrane collected in the field. (Right) $^1/_2$° min^{-1} scan of 100 μg Minusil 5 collected from aqueous suspension (88 μg/cm^2). Both membranes have 12-mm effective filter diameters. RMS noise range is estimated by the added curves at the peak bases

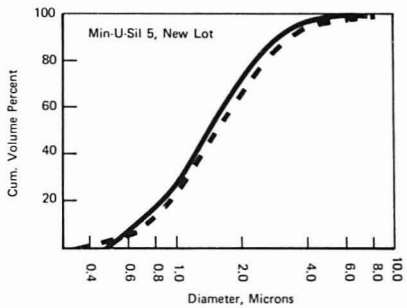

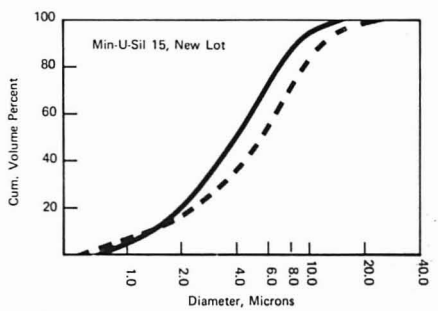

Figure 2. Comparison of particle size distributions for Minusil 5 and 15. Semilog plot; (—) Coulter Counter, (- - -) X-ray sedigraph

rms noise ($2\tilde{\sigma}$) to be considered observed.

Step scans were made by first manually determining the peak maximum, $2\theta_{max}$, and counting for 180 s. Backgrounds were counted each for 90 s at $2\theta_{max} \pm 0.5$°. Subtracting the two backgrounds from the counts for $2\theta_{max}$ gives the intensity for α-quartz, i.e., $I_c = I - (B_1 + B_2)$. The standard deviation is calculated as $\tilde{\sigma} = (\Sigma B_1 + I + B_2)^{1/2}$. $2\tilde{\sigma}$ is taken to be the detectable limit.

Particle Size Distributions. Procedures followed for separating α-quartz standards into different particle size distributions have been described (*21*). Sediments were dried and sized using the Coulter Counter.

Minusil 5 and 15 (Midland lots) were sized both by sedigraphic and Coulter Counter techniques. The particle size

Table I. α-Quartz Response for Various Particle Sizes (Midland and Freeport values not normalized)

a. Midland, Cu Kα, 35 kV/25 mA

Ag, 0.45-μm membrane	X-ray response/μg
Minusil 5	0.3
Minusil 15	0.8
Minusil 15W	1.0

b. Freeport, Cu Kα, 50 kV/35 mA, He purge

Minusil 5	0.9
Standard No. 2	1.8
Millipore, 0.6-μm PVC membrane	
Minusil 5	1.0
Standard No. 2	1.7
MSA FWS-B, 5-μm membrane	
Minusil 5	1.3
Standard No. 3	1.8
Standard No. 2	2.1

distributions are compared in Figure 2. The superposition of curves (within experimental error) for Minusil 5 is consistent with uniformly shaped particles, and indicates the validity of the Coulter Counter data for this sample. The lack of overlap for Minusil 15, however, is consistent with this sample having irregularly shaped particles in the larger sizes. The results possibly indicate different modes of manufacture for the two Minusils. Particle size distributions for standards No. 2 and No. 3 determined by optical and electron microscopy compared favorably to the Coulter Counter data.

DISCUSSION

During the process of developing x-ray diffraction methods for the analysis of silica in our Midland and Freeport laboratories, prepared PVC membranes were exchanged as a check on results due to minor differences in technique and equipment (availability of helium purge, sample spinner, choice of scan speed and standard, and effective filter area). The apparent weights of α-quartz were calculated from the x-ray diffraction intensity of the 3.34-Å line and compared to the in-house calibration curve. The weight results for one set of membranes (Midland) were uniformly low when compared to the other (Freeport) calibration curve. Since Minusil 5 had been the standard used in Midland, and a larger sized in-house standard in Texas (*21*), an investigation was begun into the effects of the particle size of the α-quartz standards on the x-ray diffraction method.

Silver membranes were selected because of low background in the region of the 3.34-Å line (*9*). From standard stock solutions (see Experimental), three membranes each were made for depositions of 20, 40, 80, and 100 μg of Minusil 15, Minusil 5, and a fraction of Minusil 15 with the fine particles removed by suspension ("Minusil 15 W").

The relative particle size distributions for the Midland Minusil 5, 15 and 15 W standards are displayed in Figure 3. Membranes were prepared in Texas according to documented procedures (*21*) using Minusil 5 (lot differing from Midland Minusil 5), and two in-house standards, No. 2 and No. 3. The relative particle size distributions are also presented in Figure 3. Depositions of standard No. 2 and Minusil 5 were also made on silver 0.45-μm membranes. The resulting x-ray diffraction intensities were averaged for each weight range for each standard, and are presented in Table I. It is clearly seen that as volume averaged particle size increases, apparent sensitivity increases because of an increase in the x-ray diffraction intensity per unit weight of α-quartz. This increase in intensity per unit weight can be due to amorphous material in the smaller size standards, shadowing of small (<2 μm) particles by the surface of the silver membranes, or particle orientation. Studies on MSA FWS-B and Millipore BD membranes with Freeport standards No. 2, No. 3, and Minusil 5 also show the same increase of x-ray intensity with increasing particle size (Table I).

Table II. Membrane Effects on α-Quartz X-ray Response (Midland and Freeport values not normalized)

a. Midland, Cu Kα, 35 kV/25 mA

Minusil 5	X-ray response/μg
Ag, 0.45 μm	0.3
MSA FWS-B, 5 μm	0.7
Minusil 15	
Ag, 0.45 μm	1.0
MSA FWS-B, 5 μm	1.3
Millipore, 0.6 μm	1.6

b. Freeport, Cu Kα, 50 kV/35 mA, He purge

Standard No. 2	
Millipore, 0.6 μm	1.7
Ag, 0.45 μm	1.8
MSA FWS-B, 5 μm	2.1

To elucidate the effects of shadowing (if predominant), the same weight depositions of Minusil 15W and standard No. 2 were made on Millipore BD, silver, and MSA FWS-B 5-μm (smooth side) membranes. The results are displayed in Table II. It is surprising to note that greater x-ray intensity above background per unit weight is obtained using the organic as opposed to the silver membrane filters. This observation led to a scanning electron microscopic examination of the membrane surfaces.

Electron micrographs were obtained for α-quartz on silver, Millipore BD, and smooth and rough faces of MSA FWS-B membranes (*21*) (Figure 4). The micrographs show irregular particles, some, but not the majority, deposited in such a way that shadowing by the silver would occur at low angles (θ = 13.3°). The Millipore BD shows a smoother surface, but at high magnification shows ~1-μm pores and a detectable unevenness. The Millipore membrane also exhibits slight differences in smoothness between front and back faces. MSA FWS-B shows cavernous openings (>100 μm) on the "rough" face, but a very smooth surface under high magnification for the "smooth" face. It has been shown that the smooth face, rather than the rough face of the MSA membrane yields much greater x-ray intensity response per unit weight of deposited silica (*21*), most likely because of silica not becoming entrapped deep into the membrane. The micrographs indicate that the MSA FWS-B "smooth" surface offers the best surface characteristics for analysis, and the x-ray studies confirm satisfactory intensity per unit weight. The difference between the "smooth" and "rough" faces of the MSA FWS-B membranes is apparent to the naked eye.

Orientation. The Minusil 5 and 15 standards were compared by depositing 100 μg each on 12-mm circular cover glasses to eliminate membrane effects and permit the entire sample to be irradiated by the x-ray beam. The resulting x-ray intensities for the 3.34-Å line ($10\bar{1}1$) averaged over three independent observations under the same conditions were not equal: $I_{Min5}/I_{Min15} = 0.6$. Additional diffraction lines were scanned for each standard on cover glasses and for thick loadings of the bulk standards, and the relative intensities calculated (Table III). While relative intensities of the bulk standards agree with published values, those for the 100-μg deposits on 12-mm cover glasses do not. Dana (*26*) indicates the preferred cleavage of α-quartz is ($10\bar{1}1$). What is being observed is that extremely thin layers of α-quartz (no matrix) exhibit a preferred orientation favoring ($10\bar{1}1$), the 3.34-Å *d*-spacing. As the deposition depth increases and gives a rougher surface, the orientation approaches random (Figure 5). Using relative intensities as indicators (Table III), it can

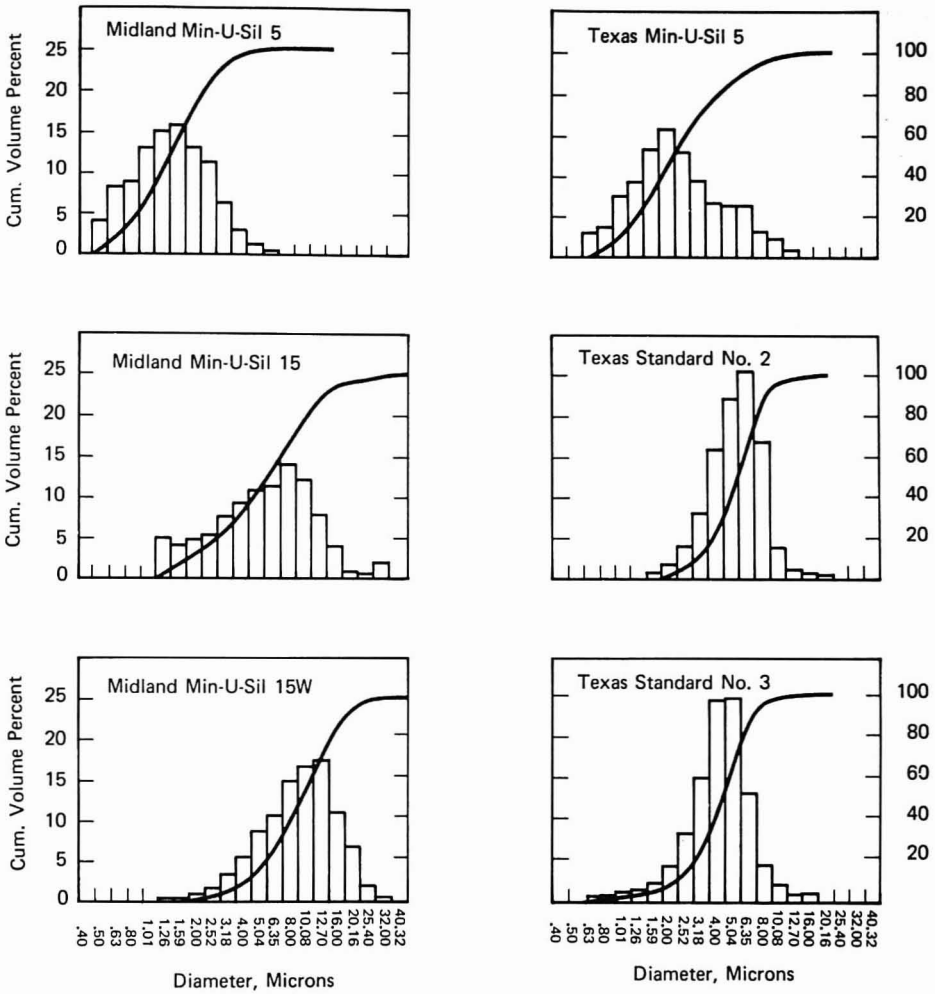

Figure 3. Comparison of Coulter Counter derived particle size distributions for α-quartz standards. Bar graph indicates volume percent for each data channel, plotted as equivalent diameter, μm. Line graph represents cumulative volume percent

be seen that preferred orientation is apparent on the MSA FWS-B membrane as well as the silver membrane.

It appears that two phenomena account for the decreased x-ray intensity response per unit weight on silver membranes. First, the smaller particles are "shadowed" (hidden from the x-ray beam) by the rougher silver membrane surface and, second, the rougher surface gives a more random orientation to the deposited α-quartz particles, i.e., preferred orientation *enhances* the ($10\bar{1}1$) diffraction line on the flat PVC membranes. This effect can be used to enhance the threshold sensitivity of an analytical method, however, if it is recognized.

The observed effect of α-quartz particle size on the calibration curves is therefore primarily due to preferred orientation. If a standard is used whose particle size is significantly larger than the particle size of the field samples, then a larger x-ray intensity per unit weight of α-quartz will be observed, a lower threshold sensitivity deduced, and the actual amount of α-quartz on a field sample will be underestimated. For example, *the error can approach a factor of three as exhibited by the different responses of Minusil 5 and 15 (Table I).*

Standards. The obvious standard to use is one which matches a "respirable" size distribution obtained by the sampling apparatus (*27*). Since this is not generally available, the best approximation is Minusil 5 or any α-quartz standard whose particle size distribution fits the field sample distributions. Unfortunately, α-quartz standards, however similar in particle size, are not identical. The pulverizing process creates an amorphous surface on the α-quartz particles approximately 0.03 μm thick (*28–35*), making in-house standard

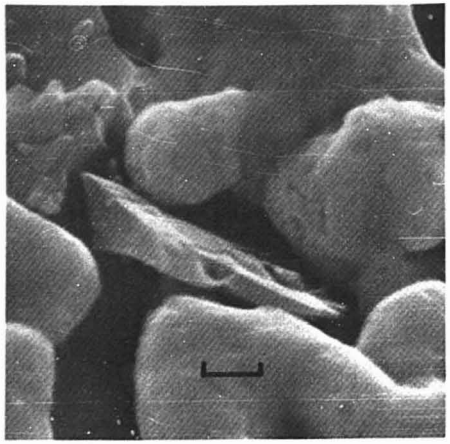

Figure 4. Electron micrograph of Minusil 5 particle deposited from liquid suspension on silver 0.45-μm membrane. The irregularly shaped particle would preferentially orient on a smooth surface, and be "shadowed" on a rough surface. Marker indicates 1 μm. (Adapted with permission from (*21*))

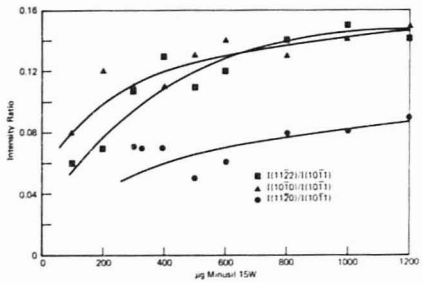

Figure 5. α-Quartz x-ray intensity ratio, $I_{(hkil)}/I_{(10\bar{1}1)}$, compared to weight of Minusil 15W deposited on 12-mm cover glass slips

Table III. $I/I_{(10\bar{1}1)}$ α-Quartz Preferred Orientation

(*hkil*)	(10$\bar{1}$0)	(11$\bar{2}$0)	(11$\bar{2}$2)
d-spacing, A	4.26	2.458	1.817
Literature	0.18–0.22	0.11	0.21
Ball milled rock quartz			
100 μg on 12-mm coverglass	0.11	...	0.10
Bulk	0.18	0.11	0.21
Minusil 5			
500 μg on Ag, 0.45 μm	0.18	0.05	0.09
Bulk	0.16	0.08	0.17
Minusil 15, air collected, MSA FWS-B			
260 μg	0.17	0.09	0.09
Bulk	0.15	0.09	0.17
Minusil 15W on coverglass			
No. 1, 100 μg	0.08	0.02	0.03
No. 2, 100 μg	0.10	0.06	0.07
Bulk	0.15	0.09	0.17
Minusil 5, 3.5% in Cabosil			
Bulk	0.16	0.08	0.19

Table IV. Relative X-ray Intensities for Various Sources of α-Quartz[a]

Quartz type	Volume averaged diameter, μm	X-ray response/ μg
Minusil 5 (new lot)	1.7	1.2
Minusil 5 (old lot)	3.8	1.1
Minusil 15 (new lot)	4.5	1.5
Minusil 15 (old lot)	7.2	1.7
Minusil 15W cut No. 1	7.7	1.9
Ball milled rock quartz	4.3	1.4

[a] 100 μg deposited on 12-mm cover glass slips.

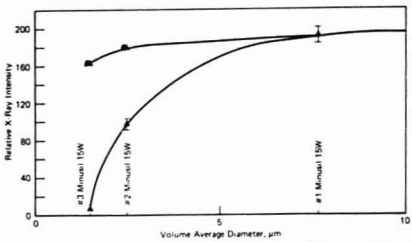

Figure 6. Relative x-ray intensities of α-quartz (10$\bar{1}$1) for particle size fractions of Minusil 15, 100 μg on 12-mm cover glass slips. Upper curve is theoretical fall off of x-ray intensity assuming a 0.03-μm amorphous shell and spherical particles in the particle size distribution

generation inadvisable. For example, pure rock quartz ball milled, sized, and scanned by x-ray diffraction is compared to commercial Minusil standards in Table IV. Treatment with 10% HF to remove the amorphous layer (*28*) is not advised, as the field samples cannot be similarly treated without complicated manipulations detrimental to a fast, reliable, direct analytical method. The physiological effects of this amorphous layer are still unclear.

The best solution appears to be the use of a universally available α-quartz standard which has a well documented particle size distribution below 5 μm. This would then permit interlaboratory exchange of membranes for verification purposes, and aid in making silica exposure data uniform for future health and environmental comparisons. One remaining problem, however, is that there exists no direct technique for determining the percent crystalline α-quartz in an x-ray diffraction standard other than x-ray diffraction. The work necessary to determine the quality of an α-quartz x-ray diffraction standard is sufficient to justify certification and availability through a single source.

The effect that the amorphous nature of the surface of the α-quartz particles in field samples will have on x-ray diffraction response is still unknown. Sandblasting may have an entirely different effect on particle surface than, for instance, foundry activities or quarrying. Errors may remain in the estimation of the amount of α-quartz from various sources, even when compared to a universal standard. It is not felt that these errors are large in the sandblasting field samples observed, where only 3% of the particles passing the cyclone are smaller than 0.4 μm and therefore have a negligible amorphous content.

The amorphous content present in Minusil 15 was investigated by sedigraphically separating various particle size ranges (see Experimental) and measuring x-ray intensities for three depositions of 100 μg of each fraction on 12-mm cover glasses. The results are displayed in Figure 6. Assuming a 0.03-μm shell of amorphous silica surrounds each α-quartz particle (*28*), a curve of x-ray intensity vs. *volume average*

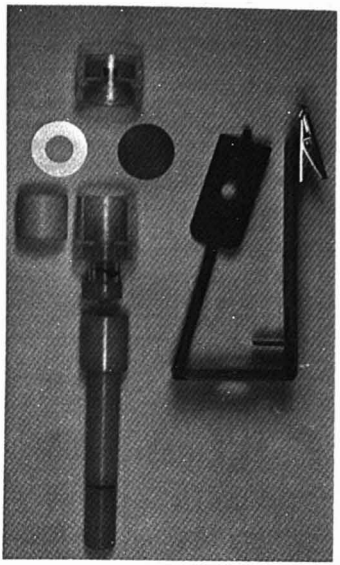

Figure 7. Exploded view of a Bendix 25-mm filter cassette and cyclone. Also shown are the Teflon pre-membrane insert and the 8-mil stainless steel post-membrane insert

diameter can be calculated using the particle size distribution for each of the three Minusil 15 sedigraphic cuts and assuming random orientation. These calculated points are normalized and also displayed in Figure 6. It can be seen that the observed x-ray intensity (*with* preferred orientation) falls off faster than expected for the smaller particle fractions of Minusil 15. While the fall off may be due in part to the loss of enhancement due to preferred orientation, the x-ray intensity should not fall to nearly zero with the smallest fraction. This indicates there is a significant fraction of noncrystalline material in the smaller particle sizes. While this size fraction may be negligible compared to the sample bulk, the percent *crystalline* silica is not 100% as presumed, but unknown. It is also indeterminable without critical assumptions. The lack of standard characterization in published methods (*1–5, 8–20, 22*) therefore makes it impossible to make a fair comparison of the sensitivities or detection limits of these methods.

Sampling. The two-stage respirable dust separator has achieved acceptance as a sampling device. The variations in available filter holders have forced most analytical methods development to deal with the collected membrane, with two exceptions (*10, 18*). It is obvious that if the x-ray or infrared beam cannot irradiate all of the deposited material, one must assume uniformity of deposition *or* redeposit the sample in order to perform the analysis. Since redeposition techniques are time consuming and prone to introduce additional error, it seems preferable to confine redeposition to cases where severe interferences must be removed.

It therefore appeared more reasonable to modify the existing cassettes than to design a separate filter holder as had been done previously (*10*). A Bendix 25-mm filter cassette and cyclone (*25*), Figure 7, were selected since the collection membrane would fit directly onto the diffractometer sample spinner attachment. This filter holder had been designed in conjunction with Gebhardt (*18*), but still retained an effective filter diameter of 21 mm, substantially greater than both the

Table V. Relative X-ray Intensities for α-Quartz ($10\bar{1}1$) for Air and Filtered Liquid Suspensions of Minusil 5 Collected on MSA FWS-B 5-μm Membranes Using a 12-mm Effective Filter Diameter

	X-ray response/μg
Air filtered	0.9 ± 0.1
Liquid filtered	1.0 ± 0.03

x-ray beam (12.5 mm square) or the liquid filtration chimney used for standard membrane preparation (~16-mm diameter). The first modification was a Teflon insert placed between the cyclone outlet and the collection membrane (Figure 7). The insert had a 15.5-mm cylindrical hole, so that deposition would cover the same effective filter area as the standard membranes from liquid filtration. α-Quartz dust was deposited on membranes in an air chamber as described under Experimental, but resulted in a nonuniform dust distribution. Since the open chamber behind the membrane and the Teflon insert appeared to control deposition, a post-membrane disk insert was fabricated from 8-mil stainless steel, 25 mm in diameter. A 12-mm hole was punched concentrically so that air flow would be forced to the membrane center and all material would be deposited in an area which would be completely irradiated by the x-ray beam. Placing the insert *behind* the membrane does not give a membrane-insert interface for α-quartz entrapment. Air expansion and convection into the chamber behind the insert might affect the uniformity of deposition, but all deposited material would be irradiated regardless.

Air chamber experiments were repeated using the post-membrane insert and Minusil 5. Membranes were treated as above and the results are displayed in Table V. The intensity curve for the air deposited membranes is quite linear for values less than 100 μg/membrane, the region of interest, and the calibration curve for filtered liquid suspensions of Minusil 5 is seen to be the same within experimental error. This is an indication that liquid filtered standard membranes can be used for analysis, thus avoiding the complications of dust feed mechanisms and air chamber equilibration.

Inserts made for the more common 37-mm cassettes have proved just as effective in field use.

Matrix Effects. Spurious effects of iron contaminants might be expected with fluorescence because of the Cu radiation and absorption. No adverse effects were observed for the x-ray intensity of α-quartz when admixed with a 1:1 mixture of Fe_2O_3 and Fe_3O_4 in a 1:4 weight ratio with α-quartz. The data points for this mixture were observed to fall on the α-quartz calibration curve (*21*). Similar results were obtained by Bradley for iron oxides (*8*) and Gebhardt with calcite and feldspar (up to 80% total sample weight) (*18*).

Field Samples and Cyclone Operation. Field sampling was made with the post-membrane insert in a two-stage cyclone separator (*25*). Flow rate checks with a membrane and insert in place indicated a 1.7 to 2.0 L/min. flow could easily be maintained for the MSA FWS-B 5-μm membrane, but a maximum of only 1.6 L/min for the Millipore BD 0.6-μm membrane. Previous studies indicate that the 10-mm cyclone passes a particle fraction in agreement with the Los Alamos curve (*27*) and that this separation efficiency does not change in the flow rate range of 1.7 to 2.1 L/min (*36*).

Field samples were collected both in the respirable zone under the sandblasters hood using the cyclone separator and in the open air adjacent to the sandblasting operation using an open faced membrane. Typical particle size distributions with and without the cyclone are displayed in Figure 8. The size selected material is seen to have a size distribution similar only to the Minusil 5 standard. The cyclone is also seen to be quite efficient at the 2.0 L/min flow rate. An x-ray dif-

Table VI. For Scanned Membranes, α-Quartz Threshold Detection Limit/Membrane at 95% Confidence Level, Cu Kα 35 kV/25 mA, 1/2°/min, 2θ scan

Membrane	Conditions[a]	Threshold (2σ), μg
Ag, 0.45 μm	Minusil 5, 15.5 mm, liquid	25
	Minusil 15, 15.5 mm, liquid	11
	Minusil 15W, 15.5 mm, liquid	7
MSA FWS-B,	Minusil 5, 15.5 mm, liquid	15
	Minusil 15W, 15.5 mm, liquid	6
	Minusil 5, 12 mm, liquid	11
	Minusil 5, 12 mm, air	11

[a] α-Quartz standard, effective filter diameter, filter mode.

Table VII. Increased Sensitivity for Three-Point Step Scans, 100 μg Minusil 5 on MSA FWS-B, Liquid Filtered Standard

	Time, s	Count	$I = P - B_1 - B_2$	$2\sigma = 2(P + B_1 + B_2)^{1/2}$	% relative error, Threshold detection limit, μg[a]
B_1	10	103			
P	20	450	229	52	23
B_2	10	118			
	30	311			
	60	1362	709	90	13
	30	342			
	90	942			
	180	4012	2073	154	7
	90	997			
	180	1919			
	360	8207	4282	220	5
	180	2006			

[a] In this example only, % relative error = threshold detection limit at 95% confidence level.

fraction scan of an open-faced sample indicates the signal to noise ratio encountered and the low level of interferences (Figure 1).

Detection Limits. The variation of threshold detection limit with particle size distribution for scanned membranes is summarized in Table VI. Table VII summarizes the increased sensitivity gained in using a three-point step scan method, in which considerable time is saved and fewer errors induced.

CONCLUSIONS

1. The tendency for α-quartz to exhibit preferred orientation in thin deposited layers on smooth surfaces is responsible for the increased x-ray diffraction intensity per unit weight on PVC membranes. The rougher surface of silver membranes tends not only to give a more random particle orientation, but also to "shadow" smaller particles from the x-ray beam, both resulting in lower unit intensity response than observed for smooth PVC membranes. This orientation effect can be used to enhance α-quartz threshold detectability on smooth PVC membranes compared to that on silver membranes. Rotation of the sample in the beam is also advisable to even out the effects of this preferred orientation.

2. The tendency to select a "pure α-quartz" standard for use in respirable silica analysis without regard for particle size distribution will lead to spurious, although internally consistent, results. For instance, maximizing threshold detection by selecting Minusil 15 over Minusil 5 can lead to almost a threefold underestimation of the amount of respirable silica on field samples collected with a cyclone size selector. Therefore, an α-quartz standard with a particle size distribution nearly 100% in the "respirable" range should be characterized and be made universally available even though this results in an apparent loss of "sensitivity" above background on selected membranes.

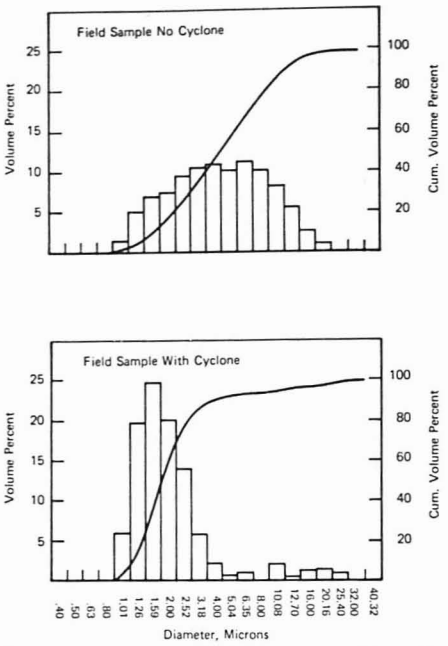

Figure 8. Comparison of Coulter Counter derived particle size distributions for field collected material with and without the 10-mm cyclone separator. Material with diameter greater than 5 μm in the lower graph is particle/membrane agglomeration

3. Simple modification of personal samplers (25- and 37-mm) to permit collection of dusts in an area (e.g., 12-mm diameter) that is entirely irradiated by an x-ray or infrared beam does not decrease the efficiency of the sampler, but will concentrate the sample for more sensitive and rapid analysis. The samplers (10-mm cyclones) can efficiently operate at flow rates from 1.7 to 2.0 L/min.

4. The availability of a "respirable" α-quartz standard and the deposition of α-quartz in an area completely irradiated would make round-robin sample exchanges a convenient reality, and provide a meaningful basis for the reported exposures to respirable silica dust.

5. The fall-off of calibration curves at ~100 μg/cm² is most likely due not to absorption but to the loss of preferred orientation favoring the 3.34-Å d-spacing of α-quartz. The deposited layer is thick enough to favor more random orientation so that the observed x-ray intensity of the $(10\bar{1}1)$ peak begins to decrease to the expected relative intensity value for a randomly oriented bulk sample.

6. Determination of the particle size distribution of selected field samples is necessary to ensure the validity of the standard used.

ACKNOWLEDGMENT

The authors thank G. R. McGowan and B. W. Pynnonen for the particle size analyses, R. E. Cook for aid in field sampling, H. O. Yakel for aid with the dust chamber work, L. R. Ruhberg for help with the initial x-ray studies, L. D. Martin, M. R. McCullogh, and D. W. Krieg for studies on the scanning electron microscope, D. C. Benefiel on the transmission electron microscope, and R. R. Langer and B. S. Horvrath for discussions and support.

LITERATURE CITED

(1) N. A. Talvitie, *Am. Ind. Hyg. Assoc. J.*, **25**, 169–178 (1964).
(2) D. V. Sweet, F. R. Wolowicz, and J. V. Crable, *Am. Ind. Hyg. Assoc. J.*, **34**, 500–506 (1973).
(3) J. W. Cares, A. S. Goldin, J. J. Lynch, and W. A. Burgess, *Am. Ind. Hyg. Assoc. J.*, **34**, 298–305 (1973).
(4) D. J. Larsen, L. J. von Doenhoff, and J. V. Crable, *Am. Ind. Hyg. Assoc. J.*, **33**, 367–372 (1972).
(5) S. Z. Toma and S. A. Goldberg, *Anal. Chem.*, **44**, 431–432 (1972).
(6) G. L. Clark and D. H. Reynolds, *Ind. Eng. Chem., Anal. Ed.*, **8**, 36–40 (1936).
(7) H. P. Klug, *Anal. Chem.*, **25**, 704–708 (1953).
(8) A. A. Bradley, *J. Sci. Instrum.*, **44**, 287–288 (1967).
(9) J. Leroux and C. A. Powers, *Staub-Reinhalt. Luft (Eng. Ed.)*, **29**, 26–31 (1969).
(10) J. Leroux, A. B. Davey, and A. Paillard, *Staub-Reinhalt. Luft (Eng. Ed.)*, **32**, 27–31 (1972).
(11) J. Leroux, A. B. Davey, and A. Paillard, *Am. Ind. Hyg. Assoc. J.*, **34**, 409–417 (1973).
(12) G. Knight, W. Stefanich, and G. Ireland, *Am. Ind. Hyg. Assoc. J.*, **33**, 469–475 (1972).
(13) G. Knight, R. Kowalchuk, and R. Yourt, *Am. Ind. Hyg. Assoc. J.*, **35**, 671–680 (1974).
(14) G. C. Allen, B. Samimi, M. Ziskind, and H. Weill, *Am. Ind. Hyg. Assoc. J.*, **35**, 711–717 (1974).
(15) H. E. Bumsted, *Am. Ind. Hyg. Assoc. J.*, **34**, 150–158 (1973).
(16) R. W. Freedman, S. Z. Toma, and H. W. Lang, *Am. Ind. Hyg. Assoc. J.*, **35**, 411–418 (1974).
(17) A. Mangia, *Anal. Chem.*, **47**, 927–929 (1975).
(18) R. F. Gebhardt, Martin Marietta Cement Technical Center, Baltimore, Md. Paper presented to the September 1975 meeting of the Portland Cement Association at Tucson, Ariz.
(19) M. T. Crosby and P. S. Hamer, *Ann. Occup. Hyg.*, **14**, 65–70 (1971).
(20) S. Altree-Williams, *Anal. Chem.*, **49**, 429–432 (1977).
(21) W. W. Henslee and R. E. Guerra, "Direct Quantitative Determination of Silica by X-ray Diffraction on PVC Membrane Filters", *Advan. X-ray Anal.*, **20**, 139–152, 1977.
(22) E. T. Peters, "Evaluation of the NIOSH X-ray Diffraction Method for the Determination of Free Silica in Respirable Dust", Contract No. CDC-99-74-51., NIOSH, 4676 Columbia Pkwy., Cincinnati, Ohio 45226, May 1976.
(23) "Occupational Exposure to Crystalline Silica, Criteria for a Recommended Standard", HEW publication No. (NIOSH) 75-120, 1974.
(24) B. M. Wright, *J. Sci. Instrum.*, **27**, 12–15 (1950).
(25) Bendix Environmental Systems, Model No. 2419107.
(26) E. S. Dana, "A System of Mineralogy", 6th ed., J. Wiley & Sons, New York, N.Y., 1937.
(27) Aerosol Technology Committee, American Industrial Hygiene Association, *Am. Ind. Hyg. Assoc. J.*, **31**, 133–137 (1970).
(28) G. Nagelschmidt, R. L. Gordon, and O. G. Griffin, *Nature (London)*, **169** (4300), 539–540 (1952).
(29) P. B. Dempster and P. D. Ritchie, *Nature (London)*, **169** (4300), 538–539 (1952).
(30) D. W. Clelland, W. M. Cumming, and P. D. Ritchie, *J. Appl. Chem. (London)*, **2**, 31–41 (1952).
(31) R. L. Gordon and G. W. Harris, *Nature (London)*, **175**, (4469), 1135 (1955).
(32) C. M. Jephcott and H. F. V. Wall, *AMA Arch. Ind. Health*, **11**, 425–430 (1955).
(33) G. Nagelschmidt, *Analyst (London)*, **81**, 210–219 (1956).
(34) G. W. Brindley and S. Udagawa, *J. Am. Ceram. Soc.*, **42** (12), 643–644 (1959).
(35) R. W. Grimshaw, "The Chemistry and Physics of Clays and Allied Ceramic Materials", 4th ed., Wiley-Interscience, New York, N.Y., 1971, p 708.
(36) G. R. McGowan, Dow Chemical Co., Midland, Mich., private communication, 1975.

RECEIVED for review April 18, 1977. Accepted August 31, 1977.

Proton Induced X-ray Emission Analysis of L-Cells Grown in Vitro

R. R. Zombola,* P. A. Kitos, and R. C. Bearse

University of Kansas, Lawrence, Kansas 66045

The trace element concentrations of L-cells grown in vitro have been determined by PIXE analysis. The precision of the technique was determined by comparing measurements of 20 targets made from a common sample. Nineteen separate cultures were analyzed to determine the variability of "identically" grown cells. The results from this latter experiment indicate that the elemental concentration in ppm of each element in L-cells is K (13033 ± 649), Ca (74.7 ± 10.7), Mn (5.0 ± 0.5), Fe (101 ± 3), Cu (12.3 ± 1.0), Zn 57.6 ± 2.8). The system was shown to be linear for variations in elemental concentration.

Proton induced x-ray emission (PIXE) has been recognized as a useful method for determining the elemental composition of small samples (*1*). A major advantage of this technique is that a sample can be analyzed quickly, and all elements between Cl and Mo are detected simultaneously if they are present in large enough quantity. The purpose of this paper is to report the details involved in applying this technique to the elemental analysis of cell cultures. These cell samples are, by their nature, small in total mass and contain several elements at concentration levels amenable to measurement by PIXE.

The cells used here, L-cells, are derived from a line of fibroblastoid mouse cells. Comparison of elemental concentrations of these L-cells to L-cells in various pathological states may be helpful in understanding the nature of these states. There is also some evidence that healthy and cancerous cells have different trace element concentrations (*2*). Thus, application of this technique could open some interesting avenues of research in cell biology.

EXPERIMENTAL

The cells used were NCTC clone 929, strain L, mouse cells which have been in continuous culture at the University of Kansas for 12 years. Growth takes place on the interior walls of glass 250-mL screw-cap milk dilution vessels, each of which contains 35 mL of a modified Waymouth's MD 705/1 nutrient medium (*3*). The cells attach themselves to the glass shortly after inoculation and remain there during incubation at 37 °C. After 7 days, the growth medium is removed, the cells are rinsed with saline solution, and 5 mL of deionized-distilled water is pipetted into each vessel to lyse the cell walls. The cells are scraped from the sides of each bottle and suspended in the distilled water. Each cell suspension is decanted into a plastic 50-mL centrifuge tube, lyopholized, and transferred into a 1-mL Pyrex beaker. After

Table I. Elemental Concentrations and Standard Deviations for L-Cells[a]

Elements	K	Ca[b]	Mn	Fe	Cu	Zn[b]
Concentration, ppm dry weight	13033	74.7	5.0	101	12.3	57.6
Relative standard deviation for 20 samples from same cell mixture	5.9%	15.9%	8.6%	3.9%	6.1%	3.8%
Relative standard deviation for 19 separately-grown cultures	16.8%	50.8%	39.3%	6.6%	33.6%	10.8%

[a] The elemental concentrations have been obtained for L-cells grown in vitro. Also displayed are the standard deviations obtained for 20 targets from a single mixture of cells and the standard deviations for 19 separately grown and analyzed cultures. The former thus represents the variations introduced in the handling and analysis steps and the latter the variations by the growing and harvesting processes. [b] Analysis performed using the Kβ line.

weighing, these beakers are placed in a Perkin-Elmer model 40 Low Temperature RF Reactor, and the cells are ashed for 24 h. The purpose of ashing is to concentrate the elements of interest by removing the light elements C, H, N, and O (*4*).

The ash from each sample is dissolved in 0.1 mL of 4% HCl spiked with molybdenum to a level of 400 ppm. The Mo is added as an internal normalization standard. The resulting acidic solution is neutralized with 0.1 mL of 9% NH_4OH. Targets are prepared by placing a 5-μL drop of this solution onto a clean Formvar foil, the preparation of which is described in Ref. 5. Instead of drying the targets in air, they are placed horizontally in a vacuum chamber and freeze dried. We have found that this method of drying leads to more reproducible results, presumably, because the resulting targets are more homogeneous than those obtained by air drying (Barrette et al., Ref. 5).

The targets are placed in an analysis chamber similar to the one used in Ref. 6. This chamber holds 9 targets on a movable vertical ladder and is evacuated to a pressure of 1×10^{-5} mm of Hg. The targets are bombarded with a beam of 2.25-MeV protons from the University of Kansas 3.75-MV Van der Graaff accelerator for 20 min at ~85 nA of beam current. The beam crossing the $\sim 1 \times 10^{-1}$ cm^2 target surface area is made uniform to within 4% by first passing it through a 10^{-5} cm thick nickel diffuser foil. The x-rays which result from proton bombardment of the sample pass through a 1.45×10^{-2} cm thick Mylar absorber and are detected by an Ortec 7416 Si(Li) detector. Overall system resolution is 225 eV for 6.4-keV x-rays. The x-ray detection system was calibrated with a series of targets prepared by mixing known amounts of the elements of interest with molybdenum. The targets were irradiated, and the yield relative to molybdenum was determined.

The x-ray spectrum is analyzed by a series of programs written for an IBM 1800 computer. The peaks in the spectrum are fitted with Gaussian curves from which the position and area of each peak is determined. The background is subtracted after it is fitted to an expression quadratic in channel number and, finally, each peak area is corrected for detector efficiency and is compared to the molybdenum peak area to find the elemental concentration. A typical spectrum is shown in Figure 1.

RESULTS AND DISCUSSION

To ensure that a change in the concentration of one element does not affect the measured concentration of other elements present, an L-cell sample was spiked with successively larger amounts of iron. The amounts of K, Ca, Fe, Cu, and Zn were determined as a function of the amount of Fe added to the sample. The measured concentrations of Fe as a function of Fe added to the sample were well fitted by a straight line. The intercept of this line with the concentration axis determines the amount of Fe in the original cell solution (i.e., before any Fe spike was added). Using the dry weight of the cell sample and the weight of the solute added, it is found that the intercept corresponds to 74 ± 40 ppm dry weight. The relatively large error is a consequence of the 4% error in each of the single data points.

Because the targets are thin (~0.5 mg/cm^2), no corrections are made for x-ray absorption in the target itself. To ensure that this assumption is valid, an ashed L-cell sample was

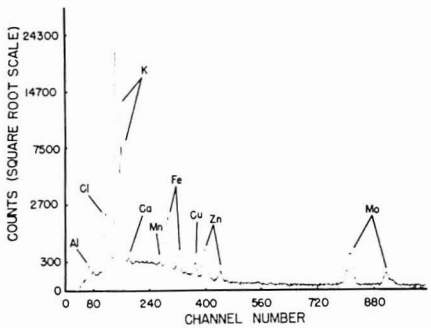

Figure 1. An x-ray spectrum produced by PIXE analysis of L-cells. The ordinate is a square-root scale. The peaks corresponding to Al, Cl, K, Ca, Mn, Fe, Cu, and Zn are clearly evident. Molybdenum, not normally present in the cells in measurable quantities, is added as an internal normalization standard.

successively diluted with 0.1 mL of distilled deionized water. If any elemental concentration increases as the target solution becomes more dilute, x-ray absorption in the target cannot be ignored. The relative amount of K, Ca, Mn, Fe, Cu, and Zn as a function of the amount of water added to the target solution was calculated. The relative concentrations of all elements present undergo no significant change except, possibly, for K which shows less than a 20% correction. We thus may safely assume that target self-absorption corrections are negligible.

System reproducibility was determined using a mixture of cells made by combining cells grown in 4 milk dilution bottles, from which 20 identical targets were made and analyzed as described above. In addition to Mo (added for calibration) we see peaks from K, Ca, Mn, Fe, Cu, and Zn. Note that the Ca Kα peak is obscured by the K Kβ, the Mn Kβ falls under the Fe Kα, and the Cu Kβ is under the Zn Kα. Because of this, analysis for Ca was performed using the Ca Kβ line, and analysis for Zn was performed using the Zn Kβ line. The extremely small amount of Mn present did not add significantly to the Fe Kα peak area, so the Fe concentration was determined using the Fe Kα line. The precision of the Ca, Mn, and Cu measurements is quite poor because of the very small peak areas. The small Al Kβ peak arises from scattered protons hitting the target frames and the walls of the aluminum target chamber. The elemental concentrations and respective standard deviations for this group of targets reflect the optimum precision obtainable for this application of PIXE and are displayed in Table I.

To determine the reproducibility of the method for separately grown cells, 19 identically grown cell cultures were harvested. One target was made and analyzed from each

bottle, and a statistical analysis was again performed on the resulting data (see Table I). The elemental concentrations and respective standard deviations thus obtained reflect the errors introduced by handling a large number of separate cell cultures. These larger standard deviations also reflect inherent variability of the cell cultures. Note that the concentration of Fe obtained, 101 ppm, is in agreement with the value calculated above using the intercept method.

CONCLUSIONS

These results indicate that the application of PIXE to L-cell samples is most successful in determining concentrations of the elements K, Fe, and Zn. Less precise results are obtained for the elements Ca, Mn, and Cu. The modest precision observed for the 19 identically-grown cell cultures is reasonable, considering the inherent variability of biological systems. Work is now underway examining the variation of L-cell trace-element content as a function of trace-element content in the nutrient medium.

LITERATURE CITED

(1) T. B. Johansson, R. Akselsson, and S. A. E. Johansson, *Nucl. Instrum. Methods*, **84**, 141 (1970).
(2) K. Samsahl, D. Brune, and P. O. Webster, *Int. J. Appl. Radiat. Isot.*, **16**, 273 (1965).
(3) P. A. Kitos, R. Sinclair, and C. Waymouth, *Exp. Cell Res.*, **27**, 307 (1962).
(4) C. J. Umbarger, R. C. Bearse, D. A. Close, and J. J. Malanify, *Adv. X-Ray Anal.*, **16**, 102 (1973).
(5) M. Barrette, G. Lamoureux, E. Lebel, R. Lecomte, P. Paradis, and S. Monaro, *Nucl. Instrum. Methods*, **134**, 189 (1976).
(6) R. C. Bearse, D. A. Close, J. J. Malanify, and C. J. Umbarger, *Anal. Chem.*, **46**, 499 (1974).

RECEIVED for review August 3, 1977. Accepted September 19, 1977. Work supported in part by the University of Kansas General Research Fund and by Biomedical Sciences Support Grant RR07037.

Pulse-Counting Techniques in Organic Mass Spectrometry

Jedidja Freudenthal* and Laurens G. Gramberg

National Institute of Public Health, Laboratory of Toxicology, P.O. Box 1, Bilthoven, The Netherlands

Pulse-counting techniques in mass spectrometry are described with which it is possible to make accurate measurements (peak matches) in gas chromatographic peaks of only a few seconds wide. An accuracy of better than 1 ppm in the mass determination can be obtained on a Varian Mat 731 mass spectrometer from an amount of less than 100 pg for most substances. The accuracy at these levels is the result of the high sensitivity with which the mass spectrometric peaks are observed. Three different quantitative methods, using gas chromatographic inlets as well as direct inlet systems, are described. These quantitative methods are also based on pulse-counting techniques. The design for the electronic circuitry for a Varian Mat 731 and a Varian Mat CH5 mass spectrometer is given.

In organic mass spectrometry, the determination of accurate masses of unknown compounds is often done with "peak match" procedures (*1*). There are restrictions in performing an accurate peak match. The unknown peak should be long enough on the oscilloscopic screen of the mass spectrometer, and the unknown compound should be present in sufficient quantity to create a peak with a reasonable intensity.

When enough of the unknown compound is available, a peak match can be made using the direct inlet of the mass spectrometer. When the unknown compound enters the mass spectrometer via a gas chromatograph, the situation becomes questionable. If the gas chromatographic peak is wide, as, for example, from a packed column, a peak match might be still possible, provided enough of the compound is available. In the case of a narrow peak, as from a capillary column, the peak match is impossible.

In this paper a pulse-counting technique will be described in which it is possible to peak match when the compound is present for only a short time. The integrating properties of the pulse-counting system make it possible also to perform a peak match from much smaller quantities of the unknown substance. Both properties make possible an exact mass determination of unknown peaks in narrow gas chromatographic peaks.

PULSE-COUNTING TECHNIQUES

In most applications in organic mass spectrometry, the signal is obtained via an electron multiplier. This signal consists of a series of pulses of only a few nanoseconds wide. The width of the pulses depends on the type of the electron multiplier used. In our experiment, we used electron multipliers supplied by Varian for the mass spectrometers Mat 731 and Mat CH5. The pulses are clouds of secondary electrons, created by the ions hitting the cathode of the electron multiplier. The ions from the mass spectrometer will arrive at the cathode of the electron multiplier randomly distributed in time, and consequently the pulses coming from the anode will do the same.

There are several ways to handle this pulse-shaped signal. The normal way in organic mass spectrometry is to couple the anode of the electron multiplier to the high impedance input of an electrometer amplifier. The pulse character of the signal disappears, and the result is an averaged analog signal.

Another approach is the pulse-counting technique. This technique is common in physics and physical chemistry, but not so in organic chemistry. In the pulse-counting technique, the single pulses (or ions) are counted (*2–5*). A current measurement consists of counting the number of ions in a certain time interval. This methodology has advantages over the electrometer methodology; it gives the maximum possible information about the signal with a minimum of noise. Since the data are already in a digital form, the data handling is easy to perform. A disadvantage of the pulse-counting system is that it cannot accept strong signals. With these signals, the interval between two pulses may become too small, such that the pulses are not separated anymore. Therefore a pulse-

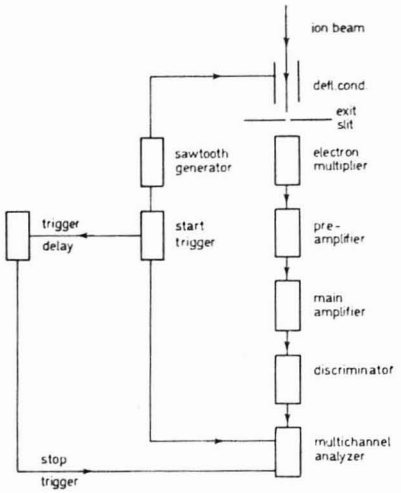

Figure 1. Block diagram of a pulse-counting system for a mass spectrometer

counting system is usually applied in cases with relatively low signal levels.

Here an electronic circuit will be given for a pulse-counting system with an upper limit of 10^5 ions/s. By using faster pulse amplifiers and other electronics, it is possible to reach an higher upper limit. Furthermore, several applications with the pulse-counting system will be given.

EXPERIMENTAL

In the pulse-counting system (Figure 1), use was made of either the electron multiplier of a Varian Mat CH5 or a Varian Mat 731 mass spectrometer.

The signal was first amplified in a pre-amplifier of the Ortec 121 type. This is a charge-sensitive amplifier. To avoid a charge buildup, a resistor of 100 K is put across the input of the pre-amplifier. The connection between the electron multiplier is shielded in order to avoid interferences.

The signal from the pre-amplifier goes to the main amplifier–discriminator of the Ortec 490A type. The output of the discriminator is given in TTL pulses. The upper limit of the signal is in our case 10^5 ions/s. If this upper limit is too low for the application at hand, the limit can be made higher by using faster amplifiers and a faster discriminator.

Up to this point, each ion arriving at the cathode is represented by a standard TTL pulse. The subsequent pulse-counting and data representation is done in a multichannel analyzer (Laben 8001) with a timing control (Laben 8190). The multichannel analyzer contains four memory subgroups of 256 channels each. The storage of the periodic signals from the mass spectrometric peaks in the multichannel analyzer requires trigger electronics (see Figure 3) not commercially available.

PEAK MATCHING

In the usual peak matching procedure, a small part of the high-resolution mass spectrum containing the unknown peak, is compared to that one containing a reference peak (*1*). This is done by switching from one accelerating voltage to the other one, such that the ion trajectories between ion source and detector are the same for the two masses. The two high-resolution mass peaks are alternately displayed on the oscilloscopic screen of the mass spectrometer. The mass spectrometric peaks on the oscilloscopic screen are created by a deflection condensor placed in front of the detector. On this condensor a saw tooth potential is applied, sweeping the ion beam in front of the exit slit of the mass spectrometer. The ratio of the accelerating voltages [and of electrostatic analyzer (ESA) voltages for double focusing instruments] of the mass spectrometer is then adjusted until the two peaks match, from which the accurate mass can be calculated. The procedure in the pulse-counting system is analogous to that of the usual peak-match procedure. The differences are that the signal is treated with pulse amplifiers and the data are represented on a multichannel analyzer.

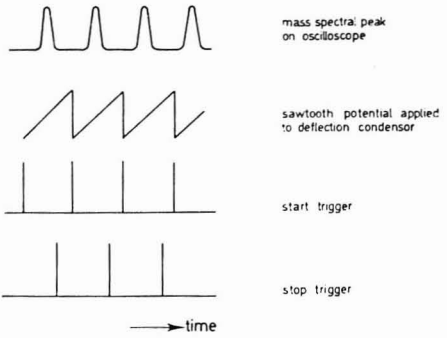

Figure 2. Timing of the trigger pulses for the multichannel analyzer in the multiscale mode. The timing is such that the periodic signal of the mass spectrometric peaks is stored on the same position in a memory subgroup of the multichannel analyzer

The storage of the unknown mass spectrometric peak is in one memory subgroup of the multichannel analyzer. The reference peak is stored in another memory subgroup. Display of the content of the two memory subgroups on the oscilloscopic screen of the multichannel analyzer makes a comparison between the two peaks possible (peak match).

A somewhat similar methodology is described in the literature, where a time averaging computer (Varian TAC 1024) is used (*6*, *7*). In this approach the signal from the mass spectrometer is in analog form and processed in the time averaging computer.

The methodology with the time averaging computer is described for quantitative applications and not for peak matches on compounds which are present for a short time.

The main advantages of a pulse-counting system over an analog system are the high speed and the better performance in signal to noise. For a peak match of a compound present for only a few seconds, these properties are important.

STORAGE OF MASS SPECTROMETRIC PEAKS IN THE MULTICHANNEL ANALYZER

The storage of the periodical signal (scan) of a mass spectrometric peak in a memory subgroup requires a proper triggering of the multichannel analyzer. The commercially available multichannel analyzers do not possess the required triggering electronics. The timing of the triggering is given in Figure 2. The electronics designed for this purpose are given in Figure 3. The properties of the electronics should be such that a trigger pulse ("start") will open the first channel of a memory subgroup at the start of the sweep through the mass spectrometric peak. Another trigger pulse ("stop") will stop the multichannel analyzer advancing through the channels in the memory subgroup in the multiscale mode. After this, the first channel of the memory subgroup will be addressed again with the next trigger start pulse. This periodic procedure repeats throughout the measuring time. The periodic signal of the mass spectral peak is stored and in-

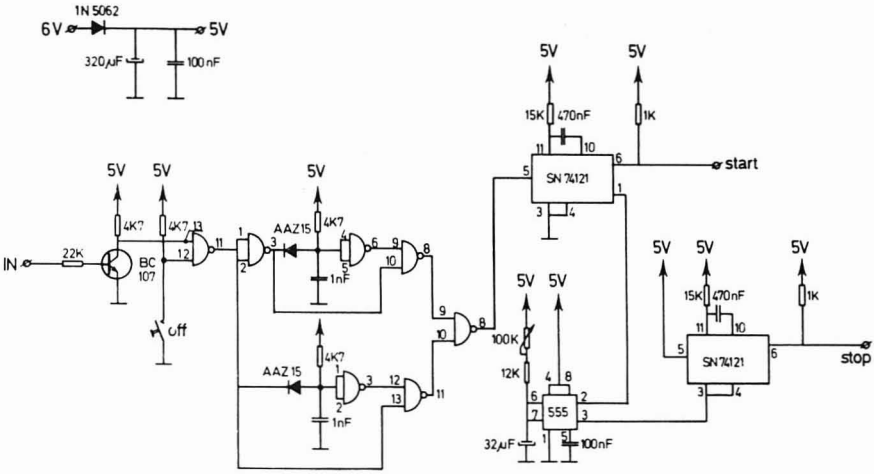

Figure 3. Electronics for triggering the multichannel analyzer. The input is a block pulse from a flip-flop in the decade bank electronics of the Varian Mat 731 mass spectrometer. The flip-flop switches when the slope of the sawtooth potential for the scope and the deflection condensor changes sign. The block pulse is then differentiated on the positive as well as the negative flanks. The differentiated pulses are shaped (in the first SN 74121) into a good trigger pulse to give the start trigger pulse. This pulse is delayed (in the 555). The variable delay time can be set with the potentiometer (100 K). This delayed pulse is shaped into a good trigger pulse (in the second SN 74121) to give the stop trigger pulse

tegrated in the memory subgroup.

The same procedure can be used for the reference peak in another memory subgroup. Both reference and unknown peaks can be displayed on the oscilloscopic screen of the multichannel analyzer. If they do not match, the reference peak is erased and recorded again using a different accelerating voltage setting, this process being repeated until a match is obtained. In our experience the whole operation can be performed within 2 min. In contrast to the usual peak-matching procedure the stability of our mass spectrometer (Varian Mat 731) was such that it allowed the unknown and reference peaks to enter one after the other into two memory subgroups of the multichannel analyzer. Compared to the alternating procedure in the usual peak matching, this gives an additional gain of two in sensitivity.

The stability of the mass spectrometer can be checked by entering a PFK peak in one of the four memory subgroups repeatedly over a 2-min time interval. A simultaneous display of the peaks should not show a shift in case of good stability. An investigation into possible sources of instabilities showed that the ESA voltages are usually highly stable. Instabilities may arise at the magnet. The reference resistor for the current regulator of the magnet should not be subjected to sudden temperature changes. Furthermore the magnet may be subjected to mechanical instabilities from pressure changes in the cooling water of the magnet. A closed circuit cooling system is a solution to this problem.

Before a peak match is performed, the ratio of the ESA voltages is checked with the help of two PFK peaks with an accurately known mass ratio with a calibration facility on the decade bank of the mass spectrometer. It was found that the precision of the peak match with the pulse-counting procedure could be performed more precisely than with the conventional peak match procedure. This improvement revealed, however, that slight position changes of the peaks could be observed in time, apparently because the calibration of the mass spectrometer decade banks changed. Keeping the temperature changes in the decade banks as low as possible is the solution to this problem.

It must be noted that in the normal peak-matching procedure the same drift is present, but remains unnoticed.

RESULTS OF PEAK MATCHING

As mentioned before, a peak match with the pulse-counting procedure can be performed with an accuracy better than with the conventional peak-match procedure. However, the main strength is that a peak match can be performed on a small amount of a compound which is present for only a few seconds, as in the gas chromatographic peak from a capillary column.

With the Varian Mat 731 mass spectrometer, peak matches were made at a resolution of 10000, 10% valley definition. For most substances, an accuracy of 1 ppm was obtained for an amount of 100 pg or less.

An example of the peak shapes is given in Figure 4 for hexachlorobenzene for the mass $m/e = 284$.

At these small amounts of substance, the number of channels used in the experiments is only around ten. This number of channels was the best compromise between peak definition and peak height. In case of more substance, the number of channels in the peak can be increased in order to get a better peak definition.

The shape of the peak is determined by the number of counts in the different channels. The variability in the numbers of counts can be obtained from ion statistics.

QUANTITATIVE MEASUREMENT WITH THE PULSE-COUNTING SYSTEM

With the pulse-counting system, the amount of substance coming from a direct inlet system or a gas chromatograph can be quantified. A mass spectrometric peak of the substance is stored and integrated in a memory subgroup in the same way as described before.

The number of counts in the peak or the peak height can be used for quantitation purposes. The interesting feature of this type of quantitation is that the exact peak position is known also. Interfering neighboring masses can be detected. This quantitation procedure has been described in the literature for an analog input signal (*6*, *7*). The advantage of the pulse-counting system compared to the analog method

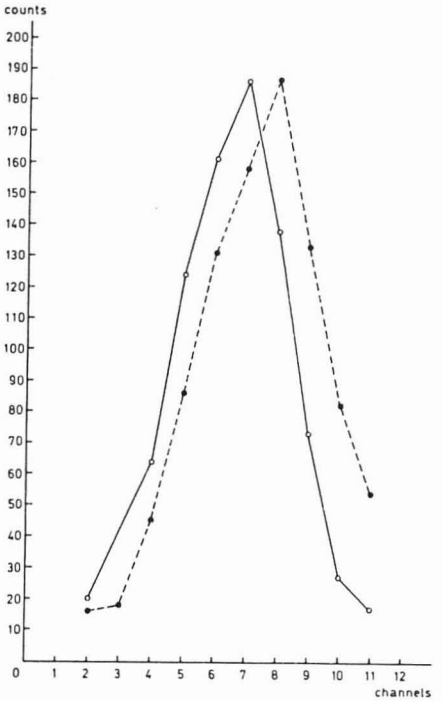

Figure 4. The peak shape of the HCB peak of m/e = 283.81017. The two peaks are shifted over a distance of 10 ppm. The resolution is 10.000 with a 10% valley definition

is again the better signal to noise ratio and the possibility to quantitate when the compound is present for only a short time.

With the mass spectrometer Varian Mat 731, we obtained 200 counts from 10 pg of hexachlorobenzene. The relative standard deviation was 15% for the quantitation (obtained from 10 measurements).

In all quantitative measurements, a solvent blank should be included. With the pulse-counting technique, the mass spectral peak from the solvent blank is stored in the same memory subgroup as the one in which the mass spectrometric peak of the sample is stored. However, the storage is done in the "subtract mode" of the multichannel analyzer. In this way an automatic correction of background influences from the blank solvent as well as from other sources is obtained.

OTHER QUANTITATIVE PROCEDURES

Mass fragmentographic procedures for single ion detection can be performed with the pulse-counting system too. The mass spectrometer is focused on one particular ion. The pulse

Table I. Sensitivities and Standard Deviations of Mass Fragmentographic Measurements, Using Pulse-Counting Techniques

Mass spectrometer	Varian Mat 731	Varian Mat 731	Varian Mat CH5
Resolution, 10% valley definition	10 000	1000	1000
Emission current[a], mA	1.5	1.5	1.0
Electron energy, eV	100	1000	70
Amount sample (HCB), pg	120	2.5	2.5
Counts	2890	700	10 400
Counts/pg HCB	32	280	4160
Rel std dev of peak area, %	6	5	2.7

[a] The emission current for the Varian Mat 731 is the electron current on the ionization chamber. The emission current for the Varian Mat CH5 is trap current. All measurements were done on the m/e = 284 peak of hexachlorobenzene. The relative standard deviations of the gas chromatographic peak areas were obtained from ten measurements.

amplifiers and discriminator handle the signal in the same way as described before. The multichannel analyzer is now used as a recorder in the multiscale mode without the trigger system. The multichannel analyzer is started and stopped by hand. The gas chromatographic peaks appear in the usual way on the oscilloscopic screen of the multichannel analyzer. With the peak-integrating feature present on the multichannel analyzer, it is possible to determine the gas chromatographic peak area. Comparison of this peak area with that one obtained from a standard gives the quantity of the substance.

In Table I the results of the quantitation are given for two mass spectrometers at two resolution settings.

The mass fragmentographic method is done usually with a gas chromatograph as the inlet system. It can be done too with the direct inlet system, for example for substances that cannot be gas chromatographed. In this case the "evaporation peak" can be recorded on the multichannel analyzer. The peak area is a measure for the quantity of the substance.

In this methodology, without a gas chromatograph, an interference from another compound may occur. Therefore this methodology is best done in high-resolution mass fragmentography and, even then, one has to check the high-resolution spectra as to whether there are interferences from other compounds.

LITERATURE CITED

(1) G. Spiteller, "Massenspektrometrische Strukturanalyse organische Verbindungen", Verlag Chemie GmbH, Weinheim, 1966, p 38.
(2) J. M. Hayes and D. A. Schoeller, 22nd Annual Conference on Mass Spectrometry and Allied Topics, Philadelphia, Pa., May 1974.
(3) D. A. Schoeller and J. M. Hayes, *Anal. Chem.*, **47** 408 (1975).
(4) W. J. Wysochansky, *Diss. Abstr.*, No. 75-10073, **35** (11), P.5275B 94B (1975).
(5) G. Goby and L-D. Nguyer, *Int. J. Mass Spectrom. Ion Phys.*, **20**, 305 (1976).
(6) R. Baughman and M. Meselson, *Adv. Chem. Ser.*, **120**, 92 (1973).
(7) L. A. Shadoff and R. A. Hummel, 170th National Meeting, American Chemical Society, Chicago, Ill., 1975.

RECEIVED for review March 28, 1977. Accepted August 29, 1977.

Analysis of Triglycerides by Gas Chromatography/Chemical Ionization Mass Spectrometry

Takeshi Murata

Analytical Application Laboratory, Kyoto Laboratory, Shimadzu Seisakusho Ltd., Nakagyo-ku, Kyoto, Japan

Peanut oil samples (having triglycerides with up to 60 carbon atoms) and rapeseed oil and mustard oil samples (both containing triglycerides with up to 62 carbon atoms) were analyzed by GC-CI-MS, and the type and distribution of triglycerides (TG) were determined. The $[MH - RCOOH]^+$ ion group showed that the major component of the C_{62} TG was the 18–22–22 type, and that the 18–22–22 type contained a largest quantity of 18:1–22:1–22:1. CI(NH_3)–mass chromatography provided detailed information on the TG structures. In the mass chromatography of C_{54} TG, which is recorded as a single peak on the total ion chromatogram, the six MC peaks, *m/e* 908 (0), *m/e* 906 (1), *m/e* 904 (2), *m/e* 902 902 (3), *m/e* 900 (4), and *m/e* 898 (5), which are QM^+ ions, gave different retention times. In the mass chromatography of triglycerides in milk fat, the existence of odd-carbon-number triglycerides was confirmed. The major component of C_{53} TG was 18–18–17, that of C_{51} TG was 18–18–15, and those of C_{49} TG were 18–18–13 and 18–16–15.

The satisfactory results obtained in analysis of triglycerides (TG) by gas chromatography–electron impact mass spectrometry (GC-EI-MS) (*1*) and direct inlet probe introduction-chemical ionization mass spectrometry (DI-CI-MS) (*2*) were reported elsewhere.

Our method is different from the method of Bugaut (*3*) or Bezard et al. (*4, 5*) who used preparative gas chromatography. In our GC-EI-MS method (*1*), the mass spectra for the GC peaks that are separated on the basis of the number of carbon atoms are obtained, and then the types of fatty acids composing a TG are determined from the $[M - RCOO]^+$, $[RCO + 128]^+$, $[RCO + 74]^+$, and RCO^+ ions, or from the M^+ ion. The compositions and the types of TG can be determined by finding three fatty acids of which the total of the carbon numbers agrees with the carbon number of the TG.

In DI-CI-MS using ammonia as the reagent gas (*2*), the $(M + NH_4)^+$ ion was recorded as the QM^+ ion and as the major ions, and it was possible to determine qualitatively and quantitatively, from the QM^+ ions, the number of carbon atoms of TG, the number of double bonds, and whether a TG is odd-carbon-number type or even-carbon-number type.

This method, however, was not satisfactory in the following points. In the case of TG larger than 54 in the number of carbon atoms, C_{58}, C_{60}, and C_{62}, for example, the GC-EI-MS method could not provide enough molecular ions to be informative. Though the method could determine odd-carbon-number TG by means of DI-CI-MS, it could not determine the type of TG, or study the behavior of TG having odd-carbon-number fatty acids.

In order to characterize TG in more details, we tried mass chromatography (MC), which is a combination of a GC-CI-MS and a computer, and obtained satisfactory results.

EXPERIMENTAL

Samples. Tristearin, tripalmitin, and trilaurin were purchased from Applied Science Laboratories, Inc. The milk fat had a purity better than 98%. The peanut oil, mustard oil, and rapeseed oil were purchased from a commercial source. Triglycerides were extracted with ethyl ether, and stored below 5 °C.

Instrumentation. The equipment was the Shimadzu-LKB 9000 gas chromatograph–mass spectrometer combined system with a electron impact/chemical ionization duel source. The gas chromatographic conditions were as follows. The column was 0.35 m × 3 mm i.d., glass with 1% OV-1 on Chromosorb W, 80–100 mesh. The chromatograph was programmed from 220–335 °C at 4 °C/min and kept isothermal at 335 °C until the last peak was recorded. The sample injection port temperature was maintained at 350 °C. The carrier gas was helium, 45 mL/min. A separator was set at 350 °C. A total ion collector was used as the detector for GC-MS. The mass spectrometric conditions for CI-MS were as follows. The ion source temperature was held at 230 °C during the CI-MS runs. The mass spectra were all obtained at 500 eV of electron energy, 500 μA of emission current, and 3.5 kV of accelerating voltage. Ammonia was used as the reagent gas; the pressure in the ion source was adjusted to 0.9 Torr. The mass spectrometric conditions for EI-MS were as follows. The ion source temperature was held at 310 °C. The mass spectra were all obtained at 20 eV of electron energy, 60 μA of trap current, and 3.5 kV of accelerating voltage. The data processing system included a GCMS-PAC 300 DG consisting of an OKITAC 4300 minicomputer with 12K core, a typewritter, an incremental plotter, a magnetic disk, and an interface to the GC-MS.

RESULTS AND DISCUSSION

Analysis of Triglycerides up to 62 in the Number of Carbon Atoms. The samples were peanut oil, rapeseed oil, and mustard oil, which contain triglycerides up to 62 in the number of carbon atoms. Figure 1 shows the gas chromatogram of mustard oil. It was necessary to raise the column temperature as high as 335 °C. Mustard oil gave peaks up to C_{62}, peanut oil up to C_{60}, and rapeseed oil up to C_{62}. In GC-CI-MS, the CI mass spectra may differ with the reagent gas used. Such is the case with TG samples. When isobutane is used, no QM^+ ions are recorded, and the $[MH - RCO_2H]^+$ ion is recorded as the base peak. When ammonia is used as the reagent gas, the $[M + NH_4]^+$ ion is recorded on the QM^+ ion, and its intensity is about 20 times higher compared with that given by GC-EI-MS. As for the fragment ions, only the $[MH - RCO_2H]$ ion is observed, and no fragment ions are recorded in the region of smaller mass numbers.

Figure 2 shows the ammonia–CI mass spectra of C_{58}, C_{60}, and C_{62} TG of mustard oil. The $[MH - RCO_2H]^+$ ion is recorded as the base peak. The QM^+ ion is intense enough to be used for structure study. This $[MH - RCO_2H]^+$ ion was used to determine the fatty acid compositions of TG groups ranging from 50 to 62 in the number of carbon atoms and to determine the distribution of the triglyceride groups and the TG types in peanut oil, rapeseed oil, and mustard oil.

Table I (*1*) shows the distribution of 17 types (6 groups) of triglycerides of peanut oil, ranging from 50 to 60 in the number of carbon atoms. Table II (*1*) shows the distribution of 40 types (7 groups) of TG of mustard oil, and Table III (*1*) that of 38 types (7 groups) of rapeseed oil.

Mustard oil and rapeseed oil are both rich in erucic acid, and their main components are 18–22–22 and 20–20–22 types. But Table II and Table III show a considerable difference.

Table I. Distribution of Triglyceride Groups and Triglyceride Type in Peanut Oil

C_{50}	14-16-20 8	C_{56}	16-18-22 20
	14-18-18 12		16-20-20 13
	16-16-18 80		18-18-20 67
C_{52}	16-16-20 9	C_{58}	16-20-22 12
	16-18-18 91		18-18-22 47
			18-20-20 41
C_{54}	16-16-22 5		
	16-18-20 6	C_{60}	16-22-22 6
	18-18-18 89		18-20-22 62
			20-20-20 32

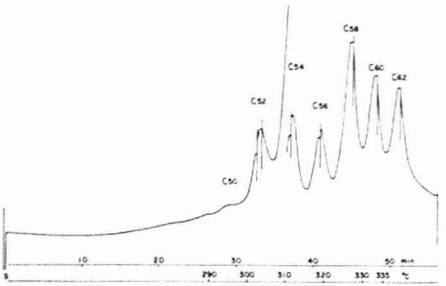

Figure 1. Gas chromatogram of mustard oil triglyceride detected by total ion chromatogram. The carbon numbers are written on the peaks

CI-MS has the advantage that the QM^+ ions are intense enough to provide useful information. It is possible to determine the number of double bonds that exist in the TG molecules from the mass numbers in the group of the same carbon number and from the ion intensities.

In the spectrum for the C_{62} TG group in mustard oil, shown in Figure 2, for example, the m/e 1014 ion is the most intense. This mass number indicates that there are three double bonds in the molecule. (If all the fatty acids are saturated, the molecular weight will be m/e 1020). The second most intense is the m/e 1010 ion indicating the existence of five double

Table II. Distribution of Triglyceride Groups and Triglyceride Types in Mustard Oil

C_{50}	10-16-24 3	C_{56}	14-16-26 2
	10-18-22 2		14-18-24 6
	10-10-20 2		14-20-22 3
	12-16-22 4		16-16-24 5
	12-18-20 3		16-18-22 25
	14-16-20 9		16-20-20 14
	14-18-18 16		18-18-20 44
	16-16-18 59	C_{58}	16-16-26 2
C_{52}	14-14-24 2		16-18-24 5
	14-16-22 2		16-20-22 8
	14-18-20 11		18-18-22 45
	16-16-20 6		18-20-20 40
	16-18-18 79	C_{60}	16-18-26 9
C_{54}	14-14-26 3		18-18-24 16
	14-16-24 3		18-20-22 44
	14-18-22 6		20-20-20 31
	14-20-20 2	C_{62}	18-18-26 5
	16-16-22 2		18-20-24 8
	16-18-20 17		18-22-22 64
	18-18-18 67		20-20-22 25

bonds. Combination of the information on the degree of unsaturation and the information on the $[MN - RCO_2H]^+$ ion group may not be able to provide quantitative data but can provide some data on the degree of unsaturation, which may be useful to presume the distribution of fatty acids.

It can be concluded from Table II that the C_{62} TG of mustard oil contains 64% of 18-22-22, 25% of 20-20-22, 8% of 18-20-24, and 5% of 18-18-26.

Let's make further consideration using the information on the intensities of the QM^+ ion and $[MH - RCO_2H]^+$ ion group.

Concerning the 18-22-22 type, which is the major component, the QM^+ ion is recorded at m/e 1014, which indicates the existence of three double bonds. The $[MH - RCOOH]^+$ is recorded at high intensities at m/e 715 and m/e 659. This shows that much $[MH - C_{18}{}^{1=}]^+$ and $[MH - C_{20}{}^{1=}]^+$ ions are contained. There are 24 possible combinations for the 18-22-22 type with varied degree of unsaturation, 18:1-22:1-22:1 being the largest quantity component and

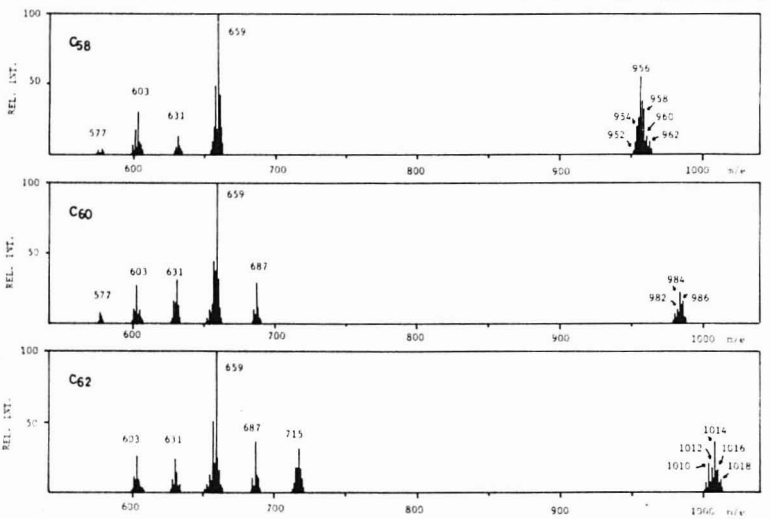

Figure 2. Ammonia chemical ionization mass spectra of C_{58}, C_{60}, C_{62} of mustard oil

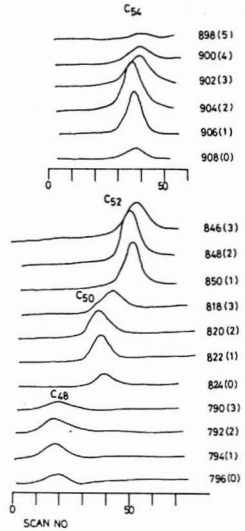

Figure 3. Ammonia chemical ionization mass chromatograms of QM^+ ion of C_{48}, C_{50}, C_{52}, C_{54} TG (The numerals show the mass numbers, and the parenthesized numerals the number of double bonds.)

Table III. Distribution of Triglyceride Groups and Triglyceride Types in Rapeseed Oil

C_{50}	10-20-20	8	C_{58}	14-18-26	4
	12-18-20	12		14-20-24	3
	14-16-20	11		14-22-22	4
	14-18-18	24		16-16-26	4
	16-16-18	45		16-18-24	8
C_{52}	12-20-20	8		16-20-22	10
	14-18-20	13		18-18-22	42
	16-16-20	19		18-20-20	25
	16-18-18	60	C_{60}	16-18-26	7
C_{54}	14-18-22	6		16-20-24	5
	14-20-20	4		16-22-22	10
	16-16-22	5		18-18-24	10
	16-18-20	15		18-20-22	43
	18-18-18	70		20-20-20	23
C_{56}	14-16-26	3	C_{62}	18-18-26	7
	14-18-24	3		18-20-24	8
	14-20-22	3		18-22-22	65
	16-16-24	4		20-20-22	20
	16-18-22	28			
	16-20-20	15			
	18-18-20	44			

18:2–22:1–22:1 being the next largest. Also, there are 17 possible combinations for the 20–20–22 type, 20:1–20:1–22:1 being the major component. We also successfully determined the possible combinations for the 18–22–22 type and the 20–20–22 type of the C_{62} group, with varied degrees of unsaturation and those of other number of carbon atoms taken into consideration.

It may be concluded that, compared with GC-EI-MS, GC-CI-MS can provide more information, because of its higher intensity of the QM^+ ion, making it possible to make more precise and more detailed study of molecular structures.

Structure Study of Triglycerides by CI(NH_3) Mass Chromatography. Mass chromatography is a technique to measure the mass spectra of a desired range of a gas chromatogram at 5 ~ 6 second intervals, store them on a disc of a computer, and then take out the MC peaks of a desired mass number (m/e) range.

Table IV. Difference of Retention Times on Mass Chromatograms of QM^+ Ions of C_{54}, C_{52}, C_{50}, C_{48} Triglycerides, and Difference of Retention Times on Mass Chromatograms of RCO^+ Ion of the C_{18} Group (the numerals show the number of double bonds in the molecule)

TG	Degree of unsaturation				
C_{54}	2	1	0	4	3	5
C_{52}	2	1	–	–	3	–
C_{50}	2	1	0	–	3	–
C_{48}	2	1	0	–	3	–
FA	Degree of unsaturation				
C_{18}	1	2	0	3		

→ retention time

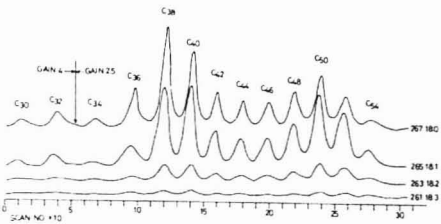

Figure 4. Electron impact ionization mass chromatograms of m/e 267 (18:0), m/e 265 (18:1), m/e 263 (18:2), and m/e 261 (18:3), which are RCO^+ ion of $C_{30 \sim 54}$ TG in milk fat

We applied this technique to analysis of triglycerides. Figure 3 shows the mass chromatograms of the C_{48}, C_{50}, C_{52}, and C_{54} TG in milk fat. On the total ion chromatogram, the four TG groups are recorded as four peaks, one peak for one group.

On the mass chromatogram, the C_{54} group gives peaks at m/e 908 (0), m/e 906 (1) m/e 904 (2), m/e 902 (3), m/e 900 (4) and m/e 898 (5). The numerals show the QM^+ ions, $[M + NH_4]^+$, and the parenthesized numerals show the number of double bonds in the molecules. These six MC peaks have slightly different retention times (t_R). The order of retention times is m/e 904 (2), m/e 906 (1), m/e 908 (0), m/e 900 (4), m/e 902 (3), and m/e 895 (5). The retention times are related to the number of double bonds in some way (See Table IV).

The C_{52} TG group gives MC peaks in the order of m/e 876 (2), m/e 878 (1), and m/e 874 (3). The C_{50} TG group gives peaks in the order of m/e 848 (2), m/e 850 (1), m/e 852 (0), and m/e 874 (3), and the C_{48} TG group in the order of m/e 820 (2), m/e 822 (1), m/e 824 (0), and m/e 818 (3).

Figures 3 and 4 are compiled in Table IV.

In order to clarify why retention times depend on the number of double bonds and why the MC peaks of C_{54} TG are eluted in the order of 2–1–0–4–3–5 (the numerals show the number of double bonds), and also why in the case of the TG other than C_{54}, the MC peaks are traced in the order of 2–1–0–3, the EI-MC were recorded at m/e 267, m/e 265, m/e 263, and m/e 261, the data being presented in Figure 4. Figure 4 shows the MC profile of the four fatty acids contained in the triglycerides ranging from 30 to 54 in the number of carbon atoms. The peaks are recorded in the order of C18:1, C18:2, C18:0, and C18:3; the retention times depend on the number of double bonds, in this case, too. The retention times of triglycerides of the same number of carbon atoms depend on the degree of unsaturation of the C_{18} group.

The larger variation of t_R in Figure 3, compared with Figure

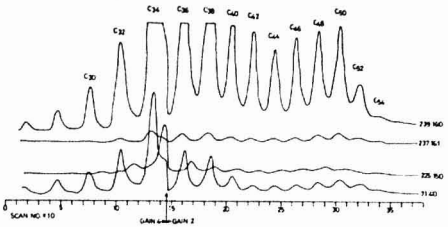

Figure 5. Electron impact ionization mass chromatograms of m/e 239 (16:0), m/e 237 (16:1), m/e 225 (15:0), and m/e 71 (4:0), which are RCO^+ ions of $C_{30} \sim {}_{54}$ TG of milk fat

4, may be accounted for by the synergetic influence of the three fatty acids. The fewer the C_{18} groups, the smaller the variation in retention time: the variation of C_{54} TG which has three C_{18} groups is larger compared with C_{52}, C_{50}, and C_{48} TG which have fewer C_{18} groups.

In the study of the MC of other fatty acids, we found that the retention time variations are not so large as that of the C_{18} group, except short-chain fatty acids such as C_4, C_6, and C_8, of which variations are of the same level as C_{18} group.

That the retention times of TG with same number of carbon atoms differ with the number of carbon atoms suggests that, though it is common to take a mass spectrum at the top of a GC peak, the MC results will differ depending on this timing, and that, to obtain a high reliability, it is necessary to calculate the quantities of QM^+ ions, fragment ions, and other ions from CI-MC or EI-MC.

The difference of retention times on MC of the QM^+ ions or RCO^+ ions of the TG having a same number of carbon atoms can be effectively used for structure study.

Concerning the C_{54} group, for example, the m/e 904 (2) ion, which has the shortest t_R, has two double bonds. This suggests 18:1–18:1–18:0 and 18:2–18:0–18–0 as the possible combinations of the three fatty acids. And it may be concluded from Table IV that 18:1–18:1–18:0 is the major component.

Similarly, it may be concluded that the major component of the m/e 906 (1) ion is [18:1–18:0–18:0], that of the m/e 908 (0) ion is [18:1–18:0–18:0], and that of the m/e 900 (4) ion is [18:1–18:3–18:0] rather than [18:1–18:1–18:2]. The major component of the m/e 902 (3) ion is [18:3–18:0–18:0] rather than [18:1–18:2–18:0] or [18:1–18:1–18:1]. We did not investigate the possibility of 18:1–18:1–18:1 or 18:1–18:2–18:0, because their QM^+ ion has a long retention time. The major component of the m/e 898 (5) ion is 18:3–18:2–18:0. The QM^+ ion ratios are 30% for m/e 904 (2) ion, 28% for m/e 906 (1) ion, 24% for m/e 902 (3) ion, 9% for m/e 908 (0) ion, 9% for m/e 900 (4) ion, and 2% for m/e 898 (5) ion. The ions m/e 904, 906, and 902 total more than 80%. The major components of the C_{52} group, which is the combination of 18–18–16, are [18:1–18:1–16:0], [18:1–18:0–16:0], and [18:1–18:2–16:0]. The major components of the C_{50} group, which is the combination of 18–16–16, are [18:1–16:0–16:0], [18:2–16:0–16:0], and [18:3–16:0–16:0], which are almost equal in quantity.

Qualitative Determination of Odd-Carbon-Number Triglycerides by CI(NH_3) Mass Chromatography and EI Mass Chromatography. When triglycerides are analyzed by gas chromatography, the peaks will be eluted in the order of the numbers of carbon atoms. It is quite difficult, however, to separate all the peaks completely: baseline resolution is quite difficult to obtain. It is said that this unsatisfactory separation is not so much due to the bleeding of the liquid phase from the column as to the existence of odd-carbon-number TG. This assertion has not so far been proved. Figure 5 shows the EI-MC of the m/e 239 ion in C16:0, m/e 237 ion in C16:1, m/e 225 ion in C15:0 and m/e 71 ion in C4:0 contained in the TG ranging from 30 to 54 in the number of carbon atoms.

The m/e 225 ion, which is the C15:0 odd-carbon-number fatty acid, is traced as a valley at the position of the peak for C4:0 ion, which is C16:0 or C16:1 even-carbon-number fatty acid. This suggests the existence of odd-carbon-number TG.

In order to confirm the existence of odd-carbon-number fatty acids, the MC of the m/e 237, 225, and 71 ions of C_{36}

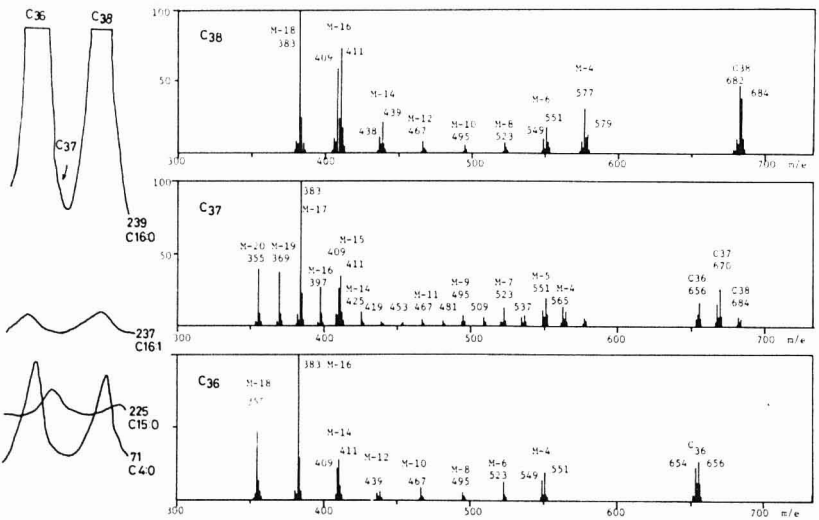

Figure 6. Electron impact ionization mass chromatograms of RCO^+ ions of C_{36}, C_{37}, C_{38} TG, and chemical ionization mass spectra of C_{36}, C_{37}, C_{38} TG

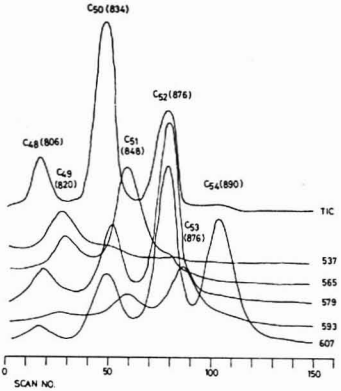

Figure 7. Identification of TG types of C_{48}, C_{49}, C_{50}, C_{51}, C_{52}, C_{53}, C_{54} TG in milk fat by chemical ionization mass chromatography using m/e 607, 593, 579, 565, and 537 ions, which are $[MH - RCO_2H]^+$ ions

and C_{38} TG were obtained, between the Scan No. 150 and Scan No. 190 shown in Figure 5. Also, the CI mass spectra of C_{36}, C_{38}, and the peak top of the m/e 225 (C15:0), which is C_{37}, were obtained. These spectra are shown in Figure 6.

It can be seen from the QM^+ ion that the C_{36} and C_{38} TG are large in quantity and, hence, there is no interference of other components.

The peak of the C_{37} TG which is quite small in quantity, is interfered with by the C_{36} and C_{38} TG.

In the case of CI mass spectra, because of the high intensity of the QM^+ ion, the m/e 670 ion which corresponds to C_{37} TG can be distinguished from the m/e 656 and 684 ions which correspond to C_{36} and C_{38} TG, respectively (Figure 6 middle chromatogram).

The $[MH\text{-}RCO_2H]^+$ ion group, however, gives a rather complicated spectrum due to the interference of C_{36} TG and C_{38} TG. The spectrum shows the existence of odd-carbon-number fatty acids such as C_5, C_9, C_{11}, C_{13} C_{15}, C_{17}, and C_{19}.

Figure 7 shows the CI-mass chromatograms of the $[MH - RCO_2H]$ ion of C_{48}, C_{49}, C_{50}, C_{51}, C_{52}, C_{53}, and C_{54} TG in milk fat. The TIC, which is also shown in Figure 7, shows no odd-carbon-number TG such as C_{49}, C_{51}, or C_{53} TG. The MC, by contrast, shows clearly how even-carbon-number TG and odd-carbon-number TG overlap each other.

On detailed study of the mass chromatograms, we found that the C_{54} TG has a molecular weight of 890 and, also we knew from the MC peaks of the m/e 607 ion that $[18\text{–}18\text{–}]^+$ ion exists. It can be concluded from these data that the C_{54} TG is of 18–18–18 type.

The C_{52} TG has a molecular weight of 876 and gives MC peaks of m/e 607 and m/e 579 ions. Calculation on $[MH - RCO_2H]^+$ shows that the m/e 607 ion corresponds to $[18\text{–}18\text{–}]^+$ ion and m/e 579 ion to $[18\text{–}16\text{–}]^+$ ion. It can be concluded that the C_{52} TG is of the 18–18–16 type.

The C_{50} TG has a molecular weight of 834 and gives MC peaks of m/e 607 and m/e 579. These ions corresponds to $[18\text{–}16\text{–}]^+$ and $[18\text{–}18\text{–}]^+$ ions. Thus it can be concluded that the C_{50} TG is of 18–16–16 and 18–18–14 types.

The C_{48} TG has a molecular weight of 806 and gives MC peaks of m/e 607 and m/e 579 ions. These ions correspond to $[18\text{–}16\text{–}]^+$ and $[18\text{–}18\text{–}]^+$ ions and suggest the existence of TG of 18–16–14 and 18–18–12 types.

As for the odd-carbon-number TG, the C_{53} TG has a molecular weight of 876 and gives the MC peak of m/e 593 ion. This ion corresponds to $[18\text{–}17\text{–}]^+$ ion and, therefore, suggests that the C_{53} TG is of the 18–18–17 type. The C_{51} TG has a molecular weight of 848 and gives MC peaks of m/e 593 and m/e 565 ions, which indicate the existence of $[18\text{–}18\text{–}]^+$ ion and $[18\text{–}15\text{–}]^+$ ion, and that the C_{51} TG is of the 18–18–15 type. The C_{49} TG has a molecular weight of 820. The MC peaks of m/e 607, m/e 565, and m/e 537 ions show the existence of $[18\text{–}15\text{–}]^+$, $[18\text{–}18\text{–}]^+$, and $[16\text{–}15\text{–}]^+$ ions and that the C_{49} TG is of the 18–18–13 and 18–16–15 types.

In Figure 7, only the important types of TG are shown; it is possible to identify trace-quantity TG, through suitable selection of $[MH\text{-}RCO_2H]^+$ ions.

Odd-carbon-number triglycerides can be identified by effective use of EI-MC, CI-MC, and CI-MS.

LITERATURE CITED

(1) T. Murata and S. Takahashi, *Anal. Chem.*, **45**, 1816 (1973).
(2) T. Murata and S. Takahashi, *Anal. Chem.*, **49**, 728 (1977).
(3) M. Bugaut and J. Bezard, *J. Chromatogr. Sci.*, **8**, 380 (1970).
(4) J. Bezard, M. Bugaut, and G. Clement, *J. Am. Oil Chem. Soc.*, **48**, 134 (1971).
(5) J. Bezard, *Lipids*, **6**, 9 (1971).

RECEIVED for review July 13, 1977. Accepted September 13, 1977.

Gas Chromatographic Determination of β-Hydroxyethylhydrazine in the Presence of Its Synthesis By-products

Philip J. Palermo

Norwich Pharmacal Company, Division of Morton-Norwich Products, Inc., Norwich, New York 13815

A rapid programmed temperature gas chromatographic analysis using thermal conductivity detection is presented for water, hydrazine, β-hydroxyethylhydrazine (HEH), and high-boilers, which are the products of the reaction between hydrazine and ethylene oxide. The HEH assay has an accuracy of ±1.3% at the 95% tolerance level. The other major reaction products are also identified and quantitated. The detection limits of the minor constituents are: water, 0.05% and hydrazine, 0.1%.

For some time a fast and accurate analysis of β-hydroxyethylhydrazine (HEH) and other components within its formation mixture has been lacking. Most laboratories use

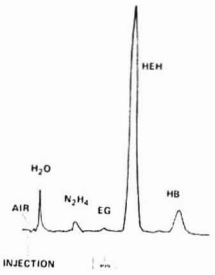

Figure 1. Typical chromatogram of technical grade HEH; 1 μL injected

a tedious vacuum distillation procedure, which employs the weighing of collected fractions. This procedure takes several hours and the components are not well separated. The first fraction contains both water and hydrazine, one of which must then be determined by another procedure. The second fraction contains HEH and small amounts of the other components, while the third fraction contains a mixture of high-boilers (HB) which are inseparable by distillation. Although an NMR procedure is also available (*1*) its precision is in doubt and NMR analysis is usually not preferred because of its expense. A colorimetric procedure has been presented (*2*) for HEH alone but the high boiling 1,1-bis(β-hydroxyethyl)hydrazine and hydrazine itself would react with cinnamaldehyde, resulting in an interference. A paper chromatography system has been reported for the detection of the reaction products but no quantitation was attempted (*3*). Gas chromatography has also been applied to these and related compounds without quantitation (*4*).

β-Hydroxyethylhydrazine is an important intermediate in the synthesis of nitrofuran antibacterial agents, especially furazolidone. Because of its effect on synthesis yields, the exact composition of the technical grade HEH used is of economic importance. HEH has also been used as a growth regulator (*5*) and pesticide (*3*). A gas chromatographic approach was desired for simultaneous determination of all the components including water, and therefore thermal conductivity detection was necessary since water is not quantitated by a flame ionization detector.

EXPERIMENTAL

Apparatus. A Hewlett-Packard Model 5750A Gas Chromatograph equipped with a thermal conductivity detector was used with a 10-μL Hamilton Model 701-N syringe. A Moseley Model 7127 Strip Chart Recorder with a Model 229 Disc Chart Integrator was used to integrate peak areas. The column was $^1/_4$-inch × $1^1/_2$-foot type 316 stainless-steel tubing filled with 100/120 mesh Chromasorb 101 installed for on-column injection. The tubing was prewashed in dilute nitric acid, followed by 25% sodium hydroxide. A glass column showed no differences in elution or peak areas. The column was conditioned overnight at 220 °C and 50 mL/min helium flow. The reference column was the same as the analytical column. The instrument parameters are: helium flow A and B, 60 mL/min; detector block temperature, 220 °C; detector filament temperature, 220 °C; detector transfer zone temperature, 220 °C; injection port temperature, 220 °C; initial column temperature, 85 °C; final column temperature, 230 °C; program rate, 30°/min; post injection time, 0; hold at limit, 4 min; bridge current, 150 mA; and injection volume, 1.0 μL.

Procedure. Technical grade HEH is a highly viscous liquid with strong reducing properties. A separate syringe was washed with HEH several times and kept for this analysis only. Because of its high viscosity, highly reproducible (2% or less) injection volumes are difficult to achieve. For this reason, an internal normalization technique was found preferable to comparison with a standard. Since HEH is very hygroscopic, care must be taken to inject as quickly and reproducibly as possible. A delayed syringe withdrawal of about 3 s was used to ensure complete vaporization of the sample from the syringe and thereby minimize the possibility of differential vaporization within the needle.

Table I. Composition of Synthetic Mixture Samples

Sample No.	HEH, g	HB, g	N_2H_4, g	H_2O, g
1	4.2270	0.8074	0	0
2	3.9280	0.8361	0.0463	0.0260
3	3.9280	0.8361	0.1370	0.0772
4	4.5222	0.7484	0.0272	0.0154
5	4.5259	0.7961	0.0906	0.0508
6	4.0094	0.9864	0.1620	0.0910

Table II. Normalized Peak Area Percentages for the Synthetic Mixtures

Sample No.	H_2O	N_2H_4	HEH	HB
1	0.46	0.04	87.21	12.29
2	1.33	1.07	84.06	13.54
3	2.82	3.89	82.36	10.93
4	0.67	0.75	87.84	10.74
5	1.97	1.91	84.72	11.40
6	3.40	3.55	79.13	13.93

A typical chromatogram of a technical grade HEH sample is shown in Figure 1. The approximate retention times are: air (0.1 min), H_2O (0.4 min), N_2H_4 (2.0 min), ethylene glycol (3.4 min), HEH (4.5 min), high-boilers (5.8 and 6.7 min). Since HEH is the major component, it is advantageous to change attenuations to give reasonable peak areas for all components. Thus, after elution of hydrazine, the attenuation is increased by a factor of four.

For an internal normalization technique, both the linearity of response of each component over the expected concentration range and the relative detector response factors were established. This was accomplished by obtaining both pure HEH and pure high-boilers (HB) from the distillation technique. The purity was established by the lack of any extraneous gas chromatographic or NMR peaks. Synthetic mixtures of HEH, HB, and pure hydrazine hydrate of known concentrations were prepared to typify technical grade samples by weighing each.

The HEH used was double distilled and showed only a minor water peak (less than 0.05%). GC and NMR data both indicated high purity. The HB used showed only the ethylene glycol (EG) peak and the high-boilers. No HEH peak was present in the high-boilers. The 100% hydrazine hydrate (HH) used showed no other GC peaks. The composition of the samples is shown in Table I.

The normalized peak area percentages are shown in Table II. To simplify the calculation, the EG peak is included with the high-boilers. Although ethylene glycol elutes before HEH, most of it stays back with the high-boilers in the distillation procedure.

When the peak percentage is plotted vs. the actual percentage of each component, the slope of the line gives the response factor of that component. Also when linear regression is performed on these data the linearity is reflected in the correlation coefficient. Table III shows these data for the six samples.

According to the slope for the four components the calculations are:

$$\text{area } H_2O \text{ peak} \div 1.83 = \text{corrected area } H_2O$$
$$\text{area } N_2H_4 \text{ peak} \div 1.13 = \text{corrected area } N_2H_4$$
$$\text{area HEH peak} \div 1.02 = \text{corrected area HEH}$$
$$\text{area HB peak} \div 0.73 = \text{corrected area HB}$$

$$\frac{}{\text{total corrected area}}$$

The percentage of each component is its (corrected area/total corrected area) × 100.

To establish the precision of the method, a technical-grade HEH sample was analyzed six times by this method. The results are shown in Table IV. From the chromatogram (Figure 1), the limit of detection of water is estimated to be about 0.05% and hydrazine about 0.1%.

Table III. Linear Regression Analysis

Component	Slope	Correlation Coefficient	Standard Error of Estimate
H_2O	1.83	0.979	0.198
N_2H_4	1.13	0.992	0.153
HEH	1.02	0.989	0.437
HB	0.73	0.963	0.331

Table IV. Analysis of a Technical Grade HEH Sample

Run	H_2O, %	N_2H_4, %	HEH, %	HB, %
1	0.64	0.39	83.95	15.02
2	0.70	0.42	83.76	15.09
3	0.86	0.38	83.55	15.21
4	0.63	0.50	82.95	15.92
5	0.61	0.49	82.92	15.97
6	0.66	0.40	83.12	15.81
$\bar{x}$	0.68	0.43	83.38	15.50
s	0.09	0.05	0.44	0.44
RSD, %	13.4	11.1	0.52	2.9

Table V. Analyses of Synthetic Samples

Component	Av % Recovery
Water	113
Hydrazine hydrate	107
HEH	99.4
HB	102.6

Five synthetic samples composed of hydrazine hydrate, β-hydroxyethylhydrazine, and high-boilers were analyzed for water (range 0–2%), hydrazine (range 0–3%), HEH (range 75–85%), and high-boilers (range 14–19%). These mixtures represent the normal variation in yields. The results are shown in Table V.

RESULTS AND DISCUSSION

The linear regression and standard deviation data show that HEH can be assayed to ±1.3% at the 95% tolerance level. The 95% tolerance level is the % RSD (0.52) multiplied by the Student t table value (2.57 for 5 degrees of freedom). Because they are minor constituents and also because HEH is hygroscopic, the error is larger for both H_2O and N_2H_4.

The major products of the synthesis were also of interest. In the first fraction of the distillation method, a trace of ethanol was found which eluted between H_2O and N_2H_4. The high-boiler residue contained mostly 1,1-bis(β-hydroxyethyl)hydrazine, as confirmed by the disappearance of its GC peak (R_t = 6.7 min) upon reaction with cinnamaldehyde in ethanol solution. The second high-boiler (R_t = 5.8 min) was 1,2-bis(β-hydroxyethyl)hydrazine (*1*). At low attenuation a third peak was barely detectable between these two. This is probably β-(β-hydroxyethoxy)ethyl hydrazine (*1*). As previously mentioned, ethylene glycol was found.

The column used in this method can be prepared in 1 h and conditioned overnight. A typical column showed no signs of deterioration after more than 200 sample analyses. Rapid and accurate analyses of the major components in the synthesis mixture, including calculations, is achieved in about 20 min. Since the relative response of these components to thermal conductivity detection has been shown to be constant (*5*), the relative response factors given should be appropriate for any gas chromatograph equipped with a thermal conductivity detector. The internal normalization technique eliminates the inconvenience of periodically preparing pure HEH for a standard by the distillation technique.

LITERATURE CITED

(1) R. G. Haber, *Chim. Anal. (Paris)*, **52**, 1394–1396 (1970).
(2) M. P. Thomas and H. J. Ackerman, *J. Agric. Food Chem.*, **12**, 432–433 (1964).
(3) L. Fishbein and M. A. Cavanaugh, *J. Chromatogr.*, **20**, 283–294 (1965).
(4) L. Fishbein and W. L. Zielinski, Jr., *J. Chromatogr.*, **28**, 418–421 (1967).
(5) A. E. Messner, D. M. Rosie, and P. A. Argabright, *Anal. Chem.*, **31**, 230–233 (1949).

RECEIVED for review July 18, 1977. Accepted September 2, 1977.

Spectroscopic Element Detector for Gas Chromatography

Cyrus Feldman* and Daniel A. Batistoni[1]

Analytical Chemistry Division, Oak Ridge National Laboratory, Oak Ridge, Tennessee 37830

A simple helium glow discharge detector with a stable but inexpensive power supply has been used to detect individual halogens, S, P, C, and metals in GC effluents. Glow chamber design prevents degradation products from coating the observation window. The monochromator is provided with an internal beam-splitter and a side-exit port. A movable exit slit mounted on the latter permits background corrections to be made at the most suitable distance from the elemental line detected. Selectivity and versatility are greatly improved by this type of background detection.

A need recently arose in this laboratory for an individual element detector for gas chromatography. The type of device desired would be highly specific, but simple and inexpensive to construct and operate. The requirement of specificity confined our search essentially to spectroscopic methods.

The spectroscopic methods used to detect specific elements in gas chromatography have been reviewed by Cram and Juvet (*1*). Almost all of the spectroscopic detectors they mention employed either a microwave discharge or a flame to generate the spectrum. The microwave devices were comparatively complex and expensive, however, and the flames not highly specific for a wide range of elements. One detector, the glow discharge tube of Braman and Dynako (*2*), had the desired simplicity: it consisted of a 50-mm length of 1-mm or 2-mm i.d., 6-mm o.d. silica tubing, with platinum wire electrodes mounted axially, a 6–18 mm electrode gap, and provision for axial flow of gas (He, Ar or He-Ar mixtures). This device's principal drawback appeared to be coating of the tube walls by decomposition products, thus attenuating the light signal as chromatographic peaks (or, by accident, solvent peaks) passed through the discharge. It appeared to us that certain changes in design and materials might result in a detector with

[1] Present address, Comisión Nacional de Energía Atómica, Avenida del Libertador 8250, Buenos Aires, Argentina.

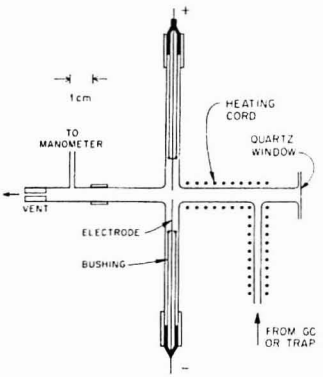

Figure 1. Glow discharge detector (schematic)

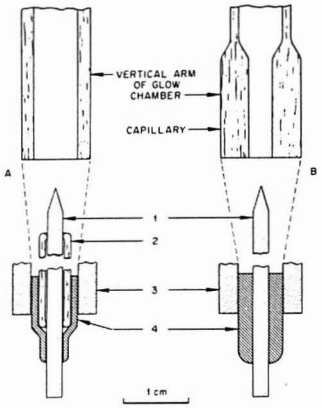

Figure 2. Electrode assemblies. (A) Bushing type. (B) Non–bushing type. (1) W–2% ThO_2 electrode. (2) Bushing. (3) Heat-resistant flexible tubing. (4) Shrinkable tubing

improved performance characteristics.

Several of the workers who have developed optical emission detectors have remarked that spectral background correction would be beneficial, but did not perform such a correction. Even when used, the possible advantages of background correction have not always been fully enjoyed, because most of the devices proposed for this purpose have had a fixed wavelength interval between the line of interest and the position at which background intensity was measured. Inevitably, occasions arise upon which these positions are occupied by other lines or bands, so that the simple background correction hoped for cannot be performed.

This difficulty can often be circumvented by making the separation of the two observation points variable, as suggested by J. D. Defreese and H. V. Malmstadt (*3*). To prevent mechanical interference between the two photomultipliers, the spectrally resolved beam is split inside the monochromator, with the normal fixed slit at one exit and the movable slit at the other. The splitting can be accomplished with a conventional beamsplitting mirror (*3*), but less ultraviolet energy is lost if instead one replaces the existing mirror by a quartz-substrate mirror with a latticework coating pattern, or if one cuts away the upper half of the existing deflecting mirror, as was done in the present case. If the latter course is chosen, the aperture of the monochromator should be filled as completely as possible, in order to minimize the effects of the stigmaticity of the optical system on the relative intensity of the beams.

EXPERIMENTAL

Construction of Glow Discharge Chamber. A schematic diagram of the discharge chamber currently in use in this laboratory is shown in Figure 1. Its body is essentially a cross made of 6-mm o.d. borosilicate glass tubing; its vertical arms are approximately 4.5 cm long. Its front end is a flange (2.5-cm diam.) to which a fused quartz window is cemented with a suitable epoxy adhesive. This window can be replaced by a plano-convex fused quartz lens, if desired.

An essential feature of this design is placement of the gas inlet between the window and the discharge. The resulting flow pattern carries any degradation products produced by the discharge away from the observation window. The gas inlet region (shown by the dotted section of Figure 1) can be heated, if necessary, by a heating cord (Catalogue No. 3122-30, Cole-Parmer Instrument Co., Chicago, Ill., or equivalent) or a suitably designed oven.

The electrodes were made from 2% thoriated tungsten helium-arc welding electrodes ($^1/_{16}$ inch × 7 inches), which are readily available (Philips Elmet Corp., Lewiston, Me., or Van Dresser and Hawkins, Inc., Atlanta, Ga.). The design of the electrode holders provides for easy removal from the chamber and for stable alignment of the cathode with the anode.

The electrode assemblies were prepared as follows (see Figure 2A). A piece of borosilicate glass tubing 4 mm o.d. × 45 mm, called the bushing, 2, was tested to make sure that it would slide easily into the 6-mm o.d. vertical arms of the chamber. A welding electrode (see above) was cut in half and tipped as illustrated, 1, with a belt sander. The glass bushing was slipped over the electrode, leaving approximately 15 mm of electrode exposed at the pointed end. To make the electrode alignment as rigid as possible, the openings at the ends of the glass bushing were now shrunk with the aid of a small flame. Any resultant local increase in the outside diameter of the bushing was removed with a belt sander. The bushing was fixed in place with a section of shrinkable tubing, 4 (Frank Markel and Sons, Inc., Norristown, Pa.). A section of thin-walled heat-resistant elastic tubing of suitable diameter (Silicone Tubing, Compound 2570-70 Durowhite, Minor Rubber Co., Bloomfield, N.J. 07003, or 70 Dino Viton Tubing, Pelmore Laboratories, Newton, Pa. 18940), called the sleeve, was fitted over the jacketed region as shown in Figure 2A, 3. The length of the sleeve was chosen so that when its free end was fitted over the vertical arm of the glow chamber (Figure 2A), the tip of the electrode was close to the center of the chamber (Figure 1). Before use, the tips of the electrodes were cleaned with 150-frit corundum paper, followed by 400-frit carborundum paper. When both electrodes were in place, the electrode gap was adjusted by sliding one or both electrode assemblies vertically. Care was taken to make the sleeve fit snugly over the vertical arms.

An alternative arrangement which eliminated the glass bushing is shown in Figure 2B. In this case the vertical arm of the glow chamber, from its free end to within 10 mm of the intersection area, was made of 7-mm o.d./2 mm-i.d. borosilicate glass tubing. Since the i.d. of this tubing is somewhat variable, the section to be used was chosen to have the minimum i.d. which would still permit the tungsten electrode to slide within the tubing. Concentric layers of shrinkable tubing, 4, were applied to the electrode until the diameter of the clad section was approximately the same as in Figure 2A. A sleeve, 3, of suitable diameter was fitted onto the clad electrode as before, and the assembly slid onto the vertical arm of the glow chamber. The electrode gap was set to approximately 3 mm.

A 50-mm section of 0.5-mm i.d. borosilicate glass capillary was attached to the exit with heat-resistant elastic tubing. A mercury manometer was inserted between the chamber and this capillary in order to monitor gas flow (Figure 1).

A more elegant if slightly less convenient arrangement for holding the electrodes is shown in Figure 3. The electrodes were held by solid Teflon ferrules with $^1/_{16}$-inch diameter holes, (Catalogue No. RF 400/100-T, Alltech Associates Inc., Arlington

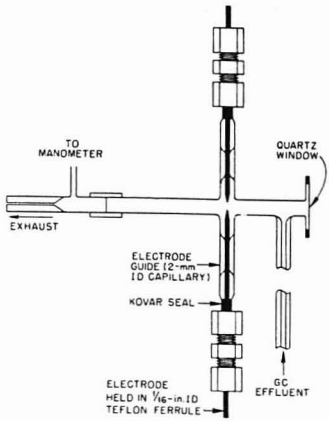

Figure 3. Stainless steel Swagelok-fitted glow chamber

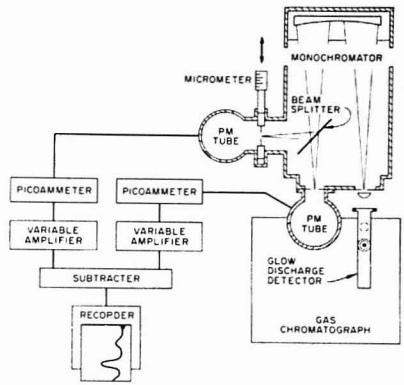

Figure 4. Experimental arrangement (schematic)

Heights, Ill. 60004) contained in the uppermost and lowest hexagonal nuts, respectively. The position of either electrode was adjusted by loosening its hexagonal nut. The short sections of capillary tubing in the vertical arms of the chamber served to align the electrodes.

Gas Conditions. All of the work with this detector was done with commercial grade helium, purified by passage through either Molecular Sieve 5A or activated charcoal and indicating silica gel. The emission spectrum of the helium showed that after this treatment, the gas still contained trace amounts of species composed of O, C, N, and/or H. The helium passed through the glow chamber slightly above atmospheric pressure, at 10–140 cm^3/min.

Electrical Conditions. The power supply for the glow discharge was a Model SSG-400 Power Supply, 1100 V, dc, 50 mA, current regulation ±0.1% or better (G. W. Gates Co., Franklin Square, Long Island, N.Y., price (1976) <$250). The high voltage was needed to effect the initial breakdown; the operating voltage across the discharge was 380-400 V, dc for a 3-mm electrode gap; the current was set at 40 mA.

Optical Conditions. A plano-convex fused quartz lens (75-mm focal length, 25-mm diameter) was placed at the slit of the Jarrell-Ash Ebert Mark V Monochromator (see Figure 4). An image of the glow discharge was focused on the center of the entrance aperture of the collimating mirror. Interchangeable gratings blazed at 1900 Å (190 nm) and 5000 Å (500 nm) were used for the ultraviolet and visible ranges of the spectrum, respectively. During measurements in the visible region, a yellow filter was placed at the slit in order to eliminate interference from second-order ultraviolet radiation. Entrance and exit slit widths were usually 50 or 75 μm (equivalent to 0.08 or 0.12 nm bandpass, respectively).

Construction of the Detection System and Background Corrector. The upper half of the internal deflecting mirror of a Jarrell-Ash Ebert Mark V 0.5-meter scanning monochromator was removed, so that the upper half of the diffracted and partially refocused exit beam went to the normal exit slit and the lower half to the side exit port. (See Figure 4). The side exit port slit housing (Catalogue No. 82-018) was modified as follows. The dovetailed end section which normally holds the bayonet-type slit was milled away and replaced by a light-tight slit holder which could be moved 15 mm horizontally by means of a micrometer screw. Dovetailed ways inside the new holder located the slit in the original focal plane of the deflected beam. The horizontal (i.e., wavelength) limits of travel of this slit holder were adjusted so that a narrow wavelength band (e.g., 0.4–1 nm) could be observed through it at any wavelength within 20 nm of the line of interest on either side. The spectral displacement of this slit relative to the normal exit slit was calibrated with the aid of a low pressure mercury discharge lamp. Each exit channel was provided with an RCA 1P28 or 4840 photomultiplier tube, a John Fluke Model 415B power supply (John Fluke Co., Mountlake Terrace, Wash. 98043), and a Gencom Model 1012 picoammeter (EMI-Gencom., Inc., Plainview, N.Y. 11803) to which a 7-stage output damping control was added. These signals were fed to a two-channel variable amplifier which amplified each signal 0- to 2.5-fold. The degree of amplification was controlled by a 10-turn potentiometer in each channel. The main channel potentiometer was usually set for maximum gain; the side exit channel potentiometer was set somewhat lower. The side-exit signal was then subtracted from the normal exit signal, and the difference signal fed to a Varian A-25 recorder (Varian Associates, Palo Alto, Calif. 94303). The side-exit signal was usually the background or reference signal, but gain-control potentiometers were provided in both channels of the amplifier in case it was ever desirable to reverse these roles.

As a preliminary check on the operation of the background corrector, a low-pressure mercury lamp, emitting light only through a pinhole in its shield, was placed on the optical bench of the monochromator; an incandescent light bulb (initially turned off) was placed immediately behind it to serve as a source of continuous background. The position of the side-exit slit was now adjusted to pass the same wavelength as the main exit slit. With the side-exit detector turned off, the monochromator was adjusted to pass the mercury green line (546.07 nm) through the main exit slit. The mercury lamp was then turned off, and the side-exit slit displaced about 0.5 nm from its previous position; e.g., to ~545.57 nm. The side-exit detector and the incandescent light were now turned on, and the amplifier gain in the appropriate channel was adjusted until the signals from the two channels exactly cancelled. The mercury lamp was turned on again, giving a signal of, for example, 80% full scale. The incandescent light was now alternately turned on and off; no change was observed in the indicated intensity of the mercury line, proving that the background common to the two signals had been compensated.

Use of the Glow Discharge Detector with Gas Chromatograph. The helium glow chamber was connected to the outlet of a Tracor Model MT-220 gas chromatograph, using a borosilicate glass connecting tube, stainless steel couplings, and Teflon ferrules. The connecting tube was heated to ~200–250 °C, using heating cord. A 4 mm i.d. × 180 cm column of 4% OV-101 on 80–100 mesh Chromosorb G(HP) was used for all chromatographic experiments. The helium flowrates tested ranged from 10 to 140 cm^3/min, but most chromatograms were obtained at a flowrate of 100 cm^3/min.

In order to select the best spectral line for the detection of each element, it is desirable to scan the spectrum while the glow chamber is continuously emitting the spectrum of that element. To accomplish this, a current of helium containing a volatile compound of the element was passed through the detector. For C, Cl, and F, a 0.0013 mol % mixture of CCl_2F_2 in He was used. For S, a current of He was passed over an 0.02% aqueous solution

of SO_2, through a desiccant trap, and into the detector. For iodine, the helium was passed over heated crystals of the element; for the remaining elements listed in Table I, helium was passed over heated crystals of an appropriate compound. In some cases (Si, As), this approach was not practical with the facilities at hand, so the most prominent lines were selected from tables (4) and measured individually.

Determination of Sensitivity Limits. The time required for passage of the solvent front was determined by means of a flame ionization detector, with the glow discharge off. A substantial amount of the substance being tested (e.g., 1 μg of 1-chloro-3-fluorobenzene in CH_2Cl_2) was then injected. After passage of the solvent front, the glow discharge was turned on, with the monochromator set to detect C 193.1 nm. The retention time for this carbon peak was noted. The monochromator was then set to detect an emission line of the element of special interest; e.g., F 685.6 nm for fluorine. The occurrence of a substantial intensity peak at this wavelength at the same retention time observed for the carbon peak was taken as probable evidence that a (in this case) fluorine-bearing compound had been detected. To guard against false positive signals due to transient band emission, each experiment was repeated at a closely neighboring wavelength. If a peak of intensity comparable to the previous peak was observed, the first peak was considered to be due principally to band emission rather than atomic line emission, and a more favorably situated line was sought. (A technique for counteracting band interference, rather than avoiding it, is described below in the section on background correction.) If the intensity vs. time peak was shown to be due to the intended atomic line, a limit of detection was established for the element in question by injecting successively smaller quantities of its compound. Background correction was not used in these determinations because the background corrector described above was not yet available.

Measurement of Selectivity. A silylized mixture of phenylarsonic acid, nonanoic acid, undecanoic acid, and three aliphatic hydrocarbons was chromatographed. The effluent was split; one stream was directed through an FID and the other through the glow discharge detector (GDD). In one set of runs, the pass band of the monochromator was 288.12–288.20 nm (to detect Si 288.16 nm). In the other, the pass band was 228.77–228.85 nm (to detect As 228.81 nm). In each case, an FID trace was obtained simultaneously with the GDD trace. The selectivity of a given Si or As line was defined as the ratio of the peak height obtained per gram atom of Si or As to the peak height obtained per gram atom of C in the form of the interfering compound tested.

Operation of the Background Corrector. The most intense lines of the element to be detected were examined to see which had the best combination of high intensity and low background. To do this, the GC was brought to baseline conditions; i.e., achievement of a stable baseline after passage of the solvent front. The GDD was turned on, and the side-exit (background) detection channel turned off. The spectrum was now scanned from 1–2 nm below the wavelength of the line being examined to 1–2 nm above it. This procedure was repeated for each of the atomic lines being considered. The traces obtained were examined to find one in which the wavelength of the atomic line (e.g., Si 288.16 nm) was unencumbered by extraneous lines or bands and in which an adjacent background region existed which was more intense than the background at the wavelength of the atomic line (to compensate for reflection losses at the internal deflection mirror) and which was separated from the latter wavelength by more than twice the spectral bandpass (to prevent overlap of the line and background spectral intervals). When the best line–background combination had been determined, the monochromator was set for the atomic line selected, and the wavelength displacement of the background channel from the signal channel was set correspondingly. Both amplifier outputs were now turned off. The power supply voltages of the photomultiplier tubes were adjusted (with no compensation current used in either channel) until equal signals were shown by the panel meters of the corresponding picoammeters. Each signal was then reduced to zero on the meter using the cancellation current on that picoammeter. Both amplifier outputs were then turned on again. Both variable amplifier potentiometers were set for maximum gain.

A solution was now prepared containing representative amounts of Si compound(s) (e.g., silyl esters of alcohols, carboxy acids, or amines) plus the extraneous compounds against which it was desired to discriminate (e.g., hydrocarbons). A GC run was made to determine the degree of over-correction of the non-Si peaks (i.e., production of negative peaks) produced with both variable amplifiers set for maximum gain. Successive identical GC runs were made, with the background correction signal reduced each time by adjusting the appropriate variable amplifier, until essentially no peak was observed for the extraneous compound, although a signal was still observed for any Si compound. An analogous procedure was followed for studying the behavior of the background corrector for P 213.62 min.

RESULTS AND DICUSSION

Detection Limits. The detection limit for a given element achieved by the present system was governed by a number of factors. These included the characteristics of the glow discharge and its chamber, characteristics of the optical system outside and inside the monochromator, and those of the electrical detection/amplification system.

One of these factors, spectral background, was dependent on the impurities present in the gas stream. The impurity level originally present in the helium used had to be low enough to permit day-long operation of the tungsten electrodes without attention, and to reduce the spectral background to a minimum. The major additional source of gas contamination was, of course, the atmosphere. Despite the fact that the pressure in the gas train was above atmospheric, back-diffusion into the discharge was possible through the exit tube of the GDD chamber, as well as through any leaks which might have existed in the gas train. The former difficulty was essentially eliminated by attaching a 50-mm section of ≲0.5-mm i.d. borosilicate glass capillary tubing to the exit, and the latter by the usual systematic searches. Once these sources of contamination were eliminated, the purity of our commercial helium supply (>99.996%) was found satisfactory for this use.

Helium flowrate was found to affect the intensities of most lines studied by factors up to 2, but no general pattern was seen at flowrates between 9 and 35 cm^3/min. In certain cases, some lines of a given element increased in intensity as the flowrate rose from 9 to 35 cm^3/min, and other lines of the same element decreased. At any given flowrate, individual line intensities were quite steady.

The discharge obtained under the conditions described was a glow, rather than an arc; i.e., it was diffuse and did not have a narrow, highly luminous central discharge channel. It was greyish pink in color and transversely banded. It was also quite stiff: in the above chamber, it was not distorted or displaced from its normal axial position by transverse helium flows of up to 600 cm^3/min, corresponding to linear rates of 9600 cm/min or 320 linear feet per minute. The tightly adhering pink cathode layer covered the terminal 3–8 mm of the cathode. The anode spot was microscopic; its location was visible only because of local incandescence.

The intensity of any individual spectral line tended to increase with the current. Above 50 mA, however, the 0.060-inch diameter cathode tended to overheat. All experiments were therefore carrried out at 40 mA. At the typical operating voltage (400 V), the discharge thus dissipated 16 W. The discharge operated very stably as long as the gas stream consisted of helium and occasional impurities such as chromatographic peaks. If substantial amounts of air, hydrogen, or organic compounds reached the chamber, the discharge was extinguished. However, it started again spontaneously as soon as helium again became the predominant component of the gas stream.

One of the optical factors limiting sensitivity was the narrow cylindrical shape of the section of the chamber between the discharge and the window (Figure 1). This design was adopted in order to force as high a fraction of the gas as possible to

Table I. Limits of Detection for Various Elements Using the Helium Glow Discharge Detector (Preliminary Values)

Atom or molecule obsd	Compound used	Wavelength of line or bandhead, nm (4)	Detection limit of element	
			ng	ng/cm³
F	1-Chloro-3-fluorobenzene	685.60	4.5	0.09
Cl	1-Chloro-3-fluorobenzene	725.67	45	0.9
CCl	1-Chloro-3-fluorobenzene	277.8	15	0.3
Br	Bromobenzene	734.85	45	0.9
I	Iodobenzene	206.24	4.5	0.09
C	*n*-Decane	193.09	120	2.4
C	*n*-Decane	247.86	5.0	0.1
P	Tributyl phosphite	213.62	6.4	0.13
P	Tributyl phosphate	213.62	18	0.4
S	Dibutyl sulfide	527.89	110	2.2
Si	BSTFA ester of undecanoic acid	251.61	10	0.2
Al	Al trifluoroacetylacetonate	396.15	12	0.2
As	AsH_3	228.81	0.3[a]	0.001
Cr	Cr acetylacetonate	425.43	1.4	0.028
Cu	Cu hexafluoroacetylacetonate	324.75	110	2.2

[a] Observed by release of AsH_3 from a liquid nitrogen-cooled trap, not by gas chromatography. Carrier gas velocity 600 cm³/min.

go through the discharge. The design necessarily produced some vignetting of the outgoing radiation, but reflection from the walls of this section probably kept some of this radiation from leaving the system.

The 75-mm focal length lens used at the slit of the monochromator produced an image of the discharge on the entrance aperture. This aperture (a mask over the incoming half of the monochromator's paraboloidal mirror) was 50 × 50 mm. The image was 15–20 mm high and ~4 mm wide. The aperture thus was not filled; the use of shorter focal length lenses and other modes of external illumination might have increased the amount of light available.

Wider slits at all three positions would also increase the amount of light available, and are advantageous if the concomitant decrease in spectral resolution is permissible.

The detection limits obtained under existing conditions without background correction are given in Table I. The quantity listed is the quantity required to give a peak twice as high as the peak-to-peak baseline noise.

Selectivity. This property of a detection system is best expressed as the ratio of the response obtained from the species one desires to detect (e.g., any compound containing Si) to the response obtained from other species. Since any one of several Si lines might have been chosen for investigation, and since different non-silicon-bearing compounds would produce different false positive signals at each of these wavelengths, we chose to state the selectivity ratio for a specific silicon emission line vs. a specific impurity, referred to the number of gram atoms of the element producing the signal in each case. (See definition of (SR) below.) The width of the spectral bandpass should also be specified, since narrower bandpasses tend to produce higher selectivity ratios.

The selection of a comparison compound for measuring a selectivity ratio need not be arbitrary. In the present investigation, the property of the detection system which interests us is the selectivity of detection for silicon-bearing compounds vis-a-vis the non-silicon-bearing species that actually exist in the mixture. Measurements of the selectivity ratio of a given Si line should be made vs. these compounds, if they are known, or against similar compounds which produce bands at the wavelength in question.

The experimental results of the selectivity runs are shown in Figure 5. The FID, as expected, detected all compounds in the mixture. The center section shows the GDD trace when the monochromator was set for Si 288.16 nm. Only those

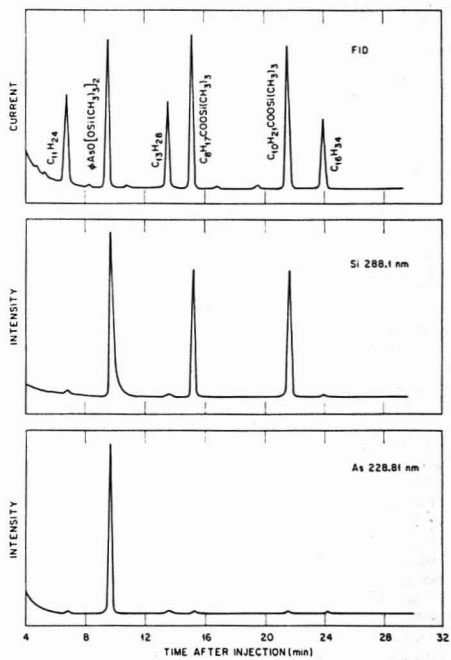

Figure 5. Gas chromatograms of a silylated mixture of aliphatic acids, phenylarsonic acid, and hydrocarbons. Top curve: Flame ionization detector (FID). Center and bottom curves: glow discharge detector (GDD), with monochromator set as indicated

compounds known to silylize showed substantial peaks; the other components produced small, but still perceptible peaks (false positives). The lower section shows the GDD trace for a second run of the same mixture, with the monochromator set for As 228.81 nm. Phenylarsonic acid was the only compound giving a pronounced peak in this case. Some other choice of compounds not containing silicon or arsenic might

have produced either larger or smaller false positives, depending on the factors discussed previously. Even under these conditions, however, this type of detection could be used to distinguish those components of a mixture which silylize (i.e., contain an active hydrogen) from those which do not, or to identify the arseniferous components of a mixture. Similar information could be gotten for other elements (see below).

In the present example, the selectivity ratio (SR) was defined to measure the ability of the system to discriminate between silicon-bearing compounds and saturated hydrocarbons, using λ_{Si} = Si 288.16 nm radiation with a bandpass of 0.08 nm or

$$(SR)^{Si/C}_{288.16,\,0.08} = \frac{\text{peak response of Si compound at } \lambda_{Si} \text{ per g-atom Si}}{\text{peak response of C compound at } \lambda_{Si} \text{ per g-atom C}}$$

Analogously, the selectivity ratio for As vs. C under the present experimental conditions would be

$$(SR)^{As/C}_{228.81,\,0.06} = \frac{\text{peak response of As compound at } \lambda_{As} \text{ per g-atom As}}{\text{peak response of C compound at } \lambda_{As} \text{ per g-atom C}}$$

The values obtained experimentally for these parameters were

$$(SR)^{Si/C}_{288.16,\,0.06} = 325 \quad (SR)^{As/C}_{288.81,\,0.06} = 2960$$

A rigorous calculation of (SR) would have required correction of the numerator response for the contribution of C atoms. Since the (SR) values are large, however, this correction would be negligible.

The present Si and As lines were favorably situated; i.e., at wavelengths where the hydrocarbons did not produce intense band emission. Other lines of these or other elements in other experiments might not be so favorably situated, and it is for cases like the latter, among others, that background correction is desirable.

Correction for Steady-State and/or Transient Background Radiation. The degree of selectivity exhibited by a spectral emission detector is intimately connected with the level and time variation of the spectral background at the wavelength observed. The situation can best be comprehended in terms of a few typical situations.

(1) *Constant Background Level.* After normal purification, commercial helium carrier gas still contains trace amounts of impurities, and may entrain additional impurities during its passage through the gas chromatograph. These impurities react in the glow discharge to produce a steady-state concentration of excited atoms, ions, molecules, molecular ions, and free radicals. The relative concentration of each species depends on the identity and pressure of the main gas components and on various physical and electrical characteristics of the discharge. Each diatomic species, when properly excited, emits a band spectrum which may cover tens of nanometers at various wavelengths and intensity levels. The situation is further complicated by the fact that if a given species exists in the discharge, the intensity with which it emits a certain band system may depend not only on the concentration of that species in the discharge, but on the concentration of other components of the mixture as well; e.g., if the species usually emits a certain band system which has a comparatively high excitation energy, this band system may not appear in the spectrum at all if the steady-state mixture contains a component having a very low excitation energy.

Whatever the shape of the steady-state spectrum, however, the ratio of the intensity of the background at a given wavelength to its intensity at some specific neighboring wavelength will be a constant.

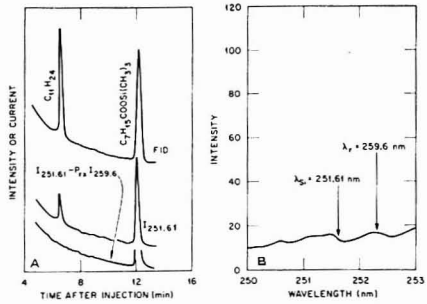

Figure 6. (A) Gas chromatogram of silylated mixture of octanoic acid and undecane. Top curve: FID trace. Center and bottom curves: GDD trace using Si 251.6 nm radiation, without and with background correction, respectively. (B) Wavelength scan of spectral region used

(2) *Variable Background Level.* It will be assumed that the monochromator has been set to pass a specific atomic line (e.g., Si 288.16 nm), that a measurable level of spectral background exists at this wavelength under GC baseline conditions, and that the discharge disintegrates any molecules passing through it and excites the fragments. As chromatographic peaks pass through the discharge, several types of signal response are possible, depending on the composition of the peak and the wavelength observed.

(a) If the substance contains the element sought (Si, in this case), strong line emission will be detected. Simultaneously, the additional molecular fragments accompanying the Si atoms will emit broad bands. If these bands cover the observed wavelength interval, the signal observed will be higher than it would have been otherwise. The total signal will consist of the transient atomic Si emission, the transient background band emission produced by other fragments of the Si-bearing molecule and/or their reaction products, and the constant background band emission due to impurities present in the helium when it entered the discharge.

(b) If the substance does not contain the element sought, its fragments will still produce a transient band emission as they pass through the discharge, and this band emission, if it covers the interval observed, will produce a false positive signal: there will be no way to tell whether this signal is due to Si or to molecular fragments not containing Si (Figure 5). The possibility also exists that particular types of transient molecular fragments might react in the discharge with the residual impurity fragments which are normally present at a steady-state concentration. Such reactions might produce new species, adding to the band emission at the location observed, but they might equally well destroy species which had previously been producing part of the steady-state band emission at that location, thus leading to a transient decrease in the total background intensity at the wavelength in question. This would produce a negative chromatographic "peak", unless compensated by simultaneous transient increases. Examples of such reactions might be the reaction of carbon with free hydroxyl radical to produce CO, or with NO to produce CN. If this occurred while a narrow interval in the OH or NO band region was being monitored, either of these events would be seen as a negative chromatographic "peak". Such events have been observed several times during this investigation.

Figures 6B and 7B show wavelength scans of two different spectral regions in which a background correction was desired. These scans were made under GC baseline conditions. Their intensity scales are the same. The atomic emission lines used

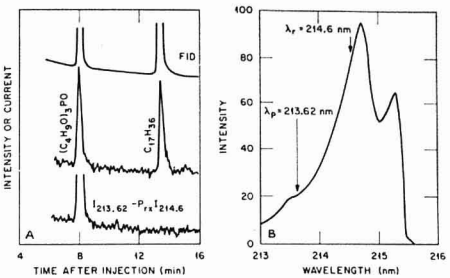

Figure 7. (A) Gas chromatogram of mixture of tributyl phosphate and heptadecane. Top curve: FID trace. Center and bottom curves: GDD trace using P 213.6 nm radiation, without and with background correction, respectively. (B) Wavelength scan of spectral region used

for detection were Si 251.61 and P 213.62, respectively; the spectral bandwidth was 0.16 nm. The reference wavelengths λ_r (i.e., the wavelengths at which background intensity was read) were located more than twice the above spectral bandwidth away from the atomic lines. In Figure 6B, the steady-state intensity at λ_r is only slightly greater than that at λ_{Si}. In Figure 7B, the intensity of λ_r is considerably greater than that at λ_p. The band in this figure is probably the (1,0) component of the λ system of NO (*5*). Thus Figure 6B shows a situation in which any transient band emission would be superimposed on a relatively smooth steady-state background; Figure 7B shows a situation in which the transient band emission would be superimposed on a relatively strong and steeply sloping background. A detailed discussion of background interferences is given by Hendrix-Jongerius and De Galan (*6*).

In the chromatograms of Figures 6A and 7A the FID traces indicate the retention times of the components. The center curve in Figure 6A shows a single-channel recording of the intensity of all radiation detected in the wavelength interval 251.57–251.65 nm, which includes λ_{Si} = 251.61 nm. No background correction was made. It is evident that, in this case, a false positive signal was produced when the $C_{11}H_{24}$ peak passed through the glow discharge. In the lowest curve, a constant fraction of the intensity at λ_r, chosen as above, was automatically subtracted from the intensity at λ_{Si}; no false positive peak was observed. The symbol P_{rx} in Figures 6A and 7A represents the fraction subtracted.

Analogously, the center curve in Figure 7A represents a single-channel recording of the intensity of all radiation detected in the wavelength interval 213.54–213.70 nm, which include λ_p = 213.62 nm. No background correction was made, and in this case the false positive signal given by the hydrocarbon peak was substantial. The lowest curve in this figure shows a chromatogram produced by the same phosphorus line, but with spectral background correction. In this case, the relatively strong and steeply sloping background has also been compensated.

Possible Effect of Detector Inlet Tubing on Bandwidth. Since the inlets of the GDD's pictured in Figures 1 and 3 were 26 cm long, with radii of 2.1 to 0.5 mm, it seemed desirable to ascertain whether diffusion occurring between the column outlet and the glow discharge itself might materially broaden the peaks produced by the GDD. A formula describing the effect of connecting tube parameters on chromatographic bandwidth was derived by R. P. W. Scott (*7*):

$$\sigma_t^2 = \frac{\pi r^4 l}{24 D_m Q}$$

where σ_t is the additional bandwidth (in seconds) at 0.607 of the peak height, contributed by diffusion in the connecting tube, r and l are the radius and length of the tube, respectively, in cm., D is the diffusivity of the pair of gases concerned (peak and carrier) in $cm^2\ s^{-1}$ and Q is the carrier gas velocity in $cm^3\ s^{-1}$. For illustrative purposes, D_m was calculated for a mixture of benzene vapor and helium from formula 16.3-1 of Bird, Stewart and Lightfoot (*8*). At 102 °C and a total pressure of 1 atmosphere, this formula gives D_m = 0.636. For r = 0.21 cm, l = 26 cm, D_m = 0.636 and Q = 1.67 $cm^3\ s^{-1}$, Scott's formula gives $\sigma_t^2 = 0.00623\ s^2$. Since the peaks obtained with the GDD had half-widths of ≥5 s (i.e., $\sigma_t^2 \geq 25\ s^2$), the additional bandwidth expected to result from diffusion in the GDD inlet tube would be negligible.

The experimental bandwidths obtained with the GDD were indistinguishable from those obtained for the same peaks with a flame ionization detector. It appears that diffusion in the tubing between effluent splitter and detector does not add materially to the bandwidth in either case.

ACKNOWLEDGMENT

The authors are grateful to T. R. Mueller for designing the variable amplifier-subtracter circuit used in the background corrector, and to A. D. Horton for helping with GC procedures and for suggesting certain design features of the GDD chamber.

LITERATURE CITED

(1) S. P. Cram, and R. S. Juvet, *Anal. Chem.*, **48**, 411R (1976).
(2) R. S. Braman, and A. Dynako, *Anal. Chem.*, **40**, 95 (1968).
(3) J. D. Defreese and H. V. Malmstadt, Paper No. 206 presented before the Federation of Analytical Chemistry and Spectroscopic Societies, Indianapolis, Ind., November 1975.
(4) A. I. Zaidel, V. K. Prokof'ev, S. M. Raiskii, V. A. Slavnyi, and E. Ya. Shreider, "Tablitsy Spektralnykh Linii", Nauka, Moscow, 1969.
(5) R. W. B. Pearse, and A. G. Gaydon, "The Identification of Molecular Spectra", 3rd ed., John Wiley & Sons, New York, N.Y., 1963, p 227.
(6) C. Hendrix–Jongerius and L. De Galan, *Anal. Chem. Acta*, **87**, 259 (1976).
(7) R. P. W. Scott, *J. Chromatogr. Sci.*, **9**, 641 (1971).
(8) R. B. Bird, W. E. Stewart, and E. N. Lightfoot, "Transport Phenomena", John Wiley & Sons, New York, N.Y., 1960, p 505.

RECEIVED for review July 22, 1977. Accepted September 19, 1977. Oak Ridge National Laboratory is Operated by Union Carbide Corp. for the U.S. Department of Energy.

Unrecognized Systematic Errors in Quantitative Analysis by Gas–Liquid Chromatography

Adam Shatkay* and Solange Flavian

Israel Institute for Biological Research, Ness-Ziona, Israel

The errors inherent in the accepted methods of quantitative gas chromatographic analysis are discussed. It is shown that in addition to the usual parameters affecting the measurements (such as temperature and gas flow), it is necessary to consider also the volume of liquid injected, and the concentration of the standards. This applies not only to the "direct" measurements using peak area vs. quantity for the calibration curve, but also to the "internal standards" technique, which is tacitly assumed to depend only on relative data, considered to be independent of quantity and concentration of the samples. Our argument is supported by experimental results obtained using various combinations of analytes and standards, various chromatographs, various columns, various detectors, and various integrators.

Gas–liquid chromatography (GLC) has become a very popular tool in quantitative analysis. In fact, the very informative and comprehensive text by Littlewood (*1*) states that gas chromatography is mainly used for quantitative analysis, as the interpretation of the data is simple, and the apparatus does not require skilled personnel. This claim appears to us rather dangerous. We shall attempt to point out that the interpretation of the GLC data is not very straight forward, and that unless the quantitative methods are tested in ways which have not been in common use up to now, the results of an analysis can easily be in error by ±10%, or more in some cases, without the investigator being aware of any deviation from accuracy.

Two methods are claimed to give reasonably accurate quantitative results in GLC analysis. One is based on the direct calibration of the quantity of pure analyte vs. the peak area, when the instrument parameters (such as temperature, gas flow, etc.) are kept constant. The other method is based on the use of internal standard or standards—it employs a calibration curve where the abscissa is the ratio of the quantity of the analyte to the quantity of the standard, while the ordinate is the corresponding ratio of the peak area of the analyte to the peak area of the standard.

These two methods have been considered at length in the literature (*1–5*), and we shall summarize here only the salient features, in order to point out the weaknesses of these methods, which have been either tacitly ignored or not realized before.

In the "direct" method, a volume of solution (v) containing a quantity of the analyte ($q_{analyte}$ grams or moles) is introduced into the column. A calibration curve of the peak areas ($A_{analyte}$) corresponding to $q_{analyte}$ is prepared; it need not be linear. When an unknown sample is analyzed, its peak area is determined, and the quantity of the analyte is read off the calibration curve. As the volume injected is known, the concentration ($C_{analyte}$) can also be calculated.

The above argument assumes that the volume of the analyte solution is adequately known. In the common quantitative analysis, the 10-μL syringe is most popular; it is graduated in 0.1-μL divisions and can be assumed accurate to within ±0.1 μL. When ca. 2 μL of liquid are introduced, this corresponds to the range of ±5%. When the quantity injected is less than 2 μL, the possible error increases. On introduction of samples greater than ca. 4 μL, the reproducibility decreases considerably, as can be seen in Figures 7 and 8. This appears to be due to the difficulty in transferring quantitatively all the volume of the liquid from the syringe to the column. When a large volume is introduced, only a small part of the piston serves as a seal, and the liquid tends to evaporate through the top of the syringe.

Next, the assumption that all the instrument parameters are constant, both during the establishment of the calibration curve and during the analysis, is not always justified. Thus a shift might occur in the temperatures of the various instrument components, or in the various gas flows. Such factors would introduce systematic errors in any continuous analysis: the duplicate samples would show only small fluctuations, so that the precision might be high, while the accuracy might be low. This is illustrated in Figure 7 and 8, where 100 measurements taken in 15 independent runs are plotted together.

As a solution to the above two problems associated with the "direct" method, the "internal standard" method is supposed to be independent of the exact volume introduced into the column, and if the effects of temperature and gas flow on the sensitivity of the instrument to analyte and standard are similar, then fluctuations in these parameters should not affect the applicability of the calibration curve, which depends only on the ratios between the analyte and the standard.

We shall attempt to show that such trust in the "internal standard" method might be misleading. Furthermore, we shall show that even in the "direct" method, in addition to the limitations listed above, the concentration itself is a parameter which cannot be neglected.

We have started our investigations in order to develop an analytic method which would assist the research carried out in our Institute on the use of ^{31}P in NMR studies. For this purpose we employed some esters of phosphoric acid. In the course of the investigation, we have extended our measurements to cover quite dissimilar substances, such as halogen derivatives of benzene, or simple hydrocarbons like dodecane. The effects described below were found in all the materials tested by us. However, for brevity, only representative experiments will be described in detail, without quoting the data for all the substances used.

EXPERIMENTAL

Materials. For analytes and standards, we have used a number of esters of phosphoric acid (trimethyl phosphate, triethyl phosphate, dimethyl methylphosphonate), 1-bromo-4-chlorobenzene, undecane, and dodecane. All these materials were commercially obtained (from Merck, B.D.H. and Aldrich); all were of analytical grade and were used without any further purification.

Instruments. (a) The following gas chromatographs were used: (a1) Packard, Oven model 804, Temp. control model 873, Electrometer model 842, H.V. supply model 838. (a2) Packard, Oven model 805, Temp. control model 873, Electrometer model 844, H.V. supply model 834. (a3) Packard, Oven model 802, Temp. control model 871, Electrometer model 840, H.V. supply model

871. (a4) Pye Unicam Series 802.

(b) The following detectors were used: (b1) Flame ionization detector, Packard model 881. (b2) Flame ionization detector, Pye model 802. (b3) Thermal conductivity detector, Packard model 839.

(c) The following integrators were used: (c1) Infotronics digital integrator model CRS-100. (c2) Honeywell Disc-chart Integrator model 201-B. (c3) Weighing of areas plotted on Leeds & Northrop Ltd. Speedomax W Recorder. (c4) Home-made capacitor-integrator, combined with Radiometer PHM-64 potentiometer. (c5) Home-made integrator based on Hewlett-Packard model 9810 Desk calculator.

(d) The following columns were used (length 2 m, diameter 5 mm): (d1) 15% Silicone oil DC 550 on Chromosorb W, DMCS 60/80 mesh. (d2) 5% Silicone oil SE 30 on Chromosorb W, DMCS 80/100 mesh. (d3) 10% Silicone oil DC 550 + 5% Polyethylene glycol succinate on Chromosorb W, DMCS 80/100 mesh.

Most of the results described below were obtained on using gas chromatograph a1 with detector b1 and integrator c1. On use of the other instruments, similar effects were observed.

Syringes. We have used the 10-μL Hamilton syringes. The reproducibility and the linearity of the volumes delivered was checked by using a number of syringes, and by extracting the same volumes from different regions of the syringe (e.g., 1 μL between the marks 1–2 or 3–4 μL).

Working Conditions. Usually we used intake temperature of 150 °C, isothermal column temperature of 110 °C, and detector temperature of 150 °C. The effects of changes in these temperatures by 50–100 °C were tested in some experiments, to study the influence of variations in temperature. While the retention times and peak shapes and areas were altered by such changes, the effects described in the following discussion were present at all the temperatures tested.

The gas flows were usually: H_2 50 cm^3/min, N_2 30 cm^3/min, air 500 cm^3/min. These also were altered in some experiments, with results similar to those stated for the temperature changes.

RESULTS AND DISCUSSION

Calibration Curve. In the "internal standard" method, a series of mixtures is prepared, each mixture containing a known quantity of the analyte and a known quantity of the standard, in a solution of a given volume. The exact amount of the solvent is considered to be immaterial. The variable of interest is the ratio

$$R_q \equiv q_{\text{analyte}}/q_{\text{standard}} \quad (1)$$

which is different for each of the solutions prepared, and serves as the independent variable in the calibration curve.

Approximately 2 μL of the various solutions are introduced into the column (the exact amount is again considered to be immaterial, as stated above). The areas of the peaks due to the analyte (A_{analyte}) and due to the standard (A_{standard}) are measured for each mixture, and the ratio

$$R_A \equiv A_{\text{analyte}}/A_{\text{standard}} \quad (2)$$

is plotted as the dependent variable in the calibration curve. This is accepted practice in analyses using the internal standard technique. When the calibration points obtained using a number of R_q's are self-consistent, no additional experiments are considered necessary to support the calibration curve. A similar experiment has been carried out by us using four solutions of dimethyl methylphosphonate in methanol, with undecane as the internal standard. The concentration of undecane was approximately constant in all the solutions, at ca. 3×10^{-3} g/cm^3. The concentration of the ester varied from 7×10^{-3} to 2×10^{-2} g/cm^3. The peak areas corresponding to each of the four solutions were determined in triplicate, and the ratio R_A was calculated. The results are summarized in Figure 1.

It can be seen that the results of the triplicate determination are reproducible and form an apparently satisfactory curve, linear and passing through the point of origin (as obviously

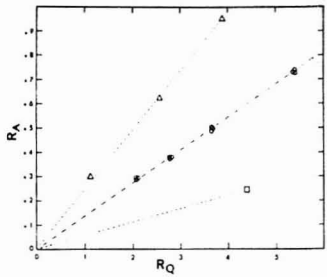

Figure 1. Calibration curve of the ratio of areas vs. ratio of weights, for dimethyl methylphosphonate and undecane. (○): experimental results for the concentration of undecane ca. 3×10^{-3} g/cm^3. (△): experimental results for the concentration of undecane ca. 1×10^{-3} g/cm^3. (□): experimental result for the concentration of undecane ca. 2×10^{-2} g/cm^3

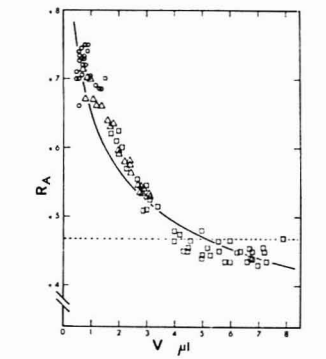

Figure 2. Effect of the volume injected into the column (v) on R_A at constant R_q and constant concentrations. Points—experimental. (○): range 3×10^{-9}. (△): range 1×10^{-8}. (□): range 3×10^{-8}. Curves—theoretical. (—): $A_{\text{ester}} = 6124 \times v^{0.856}$, $A_{\text{dodecane}} = 9396 \times v^{1.056}$. (---): $A_{\text{ester}} = 4828v$; $A_{\text{dodecane}} = 10324v$

at a constant q_{standard} and for $q_{\text{analyte}} = 0$, we should get $A_{\text{analyte}} = 0$, and $R_A = 0$).

However, when an attempt was made to reproduce the calibration curve with the undecane concentration kept at about 1×10^{-3} g/cm^3, a different curve was obtained, represented by the triangles in Figure 1.

Furthermore, keeping R_q at the value of 4.4, while increasing the concentration of undecane to about 2×10^{-2} g/cm^{-3}, the point represented by the square in Figure 1 was obtained.

It appears, therefore, that even when the instrumental conditions (temperatures, gas flows, column) are kept constant, the calibration curve of R_A vs. R_q is not uniquely defined. We shall attempt to show that two other important parameters have to be specified before a calibration curve for the internal standard method can be safely employed; these are the volume of the liquid injected (v) and the concentration of the standard (q_{standard}/v, as opposed to q_{standard} alone).

Effect of the Volume Introduced into the Column. When a mixture of analyte and standard is introduced into the column, we obtain two peaks, with a ratio of their areas R_A. The method of internal standards tacitly assumes that this ratio is independent of the volume injected. Figure 2 presents the results of an experiment aimed at testing this assumption. The mixture studied was trimethyl phosphate

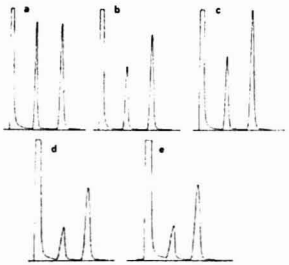

Figure 3. Effect of volume injected into the column (v) on the peaks, while R_q and concentrations are kept constant. The left peak is due to trimethylphosphate (7.19×10^{-2} g/cm^3); the right peak is due to dodecane (1.04×10^{-2} g/cm^3. (a) 0.9 μL, range 3×10^{-9}; (b) 2.4 μL, range 1×10^{-8}; (c) 2.9 μL, range 1×10^{-8}; (d) 6.8 μL, range 3×10^{-8}; (e) 7.9 μL, range 3×10^{-8}

(7.19×10^{-2} g/cm^3 and dodecane (1.04×10^{-2} g/cm^3). Not only was the R_q kept constant at 6.92 g ester/g dodecane, but the concentration of the individual components was also kept constant. The only variable was the volume v injected into the column.

It should be noted that the measurements involved the use of three sensitivity ranges, so that the data shown were obtained by use of the appropriate sensitivity factors. However, the overlap between the results obtained when the same volumes of solution were measured at different ranges shows that (in the present case at least) the dependence on range is linear within our accuracy.

The qualitative effect of v on the areas of the ester and the dodecane peaks is shown in Figure 3. The change in the peaks (shape, height, area) is quite pronounced.

The quantitative aspect of the variation in v is better seen in Figure 2. It appears that R_A is quite a sensitive function of v. Change of v from 1 μL to 2 μL causes a change of R_A (and a subsequent error in analysis) of 15%. A similar magnitude of error is produced on changing from 2 μL to 3 μL.

The advantages of linearity in the response of a detector in gas chromatography have been stressed by many authors (*1, 5–12*). If the response of the detector is linear with respect to both the analyte and the standard, then R_A should be constant and independent of v. For in such a case

$$A_{\text{analyte}} = k_1 q_{\text{analyte}} \tag{3}$$

$$A_{\text{standard}} = k_2 q_{\text{standard}} \tag{4}$$

k_1 and k_2 being some constants dependent on the experimental conditions. For our solution:

$$R_A = k_1 q_{\text{analyte}} / k_2 q_{\text{standard}} \tag{5}$$

and for a constant composition the term $q_{\text{analyte}}/q_{\text{standard}}$ is constant, so that R_A remains constant with changing v.

Thus linearity of response of the detector is a sufficient condition for the constancy of R_A. We shall show, however, that it is not a necessary condition. It is also of interest to consider how the "constancy" of R_A is affected by small deviations from linearity in the response of the detector.

It has been demonstrated by many authors that various detectors are linear, or at least approximately so (*3, 4, 6–21*). The usual test of such a linear response is an experiment where some 3 or 4 points are shown to lie fairly close to a straight line. Out of some 20 papers which we have perused (discussing the linearity of response of detectors) only one (*11*) uses as many as 10 points to support this view. This is not stated derogatively—for the purposes of the authors quoted the degree of linearity claimed was quite sufficient. However, we shall point out that for the "internal standard" method, the demand for linearity must be much stricter.

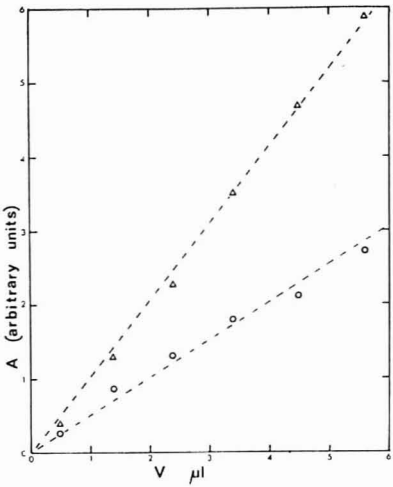

Figure 4. Peak areas of different volumes of a mixture having 7.19 $\times 10^{-2}$ g/cm^3 of trimethyl phosphate and 1.04×10^{-2} g/cm^3 of dodecane. (Δ): areas of ester. (O): areas of dodecane

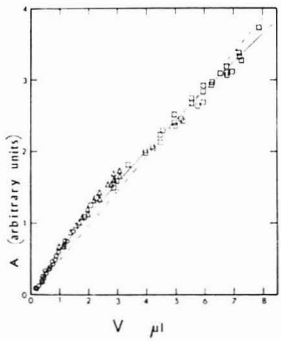

Figure 5. Peak-area vs. v for a solution of trimethyl phosphate in methanol, 7.19×10^{-2} g/cm^3. Points—experimental. (O): range 3×10^{-9}. (Δ): range 1×10^{-8}. (□): range 3×10^{-8}. Curves—theoretical. Continuous line: $A = 6124 \times v^{0.856}$. Broken line: $A = 4825\ v$

In the example described in Figure 2 we show 91 experimental points. We have chosen at random 6 values of A_{ester} and the corresponding values of A_{dodecane}, to span the range of v from 0 to 6 μL. The results are plotted in Figure 4.

It can be seen that the response to both the ester and the dodecane is fairly linear, and can be expressed as $A_{\text{ester}} = 5.10 \times 10^4 \times v$ for the ester, and as $A_{\text{dodecane}} = 1.04 \times 10^5 \times v$ for the dodecane. These values should yield a constant $R_A = 0.49$ (cf. Equation 5). Such constant R_A, is, however, quite incompatible with the experimental values of R_A, presented in Figure 2.

A more detailed picture of the change of peak area with v is presented in Figures 5 and 6, where all the 91 experimental points are shown.

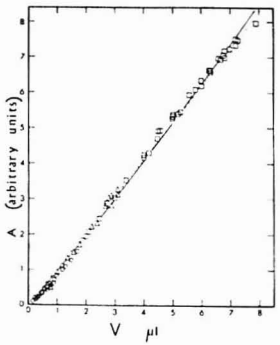

Figure 6. Peak area vs. v for a solution of dodecane in methanol. 1.04 × 10^{-2} g/cm^3. Points——experimental. (O): range 3 × 10^{-6}. (△): range 1 × 10^{-6}. (□): range 3 × 10^{-6}. Curves——theoretical. Continuous line: $A = 9396 \times v^{1.056}$. Broken line: $A = 10324\ v$

Attempt to fit all the points with a straight line by least squares (cf. Equations 3 and 4) gives for the ester the best value for $A_{ester} = 4.83 \times 10^4 \times v$, while for the dodecane the best value is $A_{dodecane} = 1.03 \times 10^5 \times v$. These two equations yield the constant $R_A = 0.47$, marked by the broken line in Figure 2. The rms deviation obtained with these values is 1.39 × 10^4 for the ester, and 1.51 × 10^4 for the dodecane.

We have attempted also to fit the 91 points with an equation of the form

$$A_i = a_i v^{b_i} \tag{6}$$

where for a substance i, a_i is a scaling factor, while b_i can be considered as "non-linearity" factor. It can be seen that when $b_i = 1$, we obtain a linear relation as in Equations 3 and 4; for b_i greater than unity the graph of A_i vs. v will be concave; for b_i less than unity the graph will be convex.

In our case, using a computer search (22) to obtain best fit by least squares to Equation 6, we find that $a_{ester} = 6.12 \times 10^4$, $b_{ester} = 0.856$, $a_{dodecane} = 9.40 \times 10^4$ and $b_{dodecane} = 1.056$. The rms deviation obtained with these values is 7.53 × 10^2 for the ester, and 1.22 × 10^4 for the dodecane. The theoretical curves obtained using these values are drawn as continuous lines in Figures 5 and 6. The fit of such exponential curves is better than that of the straight lines, though visually there does not appear to be much difference. However, the real test emerges in the compatibility of the theoretical results with the experimental values of R_A. If our exponential equations hold, then:

$$R_A = \frac{a_{ester} v^{b\,ester}}{a_{dodecane} v^{b\,dodecane}} = \frac{6.12 \times v^{0.856}}{9.40 \times v^{1.056}} \tag{7}$$

The theoretical values calculated with Equation 7 are plotted as the continuous line in Figure 2. It can be seen that qualitatively the mathematical model fits the experiment, and even quantitatively the agreement is fair.

It has been stressed by a number of authors (*3*, *8*) that it is helpful to have the standard "similar" to the analyte. The term "similar" is rather vague. To have it fit the context, we should take it to mean "almost identical with the analyte in all respects, with the sole exception of the retention time". While such a definition would theoretically enable us to use the internal standard with great accuracy, in practice it is doubtful if such standards could be found. However, using

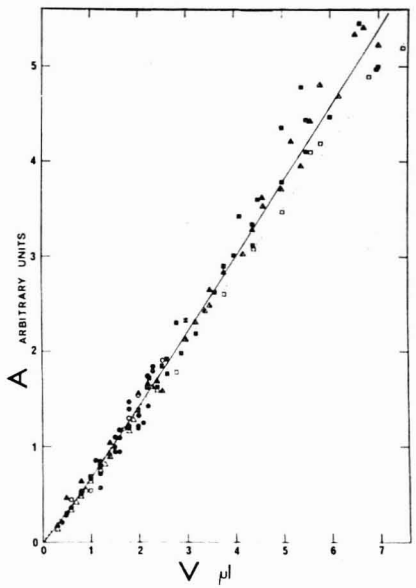

Figure 7. Peak areas as function of the volume of solution introduced into the column, for solution of undecane 1.06 × 10^{-2} g/cm^3. Points——experimental. (- - -): theoretical, using $A = 7504\ v$. (—): theoretical, using $A = 6796 \times v^{1.064}$

our "non-linearity factor" b_i, we note that when it is equal for the analyte and the standard (even when $b_i \neq 1$), Equation 7 reduces to

$$R_A = \frac{a_{analyte}}{a_{standard}} = \text{constant} \tag{8}$$

so that we get rid of the effect of v on R_A. Thus, in the terms of our discussion, we are now in a position to restate the definition of "similar": it will now mean "having a sufficiently close non-linearity factor, without any regard to any physical or chemical resemblance".

The importance of this distinction will be made plain by considering the case where dodecane is taken as the "analyte", while undecane is the "standard". By any ordinary usage the two substances can be considered as "similar". However, we shall show that their "non-linearity factors" are sufficiently dissimilar to cause deviations from Equation 8.

Figures 7 and 8 present results of 100 chromatograms, taken in 15 independent experiments on the above system, conducted on different solutions by different workers on different dates (each symbol represents a different experimental series). The scatter of points reflects the effect of small differences in the experimental conditions. The increase of scatter for large values of v has been discussed already.

In Figure 9 we summarize the effect of v on R_A (at constant R_q). While the phenomenon is much less noticeable than for the pair trimethyl phosphate–undecane (cf. Figure 2), it is still quite significant. An injection of 1 μL instead of 2 μL introduces an error of about 2%, while our experimental error in this experiment is within the range of about ±1%.

A linear fit to the experimental points of Figures 7 and 8 yields $A_{dodecane} = 7.02\ v \times 10^3$ and $A_{undecane} = 7.50\ v \times 10^3$. The rms deviation obtained with these values is 2.11 × 10^4 for the

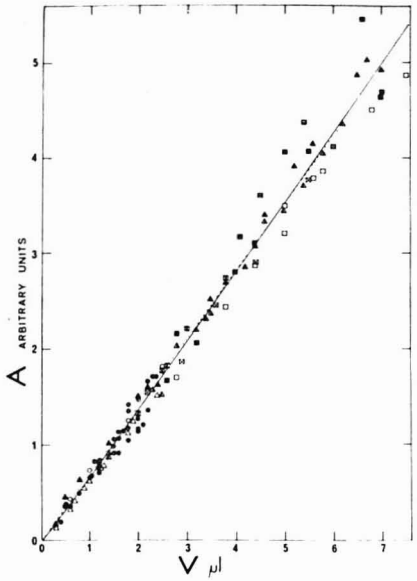

Figure 8. Peak areas as function of the volume of solution introduced into the column, for solutions of dodecane 1.02×10^{-2} g/cm^3. Points——experimental. (- - -): theoretical, using $A = 7024\ v$. (—): theoretical, using $A = 6644 \times v^{1.036}$.

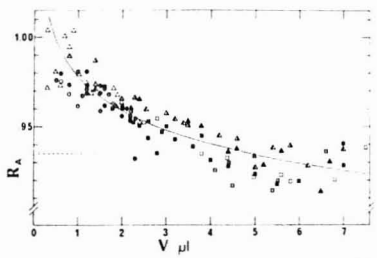

Figure 9. R_A as function of v for a solution of 1.06×10^{-2} g/cm^3 undecane and 1.02×10^{-2} g/cm^3 dodecane in methanol. Points — experimental. (- - -): theoretical, using Equation 5 with $k_{\text{dodecane}} = 7024$, and $k_{\text{undecane}} = 7504$. (—): theoretical, using Equation 7, with $a_{\text{dodecane}} = 6644$, $b_{\text{dodecane}} = 1.036$, $a_{\text{undecane}} = 6796$, $b_{\text{undecane}} = 1.064$

undecane, and 1.82×10^4 for the dodecane. These values yield in turn $R_A = 0.94$ (constant). Such a constant R_A is drawn as the dashed straight line in Figure 9, and is obviously inconsistent with the experimental results.

On trying to fit the results with Equation 6, we obtain for best fit $A_{\text{dodecane}} = 6.65 \times 10^3 \times v^{1.036}$, and $A_{\text{undecane}} = 6.80 \times 10^3 \times v^{1.064}$. The rms deviation obtained with these values is 1.98×10^4 for the undecane, and 1.04×10^4 for the dodecane. The R_A calculated using the above values appears as the continuous curve in Figure 9. It gives a fair fit to the experimental results.

One additional result can illustrate the generality of the effect described above. In Figure 10 we present the values of R_A obtained for a solution of trimethyl phosphate (9.6×10^{-3} g/cm^3) and dodecane (1.04×10^{-3} g/cm^3) in a mixture

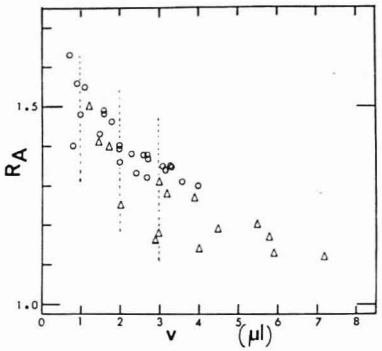

Figure 10. R_A as function of v for a solution of trimethyl phosphate and dodecane in methanol and ether. (O): range 3×10^{-6}. (Δ): range 1×10^{-6}

of methanol and ether. This solution is about 10 times more dilute than that described in Figure 2. The instrumental set-up was (cf. "Instruments" above): gas chromatograph a3; detector b1; integrator c5.

Despite the change in the setup as compared with the previous examples, the effect described in Figure 10 is seen to be similar to that described in Figures 2 and 9. Change of v from 1 µL to 3 µL causes a change of R_A from about 1.5 to about 1.3 (over 10%).

Effect of Concentration. Thus far we have dealt with the effect of the quantity of solution introduced into the column, while the composition of the solution remained constant. We shall now deal with the other source of error mentioned in our introductory remarks: the use of the same quantity of material (q_i), or the same volume of solution (v), but at different concentrations.

In the Figures 4–10, the abscissa is v, graded in microliters. This may seem rather ambiguous: only on stating the concentration (as is done in the captions to the figures or in the accompanying text) can the calibration be practically applied. The conventional procedure is to mark the abscissa in units of quantity (say grams or moles), thus giving a spurious impression that the calibration curve is unambiguous. This is, in general, incorrect. We shall demonstrate that the concentration of the solution should also be stated in order that the calibration curve can be applied unambiguously; in brief, both v and q_i have to be known. When this information is missing, the calibration curve is virtually irreproducible. If this point is not realized in a laboratory using such a calibration curve, the results can well be suffering from a systematic error—the precision can be good, but the accuracy can be poor, without the worker having any indication of this error.

The fact that for a constant R_q, the R_A can be a function of concentration has been noted already by Subbotina and Evdakov (*23*), and the use of corrective calibration has been suggested by the authors. However, the phenomenon appears to be more complicated than that, and requires discussion in some detail.

When we wish to test the effect of concentration on R_A (at constant R_q), two very different experiments can be conducted. In the more straightforward one, we take a solution containing q_{analyte} and q_{standard} in a volume v, which is injected into the column. R_A is measured, and then the solution is diluted by addition of the solvent. Again the same volume v is injected; in general, a different R_A will now be obtained (contradicting the tacit assumption of the "internal standard method" about

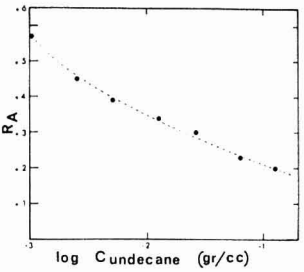

Figure 11. Change of R_A with concentration, for a mixture of undecane and dimethyl methylphosphonate. R_q kept constant at 2.27 g ester/g undecane. v kept constant at 2 μL

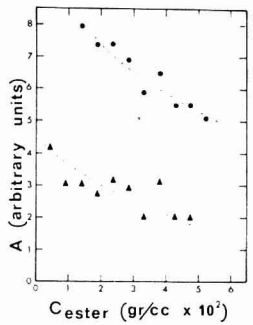

Figure 12. Change of peak urea of dimethylmethylphosphonate on change of concentration. (○): for 5×10^{-5} g of the ester. (△): for 2×10^{-5} g of the ester

the constancy of R_A). This is the experiment reported by Subbotina and Evdakov (*23*). It must be mentioned that the authors apparently were not aware of the possible effect of v itself on R_A, as demonstrated in the previous section, so that the constancy of v during the experiment is not stressed in ref. (*23*).

We present in Figure 11 the results of such an experiment.

It can be seen that R_A changes with concentration. The proper expression of this result would be $(\partial R_A/\partial C_{\text{standard}})_{R_q,v} \neq 0$.

However, this is not the only way in which R_q can be kept constant on change of concentration. We can also conduct an experiment in which q_{standard} is kept constant while v is changed, so that the resulting concentration is changing. For each such C_{standard}, a series of solutions of varying q_{analyte} can be prepared, and R_A can be determined for any required R_q. To make this clearer, let us consider the effect on A_i of change of concentration, when q_i remains constant (obviously v will have to change, to give different C_i for the same q_i). Such an experiment is described in Figure 12.

Each point drawn in Figure 12 is obtained from a curve similar to those drawn in Figures 5, 6, 7, and 8. It can be seen that 5×10^{-5} g of the ester yields very different peak areas at different concentrations; in fact, doubling the concentration reduces the peak area by some 20%. When the quantity of the ester is reduced (as shown by the triangles in Figure 12), the peak areas are reduced correspondingly, and the effect of change of concentration is less pronounced. In this case also the errors become more effective, so that the experimenter can fail to notice the phenomenon.

When R_q is kept constant, both q_{analyte} and q_{standard} remain constant in our present experiment (for any change in concentration). Thus A_{analyte} will change as described in Figure 11, and A_{standard} will also change, but not necessarily at the same rate. It follows that the ratio R_A at constant q_i can also change with concentration. However, the quantity now measured is $(\partial R_A/\partial C_i)_{R_q,q_i}$ which need not be equal to $(\partial R_A/\partial C_i)_{R_q,v}$ shown in Figure 11. Formally, the two experiments described above might be compared to the difference between heat capacity at constant pressure or at constant volume—the term "heat capacity" alone is indeterminate, and so is the idea of the change of R_A with concentration, unless the constancy of q_i or of v is stated.

Our experimental results show that in fact there is a dependence of R_A on concentration, both a constant q_i and at constant v. Practically, this means that even on using the "direct" calibration method, a graph of A_{analyte} vs. q_{analyte} is valueless unless also C_{analyte} is stated, and v is kept constant. Similarly a graph of A_{analyte} vs. C_{analyte} is suspect, unless q_{analyte} is stated (v being given, and kept constant, or q_{analyte} being constant for a varying v). The unknown solution has to be introduced into the column so as to satisfy the conditions of the appropriate calibration curve.

Similarly, when the "internal standard" technique is used, the correct dependence on concentration has to be considered. It follows that the curve of R_A vs. R_q requires, in addition to the specification of the volume of liquid injected, also the statement of the concentration of either the analyte or of the standard. Formally, the two are equivalent. Practically, the concentration of the analyte in the sample is unknown, while the concentration of the standard is within our control. Thus it is advisable to state the concentration of the standard used for a given calibration curve, and to use the same concentration for the preparation of the samples.

CONCLUSIONS

We suggest that the above discussion warrants the following conclusions.

(a) One should be careful to distinguish between the volume of the solution introduced into the column (v), the quantity of the substance introduced (q_i), and the concentration (C_i). In particular, the ratio $C_{\text{analyte}}/C_{\text{standard}}$, in which v cancels out, is an ambiguous quantity, and insufficient to specify a calibration curve.

(b) Generally the graph of R_A vs. R_q, as usually reported for calibration curves, is insufficient for use in the "internal standard" technique. Injudicious construction and use of such calibration curves can cause serious systematic errors in quantitative analysis.

(c) Generally the graph of A_{analyte} vs. q_{analyte}, as usually reported, is ambiguous. It should be supported by an explicit statement of C_{analyte}.

(d) The system analyte/standard should be tested in each case to see whether for a constant R_q the R_A is independent of v and of C_{standard}.

(e) It will often be found that the system is significantly dependent on v and on C_{standard}. In such a case the R_A vs. R_q curve should be constructed for a definite concentration of standard, and for a definite volume of injection. The samples have to be prepared so as to reach the same C_{standard}, and the ratio R_A has to be corrected by interpolation to yield the value corresponding to the v employed in the calibration curve.

ACKNOWLEDGMENT

We are very grateful to Pnina Bloch and to Ruth Sarenga for their devoted technical assistance.

LITERATURE CITED

(1) A. B. Littlewood, "Gas Chromatography", 2nd ed., Academic Press, New York, N.Y., 1970.

(2) J. Tranchant, Editor., "Practical Manual of Gas Chromatography", Elsevier, New York, N.Y., 1969.
(3) G. Shomburg, *Z. Anal. Chem.*, **164**, 147 (1958).
(4) H. F. Walton and J. Reyes, "Modern Chemical Analysis and Instrumentation", Marcel Dekker New York, N.Y., 1973, Chapter 9.
(5) J. Novak, "Quantitative Analysis by Gas Chromatography", Marcel Dekker, New York, N.Y., 1975.
(6) H. Bruderreck, W. Schneider, and I. Halasz, *Anal. Chem.*, **36** 461 (1964).
(7) D. H. Desty, C. J. Geach, and A. Goldup, in "Gas Chromatography 1960", R. W. P. Scott, Ed., Proc. 3rd Intl. Symp., Academic Press, New York, N.Y., 1961, p 46.
(8) M. Dimbat, P. E. Porter, and F. H. Stross, *Anal. Chem.*, **28**, 290 (1956).
(9) D. W. Grant in "Gas Chromatography", D. H Desty, Ed., Proc. 2nd Intl. Symp., Butterworths, London, 1958, p 153.
(10) A. I. M. Keulemans, A. Kwantes, and G. W. A. Rijnders, *Anal. Chim. Acta*, **16** 29 (1957).
(11) I. G. McWilliam and R. A. Dewar, in "Gas Chromatography", D. H. Desty, Ed., Proc. 2nd Intl. Symp., Butterworths, London, 1958, p 142.
(12) L. J. Schmauch and R. A. Dinerstein, *Anal. Chem.*, **32**, 343 (1960).
(13) H. Cherdron, L. Hoehr, and W. Kern, *Z. Angew. Chem.*, **73**, 215 (1961).
(14) R. D. Condon, P. R. Scholly and W. Averill, in "Gas Chromatography 1960", R. P. W. Scott, Ed., Proc. 3rd Intl. Symp., Butterworths, London, 1960, p 30.
(15) K. Edelman and J. Srnensky, *Kautch. Gummi Kunstst.*, **27**, 422 (1974).
(16) L. B. Foster and C. S. Frings, *Clin. Chem. (Winston-Salem, N.C.)*, **16**, 177 (1970).
(17) D. J. Freed and A. M. Mujsce, *Anal. Chem.*, **49** 139 (1977).
(18) M. A. Harmon and H. W. Doelle, *J. Chromatogr.*, **42** 157 (1969).
(19) D. Jentzsch and K. Friedrich, *Z. Anal. Chem.*, **180** 96 (1961).
(20) H. Joseph, *Isr. J. Chem.*, **8** 575 (1970).
(21) H. F. Proells and H. J. Lohmann, *Clin. Chem. (Winston-Salem, N.C.)*, **17**, 222 (1971).
(22) A. Shatkay, *Anal. Chem.*, **48** 1039 (1976).
(23) L. S. Subbotina and V. P. Evdakov, *J. Anal. Chem. USSR*, **29**, 1923 (1974).

RECEIVED for review May 27, 1977. Accepted September 7, 1977.

Determination of Sulfobetaine Amphoteric Surfactants by Reverse Phase High Performance Liquid Chromatography

Nicholas Parris, Warner M. Linfield, and Robert A. Barford*

Eastern Regional Research Center, Agricultural Research Service, U.S. Department of Agriculture, 600 East Mermaid Lane, Philadelphia, Pennsylvania 19118

We have developed a method for the direct analysis of sulfobetaine amphoteric surfactants by reverse phase HPLC using methanol/water 80/20 (v/v) as the mobile phase. Elution order correlated with the surface properties of the solutes. This method for determination of (2-hydroxy-3-sulfopropyl) and (sulfopropyl) dimethyl (alkyl) ammonium inner salts was more reliable than indirect determinations of reactants. The accuracy for analysis of sulfobetaines in the reaction mixture was estimated to be 3%. The development of this method expedited studies of reaction conditions so that optimum yields of lime soap dispersants could be obtained. Commercial samples of tallow- and coconut oil-derived amido sulfobetaines were analyzed.

Fat-derived sulfobetaines such as sulfopropylated long chain alkyl quaternary ammonium compounds have been reported elsewhere to be useful as lime soap dispersing agents (*1–3*). However, research studies on such materials have been severely hampered by the lack of a reliable direct method of analysis. Gas chromatographic methods are not applicable because the materials are essentially nonvolatile and cannot be readily derivatized. Reverse phase high performance liquid chromatographic separation (HPLC) and analysis of fatty derivatives such a methyl and phenacyl esters (*4, 5*), methoxy anilides (*6*), or fatty alcohol acetates (*7*) have been reported. Specifically, methanol–water and acetonitrile–water mobile phases have been used for the separation of such nonionized solutes by several workers (*4–7*). The mechanism of liquid chromatographic separations considering surface phenomena were studied by Albertsson (*8*), Guiochon (*9*), and Horvath (*10, 11*). It was of interest to determine in the present study whether the separation mechanism of amphoteric surfactants also involved interfacial phenomena.

The amphoteric surfactants subjected to HPLC separation in the present study were obtained via two different synthetic routes which have been described in detail elsewhere (*2, 3*). They are represented by the following two schemes:

$$ZN(CH_3)_2 + ClCH_2CHOHCH_2SO_3Na \rightarrow ZN^+(CH_3)_2CH_2CHOHCH_2SO_3^- + NaCl \quad (I)$$

and

$$ZN^+(CH_3)_2CH_2CH{=}CH_2 \cdot Cl^- + NaHSO_3 \rightarrow ZN^+(CH_3)_2CH_2CH(H)CH_2SO_3^- + NaCl \quad (II)$$

where Z is either a long chain alkyl group or a fatty acid derived long chain amido group of the structure $RCONHCH_2CH_2CH_2-$. The position of the sulfo group of scheme II is not certain, and the resulting amphoteric surfactants are thought to be a mixture of the 2- and 3-sulfopropylated quaternary ammonium compounds.

EXPERIMENTAL

HPLC Apparatus and Operating Conditions. Chromatographic separation of the amphoteric compounds was carried out with the aid of a pneumatically operated pumping system (du Pont 820) fitted with a loop injector (Waters Associates U6K) with a μ-Bondapak-C_{18} column (Waters Associates). A refractometer (Waters Associates Model R-401) was used as a detector. The flow rate was maintained at 1 mL/min. The mobile phase was 80/20 methanol/water.

The test surfactant samples were diluted with 80/20 methanol/water (v/v) or with pure methanol to bring the solvent to this ratio in preparation for HPLC analysis. A 200-μL sample containing up to 1.0 mg pure amphoteric or mixtures of amphoterics was then injected. Standard curves relating peak height to concentration were prepared with the aid of sulfobetaines prepared previously (*1, 2*). Degree of purity for homologous mixtures of sulfobetaines was found by relating the areas of chromatographic peaks run before and after spiking with a known weight of a pure individual amphoteric homolog.

Materials. *N,N*-dimethyldodecylamine (Armeen DM 12D) and *N,N*-dimethylhexadecylamine (Armeen DM 16D), obtained

from Armak Chemical Division, Akzona Inc. (Chicago, Ill.), were better than 99% pure by GLC. The methyl esters of fatty acids were prepared from the appropriate natural products by standard techniques and their purity was determined to be >98% by GLC. The synthesis of sodium 3-chloro-2-hydroxy-1-propanesulfonate and the procedures for the preparation of

$$RN^+(CH_3)_2CH_2CHOHCH_2SO_3^- \text{ and } RN^+(CH_3)_2CH_2CH(H)CH_2 \quad (SO_3^-)$$

are described by Parris et al. (2). The amido compounds

$$RCONHCH_2CH_2CH_2N^+(CH_3)_2CH_2CHOHCH_2SO_3^- \text{ and}$$

$$RCONHCH_2CH_2CH_2N^+(CH_3)_2CH_2CH(H)CH_2 \quad (SO_3^-)$$

were prepared in accordance with the procedure of Parris et al. (3).

Pilot plant samples of the amido compounds $RCONHCH_2CH_2CH_2N^+(CH_3)_2CH_2CHOHCH_2SO_3^-$ prepared from coco and tallow fatty acids, respectively, were obtained through the courtesy of the Ashland Chemical Co. (Columbus, Ohio). A 1- mg sample of these two amido compounds was separated by HPLC as shown in Figure 1 (attenuation 16X). The capacity factors for the individual homologues separated were calculated with the use of retention volumes from the chromatograms (Figure 1) and plotted vs. chain length.

Physical Measurements. The amphoteric surfactants of this study were dissolved in a blend of methanol/water 80/20 (v/v), whereas the methyl esters of fatty acids were dissolved in a blend of methanol/water 85/15 (v/v). All physical measurements and HPLC determinations were carried out with the test materials dissolved in the above solvents. Hexane was used to simulate the chromatographic nonpolar stationary phase.

Interfacial tension measurements were carried out with hexane and solutions of test material, at various concentrations, in the appropriate aqueous methanol mixture with the aid of a Du Noüy tensiometer equipped with a 6.0-cm platinum ring.

Distribution coefficients were determined by carrying out batch equilibrations of solutes between hexane and aqueous methanol using previously described methods (*12*).

Monitoring of Sulfobetaine Formation. The following two types of reactions were monitored by HPLC.

(I) *N,N*-dimethyldodecylamine (4.27 g, 0.020 mol) was dissolved in 48 mL methanol followed by the addition of sodium 3-chloro-2-hydroxy-1-propanesulfonate (the addition product of sodium bisulfite to epichlorohydrin) (3.03 g, 0.020 mol) and sodium carbonate (0.42 g, 0.004 mol) dissolved in 12 mL water. The solution was placed in a reaction flask heated to 65 °C with constant temperature bath. The concentration of the reaction mixture was 0.30 M with respect to reactants and contained 20 mol % sodium carbonate. Samples for HPLC analysis were withdrawn at roughly 1-h intervals and % yield of amphoteric surfactant was determined as a function of reaction time as shown in Table III.

The same synthetic procedure was repeated at a concentration of 0.10 M with and without 20 mol % of sodium carbonate. The results are also shown in Table III.

(II) To (allyl) dimethyl (hexadecyl) ammonium chloride (*2*) (13.84 g, 0.040 mol) dissolved in 20 mL methanol was added sodium bisulfite (5.00 g, 0.048 mol) in 20 mL H_2O and the solution was kept at 22 °C. *tert*-Butylperbenzoate (0.194 g, 0.001 mol) was added immediately after mixing to initiate the reaction. The initial concentration of the allyl quaternary compound in the reaction mixture was 0.73 M.

Samples were withdrawn at periodic intervals. The bisulfite content was determined iodimetrically and is discussed later with reference to Figure 2. The methanol/water ratio of the samples had to be adjusted from 50/50 to 80/20 (v/v) by addition of methanol prior to the HPLC determination of sulfobetaine content.

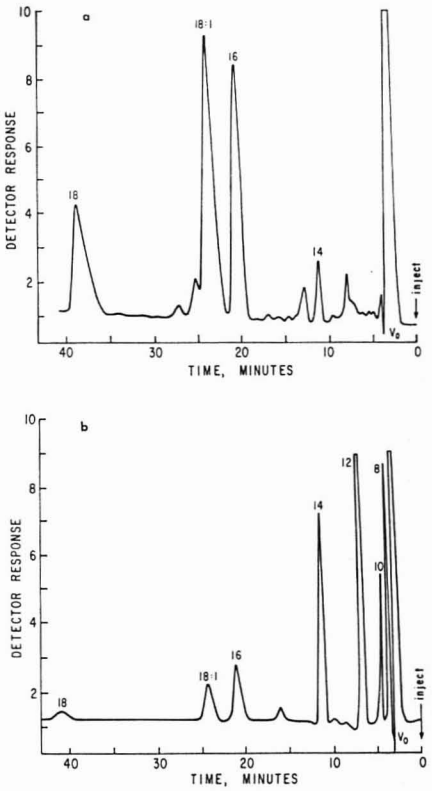

Figure 1. (a) Chromatogram of tallow–derived sulfobetaine. Tal–$CONHC_3H_6N^+(CH_3)_2CH_2CH(OH)CH_2SO_3^-$. (b) Chromatogram of coconut oil-derived sulfobetaine. Coco–$CONHC_3H_6N^+(CH_3)_2CH_2CH(OH)CH_2SO_3^-$

RESULTS AND DISCUSSION

Reverse phase HPLC proved to be a satisfactory method for the separation and identification of several individual homologues of fat-derived sulfobetaines. A refractive index detector was used in this study, since the absence of a suitable chromophore in the test compounds precludes the use of a UV detector. The behavior of these amphoteric surfactants on the HPLC column appeared to differ markedly from that of a homologous series of fatty acid methyl esters. Capacity factors k', calculated from HPLC chromatograms of the methyl esters correlate roughly with distribution coefficients (K) determined in bulk phase equilibrium experiments using hexane to simulte the stationary phase (Table I). The distribution coefficients of the sulfobetaines, $RN^+(CH_3)_2CH_2CH_2CH_2SO_3^-$, on the other hand do not correlate with elution order. The observed capacity factors were much larger than those predicted by Equation 1 using the batch distribution coefficients and considering the fact that the same column was used for both esters and amphoterics, so that V_s/V_m may be considered the same for both series. These relationships are given by:

$$k' = (V_R - V_m)/V_m = KV_s/V_m \quad (1)$$

where V_s is the volume of the stationary phase within the

Table I. Properties of Solutes in Model and Chromatographic Systems

R[a]	Capacity[b] factor (k')	Distribution[c] coefficient (K)	Interfacial[d] tension (dyne/cm)
$RN^+(CH_3)_2C_3H_6SO_3^-$			
Blank			7.5
C_{12}	1.1	4×10^{-3}	4.6
C_{14}	2.4	6×10^{-4}	2.4
C_{16}	5.1	1×10^{-3}	0.1
RCO_2CH_3			
Blank			6.4
C_{16}	6.6	58	5.1
$C_{18:1}$	7.3	71	4.6
C_{18}	12.4	154	4.9

[a] Fatty acid portion. [b] Determined from chromatogram (Equation 1). [c] Determined in equilibrium experiments with model systems (hexane—80/20 methanol/water (v/v) for sulfobetaines, 85/15 methanol/water (v/v) for esters). Precision was ±5% for esters, ±10% for sulfobetaines. [d] At same solute concentration (1.3%).

column, V_R is retention volume of the solute, V_m is the volume of the mobile phase, and K is the distribution coefficient. The interactions between solute, mobile phase, and bound-monolayer stationary phases where the interacting moieties have fewer degrees of motion, differ from those in bulk systems. However, as evidenced by the esters, trends in K values determined in model two-phase systems may be similar to those determined in chromatography. Such similarity was not found for the sulfobetaines.

Since the successful separation of these sulfobetaines by HPLC obviously was unrelated to the bulk distribution coefficients, it was surmised that surface activity contributed significantly to the elution order. Interfacial tension measurements of hexane–aqueous methanol systems containing homologues of $RN^+(CH_3)_2CH_2CH_2CH_2SO_3^-$ as well as of those containing methyl esters are given in Table I. The esters possess essentially no surface activity, whereas the surface activity of the sulfobetaines increases dramatically (i.e., interfacial tension decreases) as the chain length increases. Several researchers have discussed retention mechanisms using models in which surface or interfacial tensions are important contributors (*8–11*). All of the models predict trends in retention similar to those in this study. However, more research is needed to explore the quantitative differences observed and the application of these approaches to surface active compounds.

The differences in surface activity between members of a longer series of sulfobetaine homologues are large enough to effect chromatographic separation. A straight line was obtained when logarithm of capacity factor was plotted as a function of chainlength of R in a homologous series of $RCONHCH_2CH_2CH_2N^+(CH_3)_2CH_2CH(OH)CH_2SO_3^-$.

Chromatograms of commercial samples of a tallow-derived sulfobetaine and a coconut oil-derived sulfobetaine show that good separation of complex mixtures of these surfactants can be achieved (Figure 1). The slight differences in retention times of common components in the chromatograms are due to changes in the column which took place after repeated use over a long time span. The peaks for the saturated homologues were identified by comparison with the retention volumes for the purified homologous sulfobetaines (*2*). Although not identified directly, it is assumed that the peak following the C_{14} compound in Figure 1b is $C_{18:2}$. Comparison of such chromatograms before and after spiking with a known amount of a single solute permits quantification of the amount of total amphoteric in commercial lime soap dispersants. Total area varied by <4%, depending on whether a C_{14} or C_{18} spike was used. Thus while the solutes differ in refractive index, a direct

Table II. Fatty Acid Distribution of Coconut Oil- and Tallow-Derived Sulfobetaines of the Structure $RCONHC_3H_6N^+(CH_3)_2CH_2CH(OH)CH_2SO_3^-$

Fatty acid	Percent homologue in: Tallow-derived sulfobetaines	Tallow (*12*)	Coconut oil-derived sulfobetaines	Coconut oil (*12*)
C_8			12	5-9
C_{10}			8	6-10
C_{12}			49	44-52
C_{14}	4	2-8	15	13-19
$C_{18:2}$	3	1-5	1	0-2.5
C_{16}	31	24-37	8	8-11
$C_{18:1}$	41	40-50	5	5-8
C_{18}	21	14-29	2	1-3

Table III. Effect of Conditions on Reaction I

Time, h	Percent reaction: 0.30 M Reactants, 0.06 M Na_2CO_3	0.10 M Reactants, 0.02 M Na_2CO_3	0.10 M Reactants
0.5	7	...	...
1.5	24	7	2
2.5	41	13	6
7.5	90	44	22

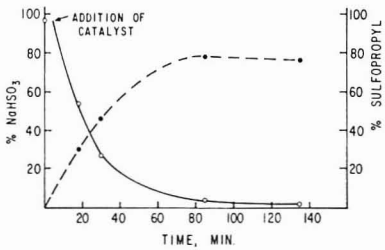

Figure 2. Monitoring of reaction II. (●) % sulfopropylated amphoteric surfactant by HPLC. (○) % $NaHSO_3$ by iodimetric titration

and good estimation of the purity of commercial preparations can be obtained.

The composition of the two commercial samples is shown in Table II. The values obtained are within the range for tallow and coconut oil in a standard reference work (*13*).

On the strength of the above chromatographic separation by HPLC, this technique was applied also to process studies of the synthesis of two types of sulfobetaines. In the process study described elsewhere (*3*), it was pointed out that the formation of the sulfobetaines could not be monitored by conventional means; however we have now shown that monitoring of the sulfobetaine could be successfully carried out by HPLC. Table III shows the rate of formation of the surfactant $C_{12}H_{25}N^+(CH_3)_2CH_2CHOHCH_2SO_3^-$ according to reaction scheme I above under three different conditions. Presence of carbonate buffer and higher concentration of reactants clearly accelerate the reaction.

Bisulfite addition to an alkyl dimethyl allyl ammonium chloride according to scheme II is shown graphically in Figure 2. Here the rate of formation of sulfobetaine is monitored by HPLC while the rate of disappearance of bisulfite is determined by iodimetric titration. Whereas disappearance of bisulfite had been used previously (*3*) as a criterion of completeness of reaction, the HPLC monitoring curve clearly shows a discrepancy between formation of sulfobetaine and disappearance of bisulfite. At the point where all bisulfite

has been consumed, the reaction is only about 78% complete. Thus iodimetric titration is an unreliable means of following the reaction. The accuracy of analysis for both reactions was ±3% when determined for known reaction mixtures.

The significance of the present research lies in the finding that amphoteric surfactants can now be analyzed directly and nondestructively by HPLC. Since a number of analytical methods for the direct determination of all other types of surfactants have been developed in the past, a major gap in analytical methodology has now been filled.

ACKNOWLEDGMENT

The authors thank Bernadene Sliwinski for determining distribution coefficients and Bruce Newman for his assistance in measuring interfacial tensions.

LITERATURE CITED

(1) N. Parris, J. K. Weil, and W. M. Linfield, *J. Am. Oil Chem. Soc.*, **50**, 509 (1973).
(2) N. Parris, J. K. Weil, and W. M. Linfield, *J. Am. Oil Chem. Soc.*, **53**, 60 (1976).
(3) N. Parris, C. Pierce, and W. M. Linfield, *J. Am. Oil Chem. Soc.*, **54**, 294 (1977).
(4) C. R. Schofield, *J. Am. Oil Chem. Soc.*, **52**, 36 (1975).
(5) H. D. Durst, M. Milano, E. J. Kikta, S. A. Connelly, and E. Grushka, *Anal. Chem.*, **47**, 1797 (1975).
(6) N. E. Hoffman, *Anal. Chem.*, **48**, 1104 (1976).
(7) J. D. Warthen, *J. Am. Oil Chem. Soc.*, **52**, 151 (1975).
(8) P. A. Albertsson, "Partition of Cell Particles and Macromolecules," 2nd ed., Wiley-Interscience, New York, N.Y., 1971, Chapter 3.
(9) C. Eon, B. Novosel, and G. Guiochon, *J. Chromatogr.*, **83**, 77 (1973).
(10) C. Horvath, W. Melander, and I. Molnar, *J. Chromatogr.*, **125**, 129, (1976).
(11) C. Horvath, W. Melander, and I. Molnar, *Anal. Chem.*, **49**, 142, (1977).
(12) J. F. Rusling, R. J. Bertsch, R. A. Barford, and H. L. Rothbart, *J. Chem. Eng. Data*, **14**, 169 (1969).
(13) "Bailey's Industrial Oil and Fat Products", 3rd ed., D. Swern, Ed., Interscience Publishers, New York, N.Y., 1964, pp 176, 192.

RECEIVED for review May 12, 1977. Accepted September 15, 1977. Reference to brand or firm name does not constitute endorsement by the U.S. Department of Agriculture over others of a similar nature not mentioned.

Reversed Phase High Performance Liquid Chromatographic Separations of Nucleotides in the Presence of Solvophobic Ions

Norman E. Hoffman* and John C. Liao

Todd Wehr Chemistry Building, Marquette University, Milwaukee, Wisconsin 53233

The groups UMP, CMP, AMP, and GMP; UDP, CDP, ADP, and GDP; UTP, CTP, ATP, and GTP; and AMP, ADP, and ATP were separated by high performance liquid chromatography isocratically on a reversed phase column in the presence of tetra-*n*-butylammonium ion. The 12 nucleoside phosphates and cyclic AMP could not be separated isocratically but could be separated by gradient elution with increasing ionic strength and methanol concentration. Uracil, cytosine, adenine, and guanine were separated in the presence of 10-camphorsulfonate ion. The ribonucleosides of these bases also were separated in the presence of the latter ion.

High performance liquid chromatography methods for nucleotides, nucleosides, and their bases have been reviewed in several papers by Brown et al. (*1–3*) and Anderson and Murphy (*4*). Nucleotides have usually been separated by anion exchange, but recently reversed phase chromatography has been used with these phosphate esters. The unphosphorylated compounds have been separated by both cation- and anion-exchange columns, and, more recently, by reversed phase chromatography.

The addition to the mobile phase of solvophobic ions of opposite charge to the charge on the ions to be separated has proved successful in the resolution of a variety of charged species (*5–15*). Both reversed phase and uncoated silica have been employed as stationary phases. This kind of system appeared attractive for the separation of nucleotides, nucleosides, and bases because the nucleotides are negatively charged over a wide range of pH, and many of the nucleosides and bases take on a positive charge at low pH. Furthermore, the technique lends itself to the manipulation of several parameters, solvophobic ion concentration, ionic strength, pH, and mixing of solvents in order to change retention volumes so as to succeed with a particular separation. We wish to report separations of ribonucleotides with a reversed phase column using tetra-*n*-butylammonium ion. Ribonucleosides also were separated from each other and bases from each other in the presence of 10-camphorsulfonate ion.

EXPERIMENTAL

Materials. Spherisorb 10 μ ODS was purchased from Spectra-Physics (Santa Clara, Calif.). Nucleosides, nucleotides, and their bases were purchased from Aldrich Chemical (Milwaukee, Wis.) or P-L Biochemicals (Milwaukee, Wis.). All other chemicals were purchased either from Aldrich Chemical or Fisher Scientific (Fairlawn, N.J.). All nucleotides except cyclic AMP were 5′- ribonucleoside phophates.

Mobile phase solutions were prepared by adding buffer reagent(s) and solvophobic species to about 80% of the final volume of water. Tetra-*n*-butylammonium hydrogen sulfate (TBHS) and 10-camphorsulfonic acid gave the solution a low pH at this point. Therefore, 0.75 N NaOH was added to raise the pH to the desired point. Then water was added to reach the final volume of the mobile phase. The pH was again measured and, as expected, the pH never changed.

The only exception to the above procedure for preparing mobile phase solutions was the preparation of the solution for nucleoside isocratic separation. In this case, a solution of acetic acid and 10-camphorsulfonic acid was adjusted for pH by adding dropwise 20% NaOH.

Mixed aqueous buffer and methyl alcohol solutions in isocratic runs were prepared in the chromatograph by pumping methanol from one pump and buffer from the other. Premixing buffer and methanol and using only one pump gave the same result in several test cases. All concentrations presented in this paper represent water concentrations and are not corrected for added methanol. Solvophobic ions in the mobil phase always were 0.025 M in water.

Table I. Isocratic Separation

Chromatographic separation	Peak	k^a	Buffer[b]	Mobile phase pH[c]	Vol % MeOH
A	CMP	0.40	0.10 M KH_2PO_4	3.90	0
	UMP	2.04			
	GMP	3.20			
	AMP	4.92			
B	GMP	0.52	0.10 M KH_2PO_4	7.00	25
	AMP	0.84			
	cAMP	2.40			
C	CDP	1.12			
	UDP	1.84	0.10 M KH_2PO_4	5.45	0
	GDP	2.96	0.10 M NH_4OAc		
	ADP	7.28			
D	CTP	0.44	0.10 M KH_2PO_4		
	UTP	0.76	0.30 M NH_4Cl	7.00	0
	GTP	1.12			
	ATP	2.88			
E	AMP	1.02	0.10 M KH_2PO_4		
	ADP	1.88		7.20	18
	ATP	2.52			
F	Uridine	0.40			
	Cytidine	0.64	0.20 M HOAc		
	Guanosine	0.92		4.60	15
	Adenosine	2.56			
G	Uracil	0.32			
	Cytosine	0.68	0.20 M KH_2PO_4	3.00	15
	Guanine	0.92			
	Adenine	1.52			

[a] Capacity ratio. [b] TBHS and *d*-camphorsulfonic acid, 0.025 M, were in the aqueous buffer for chromatographic separations A-E and F-G, respectively. [c] NaOH was added to give the pH shown.

Apparatus. A model ALC 202 liquid chromatograph equipped with a model 660 solvent programmer, model 6000 pumps, a 254-nm UV detector and a model 400 loop (30 μL size) injector (Waters Associates, Milford, Mass.) was used. The 10-mV recorder used was purchased from Sargent-Welch Scientific Co. (Skokie, Ill.). The ultrasonic vibrator used in column packing was bought from L & R Manufacturing Co. (Kearny, N.J.). A Vortex Jr. vibrator from Scientific Industries, Inc. (Queens Village, N.Y.) was used. A Zeromatic pH meter from Beckman Instruments, Inc. (Fullerton, Calif.) was used.

Column Preparation. *Column Packing.* Spherisorb ODS was coated twice again using trichlorooctadecylsilane reagent (*16*). The carbon content of the doubly recoated packing was 13.9% by wt. (Chemalytics, Tempe, Ariz.).

A viscosity packing method was used (*17*). A mixture of 5 g of the treated Spherisorb ODS and 10 mL methanol was vibrated in an ultrasonic vibrator for 10 min. The methanol was decanted, and 25 mL of cyclohexanol was added to the Spherisorb. The methanol helped wet the solid particles and depressed the freezing point of the cyclohexanol. The mixture was stirred with a vortex mixer and then degassed by ultrasonic, vibration, each for 10 min. The mixture was slurry packed using the Waters 6000 pump at or near its pressure limit of 6000 psi into a 4.6 mm i.d. × 25 cm long stainless steel column equipped with frits and no dead volume unions. The plate number of the column was 3500 as measured with naphthalene as solute and methanol/water (80/20) as mobile phase.

Solvophobic Ion Introduction and Removal. The mobile phase containing the solvophobic ion was pumped through the reversed phase column for 60 min at a flow rate of 1 mL/min prior to the first time it was used. This time was more than enough to reach equilibrium between ion in the mobile and stationary phases. It was our experience that if the columns were flushed by pumping water through for 20 min at a rate of 1 mL/min and the ends then plugged, they could be stored and then regenerated to give the same characteristics, provided the storage time did not exceed one week. Removal of the last small amounts of solvophobic ion was accomplished by pumping 0.50 M ammonium acetate for 10 min and then methanol for 60 min both at a 1 mL/min flow rate. The column then had the same characteristics as the original reversed phase column.

In gradient elution, initial solvent was pumped between runs for 10 min at a rate of 1 mL/min. In this time, the column was reequilibrated for the next separation.

Procedure. Injections of 5–20 μL of solutions were made in isocratic studies. The concentrations of nucleotides, nucleosides, and their bases in these solutions were chosen so as to give chromatographic peaks of 30–80% full scale at 0.16 to 0.32 aufs. Normally, this meant 3–10 μg of each solute injected. In gradient elution, 10–40 μg of each solute was injected, and the attenuation was adjusted to give 0.64 aufs.

Gradient elution followed a concave curve (curve 8 on the Waters programmer).

Final chromatographic conditions reported in this paper were the result of changes in concentration of buffers, pH, and methanol concentrations that followed runs which were unsatisfactory because retentions were too short or long or there was too much band spreading.

Quantitative Studies. All the nucleotides, nucleosides, and bases reported in this paper were chromatographed isocratically over a range of injection amount of 0.1–1 nmol. Injection volume was the same but the concentration of solute was varied. In gradient elution chromatography only UMP, ADP, and cAMP were quantitatively studied over the same injection range.

Four injections were made. In all cases, a plot of peak height vs. amount injected gave a straight line with zero ordinate–abscissa intercepts.

RESULTS

Table I presents the mobile phase composition and capacity ratios in isocratic separations of nucleotides, nucleosides, and their bases. In the great majority of separations, baseline peak resolution was achieved.

In separation A, monophosphate separation, the capacity ratios were significantly different. At the pH of the eluent,

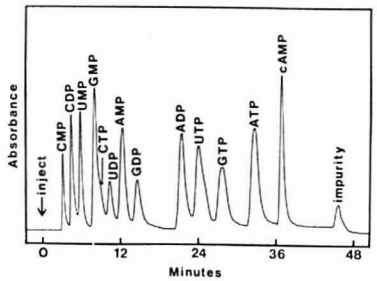

Figure 1. Gradient elution separation of ribonucleotides. Mobile phase: (A) 0.025 M TBHS, 0.050 M KH_2PO_4, 0.080 M NH_4Cl buffer at pH 3.90. (B) 0.025 M TBHS, 0.10 M KH_2PO_4, 0.20 M NH_4Cl buffer at pH 3.40, 30% methanol. Operating conditions: 40-min gradient program

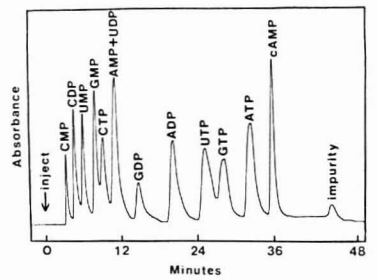

Figure 2. Gradient elution separation of ribonucleotides. Mobile phase: (A) 0.025 M TBHS, 0.050 M KH_2PO_4, 0.070 M NH_4Cl buffer at pH 3.90. (B) Same as in Figure 1 B. Operating conditions: 40-min gradient program

3.90, the pK_as (*18*) of the nucleotides dictate that CMP was slightly negatively charged, UMP and GMP were predominantly negatively charged, and AMP was about half negatively charged. Under conditions used to produce this separation, cyclic AMP had a very long retention time. Therefore, conditions were altered to produce separation B. Here GMP had a double negative charge; AMP had slightly more than a single negative charge, and cyclic AMP probably had slightly more than one negative charge. Under these conditions GMP, UMP, and CMP were not resolved.

In separation C, all of the diphosphates were negatively charged, and their order of appearance was the same as that found for the monophosphates. Likewise the triphosphates, listed as separation D, were all negatively charged and were separated in the same order as the monophosphates.

Because of the interest in 5′-adenosine phosphates, the mono-, di-, and triphosphate derivatives were separated as a group as shown under separation E. Although at the pH of this experiment all were negatively charged, the magnitude of the charge increased with increasing retention time.

Figures 1 and 2 show a gradient elution separation of the 12 nucleoside 5′-phosphates and cyclic AMP. The separation of all of these could not be done isocratically. Even with gradient elution, the separation of the GMP and CTP pair and the AMP and UDP pair required two sets of chromatographic conditions.

Separation F was a separation of the nucleosides themselves. At pH 4.60, U, G, and A are electrically neutral, and C is predominantly neutral with some positively charged species in equilibrium (*19*). The bases were separated in separation G. At pH 3.0, uracil is neutral, guanine is predominantly positive, and cytosine and adenine are completely positive for all practical purposes (*19*).

DISCUSSION

Knox (*20*) and more recently Kissinger (*21*) have pointed out that reversed phase ion pair chromatography can be viewed as an ion-exchange phenomenon. In fact, Kissinger suggests the concept of a solvophobic ion complexing with a solute ion and partitioning between the polar mobile and the nonpolar stationary phase is in general incorrect. Instead, the solvophobic ion should be viewed as equilibrating between the two phases, and its presence in the stationary phase makes it the analogue of a nonexchangeable ion. In this condition, it attracts the solute oppositely charged ion as would an ionic site on a permanent ion exchange column.

We have found this model very helpful in selecting experimental conditions for separating charged solutes. And it was this model that helped us choose conditions for the separation of nucleotides, nucleosides, and their bases reported in this paper. Additional evidence that this model better describes what is happening than ion pair partition is that we observe a lasting effect of the solvophobic ion after it has been removed from the mobile phase. After using the solvophobic ion in a column, only slowly does the chromatogram change to that observed when no solvophobic ion is used. Many retention volumes are required to remove the solvophobic ion effect. We interpret this to mean the solvophobic ion is retained by the column for a long time. While it is there, it is causing, or at least contributes to, the affinity for the solute.

Our results in nucleotide, nucleoside, and base chromatography can in large part be rationalized with this view of the separation process in mind. With the exception of AMP, the order of nucleotide retention times in separation A of Table I follows the predicted order for a positively charged column surface. CMP is retained least because it is least negatively charged, and GMP, being negatively charged, has significant retention. AMP's strong retention is probably the result of strong solvophobic interaction with the stationary reversed phase not connected with ion affinity.

Cyclic AMP is formed structurally from AMP by removal of hydroxyl groups of the phosphoric acid and monosaccharide 3′-alcohol moieties and replacing them with an ester oxygen linkage. This should lower the polar interaction of cyclic AMP with the mobile phase and, thereby, raise its concentration in the stationary phase compared to AMP. Thus, cyclic AMP had a longer retention time than AMP as shown in separation B of Table I. Brown also found, when using an anion-exchange column, that cyclic AMP is retained longer than AMP (*22*).

Separations C and D indicate that the number of negative charges on the nucleotide and the stationary reversed phase interaction govern the retention of di- and triphosphate nucleosides. Separation E shows exactly what is expected for an anion-exchange separation of mono-, di-, and triphosphates of adenosine (*23, 24*). The order is opposite of that observed in reversed phase chromatography alone (*4*).

The order of appearance of peaks in the gradient elution chromatograms shown in Figures 1 and 2 can be rationalized in terms of charge and stationary reversed phase interaction. The impurity peak has been observed by others (*25*) and results from a KH_2PO_4 impurity.

The nucleoside separation F was done under conditions of almost complete electrical neutrality for the solutes. Adenosine was again strongly attracted, and this can be viewed as a solvophobic interaction with the stationary reversed phase. The slight positive nature of cytidine may explain its exchange of chromatogram positions with uridine as compared to nucleoside separations with a reversed phase column (*3*). Over a pH range of 4.2–5.0, cytidine's peak could be moved, but

it always remained between uridine and guanosine. As predicted for uncharged species, the other three peaks did not move over this pH range. The separation of bases G was consistent with the nucleoside separation F. Ion exchange alone does not tell the whole story. Stationary reversed phase interaction also plays a role.

Methanol was used as a co-solvent in the majority of the separations shown in Table I and Figures 1 and 2. Methanol always reduced the solutes' retention times. Of course, too much methanol led to loss of resolution. Although methanol concentration was not investigated in detail, it appeared that there was a concentration range of methanol below which loss of resolution occurred too.

In some instances, salt effects were observed. For example, the retention times of the monophosphates in separation A could be reduced considerably by the addition of ammonium chloride to make the mobile phase 0.10 M in it. CTP, UTP, and GTP could be better resolved than in separation D by a decrease of ammonium chloride to 0.20 M; however, ATP's retention time then became very long. The changes in separation, e.g. of AMP and UDP, in Figures 1 and 2 were effected by merely changing the ammonium chloride concentration in one of the mobile phases from 0.080 to 0.070 M.

The packing was coated three times with octadecyl groups in order to provide a stationary phase surface rich in nonpolar groups. This was done to increase the stationary phase surface concentration of solvophobic ions.

To test whether the conditions used for isocratic chromatography permitted quantitative determination of nucleotides, nucleosides, and bases, plots of peak height vs. amount injected were made for all the conditions used. In all cases, straight lines with zero intercepts were obtained. Thus, the chromatographic conditions gave quantitation. UMP, ADP, and cyclic AMP gave similar plots under gradient elution conditions. It was assumed that all of the nucleoside phosphates could be quantitatively determined by gradient elution since these three indicated no problems were present.

CONCLUSION

The reversed phase column has become the most useful column in high performance liquid chromatography. With this column, the chromatographer can successfully separate nucleotides in the normal mode. As an alternative, tetra-*n*-butylammonium ion can be introduced into the mobile phase to obtain a different separation. The order of nucleotide elutions is different in the two modes. Likewise, the same column can be used with or without 10-camphorsulfonate ion to obtain two different orders of separation of either a group of nucleosides or a group of their bases. Thus, the use of solvophobic ions gives an added dimension to separations of nucleotides, nucleosides, and their bases by reversed phase columns.

LITERATURE CITED

(1) P. R. Brown, S. Bobick, and F. L. Hanley, *J. Chromatogr.*, **99**, 587 (1974).
(2) R. A. Hartwick and P. R. Brown, *J. Chromatogr.*, **112**, 651 (1975).
(3) R. A. Hartwick and P. R. Brown, *J. Chromatogr.*, **126**, 679 (1976).
(4) F. S. Anderson and R. C. Murphy, *J. Chromatogr.*, **121**, 251 (1976).
(5) S. Eksborg, P. Lagerström, R. Modin, and G. Schill, *J. Chromatogr.*, **83**, 99 (1973).
(6) J. H. Knox and J. Jurand, *J. Chromatogr.*, **103**, 311 (1975).
(7) K.-G. Wahlund, *J. Chromatogr.*, **115**, 411 (1975).
(8) W. Santi, J. M. Huen, and R. W. Frei, *J. Chromatogr.*, **115**, 423 (1975).
(9) B.-A. Persson and P.-O. Lagerström, *J. Chromatogr.*, **122**, 305 (1976).
(10) B. Fransson, K.-G. Wahlund, I. M. Johansson, and G. Schill, *J. Chromatogr.*, **125**, 327 (1976).
(11) K.-G. Wahlund and U. Lund, *J. Chromatogr.*, **122**, 269 (1976).
(12) S. C. Su, A. V. Hartkopf, and B. L. Karger, *J. Chromatogr.*, **119**, 523 (1976).
(13) J. H. Knox and G. R. Laird, *J. Chromatogr.*, **122**, 17 (1976).
(14) J. H. Knox and J. Jurand, *J. Chromatogr.*, **125**, 89 (1976).
(15) E. Fitzgerald, *Anal. Chem.*, **48**, 1735 (1976).
(16) R. K. Gilpin, J. A. Korpi, and C. A. Janicki, *Anal. Chem.*, **47**, 1498 (1975).
(17) J. Asshauer and I. Halász, *J. Chromatogr. Sci.*, **12**, 139 (1974).
(18) W. E. Cohn, *J. Am. Chem. Soc.*, **72**, 1471 (1950).
(19) E. Harbers, G. F. Domagk, and W. Müller, "Introduction to Nucleic Acids", Reinhold Book Corp., New York, N.Y., 1968, pp 25–26.
(20) J. H. Knox in "High Pressure Liquid Chromatography in Clinical Chemistry", P. F. Dixon, C. H. Gray, C. K. Lim, and M. S. Stoll, Ed., Academic Press, New York, N.Y., 1976, p 6.
(21) P. T. Kissinger, *Anal. Chem.*, **49**, 883 (1977).
(22) P. R. Brown, *J. Chromatogr.*, **52**, 257 (1970).
(23) P. R. Brown, R. E. Parks, and J. Herod, *Clin. Chem.* (*Winston-Salem, N.C.*), **19**, 919 (1973).
(24) R. A. Henry, J. A. Schmit, and R. C. Williams, *J. Chromatogr. Sci.*, **11**, 358 (1973).
(25) H. W. Shmukler, *J. Chromatogr. Sci.*, **8**, 581 (1970).

RECEIVED for review May 20, 1977. Accepted September 16, 1977. One of the authors (J.C.L.) thanks Marquette University for a University Fellowship.

Simultaneous Determination of Chlordiazepoxide and Its *N*-Demethyl Metabolite in 50-μL Blood Samples by High Pressure Liquid Chromatography

Hebe B. Greizerstein* and Caryn Wojtowicz

Research Institute on Alcoholism, New York State Department of Mental Hygiene, 1021 Main Street, Buffalo, New York 14203

A method for the determination of chlordiazepoxide and its *N*-demethyl metabolite in 50-μL samples of mice blood by high pressure liquid chromatography has been developed. The drugs together with an internal standard (chlorpromazine) were extracted from alkalinized whole blood with heptane containing 1.5% isoamyl alcohol. The separation was achieved by the use of a solvent gradient program where the eluant was a mixture of 1 mM KH_2PO_4 (pH 8.0) and methanol. The method was reproducible at levels ranging from 0.1 to 10 μg/mL and it is routinely possible to detect as little as 0.1 μg/mL of the compounds in a 50-μL sample. The use of a small volume of sample allowed for the serial sampling of blood from the same animal. The method was tested to determine the concentration of these substances in blood of mice injected ip with a 30 mg/kg dose of chlordiazepoxide.

There is an increasing need for sensitive and precise methods for measuring the concentration of chlordiazepoxide (7-chloro-2-methylamino-5-phenyl-3*H*-1,4-benzodiazepine-4-oxide) and its *N*-demethyl metabolite (7-chloro-2-amino-5-phenyl-3*H*-1,4-benzodiazepine-4-oxide) in blood and biological fluids both for research purposes and for monitoring therapy.

Several methods using colorimetry (*1*, *2*), fluorometry (*3*), gas chromatography (*4–8*) and differential pulse polarography (*9*) have been reported. These methods are directed specifically toward the determination of chlordiazepoxide and are not suited for small volume samples.

Work in our laboratory required a microscale method for accurate measurement of chlordiazepoxide and its *N*-demethyl metabolite levels in serial small samples of blood from a single mouse. This report presents a simple and accurate method of quantification using reverse phase high pressure liquid chromatography and the addition of an internal standard.

EXPERIMENTAL

Apparatus. The analyses were carried out in a Waters Associates Liquid Chromatograph equipped with a Model 440 Absorbance Detector (254 nm fixed wavelength), a dual pumping and solvent programmer system, a U6K Universal injector, and a 10-mV recorder. The separation of the drug and its metabolite was achieved using a 4 mm i.d. × 30 cm μ Bondapak C_{18} column (Waters Associates) and the programmed elution of solvent (curve 2) at a flow rate of 2 mL/min. The eluant used was a solution consisting of 1 mM KH_2PO_4 buffer (pH 8.0) and methanol at an initial composition of 60:40 v/v that changed to 10:90 v/v final solution in a 3-min period. After the completion of a run, the program was reversed and an additional 2-min period was required for the column to stabilize before the next injection was made.

Reagents. Methyl alcohol was acquired from Burdick & Jackson; all the other chemicals used were reagent grade. The drug standards were obtained from Applied Science Laboratories (chlorpromazine, chlordiazepoxide) and Hoffmann-LaRoche (*N*-demethyl chlordiazepoxide).

Sensitivity and Linearity Response of the Detector. Standard solutions were prepared by volumetric dilution in methanol of stock solutions of the drugs to produce concentrations of chlordiazepoxide and *N*-demethyl chlordiazepoxide in the range of 0 to 5 μg/mL. The concentration of chlorpromazine (internal standard) was kept constant at a 1 μg/mL level. Aliquots of the samples (20 μL) were injected in duplicate into the chromatograph.

Recovery. Whole blood standards were prepared by adding to a series of 50-μL drug-free blood samples, 10 μL of methanol solutions containing different amounts of the compounds of interest. The final concentrations achieved were in the 0.1 to 10 μg/mL range. These standards were extracted as in the procedure for blood samples.

Extraction Procedure. To 50 μL of blood in a Teflon lined, screw capped test tube, 10 μL of a 50 μg/mL chlorpromazine HCl methanol solution (internal standard) was added. The pH of the mixture was adjusted to 9.0 with 125 μL of 0.1 N NaOH. The extraction was carried out by the addition of 3 mL of heptane containing 1.5% isoamyl alcohol. The mixture was vortexed for 2 min and centrifuged on a clinical bench centrifuge for 15 min. The organic layer was removed to a second test tube and evaporated to dryness under a gentle stream of nitrogen. The dried extract was reconstituted with 100 μL of methyl alcohol, vortexed, and 20-μL aliquots were injected twice into the liquid chromatograph.

At the beginning of our studies, we used phosphate buffer (pH 9.0) instead of NaOH to achieve the right pH in the aqueous solution previous to its extraction with the organic solvent. The chromatograms of those extracts showed interfering peaks that made difficult the identification and quantitation of the compounds of interest. Presently, we do not have an explanation on the nature of those interferences.

Drug Blood Levels in Mice. A group of 15 male CF-1 mice 25–34 g in weight, were injected ip with 30 mg/kg chlordiazepoxide HCl in isotonic saline solution. Tail vein samples, each 50 μL in volume, were obtained only twice from each mouse allowing an interval of 2 h between samples. The time periods studied were 10, 30, 60, 120, and 180 min and 5 blood samples were collected for each point. A parallel set of whole blood standards was prepared by adding to drug-free blood known amounts of chlordiazepoxide and *N*-demethyl metabolite in methanol to produce concentrations in the range of 0 to 10 μg/mL. The blood standards and samples were extracted simultaneously. The concentrations of the compounds in the blood samples were determined using the blood standards as the calibrating solutions. This procedure minimizes the differences in recovery rates.

Calculations. Peaks on the chromatogram were identified by their retention times relative to the internal standard. The concentration of the drugs was calculated on the basis of the ratio of their peak heights to that of the chlorpromazine internal standard.

RESULTS AND DISCUSSION

Sensitivity and Linearity. The detection limit for chlordiazepoxide and its *N*-demethyl metabolite is 2 ng of compound injected in the chromatograph. The response curves for chlordiazepoxide and *N*-demethyl chlordiazepoxide were found to be linear ($y = -0.024 + 0.596\,x$ and $y = -0.171 + 0.935\,x$, respectively) from the limit of detection near 2 ng to the higher sample size studied. The correlation coefficients calculated for the regression lines were 0.99 and 0.97, respectively. Using a sample size of 50 μL of blood, the drug and its metabolite were readily quantitated to 0.1 μg/mL.

Recovery. These data were calculated by the amount of drug detected after extraction of blood samples to which the pure compounds were added in relation to the concentration

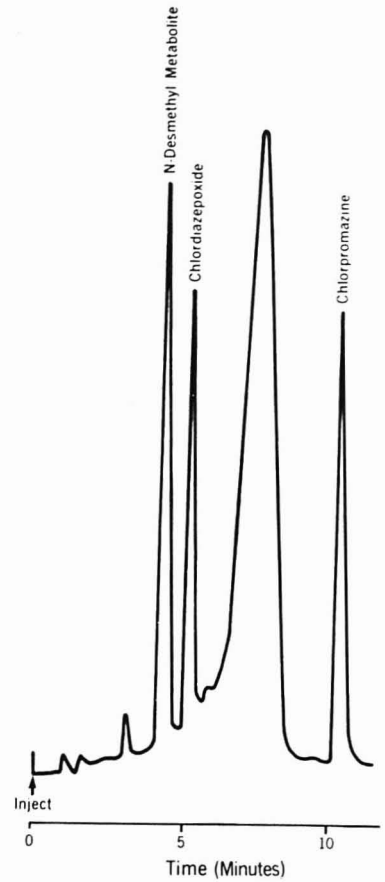

Figure 1. Chromatogram of the extract of a blood sample taken from a mouse injected with chlordiazepoxide

of these pure compounds in methanol solutions. Recovery was found to be 89 ± 3, 68 ± 2, and 94 ± 4% for chlordiazepoxide, *N*-demethyl chlordiazepoxide, and chlorpromazine, respectively.

Drug-Blood Levels in Mice. A characteristic chromatogram of a blood sample taken 10 min after the administration of chlordiazepoxide is shown in Figure 1. The peak appearing between the chlordiazepoxide and chlorpromazine peaks was due to the solvent program used for the separation. The run was completed in 20 min and interfering peaks were not observed in the series of blood samples. Calibration curves were calculated from the set of blood standards, $0.014 + 1.27\ x$, and $-0.023 + 119\ x$ for the drug and the *N*-demethyl metabolite. Although chlorpromazine eluted after the large peak because of some impurity, the reproducibility of the results provides enough justification for its use as the internal standard.

The concentrations of drug in blood of mice injected with chlordiazepoxide solutions are represented in Figure 2. Chlordiazepoxide was not detected in the samples taken 2 and

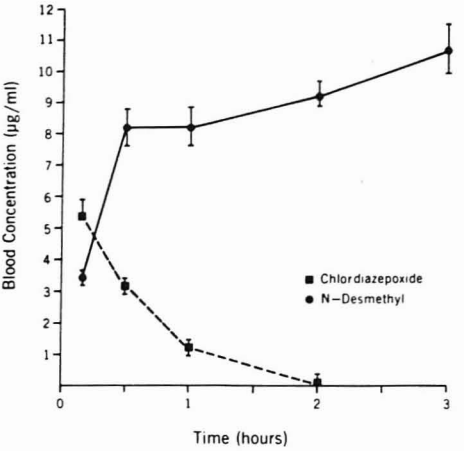

Figure 2. Drug concentration curves in blood of mice after administration ip of 30 mg/kg chlordiazepoxide. Each point represents the mean of 5 samples ± S.E.M.

3 h after administration of the drug, while the *N*-demethyl metabolite had reached a plateau level after 30 min.

We have attempted the identification of demoxepam, another of the metabolites of chlordiazepoxide. Under the described chromatographic conditions, this substance has a shorter retention time and similar limit of detection as *N*-demethyl chlordiazepoxide. However, its recovery from blood by the extraction procedure here presented is very low (<5%). A second extraction at a different pH value is required to improve its recovery. Demoxepam was not detected in the blood samples obtained from mice injected with chlordiazepoxide and extracted as described in the method section.

The small volume of sample needed for the present method allows the determination of complete curves for the concentration of chlordiazepoxide and its *N*-demethyl metabolite in individual animals at reasonable times without significant risks. The number of samples taken from the same animal in this report was kept to a minimum of two; however, more frequent sampling is possible. Presently, this study is being extended to follow the concentration curves for longer periods of time by obtaining 50-µL blood samples from the same mice every hour.

ACKNOWLEDGMENT

The authors gratefully thank Iris G. McLaughlin for her technical assistance and Hoffmann-LaRoche for the supply of *N*-demethylchlordiazepoxide.

LITERATURE CITED

(1) P. Jatlow, *Clin. Chem.* (*Winston-Salem, N.C.*), **18**, 516 (1972).
(2) C. S. Frings and P. S. Cohen, *Am. J. Clin. Pathol.*, **58**, 216 (1971).
(3) B. A. Koechlin and L. D'Arconte, *Anal. Biochem.*, **5**, 195 (1963).
(4) F. Marcucci, R. Fanelli, and E. Mussini, *J. Chromatogr.*, **37**, 318 (1968).
(5) L. B. Foster and C. S. Frings, *Clin. Chem.* (*Winston-Salem, N.C.*), **16**, 177 (1970).
(6) H. F. Proelss and H. J. Lohmann, *Clin. Chem.* (*Winston-Salem, N.C.*), **17** 222 (1971).
(7) I. A. Zingales, *J. Chromatogr.*, **61**, 237 (1971).
(8) J. A. F. deSilva, I. Bekersky, C. V. Puglisi, M. A. Brooks, and R. E. Weinfeld, *Anal. Chem.*, **48**, 10 (1976).
(9) M. R. Hackman, M. A. Brooks, J. A. F. deSilva, and T. S. Ma, *Anal. Chem.*, **46**, 1075 (1974).

RECEIVED for review June 10, 1977. Accepted September 1, 1977.

Identification of Nucleosides and Bases in Serum and Plasma Samples by Reverse-Phase High Performance Liquid Chromatography

Anté M. Krstulovic, Phyllis R. Brown,* and Douglas M. Rosie

Department of Chemistry, University of Rhode Island, Kingston, Rhode Island 02881

Nucleosides and bases in plasma and serum samples were identified using multiple or variable wavelength detectors by two techniques: absorbance ratios and the enzymatic peak shift. Compounds such as uric acid and xanthine, which fluoresce, were further identified using a fluorescence detector with an excitation wavelength of 325 nm and a cut-off filter at 340 nm. A peak which appeared in all the samples and was not a nucleic acid component was identified as tryptophan by using the fluorescence detector. These techniques can be used alone or in combination for peak identification.

Sensitive analyses of nucleosides and bases can now be achieved rapidly and accurately by the reverse-phase partition mode of high pressure liquid chromatography (HPLC) (*1–4*). In preliminary work it was found that nucleoside and base composition and levels vary in serum and plasma samples from patients suffering from various diseases (*1*, *2*). For the chromatograms of biological samples to be useful, the peaks in the chromatograms must be identified unambiguously. If possible, on-line identification is preferred to minimize post-chromatographic handling errors. Retention times alone are not sufficient for positive identification and other corroborative information is needed. Mass spectrometry can provide unambiguous identification of many compounds, but its use is limited in the analysis of nucleic acid components because of their low volatility. IR and NMR spectra of collected fractions have limited applicability since these techniques require relatively large amounts of pure compounds. UV spectra have been used for many years in identification of nucleic acid components. However, UV spectra taken alone are sometimes difficult to interpret, especially when dealing with closely related compounds or mixtures of these compounds.

The development of the dual and variable wavelength UV detectors for HPLC has opened up new possibilities for the characterization of peaks in HPLC eluates. Peaks in serum chromatograms which were detected by UV spectroscopy can be characterized using two different techniques: absorbance ratios and the enzymatic peak shift technique. By measuring absorbances at different wavelengths, it is possible to use the computed ratios for determination of peak identity and purity. This technique has proved to be useful in other studies of UV-absorbing species in HPLC eluates (*5*). The enzymatic peak shift has been shown to be a simple and elegant method of peak identification for nucleotides (*6–8*) and preliminary work has been done with nucleosides and bases (*1*, *2*). This technique utilizes the specificity of an enzyme in catalyzing a reaction. It can be used to identify either a specific compound, or a group of compounds.

Although fluorescence detectors are extremely sensitive, they have not been used widely with nucleic acid components because the majority of the nucleosides and bases do not fluoresce. However, uric acid which may be present in serum or plasma fluoresces and derivatization of compounds which ordinarily do not fluoresce makes possible very sensitive detection and identification of these compounds (*9–12*).

This technique has recently been applied to studies involving low levels of adenosine in biological samples (*13*).

In this article, the use of absorbance ratios, enzymatic peak shifts, and fluorescence is reported for the identification of peaks in chromatograms of the cold acid extracts of serum and plasma samples.

EXPERIMENTAL

A Waters Associates Model 6000 A Solvent Delivery System, Model U6K Universal Injector, and a dual wavelength (254 nm/280 nm) Model 440 Absorbance Detector were used in all determinations. A variable wavelength detector Model SF 770 Spectroflow Monitor and a FS 970 L. C. Fluorometer (Schoeffel Instrument Corp., Westwood, N.J.) were also used. The column was a microparticle reverse-phase μ Bondapak/C_{18} from Waters Associates. Gradients were electronically generated by means of a solvent programmer. Peak heights at 254 nm and 280 nm were simultaneously recorded on a two-pen recorder, and areas were electronically integrated using a Hewlett-Packard Model 3380 Integrator (Hewlett-Packard, Avondale, Pa.).

Chromatographic conditions: Reagent grade potassium dihydrogen phosphate was obtained from Mallinckrodt Chemical Works (St. Louis, Mo.). The low concentration eluent of 0.02 F KH_2PO_4 prepared in distilled water, was filtered through a millipore membrane filter, type HA, pore size 0.45 μm, (Millipore Corporation, Bedford, Mass. 01730). The pH of the solution was adjusted to 5.5 with a dilute potassium hydroxide solution. Methanol, which was used in the preparation of the high concentration eluent, was distilled in glass (Burdick & Jackson, Inc., Muskegon, Mich.). A 60/40 methanol–water solution was prepared by mixing appropriate volumes of each solvent after which the mixture was degassed under vacuum. A 35-min linear gradient from 0% of the low concentration eluent to 40% of the high concentration eluent was used in all determinations.

The full strength high concentration eluent was used to purge the column periodically. The flow rate was 1.5 mL/min and the analyses were carried out at ambient temperature.

Materials. 1,1,2-Trichlorotrifluoroethane (Freon) was purchased from Matheson Gas Products, (East Rutherford, N.J.), tri-*n*-octylamine (amine) from ICN Pharmaceuticals, Inc., (Plainview, N.Y.) and trichloroacetic acid and trizma base from Sigma Chemical Co., (St. Louis, Mo.). The enzymes, xanthine oxidase (E.C. No. 1.2.3.2.), purine nucleoside phosphorylase (E.C. No. 2.4.2.1.), guanase (E.C. No. 3.5.4.3.), and adenosine deaminase (E.C. No. 3.5.4.4.) and the standards, adenosine (ADO), *N*-methyladenosine (6 MeADO), guanosine (GUO), N^2-methylguanosine (2 MeGUO), inosine (INO), 1-methylinosine (1 MeINO), xanthosine (XAO), thymidine (*d*-THD), uridine (URD), and cytidine (CYD), and the bases, adenine (ADE), guanine (GUA), hypoxanthine (HYP), xanthine (XAN), 1,3-dimethylxanthine (1,3-Me_2XAN), 3,7-dimethylxanthine (3,7-Me_2XAN), as well as uric acid, caffeine and L-tryptophan (L-TRP) were purchased from Sigma Chemical Co. (St. Louis, Mo.). N^2,N^2-dimethylguanosine (2-Me GUO) was purchased from Vega-Fox Biochemicals (Tuscon, Ariz.). Standard solutions were prepared at a concentration of 1 mM in a solution of 0.01 F KH_2PO_4, pH 5.5.

Table I. Reactions and Conditions for Some Enzymatic Peak Shifts Used in This Study; XOD, Xanthine Oxidase; PNP, Purine Nucleoside Phosphorylase; and Guanase

HYPOXANTHINE + H_2O + O_2 $\xrightarrow[pH 7.8, 25°C]{XOD}$ XANTHINE + H_2O_2

XANTHINE + H_2O + O_2 $\xrightarrow[pH 7.8, 25°C]{XOD}$ URIC ACID + H_2O_2

INOSINE + PHOSPHATE $\xrightarrow[pH 7.4, 25°C]{PNP}$ HYPOXANTHINE + RIBOSE-1-PHOSPHATE

GUANOSINE + PHOSPHATE $\xrightarrow{PNP}$ GUANINE + RIBOSE-1-PHOSPHATE

XANTHOSINE + PHOSPHATE $\xrightarrow{PNP}$ XANTHINE + RIBOSE-1-PHOSPHATE

ADENOSINE + PHOSPHATE $\xrightarrow{PNP}$ ADENINE + RIBOSE-1-PHOSPHATE

GUANINE + H_2O $\xrightarrow[pH 8.0, 25°C]{GUANASE}$ XANTHINE + NH_3

Sample Preparation. To obtain serum samples, freshly drawn blood was transferred to a tube without anticoagulant. The blood clotted spontaneously when it was allowed to stand for 10 to 15 min at room temperature. The supernatant fluid was then spun down at 630 × *g* for 10 min to remove any contaminating white cells. To each milliliter of serum, 2 mL of cold trichloroacetic acid (TCA), 6% by weight, were added dropwise, while the tube was being vortexed at a moderate speed. After all the TCA had been added, the tube was vortexed for 5 more seconds and then allowed to stand. The solution was then centrifuged for 3 min at 630 × *g* to separate the cell protein. The supernatant fluid was filtered through a plastic Millipore filter (Swinnex-25). The filtrate was transferred to another test tube and 1 mL of a 0.5 F amine–Freon solution was added for every milliliter of filtrate. The mixture was vortexed for 3 min and then centrifuged for 3 min at 50 × *g*. The top layer, which contained the nucleosides and bases, was transferred to a plastic vial and its pH adjusted with solid trizma base to approximately 7.

For the preparation of plasma samples, freshly drawn blood was collected in Vacutainer tubes containing either acid–citrate–dextrose or heparin as the anticoagulant. To 9 mL of whole blood, 1 mL of a sterile 6% solution of dextran in normal saline was added and the mixture stirred gently but thoroughly. The mixture was then transferred to a 30-mL plastic syringe held at a 45° slant and allowed to stand for 30 min. After the red cells were completely precipitated, the top layer containing plasma and white cells was withdrawn and centrifuged at 50 × *g* for 10 min. The supernatant plasma was separated from the white cell pellet and the nucleic acid components were extracted from the plasma using the same procedure as with the serum.

Absorbance Ratios. Ratios of absorbance at 254 nm and 280 nm were computed for the standards and compared with the ratios for the peaks of interest in the serum and plasma chromatograms.

Enzymatic Peak Shift. In carrying out enzymatic reactions, an aliquot (50–75 μL) of the deproteinized serum or plasma sample was first chromatographed. To another aliquot of the same volume, 5–10 μL of an enzyme solution was added after the solution was buffered to a pH needed for carrying out the enzymatic reaction. The conditions of analysis and the reactions catalyzed are listed in Table I. An appropriate volume of the incubated sample was analyzed by HPLC, taking into account the dilution of the solution. In some cases where the specific enzyme for a particular reaction was not commercially available, a general enzyme was used, and the product of that reaction was then reacted with a specific enzyme.

Fluorescence Detection. Fluorescence was used to detect selectively and identify uric acid which was not resolved from other early eluting compounds in serum or plasma samples. Since very few naturally occurring serum constituents fluoresce, by using the excitation wavelength for uric acid (325 nm) it is possible to detect this biologically important compound sensitively and selectively. Fluorescence was also used to characterize an unknown peak in serum and plasma chromatogram which was found to be L-tryptophan.

Peak Identification. Chromatographic peaks of the serum and plasma samples were first identified tentatively on the basis of retention times and comparison with standards. A known quantity of standards was then added to the sample and a quantitative increase in the area of a specific peak was taken as a further characterization of the peak. Absorbance ratios of the standards were compared to those of the unknown peaks. To support the findings, the enzymatic peak shift was used to identify peaks whenever an appropriate enzyme was commercially available. Further identification was obtained where possible by use of a fluorescence detector.

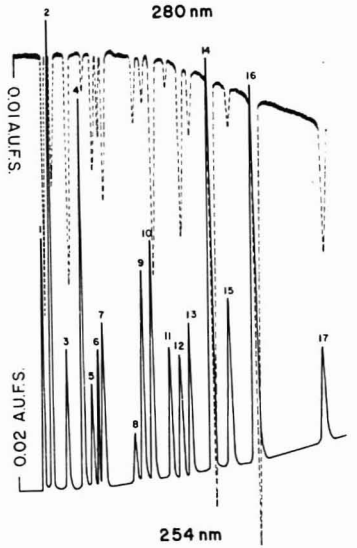

Figure 1. Separation of some nucleosides and bases detected at 254 nm and 280 nm; (1) cytosine, (2) uracil, (3) cytidine, (4) hypoxanthine, (5) xanthine, (6) uridine, (7) thymine, (8) xanthosine, (9) inosine, (10) guanosine, (11) adenosine, (12) thymidine, (13) 1-methylinosine, (14) N^2-methylguanosine, (15) adenosine, (16) N^2,N^2-dimethylguanosine, and (17) N^6-methyladenosine. Chromatographic conditions: column, μ Bondapak/C_{18}, gradient, linear in 35 min from 0% of 0.02 F KH_2PO_4; pH 5.5 to 40% of 60/40 (v/v) CH_3OH/H_2O; flow rate, 1.5 mL/min; temperature, ambient

Table II. Peak Height Ratios (254 nm/280 nm) for Some Standard Nucleosides and Bases. Ratios Were Averaged from Triplicate Runs

1	CYT	1.91 ± 0.02	10	GUO	2.18 ± 0.03
2	URA	3.02 ± 0.04	11	ADE	11.00 ± 0.04
3	CYD	1.20 ± 0.03	12	dTHD	1.42 ± 0.04
4	HYP	19.70 ± 0.02	13	1MeINO	4.61 ± 0.02
5	XAN	1.73 ± 0.03	14	2MeGUO	1.94 ± 0.03
6	URD	3.42 ± 0.02	15	ADO	8.03 ± 0.04
7	THY	2.22 0.04	16	$2Me_2$GUO	1.68 ± 0.05
8	XAO	1.57 ± 0.03	17	6MeADO	1.45 ± 0.02
9	INO	8.52 ± 0.01			

RESULTS

Chromatograms of standards were obtained using the UV detector at wavelengths of 254 nm and 280 nm (Figure 1). The ratios of the peak heights were averaged from triplicate runs (Table II) and used for comparison with the ratios of unknown peaks in serum and plasma extracts. The peak height ratios vary significantly from compound to compound. In the case of thymidine (Figure 1, peak 12) and 6-methyladenosine (Figure 1, peak 17), the peak height ratios are similar, but since the retention times of the two compounds are different, there is no possibility of confusing the two compounds. Absorbance ratios are particularly useful to distinguish closely eluting compounds like hypoxanthine,

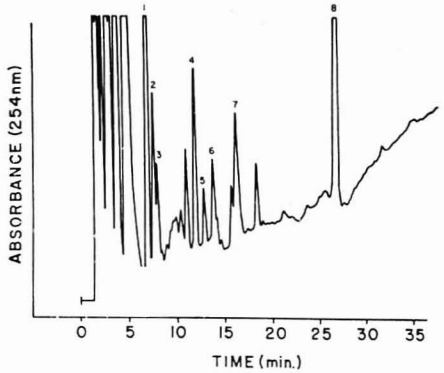

Figure 2. Separation of components in a serum sample from a patient with congestive heart failure. Chromatographic conditions same as in Figure 1

Table III. Peak Height Ratios (254 nm/280 nm) for Some Standards and Peaks with the Same Retention Time Characteristics in a Serum Sample from a Patient with Congestive Heart Failure. Ratios Are Averaged Values of Triplicate Runs

PEAK No.		STANDARD	
1.	19.00 ± 0.03	HYP	19.70 ± 0.02
2.	3.56 ± 0.02	URD	3.42 ± 0.02
3.	1.78 ± 0.03	XAN	1.73 ± 0.03
4.	1.62 ± 0.02	XAO	1.57 ± 0.03
5.	8.41 ± 0.04	INO	8.52 ± 0.01
6.	2.25 ± 0.01	GUO	2.18 ± 0.03
7	0.60 ± 0.03	L-TRP	0.54 ± 0.06
8	0.83 ± 0.03	$1,3Me_2XAN$	0.83 ± 0.02

uridine, and xanthine which have very different ratios (19.70, 3.42, and 1.73, respectively).

The complete identification procedure using retention time analysis, co-injection with standards, absorbance ratios, and enzymatic peak shift technique is illustrated with a serum sample from a patient suffering from congestive heart failure (Figure 2). The peaks were tentatively identified on the basis of retention times and comparison with standards. Standards were then co-injected with the sample and an increase in the area was taken as further characterization of the identity of the peak (Figure 3). Peaks were further characterized by determining the absorbance ratios. Table III contains the absorbance ratios for the standards and unknown peaks in the chromatogram. A portion of the same deproteinized sample was then incubated with xanthine oxidase, and the resulting chromatogram (Figure 4) shows the disappearance of peaks number 1 and 3, corresponding to hypoxanthine and xanthine, respectively. Finally, chromatograms using fluorescence detection were obtained and only the L-tryptophan fluoresced when the exciting wavelength was 295 nm. On the basis of the combined data, the peaks in Figure 2 were identified as hypoxanthine (peak 1), uridine (peak 2), xanthine (peak 3), xanthosine (peak 4), inosine (peak 5), guanosine (peak 6), L-tryptophan (peak 7), and 1,3-dimethylxanthine (peak 8). In cases where the enzyme for a specific nucleoside was not commercially available, it was possible to identify the desired compound by using a nonspecific enzyme, purine nucleoside phosphorylase, to convert the nucleosides to bases. A specific enzyme is then used to identify the base formed. For example, since specific enzymes for inosine, xanthosine, and guanosine are not commercially available, it is possible

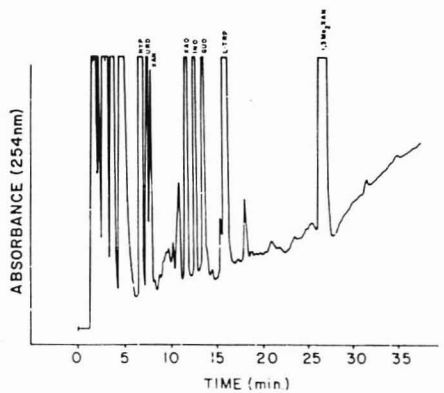

Figure 3. Chromatogram of a serum sample from a patient with congestive heart failure with co-injected standards of hypoxanthine, uridine, xanthine, inosine, guanosine, L-tryptophan and 1,3-dimethylxanthine. Chromatographic conditions same as in Figure 1

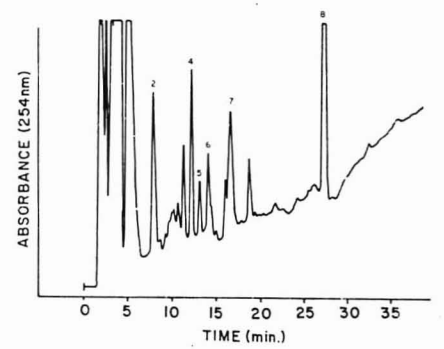

Figure 4. Xanthine oxidase peak shift carried out on a sample from a patient with congestive heart failure. Chromatographic conditions same as in Figure 1

to identify these nucleosides by converting them to the bases, hypoxanthine, xanthine, and guanine, respectively. Specific enzymes, xanthine oxidase and guanase are then used to distinguish the hypoxanthine and xanthine from the guanine and to identify selectively the guanine.

The use of a coupled-enzyme peak shift is illustrated on a serum sample from a normal subject (Figure 5A). A portion of the sample was first incubated with xanthine oxidase to remove hypoxanthine and xanthine already present in the sample as was illustrated in Figures 2 and 4. Further incubation of the same sample with purine nucleoside phosphorylase caused conversion of peaks 5, 6, and 7 (retention times of inosine, xanthosine, and guanosine, respectively) to peaks 1, 3, and 4 with retention times of the hypoxanthine, xanthine, and guanine (Figure 5B). Thus, hypoxanthine (peak 1) is formed from the conversion of inosine (peak 6), xanthine (peak 3) from xanthosine (peak 5), and guanine (peak 4) from guanosine (peak 7). Further incubation of the same sample with guanase resulted in the disappearance of the guanine peak (peak 4) and an increase in the xanthine peak (peak 3). Thus, based on the accumulated evidence from retention times, absorbance ratios and coupled-enzyme peak shifts,

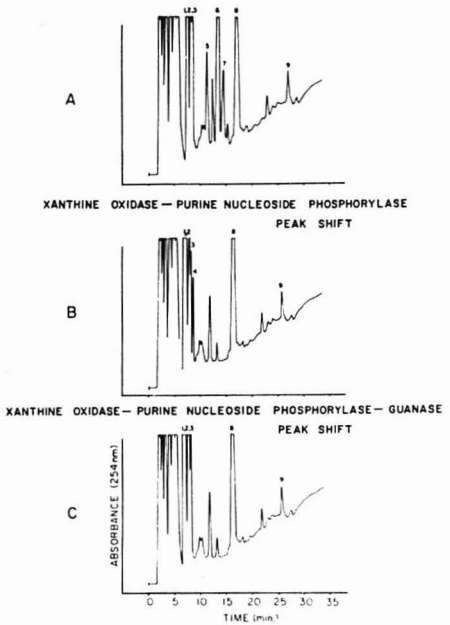

Figure 5. (A) Chromatogram of a serum sample from a normal subject. Chromatographic conditions same as in Figure 1. (B) Chromatogram of a serum sample shown in (A), incubated with xanthine oxidase and purine nucleoside phosphorylase. Chromatographic conditions same as in Figure 1. (C) Chromatogram of a serum sample shown in (A), incubated with xanthine oxidase, purine nucleoside phosphorylase, and guanase. Chromatographic conditions same as in Figure 1

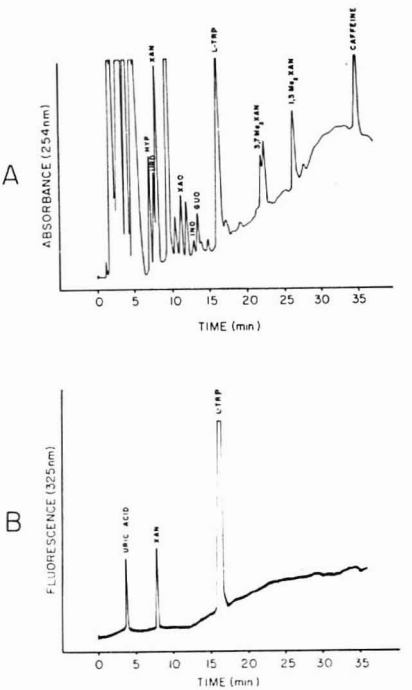

Figure 6. (A) Chromatogram of a plasma sample from a patient with gout. Chromatogram conditions same as in Figure 1. Detector, UV at 254 nm. (B) Chromatogram of a plasma sample from a patient with gout. Chromatographic conditions same as in Figure 1. Fluorescence detector, length at 325 nm (340 nm cut-off filter)

peaks in the chromatogram (Figure 5A) were identified as: hypoxanthine (peak 1), uridine (peak 2), xanthine (peak 3), guanine (peak 4), xanthosine (peak 5), inosine (peak 6), guanosine (peak 7), L-tryptophan (peak 8), and 1,3-dimethylxanthine (peak 9).

Fluorescence characteristics can also be used for the sensitive determination and identification of certain compounds present in serum samples. By choosing the proper excitation and emission wavelengths, it is possible to identify a specific compound such as uric acid, which is very important in studying purine metabolism disorders. For example, Figure 6A shows a chromatogram of a plasma sample from a patient suffering from clinically diagnosed gout. This patient was treated with a xanthine oxidase inhibitor, 4-hydroxpyrazolo(3,4-*d*)pyrimidine (Allopurinol). This drug is known to reduce the formation of uric acid. Thus, the hazard of hyperuricosuria is avoided in patients with gouty nephropathy or with a predisposition to the formation of uric acid stones. In this case, the uric acid peak as well as that of xanthine and hypoxanthine were of interest. Uric acid, however, was not resolved from other UV-absorbing constituents of plasma which elute immediately after the void volume. Therefore, in order to detect and identify uric acid in the sample, a fluorescence chromatogram was obtained using an excitation wavelength of 325 nm with the emission cut-off filter of 340 nm (Figure 6B). In addition, this chromatogram was also taken as corroborative evidence for the presence of tryptophan since the wavelength used is close to the excitation maximum for tryptophan (295 nm).

Hypoxanthine and xanthine were identified enzymatically with xanthine oxidase. The remaining peaks were identified on the basis of retention times, co-injection with standards and the absorbance ratios. A major peak with the retention time of 9 min was not identified because of the lack of correlation with the standards. It is possible that this peak is a metabolite of Allopurinol.

In summary, absorbance ratios, enzymatic peak shift, and fluorescence spectra alone or in combination can be used to unambiguously identify HPLC peaks in the cold acid extracts of serum and plasma samples. Absorbance ratios alone can provide a simple, reliable, and on-line method for routine determination of both the identity and the purity of HPLC peaks. Enzymatic peak shift can also be used alone, providing the enzymes are commercially available. This technique can be used with very small sample sizes and is highly specific.

Chromatograms in which fluorescence detection is used are valuable for the identification of certain peaks since it is possible to take advantage of the specific excitation maxima required for various compounds. This specificity enables selective detection and identification and eliminates interferences from undesired compounds that either do not fluoresce or cannot be excited at the wavelength used.

Although the methods of peak identification described have been used mainly for nucleosides and bases in serum and plasma samples, they can also be applied to other types of compounds in biological samples, providing the compounds of interest absorb in the UV or fluoresce.

ACKNOWLEDGMENT

The authors thank Waters Associates, Inc., and Schoeffel Instrument Corporation for the use of their instruments; Hilaire Meuwisen of the Albany Medical School of University College for the serum samples from normal subjects; Rhode Island Hospital for the serum sample from the patient with congestive heart failure; Steven Kaplan, Roger Williams Hospital, Providence, R.I., for the gout sample; and Malcolm McKeag for his work on the extraction procedures.

LITERATURE CITED

(1) R. A. Hartwick and P. R. Brown, *J. Chromatogr.*, **126**, 679 (1976).
(2) P. R. Brown, A. M. Krstulovic, and R. A. Hartwick, *J. Clin. Chem. Biochem.*, **14**, 282 (1976).
(3) R. F. Adams, F. L. Vandemark, and G. J. Schmidt, *Clin. Chem. (Winston-Salem, N.C.)*, **22**, 1903 (1976).
(4) J. J. Orcutt, P. P. Kozak, Jr., S. A. Gillman, and L. H. Cummings, *Clin. Chem. (Winston-Salem, N.C.)*, **23**, 599 (1977).
(5) A. M. Krstulovic, P. R. Brown, and D. M. Rosie, *Anal. Chem.*, **48**, 1383 (1976).
(6) P. R. Brown, *J. Chromatogr.*, **52**, 257 (1970).
(7) B. L. Akiri, *Ind. J. Biochem.*, **5**, 25 (1968).
(8) T. Myazaki and N. Nakamura, *Jpn. Heart J.*, **10**, 259 (1969).
(9) G. C. Mills, F. C. Schmalstieg, K. B. Trimmer, A. S. Goldman, and R. M. Goldblum, *Proc. Natl. Acad. Sci., USA*, **73**, 2867 (1976).
(10) G. Avigard and S. Damie, *Anal. Biochem.*, **50**, 321 (1972).
(11) J. R. Barrio, J. A. Secrist III, and N. J. Leonard, *Biochem. Biophys. Res. Commun.*, **46**, 597 (1972).
(12) R. A. Hartwick and P. R. Brown, *J. Chromatogr., Biomed. Appl.*, **143**, 383 (1977).
(13) J. Arley Nelson, private communication.

RECEIVED for review June 6, 1977. Accepted September 12, 1977. This work was supported by Grant No. 17603-02 from the National Cancer Institute.

Separation and Determination of Copper(II) and Iron(II) as Their Monothiothenoyltrifluoroacetone Complexes with Pyridine by Extraction Spectrophotometry and Reversed-Phase Thin-Layer Chromatography

Takaharu Honjo,* Yoshinori Fujioka, Hitoshi Itoh, and Toshiyasu Kiba

Department of Chemistry, Faculty of Science, Kanazawa University, Kanazawa, Ishikawa, 920, Japan

The separation and determination of copper(II) up to 0–12 μg/mL and iron(II) up to 0–100 μg/mL with monothiothenoyltrifluoroacetone (STTA) in cyclohexane with or without pyridine (Py) by extraction spectrophotometry has been established. The molar absorptivity expressed in cm^2 L mol^{-1} was found to be 4.65×10^4 (390 nm) for $Cu(STTA)_2$ and 5.59×10^3 (810 nm) for $Fe(STTA)_2Py$, respectively. Anions such as hexacyanoferrate(II), cyanide, and citrate, as well as EDTA interfered. A set of two and five components of manganese(II), iron(II), cobalt(II), nickel(II), copper(II), zinc(II), mercury(II), lead(II), cadmium(II), and palladium(II) spotted on the thin-layer of cellulose impregnated with STTA could be separated by an aqueous solution containing pyridine adjusted to pH 5. The content of copper and iron of a few micrograms in chalcopyrite and in beryllium chloride of commercial reagent could be determined.

It has been generally known that monothio β-diketones are useful chelating reagents in coordination and analytical chemistry (*1*, *2*). Fluorinated monothio β-diketones such as STTA(monothiothenoyltrifluoroacetone) are especially useful for the solvent extraction of various metal ions (*3*, *4*). The extraction behavior of the TOPO (tri-*n*-octylphosphine oxide) adducts of cobalt(II), nickel(II), and zinc(II) complexes of STTA in cyclohexane (*4*), and of the pyridine (Py) adduct of iron(II) complexes of STTA in benzene (*5*) was previously reported, while the adducts of nickel(II), zinc(II), and cadmium(II) complexes of STTA with pyridine or γ-picoline were also investigated and characterized by the crystallization of their complexes (*6*). After preliminary experiments on the extraction behavior of adducts of beryllium(II), cadmium(II), cobalt(II), copper(II), iron(II, III), mercury(II), manganese(II), nickel(II), lead(II), palladium(II), platinum(II), vanadium(V), and zinc(II) complexes of STTA with some representative organic bases, the STTA chelates of copper(II) and iron(II) in cyclohexane were found to form stable adducts with pyridine than with TOPO, TBP (tributyl phosphate), tri-*n*-octylamine, and quinoline and to give higher absorbance at 500–560 nm for Cu(II) and 700–830 nm for Fe(II) than those in benzene, chloroform, ethylacetate, and methyl isobutyl ketone. On the basis of these results, the extraction behavior of STTA chelates of copper(II) and iron(II) in cyclohexane with or without pyridine has been investigated in detail and a new method for mutual separation and spectrophotometric determination of copper(II) and iron(II) by extraction and back-extraction methods has been proposed. On the other hand, the reversed-phase thin-layer chromatography of inorganic compounds has become a well established technique in analytical chemistry (*7*). Taking advantage of this method, the separation of metals has been achieved on the thin-layers of cellulose impregnated with various exchangers such as TBP (tributyl phosphate), alkyl amine, or quaternary ammonium salt (*8*, *9*). However, little has been reported on the reversed-phase thin-layer chromatography of metal ions with chelating reagents. In this investigation, metal mixtures of manganese(II), iron(II), cobalt(II), nickel(II), copper(II), zinc(II), mercury(II), lead(II), cadmium(II), and palladium(II) have been spotted on the thin-layers of cellulose impregnated with STTA (monothiothenoyltrifluoroacetone) and the spots were developed by an aqueous solution adjusted to a desired pH for the mutual separation of these metal ions. By using the proposed methods, the content of copper and iron of a

few μg in chalcopyrite and in beryllium chloride of commercial reagent could be determined.

EXPERIMENTAL

Apparatus. A 323 Hitachi Recording Spectrophotometer; 239 Hitachi Digital Spectrophotometer; Hitachi-Horiba glass electrode pH meter, Model M-5; Iwaki shaking machine, type KM; Kubota centrifuge machine; and a Yanagimoto Micro Melting-point Apparatus, Model MP-J2, were used. The thin-layer chromatograph: TLC developing apparatus, model TL-IS, is made by Yamato Scientific Instruments.

Materials. The solutions of metal ions were prepared by dissolving their salts such as $FeSO_4 \cdot 7H_2O$, $Fe(NO_3)_3 \cdot 9H_2O$, $CdCl_2$, $Pb(NO_3)_2$, $MnSO_4$, $CoSO_4$, $NiSO_4$, $CuSO_4 \cdot 5H_2O$, $Zn(CH_3COO)_2$, $HgCl_2$, and $PdCl_2$ of reagent grade in distilled water or in a slightly acidic solution to make a 10^{-2} M aqueous solution of each metal ion. The concentration of these metal ions was standardized complexometrically and the solutions were diluted as required with distilled water. The STTA was synthesized in our laboratory (*10*) and purified by the back-extraction method: the crude crystal of STTA synthesized was dissolved in the petroleum ether and the organic solution was shaken with 1 M sodium hydroxide solution to transfer most of STTA from the organic phase into an aqueous solution. After adding 1–6 M hydrochloric acid to the aqueous solution, the STTA was again extracted with pure petroleum ether. The excess solvent was evaporated off in air, yielding the pure compound of a needle red crystal. The STTA purified by this method showed a melting point of 72–74 °C. Yield: crude crystal 89%, pure crystal 69%. The elemental analysis of sulfur in STTA was carried out by using the Sn(II)–strong phosphoric acid method (*11*, *12*). Sulfur in the STTA (about 5–6 mg) was reduced to hydrogen sulfide by heating the STTA with tin(II)–strong phosphoric acid (30 g) on an electric heater at 300 °C for 30–60 min after oxidizing the STTA with chromium(VI)–strong phosphoric acid (15 g) on a water bath for 30–60 min followed by decomposing the excess chromium on an electric heater. The liberated hydrogen sulfide was absorbed in zinc acetate solution to form zinc sulfide. Next 20 mL of a 2×10^{-2} M I_2 solution was added to the solution and the iodine consumed for liberating sulfur in zinc sulfide was estimated by back-titration with a 2×10^{-2} M sodium thiosulfate solution. S(%): calcd 26.91, found 27.68. The stock solution of 10^{-3}–10^{-2} M STTA in cyclohexane or carbon tetrachloride was used and the solution was usually preserved in a refrigerator at 5 °C before use. All the other chemicals were of a guaranteed reagent grade.

Extraction Spectrophotometry. An aqueous solution containing 10^{-6}–10^{-2} M metal ions of copper(II) and iron(II, III) was made to have 10^{-2} M acetic acid (in the region of pH 0–7) or 10^{-2} M boric acid (in the region of pH 7–13) with or without 10^{-4}–10^{-1} M pyridine, and its pH was adjusted to a desired value by 0.1–1 M sodium hydroxide or hydrochloric acid solution. Ten milliliters of this solution and 10 mL of 10^{-3} M STTA in cyclohexane were then introduced into a 50-mL glass-stoppered centrifuge tube and equilibrated for 1–30 min and the phases were separated by centrifugation. In order to remove free STTA ligand and to investigate the stability of the STTA chelates and their pyridine adducts in cyclohexane solution, the back-extraction was also attempted by shaking 5 mL of the organic phase after extraction with 5 mL of boric acid solution of about pH 10 for 30 min. All iron(III) was reduced to iron(II) by 0.1 M hydroxylamine prior to the extraction of iron.

Reversed-Phase Thin-Layer Chromatography. A 6-g portion of cellulose powder was mixed with 30 mL of 10^{-3} M STTA in carbon tetrachloride to give a homogeneous slurry. This slurry was spread so as to be an even layer 0.25 mm thick on two 5 × 20 cm and two 20 × 20 cm plates by using a spreading device available from Yamato Kagaku Co. The plates were air-dried for 15–20 min at room temperature (20 °C) and were stored in the plastic box containing silica gel. The content of the STTA on a thin-layer of cellulose was estimated by conventional spectrophotometry after scooping up a definite amount of cellulose layer followed by dissolving the STTA on the plate into carbon tetrachloride. The STTA in carbon tetrachloride showed its absorption maximum at 365 nm. The change of the STTA content ($\mu g/cm^2$) on the thin-layer of cellulose after preparation was as follows: 0.92 (immediately), 0.68 (after 1 day), and 0.60 (after 2 days). When the standing time of the cellulose plates increases, the content of the STTA on the thin-layers decreases and the length of run of metal ions increases. The STTA was gradually oxidized by air and then the plates should be used within 1 day. In this thin-layer chromatography, the cellulose containing STTA is always in contact with the fresh aqueous solution on the plates; the STTA on the thin-layer will gradually dissolve in the aqueous phase and may be taken away from the chromatographic system. Therefore, the eluting solutions should be pre-equilibrated with the STTA in carbon tetrachloride. A 2–3 μL quantity of 0–3 μg of metal ion solution was spotted on the starting position of the plate in a distance of 1 cm straight line within about 1.5 cm from the bottom of the plates by using a glass capillary. After air-drying the spots for about 15 min at room temperature, the plates were dipped into the eluting solution up to 1 cm below the sample spots. The chromatographic chamber was saturated with carbon tetrachloride vapor for 1 h in order to protect the evaporation of the eluting solution from the plate, and the spots were developed by the usual ascending method with a 25-mL buffer solution of 10^{-2} M CH_3COONa adjusted to a desired pH with or without 10^{-3} M pyridine by 0.1 M HCl. A 25-mL aliquot of the eluting solution was always pre-equilibrated with the same volume of the STTA in carbon tetrachloride for 1 h. Developing was continued till the front of the solvent reached 10–20 cm from the distance of the original spots. When the elution was completed, the plates were dried under an infrared lamp to remove any remaining eluting solution. The location of the metal ions was confirmed by spraying a carbon tetrachloride solution of 0.05% dithizone on the plates followed by exposing the layers to concentrated ammonia vapor. After a while, the position of each metal appeared on the plates as the specific colored bands of dithizonates by the ligand exchange reaction between STTA chelates and dithizone.

Table I. Extraction pH, Color, Absorption Peak, Molar Absorptivity of Cu(II) and Fe(II) STTA Chelates, and Those of Their Pyridine Adducts

STTA Chelates

Metal	pH	Color	λ(nm)	ε(cm² × L/mol)
Cu(II)	2	Brown	390	4.65×10^4
Fe(II)	5–6	Brown	364	1.79×10^3

Pyridine Adducts

Metal	pH	Color	λ(nm)	λ(nm)	ε(cm² × L/mol)
Cu(II)	5–6	Greenish brown	386	620	6.85×10^2
Fe(II)	5–6	Green	370	810	5.59×10^3

RESULTS AND DISCUSSION

Extraction Spectrophotometry. *Absorption Spectra.* The absorption spectra of STTA, its chelates of copper(II) and iron(II), and their pyridine adducts in cyclohexane are shown in Figure 1. The absorption maxima, absorbance, and color of these complexes in cyclohexane solution and the pH in an aqueous phase after the extraction and back-extraction of copper(II) and iron(II) with STTA in cyclohexane with or without pyridine are summarized in Table I. It was found that the complexes of iron(II) and copper(II) extracted showed a distinct change of intensity of the absorption spectra and an absorption maxima in wavelength by the adduct formation between their STTA chelates and pyridine in cyclohexane. The molar absorptivity of Cu–STTA chelate at 390 nm was 4.65×10^4 and this value was larger than that of the Cu–STTA–pyridine adduct of 6.85×10^2 at 386 nm. Therefore the peak of Cu–STTA chelate at 390 nm was used for the determination of copper by extraction spectrophotometry. Some decrease of the absorbance of the organic solution which appeared after back-extraction is due to the transfer of the free STTA ligand into an aqueous solution. The spectrophotometric determination of copper with STTA (*13*, *14*) may be less sensitive and less accurate as compared to the present

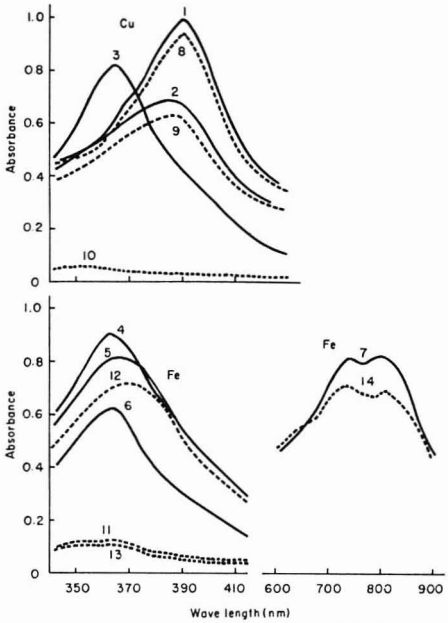

Figure 1. Absorption curves of copper(II) and iron(II) STTA chelates and their pyridine adducts in cyclohexane. Extraction: (1) Ca. 5×10^{-5} M Cu(II)–STTA chelate, pH 3.00; (2) Ca. 5×10^{-5} M Cu(II)–STTA–Py adduct, pH 5.40; (3) Ca. 10^{-4} M STTA, pH 3.20; (4) Ca. 5×10^{-5} M Fe(II)–STTA chelate, pH 5.07; (5) Ca. 5×10^{-5} M Fe(II)–STTA–Py adduct, pH 5.71; (6) Ca. 10^{-4} M STTA, pH 6.92; (7) Ca. 10^{-3} M Fe(II)–STTA–Py adduct, pH 4.79. Back-extraction: (8) (1), pH 9.25; (9) (2), pH 9.29; (10) (3), pH 9.20; (11) (4), pH 8.90; (12) (5), pH 8.95; (13) (6), pH 8.90; (14) (7), pH 9.65. Shaking time: 30 min. Blank: cyclohexane

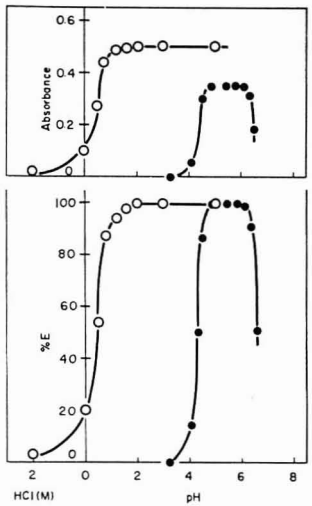

Figure 2. Dependence of pH on the extraction of Cu(II)–STTA chelate and Fe(II)–STTA–Py adduct in cyclohexane. Cu(II): —○—, 10^{-5} M, 390 nm; Fe(II): —●—, 10^{-4} M, 810 nm. STTA: 10^{-3} M, Py: 0.1 M. Shaking time: 30 min

method, because the excess STTA is not removed from the extract and the spectrum of the reagent overlaps that of the chelate. In the case of iron(II), the molar absorptivity of Fe–STTA chelate at 364 nm was 1.79×10^5. The Fe–STTA chelate in cyclohexane was easily decomposed by washing it with an aqueous solution of about pH 9, but the Fe–STTA–pyridine adduct was left in the organic phase. The free STTA ligand was almost removed from an organic phase under the same condition. The Fe–STTA–pyridine adduct showed a new peak having molar absorptivity of 5.59×10^3 at 810 nm and this peak did not overlap on the spectrum of STTA and was used for the direct spectrophotometric determination of iron(II) as its pyridine adduct without any other treatment like back-extraction. A similar new peak was also observed in the Fe(II)–STTA–pyridine–benzene extraction system (5).

Effect of pH. The pH dependence of the extractability of copper(II) with 10^{-3} M STTA in cyclohexane and of iron(II) with 10^{-3} M STTA in cyclohexane in the presence of 0.1 M pyridine was examined in the region of 3 M hydrochloric acid to pH 7. The results are shown in Figure 2 in terms of the absorbance and % E vs. pH plots of copper(II) chelate and iron(II) adduct with pyridine extracted in cyclohexane. The quantitative extraction of the STTA chelate with copper(II) and the adduct of iron(II) with pyridine in cyclohexane were achieved rapidly in the region of pH 5–6 for iron(II) and over about pH 2 for copper(II). In this experiment, all iron(III) was reduced to iron(II) by 0.1 M hydroxylamine prior to the extraction of iron, because the extraction of iron(III) with STTA with or without pyridine was slow and not quantitative under the conditions studied. It was also reported that iron(III) was reduced partially to form the green pyridine adduct of iron(II) chelate in the iron(III)–STTA–pyridine–benzene system and this reaction was slow and not quantitative (5).

Effect of Shaking Time. The extractability of 10^{-5} M copper(II) with 10^{-3} M STTA in cyclohexane at pH 3.2 and 10^{-4} M iron(II) with 10^{-3} M STTA in cyclohexane in the presence of 0.1 M pyridine at pH 5.8 was examined by shaking the two phases for from 1 min to 2 h. The complete and quantitative extraction was attained in over 1 min of shaking.

Effect of the Volume of the Aqueous Solution. When the volume of the organic phase of 10^{-3} M STTA in cyclohexane was kept at 10 mL, when that of the aqueous phase was varied from 10 to 1000 mL, and when the absorbance of the organic phase was measured at 390 nm for Cu(II) and 810 nm for Fe(II) after every extraction, almost the same absorbance was obtained in each case. Ten mL of 10^{-3} M STTA in cyclohexane was quite adequate for quantitative extraction of copper(II) and iron(II).

Stability of the Color and the Stoichiometry of the Extracted Complex. When the absorbance of the Cu(II)–STTA complex and Fe(II)–STTA–pyridine adduct in cyclohexane was measured at intervals of several days, no change in their absorbance could be found at least for a few days. The absorbance of the Cu–STTA and Fe–STTA–pyridine complexes extracted was examined in terms of the mole ratio of STTA to copper(II) and iron(II); the absorbance was found to be constant in the region above the 2:1 ratio, as is shown in Figure 3. This result confirms that the mole ratio of STTA to copper(II) and iron(II) in the complex formation was 2:1. The composition of the pyridine adduct of iron(II)–STTA chelate was determined by use of the slope ratio method as shown in Figure 4. The equilibrium concentration of pyridine was evaluated by measuring the absorbance of pyridine at 256

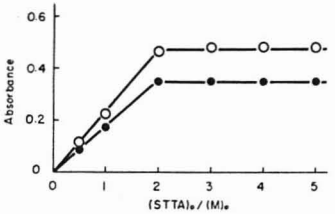

Figure 3. Composition of Cu(II)–STTA chelate and Fe(II)–STTA–Py adduct in cyclohexane. Cu(II): —O—, 10^{-5} M, pH 2.7, 390 nm; Fe(II): —●—, 10^{-4} M, pH 5.9, 810 nm. Py: 0.1 M, STTA: 10^{-3} M

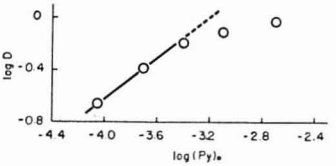

Figure 4. Variation of the distribution ratio of iron(II) as a function of pyridine in cyclohexane. Fe(II): 10^{-4} M, 810 nm, pH 5.4. STTA: 10^{-3} M

nm in an organic and aqueous phase after shaking the cyclohexane solution with an aqueous solution containing a definite concentration of pyridine at varying pH values. The amount of pyridine in the organic phase can then be computed from the calibration curve, the plots of absorbance vs. the concentration of pyridine in cyclohexane at 256 nm. It was assumed that the distribution of pyridine with or without STTA in cyclohexane was not so different because the absorption spectra of STTA in cyclohexane with or without pyridine gave almost the same curves. From the slope of log D vs. log $[Py]_0$, that is unity, the composition of the extracted species was estimated to be $Fe(STTA)_2Py$. The reaction of the adduct formation of iron(II) may be expressed as follows; $Fe(II) + 2HSTTA + Py \rightleftarrows Fe(STTA)_2Py + 2H^+$.

Recommended Procedure and Working Curve. From the experimental results described above, a useful systematic procedure for the mutual separation and determination of copper(II) and iron(II) could be proposed as Figure 5.

Table II. Effect of Foreign Ions

Effect of anions on the extraction of copper at pH 3.0 with 10^{-3}M STTA in cyclohexane

Anions	Absorbance at 390 nm	Anions	Absorbance at 390 nm
None	0.465	EDTA	0.006
$Fe(CN)_6^{4-}$	0.053	$C_2O_4^{2-}$	0.462
CN^-	0.030	SCN^-	0.469
SO_4^{2-}	0.432	MoO_4^{2-}	0.447
Cl^-	0.465	NO_3^-	0.443
$C_6H_5O_7^{3-}$	0.459		

Cu^{2+}: 10^{-5} M, anion: 10^{-3} M.

Effect of anions on the extraction of iron at pH 6.1 with 10^{-3}M STTA in cyclohexane

Anions	Absorbance at 810 nm	Anions	Absorbance at 810 nm
None	0.177	EDTA	0.002
$Fe(CN)_6^{4-}$	0.003	$C_2O_4^{2-}$	0.143
CN^-	0.163	SCN^-	0.172
SO_4^{2-}	0.177	MoO_4^{2-}	0.175
Cl^-	0.176	NO_3^-	0.168
$C_6H_5O_7^{3-}$	0.062		

Fe^{2+}: 5×10^{-5} M, Py: 0.1 M, anion: 10^{-3} M.

The system conforms to Beer's law over the concentration range of 0–12 μg/mL of copper(II) and 0–100 μg/mL of iron(II). The molar absorptivity expressed in cm^2 L mol^{-1} of the chelate with STTA and its pyridine adduct in cyclohexane were found to be 4.65×10^4 (at 390 nm) for $Cu(STTA)_2$ and 5.59×10^3 (at 810 nm) for $Fe(STTA)_2Py$, respectively.

Effect of Diverse Ions. The effect of the presence of foreign ions on the extraction behavior of Cu(II) and Fe(II) is given in Table II. Anions, such as EDTA, $Fe(CN)_6^{4-}$, and CN^- for copper(II), and EDTA, $Fe(CN)_6^{4-}$, and $C_2O_4^{2-}$ for iron(II) interfered with the decrease of the extractability of these metal ions.

Application of the Recommended Method. The extraction spectrophotometry of the systematic procedure described above has been applied to the determination of iron and copper in chalcopyrite and in beryllium chloride of commercial reagent grade. The results are shown in Table III. The present method was found to be suitable for the mutual

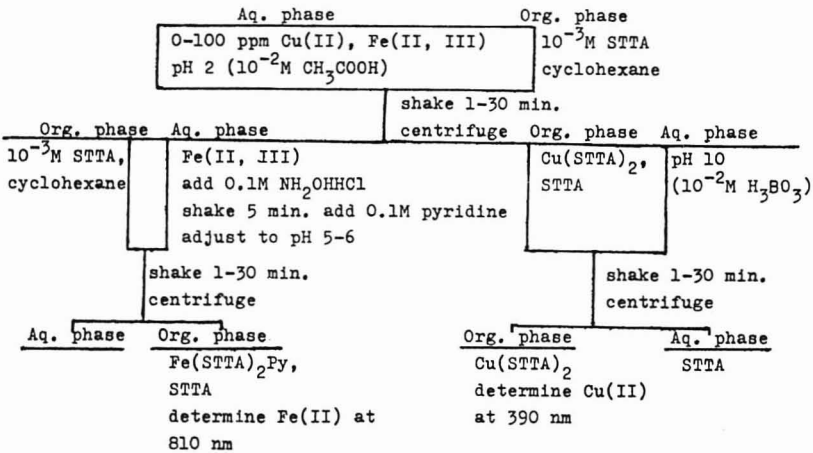

Figure 5. Scheme for the separation and determination of copper(II) and iron(II)

Table III. Determination of Fe(II) and Cu(II) in Chalcopyrite and Beryllium Chloride

Sample	Taken, mL	Fe(II), %	Cu(II), %
$FeCuS_2$[a]	1.0	36.2	31.3
$BeCl_2$[b]	1.0	0.016	0.205

[a] 0.357 g of chalcopyrite was dissolved in concd HNO_3 and diluted to 10^3 mL with water. [b] 7.99 g of $BeCl_2$ was dissolved in HCl and diluted to 10^3 mL for Cu(II) and 10^3 mL for Fe(II).

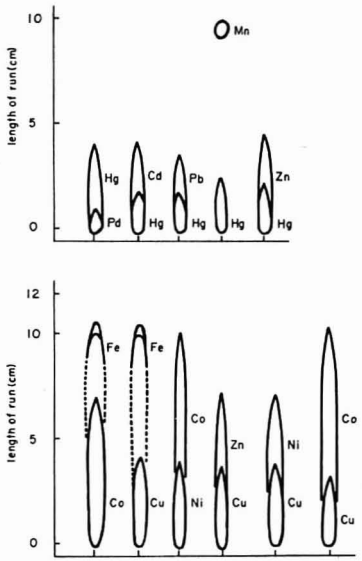

Figure 6. Chromatograms of binary mixtures. Eluent: pH 5 (10^{-2} M CH_3COONa–10^{-3} M Pyridine–HCl). Developing time: 60 min. Length of the run of eluent from origin: 12 cm

separation and direct colorimetric determination of copper(II) and iron(II, III) in these samples.

Reversed-Phase Thin-Layer Chromatography. *The Chromatographic Behavior of Metal Ions.* A series of runs of each metal ion such as cobalt(II), nickel(II), copper(II), zinc(II), cadmium(II), mercury(II), and palladium(II) with the eluting solution of pH 1, 2, 3, 4, 5, 6, and 8.2 always caused the pronounced tailing rising up the plate from the origin. These tailings were decreased by using the eluting solution containing pyridine. The most widely applicable developing solution was the buffer solution of pH 5 and the developing solution thus prepared was used throughout this study. The chromatographic behavior of each metal ion always gave rise to some tailing which would be overlapped on each band, and the separation of each metal ion seems to be difficult under this condition. However, the binary mixtures of metal ions were found to be effectively separated under the same condition. The results are summarized in Figure 6. From these chromatograms, it is easily seen that the resolution among metals was achieved in the case of binary mixtures of Pd(II)–Hg(II), Hg(II)–Cd(II), Hg(II)–Pb(II), Hg(II)–Mn(II), Hg(II)–Zn(II), Cu(II)–Fe(II), Cu(II)–Zn(II), Cu(II)–Co(II), Cu(II)–Ni(II), Ni(II)–Co(II), and Co(II)–Fe(II). The representative separation chromatograms of each metal ion from the quinary mixtures with an eluting solution of pH 5 are shown in Figure 7. It was found that a set of five components

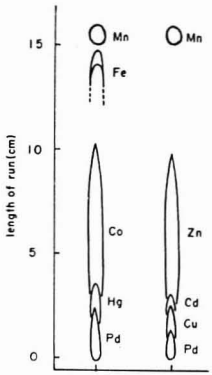

Figure 7. Chromatograms of quinary mixtures. Eluent: pH 5 (10^{-2} M CH_3COONa–10^{-3} M Pyridine–HCl). Developing time: 100 min. Length of the run of eluent from origin: 16 cm

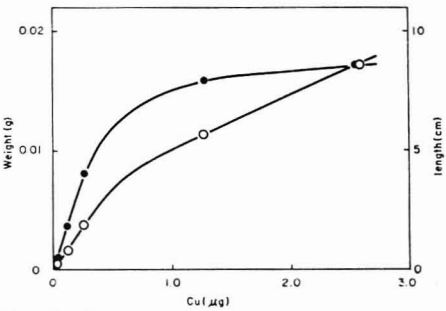

Figure 8. Calibration curves of copper. —O— weight, —●— length

could be separated in the following order: Pd(II) → Hg(II) → Co(II) → Fe(II) → Mn(II), Pd(II) → Cu(II) → Cd(II) → Zn(II) → Mn(II). There was considerable evidence to support the migration of divalent cations in the form of positively charged complexes such as $M(STTA)^+$, $M(STTA)(Pyridine)_n^+$, $M(Pyridine)_n^{2+}$, $M(CH_3COO)(Pyridine)_n^+$, and $M(CH_3COO)^+$, which would stop with the formation of neutral complexes as $M(STTA)_2$ and $M(STTA)_2(Pyridine)_n$ (n = 1–2) on the plates. The separation appearance of the chromatograms of each metal ion from mixtures of several metal ions seems to be caused by the successive competition reaction in the chelate formation among metals with STTA on the plate, which may depend on their stability and on the rate of their chelate formation. Metals having higher stability constants may predominantly form stable chelates with STTA and the reaction will make it possible to separate the bands of various metal cations. The complex formation of iron(II) and manganese(II) with STTA is slow and their stability constants are low and these metals may run at the front of the eluting solution. It is interesting that the migration order of metal ions on the plates follows the order of Irving and William (*15*) for the complex stability of first transition elements, that is, Mn(II) < Fe(II) < Co(II) < Ni(II) < Cu(II) > Zn(II). After chelate formation, the position of the tailing was not changed even though the eluting solution was developed for a long time. Thus, the general R_f value used in thin-layer or paper chromatography cannot be applied to this experiment, and we would like to name this phenomenon "reaction

Table IV. Determination of Copper in Chalcopyrite and in Beryllium Chloride

Sample	Taken, μL	Cu(II), μg	Found, %	Method
$FeCuS_2$[a]	0.4	0.223	32.2	length
	0.4	0.235	32.9	length
	0.4	0.215	30.2	length
	0.4	0.220	30.8	weight
	0.4	0.221	30.9	weight
	0.4	0.216	30.2	weight
			31.3	extraction spectrophotometry
$BeCl_2$[b]	0.4	0.07	0.22	length
			0.21	extraction spectrophotometry

[a] 0.275 g of chalcopyrite was dissolved in concd HNO_3 and diluted to 100 mL with water. [b] 7.99 g of $BeCl_2$ was dissolved in HCl and diluted to 100 mL with water. The standard deviation was 1.4 (with the length method) and 0.37 (with the weight method).

chromatography" or "candle chromatography" by judging from the mechanism of this chromatography or the shape of the chromatograms which is similar to the flame of a candle. A similar phenomenon was observed in the precipitation chromatography of several metal ions such as Hg(II), Ag(I), Pd(II), Cu(II), Bi(III), Cd(II), Zn(II), and Fe(III) with thiooxine impregnated filter paper (*16*).

Application of the Proposed Thin-Layer Chromatography. The possibility of the direct quantitative determination of copper(II) has been investigated by measuring the length of tailing on the plate or weighing the paper equal to the area of tailing drawn on a millimeter-graph sheet. The calibration curves thus obtained are shown in Figure 8. The length of the tailing or the weight of the area equivalent to the graph sheet depends on the amount of copper(II) initially taken. By using these calibration curves, the separation and the determination of a few micrograms of copper(II) in chalcopyrite and in beryllium chloride of commercial reagent grade were achieved on the plate of the STTA-impregnated cellulose. The results are shown in Table IV. These values were in quite good agreement with those obtained by the extraction spectrophotometry of copper(II) with STTA in cyclohexane.

LITERATURE CITED

(1) M. Cox and J. Darken, *Coord. Chem. Rev.*, 7, 29 (1971).
(2) S. E. Livingstone, *Coord. Chem. Rev.*, 7, 59 (1971).
(3) T. Honjo and T. Kiba, *Bunseki Kagaku*, 21, 676 (1972).
(4) T. Honjo, S. Yashima, and T. Kiba, *Bull. Chem. Soc. Jpn.*, 46, 3772 (1973).
(5) M. Chikuma, A. Yokoyama, Y. Ooi, and H. Tanaka, *Chem. Pharm. Bull.*, 23 (3), 507 (1975).
(6) R. K. Y. Ho, S. E. Livingstone, and T. N. Lockyer, *Aust. J. Chem.*, 21, 103 (1968).
(7) T. Honjo and T. Kiba, *Bull. Chem. Soc. Jpn.*, 45, 185 (1972).
(8) S. Ohashi, *Bull. Chem. Soc. Jpn.*, 28, 645 (1955).
(9) T. Kiba, I. Akaza, and S. Taki, *Bull. Chem. Soc. Jpn.*, 30, 482 (1957).
(10) V. M. Shinde and S. M. Khopkar, *Anal. Chem.*, 41, 342 (1969).
(11) M. Deguchi and M. Yashiki, *Bunseki Kagaku*, 20, 317 (1971).
(12) T. Braun and G. Ghersini, "Extraction Chromatography", Elsevier Scientific Publishing Company, Amsterdam, The Netherlands, 1975.
(13) L. S. Bark, G. Duncan and R. J. T. Graham, *Analyst (London)*, 92, 31, 347 (1967).
(14) R. W. Murray and R. J. Passarelli, *Anal. Chem.*, 39, 282 (1967).
(15) H. Irving and R. J. P. Williams, *J. Chem. Soc.*, 1953, 3192.
(16) H. Nagai, T. Deguchi, and N. Narahara, *Bunseki Kagaku*, 24, 184 (1975).

RECEIVED for review April 26, 1977. Accepted August 23, 1977.

Solvent Effect on the Liquid-Liquid Distribution of Monothiothenoyltrifluoroacetone and Its Metal Chelates of Copper(II), Cobalt(II), and Zinc(II)

Takaharu Honjo,* Ryumon Honda, and Toshiyasu Kiba

Department of Chemistry, Faculty of Science, Kanazawa University, Marunouchi, Kanazawa, Ishikawa 920, Japan

The solvent effect on the liquid–liquid distribution of STTA (monothiothenoyltrifluoroacetone) and its metal chelates of copper(II), cobalt(II), and zinc(II) is investigated. The correlation between the distribution coefficient of STTA (P_{HA}) and the distribution ratio of its metal chelates (D_M) expressed by $\log D_M = n \log P_{HA}$ + constant at a fixed pA is valid in nine solvents for all chelate systems except for the Co–STTA system. The difference of the relationship for oxygen containing solvents from that for inert solvents is also discussed. The data for TTA and its metal chelates of copper(II), cobalt(II), and zinc(II) are also reported for comparison.

The organic solvents play an important role in the distribution of extractable species; however, the theoretical treatment of the solvent effect has not yet been fully elucidated. Recently, the regular solution theory (*1*) has been found useful for interpreting the solvent effect on the chelate extraction systems such as the liquid–liquid distribution of TTA (thenoyltrifluoroacetone), its zinc(II) chelate and adduct with TBP (*2*), oxine derivatives and their copper(II) chelates (*3*, *4*), and nickel(II) dimethylglyoxine chelate (*5*). The viscosity of dilute solutions of chromium(III) acetylacetonate in organic solvents was also explained by this theory (*6*). The following empirical equation derived from the regular solution theory has been found to be established in various β-diketones and their metal chelates at a fixed pA (*7*):

$$\log D_M = n \log P_{HA} + \text{constant}$$

where n is the ratio of the molar volume of the metal chelate to that of the chelating agent, D_M is the distribution ratio of metal chelate, and P_{HA} is the distribution coefficient of the chelating agent, respectively. In the present paper, the effect of the solvents on the liquid–liquid distribution of STTA (monothiothenoyltrifluoroacetone) and its metal chelates of copper(II), cobalt(II), and zinc(II) is examined with the use of the equations derived from the regular solution theory. The

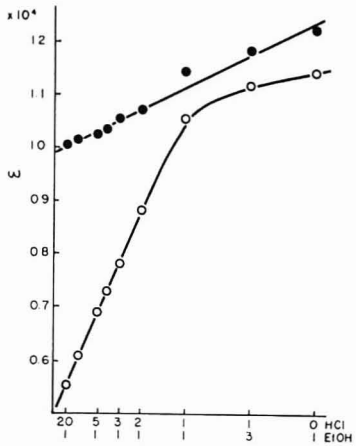

Figure 1. Molar absorptivity, ϵ, of STTA in the solutions containing 1 M hydrochloric acid and 99.5% ethanol in various ratios. (●) STTA solutions after standing for 2–3 min. (○) STTA solutions after standing for 17 h

data for TTA and its metal chelates of copper(II), cobalt(II), and zinc(II) are also presented for comparison.

EXPERIMENTAL

Materials. The STTA was synthesized by the reaction of hydrogen sulfide with TTA in absolute ethanol in the presence of hydrogen chloride (*8*). The TTA of the guaranteed-grade reagent was supplied from Dojindo Co., Ltd. The chlorides of radioisotopes of ^{60}Co and ^{65}Zn were purchased from New England Nuclear Corporation (U.S.A) and The Radio Chemical Centre (England). Organic solvents were of the highest purity commercially available, and were purified further in the ordinal manner if necessary. Other reagents used were all of guaranteed-grade materials.

Apparatus. The visible and ultraviolet spectra were scanned with a Hitachi 323 Type automatic recording spectrophotometer and a Hitachi 239 Type digital spectrophotometer. Radioactivity was counted with a Kobe Kogyo NaI(Tl) well-type scintillation counter, Mount Model EA-14, connected to a scaler, SA-250 and to a Dual Timer, TM-2. A Hitachi-Horiba M-5 pH meter was employed for the pH measurement. A Iwaki KM shaker was used for the agitation (54 strokes/min) of aqueous and organic phases.

Distribution of STTA. An equal volume of 10^{-2} M STTA organic solution and 1 M hydrochloric acid solution was equilibrated by shaking both phases for 30 min. After centrifugation, the absorbance of the hydrochloric acid solution was measured, and the concentration of the neutral STTA in an aqueous phase was determined spectrophotometrically by using the molar absorptivity of STTA of $\epsilon = 9.89 \times 10^3$ at 375 nm. This value was estimated by extrapolation of the plots of ϵ values of mixtures of 1 M hydrochloric acid and 99.5% ethanol in various ratios as is shown in Figure 1. As can be seen from Figure 1, STTA may be decomposed relatively fast in higher concentrations of hydrochloric acid, and the above procedure was carried out as quickly as possible. The distribution coefficient of STTA, P_{HA}, could also be determined by using the equation,

$$P_{HA} = \{[HA]_{org.\ init.} - [HA]_{HCl}\}/[HA]_{HCl}$$

where $[HA]_{org.init.}$ is the initial concentration of chelating reagent in the organic phase, and $[HA]_{HCl}$ is the concentration of chelating reagent in 1 M hydrochloric acid solution after equilibrium, respectively. The distribution coefficient of STTA in some organic solvents was obtained by another method in which the extraction curves of STTA were determined spectrophotometrically. The shaking time of 30 min was enough to reach the distribution equilibrium of STTA. It should be noticed that a little error can accompany this, owing to the decomposition of STTA during the shaking. The P_{HA} value was calculated by using the equation

$$P_{HA} = D_{HA}(1 + K_a/[H^+])$$

where D_{HA} is the distribution ratio of STTA calculated on several points on the extraction curves. K_a is an acid dissociation constant of STTA. Although the pK_a value is reported to be 3.96 (*9*), 4.05 (*9*), and 4.31 (*10*), the value of 4.00 was adopted in this study.

Distribution of Copper(II). Ten milliliters of an aqueous solution containing 10^{-5} M copper(II) in the region of pH 0–5 were shaken with the equal volume of 10^{-3} M STTA in an organic solvent. A shaking time of 30 min was enough to attain equilibrium. After extraction, a 5-mL portion of the organic phase was furthermore shaken with an equal volume of boric acid buffer of pH 10–10.5 for about 30–40 min to remove the excess of the chelating agent from the organic phase. In order to check the extractability of copper(II), 5-mL portion of the aqueous phase was taken out, adjusted again to pH 3–5, and shaken with an equal volume of 10^{-3} M STTA solution to extract copper(II) completely. In these experiments, the aqueous buffer solution consisted of 0.01 M sodium acetate (in the acidic region, pH 4–7) or 0.01 M boric acid (in the basic region pH 7–10). The STTA in cyclohexane, carbon tetrachloride, chloroform, and benzene was confirmed to be almost stripped out from the organic phase by shaking it with the solution of pH 10–10.5; however, the chelating reagent could only be stripped out as far as about one third of the total amount from the MIBK (methyl isobutyl ketone) solution. When the higher pH solution was used for stripping the excess chelating reagent, decomposition of copper chelate occurred; therefore, pH 10–10.5 seemed to be the limit to remove the excess of STTA from organic solvents as well as MIBK. After centrifugation, the distribution of copper(II) was determined by measuring the absorbance of the wavelength in the vicinity of the maximum absorption of the copper chelate in each solvent. The distribution of copper(II) with 10^{-1} M TTA in organic solvents was also determined by the same procedure.

Distribution of Cobalt(II) and Zinc(II). Ten milliliters of 0.01 M acetate buffer solution containing ^{65}Zn and ^{60}Co in a trace amount (<10^{-5} M) adjusted to an adequate pH were shaken with 10 mL of the organic solution of 10^{-3} M STTA for about 40–50 min. After centrifugation, 3-mL portions were taken from both phases, and the γ-activity was counted by a scintillation counter to determine the distribution of the metals. The pH of the aqueous solution was checked again after extraction. The distribution of cobalt and zinc with 10^{-1} M TTA in organic solvents was also determined by the same procedure. In all experiments described above, the aqueous phase was maintained at an ionic strength of 0.10 with $NaClO_4$. All investigations were carried out at room temperature (25 °C).

RESULTS AND DISCUSSION

The values of the distribution coefficient of STTA, P_{HA}, between an aqueous solution and various organic solvents obtained from the two methods are given in Table I together with those of TTA. It was found that the distribution coefficient of STTA was larger than that of TTA, and the solvents having higher dielectric constant gave larger distribution coefficients. The interaction between STTA and the more polar solvents, e.g., the hydrogen bonding or the dipole–dipole interaction may take place in the solution (*10*). When the metal chelate in the aqueous phase seems to be in negligible amount, the distribution ratio of divalent metal ion can be expressed as

$$D_M = \frac{\beta_2 P_M K_a^2}{P_{HA}} \frac{[HA]^2_{org.}}{[H^+]^2}$$

where β_2 is overall stability constant of metal chelates, P_M is the distribution coefficient of metal chelates, K_a is an acid dissociation constant of the chelating agent HA, and the suffix "org" is an organic phase, respectively. The plots of the log D_M of Cu(II), Co(II), and Zn(II) vs. pH for regular extraction

Table I. Distribution Coefficients of STTA and TTA

No.	Solvent	Dielectric constant	Solubility parameter	log P_{HA} STTA	log P_{HA} TTA (*2, 7, 12, 13*)
1	Cyclohexane	2.1	8.2	3.10, 3.44[a]	0.56
2	Carbon tetrachloride	2.2	8.6	3.49[a]	1.30
3	Chloroform	4.8	9.3	4.29[a]	1.73
4	Benzene	2.3	9.2	4.30[a]	1.62
5	Methyl isobutyl ketone	13.1	8.8	4.00	2.30
6	Isopropyl ether	3.9	7.0	3.58	1.51
7	*n*-Butyl ether	3.1	7.6	3.74	1.29
8	Ethyl acetate	6.0	9.1	3.35	2.27
9	*n*-Butyl acetate	5.1	8.5	3.65	2.22

[a] Values obtained from the distribution curves.

Table II. Distribution Ratios of STTA and TTA Chelates of Copper(II), Cobalt(II), and Zinc(II) at a Fixed p*A*

No.	Solvent	log D_M STTA Cu(II), p*A* 10.0	STTA Co(III), p*A* 6.0	STTA Zn(II), p*A* 6.0	TTA Cu(II), p*A* 7.0	TTA Co(II), p*A* 4.0	TTA Zn(II), p*A* 4.0
1	Cyclohexane	−0.80	0.84	−1.95	−1.20	−2.80	−2.77
2	Carbon tetrachloride	0.84	2.19	−0.17	−0.08	−1.82	−0.93
3	Chloroform	0.76	−0.30	0.51	0.94	−1.38	−0.11
4	Benzene	0.78	1.65	0.24	0.76	−0.50	−0.36
5	Methyl isobutyl ketone	−0.60	2.57	1.46	2.64	2.80	3.39
6	Isopropyl ether		1.86	0.19		0.85	1.35
7	*n*-Butyl ether		2.94	0.40		1.12	1.30
8	Ethyl acetate		−0.03	0.36		2.65	2.48
9	*n*-Butyl acetate		1.41	0.47		3.31	2.60

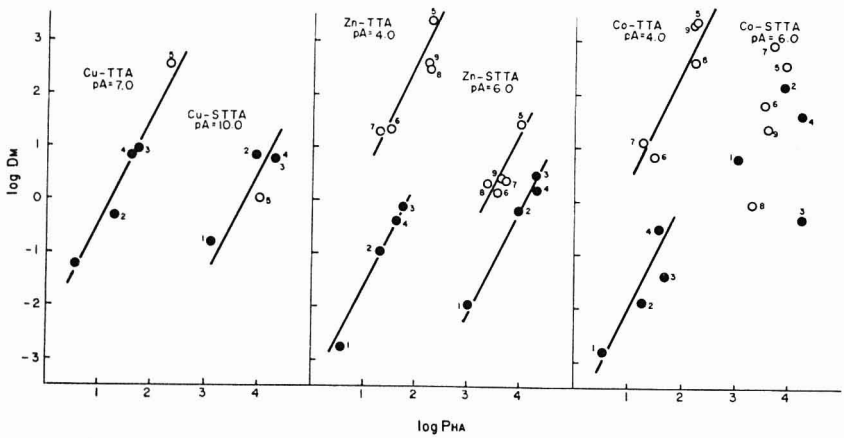

Figure 2. Correlation between the distribution coefficients of STTA and TTA, and the distribution ratios of their metal chelates of copper(II), cobalt(II), and zinc(II) at a fixed p*A*. (●) Inert solvents: 1, Cyclohexane; 2, Carbon tetrachloride; 3, Chloroform; 4, Benzene (○) Oxygen containing solvents: 5, Methyl isobutyl ketone; 6, Isopropyl ether; 7, *n*-Butyl ether; 8, Ethyl acetate; 9, *n*-Butyl acetate

in the STTA and TTA systems were approximately in agreement with the lines with the slope of 2 and the extracted species may be of $M(STTA)_2$ and $M(TTA)_2$ chelates except for the Co(II)–STTA system in which the valence of cobalt changed from 2 to 3 to form $Co(STTA)_3$ chelate (*10, 11*). The following relation between the distribution coefficient of the chelating agent and the distribution ratio of metal chelates at a fixed pA has been derived from the regular solution theory (*2, 7*):

$$\log D_M = n \log P_{HA} + \text{constant}$$

where n is the ratio of the molar volume of metal chelate to that of chelating agent. The pA = −log [A^-] could be calculated by the equation

$$[A^-] = \frac{[HA]_{org.\ init.}}{(P_{HA} + 1)[H^+]/K_a + 1}$$

where A^- is the concentration of anion of the chelating agent in an aqueous solution. It has been found that the distribution ratio of copper(II), cobalt(II), and zinc(II) at a constant pA is proportional to the distribution coefficient of their metal chelates in each solvent, and the results are summarized in Table II. The plots of log D_M at a fixed pA vs. log P_{HA} gave a straight line with a slope of about 2 except for the Co–STTA

system as shown in Figure 2. The results of the Zn–TTA system are in good agreement with those in previous papers (*12, 13*). It is reasonable that the ratio of the molar volume of the chelate to that of the ligand is about two, because two molecules of chelating reagent combine with a divalent metal ion. In the case of the Zn–STTA, Zn–TTA, and Co–TTA systems, the plots for polar solvents containing an oxygen atom are generally far apart from the lines for inert solvents as is shown in Figure 2. This may be due to the solvation effect of polar solvents (*13*). The difference of the lines for oxygen containing solvents from those for inert solvents increased in the order of Cu(II) < Zn(II) < Co(II), showing the magnitude of the residual coordination power of a metal ion with polar solvent (*14*). The solvation effect concerning oxygen containing solvents in the TTA system is relatively larger than that in the STTA system, as can be seen in Figure 2. This may be attributed to the enhancement of the stability of the metal STTA chelates due to the strong covalent bonding between metal and sulfur atoms such as $d\pi$–$d\pi$ back donation, and the participation of solvation to the STTA chelates may become relatively smaller.

LITERATURE CITED

(1) J. H. Hildebrand and R. L. Scott, "The Solubility of Non-Electrolytes", Dover Publications, New York, N.Y., 3rd ed., 1964.
(2) K. Akiba, N. Suzuki, and T. Kanno, *Bull. Chem. Soc. Jpn.*, **42**, 2537 (1969).
(3) H. A. Mottola and H. Freiser, *Talanta*, **13**, 55 (1966); **14**, 864 (1967).
(4) T. Wakabayashi, *Bull. Chem. Soc. Jpn.*, **40**, 2836 (1967).
(5) S. Oki, *Talanta*, **18**, 1233 (1971).
(6) H. M. N. H. Irving and J. S. Smith, *J. Inorg. Nucl. Chem.*, **30**, 1873 (1968).
(7) T. Omori, T. Wakabayashi, S. Oki, and N. Suzuki, *J. Inorg. Nucl. Chem.*, **26**, 2265 (1964).
(8) T. Honjo and T. Kiba, *Bull. Chem. Soc. Jpn.*, **45**, 185 (1972).
(9) E. Uhlemann and H. Müller, *Z. Chem.*, **8**, 185 (1968).
(10) T. Honjo, S. Yashima, and T. Kiba, *Bull. Chem. Soc. Jpn.*, **46**, 3772 (1973).
(11) T. Honjo, M. Horiuchi, and T. Kiba, *Bull. Chem. Soc. Jpn.*, **47**, 1176 (1974).
(12) N. Suzuki, K. Akiba, and H. Asano, *Anal. Chim. Acta.*, **52**, 115 (1970).
(13) N. Suzuki and K. Akiba, *J. Inorg. Nucl. Chem.*, **33**, 1897 (1971).
(14) T. Sekine and D. Dyrssen, *J. Inorg. Nucl. Chem.*, **26**, 1727 (1964).

RECEIVED for review April 26, 1977. Accepted August 23, 1977.

Determination of Trace Levels of Nitrates by an Extraction-Photometric Method

Philip Baca and Henry Freiser*

Department of Chemistry, University of Arizona, Tucson, Arizona 85721

Trace levels of nitrates may be quantitatively and selectively extracted as an ion pair with crystal violet using chlorobenzene. The results in the range of 60–720 ppb agree within a standard deviation of 28 ppb. The interference of bromide was substantially reduced by the use of hydrazine. It was surprising to learn that oxidation of bromide to tribromide under the mild extraction conditions will occur unless a reducing agent is added.

The most widely accepted methods currently available for analysis of nitrate ion generally involve either nitration of a phenol derivative, oxidation of an organic reagent, or reduction to nitrite followed by production of an azo dye (*1*). These methods frequently give poor reproducibility because of the difficulty of maintaining proper control of the chemical reaction involved. Results may be affected directly by substances whose behavior is similar to that of nitrate or indirectly by substances which affect the reactivity of the reagents or the stability of the products, as well as by substances that react with nitrate under the reaction conditions used.

Ion pair formation is another useful basis for nitrate analysis. The nitrate ion because of its size and relatively weak hydration readily forms extractable ion pair complexes with large organic cations. Although ions of similar charge and geometry interfere, very few such interferences occur in atmospheric particulate samples.

Yamamoto et al. (*2*) introduced a procedure based on the extraction of the ion pair complex between nitrate ion and the cation of crystal violet into chlorobenzene at pH 5–7, which has a working range of 0.24 to 1.20 ppm nitrate. When we examined the suitability of the method for analysis of nitrate in atmospheric particulate matter, we found it possible to substantially improve both the sensitivity and selectivity of the crystal violet method.

EXPERIMENTAL

Apparatus. Absorbances were measured with a Gilford 2400 spectrophotometer using matched 1-cm path length glass cells.

Reagents. Crystal violet chloride (Matheson Coleman and Bell) was used as received. Hydrazine sulfate (Fisher Scientific Company), potassium monobasic phosphate and chlorobenzene (Mallinckrodt Chemical Works) were reagent grade. Deionized water was used.

Procedure. The following reagents were added to 50-mL volumetric flasks: 10.0 mL crystal violet chloride (1.3×10^{-3} M aqueous solution), 4.0 mL potassium monobasic phosphate (pH 6.0), 5.0 mL of 1.4×10^{-3} M hydrazine sulfate, and 1.0–12.0 mL of 3.00 ppm nitrate (prepared with KNO_3) working solution. Aliquots of 10.0 mL were transferred from each flask to separatory funnels, 10.0 mL of chlorobenzene were added to each funnel, and the funnels were shaken for 2 min. Absorbances of the organic phase were measured at 595 nm against a chlorobenzene reference.

RESULTS AND DISCUSSION

A number of anions, including perchlorate, chlorate, and halides compete with nitrate for pairing with cations. Of these, only bromide ion and, to a lesser extent, chloride ion, were expected to present interference problems since the other interfering ions are not usually present in atmospheric particulate samples.

In the course of a bromide interference study, absorbances were observed to continually increase with repeated shaking of the extraction vessels (Table I) or merely on prolonged contact (Table II) of organic phases with aqueous phases containing bromide ion. In contrast, absorbances remained constant when bromide was not added to the standard solutions.

The results are consistent with atmospheric oxidation of bromide to tribromide, a large and poorly solvated ion which

Table I. Effect of Repeated Shaking of Extraction Vessels on Br^- Interference

Set A

Sample No.	Concn NO_3^-, ppm	Concn Br^-, ppm	Absorbance	Absorbance after second shaking of extraction vessel[a]	Absorbance after third shaking of extraction vessel
1	0.00	0.00	0.463	0.464	0.464
2	0.48	0.00	0.577	0.576	0.578
3	0.48	0.32	0.578	0.580	0.585
4	0.48	0.64	0.590	0.608	0.611
5	0.48	0.96	0.604	0.610	0.614
6	0.48	1.28	0.616	0.622	0.631

[a] Extraction vessels were shaken for 5 min each time.

Table II. Effect of Prolonged Contact of Phases on Br^- Interference

Set B

Sample No.	Concn NO_3^-, ppm	Concn Br^-, ppm	Absorbance of organic phase	Absorbance of organic phase after 30 hours in contact with aqueous phase
1	0.00	0.00	0.464	0.464
2	0.48	0.00	0.578	0.577
3	0.48	0.32	0.579	0.582
4	0.48	0.64	0.591	0.595
5	0.48	0.96	0.606	0.612
6	0.48	1.28	0.613	0.622

Table III. Effect of Hydrazine Sulfate on Br^- Interference

Sample No.	Concn hydrazine sulfate, mol/L	Concn Br^- ppm	Concn NO_3^-, ppm	Absorbance
1	0.0	0.00	0.00	0.476
2	0.0	1.28	0.00	0.508
3	4.0×10^{-5}	1.28	0.00	0.501
4	8.0×10^{-5}	1.28	0.00	0.476
5	8.0×10^{-5}	1.60	0.00	0.489
6	1.2×10^{-4}	1.60	0.00	0.479
7	0.0	0.00	0.36	0.599
8	8.0×10^{-5}	1.28	0.36	0.605
9	0.0	0.00	0.48	0.630
10	8.0×10^{-5}	1.28	0.48	0.632

has a greater tendency to form an extractable ion pair than does the smaller bromide ion. In this event, use of a reducing agent should correct the problem.

Hydrazine sulfate, a reducing agent which was considered as likely not to interfere (e.g., by reducing the dye to the leuco form), was therefore added to the calibration standards to determine its effect on the extent of interference in solutions containing bromide ion. The data in Table III indicate a decrease in the extent of interference. In the presence of the reducing agent, variation of absorbance with nitrate concentration was approximately constant regardless of whether or not bromide ion was added to the standards.

Because addition of hydrazine sulfate similarly improved selectivity with respect to chloride, the concentration of crystal violet chloride reagent was increased in an attempt to achieve higher sensitivity to nitrate. Linear and reproducible calibration curves with working range 0.06–0.72 ppm nitrate were obtained when the crystal violet concentration was 1.3×10^{-3} M and the hydrazine sulfate concentration in the standards was 1.4×10^{-4} M. From a typical calibration run, illustrated in Table IV, it may be seen that the method may be successfully applied to nitrate solutions from 60–720 ppb NO_3 with a standard deviation of 28 ppb.

Table IV. Crystal Violet Method for Nitrate Calibration Run

Solution No.	Absorbance reading		Nitrate concentration, ppb		
	Obsd	Calcd[a]	Taken	Calcd[a]	Error, ppb
1	0.507	0.499	60	79	+19
2	0.534	0.524	120	144	+24
3	0.543	0.549	180	166	−14
4	0.566	0.574	240	221	−19
5	0.587	0.598	300	272	−28
6	0.613	0.623	360	336	−24
7	0.708	0.697	540	566	+26
8	0.740	0.722	600	643	+43
9	0.760	0.772	720	692	−28

$S = 28$ ppb

[a] Calculated from least squares equation: $A = (412.5 \pm 12)C_{NO_3} + 474.6 \pm 7.4$ where A is absorbance and C_{NO_3} is expressed in ppb.

CONCLUSION

Modification of the crystal violet procedure to include hydrazine sulfate reagent and an increased concentration of crystal violet chloride reagent has resulted in greater sensitivity and selectivity. The method is reliable and simple enough to use routinely. Finally, the surprising ease of oxidation of bromide to tribromide suggests that much more care in dealing with samples containing bromide (and of course iodide) need be exercised.

LITERATURE CITED

(1) M. J. Taras, "Colorimetric Determination of Nonmetals", D. F. Boltz, Ed., Interscience, New York, N.Y., 1958, pp 135–147.
(2) Y. Yamamoto, S. Ushikawa, and K. Akabori, *Bull. Chem. Soc. Jpn.*, **37**, 1718 (1964).

RECEIVED for review July 25, 1977. Accepted August 15, 1977. This work was supported by a grant from the Environmental Protection Agency.

Detection of Trinitrotoluene in Water by Fluorescent Ion-Exchange Resins

Carl A. Heller,* Robert R. McBride,[1] and Matthew A. Ronning[2]

Chemistry Division (Code 385), Naval Weapons Center, China Lake, California 93555

A system is described for monitoring the effluent water from the purification apparatus of ammunition plants. This system will give warning of any colored species, but is mainly valuable for detecting trinitrotoluene (TNT) at low levels (70 ppb). The heart of the system is a fluorescent-dyed quaternary ammonium ion-exchange resin which darkens in contact with TNT. The resin is irradiated with ultraviolet radiation and the fluorescent output is monitored by a photomultiplier.

The detection of TNT (2,4,6-trinitrotoluene) in effluent water from ammunition plants is necessary for controlling this pollutant (*1*). This paper describes a detection system which is presently usable at 0.07 ppm and could be made more sensitive. The basis of the method is the absorption of TNT on a quaternary ammonium ion-exchange resin. The original thought was to absorb a fluorescent molecule on an ionic site and then the TNT on the same site. It was thought that the quenching of the fluorescence could be used to measure the TNT. As it happened, the fluorescence was quenched, but probably only in the trivial sense that a colored product formed on the resin and filtered both the ultraviolet exciting light and the emitted light. This did turn out to be sensitive at low levels since the colored compounds are held on the surface of a resin bead and quickly form an effective light filter.

The reactions of TNT to give colored products are well known (*2, 3*). Reactions of TNT with quaternary amines are not known and indeed we saw no reaction in aqueous solution. However, it appears likely that Meisenheimer anions are formed in the resins to give the dark colored products. Several structures, including dimers of two TNT molecules, have been suggested for Meisenheimer anions. Our major new evidence involves the strong binding of these colored species in the resin.

Ammunition plants purify the effluent water with various absorbing columns and need methods to detect breakthrough. TNT is one of the more toxic materials as are some of its decomposition products in the so-called "pink water". These colored breakdown products also given a signal on the resins. Colorless organic compounds or inorganic ions will not be detected.

EXPERIMENTAL

Apparatus. The essentials of our apparatus (Figure 1) consist of the liquid flow system and an optical system for illuminating and viewing the beads immersed in the liquid system. This portion contains beads of commercial ion-exchange resin dyed with a fluorescent dye. Initially the beads glow brightly under UV irradiation and this glow is detected photometrically and registered on a strip chart recorder. TNT in the water causes the resin beads to darken on the surface and the measured light output immediately decreases.

The flow system uses a Cole-Parmer Masterflo pump in which only Viton tubing touches the solution until it reaches the Pyrex U-tube containing Pyrex wool and the resin beads. Viton was the only tubing tested which did not absorb TNT from solutions. The beads clearly absorb TNT, but at such low capacity that we can't detect any decrease of concentration spectrometrically. On the other hand, when water is recycled over beads, it picks up material which can be detected spectrometrically at 230 nm in a 10-cm path cell.

The Pyrex U-tube was held in the cell compartment of a filter fluorimeter by a special holder. The fluorimeter was a Photovolt 540 using a primary filter for the mercury 365-nm light (Corning CS-7-60) and a secondary filter for fluorescein (Corning CS-3-67). A General Electric S-4 medium pressure mercury lamp was used. The output was detected with a 1P21 RCA Photomultiplier using a Photovolt 540 M Photometer and recorded using a Hewlett-Packard 7100A potentiometric recorder.

Material. Resins of various manufacturers were tried and several quaternary salt polystyrenes gave positive results. Dowex-2, which was used for most of the work, is a cross-linked polystyrene which has been amminated on the phenyl rings. The amine is dimethyl ethanol benzyl quaternary ion with chloride as the counteranion. The exchange capacity is 3.15 mequiv g^{-1} of dry resin which means there is an amine group on about every other unit of the polymer chain. The cross-linking varies according to the percent of divinylbenzene—we tried materials listed as X4, X8, and X10. The bead sizes varied and we separated special sizes for our own use by sieving. We also separated the spherical beads from broken material by rolling down an inclined board.

We treated the beads with concentrated NaOH or NaCN to change the counterion from Cl^- to OH^- or CN^-. The resin was water-washed to remove excess electrolyte. Rhodamine B was the first dye used. It gave positive results and moderate sensitivity but it was felt that this red fluorescer would be inherently less useful since photomultipliers lose sensitivity in the red. Uranine, a yellow fluorescer, was introduced quantitatively by placing beads into a aqueous uranine solution at concentrations where more than 99% was absorbed. The dye colored only an outer shell of the beads as could be observed by microscopic examination of sliced beads. The total capacity of some chloride beads was measured as 55.4 mmol g^{-1}. The beads were dried before being loaded into the U-tubes.

We used military grade α-TNT and RDX (2,4,6-trinitro-2,4,6-triazacyclohexane) as available in our laboratory. Aqueous solutions of α-TNT were made 100 μM and stored in glass bottles in the dark. The ultraviolet absorption spectra remained constant for months with only one peak at 233 nm where the molecular absorbance was $\epsilon = 19\,600\ M^{-1}\ cm^{-1}$.

Procedures. Three chemical forms of the resin were tried—the original chloride, the hydroxide, and the cyanide. Many physical configurations of the beads in various tube shapes were tried. The final and best material was with cyanide counterions using 35–60 mesh beads of Dowex-2 X10 with 50 μmol g^{-1} of uranine.

The U tubes (Figure 1) were made of 3-mm o.d. standard wall Pyrex. The U was 68 mm long with one arm bent outward 45° for the upper 20 mm. The ends were flared to hold the Viton tubing. The tubes were reinforced at the bottom and top with epoxy resin to prevent breakage.

Loading was in the straight arm using Pyrex glass wool at the bend, then beads for about 10 mm, and then another wool plug. Water was run into the straight arm. The tube was constricted at the bottom bend to prevent the glass wool plug from being moved by the water.

Water or solutions were pumped through the Viton tubing and U tube at rates of 10–50 mL min^{-1}. The fluorescence was monitored on the strip chart recorder. Solutions were changed

[1] Present address, Harvey Mudd College, Claremont, Calif.
[2] Present address, California Institute of Technology, Pasadena, Calif.

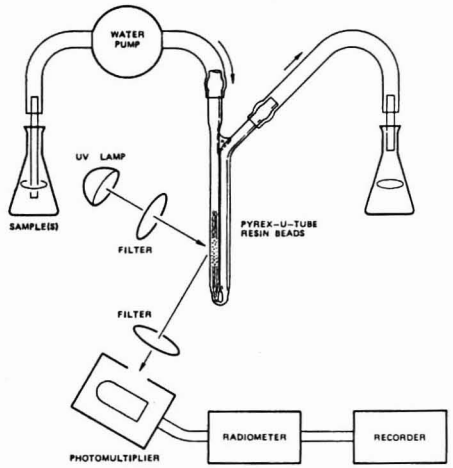

Figure 1. Schematic of apparatus

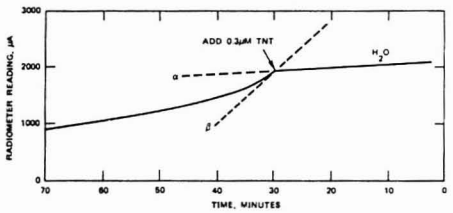

Figure 2. Recorder chart. The 0.3 μM TNT is 68 ppb

by moving the Viton tubes from one Erlenmeyer flask to another.

TNT concentrations in solutions were monitored using the absorbance at 233 nm in cells from 0.3 mm to 10 cm in length. With dilute solutions, the resin gave off absorbing materials which interfered with this technique. It is this type of interference which negates the use of spectral absorbance for monitoring TNT in the presence of less toxic organic materials.

RESULTS AND DISCUSSION

Analytical Runs. Figure 2 shows a reproduction of the chart record run with a solution using 0.30 μM TNT (0.068 ppm). The break in the curve is a quick indication of the presence of TNT. Figure 2 shows two drawbacks of the present method. There is a small drop in light output (radiometer reading) even with distilled water The decrease in light with TNT solution is not linear, but instead the light asymptotically approaches a lower limiting value. This lower limit depends upon the concentration of TNT as does the slope of the initial dropping curve.

Table I gives the slopes of the fluorescence decay for water (α) and for the initial drop with solutions of TNT (β). Figure 2 defines these slopes. The magnitude of the slopes will clearly depend upon the apparatus, the UV lamp irradiance, etc., but should stay in the same relative ratios. The material used in these runs was the most sensitive made to date, but batches of equivalent sensitivity have been made since.

It is also possible to measure the total decrease in light when the beads have become black and opaque. Only a few runs of this length were made and the results are shown in Table II.

Table I. Summary of TNT Concentration and Flow Rate Runs

Run No.	Flow, mL min^{-1}	α, μA min^{-1} [a]	TNT, μm	β, μA min^{-1} [b]
23A	13	0.7	10	1000
23B	30	12	5	2800
23C	14	48	2.1	890
23D	30	15	0.82	236
23F	33	0	10	1800
23G	30	14	10	2000
23H	30	7	5	1000
23I	34	8	2.1	260
23J	31	9	0.82	320
23K	25	16	0.3	186
29-1	43	4.2	9	741
29-2	30	4.2	9	1060

[a] α is the slope with distilled water running at the flow rate indicated. [b] β is the slope with TNT solution running at the same flow rate.

Table II. Radiometer Readings

TNT, μM	I_0, [a] mA	I_∞, [b] mA	t, hour
0	5 900	5 100	24
5	12 000	50	3
20	7 500	400	3
50	65 000	8 000	3

[a] I_0 = Initial reading. [b] I_∞ = Reading after reaching lower plateau.

In another run, a low concentration of TNT (0.82 μM) was passed over the beads for 20 min. Then a higher concentration (2.1 μM) caused a clear break in the slope. When periods of water flow were intermixed with sections of TNT solution flow, there were flat portions for the water while the TNT curves looked like portions of an unbroken curve. Sometimes there was a slight upward recovery during the water flow period but this never approximated the original light level although the resin seemed to "wash out" more when the TNT periods were very short, i.e., when the products were "fresh".

The runs with rhodamine B are of interest since it is a cationic dye. The fluorescein dianions of uranine can be associated with the cations of the resin at least up to the 3.15 mequiv g^{-1} level. The rhodamine cations must be located in the neutral portions of the polymer chains. The fluorescein anions can be displaced by Meisenheimer anions and presumably would give higher sensitivity. Some efforts to determine this effect were unsuccessful.

Chemical Experiments. To learn more about the chemical reactions, resin beads without fluorescer were reacted with TNT solutions. They start out looking amber, turn red, and then black. Attempts to take absorption spectra by immersing the beads in solutions of matching index of refraction were unsuccessful.

Reacted beads were sliced and viewed through a microscope which showed that only an outside shell was colored. Beads were stirred with TNT solutions for several days and only about 25% of the reactive sites had taken up TNT. Hoffsummer (*4*) tells us that he observed the same thing when he tried to use resin beads to clean up TNT from water. He also observed that RDX, an equally large molecule, did seem to penetrate resin beads to react with an OH^- counteranion. In our work the uranine molecules penetrate completely when at high concentration; perhaps the Meisenheimer anions formed from TNT block the pores of the resin.

It should be noted that the initial reaction is very fast, as shown in Figure 2. The outer surface darkens very rapidly. We followed the uptake of TNT by 35–60 mesh beads for

several days. The curve of uptake starts rapidly and becomes very slow. Thus reaction 1 must be very rapid, but diffusion is very slow for some reason.

A point of interest is that quaternary amines which are soluble in water do not give colored products with TNT. We tested benzyl triethyl ammonium chloride and benzyl dimethyl ethanol ammonium chloride with TNT-saturated water and obtained no visible reaction. The environment in the polymer beads must shift the reaction equilibrium toward the colored species.

Interferences. Any colored anion, organic "dye" or dark particulate matter will give a signal. We obtained signals with "pink water" from TNT photolysis and from rusty tap water. For the intended use, this is not a drawback since any of these in the purified water is a reason to make adjustments in the purification system. Batch analytical methods exist to separate and identify the impurities (*5*). Most noncolored organic or inorganic materials will not give a signal. We specifically tested RDX, NH_4NO_3, and two sulfonated dinitro toluenes formed from β- and γ-TNT plus sodium sulfite (*6*).

The really bad case would be any poisons which lowered the sensitivity to TNT without darkening the resin. RDX, a likely contaminant, did not do this. Since the water is generally low in other contaminants after passage through a carbon or resin column, we think this danger is low, but it can be checked periodically by adding known TNT solutions or can be taken care of by replacing the beads daily.

CONCLUSIONS

A sensitive method for detecting TNT in water has been found. A reaction to form a colored material is used as has been used elsewhere (*1*). However, in the present case, the colored compound is immobilized from the flowing water and held in front of the detector, thereby increasing the sensitivity.

This method might be used as a semicontinuous monitoring system by flowing distilled or tap water 99% of the time with samples of effluent water for 50 out of every 100 s. The sudden break in the record could be monitored visually or with an electronic system. The beads will become less sensitive once TNT is initially detected but the beads are inexpensive and easily replaced. Different batches of beads have given similar responses to TNT so a semiquantitative estimate of concentration is possible although simple detection may be all that is needed.

ACKNOWLEDGMENT

Discussions with Ronald Henry, William Norris, Eugene Martin, and Donald Moore were very helpful. Ronald Henry and Taylor Joyner also supplied us with several chemicals not easily available elsewhere.

LITERATURE CITED

(1) D. H. Rosenblatt, M. J. Small, and J. J. Barkley, Edgewood Arsenal Report No. 73-07 USAMEERU, AD-912752 (June 1973).
(2) C. A. Fyfe, C. D. Malkiewich, S. W. H. Damji, and A. R. Norris, *J. Am. Chem. Soc.*, **98**, 6983 (1976).
(3) C. F. Bernasconi, *J. Org. Chem.*, **36**, 1671 (1971).
(4) J. C. Hoffsummer, Naval Surface Weapons Center, White Oak, Md., personal communication.
(5) J. C. Hoffsummer and J. M. Rosen, Naval Ordnance Laboratory, Technical Report 71-151 (1971); J. C. Hoffsummer, *J. Chromatogr.*, **51**, 243 (1970).
(6) T. Urbanski, "Chemistry and Technology of Explosives", Macmillan, New York, N.Y., 1964, Vol. I, pp 332–333.

RECEIVED for review July 14, 1977. Accepted September 12, 1977. R.R.M. and M.A.R. were work experience students from Burroughs High School, Ridgecrest, Calif.

Separation of Hydroaromatics and Polycyclic Aromatic Hydrocarbons and Determination of Tetralin and Naphthalene in Coal-Derived Solvents

J. F. Schabron and R. J. Hurtubise*

Department of Chemistry, University of Wyoming, Laramie, Wyoming 82071

H. F. Silver

Mineral Engineering Department, University of Wyoming, Laramie, Wyoming 82071

Tetralin and naphthalene in a coal liquefaction recycle solvent were determined by high performance liquid chromatography (HPLC) with a μ-Bondapak C_{18} stationary phase and a methanol:water mobile phase. Initially two fractions were collected from an aluminum oxide open column. The first fraction contained tetralin and the second naphthalene. The standard addition method was employed to determine tetralin and naphthalene. The standard deviation was 0.024% for tetralin and 0.035% for naphthalene. Several aromatic and hydroaromatic compounds were identified by their chromatographic behavior and by their fluorescence excitation and emission spectra. A correlation factor which relates the log k' values for polycyclic aromatic hydrocarbons (PAH), alkyl-substituted aromatic hydrocarbons, and hydroaromatics to certain structural features was developed. The results from this work show the possibility of developing an overall separation and characterization scheme for complex mixtures of aromatic and hydroaromatic compounds.

Table I. Precision of the Method with F-3

Sample weight, mg	Tetralin, % w/w	Naphthalene, % w/w
97.92	6.08	6.36
97.92	6.13	6.40
97.92	6.10	6.38
96.67	6.10	6.31
96.67	6.14	6.34
	$\bar{x}$ = 6.11	$\bar{x}$ = 6.36
	s = 0.024	s = 0.035

95% confidence level
tetralin: 6.11 ± 0.030%
naphthalene: 6.36 ± 0.043%

There are a variety of methods currently in use for the separation and characterization of components in coal liquids. Most involve fractionation into various classes of compounds

which are subjected to further analysis. Sternberg et at. (*1*, *2*) divided coal conversion products into asphaltenes and oils. These main constituents were further subdivided by column chromatography and precipitation. Slightly modified separation and characterization methods developed by the Bureau of Mines–API Research Project 60 for characterizing heavy ends of petroleum were used successfully in analyzing coal liquid distillates within the boiling range 200 to 540 °C (*3*). Farcasiu (*4*) developed an alternative scheme based on separation of fractions of different chemical functionality using sequential elution of the fractions from silica gel. Process solvents and liquefaction products were separated into saturates, aromatics, and various polar materials with neutral alumina by Schiller (*5*) and then subjected to GC/MS analyses. After preparative separation using gel permeation chromatography, various coal liquid fractions were studied by quantitative ^1H and ^{13}C Fourier transform nuclear magnetic resonance techniques by Dorn et al. (*6*, *7*). Raw anthracene oil was separated using cation, anion, and complexation chromatography by Scheppele et al. (*8*, *9*). They studied some of the fractions with low- and high-resolution field ionization mass spectrometry. Prather et al. (*10*) used HPLC to characterize creosote oil during hydrogenation/hydrodesulfurization of the oil.

Aluminum oxide separations with the appropriate mobile phase occur mainly by aromatic ring number (*11*). Compounds with the greater number of aromatic rings are retained more strongly. This has proved useful for the separation of various classes of polycyclic aromatic hydrocarbons (PAH) from complex samples such as shale oil (*12*). The separation mechanism on a μ-Bondapak C_{18} column is not as clear (*13*). Sleight (*14*) showed that the retention volumes of aromatic hydrocarbons generally increase with increasing carbon number on columns of Zipax Permaphase ODS in water–methanol mixed solvents. Sleight also showed that the retention volumes of alkyl-substituted aromatic hydrocarbons increased with increasing aliphatic carbon number. Without prior information as to the parent compound type, however, approximate capacity factors (k') were difficult to estimate. In this study, an analytical method was developed to determine specifically tetralin and naphthalene in a coal-derived solvent. Tetralin is important in the study of the hydrogen donor capacity of recycle solvents (*15–19*). A measure of tetralin in recycle solvents can be obtained by gas–liquid chromatography using a Dexsil 300 liquid phase to obtain simulated boiling-point distributions (*15*). This type of approach is useful but can result in complex chromatograms and is subject to interferences (*20*). Aluminum oxide open-column chromatography, μ-Bondapak C_{18} HPLC, and fluorescence spectroscopy were combined in this work to give qualitative and quantitative information on tetralin and naphthalene in the coal-derived solvent which was hydrogenated under different conditions. Several other hydroaromatic and polycyclic aromatic hydrocarbons were also separated from the solvent and identified. An empirical correlation factor which relates the structures of alkyl-substituted and unsubstituted aromatic hydrocarbons and alkyl-substituted and unsubstituted hydroaromatics to log k' values on a μ-Bondapak C_{18} column was developed.

EXPERIMENTAL

High Performance Liquid Chromatography. The liquid chromatograph used was a Waters model ALC/GPC 244 equipped with a model 6000-A pump, a U6K injector, and a free standing ultraviolet detector set at 254 nm. A stainless steel tube 11 cm × 0.23 mm i.d. attached to the exit port of the detector cell was used in sample collection. A Waters μ-Bondapak C_{18} 3.9 mm i.d. × 30 cm column was employed. This column has a monomolecular layer of octadecyltrichlorosilane chemically bonded to Waters μ-Porasil. Methanol:water (65:35) at a flow rate of 1 mL/min was employed, and a 10 mV recorder completed the system.

Open-Column and Thin-Layer Chromatography. The columns used were 50 cm × 11 mm i.d. Pyrex (Corning No. 2145) and were dry packed to a height of 35 cm with aluminum oxide activity II–III according to Brockmann (aluminum oxide from I.C.N. Life Sciences, Cleveland, Ohio, and Brinkmann, Westbury, N.Y. were used interchangeably). Columns packed with silica gel (0.1–0.2 mm, 130–170 mesh, Brinkmann) were prepared in the same manner. Brinkmann ALOX N/UV 254 thin-layer chromatoplates were used in the thin-layer chromatography (TLC) work with *n*-hexane as the mobile phase.

Reagents. Pure grade (99% min.) *n*-hexane was obtained from Phillips Chemical, Borger, Texas. Glass distilled methanol from Burdick and Jackson, Muskegon, Mich., was filtered through a Millipore type F-H 0.5-μm filter. Distilled water was filtered through a Millipore type G-S 0.22-μm filter.

Naphthalene (99+%) and Tetralin (99%) were obtained from Aldrich and used as received. All other chemicals were obtained from commercially available sources and were purified when necessary.

Recycle Solvents. Recycle solvent from the liquefaction of Wyodak Coal at Wilsonville, Ala., (designated F-1) was hydrogenated at 2000-psi initial hydrogen pressure at 700 °F for 1 h over a Co–Mo on Al_2O_3 catalyst (Nalcomo 471). The product was designated F-2. Hydrogenation of F-1 solvent at 3000-psi initial hydrogen pressure at 800 °F for 1 h over the same catalyst resulted in a product designated F-3. The nominal boiling range of the three solvents was from 177–427 °C (350–800 °F).

Procedure. *Preparation of Samples with No Hexane Insolubles (F-3).* A 20-g sample was brought to volume with *n*-hexane in a 100-mL volumetric flask. Aliquots of 25 mL were added to each of three 50-mL volumetric flasks. Standard additions of 50 mg and 100 mg each of tetralin and naphthalene were added volumetrically to two of the flasks, respectively. All three flasks were diluted to volume with *n*-hexane. Aliquots of 1 mL of each of the solutions were pipetted onto the top of each of three aluminum oxide columns. Elution was performed with *n*-hexane. Work with standards showed that the tetralin was eluted totally in the first 15 mL (Fraction 1) and the naphthalene in the next 40 mL (Fraction 2). Fractions 1 corresponding to the unknown and two standard additions were collected in 25-mL volumetric flasks. Fractions 2 corresponding to the unknown and two standard additions were collected in 50-mL volumetric flasks. Prior to collection, 10 mL of *n*-hexane was pipetted into each of the six flasks. The fractions were collected until the appropriate volumes were obtained. These solutions were ready for injection onto the μ-Bondapak C_{18} column.

Preparation of Samples with Hexane Insolubles (F-1 and F-2). Hexane insolubles from F-1 or F-2 coat the volumetric glassware when the sample solution is less than about 25% w/v in *n*-hexane. The volume displacement was found to be approximately 0.5 mL for a 20-g sample. To minimize this source of error, a solution of 20 g sample in approximately 120 mL *n*-hexane was made and swirled in a sealed flask. After at least 2 h, most of the solid material coated the flask, and the remaining solution was rinsed into a 250-mL volumetric flask, then diluted to volume. Three aliquots of 25 mL each of the diluted solution were prepared as before, but the standard addition quantities were 20 mg and 50 mg for both tetralin and naphthalene. Aliquots of 2 mL each were pipetted onto the aluminum oxide columns. Fractions 1 and Fractions 2 were collected and diluted in the same manner as described above. These solutions were ready for injection onto the μ-Bondapak C_{18} column.

Determination of Tetralin and Naphthalene. Determination of tetralin in F-1, F-2, and F-3 was accomplished by an injection of 10 μL of each of the unknown and two standard addition solutions onto the μ-Bondapak C_{18} column with the detector at 0.01 absorbance unit. The heights of the tetralin peaks were all measured and were "normalized" to the peak height of the only other predominant chromatographic peak in Fraction 1 which was identified as indan. This internal reference peak represented a constant amount of indan present in the unknown and two standard addition solutions for a given sample. Normalization of all the tetralin peak heights to a constant indan peak height compensated for the nonreproducible injections inherent in the HPLC system. A standard addition curve was prepared by

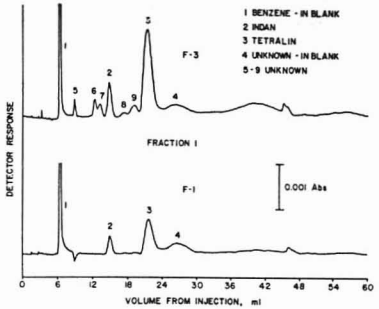

Figure 1. HPLC chromatograms of 10-μL injections of Fraction 1 from 85 mg F-1 and 97 mg F-3, obtained with a μ-Bondapak C_{18} column with methanol:water (65:35) at 1 mL/min

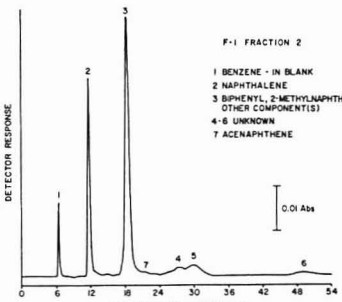

Figure 2. HPLC chromatogram of a 10-μL injection of Fraction 2 from 85 mg F-1. Conditions as in Figure 1

plotting peak height vs. mg tetralin added. The line intersecting the peak height axis was extrapolated to zero peak height to obtain the tetralin concentration in the prepared solution. From this value, the percentage tetralin was calculated.

Injections of 10 μL at 0.1 absorbance unit were used for the determination of naphthalene. Peak heights were normalized to the predominant peak at 18.4-mL. retention volume, which from fluorescence studies with F-1, was believed to be composed mainly of biphenyl and 2-methylnaphthalene. The percentage naphthalene was calculated in the same manner as tetralin.

HPLC chromatograms of Fraction 1 from F-1 and F-3 and Fraction 2 from F-1 show the positions of the internal reference peaks, tetralin peak, and naphthalene peak (Figures 1 and 2). The peaks in the chromatograms due to benzene resulted from approximately 0.016% w/v benzene present in the *n*-hexane.

Peak Identification. An appropriate amount of sample or standard solution was injected onto the μ-Bondapak C_{18} column, and peaks were collected directly into a 1 × 1 cm quartz cuvette. Final volume was adjusted between 3–4 mL with methanol:water (65:35), and fluorescence excitation and emission spectra taken. Spectra were then compared with standard spectra taken from standards run through the aluminum oxide–HPLC system. A Perkin-Elmer MPF-2A Spectrophotofluorometer was used for obtaining the fluorescence spectra. Both excitation and emission slits were set at 6 nm for all the emission spectra. The emission slit was set at 10 nm and the excitation slit at 2 nm for all the excitation spectra. The sensitivity for each spectrum was adjusted to a level which yielded spectra of comparable peak heights.

RESULTS AND DISCUSSION

Initial Experiments. Fluorescence spectra were employed for chromatographic peak identification, as very dilute samples can be analyzed without any preconcentration steps. Samples

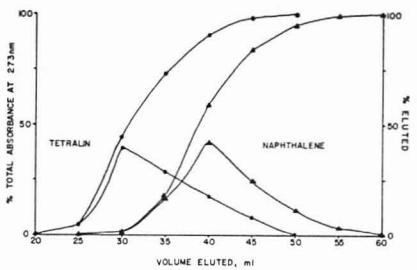

Figure 3. Elution of 9.7 mg tetralin and 9.6 mg naphthalene from silica gel columns

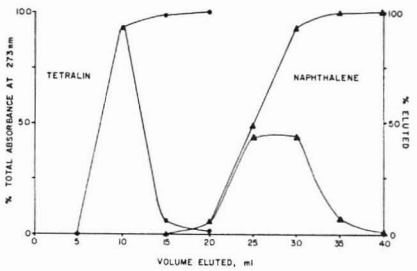

Figure 4. Elution of 9.7 mg tetralin and 9.6 mg naphthalene from aluminum oxide columns

thought to contain tetralin were first separated with either silica gel or aluminum oxide dry columns using *n*-hexane as the mobile phase. Fluorescence spectra showed two components present in the HPLC samples collected at the retention volume for tetralin. Tetralin was one component with an emission maximum at 286 nm, and an unknown, with emission maxima at 324 and 339 nm. An excitation spectrum of the interfering component was taken and compared with the maxima of several published ultraviolet absorption spectra (*21*), leading to the assumption that the unknown was an alkyl-substituted naphthalene. Later, after it was separated from tetralin, the unknown was identified as acenaphthene by fluorescence spectroscopy. In order to remove this interfering component, two separate fractions had to be collected, one containing tetralin and the other acenaphthene. Both silica gel and aluminum oxide columns, prepared as before, were investigated. It was assumed that in both systems tetralin would elute first, naphthalene and acenaphthene second, with naphthalene eluting slightly before acenaphthene. The desired separation would, therefore, provide a fraction containing all the tetralin (Fraction 1), and a second fraction containing naphthalene and acenaphthene (Fraction 2).

Approximately 10 mg each of tetralin and naphthalene were placed on top of individual columns packed with each adsorbent. Samples were collected every 5 mL, diluted to an appropriate volume, and absorbance data obtained. Results were plotted as percentage of the total absorbance of all samples at 273 nm for each sample vs. mL eluted (Figures 3 and 4). 98.5% of the tetralin eluted from the aluminum oxide column before the naphthalene started to elute. Thus, aluminum oxide provided a relatively clean separation of tetralin and naphthalene, whereas silica gel did not. Experiments also showed that the μ-Bondapak C_{18} column with methanol–water mobile phase readily separated naphthalene and acenaphthene. To check if tetralin was separated from acenaphthene with the aluminum oxide system, samples

Table II. Variation of Sample Size

Sample	Weight, mg	Tetralin, % w/w	Average	Naphthalene, % w/w	Average
F-3	96.67	6.10		6.31	
	96.67	6.14	6.12	6.34	6.32
	48.93	6.13		6.40	
	48.93	6.15	6.14	6.36	6.38
F-2	81.20	2.71		7.09	
	81.20	2.73	2.72	7.03	7.06
	43.61	2.77		7.08	
	43.61	2.73	2.75	7.04	7.06
F-1	85.29	2.24		7.27	
	85.29	2.32	2.28	7.33	7.30
	44.24	2.24		7.28	
	44.24	2.28	2.26	7.32	7.30

corresponding to the chromatographic peaks at the retention volume of tetralin from a μ-Bondapak C_{18} column were collected for both Fractions 1 and 2 from F-1. Fluorescence excitation and emission spectra were obtained from each sample. The fluorescence spectra indicated the chromatographic peak from Fraction 1 was tetralin, and the chromatographic peak from Fraction 2 was acenaphthene. These results indicated that tetralin was separated from acenaphthene.

Sample Size. Sample size studies were performed with aluminum oxide columns with F-1. Sample sizes of 1000, 500, and 200 mg overloaded the column to the extent that naphthalene was present in Fraction 1. Acenaphthene was also present in Fraction 1 with sample sizes of 1000 and 500 mg, but not 200 mg. Sample sizes of 100 and 50 mg resulted in a clean separation of tetralin and naphthalene with no interference from acenaphthene. For all quantitative HPLC work, 10-μL injections of the aluminum oxide fractions were made. Injection of more than 10 μL of these hexane solutions into the methanol:water mobile phase resulted in distorted chromatographic peaks. The peak distortion did not affect peak collections for qualitative fluorescence work when more than 10-μL samples from Fraction 1 were injected.

Precision and Accuracy of the Method. The precision of the method for five replicate determinations of tetralin and naphthalene on F-3 was quite good, yielding results at the 95% confidence level of 6.11 ± 0.030% for tetralin and 6.36 ± 0.043% for naphthalene (Table I).

Results of analysis of F-1, F-2, and F-3 at two different sample size levels illustrate the absence of any significant constant error (Table II). Spiking experiments for each sample at two levels of tetralin and naphthalene indicated good percentage recovery (Tables III and IV).

Limits of Detection. Limits of detection were calculated at maximum detector absorbance settings of 0.01 for tetralin and 0.1 for naphthalene. Since baseline noise at these settings is minimal, the smallest practical measurable peak height was chosen arbitrarily to be 2 mm. Typically observed standard addition curve slopes of 10 mm/mg for tetralin and 17 mm/mg for naphthalene were used. For a 100-mg sample, this would correspond to limits of detection for the method as described of 0.2 mg tetralin, or 0.2% tetralin, and 0.1 mg naphthalene, or 0.1% naphthalene. These limits could be lowered by increasing the detector sensitivity or concentrating the hexane fractions. All anticipated samples fall well above these limits.

Identification of Tetralin, Indan, and Naphthalene. Chromatographic peaks corresponding to tetralin, indan, and naphthalene each from F-1, F-2, and F-3 were all collected from the μ-Bondapak C_{18} column after separation on aluminum oxide columns. The fluorescence excitation and emission spectra were obtained and were compared with excitation and emission spectra of standards treated chromatographically in an identical manner. Comparison of the sample excitation and emission spectra with the corresponding standard excitation and emission spectra showed almost exact comparison for the respective compounds. The fluorescence excitation and emission spectra of tetralin and indan were identical. However, because of the chromatographic systems used, these compounds are separated completely. These results show how fluorescence spectroscopy can be used in combination with chromatographic techniques in the analysis of complex samples like coal-derived solvents.

Internal Reference Component. A basic assumption in using an internal reference peak from the sample chromatogram for the standard addition method is that the reference peak represents the same amount of internal reference compound in all solutions used in a determination. At one point, a new batch of aluminum oxide was used and erratic reference peak heights in the naphthalene fraction were

Table III. Percentage Tetralin Recovery in Spiked Samples

Sample	Weight, mg	Tetralin present, mg[a]	Tetralin added, mg	Tetralin found, mg[b]	Recovery, %
F-3	95.79	5.86	0.96	0.96	100
	95.79	5.86	0.96	1.01	105
	96.67	5.92	2.41	2.33	97
	96.67	5.92	2.41	2.46	102
					$\bar{x}$ = 101
F-2	86.32	2.36	0.77	0.77	100
	86.32	2.36	0.77	0.74	96
	84.60	2.32	1.93	1.98	102
	84.60	2.32	1.93	1.91	99
					$\bar{x}$ = 99
F-1	84.98	1.93	0.78	0.72	92
	84.98	1.93	0.78	0.73	94
	81.02	1.84	1.95	1.92	98
	81.02	1.84	1.95	1.89	97
					$\bar{x}$ = 95

[a] Results obtained from the standard addition method. [b] Results corrected for original tetralin content present in the sample.

Table IV. Percentage Naphthalene Recovery in Spiked Samples

Sample	Weight, mg	Naphthalene present, mg[a]	Naphthalene added, mg	Naphthalene found, mg[b]	Recovery, %
F-3	95.79	6.09	0.87	0.85	98
	95.79	6.09	0.87	0.83	95
	96.67	6.15	2.18	1.98	91
	96.67	6.15	2.18	2.02	93
					$\bar{x}$ = 94
F-2	86.32	6.09	0.70	0.65	93
	86.32	6.09	0.70	0.71	101
	84.60	5.97	1.75	1.81	103
	84.60	5.97	1.75	1.80	103
					$\bar{x}$ = 100
F-1	84.98	6.20	0.69	0.68	99
	84.98	6.20	0.69	0.66	96
	81.02	5.91	1.73	1.66	96
	81.02	5.91	1.73	1.69	98
					$\bar{x}$ = 97

[a] Results obtained from standard addition method. [b] Results corrected for original naphthalene content present in the sample.

Table V. R_f Values[a] and Retention Volumes[b] of Hydroaromatic and Polycyclic Aromatic Hydrocarbons

Compound	R_f value	Retention vol., mL
1) Benzene	--	6.3
2) 1,2,4-Trimethylbenzene	--	19.5
3) 1-Phenyldodecane		No indication of elution
4) Tetralin	0.74	21.5
5) Indan	--	14.8
6) 5-Methyltetralin	--	33.0
7) Indene	0.55	10.5
8) Naphthalene	0.50	11.7
9) Acenaphthene	0.44	21.5
10) 1,5-Dimethylnaphthalene	0.43	26.8
11) 1-Methylnaphthalene	0.43	17.6
12) Biphenyl	0.43	18.3
13) 2-Methylnaphthalene	0.42	18.4
14) 2,3-Dimethylnaphthalene	0.40	27.3
15) 1-Phenyl-3,4-dihydronaphthalene	0.38	55.2
16) 9,10-Dihydroanthracene	0.34	26.1
17) Acenaphthylene	0.32	14.6
18) 9,10-Dihydrophenanthrene	0.27	30.3
19) [2.2]Paracyclophane	0.24	32.8
20) Fluorene	0.20	25.2
21) Anthracene	0.14	28.0
22) Phenanthrene	0.13	25.0
23) Pyrene	0.069	39.6
24) Fluoranthene	0.056	36.9
25) Chrysene	0.054	62.1

[a] Aluminum oxide TLC with *n*-hexane eluent. [b] One μ-Bondapak C_{18} column with methanol:water (65:35) at 1 mL/min.

noticed. The collection of Fraction 2 was made from 15–50 mL, and a change to 15–55 mL rectified the problem, indicating that all the internal reference compound was not obtained in the first collection. As a precaution against nonuniformity within a given standard addition series, the amount of aluminum oxide placed in the glass column was weighed. This weight, about 38 g, was kept constant for a given batch of adsorbent.

R_f Values and Retention Volumes. The R_f values and retention volumes obtained in this work (Table V) suggest the possibility of developing an overall characterization scheme for aromatic and hydroaromatic hydrocarbons in coal liquid samples. For example, with the compounds in Table V, four main fractions could be separated initially with aluminum oxide. These fractions would contain compounds 1–6, 7–19, 20–22, 23–25, respectively. Further separation of each fraction with μ-Bondapak C_{18} would give almost complete separation of each compound in a given fraction. Phenanthrene and fluorene would have nearly the same retention volumes and 2-methylnaphthalene and biphenyl would have nearly the same retention volumes. However, with refinements in the chromatographic systems, it should be possible to achieve complete separation of these compounds.

The results in Table V show that it was necessary to obtain two fractions from the coal-derived solvents to determine tetralin and naphthalene. Acenaphthene and tetralin have identical retention volumes on μ-Bondapak C_{18}, thus necessitating the initial separation step with aluminum oxide.

Reversed-Phase Retention. The log k' values of several alkyl-substituted aromatic hydrocarbons have been shown to increase linearly with increasing aliphatic carbon number on Zipax Permaphase ODS and a methanol:water (7:3) mobile phase (*14*). A separate graph, however, had to be made for the alkyl derivatives of each parent aromatic hydrocarbon. In this work, attempts were made to correlate retention volumes of hydroaromatic compounds with retention volumes

Table VI. Log k' Values and Aromatic and Aliphatic Carbon Numbers for Aromatic and Hydroaromatic Hydrocarbons

Compound	log k'[a]	Aromatic carbon number	Aliphatic carbon number
Benzene	−0.041	6	0
Toluene	0.24	6	1
o-Xylene	0.46	6	2
p-Xylene	0.50	6	2
1,2,4-Trimethylbenzene	0.69	6	3
Indene	0.34	6	2[b]
Indan	0.54	6	3
Tetralin	0.74	6	4
5-Methyltetralin	0.95	6	5
Naphthalene	0.41	10	0
1-Methylnaphthalene	0.64	10	1
2-Methylnaphthalene	0.66	10	1
1,5-Dimethylnaphthalene	0.85	10	2
2,3-Dimethylnaphthalene	0.86	10	2
Acenaphthylene	0.53	10	1[b]
Acenaphthene	0.74	10	2

[a] μ-Bondapak C_{18} with methanol:water (65:35) at 1 mL/min. [b] It is assumed a nonaromatic double bond is equivalent to one aliphatic carbon. See text.

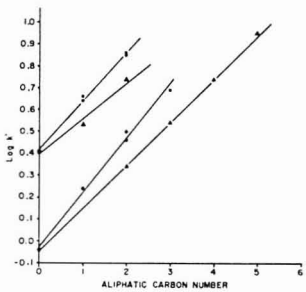

Figure 5. Plot of log k' vs. aliphatic carbon number for the compounds listed in Table VI. Unsubstituted compounds (O), alkyl-substituted compounds (●), hydroaromatics (▲). Chromatographic conditions are as in Figure 1

of alkyl-substituted derivatives with the same aromatic carbon number on a μ-Bondapak C_{18} column and a methanol:water (65:35) mobile phase. Table VI gives the data for the compounds investigated and Figure 5 shows several curves of log k' vs. aliphatic carbon number. The capacity factor, k', was calculated by $k' = (V_R - V_m)/V_m$ where V_R (mL) is the measured retention volume and V_m (mL) is the column void volume, which was determined by eluting methanol. Methanol had no retention at the eluting conditions employed. Separate curves were made for alkyl-substituted aromatic and hydroaromatic hydrocarbons with a different parent compound. As Figure 5 shows, curves of hydroaromatic compounds with a given aromatic carbon number exhibit different slopes compared to the slopes observed for curves of alkyl-substituted derivatives with the same aromatic carbon number. The compounds containing a nonaromatic double bond, such as indene and acenaphthylene, fall on the hydroaromatic curves if the two double-bonded carbons are considered to be equivalent in affecting retention to one aliphatic carbon. This assumption was also important in the development of an empirical correlation factor which is discussed later. Figure 5 shows that a correlation of a log k' value of an alkyl-substituted aromatic hydrocarbon with a hydroaromatic compound can be difficult without prior knowledge as to the

aromatic ring type. Knowledge of the aromatic ring type can be obtained by an initial aromatic class separation with aluminum oxide open-column chromatography using a *n*-hexane mobile phase, as was done in this work. If an initial aromatic class separation is carried out, then the curves in Figure 5 would be useful in predicting approximate retention volumes for both alkyl-substituted and hydroaromatic hydrocarbons in a given class. Also, the slopes of the hydroaromatic curves are less than the slopes of the corresponding alkyl-substituted aromatic curves. This indicates that hydroaromatic compounds with a given number of aromatic carbons interact less with the μ-Bondapak C_{18} stationary phase than the corresponding alkyl-substituted compounds.

The Correlation Factor. An empirical correlation factor was developed, which applies to alkyl-substituted and unsubstituted aromatic hydrocarbons and alkyl-substituted and unsubstituted hydroaromatics. This factor relates log k' values to certain structural features of the compounds. Use of an overall correlation factor would eliminate the need to plot a separate graph for a series of compounds with the same parent structure. One graph could then be used for all the compound types mentioned above. Our observations show that two aromatic or double-bonded carbons are approximately the same in affecting log k' as one methyl or methylene carbon. Tertiary and quaternary carbons, such as in an isopropyl or *tert*-butyl group, respectively, appear to have a negligible effect on retention. They seem to be insulated from interaction with the stationary phase. For example, the log k' values obtained by Sleight (*14*) for ethylbenzene and isopropyl benzene on Zipax Permaphase ODS with a methanol–water mobile phase are −0.64 and −0.62, respectively. Sleight included tertiary and quaternary carbons in his plot of log k' vs. alkyl chain carbon number and obtained a straight line for the benzene series with a slope of 0.100 and an intercept of −0.83. We plotted the same log k' values against "corrected aliphatic carbon number", a term which we defined as the number of aliphatic carbon numbers excluding tertiary or quaternary aliphatic carbons. A reasonably good straight line resulted. A linear regression slope of 0.17 and an intercept of −0.99 were calculated excluding the data point for hexaethylbenzene. The correlation coefficient was calculated to be 0.99. The intercept came closer to the log k' of −1.05 for benzene than the intercept of −0.83 reported by Sleight. This indicates a better correlation when tertiary or quaternary aliphatic carbons are assumed not to interact with the stationary phase. Hexaethylbenzene, with a "corrected aliphatic carbon number" of 12 did not fall near our graph. According to Sleight, hexaethylbenzene and 1,2,4,5,-tetraisopropylbenzene have identical log k' values. This suggests that the solubility characteristics of these compounds are the same. It appears with hexaethylbenzene the methylene carbons are insulated because of steric crowding by methyl groups and cannot interact readily with the stationary phase. In order to eliminate the need of initially knowing the parent compound, an empirical correlation factor was defined at first as the number of double bonds plus the number of primary and secondary aliphatic carbons. With this factor it was assumed that tertiary and quaternary carbons have no effect on retention, and thus they were not included. It was also assumed that an aromatic double bond affects retention to a degree identical to a nonaromatic double bond. Another assumption was that the various structural effects were additive. It was discovered, however, that the presence of a nonaromatic ring in a molecule resulted in less retention than predicted by the factor, and thus a correction had to be made for this. As mentioned earlier, the aliphatic ring part of a hydroaromatic compound probably cannot interact with the stationary phase as readily as an open aliphatic group. This effect was also assumed to be additive. With this correction, a new correlation factor, F, was defined finally as: F = number of double bonds + the number of primary and secondary carbons − 0.5 for a nonaromatic ring. To test the assumption of the lack of effect of tertiary or quaternary carbons on retention, another correlation factor, F', was defined as being equal to F plus the number of tertiary and quaternary carbons. Sleight's log k' values for several unsubstituted and alkyl-substituted aromatic hydrocarbons listed in Table VII were plotted vs. F'. A considerable amount of scatter was evident in the graph. The linear regression slope was 0.12 and the intercept at $F' = 3$ was −0.77. The correlation coefficient was 0.86. Finally, a plot of the same log k' values vs. our final correlation factor, F, was made. A reasonably good linear relationship was evident. This graph showed that separate curves are not needed for compounds with different parent structures. A linear regression slope of 0.19 and an intercept of −1.03 at $F = 3$ were calculated excluding the data point for hexaethylbenzene. The correlation coefficient was calculated to be 0.98. The results support the assumption that tertiary and quaternary carbons are effectively insulated from interaction with the stationary phase. Again, hexaethylbenzene, with an F value of 15, does not fall near the graph. If the six methylene carbons in this molecule are considered to be insulated from interaction with the stationary phase, and not included in the calculation of F, the resultant F value of 9 seems better. With an F value of 10 the data point lies on the curve, implying that the methylene carbons interact a slight extent with the stationary phase. The correlation is illustrated in Figure 6 for data obtained in this work on a μ-Bondapak C_{18} column (Table VIII). The value of V_m used in the calculations of k' was taken to be 3.3 mL, the elution volume of methanol. The values of log k' differ from those in Table VII since a different chromatographic system was used. Several hydroaromatic structures are included in Figure

Table VII. Values of log k' and the Correlation Factor, F, for Some Aromatic Hydrocarbons

Compound	log k'[a]	Correlation factor, F
Benzene	−1.05	3.0
Toluene	−0.77	4.0
Ethylbenzene	−0.64	5.0
Naphthalene	−0.64	5.0
Isopropylbenzene	−0.62	5.0
2-Methylnaphthalene	−0.49	6.0
Biphenyl	−0.47	6.0
n-Butylbenzene	−0.39	7.0
Fluorene	−0.36	6.5
Durene	−0.36	7.0
1,3-Diisopropylbenzene	−0.27	7.0
Phenanthrene	−0.26	7.0
2-Isopropylnaphthalene	−0.24	7.0
Anthracene	−0.17	7.0
2-Methylfluorene	−0.15	7.5
Diisopropyltoluene	−0.12	8.0
Methylphenanthrene	−0.09	8.0
Fluoranthene	−0.05	8.0
Pyrene	−0.03	8.0
1,4-Di-*tert*-butylbenzene	−0.01	9.0
Dimethylphenanthrene	0.09	9.0
1,3,5-Triisopropylbenzene	0.17	9.0
Naphthacene	0.23	9.0
Chrysene	0.24	9.0
Trimethylphenanthrene	0.24	10.0
1,2,4,5-Tetraisopropylbenzene	0.31	11.0
Hexaethylbenzene	0.31	15.0
1-Methyl-7-isopropylphenanthrene	0.38	10.0
1,3-Dimethylpyrene	0.40	10.0
2,6-Di-*tert*-butylnaphthalene	0.40	11.0
Perylene	0.44	10.0
3,4-Benzopyrene	0.49	10.0

[a] Values of log k' from Sleight (*14*).

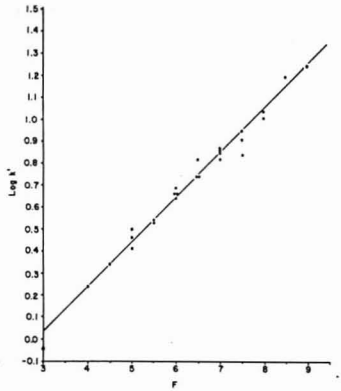

Figure 6. Plot of log k' vs. F for the compounds listed in Table VIII. Chromatographic conditions are as in Figure 1

Table VIII. Values of log k' and the Correlation Factor, F, for Some Aromatic and Hydroaromatic Hydrocarbons

Compound	log k'[a]	Correlation factor, F
Benzene	−0.041	3.0
Toluene	0.24	4.0
Indene	0.34	4.5
Naphthalene	0.41	5.0
o-Xylene	0.46	5.0
p-Xylene	0.50	5.0
Acenaphthylene	0.53	5.5
Indan	0.54	5.5
1-Methylnaphthalene	0.64	6.0
Biphenyl	0.66	6.0
2-Methylnaphthalene	0.66	6.0
1,2,4-Trimethylbenzene	0.69	6.0
Tetralin	0.74	6.5
Acenaphthene	0.74	6.5
Phenanthrene	0.82	7.0
Fluorene	0.82	6.5
9,10-Dihydroanthracene	0.84	7.5
1,5-Dimethylnaphthalene	0.85	7.0
2,3-Dimethylnaphthalene	0.86	7.0
Anthracene	0.87	7.0
9,10-Dihydrophenanthrene	0.91	7.5
[2.2]Paracyclophane	0.95	9.5
5-Methyltetralin	0.95	7.5
Fluoranthene	1.01	8.0
Pyrene	1.04	8.0
1-Phenyl-3,4-dihydronaphthalene	1.20	8.5
Chrysene	1.25	9.0

[a] μ-Bondapak C_{18} column with methanol:water (65:35) at 1 mL/min.

6. From examination of Figure 6 and the data in Table VIII, it is apparent that the correlation for the compounds with a nonaromatic ring would be poor without the correction of 0.5 F unit. Again, a reasonably good linear relationship is evident. An exception is [2.2]paracyclophane, which has a strained ring system with transannular interaction (*22*), and is not similar to the other compounds studied. A calculated linear regression slope of 0.20 and an intercept of 0.032 at $F = 3$ were obtained excluding the data point for [2.2]paracyclophane. The correlation coefficient was calculated to be 0.99. The log k' of 1-phenyl-3,4-dihydronaphthalene, with an F value of 8.5, is predicted from Figure 6 to be 1.15, which is very near to the experimental value of 1.20. Its structure includes a nonaromatic double bond and a nonaromatic ring. This correlation between predicted and observed log k' values suggests that the assumptions concerning nonaromatic double bonds and nonaromatic rings are valid.

In this study no attempt was made to elucidate the mechanism of the observed retention behavior, as this is beyond the scope of the work. A recent study by Kitka and Grushka (*13*) has shown that the retention mechanism on alkyl-bonded stationary phases is a complex phenomenon depending on several factors. Locke (*23*) has proposed that retention of compounds of similar type is a function mainly of solute solubilities in the mobile phase. With the empirical correlation factor developed in this work, the exact order of elution of compounds with the same or similar F values cannot be predicted. As an example, the log k' value of 0.84 for 9,10-dihydroanthracene with an F value of 7.5 is very close to the log k' value of 0.87 for anthracene, which has an F value of 7.0. The log k' of 0.91 for 9,10-dihydrophenanthrene, with an F value of 7.5 is 0.09 unit higher than the log k' of 0.82 for phenanthrene, which has an F value of 7.0. The observed difference in retention behavior of the two hydroaromatics is probably due to the nonlinear structure of 9,10-dihydrophenanthrene which exposes the two methylene groups to more interaction with the stationary phase than the two methylene groups in 9,10-dihydroanthracene. Also, it has been suggested that the nonplanar spatial arrangement of 9,10-dihydroanthracene causes it to be solvated more easily by methanol (*24*). This could cause it to be eluted sooner than most other compounds with the same F. Although the correlation factor has been demonstrated to work well with a methanol:water mobile phase, it has not been tried with water mixtures of acetonitrile, ethanol, or tetrahydrofuran.

In practice, the correlation factor, F, can be used to predict the approximate retention volume region in a reversed-phase HPLC system for a sought-after compound. Collection of various samples corresponding to the chromatographic peaks in the region of interest could be made, followed by sample identification. Alternatively, speculation as to the identity of a chromatographic peak from the injection of a sample from an aluminum oxide aromatic ring class separation could be performed. For example, speculation as to the identity of the unknown peaks in the HPLC chromatogram of Fraction 1 from F-3 in Figure 1 could be made. Peaks 5 through 9 have log k' and F values of 0.24 and 4.0, 0.44 and 5.0, 0.49 and 5.0, 0.64 and 6.0, and 0.69 and 6.0 or 6.5, respectively. The F values were obtained from Figure 6. Since the aluminum oxide separation limits the possibilities to one aromatic ring, 3.0 F units are accounted for. The speculation based on F values leads to some of the following as possible structures: peak 5, toluene; peaks 6 and 7, xylenes, ethyl benzene, or isopropylbenzene; peaks 8 and 9, trimethylbenzene, ethyltoluene, or *tert*-butylbenzene, and peak 9, methylindan. Speculation based on F as to the identity of peaks 4 through 6 in Fraction 2 from F-1 (Figure 2) is more difficult, but can be useful. The log k' values and F values for peaks 4 through 6 are 0.86 and 7.0, 0.90 and 7.0 or 7.5, and 1.14 and 8.5, respectively. Some possible structures are: peak 4, ethyl- or dimethylnaphthalene, or methylbiphenyl; peak 5, trimethylnaphthalene, methylacenaphthene, or methylfluorene; peak 6, 1,2,3,4-tetrahydroanthracene or 1,2,3,4-tetrahydrophenanthrene. The above lists do not include all possible structures; rather, they serve as examples of how F can be used. The number of possible structures increases as F increases. It may be more practical to use F to predict the approximate retention for a chemical structure than to predict chemical structures from retention data and F values, but both possibilities exist.

With some prior knowledge as to the structural features affecting retention on a reversed-phase HPLC column, the overall problem of isolation and identification is made easier.

Even though the correlation factor can be used without prior knowledge of the parent compound, coupling the use of this correlation factor for a C_{18} separation with an aluminum oxide aromatic ring class preparation step should provide a powerful analytical tool for overall characterization of hydroaromatics and aromatic hydrocarbons in complex samples.

LITERATURE CITED

(1) H. W. Sternberg, R. Raymond, and F. K. Schweighardt, *Science*, **188**, 49 (1975).
(2) H. W. Sternberg, R. Raymond, and F. K. Schweighardt, *Prepr., Div. Pet. Chem., Am. Chem. Soc.*, **21** (1), 198 (1976).
(3) S. A. Holmes, P. W. Woodward, G. P. Sturm, J. W. Vogh, and J. E. Dooley, ERDA BERC RI-76/10, 1976.
(4) M. Farcasiu, *Fuel*, **56**, 9 (1977).
(5) J. E. Schiller, *Prepr., Div. Pet. Chem., Am. Chem. Soc.*, **22** (2), 638 (1977).
(6) D. L. Wooton, W. M. Coleman, H. C. Dorn, and L. T. Taylor, *Prepr., Div. Pet. Chem., Am. Chem. Soc.*, **22** (2), 634 (1977).
(7) H. C. Dorn and D. L. Wooton, *Anal Chem.*, **48**, 2146 (1976).
(8) S. E. Scheppele, G. J. Greenwood, P. L. Grizzle, T. D. Marriott, C. S. Hsu, N. B. Perreira, P. A. Benson, K. N. Detwiler, and G. M. Stewart, *Prepr., Div. Pet. Chem., Am. Chem. Soc.*, **22** (2), 665 (1977).
(9) S. E. Scheppele, P. L. Grizzle, G. J. Greenwood, T. D. Marriott, and N. B. Perreira, *Anal. Chem.*, **48**, 2105 (1976).
(10) J. W. Prather, A. R. Tarrer, J. A. Guin, D. R. Johnson, and W. C. Neely, *Prepr., Div. Fuel Chem., Am. Chem. Soc.*, **21** (5), 144 (1976).
(11) L. R. Snyder, "Principles of Adsorption Chromatography", Marcel Dekker, New York, N.Y., 1968.
(12) R. J. Hurtubise, J. F. Schabron, J. D. Feaster, D. H. Therkildsen, and R. E. Poulson, *Anal Chim. Acta*, **89**, 377 (1977).
(13) E. J. Kitka, Jr., and E. Grushka, *Anal. Chem.*, **48**, 1098 (1976).
(14) R. B. Sleight, *J. Chromatogr.*, **83**, 31 (1973).
(15) Mobil R&D Corp., EPRI Project RP 410-1 (1976).
(16) L. E. Furlong, E. Effron, L. W. Vernon, and E. L. Wilson, *Chem. Eng. Progr.*, August, pp 69–75 (1976).
(17) Hydrocarbon Research, Inc., EPRI Project FR 389 (1976).
(18) G. Doyle, *Prepr., Div. Pet. Chem., Am. Chem. Soc.*, **21** (1), 165 (1976).
(19) R. C. Neavel, *Fuel*, **55**, 237 (1976).
(20) W. Bertsch, E. Anderson, and G. Holzer, *J. Chromatogr.*, **126**, 213 (1976).
(21) R. A. Friedel and M. Orchin, "Ultraviolet Spectra of Aromatic Compounds", John Wiley & Sons, New York, N.Y., 1951.
(22) E. L. Eliel, "Stereochemistry of Carbon Compounds", McGraw-Hill Book Company, New York, N.Y., 1962, p 195.
(23) D. C. Locke, *J. Chromatogr. Sci.*, **12**, 433 (1974).
(24) V. Martinù and J. Janák, *J. Chromatogr.*, **65**, 477 (1972).

RECEIVED for review June 21, 1977. Accepted August 30, 1977. Presented in part at the 174th National Meeting of the American Chemical Society, Chicago, Ill., August 1977. Financial support was provided by United States Energy Research and Development Administration, Washington, D.C., Contract No. E (49 -18)-2367.

Open-Pore Polyurethane Columns for Collection and Preconcentration of Polynuclear Aromatic Hydrocarbons from Water

James D. Navratil

Rockwell International, Rocky Flats Plant, Golden, Colorado 80401

Robert E. Sievers* and Harold F. Walton

Department of Chemistry, University of Colorado, Boulder, Colorado 80309

Open-pore polyurethane (OPP) columns are prepared by in-situ polymerization of toluene–carbon tetrachloride solutions of an isocyanate and a polyol. Columns of OPP have been tested for ion-exchange properties, solvent compatibilities, and ability to remove and concentrate polynuclear aromatic hydrocarbons (PAH) from water. Solutions containing 1 μg of pyrene per liter of water have been concentrated 200-fold by passing 1000 mL through a 0.3 × 5 cm column and eluting the pyrene with 5 mL of methanol. Recovery of pyrene was approximately 100%. Results of comparisons of breakthrough capacities and elution rates for PAH on OPP, Amberlite XAD-2, and Bio-Rad AG MP-50 are presented.

This paper deals with the comparison of in-situ formed open-pore polyurethane (OPP) with other new materials for the removal and concentration of polynuclear aromatic hydrocarbons (PAH) from water. OPP has also been tested for ion-exchange properties, solvent compatibilities, and other characteristics.

OPP is composed of agglomerated spherical particles (1 to 10 μm in diameter) bonded to each other in a rigid, highly permeable structure (*1–4*). We have shown scanning electron micrographs of OPP in a recent publication (*4*). It was first used in a column by Ross and Jefferson in 1970 (*1*). OPP was also used as an efficient gas chromatographic support (*2*) and for liquid chromatography separations with nonaqueous solvents (*3, 4*). No study has been reported, to the best of our knowledge, in which OPP has been used for removing organic compounds from water.

Much work has been reported, however, on the use of cellular (foamed) polyurethane for the collection, separation, and recovery of various inorganic and organic components from aqueous solution (*5*). Polyurethane foam plugs were investigated as a replacement for carbon as a sorbent for preconcentration of organics prior to analysis (*6*) and for removal of organics from wastewater (*7*). Foam plugs were used successfully for the preconcentration of polychlorinated biphenyls (*8–10*) and chlorinated insecticides (*10*) from water. For oil concentration from water, polyurethane gave a lower collection efficiency than liquid–liquid extraction (*11*), and for several organic compounds including naphthalene, polyurethane foams were not as effective as chloroform extraction and Amberlite XAD resin sorption (*12*). Other than naphthalene, sorbtion of PAH on polyurethanes has not been tested.

Table I shows the structures of the PAH studied. Carbon adsorption, liquid–liquid extraction, reverse osmosis, and macroreticular resins have been studied for the preconcentration of PAH from water (*7, 13*). The most popular methods have been the use of Amberlite XAD macroreticular resins

Table I. Polycyclic Aromatic Hydrocarbons Studied.

Compound	Structure
Benzo [a] pyrene (Aldrich, 98%)	
Biphenyl	
Fluoranthene (Aldrich, 98%)	
Naphthalene (Baker, reagent)	
Phenanthrene (Matheson, technical[a])	
Pyrene (K&K, reagent[a])	

[a] Purified further by sublimation.

Table II. Materials and Reaction for Preparation of Open-Pore Polyurethane of Various Compositions.

Trade Name	Structure	Grams of Material per 25 ml Solvent OH/NCO=1.0	OH/NCO=2.2
Mondur MR (Mobay Chemical Co.)	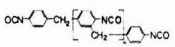	3.16	2.00
LA-475 (Union Carbide Corp.)	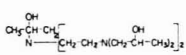	2.84	4.00

Reaction: 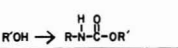

(*14*), Tenax GC (a polymer of phenylene oxide) (*15*, *16*), and ion exchange resins (*17*).

Several general analytical techniques have been used with the popular preconcentration methods. After the water sample is passed through the sorbent material, the PAH are stripped from the sorbent material two different ways. Either the PAH are removed with a small volume of solvent (*14*) or the PAH are thermally desorbed directly into a gas chromatograph–mass spectrograph (GC-MS) (*18*, *19*). The stripping solvent containing the PAH can be analyzed by ultraviolet (UV) spectrophotometry or the sample concentrated and injected into a GC-MS. Other techniques under investigation include liquid chromatography (LC) (*17*).

We have been exploring the use of OPP for LC. It is envisioned that a small OPP column could be used to concentrate the PAH, then used as a precolumn in LC, or the PAH could be stripped with a small volume of solvent and injected into a GC-MS. Another objective was to compare OPP to some of the popular sorbent materials for the preconcentration of PAH from water.

EXPERIMENTAL

Table II shows the materials for OPP preparation. The OPP columns were prepared by in-situ polymerization of 60–40 vol % toluene–carbon tetrachloride solutions of an isocyanate and a polyol (*4*). The isocyanate is a mixture of 4,4'-diphenylmethane–diisocyanate with lesser amounts of the tri-, tetra-, and pentaisocyanates, and the polyol was principally a pentahydroxy compound resulting from the total oxypropylation of diethylenetriamine. OPP made from monomer formulations with OH–NCO ratios of 1.0 and 2.2 was prepared in glass columns (5 or 10 cm in length and 3.2 mm in diameter). The reaction mode involves the addition of a hydroxy group to an isocyanate to yield a substituted amide ester of carbonic acid (polyurethane). The density of the OPP formed was 0.197 g/mL. Three different batches of Mondur MR were employed for the syntheses. No appreciable differences were observed in the properties of the columns prepared from different lots of the isocyanate.

Prior to use, the OPP columns were rinsed with 100 mL of heptane, 20 mL of methanol, and 10 mL of deionized-distilled water.

For breakthrough studies the aqueous pyrene solutions were prepared in volumetric flasks by dilution of a stock methanol solution with water. The stock solution containing 9 μg/mL pyrene in methanol was pipetted into a flask partially filled with water by placing the pipet tip under the water surface. The flask was then filled to volume with water and shaken. The aqueous solutions were used immediately because they are not stable over long periods of time.

Table III. Compatibility of OPP with Various Solvents

Solvent	Maximum pump pressure, lb/in.^{2} [a]	Weight loss, % [b]
Acetone	330 ± 10	...
Heptane	>330	−1.2
Ethanol	>330	−1.2
Methanol	>330	−1.2
1 M HCl	175 ± 5	−7.6
1 M HNO_3	330 ± 10	+1.2
1 M H_2SO_4	113 ± 47	...
H_2O	250 ± 12	−2.5
0.1 M NH_3	15 ± 5	...
1 M NH_3	85 ± 15	−3.5
1 M NaOH	<10	−1.1

[a] Pressure to break the OPP to glass column bond after storage of OPP columns (5 cm long) in solvent for 1 week. [b] After passage of 1 L of solvent through OPP column 10 cm long.

RESULTS AND DISCUSSION

Compatibility of Solvents with OPP. Compatibilities of OPP with various solvents were determined by checking the strength of the OPP to glass column bond and the weight loss of OPP. The first method consisted of storing columns (5 cm long) of OPP (monomer OH/NCO = 2.2) in the solvents for 1 week. Then, one end of the column was connected to a stainless steel cylinder pump (500-mL volume) with Cheminert fittings and tubing (Chromatronix). The pump containing water was pressurized with nitrogen from 0 to 330 lb/in.^{2} in 5 lb/in.^{2} increments. The pressure at which the cylinder of dislodged OPP came out the open end of the glass column is given in Table III. The error limits are the standard deviations between three different tests with OPP prepared on different occasions.

The other method consisted of passing 1 L of solvent from the cylinder pump through a dried, tared OPP column (10 cm long) under low pressure (50 lb/in.^{2}). Afterwards the OPP was dried, weighed, and the weight difference divided by the initial weight of the OPP was taken as the weight loss ratio.

The results of the compatibility tests (Table III) show that the OPP (OH/NCO = 2.2) is compatible with organic solvents, water, and dilute acids. However, bases appeared to break the OPP to glass column bond easily.

OPP (OH/NCO = 2.2) columns used routinely for the preconcentration of PAH had a limited life. Passing large volumes of water (a total of 12–24 L) through the 5-cm columns at 50-100 lb/in.^{2} pressure eventually broke the OPP-column bond (over a period of several weeks). Etching the inside of the glass columns with hydrofluoric acid prior to formation of OPP appeared to increase the useful life of

Table IV. Distribution Coefficients for OPP

Material	K_D (Ca^{2+})	K_D ($CdCl_4^{2-}$)
OPP (OH/NCO = 1.0)	<0.1	7 ± 2
OPP (OH/NCO = 2.2)	<0.1	64 ± 6
Dowex 50	150 ± 15	...
Dowex 1	...	700 ± 70

the OPP columns. Perhaps the life of the OPP columns could also be lengthened by lowering the pH of the water samples.

Ion-Exchange Properties of OPP. Batch equilibrium tests were performed to determine the distribution coefficients of several anions and cations with OPP. Dried 1.0-g batches of OPP, Dowex 50, and Dowex 1 were weighed and mixed with 1 M HCl solutions (25 mL) of calcium (1.0 g/L) and cadmium (1.1 g/L) in sealed polyethylene bottles. The batches were stirred for 12 and 15 days. After the mixing period, the solutions were filtered through Whatman No. 42 filter paper. The metal ion concentrations in the solutions were determined by atomic absorption before and after equilibration with the various polymers.

The results shown in Table IV are an average of equilibration for the two different times, and indicate that both formulations of OPP have no cation-exchange properties, but indeed have anion-exchange properties. The latter result is not surprising since one might expect that OPP would be a weak base anion-exchanger from examining its structure.

The anion-exchange capacity was also determined. The determination involved passing 100 mL of 2 M HCl through a column (10 cm long) of OPP (OH/NCO = 2.2), then 25 mL H_2O, and finally 50 mL of 1 M NaOH. The sodium hydroxide solution was analyzed for chloride. Duplicate experiments showed the chloride capacity of OPP to be about 1.2 mequiv/g.

Preconcentration of PAH from Water. OPP (OH/NCO = 1.0 and 2.2) was compared to Amberlite XAD-2 (20–50 mesh macroreticular beads, Polysciences, Inc.) and Bio-Rad AG MP-50 (Ca^{2+} form, 100–200 mesh macroreticular beads, Bio-Rad Laboratories) for PAH breakthrough capacity and elution behavior. The recovery efficiency was also determined for the PAH on OPP.

Pyrene Breakthrough. In a comparison of the capacity of the three materials, solutions of pyrene (0.9 μg/mL) were passed through columns (5 cm long) of all four materials at various flow rates, and fractions were analyzed by UV spectrophotometry on a Cary 14 or Cary 17 spectrophotometer using 10-cm cells. The absorbance peak of pyrene at 335 nm was used for the measurements.

The results of the breakthrough capacities of the materials are shown in Figure 1. C/C_0 is defined as the concentration of pyrene in the column effluent divided by the pyrene concentration in the influent (0.9 μg/mL). Breakthrough capacity is defined for present purposes as the weight of the test substance that can be sorbed by the polymer before C/C_0 becomes greater than 0.1. When less than 90% of the compound in the incoming stream is being sorbed, the polymer is judged to be no longer effective as a collection medium. The data show that OPP with OH/NCO = 1.0 had a much lower capacity than OPP with OH/NCO = 2.2. The latter OPP formulation had the highest breakthrough capacity, followed by Bio-Rad AG MP-50. Amberlite XAD-2 had a fairly low breakthrough capacity. As expected, the breakthrough capacity increases as the flow rates are decreased.

Pyrene Elution. The volume of organic solvent required to quantitatively elute pyrene from the four materials was determined. Anhydrous methanol (Mallinckrodt, Analytical Reagent) or anhydrous ethanol (J. T. Baker, reagent grade) was pumped at 1 mL/min through 5-cm columns of the materials, previously loaded with 5 μg of pyrene (dissolved in water). The effluent stream was passed through a

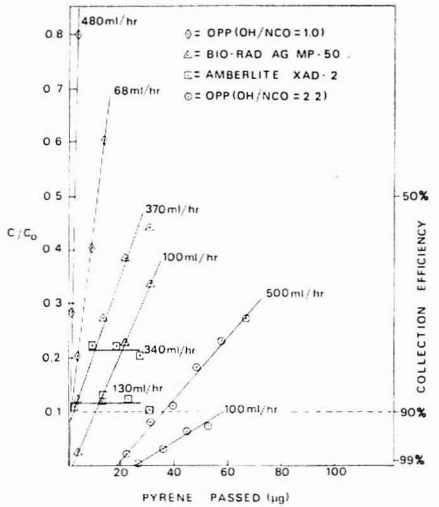

Figure 1. Breakthrough results for pyrene on various polymers

Table V. Volumes of Methanol and Ethanol Required to Elute Pyrene from Various Polymers[a]

Material	MeOH, mL	EtOH, mL
OPP (OH/NCO = 2.2)	2.0 ± 0.6	1.4 ± 0.2
OPP (OH/NCO = 1.0)	2.3 ± 0.5	...
Bio-Rad AG MP-50	3.4 ± 0.6	...
Amberlite XAD-2	5.9 ± 1.2	5.4 ± 1.4

[a] Columns 5 cm long, loaded with 5 μg of pyrene.

Chromatronix Model 220 (254 nm) detector and the pyrene peak was recorded on a dual input Omniscribe recorder (Houston Instrument Corp.). The solvent volume required to quantitatively elute the pyrene (>99% recovery) was determined 3 to 5 times for each material.

The results, shown in Table V, are the average values and the standard deviations of the elution volumes. The results show little significant difference between the two different formulations of OPP and between methanol and ethanol eluent. The OPP allowed faster elution of pyrene with smaller volumes of eluent than did Bio-Rad AG MP-50 and Amberlite XAD-2.

Recovery of PAH. Synthetic samples of PAH were prepared freshly each day by diluting 1–5 mL of stock PAH solution in methanol to 2 L of deionized-distilled water. The PAH solutions were then placed in the cylinder pump (50–100 lb/in.^{2} N_2) and passed through 5-cm columns of OPP (or, in one case, Amberlite XAD-2). After 1 L of the solution was passed through the column, the PAH were eluted from the column with methanol. Two, and sometimes three, 5-mL volumetric flasks of eluate were collected and the concentration of PAH was determined by UV spectrophotometry. For each of the PAH, 3 to 5 recovery determinations were performed.

The average and standard deviation of the determinations are shown in Table VI. The results show that excellent recovery of PAH was achieved using OPP under a variety of conditions. Fluoranthene, naphthalene, and phenanthrene had good recovery when the capacity of the OPP for these PAH was not reached (~3 μg). Pyrene recovery from Amberlite XAD-2 was not as good as OPP, which is in agreement

Table VI. Recovery of PAH with OPP (OH/NCO = 2.2)

PAH	Flow rate, L/h	PAH Loaded, μg	Recovery, %
Benzo[*a*]pyrene	1.8	4	95 ± 6
Biphenyl	0.9–1.5	5–6	98 ± 5
Fluoranthene	0.5–1.0	4–5	77 ± 4
	0.5–1.0	1–2.5	97 ± 3
Naphthalene[a]	0.1	5	56 ± 3
	0.1–1.0	1–2.5	98 ± 10
Phenanthrene	0.8–1.0	5	58 ± 7
	0.8–1.0	1–2.5	92 ± 9
Pyrene	0.6–0.8	1–4	100 ± 2
	1.2–1.7	4–5	89 ± 3
Pyrene (XAD-2)[a]	0.6	4	79 ± 8

[a] Required 10 mL of methanol to elute quantitatively; others needed only 5 mL.

Table VII. Flow Rate Tests

Material, 5 cm	Flow rate, mL/h 10 psi	50 psi
Amberlite XAD-2	360 ± 24	1040 ± 0
OPP (OH/NCO = 2.2)[a]	230 ± 80	780 ± 200
OPP (prepared at 0 °C)	560 ± 220	1670 ± 490

[a] Gravity flow rate = 10 mL/h with 10-cm head.

with the breakthrough capacity results.

A second 5-mL fraction of methanol was required to quantitatively elute (>99%) naphthalene from OPP and pyrene from XAD-2. The remainder of the PAH were eluted with 5 mL of methanol.

Possible Interferences in UV Determinations of PAH. Humic substances could interfere with the UV determination of PAH in actual water samples if they sorb on OPP and then are subsequently eluted by methanol. To check the retention and UV interference of humic substances, the water used to make up the synthetic pyrene solutions was boiled for 1 h in the presence of peat moss and filtered with Whatman No. 1 filter paper. The pyrene solution containing humic and fulvic acids was then concentrated in the same manner as in the recovery experiments. The methanol eluate gave an identical spectrum, with no additional baseline noise, to that of a solution containing no humic substances. This showed that the humic substances would not interfere with the UV determination of PAH after preconcentration on OPP. Either the humic acids are not sorbed or they are not eluted by methanol to cause interference in measurements with UV detectors.

Pressure Drop. One apparent disadvantage of the OPP in comparison to Amberlite XAD-2 is the additional pressure drop across a 5-cm column. Table VII shows the flow rates at two different cylinder pump pressures of water through the materials. The flow rates are an average of 6 different tests. The results show that OPP prepared at 0 °C instead of 23–25 °C gave a higher flow rate, even better than XAD-2. This is believed to be due to the larger microspherules formed at 0 °C relative to those synthesized at higher temperatures. The recovery of pyrene was not significantly different with the OPP prepared at 0 °C as compared to the room temperature OPP preparation.

LITERATURE CITED

(1) W. D. Ross and R. T. Jefferson, *J. Chromatogr. Sci.*, **8**, 386 (1970).
(2) F. D. Hileman, R. E. Sievers, G. G. Hess, and W. D. Ross, *Anal. Chem.*, **45**, 1126 (1973).
(3) T. R. Lynn, D. R. Rushneck, and A. R. Cooper, *J. Chromatogr. Sci.*, **12**, 76 (1974).
(4) L. C. Hansen and R. E. Sievers, *J. Chromatogr.*, **99**, 123 (1974).
(5) T. Braun and A. B. Farag, *Talanta*, **22**, 699 (1975).
(6) H. D. Gesser, et al., *J. Am. Water Works Assoc.*, **65**, 220 (1973).
(7) I. H. Suffet, S. Friant, C. Marcinkiewicz, M. J. McGuire, and D. T. L. Wong, *J. Water Pollut. Control Fed.*, **47**, 1169 (1975).
(8) J. W. Bedford, *Bull. Environ. Contam. Toxicol.*, **12**, 622 (1974).
(9) H. D. Gesser, A. Chow, F. C. Davis, J. F. Uthe, and J. Reinke, *Anal. Lett.*, **4**, 883 (1971).
(10) P. R. Musty and G. Nickless, *J. Chromatogr.*, **100**, 83 (1974).
(11) S. M. Ahmed, M. D. Beasley, A. C. Efromson, and R. A. Hites, *Anal. Chem.*, **46**, 1858 (1974).
(12) R. G. Webb, "Isolating Organic Water Pollutants: XAD Resins, Urethane Foams, Solvent Extraction", EPA-660/4-75-003, June 1975.
(13) R. M. Harrison, R. Perry, and R. A. Wellings, *Water Res.*, **9**, 331 (1975).
(14) G. A. Junk, J. J. Richard, M. D. Grieser, D. Witiak, J. L. Witiak, M. D. Arguello, R. Vick, H. J. Svec, J. S. Fritz, and G. V. Calder, *J. Chromatogr.*, **99**, 745 (1974).
(15) V. Leoni, G. Puccetti, and A. Girella, *J. Chromatogr.*, **106**, 119 (1975).
(16) W. E. May, S. N. Chesler, S. P. Cram, B. H. Gump, H. S. Hertz, D. P. Enagonio, S. M. Dyszel, *J. Chromatogr. Sci.*, **13**, 535 (1975).
(17) P. A. Larson, Ph.D. thesis, University of Colorado, Boulder, Colo., May 1976.
(18) R. C. Lao, R. S. Thomas, and J. L. Monkman, *J. Chromatogr.*, **112**, 681 (1975).
(19) W. Bertsch, E. Anderson, and G. Holzer, *J. Chromatogr.*, **112**, 701 (1975).

RECEIVED for review March 25, 1977. Accepted September 19, 1977. This research was supported in party by the Air Force Office of Scientific Research under Contract No. AF 44620-76-C-0031 and by the Environmental Protection Agency under Grant No. R804472-01-1.

Selection and Cleaning of Plastic Containers for Storage of Trace Element Samples

John R. Moody* and Richard M. Lindstrom

National Bureau of Standards, Institute for Materials Research, Analytical Chemistry Division, Washington, D.C. 20234

Since the sample container represents one of the earliest and potentially one of the largest sources of sample contamination, much of the analytical accuracy will depend upon the choice of container materials and the method of cleaning containers. Twelve different plastics have been examined by gravimetry, isotope dilution mass spectrometry, and neutron activation analysis. The present study examines the levels of impurities present in the various plastics as well as the quantities of impurities leached from the plastics by acid cleaning. A suggested method of cleaning containers is presented.

The determination of trace elements at very low levels, particularly in liquid samples, has been found to be biased by the analytical blank and can often be attributed in large part to contamination from sampling and storage containers (*1–4*). Synthetic polymeric materials are often employed as containers in the expectation that contamination will be less than if glass or metallic containers were used. The degree of improvement depends on the plastic and on the cleaning procedure (if any) employed to clean the plastic before use. The literature is contradictory on this topic (*1*). The present work examines several materials and cleaning methods in an effort to define a set of materials and procedures adequate for most work at the ng/g level.

For long term storage of liquid samples, an important consideration together with low contamination levels is a low rate of loss of water vapor. Factors to be considered include permeability, wall thickness, and closure integrity and are best determined by experiment. The rate of loss which can be tolerated is dependent upon both the accuracy desired and the amount of time during which the sample must be stored. For high accuracy work over a storage period of 10 years, an annual rate of loss of 0.1% or less per year is necessary.

EXPERIMENTAL

A number of plastic materials were studied, including bottles constructed of conventional polyethylene (CPE), linear polyethylene (LPE), polypropylene (PP), polymethylpentane (PMP), polycarbonate (PC), poly(vinyl chloride) (PVC), and several types of Teflon (TFE, FEP). In addition specimens of ethylene-tetrafluoroethylene copolymer (Tefzel or ETFE), Teflon PFA, polystyrene (PS), and Teflon pipe sealing tape (TPT) were examined. The containers used for these studies were carefully selected to be free from visible inclusions and were average in wall thickness, weight, and other characteristics. The studies of these materials may comprise three types of experiments: a gravimetric study of the rate of loss of water from bottles, isotope dilution mass spectrometric (IDMS) analysis of the impurities leached from a bottle during a cleaning process, and neutron activation analysis (NAA) of the impurities contained within and leached from the plastics.

Gravimetric Studies. Two bottles each of CPE, PP, PVC, PMP, and PC were obtained from commercial sources (Bel Art, Nalge, or equivalent). The bottles were 1-L or 500-mL capacity and, except for rinsing with 95% ethanol followed by distilled water, they were not subjected to a special cleaning procedure. All of the containers were weighed, then were filled to the same relative level with distilled water and re-weighed. The second container of each type was retained as a weighing tare to correct for the influence of changes in the barometric pressure, relative humidity and temperature, and loss of plasticizer. The samples were re-weighed after 17 days and 66 days to establish a rate of loss of moisture.

IDMS Studies. Leach solutions from 1-L or 500-mL size bottles of FEP, CPE, LPE, and PC were examined by spark source IDMS (multielement) and by thermal emission IDMS (for lead only). The general principles and techniques used have been given elsewhere (*5, 6*). The bottles were rinsed with distilled water to remove any surface contamination and three sets of bottles were filled with a (1 + 1) mixture of ultra-pure HCl or ultra-pure HNO_3 and ultra-pure water (*7*). The bottles were allowed to stand at room temperature for one week, with the exception of the FEP bottle which was heated to 80 °C for one week.

Aliquots of the contents of one set of bottles leached by (1 + 1) HCl were spiked with ^{206}Pb. Aliquots from two other sets of bottles, leached by (1 + 1) HCl and (1 + 1) HNO_3 respectively, were spiked with a 19-element multispike (*7*) for the spark source mass spectrometer (SSMS). The spiked solutions were then evaporated to several drops under a Class 100 laminar flow clean hood. The sample solutions were analyzed in the SSMS (multielement) or thermal source mass spectrometer (for Pb only).

The first set of bottles were then re-filled with a (1 + 1) mixture of ultra-pure HNO_3 and ultra-pure water and the entire cleaning, sampling, spiking, analysis sequence was repeated as before. Finally, the bottles were filled with high purity 0.5% (w/w) HNO_3, sampled after one week and again after two months, and then the aliquots were spiked with ^{206}Pb and subsequently analyzed.

NAA Studies. Specimens of 0.2–2 g (4–12 cm^2) were cut from new 0.5–1 L plastic bottles (CPE, LPE, PP, PMP, PC, PVC, and FEP), sheet (TFE and PFA), bottle caps (ETFE), boxes (PS), or tape (TPT). The samples were pre-cleaned by rinsing lightly with 95% ethanol followed by distilled water. All irradiations were performed at a thermal neutron flux of 1.3×10^{13} n cm^{-2} s^{-1} and a γ flux of 2×10^7 rad/h (*8*). Other positions in the reactor offer higher neutron flux, but at the expense of a much higher γ flux per neutron, and hence a much higher radiation damage to the samples.

NAA Experiment 1. The samples packaged in high purity LPE film (*9*) were irradiated for 2 min, the edges trimmed, and the induced radioactivity determined by counting on a Ge(Li) γ detector. The samples were weighed, cleaned in (1 + 1) HCl by heating at 100 °C for 2 h, rinsed with high purity water, dried, repackaged, and irradiated and counted again. After a similar 2-h leach in hot (1 + 1) HNO_3, the plastics were analyzed a third time.

NAA Experiment 2. Different samples of the same plastics were used in measurements of long-lived activation products. After irradiation (4–6 h) and decay of short-lived activities, the remaining radioactivation products were counted. The samples were then leached in (1 + 1) HCl at 100 °C, rinsed, and then leached in hot (1 + 1) HNO_3. Both leach solutions and the cleaned plastics were then counted on a γ-ray detection system.

RESULTS AND DISCUSSION

Gravimetric Studies. The results are summarized in Table I. Two of the bottles (PP and CPE) have water loss rates which are compatible with the long term storage of aqueous samples. In addition, data previously obtained by Moody et al. (*10*) indicated an annual rate of water loss of ~0.05% from 1-L Teflon FEP bottles. PVC, PMP, and PC

Table I. Annual Rate of Loss of Water from Container Materials

Container	Calculated % loss/year After 17 days	After 66 days
CPE	0.116	0.109
PP	0.034	0.049
PVC	0.429	0.601
PMP	0.988	1.018
PC	1.65	2.00

Table II. Lead Leached from Containers (ng/cm²) Determined by IDMS

Bottle	(1 + 1) HCl 1 week	(1 + 1) HNO_3 1 week	0.5% HNO_3 1 week	0.5% HNO_3 2 months
FEP	0.41	0.014	...[a]	...
LPE	0.20	...	...	...
CPE	0.18	...	...	...
PC	0.36	0.023	0.023	...

[a] ... No significant amount over blank level.

bottles may be adequate for storage over short time periods. Losses due to transpiration may be reduced by sealing the bottle in a commercially available vapor barrier, e.g., a polyethylene-coated film of aluminized Mylar. The practice of using a desiccator partially filled with water to act as a humidity chamber to slow transpiration losses is recommended although one must be careful that high humidity conditions do not cause a weight gain (absorption of moisture).

None of the observed loss rates should be construed as permeability data since the closure may have been responsible for a significant portion of the total water loss. The results obtained in this work for CPE are similar to those observed by Curtis et al. (*11*).

IDMS Studies. The results obtained for the leaching of lead from FEP, LPE, CPE, and PC containers are listed in Table II. Lead was chosen as a model element for this study, partly because of the high accuracy obtainable by thermal source isotope dilution mass spectrometry and partly because lead is a common contaminant. The practice of cleaning bottles first with HCl and then with HNO_3 has been proved to be an effective procedure in our laboratories (*7*). Most of the cleaning of these containers is accomplished by only one week of soaking in HCl. The additional week of soaking in (1 + 1) HNO_3 removes additional lead only from FEP and PC. Patterson (*2*) has suggested that 0.5% HNO_3 is more efficient for the long term cleaning of Teflon containers from Pb contamination than is (1 + 1) HNO_3. In these experiments no further leaching of lead was detected after leaching with (1 + 1) HNO_3 except from the PC container. After one month of leaching with 0.5% HNO_3, no further lead was leached even from the PC container.

Data obtained by SSMS is compiled in Tables III and IV for impurities leached by (1 + 1) HCl and (1 + 1) HNO_3 respectively. Again, the Teflon FEP bottles were heated to 80 °C while the others were leached at room temperature. The (1 + 1) HCl leached more than the (1 + 1) HNO_3 except for the FEP containers. A single element, Ca, is responsible for most of the difference between the (1 + 1) HCl and (1 + 1) HNO_3 in leaching Teflon FEP. Values which are below 2 ng/cm² or which are prefixed by ≤ are upper limits. That is, the concentration is below the optimum concentration range for the amount of spike isotope used or the concentration is near the blank or detection limit. The greater total quantity of various elements leached from FEP may be partially explained by the higher temperature (80 °C vs. room temperature) used to clean the Teflon FEP container.

Table III. Impurities Leached from Plastic Containers in One Week by (1 + 1) HCl (ng/cm²) Determined by IDMS

Elements	Teflon FEP	LPE	CPE	PC
Pb	2	0.6	18	10
Tl	≤1	≤0.6	3	0.7
Ba	2	1	0.3	3
Te	2	...	0.7	...
Sn	1	≤1	≤0.8	13
Cd	0.6	0.2	0.2	≤8
Ag	≤6	...	...	...
Sr	≤1	0.2	0.2	0.3
Se	0.8	0.4	≤0.3	≤0.5
Zn	4	9	1.0	...
Cu	6	1	0.7	≤6
Ni	0.8	0.8	0.3	0.3
Fe	16	1	1.0	≤49
Cr	4	0.8	0.3	≤5
Ca	2	60	0.8	≤16
K	1.6	1	0.7	≤5
Mg	1.0	0.4	0.7	0.8
Al	4	4	10	3
Na	2	6	42	8
	Σ 58	Σ 89	Σ 81	Σ 130

Table IV. Impurities Leached from Plastic Containers in One Week by (1 + 1) HNO_3 (ng/cm²) Determined by IDMS

Elements	Teflon FEP	LPE	CPE	PC
Pb	2	2	0.7	0.3
Tl	≤1	≤1	1	≤0.8
Ba	4	≤0.2	2	0.3
Te	0.6	0.2	≤0.5	0.3
Sn	1	1	≤0.8	0.2
Cd	0.4	0.2	0.2	0.3
Ag	≤8	0.2	...	...
Sr	0.2	1	0.2	≤0.2
Se	0.2	0.4	3	0.5
Zn	4	8	2	0.8
Cu	2	0.4	2	0.8
Ni	2	1.6	0.5	0.7
Fe	20	3	3	3
Cr	0.8	0.2	0.8	0.3
Ca	80	0.6	10	3
K	2	2	2	2
Mg	8	0.6	0.7	2
Al	6	1	1	5
Na	6	10	8	3
	Σ 148	Σ 50	Σ 38	Σ 23

NAA Studies. The amount of impurities found in the uncleaned plastics as determined in NAA experiments 1 and 2 are summarized in Table V. A comparison of the impurities found in CPE in this study shows agreement with that found by other workers (*4, 9, 12–15*) to approximately an order of magnitude. It is interesting to note that there has been no clear change in trace elemental impurities in over 25 years of manufacture (*12*). The ten materials studied show striking differences in trace element composition. The purest materials are TFE and CPE, in agreement with the experience of numerous workers (*1*). Polystyrene was also very clean. Many materials showed easily detectable amounts of a few elements. Some of these elements are residues of polymerization catalysts (*16*).

Interpretation of the acid-leaching experiments is complicated, particularly with the long irradiation in the second experiment, by the fact that the experiments are imperfect

Table V. Concentrations of Trace Elements in Plastics Determined by NAA (ng/g)

	CPE	LPE	PP	PMP	PS	PC	PVC	TFE	FEP	PFA	TPT	ETFE
Na	1.3E3[a]	15E3	4.8E3	200	2.2E3	2.7E3	20E3	160	400	100	2.3E3	600
Al	500	30E3	55E3	6.2E3	500	3.0E3		230	200		29E3	
Cl	7E3	30E3	180E3			50E3	major		800	50E3	7E3	1E6
K	>5E3	>600		>200					90E3		3E3	1.1E3
Ca		800E3										
Ti		5E3	60E3	5E3	1E3						2E6	
Mn		10	20	10	20				60	20	20	
Co			40			6				90		
Zn		520E3		33E3							14E3	
Br	>20	800	>5	>2	>1	29E3	>6	>2		16E3		240
Sn							2.4E6					
Sb	5	200	600									
La					0.3			0.6				1
W									700			
Au			0.1	0.6	0.04	0.03		0.4			0.2	0.4

[a] 1.3E3 = 1.3 × 10^3 ng/g. When lower limits are quoted, the element sought was short-lived and found only in the leachate or leached sample. Hence the concentration in the unleached plastic may have been greater but was not visible in the presence of large quantities of short-lived interfering radioactivities. Blanks in the table represent the extreme where the element sought for was not visible. Detection limits may be roughly judged from values in adjacent columns.

Table VI. Removal of Sodium from Plastics[a]

	Expt 1. Short irradiation			Expt 2. Long irradiation			
Matrix	Before cleaning	Post HCl	Post HCl + HNO_3	Before cleaning	HCl leach liquid	HNO_3 leach liquid	Post cleaning
CPE	600 ±100			1290 ±30	1480 ±10	2.0 ±0.3	330 ±20
LPE	17000 ±3000	15000 ±3000	14000 ±1000	13200 ±200	273 ±2	5.9 ±0.5	13200 ±100
PP	5000 ±1000			4640 ±70	480 ±3	32 ±1	4330 ±60
PMP	220 ±50			160 ±5	52 ±1	1.0 ±0.1	120 ±10
PS	2000 ±400	1500 ±400		2450 ±40	60 ±1	9 ±1	2430 ±70
PC	2400 ±400			2860 ±50	68 ±1	4 ±1	2850 ±100
PVC				19500 ±400	190 ±10	28 ±3	21000 ±900
TFE	170 ±40			160 ±10	111 ±2		
FEP				400 ±20	242 ±3		
PFA	180 ±50			39 ±4	15 ±1		10 ±10
TPT	2900 ±600		1900 ±200	2270 ±50	1890 ±20	144 ±3	380 ±40
ETFE				575 ±15	427 ±3	1.2 ±0.1	208 ±3

[a] Concentrations are in ng/g plastic. Errors quoted reflect counting statistics only, and so underestimate the total error of measurement. Note that the two "leach liquid" columns give directly the amount of Na *removed* by the leach step; all other columns give the amount *present* in the plastic sample. Blanks imply that Na was not detected.

models of a reagent or analyte stored in a bottle. Those atoms of trace elements leached and detected in the leachate in the second experiment are precisely those not representative of undisturbed trace elements in an undisturbed matrix. The radioactive atoms underwent recoil on absorption of a neutron and thus may have been more labile than their inactive neighbors. In addition, the matrix suffered radiation damage from some 10^8 rads of γ radiation and the halocarbons were damaged additionally by the absorption of nuclear recoil energy and β radiation induced in major constituents of the matrix. However, detailed examination of the leaching results for sodium, the only element common to the two experiments, shows that radiation damage does not seem to greatly affect the general conclusions (Table VI) which are discussed below.

The results of the acid leaching experiments for all elements (Table VII) are compiled from the differences in trace element composition of the plastic before and after leaching in the first and second NAA experiments, and from direct measurement of leached tracer in the second, in a manner similar to the sodium results in Table VI.

With the exception of Na in pipe tape, (perhaps a special case because of its high surface/volume ratio), and to a lesser extent Na in CPE, the trace elements studied are in general not leached from the polymer matrix even with the rather severe acid treatment used here. It may be inferred that the bulk of most trace elements present is distributed throughout

Table VII. Sequential Leaching of Trace Elements from Plastics (ng/cm²)[a]

	CPE	LPE	PP	PMP	PS	PC	PVC	TFE	FEP	PFA	TPT	ETFE
Al	200 + 0.4	70 + 1	100 + 7	20 + 0.4	20 + 8	20 + 1	30 + 10	80+	60+	20+	50 + 4	300 + 1
K	50+											
Co	1000+	100+		80+					90+			400+
Zn						+2						
Br		50 + 30									20+	
Sb	3+	2 + 0.5	1+	1+	0.3 + 0.1	7 + 20	2+	10+				
La	1+	3+										
W					0.1+			0.4+				0.7+
Au									4 + 0.2			
			0.03 + 0.01		0.01+	0.01+		0.3+			0.01+	0.3 + 0.01

[a] Determined by NAA. The two numbers given (in ng/cm²) are respectively the amount leached by 1:1 HCl and by 1:1 HNO_3 in 2 h at 100 °C. A blank means that the constituent was not detected. See also footnote to Table V.

Table VIII. Suggested Method for Cleaning Plastic Containers

1. Fill with 1 + 1 HCl (AR grade).
2. Allow to stand one week at room temperature (80 °C for Teflon).
3. Empty and rinse, with distilled water.
4. Fill with 1 + 1 HNO_3 (AR grade).
5. Allow to stand one week at room temperature (80 °C for Teflon).
6. Empty and rinse with distilled water.
7. Fill with purest available distilled water.
8. Allow to stand several weeks or until needed, changing water periodically to ensure continued cleaning.
9. Rinse with purest water and allow to dry in a particle- and fume-free environment.

the matrix, and not merely on the surface.

The hydrochloric acid leach in experiment 1 increased the chloride concentration in all the plastics corresponding to a 10^{-4} cm thickness of 1 + 1 HCl in the surface of polypropylene, and less in the other materials. This inward diffusion of HCl is in accord with the water loss measurements, both experiments leading to a diffusion coefficient for aqueous solutions in polyolefin of the order of $D = 10^{-12}$ cm²/s. With this value of D, the rms diffusion length in one year is 0.1 mm.

CONCLUSIONS

Differences were observed between NAA and IDMS results for trace elements leached from the plastics. At least some of these differences may be in the way the samples were leached. For IDMS work, the leaching was carried out within intact bottles. In contrast, the NAA studies examined the trace elements leached from both sides of a small sample of plastic immersed in acid. Since at least some containers are known to be blow molded, the higher results obtained by NAA may simply reflect a difference in contamination levels between inside and outside walls, the NAA data probably including contamination from the mold.

With the exception of Teflon FEP, (1 + 1) HCl has been found to be the better cleaning agent. However, HCl and HNO_3 appear to leach various elements with different efficiencies; thus, the use of both acids, one after the other, is recommended. The various Teflons and CPE bottles have been found to be the least contaminating bottles, once they have been cleaned. Many methods have been suggested and several have been shown to be sufficient for the purpose at hand (*1*, *2*, *7*).

Suggested Method for Cleaning Bottles. From the present work, that of Karin et al. (*15*), and earlier work in this laboratory (*3*, *7*), a procedure is suggested which may be suitable for most contemporary trace element work. The procedure is outlined in Table VIII. Only reagent grade acid is necessary for the acid leaching; but ultrapure distilled water should be used for the final step.

ACKNOWLEDGMENT

The authors acknowledge the contributions of T. J. Murphy, P. J. Paulsen, and J. W. Gramlich for the IDMS analysis of solutions stored in plastic containers, and of D. A. Becker for numerous constructive suggestions.

LITERATURE CITED

(1) E. J. Maienthal and D. A. Becker, "A Survey of Current Literature on Sampling, Sample Handling and Long Term Storage for Environmental Materials", *Natl. Bur. Stand. (U.S.) Tech. Note*, **929** (1976).
(2) C. C. Patterson and D. M. Settle, in "Accuracy in Trace Analysis: Sampling, Sample Handling, and Analysis", Proceedings of the 7th IMR Symposium, P. D. LaFleur, Ed., *Natl. Bur. Stand. (U.S.) Spec. Publ.*, **422**, 321 (1976).
(3) T. J. Murphy, in "Accuracy in Trace Analysis: Sampling, Sample Handling, and Analysis", Proceedings of the 7th IMR Symposium, P. D. LaFleur, Ed., *Natl. Bur. Stand. (U.S.) Spec. Publ.*, **422**, 509 (1976).
(4) D. E. Robertson, *Anal. Chem.*, **40**, 1067 (1968).
(5) P. J. Paulsen, R. Alvarez, and C. W. Mueller, *Appl. Spectrosc.*, **30**, 42 (1976).
(6) I. L. Barnes, T. J. Murphy, J. W. Gramlich, and W. R. Shields, *Anal. Chem.*, **45**, 1881 (1973).
(7) E. C. Kuehner, R. Alvarez, P. J. Paulsen, and T. J. Murphy, *Anal. Chem.*, **44**, 2050 (1972).
(8) H. E. Despain, National Bureau of Standards, private communication, 1976.
(9) S. H. Harrison, P. D. LaFleur, and W. H. Zoller, *Anal. Chem.*, **47**, 1685 (1975).
(10) J. R. Moody, H. L. Rook, T. C. Rains, and P. J. Paulsen, unpublished data from the preparation of SRM 1642.
(11) G. J. Curtis, J. E. Rein, and S. S. Yamamura, *Anal. Chem.*, **45**, 996 (1973).
(12) R. E. Thiers, *Methods Biochem. Anal.*, **5**, 274–309, (1957).
(13) J. W. Mitchell, *Anal. Chem.*, **45**, 429A (1973).
(14) H. Sorantin and P. Patek, *Fresenius Z. Anal. Chem.*, **211**, 99 (1965).
(15) R. W. Karin, J. A. Buono, and J. L. Fasching, *Anal. Chem.*, **47**, 2296 (1975).
(16) E. C. Kuehner and D. H. Freeman, in "Purification of Inorganic and Organic Materials", M. Zief, Ed., Marcel Dekker, New York, N.Y., 1969, pp 297–306.

RECEIVED for review April 8, 1977. Accepted August 29, 1977. In order to adequately describe materials and experimental procedures, it was occasionally necessary to identify commercial products by manufacturer's name or label. In no instance does such identification imply endorsement by the National Bureau of Standards nor does it imply that the particular products or equipment is necessarily the best available for that purpose.

Principles of Nephelometric Titrations and Application to Titration of Dilute Solutions of Bromide

E. J. Meehan* and S. Yamaguchi[1]

Department of Chemistry, University of Minnesota, Minneapolis, Minnesota 55455

Calculations are presented of the variation of intensity of light scattered during a titration in which a nonabsorbing colloidal suspension is formed. The calculations are based on exact Mie theory for monodisperse homogeneous spheres of various refractive indices and illustrate the choice of optimum particle size and optimum angle for measurement of scattering, as well as the effect of addition of preformed colloidal material before the titration. The principles are illustrated by the titration of bromide, as dilute as 5×10^{-7} M in mixtures of 2-propanol and water with an average accuracy of 1–2%.

The term "nephelometric titration" as used in this paper means a titration in which the relative intensity of light scattered by the suspension which is formed in the titration is measured at a specific well defined angle from the direction of the monochromatic incident beam. The general principles have been presented earlier (*1*). The present paper consists of two parts. The first part is entirely optical in nature. It summarizes the results of extensive theoretical calculations based on exact Mie theory for scattering by homogeneous spheres. The calculations illustrate the choice of optimum scattering angle and of optimum particle size of the colloidal material, and show the effect of addition of "seed"—that is, preformed colloidal material of a given particle size—before the titration. Many of the calculations apply to a refractive index ratio (defined below) around 1.76, which corresponds to a suspension of silver bromide in water at wavelength 436 nm, but illustrative calculations are summarized for other ratios. In the calculations, the suspensions are assumed to consist of monodisperse spheres which scatter independently. The effects of nonsphericity and polydispersity are referred to later. The assumption of independent scattering is valid for the dilute suspensions which are used in practice. The second part of the paper presents results of titration of dilute solutions of bromide with silver nitrate. It indicates to what extent the theoretically optimum situation may be approached in practice for this particular system.

Calculated Titration Curves. The quantity $i_1(\theta)$ is proportional to the intensity scattered per particle at angle θ from the direction of the incident beam, which is unpolarized and of unit intensity. The electric vector in the scattered beam is perpendicular to the plane containing the incident beam and the direction of observation. $V_{\theta u}$ (dimension cm^{-1}) is given by Equation 1:

$$V_{\theta u} = \frac{N\lambda^2 i_1(\theta)}{8\pi^2} \tag{1}$$

where N is the number of particles per mL and λ is wavelength in the medium surrounding the particles. $V_{\theta u}$ is the vertically polarized component of the Rayleigh Ratio (see Ref. 3, p 38, p 503) at scattering angle θ. The concentration of suspended material, g-mL^{-1}, is c. The density of the colloidal material is assumed to be the same as that of the bulk material in the calculation of c from N and radius r. The *specific scattering* is $V_{\theta u}/c$. For the method of calculation of $i_1(\theta)$ and $V_{\theta u}$ and their relation to the Mie scattering functions, see Ref. 2 or 3. In a nephelometric titration, it is sufficient to measure the relative, not absolute, intensity. However, knowledge of the absolute scattered intensity is useful because it allows comparison of the scattering by a suspension of given c with the scattering by water, or other suspending medium; the latter quantity determines the ultimate limit of detection of suspended material.

The scattering by pure, dust-free water with the same state of polarization specified above for $i_1(\theta)$ is independent of θ. The quantity which for a pure liquid corresponds to $V_{90,u}$ for a suspension is the Rayleigh Ratio R_{90} referred to above. For water R_{90} is equal to 2.32×10^{-6} cm^{-1} and 8.65×10^{-7} cm^{-1} at wavelengths 436 and 546 nm, respectively. (It may be mentioned that the scattering of water is less than that of many organic liquids, being $^1/_{20}$ that of benzene for example. In the Experimental section it is shown that the use of 2-propanol as co-solvent is beneficial in the case of silver bromide. R_{90} for this substance has not been measured but it may be expected to be roughly the same as that of methyl ethyl ketone, which is about twice that of water.) R_{90} is compared later with $V_{\theta u}$ of various suspensions.

The quantity α is $2\pi r/\lambda$; λ is λ_v/n_m, where λ_v is vacuum wavelength and n_m is the refractive index of the medium. The refractive index ratio m is n/n_m, where n is the refractive index of the colloidal material. The present paper is restricted to real values of n, corresponding to nonabsorbing substances. Because it is conventional to use a relatively concentrated solution of titrant, it is not necessary to correct for the change of volume during titration. (Such correction, of course, is trivial.)

Silver bromide absorbs slightly at 436 nm. In earlier work (*4*), it has been shown that the value of k in the complex refractive index ratio $m(1 - ik)$ at 436 nm in small-particle suspensions is $3\text{–}5 \times 10^{-4}$, which is small enough that in respect to scattering the particles behave as nonabsorbing.

The two limiting cases of these titrations correspond to (a) constant particle size and increasing number of particles and (b) constant number and increasing size, in both cases with no agglomeration or flocculation between additions of titrant before or after the equivalence point (EP). If case (a) existed, it is obvious without calculation that the titration curve (TC), that is, relative intensity vs. volume of titrant, would consist of a rising straight line intersecting a horizontal straight line at EP, regardless of particle size. Actually the truth lies between (a) and (b) but is closer to (b). Therefore in the calculations it is assumed that when no seed is added, all the particles are formed upon addition of the first increment and these grow upon subsequent additions. It is assumed that when seed is added, the number of particles remains equal to the number added as seed.

Consider first the situation in which no seed is added and denote the fraction of equivalent amount of titrant added as f. The particle radius up to $f = 1$ is given by Equation 2,

$$r_f = r_0\left(\frac{f}{f_0}\right)^{1/3} \tag{2}$$

[1] Present address, Kao Soap Co. Ltd., Wakayama-shi, Japan.

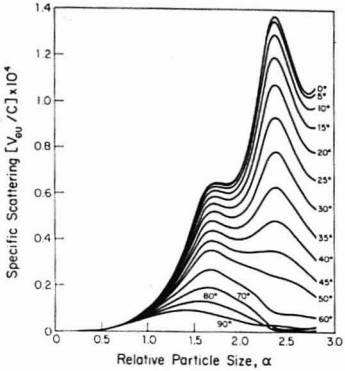

Figure 1. Specific scattering vs. α at various angles; $m = 1.76$

in which r_0 and f_0 correspond to the initial increment. A similar relation connects α_f and α_0.

For small ("Rayleigh") particles with $r \leq \lambda/20$, corresponding to $\alpha \leq 0.314$, $i_1(\theta)$ is independent of θ and proportional to r^6:

$$i_1(\theta) = \left(\frac{m^2 - 1}{m^2 + 2}\right)^2 \alpha^6 \qquad (3)$$

Therefore $V_{\theta u}/c$ varies as f, and because c also varies as t, the scattered intensity at any θ increases as f^2 up to $f = 1$. This is the optimum situation in regard to shape of TC and location of EP, but the sensitivity is not as great as it is for somewhat larger sizes. For example, suspensions of silver bromide and barium sulfate in water at $\lambda_v = 436$ nm have m values equal to 1.76 and 1.23, respectively. The respective densities are 6.47 and 4.50 g-mL^{-1}. From Equations 1 and 3 the respective values of $V_{\theta u}/c$ are found to be 18.7 and 3.39 for $\alpha = 0.314$. Comparison of the former with R_{90} for water shows that this silver bromide suspension scatters as strongly as water for c about 10^{-7} g-mL^{-1}. The corresponding c for barium sulfate is about 6×10^{-7} g-mL^{-1}.

As α increases above the Rayleigh region, the scattering becomes concentrated in the forward direction and depends in an increasingly complex way upon α and m. Figure 1 illustrates the situation for $m = 1.76$ up to $\alpha = 3.0$ (Figures 1–6 are derived from computer-generated plots. The plotting increment of α in Figure 1 is 0.05.) For smaller or larger values of m, the curves are generally similar to those of Figure 1 but are displaced to larger or smaller α, respectively; some representative TC's for other m are given later. Specifically for $m = 1.76$, a maximum specific scattering occurs at α about 2.4 for angles close to zero, which angles are easily accessible experimentally with a laser source. Beyond $\alpha = 3$, fluctuations become increasingly more pronounced. Evidently up to $\alpha = 2.4$, there is a great increase in sensitivity with increasing α, especially at the forward angles. For example at $\theta = 30°$, $V_{\theta u}$ is about 8000 at $\alpha = 2.4$, about 400 times as great as the value at $\alpha = 0.314$. However, if α at EP is too large, the TC has an oscillatory and practically useless character as is shown in Figure 2. (In this and Figures 3–6 the curves are calculated with titration increments of 2%.) Figure 2 is calculated on the assumption that all the particles are formed on addition of 1% of titrant; $f_0 = 0.01$ and $\alpha_0 = 0.1(0.1)1.0$. In this case $\alpha_1 = (100)^{1/3} = 4.64$. For α_0 up to 0.5, the TC's have positive slopes up to EP and the location of EP is easy. A value of α_0 about 0.5, corresponding to α_1 about 2.3, is preferred for

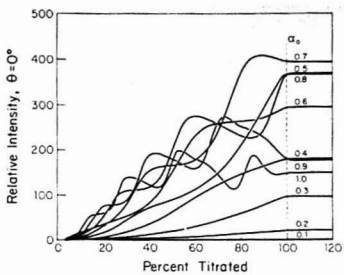

Figure 2. Calculated titration curves, constant number of particles after addition of 1% of titrant; $m = 1.76$

maximum sensitivity. For larger α_0 the location of EP is difficult or impossible.

As mentioned earlier, these calculations apply to monodisperse spheres. If the system is heterodisperse, the fluctuations would be masked to some extent, the more so the greater the heterodispersity. Theoretical calculations can be made easily for any assumed distribution of sizes, but would not be of general value. The angular scattering pattern for nonspherical particles is generally similar to that of spheres, but a nonsphere of given volume in general has an angular pattern corresponding to a sphere of somewhat larger volume. Thus the same general conclusions drawn from Figure 2 apply to nonspheres.

In the calculation of Figure 2 it is assumed that the value of α_0 can be chosen by the experimenter. Actually this usually is not possible, because particle sizes in colloidal suspensions depend in general upon reactant concentrations, mode of mixing, and other factors which need not be listed here. Moreover the samples may contain constituents which affect particle size. For this reason it may be a great practical advantage to add seed material which has been prepared separately under such conditions as yield the desired size. Assuming as stated earlier that N remains equal to the value added as seed, the increase in α during titration is given by

$$\alpha_f = \left(\frac{f + w}{w}\right)^{1/3} \alpha_s \qquad (4)$$

where α_s and α_f refer to seed and suspension, respectively, and w is weight fraction added as seed with respect to the constituent being formed in the titration. At EP,

$$\alpha_1 = \left(\frac{1 + w}{w}\right)^{1/3} \alpha_s \qquad (5)$$

Thus $\alpha_1/\alpha_s = 4.7$, 2.2, and 1.3 for $w = 0.01$, 0.1, and 1, respectively. Figures 3–5 give curves at various θ for these values of w. All the curves apply to $m = 1.76$ and α_s in each case is chosen such that $\alpha_1 = 2.3$ so that there are no oscillations at the forward angles. In fact up to $\theta = 40°$, the curves rise smoothly to EP. It is of interest to note that for $\theta \geq 50°$, there is a pronounced maximum before EP. This arises from the first maximum visible in Figure 2 which is not compensated by the second maximum as it is for $\theta \leq 40°$. The total scattered intensity at a given θ increases with increase of w, but too large a value of w obviously is undesirable because it would correspond to a small relative change in scattering. From Figures 3–5 it appears that values of w up to around 1 would be appropriate with $\theta \leq 40°$; the smallest θ consistent with the instrumental optics should be chosen. Figure 6 gives calculated TC's for $w = 0.01$, $\alpha_s = 1.0$ and $m = 1.3$. Curves (not shown) for $m = 1.5$ and 1.2 are generally similar, being

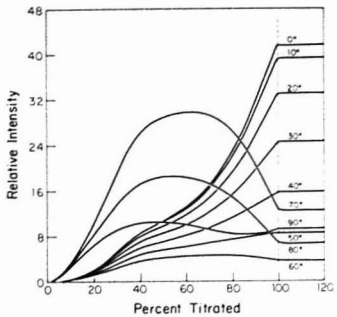

Figure 3. Calculated titration curves, constant number of particles after addition of 1% seed of $\alpha_s = 0.493$; $m = 1.76$ (scale × 10 for $\theta \geq 70°$)

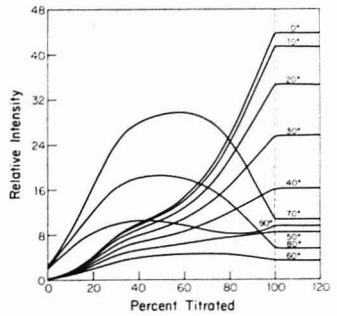

Figure 4. As Figure 3, but 10% seed of $\alpha_s = 1.04$

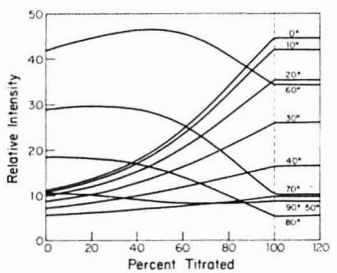

Figure 5. As Figure 3, but 100% seed of $\alpha_s = 1.83$ (scale × 10 for $\theta \geq 60°$)

more and less structured respectively. For $m = 1.3$ and 1.2, satisfactory titrations are theoretically possible at small θ, with a wide latitude in the choice of w and α_s. For the same w and α_s as in Figure 6, the TC's for $m = 1.76$ (not shown) are very complex with several maxima and minima before EP.

All the above conclusions are entirely optical in character and are based on the assumptions of monodisperse spheres of negligible solubility in the surrounding medium, all of which being formed on addition of the first increment or added as seed, with no agglomeration or growth between additions of titrant. These are matters of colloid chemistry rather than optics and will be characteristic for each chemical system. The experimental part which follows considers the specific case of silver bromide.

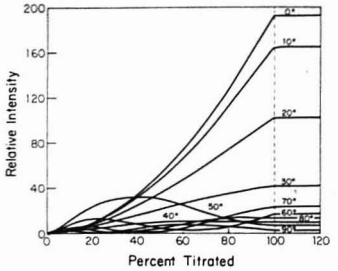

Figure 6. As Figure 3, but 1% seed of $\alpha_s = 1.00$; $m = 1.3$ (scale × 10 for $\theta \geq 50°$)

Table I. Solubility of Silver Bromide in Solvents of Dielectric Constant D at 25 °C

Solvent	pK_{sp}	D	Ref
water	12.3	80.4	5
30% ethanol[a]	13.2[b]	62.6	6
62% methanol	13.7[b]	50.4	6
50% ethanol	13.7[b]	50.4	6
48.5% acetone	13.7[b]	50.4	6
70% ethanol	14.4[b]	39.1	6
methanol	15.2	32.6	7, 8
90% ethanol	15.2[b]	29.0	6
82% acetone	15.2	29.0	6
ethanol	16.1	24.3	5
acetone	18.7[c]	20.7	9

[a] Weight percent (w/w). [b] At 20 °C. [c] At 23 °C.

Titration of Bromide with Silver. In titrations in which complexation reactions are unimportant, the solubility is greatest at EP. From the solubility of silver bromide in water ($pK_{sp} = 12.3$ at 25 °C), it is calculated that 0.7, 7, or 70% of silver bromide is dissolved at EP when initial $[Br^-]$ is 10^{-5}, 10^{-6}, or 10^{-7} M, respectively (negligible volume change). Since the present interest is in methods applicable at great dilution, solvents in which the solubility is substantially smaller than in water must be used. For initial $[Br^-] = 10^{-7}$ M, a $pK_{sp} \geq 18$ corresponds to solubility at EP ≤ 1%. Table I lists pK_{sp} in solvents of various dielectric constants D. While the solubility in 1-propanol, 2-propanol and *tert*-butanol apparently has not been measured, the values of D of these solvents (20.1, 18.3, and 10.9, respectively) indicate that mixtures with water should be suitable for titrations of very dilute solutions. All the experiments reported in this paper were done in mixtures of water–organic solvent. The refractive index ratios in these mixtures range from 1.70 to 1.74 and thus the calculated scattering is very similar to that in water.

Under most conditions the addition of silver nitrate to dilute aqueous solutions of bromide yields suspensions in which the particle size increases rapidly for several minutes (*10*). Such systems obviously are useless for titrations and it was necessary to establish conditions such that a practically constant size and scattering intensity would be reached within some seconds after addition of titrant. Such suspensions are called "stable" for the present purpose.

EXPERIMENTAL

Reagents. Analytical reagent grade potassium bromide and silver nitrate dried at 110 °C for 2 h were used to prepare 0.1 M stock solutions in distilled water. The silver nitrate solution, standardized against sodium chloride and stored in the dark, was used to standardize the potassium bromide solution. All organic solvents were analytical grade except isopropanol which was obtained by distilling the technical grade. No substances reacting with silver nitrate were present in any of the organic solvents.

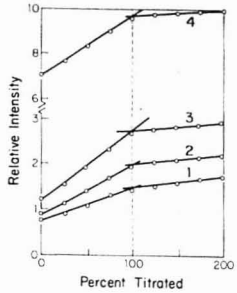

Figure 7. Experimental curves in 80% 2-propanol, $[Br^-] = 10^{-6}$ M, $\Delta t = 30$ s, $\theta = 25°$. Amount of seed: (1) none, (2) 1%, (3) 10%, (4) 100%

The compositions of the mixtures are expressed as volume-percent. Wool violet and polyvinylpyrrolidone (PVP) and various commercially available surfactants, including polyethylene glycol 4000, Tween 40 (sorbitan monopalmitate ethyleneoxide adducts) and Tergital (nonylphenol ethyleneoxide adducts) were tested as protective colloids.

Apparatus. Scattering measurements were made with a Brice-Phoenix light scattering photometer equipped with a Virtis digital voltmeter. The instrument was calibrated in the usual manner with Ludox (*11*). A cylindrical cell, 4-cm diameter, with flat entrance and exit windows, and with the back painted black, was used. A dilute solution of fluorescein was used to check the angular symmetry of the instrument.

Titrations. Forty mL of the bromide solution were pipetted into the cell described above. Silver bromide seed, prepared as described below, was added in specified amounts. The silver nitrate solution was added from a 2-mL or 5-mL microburet, with the tip immersed into the solution. The delivery of 0.1 mL titrant took from 3 to 5 s. The solution was stirred at 400 rpm during addition and for 10 s after addition. The time interval (s) between addition of increments of titrant is referred to later as Δt. Most of the scattering measurements were made at $\theta = 25°$ and 40°.

Preparation of Seed. Tem mL of 10^{-3} M silver nitrate were pipetted into a 50-mL beaker containing 10 mL of 10^{-3} M potassium bromide being stirred at 400 rpm. Ten after delivery, 2 mL of the suspension were pipetted into a 100-mL volumetric flask containing 80 mL of isopropanol, and water was added to the mark. The 10^{-5} M seed thus prepared was stable, as measured by scattering, for at least 100 h. Electron microscopy using carbon replicas (*12*) showed that the particles were practically monodisperse and approximately spherical with an average radius of 46 nm, which corresponds to $\alpha_s = 0.9$ at $\lambda_v = 436$ nm.

RESULTS AND DISCUSSION

Stability studies at 10^{-6} M bromide with less and more than the equivalent amount of bromide gave the following results. Unstable suspensions are formed in acetone (50%) in the absence and presence of any of the protective colloids listed in Experimental, methanol (50%) in the absence and presence of PVP, and ethanol (50%, 70%). Suspensions stable within 30 s or less are formed in methanol (80%), ethanol (80%, 90%), 1-propanol (80%), and 2-propanol (80%, 90%); in the latter group, the addition of protective colloids is unnecessary.

Effect of Amount of Seed. Figure 7 gives the results of titrations in 2-propanol (80%, $\Delta t = 30$, $[Br^-] = 10^{-6}$ M) with 0, 1, 10, and 100% seed. The end points are located more easily in the presence than absence of seed because of the increased slope before EP. In these four and most other titrations, there is a small positive slope after EP, which undoubtedly is due to a slight agglomeration upon increase of concentration of silver ion.

The TC with 1% seed, $\alpha_s = 0.9$, is drastically different from the theoretical one, which as mentioned shows maxima and minima before EP. The agreement is fair with 10% and good with 100%. Maxima and minima are not observed with 1% seed because this amount of seed is not sufficient to prevent nucleation during the titration, with the result that the particles do not grow as large as assumed in the calculation. This is shown very clearly by comparison of initial and final particle sizes (measured by specific scattering (2)), given in Table II. Apparently 100% seed is completely effective in preventing nucleation, and 10% seed much less so. As a practical matter, the use of 10% is preferable to a much larger amount, because the total variation in the measured scattering is larger with the smaller amount. The location of the EP is entirely satisfactory in this case.

Table II. Particle Growth in Titration in Presence of Seed, $r_s = 46$ nm

	% seed			
	0	1	10	100
r_i, nm (calcd)	...	213	103	58
r_i, nm (obsd)	40	51	53	57

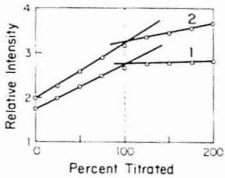

Figure 8. As Figure 7, but 90% 2-propanol; curve 1, 10^{-6} M Br^-, 10% seed; curve 2, 5×10^{-7} M Br^-, 20% seed

Other alcohols tested include methanol (70%), ethanol (70–90%), 1-propanol (80%) and *tert*-butanol (70–90%). Of these the latter two are useful with 10^{-6} M Br^-, but generally 2-propanol is to be preferred and the further remarks apply to this substance.

When specially prepared dust-free water is used instead of ordinary deionized water to prepare the seed and solutions, the initial scattering is reduced somewhat but the shape of the TC is unchanged. Increase of Δt to 60 or 120 s causes virtually no change in the shape at 10^{-6} M Br^-. As expected, $\theta = 25°$ gives a better curve (larger slope before EP) than 40°. Even 5×10^{-7} M Br^- can be titrated accurately in 90% 2-propanol (Figure 8).

The accuracy of the method was tested at $[Br^-] = 10^{-5}$, 5×10^{-6}, 10^{-6}, and 5×10^{-7} M at alcohol contents respectively 30, 50, 80, and 90%. In 20 such tests, the maximum deviation from the true value was 2.5%, and the precision (standard deviation) was 1.3%, which is scarcely larger than the precision in the buret reading. The titration time is less than 5 min. As compared to previous nephelometric procedures (see Ref. 1 and references contained therein), the use of the water-miscible organic solvent and of seed have made a substantial improvement in the accuracy and reduction of the time required for titration of such dilute solutions. The titrations are for obvious reasons much more sensitive than turbidimetric ones, in which transmission is measured, and compare favorably with any other method at the 10^{-6} M level.

LITERATURE CITED

(1) E. J. Meehan and Grace Chiu, *Anal. Chem.*, **36**, 536 (1964).
(2) E. J. Meehan and W. H. Beattie, *J. Phys. Chem.*, **64**, 1006 (1960).
(3) M. Kerker, "The Scattering of Light and Other Electromagnetic Radiation", Academic Press, New York, N.Y., 1969, Chapter 7.
(4) E. J. Meehan and Jerry K. Miller, *J. Phys. Chem.*, **72**, 1523 (1965).
(5) L. G. Sillén and A. E. Martell, "Stability Constants of Metal-Ion Complexes", The Chemical Society, London, 1964.
(6) J. Kratohvil and B. Težak, *Ark. Kemi.*, **26**, 243 (1954).

(7) R. Alexander, E. C. F. Ko, A. J. Parker, and T. J. Broxton, *J. Am. Chem. Soc.*, **89**, 3703 (1967).
(8) P. S. Buckley and H. Hartley, *Phil. Mag.*, **8**, 320 (1929).
(9) D. C. Luehrs, R. T. Iwamoto, and J. Kleinberg, *J. Inorg. Chem.*, **5**, 201 (1966).
(10) E. J. Meehan and Grace Chiu, *J. Phys. Chem.*, **70**, 1384 (1966).
(11) M. B. Huglin, "Light Scattering from Polymer Solutions", Academic Press, London, 1972, Chapter 4.
(12) E. J. Meehan and W. H. Beattie, *J. Colloid Sci.*, **15**, 183 (1960).

RECEIVED for review August 11, 1977. Accepted September 19, 1977.

Determination of Nitrite Ion Using Differential Pulse Polarography

Shaw-Kong Chang, Raymond Kozeniauskas, and George W. Harrington*

Department of Chemistry, Temple University, Philadelphia, Pennsylvania 19122

Nitrite ion can be determined with a high degree of accuracy and sensitivity by differential pulse polarography utilizing the rapid and quantitative reaction between nitrite ion and diphenylamine at low pH with thiocyanate ion as catalyst. The calculated detection limit is shown to be 0.3 (as NO_2^-) ppb in simple aqueous solution. The method is further used to determine nitrite in processed meats and human saliva. The results for processed meat are compared to those obtained by the AOAC method. The agreement is excellent.

Because of the role of nitrite ion as an important precursor in the formation of *N*-nitrosamines, many of which have been shown to be potent carcinogens (*1–3*), and it widespread occurrence in our environment, either naturally (*1*) or by its use as a food preservative (*2*), it is important that sensitive and accurate methods be available for the determination of this ion. Such methods should also be simple and quick and capable of determining nitrite ion in various types of real samples. It is the purpose of this paper to demonstrate that differential pulse polarography (DPP) coupled with an appropriate chemical reaction satisfies these requirements.

A large number of methods for the determination of nitrite have been reported, principally involving colorimetric methods. These methods have been summarized and compared by Szekely (*4*) and Sawicki et al. (*5*). The methods all have limited sensitivity and dynamic range. They frequently depend on unstable colors and involve long reaction times.

Determination of nitrite by differential pulse polarography has been previously reported. In the first instance (*6*) nitrite was determined as nitrous acid in a citrate buffer. However, since nitrous acid is unstable and its reduction potential is close to that of oxygen, the sensitivity of the method was limited to 0.5 ppm. A second report appeared by O'Laughlin et al. (*7*), in which nitrite and nitrate were determined by DPP using the enhancement of the ytterbium peak current. A detection limit of 14 ppb nitrate, or nitrite, nitrogen was achieved under ideal conditions.

As part of a continuing study of *N*-nitrosamines (*8–11*) the authors have discovered that diphenylamine (DPA) reacts instantaneously and quantitatively with nitrite under appropriate conditions to yield diphenylnitrosamine (DPN). This nitrosamine, which has been found *not* to be a carcinogen (*12–15*), yields a very sharp differential pulse polarogram with $E_p = -0.55$ to -0.60 V vs. SCE at pH 1–2. The polarographic behavior of DPN has been well studied (*16, 17*). The purpose of this paper is to demonstrate that the formation of DPN can serve as the basis for a useful analytical method.

EXPERIMENTAL

Apparatus. The instrumentation, cells, etc. were previously reported (*11*). The drop time was 1 s, pulse height, 50 mV; and scan rate, 2 mV/s. Hg flow rate was 1.26 mg/s. Hg column height was 82.4 cm. All microliter pipets were calibrated in terms of precision and accuracy. pH was measured with a Leeds and Northup Expanded Scale pH meter.

Reagents. All inorganic chemicals used were reagent grade and used without further purification. *N*-1-Napthylenediamine used for modified Griess Reagent was obtained from the Eastern Regional Research Laboratory of the U.S. Department of Agriculture. Diphenylamine (Aldrich Chemical Co.) was recrystallized from water and methanol. All distilled water used was triple-distilled. Dilute solutions of nitrite were prepared from stock solutions, which were 1.00×10^{-2} M in $NaNO_2$, by appropriate quantitative dilution or by direct pipetting into samples. High purity nitrogen further purified by passage through a chromous scrubber was used for degassing solutions having concentrations of 0.1 μM or higher. Helium was used for lower concentrations. Irreproducibile results were obtained when nitrogen was used for the more dilute solutions, possibly because of trace amounts of nitrogen oxides present in the gas.

Saliva was collected by expectoration into clean vials. Approximately 1 mL was obtained from each subject. Filtration, if necessary, was performed using nitrite-free No. 1 filter paper; the filtrate, or clear saliva, was used directly as the sample.

Frankfurters were prepared for analysis using the AOAC method (*18, 19*).

Procedure. A differential pulse polarogram was run on a degassed solution containing diphenylamine, percholoric acid, and NaSCN, as a catalyst. Details are given below. The background current was recorded. To this solution was added an appropriate aliquot of sample and the current–voltage curve recorded again. The background current was subtracted from the current observed after addition of sample, yielding the desired current signal. Nitrite was then determined by the method of standard addition. For the analysis using the AOAC method, a working curve was established.

RESULTS

In order to determine those solution conditions yielding the fastest reaction time, several solutions of varying composition were examined. The DME was potentiostated at the peak of DPN and the current recorded as a function of time. A voltage integrator was used to drive the *X*-axis of the recorder. The reaction rate was followed from time of addition of the known amount of nitrite solution. After the desired interval of reaction time had passed, a large concentration of SCN^-

Table I. Rate of Formation of Diphenylnitrosamine (DPA) for Various Solutions Conditions (t = 25.0 °C)

Solution No.	pH	DPA, μM	Nitrite concn, μM	SCN^- concn, μM	$t_{1/2}$, min^{-1}
1	1.00	200	25.0	0	0.777
2	1.50	200	25.0	0	2.42
3	2.00	200	25.0	0	7.03
4	2.50	200	25.0	0	21.3
5	1.50	200	10.0	0	2.35
6	1.50	200	5.00	0	2.40
7	1.00	100	25.0	0	1.01
8	1.00	300	25.0	0	0.694
9	1.00	400	25.0	0	0.648
10	2.00	200	25.0	125	3.52
11	2.00	200	25.0	250	2.44
12	2.00	200	25.0	375	1.80
13	2.00	200	25.0	500	1.47
14	2.00	200	25.0	1000	0.811

was added to the solution. This was done simply to accelerate the reactions. When there was no further increase in current, the value was recorded as the 100% current ($I_{100\%}$). This current was further checked by determining the peak of an equimolar amount of DPN under the same solution conditions. In all cases plots of $\ln (1 - I_p/I_{100\%})$ vs. time were linear; hence, $t_{1/2}$ could be calculated. Results are shown in Table I. $NaClO_4$ was added in appropriate amounts to maintain constant ionic strength. Acid was added as $HClO_4$.

From the results for solutions 1, 2, 3, and 4 in Table I is seen that the reaction is fastest at low pH. This is in contrast to the rate of formation of other nitrosamines which have maximum rates at pH 3 (*20–22*). This may be associated with the fact that DPA is a very weak base. From the results for solutions 2, 5, and 6 it is obvious the $t_{1/2}$ is independent of nitrite concentration over the range studied. This observation agrees with previous reports (*23, 24*) that the rate of formation of aromatic nitrosamines is frequently first order with respect to nitrite ion. The results for solutions 1, 7, 8, and 9 yield the expected result that the rate increases with increasing concentration of DPA. The results for solutions 3, 10, 11, 12, 13, and 14 confirm the previously reported observation (*20, 25*) that thiocyanate ion greatly enhances the rate of the reaction. It has been suggested that this effect is due to the conversion of the HNO_2 to NOSCN (*26*), thus increasing the concentration of the nitrosyl ion which is the actual nitrosating agent. From these experments we can expect that the half-time of the reaction will be less than 3 s if DPA concentration is greater than 100 μM, thiocyanate concentration is greater than 7000 μM, and the pH $\simeq$ 1.5. Using these conditions, the reaction rate was too fast to measure by monitoring the increase of peak current. Addition of NO_2^- to this solution after 10-s stirring resulted in a peak current that did not change with time, indicating that the reaction was complete before the measurement could be made. The rapid rate of reaction for DPA agrees with predictions based on kinetic studies of other secondary amines by Mirvish (*21*). It should be noted that neither DPA nor thiocyanate is electroactive; hence, the presence of excesses of these compounds had no effect on the determination. The reagent solution was thus prepared from the following stock solutions:

Solution A: 2.60×10^{-3} M diphenylamine in 40% methanol (methanol is required to ensure solubility of the amine).

Solution B: 0.100 M NaSCN.

Solution C : 0.40 M $HClO_4$.

The reagent solution was prepared by adding 5.00 mL of A and 10.00 mL each of B and C to 100.0 mL distilled water. The reagent solution prepared in this fashion yielded the best background i–E curves in terms of slope and noise level and also provided the necessary constant ionic strength buffer.

Table II. Nitrite Determination in Aqueous Solution

NO_2^- concn, μM	NO_2^- found: Colorimetry (n = 4) (Griess reagent)	NO_2^- found: DDP (n = 4)
4.00	4.05 ± 0.19	4.00 ± 0.02
8.00	8.05 ± 0.33	8.00 ± 0.05
12.00	12.20 ± 0.20	12.12 ± 0.06

Table III. Nitrite Determination in Aqueous Solution

NO_2^- concn ($\times 10^{-7}$ M)	I_p (corr.) nA	n
0.200	3.3 ± 0.4[a]	5
0.400	6.3 ± 0.4	5
0.600	9.3 ± 0.4	5
0.800	12.2 ± 0.5	5
1.00	15.4 ± 0.3	5
1.20	18.4 ± 0.4	5
2.00	30.8 ± 0.4	4
3.00	46.0 ± 0.3	3
4.00	61.0 ± 0.5	3
5.00	76.2 ± 0.6	3
6.00	91.6 ± 0.4	3
7.00	106.2 ± 0.6	2
8.00	121.0 ± 0.6	2
10.0	151.0 ± 1.4	4

[a] Standard deviation.

The solution was prepared fresh each day and stored in a dark bottle containing a small amount (ca. 1 g) of zinc metal shot to destroy any DPN that might form simply on standing after exposure to air. This solution was used as described above in the Experimental section.

Aqueous Solutions. Some typical results for simple aqueous solutions are shown in Tables II and III. In Table II and others, n values refer to the number of independent determinations. Table II shows the results of comparisons between the usual colorimetric method using Griess reagent and the differential pulse method. It will be noted that the agreement is excellent. Table III shows the results of the differential pulse method for a series of known nitrite solutions. These solutions were prepared by adding an appropriate aliquot of nitrite stock solution to 10.00 mL of reagent solution described above. The data appear to be quite good. Peak current is linearly related to concentration with a correlation coefficient (r^2) = 0.999. Using the data in Table III for the concentration range 1.20×10^{-7} M to the lowest value determined, the detection limit calculated by the method of Skogerboe and Grant (*27*) is 6×10^{-9} M (0.3 ppb as NO_2^-). The calculation uses the formula, d.l. = $t\delta x/m$ where δx is the pooled standard deviation, m = slope (151 nA/μM), and t is the one-tailed statistic constant at 99% confidence level for 30 independent determinations.

A solution 6.3×10^{-9} M NO_2^- was run to check the reasonableness of the calculated detection limit. A corrected current of 0.8 ± 0.3 nA was observed. The error of approximately 40% at this concentration agrees with the meaning of detection limit according to Ingle (*28*).

At the lowest concentration in Table III, 2.00×10^{-8} M, the standard deviation is about 12%. If a standard deviation of 2% or better is desired, 1.00×10^{-7} M (4.6 ppb) should be considered the practical working limit. The samples to be discussed below were all examined at concentrations above 0.1 μM.

In the potential region used in this study, –0.4 to –0.7 V, a noise level of about 3 nA or higher is not uncommon. The presence of DPA, however, at the recommended level, has a marked smoothing effect on the i–e curve. Essentially no noise was observed in background even at 50-nA full scale deflection.

Table IV. Stability of Diphenylnitrosamine Under Conditions of Analysis

Time	NO_2^- found as DPN[a]
20 min	4.97 μM
23 h	5.03 μM
46 h	4.92 μM

[a] = 5.00 μM NO_2^- added as $NaNO_2$.

This is most likely a surfactant effect due to the DPA which apparently, from our data, does not negatively effect the analytical method.

Table IV shows data that indicate the stability of the nitrosated product as a function of time. It can be seen from Table IV that DPN is quite stable under these conditions.

Saliva. Fifty to two-hundred microliters of either clear saliva or saliva filtrate were added to 10.00 mL of the reagent solution. Results are shown in Table V. In samples C and D, known amounts of nitrite were added to check recovery. The original nitrite found in each sample was within the range previously reported for human saliva (*29*). Total analysis time per 5 samples was approximately 20 min.

Processed Meat (Frankfurters). Frankfurters from three different manufacturers were examined. The suspensions prepared by the AOAC method were divided into two portions. One was analyzed by the DDP method and the other by the AOAC method using *N*-1-naphthylenediamine as reagent. Fifty to five-hundred microliter aliquots were used for the DPP method. Exactly 10.00 mL of reagent solution were used. In addition to determination of residual nitrite, a known amount was added to each sample and recovery checked. The results are shown in Table VI. It is apparent that the agreement is quite good and that the small amounts of miscellaneous material present in the frankfurther extract do not affect the electoanalytical determination under the conditions used. Table VII contains data comparing the results for the DPP method at two different dilutions. The AOAC method of sample preparation requires a dilution of 1:100. The DPP method, however, can be used at 1:10 dilution. At the lower dilution, the DPP method yields better accuracy as seen from data in Table VII.

Interferences. There are relatively few interfering substances in the type of samples studied in this investigation. Since the method basically determines the amount of nitrosating agent present, any NO in the air will also give rise to a peak. The *N*-1-naphthyldiamine used for Griess reagent will also react with nitrosating agents. It was observed that prolonged exposure of the reagent solution to laboratory air resulted in development of a small peak as seen during the background scan if the solution was not stored over zinc. Nitrate is not electroactive under the conditions used in these determinations, and hence does not interfere. In fact, additions of nitrate up to 500 times the concentration of nitrite did not affect the observed currents. The peak potential of DPN is sufficiently different from that of oxygen at this pH that oxygen is not a serious interference. The usual degassing and blanketing procedures are sufficient except as noted in the Experimental section concerning very dilute solutions.

Diphenylnitrosamine already present in the sample could, of course, yield erroneous results. Its presence is unlikely in the type of samples studied since it has not been found to be a naturally occuring nitrosamine (*30*). If there is reason to suspect the presence of this nitrosamine, its presence and concentration could be checked by a variety of methods. A portion of the sample could be treated with urea to destroy the nitrite and an aliquot then run in the reagent solution. Alternatively, one could simply add an aliquot of the sample to the reagent solution prepared without the DPA and then scan the potential region. If necessary, corrections could then be made in the final results. This check was performed in the samples used in this study and no electroactive species were observed in the potential range −0.4 to −0.7 V.

DISCUSSION

From the results given in Tables I–VII, it seems clear that utilization of the nitrosation of diphenylamine provides the basis for a sensitive and rapid analytical method for determining nitrite ion using differential pulse polarography. Analysis times are short and the reagents required are readily available and relatively non-toxic. DPN, although not a carcinogen, may under certain conditions act as a nitrosating agent via transnitrosation. DPN solutions should, therefore, be disposed of properly using a denitrosating solution such as 10% NaOH (aqueous) containing aluminum metal. In the case of saliva, very minor sample pretreatment is required. In some instances, raw saliva could be used directly. This method should be especially useful for studies involving the effect of diet and other parameters on nitrite concentrations in human saliva or for monitoring nitrite levels in processed meats.

The method is currently being extended to include nitrate determination subsequent to nitrite determination. Results of these studies will be reported later.

Table V. Nitrite in Saliva

Sample	Nitrite found, ppm 1	2	3	4	5	Average
A (1/14/77) (S.K.C.)	3.20	3.24	3.15	3.23	3.26	3.22 ± 0.04
B (1/18/77) (S.K.C.)	3.52	3.57	3.61	3.55	3.66	3.58 ± 0.05
C (G.W.H.)	0.25	0.23	0.28			0.25 ± 0.03
C + 1.74 ppm Recovery = 95 ± 3%	1.87	1.95	1.90			1.91 ± 0.04
D (B.W.L.)	5.18	5.30	5.34			5.27 ± 0.08
D + 5.00 ppm Recovery = 99.0 ± 3.0%	10.12	10.31	10.24			10.22 ± 0.10

Table VI. Residual Nitrite in Frankfurter: Comparison of AOAC Methods vs. DPP Method

	Concentration, μmol AOAC (n = 5)	Recovery of added NO_2^-[a]	DPP (n = 4)	Recovery of added NO_2^-[a]
Sample A	6.73 ± 0.20	95.7 ± 6.1%	6.55 ± 0.07	101.7 ± 2.4%
Sample B	2.25 ± 0.08	98.4 ± 2.4%	2.37 ± 0.03	98.8 ± 1.6%
Sample C	5.46 ± 0.11	98.8 ± 4.0%	5.39 ± 0.07	99.0 ± 2.4%

[a] 5 μM NO_2^- was added in all cases.

Table VII. Concentration (ppm) of $NANO_2$ in Frankfurter: Comparison of 1:10 vs. 1:100 Dilution

	Concentration (ppm) of $NANO_2$ in frankfurter	
	1:10 (n = 4)	1:100 (n = 4)
Sample D	23.44 ± 0.10	23.56 ± 0.28
Sample E	25.44 ± 0.09	25.49 ± 0.24

ACKNOWLEDGMENT

The authors thank Walter Fiddler of The Eastern Regional Research Laboratories of the U.S. Department of Agriculture for his generous contribution of materials for Griess reagent.

LITERATURE CITED

(1) P. N. Magee and J. M. Barnes, *Brit. J. Cancer*, **10**, 11 (1956).
(2) W. Lijinsky and S. S. Epstein, *Nature (London)*, **225**, 21 (1970).
(3) I. A. Wolff and A. E. Wasserman, *Science*, **177**, 15 (1972).
(4) E. Szekely, *Talanta* **15**, 795 (1968).
(5) E. Sawicki, T. W. Stanley, I. Pfaff, and A. Damico, *Talanta*, **10**, 641 (1963).
(6) Princeton Applied Research Application Brief N-1, Princeton, N.J., 1974.
(7) S. W. Boese, V. S. Archer, and J. W. O'Laughlin, *Anal. Chem.*, **49**, 479 (1977).
(8) S. Yanagida, D. J. Barsotti, G. W. Harrington, and D. Swern, *Tetrahedon Lett.*, **29**, 2671 (1973).
(9) S. K. Chang and G. W. Harrington, *Anal. Chem.*, **47**, 1857 (1975).
(10) S. E. Abanoli, J. A. Popp, S. K. Chang, G. W. Harrington, P. D. Lotlikar, D. Hadjiolov, M. Levitt, S. Rajalakshmi, and D. S. R. Sarma, *J. Natl. Cancer Inst.*, **58**, 263 (1977).
(11) S. K. Chang, G. W. Harrington, H. S. Veale, and D. Swern, *J. Org. Chem.*, **41**, 3752 (1976).
(12) R. Druckery, S. Preussmann, D. Ivankovic, and Z. Schmahl, *Krebsforsch.*, **69**, 103 (1967).
(13) M. F. Argus and C. Hoch-Ligeti, *J. Natl. Cancer Inst.*, **27**, 695 (1961).
(14) H. Druckery, R. Preussman, D. Schmahl, and M. Miller, *Naturwissenschaften*, **48**, 134 (1961).
(15) E. Boyland, R. L. Carter, J. W. Gorrod, and F. J. C. Roe, *Eur. J. Cancer*, **4**, 233 (1968).
(16) H. Lund, *Acta Chem. Scand.*, **11**, 990 (1957).
(17) L. Holleck and R. Schindler, *Z. Electrochem.*, **62**, 942 (1958).
(18) "Official Methods of Analysis", 12th ed., Association of Official Analytical Chemistry Washington, D.C., 1975.
(19) R. A. Nicholas, and J. B. Fox, Jr., *J. Assoc. Off. Anal. Chem.*, **56**, 922 (1973).
(20) S. S. Mirvish, J. Sams, T. Y. Fan, and S. R. Tannenbaum, *J. Natl. Cancer Inst.*, **51**, 1833 (1973).
(21) S. Mirvish, *Toxicol. Appl. Pharmacol.*, **31**, 325 (1975).
(22) S. Mirvish, *J. Natl. Cancer Inst.*, **44**, 633 (1970).
(23) J. H. Ridd, *Quart. Rev., Chem. Soc.*, **15**, 418 (1961).
(24) E. Kalatzis and J. H. Ridd, *J. Chem. Soc. B*, 529 (1966).
(25) T. Y. Fan and S. R. Tannenbaum, *J. Agric. Food Chem.*, **21**, 237 (1973).
(26) C. A. Bunton, D. R. Llewellyn, and G. Stedman, *J. Chem Soc.*, 568 (1959).
(27) R. K. Skogerboe and C. L. Grant, *Spectrosc. Lett.*, **3**, 215 (1970).
(28) J. D. Ingle, Jr., *J. Chem. Educ.*, **51**, 101 (1974).
(29) S. R. Tannenbaum, A. J. Sinskey, M. Weisman, and W. Bishop, *J. Natl. Cancer Inst.*, **53**, 79 (1974).
(30) P. N. Magee, R. Montesano, and R. Pruessmann in "Chemical Carcinogens," ACS Monograph, No. 173, C. E. Searle, Ed., 1976, Chapter 11.

RECEIVED for review March 31, 1977. Resubmitted July 18, 1977. Accepted September 12, 1977. Presented at the 11th MARM, April 1977, Newark, Del. The investigation was supported by PHS Research Grant CA-18618 from the National Cancer Institute.

Fourier Transform Infrared Analysis below the One-Nanogram Level

R. Cournoyer,* J. C. Shearer, and D. H. Anderson

Industrial Laboratory, Eastman Kodak Company, Rochester, New York 14650

The interfacing of microscopy with Fourier Transform infrared (FTIR) spectroscopy is a useful combination allowing samples of less than 1 ng to be identified. The sample, usually supported by a thin sodium chloride plate, is centered in a aperture 50 to 200 μm in diameter. The sample mount is oriented in an 8X beam condenser in an FTIR spectrometer where multiscan signal averaging techniques produce a spectrum with the desired signal-to-noise ratio. One or two hours of total analysis time is generally required. Polymers and other solids as well as oils and various liquids have been identified. The small amounts of material require that the entire sample preparation be done under a microscope.

The characterization of samples too small to be visible to the naked eye is restricted to the domain of the microscope. In many cases characterizations can be made accurately and quickly with the microscope alone, but some microsamples do not yield to such analysis or do so only with great difficulty. These samples require the interfacing of modern instrumental techniques with classical microscopic analysis. The interfacing of microscopy with Fourier Transform infrared (FTIR) spectroscopy is a useful combination allowing preparations of less than 1 ng of sample to be identified. The sample, usually supported by a thin sodium chloride plate, is centered in an aperture 50 to 200 μm in diameter. The sample mount is oriented in an 8X beam condenser in an FTIR spectrometer where multiscan signal averaging techniques produce a spectrum with the desired signal-to-noise ratio. One or two hours of total analysis time is generally required. Polymers and other solids as well as oils and various liquids have been identified using this approach.

EXPERIMENTAL

Instrumentation. A stereo and compound microscope as well as microtomes, hot stages, or any other apparatus appropriate for the particular samples at hand are required. A fine pointed probe (dissecting needle), forceps, and other paraphernalia suitable for micromanipulation are also necessary. A Digilab FTS-14 Fourier Transform spectrometer equipped with the standard nichrome wire source and TGS detector, and a Perkin-Elmer 8X reflecting beam condenser were used to produce the spectra.

Sodium Chloride Plates. Thin sodium chloride plates (200–500 μm thick) are prepared by cleaving rock salt used in standard infrared work. The salt crystals are first cut into rectangles (approximately $^1/_4 \times {}^1/_2$ cm) with a clean, single edged stainless steel blade. This rectangle is transferred with forceps to a clean microscope slide and placed under a stereo microscope. The rectangle is stood on edge and cleaved into two plates of equal thickness with a clean, unused single edged blade. The process is repeated until plates of the desired thickness are obtained. Plates without both faces freshly cleaved are discarded to avoid possible contamination. A plate is selected that is flat and has flawless domains, and is trimmed to 1–2 × 3–4 mm. Some infrared

salt plates will not cleave satisfactorily and much aggravation can be avoided by searching out plates that are easily cleaved. A single (38 × 19 × 4 mm) infrared rock salt crystal will provide scores of the desired thin plates. Cleanliness throughout the preparation is imperative because of the small amount of sample involved in the analysis.

Aperture Disk. Perkin-Elmer micropellet disks with 250 or 500 μm apertures are the bases for sample mounts. Apertures, 50 to 200 μm, are fashioned under the microscope by punching holes of appropriate diameter in 1-mil brass or stainless steel shim stock with tapered watchmaker's reamers. The apertures should be flat and have clean edges. Some polishing is necessary with an Arkansas stone. The aperture, centered on the micropellet disk, is attached with glue or adhesive tape. The aperture disk surface and aperture should be inspected under the microscope for cleanliness prior to use.

Sample Preparation. The technique used for sample preparation is determined by the nature of the sample, the available equipment, and the manipulative skills and preferences of the microscopist. The sample should be prepared so that it will approximately fill the aperture, and so that it is only several micrometers thick. The thin salt plates are used to support the sample in an aperture of appropriate diameter. The smaller samples require the use of the smaller apertures. The sample may be too thin or, as more often the case, too thick. A general approach has been to make the sample as thin as possible. One approach for solids has been to place the sample on a microscope slide and roll it under a fine pointed probe tip; another approach is to press the sample between two clean microscope slides or a slide and a coverslip, then use a new, solvent washed razor blade to peel the material from the glass surface. Another technique which is suitable for solids and liquids is to place the sample between two freshly cleaved thin salt plates and apply gentle pressure with a probe. The plates must be flat and without irregularities; otherwise the pressure applied will crack the plates. When the two salt plates are separated, most or all of the sample generally remains on one of the plates. If the sample will not stay flat because of elasticity or surface tension, the plates need not be separated. Troublesome samples sometimes require the use of a small vise to hold the salt plates together.

Liquid sample handling is sometimes facilitated by transferring the liquid to a flexible film. The film is then arched with the liquid at the high point, and the sample transferred by touching the salt plate to the droplet. These are only the most generally applicable sample preparation techniques used in our laboratory. Other techniques exist and additional ones are continually being developed as different samples require. Small amounts of volatile materials may be handled by adapting cryogenic techniques familiar to many microscopists and other workers involved with low temperature sample manipulation.

Sample Mounting. The sample side of the salt plate is placed against the aperture disk surface when a single salt plate is being used. With this orientation, the sample sits in the aperture rather than some distance above it. The thin salt plates with the samples attached are secured to the aperture disks with a small amount of soft wax. The wax is applied to the end of the salt plate surfaces with a fine pointed probe. An aperture disk containing the sample is then placed in the FTIR spectrometer, and aligned by adjusting the disk position until the detector signal is maximized. FTIR spectra are accumulated until a spectrum with usable signal to noise ratio results. Higher gains and longer scanning times are required as the sample or aperture size decreases. We have found 50 μm to be the smallest usable aperture for our instrument. A Globar source and/or Mercury–Cadmium–Telluride detector will enable the use of somewhat smaller apertures; however, diffraction effects will prevent the use of apertures less than 30 μm.

RESULTS AND DISCUSSION

The sensitivity of the FTIR spectrometer has enabled infrared identification of increasingly smaller amounts of material (*1–3*). The exploitation of this sensitivity requires new approaches for sample presentation to the instrument. Investigations carried out in this laboratory indicate that miniaturization of the familiar KBr pellet would not give suitable preparations for samples at the nanogram level because of dilution and loss of sample, or impurities in the KBr or solvents. Even when these limitations were overcome, atmospheric contamination would often swamp out the sample signal. A single atmospheric "dust speck" is frequently 10

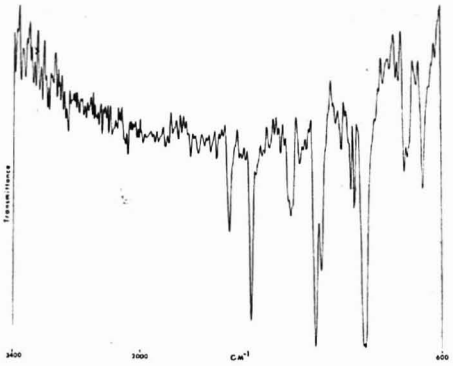

Figure 1. Spectrum of 6 ng of triphenyl phosphate in a 100-μm aperture scanned 1000 times at 8 cm^{-1} resolution

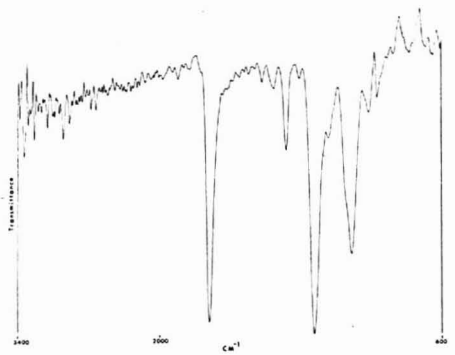

Figure 2. Spectrum of 3.4 ng of cellulose acetate with 10% triphenyl phosphate in a 100-μm aperture scanned 2000 times at 8 cm^{-1} resolution

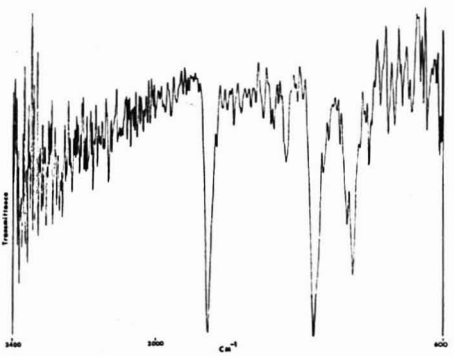

Figure 3. Spectrum of 0.9 ng of cellulose acetate with 10% triphenyl phosphate in a 50-μm aperture scanned 2000 times at 8 cm^{-1} resolution

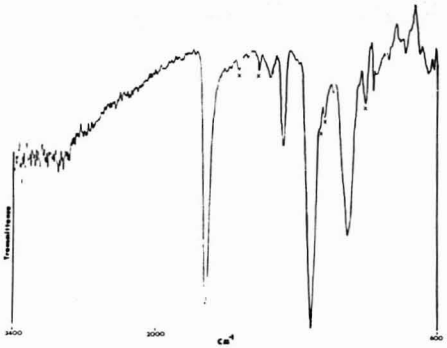

Figure 4. Spectrum of 0.9 ng of cellulose acetate with 10% triphenyl phosphate in a 50-μm aperture scanned 96 000 times at 8 cm^{-1} resolution

to 100 times the weight of the samples being considered. It was decided for these reasons that the samples would have to be examined neat. Sodium chloride was chosen as the most suitable support for the sample because of its infrared transmission and ease of cleavage. The use of microscopic techniques throughout the sample preparation has two advantages; the analyst is able to work with materials not visible to the naked eye, and microscopic physical and chemical separations enable relatively pure samples to be used, which greatly increases the probability of successful identification by infrared spectroscopy.

Figure 1 is an infrared curve of 6 ng of triphenyl phosphate. This curve was used to identify an isolated 6-ng sample found in a manufacturing environment. Total analysis time was approximately 2 h of which 80% involved sample preparation.

Figure 2 is the spectrum of 3.4 ng of cellulose acetate film base in a 100-μm aperture, and that in Figure 3 is of 0.9 ng of the same sample in a 50-μm aperture. Both of these spectra are unsmoothed and were recorded after 2000 scans. The increased noise in Figure 3 shows a reduction in sample size and aperture. The spectrum in Figure 3 is identifiable as cellulose acetate even though less than 1 h of spectrometer time and less than 1 ng of sample were used. Figure 4 shows the improvement obtained by prolonged scanning (~40 h) of the sample described in Figure 3. The noise has been reduced to the extent that absorptions due to 90 pg of triphenyl phosphate, which is present at approximately 10% in the film base, are recognizable. These absorptions have been marked with x's and may be compared with those in Figure 1.

Microscopic sample manipulation combined with the sensitivity of FTIR spectroscopy allows us to identify previously unidentifiably small amounts of material. Work is under way to construct a stronger beam condenser to reduce data collection time and to improve sensitivity. The combination of this condenser with refinements in sample preparation should result in at least an additional 10-fold reduction in minimum identifiable sample size. The obtainable spectra are of sufficiently high quality that spectral subtractions will be feasible. Work is now under way to demonstrate the practicality and utility of this technique. Successful infrared spectroscopic analysis of materials at the nanogram to picogram level indicates that this technique, with all its advantages, can be considered as an ultra micro method.

ACKNOWLEDGMENT

We thank Rex Wooton for his assistance in producing the spectra in Figures 1 through 4.

LITERATURE CITED

(1) P. R. Griffiths and F. Block, Paper 329, 23rd Pittsburgh Conference on Analytical Chemistry and Applied Spectroscopy, Cleveland, Ohio, 1972.
(2) S. S. T. King, *J. Agric. Food Chem.*, **21**, 526 (1973).
(3) D. H. Anderson and T. E. Wilson, *Anal. Chem.*, **47**, 2482 (1975).

RECEIVED for review July 18, 1977. Accepted September 26, 1977.

Spectrophotometric Determination of Acrylonitrile

Maynard E. Hall* and John W. Stevens, Jr.[1]

Univeristy of Arkansas, Graduate Institute of Technology, Post Office Box 3017, Little Rock, Arkansas 72203

A spectrophotometric method for the determination of acrylonitrile based on the absorbance of visible light of a pyridine–acrylonitrile complex at 411 nm has been developed. This complex is formed in the presence of a basic hypochlorite solution at 60–65 °C. The molar absorptivity, based on acrylonitrile concentration, is 635.4. The precision of the method is ±3.18% of the acrylonitrile present in the 5–30 ppm range. The complex color is stable for at least 20 min after development.

The usefulness underlying the chemical analysis of acrylonitrile lies in the fact that it is widely used in the synthetic rubber, fiber, and plastic industries. In the United States alone in 1976 over 1.5 billion pounds were produced (*1*). Sensitive and reliable analytical methods for acrylonitrile are necessary for economic and toxicological purposes. Acrylonitrile is known to be toxic when ingested, inhaled, or applied to the skin, and the U.S. Public Health Service has set the maximum allowable limit for the monomer in the air at 20 ppm (*2*). Recent studies by Du Pont have linked acrylonitrile to cancer in workers and steps are being taken by Du Pont to reduce exposure to workers to 2 ppm (*3*). Analytical procedures which have been used most for acrylonitrile are titrimetric (*4–6*), gas chromatographic (*7–9*), and polarographic (*10–13*). The titrimetric procedures are good for relatively high concentrations while the others can measure as little as 5 ppm in aqueous solutions. The few gas chromatographic procedures reported are sensitive but have been limited to nonaqueous systems. Polarographic methods

[1] Present address, Dow Chemical Company, P.O. Box 520, Magnolia, Ark. 72753.

are subject to many interferences and lack the necessary sensitivity at the ppm level.

It was found in this laboratory that acrylonitrile forms at elevated temperatures, a highly colored (yellow) complex in the presence of pyridine, hydroxyl ions, water, and sodium hypochlorite. This report describes a sensitive method developed for the quantitative determination of acrylonitrile in aqueous systems based on the yellow colored pyridine complex.

EXPERIMENTAL

Apparatus. The recorded spectra were obtained with a Bausch and Lomb SP 600 spectrophotometer in conjunction with a Sargent SRL recorder. Some single wavelength absorbances were made with the Bausch and Lomb 70 Manual spectrophotometer. Absorption cells were mainly 2.5-cm path length and in some work 1-cm cells were used. Ten-mL volumetric flasks were used for all sample solutions on which absorbances were measured.

Reagents. Pyridine, obtained from Fisher Scientific Company, was purified by distillation over potassium hydroxide. The first 12% and last 20% were discarded.

Lithium hydroxide, purified grade, was obtained from Fisher Scientific Company. Solutions were prepared in molar strengths as specified.

Sodium hypochlorite, brand name Purex Bleach, was obtained from a grocery store as a 6% solution in water.

Acrylonitrile, Chromatographic grade 99+ mol %, was obtained from Analabs Incorporated.

Preparation of Stock Solution of Acrylonitrile. Stock solutions of acrylonitrile were made by pipetting approximately 0.5 mL into a tared 100-mL volumetric flask containing 25 to 50 mL of distilled water, and reweighing to obtain the weight of acrylonitrile. In order to ensure the accuracy of weighing and the purity of the acrylonitrile, the titration method reported by R. P. Taubinger (*4*) was used to analyze the stock solutions.

Procedure. To a 10-mL volumetric flask, add 7.5 mL of pyridine, 1 mL of 0.05 N lithium hydroxide solution, and 0.1 mL of 0.6% solution of sodium hypochlorite. To this mixture add 1.0 mL of the unknown acrylonitrile solution and then dilute to volume with distilled water. Mix thoroughly, and place in a water bath at 65 °C for 10 min. After cooling, absorbance values were taken as the difference between absorbances at 411 and 500 nm. This technique of measuring absorbances was chosen so that it could be readily adapted to nonrecording spectrophotometers.

DISCUSSION AND RESULTS

Pyridine is known to react with several substances in the presence of base and hypochlorite to form highly colored complexes. The Fujiwara (*14*) reaction as reported by Fugg (*15*) is probably the best known. The Fujiwara reaction employs sodium hydroxide and pyridine in the determination of chlorinated hydrocarbons. A complex between the pyridine and the chlorinated hydrocarbons is formed which absorbs at a wavelength of 535 nm. The complex formed is not very well understood but the method is quite sensitive for some chlorinated hydrocarbons. The complex formed by acrylonitrile and pyridine under similar conditions described for chlorinated hydrocarbons absorbs at a much lower wavelength, 411 nm, and is probably quite different. The color forming complex with acrylonitrile is believed to be more similar to cyanogen chloride complexes formed with pyridine (*16*). Attempts were made to isolate the complex by extraction and column chromatography to establish its composition, but it became unstable when removed from the pyridine-water solution. The acrylonitrile complex absorbs at only a slightly higher wavelength than the cyanogen chloride complex shown below.

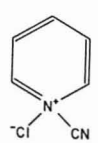

Table I. Effect of Concentration of Water on Absorbance

Sample	% H_2O	% Pyridine	Absorbance
1	20	80	0.32
2	25	75	0.35
3	30	70	0.31
4	40	60	0.19
5	50	50	0.09
6	60	40	0.04
7	70	30	0.03

Table II. Effect of Base Strength on Absorbance

Sample	Final LiOH concn, N	Absorbance
1	0.0025	0.517
2	0.0050	0.580
3	0.0100	0.527
4	0.0200	0.410
5	0.0250	0.370

Effect of Water Concentration. The solvent system for the acrylonitrile determination is a mixture of pyridine and water with pyridine being present in the greatest amount. The ratio of pyridine to water affects the amount of color forming species produced and this, of course, affects the sensitivity of the method. In order to achieve maximum sensitivity, the amount of water in the analysis mixture must be controlled.

Seven solutions were prepared where the pyridine–water ratio was varied, but the amounts of lithium hydroxide and sodium hypochlorite were held constant. The absorbance values were measured for these seven solutions and are listed in Table I. The data show that approximately 25% water in the reaction mixture gives maximum color formation.

Effect of Lithium Hydroxide Concentration. In order for the yellow color reaction to develop for acrylonitrile in the presence of pyridine, water, and sodium hypochlorite, the solution must be basic. Lithium hydroxide was chosen as the base because of its greater solubility in organic solvents than sodium hydroxide. The pyridine–water ratio was held constant at a 75–25 vol %, the hypochlorite was kept constant at 0.2%, and the amount of acrylonitrile was kept constant at 45 μg. One mL of base was added to each solution but the amount of base was varied by using LiOH solutions of different concentrations. At lithium hydroxide concentrations of 0.25 N and higher, the LiOH precipitated when added to the 75–25 pyridine–water solvent. All solutions were made up to a 10-mL volume just as described in the study of water effects. The results of the base concentration studies are given in Table II. These data indicate that a concentration of 0.005 N lithium hydroxide gives the maximum absorbance.

Effect of Sodium Hypochlorite Concentration. The formation of the yellow pyridine–acrylonitrile complex is more sensitive to the hypochlorite concentration than to the concentration of the other variables. In order to achieve maximum sensitivity, linearity, and reproducibility, the required amount of hypochlorite is very small and must be carefully controlled.

The hypochlorite studies were made on several solutions of different acrylonitrile concentrations since the amount of hypochlorite is so critical. The pyridine–water ratio and the amount of base were held constant. The acrylonitrile concentrations ranged from 48 down to 10 ppm. One-tenth mL of sodium hypochlorite solution was added to each test solution and the amount of hypochlorite was varied by using hypochlorite solutions of different strengths. The results of these tests are given in Table III.

Effect of Time and Temperature of Heating. Elevated temperatures were necessary to produce a colored complex,

Table III. Effect of Sodium Hypochlorite Concentration on Absorbance Values

Final concn of NaOCl x 100, %	48 ppm Absorbance $A_{411}-A_{500}$
1.00	1.36
0.85	1.35
0.75	1.41
0.66	1.28
0.60	1.22
	25 ppm
2.00	0.44
1.20	0.56
1.00	0.57
0.85	0.64
0.75	0.68
0.66	0.69
0.54	0.70
	20 ppm
2.00	0.36
1.20	0.47
1.00	0.52
0.85	0.54
0.75	0.60
0.66	0.59
0.54	0.61
	10 ppm
2.00	0.16
1.20	0.21
1.00	0.25
0.85	0.26
0.75	0.27
0.66	0.29
0.54	0.29

but if the temperature became too high, side reactions apparently developed. At temperatures of 75 to 80 °C, the products of the acrylonitrile pyridine complex broke down and the resulting red solution showed no linearity with concentration.

In order to study the effects of temperature, stock solutions were prepared as described earlier, then the samples were treated with the remaining reagents and heated in a water bath. The time of heating and temperature were carefully monitored and controlled.

It was found that heating at 60–65 °C developed the color quite satisfactorily and heating time from 5–10 min made very little difference in the absorbance value of 30 ppm acrylonitrile sample.

A more detailed study at 65 °C showed that over a concentration range of 0 to 25 ppm a heating time of 10 min gave the best reproducibility.

Time Stability of the Complex. Immediately after development of the complex as described, absorbances were monitored for a period of 20 min for samples containing 5 to 15.5 ppm acrylonitrile. Absorbance values remained constant over this time period.

Interferences. The following interferences were studied because these compounds, or similar types in small concentrations, are known to accompany pyridine and acrylonitrile in their manufacture.

Cyanide. The cyanide standard solution was prepared by dissolving 3.77 g of potassium cyanide into 500 mL of water to which 1 mL 1.0 N sodium hydroxide had been added. This solution was then diluted down to a concentration of 3 ppm cyanide ion.

The absorbance for a 3 ppm cyanide solution was 0.66 at 411 nm. The absorbance for a 3 ppm acrylonitrile solution was 0.087, thus the cyanide was 7.6 times as sensitive as acrylonitrile to this reaction. This means, of course, that cyanide ion is a serious interference and a separation procedure has to be found to eliminate cyanide interference if the latter is present.

Fortunately the interference of cyanide in solution is easily detected because of the characteristic green color which is formed on the addition of the sodium hypochlorite at room temperatures. Acrylonitrile does not react in these solutions at room temperature. This warning enables one to detect the presence of cyanide before any analysis is made for acrylonitrile. In the analytical procedure reported by Kroeller (*17*), he describes a method for the separation of cyanide from acrylonitrile samples using cotton wool and copper sulfate. This method may be used to remove cyanide from acrylonitrile samples.

Acetone. The acetone standard solutions were prepared in the same manner as the acrylonitrile standards. One-half mL of acetone was placed in approximately 50 mL of distilled water contained in a 100-mL volumetric flask which had been weighed. The resulting solution was then reweighed to ascertain the amount of acetone. The stock solution was diluted 500-fold to yield a standard solution of 10 ppm.

The test was then carried out as in the acrylonitrile determination. Acetone gave no indication of interference either at the 10 or 100 ppm level.

Ammonia. The ammonia standard solutions were prepared by dissolving 0.3141 g of ammonium chloride into 50 mL of water. This solution was then diluted to one hundred mL to yield a stock solution to 100 ppm in ammonia. This initial stock solution was then diluted ten fold to yield a 10 ppm stock solution.

After preparation of the stock solution the ammonia sample was tested in the same manner as acrylonitrile samples. The tests gave no indication of interference from ammonia either at the 10 or 100 ppm level.

Reproducibility and Statistics. Statistical calculations were made in accordance with the method of Smith and Mathews (*18*), assuming a constant percentage error in the data. According to this method, the percentage error instead of absolute error is assumed to be constant. In chemical analyses, the experimental conditions are generally controlled so as to make the percentage error a constant. In this case the sum of the weighted squares of the deviations from the least squares line is minimized. The standard deviation was found to be ±0.255, and is the fractional error along the calibration line. In terms of percent, the standard deviation is ±3.18. The lowest concentration of acrylonitrile measured in this work was 5 ppm using 2.5-cm cells. Obviously, by using 10-cm path length cells, a concentration approaching 1 ppm could be measured.

Molar Absorptivity. The molar absorptivity of the acrylonitrile–pyridine complex, based on the acrylonitrile concentration, was calculated to be 635.4.

Applications. Analysis of Acetonitrile. The method developed in this report was applied to the analysis of acetonitrile (Fisher Scientific Company) for its acrylonitrile content. A content of 250 ppm acrylonitrile was found. This compares favorably with 230 ppm found on the same sample by gas chromatographic techniques developed in this laboratory.

ACKNOWLEDGMENT

We appreciate the assistance of E. D. Smith in making the gas chromatographic analyses.

LITERATURE CITED

(1) *Chem. Eng. News*, **55** (18), 37 (1977).
(2) H. Brieger, W. A. Hodes, and F. Reiders, *Ind. Hyg. Occup. Med.*, **6** 128-140 (1952).

(3) *Chem. Eng. News*, **55** (21), 6 (1977).
(4) R. P. Taubinger, *Analyst* (London), **94**, 628–633 (1969).
(5) D. W. Beesing, W. P. Tyler, D. M. Kurtz, and S. A. Harrison, *Anal. Chem.*, **21**, 1073 (1949).
(6) M. Wronski, and E. Bald, *Chem. Anal. (Warsaw)*, **15**, 357–359 (1970).
(7) A. J. Gorerea, *Gas Chromatogr.*, **3**, 138 (1965).
(8) C. E. R. Jones, *Proc. Gas Chromatogr. Symp., 3rd, Edinburgh*, 501 (1960).
(9) H. Nestler and W. Berger, *Chem. Tech. (Berlin)*, **17**, 169 (1965).
(10) W. L. Bird, and C. H. Hale, *Anal. Chem.*, **24**, 586–587 (1952).
(11) S. I. Meklev, *Aferbneft Kohz.*, **6**, 33-34 (1968).
(12) I. G. Sevast and A. P. Tomilov, *Zavod. Lab.*, **32** 1210 (1966).
(13) D. Buckley and T. R. Crompton, *Analyst (London)*, **99**, 76 (1968).
(14) L. Fujiwara, *Sitzungsber. Abh. Naturforsch. Ges. Rostock*, **6**, 33 (1914).
(15) G. A. Fugg, *Anal. Chem.*, **36**, 1532 (1966).
(16) F. Feigl, "Spot Tests in Organic Analysis", Van Nostrand Company, Inc., Princeton, N.J. 1956, p 280.
(17) E. Kroeller, *Dtsche Lebensm-Rundsch.*, **66**, 11 (1970).
(18) E. D. Smith, and D. M. Mathews, *J. Chem. Educ.*, **44**, 757 (1967).

RECEIVED for review June 28, 1977. Accepted October 3, 1977.

Determination of Optimum Compromise Flame Conditions in Simultaneous Multielement Flame Spectrometry

D. F. Brost, B. Malloy, and K. W. Busch*

Department of Chemistry, Baylor University, Waco, Texas 76703

A composite response parameter, P_J, is developed for optimization of compromise excitation conditions in simultaneous multielement flame spectrometry. P_J is a direct measure of overall instrumental response for a particular multielement sample and is therefore sensitive to the detection powers and concentrations of each analyte species. Optimum compromise conditions are selected by simple maximization of the P_J response surface. The behavior of P_J is illustrated with experimental measurements made with a vidicon flame spectrometer on an ideal sample containing the spectrochemically divergent elements manganese and molybdenum. Practical application to several types of multielement samples is discussed on the basis of these measurements.

Simultaneous multielement analytical methods have played an important role in survey analyses where information on a large number of elements is desired. Traditionally, this role has been filled by such techniques as spark-source mass spectrometry, neutron activation analysis, wavelength dispersive x-ray fluorescence, and emission spectrometry. Recently, there has been an interest in extending the capability of traditionally single element methods, such as flame techniques, to include simultaneous multielement determinations (*1*, *2*).

One of the problems inherent in multielement flame spectrometry is the selection of the optimum compromise excitation conditions for the elements under consideration. Although several statistical methods could be applied to this problem, the simplest technique would involve some form of response surface analysis utilizing a single response parameter which directly measures the overall effectiveness of the instrument for the simultaneous multielement determination of all analytes in the sample. If such a composite parameter were available, simple maximization of the response surface would lead directly to the optimum compromise conditions without going through complex mathematical analysis of individual linear regression equations. This paper describes an effective joint response parameter, developed from probability considerations, as well as a simple method for its use in the optimization of excitation conditions for simultaneous multielement determinations by flame emission.

THEORY

The need for the determination of compromise excitation conditions in simultaneous multielement flame emission spectrometry arises from differences in the chemical and physical behavior of elements in the flame. Because of these differences, optimum detection power for some elements may be obtained by observing a volume element close to the burner top in a fuel-lean flame, while others may require observation higher in the same flame, or under more fuel-rich conditions. Since the simultaneous determination of all elements in a given sample is presently restricted to one set of conditions, a compromise must be found which provides adequate detection power for all analyte species.

The severity of the necessary compromise depends upon the spectrochemical behavior of the individual elements as well as their respective concentrations in the sample. If all the elements are present in concentrations far in excess of their poorest detection limits over the useful range of experimental conditions, the selection of a particular set of conditions is not critical for their determination. On the other hand, if two or more spectrochemically divergent elements are present in a sample in low concentrations, the selection of an appropriate compromise becomes very important.

The optimum excitation conditions for any element in flame emission spectrometry are those which yield the minimum possible detection limit. Under these conditions, the signal-to-noise ratio (S/N) is at a maximum for a given concentration, and the emitted intensity at the wavelength of interest is measured with the greatest possible precision. All that is needed, therefore, for optimization in single element determinations is the location of the minimum experimentally obtainable detection limit. For the case of multielement optimization, the problem becomes more complex.

In order for a response parameter to be useful for optimization of multielement systems, it must satisfy two criteria. First, the parameter must be a function of the detection power of the instrument for each element just as in the single element case. Second, it must be sensitive to the prevailing concentrations of the analyte species. The necessity of concentration dependence is a direct consequence of the basic need to compromise.

Consider a model sample containing two elements whose hypothetically divergent spectrochemical behaviors are shown in Figure 1 for various oxidant-to-fuel ratios (Ox/Fuel) at a constant observation height. The individual optimum for element X occurs at low values (fuel-rich), while that for element Y occurs at high values (fuel-lean). If element X is present in very high concentration in the sample (e.g., 100 ppm), its presence will easily be detected at any Ox/Fuel setting. If element Y is present at very low concentration (e.g.,

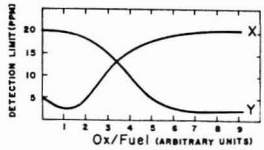

Figure 1. Hypothetical variation of detection limit with oxidant-to-fuel ratio at constant observation height for elements X and Y

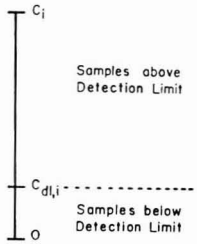

Figure 2. Line segment diagram for element i

5 ppm), it will only be detected at Ox/Fuel settings above six. Clearly, for elements X and Y to be determined simultaneously, the detection power of X will have to be sacrificed in order to observe *both* elements.

Before describing a multielement optimization parameter, it is necessary to analyze the single element case from a probability viewpoint. Consider the line segment diagram in Figure 2 for element i. The entire length of the line represents the total number of possible samples of different concentration which can occur within the sample space from 0 to C_i. The segment from $C_{dl,i}$ to C_i represents the total number of possible samples which are greater than or equal to the detection limit. In other words, element i will be "observed" only in those samples where the concentration is above $C_{dl,i}$. The probability of detecting the presence of element i in a random sample increases or decreases with the length of $\overline{C_{dl,i}C_i}$. The following response parameter can now be defined:

$$P_i = \frac{C_i - C_{dl,i}}{C_i}; P_i = 0 \text{ when } C_{dl,i} > C_i \qquad (1)$$

P_i is confined to values from 0 to 1 and represents the probability of observing element i in a randomly selected sample, if all concentrations are equiprobable.

As a single element response parameter, P_i is a maximum when $C_{dl,i}$ has its lowest value. Since this condition corresponds to the best possible reproducibility of measurement, the maximum in the P_i surface, computed from detection limit measurements at each set of excitation conditions, represents the optimum conditions for the determination of element i.

For a sample containing n elements, the joint probability of observing all the analyte species simultaneously in a random sample can be computed from

$$P_J = \prod_{i=1}^{n} P_i \qquad (2)$$

where P_J at a given set of conditions is the product of the individual response functions, P_i, computed from detection limit measurements at the same set of conditions.

Analysis of Equation 2 reveals that the joint probability of observation, P_J, fulfills all the requirements of a multielement response parameter as discussed above. That is, P_J is calculated from the individual detection limits of the elements in the sample and from an appropriate estimate of their respective concentrations. A joint response surface for any multielement sample can thus be constructed by simply computing P_J for several combinations of Ox/Fuel and observation height. The maximum in this surface will correspond to that set of conditions giving the greatest possible compromise detection power for all elements in the sample.

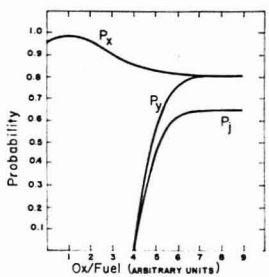

Figure 3. Response parameter curves for elements X and Y

Table I. Experimental Facilities

External optics	5-cm UV-grade fused silica lens with 10-cm focal length, Oriel Corp.
Burner	Varian Techtron 5-cm slot burner for nitrous oxide–acetylene
Monochromator	Spex, Model 1870, 0.5-cm Czerny-Turner spectrograph, *f*/6.9, with 1200 grooves/mm grating blazed for 300 nm. Reciprocal linear dispersion 1.6 nm/mm in the first order
Detector	Model 1205D silicon intensified target detector head, Princeton Applied Research Corp.
Optical multichannel analyzer	Model 1205A, Princeton Applied Research Corp.
Readout	Tektronix oscilloscope, 604 Monitor
Flow meters	Brooks Full-View rotameters calibrated for nitrous oxide and acetylene, Brooks Instrument Division

The degree to which a given element influences the location of the optimum depends upon the proximity of its expected sample concentration, C_i, to its detection limit, $C_{dl,i}$. Consider again the model binary system depicted in Figure 1. The response parameter curves P_X and P_Y, computed from these detection limits, are shown in Figure 3 for a sample where C_X = 100 ppm and C_Y = 10 ppm. P_J is also shown. Since C_X is much greater than $C_{dl,X}$ at every Ox/Fuel setting, P_X remains relatively constant and at high values. On the other hand, C_Y is either close to or less than $C_{dl,Y}$. Because of this P_Y is quite sensitive to Ox/Fuel and therefore is the determining factor in the shape and maximum of P_J.

The practical use of P_J for flame emission will be discussed on the basis of experimental measurements on the spectrochemically divergent elements manganese and molybdenum.

EXPERIMENTAL

Apparatus and Experimental Conditions. The vidicon flame spectrometer used in this study was similar to that described previously (*3–5*). Details of the operation of this system can be found in the cited references. A description of the spectrometer components can be found in Table I.

This investigation requires the determination of reproducible detection limits which are functions only of the oxidant-to-fuel ratio and the flame volume element observed by the optical system. In order to accomplish this, the other instrumental variables were held constant at settings which were known to be compatible with good general sensitivity.

The monochromator was adjusted so that the wavelength range between 390 and 410 nm was focused on the detector faceplate.

Table II. Experimental Flame Conditions

Flow rates (L/min)		Molar oxidant-to-fuel ratio
N_2O	C_2H_2	
9.5	5.3	1.8
9.5	5.7	1.7
9.5	6.0	1.6
9.5	6.5	1.5

The lens and burner assembly were positioned to produce a 1:1 image of the flame on the entrance slit. The slit was set at 5 μm and the height was maintained at 2 mm. A neutral density filter with an absorbance of 0.3 was placed in front of the entrance slit. This filter, in combination with the slit dimensions, provided a light level such that 500 frame scans could be accumulated over the entire range of measurement conditions without exceeding the capacity of the optical multichannel analyzer memory.

A premixed nitrous oxide–acetylene flame was used in this investigation. The flame conditions were altered by varying the fuel flow while maintaining the oxidant flow at 9.5 L/min. Table II gives the fuel and oxidant flow rates as well as the molar oxidant-to-fuel ratios, ρ, for the various flame conditions employed. A stoichiometric nitrous oxide–acetylene flame has a ρ value of 3.0 (*6*). The oxidant flow produced a constant solution aspiration rate of 5.4 mL/min.

Determination of Detection Limits. *Signal-to-Noise Ratios.* S/N vs. concentration curves were constructed for manganese and molybdenum at each combination of observation height and oxidant-to-fuel ratio from the background-corrected spectra of two single-element standard solutions. Each spectrum was obtained as follows. A blank spectrum was collected by nebulizing a distilled water blank containing 1000 ppm Cs into the flame for 500 accumulation cycles and storing the resulting spectrum in memory B. The sample spectrum was similarly obtained and stored in memory A using a simple aqueous standard solution of the element in question which also contained 1000 ppm Cs as an ionization buffer. The background-corrected spectrum was observed using the A minus B mode of the optical multichannel analyzer.

The signal-to-noise ratio in a given spectrum was determined from the number of counts accumulated in the channel corresponding to the peak of the spectral line, and the counts in the ten adjacent channels on either side of the spectral line. The average of the counts in the 20 background channels was taken and subtracted from the counts at the line peak to yield the signal. The rms noise was taken as the standard deviation of the counts in the background channels.

Concentrations were chosen which yielded a maximum S/N of 25 at each set of measurement conditions for each element investigated. This resulted in greater reproducibility when extrapolating the curve back to the detection limit. In order to ensure linearity of the standard curve, the intercept on the S/N axis was monitored. Concentrations were taken as acceptable when the intercept was within ±1 S/N unit of the origin.

Detection Limits. The best linear relationship passing through the origin of the S/N vs. concentration plot was determined by using a slope averaging procedure. The detection limit was obtained from this line and was taken as the concentration corresponding to a S/N of 2. Each detection limit was determined in this manner a minimum of 5 times for each set of measurement conditions.

RESULTS AND DISCUSSION

Experimentally determined detection limits for manganese and molybdenum are shown in Table III. Single element response parameter values, P_{Mn} and P_{Mo}, were calculated using Equation 1 for several arbitrary concentrations which may be encountered in an analytical sample solution. P_{Mn} for manganese concentrations of 0.03 and 1.0 ppm and P_{Mo} for molybdenum concentrations of 0.5 and 10 ppm are given in Table IV.

Examination of the individual detection limit surfaces (Table III), reveals that maximum detection power occurs at different sets of conditions for the two elements. Manganese response is best in a fuel-lean flame (ρ = 1.80–1.70) at observation heights between 5 and 10 mm. Optimum conditions for molybdenum occur in a fuel-rich flame (ρ = 1.60–1.50) at approximately the same range of observation heights. As has been previously indicated, this behavior is reflected in P_{Mn} and P_{Mo} (Table IV) for all the chosen sample concentrations.

The response toward both elements changes slowly and evenly as conditions are varied about the individual optima. Also, as is indicated in Table IV, each point on the response surfaces has its own degree of uncertainty arising from the uncertainties in the corresponding detection limit measurements. For these reasons, it is more realistic to simply locate the *region* of optimum joint response than to attempt to identify a single set of conditions which represents a statistically unique optimum.

Joint response surfaces are shown in Table V for three combinations of P_{Mn} and P_{Mo}. The uncertainties shown represent the most probable error in P_J computed from the precision indices of P_{Mn} and P_{Mo}. These results clearly demonstrate the response of P_J to samples of varying composition. When C_{Mn} is low and C_{Mo} is high in relation to their respective detection limits (Table Va), optimum compromise conditions are located in the region of maximum detection power for manganese. Likewise, when only molybdenum is present in critically low concentration (Table Vb), P_J indicates optimum conditions which overwhelmingly favor molybdenum response. In a sample which contains both elements in low amounts (Table Vc), the maximum in P_J moves toward conditions which partially sacrifice the individual detection powers of each in order to indicate the best compromise for the determination of the multielement system.

Table III. Manganese and Molybdenum Detection Limits

	Observation height (mm above burner top)			
ρ	5	10	15	20
	Mn detection limit surface			
1.50	0.06 ± 0.01[a,b]	0.06 ± 0.01	0.06 ± 0.01	0.05 ± 0.01
1.60	0.027 ± 0.005	0.022 ± 0.006	0.024 ± 0.005	0.028 ± 0.003
1.70	0.012 ± 0.002	0.016 ± 0.002	0.021 ± 0.003	0.027 ± 0.005
1.80	0.010 ± 0.002	0.016 ± 0.003	0.020 ± 0.003	0.029 ± 0.003
	Mo detection limit surface			
1.50	0.12 ± 0.02	0.09 ± 0.02	0.13 ± 0.04	0.20 ± 0.01
1.60	0.11 ± 0.03	0.12 ± 0.03	0.3 ± 0.1	1.1 ± 0.2
1.70	0.18 ± 0.04	0.35 ± 0.07	2.7 ± 0.3	13 ± 3
1.80	0.53 ± 0.06	3 ± 1	14 ± 2	39 ± 6

[a] All uncertainties are represented as the standard deviation of the mean of replicate measurements at the 95% confidence level. [b] All detection limits are in parts per million.

Table IV. Single Element Response Parameter Values

ρ	Observation height (mm above burner) 5	10	15	20
	Mn response surface for C_{Mn} = 0.03 ppm			
1.50	0	0	0	0
1.60	0.10 ± 0.17[a]	0.27 ± 0.20	0.20 ± 0.17	0.07 ± 0.10
1.70	0.60 ± 0.07	0.47 ± 0.07	0.30 ± 0.10	0.10 ± 0.17
1.80	0.67 ± 0.07	0.47 ± 0.10	0.33 ± 0.10	0.03 ± 0.10
	Mn response surface for C_{Mn} = 1.0 ppm			
1.50	0.94 ± 0.01	0.94 ± 0.01	0.94 ± 0.01	0.95 ± 0.01
1.60	0.973 ± 0.005	0.978 ± 0.006	0.976 ± 0.005	0.972 ± 0.003
1.70	0.988 ± 0.002	0.984 ± 0.002	0.979 ± 0.003	0.973 ± 0.005
1.80	0.990 ± 0.002	0.984 ± 0.003	0.980 ± 0.003	0.971 ± 0.003
	Mo response surface for C_{Mo} = 0.5 ppm			
1.50	0.76 ± 0.04	0.82 ± 0.04	0.74 ± 0.08	0.60 ± 0.02
1.60	0.78 ± 0.06	0.76 ± 0.06	0.40 ± 0.20	0
1.70	0.64 ± 0.08	0.30 ± 0.14	0	0
1.80	0	0	0	0
	Mo response surface for C_{Mo} = 10.0 ppm			
1.50	0.988 ± 0.002	0.991 ± 0.002	0.987 ± 0.004	0.980 ± 0.001
1.60	0.989 ± 0.003	0.988 ± 0.003	0.97 ± 0.01	0.89 ± 0.02
1.70	0.982 ± 0.004	0.965 ± 0.007	0.73 ± 0.03	0
1.80	0.947 ± 0.006	0.70 ± 0.10	0	0

[a] All uncertainties are represented as the standard deviation of the mean at the 95% confidence level.

Table V. Multielement Response Parameter Values

ρ	Observation height (mm above burner) 5	10	15	20
	A. Response surface for C_{Mn} = 0.03 ppm and C_{Mo} = 10 ppm			
1.50	0	0	0	0
1.60	0.10 ± 0.17[a]	0.26 ± 0.20	0.19 ± 0.16	0.06 ± 0.09
1.70	0.59 ± 0.07	0.45 ± 0.06	0.22 ± 0.07	0
1.80	0.63 ± 0.07	0.33 ± 0.08	0	0
	B. Response surface for C_{Mn} = 1.0 ppm and C_{Mo} = 0.5 ppm			
1.50	0.71 ± 0.04	0.77 ± 0.04	0.70 ± 0.08	0.57 ± 0.02
1.60	0.76 ± 0.06	0.74 ± 0.06	0.39 ± 0.20	0
1.70	0.63 ± 0.08	0.30 ± 0.14	0	0
1.80	0	0	0	0
	C. Response surface for C_{Mn} = 0.03 ppm and C_{Mo} = 0.5 ppm			
1.50	0	0	0	0
1.60	0.08 ± 0.13	0.20 ± 0.15	0.08 ± 0.08	0
1.70	0.38 ± 0.06	0.14 ± 0.07	0	0
1.80	0	0	0	0

[a] $\sigma_{P_J} = [(\sigma_{P_{Mn}}/P_{Mn})^2 + (\sigma_{P_{Mo}}/P_{Mo})^2]^{1/2} P_J$

Interferences. In order to correctly apply Equations 1 and 2 to locate the optimum compromise conditions for the simultaneous determination of a particular set of elements, care must be taken in the determination of the detection limits. It is well known that many general and specific interferences may be present in a sample which could alter instrumental response toward one or more of the analyte species. For this reason, the optimum obtained by maximizing P_J is valid only if the detection limits are measured in the presence of the sample interferences. This, however, does not present a significant problem, since the primary requirement of a multielement analysis is the capability of preparing multielement standards which mimic the behavior of all analytes in the sample. These standards can then be used to determine the detection power of the instrument for each element. Thus the location of the correct optimum compromise conditions by the joint probability of observation and the accurate determination of analyte concentrations in the final analysis are dependent upon the same basic capability.

Selection of C_i. As has previously been discussed, the determination of the optimum compromise conditions via P_J requires that an estimate of each analyte concentration, C_i, be available. The closer these estimates are to the actual case, the more accurate will be the selected optimum.

There are several practical approaches to the selection of C_i and each has its own degree of complexity and reliability. First, if typical concentration ranges are available for samples of a given type and origin, the central value in the range for each element can be used as its C_i. Since no measurements are required, this method is by far the simplest, and can be sufficiently accurate when the expected concentration ranges are narrow. Serious error may result in the determination of P_J if actual analyte concentrations are at the extremes of a wide range for one or more elements. Second, a rough survey determination of the elements in a given sample could be carried out by any analytical technique, and the results used as C_i. Although this approach is more time-consuming, the results are usually more reliable than the above technique, even if the analysis is accurate to only 10–20%. Finally, if enough sample is available, the sample dilution method as discussed below can be employed to eliminate C_i from Equation 1.

Sample Dilution Technique for Relative Detection Limit Determination. As stated above, C_i represents an analyte concentration in the actual sample solution. If this solution (where C_i is assumed to be on the linear portion of the calibration curve) is serially diluted, and S/N measurements are made at each dilution, a curve of S/N vs. the fraction of C_i can be constructed. As indicated in Figure 4, point A represents the fraction of the original concentration which yields a S/N of 2. At this point, the element in question is present in the sample at its detection limit. Mathematically,

$$C_{dl,i} = AC_i \tag{3}$$

where A is the factor by which C_i must be diluted to give $C_{dl,i}$.

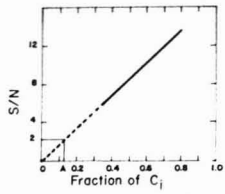

Figure 4. Signal-to-noise ratio vs. fraction of C_i

Combination of Equations 1 and 3 leads to the following relation,

$$P_i = 1 - A \tag{4}$$

The individual response parameters for each analyte can therefore be accurately computed without knowing their respective absolute concentrations.

In addition to eliminating all possible errors arising from inaccurate selection of C_i, the sample dilution technique offers the distinct advantage of interference compensation. That is, the relative detection limit of an analyte will be determined in the presence of any general or specific interferences which might be unique to a particular sample. Although this can be accomplished using correctly prepared multielement standards as discussed above, the present approach circumvents the necessity of specifically identifying each interference for the purpose of optimization.

The major limitation to the general usefulness of this approach is obviously the relatively large sample requirement. For the sample and spectrometer used in this investigation, a single determination of the 20 point detection limit surfaces consumed approximately 80 mL when the S/N of both Mn and Mo were measured in two sample dilutions. This amount, however, represents the total aspirated volume of the dilutions employed, and does not indicate the amount of actual sample solution which would be consumed. The worst possible case would correspond to a situation where the undiluted sample solution is used for one set of S/N measurements. The dilution required for the next set of measurements determines the total amount of sample solution required. If half the original concentration is used, the total sample volume required would equal about 60 mL. Since S/N measurements for all elements are made simultaneously, the sample requirement remains constant regardless of the number of analytes considered.

Because of the sample volume limitation, optimum conditions for the determination of small samples which cannot be diluted without reducing analyte concentrations to undetectable levels, must be found using C_i's estimated by one of the alternatives discussed above. A large number of analytical samples do, however, easily satisfy the volume requirement of the sample dilution technique.

Practical Considerations. Several variables mediate the practical application of P_J to multielement optimization. Due consideration must be given to such factors as the presence or absence of interferences, the amount of available sample, the time allotted to optimization, and the degree of instrumental mechanization before a viable approach to a given problem can be decided upon.

Rigorous optimization, according to the methods discussed above, can be carried out if the requirements of sample size and optimization time are met. For a spectrometer like the one used here, which was not computer interfaced or mechanized in any way, a single determination of the 20 point detection limit surfaces would require about 1 day. The same is true for relative detection limit measurements by the sample dilution technique. Once these data are obtained, it is then a simple matter to compute P_J for the particular sample. If a computer-interfaced spectrometer were available, optimization of conditions for nearly any multielement sample could probably be accomplished in an afternoon.

Fortunately, the use of P_J provides an alternative to pure guesswork when one or more of the above mediating factors make rigorous optimization impractical. When sample size is small, time is short, or the presence or absence of interferences is impossible to determine, P_J can be approximated if detection limit surfaces were previously measured using simple aqueous solutions of the individual elements. If these surfaces were stored in a computer, as was done for manganese and molybdenum in this paper, P_J could be computed and maximized in a matter of minutes. For a sample containing no significant interferences, the optimum obtained by this method would be as accurate as the estimates of C_i. If unknown interferences were present, the maximum in P_J would still indicate a first approximation of the actual optimum conditions for the sample. Even though the accuracy of this ideal approach may be lacking for some samples, it is important to remember that only one determination of the detection limit surface for each element is necessary. These results can then be used again and again, no matter what combination of elements is under consideration, and may indeed provide the only possible route to the approximate optimum conditions for the determination of many critical samples.

ACKNOWLEDGMENT

The authors thank M. A. Busch for many helpful discussions.

LITERATURE CITED

(1) K. W. Busch and G. H. Morrison, *Anal. Chem.*, **45**, 712A (1973).
(2) J. D. Winefordner, J. J. Fitzgerald, and N. Omenetto, *Appl. Spectrosc.*, **29**, 369 (1975).
(3) K. W. Busch, N. G. Howell, and G. H. Morrison, *Anal. Chem.*, **46**, 575 (1974).
(4) K. W. Busch, N. G. Howell, and G. H. Morrison, *Anal. Chem.*, **46**, 1231 (1974).
(5) K. W. Busch, N. G. Howell, and G. H. Morrison, *Anal. Chem.*, **46**, 2074 (1974).
(6) J. O. Rasmuson, V. A. Fassel, and R. N. Kniseley, *Spectrochim. Acta, Part B*, **28**, 365 (1973).

RECEIVED for review January 26, 1977. Accepted October 3, 1977. This paper was presented at the November 1976 Pacific Conference on Chemistry and Spectroscopy in Phoenix, Ariz. Acknowledgment is made to the Donors of The Petroleum Research Fund, administered by the American Chemical Society, for partial support of this research. Acknowledgment is also made to the Robert A. Welch Foundation for partial support of this research.

Categorization of Papers by Trace Metal Content Using Atomic Absorption Spectrometric and Pattern Recognition Techniques

P. J. Simon,[1] B. C. Giessen, and T. R. Copeland*

Department of Chemistry and The Institute for Chemical Analysis, Applications, and Forensic Science, Northeastern University, Boston, Massachusetts 02115

Nineteen paper samples representing eleven different types of paper from seven manufacturers were analyzed for Cu, Mn, Sb, Cd, Cr, Co, Ag, Pb, Mg, and Fe using electrothermal atomization atomic absorption spectrometry. Unsupervised learning pattern recognition techniques were utilized for data analysis. Only six features were needed to identify 16 of 19 papers completely. The three not completely separated came from different manufacturing runs of the same type of paper. The five elements found to be most powerful in classifying papers were Cu, Mn, Sb, Cr, and Co. For Pb, high correlation with Mn, Cr, and Co was found. Mg, Fe, and Cd exhibited high intra-sheet scatter. The sixth feature used was density. These results indicate that papers can be characterized using trace metal data.

The identity and source of paper is quite important to the forensic scientist in judicial problems encountered in forgery, counterfeiting, and felonious use of certificates, securities, wills, etc. It is, therefore, important to be able to state conclusively whether an unknown paper sample does or does not come from a particular batch.

The primary source of trace metals in paper is contamination of the chemicals used as additives such as alumina, TiO_2, talc, clay, ZnO, and others (*1*, *2*). Trace metals may also originate in the wood pulp, process water, or process equipment. Characterization of papers has utilized colorimetric methods for certain metals (*3*), often in conjunction with paper or thin-layer chromatographic separation procedures. These techniques are time consuming and semiquantitative at best.

The potential for characterizing paper by neutron activation analysis has been shown by two independent laboratories (*2*, *4*). In one study (*2*) where 600 paper samples were investigated for 23 elements, it was found that certain elements such as Na, Mn, Ag, and Cu have a high frequency of occurrence whereas Ta, As, and Sb have a qualitative significance because of their low frequency of occurrence. These results indicated that papers were uniform in regards to their trace element concentration and papers from different manufacturers could be distinguished by qualitative and quantitative tests.

Barnard et al. (*5*, *6*) used the scanning electron microscope (SEM) for elemental analysis. The SEM x-ray microanalysis technique examined individual particles near the paper surface. Studies on the variation within a sheet and within a box were performed. Better results were obtained if the samples were ashed before examining them under the SEM. These results on 54 different samples for major elements seem to indicate that SEM data can be used for identification purposes. All elemental amounts determined are relative amounts and not absolute concentrations making these results difficult to compare directly to other techniques which give actual concentrations.

[1] Present address, Food and Drug Administration District Laboratory, 585 Commercial Street, Boston, Mass.

Previous work by Langmyhr et al. (*7*) using atomic absorption spectroscopy for the determination of Cu, Pb, Cd, and Mn suggested that papers could be identified by trace metal content determined by atomic absorption spectrometry using a graphite furnace. These results suggest that further work in atomic absorption spectrometry to determine the number of elements needed to identify papers is appropriate. Electrothermal atomization (nonflame) atomic absorption spectrometry requires minimal analysis time and therefore was used in this study. Using electrothermal atomization, wet digestion of the samples was unnecessary, the papers were ashed and analyzed directly. The 19 paper samples investigated represent 11 different types of paper and seven manufacturers and are all white bond or thesis paper including the same samples previously investigated using the SEM (*5*, *6*).

Data analysis was performed using pattern recognition which has been shown to be quite successful in solving various chemical problems (*8–11*). In fact, Duewer and Kowalski (*12*) used pattern recognition to identify papers from the data collected by neutron activation analysis (*4*) where separation was achieved by paper grade and by paper manufacturer using the concentrations of 10 elements.

EXPERIMENTAL

Standards and Reagents. All glassware was first cleaned in hot 1:1 (v/v) nitric acid:water for a period of at least 4 h. For subsequent use, glassware and polyethylene bottles were allowed to sit overnight in approximately 10% (v/v) nitric acid. All standard solutions were made with distilled deionized water. Acids were Baker Analyzed, Reagent grade. Standard stock solutions of 1 mg/mL concentrations were made using the respective metals (Alfa products) except for cobalt where anhydrous $CoCl_2$ (Alfa products) was used. Cu, Pb, Mn, Cd, Co, Ag, and Mg stock solutions were kept in approximately 1% HNO_3 and Sb, Cr, and Fe in 1% HCl. All solutions were stored in polyethylene bottles. Dilutions were made for each element the same day that they were used and were either 1% nitric acid or 1% hydrochloric acid.

Instrumentation. A Cahn electrobalance model No. 4100 was used for weighing all of the paper dots.

A Varian-Techtron Atomic Absorption Spectrophotometer Model AA-6 in conjunction with a carbon rod atomizer (CRA-63), a carbon cup, a background corrector, and a Varian Aerograph A-25 recorder was used exclusively in this work.

The CRA control module controlled the time and temperature for the dry, ash, and atomize cycles. When analyzing any particular element, the voltages for the three cycles were kept constant but the times for the dry and ash cycle varied (i.e., a longer dry cycle for solutions and a longer ash for the papers). The atomization time and temperature were kept constant for both samples and standards. A hydrogen continuum lamp was used for the background correction spectral source. For the wavelengths selected for manganese (403.2 nm) and chromium (357.9 nm), the hydrogen continuum lamp output is quite weak and, consequently, was not used. However, it was found that scattering or nonspecific absorption was not a major factor for these elements.

Sample Preparation. Up to four sheets of paper were taken consecutively from each of 19 reams of paper. From each sheet, using a small paper punch, 150 small dots about 3 mm in diameter were punched out and placed in a small plastic tray. Care was

Table I. AA Instrumental Parameters

Element	Wavelength, nm	Lamp current, mA	Spectral band pass, nm	Photomultiplier voltage, V	Ash temperature (°C)/time (s)
Cu	328.4	2.5	0.5	380	1100/3
Pb	283.4	3.0	0.5	343	550/3
Mn	403.2	4.0	0.5	280	800/3
Sb	217.6	10.0	0.2	440	800/3
Cr	425.5	5.0	0.2	368	1100/3
Co	240.8	5.0	0.5	350	1100/3
Cd	228.7	2.5	0.5	306	550/2
Fe	248.3	5.0	0.2	500	1100/2.5
Mg	202.5	10.0	0.5	522	1100/3
Ag	328.1	2.5	0.5	253	550/3

taken to keep contamination of the papers to a minimum. The sheet being punched was held in the corners where no sample dots were taken for analysis. Also, the first ten dots from each sheet were discarded to eliminate any possibility of cross-contamination. To eliminate variations in moisture content for different types of paper, all paper dots were dried in a vacuum oven at 70 °C for at least 4 h. Samples were then placed in a desiccator. Each dot was weighed individually using a Cahn Balance. In order to eliminate moisture errors due to changes in humidity over the period of weighing, "standard" dots were weighed before and after each sample. It was found that, at most, the weight difference for the "standard" dots during weighing a sample (over a period of about 2 h) was generally 0.1–0.3 μg and over a complete day no more than 2 μg which is insignificant when compared to sample weights in the range of 0.3 to 0.6 mg. Sample dots were stored in small plastic trays with appropriate identification (sample, sheet, and tray). A 50-μg range was used for each tray. The sample weight used for a particular tray was the average weight of all the dots in the tray.

Because of the relatively high concentrations of iron and magnesium in papers, a digestive method was used. The same sheets that were used to obtain the other samples were torn into small squares (ca. 5 cm^2) using a piece of nitric acid cleaned glass and Teflon-coated tweezers. These papers were dried in the same manner as the dots, weighed on a Mettler type H-15 single pan balance, placed in porcelain crucibles and then into a muffle furnace at 260 °C overnight. Five mL of concentrated nitric acid were added, placed on a hot plate, and simmered on low to dryness. After cooling, 3 mL of concentrated nitric acid were added to the residues and the digests were brought to a volume of 25-mL with distilled, deionized water and stored in polyethylene bottles. Reagent blanks were also prepared following the same procedure.

Analytical Procedure. After instrument warmup and signal optimization, standards and samples were added directly to the graphite cup. The standards were pipetted into the cup using a 5-μL Eppendorf pipet and the papers were placed inside the cup using tweezers and a glass tamping rod to ensure uniform sample ashing. The time between injections was held constant (90 s) throughout a run.

Some of the instrument parameters used in this study are shown in Table I. The ash voltage and time were set high and long enough to eliminate any memory effects from the highest standard run. Five or more replicates were run for each element from each sheet of paper. The elemental concentration ranges are given in Table II.

RESULTS AND DISCUSSION

The data analysis was accomplished using ARTHUR, a program obtained from the Laboratory for Chemometrics at the University of Washington and modified for use on Northeastern's CDC Cyber 70. Unsupervised learning routines employing hierarchial clustering or Q mode clustering (HIER) and Zahn minimal spanning tree clustering (TREE) (*13, 14*) were used. For these clustering algorithms, each group of measurements made on a paper is represented as a point in *n*-dimensional space. TREE connects all the points by drawing a "tree" of minimum length in *n*-dimensional space. Clusters are groups of points whose intrapoint "distance" is significantly smaller than the distance to a neighboring cluster i.e., high density clusters of points (leaves) are (hopefully) widely separated on bare branches. HIER initially assumes each point (in this case each sheet of paper) is a separate cluster. An interpattern similarity matrix is then generated and the two points with the smallest similarity coefficient are identified. These two points (the most similar) are then represented as a single point (their center of gravity) and the similarity matrix is regenerated. The result is a dendogram where each point is connected to all others at some level of similarity (see Figure 1). The length of the interconnecting line is an indication of similarity. A length of 0.0 implies that the samples are identical, a length of 1.0 the least similar. A coefficient of <0.1 was arbitrarily used as the definition of a cluster in this work.

Table II. Elemental Concentration Ranges

Element	Range, μg/g
Cu	1.7–9
Pb	0.2–17
Mn	0.3–20
Sb	0.1–14
Cr	5–22
Co	0.01–0.36
Cd	0.001–0.020
Fe	4–158
Mg	0.5–520

Several supervised learning routines are also available in the ARTHUR package. These techniques were not used in the present analysis since they require a training set of papers and some a priori knowledge of which elements are good classifiers. For typical samples of forensic interest, such information is not available making the cluster analysis approach used here far more attractive.

Several of the elements determined in the papers were eliminated from the pattern recognition analysis. Fe and Mg exhibited high intrasheet variances regardless of the fact that these analyses were performed on much larger digested samples. Acid blanks carried through the same digestion procedure did not exhibit high variation in Fe or Mg concentration implying a nonuniform distribution of these elements in the papers and not contamination during digestion. Silver was found in only one paper at a level above 0.05 μg/g and was, therefore, omitted from the pattern recognition data set since it would have unduly biased the separation of that one paper. The relative standard deviations for the other elements determined are shown in Table III. These deviations indicate that the cadmium analyses were of little utility in separation of the papers. One ream of paper (19E) exhibited high relative standard deviations for Mn and Sb. These deviations are indicated by asterisks in Table III. Alternate sheets of paper from this ream exhibited relative standard deviations of less than 5% implying an interleaving of two batches of paper. Such interleaving is not uncommon in paper manufacture and periodic variations of major element concentrations in one ream of paper have been reported (*15*). All data analyses were performed using autoscaled data. Autoscaling transforms each old feature (concentration) into a new feature with a mean of 0.0 and a variance of 1.0 to eliminate undue bias of higher concentrations. Preliminary data analyses indicated high correlations between Pb content and the Mn, Co, and Cr concentrations. Subsequent computer trials confirmed that the Pb analyses could be eliminated from the data with no change in the clusters formed. Using the five remaining elemental concentrations (Co, Cr, Cu, Mn, Sb) as features for the pattern recognition routines, 12 paper samples were completely separated into individual clusters.

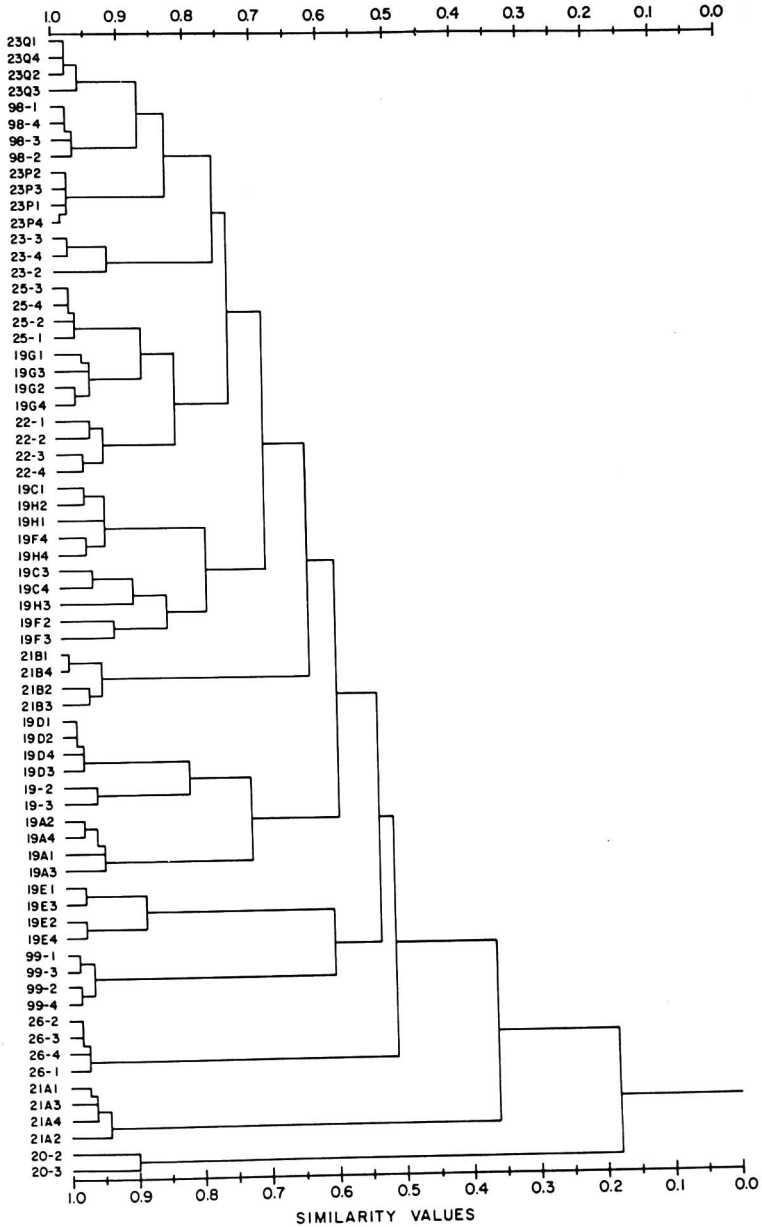

Figure 1. Dendogram of similarity matrix

Two other clusters each contained two paper samples and a final cluster (HIER) or group of three clusters (TREE) contained all the sheets from three different manufacturing batches of the same paper type. The pairing of two of the papers into one cluster was explicable—they were samples of the same paper, one being made from recycled stock, the other from nonrecycled stock. However, the other paired cluster contained a thesis bond paper and an onion skin typing paper.

Table III. Relative Standard Deviations %

Paper	Element Cu	Pb	Mn	Sb	Cr	Co	Cd
19	15	17	7	7	9	13	64
19A	5	14	7	20	9	11	68
19C	12	20	12	15	4	<d1	69
19D	5	21	6	6	ND	12	35
19E	8	19	24*[a]	29*	23	10	50
19F	16	23	20	<d1[b]	42	<d1	50
19G	7	21	5	11	8	13	61
19H	10	24	10	<d1	47	<d1	95
20	8	19	ND[c]	25	31	17	31
21A	3	16	10	<d1	17	4	62
21B	2	ND	10	27	23	24	40
22	8	29	7	18	28	30	32
23	4	9	16	54	25	<d1	43
23P	3	10	11	13	7	<d1	60
23Q	3	11	9	9	11	<d1	53
25	8	17	7	10	8	16	55
26	9	18	11	7	11	<d1	39
98	4	32	21	11	10	<d1	76
99	4	15	11	36	11	<d1	43
Pooled	7	19	11	18	19	15	85

[a] * see text. [b] <d1 = not detected. [c] N.D = not determined, concentrations above linear range.

This indicates that although the trace metal contents of the papers are extremely useful in separating and identifying different papers, use of only these data alone is not infallible. Other parameters such as physical appearance, rag content, major elemental concentrations, etc. are undoubtedly additional features in the pattern recognition routine. The most easily defined physical characteristic of the papers is their density (actually the weight of a $^1/_8$-inch diameter "dot"). This weight was added as a sixth feature in ARTHUR. HIER was successful in identifying 16 of the 19 papers using these six features. The dendogram shown in Figure 1 was generated using HIER and average values for the concentrations from 5 separate sets of 4 determinations for each sheet of paper. The numbers in the left column indicate the paper and sheet e.g. 23Q1 is paper sample 23Q sheet 1 of the 4 consecutive sheets analyzed Papers 19C, 19F, and 19H are from 3 different batches of the same paper and were not separated on the basis of the 6 parameters used. The major element concentrations of these papers are somewhat different (*15*) and may afford the ability to discriminate between batches, although of the 10 elements analyzed by SEM (*15*) only the Na, Al, and Ti concentrations are obviously different.

TREE was less powerful in separating the papers using the six features. Two papers (one recycled 23P and one not 23) remained unresolved as well as 3 clusters containing various sheets of 19C, 19F, and 19H. TREE has several user-defined parameters dealing with the number of edges allowed between patterns and the length of the "bare branches" between patterns. Although several combinations of these were tried, the recommended values allowing 3 edges and branches twice the size of a pattern edge afforded the best separation. This indicates that the hierarchial clustering technique is more powerful than the minimal spanning (TREE) algorithm in its ability to identify the papers. HIER also requires approximately 33% more computer time. The dendogram in Figure 1 required 27 seconds execution time.

These results indicate that a relatively small number of trace elements may be used to classify papers. Combining these data with physical evidence such as rag content, density, color, etc. may afford a rapid method of paper identification. Some of these data used in conjunction with major element concentrations may also prove a powerful classification procedure. For example, this study found Co, Cr, Cu, Mn, and Sb the most powerful features. Duewer and Kowalski (*12*) found Al, Cl, Ti, Cr, and Sb most powerful. Thus, their data are in agreement with the present study insofar as both found the trace elements Cr and Sb to be significant. In addition, the papers which were inseparable using the trace element data (19C, F, and H) have significantly different Al and Ti concentrations (*15*).

Combining data from this study with SEM data as one pattern recognition data set would be of little utility since the probability of isolating each sheet of paper as a separate category is high (*12*).

LITERATURE CITED

(1) B. L. Browning, "Analysis of Paper", Marcel Dekker, New York, N.Y. 1969, pp 122, 178–184, 199, 202–209, 319–326.
(2) R. L. Brunelle, W. O. Washington, C. M. Hoffman, and M. J. Pro, *J. Assoc. Offic. Anal. Chem.*, **54**, 920 (1971).
(3) E. Martin, "An Analytical Technique for Determining the Origin of Unidentified Paper in Methods of Forensic Science", Vol. 11, F. Lundquist, Ed., Interscience, New York, N.Y., 1963, pp 1–33.
(4) H. R. Lukens, H. L. Schlesinger, D. M. Settle, and V. P. Guinn, "Forensic Neutron Activation Analysis of Paper", USAEC GA-10113, 1970.
(5) J. A. W. Barnard, D. E. Polk, and B. C. Giessen, "Forensic Identification of Papers by Elemental Analysis Using Scanning Electron Microscope", Paper presented at the Workshop on Scanning Electron Microscopy and the Law, IIT Research Institute, Chicago, Ill., April 1975.
(6) B. C. Giessen, D. E. Polk, and J. A. W. Barnard, "The Applications of Material Science Methods to Forensic Problems: Principles, Serial Number Recovery and Paper Identification", in "Education and Scientific Progress in Forensic Science", G. Davies, Ed., ACS Symposium Series, 1975.
(7) F. J. Langmyhr, Y. Thomassen, and A. Massoumi, *Anal. Chim. Acta*, **68**, 305 (1974).
(8) P. C. Jurs, B. R. Kowalski, and T. I. Isenhour, *Anal. Chem.*, **41**, 1949 (1969).
(9) B. R. Kowalski, T. F. Schatzki, and F. H. Stross, *Anal. Chem.*, **44**, 2176 (1972).
(10) D. D. Tunnicliff and P. A. Wadsworth, *Anal. Chem.*, **45**, 12 (1973).
(11) J. Schechter and P. C. Jurs, *Appl. Spectrosc.*, **27**, 30 (1973).
(12) D. L. Duewer and B. R. Kowalski, *Anal. Chem.*, **47**, 526 (1975).
(13) B. R. Kowalski, *Anal. Chem.*, **47**, 1152A (1975).
(14) D. L. Duewer, J. R. Koskinene, and B. R. Kowalski, ARTHUR, available from B. R. Kowalski, Department of Chemistry, BG-10, University of Washington, Seattle, Wash., 98195.
(15) D. E. Polk, A. E. Attard, and B. C. Giessen, *J. Forensic Sci.*, **22**, 524 (1977).

RECEIVED for review August 3, 1977. Accepted September 22, 1977. The authors gratefully acknowledge the Dreyfus Foundation and the Law Enforcement Assistance Administration for partial support of this work.

Flameless Atomic Absorption Spectrometric Determination of Ultratrace Elements in Silicon Tetrachloride

T. Y. Kometani

Bell Laboratories, 600 Mountain Avenue, Murray Hill, New Jersey 07974

Nanogram per gram levels of Fe, Ni, Cr, Cu, Co, Mn, and Zn in silicon tetrachloride ($SiCl_4$) have been determined quantitatively by flameless atomic absorption spectrometry with a carbon rod atomizer (CRA). Various procedures for preparing samples prior to analysis and for preventing contamination errors are described in detail. The most effective sampling procedure was evaporation of $SiCl_4$ at low temperature and dissolution of the residue in high purity hydrofluoric acid. Losses of trace elements and interferences from inter-elemental or chemical effects in the CRA were negligible. The precisions and accuracies of the method for the seven metals based on the analysis of a silica standard, ranged from ±1.4 to ±13% and ±4.5 to ±18%, respectively.

Ultratrace concentrations of certain transition elements cause unacceptable attenuation of light transmitted through optical glass fibers. Nevertheless, fibers virtually free of absorption losses have been fabricated by introducing modified chemical vapor deposition (MCVD) techniques (*1*). With this method low-loss fibers are now produced routinely using commercially available reagents, particularly silicon tetrachloride ($SiCl_4$). Although monitoring the initial purity of MCVD reagents is not critical for production of acceptable fibers, suitable analytical techniques are required to determine whether impurities are causitive factors for the periodic production of high-loss fibers and to determine the maximum impurity levels that can be tolerated without noticeable optical effects. A procedure has been described previously for the semiquantitative emission spectrometric analysis of $SiCl_4$ (*2*). However, quantitative methods are needed to evaluate the effects mentioned above. The high sensitivity of flameless atomic absorption methods (10 to 100 times more sensitive than conventional flame atomic absorption methods) permits the quantitative determination of ng/g concentrations of metals in solution. This paper describes methods in which a carbon rod atomizer (CRA) is used for the atomic absorption spectrometric determination of Fe, Cu, Ni, Co, Cr, Mn, and Zn. Reliable quantitative data have been obtained by carefully controlling conditions to minimize contamination and interference effects.

EXPERIMENTAL

Apparatus. The atomic absorption spectrometer consisted of a Jarrell-Ash 0.5-m monochromator with Varian-Techtron IM-6 amplifier-readout and power supply. A Varian-Techtron Model 63 carbon rod atomizer with pyrolytic graphite coated tubes was used. The life of the tubes was about 100 firings for HF solutions. A Varian-Techtron BC-6 background corrector accessory was used to check for nonspecific absorption. Absorbance peaks were recorded in the peak-read mode in order to avoid errors due to pen lag. An exhaust fan was attached to the rear of the CRA power supply chassis to avoid overheating. Five microliters (μL) of sample solution were injected into the graphite tube with an Excaliber pipet equipped with plastic tips supplied by Varian-Techtron. Instrumental conditions for each element are given in Table I.

The choice of voltage/time settings for the dry, ash and atomize stages was dictated by several considerations.

1. During the dry stage the furnace was maintained at ~90 °C for a sufficient time interval to completely evaporate the solvent.
2. Ashing was unnecessary in the absence of an organic matrix. However, the ash stage was used to heat the furnace (600 °C) prior to the atomize stage.
3. Conditions for the atomize stage were chosen so that maximum sensitivity was obtained while completely volatilizing the analyte with a single power sequence.

Contamination Control. Because of the low concentration of element being determined (1–500 ng/g), it was necessary to take precautions to minimize contamination errors during all phases of the analysis. Procedures for preventing contamination from labware, reagents, and atmospheric fallout are described below.

Disposable polystyrene serological pipets from Falcon were used for volumetric measurements. Sample solutions were prepared in Teflon beakers. Since polystyrene is attacked by $SiCl_4$, glass pipets were used for measuring and transferring the sample. All labware was cleaned thoroughly by alternate leachings in hot HCl (1:1) and hot HNO_3 (1:1) followed by a thorough distilled water rinse. The plastic injection pipettor tip was a serious source of Fe contamination. HF was found to be more effective then HCl and HNO_3 in removing Fe from the plastic tips. Tips were cleaned prior to each use by repeatedly drawing in and expelling concentrated HF followed by rinsing with distilled water. Precleaning in this manner allowed each tip to be reused many times without introducing contamination. Aqueous sample solutions were prepared in Teflon beakers and stored in a covered container. Standard solutions were prepared and stored in 15-mL capped polystyrene vials.

Acids were purified by double sub-boiling distillation. All rinses and dilutions were made with water purified by demineralization followed by double distillation in a quartz still. The concentration of impurities in acids and water determined by direct injection into the CRA was <1 ng/mL with respect to each metal of interest.

In order to minimize errors due to particulate fallout, sample and standard solutions were prepared in a class 10 laminar-flow exhaust hood located within a class 1000 clean room (*3*). The absorption measurements were made in a conventional laboratory. The fall-out contamination on the graphite tube was negligible for the duration of the cycle time between injections, which was about 1 min.

Overall contamination blanks due to labware, reagents, and fall-out were determined by analyzing 1.0 mL of HF/H_2O (1:4) solution which was added to 5-mL Teflon beakers and treated in the same manner as samples. These blanks, which ranged from 0.4 ng/mL for Zn to 5 ng/mL for Co, were used to correct for contamination during analysis.

Procedure. Add 2.0 mL of $SiCl_4$ to a 5-mL Teflon beaker on a hot plate (~50 °C) and evaporate to dryness with the aid of an infrared heat lamp. Using a 1-mL graduated plastic pipet, add 0.2 mL HF and slowly rotate the beaker until all residue is dissolved. Dilute to 1.0 mL by adding 0.8 mL of H_2O and reserve for measurement. Prepare standard metal solutions containing 0, 10, 50, and 100 ng/mL cation in HF/H_2O (1:4). Prepare blanks for both standard and sample solutions. Blanks for sample and standard solutions are not equivalent since different conditions are used during their preparation. Inject 5.0 μL of solution into the carbon rod atomizer and record peak absorbance without scale expansion. Average the absorbance of at least two injections for

Table I. Instrumental Conditions for Atomic Absorption Analysis by CRA

	Fe	Ni	Mn	Co	Cr	Cu	Zn
Lamp current, mA	5	5	5	5	5	5	3
Wavelength, nm	248.3	232.0	279.5	240.7	357.9	324.7	213.9
Spectral slit, nm	0.2	0.2	0.2	0.2	0.2	0.2	0.2
N_2, L/min	5.5	5.5	5.5	5.5	5.5	5.5	5.5
Dry[a], 10 s	8.0	8.0	8.0	8.0	8.0	8.0	8.0
Ash[a] 5 s	7.5	7.5	7.5	7.5	7.5	7.5	7.5
Atomize[a] 3 s	8	8	7.0	7.0	7.0	7.0	7.0

[a] Arbitrary dial settings on the M-63 power supply.

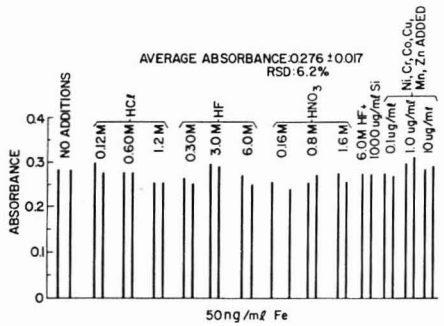

Figure 1. Effect of acids and cations on absorption of 50 ng/mL Fe solution

each solution. Subtract the appropriate blank absorbance from each standard and sample absorbance and prepare a calibration curve. Read the concentration of the metal from the curve and calculate the ng/g metal in $SiCl_4$ with the formula:

$$\text{ng/g} = \frac{AB}{C}$$

where A = concentration of metal in sample solution, ng/mL; B = concentration factor, 1/2; and C = density of $SiCl_4$, 1.5 g/mL.

RESULTS AND DISCUSSIONS

$SiCl_4$ is highly volatile at 25 °C and reacts exothermally with water to produce silicic acid and HCl. Thus, special sampling and analytical procedures were necessary to prevent possible losses by volatilization of metal chlorides during sample treatment. It was also necessary to systematically investigate interference effects due to the acid matrix and metal ions.

Interferences. The effect of various acids and matrix components, which may be present after sample preparation, on absorbance was investigated. The absorbance peaks of 50 ng/mL Fe in the presence of different concentrations of HF, HCl, HNO_3, Si, and metal ions are shown in Figure 1. The close agreement of the absorbance values (relative standard deviation of 6.2%) indicates that interference effects were negligible. Similarly, studies of Ni, Cr, Co, Cu, Mn, and Zn (summarized in Table II) indicate that interelemental and chemical effects were negligible for each cation. Nonspecific absorption due to light scattering and/or molecular absorption was not observed in these solutions.

Precision and Accuracy. A linear calibration curve was obtained for Fe standards in HF/H_2O (1:4) using the average of 10 replicate absorbance measurements for each standard. The RSD for absorbance varied from 11% for the 10 ng/mL Fe solution to 4.4% for the 100 ng/mL Fe solution. Similar results were obtained for other cations examined. The precision of results was found to be dependent primarily on the analyst's ability to deposit a measured volume of solution at the same position in the graphite tube for each heating cycle.

Table II. Effect of Metals and Acids on Absorbance of 50 ng/mL Metal Solutions

	Mean absorbance[a]	Std dev	Rel std dev, %
Ni	0.079	± 0.004	5.3
Cr	0.016	± 0.008	7.4
Cu	0.120	± 0.006	5.3
Co	0.110	± 0.004	4.1
Mn	0.55	± 0.04	7.3
Zn	0.76	± 0.06	7.9

[a] Mean absorbance of 5 solutions containing (1) no additions; (2) 1.2 M HCl; (3) 3.0 M HF; (4) 1.6 M HNO_3; (5) 3.0 M HF and 10 μg/mL of the six alternate cations.

Table III. CRA Analysis of NBS SRM 57 Refined Silicon in Triplicate

	Weight % CRA	Weight % NBS value	Precision, RSD %	Accuracy, %
Fe	0.71 ± 0.03	0.65	4.2	9.2
Mn	0.029 ± 0.002	0.034	6.9	19
Cr	0.027 ± 0.001	0.024	3.7	12
Cu	0.015 ± 0.001	0.02	6.7	21
Zn	0.0089 ± 0.00003	...		
Ni	0.00130 ± 0.00002	0.002	15	35
Co	0.00050 ± 0.00001	...		

The reliability of the CRA technique was assessed by determining the precision and accuracy on analyses of standard materials. National Bureau of Standards SRM 57, refined silicon, and a homogeneously doped silica prepared as a trace element standard for neutron activation analysis (*4*) were analyzed by CRA. These standard materials were prepared for analysis by dissolving in $HF–HNO_3$ solution and diluting to appropriate volumes with water. The CRA results for SRM 57, compared with recommended NBS values in Table III, indicate precisions of ±4.2 to ±15% and accuracies of ±9 to ±35% for five of the metals. The results for the doped silica trace standard are given in Table IV and compare favorably with data obtained by neutron activation analysis and flame AAS. Precisions and accuracies of ±1.4 to ±13% and ±4.5 to ±18%, respectively, were obtained for the seven metals.

Volatilization of Iron. The extent of losses of trace elements during sample preparation and during the heating cycle was unknown. Since the volatility of $FeCl_3$ in $SiCl_4$ has been reported (*5*), it was necessary to establish a sampling procedure with minimum susceptibility to losses of trace elements. The high volatility of $SiCl_4$ obviated direct injection into the CRA since quantitative introduction of the sample was not possible. The effectiveness of various procedures for converting $SiCl_4$ to aqueous solutions for injection into the CRA was evaluated. Two samples of $SiCl_4$ were doped with "low" and "high" levels of anhydrous $FeCl_3$ and analyzed in

Table IV. Analysis of Trace Element Silica Standard[a] by CRA

	μg/g			Precision, RSD, %	Accuracy, %
	CRA[d]	Flame[b]	NAA[c]		
Fe	70 ± 1	67 ± 3		1.4	4.5
Mn	2.3 ± 0.2	2.5 ± 0.1	2.69 ± 0.17	8.7	15
Cr	8.9 ± 0.8	11.5 ± 0.1	9.47 ± 0.53	9.0	6.3
Cu	3.6 ± 0.2	4.2 ± 0.1	4.11 ± 0.04	5.6	12
Zn	0.40 ± 0.05	.49 ± 0.07	...	13	18
Ni	8.8 ± 0.2	8.2 ± 0.4	...	2.3	7.3
Co	6.2 ± 0.2	6.7 ± 0.1	6.87 ± 2.1	3.2	9.8

[a] Preparation and standardization described in Reference 4. [b] Atomic absorption analysis at Bell Laboratories. [c] Neutron activation analysis at NBS. [d] Mean of triplicate determinations.

Table V. Determination of Fe in $SiCl_4$ Using Different Sample Preparation Methods

	Fe, ng/g	
Method[a]	Low	High
1	16 ± 0.5	358 ± 2
2	16 ± 1	334 ± 6
3	14 ± 1	367 ± 20
4	16 ± 0	337 ± 4
Mean	16	349

[a] See Results and Discussion for description of sample preparations 1-4.

duplicate using the following procedures:

1. Hydrolysis. $SiCl_4$ was slowly added to water at 0 °C and the resulting mixture of silicic acid and HCl was dried. The matrix was then destroyed with HF and the solution evaporated to dryness. The residue was dissolved in dilute HNO_3. The conditions of this procedure were such that volatilization losses of hydrated metal chlorides were minimized.

2. Direct reaction with HF. $SiCl_4$ was added to concentrated HF at 0 °C to yield a solution of SiF_4 and $FeCl_3$ in HF-HCl. The method was included to test the effect of this matrix on the volatility of $FeCl_3$.

3. Reaction with HF and evaporation. $SiCl_4$ was reacted with HF at 0 °C and evaporated to dryness. The residue was dissolved in dilute HNO_3. This procedure was included to detect any loss of Fe during evaporation of HF.

4. Evaporation. $SiCl_4$ was evaporated to dryness and the residue dissolved in dilute HF. With this procedure, losses of iron by volatilization as $FeCl_3$ in the presence of $SiCl_4$ could be determined.

It is evident from the results in Table V that $FeCl_3$ was not lost during the various sampling procedures. The evaporation method (*4*), which was described in the Experimental section, proved most effective because it was rapid, had extremely low blanks, and provided increased sensitivity via a concentration step. Determination of impurities in $SiCl_4$ at <1 ng/g was thus obtainable.

Application of Method. Cation impurities found in commercially available $SiCl_4$ samples are reported in Table VI. Sample A, epitaxial grade, was bottled in glass. Sample B, impure grade, was contained in a stainless steel cylinder. Sample C was Sample A which had been in contact with

Table VI. CRA Analysis of $SiCl_4$, ng/g

Element	A[a]	B[a]	C[a,b]	RSD, %
Fe	1.1	33	42.5 ± 2.3	5.4
Cr	<0.3	0.5	0.4 ± 0.1	25
Ni	<0.5	<0.5	<0.5	...
Mn	<0.2	<0.2	<0.2	...
Cu	1.0	<0.5	<0.5	...
Co	<0.5	<0.5	<0.5	...
Zn	0.06	0.14	0.063 ± 0.004	6.3

[a] A = Epitaxial Grade, B = Impure Grade, C = A in contact with stainless steel chips. [b] Mean of four replicate determinations.

stainless steel chips for three days. The epitaxial grade was extremely pure as expected. The "high" Fe concentration in Sample B indicated contamination from the stainless steel container. The RSD of Fe and Zn results for Sample C approached the reproducibility expected for CRA determinations (~5%). Analysis of $SiCl_4$ with various histories of exposure to contamination gave results similar to those in Table VI. It was important to avoid particulate residue which may be present in the $SiCl_4$ by sampling only the supernatant liquid. Since Fe, by far, was the most prevalent impurity in all $SiCl_4$ tested, the monitoring of impurities was greatly simplified by determining only Fe.

The method was adequately sensitive and quantitative to identify sources of metal contamination in the MCVD process. In addition to evaluating the starting materials, the method was equally applicable for analyzing $SiCl_4$ vapor condensates from various parts of the MCVD apparatus.

LITERATURE CITED

(1) W. G. French, J. B. MacChesney, and A. D. Pearson, *Ann. Rev. Mater. Sci.*, **5**, 373 (1975).
(2) L. Versernyes, *Acta. Chim. Acad. Sci. Hung.*, **28**, 111 (1961).
(3) Federal Standard 209A, "Cleanroom and Work Station Requirements", U.S. General Services Administration, Business Service Centers, Aug. 10, 1966.
(4) J. W. Mitchell, L. D. Blitzer, J. Gills, T. Y. Kometani, and L. Clark, *Mod. Trends Act. Anal.*, **2**, 781 (1976).
(5) M. Seider, Manfred Schoenherr, and Erich Wolf, Int. Symp. "Reinstoffe Wiss. Tech.", Tagungsber., 2nd (1965).

RECEIVED for review June 3, 1977. Accepted September 16, 1977.

Nitrogen Compounds in Coal Derived Liquids

Joseph E. Schiller

Grand Forks Energy Research Center, Energy Research and Development Administration, Box 8213, University Station, Grand Forks, North Dakota 58202

Five liquid products from different pilot plant scale coal liquefaction processes were examined. Column chromatography was used to isolate a fraction of each sample that contained the nitrogen compounds, and this fraction was subjected to gas chromatography–mass spectrometry (GC/MS), low voltage mass spectrometry, and high resolution mass spectrometry. The major compound types seen were quinolines, benzoquinolines, and carbazoles. Benzocarbazoles and compounds in the mass *Z* series −13 *N* (phenylpyridines, diphenylamines, and aminobiphenyls) were also major constituents in some liquids studied. The composition of the liquids reflected differences in process conditions. A broader range of compounds resulted from more vigorous liquefaction conditions (higher pressure, higher temperature, longer reaction time, or recycle).

Some analyses of nitrogen compounds in materials related to coal liquefaction products have been reported previously. Early studies on low temperature coal tar (*1*) and shale oil (*2*) relied on countercurrent extraction and gas chromatography. Many individual pyridines and pyridine benzologs, as well as several aminoaromatics, were identified. More recent work on coal tar products has used refined chromatographic methods and has relied on mass spectrometry for characterization of the mixtures encountered (*3–5*). Tentative identification of carbazoles, pyridines, and pyridine benzologs was made.

Some excellent work on nitrogen compounds has been done at the ERDA Laramie Energy Research Center. Compound type characterization of acidic and basic nitrogen species in high boiling petroleum distillates showed carbazoles, amides, pyridine benzologs, and diaza compounds to be present (*6, 7*). Syncrude from hydrotreating crude shale oil distillates exhibits a wider range of nitrogen compound types (*8*). Specific nitrogen compounds in tar produced from underground gasification of coal were isolated by preparative GC and identified as alkyl pyridines, quinolines, and anilines (*9*). A recent report from the ERDA Pittsburgh Energy Research Center described the identification of some basic nitrogen compounds in one coal liquid (*10*).

Nitrogen compounds in coal liquefaction products are present in various chemical forms, and it is important to know the type and amount of these species. If the liquid is to be used directly as a fuel, the chemical form of the nitrogen may affect the extent of formation of nitrogen oxides in the effluent gas (*11*). If a coal liquefaction product is to be upgraded to motor fuel or home heating oil, the character and content of nitrogen compounds must be known in order to choose appropriate catalysts and conditions for the nitrogen compound removal during refining. The health hazards involved in working with coal liquids may be better defined by knowing which nitrogen compounds are present (*12*). There may also be contained in these liquids some valuable chemicals, and their isolation from the coal liquid will be economically desirable if they are present in sufficiently high concentrations. This study is intended to shed light on the nature of the nitrogen compounds present in coal liquids.

Coal liquefaction by direct hydrogenation (*13, 14*) and solvent refining (*15, 16*) involves high temperature, high pressure reaction of a coal/oil slurry with hydrogen or synthesis gas. In SRC processes, the crude product is filtered to remove mineral matter and unreacted coal; vacuum distillation of the filtrate yields a liquid distillate used as the slurry vehicle oil and a solid "solvent refined" coal (SRC) as the distillation residue. In coal liquefaction, higher temperature and pressure or a catalyst are used to give a liquid product, and some of the product is recycled as vehicle. Materials analyzed in this work represent four recycle solvents from three SRC pilot plants and one coal liquid from the CO-Steam (*13*) pilot plant at the Pittsburgh Energy Research Center (see Table I). In all cases, "lined out" operation has been achieved so that the materials analyzed indeed represent coal-derived liquids from each process rather than start-up solvent.

EXPERIMENTAL

Column Chromatography. The column chromatographic procedure described previously was employed (*17*). Activity I neutral alumina was packed into a 11-mm i.d. column, and the sample was eluted from the column with hexane and toluene, followed by chloroform to remove the nitrogen-containing compounds. The percent nitrogen in the chloroform fractions and whole liquids is summarized in Table I. (Elemental analysis for nitrogen was performed by Huffman Laboratories, Inc., Wheatridge, Colo. 80033.)

GC/MS. Fractions obtained from the column chromatographic separation were subjected to GC/MS analysis. The column used was 3% OV 17 on Chromosorb W-HP packed in a $^1/_8$-inch o.d. by 10-foot stainless steel column. The chromatograph was a Varian model 2740 with a glass splitter which directed $^1/_3$ of the column effluent to the flame ionization detector and $^2/_3$ to a duPont model 21-491B low resolution mass spectrometer. Mass spectra were recorded for large peaks which appeared in each chromatogram. A typical chromatogram is shown in Figure 1. Compounds were identified by their mass spectra or retention times and mass spectra. The temperature employed during the GC separation was programmed from 100–275 °C at 8°/min, and the flow rate of helium carrier gas was 30 mL/min through the column. The amount of sample solution injected was varied to give a chromatogram where the most intense peak was almost full scale.

Mass Spectrometry. Low voltage mass spectrometry (LVMS) was performed using an AEI MS30 mass spectrometer equipped with a heated glass inlet operated at 325 °C. A weighted amount of sample (2–3 mg) was introduced into the mass spectrometer and vaporized. After the intensities had attained stable values, at least 6 spectra were recorded and intensities were averaged. Relative intensities were corrected for differences in sensitivity and normalized to give the quantitative data shown in Table III. The source pressure was approximately 2×10^{-5} Torr and an ionizing voltage of 10.0 V was used for obtaining low voltage spectra at a resolution of 1000. High resolution spectra were obtained at a resolving power of approximately 7000 and an ionizing voltage of 70 V. An AEI DS 50 data system was used for collecting and minipulating low voltage and high resolution data. The high resolution mass spectra confirmed the presence of nitrogen compounds indicated by GC/MS analysis, and peaks

Table I. Summary of Materials Analyzed in This Study

	Source of sample				
	Pittsburgh & Midway Coal Co., Research & Dev. Dept., Solvent Refined Coal Pilot Plant, Dupont, Wash. 98327 (near Tacoma, Wash.)	Pittsburgh & Midway Coal Co. Research & Dev. Dept., 9009 W. 67th St., Merriam, Kan. 66202		Southern Services, Inc., P. O. Box 2625, Birmingham, Ala. 35202 (pilot plant at Wilsonville, Ala.)	Pittsburgh Energy Research Center, 4800 Forbes Ave., Pittsburgh, Pa. 15213
Sample type	SRC process solvent, No. 307	SRC process solvent, No. 122[a]	SRC II process solvent, No. 115R[a,b]	SRC process solvent	CO-Steam product[c]
Type of coal used	Ky. 14 Bit.	Ky. 14 Bit.	Ky. 14 Bit.	Wyo., Sub-Bit.	N.D. Lignite
% N in whole liquid	0.97	1.06	1.15	0.64	1.34
% N in chloroform fraction from column chromatography	5.64	5.53	6.03	4.98	2.72
Weight % of chloroform eluate from the whole liquid	11	17	14	10	24

[a] Solvent was removed by batch distillation. [b] SRC II involves higher pressure and product recycle in order to generate excess process solvent. [c] In the CO-Steam process, no distillation step is involved after the reaction, so the product is 40% nonvolatile.

Table II. Compound Names That Correspond to Abbreviations in Figure 1

Abbreviation	Identification	Compound
Q	a	Quinoline
iQ	a	Isoquinoline
I	a	Indole
MQ	b	Methylquinoline
C_2Q	b	Dimethylquinoline or Ethylquinoline
PP	a	2-Phenyl pyridine
34BQ	a	3,4-Benzoquinoline
56BQ	a	5,6-Benzoquinoline
78BQ	a	7,8-Benzoquinoline
A	a	Acridine
C	a	Carbazole
MC	b	Methylcarbazole
MBQ	b	Methylbenzoquinoline
AP	a	1-Azapyrene

[a] Identified by GC retention time and MS. [b] Identified by MS only, since standards were not available.

at nominal mass 217 and 231 were shown to have molecular formulas corresponding to benzocarbazole and methyl benzocarbazole.

RESULTS AND DISCUSSION

Results of GC/MS analysis shown by a typical chromatogram of the nitrogen-rich fraction from one SRC solvent are given in Figure 1. The specific compounds corresponding to the symbols identifying the chromatographic peaks are listed in Table II. Preliminary inspection of five such chromatograms and the corresponding LVMS data in Table III indicates the following:

1. SRC solvents No. 307 and No. 122 (see Table I) have almost the identical composition of major nitrogen compounds. This may be expected, since both were made from the same coal under conditions designed to give duplicate product. Solvent No. 122, however, shows a somewhat larger amount of unresolved minor constituents in the chromatogram.

2. The SRC solvent from Wilsonville exhibits a much larger concentration of light components. This is reflective of the

Table III. Quantitative Data from LVMS Analysis of the *N*-Rich Fractions. Numbers in the Table Are Weight Percent of the Fraction

Probable compound type	Mass *Z* series	SRC solvent (307)	SRC solvent (122)	SRC II solvent (115R)	SRC solvent, Wilsonville	CO-Steam product
Pyridines, anilines	$-5\ N$	0.0	2.2	3.9	7.9	1.0
Tetrahydroquinilines	$-7\ N$	1.8	5.2	8.3	5.0	1.9
Indoles	$-9\ N$	0.0	0.5	1.3	0.6	0.5
Quinolines	$-11\ N$	20.0	16.9	8.2	22.5	5.2
Phenylpyridines, diphenylamines, amino biphenyls	$-13\ N$	10.3	14.5	18.1	8.9	5.8
Carbazoles	$-15\ N$	19.7	10.5	10.5	6.9	7.0
Benzoquinolines	$-17\ N$	15.5	12.0	8.2	8.2	8.1
Naphthenobenzoquinolines	$-19\ N$	1.2	2.3	2.8	0.8	2.8
Azapyrene, azafluoranthenes	$-21\ N$	1.1	2.0	3.5	1.3	1.8
Benzocarbazoles	$-21\ N$	3.5	2.0	1.4	0.7	3.8
Azachrysenes	$-23\ N$	0.6	0.6	0.3	0.5	2.4
Naphthenoazachrysenes	$-25\ N$	0.0	0.0	0.0	0.0	1.2
Dibenzocarbazoles	$-27\ N$	0.0	0.0	0.0	0.0	2.2
Nonvolatile		8.3	4.1	5.1	7.6	35.1
Non-nitrogen compounds		18.0	27.2	28.4	31.7	21.2

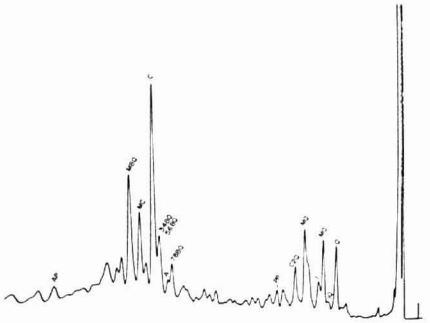

Figure 1. Gas chromatogram of the nitrogen compound fraction from an SRC solvent No. 307 made at the Tacoma pilot plant

low temperature used for solvent stripping in removing recycle solvent after reaction (*18*).

3. The CO-Steam product and the SRC II process solvent (115R) show carbazole and methylcarbazole as major peaks in the chromatograms, while many smaller peaks of about the same size are seen throughout the elution. This indicates a more complicated mixture with more individual compounds and compound types. Since more vigorous reaction conditions were used in these reactions than for the other three samples, a broader range of compounds could be expected.

Because of the many possible isomers of alkylated compounds, no attempt was made to distinguish the isomeric methylated quinolines, methylated benzoquinolines, or methylated carbazoles. However, with the chromatographic system used, quinoline and isoquinoline are resolved, and acridine is separated from other benzoquinolines. All of the liquids studied contain several times as much quinoline as isoquinoline, and acridine is only a small fraction of the total benzoquinolines. Also identified were 1-azapyrene, indole, 2-phenyl pyridine, and carbazole.

Quantitative analysis for nitrogen compounds in the coal liquids studied obtained by LVMS are given in Table III. For the four SRC process solvents, 67.7 to 88.8% of the volatile nitrogen compounds are in the mass Z series -11 N to -17 N, and 59.8% of the volatile material in the CO-Steam product is in the same range. These are two- and three-ring heterocyclics. Differences among the nitrogen compounds may generally be explained by differences in the process used.

Solvent 115R shows an unusually large quantity of tetrahydroquinolines and pyridines/anilines. These species are hydrogenation products of quinoline (*19*), and they result from the vigorous reaction conditions used in the SRC II process.

The solvent from Wilsonville contains relatively more low molecular weight compounds (quinolines, tetrahydroquinolines, and pyridines/anilines). As indicated in the discussion on GC/MS analysis of these mixtures, a rather low temperature was used for solvent flash, and this causes the observed tendency toward lighter compounds.

The CO-Steam product is the only sample studied that is not a distillate. As a result, a rather large portion of the nitrogen-rich fraction is nonvolatile, and four- and five-ring heterocyclics are present in significant concentration. Work is in progress to further characterize these heavy nitrogen compounds in CO-Steam product.

ACKNOWLEDGMENT

The author thanks Lu Ann Sidney and David J. Miller who performed some of the experimental work in this study. The organizations listed in Table I which supplied samples are also appreciated.

LITERATURE CITED

(1) C. Karr, Jr., P. A. Estep, T-C. L. Chang, and J. R. Comberiatl, *U.S. Bur. Mines, Bull.*, **591** (1961).
(2) A. W. Decora and G. U. Dinneen, *U.S. Bur. Mines, Rep. Invest.*, **5768** (1961).
(3) K. D. Bartle, D. W. Jones, T. G. Martin, and W. S. Wise, *J. Appl. Chem.*, **20**, 197 (1974).
(4) K. Tesari and S. Chyczy, *J. Chromatogr.*, **91**, 723 (1974).
(5) B. L. Chrynes, *Quart. Tech. Prog. Rep.*, **FE-2011-4** under ERDA Contract E(49-18)-2011, June 1976.
(6) J. F. McKay, T. E. Cogswell, J. H. Weber, and D. R. Latham, *Fuel*, **54**, 50-61 (1975).
(7) J. F. McKay, J. H. Weber, and D. R. Latham, *Anal. Chem.*, **48**, 891-898 (1976).
(8) R. E. Paulson, C. M. Frost, and H. B. Jensen, *Am. Chem. Soc., Fuel Div., Prepr.*, **19** (2), 175-182 (1974).
(9) S. B. King, C. F. Brandenburg, and W. J. Lanum, *Am. Chem. Soc., Fuel Div. Prepr.*, **20** (2), 131-139 (1975).
(10) J. L. Shultz, C. M. White, F. K. Schweighardt, and A. G. Sharkey, Jr., *ERDA Rep. Invest.*, **Perc/RI-77/7**, 1977, 25 pp.
(11) A. E. Axworthy, G. R. Schneider, M. D. Shuman, and V. H. Dahan, *U.S. NTIS PB Rep.*, 1976, **Pb 250373**, 35 pp.
(12) "Suspected Carcinogens—A Subfile of the NIOSH Toxic Substances List", Herbert E. Christiansen, D.S.C., and Thomas T. Lugenbill, Ed., Department of Health, Education and Welfare, Public Health Service, Rockville, Md., June 1975.
(13) H. R. Appell and I. Wender, *Am. Chem. Soc., Fuel Div. Prepr.*, **12**, (3), 220 (1968).
(14) D. L. Klass, *Chemtech*, **5** (8) 499 (1975).
(15) D. E. Severson, A. M. Souby, and W. R. Kube, *U.S. Bur. Mines, Inf. Circ.*, **8650**, 236 (1974).
(16) Interim Report for Research Project No. 1234, Electric Power Research Institute, 3412 Hillview Ave., Palo Alto, Calif., May 1975.
(17) J. E. Schiller and D. M. Mathiason, *Anal. Chem.*, **49**, 1225 (1977).
(18) J. E. Schiller, *Hydrocarbon Process.*, **56** 147-152 (1977).
(19) J. R. Katzer, B. C. Gates, J. H. Olson, H. Kwart, and A. B. Stiles, *Quart. Tech. Progr. Rep.*, **FE 2028-3** under ERDA contract E(48-19)-2028, March 1976.

RECEIVED for review July 21, 1977. Accepted September 19, 1977. Reference to specific brands or models is for identification only and does not represent endorsement by ERDA.

Enhancement of Retention by Ion-Pair Formation in Liquid Chromatography with Nonpolar Stationary Phases

Csaba Horvath,* Wayne Melander, Imre Molnar,[1] and Petra Molnar

Chemical Engineering Group, Department of Engineering and Applied Science, Yale University, New Haven, Connecticut 06520

In ion-pair reversed-phase chromatography, the retention of ionized analytes on a nonpolar bonded stationary phase is enhanced by the presence of a "hydrophobic" counterion (hetaeron) in the mobile phase. Either ion-pair formation in the mobile phase with relatively strong retention of the complex or the conversion of the stationary phase into an ion-exchanger may explain the phenomenon. Analysis of the pertinent equilibria shows that the observed hyperbolic or parabolic dependence of the capacity factors on the hetaeron concentration cannot shed light on the mechanism. The experimental data obtained for the retention of catecholamines by using C_4–C_{10} alkyl sulfates and other similar hetaerons in a wide concentration range, however, could be mechanistically interpreted from the chain length dependence of the parameters for the relationship between the capacity factors and hetaeron concentration. Although the results clearly demonstrate that in the system investigated, ion-pair formation governs retention, ion-exchange mechanism can be operative under certain conditions. Changes in retention upon addition of salt to the eluent are treated both theoretically and experimentally. The effect of organic solvents on the behavior of the chromatographic system is discussed in view of the proposed theory.

According to the popular notion, the selectivity in chromatographic separations is determined by the differences in the equilibrium distribution of eluite molecules, i.e. analytes, between the stationary and mobile phases. Quite frequently, however, secondary equilibria between the eluites and certain species present in the eluent can drastically affect retention (*1*). In a recent paper (*2*) we analyzed the effect of protonic equilibria in the mobile phase on retention in liquid chromatography with nonpolar stationary phases. The selectivity of the chromatographic system for ionogenic eluites was shown to be greatly influenced by their dissociation constant and the hydrogen ion concentration in the eluent because the binding of protons increases and decreases the retention of weak acids and bases, respectively.

Recent work has demonstrated that retention of charged eluites on nonpolar bonded stationary phases can be augmented by the presence of suitable counterions, which have a substantial hydrophobic moiety, in the mobile phase (*3–5*). This technique is often referred to as "soap" or "ion-pair reversed-phase" chromatography. The counterions used in the mobile phase belong in the group of detergents such as alkyl sulfonates and sulfates or tetraalkylammonium compounds, and ion-pair formation between the eluite and counterion is assumed to be responsible for the increase in retention (*6*).

This approach is particularly interesting because the use of nonpolar bonded stationary phases for liquid chromatographic separations has a wide currency (*7*). In most cases octadecyl-silica is the stationary phase and hydro-organic mixtures with methanol or acetonitrile as well as neat aqueous or organic solvents are used as eluents. The technique is simple and can be used for the separation of a wide variety of substances. For this reason it is the most popular method in high performance liquid chromatography. The mechanism of retention is believed to be the same as involved in the so-called hydrophobic effect (*8*) and we recently adapted the solvophobic theory (*9*) to treat the interaction of eluites with the hydrocarbonaceous functions of bonded phases in a rigorous thermodynamic fashion (*2, 10*). We have shown that the magnitude of retention is governed by the effect of the solvent on these species and their adducts.

The increasing popularity of using an ion-pair forming agent in the mobile phase to increase the retention of oppositely charged eluites prompted us to investigate the fundamental aspects of this technique. Our treatment, however, is quite general and applicable to a variety of cases where the retention of an eluite on nonpolar bonded phases is enhanced by complex formation with a component of the eluent. For sake of convenience we propose to call the complexing agent *hetaeron*, a term derived from the Greek work for companion (εταιρον). Thus "hetaeric" chromatography would denote a technique in which a certain concentration of a complexing agent is intentionally maintained in the mobile phase in order to affect the selectivity of the chromatographic system by secondary equilibria. The name should be restricted to situations where the eluite–hetaeron complex is formed in the mobile phase and distributed between the two phases. Of course, secondary equilibria may change the properties of the stationary phase. Indeed, it was recently suggested (*11*) that in ion-pair reversed-phase chromatography the stationary phase acts as a dynamically coated ion exchanger because of the adsorption of the detergent ions. By using extensive experimental data and applying the solvophobic theory for the interpretation of the results, we intend to demonstrate in this article that in the situations examined the mechanism of the chromatographic process entails ion-pair formation in the mobile phase and binding of the neutral complex to the stationary phase.

THEORY

Phenomenological Treatment. In order to shed light on the relationship between the capacity factor, which is a convenient measure of retention, and the equilibrium constants, which govern the retention on nonpolar bonded stationary phases in the presence of various concentrations of a complexing agent (hetaeron) in the mobile phase, the process first will be treated phenomenologically.

Figure 1 illustrates the various equilibria which are involved in the chromatographic process. The eluite, E, whose retention is of interest, can interact with the hetaeron, *H*, to form a complex, E*H*, which is bound to the hydrocarbonaceous ligand, L, of the stationary phase to form LE*H*. Alternatively, the hetaeron may bind first to the stationary phase and then form LE*H*. In addition the species E and *H* can individually form the adducts LE and L*H* with the ligands of the stationary phase. It is assumed that binding of the eluite and the heteron

[1] Present address, K. G. Dr. Herbert Knauer, Hegauer Weg 38, Berlin 37, West Germany.

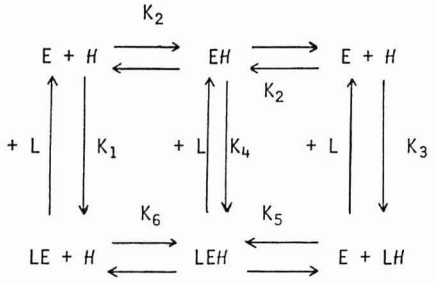

Figure 1. Schematic illustration of the equilibria involved in the chromatographic process with nonpolar bonded stationary phases and a complexing agent in the mobile phase. The meaning of the symbols is: E, eluite; *H*, complexing agent (hetaeron); L, hydrocarbonaceous ligand bound to the support; K_1 to K_6 are the corresponding equilibrium constants

to the stationary phase ligands takes place independently.

The equilibrium constants are expressed by the following set of equations in which the species concentrations in the mobile and stationary phase are denoted by the subscripts m and s, respectively. The concentration of L is defined as the accessible ligand concentration in the stationary phase.

$$K_1 = [LE]_s/[E]_m[L]_s \quad (1)$$

$$K_2 = [EH]_m/[E]_m[H]_m \quad (2)$$

$$K_3 = [LH]_s/[H]_m[L]_s \quad (3)$$

$$K_4 = [LEH]_s/[EH]_m[L]_s \quad (4)$$

$$K_5 = [LEH]_s/[LH]_s[E]_m \quad (5)$$

$$K_6 = [LEH]_s/[LE]_s[H]_m \quad (6)$$

The capacity factor of the eluite, k, is defined in the usual way as

$$k = \phi([LEH]_s + [LE]_s)/([E]_m + [EH]_m) \quad (7)$$

where ϕ is the phase ratio, i.e. the ratio of the volume of stationary phase to the volume of the mobile phase in the column.

In chromatographic practice when the column is equilibrated with the eluent the hetaeron concentration in the mobile phase is constant. If $[E] \ll [H]_m$, only a negligible fraction of the hetaeron is in the form of a complex so that the hetaeron concentration can be considered invariant and we can write

$$[H]_m \equiv [H] \quad (8)$$

Since the extent of binding of the eluite by the stationary phase is expected to be small and the total ligand concentration $[L]_T$ is conserved, we may write that

$$[L]_T = [L]_s + [LH]_s \equiv [L] \quad (9)$$

There are several ways to evaluate from Equations 1–6 a combination of the equilibrium constants which govern the chromatographic process. If we assume that the eluite is bound by the stationary phase as its complex with the hetaeron, which is formed in the mobile phase, then the combination of Equations 1–4 and 7–9 yields the following expression for the capacity factor

$$k = \phi[L](K_1 + K_2K_4[H])/(1 + K_2[H])(1 + K_3[H]) \quad (10)$$

The assumption that complex formation occurs with the hetaeron already bound to the stationary phase yields, by the combination of Equations 1–3, 5 and 7–9 the following expression for the capacity factor.

$$k = \phi[L](K_1 + K_3K_5[H])/(1 + K_2[H])(1 + K_3[H]) \quad (11)$$

A third possible combination uses Equations 1–3 and 6–9 and yields

$$k = \phi[L](K_1 + K_1K_6[H])/(1 + K_2[H])(1 + K_3[H]) \quad (12)$$

Equation 12 would imply that the eluite first binds to the stationary phase and then forms a complex with the hetaeron.

Equations 10–12 all express the dependence of the capacity factor on the hetaeron concentration and have the general form

$$k = (k_0 + B[H])/(1 + K_2[H])(1 + K_3[H]) \quad (13)$$

where k_0 is the capacity factor of the eluite in the absence of hetaeron, K_2 is the association constant for the eluite and the hetaeron, K_3 is the binding constant of the hetaeron to the stationary phase and B is the product of the two equilibrium constants as shown in Equations 10–12. A plot of k vs. $[H]$ according to Equation 13 yields a parabola provided $1/K_3[H] < 1/K_2$.

If either $K_2[H] \ll 1$ or $K_3[H] \ll 1$, Equation 13 can be written as

$$k = (k_0 + B[H])/(1 + P[H]) \quad (14)$$

where P can be either K_2 or K_3. Equation 14 is the equation of a rectangular hyperbola, for the dependence of the capacity factor on the hetaeron concentration. Both parabolic and hyperbolic dependence of the capacity factor on the hetaeron concentration have been observed in ion-pair reversed phase chromatography (*5*, *6*).

When the complex is an ion-pair, both the eluite and the hetaeron have to be fully ionized for the above treatment to be valid. Whereas the hetaeron is usually a strong electrolyte in ion-pair chromatography, the eluites are often weak bases or acids and therefore the pH of the eluent can have an influence on the retention. The corresponding protonic equilibria can readily be incorporated into the above model as will be shown by the example of a weakly basic eluite.

The protonation of the neutral eluite, E^0, is characterized by its acid dissociation constant, K_a, related to the equilibrium

$$E^0 + H^+ \rightleftarrows EH^+ \quad (15)$$

Both forms, E^0 and EH^+, can bind to the ligands of the stationary phase according to the following equilibria

$$E^0 + L \rightleftarrows LE^0 \quad (16)$$

and

$$EH^+ + L \rightleftarrows LEH^+ \quad (17)$$

The equilibrium constants corresponding to Equations 16 and 17 are denoted by K_1^0 and K_1, respectively.

In this case, however, only the protonated eluite molecules can form an ion-pair [HE*H*] with the hetaeron–counterion and bind as a complex, [LHE*H*], to the stationary phase. Consequently, mass balance yields the following expression for the capacity factor

$$k = \phi \frac{[LHEH]_s + [LE]_s + [LEH^+]_s}{[E]_m + [EH^+]_m + [HEH]_m} \quad (18)$$

Following the previous approach and using Equations 1–4 and 15–17 to substitute the equilibrium constants into Equation 18, we obtain for the capacity factor the expression

$$k = \phi[\mathrm{L}]\frac{\dfrac{K_1^0 K_a}{(K_1 + [\mathrm{H}^+] + K_2K_4[H])}}{(1 + \dfrac{K_a}{[\mathrm{H}^+]} + K_2[H])(1 + K_3[H])} \qquad (19)$$

Equation 19 can also be written in a form similar to that of Equation 13, but in this case the magnitude of the parameters would also be dependent on the acid dissociation constant of the eluite and the hydrogen ion concentration in the mobile phase.

Enhancement Factor. Experimental data show that in ion-pair reversed phase chromatography the dependence of the capacity factor on the detergent concentration often follows hyperbolic behavior (*6*) such as represented by Equation 14. According to this expression the two limiting values of the capacity factor are k_0 and B/P at zero and at sufficiently high hetaeron concentrations, respectively. The ratio of the two quantities gives the highest possible amplification of the capacity factor due to the presence of the hetaeron. It is termed the enhancement factor, η, and given by

$$\eta = B/k_0P \qquad (20)$$

where k_0 is the capacity factor of an eluite in the absence of hetaeron, P is either the stability constant of the eluite–hetaeron complex or the equilibrium constant for the binding of the hetaeron to the stationary phase and the physical meaning of B also depends on the particular mechanism which governs eluite retention in the presence of the hetaeron. We shall see later how η can be used for both the elucidation of mechanism and the practical selection of a hetaeron.

Mechanistic Implications of the Solvophobic Theory. In view of the preceding section, on a closer examination of the process, the retention of the eluite in ion-pair chromatography on nonpolar bonded phases can occur either by "*dynamic ion-exchange*", i.e., ion-pair formation takes place between the eluite and the hetaeron bound to the stationary phase, or by *ion-pair formation in the mobile phase* and binding of the complex to the nonpolar stationary phase. Since a phenomenological approach cannot distinguish between the two cases on the basis of the dependence of the capacity factor on the hetaeron concentration, we shall use the solvophobic theory to estimate the relative magnitude of the equilibrium constants on the basis of the molecular properties of the hetaeron and eluites.

The solvophobic theory was developed to describe the effect of solvent on chemical phenomena (*9*) and has successfully accounted for inter alia, the solubility of small nonelectrolytes in water and other solvents (*12*) and the effect of solvent variation on reaction rates for several different chemical reactions (*13*). It is not restricted to water as the solvent and expresses the energetics of the solvent effect in terms of, at least in principle, measurable properties of the solute and solvent, unlike other theories for the hydrophobic effect.

We have recently adapted this approach to quantitatively treat the effect of eluite and eluent properties on chromatographic retention using polar solvents, especially water, and a nonpolar stationary phase (*2, 10*). In our model, we assumed that the chromatographic process entails a reversible association of a solute, S, with the hydrocarbonaceous ligand, L, of the stationary phase to form a complex SL. The logarithm of the corresponding equilibrium constant for a nonionized solute, K_1^0, was expressed for fixed column and eluent properties at a given temperature by Equation 47 in Ref. (*10*) which for our purpose can be written in a simplified form as

$$\ln K_1^0 \approx a - b + c\Delta A \qquad (21)$$

where a, b, and c can be regarded as constants dependent upon solvent and column properties; b also depends on the eluite properties such as dipole moment, polarizability and molecular volume. ΔA is the difference between the molecular surface area of the complex, A_{SL}, and those of the eluite, A_S, and the hydrocarbonaceous ligand, A_L, so that

$$\Delta A = A_{SL} - A_S - A_L \qquad (22)$$

For the capacity factor of an ionized solute, the following simplified expression can be derived from Equation 20g of Ref. (*2*)

$$\ln K_1 \approx a' + b'\,f(Z) + c'\Delta A \qquad (23)$$

where a', b', and c' are again solvent and column dependent parameters. The effect of charge on the solute molecule is represented by the function $f(Z)$ which goes approximately as the absolute value of the product of charges on the ion and its counterion.

The simplified expressions in Equations 21 and 23 allow us to make some qualitative and semiquantitative statements regarding the constants lumped together in the enhancement factor as far as the mechanism of ion-pair reversed-phase chromatography is concerned. It is recalled that the parameters k_0, B, and P in Equation 20 are directly related to the equilibrium constants defined in Equations 1–5.

As k_0 is the capacity factor of the eluite in the absence of hetaeron, in view of Equations 1, 10, and 14 we may write that

$$\ln k_0 = \ln(\phi[\mathrm{L}]K_1) = a' + b'\,f(Z) + c\Delta A \qquad (24)$$

Obviously the value of k_0 is independent of any kind of ion-pair formation. On the other hand, the meaning of the constants B and P in Equation 20 is dependent on the actual mechanism of the chromatographic process.

The energy of any electrostatic interaction and hence the logarithm of the corresponding equilibrium constant depends upon the product of the charges on the interacting species. Thus, for the ion-pair formation in the mobile phase the equilibrium constant, K_2, in Equation 2 can be expressed by

$$\ln K_2 = f'(Z_E Z_H) + \text{const.} \qquad (25)$$

where Z_E and Z_H are the charges on the eluite and hetaeron, respectively. Similarly, in the case of dynamic ion-exchange, represented by Equation 5, the equilibrium constant, K_5, for the interaction between the eluite and the hetaeron bound to the stationary phase can be expressed by

$$\ln K_5 = f''(Z_E Z_H) + \text{const.} \qquad (26)$$

The other equilibrium constants of interest, K_3 and K_4, correspond to the binding of the hetaeron and the complex to the stationary phase ligands, as shown by Equations 3 and 4, respectively. According to the solvophobic theory, both equilibrium constants can be expressed as a function of the decrease in the molecular surface area upon binding of the species to the stationary phase. Thus, by using Equation 23, we can write for the equilibrium constant representing the binding of the charged hetaeron, that

$$\ln K_3 = a' + b'\,f(Z_H) + c'\Delta A_3 \qquad (27)$$

On the other hand, the equilibrium constant for the binding of the neutral ion-pair can be expressed from Equation 21 as

$$\ln K_4 = a - b + c\Delta A_4 \qquad (28)$$

Table I. Relationship between Hetaeron Properties and the Parameters of Equation 14 as Predicted for the Two Limiting Mechanisms in Ion-Pair Reversed-Phase Chromatography

Parameter	Ion-pair formation occurs in the mobile phase	Ion-pair formation occurs in the stationary phase
k_0	...	...
B	hydrophobic surface area (carbon number)	hydrophobic surface area (carbon number)
P	charge type ($P = K_1$)	hydrophobic surface (carbon number) area + charge type ($P = K_3$)
B/k_0P	hydrophobic surface area (carbon number)	charge type

According to the previous discussion the meanings of ΔA_3 and ΔA_4 in Equations 27 and 28 are different and given by

$$\Delta A_3 = A_{HL} - A_H - A_L \quad (29)$$

and

$$\Delta A_4 = A_{HEL} - A_L - A_{HE} \quad (30)$$

where A_i is the molecular surface area of the species i denoted by the subscripts.

We can express the enhancement factor, η, by two different combinations of the equilibrium constants. In the first case, assuming dynamic ion exchange we obtain from Equations 11, 14, 20, 24, and 26 that

$$\ln \eta = \ln (K_5/K_1) = \text{const.} + f''(Z_E Z_H) - f(Z_E) - c(A_{LEH} - A_{EL} - A_{LH}) \quad (31)$$

In the second case, when ion-pair formation in the mobile phase dominates, the enhancement factor can be expressed by using a similar combination of the pertinent equations as

$$\ln \eta = \ln (K_4/K_1) = \text{const.} - f(Z_E) + c(A_{HEL} - A_{HE} + A_E - A_{LE}) \quad (32)$$

From the results presented earlier (2) we know that

$$A_{EL} - A_E - A_L \propto A_E \quad (33)$$

Since this relationship is expected to hold for all species under investigation we can write for the last term in Equation 32 that

$$A_{HEL} - A_{HE} + A_E - A_{LE} \propto (A_{HE} - A_E) \quad (34)$$

In other words the last term in Equation 32 depends upon the difference in the surface area of the complex and eluite. If the complex is formed to maximize the electrostatic effect, this difference is very nearly the surface area of the hetaeron, A_H, alone. Hence, if the retention proceeds primarily by the formation of ion-pairs in the mobile phase, the enhancement factor will depend upon the surface area of the hetaeron as

$$\log \eta \propto A_H \quad (35)$$

Consequently, in the case of normal alkyl sulfates or sulfonates $\log \eta$ is expected to be proportional to the carbon number of the hetaeron.

On the other hand, no such a dependence is expected in the "ion-exchange" mechanism. Indeed, the relevant hetaeron property, as seen from Equation 30, is a function of its charge, $f(Z_H Z_E)$, only. In view of these relationships, the analysis of

Table II. Relationship between Eluite Properties and the Parameters of Equation 14 as Predicted for the Two Limiting Mechanisms with Ion-Pair Formation

Parameter	Ion-pair formation occurs in mobile phase	Ion-pair formation occurs in stationary phase
k_0	charge and hydrophobic surface area	charge and hydrophobic surface area
B	charge and hydrophobic surface area	charge and hydrophobic surface area
P	charge ($P = K_1$)	...
B/k_0P	charge	charge and hydrophobic surface area

experimental data obtained with hetaerons containing the same ionic groups but different alkyl chain lengths can shed light on the actual mechanism of the process. The dependence of the enhancement factor on the properties of the hetaeron and eluite is shown in Tables I and II, which summarize the conclusions of this approach.

EXPERIMENTAL

A Model 601 (Perkin-Elmer, Norwalk, Conn.) high pressure liquid chromatograph was used with a Model 7010 sampling valve (Rheodyne, Berkeley, Calif.), a Model FS 770 (Schoeffel, Westwood, N.J.) variable wavelength detector at 254 nm, and a Perkin-Elmer Model R-56 recorder were used. Partisil 1025 ODS (Whatman, Clifton, N.J.) columns packed with 10-μm octadecyl-silica containing about 5% (w/w) carbon were used in the study of hetaeron behavior. The chromatogram in Figure 2 was obtained with a LiChrosorb RP-18 column (Rainin, Boston, Mass.) packed with 5-μm octadecyl-silica. All columns were 250 mm long and had 6.4 mm o.d. and 4.6 mm i.d. Most experiments were carried out by isocratic elution using neat aqueous 5×10^{-2} M phosphate buffer, pH 2.5, and the hetaerons were also dissolved in this buffer. In most cases the flow rate and the column temperature were 2 mL/min and 40 °C, respectively. Some experiments were carried out with hetaerons dissolved in mixtures of methanol and the above mentioned phosphate buffer as the eluent.

Catecholamine derivatives were obtained from Aldrich (Milwaukee, Wis.) or Schwartz/Mann (Orangeburg, N.Y.) and reagent grade H_3PO_4 and KH_2PO_4 were supplied by Fisher (Pittsburgh, Pa.). The alkyl sulfates and hexylsulfonate used were Eastman products (Rochester, N.Y.), whereas the alkyl phosphates were gifts from Hooker Chemicals Corp. (Buffalo, N.Y.). The perfluorated carboxylic acids were purchased from Aldrich. Methanol was "distilled in glass" from Burdick and Jackson (Muskegon, Mich.).

Retention times were measured from the distance between the injection point and the peak maxima on the chromatogram. The mobile phase hold-up times were measured as described previously (2) and the capacity factors have been calculated in the usual way (14).

The analysis of the data was performed on a PDP 11/10 minicomputer equipped with a RX01 floppy disc, a VT55 display unit, and a Decwriter. The computer program used for parameter estimation by the least squares method was written in BASIC language.

The symbols used in this study for the sample components are as follows: DOPA, 3,4-dihydroxyphenylethylamine (dopamine); EP, 1-(3,4-dihydroxyphenyl)-2-(methylamino)ethanol (epinephrine, adrenaline); OP, 1-(4-hydroxyphenyl)-2-aminoethane (octopamine); NE, 2-amino-1-(3,4-dihydroxyphenyl)ethanol (norepinephrine, noradrenaline); DOS, 3,4-dihydroxyphenylserine.

RESULTS AND DISCUSSION

A typical chromatogram in Figure 2 illustrates the separation of certain catecholamines on octadecyl-silica in the absence and in the presence of n-octylsulfate in the neat aqueous phosphate buffer used as the eluent. As the chemical nature and concentration of the alkyl sulfate have great

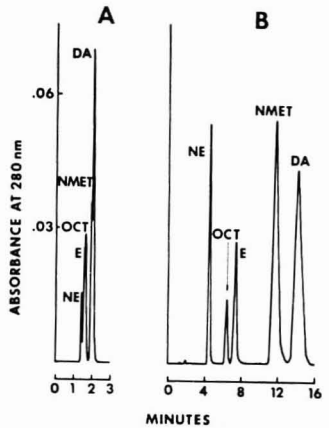

Figure 2. Chromatograms illustrating the effect of ion-pair formation with *n*-octylsulfate in the eluent on the separation of catecholamines by reversed-phase chromatography. Column, 5 μm LIChrosorb RP18; flow rate, 2.0 mL/min; temp., 70 °C; inlet pressure, 2200 psi. Eluents: A, 5×10^{-2} M phosphate in water, pH 2.2; B, 5×10^{-2} M phosphate and 3×10^{-3} M octylsulfate in water, pH 2.2

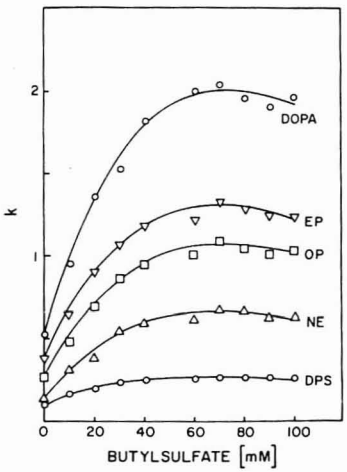

Figure 3. Dependence of the capacity factor of protonated catechol amine derivatives on the concentration of *n*-butylsulfate in the eluent. Column, 10 μm Partisil ODS; flow rate, 2.0 mL/min; temp., 40 °C; inlet pressure, 400 psi; eluent, 5×10^2 M phosphate in water, pH 2.55, containing various concentrations of the hetaeron

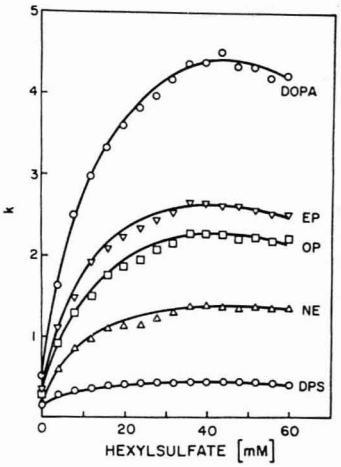

Figure 4. Dependence of the capacity factor of charged catecholamine derivatives on the concentration of *n*-hexylsulfate in the neat aqueous mobile phase. Conditions are given in Figure 3

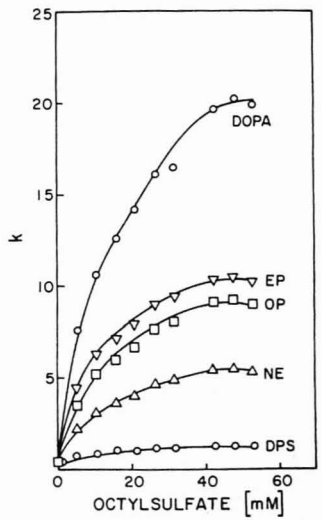

Figure 5. Dependence of the capacity factor of charged catecholamine derivatives on the concentration of *n*-octylsulfate in the neat aqueous mobile phase. Conditions are given in Figure 3

influence on the retention of the eluites, experiments were carried out in a wide range of conditions in order to shed light on the chromatographic process in view of the preceding theoretical anaysis. In addition to alkylsulfates of different chain lengths, hexylsulfonate as well as butyl- and amylphosphates were also employed.

Equation 13 predicts that the observed capacity factor will initially increase with increasing hetaeron concentration followed by a monotonic decrease at high hetaeron concentrations. However, if over the experimentally accessible range of hetaeron concentrations, either the binding of hetaeron to the stationary phase, $K_3[H]$, or the extent of ion-pair formation in the mobile phase, $K_2[H]$, is negligible, the capacity factor can be expressed by Equation 14. In this case the capacity factor first rises and eventually becomes practically independent of the hetaeron concentration. Therefore, if Equation 14 holds over the experimental range of hetaeron concentration, a plot of k vs. $[H]$ yields a rectangular hyperbola.

The capacity factor of four catecholamines and the amino acid, 3,4-dihydroxyphenylserine, as a function of the concentration of various *n*-alkyl sulfates in the eluent is shown

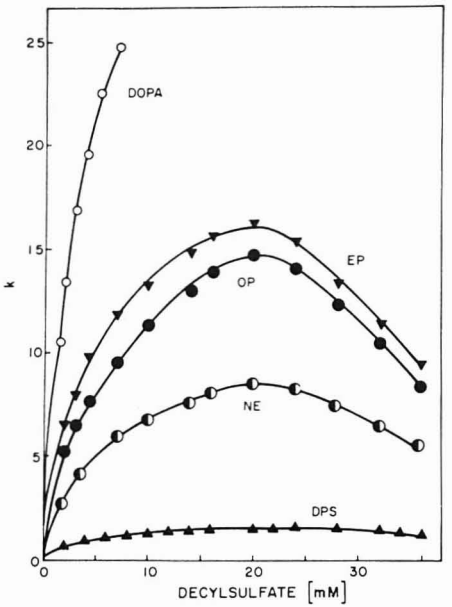

Figure 6. Dependence of the capacity factor of charged catecholamine derivatives on the concentration of *n*-decylsulfate in the neat aqueous mobile phase. Conditions are given in Figure 3

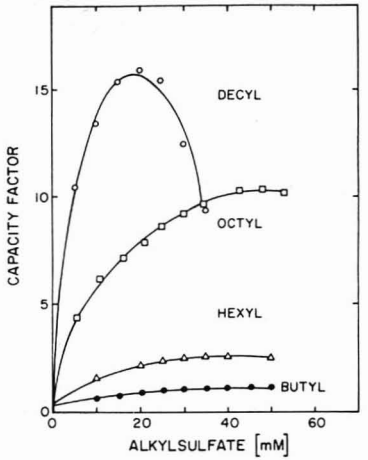

Figure 7. Plots of the capacity factor of adrenaline vs. the hetaeron concentration for various *n*-alkylsulfates. Conditions are given in Figure 3

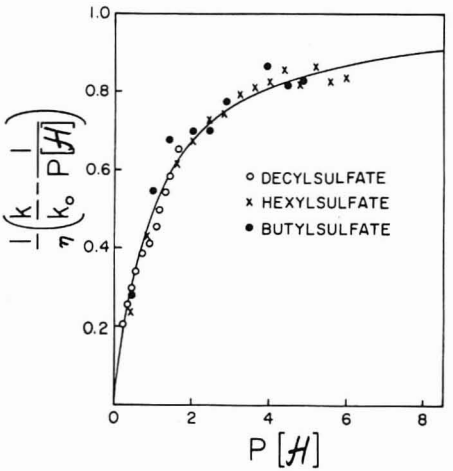

Figure 8. Normalized plot of the capacity factor data obtained for dopamine using three different *n*-alkyl sulfates as the hetaerons. The theoretical curve calculated from Equation 41 is given by the solid line. The data were obtained under conditions described in Figure 3

in Figures 3–6. The alkyl chain of the hetaerons ranges from butyl to decyl groups and the upper limit of the concentration range was usually determined by the solubility of the hetaeron in the neat aqueous eluent.

Inspection of the data shows that with butyl-, hexyl-, and decylsulfates the capacity factor in most cases rises with increasing hetaeron concentration to a constant value from which it does not decline significantly. On the other hand when decylsulfate is used, the capacity factor increases to a maximum from which it rapidly decreases with further increase in the hetaeron concentration. Thus, the qualitative predictions are supported by the data as is also illustrated by the dependence of the capacity factor of adrenaline on the concentration of the hetaerons in Figure 7.

In order to test the validity of Equations 13 and 14, the data shown in Figures 3–6 were analyzed by a least-square fit. The data obtained using butyl-, hexyl-, and octylsulfates did not converge by using Equation 13 but they did fit Equation 14. On the other hand, the data obtained using decylsulfate could be well fitted to Equation 13, whereas the fit to Equation 14, was very poor.

The quality of the fit can be illustrated by a generalized plot of the data. Equation 14 is divided by k_0, the expression can be rearranged to obtain

$$(k/k_0\eta) - [1/\eta(1 + P[H])] = P[H]/(1 + P[H]) \quad (36)$$

The RHS of Equation 36 represents a normalized capacity factor corrected for the effect of unconjugated eluite binding. When it is plotted against the normalized hetaeron concentration, $P[H]$, a rectangular hyperbola should be obtained. Such a plot of data obtained with butylsulfate, hexylsulfate, and decylsulfate as hetaerons and DOPA as the eluite is shown in Figure 8. In the case of other acidic hetaerons such as hexylsulfonate, butyl- and amylphosphates in neat aqueous eluents, the relationship between the capacity factors measured with these eluites and the hetaeron concentration was found to conform well to Equation 13.

We noted in the theoretical section that the dependence of the capacity factor on the hetaeron concentration alone does not shed light on the actual mechanism of the process. However, as one changes from one hetaeron to another, both representing the same type of compounds, predictions of the effect on the capacity factor can be made by recourse to solvophobic theory as shown in Tables I and II. If ion-pair formation occurs in the mobile phase, the enhancement factor will depend strongly on the hydrophobic area of the hetaeron

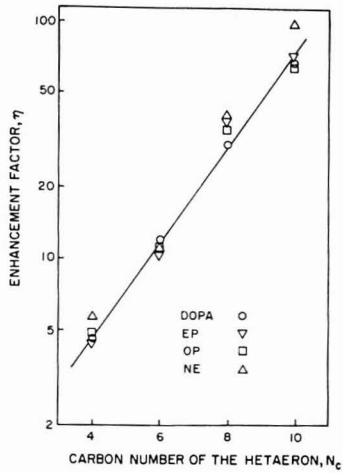

Figure 9. The dependence of the enhancement factor of catecholamine derivatives on the carbon number of *n*-alkyl sulfates as the hetaerons. The straight line obtained by least squares analysis fits the expression, $\log \eta = 0.225\ (\pm 0.0317)\ N_c$, where η is the enhancement factor and N_c is the carbon number. The intercept is zero within experimental error

and the charge of eluite but it will be independent of the size of the eluite. On the other hand, if ion-pair formation occurs on the stationary phase, i.e., in the case of the ion-exchange mechanism, the enhancement factor will depend on the charge of the hetaeron and the charge and size of the eluite.

The predictions based on the solvophobic treatment of chromatographic retention support the concept that in our experiments soap chromatography proceeds through the formation of ion-pairs in the mobile phase followed by adsorption onto the nonpolar stationary phase. The logarithm of the enhancement factor evaluated with the least-squares parameters of Equation 14 is linear in the carbon number of the hetaeron and largely independent of the size of the eluite as illustrated in Figure 9. This is predicted for the ion-pairing mechanism according to Equation 35, whereas no dependence on the hetaeron size but a dependence on the molecular area of the eluite is expected for the ion-exchange mechanism. The constant P of Equation 14 should be equal to K_2 and independent of hetaeron size in the ion-pair mechanism but will depend upon the charge of both eluite and hetaeron. It will also be dependent upon the charge type since the distance of closest approach of the two ions is implicitly included in the function $f(Z_E Z_H)$ in Equation 25 and 26.

The mean values of the pertinent parameters as obtained by least squares analysis are shown in Table III. The standard deviation of the values is also indicated. The capacity factor of the eluite in the absence of hetaeron, k_0, is not shown because it is not a property of the hetaeron. It is seen from the data in Table III that the enhancement factors are fairly independent of the eluite, but they strongly depend and, in fact, increase exponentially with the carbon number of the hetaeron in agreement with the data shown in Figure 9. The only exception to this rule is 3,4-dihydroxyphenylserine which was not entirely in the cationic form at the eluent pH employed. However, we can estimate the enhancement factor of the cationic form by using Equation 19. Assuming a value of 2.8 for K_1^0/K_1 on the basis of data obtained with similar eluites in a previous work (2), we obtain corrected enhancement factors for the amino acid which fall into the range of η shown in Table III for the fully protonated amines.

Table III. List of the Parameters of Equation 13 and the Enhancement Factors as Evaluated from Experimental Data Obtained at Various Hetaeron Concentrations in the Mobile Phase on Octadecyl-Silica Column. The Eluites Were the Same as Those in Figures 3–7

Hetaeron	$K_2[M]^{-1}$, Ion-pair formation constant	$K_3[M]^{-1}$, Hetaeron binding constant	$\eta = B/k_0K_2$, Enhancement factor
Alkyl sulfates			
Butyl	46 ± 3	...	4.9 ± 0.6
Hexyl	107 ± 8	...	11.1 ± 0.6
Octyl	68 ± 10	...	36.6 ± 3.8
Decyl	125 ± 40	12	104 ± 30
Hexylsulfonate	68 ± 3	...	12.1 ± 1.3
Alkyl phosphates			
Butyl	270 ± 77	...	6 ± 1.4
Amyl	341 ± 72	...	15.5 ± 3.7

On the other hand, in the ion-exchange mechanism, the constant P will depend upon the charge of the hetaeron and the size of the hetaeron. Even though the experimentally determined value of P ranges widely, it is apparent from an inspection of the data for the alkyl sulfates in Table III that the value of P does not depend upon hetaeron size in a strong fashion, if at all. If we consider the data obtained with hetaerons other than alkyl sulfates, this conclusion is reinforced. The value of the enhancement factor for hexylsulfonic acid is virtually identical to that for hexylsulfate in accord with their identical carbon numbers.

The results of the preceding analysis can be sustained without an explicit dependence on the solvophobic theory. In interactions between ionized species, one expects the magnitude of the effect to be determined by the charges on the species. On the other hand, retention by the hydrocarbonaceous stationary phase should depend upon the "hydrophobicity" of the species, i.e. on the carbon number or some related parameter. As a consequence, we expect the parameter P of Equation 14 to depend upon the charge and not the size of the hetaeron if ion-pair formation occurs in the mobile phase, whereas in the dynamic ion-exchange a strong size-dependence would be expected. The enhancement factor for ion-pairing depends upon the difference between the carbon number of the hetaeron–eluite complex and the carbon number of the eluite, since the ratio K_4/K_1 depends upon two binding constants. On the other hand the enhancement factor for ion-exchange would depend upon the ratio K_5/K_1 which corresponds to the process of ion-pairing in the stationary phase and eluite binding. As a consequence, the only hetaeron property affecting this ratio would be the charge.

The Enhancement Factor. As shown above, the enhancement factor may be justifiably regarded as a property peculiar to the hetaeron and largely independent of eluite properties. This conclusion is supported by both experimental results and theoretical considerations. As a consequence, it may be used as a guide to hetaeron selection or to extract information about the eluite which is otherwise experimentally inaccessible. In the following development, it is assumed that chromatographic experiments are carried out in the range of hetaeron concentration where the capacity factor is at the maximum or in the plateau region of the saturation curves where the effect of the hetaeron on the retention is the greatest. The advantage of working at saturation concentration is that the capacity factors are least sensitive to small errors in hetaeron concentration. On the other hand an error in the hetaeron concentration can generate a large error in the capacity factor at low hetaeron concentrations where the curve is almost linear. The capacity factor obtained with a

given hetaeron at the saturation level may be too great or too small or the eluite–hetaeron complex may elute together with another species whose retention is unaffected by the hetaeron under such conditions. The retention of the complex may be affected by choosing another hetaeron with a shorter or longer aliphatic sidechain, respectively, rather than by changing the hetaeron concentration.

By use of the enhancement factor, determined in an appropriate solvent system, one can readily calculate the effect of the alkyl chain length of the hetaeron upon the capacity factor of the eluite complex. In the example of the alkyl sulfates examined here in water, the effect of two additional carbons is to increase the capacity factor by a factor of 2.5. Thus, increasing or decreasing the carbon number of the alkyl chain can shift the capacity factor into the usually favored range of 1–10.

The analysis of the enhancement factor also allows the effect of simultaneously using two hetaerons of the same kind but having different chain lengths to be explicated. If the mobile phase contains two such hetaerons of equal concentration, the capacity factor is the arithmetic mean of the capacity factors which are obtained when the two are used alone at the same total molar concentration. On the other hand from the data shown in Figure 9 it follows that the capacity factor of a hetaeron, which has the arithmetic mean alkyl chain length of the two hetaerons, is given by the geometric mean of their capacity factors. If the chain lengths of the two hetaerons are not too different, the arithmetic and geometric mean capacity factors are about the same. For example, a 1:1 mixture of hexyl- and octylsulfates would have an enhancement factor of 24, whereas heptylsulfate at the same total hetaeron concentration would show an enhancement of 20. Therefore, a safe rule of thumb is that at the same molar concentration a mixture of hetaerons has the same capacity factor as that of a hetaeron which has their mean chain length.

In many cases it is difficult to obtain precise values for the capacity factors of eluites poorly retarded in the absence of a hetaeron. However, it may be desirable to determine the value of these capacity factors in physicochemical measurements. If the enhancement factor is available from experiments, the capacity factor in the absence of hetaeron can be estimated as the quotient of the observed capacity factor to the enhancement factor. Alternatively, an equivalent calculation is

$$k_0 \approx kk_{0,R}/k_R \tag{37}$$

where k_0 is the capacity factor in the absence of hetaeron, $k_{0,R}$ is the capacity factor of a reference eluite obtained in the absence of hetaeron, and k and k_R are the observed capacity factors of the test and reference eluite in the presence of hetaeron.

Depletion of Hetaeron. In one case we have observed a sigmoidal dependence of the capacity factors on the hetaeron concentration as shown in Figure 10. Under the conditions of the experiment, the concentration of dodecysulfate, which is sparingly soluble in aqueous salt solutions, was below the concentration range used in this study for the other alkylsulfates having relatively short hydrocarbon chains.

The observed behavior can readily be explained by a break-down of the theoretical model at sufficiently low hetaeron concentrations. When the concentrations of the hetaeron and eluite are commensurable, a significant fraction of the hetaeron can be complexed so that the total hetaeron concentration in the mobile phase is not conserved, i.e., the assumption stated in Equation 8 is not fulfilled. The nonlinearity arising from a depletion of the dodecylsulfate ions by the eluites at very low hetaeron concentrations can be responsible for the observed sigmoidal behavior.

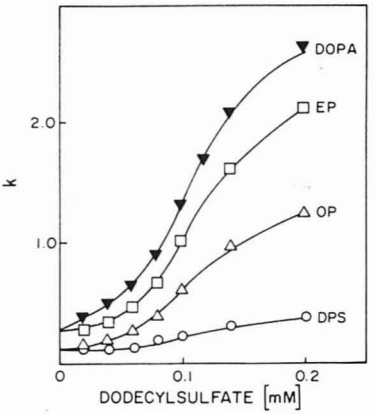

Figure 10. Plots of the capacity factors of catecholamine derivatives against the concentration of *n*-dodecylsulfate as the hetaeron. Conditions are stated in Figure 3

Salt Effects. If salt is added to the eluent, the model shown in Figure 1 can be extended by the equilibria related to the salt–eluite complex. In general, added salts would tend to reduce the capacity factor because they would compete with the hetaeron in forming ion-pairs with the eluite. Equation 10 can be modified in order to take into account salt competition in the calculation of the capacity factor as follows:

$$k = \phi[\mathrm{L}](K_1 + K_2K_4[H] + K_7K_8[\mathrm{S}])/(1 + K_7[\mathrm{S}] + K_2[H]) \tag{38}$$

where K_7 is the equilibrium constant for the formation of salt–eluite complexes, K_8 is the binding constant of the complex to the stationary phase, and [S] is the salt concentration. The values of K_7 and K_8 are unknown. We can estimate, on the basis of the change in capacity factor of acids upon ionization, that $K_8/K_1 \approx 3.5$ (2). Since in the case of the hydrophobic hetaerons investigated the capacity factor is much greater than this value, according to Equation 38, the capacity factor is expected to fall precipitously with addition of salts until it descends to a value which is unaffected by the addition of more salts. Data obtained with several eluites and the use of decylsufate as the hetaeron are shown in Figure 11, where the capacity factor is plotted as a function of $(NH_4)_2SO_4$ concentration. As expected from Equation 38 and the above discussion, the capacity factors rapidly decrease with the salt concentration. However, the capacity factor at high salt concentrations does not reach a constant value but increases somewhat. The increase of retention on nonpolar stationary phases with increasing salt concentration has already been observed and explained in the rubric of the solvophobic theory by the increase in the surface tension of the mobile phase (2, 10). In a rigorous treatment, each term of Equation 38 should be treated for ionic strength effects by an expression which has been used previously, Equation 20 in Ref. (2) and can be written as

$$\ln K = \ln K^0 + \alpha[BI^{1/3} + CI) + \beta I \tag{39}$$

where B, C, α, and β are constants, I is the ionic strength, and K and K^0 are the equilibrium constants in the presence and absence of salt, respectively. However, at high salt and hetaeron concentrations we can assume that practically only

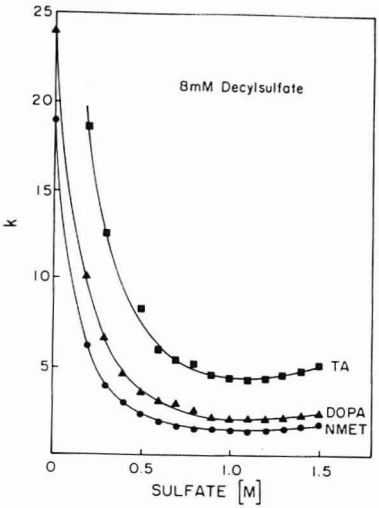

Figure 11. Effect of salt on the retention in ion-pair reversed phase chromatography with 8×10^{-3} M *n*-decylsulfate in the neat aqueous eluent. The chromatographic conditions are the same as those described in Figure 3 except that in addition various concentrations of Na_2SO_4 were used in the eluent

neutral complexes bind and, as a consequence, the expression can be rewritten as

$$\ln K = \ln K^0 + \beta' I \tag{40}$$

where

$$\beta' = \beta + \alpha C \tag{41}$$

Since the value of β' is practically constant for different eluites (*2*) Equation 38 can be rewritten as

$$k = \phi[\mathrm{L}][(1 + K_2K_4[H] + K_7K_8[\mathrm{S}])/(1 + K_7[\mathrm{S}] + K_2[H])] \exp(\beta' I) \tag{42}$$

The inspection of Figure 11 shows that the data conform to this expression.

The addition of inorganic acids such as H_2SO_4 and H_3PO_4 to the eluent has been observed to have an effect similar to that of added salt in agreement with the findings of others (*5*). The decrease in the capacity factors can be readily explained by the competition between the organic and inorganic anions to form ion-pairs with the eluites. At sufficiently high concentrations, however, a strong inorganic acid may also reduce the degree of dissociation of the hetaeron acid, and thereby further diminish retention. Of course, if such a hetaeron would be used for the separation of basic eluites at an eluent pH where they are partially or fully undissociated, the addition of an acid first would result in a reduction of pH and a concommitant protonation of the eluites. Under such conditions the observed capacity factors would increase as expressed by Equation 19 before a decrease occurs upon further increasing the acid concentration.

Nature of the Hetaeron. Among the anionic hetaerons investigated, the use of alkyl sulfates and sulfonates is the most convenient according to our experience. As shown previously, commercially available compounds can provide a sufficiently broad scale of enhancement factors to meet the requirements in chromatographic practice.

The alkyl phosphates used were mixtures of the corresponding mono- and dialkyl derivatives. These substances have a very low solubility in water but they can be used in hydro-organic eluents. Nevertheless we have not observed in our chromatographic system any specific effect which would warrant the use of such hetaerons over that of alkyl sulfates or sulfonates.

A number of experiments were carried out with perfluorooctanoic and decanoic acids. The enhancement factors of these hetaerons, which are almost fully dissociated above pH 2, were estimated to be commensurable to those obtained with alkyl sulfates having the same chain length. An accurate evaluation of the properties of the perfluorated hetaerons, however, was not possible because of an instability of the chromatographic system which gave rise to poor reproducibility. We cannot close out the possibility that the mechanism of retention with such bulky and highly hydrophobic hetaerons would involve dynamic ion exchange rather than ion pairing in the mobile phase. It should be emphasized, therefore, that the conclusions from the experimental data obtained with alkyl sulfates and similar compounds, together with the predictions therefrom, may not be applicable to ion-pairing agents of greatly different chemical makeup. On the other hand, alkyl sulfonates and sulfates enjoy great popularity in ion-pair reversed phase chromatography so that the results can be of wide interest.

Hydro-organic Eluents. The effect of an organic solvent in eluents containing the hetaerons investigated can be estimated in a general fashion. The predictions are based on our knowledge of the behavior of the individual terms in Equation 11 upon the dielectric properties of the medium. The effect of the organic solvent is qualitatively illustrated in Figure 12, where the solid curve represents the dependence of the capacity factor on the hetaeron concentration in neat aqueous eluents. When an organic solvent is added to the eluent, the relationship is modified as shown by the dashed curve. At low hetaeron concentrations, the increase in capacity factor with increasing hetaeron concentration is expected to be greater in the hydro-organic mixture than in the neat aqueous eluent. According to Equation 11, the rise of k in this domain is determined by the stability constant for ion-pair formation, K_2, whose magnitude increases with decreasing dielectric constant of the medium. Hence, the addition of organic components, and the attendent depression of the dielectric constant of the eluent, causes the left side of the curve to shift to the left.

The magnitude of the change as a function of the organic solvent concentration in the eluent is illustrated in Figure 13 for methanol and acetonitrile. The dependence of K_2 on the medium dielectric has been estimated using the Born approximation for the energy of an ion in solution which is given by

$$K_2 = A \exp(-2Z_1Z_2e^2/a\epsilon kT) \tag{43}$$

where Z_1 and Z_2 are the charges of the ions, e is the charge of the electron, a is the radius, ϵ is the dielectric constant of the medium, and A is a preexponential. The results illustrated in Figure 13 show the maximum change in K_2 one would expect due to solvent variation on the basis of Equation 43. With acetonitrile of methanol as solvent, the ion pair formation constant, K_2, may be enhanced by three orders of magnitude with respect to the value in neat aqueous medium, K_2^0. Similar results can be expected with other solvents of chromatographic interest.

On the other hand the value of the capacity factor at the maximum or plateau region of the curve is expected to decrease as shown in Figure 13. According to Equation 11, the saturation value of k is determined by the association constant

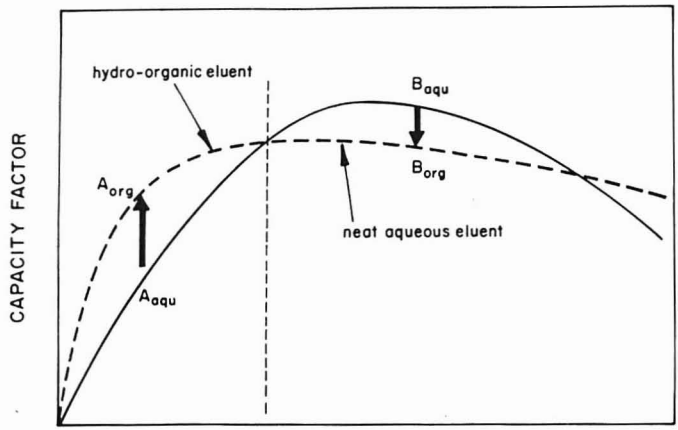

Figure 12. Schematic illustration of the effect obtained when instead of neat aqueous eluent a hydro-organic mixture is used in ion-pair reversed-phase chromatography

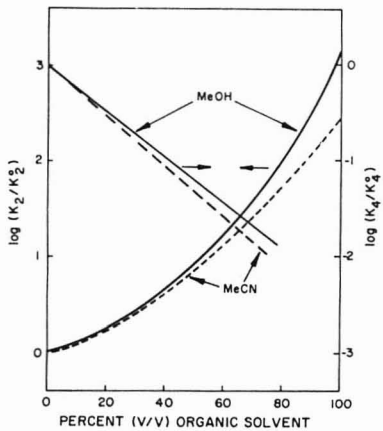

Figure 13. Variation of the normalized stability constant, K_2/K_2^0, of the ion-pair and that of the normalized binding constant K_4/K_4^0, of the complex with the organic solvent content of the eluent in ion-pair reversed-phase chromatography. The equilibrium constants K_2^0 and K_4^0 are obtained with neat aqueous eluents under otherwise identical conditions. The dielectric constants for water–methanol and water–acetonitrile mixtures were taken from Åkerlof (*15*) and Douhéret and Morénas (*16*), respectively. The dependence of the normalized binding constant on the solvent composition is taken from various sources (*10*, *17*, *18*)

for the hetaeron–eluite complex and the ligand of the stationary phase, K_4. The magnitude of this term is primarily determined, in the hermeneutics of the solvophobic theory, by the surface tension of the mobile phase and the eluite surface area. As the addition of an organic solvent reduces the surface tension of the eluent, this term is also reduced in magnitude. In fact, properties other than the surface tension are also involved but the chief effects come from the surface tension and a closely related solvent property as discussed in previous work (*10*). The constant K_3 in Equation 11 is the association constant of the hetaeron and the hydrocarbonaceous ligand. Therefore, it is affected by the organic solvent in a similar way, i.e., K_3 also decreases with added organic component. The effect of organic solvent concentration on K_3 or K_4 can be estimated on the basis of prior results (*10*, *17*, *18*) and is shown for K_4 in Figure 13. It is seen that with methanol or acetonitrile as cosolvents with water, the binding constant of the hetaeron to the stationary phase, K_4 (or the maximum capacity factor) may be reduced as much as two or three orders of magnitude with respect to the corresponding value, K_4^0, in neat aqueous eluent.

The result of these effects is that the capacity factor vs. hetaeron concentration curve will be broadened and flattened. This analysis implies that quite contradictory observations can be made with regard to the effect of the added organic solvent on retention in this type of chromatography. If, with neat aqueous eluents, one is operating in the quasilinear portion of the curve, marked A_{aqu}, the effect of the organic component will be to enhance the retention because a larger fraction of the eluite will be complexed by the hetaeron and the capacity factor will change from A_{aqu} to A_{org}. On the other hand, in the plateau region an addition of organic component will cause a decrease in the capacity factor for the reasons already adduced. This is illustrated schematically by the shift of point B_{aqu} to B_{org} in Figure 12. At higher hetaeron concentration levels, it is even possible to enhance the retention by increasing the organic solvent concentration. It should be noted that this analysis assumes that the retention is achieved primarily by the ion-pair mechanism. If the ion-exchange mechanism predominates, a different set of predictions will hold. In general, the curve will become narrower and the maximum may become greater. The effect depends upon the relative magnitudes of the two association constants.

Possibility of Dynamic Ion-Exchange. Whereas the analysis of our experimental data clearly shows that chromatographic retention is enhanced by ion-pair formation in the mobile phase and subsequent binding of the complex to the nonpolar stationary phase, dynamic ion-exchange can be the underlying mechanism under some other conditions as has been pointed out earlier.

With alkyl sulfates, the mechanism may be expected to change when the size of the hetaeron increases which results in an increase in its binding constant, K_3. An arbitrary but reasonable definition of the point where the mechanism changes from ion-pairing in the mobile phase to ion-exchange or vice versa is where K_3 is equal to the ion-pair formation constant, K_2. Given that the enhancement factor increases by a factor of 2.5 per ethylene group, a change in mechanism in neat aqueous solutions is expected to occur when the number of carbon atoms in the aliphatic chain is 14 or greater because with such very hydrophobic hetaerons the value of K_2 approaches that of K_3. However, such a situation is difficult to observe experimentally because of the low solubility of long-chain alkyl sulfates. In practice such long-chain species would be used with hydro-organic eluents and under such conditions the various terms are expected to change differently with respect to the neat aqueous solvent. If one considers 50% methanol/water as a "typical" eluent and uses the same criterion for the change in the mechanism, i.e., the ion-pair formation constant equals the hetaeron binding constant, one finds upon recourse to Figure 13 and the data in Table I that the mechanism will be essentially the same as in a neat aqueous eluent unless the carbon number of the hetaeron exceeds 22. This calculation is necessarily crude but it does suggest that in most normally encountered situations with alkyl sulfates or sulfonates the dominant mechanism of "soap" chromatography will be via ion-pairing in the mobile phase.

However, it must be pointed out that a rapid change of mechanism is to be expected with increased molecular size with certain other hetaerons, e.g., with tetraalkylammonium ions of formula R_4N^+. As the number of methylene groups in the alkyl chains increases, the ion-pair formation as measured by K_2 will decrease because the distance between charge centers increases, cf. Equation 43. On the other hand the hetaeron binding constant, K_3, will increase with the chain length since the hydrophobic surface area of the hetaeron increases. As a consequence, the change of mechanism from ion-pairing in the mobile phase to dynamic ion-exchange will be more rapid with increasing size of the hetaeron when the charged group is in the center of the molecule rather than in the ω-position as in the case of alkyl sulfates and sulfonates. A rough calculation, similar to those given in the preceding analyses, indicates that in neat aqueous eluents the onset of dynamic ion-exchange occurs when the hetaeron is changed from tetrapropylammonium to tetrabutylammonium salts.

Since the introduction of ion-pair chromatography for the separation of organic compounds by Horvath and Lipsky in 1966 (*19*), column chromatography with ion-pairing agents present in the liquid stationary phase has been widely used and investigated from the mechanistic point of view (*20–26*). The results obtained in this type of partition chromatography have usually been interpreted by using an extraction model. The predicted linear dependence of the capacity factor on the concentration of the complexing agent, however, was not strictly observed and secondary equilibria have been invoked in order to explain the results.

In ion-pair reversed-phase chromatography, the complexing agent is present in the mobile phase; consequently, the physico-chemical phenomena involved in the separation process are significantly different from those which govern chromatographic retention when a "liquid ion-exchanger" is used as the stationary phase. Therefore, the two techniques have to be clearly distinguished. With suitable bonded phases, ion-pair reversed-phase chromatography offers numerous advantages as far as the versatility of the technique is concerned (*27*). It can greatly expand the scope of reversed-phase chromatography, which has already become the most popular type of high performance liquid chromatography (*27*).

ACKNOWLEDGMENT

We are grateful to Glenn Laub, a participant in the Summer Research Program of the Department of Engineering and Applied Science for writing the computer program and performing the least-squares analysis.

LITERATURE CITED

(1) B. L. Karger, L. R. Snyder, and C. Horvath, "An Introduction to Separation Science", Wiley, New York, N.Y., 1973, pp 28–30.
(2) C. Horvath, W. Melander, and I. Molnar, *Anal. Chem.* **49**, 142 (1977).
(3) D. P. Wittmer, N. O. Nuessle, and W. G. Haney, Jr., *Anal. Chem.*, **47**, 1422 (1975).
(4) J. H. Knox and G. R. Laird, *J. Chromatogr.*, **122**, 17 (1976).
(5) J. H. Knox and J. Jurand, *J. Chromatogr.*, **125**, 89 (1976).
(6) J. H. Knox and J. Jurand, *J. Chromatogr.*, **103**, 311 (1975).
(7) C. Horvath, and W. Melander, *J. Chromatogr. Sci.*, **15**, 393 (1977).
(8) C. Tanford, "The Hydrophobic Effect", Wiley-Interscience, New York, N.Y., 1973.
(9) O. Sinanoğlu, "Molecular Associations in Biology", B. Pullmann, Ed., Academic Press, New York, N.Y., 1968, pp 427–445.
(10) C. Horvath, W. Melander, and I. Molnar, *J. Chromatogr.*, **125**, 129 (1976).
(11) P. T. Kissinger, *Anal. Chem.*, **49**, 883 (1977).
(12) O. Sinanoğlu and S. Abdulnur, *Fed. Proc.*, **24** (2), 12 (1965).
(13) T. Halicioğlu and O. Sinanoğlu, *Ann. N.Y. Acad. Sci.*, **158**, 308 (1969).
(14) C. Horvath, *Methods Biochem. Anal.*, **21**, 79 (1973).
(15) G. Åkerlof, *J. Am. Chem. Soc.*, **54**, 4125 (1932).
(16) G. Douhéret and M. Morênas, *C.R. Acad. Hebd. Seances Acad. Sci., Ser. C*, **264**, 729 (1967).
(17) S. R. Abbott, J. R. Berg, P. Achener, and R. L. Stevenson, *J. Chromatogr.*, **126**, 421 (1973).
(18) B. L. Karger, J. R. Gant, A. Hartkopf, and P. H. Weiner, *J. Chromatogr.*, **128**, 65 (1976).
(19) C. Horvath and S. R. Lipsky, *Nature (London)*, **211**, 748 (1966).
(20) S. Eksborg, P. O. Lagerström, R. Modin, and G. Schill, *J. Chromatogr.*, **83**, 99 (1973).
(21) S. Eksborg and G. Schill, *Anal. Chem.*, **45**, 2092 (1973).
(22) J. C. Kraak and J. F. K. Huber, *J. Chromatogr.*, **102**, 333 (1974).
(23) B. L. Karger, S. C. Su, S. Marchese, and B. A. Persson, *J. Chromatogr. Sci.*, **12**, 678 (1974).
(24) B. A. Persson and B. L. Karger, *J. Chromatogr. Sci.*, **12**, 521 (1974).
(25) B. Fransson, K. G. Wahlund, I. M. Johansson, and G. Schill, *J. Chromatogr.*, **125**, 327 (1976).
(26) S. C. Su, A. V. Hartkopf, and B. L. Karger, *J. Chromatogr.*, **119**, 523 (1976).
(27) R. Gloor and E. Johnson, *J. Chromatogr. Sci.*, **15**, 413 (1977).

RECEIVED for review August 1, 1977. Accepted September 29, 1977. This work was supported by grants No. GM 20993 and GM 22735 from the National Institutes of Health, U.S. Public Health Service. This paper was presented in part at the 173rd National Meeting of the American Chemical Society, New Orleans, La., March 1977.

Chemically-Bonded Aminosilane Stationary Phase for the High-Performance Liquid Chromatographic Separation of Polynuclear Aromatic Compounds

S. A. Wise,* S. N. Chesler, H. S. Hertz, L. R. Hilpert, and W. E. May

Institute for Materials Research, Analytical Chemistry Division, National Bureau of Standards, Washington, D.C. 20234

A commercially available, chemically-bonded aminosilane liquid chromatographic packing material, μBondapak NH_2, was used as a substitute for silica or alumina for the normal-phase high-performance liquid chromatographic (HPLC) separation of aliphatic hydrocarbons and polynuclear aromatic compounds. The μBondapak NH_2 provides a more distinct separation of polynuclear aromatic compounds based on the number of condensed rings than the classical adsorbents because the addition of alkyl groups to the aromatic rings has very little effect on their retention. The retention characteristics of polynuclear aromatic compounds on μBondapak NH_2, classical adsorbents, and a reversed-phase packing material were compared. The application of μBondapak NH_2 to isolate polynuclear aromatic compounds according to the number of condensed rings prior to analysis by gas chromatography–mass spectrometry (GC-MS) and/or reversed-phase HPLC with fluorescence emission spectral identification is described.

A large number of laboratories are currently involved in the analysis of hydrocarbons in the environment. In the past, research has focused primarily on the determination of the low molecular weight (less than 300) aliphatic and olefinic hydrocarbons because of their relative ease of analysis by gas chromatography (GC). Of more recent interest are the polynuclear aromatic hydrocarbons (PAHs) because of their possible carcinogenic and mutagenic properties. The current increasing use of fossil fuels and the potential use of liquified coal and shale oil require the development of meaningful analytical methodologies for the determination of PAHs in the environment. Fossil fuels contain a wide range of aromatic hydrocarbons with the alkylated PAHs generally being more abundant than the unsubstituted parent PAHs (*1*). Soils and recent sediments from presumably unpolluted environments have also been reported to contain series of alkylated aromatics (*2*). The complexity of such samples necessitates the combination of several chromatographic techniques to achieve suitable separations.

The typical analytical scheme for hydrocarbon analysis in environmental samples involves extraction, fractionation of aliphatic and aromatic hydrocarbons by column chromatography on silica and/or alumina, and finally quantitative and qualitative analysis by GC and GC-MS. Several problems are encountered when using classical adsorbents such as silica or alumina. For example, the retention characteristics of these adsorbents with nonpolar mobile phases are strongly influenced by the water content of the eluent. Thus, small changes in the water content of the eluent result in nonreproducible separations (*3*, *4*). In addition, the high adsorptivity of the classical adsorbents can result in the loss of trace components and the tailing of late-eluting components. These difficulties make the use of silica or alumina for routine fractionation of PAHs unreliable.

Recently, Giger and Blumer (*5*) described an analytical procedure for isolating PAHs which utilized gel filtration on Sephadex LH-20, adsorption chromatography on silica gel–alumina, and charge-transfer complexation. Novotny et al. (*6–8*) employed Sephadex LH-20 for purification and bulk separations, but utilized a polar, chemically-bonded stationary phase (oxypropionitrile) instead of adsorption chromatography for further fractionation of the PAHs prior to GC-MS analysis. Other workers (*9*, *10*) have described the combination of adsorption or gel chromatography and reversed-phase HPLC to resolve complex mixtures.

Recent work in this laboratory has involved the use of μBondapak NH_2, a polar chemically-bonded stationary phase, as a substitute for silica to remove interfering polar compounds in the analysis of hydrocarbons in marine biota (*11*). In the present paper the retention characteristics of μBondapak NH_2 and a reversed-phase HPLC material for aromatic hydrocarbons are compared with literature data on retention by classical adsorbents. In addition, the use of μBondapak NH_2 to fractionate PAHs which were extracted from a marine sediment is reported. The μBondapak NH_2 yielded separations according to the number of condensed rings. Each PAH fraction was subsequently analyzed by reversed-phase HPLC to separate the alkyl homologues within each fraction. Fluorescence emission spectroscopy and GC-MS were utilized for identification of the individual components. The application of μBondapak NH_2 for bulk fractionation of PAHs in crude oil prior to analysis by GC-MS is also described.

EXPERIMENTAL

Column Comparison. The retention characteristics of μBondapak NH_2 and μBondapak C_{18} for a number of aromatic hydrocarbons were determined. Hexane was used as the mobile phase for the μBondapak NH_2 and mixtures of 50–70% acetonitrile in water were used for the μBondapak C_{18}.

Marine Sediment Sample. An extract of a petroleum-contaminated sediment was obtained by ultrasonic agitation (~2 h) of the sediment (990 g) with ether. The extract was concentrated by evaporation, diluted with freshly distilled pentane, and gently heated to remove the remaining ether. The pentane solution was concentrated to approximately 1 mL, and the latter was injected onto a 30 cm × 4 mm i.d. μBondapak NH_2 column (Waters Associates, Milford, Mass.). The PAHs were eluted using freshly distilled pentane as the mobile phase. A small volume of acetonitrile was added to the PAH fractions and the pentane removed by evaporation. The concentrated fractions were analyzed by reversed-phase HPLC on a 30 cm × 4 mm i.d. μBondapak C_{18} column utilizing a linear gradient of 50–100% acetonitrile in water in 30 min. The column effluent was monitored with a UV absorption detector at 254 nm (Waters Associates, Milford, Mass.) and a fluorescence spectrophotometer (Model FP-4, JASCO Incorporated, Easton, Md.) in series. The fluorescence spectrophotometer had been previously modified by decreasing the slits of the excitation monochromator and increasing the cell volume from 9 to 36 μL (*12*). In order to obtain a fluorescence emission spectrum on an eluting component, the mobile phase flow was diverted (by means of a valve) at the maximum fluorescence response, thereby leaving the peak sample trapped in the flow cell. This procedure allowed continuous monitoring of the chromatogram with the UV absorption detector while scanning to obtain the fluorescence emission spectrum of the component trapped in the fluorescence spectrophotometer flow cell.

Table I. Comparison of Retention Indices (I) of Aromatic Hydrocarbons on Several Liquid Chromatographic Packing Materials

Compounds	Logarithm of the retention index (log I)				
	μBondapak NH_2 (hexane)[a]	Silica (*13*) (pentane)	Alumina (*14*) (pentane)	Polystyrene gel (*15*) (water–methanol–diethylether)	μBondapak C_{18} (aceto-nitrile–water)
One-ring aromatics					
Benzene	1.00	1.00	1.00	1.00	1.00
Toluene	1.00	1.30	1.05	1.22	1.51
m-Xylene	1.00	1.43	1.08	1.32	2.16
1,2,4-Trimethylbenzene	1.00	...	1.23	1.60	2.65
n-Pentylbenzene	0.71	...	1.08	1.81	3.80
Nonadecylbenzene	0.50	...	...	...	...
Two-ring aromatics					
Naphthalene	2.00	2.00	2.00	2.00	2.00
2-Methylnaphthalene	1.96	2.25	2.11	2.25	2.59
2,3-Dimethylnaphthalene	2.08	2.50	2.32	...	3.47
2,6-Dimethylnaphthalene	1.94	...	...	...	3.15
1,5-Dimethylnaphthalene	1.93	2.32	2.04	...	3.00
2,3,6-Trimethylnaphthalene	2.00	...	...	...	3.54
1,4,6,7-Tetramethylnaphthalene	2.05	...	...	...	3.86
2-Ethylnaphthalene	1.92	2.21	2.09	2.31	3.14
Biphenyl	2.25	2.92	2.23	2.25	2.57
3-Ethylbiphenyl	2.20	...	...	...	3.46
Acenaphthalene	2.00	...	...	2.58	2.73
Three-ring aromatics					
Fluorene	2.61	3.26	2.79	2.70	2.78
Dibenzothiophene	2.75	...	...	...	2.98
Anthracene	2.95	2.95	3.00	3.09	3.02
2-Methylanthracene	2.92	2.97	...	...	3.63
9,10-Dimethylanthracene	2.95	...	...	...	3.82
Phenanthrene	3.00	3.00	3.00	3.00	3.00
1-Methylphenanthrene	2.98	3.26	3.18	...	3.43
p-Terphenyl	3.40	4.57	3.44	3.66	3.94
Four-ring aromatics					
Fluoranthene	3.39	3.42	3.41	3.36	3.42
Benzo[*a*]fluorene	3.46	3.95	...	...	3.74
Benzo[*b*]fluorene	3.53	4.14	...	...	3.78
Pyrene	3.68	3.06	3.31	3.45	3.51
Naphthacene	3.93	3.95	...	...	...
Benzo[*a*]anthracene	4.00	4.00	4.00	4.00	4.00
Triphenylene	4.00	4.04	...	...	3.82
Chrysene	4.03	4.00	4.06	3.95	3.94
Five-ring and larger aromatics					
Benzo[*a*]pyrene	4.30	4.11	...	...	4.57
Perylene	4.47	4.20	...	4.63	4.43
Benzo[*g,h,i*]perylene	4.61	4.21	...	...	>5
Indeno[*1,2,3-c,d*]pyrene	4.72	...	...	...	>5
Dibenzo[*a,c*]anthracene	4.93	4.92	...	...	4.84
Dibenzo[*a,h*]anthracene	4.93	...	...	...	>5
Picene	>5	5.07	...	...	4.93
Benzo[*b*]chrysene	5.00	5.00	5.00	5.00	5.00

[a] Hexane was used as the mobile phase because of poor flow reproducibility with pentane. However, both solvents produce identical chromatographic results using μBondapak NH_2 for normal-phase HPLC.

Crude Oil Sample. A crude oil sample was diluted with pentane and was then fractionated on a 61 cm × 7 mm i.d. μBondapak NH_2 column using freshly distilled pentane as the eluent. After the individual fractions were concentrated by gentle evaporation in a heated sandbath, GC analyses were performed on a glass SE-30 coated, SCOT analytical column (100 m × 0.65 mm i.d.). A gas chromatograph–mass spectrometer computer system (Model 5930, Hewlett-Packard, Palo Alto, Calif.) was utilized for GC-MS analysis of these samples.

RESULTS AND DISCUSSION

μBondapak NH_2 consists of an aminopropylsilane chemically bonded to 10-μm fully porous silica particles. The highly polar, strongly basic surface of the μBondapak NH_2 material makes it useful for the separation of polar compounds. However, when a nonpolar mobile phase such as hexane is used, a hydrocarbon class separation similar to that obtained on a silica or alumina column is achieved, i.e., saturated hydrocarbons elute before olefinic and aromatic hydrocarbons, and the elution volumes for the aromatic hydrocarbons increase with the number of condensed rings. The addition of approximately 10% of a more polar solvent such as methylene chloride to the mobile phase results in the elution of 5–7 condensed-ring PAHs as sharp peaks in less than 10 min.

Logarithms of the retention indices (I) for a number of aromatic hydrocarbons on μBondapak NH_2, silica (*13*), alumina (*14*), polystyrene gel (*15*), and μBondapak C_{18}, a reversed-phase packing, are given in Table I. The retention indices were calculated as previously described by Popl et al. (*13*), with the hydrocarbon standards being assigned the following retention indices: benzene 10, naphthalene 100, phenanthrene 1000, benzo[*a*]anthracene 10 000, and benzo[*b*]chrysene 100 000. The retention index of an aromatic hydrocarbon was then calculated in a manner analogous to the calculation of Kováts indices for gas chromatography.

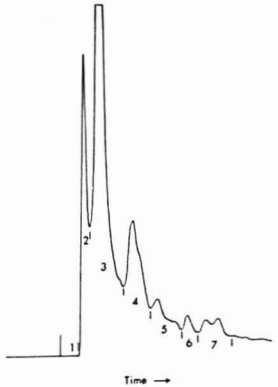

Figure 1. HPLC analysis of a sediment extract on μBondapak NH_2. Numbers refer to the fractions collected for subsequent analysis. Conditions: pentane at 3 mL/min, 1.0 absorbance unit full-scale (aufs), 1.0 mL injected

With the classical adsorbents, the addition of alkyl groups to an aromatic ring generally increases the retention of the compound. In contrast, when using μBondapak NH_2 the presence of an alkyl group on the PAH has only a slight effect on retention; for example in Table I, compare the retention of *m*-xylene, 2-methylnaphthalene, and 1-methylphenanthrene with the unsubstituted parent aromatic hydrocarbon on silica, alumina, and μBondapak NH_2. The μBondapak NH_2 provides a more distinct class fractionation than achieved with silica or alumina. In normal-phase HPLC with μBondapak NH_2, the retention is based primarily on the interaction between the aromatic π electrons of the PAH and the polar amino group of the stationary phase. Since the addition of alkyl substituents to the aromatic rings would affect the π electron system only slightly, alkyl substitution would also affect the retention on μBondapak NH_2 only slightly. Popl et al. (*15*) studied the retention characteristics of PAHs on a macroporous polystyrene gel and found that the presence of alkyl groups increased the retention approximately to the same degree as on silica. Streuli (*16*) found the retention of PAHs on Sephadex LH-20 to decrease slightly with alkyl substitution. The data summarized in Table I indicate that the presence of alkyl groups affects the retention of the PAHs more on silica than on alumina. Martin et al. (*17*) also observed this behavior for alkylbenzenes.

The reversed-phase packing material, μBondapak C_{18}, provides a separation for unsubstituted PAHs similar to silica, alumina, and μBondapak NH_2. However, the presence of an alkyl side chain on the aromatic ring significantly increases its retention on the reversed-phase material. Reversed-phase liquid chromatographic separations are largely dependent on the relative solubilities of the components in the polar mobile phase (*18, 19*). The addition of an aliphatic side chain results in a significant reduction in the solubility and, as a consequence, a large increase in the retention volume (see Table I). In complex samples containing alkyl-substituted PAHs as well as the unsubstituted parent PAHs, the use of reversed-phase HPLC could therefore yield misleading results due to overlapping alkyl homologues; for example, 1,3,5-trimethylnaphthalene, 1-methylphenanthrene, and fluoranthene elute simultaneously even though these compounds consist of two, three, and four rings, respectively (see Table I).

The combination of separations, first with μBondapak NH_2 to achieve a PAH fractionation based on the number of condensed aromatic rings, and then with reversed-phase HPLC to obtain the separation of the alkyl homologues within each fraction, provides a powerful technique for the LC analysis of complex mixtures of PAHs. This combination was applied to the analysis of a marine sediment collected near a natural oil seep. Figure 1 is the liquid chromatogram obtained on μBondapak NH_2 of an extract of the sediment. Numbers on the chromatogram identify the fractions which were collected for subsequent reversed-phase HPLC analysis. A reversed-phase HPLC analysis of fraction 4 is shown in Figure 2. In addition to both the UV absorption and fluorescence emission response, Figure 2 also contains the fluorescence emission spectra obtained for several of the

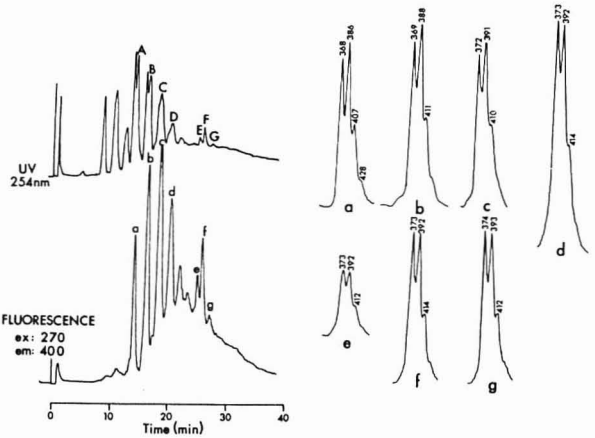

Figure 2. Reversed-phase analysis of sediment fraction 4 (Figure 1). Conditions: 50–100% acetonitrile in water, linear gradient in 30 min at 2 mL/min., 0.05 aufs, 200 μL injected (~20% of fraction 4). Upper chromatogram: UV absorption detection at 254 nm. Lower chromatogram: Fluorescence emission detection at 400 nm with excitation at 270 nm. Spectra *a* thru *g*: Fluorescence emission spectra at 270-nm excitation (numbers indicate wavelengths in nm)

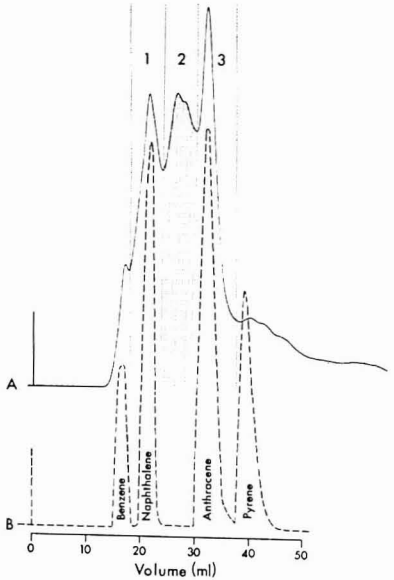

Figure 3. HPLC analysis of crude oil on μBondapak NH_2. (A) crude oil, (B) separation of a synthetic mixture of aromatic hydrocarbons. Conditions: pentane at 2 mL/min, 2.0 aufs, 1.0 mL injected

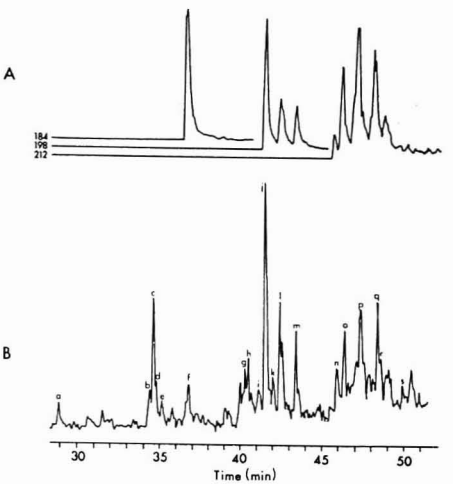

Figure 4. GC-MS analysis of crude oil fraction 2 (Figure 3A). (A) single ion records *m/e* 184, 198, and 212. (B) total ion chromatogram. Tenative GC-MS identifications: (*a*) fluorene, (*b*, *c*, *d* and *e*) methylfluorenes, (*f*) dibenzothiophene, (*g*, *h*, *i*, and *k*) C_2-substituted fluorenes, (*j*, *l*, and *m*) methyldibenzothiophenes, (*n*, *o*, *p*, *q*, *r*, and *s*) C_2-substituted dibenzothiophene. Column: 100m × 0.65 mm I.d. glass SE-30 coated SCOT. Conditions: Helium flow at 5 mL/min., temperature program from initial temperature of 80 °C for 8 min to 275 °C at 4°/min

chromatographic peaks. Peak *a* is tentatively identified as chrysene based on the retention volume and the fluorescence spectrum. The spectra for peaks *b* thru *g* are similar in shape to the fluorescence emission spectrum of chrysene, but the fluorescence maxima are shifted slightly to higher wavelengths. Since the addition of alkyl groups, particularly methyl groups, to the aromatic ring produces a displacement in the fluorescence spectrum towards higher wavelengths (*20*), these fluorescence spectra and the chromatographic retention data indicate that a series of alkyl (probably methyl) substituted chrysenes is present in this fraction.

The largest peak in Figure 1 (fraction 3) is in the three-ring PAH region. Reversed-phase HPLC/fluorescence emission spectroscopy and GC/MS indicated that the compounds in this fraction were primarily phenanthrene and C_1-, C_2-, and C_3-substituted phenanthrenes with no detectable amounts of anthracene or alkyl-anthrancenes. This is not unexpected as Pancirov and Brown (*1*) have reported that phenanthrene and alkyl-phenanthrene homologues are the most abundant PAHs in several crude oils, and other investigators (*21*, *22*) have reported that phenanthrenes are present in some crude oils in much greater quantities than anthracenes. In addition, GC-MS analysis indicated the presence of dibenzothiophene and C_1- and C_2-substituted dibenzothiophenes in fraction 3. The aliphatic hydrocarbons, which are often used as an indication of the presence of petroleum, were identified in fraction 1 by GC-MS analysis.

The application of μBondapak NH_2 to fractionate crude oil prior to GC-MS analysis was also investigated. Chromatograms obtained on μBondapak NH_2 for a synthetic aromatic hydrocarbon mixture and a crude oil are shown in Figure 3. A GC-MS analysis performed on the fraction between the naphthalene and anthracene fractions is shown in Figure 4. This fraction was found to consist primarily of three-ring compounds containing a five-member ring (i.e., dibenzothiophenes, dibenzofurans, and fluorenes). Figure 4 contains a total ion chromatogram and the single ion records for *m/e* 184, 198, and 212 which indicate the presence of dibenzothiophene, C_1-substituted dibenzothiophenes, and C_2-substituted dibenzothiophenes. A series of alkylated fluorenes and another of alkylated dibenzofurans were also identified. The predominant components of the naphthalene region (fraction 1 in Figure 3) were identified as C_1- through C_4-substituted naphthalenes. The most abundant compounds present in the anthracene region (fraction 3 in Figure 3) were identified by GC-MS as C_1- through C_4-substituted phenanthrenes/anthracenes. Thus, the μBondapak NH_2 not only provides a separation according to the number of condensed aromatic rings, but is also capable of separating three-ring components containing a five-membered ring from three-ring components consisting only of six-membered rings.

Three-ring nitrogen heterocyclic compounds are more polar than sulfur and oxygen heterocyclic compounds and, therefore, require a more polar mobile phase composition for elution from the μBondapak NH_2. We are presently investigating the applicability of μBondapak NH_2 for the separation of more polar compounds such as the *N*-heterocyclic compounds and the phenols, which are found in crude petroleum and other fossil-derived oils.

High-performance liquid chromatography using μBondapak NH_2 provides a versatile, convenient method for the isolation of various hydrocarbon classes prior to analysis by other techniques. In addition to separating aliphatic hydrocarbons from the aromatic hydrocarbons, μBondapak NH_2 provides a convenient, reproducible HPLC fractionation of PAHs according to number of condensed aromatic rings. The use of this material eliminates one of the major difficulties encountered with classical adsorbents, i.e., nonreproducible retention due to small changes in the moisture content of the eluent.

LITERATURE CITED

(1) R. J. Pancirov and R. A. Brown, "Proceedings of the 1975 Conference on Prevention and Control of Oil Pollution", American Petroleum Institute, Washington, D.C., 1975, p 103.
(2) W. W. Youngblood and M. Blumer, *Geochim. Cosmochim. Acta*, **39**, 1303 (1975).
(3) L. R. Snyder, "Principles of Adsorption Chromatography", Marcel Dekker, New York, N.Y., 1968.
(4) T. Doran and N. G. McTaggart, *J. Chromatogr. Sci.*, **12**, 715 (1974).
(5) W. Giger and M. Blumer, *Anal. Chem.*, **46**, 1663 (1974).
(6) M. Novotny, M. L. Lee, and K. D. Bartle, *J. Chromatogr. Sci.*, **12**, 606 (1974).
(7) M. L. Lee, M. Novotny, and K. D. Bartle, *Anal. Chem.*, **48**, 405 (1976).
(8) M. L. Lee, M. Novotny, and K. D. Bartle, *Anal. Chem.*, **48**, 1566 (1976).
(9) J. A. Schmit, R. A. Henry, R. C. Williams, and J. F. Dieckman, *J. Chromatogr. Sci.*, **9**, 645 (1971).
(10) C. Golden and E. Sawicki, *Anal. Lett.*, **9**, 957 (1976).
(11) S. N. Chesler, B. H. Gump, H. S. Hertz, W. E. May, and S. A. Wise, manuscript in preparation.
(12) W. E. May and R. G. Christensen, manuscript in preparation.
(13) M. Popl, V. Dolanský, and J. Mostecky, *J. Chromatogr.*, **117**, 117 (1976).
(14) M. Popl, V. Dolanský, and J. Mostecky, *J. Chromatogr.*, **91**, 649 (1974).
(15) M. Popl, V. Dolanský, and J. Čõupek, *J. Chromatogr.*, **130**, 195 (1977).
(16) C. A. Streuli, *J. Chromatogr.*, **56**, 219 (1971).
(17) M. Martin, J. Lohéac, and G. Guiochon, *Chromatographia*, **5**, 33 (1972).
(18) D. C. Locke, *J. Chromatogr. Sci.*, **12**, 433 (1974).
(19) R. B. Sleight, *J. Chromatogr.*, **83**, 31 (1973).
(20) I. B. Berlman, "Handbook of Fluorescence Spectra of Aromatic Molecules", 2nd ed., Academic Press, New York, N.Y., 1971, p 70.
(21) K. W. Bartz, T. Aczel, H. E. Lumpkin, and F. C. Stehling, *Anal. Chem.*, **34**, 1814 (1962).
(22) B. J. Mair, J. L. Martinez-Pico, *Proc. Am. Pet. Inst.*, **42**, 173 (1962).

RECEIVED for review August 9, 1977. Accepted September 22, 1977. The authors acknowledge partial financial support from the Office of Energy, Minerals, and Industry within the Office of Research and Development of the U.S. Environmental Protection Agency under the Interagency Energy/Environment Research and Development Program. Identification of any commercial product does not imply recommendation or endorsement by the National Bureau of Standards, nor does it imply that the material or equipment identified is necessarily the best available for the purpose.

Determination of Some Thiourea-Containing Pesticides by Pulse Voltammetric Methods of Analysis

Malcolm R. Smyth* and Janet G. Osteryoung

Department of Microbiology, Colorado State University, Fort Collins, Colorado 80523

The polarographic behavior of thiourea, phenylthiourea, α-naphthylthiourea and benzyl(iso)thiourea has been investigated in Britton–Robinson buffer and sodium hydroxide solutions. The waves obtained for these compounds in 1 M NaOH are recommended for analytical purposes. In particular, differential pulse polarography has been used to resolve a mixture containing thiourea, phenylthiourea or α-naphthylthiourea and benzyl(iso)thiourea. This technique can be used to determine concentrations of thiourea and phenylthiourea down to 1×10^{-7} M, α-naphthylthiourea down to 2×10^{-7} M and benzyl(iso)thiourea down to 5×10^{-7} M under optimum conditions. Since thiourea, phenylthiourea, and α-naphthylthiourea form insoluble complexes with mercury, these compounds can also be determined by cathodic stripping voltammetry at a hanging mercury drop electrode. This method of analysis can determine concentrations of these compounds down to 1 ng mL^{-1} and has been applied to the direct determination of thiourea in urine.

During the past 20 years, thiourea (TU; I) has found widespread use in a variety of industrial and biological applications (*1*). In agriculture it has been employed as a fungicide (*2*) [although its use as such has been shown to be harmful in citrus growing areas (*3*)], as an accelerator of sprouting in dormant tubers (*2*), and to decrease the content of nitrifying bacteria in the soil (*4*). It has been isolated as a urinary metabolite both of CS_2 (*5*) and of a S-containing heterocycle (*6*). Its presence in urine has also been taken as a nonspecific indicator of cancer (*7*). Several derivatives of thiourea, i.e., phenylthiourea (PTU; II) and α-naphthylthiourea (ANTU; III) have also been used as pesticides and exhibit properties harmful to man. PTU exhibits both herbicidal (*8*) and rodenticidal (*9*) activity and causes chronic goitrogenic and other glandular difficulties in man (*10*). The rodenticidal activity of ANTU was first demonstrated in 1945 (*11*). These thioureas appear to exert their toxic effects by disturbing carbohydrate metabolism (*12*) and they have been shown to produce a tolerance to their own toxic action (*13*).

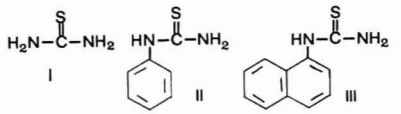

There are many published methods for the determination of TU and PTU based on titrimetric procedures (*14*, *15*) but these are not applicable for the analysis of trace quantities of these compounds in biological fluids. Colorimetric methods have been described for the determination of PTU which are based on its reaction with Folin–Ciocalteau reagent (*16*, *17*), but these methods are usually slow (it takes 1.5 h for the color to develop), offer little selectivity, and have high limits of detection (ca. 3×10^{-5} M) (*16*). The electrochemical methods that have most been applied to the determination of TU include microcoulometric argentimetric titration (*18*), ion selective electrode potentiometry (*19*), amperometric titration (*20*), and hydrogen overvoltage measurements (*21*). The latter procedure could be used to quantitatively determine TU down to 1×10^{-7} M, but it is not foreseen that this procedure could provide a convenient method for the determination of TU in biological fluids. Although polarographic methods have also been applied to the determination of TU, these have been based either on the liberation of the S atom and subsequent measurement as H_2S (*22*) or on the catalytic wave produced by TU in the presence of Cu^{2+} ions (*23*). We have therefore studied the inherent polarographic behavior of TU, PTU, and

ANTU to see if a direct method could provide the sensitivity and selectivity required for the determination of trace quantities of these compounds in situations of environmental importance.

The polarographic behavior of TU has previously been studied by several authors (*24*, *25*) and it is generally agreed that the mechanism involves mercury salt formation according to:

$$Hg \rightleftharpoons Hg^{2+} + 2e^-$$

$$Hg^{2+} + j[TU] \rightleftharpoons Hg[TU]_j^{2+}$$

where $j = 2$, 3, or 4. In strongly acidic media, TU is oxidized (on standing) to form the disulfide, the reduction of which obscures any anodic wave obtained for TU at the dropping mercury electrode (*25*). In weakly acidic or neutral solutions, the wave obtained for TU is independent of pH. Nyman and Parry (*25*) have calculated the formation constants for mercury–thiourea complexes for $j = 2$ ($k = 1.5 \times 10^{22}$), $j = 3$ ($k = 5 \times 10^{24}$), and $j = 4$ ($k = 6.3 \times 10^{26}$). They have suggested that the $Hg[TU]_2^{2+}$ form is the predominant species formed on the oxidation of TU in weakly acidic and neutral media and that it is the uncharged form of TU which participates in this reaction. TU also exhibits an anodic wave in alkaline media (*24*) which has been shown to be due to mercury salt formation. In this case, however, the $E_{1/2}$ value was shown to be dependent on pH, indicating that a different process is operative in alkaline media. Similar results have been obtained for some substituted phenylthioureas in Britton–Robinson (BR) buffer and sodium hydroxide solutions (*26*). It was our intention, therefore, to further investigate the processes exhibited by TU, PTU, and ANTU in these media using direct current (DC), normal pulse (NPP), and differential pulse (DPP) polarographic techniques. The oxidation of benzyl(iso)thiourea (BITU; IV) was also investigated. This compound can be regarded as a thioether and should be oxidized according to:

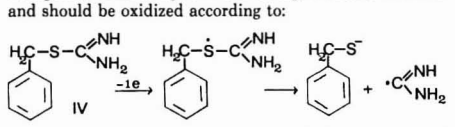

Since TU, PTU, and ANTU form insoluble complexes with mercury, these compounds are amenable to cathodic stripping voltammetry (CSV) at a hanging mercury drop electrode (HMDE). This method of analysis will be discussed in relation to the DPP procedure and preliminary results on its application to the direct determination of TU in urine will be reported.

EXPERIMENTAL

Apparatus. Polarographic curves were recorded using a PAR Model 174 Polarographic Analyzer in conjunction with a three-electrode cell system having a saturated calomel (SCE) as the reference and platinum as the counter electrode. The polarograms were recorded on a Omnigraphic Model 2000 X-Y recorder. The dropping mercury electrode used had a flow rate of 0.83 mg s^{-1} and a drop time of 8.05 s in 1 M NaOH and at a mercury head of 76 cm. Variation of pulse widths was obtained using the modification of the PAR 174 instrument described elsewhere (*27*). For the cathodic stripping voltammetric experiments, the PAR Model 9323 hanging mercury drop electrode was used in conjunction with the PAR Model 174. Drop times were controlled using a PAR Model 172 drop knocker.

Reagents. Samples of thiourea, phenylthiourea, and benzyl(iso)thiourea were obtained from Pfaltz and Bauer, Inc. A sample of α-naphthylthiourea was obtained from the Quality Assurance Section, Environmental Toxicology Division of the Environmental Protection Agency. Stock solutions of these compounds (10^{-3} M) were prepared in distilled water and stored under refrigeration. A 1 M sodium hydroxide solution was prepared from electrolytic grade pellets and made up in triple distilled water. A stock Britton–Robinson buffer solution (pH 1.8) composed of a mixture of boric acid, orthophosphoric acid, and glacial acetic acid, all 0.04 M, was prepared from analytical grade reagents. From this stock solution, buffer solutions of varying pH were prepared by the addition of 0.2 M sodium hydroxide solution and measuring the pH using a glass electrode.

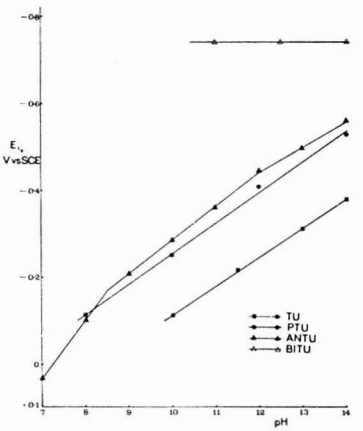

Figure 1. Plot of $E_{1/2}$ vs. pH for main wave, i_a, exhibited by TU, PTU, ANTU, and BITU

Techniques. Polarographic investigations were carried out on solutions that had previously been deaerated using oxygen-free nitrogen for 10 min. Current–potential curves were recorded in the DC, NPP, and DPP modes. The solutions were blanketed by an atmosphere of nitrogen during analysis and each solution was scanned between −0.8 V and the potential relating to the oxidation of mercury. A scan rate of 2 mV s^{-1}, drop time of 1 s (NPP and DPP), and a modulation amplitude of 100 mV (DPP) were typically employed in most investigations. Variation of pulse width was achieved by using the PAR 174 modification described elsewhere (*27*). For pulse widths of 20, 50, and 100 ms, sample widths of 2, 5, and 10 ms, respectively, were employed.

For the cathodic stripping voltammetric experiments, reproducible hanging mercury drops were obtained by dialing out four half divisions on the micrometer screw gauge of the PAR Model 9323 hanging mercury drop electrode. A constant rate of stirring was achieved using a Thermolyne Model S-7895 "Stir-Mate". The solutions to be analyzed were first degassed using oxygen-free N_2 for 10 min. The stirring motor was then switched on and a constant rate of stirring allowed to build up in the cell. A fresh drop of mercury was then dialed out and dislodged. This was then repeated and the next drop used for the experiment. In most investigations, the potential was set between −0.2 V to −0.3 V prior to plating for 2 min. With the initial potential still being exerted on the cell, the stirring motor was switched off and the solution allowed to come to rest for another 20 s. The solution was then scanned in a cathodic direction using scan rates of 25–100 mV s^{-1} in the linear potential sweep cathodic stripping (LPSCSV) experiments and 2–20 mV s^{-1} in the differential pulse cathodic stripping (DPSCV) runs. In the latter case a "drop time" of 1 s and a modulation amplitude of 100 mV was employed in most investigations.

RESULTS AND DISCUSSION

Effect of pH. The effect of pH on the $E_{1/2}$ values of the main wave exhibited by TU, PTU, ANTU, and BITU in DC polarography is shown in Figure 1. Whereas TU and PTU show linear portions of similar slope (67.5 and 70 mV pH^{-1}, respectively), ANTU shows two breaks from greater to lesser slope (at pH's 8.45 and 12.0) on increasing pH. BITU on the

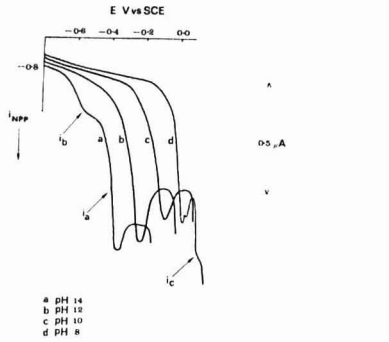

Figure 2. Effect of pH on NPP wave exhibited by PTU (5×10^{-5} M)

other hand shows no dependence on pH. This reflects that no protons or OH^- ions are involved in the electron consuming process and supports the mechanism shown previously.

In the case of TU, only the wave related to the formation of the mercury complex (i_a) is exhibited across the pH range 10–14. PTU, on the other hand, exhibits a prewave (i_b) in a solution of 1 M NaOH which disappears on lowering the pH. It also exhibits a postwave (i_c) in solutions of BR buffer of pH ≤ 8. ANTU also exhibits the postwave in solutions of pH ≤ 8 and retains the prewave throughout the pH range 7–14.

The effect of pH on the NPP behavior of PTU is shown in Figure 2. The maximum shown on the main wave (i_a) is characteristic of reactant adsorption (*28*). The pre- and postwaves are indicative that the adsorption isotherms give rise to saturation coverage over a relatively narrow range of concentration (*29*). TU also exhibits maxima on its NPP waves in sodium hydroxide solutions but no limiting current value is reached because the wave obtained for TU is followed closely by the direct oxidation of mercury. In the case of ANTU, however, the NPP behavior shows both a maximum on the main wave (i_a) and a severe depression of the limiting current. This behavior indicates that ANTU is more strongly adsorbed than either TU or PTU.

The best defined waves are obtained for TU in the pH range 12–14 and for PTU and ANTU in the pH range 10–14. At lower pH values, adsorption markedly affects the shape of the DC, NPP, and DPP polarograms. In the case of ANTU, the effects of adsorption are also seen to a certain degree at these higher pH values, but at pH values below 10 this effect becomes more pronounced. This is illustrated in Figure 3 for the DC, NPP, and DPP behavior of ANTU in BR buffer pH 7. Although the DC wave is markedly distorted by adsorption, the NPP and DPP waves show well defined prewaves followed by very sharp adsorption peaks.

The best defined waves for analytical purposes were therefore obtained in 1 M NaOH solution.

Effect of Concentration. The DPP calibration curves obtained for TU, PTU, and ANTU in 1 M NaOH are shown in Figure 4. From this it can be seen that TU shows two breaks from lesser to greater slope corresponding to concentrations 5×10^{-6} M and 3×10^{-5} M. PTU on the other hand shows no break in its calibration curve between $0–5 \times 10^{-5}$ M whereas ANTU shows one break corresponding to a concentration of 3.75×10^{-5} M. The marked differences in peak currents obtained for these compounds using DPP is not reflected in DC polarography where the ratio of i_{lim} values for TU:PTU:ANTU:BITU at the 3×10^{-5} M level is 2.4:2.1:1.7:1 (assuming BITU is oxidized in a 1 e^- process). These differences in magnitude are attributed to the increasing adsorption in the series ANTU > PTU > TU.

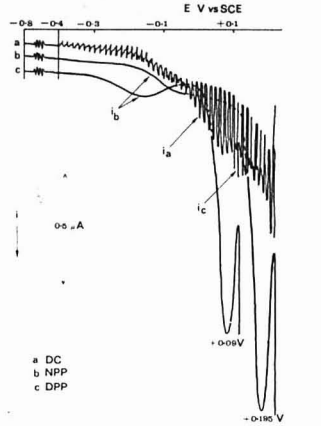

Figure 3. DC, NPP, and DPP waves obtained for 7×10^{-5} M ANTU in BR buffer pH 7

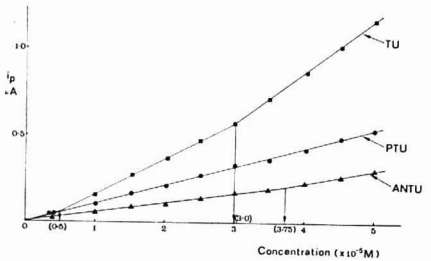

Figure 4. Calibration curves obtained for TU, PTU, and ANTU in 1 M NaOH using DPP

For all three compounds, their E_p values (in DPP) move to more negative values on increasing concentration. In the case of TU, a plot of E_p vs. log [TU] in the concentration range 8×10^{-6}–5×10^{-5} M proved linear with slope equal to 29.75 mV. Deviations from linearity were exhibited at lower concentrations due to the interference caused by the direct oxidation of mercury. Assuming the slope to be equal to $-RT/nF$ (*25*), a value for n of 1.988 is obtained indicating that although the DPP calibration curve shows two breaks from lesser to greater slope, these do not reflect a change in the number of electrons involved in the electrode process. ANTU also exhibits a linear plot of E_p vs. log [ANTU] over the concentration range 10^{-6} M to 5×10^{-5} M with a slope of 39.6 mV. PTU on the other hand, showed no variation in its E_p value up to 7×10^{-6} M. At higher concentrations the slope of the E_p vs. log [PTU] plot was found to be 56 mV.

The waves obtained for TU and PTU in 1 M NaOH were shown to be overall diffusion-controlled since plots of i_{NPP} vs. $1/\tau^{1/2}$ (where τ = pulse width) gave straight lines (of slope 17.4 and 14.2 $\mu A\ ms^{-1}$, respectively) which passed through the origin. The effect of varying pulse width on the NPP behavior of TU in 1 M NaOH is shown in Figure 5. With increasing pulse width, increased resolution is obtained on the maximum relating to reactant adsorption. For ANTU in 1 M NaOH, the NPP wave is nearly completely suppressed but measurements of peak heights as a function of pulse width showed the peak current to be directly proportional to $1/\tau$ with a slope

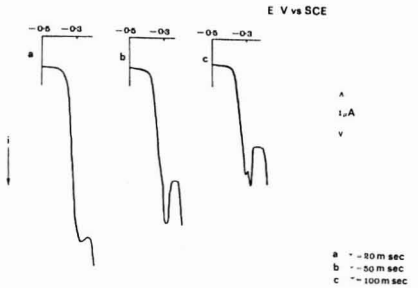

Figure 5. Effect of varying pulse width on NPP wave obtained for 2 × 10^{-4} M TU in 1 M NaOH: conditions, 2 mV s^{-1}, 1-s drop time

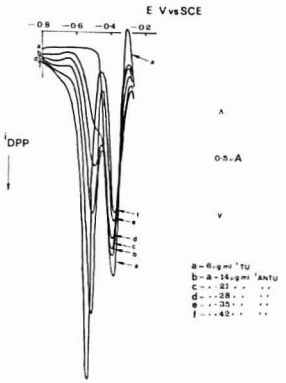

Figure 6. Effect of varying concentrations of ANTU on DPP peak of TU in 1 M NaOH

of 7.26 μA ms^{-1} (for a concentration of 5 × 10^{-5} M). This is attributed to the strong adsorption properties of the naphthalene moiety at the mercury surface.

It would appear, therefore, that in the case of TU, the breaks observed in the calibration plot reflect the successive formation of different complexes of thiourea with Hg^{2+}. Since the $E_{1/2}$ value is dependent on pH, it appears that complexes of the form $Hg^{II}(OH)_2[TU]j$ (where j = 2, 3, or 4) are being formed by the oxidation of TU in alkaline media and that increasing the concentration of TU in this medium favors the formation of the succeedingly higher complex. It is likely that PTU and ANTU will exhibit similar behavior over a wider concentration range than that examined in the present investigation.

As can be seen from the plots of $E_{1/2}$ vs. pH in Figure 1, it is possible to differentiate between TU and either PTU or ANTU. The effect of varying ANTU concentration on the DPP peak of TU in 1 M NaOH is shown in Figure 6. The addition of succeeding amounts of ANTU causes subsequent small decreases in the peak height of TU.

Although DPP cannot be used to resolve PTU and ANTU in a 1 M NaOH solution, a degree of differentiation is obtained in BR buffer, pH 10, where although PTU gives rise to a well defined DPP peak at −0.2 V, ANTU gives rise to a badly defined double peak (E_p = −0.15 and −0.1 V, respectively). BITU can be resolved from TU, PTU, and ANTU in 1 M NaOH since its E_p value (−0.79 V) is well removed from those of PTU or ANTU (−0.5 to −0.55 V) or TU (−0.39 V).

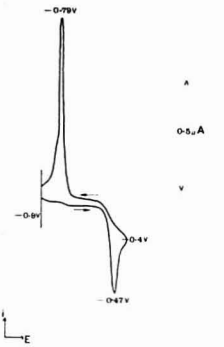

Figure 7. Cyclic voltammogram of 5 × 10^{-5} M PTU in 1 M NaOH

These compounds can be determined using DPP down to about 1 × 10^{-7} M for TU and PTU, 2 × 10^{-7} M for ANTU, and 5 × 10^{-7} M for BITU. In each case the detection limit (dl) was obtained from the expression dl = $3S_b/m$ where S_b is the standard deviation of the background current and m is the slope of the calibration curve. The limits of sensitivity given above were calculated as 3 × dl.

Cathodic Stripping Voltammetry. The application of cathodic stripping voltammetry (CSV) to the determination of TU, PTU, and ANTU is based on their ability to form insoluble complexes with mercury. This is a very sensitive method of analysis as has been reported for some aryl thioamides of pharmaceutical importance (*30*) and for 2-mercaptopyridine-1-oxide (*31*). It is performed by first concentrating ("plating") the substance of interest at the mercury surface at a potential where it forms an insoluble mercury complex. The complex is then "stripped" out by scanning in a negative (i.e., cathodic) direction. Since DPP can be used to determine concentration of TU, PTU, and ANTU down to 1 × 10^{-7} M, it was decided to limit this CSV investigation to concentrations lower than 2 × 10^{-7} M. Since the polarographic investigation indicated that different complexes of TU (and PTU and ANTU) were being formed at higher concentrations, we were unable to study in detail the "stripping" of trace quantities of these compounds using techniques such as chronopotentiometry which are limited to the mM range.

At these low concentrations, it was assumed that the $Hg^{II}(OH)_2[TU]_2$ (or $Hg^{II}(OH)_2[PTU]_2$ or $Hg^{II}(OH)_2[ANTU]_2$) species were predominant. In the case of PTU, which does not show a break in its DPP calibration curve up to 5 × 10^{-5} M, we investigated its behavior at the HMDE in 1 M NaOH using cyclic voltammetry (Figure 7). The peak obtained on scanning anodically is due to the formation of the $Hg^{II}(OH)_2[PTU]_2$ salt which is subsequently "stripped" out on scanning cathodic. The system cannot be considered to be reversible, however, since the anodic and cathodic $E_{1/2}$ values are separated by over 300 mV.

The effect of scan rate on the LPSCSV obtained for 12 ng mL^{-1} TU in 1 M NaOH solution is shown in Figure 8. At low scan rates (10–20 mV s^{-1}) two processes are observed. At higher scan rates, however, the double wave form is replaced by a single wave and this, coupled with the resulting increase in sensitivity, makes the wave obtained at 50 mV s^{-1} most suitable for the determination of TU (or PTU or ANTU, both of which exhibit similar behavior to TU under these conditions) in the 5–20 ng mL^{-1} range. In the lower concentration range (1–5 ng mL^{-1}), the double peak behavior is also manifested at 50 mV s^{-1} and a scan rate of 100 mV s^{-1} must

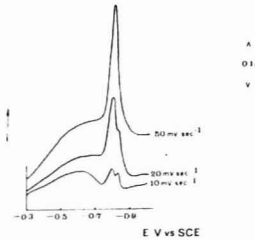

Figure 8. Effect of scan rate on LPSCSV of 12 ng mL^{-1} TU in 1 M NaOH

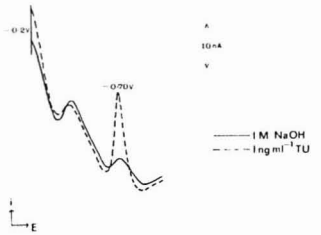

Figure 9. DPCSV of 1 ng mL^{-1} TU in 1 M NaOH

be employed for these lower concentrations. A calibration graph obtained for LPSCSV of 1–5 ng mL^{-1} TU using a scan rate of 100 mV s^{-1} proved linear with a slope of 26 nA ng^{-1} mL. Under these conditions the limit of sensitivity of the technique is 1 ng mL^{-1}.

Although differential pulse cathodic stripping voltammetry (DPSCV) is potentially a more sensitive technique than LPSCSV, in this case the limit of sensitivity of the DPCSV method is limited by the background interference. This is illustrated in Figure 9 for a DPCSV scan of 1 ng mL^{-1} TU in 1 M NaOH. It is our experience that the "blank" current obtained for DPCSV scans of 1 M NaOH solutions can change from day to day and calibration graphs must be constructed prior to running an unknown solution. Although DPCSV has the ability to measure down to 100 pg mL^{-1}, fluctuations in the "blank" measurement affect both the precision and accuracy of the results in this low concentration range. It is suggested therefore that this method of analysis also be restricted to concentrations >1 ng mL^{-1} for use in routine situations.

Although both LPSCSV and DPCSV offer greater sensitivity over the DPP method for the determination of TU, PTU, and ANTU, these techniques are unable to differentiate between these compounds in mixtures. The choice of operating technique should therefore be made on a consideration of (i) the range of concentrations likely to be present in the sample; (ii) the constituents of the mixture; and (iii) the time required for the analysis.

Application of LPSCSV to the Direct Determination of TU in urine. Because of the high sensitivity and rapid time of analysis offered by LPSCSV for the determination of TU, it was decided to apply this technique to the direct determination of this substance in urine. The preliminary results of this investigation are shown in Figure 10 where it can be seen that an interfering substance in the urine is stripped at the same potential as TU. The spiked addition of TU resulted in an enhancement of the peak around -0.8

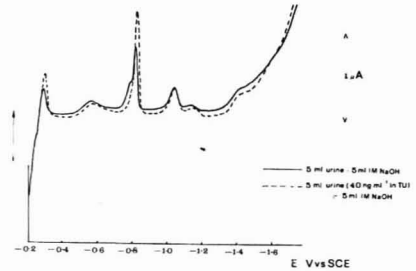

Figure 10. LPSCSV of normal urine spiked with 40 ng mL^{-1} TU

V and in the disappearance of the shoulder which accompanied this peak. Work is in progress to identify the nature of this interfering substance and to develop a convenient method of analysis for the direct determination of TU in urine. It is foreseen that such a method could prove useful in the screening of patients who suffer from defects in sulfur metabolism or who have been exposed to foreign sulfur compounds in the environment.

LITERATURE CITED

(1) "IARC Monographs on the Evaluation of Carcinogenic Risk of Chemicals to Man", Vol. 7, Lyon, 1974, pp 95–109.
(2) W. C. Heuper, and W. D. Conway, Ed., "Chemical Carcinogenesis and Cancer", C. C Thomas, Springfield, Ill., 1964, p 37.
(3) Plant Protection Ltd., Plant Protection Conference, 1956, "Proceedings of the 2nd International Conference at Fernhurst Research Station", Butterworth, London, England, 1957, p 199.
(4) T. I. Kolyada, *Ispol' z Mikroorg. Ikh. Metab. Nan. Khoz.*, 167 (1972).
(5) M. Pergal, N. Vukojevic, and D. Djuric, *Arch. Environ. Health*, **25**, 42 (1972).
(6) W. A. Creasey, K. C. Agrawal, R. L. Capizzi, K. H. Stinson, and A. C. Sartorelli, *Cancer Res.*, **32**, 565 (1972).
(7) K. Okazaki, M. Murakami, H. Kawada, and A. Okada, Japan Kokai 75 97, 394 (Cl. GOIN), (Aug 2, 1975); Appl. 74, 1,427; from *Chem. Abstr.*, **83**, 175159z (1975).
(8) K. A. Nuridzhanyan, V. G. Blinova, L. D. Stonov, L. A. Bakumenko, and N. M. Usacheva, *Khim. Sredstva Zashch. Rast.*, No. 1, 197 (1970).
(9) T. Kusano, Y. Kasahava, and Y. Kawamura, *Appl. Entomol. Zool.*, **10**, 19 (1975).
(10) P. E. J. Wheatcroft, and C. C. Thornburn, *Nature (London) New Biol.*, **235**, 93 (1972).
(11) C. P. Richter, *J. Am. Med. Assoc.*, **129**, 927 (1945).
(12) S. N. Giri and A. B. Combs, *Toxicol. Appl. Pharmacol.*, **16**, 709 (1967).
(13) E. J. Fairchild, *Arch. Environ. Health*, **14**, 111 (1967).
(14) A. Kurian and C. V. Suryanavayana, *Analyst (London)*, **97**, 576 (1972).
(15) A. A. D. Gol'tman, *Khim. Issled. Farm.*, 83 (1970).
(16) A. B. Combs, S. N. Giri, and S. A. Peoples, *Anal. Biochem.*, **44**, 570 (1971).
(17) E. T. Rakitzis, *Anal. Chim. Acta*, **78**, 495 (1975).
(18) J. H. Ladenson, and W. C. Purdy, *Anal. Chim. Acta*, **58**, 465 (1971).
(19) M. K. Papay, K. Toth, and E. Pungor, *Anal. Chim. Acta*, **56**, 291 (1971).
(20) S. Ikeda, and H. Satake, *Bunseki Kagaku*, **22**, 107 (1973).
(21) P. E. Holland, J. T. Peeler, and A. J. Wehby, *Anal. Chem.*, **41**, 153 (1969).
(22) E. S. Kosmatyi and V. N. Kavetskii, *Zh. Anal. Khim.*, **28**, 1028 (1973).
(23) H. Sohr and K. Wienhold, *Anal. Chim. Acta*, **83**, 415 (1976).
(24) M. Fedoronko, O. Manousek, and P. Zuman, *Chem. Listy*, **49**, 1494 (1953).
(25) C. J. Nyman and E. P. Parry, *Anal. Chem.*, **30**, 1255 (1958).
(26) W. U. Malik and R. N. Goyal, *Indian J. Chem.*, **14A**, 144 (1976).
(27) R. H. Abel, J. H. Christie, L. L. Jackson, J. G. Osteryoung, and R. A. Osteryoung, *Chem. Instrum.*, **7**, 123 (1976).
(28) J. B. Flanagan, K. Takahashi, and F. C. Anson, *J. Electroanal. Chem.*, (1977) to be published.
(29) A. M. Frumkin and B. B. Damaskin in "Modern Aspects of Electrochemistry", Vol. 3, J. O'M Bockris and B. E. Conway, Ed., Butterworth, London, 1964, Chapter 3.
(30) I. E. Davidson and W. Franklin Smyth, *Anal. Chem.*, **49**, 1195 (1977).
(31) D. A. Csejka, S. T. Nakos, and E. W. DuBord, *Anal. Chem.*, **47**, 322 (1975).

RECEIVED for review August 5, 1977. Accepted October 4, 1977. This paper was presented at the 174th National Meeting, American Chemical Society, Chicago, Ill., August 29–September 2, 1977. Partial financial support for this work was provided through NSF Grant Number MPS 75-00332.

Field Effect Potentiometric Sensors

Richard P. Buck* and David E. Hackleman

William R. Kenan, Jr., Laboratories of Chemistry, The University of North Carolina, Chapel Hill, North Carolina 27514

Vacuum deposition of AgBr on thin silicon dioxide films prepared on silicon substrates was shown to provide stable, rapid-response potentiometric sensors for component-ion activities. Limiting high dc impedances from impedance-frequency responses and external charge-activity measurements indicate displacement current (field-effect) as the probable cause for electrochemical responses. Implications of the mechanism (invoking Volta potential arguments) on the processes of potential generation and potential communication to underlying semiconductor substrates in ISFETs and CHEMFETs are analyzed diagrammatically and theoretically. The essential role of reference electrodes is strongly indicated.

Ion selective field effect transistors (ISFETs), introduced by Bergveld (*1, 2*) have been the subject of both theoretical (*3*) and practical studies (*4–6*). The concept has also been generalized to include sensors for uncharged chemical species (CHEMFETs) via surface electron (or hole) exchange, or adsorption (*7–9*), within a broader category of chemically sensitive semiconductor devices (CSSDs) (*3*). From the theory and practice of MOS capacitors, gate-controlled diodes and MOSFETs (*10*), a necessary condition for the sensitivity of the devices is that a field be transmitted through an insulating gate and be terminated in a space charge region at the gate/semiconductor interface. Whereas in MOSFETs the field is created by the charge on the metal gate, fields can be created in OSFETs (MOSFETs without metal) by any of the several processes of ion exchange (*11*), including ionization of neutral groups, such as SiOH (*12, 13*), electron exchange, adsorption of charged species or alignment of dipoles at the external gate surface (*14*). These processes can be enhanced, controlled, or made to occur by exposing the OSFET with reactive gases, solvents and electrolytes, and by coating the OSFET with reactive materials such as ion exchangers and redox-sensitive layers. In this paper, a specific MOS capacitor system is studied to demonstrate that a solution-ion exchanger gate behaves electrically in a highly analogous fashion to a metal gate. The system uses the well-known, reversible ion exchanging substance AgBr (*15, 16*) on SiO_2-coated silicon.

Modern ion selective electrodes of membrane type, and classical electrodes of first, second, and third kinds, make use of rapid, reversible charge exchange (ion or electron exchange) at each interface. Electrochemical reversibility assures development of interfacial electric fields and thermodynamically significant responses (interfacial, diffusion, and net potential differences) to bathing solution activities (*11, 15–17*). In contrast, proposed ISFETs contain blocked interfaces as well as reversible interfaces of the types:

$$\underset{\text{(reversible)}}{\text{electrolyte}}\,|\,\underset{\text{(blocked)}}{\text{membrane}}\,|\,\underset{\text{(blocked)}}{\text{insulator}}\,|\,\text{metal} \qquad \text{(I)}$$

and

$$\underset{\text{(reversible)}}{\text{electrolyte}}\,|\,\underset{\text{(blocked)}}{\text{membrane}}\,|\,\underset{\text{(blocked)}}{\text{insulator}}\,|\,\text{semiconductor} \qquad \text{(II)}$$

In addition, totally blocked systems have been proposed as chemical sensors (*14*):

$$\underset{\text{(blocked)}}{\text{electrolyte}}\,|\,\underset{\text{(blocked)}}{\text{insulator}}\,|\,\text{semiconductor} \qquad \text{(III)}$$

At ideally blocked interfaces, no net charge transfer can occur. While conventional ISEs are resistive at dc (*18–20*), cells (I–III), completed by use of reversible reference electrodes in the electrolyte, would show entirely capacitive behavior at dc. Use of an ion-exchange membrane, a chemical coating or a metal in Cell I provides the opportunity for generation of an interfacial potential difference by a charge transfer, or faradaic process (*21*). If the charge transfer is reversible, the generated potential difference can be Nernstian and determined within an additive constant by the equality of electrochemical potential of the transferring species (*11, 22*). At the other extreme of very slow, or no charge exchange, the interfacial potential difference at an ideally blocked interface depends on adsorption and dipole alignment. Interfacial potential and charge are related. The latter is established by transient external current flow, by adsorption of charged species, and by chemical generation of charged surface species (*23, 24*).

The hypothesis is made that fields are generated at an electrolyte/ion exchanger, or electrolyte/metal interface by net ion or electron transfer. As a test, potentials at open circuit and charge accumulation for externally shorted cells have been measured. These are equilibrium measurements: the first by classical potentiometric compensation (Volta potential or flat band shifts), and the second by integration of transient current after a fresh cell has been shorted externally. In addition, cell impedances have been measured to demonstrate and confirm capacitive behavior.

EXPERIMENTAL

Starting materials: n(111) and p(100), 2–6 ohm-cm silicon wafers of electronic purity, "Airco" electronic grade oxygen, distilled, deionized water, electronic grade HF (48%), and reagent grade salts and solvents (AgBr, $AgNO_3$, KNO_3, KCl, KBr, trichloroethane, acetone, and methanol) were used.

For the SiO_2 thickness-dependence tests, *n*-type silicon wafers were scribed into rectangular portions of 2-cm width to fit into a tube furnace. The wafers were cleaned in trichloroethane, methanol, acetone, methanol, and blown dry with filtered nitrogen. After 1-h purge of the 1100 °C furnace with steam, water temperature was adjusted to just below boiling, and ~4 ft^3/h of oxygen were passed through the water and into the furnace.

Thickness of oxidized films was established by known oxide growth rates for the time and conditions used (*25*), comparison of expected and actual color (*10*), and the use of the C-V (capacitance-voltage technique) as presented by Zaininger and Heiman (*26*). The C-V technique also produced information of the concentration of impurities and their location in the films.

The SiO_2-Si pieces were scribed on a grid of 0.25-cm centers; Draftsman's black tape (0.05-in.) protected the scribe lines from AgBr during deposition. The pieces were placed, three at a time, into the vacuum bell jar assembly of the evaporator, with approximately 0.1 g AgBr in a tantalum boat. The system was pumped down to 10^{-6} Torr, the AgBr heated slowly to liquification, and evaporated onto the SiO_2/Si substrates. This process required at least 90 min per run of three pieces. The finished pieces, with

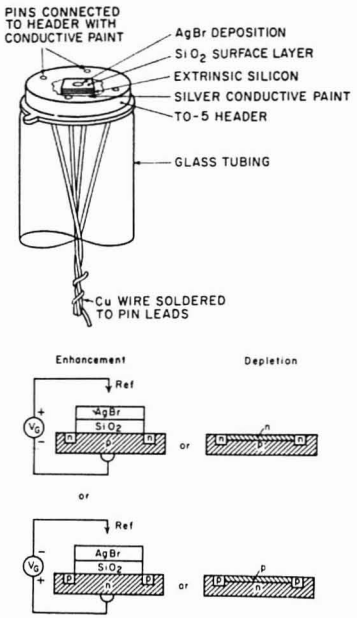

Figure 1. (Upper) Experimental field effect sensor. Note: Semiconductor junction coating and Apeizon "W" wax used to seal and isolate all except the AgBr top surface from solution contact. (Lower) Idealized layouts for ISFETs and CHEMFETs sensors. V_G is the applied bias between FET body and reference electrode. FETs may be n or p type using enhancement or depletion modes. Diffused wells of carrier type opposite to the underlying semiconductor are the contacts for passage of current along the semiconductor/gate interface. An SiO_2 gate is shown and an AgBr sensor membrane is used in this example

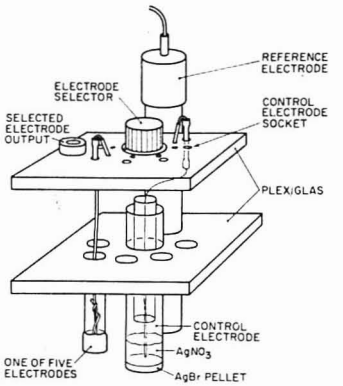

Figure 2. Field effect sensor test assembly

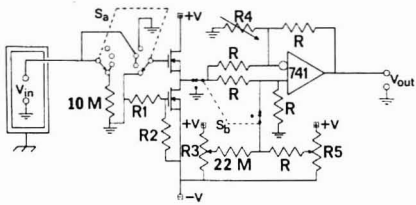

Figure 3. High impedance non-inverting amplifier schematic. R: 10 KΩ. R_1,R_2: designed to allow I_{DS} of MOSFET stages to be near midrange at V_{in} = 0.0V. R_3: 10 K Ω (1 turn) fine zero adjust. R_4: 100 K Ω (10 turn) gain adjust. R_5: 10 K Ω (10 turn) coarse zero adjust. S_a: position: (1) Input 10^7 Ω to ground, amplifier grounded (shown). (2) Input 10^7 Ω to ground, amplifier to input. (3) Input open, amplifier to input. (4) Input open, amplifier grounded. S_b: position: (1) Operate (shown). (2) Balance. ±V: ±15 V dc

typically 100 nm AgBr deposited, were etched free from back side SiO_2, and standard copper deposition solution was used to provide an ohmic contact to the silicon. Pieces separated on the scribe lines produced about 100 sensors of 0.25 × 0.25 cm from each wafer. Ten of each thickness of SiO_2 were mounted on transistor headers as shown in Figure 1.

A second series of sensors was prepared from silicon oxidized in a muffle furnace at 1000 °C in air. This type of oxidation provides a mixed layer of SiO_2 and Si_3N_4 (*27*). For a series of studies involving controlled thicknesses of AgBr and constant SiO_2 thickness, these substrates were subjected to vacuum evaporated AgBr through a molybdenum mask to provide coated areas with 0.95-mm diameters. Thicknesses of AgBr were determined by calculation of consumed AgBr, most probable density of deposit from a distributed source (*28*), and use of color comparison (*10*), with correction for the index of refraction of AgBr.

Testing of these sensor devices of physically small size and Gigohm impedances required construction of a shielded test fixture to accommodate more than one sensor in solution at one time. To monitor the test solutions and proper functioning of the reference electrode with bridge, a standardized, pressed pellet electrode was tested with each set of sensors. Figure 2 shows the test mounting used with five sample sensors, one pressed pellet AgBr electrode and an Orion double junction 90-02-00 reference electrode. Protection of the wires against solution contact was accomplished by dipping all leads in melted Apiezon "W" wax. All of the sensor samples were also coated to leave only the AgBr exposed to electrolyte solutions. Transene semiconductor junction coating, Type 1, a commercial coating designed to passify and insulate semiconductor materials was used (*29*) underneath the Apezion "W" wax.

Decade concentrations of KCl, KBr, and $AgNO_3$ from 10^{-1} to 10^{-5} M at constant ionic strength of 10^{-1} M adjusted with KNO_3, were used. The outer filling solution of the double junction reference electrode was 10^{-1} M KNO_3, and it was replaced daily and between runs. All solutions were saturated with AgBr by placing a known excess in each container, mixing, and allowing to settle one day before use. All concentration studies were done at 25 ± 1 °C. Decade solution tests were started at the lowest concentration, with thorough washing between sets of solutions. Separate beakers and containers were dedicated to each ion concentration, with rinsing of beakers only in aliquots of the solution to be eventually left in each. Replicate sets of data were made on all sensors to provide a measure of data precision.

Because of the extremely high impedances of the sample sensors, a simple impedance converting unity gain amplifier was constructed as shown in Figure 3. The MOSFETs used in this amplifier were of the unprotected gate variety, to enhance the input impedance, and were found to have less than 0.1 pA input current at 10 volts (V_{gs}). Use of an active load device extended the linear range of the otherwise nonlinear saturated mode of operation (*30*). The operational amplifier circuit offers a relatively constant input impedance to the output of the MOSFET stage, has greater than unity voltage gain, is non-inverting, has level offset, provides a high frequency filtering effect, and is stable to ±1 mV/h (*31*). The long term stability of the amplifier has been established at ±30 mV., for periods up to two weeks. The input impedance of the amplifier was not measurable. However, placing a cleaned 10^{10} Ω resistor at the input caused a discharge rate of a voltage reading to be 1000 times as fast as without it. This test indicates an input impedance on the order of 10^{13} Ω.

Impedance-frequency information was obtained using an impedance bridge described elsewhere (*32*, *33*). Bathing solutions

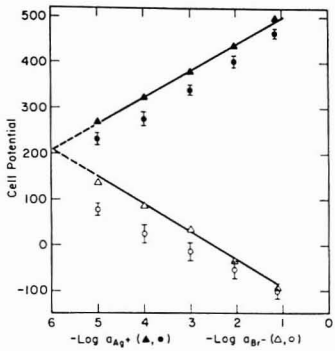

Figure 4. Folded response plots of potential (body vs. reference) as a function of silver ion and bromide ion activities. Fiducial marks are statistical 95% confidence limit ranges for 195 sensors from different chips ○ and ●); silver bromide pressed pellet electrode response (△ and ▲); solid line is the theoretical Ag/AgBr response

were 10^{-2} M $AgNO_3$ and KBr, respectively, with a reference electrode of Ag/AgBr wire. The entire assembly was thermostated at 25.0 ± 0.1 °C, and allowed to attain thermal equilibrium with the sample before proceeding with measurements. A signal excitation voltage of 100 mV p-p was used. Impedance measurements from 10 KHz to 10^{-2} Hz were made before the potentiometric study to provide an initial screening of sensors impedances. Those with less than 10^7 Ω values at 1 Hz were rejected. In addition, impedance-frequency plots were required to show ω^{-1} dependence at the lowest frequencies (10^{-2} Hz).

RESULTS

Activity-Potential dc Responses. Measured potentials, $\phi^{rt} - \phi^{left}$, for a wide range of silver ion activities are summarized in Figure 4. Not surprisingly, for all thicknesses of SiO_2 between 50 and 1300 nm with 100-nm coating of AgBr, the potential responses at each activity lie within ±20 mV of the mean value of a 95% confidence limit. Any other thickness dependence in these data would require explanation by a transport process through the oxide or mixed oxide–nitride layer. A line with theoretical Nernstian slope, but displaced about 40 mV negatively, passes through the experimental points for all data obtained in excess Ag^+ solutions, and most of the data obtained in excess Br^- solutions. For comparison, the theoretical Nernstian response for an equilibrium Ag/AgBr electrode is illustrated. The theoretical curve obeys:

$$\phi^{rt} - \phi^{left} = \phi_{Ag/Ag^+} + \Delta\phi_J - \Delta\phi ref = 0.557 + 0.059 \log a_{Ag^+} + \Delta\phi_J \text{ (volts at 25 °C)} \quad (1)$$

A folded plot is used to cover the wide range of silver ion activities in the concentration range 0.1 M $AgNO_3$ to 0.1 M KBr. Experimental points should lie parallel to the normal electrochemical, Nernstian response but displaced by the work function difference $-\alpha_e^{Si} + \alpha_e^{Ag}$ as derived below. Contact potential measurements (*34*), give a range of values for the difference (−0.01 to −0.27 V); photoelectric effect work functions give a comparable range. Despite the inevitable scatter in literature work function data, the Volta Potential measurements should be more negative than the equilibrium, electrochemical measurements. The data in Br^- solutions are noisier, less reproducible, and deviate from theoretical values at high activities.

The potentiometric sensor, or gate section of an ISFET, can be written out as a cell in the form:

$$Cu^{left}|Ag^{ref}|Ag^+ \text{ in}||Ag^+(\text{and/or } Br^-)|Si|Cu^{right} \quad (IV)$$

AgBr/Br^- ref soln (inert supporting electrolyte); in test soln (inert supporting electrolyte); AgBr|SiO_2|Si|

and it is historically recognized, from the theory and practice of contact or Volta Potential measurements, that the probable condition for zero current is zero field across the SiO_2 (*22*). The measurement of potential at zero current is analogous to a classical Volta Potential measurement, provided any charge carriers in the SiO_2 are *not* in equilibrium at the AgBr and Si interfaces. By equating electrochemical potentials (*35*) of electrons (Fermi levels) at each of the metal/metal and metal/semiconductor interfaces, and by equating electrochemical potentials of Ag^+ at solution/Ag and solution/AgBr interfaces, then

$$\phi^{rt} - \phi^{left} = \frac{1}{F}(\tilde{\mu}_e^{Si} - \tilde{\mu}_{Ag^+}^{AgBr} + \mu_{Ag^+}^{test}) + \Delta\phi_J - \Delta\phi_{ref} \quad (2a)$$

where

$$-\Delta\phi_{ref} = \frac{1}{F}(\mu_{Ag} - \mu_{Ag^+}^{ref}) \quad (3)$$

or

$$\phi^{rt} - \phi^{left} = -\alpha_e^{Si} - \alpha_{Ag^+}^{AgBr} + \frac{\mu_{Ag^+}^{test}}{F} + \Delta\phi_J - \Delta\phi_{ref} \quad (2b)$$

where $-\alpha$'s are the electronic and ionic work functions, because the outer potentials at the SiO_2 interfaces cancel out. This derivation follows Lange's treatment as modified by Parsons (*22*).

Because of the internal equilibrium between ions and electrons (*36*) in AgBr,

$$\tilde{\mu}_{Ag^+}^{AgBr} + \tilde{\mu}_e^{AgBr} = \tilde{\mu}_{Ag}^{AgBr} \quad (4)$$

the more conventional expression for the cell potential is:

$$\phi^{rt} - \phi^{left} = \frac{1}{F}(-\tilde{\mu}_e^{Si} + \tilde{\mu}_e^{AgBr}) + \phi^\circ_{Ag/Ag^+} + \frac{RT}{F}\ln\left[\frac{a_{Ag^+}^{test}}{a_{Ag}^{AgBr}}\right] + \Delta\phi_J - \Delta\phi_{ref} \quad (5a)$$

$$= -\alpha_e^{Si} + \alpha_e^{AgBr} + \phi^\circ_{Ag/Ag^+} + \frac{RT}{F}\ln\left[\frac{a_{Ag^+}^{test}}{a_{Ag}^{AgBr}}\right] + \Delta\phi_J - \Delta\phi_{ref} \quad (5b)$$

In the usual case that the AgBr is saturated with silver metal,

$$\phi^{rt} - \phi^{left} = -\alpha_e^{Si} + \alpha_e^{Ag} + \phi_{Ag/Ag^+} + \Delta\phi_J - \Delta\phi_{ref} \quad (6a)$$

$$= -V_G(\text{Pot}) \quad (6b)$$

where V_G(Pot) is the measured, zero current potentiometric cell voltage.

In the application of this type of cell to the sensor portion of an ISFET, V_G is considered as an adjustable bias applied such that $V_G > V_G$(Pot). Since the reversible interface potential differences retain constant values regardless of bias, all of the excess applied voltage appears as voltage drops across the SiO_2 and across the space charge created at the AgBr/SiO_2 and SiO_2/Si interfaces. Any additional charge induced by bias

is presumed to be linearly additive to the total charge. The additional voltage drops are written in terms of space charge:

$$V_G - V_G(\text{Pot}) = -Q\left[\frac{1}{\kappa\epsilon(\text{AgBr})} + \frac{1}{\kappa\epsilon(\text{Si})} + \frac{1}{C(\text{oxide})}\right] \quad (7)$$

where Q is the total space charge (a negative quantity) in the depletion layer of the silicon. The denominators in the right side of Equation 7 are Gouy–Chapman capacitances of the space charge regions in AgBr and silicon, respectively, while C(oxide) is the geometrical capacitance of the oxide film. κ's are Debye thicknesses and ϵ is the permittivity of free space multiplied by the appropriate dielectric constant. In a practical device, $V_G - V_G$(Pot) also contains terms of the same form as Equation 7 resulting from any fixed charge (surface states) at the SiO_2 interfaces. This term can be added into Equation 7 for completeness, if necessary.

The magnitude of V_G is chosen, such that Q is negative enough to cause the surface to be inverted (charge carriers at the surface with concentrations opposite to that observed in the bulk). The required minimum potential drop between the SiO_2/Si interface and the bulk Si is $(1/F)(E_F - E_i)$, i.e., the difference between the Fermi levels in the actual piece of doped silicon and in an intrinsic piece of silicon. This quantity is computed for the condition that $n(\text{surf}) = p(\text{surf}) = n_i$ or p_i, the intrinsic concentrations. This threshold condition is rather weak and a stronger condition is $(2/F)(E_F - E_i)$, where $n(\text{surf}) = p(\text{bulk}) = N_A$ and $p(\text{surf}) = n_i^2/N_A$, and N_A is the acceptor concentration. The threshold bias for an arbitrary minimum detectable level of Ag^+ in the test solution is written by combining Equations 6 and 7:

$$V_T = \alpha_e^{Si} - \alpha_e^{Ag} - \phi_{Ag/Ag^+}{}^{min} + \Delta\phi_{ref} - \Delta\phi_J - Q^{min}\left[\frac{1}{\kappa\epsilon(\text{AgBr})} + \frac{1}{C(\text{oxide})}\right] + \frac{2}{F}(E_F - E_i) \quad (8)$$

where Q^{min} is the generated space charge (and fixed charge) at "surface inversion" and $\phi_{Ag/Ag^+}{}^{min}$ is the value at the lowest activity level of Ag^+ to be detected.

By fixing V_G, the external bias, charges at interfaces, particularly Q at the SiO_2/Si interface, are established in relation to the silver ion activity. This result follows by eliminating V_G(Pot) between Equations 6 and 7, and taking the difference between the resulting expression for V_G and V_T using Equation 7.

$$V_G - V_T = \text{constant} = \phi_{Ag/Ag^+}{}^{min} - \phi_{Ag/Ag^+} + (Q^{min} - Q)\left[\frac{1}{\kappa\epsilon(\text{AgBr})} + \frac{1}{C(\text{oxide})}\right] + \frac{2}{F}(E_F - E_i) - \frac{Q}{\kappa\epsilon(\text{Si})} + \Delta\Delta\phi_J \quad (9)$$

This equation expresses the theoretical result for MOSFET operation, viz., the external voltage source (ϕ_{Ag/Ag^+} in this case) controls the charge at the SiO_2/Si interface, i.e. the quantity

$$\frac{2}{F}(E_F - E_i) - \frac{Q}{\kappa\epsilon(\text{Si})} \quad (10)$$

If the ISFET is designed to use (1) a surface coating with large Debye thickness, which implies a high resistance coating with low concentration of charge carriers; and (2) a thin oxide or nitride gate so that C(oxide) is large compared with the Debye thickness of the doped Si substrate; then, the charge at the SiO_2/Si interface "tracks" the external voltage. The source-to-drain current, which is proportional to the lateral conductivity, and therefore proportional to the number of charge carriers, is approximately given (in the linear range) by:

$$I \propto (V_G - V_T + \phi_{Ag/Ag^+} - \phi_{Ag/Ag^+}{}^{min} - \Delta\Delta\phi_J - V_D/2) \quad (11)$$

where V_D is the source-to-drain voltage which influences the uniformity of the space charge from one well to the other (*10*).

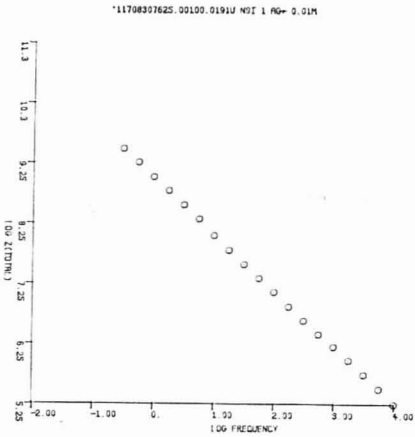

Figure 5. Impedance–frequency response of a field effect sensor. Electrode No. 117 at 25 °C using 100 mV p–p. Electrode used n-type silicon with 1000 nm SiO_2 and 100 nm AgBr. Electrolyte: 0.01 M $AgNO_3$

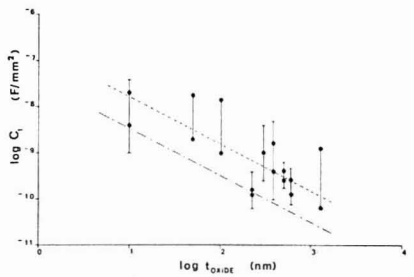

Figure 6. Low frequency capacitance vs. thickness of oxide. Substrates were both n- and p- type silicon

Time-Response Dependence on Oxide Thickness. Although oxide thicknesses in the range 50–1300 nm show no statistically significant differences on either slope or intercept of steady state Ag^+ and Br^- potential responses, thickness variations have a marked effect on time responses. Impedance–frequency plots of the isolated potentiometric sensor show typical capacitive i.e., reactive impedance behavior. One run for a 1000-nm oxide coat is shown in Figure 5. Measured capacitances, calculated from measured impedances vs. oxide thicknesses are shown in Figure 6 for both n and p-type substrates. The uncertainty in the correlation arises from the variable thicknesses of the AgBr coatings. Because the AgBr coatings are of comparable thickness with the SiO_2 films, and the AgBr films have much higher conductivities than the SiO_2

Table I. Response Characteristics with Oxide Thickness Variation

t_{oxide}, nm	Ag^+ Response			Br^- Response		
	Slope, mV/decade	log C_1, F/mm^2	log C_2, F/mm^2	Slope, mV/decade	log C_1, F/mm^2	log C_2, F/mm^2
0–10	63 ± 2	−7.7 ± 0.3	−10 ± 0.2	−49 ± 6	−8.4 ± 0.6	−10 ± 0.8
50–70	60 ± 2	−7.75		−56 ± 1	−8.7	
100 ± 5	59 ± 2	−7.85	−10.	−61 ± 8		
110 ± 5	60 ± 1	−9.0 ± 0.2	−10 ± 0.1	−62 ± 5	−9.0 ± 0.2	−9.9 ± 0.1
180 ± 5	60 ± 1	−9.8 ± 0.4	−10 ± 0.1	−53 ± 8	−9.9	−10.
300 ± 5	60 ± 5	−9.0 ± 0.6	−10.	−40 ± 6		
380 ± 5	58 ± 4	−8.8 ± 0.5	−9.6 ± 0.3	−52 ± 2	−9.4 ± 0.6	−9.9 ± 0.3
500 ± 5	59 ± 4	−9.5 ± 0.2	−9.9	−57 ± 4	−9.6 ± 0.1	−10.
600 ± 6	59 ± 0.6	−9.9 ± 0.2		−54 ± 2	−9.7 ± 0.1	
1300 ± 50	58 ± 1	−8.9	−11.	−56 ± 1	−10.2	−10.6 ± 0.1
ideal:	59			−59		

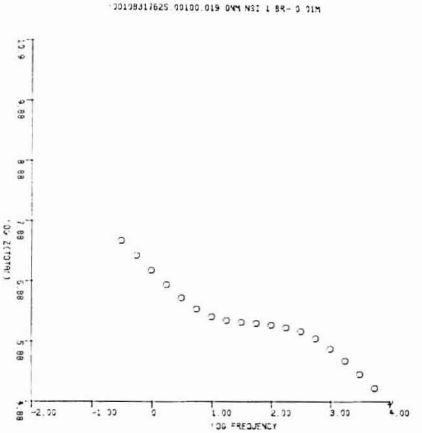

Figure 7. Impedance–frequency response of a very thin oxide coated sensor. Electrode No. 1 at 25 °C using 100 mV p–p. Electrode used n-type silicon with approximately 10 nm SiO_2. Electrolyte: 0.01 M KBr

films, the low frequency capacitance is dominated by the SiO_2 film. At high frequencies for thin oxides, a resistive break in the impedance plot occurs followed by another purely reactive region of characteristic capacitance about 100 times less, as illustrated in Figure 7. For higher oxide thicknesses, the low frequency reactive impedance line shifts to higher frequencies and the resistive arrest shortens and disappears. This result suggests that the high frequency capacitance is dominated by the depletion region. The depletion region capacitance is defined as (*25*, *37*)

$$C_{depl} \approx \left\{ \frac{N_{A,D} q K_{Si} \epsilon_0}{\phi_g} \right\}^{1/2} \quad (12)$$

where $N_{A,D}$ is the acceptor/donor density, q is the electronic charge, K_{Si} is the Si dielectric constant, ϕ_g is the Si bandgap in volts, and ϵ_0 is the permittivity of free space. For the materials used (2–6 ohm-cm), $N_{A,D} \simeq 10^{15}/cm^3$, $q = 1.6 \times 10^{-19}$ C, $K_{Si} \simeq 11.6$, $\epsilon_0 = 10^{-11}/36\pi F/cm$, and $\phi_g \simeq 1.0$ V, then

$$C_{depl} \simeq 1.1 \times 10^{-10}\ F/mm^2 \quad (13)$$

which is in agreement with the observed values.

Response data, including measured low frequency capacitance values C_1, and high-frequency capacitances C_2 are given in Table I. As further evidence that the AgBr layer is sufficiently conducting that it does not interfere with capacitance correlations with depletion region thickness, a series of measurements were made at constant oxide thickness and variable AgBr thicknesses. These results are given in Table II.

Table II. Response Characteristics with AgBr Thickness Variation

t_{AgBr}, nm	Ag^+ response		Br^- response	
	Slope, mV/decade	log C_1, F/mm^2	Slope, mV/decade	log C_1, F/mm^2
55 ± 5	60 ± 6	−9.6 ± 0.3	−57 ± 1	−9.5 ± 0.2
77 ± 7	56 ± 4	−9.8 ± 0.3	−52 ± 9	−9.7 ± 0.3
110 ± 10	60 ± 12	−10. ± 0.9	−48 ± 4	−9.5 ± 0.2
130 ± 10	59 ± 2	−9.4 ± 0.4	−61 ± 6	−9.8 ± 0.9

Table III. Externally Transferred Charge

p_{Ag^+}	Potential (mV) $\phi^{rt} - \phi^{left}$	Q(Cs × 10^{12})
5	55	−3
4	60	1
3	76	1.8
2	100	3
1	200	10

Charge Flow under Shorted Conditions. After potentiometric Volta potential measurements in silver ion concentrations 10^{-5} to 10^{-1} M, with supporting electrolyte, total charge flows under shorting conditions were measured. These results are in Table III.

MODEL AND DISCUSSION

Application of space charge theory to a model for potential, field, and space charge profiles is illustrated in Figure 8. This model, for open circuit potentiometric responses is not unique; it avoids complications from fixed charge surface sites; it is consistent with the experimental potentiometric (Volta potential) results and with the classical theory of potential generation at an ion exchanger/electrolyte interface. The interfacial potential, in the lowest panel, established by ion exchange between the electrolyte and AgBr, is accompanied by generation of space charge and field (displacement) as required by Poisson's equation. When the AgBr layer is thick compared with the Debye thickness, space charge and field (displacement) can decrease to zero at the gate surface when there is no charge penetration in the SiO_2. The generated potential is transmitted through the gate to change the energy (electrochemical potential) of charge carriers in the semiconductor and the attached metal contact. A positive-going interfacial p.d. at the AgBr occurs upon increase of a_{Ag^+}(soln). The corresponding effect at the gate/semiconductor interface is a tendency to repel positive carriers (holes) and thereby to reduce the potential in the semiconductor. However, at open circuit, or in potentiometric measurements where no current

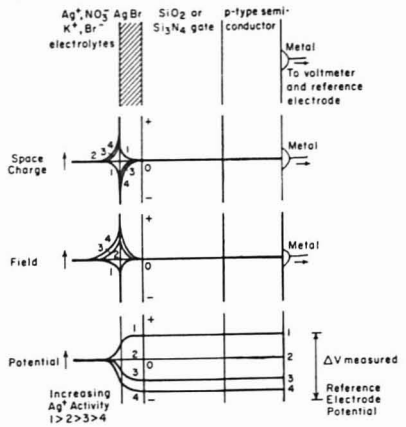

Figure 8. Electrical parameters distribution for the active ion-sensing region of an ISFET. Upper: View including bathing solution, ion sensing membrane (AgBr), insulating layer (gate) and underlying semiconductor. Lower panels: open circuit distribution of space charge, field, and potential

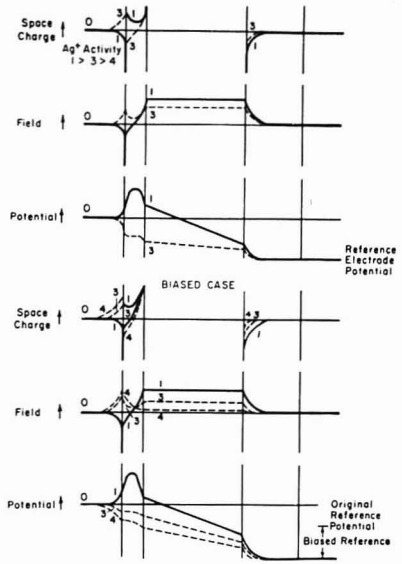

Figure 9. Electrical parameter distribution for the active ion-sensing region of an ISFET. Upper: shorted case—the reference electrode is shorted (connected) to the FET body and space charge is allowed to develop at the FET/gate interface in response to changing Ag^+ activities at the solution/membrane interface (left). Lower: Biased case—in which the reference electrode is biased so that small changes in space charge at the solution/membrane interface (left) still produce p-carrier depletion at the semiconductor/gate interface

can flow, the overall ratio of carriers at the surface does not change in the semiconductor, and there is only minimal buildup of space charge at the semiconductor interface.

When the metal contact is shorted (or biased) to the reference electrode, transient current flows within the semiconductor, and possibly in the AgBr, to charge the gate capacitor. This charging will always occur, because it is necessary to cause the semiconductor potential to reach the reference potential, or reference potential less bias value. This case is shown in Figure 9. Because the reference potential was chosen to be more negative than the AgBr interfacial potential, the gate/semiconductor interface is charged negative (p-depleted, while the AgBr is charged positively. Some of the positive charge is shown to have migrated to the AgBr gate interface, but this effect is not essential to the model. Increasing Ag^+ activity further depletes p-carriers (increases n-carriers), and the gate field is constant and nonzero. The potential profiles are linear in the gate and level off at the reference potential. There is, however, some lower level of Ag^+ activity, below which the semiconductor remains p-type at the surface. To tailor the system to give n-carriers at any desired low activity of Ag^+, one either builds more negative reference electrodes or biases the reference positive with respect to the semiconductor body. The latter is usually done.

From this study and analysis, the behavior of MOS capacitors and electrolyte/ion exchanger capacitors are analogous. Fields generated from net electron or ion transfer at electrolyte/metal and electrolyte/ion exchanger interfaces are the sources of the observed potential responses. Space charge has been shown to play an important role in the establishment of the measured potentials in both types of interfacial process. The field, transmitted through the coating, becomes modified at the coating/gate interface by surface charge or dipoles, and continues through the gate to influence the distribution of electrons and holes at the gate/semiconductor interface. Bringing the field from zero in an external electrolyte medium through positive or negative values at the interfaces and back to zero in the semiconductor bulk is a necessary condition for equilibrium in a static electrochemical cell. To achieve this equilibrium condition, the required process is passage of transient charge through an external circuit (from reference electrode to semiconductor bulk) with resulting localization of space charge, large transverse conductivity change, and corresponding bent energy bands at the gate/semiconductor interface.

Bergvelt's contention that ISFETs are single terminal devices can be criticized from the findings of this study. In the absence of a reference electrode, the cell is isolated at the back of the semiconductor and no external charge can flow to compensate the field and potential generated at the electrolyte/ion exchanger interface. In that event, only small changes in the charge carrier composition at the gate/semiconductor interface and small changes in lateral conductivity can be anticipated (*38–40*). The amount of charge separation in the semiconductor, in the absence of external charging corresponds to generation of quadrupole sheets.

SUMMARY

This paper explores the mode of potential generation for ion exchanging-gate ISFETs by measuring the potential across an SiO_2 gate device, and by showing that charge passes the external circuit to generate the necessary field-cancelling space charge. An analogy is drawn between the potential measurement across a $Cu/Ag/AgBr/SiO_2/Si/Cu$ cell, and the corresponding classical measurement of the Volta Potential (*22*) across the cell $Cu/Ag/AgBr/vacuum/Si/Cu$. Evidence that the field is not caused by impurity charge carriers in the SiO_2 gate, is inferred from impedance measurements for gates of varying thickness, and from the external charge flow.

To answer questions concerning mode of potential generation, the relationship of the potential through the oxide or nitride layer, and need for a reference electrode shorted to the ISFET body, we have used potentiometric methods on

the isolated gate section of nonintegrated FETs (analogous to MOS capacitors). The simpler test sensor structures $AgBr/SiO_2/Si/Cu$, were compared in electrical responses with the standard pressed-AgBr-pellet electrode responses. Intercomparison allowed some conclusions on the important processes and dimensions required for full field effect devices. In addition to concentration–potential response curves, selectivities, impedance–frequency curves and capacitance–voltage curves for isolated field effect sensors were measured. Statistical data treatment of 200 preparations was used to distinguish normal responses.

ACKNOWLEDGMENT

The authors offer their appreciation for the use of vacuum evaporation equipment at the Department of Physics, University of North Carolina at Chapel Hill, and the use of semiconductor processing laboratories at North Carolina State University, Raleigh, N.C., and Oregon State University, Corvallis, Ore.

SYMBOLS

α_i^β	real potential or work function of species i in phase β
C_{depl}	depletion layer capacitance of Si/SiO_2 interface
C	capacitance (geometric) of SiO_2 gate
E_i	Fermi level of intrinsic Si
E_F	Fermi level of actual Si
ϵ	dielectric permittivity = $K\epsilon_0$
ϵ_0	permittivity of free space
F	faraday
μ_i^β	chemical potential of species i in phase β
$\tilde{\mu}^\beta$	electrochemical potential of species i in phase β
κ	reciprocal Debye thickness
K	dielectric constant (dimensionless)
$N_{A,D}$	acceptor or donor concentrations
ϕ	inner potential of a phase
ϕ°_{Ag/Ag^+}	standard half cell potential difference
ϕ_{Ag/Ag^+}	half cell potential difference
$\Delta\phi_J$	electrolyte junction potential
ϕ_g	band gap
$\Delta\phi_{ref}$	reversible reference electrode half cell potential difference
Q	charge stored at the depletion layer Si/SiO_2 interface
q	electronic charge
R	gas constant
T	absolute temperature
V_T	threshhold voltage applied to cell IV to invert surface carriers at a given activity of Ag^+
V_G	applied voltage across cell IV
$V_{G(Pot)}$	zero current applied voltage across Cell IV
ω	angular frequency

LITERATURE CITED

(1) P. Bergveld, *IEEE Trans. Biomed. Eng.*, **17**, 70 (1970).
(2) P. Bergveld, *IEEE Trans, Biomed. Eng.*, **19**, 342 (1972).
(3) J. N. Zemel, *Anal. Chem.*, **47**, 255A (1975).
(4) S. D. Moss, J. Janata, and C. C. Johnson, *Anal. Chem.*, **47**, 2238 (1975).
(5) T. Matsuo and D. K. Wise, *IEEE Trans. Biomed. Eng.*, **21**, 485 (1974).
(6) R. G. Kelley, *Electrochim. Acta*, **22**, 1 (1977).
(7) J. Janata and S. D. Moss, *IEEE Trans. Biomed. Eng.*, **23**, 241 (1976).
(8) U.S. Patent, 3,831,432, P. F. Cox (Texas Instruments) "Environmental Monitoring Device and System", Aug. 27, 1974.
(9) K. I. Lundstrom, M. S. Shiravaman, and C. M. Svensson, *J. Appl. Phys.*, **46**, 3876 (1975).
(10) S. M. Sze, "Physics of Semiconductor Devices", Wiley-Interscience, New York, N.Y., 1969.
(11) R. P. Buck, "Electroanalytical Chemistry of Membranes", *Crit. Rev. Anal. Chem.*, **5** (4), 323 (1975).
(12) G. Brouwer, *Phys. Lett.*, **21**, 399 (1966).
(13) G. Brouwer, *J. Electrochem. Soc.*, **114**, 743 (1967).
(14) J. Janata, "Proceedings of Workshop on Theory, Design and Biomedical Application of Solid State Chemical Sensors", March 28–30, 1977, Case Western Reserve University, P. Cheung, Ed., C.R.C. Press, Cleveland, Ohio, (In press, August 1977).
(15) R. P. Buck, "Physical Methods of Chemistry, Part IIA", A. Weissberger and B. Rossiter, Ed., Interscience, New York, N.Y., 1971, Chapter 2.
(16) J. Koryta, "Ion Selective Electrodes", Cambridge University Press, Cambridge 1975.
(17) G. Eisenman, "Ion Selective Electrodes", R. A. Durst, Ed., *Spec. Publ.* **314**, National Bureau of Standards, U.S. Government Printing Office, Washington, D.C., 1969, Chapter 1.
(18) J. R. Macdonald, *J. Chem. Phys.*, **61**, 3977, 1974.
(19) J. R. Sandifer and R. P. Buck, *J. Electroanal. Chem. Interfacial Electrochem.*, **56**, 385 (1974).
(20) R. P. Buck, D. E. Mathis, and R. K. Rhodes, *J. Electroanal. Chem. Interfacial Electrochem.*, **80**, 245, 1977.
(21) J. O'M. Bockris, and A. K. N. Reddy, "Modern Electrochemistry", Plenum Press, New York, N.Y., 1970.
(22) R. Parsons, "Modern Aspects of Electrochemistry", J. O. Bockris and B. E. Conway, Ed., Butterworth, London, 1954, Chapter 3, p 103.
(23) Presented in part at: Workshop on Theory, Design and Biomedical Application of Solid State Chemical Sensors, March 28–30, 1977, Case Western Reserve University.
(24) P. Delahay, "Double Layer and Electrode Kinetics", Interscience, New York, N.Y., 1965.
(25) A. S. Grove, "Physics and Technology of Semiconductor Devices", Wiley and Sons, New York, N.Y., 1967.
(26) K. H. Zaininger and F. P. Heiman, *Solid State Technol.*, Part I, May, **13**, 44 (1970); Part II, June, **13**, 46 (1970).
(27) R. G. Frieser, *J. Electrochem Soc. Solid State Sci.*, **115**, 1092 (1968).
(28) F. Reif, "Fundamentals of Statistical and Thermal Physics", McGraw-Hill, New York, N.Y., 1965.
(29) Transene Company, Inc., Route One, Rowley, Mass.
(30) R. H. Crawford, "MOSFET in Circuit Design", McGraw-Hill, New York, N.Y., 1967.
(31) U. S. Ganguly, *Proc. IEEE*, **64**, 1010 (1976).
(32) A. J. Bentz, J. R. Sandifer, and R. P. Buck, *Anal. Chem.*, **48**, 543 (1974).
(33) D. E. Mathis and R. P. Buck, *Anal. Chem.*, **48**, 2033 (1976).
(34) "Handbook of Chemistry and Physics", CRC Press, Cleveland, Ohio, 1975–1976 Ed.
(35) E. A. Guggenheim, "Thermodynamics", North-Holland Publishing Co., Amsterdam, 1950, pp 331–334.
(36) Ref. 21, p 864.
(37) J. N. Zemel, private communication.
(38) S. R. Morrison, *Surf. Sci.*, **27**, 586 (1971).
(39) S. R. Morrison, *Surf. Sci.*, **50**, 329 (1975).
(40) S. R. Morrison, "The Chemical Physics of Surfaces", Plenum Press, New York, N.Y., 1977.

RECEIVED April 21, 1977. Accepted September 26, 1977. This work was supported by National Science Foundation grants CHE-75-00970-A01 and DMR 720-3024.

Quantitation of Secondary Ion Mass Spectrometric Images by Microphotodensitometry and Digital Image Processing

J. D. Fassett, J. R. Roth, and G. H. Morrison*

Department of Chemistry, Cornell University, Ithaca, New York 14853

The quantitation of secondary ion mass spectrometric images produced by an ion microscope is accomplished by microphotodensitometry and digital image processing. The film negative of the ion image is converted into a matrix of point densities which maintains the spatial resolution of the original image. The image matrix in density space is converted into intensity space and concentration space with the use of standards. Image analysis techniques are demonstrated, including feature analysis and cross-correlation using the fast Fourier transform.

The ion microscope is a unique analytical tool combining ion sputtering, mass spectrometric filtering, and ion optics to give a spatially resolved mass analysis of the surface of a solid. As a microscope the instrument analyzes morphology in terms of elemental composition. The ion optics provide this direct microscopic imaging by retaining a one-to-one correspondence between the point of origin of an ion sputtered from the surface of a sample and its location in the final mass-filtered beam. The ion micrograph that is produced contains information about the spatial distribution of any selected element in a sample within a diameter of 250 μm or less and with a spatial point-to-point resolution of about a micrometer.

The ion microprobe (*1, 2*), electron microprobe (*3, 4*), and Auger-ion sputtering spectrometer (*5, 6*) all have the proven capability to do compositional spatial analysis and elemental imaging of the surface of a sample. The imaging process in all these cases can be generalized as the sum of sequential point analyses with the probes operating in the scanning mode. This process is in contrast to the ion microscope which produces a micrograph by what can be considered as simultaneous multipoint detection. This contrast means that there is a substantial decrease of time for the ion microscope to produce the same type of information as these scanning microprobes or, conversely, the substantial increase in information produced in the same amount of time by the ion microscope. The compromise commonly made in microprobe imaging between time and total number of counts often results in strong statistical intensity variations which adversely affect the apparent resolution and quality of scanning microprobe images relative to ion images.

The production of the compositional image is different in the scanning probe techniques from that of the ion microscope, and thus quantitation is achieved by differing paths. The image in the sequential point mode is created by the counting of appropriate radiation (ion, electron, or x-ray) for a particular point; storing the data; moving to the next point; and repeating until the desired field is covered. The final image is typically produced by modulation of the intensity on an oscilloscope with the photograph of the oscilloscope resulting in the permanent combination of all the point analyses. With the ion microscope, recording of all the data points is simultaneous; the image is directly produced on photographic film. Quantitation as described in this paper is accomplished by microphotodensitometry of the ion micrograph negative.

As has been done in other techniques in chemical analysis such as emission spectroscopy or spark source mass spectrometry which utilize photographic detection, quantitation in ion microscopy is achieved by the determination of the characteristic curve for the film and the conversion of darkening to intensity (*7–9*). Darkening at any point on the photographic film can be correlated to the ion intensity produced from the analogous point on the surface of the sample. As opposed to these other analytical techniques, however, the determination of the characteristic curve is simplified by the fact that the photographic process is equivalent at all points on the image and film due to the conversion of the secondary ions into monoenergetic electrons. There are no corrections necessary for mass or wavelength differences, thus making the analysis and application of the characteristic curve to the image straightforward.

Until this time ion micrographs have been utilized only for the qualitative data they contain (*2, 10–14*). This paper describes how, by means of microphotodensitometry and computer analysis, image information is made quantitative. Image analysis through digitization of images is now widespread. Gaining its initial impetus from the work of Mariner (*15*) and subsequent extraterrestrial exploration, it is now routinely used in light microscopy, x-ray diffraction, electron microscopy, astronomy, as well as many of the other photographic techniques that have large amounts of information to be processed (*16–18*).

In this paper, procedures are developed to quantify ion micrographs in terms of ion intensity. Given standards, it is shown how this quantitation can be utilized to convert ion intensity into concentration. A simple bimetallic Ni-Cu composite system is used to illustrate the applicability of this procedure. Examples also are presented that illustrate two aspects of image analysis. The first, feature analysis, is used to evaluate heterogeneity in standards. The second, cross-correlation is used to compare and combine information from two related images. Further, cross-correlation shows the use of image transforms and the possibilities that these procedures present. Both feature analysis and cross-correlation are illustrated by micrographs of NBS-660 steels. The above procedures and illustrative images represent only a brief introduction to digital image analysis and its potential application to ion microscopy. The broader application of image analysis techniques to more complex ion micrographs is being studied.

EXPERIMENTAL

Instrumentation. The instrument layout is schematicized in the block diagram, Figure 1. The CAMECA IMS-300 ion microscope used was developed by Castaing and Slodzian (*19*) and described in detail elsewhere (*20*). Instrument operating parameters are given in Table I.

The camera assembly which makes the photographic detection is contained within the converter section of the instrument and is subject to the vacuum in the converter. Actual detection is of an electron image as the final mass filtered beam is projected onto the cathode of an ion-to-electron image converter and the secondary electrons emitted from the converter are accelerated to

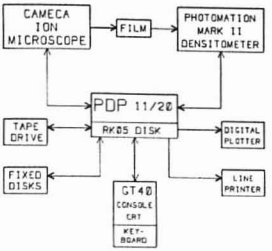

Figure 1. Block diagram of system layout

Table I. Instrument Operating Conditions

Primary ion gases	Oxygen, argon
Primary ion energy	Positive, 5.5 KeV Negative, 14.5 KeV
Primary ion current	10^{-5} to 10^{-3} A/cm^2
Sputtered area of sample	2.5×10^{-3} cm^2
Secondary ion mass range	1-250
Mass resolution	300
Secondary ion polarity	Positive Negative
Image field of view	250 μm or less
Point-to-point resolution	1 μm
Image size to film	28 mm
Magnification	110
Vacuum	10^{-7} Torr

Table II. Photographic Parameters

Film	Agfa Gavaert 37C50, 35 mm
Camera capacity	40 images
Developer	Acufine (7 min)
Rinse	Running water (30 s)
Fixer	Kodak Rapid Fixer (2 min)
Wash	Running water (10 min)

20 keV and focused onto the film. Electron sensitive roll film is used (Agfa Gavaert 37C50). Standard development procedures for the film are used and summarized in Table II.

A Photomation Mark II scanning microphotodensitometer interfaced to a PDP 11/20 computer is used to digitize the images. The film is placed in an opening in a cylindrical drum which rotates at high speed. Density is read by an incoherent optical system that is always on axis which guarantees linearity and fixed position. After each circumferential record has been scanned, the entire optical system (illumination and detection) is stepped along the axis of the drum in preparation for the next record. Zero density is electronically corrected with each revolution of the drum by the introduction of an open slit in the light path. The sampled density is amplified in a logarithmic amplifier and fed to the analog-to-digital converter. Digital data are transferred to the computer through the interface and control circuits. Table III summarizes the densitometer specifications.

The computer facilities consist of a PDP 11/20 with a 24K word memory; a 1.2-M word cartridge disk used for the RT-11 operating system, software development, and storage; a dual fixed disk assembly and a 9-track magnetic tape unit, which offer potentially unlimited data storage space; a 600-line-per-minute line printer for hard copies of program computations; an incremental plotter for contour plotting, calibration curves, and histographs; and a GT 40 graphics display and processor.

The computer is used in this study entirely as a processor of image data matrices. However, through a computer–ion microscope interface, the computer also can be dedicated to the operation of the ion microscope. Although the contemporaneous use of the computer is not possible, the potential exists for dual use and is being investigated.

Computer Programs. Programming was done primarily in FORTRAN and stored on disk. The PDP 11/20 controls all acquisition and calculation programs. The acquisition programs

Table III. Microphotodensitometer Specifications

Data format	8 bits
Raster setting	100 μm × 100 μm
Drum speed	4 rps
Positional accuracy	± 2 μm/cm on film
Density range	0-3D or 0-2D
Time to acquire image (256 × 256)	128 s

which create the primary image data files are designed to store the data in a minimum amount of space. Each image point has 8-bit resolution (0–255) and is packed into a single byte of 8 bits in the image data file. The total amount of disk space required by a 256 × 256 point image, the maximum size for which the system is designed, is 33K words.

The calculation and manipulation of image data is done by a general program, IONPIX, consisting of a keyboard command interpreter which supervises calls to the main FORTRAN subroutines. IONPIX is much larger than the available memory space in the computer but is made operable by the overlay facility of the executive monitor, RT-11. The subroutines presently callable by IONPIX are classified in several broad functional categories which include mathematical, single file examining, image analysis, file shuffling, and ion micrograph specific. These subprograms represent a basic set of useful image file handling routines expanded by subprograms designed specifically for ion images. The structure of IONPIX is such that expansion and change is readily facilitated.

Details concerning the operation and structure of IONPIX and its subroutines are available from the authors.

RESULTS AND DISCUSSION

A typical ion image has a 250-μm diameter circular field of view with a point-to-point resolution of 1 μm. Thus, there are 50 000 information bits in a typical ion image with each information bit representing the total number of ions of a particular mass being extracted from a 1-μm^2 area of the surface of a sample. The analysis of the information bits in an ion image is readily accomplished via computerization.

The ion micrograph is 28 mm in diameter and is digitized into a 256 × 256 square point matrix using the 100-μm^2 aperture of the microphotodensitometer. If the image is centered, digitization results in the loss of about 6% of the total image with no loss of point-to-point resolution. One of the results of digitizing a circular image into a square data file is the inclusion of non-ion image points in the file. About 10% of the digitized points in the image file are background points to the ion image field. This background is used in making background corrections on image points.

Each datum in the primary image is acquired in the range of 0–2D (100% to 1% transmittance) or 0–3D (100% to 0.1% transmittance). In both cases, the number of steps measureable is 256. The point density resolution is therefore inversely proportional to the range. The experimenter has the choice of increasing the resolution on images that do not exceed a maximum density of two. However, the increased dynamic range in an image that has a maximum density that approaches three is more important than higher point resolution. The experimenter aims to satisfy this condition in the determination of the exposure times in the images that are taken.

The pivotal step in quantitation of the ion image is the determination of the characteristic curve of the film and the conversion of film darkening per information bit to ions extracted per information bit. The characteristic curve is determined by the taking of a series of standard images of known intensity and of graded exposures from background to saturation for each roll of film to be quantized. These standard images define the curve of density vs. intensity. The intensity of image points of experimental images are extrapolated from this curve.

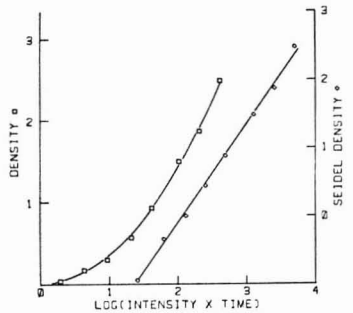

Figure 2. Characteristic curve for ion microscope film: (□) density vs. logarithm of the exposure; (◇) Seidel density vs. logarithm of exposure. The exposure is in arbitrary units of intensity–time

As previously described, the recorded ion image is produced on film by an electron beam, with the electrons accelerated to 20 keV. The response of photographic emulsions to electrons is well understood and can be described as a single hit process whereas the exposure to light requires the cooperative action of several photons (*21*). One result of this single hit process is that density is proportional to exposure in the low density range $D < D_s/4$, where D_s is the saturation density of the film. Experimentally, it was found that the useful density range where this linearity manifested itself was extremely limiting and large deviations occurred for densities greater than 1. It was decided, therefore, to analyze the characteristic curve in the more familiar manner of density vs. the logarithm of the exposure (Hurter and Driffield curve). This curve for electrons is similar to that of light with a toe region at low densities. Although not as large as that for light, the central region of the curve is linear.

Empirically, it was found that the linear region of the D vs. $\log_{10} E$ curve extended through the uppermost digitized density of 3. It was found that the linear range could be extended significantly in the toe region by the modification of densities according to Seidel (*22*):

$$D_c = \log (1/T_c - 1) \qquad (1)$$

where D_c is the Seidel density and T_c is the background corrected transmittance. This correction has little effect on the higher density values but succeeds in straightening the toe of the curve so that essentially the entire range of densities is linearly calibrated. Figure 2 illustrates a typical D vs. $\log_{10} E$ curve for a roll of ion microscope film, as well as the results of the Seidel correction. Experimentation was done also on the modification of the recorded densities according to the procedure of Arrak (*23*), where the 1 in the Seidel equation is an adjustable parameter. It was found that significantly better results were not obtained by changing the parameter from being equal to 1.

The standard images are made of an aluminum disk in which the field of view is limited by a 35-μm diameter circular field aperture. The aluminum disk is defocused to ensure a homogeneous intensity across the field of view. The intensity level can either be read in terms of current off the photomultiplier or converted into counts per second. Since the total number of information bits is fixed and equivalent for each individual bit, the ion intensity per information bit is readily calculated.

The field of view is limited to 35 μm for two reasons. The first is that it guarantees complete measurement (integration) of the signal by the photomultiplier which nominally sees a

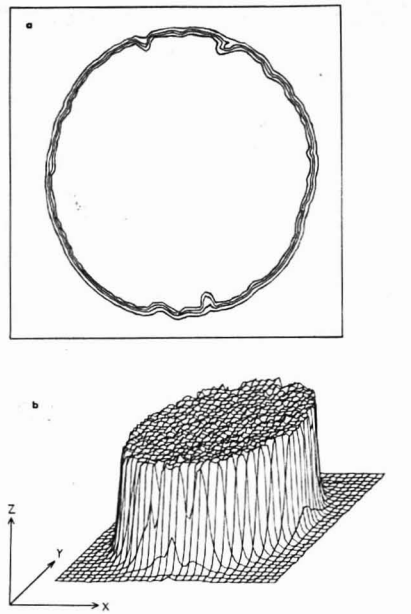

Figure 3. Standard image. (a) Contour plot with equidistant isodensity levels from maximum to minimum densities of the image. (b) Three-dimensional representation where the Z-axis represents density and X and Y-axes, position. Size of image file: 64 × 64

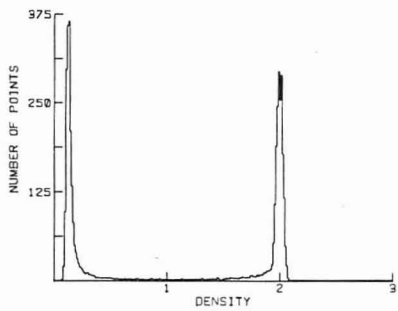

Figure 4. Histogram of standard image in Figure 3

125-μm diameter field of view and which has a slight loss of light collection efficiency around the edges due to the optics that carry the light to the photomultiplier. The second reason is that it produces an image on the film of 3.9 mm and this size can be conveniently digitized into a 64 × 64 image disk file. An iso-density contour plot and a three-dimensional representation of a standard image are illustrated by Figure 3. It should be noted that there is present a large amount of background as well as foreground area in each standard image file.

A computer routine is used to extract the average background and foreground densities and estimate the standard deviations for these values from the standard images. Figure 4 illustrates a histogram of a typical standard image. The background and foreground are assigned to the maxima of the

low and high density peaks, respectively. The standard deviations are estimated from the points to the low density side of the background and to the high density side of the foreground. The points in between the two peaks are those that lie in the foreground–background edge region and thus would be expected to cause deviation from Gaussian character for the peaks.

The data file consisting of the background and foreground densities and exposure values for the standard images is input to the routine that determines the characteristic curve. The computer calculates the best linear fit for the logarithm of exposure vs. the background corrected, Seidel modified density values, and outputs the coefficients for the line and the deviation from this line that each point suffers.

The experimental image is converted from density space to ion intensity space by application of the characteristic curve on the background corrected and exposure-time corrected densities. The process involves the determination of the center of the ion image circle which delineates the ion image field in the entire image file. This determination is accomplished by an iterative computer routine that finds the center point of the image by minimizing points over the background threshold in the background. The center point is typically within 5 pixels (picture elements) of the center of the square image file and varies according to where the photomultiplier head was manually stationed at digitization time.

Each ion image file consists of the image field and background to the image field in a ratio of digitized points of about 9 to 1. The film background, which is a function of the history of the film, is in the density range 0.07 to 0.15 (85% to 70% transmittance). The determination of the ion image field and consequently the background field allows the determination of the background in the immediate vicinity of the image and background correction of image field points.

The effective range of the analytical curve is limited at the upper end by saturation of the microphotodensitometer. The saturation density of the microphotodensitometer is sufficiently less than the saturation density of the film so that all the upper points lie on the straight line region of the characteristic curve. It is found that for the low end of the density range the deviations from the characteristic curve begin to become significant at approximately twice the background level. The lowest density quantitative point of the characteristic curve is designated the low limit to the analytical range, and it is typically twice the background level or slightly higher. Thus, the analytical range in this quantitation process extends over a density range of greater than 2.5 with more than 200 levels. Since density is related exponentially to intensity with a slope approximately of 1, the analytical intensities extend over a range between 100 and 1000.

Precision and Accuracy. A discussion of the precision and accuracy involved in ion image quantization encompasses the digitization process, the film darkening and development, and the determination and application of the characteristic curve. Integral to this discussion is the question of what minimum change in ion intensity produces a detectible change in density (contrast) for the process. Also important to the discussion is the effective analytical range of the process, as well as the ramifications of the conversion from a logarithmic to linear quantized image.

The accuracy of the digitization process can be characterized by the quantization error, the error due to the quantized steps into which the density range is divided. This error is constant at each step and is equal to $0.289 \times DR/QL$, where DR is the density range and QL are the number of quantized levels (*24*). Therefore, the relative error is inversely proportional to the density and only at low density levels does it become truly significant. As illustrated in Figure 5, it is less than 5% for densities greater than 0.1 and less than 1% for densities greater than 0.5.

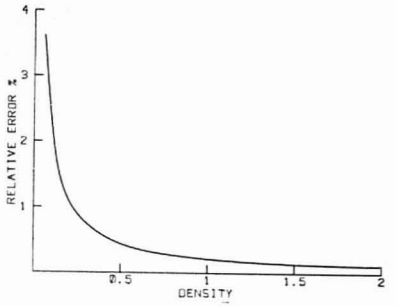

Figure 5. Quantization error for digitization range 0–2D with 256 steps

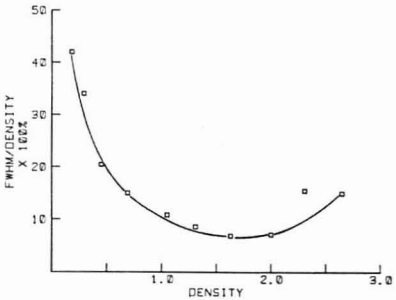

Figure 6. Histogram peak resolution as measured by normalized peak width at half maximum vs. density

The precision of the digitization process was estimated by the repetitive scanning of images with no adjustments to the densitometer. The standard deviation of the process was determined by averaging the standard deviations for corresponding points on different image files. This average standard deviation was equal to 0.65 of one density step for both low and high average density images.

The precision associated with the image formation process can be estimated conveniently from the standard images used to determine the characteristic curve. The histogram of the foreground field produces a symmetrical Gaussian-like peak whose width is relatively independent of the exposure except at maximum density levels. Figure 6 shows the effect of measurement precision on the resolution of histogram peaks. The major sources of imprecision in the imaging process are probably nonhomogeneity in the standard source for the image and statistical variations in the film. There is no way to distinguish the relative contribution of these effects to the overall spreading of densities. The fact that the eye is the final judge of the homogeneity of the image being photographed, and the variation in the measured densities would be indistinguishable to the eye, suggests that the primary component to measurement imprecision could be from the sample itself.

The characteristic curve least-squares linear fit shows typically an average deviation of points of 5%. The accuracy of conversion of the experimental density points from density space to ion intensity space by the application of this characteristic curve must be considered to have a similar accuracy. The fact that the conversion is made from the

Table IV. Calculated Concentrations of Composite Features

Image	Isotope	Exposure time, s	Feature	Average density	Background	Concn[a]	Relative error, %
1	^{58}Ni	5	1	0.625	0.094	0.939	−3.1
			2	0.647		1.046	4.6
2	^{63}Cu	20		0.780	0.103	1.099	9.9
3	^{60}Ni	20	1	0.759	0.099	0.960	−4.0
			2	0.814		1.138	13.8

[a] Cu characteristic curve; $D_c = 0.661 + 0.921 \log (Ct)$. Ni characteristic curve; $D_c = 0.264 + 0.938 \log (Ct)$, corrected for isotopic abundance.

logarithm of the exposure to the time-corrected intensity results in a larger relative error and a nonsymmetrical error bar in intensity space. Furthermore, conversion of a Gaussian distribution of densities into intensity space results in a skewed peak in intensity space by the nonequivalent widths of the quantized steps. The result of this conversion, then, is the disproportionate weighting of higher intensities which causes an overestimate for the average intensity value for a feature with a Gaussian distribution of densities. The error is dependent upon the slope of the characteristic curve, which determines the intensity range, the width of the peak, and the number of quantized levels which is constant. This error was measured on a series of test images and was always less than 8% for a typical characteristic curve of slope 1.0. This error, however, is potentially correctable by the recognition and smoothing of features prior to conversion into intensity space.

Applications. *I. Concentration Mapping.* The fundamental limitation to quantitative analysis by SIMS is the variability of the secondary ion yield which is dependent upon the state of the surface, the chemical environment (matrix effect), and effects induced by the primary ion sputtering. Thus, a compositional micrograph in ion intensity space is not necessarily directly convertible into concentration space. However, it has been shown that by using closely matched standards quantitative accuracies of 10% and better can be achieved (*25, 26*). The limitation that exists here is the general nonavailability of suitable standards.

From Morrison and Slodzian (*20*) the relationship between concentration and ion intensity is:

$$i = \tau C_m S i_p G^{-2} \qquad (2)$$

where i is the illumination, ions collected per unit area of surface times time; τ is the practical ion yield, number of M^+ ions collected per number of M atoms removed from sample; C_m is the atomic concentration corrected for isotopic abundance; S is the sputtering yield, number of atoms removed per incoming particle; i_p is the primary ion density; and G is the degree of magnification. If the practical ion yields and sputtering yields of a sample and standard are equal, the ion intensity or illumination is directly proportional to concentration when the analyses of both are made under similar conditions.

When the assumptions that sputtering yields and practical ion yields are equal for sample and standard are made, the characteristic curve can be calibrated in terms of concentration of the standard element rather than in ion intensity. The characteristic curve as previously analyzed exhibits a linear relationship between Seidel densities and the logarithm of the product of ion intensity and time, or of $\tau C_m S i_p G^{-2}$ and time. For images exposed under similar conditions and of similar materials the logarithm of $\tau C_m S i_p G^{-2}$ is equal to the logarithm of $C_m t$ plus the logarithm of $\tau S i_p G^{-2}$ which is constant. Thus, given the characteristic curve for the film and the density of the image exposed for a time, t, of a standard material, the curve can be recalibrated to the logarithm of the product of concentration and time vs. Seidel density. Alternatively, the characteristic curve can be constructed from a series of graded exposure images of the standard in the same manner as prescribed for ion intensity.

As a case in point of how standards can be used in the determination of elemental concentrations of micrographic features, a sample was prepared from nickel and copper foils consisting of two alternating layers of the foils, each with a nominal thickness of 100 μm, clad together by heat and pressure. Images were taken of this composite and of the individual standard foils, all under similar conditions. The characteristic curves for both elements were determined from graded exposures of 0.5 to 10 s. The curves are linear with correlation coefficients of 0.9969 for copper and 0.9991 for nickel. The slopes of the curves are equal within experimental error. From these curves the images of the composite were converted into concentration space by the extrapolation of the background and time-corrected Seidel densities to concentrations.

The results of this procedure as illustrated by the three related ion images of $^{58}Ni^+$, $^{63}Cu^+$, and $^{60}Ni^+$ of the composite in Figure 7 are summarized in Table IV. It is seen that the average concentrations of the features are equal to 1.00, the nominal concentration, within experimental precision. The average relative error in accuracy is 7%. The average precision equals 17%. Much of the imprecision can be ascribed to the materials; for instance, obvious crystal grain structure for the copper and topography induced by ion sputtering at the interfaces of the composite and the mounting material. The contour plots of the images in concentration space also are illustrated in Figure 7. Although simply designed, this example shows the applicability of concentration mapping. Furthermore, the interchangeability of isotopic images is also shown.

II. Sampling Constants. As previously stated, a major limitation to quantitative analysis with the ion microprobe is the lack of suitable standards. It is common practice to calibrate signals with standards that have been certified for bulk concentrations using techniques that are insensitive to microscale variations in concentration. As opposed to bulk techniques in which homogenization of large amounts of material will eliminate sampling problems, probe techniques are constrained by their intrinsic nature to microsampling of materials that may or may not be homogeneous on the micro-scale. As a result of this constraint, sampling error can assume the preeminent fraction of the total error in the microprobe measurement.

The level and range of heterogeneity of a sample can be estimated by the application of statistical techniques to the microprobe data (*27*). The procedure involves the compilation of single point analyses and the determination of the coefficient of variance for these points. The result of this analysis is that for a given probe diameter, a level of confidence can be assigned that sampling is of a homogenous area.

Whereas the previous method of analysis gives an indirect indication of homogeneity, an ion micrograph (which can be considered a compilation of one μm^2 point analyses) gives all the information necessary to directly determine the feasibility

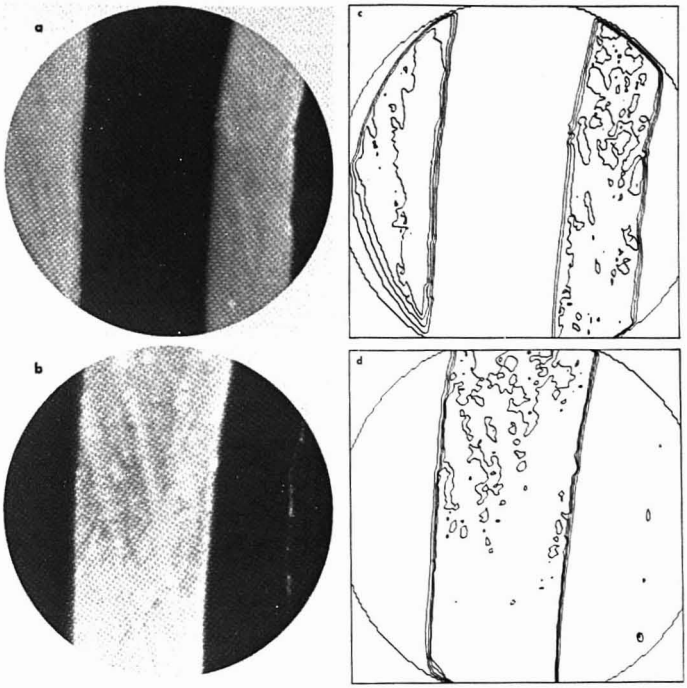

Figure 7. Bimetallic composite sample: (a) $^{58}Ni^+$ ion micrograph, 5-s exposure. (b) $^{63}Cu^+$ ion micrograph, 20-s exposure. Fields of view: 225 μm. The ^{60}Ni image is similar to $^{58}Ni^+$ and is not shown. (c) and (d) Isoconcentration contour plots of (a) and (b), respectively. Contour levels: 1. Calculated ion image field; 2–5. Concentration levels 25%, 50%, 75%, and 100%. Size of image files 256 × 256

of probe analyses to the level of resolution of the image by showing the presence or absence of inclusions or secondary phases. Scilla and Morrison (*28*) have illustrated how images can be so utilized. Here, it is illustrated how the formulas they have derived can be combined with digital image analysis to determine the sampling constant for any material. This sampling constant, as they have shown, is related to the degree of uncertainty expected (sampling error) at a given confidence level for a probe measurement of a given area of the sample.

The sampling constant of Scilla and Morrison is applicable when the element of interest is randomly dispersed as inclusions in the material under study. The greater the density of the elemental inclusions in number per volume, the greater is the homogeneity of the element in the material, and the smaller is this element's sampling constant. In their determination of the sampling constant, Scilla and Morrison utilized absolute feature counting, making the assumption that all inclusions are of relatively constant size and intensity. With digital processing of the image, a more exact determination of the sampling constant can be made by utilizing the intensity information in the image. It can be shown that:

$$K_s = (1/I_T)(A_T \sum_{i=1}^{N} i_i^2)^{1/2} (1 - A_I/A_T)^{-1/2} \quad (3)$$

where K_s is the sampling constant in micrometers; i_i is the intensity of inclusion i; N is the total number of inclusions; I_T is the total intensity of the ion image; A_T is the total area of the image, in μm^2; and A_I is the total area of inclusions. Assuming constant intensity for each inclusion, this equation reduces to the equation of Scilla and Morrison:

$$K_s = (I_I/I_T)\,\bar{n}^{-1/2}\,(1 - A_I/A_T)^{-1/2} \quad (4)$$

where $\bar{n}$ is the number of inclusions per unit area. I_I/I_T is the fraction of the signal produced by the inclusions. If there is a background signal, that is, if the element studied is present in two phases, one of which is homogeneous, the sampling constant is reduced proportionately. The term $(1 - A_I/A_T)$ is a correction due to the surface coverage by inclusions. Assuming that the fraction occupied by inclusions is small eliminates this term.

It should be pointed out that although homogeneity encompasses the three-dimensional distribution of phases, the ion microprobe is essentially a two-dimensional analyzer of an elemental surface. Thus, the two-dimensional description of homogeneity, inclusions per unit area, is more appropriate to the ion microprobe measurement. It is true that in making the image, exposure time represents integration over depth. However, the depth of field vs. the breadth of field is insignificant (Angstroms vs. micrometers) justifying the assumption that the image represents an elemental projection of the surface.

The determination of sampling constants is exemplified using the two images of titanium, Figure 8, in NBS-662 and 664 steels. Titanium is one of the most notoriously inhomogeneous elements in the NBS steels. These images were digitized, the image field was determined, and the image density points were converted to ion intensities. The in-

Table V. Determination of Sampling Constant

Element/ standard	Total intensity of image, I_T	Total area, A_T	Total intensity of inclusions I_I	I_I/I_T	A_I/A_T	$K_s(\mu m)$
Titanium/ NBS-664	9420	37100	8400	0.894	0.083	56.6
Titanium/ NBS-662	20998	36200	17585	0.838	0.105	46.8

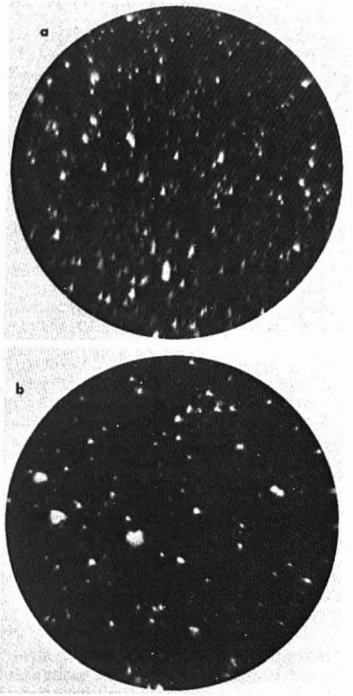

Figure 8. $^{48}Ti^+$ ion images from: (a) NBS-662 steel, 2-s exposure; (b) NBS-664 steel, 20-s exposure. Fields of view: 250 μm

clusions are identified in the image field by thresholding. The threshold value is arbitrarily chosen as the average value of the image. At this intensity, the partial derivative of integrated intensity equals the partial derivative of integrated area. Once the inclusions are isolated, K_s as defined in Equation 3 is straightforwardly found as all variables are calculable. The results of this calculation are listed in Table V. The application of sampling constants is described in the paper by Scilla and Morrison. In brief, it can be said that to achieve less than 25% sampling error at the 95% confidence limit using a 100-μm diameter circular probe there are required 26 probe analyses for titanium in NBS-664 steel and 18 probe analyses of titanium in NBS-662 steel.

III. Image Cross-Correlation. The theory of digital image processing is rapidly expanding, as well as the application of this theory in all fields. The ability to compress, enhance, and amend the information contained in images is made possible through the use of image transforms and complex mathematical procedures. One of the most commonly used image transforms is the discrete Fourier transform. Here, it is illustrated how the discrete Fourier transform can be applied to ion images to cross-correlate similar images of different elements from the same spot on a sample. Combining information in two cross-correlated images produces a four-dimensional array of information, containing two spatial dimensions and two elemental ion intensity dimensions.

The cross-correlation function is a traditional method of matching two images. The basis for the operation of this function is that for aligned images of similar object fields, the cross-correlation is the sum of large values multiplied by large values and small values multiplied by small values. When the images are of improperly oriented similar fields, or of different object fields, the value of the cross-correlation function is the sum of large values multiplied by small values and small values multiplied by large values. The former case will always yield a higher number than the latter case, and therefore the cross-correlation function will reach a maximum for properly oriented, related pictures. The formula for the discrete cross-correlation function (CCF) of two images, I_1 and I_2, is:

$$CCF(MX,MY) = \sum_{JY}\sum_{JX} I_1(JX,JY)I_2(JX + MX, JY + MY) \quad (5)$$

To get a matrix of $N \times N$ CCF values for two image arrays that are each $N \times N$, a total of N^4 operations must be executed. It can be shown, however, that:

$$FT(CCF) = FT(I_1)FT^*(I_2) \quad (6)$$

where FT is the Fourier transform function. Whereas the number of operations required by the discrete CCF is prohibitive on large image arrays, the Fourier transform reduces the number of operations by two to three orders of magnitude making the calculation feasible.

The application of Fourier transforms and their subsequent use in cross-correlation is accomplished by specific subroutines of IONPIX. It is impossible to perform a continuous Fourier transform with a digital computer forcing the use of the discrete Fourier transform. The discrete Fourier transform of an $N \times N$ array, $A(IX,IY)$ is:

$$B(IKX,IKY) = \sum_{IX=0}^{N-1}\sum_{IY=0}^{N-1} A(IX,IY)e^{(2\pi i/N)(IKX\cdot IX + IKY\cdot IY)} \quad (7)$$

for IKX, IKY from zero to $n - 1$. An advantage of the discrete Fourier transform is that the Cooley–Tukey or "fast Fourier transform" algorithm allows this function to be calculated relatively quickly (*29*). There is required for the Fourier transform a conversion of the image array from real to complex numbers, as each datum in the Fourier space has a real and imaginary part. This conversion results in a doubling of computer memory required to contain the image. The maximum image size is then reduced to 128 × 128. The procedural steps in the cross-correlation of two real image files are the conversion of each image file from real to complex space; the Fourier transform of each complex file; the complex multiplication of the two Fourier transforms; and finally the inverse Fourier transform of the product. The cross-corre-

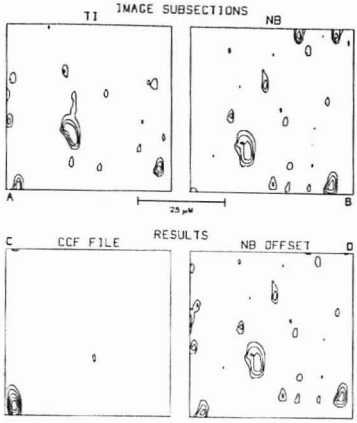

Figure 9. Cross-correlation of ion images. (a) and (b) are contour plots of $^{48}Ti^+$ and $^{93}Nb^+$ in NBS-662 (2-s and 100-s exposures, respectively). Size of files 64 × 64; subsections of full field 256 × 256 images. (c) Contour plot of the CCF of (a) and (b). Peak at (X,Y) = (5,60) indicates offset (−4,+5) for image (b). (d) $^{93}Nb^+$ image subsection with indicated offset

lation file is then searched for the maximum point and position of the maximum point. The height or magnitude of the maximum point is a measure of absolute correlation. The offset position indicates whether the files are properly oriented relative to each other. If the maximum is at point (1,1) either the images are best matched relative to each other or there is no better match calculable. The images must be within an absolute distance apart for a meaningful offset to be calculated, if they are related. This distance, known as the capture radius, is about $N/3$, where N is the number of picture elements to a side. For a precise determination of the offset, the original images should be within $N/4$ picture elements. If the indicated offset is made to the original picture and another cross-correlation to the reference image made, either a perfect or very close to perfect match can be expected with an increased height of the correlation peak. Images can be expected to be positioned within one-half picture element relative to each other.

To illustrate the application of cross-correlation, two images of NBS-662 steel of titanium and niobium were used. It is well known that Ti and Nb are strong carbide formers in steels, and that both elements are strongly heterogeneous (*30*). Therefore, there should exist a strong correlation between the images. Correlation was made on sub-images of the two ion images of size 64 × 64, or 1/16 the total image field. Contour plots of the sub-images, the resultant cross-correlation file, and the offset image indicated by the correlation peak are illustrated in Figure 9. The height of the correlation peak is indicative of the strong correlation between the images.

CONCLUSION

Ion microscopy is a multidimensional analytical technique producing simultaneous spatial (3 dimensions) and elemental (n dimensions) information about a sample. As a result, ion microscopy is a very powerful but also a very complex technique. The fact that the power of the technique has not been fully exploited is probably due to its complexities. The use of the digital computer with ion imaging challenges the complexities with its multidimensional information handling. The applications in this article illustrate differing aspects of ion image quantitation but only scratch the surface. The exercise of the technique as an analytical tool to problems in such disparate fields as biology, metallurgy, and semiconductor technology is extremely promising.

ACKNOWLEDGMENT

The authors are grateful to B. F. Addis for preparation of the composite sample and to B. F. Siegel, E. Kirkland, and K. Welles for their helpful discussions in the course of this project.

LITERATURE CITED

(1) H. Liebl, *J. Appl. Phys.*, **38**, 5277 (1967).
(2) P. Williams, C. A. Evans, M. L. Grossbeck, and H. K. Birnbaum, *Anal. Chem.*, **48**, 964 (1976).
(3) K. Heinrich, *Adv. Opt. Electron Microsc.*, **6**, 275 (1977).
(4) H. Yakowitz and J. I. Goldstein, in "Practical Scanning Electron Microscopy", J. I. Goldstein and H. Yakowitz, Ed., Plenum Press, New York, N.Y., 1975.
(5) B. D. Powell, D. P. Woodruff, and B. W. Griffiths, *J. Phys. E.*, **8**, 548 (1975).
(6) N. C. McDonald, in "Electron Microscopy: Physical Aspects", D. Beaman and B. Siegel, Ed., Wiley, New York, N.Y., 1974.
(7) M. Margoshes and S. Rasberry, *Spectrochim. Acta*, **24**, 497 (1969).
(8) R. Decker and D. Eve, *Spectrochim. Acta, Part B*, **25**, 479 (1970).
(9) R. E. Honig, in "Trace Analysis by Mass Spectrometry", A. J. Ahearn, Ed., Academic Press, New York, N.Y., 1972.
(10) J. M. Rouberol, P. Basseville, and J. P. Lenoir, *J. Radioanal. Chem.*, **12**, 59 (1967).
(11) A. J. Socha, *Surf. Sci.*, **25**, 147 (1971).
(12) E. Berkey, G. G. Sweeney, and W. M. Hickam, *Nucl. Technol.*, **16**, 263 (1973).
(13) D. Maltrepierre, D. Thivellier, and R. Tricot, *Metall. Trans.*, **6A**, 287 (1975).
(14) A. Pebler, G. G. Sweeney, and P. M. Castle, *Metall. Trans.*, **6A**, 991 (1975).
(15) R. B. Leighton, N. H. Horowitz, B. C. Murray, R. P. Sharp, A. G. Herriman, A. T. Young, B. A. Smith, M. E. Davies, and C. B. Leovy, *Science*, **165**, 684 (1969).
(16) M. Mendelsohn, B. H. Mayall, and J. M. S. Prewitt, *Adv. Opt. Electron. Microsc.*, **2**, 77 (1968).
(17) A. Rosenfeld, Ed., "Digital Picture Analysis", Springer-Verlag, New York, N.Y., 1976.
(18) A. Rosenfeld and A. Kak, "Digital Picture Processing", Academic Press, New York, N.Y., 1976.
(19) R. Castaing and G. Slodzian, *J. Microsc.*, **1**, 395 (1962).
(20) G. H. Morrison and G. Slodzian, *Anal. Chem.*, **47**, 932A (1975).
(21) R. C. Valentine, *Adv. Opt. Electron. Microsc.*, **1**, 180 (1966).
(22) H. Kaiser, *Spectrochim., Acta*, **2**, 1 (1941).
(23) A. Arrak, *Appl. Spectrosc.*, **11**, 38 (1957).
(24) C. R. Walli, *Proc. Fall Joint Computer Cong.*, **25**, 545 (1964).
(25) J. A. McHugh, in "Methods and Phenomena, Methods of Surface Analysis", S. P. Wolski and A. W. Czanderna, Ed., Elsevier Publishing Co., Amsterdam, 1976.
(26) J. D. Ganjei, D. P. Leta, and G. H. Morrison, accepted for publication in *Anal. Chem.*
(27) J. I. Goldstein and J. W. Colby, in "Practical Scanning Electron Microscopy", J. I. Goldstein and H. Yakowitz, Ed., Plenum Press, New York, N.Y., 1975.
(28) G. J. Scilla and G. H. Morrison, *Anal. Chem.*, **49**, 1529 (1977).
(29) J. W. Cooley and J. W. Tukey, *Math. Comp.*, **19**, 297 (1965).
(30) E. C. Bain, "Functions of the Alloying Elements in Steel", American Society for Metals (1939).

RECEIVED for review August 22, 1977. Accepted September 27, 1977. Financial support was provided by the National Science Foundation under Grant No. CHE-7608533 and through the Cornell Materials Science Center. One of the authors (J.D.F.) was the recipient of the Edwin Dowzard Summer Fellowship of the Analytical Division, American Chemical Society.

Quantitative Elemental Analysis of Substituted Hydrocarbon Monolayers on Platinum by Auger Electron Spectroscopy with Electrochemical Calibration

James A. Schoeffel

Varian Associates, Vacuum Division, 25 Route 22, Springfield, New Jersey 07081

Arthur T. Hubbard*

Department of Chemistry, University of California, Santa Barbara, California 93106

Clean, structurally ordered Pt(100) surfaces were prepared in ultrahigh vacuum and characterized by means of low energy electron diffraction and Auger electron spectroscopy. The Pt(100) surfaces were treated with ethylene, allylamine, allylacetic acid, chlorotrifluoroethylene, or thiophene which formed a chemisorbed layer of known stoichiometric composition containing the elements, C, N, O, F, Cl, or S in various combinations. Second harmonic Auger electron spectra of these layers were obtained in absolute units (A/eV^2) and stored in digital form by computer. The spectra were integrated numerically to obtain the total Auger electron current for each element in the adsorbed layer. The interfacial concentration of each adsorbed layer was determined by means of thin-layer coulometry. The proportionality constant relating Auger electron current to adsorbed amount was thus determined. Equations permitting calculation of Auger electron current were developed and compared with experiment. The results indicate that Auger electron current is generally rather insensitive to the chemical environment of the emitting atom. Calculated intensities correspond to the measured values within 10% in most instances.

A number of experiments to calibrate Auger electron spectrometers for various applications have been reported (*1–8*). Each of those studies has furthered the understanding of the quantitative aspects of Auger spectra. In particular, there is a linear relationship between Auger electron emission intensity and coverage, up to a monolayer (*8*). There remain several obstacles to quantitative interpretation of Auger spectra obtained for chemisorbed layers, as pointed out in Ref. *9*. Spectral intensities have usually been obtained in terms of arbitrary units, thus preventing quantitative interpretation. The data are commonly presented in the form of graphs of second derivative spectra, which cannot be twice integrated quantitatively by the reader. The equations employed to analyze the spectral data were generally approximate, incomplete, or incorrect. Methods employed for spectrometer calibration have not been methods noted for absolute analytical accuracy. In the present article these problems are remedied somewhat: Auger electron current is stated in amperes; equations are derived which relate Auger electron current emitted from an adsorbed layer to all variables known to have an appreciable effect; and calibration is based upon a quantitative technique, thin-layer coulometry. (Previous articles in this series are Ref. *10* and *11*.)

EXPERIMENTAL

Single-crystal rods of Pt approximately 9 mm in diameter were obtained from the Materials Research Corp., Orangeburg, N.Y. 10962 (Marz Grade, 99.99% minimum nominal purity). These were polished preliminarily, oriented by means of Lauë x-ray reflection photography (*12–14*), and cut into prisms (each face of which had identical crystallographic symmetry) by means of a diamond saw. The disks were mounted in resin and polished with successively finer grades of abrasive, finishing with 0.05 μm alumina (Buehler Ltd., Evanston, Ill. 60204). The finished disks were spot welded onto a pair of 26-gauge Pt wires and etched for 2 min in hot aqua regia.

After insertion of the samples, the vacuum system was baked at 250 °C for several days, during which the pressure decreased from 10^{-5} to 10^{-7} Torr; after cooling, the pressure dropped to 10^{-10} Torr. The vacuum system for combined electrochemistry and LEED was described in Ref. *10*.

The Pt sample surface was cleaned (*15*) by heating in pure O_2 (1000 °C at 10^{-7} Torr for 8 h), followed by Ar^+ bombardment (10 μA cm^{-2} at 600 eV in 4×10^{-5} Torr Ar for 1 h) and annealing (600 °C for 10 min).

Auger electron spectra were recorded after sample preparation in order to verify that the surface was clean. The detection limit for C atoms was about 10^{13} atoms per cm^2, based upon the calibration described below. The sensitivity of Auger spectroscopy varies from element to element as indicated in Tables I–III.

A four-grid LEED apparatus was employed as a retarding field electron energy analyzer (Varian Associates, model 981-0127, Palo Alto, Calif. 94303). Transmittance of the grid system was 0.43; the acceptance angles were: maximum, $\theta_2 = 60°$, and minimum, $\theta_1 = 4°$ (due to the presence of the normal incidence LEED electron gun at the center of the grid system). Electronic control of the analyzer optics was provided by an electrometer and power supply (Varian, 981-2145 and 981-2148) and lock-in amplifier (Princeton Applied Research, modified model 128, Princeton, N.J. 08540). This detection system is functionally equivalent to the design described in Ref. *16*. The modulation frequency was 1 kHz. Collected electrons were returned to ground through an audiotransformer (Ouncer, UTC 0-26) which converted current of amplitude A_j into a voltage V_j. The voltage was sensed by a lock-in amplifier, which produced a dc voltage proportional to the ac signal amplitude, Equation 1.

$$|V_j| = \frac{A_j}{|Z_j|} \tag{1}$$

The effective impedance was $Z_1 = 9.0 \times 10^4\ \Omega$ at 1 kHz and $Z_2 = 2.74 \times 10^5\ \Omega$ at 2 kHz ($j \equiv 2$). This Auger electron signal, $|V_j|$, was sampled once each millisecond by a 12-bit successive A/D converter during a 100-s scan period; the digital data were averaged numerically in groups of 50, and the resulting 2000 average values stored on a disk memory of a digital converter. A technique for analog integration of Auger spectra has been described (*17*) which would be advantageous if the energy dependence of the background normalization function, ϕ_b, were known in advance.

Every precaution was taken to minimize damage of the adsorbed layer by the incident electron beams: The incident current was 10 μA distributed over a 17° ellipse (minor axis, 1 mm; major axis, 3.4 mm), and was interrupted when not in use; the total duration of irradiation was 100 s. Control experiments were

Table I. Proportionality Constant, G, between Auger Electron Current and Interfacial Coverage. Experimental and Theoretical Values

Element	Kinetic energy, eV	Compound chemisorbed	Γ, 10^{14} atoms/cm^2	I_a, experimental, 10^{-10} A	G, experimental, 10^{-19} cm^2	G, calculated, 10^{-19} cm^2
C	268	Ethylene	8.4 ± 0.2	16 ± 2	19 ± 2	17.0
C	268	Allylamine	15.9 ± 0.5	26 ± 6	17 ± 4	17.0
C	268	Allyacetic acid	9.5 ± 0.6	16 ± 2	17 ± 2	17.0
C	268	Thiophene	8.8 ± 0.5	17 ± 1	19 ± 1	17.0
C	268	Chlorotrifluoroethylene	3.8 ± 0.1	6.0 ± 0.5	16 ± 1	17.0
N	383	Allylamine	5.3 ± 0.2	3.2 ± 0.04	6.0 ± 0.2	8.7
O	516	Allylacetic acid	3.8 ± 0.2	1.4 ± 0.3	3.6 ± 0.2	4.7
F	659	Chlorotrifluoroethylene	5.8 ± 0.2	0.55 ± 0.07	0.9 ± 0.1	2.5
S	149	Thiophene	2.2 ± 0.1	20 ± 3	96 ± 13	140.0
Cl	181	Chlorotrifluoroethylene	1.92 ± 0.05	17 ± 0.6	93 ± 2	97.0

Experimental conditions: $K = 0.43$; $\theta_1 = 4°$; $\theta_2 = 60°$; $E_p = 2000$ eV; $I_p = 10$ μA; $\theta_i = 73°$. The range of integration of Equation 2 was 50 eV, centered on the Auger electron kinetic energy.

Table II. Calculated Collection Efficiency, ϕ_c, of Electron Energy Analyzer for Auger Electrons Emitted from a Chemisorbed Layer. Background Correction Weighting Factor, ϕ_b, from Equation 11

Element	Kinetic energy eV	Q, 10^{-16} cm^2	$Q\Gamma$	ϕ_c	ϕ_b
Li	51.8	3.03	0.43	0.091	0.568
Be	103.8	2.84	0.40	0.092	0.590
B	168.0	2.26	0.32	0.095	0.656
C	268.0	1.68	0.24	0.098	0.729
N	383	1.30	0.18	0.100	0.789
O	516	1.03	0.15	0.101	0.821
F	659	0.844	0.12	0.102	0.854
S	149	2.42	0.34	0.094	0.639
Cl	181	2.17	0.31	0.095	0.665
I	507	1.04	0.15	0.101	0.821

Auger electron kinetic energies from Ref. *49*. Scattering cross section, Q, for Auger electrons in hydrocarbon layer calculated by means of Equation 4 with $E_w = 16$ eV and $n = 6$. Parametric values: $K = 0.43$; $\theta_1 = 4°$; $\theta_2 = 60°$. For the sake of example, Γ was assumed equal to 1.4×10^{15} atoms/cm^2 in calculation of the entries appearing in this Table.

Table III. Calculated Values of Ionization Cross Section, Q, Backscattering Factor, s, and Auger Electron Yield, G, for Chemisorbed Layers on Pt

Element	n	E_w, eV	Q, 10^{-19} cm^2	S, 10^{-19} cm^2	G, 10^{-19} cm^2
Li	2	55	26.5	279.0	369.0
Be	2	110	11.4	58.7	97.7
B	2	188	5.57	17.7	36.7
C	2	284	3.03	6.68	17.0
N	2	399	1.73	2.79	8.70
O	2	532	1.008	1.22	4.67
F	2	682	0.582	0.539	2.53
S	6	164	20.1	71.3	140.0
Cl	6	201	15.2	45.4	97.4
I	10	685	3.58	3.66	15.9

Parametric values: $E_p = 2000$ eV; $K = 0.43$; $\theta_1 = 4°$; $\theta_2 = 60°$; $\theta_i = 73°$ from surface normal; $\phi_i = 27°$ from (010) zone; E_w values were obtained from Ref. *50*.

performed, in which the maximum Auger electron intensity was measured at constant energy, to verify that the signal strength did not vary detectably as a result of irradiation during the recording of these spectra. In our experience, electron analyzers of the cylindrical mirror design (*18*, *19*) give better Auger spectra than the retarding field type, from the same manufacturer; use of the latter for this work, however, allowed LEED patterns to be obtained concurrently.

Auger electron emission was stimulated by irradiation of the sample at grazing incidence ($\theta_i = 73°$, measured from the surface normal) by means of a precisely focused and deflected electron beam (10 μA at 2000 eV). The electron gun was Varian 981-2454 and control unit 981-2145 plus 981-2147.

The substances were introduced onto the sample surface by means of a nozzle beam (*20*) which permitted sample exposure equivalent to a partial pressure of approximately 10 Torr while maintaining tolerably low pressure (10^{-6} Torr) in the remainder of the apparatus. This procedure invariably resulted in saturation of the surface with the strongly chemisorbing substances investigated in this study.

Electrochemical analysis of the chemisorbed layer to calibrate the Auger spectrometer was accomplished as follows: A polycrystalline Pt thin-layer electrode such as described in Ref. *21* was exposed for 60 s to argon containing the adsorbing hydrocarbon at partial pressure comparable to that employed in the vacuum. An aliquot of 1 M $HClO_4$ was then introduced into the thin-layer cavity of 0.15 V vs. NaCE (a calomel electrode prepared with 1 M NaCl). The potential was then adjusted to 1.3 V NaCE, with integration of the resulting current (*22*, *23*). Oxidation of the hydrocarbon layer and the Pt surface took place rapidly. The same degree of surface oxidation occurred as when the surface was initially clean (i.e., the change required for electrode reduction was the same in both cases). Therefore, the background correction was determined by repeating the procedure in the absence of adsorbed hydrocarbon and subtracting the resulting coulometric charge, q_B, from that obtained with the coated surface, q, Equation 2.

$$\Gamma = (q - q_B)/nFA \tag{2}$$

The standard deviation was 10% for eight trials, due primarily to variation of the hydrocarbon coverage. The magnitude of n was determined for allylacetic acid and allylamine as follows: An aliquot of 10^{-5} M solution of the surfactant in 1 M $HClO_4$ was added to the clean thin-layer cell, after which coulometric oxidation was carried out as described above. The magnitude of n was calculated from the Faraday law, Equation 3.

$$n = (q - q_B)/FVC^\circ \tag{3}$$

For allylacetic acid and allylamine, $n = 10$. The same result was obtained by another method in Ref. *24*. Although the oxidation products were not isolated, $n = 10$ implies the following net reactions:

$$CH_2{=}CHCH_2NH_2 + 4H_2O \rightarrow CO_2 + HO_2CCH_2NH_2 + 10H^+ + 10e^- \tag{4}$$

$$CH_2{=}CHCH_2CH_2CO_2H + 4H_2O \rightarrow CO_2 + HO_2CCH_2CH_2CO_2H + 10H^+ + 10e^- \tag{5}$$

The limited solubility of thiophene, ethylene, and chlorotrifluoroethylene precluded preparation of standard solutions necessary for precise determination of n-values. Therefore, it was necessary to make the assumption that these compounds react analogously to Equations 4 and 5, as follows:

$$CH_2{=}CH_2 + 4H_2O \rightarrow 2CO_2 + 12H^+ + 12e^- \quad (6)$$

$$+ 12H_2O \rightarrow 4CO_2 + H_2SO_4 + 26H^+ + 26e^- \quad (7)$$

$$F_2C{=}CFCl + 4H_2O \rightarrow 2CO_2 + 3HF + {}^1/_2Cl_2 + 5H^+ + 5e^- \quad (8)$$

i.e., the terminal adsorbed carbon is oxidized to CO_2, and the geminal olefinic carbon to carboxylate. Current–potential data concerning adsorption of atomic hydrogen on single-crystal and polycrystalline Pt electrodes (*25*) indicate that the polycrystalline thin-layer electrode consists of Pt(111) facets (55%) and Pt(100) facets (45%). As a result, the polycrystalline surface contains 1.42×10^{15} Pt atoms per cm^2, compared with 1.30×10^{15} for Pt(100). Values of Γ obtained with the polycrystalline electrode were normalized for this difference in site density (1.30/1.42 = 0.92) for purposes of comparison with Auger spectra of the Pt(100) surface. The electrolyte does not desorb the chemisorbed alkenes at open circuit (*24*); in fact, none of the materials would escape detection, even if it were to desorb, in that all of the reactant in the thin-layer cavity, whether adsorbed or otherwise, undergoes electrolysis.

RESULTS AND DISCUSSION

Determination of Auger Electron Current from a Chemisorbed Layer. Quantitative Auger electron spectra were obtained by electron beam excitation of a Pt(100) surface containing a chemisorbed layer of ethylene, I; allylamine, II; allylacetic acid, III; chlorotrifluoroethylene, IV; and thiophene, V.

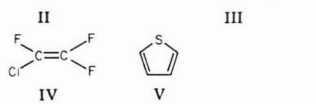

These compounds chemisorb readily and reproducibly on Pt surfaces. The resulting adsorbed material is not removed at room temperature by evacuation, rinsing, or electrolysis apart from extremely oxidizing or reducing conditions at which oxidation or hydrogenation occurs (*24*). It appears that compounds such as these remain structurally intact during chemisorption at room temperature (*24*). The interfacial concentration of adsorbed molecules can be determined by a coulometric method. Compounds I–V thus provide an opportunity to determine the yield of Auger electrons of the elements C, N, O, F Cl, and S present in an adsorbed layer in a well defined oxidation state at known coverage and relative abundance. The resulting data allow the proportionality constant relating Auger electron yield to surface concentration to be estimated and permit the reliability of various experimental equations for Auger yield to be evaluated. The potential variability of Auger electron kinetic energy with chemical environment has received attention (*8, 9, 12–24, 26–33*), but little is known about the corresponding variation in the emitted intensity. Auger electron spectra of compounds I–V are presented in Figure 1. Spectra were recorded in digital form for accuracy and convenience. The entire spectrum from 0 to 2020 eV was obtained in each case. Figure 1 was obtained by automated replotting of data over intensity and energy ranges convenient for making graphs. Other settings were employed when mathematical analysis of the data was the primary objective.

Auger electrons constitute only about 0.01% of the electrons emitted by the sample (*34*). Accordingly, selective amplification of the Auger electron component is a central aspect of experiment design (*8, 35, 36*). To that end, advantage has been

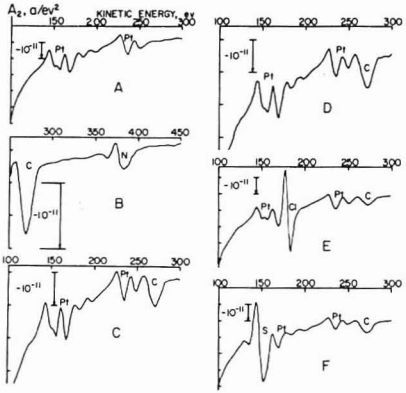

Figure 1. Auger electron spectra of substituted hydrocarbons chemisorbed on Pt(100). (A) Clean surface. (B) Allylamine. (C) Ethylene. (D) Allylacetic acid. (E) Chlorotrifluoroethylene. (F) Thiophene. Experimental conditions: sinusoidal modulation peak amplitude, k = 5 V; frequency, f = 1 kHz; primary beam current, I_p = 10 μA; primary beam energy, E_p = 2000 eV; time per scan, 90 s; filter time constant, RC = 0.1 s

taken of the fact that most of the background electron emission occurs with energies below 40 eV where it obscures relatively few Auger transitions and is distributed relatively uniformly from 40 eV up to E_p (*37–39*). Accordingly, the first derivative, $N(E)$ A/eV, of the total emitted current, I, exhibits noticeable peaks at energies characteristic of Auger processes, and the second derivative, $N'(E)$ A/eV², displays these features prominently (*35*). In the present study, $N'(E)$ was monitored by detecting the second harmonic amplitude, A_2, of the emitted current by means of LEED optics (*8*) noting that A_2 is a measure of $N'(E)$ (*34*).

Equation 9, relating A_2 to the Auger electron current, I_a, was derived by Houston (*40*) and confirmed experimentally for modulation amplitude, k, from 0.1 to 25 eV (*41*).

$$I_a = \frac{4}{k_2}\int_{E_1}^{E_2}\int_{E_1}^{E} A_2 \text{ (corrected for background) } dE'dE \quad (9)$$

Accordingly, the second-harmonic spectra, A_2, were corrected for contributions due to background and twice integrated automatically by means of a digital computer to obtain the Auger electron current. As pointed out by Houston (*40, 41*), this procedure gives the correct result regardless of modulation amplitude, peak shape, or the small energy losses resulting from plasma or valence electronic transitions.

To correct the second harmonic amplitude, A_2, of the coated surface for contributions due to background, the corresponding amplitude, A_{2c}, is measured for the clean surface, decreased by a factor ϕ_b corresponding to the absorptivity of the adsorbed layer toward electrons of the specified energy, and subtracted from A_2.

$$I_a = \frac{4}{k_2}\int_{0}^{E_p}\int_{0}^{E} (A_2 - \phi_b A_{2c})dE'dE \quad (10)$$

The factor ϕ_b is, in other words, the fraction of electrons emitted from within the substrate in a cosinusoidal distribution (*42*), transmitted by a Beer–Lambert absorber and registered by the detector. Exact values of ϕ_b cannot be calculated a priori without specifying the geometry and electron scattering characteristics of the adsorbed layer (*43*).

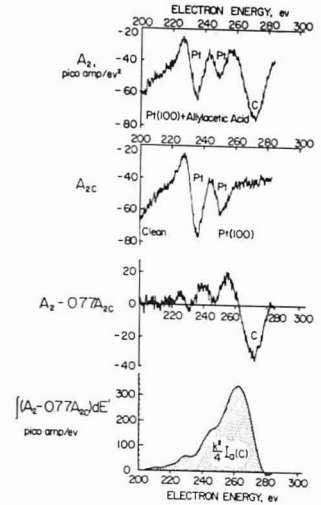

Figure 2. Integration of an Auger electron spectrum. From top: Second harmonic signal from allylacetic acid on Pt(100), A_2. Second harmonic signal from clean Pt(100), A_{2c}. Second harmonic signal after correction for background, $A_2 - 0.77\ A_{2c}$. Integral of net second harmonic signal, $\int(A_2 - \phi_b A_{2c})dE'$

However, a calculation based upon single scattering by a uniform carbon film does correctly predict the mathematical form of the energy dependence of ϕ_b, Equation 11,

$$\phi_b = \frac{r^2}{2\pi r^2}\int_0^{2\pi}\int_{\theta_1}^{\theta_2} \exp(-\sigma \sec\theta)\cos\theta \sin\theta \, d\theta \, d\alpha \Big/ \int_{\theta_1}^{\theta_2} \cos\theta \sin\theta \, d\theta$$

$$\phi_b = 2\int_{\theta_1}^{\theta_2} \exp(-\sigma \sec\theta)\cos\theta \sin\theta \, d\theta \Big/ (\sin^2\theta_2 - \sin^2\theta_1) \quad (11)$$

where σ is the average absorption cross section of the adsorbed layer (about 0.2) and the differential area increment, $\sin\theta\, d\theta\, d\alpha$, is integrated over the hemispherical surface of area $2\pi r^2$ encompassing all azimuthal angles, α, and vectorial angles limited by the LEED gun at center screen and the outer boundary of the hemispherical analyzing grids. In practice, Equation 11 is linear in kinetic energy, with a coefficient of determination of 0.99, over the energy range of a typical Auger peak, about 100 eV, Equation 12.

$$\phi_b = mE + b \quad (12)$$

The slope, m, is small, typically 10^{-3} eV^{-1}, and the intercept, b, is generally in the range from 0.75 to 1.25. Since $A_2 = \phi_b A_{2c}$ in regions of the electron energy spectrum over which there is an absence of Auger transitions of the adsorbed layer, the slope and intercept leading to ϕ_b in Equation 12 were evaluated empirically by linear least squares analysis of A_2/A_{2c} values over a 50-eV range on either side of the given Auger peak. The coefficient of determination was 0.7 or greater in all cases. Background correction assuming $\phi_b = 1$ was described in Ref. *44*. The accuracy of Equation 12 was verified by comparing calculated and observed variation of the areas of the platinum Auger peaks in the presence of an adsorbed layer. The background correction process and double integration are illustrated in Figure 2. Values of the Auger electron current, I_a, extracted from the experimental data, A_2 and A_{2c}, by means of Equation 1 and 10, appear in Table I. As can be seen from these data, the Auger electron currents from chemisorbed monolayers are on the order of 10^{-9} A. The yields differ from element to element by a factor of 40 or more. As a result, the sensitivity of Auger electron spectroscopy to various surface constituents varies widely. Qualitative detection of the Auger electron current and a knowledge of the factor relating current to coverage is thus essential for interpretation of Auger spectra.

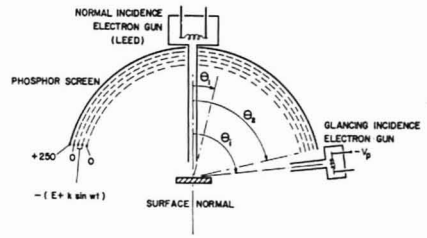

Figure 3. Retarding field energy analyzer used for Auger electron spectroscopy

Experimental Equations for Auger Electron Current. The current resulting from a given Auger transition occurring in a chemisorbed layer is expected to follow an equation of the form (*45–47*)

$$I_a = I_p \phi_c G \Gamma \quad (13)$$

where I_p is the primary beam current incident on the sample surface; ϕ_c is the collection efficiency of the electron detector; Γ, atoms cm^2, is the interfacial concentration of adsorbed atoms undergoing the specified Auger transitions; and G is a proportionality constant determined empirically and compared with values calculated from first principles in this work.

The detector employed in this study was a four-grid hemispherical LEED display system, Figure 3, the collection efficiency of which is given by Equation 14.

$$\phi_c = \frac{K}{2}\int_{\theta_1}^{\theta_2} \exp[Q\Gamma(1 - \sec\theta)]\sin\theta d\theta \quad (14)$$

That is, one-half of the Auger electrons are emitted in the direction of the vacuum hemisphere, of which a fraction K (equal to 0.43 in this work) are transmitted by the series of four analyzing grids. The angular distribution of Auger electrons emitted from a hydrocarbon monolayer on a molybdenum substrate (*42*) conforms rather closely to the function $\exp[Q\Gamma(1 - \sec\theta)]$ for vectorial angles less than about 60° from the normal, as shown in Figure 4. An inelastic scattering coefficient, $Q\Gamma$, of 0.24 gave best fit with the data. Based upon this observation, values of $Q\Gamma$ for the systems encountered in the present work were calculated as follows: The scattering cross section, Q cm^2, was calculated by means of a procedure derived and tested by Gryzinski (*48*), Equation 15. The average binding energy, E_w, of electrons in the hydrocarbon layer was taken to be 16 eV. Calculation of Q thusly for the situation depicted in Figure 4 implies that Γ equals 1.42×10^{15} carbon atoms per cm^2; the composition of the hydrocarbon layer was not specified in Reference *42* but the implied coverage falls amid those observed in other experiments (*24*). Evaluation of ϕ_c was accomplished by integrating the angular distribution over the hemispherical region between the shadow of the LEED electron gun (θ_1 =

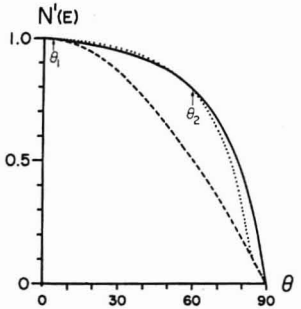

Figure 4. Angular distribution of Auger electrons emitted from a chemisorbed layer. (——) Solid curve: experimental data of Harris (*37*) for Auger electrons from hydrocarbons adsorbed on a Mo substrate. (...) Dotted curve: graph of exp[0.24(1 – sec θ)]. (---) Dashed curve: graph of cos θ. $N'(E)$ was normalized to unit emission along the surface normal

4°) and the perimeter of the energy analyzer (θ_2 = 60°), Equation 14. Values of ϕ_b thus obtained are presented in Table II. As can be seen from the Table, ϕ_c varies less than 2% over the energy range (50 eV) of typical Auger processes. Accordingly, ϕ_c may be treated as a constant for a given Auger process. Since ϕ_c depends upon Γ, extraction of the magnitude of Γ from the measured value of I_a by means of Equation 13 requires iteration of self-consistency in Γ, or use of a working curve, $\phi_c = f(Q\Gamma)$. Fortunately, the variation of ϕ_c with Γ is gradual and the solution converges after one or two iterations. As can be seen from Table II, ϕ_c ranges from 0.091 to 0.102 in the row Li to F. In Ref. *47* a constant value equivalent to ϕ_c = 0.073 was employed, based upon the approximation that Auger electrons are emitted uniformly with respect to θ.

Scattering cross sections, Q, were calculated by means of Equation 15, developed by Gryzinski (*48*).

$$Q = 6.56 \times 10^{-14} \frac{n}{E_p E_w} \left[\frac{(E_p/E_w) - 1}{(E_p/E_w) + 1}\right]^{3/2} \left\{1 + \frac{2}{3}\left(1 - \frac{E_w}{2E_p}\right) \ln\left[2.7 + \left(\frac{E_p}{E_w} - 1\right)^{1/2}\right]\right. \quad (15)$$

When ϕ_c is the object of the calculation, E_w is equal to the energy to ionize the bound electrons in the outermost shell, occupied by n electrons (inner electrons contribute negligibly, as can be seen by substituting their respective values of E_w into Equation 15), and E_p is the energy of the Auger electron. The values of E_w employed were obtained from Ref. *50*. Values of Q thus calculated appear in Table II.

Values of G extracted from the experimental data, A_2 and A_{2c}, by means of the above equations are given in Table I. The magnitude of G observed for the element carbon is similar for compounds I–V and corresponds to 1.7×10^{-18} cm^2. These data suggest that the Auger electron yield for carbon is not a sensitive function of molecular environment. Reported variations of Auger electron yield with oxidation state (*47, 51*) may have been due to structural reorganization of the surface region, as noted in Ref. *52*. Accordingly, it appears worthwhile to devote further attention to Auger electron spectroscopy as a potential method for quantitative elemental analysis of chemisorbed molecules.

Governing Equations for Auger Electron Yield Factor, *G*. As described below, the proportionality constant, G, between Auger electron current, I_a, and interfacial concentration, Γ, Equation 13, is given by Equation 16.

$$G = (Q \sec \theta_i + s)\phi_a\phi_t \quad (16)$$

The quantity (Q sec $\theta_i + s$) describes the probability that an electron of energy E_p incident on the sample at an angle θ_i (measured from the surface normal) will cause ionization of a specific core level, W, whose cross section is Q. Based upon geometric considerations, the path length of the electron through the adsorbed layer varies as sec θ_i. (For example, sec θ_i = sec 73° = 3.42, corresponds to a pathlength equivalent to 3.4 molecular layers or approximately 10 Å.) Normalization of I_p for variation within the layer is not necessary, in the present instance, as can be seen by use of the Beer-Lambert Law, Equation 17,

$$\Delta I_p/I_p = 1 - \exp[-\Delta L(0.693)/L] = 4\% \quad (17)$$

in which L is calculated, Equation 18, as described in Ref. *53*.

$$L = 1 + (E_p/150)^2 = 178 \text{ Å} \quad (18)$$

Ionization cross section, Q, was calculated by means of Equation 15, in which E_p was the kinetic energy of the incident electron and E_w was the binding energy of the initially ionized core level. Values of Q thus calculated appear in Table III. A graph of Q vs. incident electron kinetic energy for the element carbon appears in Figure 5. These values of Q agree with those of Ref. *47* within ±3%.

The back-scattering factor, S, specifies the number of w-level ionization events in the adsorbed layer which result from the flux of scattered electrons. As such, S is the ionization cross section, $Q(E)$, multiplied by the energy distribution of secondary electrons doing the ionizing, $N_s(E)$, in-

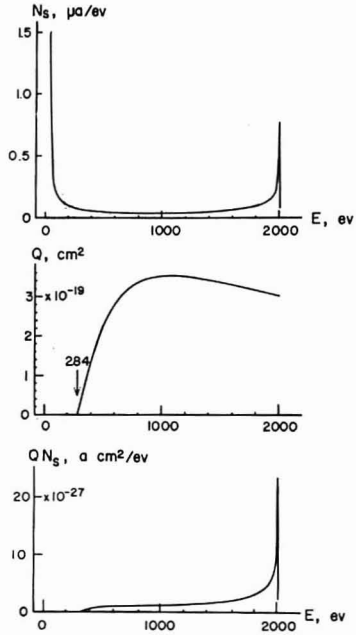

Figure 5. Calculation of backscattering factor, S, by integration of $N_s(E)$ $Q(E)$. Carbon present in an adsorbed layer on Pt(100). Experimental conditions: as in Figure 1

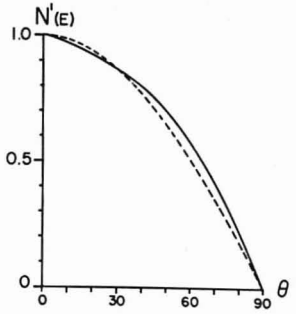

Figure 6. Angular distribution of Auger electrons emitted from a substrate. (——) Solid curve: experimental data of Harris (*37*) for Auger electrons from Mo (190 eV) containing an adsorbed hydrocarbon overlayer. (---) Dashed curve: graph of cos θ. ($N'(E)$ was normalized to unit emission along the surface normal

tegrated over all energies in the distribution and normalized by the total flow of scattered electrons (that is, by the primary beam current, I_p):

$$S = \frac{1}{I_p} \int_0^{\infty} \int_0^{\pi/2} Q(E) N_s(E) \sec\theta \cos\theta \sin\theta \, d\theta \, dE$$

$$= \frac{1}{I_p} \int_{E_w}^{E_p} Q(E) N_s(E) dE \qquad (19)$$

The integrand is zero for E outside the range $E_w \leq E \leq E_p$ because the secondary electron cannot possess energy greater than that of the primary electron [that is, $N_s(E) = 0$ for $E > E_p$] and ionization of the w-level cannot occur when $E_p < E_w$ [that is, $Q(E) = 0$ when $E_p < E_w$]. Integration over an angular distribution is necessary because electrons are scattered by the substrate in a cosinusoidal distribution (*42*), Figure 6, after which they travel a distance proportional to sec θ in the adsorbed layer. The secondary electron energy distribution, $N_s(E)$, was determined directly by measurement of the first harmonic of the modulated electron emission current, $A_1(E)$, for the clean surface, over the entire energy range from 0 to E_p. Normalization of $A_1(E)$ for collection efficiency of the analyzer was done by means of Equation 20,

$$N_s(E)/A_1(E) = 1/[kK \int_{\theta_2}^{\theta_2} \cos\theta \sin\theta \, d\theta]$$

$$= 4/[kK(\sin^2\theta_2 - \sin^2\theta_1)] \qquad (20)$$

$$= \frac{12.48}{k}$$

the derivation of which is analogous to Equations 11 and 14. The ionization cross section, $Q(E)$, was calculated from Equation 15, by setting $E_p = E$. The integral in Equation 19 was evaluated by computerized application of Simpson's rule. The calculation procedure is illustrated in Figure 4. Values of S obtained in this manner are listed in Table III. A graph of calculated S vs. E_w, the ionization energy of the w-level, appears in Figure 7. As can be seen, S is predicted to decrease sharply in magnitude with increasing E_w. Secondary electron emission varies by about 10% with vectorial and azimuthal angles, θ_i and Φ_i. Accordingly, the S-values reported in Table III are exact only for the angles employed in this work.

Some earlier workers resorted to the use of equations developed for electrons in the 10-keV energy range (*46*) to calculate S (*45, 52*). An iterative, empirical procedure has been suggested (*54*) which has the drawback that it requires tedious experiments which must be repeated for each combination

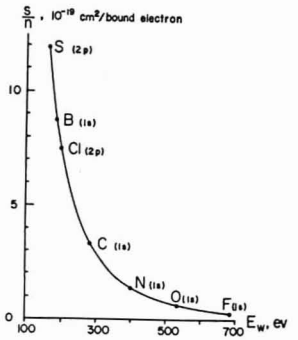

Figure 7. Backscattering factor per electron, S/n, for elements present as an adsorbed layer on Pt(100). Parametric quantities are as in Table I and Figure 1

of incident energy, substrate, and adsorbed layer. Equation 19 differs from the expression employed in Ref. *47*,

$$\int_{E_w}^{E_p} \int_0^{\pi/2} N_s(E) Q(E) \sec\theta \, dE \, d\theta / [I_p Q(E_p)]$$

which neglects the angular distribution of secondary electrons (cos θ) and omits one part (sin θ) of the expression for the differential area increment in spherical polar coordinates. The expression employed subsequently by the same authors (*52*) is equivalent to Equation 11, however.

The fraction of ionization events leading to processes other than x-ray emission, ϕ_a, is nearly unity for incident energies less than about 3000 eV, and follows Equation 21 described in Ref. *55*,

$$\phi_a = \frac{g}{g + Z^4} \qquad (21)$$

where Z is the atomic number of the emitting element, and $g = 1.12 \times 10^6$ for K shells and 6.40×10^7 for L shells.

The fraction of Auger processes, ϕ_a, leading to an Auger transition of a specific type is denoted by ϕ_t. For KLL Auger transitions of the first row elements Li through Ne and for LMM transitions of S and Cl, the Auger electron kinetic energies are grouped into bands or closely spaced multiplets. Since, for analytical purposes, the intensities due to a given element are lumped together in the process of integrating the spectra, ϕ_t can be set equal to unity for these elements.

Introducing Q, S, and ϕ_a from Equations 15, 19, and 21 into Equation 16 yields the calculated values of G listed in Tables I and III. These calculations indicate that most of the observed differences in Auger electron yield from element to element in a chemisorbed layer are due to differences in ionization cross section, Q. Accordingly, Q should be the focal point of future attempts to refine the theory.

Comparison of Data with Theory. Although the data are sparse, it is interesting to compare experimental values of G with those predicted by the equations, within either a relative or an absolute framework. For instance, comparison of the ratios of G values for elements within an adsorbed layer tests the ability of experiment and theory to produce correct relative elemental compositions. Table IV compares observed and calculated G ratios. As can be seen, theory and experiment correlate within the limits imposed by the experimental precision except in the case of fluorine. It is probable that the very low signal level for fluorine, due to its relatively low 1s ionization cross section, thwarted its accurate determination in these experiments; future spectra, in which a 10 keV in-

Table IV. Relative Auger Electron Yields

Compound chemisorbed	Experimental ratio	Theoretical ratio
Allylamine	$G_C:G_N = 2.8 \pm 0.6$	2.0
Allylacetic acid	$G_C:G_O = 4.7 \pm 0.5$	3.6
Chlorotrifluoroethylene	$G_C:G_{Cl} = 0.17 \pm 0.02$	0.175
	$G_C:G_F = 17 \pm 3$	6.8
Thiophene	$G_C:G_S = 0.20 \pm 0.03$	0.12

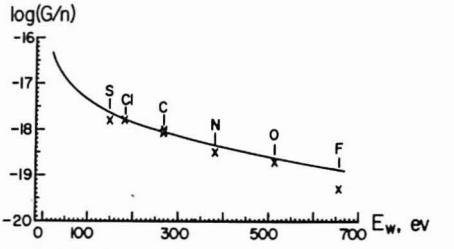

Figure 8. Calibration factor, G, for Auger electron emission from atoms present as substituted hydrocarbons chemisorbed on Pt(100). (——) Solid curve: theory. (x x x) Individual points: experimental values. Experimental conditions: as in Figure 1 and Table I

cident electron gun is employed, should resolve this question.

Absolute magnitudes of experimental and theoretical Auger efficiencies, G, are compared in Table I. As can be seen, there is strong qualitative correlation in all cases and agreement to better than ±10% is observed in about half of the examples; of the remainder only one pair displays a difference of more than 30%, the probable cause of which was discussed earlier. A graph of experimental and theoretical values of G vs. E_w appears in Figure 8. The degree to which factors such as valence state and molecular conformation influence Auger electron yield is of interest in this regard and will be the subject of future investigation. However, at present it appears that the accuracy of the theory is comparable to that of the techniques available to test it, and that with suitable calibration of the spectrometer, elemental analyses accurate to within 10% or better are to be expected.

ACKNOWLEDGMENT

Assistance was provided by Gerald Gulden and Lance Nakamura in computerization of the data handling process. Roy M. Ishikawa prepared the single crystal samples. Mark Green provided valuable assistance with the experiments.

LITERATURE CITED

(1) J. V. Florio and W. O. Robertson, *Surf. Sci.*, **18**, 398 (1969).
(2) B. J. Pollard, *Surf. Sci.*, **20**, 269 (1970).
(3) S. Thomas and T. W. Haas, *J. Vac. Sci. Technol.*, **9**, 840 (1971).
(4) M. Perdereau, *Surf. Sci.*, **24**, 239 (1971).
(5) J. W. T. Ridgway and D. Haneman, *Surf. Sci.*, **26**, 683 (1971); **24**, 451 (1971).
(6) D. T. Quinto, V. S. Sundaram, and W. D. Robertson, *Surf. Sci.*, **28**, 504 (1971).
(7) J. J. Vrakking and F. Meyer, *Appl. Phys. Lett.*, **18**, 226 (1971).
(8) R. E. Weber and W. T. Peria, *J. Appl. Phys.*, **38**, 4355 (1967).
(9) J. M. Morabito, *Surf. Sci.*, **49**, 318 (1975).
(10) R. M. Ishikawa and A. T. Hubbard, *J. Electroanal. Chem.*, **69**, 317 (1976).
(11) A. T. Hubbard, R. M. Ishikawa, and J. Katekaru, *J. Electroanal. Chem.*, in press.
(12) C. S. Barrett, "Structure of Metals", 3rd ed., McGraw-Hill, New York, N.Y., 1977.
(13) E. Wood, "Crystal Orientation Manual", Columbia University Press, New York, N.Y., 1963.
(14) L. L. Levenson et al., *J. Vac. Sci. Technol.*, **9**, 608 (1971).
(15) P. W. Palmberg, in "The Structure and Chemistry of Solid Surfaces", G. A. Somorjai, Ed., John Wiley, New York, N.Y., 1979, Article 29.
(16) R. Nathan and B. J. Hopkins, *J. Phys. E*, **6**, 1040 (1973).
(17) J. T. Grant, M. P. Hooker, and T. W. Haas, *Surf. Sci.*, **46**, 672 (1974).
(18) H. Z. Sar-el, *Rev. Sci. Instrum.*, **38**, 1210 (1967).
(19) H. Hafner, J. A. Simpson, and C. E. Kuyatt, *Rev. Sci. Instrum.*, **39**, 33 (1968).
(20) A. E. Morgan and G. A. Somorjai, *J. Chem. Phys.*, **51**, 3309 (1969).
(21) C. N. Lai and A. T. Hubbard, *Inorg. Chem.*, **11**, 2081 (1972).
(22) A. T. Hubbard, *Crit. Rev. Anal. Chem.*, **3**, 201 (1973).
(23) A. T. Hubbard and F. C. Anson, *Electroanal. Chem.*, **4**, 129 (1970).
(24) R. F. Lane and A. T. Hubbard, *J. Phys. Chem.*, **77**, 1401, 1411 (1973); **79**, 809 (1975).
(25) R. M. Ishikawa, Ph.D. dissertation, University of Hawaii, 1976.
(26) K. Ueda and R. Shimizu, *Surf. Sci.*, **36**, 789 (1973).
(27) A. M. Horgan and I. Dalins, *J. Vac. Sci. Technol.*, **10**, 523 (1973).
(28) R. J. Szalkowski and G. A. Somorjai, *J. Chem. Phys.*, **56**, 6097 (1972).
(29) H. H. Farrell, *Surf. Sci.*, **34**, 405 (1973).
(30) T. W. Haas and J. T. Grant, *Phys. Lett.*, **30A**, 272 (1969).
(31) T. W. Haas, J. T. Grant, and G. J. Dooley III, *J. Appl. Phys.*, **43**, 1853 (1972).
(32) D. A. Shirley, *Chem. Phys. Lett.*, **17**, 312 (1972).
(33) E. N. Sikafus, *Surf. Sci.*, **36**, 472 (1973).
(34) J. J. Lander, *Phys. Rev.*, **91**, 1382 (1953).
(35) L. A. Harris, *J. Appl. Phys.*, **39**, 1419 (1968).
(36) L. N. Tharp and E. J. Scheibner, *J. Appl. Phys.*, **38**, 3320 (1967).
(37) C. C. Chang, *Surf. Sci.*, **25**, 53 (1971).
(38) G. A. Somorjai and F. J. Szalkowski, *Adv. High Temp. Chem.*, **4**, 137 (1971).
(39) N. J. Taylor, *Tech. Met. Res.*, **7**, 117 (1971).
(40) J. E. Houston, *Surf. Sci.*, **38**, 283 (1973).
(41) J. T. Grant, T. W. Haas, and J. E. Houston, *Surf. Sci.*, **42**, 1 (1974).
(42) L. A. Harris, *Surf. Sci.*, **15**, 77 (1969).
(43) C. C. Chang, *Surf. Sci.*, **48**, 9 (1975).
(44) J. T. Grant, M. P. Hooker, and T. W. Haas, *Surf. Sci.*, **51**, 318 (1975).
(45) H. G. Bishop and J. C. Riviere, *J. Appl. Phys.*, **40**, 1740 (1969).
(46) H. G. Bishop, *Br. J. Appl. Phys.*, **18**, 203 (1967).
(47) F. Meyer and J. J. Vrakking, *Surf. Sci.* **33**, 271 (1972).
(48) M. Gryzinski, *Phys. Rev. A*, **138**, 305, 322, 336 (1965).
(49) W. A. Coghlan and R. E. Clausing, *At. Data*, **5**, 317 (1973).
(50) K. Siegbahn et al., "ESCA: Atomic, Molecular and Solid State Structure Studies by Means of Electron Spectroscopy", Almqvist-Wiksell Boktryckeri, Uppsala, Sweden, 1967.
(51) R. J. Fortner and R. G. Musket, *Surf. Sci.*, **28**, 339 (1971).
(52) J. J. Vrakking and F. Meyer, *Surf. Sci.*, **35**, 34 (1973).
(53) G. A. Somorjai and H. H. Farrell, *Adv. Chem. Phys.*, **20**, 215 (1971).
(54) T. E. Gallon, *J. Phys. D*, **5**, 822 (1972); **7**, 151 (1974).
(55) E. S. H. Bishop, "The Auger Effect and Other Radiationless Transitions", University Press, Cambridge, England, 1952.

RECEIVED for review August 26, 1977. Accepted October 3, 1977. Acknowledgment is made to the donors of the Petroleum Research Fund administered by the American Chemical Society, and to the National Science Foundation for support of this research.

Determination of Carboxylic Esters by Acid Fusion Reaction Gas Chromatography

Richard J. Williams[1] and Sidney Siggia*

Department of Chemistry, University of Massachusetts, Amherst, Massachusetts 01003

A quantitative method has been developed to determine the carboxylic acid content of nonvolatile esters. The determination is carried out in one piece of apparatus by coupling a reaction chamber through a trap-loop to a gas chromatograph. The method involves hydrolysis of the ester in molten phosphoric acid at 200–300 °C for 15 min. The volatile reaction products are concentrated in the trap-loop prior to gas chromatographic analysis. The precision of the method is ±0.1 to 3.0% using a 1- to 10-mg sample. Quantitative results were obtained with cholesteryl esters, carbohydrate esters, cellulose esters, poly(vinyl ester), and vinyl acetate copolymers.

Several gas chromatographic methods have been introduced for the determination of the combined carboxylic acid content of poly(vinyl esters) and cellulose esters. The methods are based on a preliminary chemical reaction to release the carboxylic acid from the ester functional group followed by a gas chromatographic analysis of the reaction products. Wandel and Tengler developed a method involving the transesterification of cellulose esters with 10% BF_3 in absolute methanol (*1*). The analysis was carried out in a sealed tube at 140 °C for 3 h. The methyl esters formed in the transesterification were analyzed on a poly(ethylene glycol) column. Esposito and Swann reported a procedure involving a 2-h saponification of the sample followed by acidification with hydrochloric acid and gas chromatographic determination (*2*). Aydin et al. used acid hydrolysis to determine the total and individual carboxylic acid content of vinyl acetate–vinyl propionate copolymers (*3*). The total aliphatic acid content was measured by potentiometric titration after hydrolysis with excess *p*-toluenesulfonic acid. The acetic and propionic acids liberated by hydrolysis were identified and their relative amounts determined by gas chromatography.

This paper describes the determination of the carboxylic acid content of nonvolatile esters by acid fusion reaction gas chromatography. In the present work, the carboxylic acid is liberated by hydrolysis in molten phosphoric acid at an elevated temperature. The reaction conditions promote a rapid analysis. The proposed method is free of solvent limitations which is particularly important in polymer analysis. Another advantage of the method is that the reaction, separation, and quantitative determination are performed in one piece of apparatus. This reduces sample manipulation and losses to a minimum. The entire determination can be completed in 30–35 min on a 1- to 10-mg sample.

EXPERIMENTAL

Reagents. Solid orthophosphoric acid, H_3PO_4, was found to be an ideal reagent for acid fusion. The reagent was obtained from K & K Laboratories and required further drying before using. This was accomplished by drying in vacuo for 24–48 h using phosphorus pentoxide as desiccant. After drying, the reagent was stored in a glove box.

A number of other acids were investigated as possible acid fusion reagents. Sodium bisulfate monohydrate, $NaHSO_4 \cdot H_2O$, was obtained from J. T. Baker Chemical Co. Phosphorous acid, H_3PO_3, was obtained from Fisher Scientific Co. Benzenephosphonic acid, $C_6H_5PO_3H_2$, and *p*-toluenesulfonic acid monohydrate, $C_7H_7SO_3H \cdot H_2O$, were obtained from Eastman Organic Chemicals. All were used without further purification.

Cellulose acetate, cellulose acetate propionate, cellulose acetate butyrate, and cellulose acetate hydrogen phthalate were obtained from Eastman Organic Chemicals. Cellulose triacetate was supplied by Polyscience. The carbohydrate esters were obtained from either Aldrich Chemical Co. or Eastman Organic Chemicals. Sucrose benzoate was supplied by Pfaltz & Bauer. The cellulose and carbohydrate esters had a 1–3% adsorbed water content and were analyzed wet for their carboxylic acid content by acid fusion. This was necessary since dried samples readsorbed moisture during weighing. Sample weight was corrected by determining the water content of each sample analyzed. This was usually accomplished by oven drying at 100–105 °C for 2 h.

Poly(vinyl acetate) and poly(vinyl propionate) were prepared from 99–100% hydrolyzed poly(vinyl alcohol) obtained from Aldrich Chemical Co. and the corresponding carboxylic acid anhydride also obtained from Aldrich Chemical Co. according to the procedure outlined by Sorenson and Campbell (*4*). A commercial sample of poly(vinyl acetate) was also obtained from Polyscience. Poly(ethylene–vinyl acetate), 18% vinyl acetate, and poly(vinyl pyrrolidone–vinyl acetate) were supplied by Polyscience. Cholesteryl acetate and cholesteryl *n*-butyrate were obtained from Aldrich Chemical Co. Cholesteryl propionate was obtained from Applied Science. Ethynodiol diacetate was furnished by Searle Pharmaceutical Co.

The C_2–C_4 carboxylic acids used in calibration were obtained from the following sources: glacial acetic acid from J. T. Baker, propionic acid from Mallinckrodt Chemical, isobutyric acid from Aldrich Chemical Co., and *n*-butyric acid from Eastman Organic Chemicals. Benzoic acid, analytical reagent grade, was supplied by Mallinckrodt.

Apparatus. Gas chromatographic separations were performed using either a Perkin-Elmer 900 or 990 gas chromatograph equipped with thermal conductivity detectors and linear temperature programming. The chromatograms were recorded on a Varian A-25 and in some cases a Leeds & Northup Speedomax W recorder. A Vidar 6300 digital integrator was used for retention time and peak area measurements. The columns and chromatographic conditions used in this investigation are listed in Table I. The Chromosorb 101 and 105 columns were used to separate the C_2–C_4 carboxylic acids. The Free Fatty Acid Phase (FFAP) column was employed for separating benzoic acid from water. Since the free carboxylic acids were chromatographed, every effort was made to reduce or eliminate possible adsorption sites (*5, 6*). Glass tubing was substituted whenever possible for stainless steel. The glass tubing was silanized with trimethylchlorosilane to remove surface silanol groups (*7*). Teflon wool (Supelco, Inc.) was used for column end plugs instead of the usual glass wool.

The reaction unit consisted of a pyrolysis apparatus obtained from Perkin-Elmer Corp. (Pyrolysis Accessory 154-0825) and modified for analytical reaction gas chromatography by Siggia et al. (*8–10*). A detailed diagram of the reaction unit used in this investigation including all major modifications is given by Frankoski and Siggia (*9*). Two modifications in the reaction apparatus were made during this investigation. The trap-loop

[1] Present address, Allied Chemical Corp., Box 1021R- Bldg. CRL, Morristown, N.J. 07960.

Table I. Columns and Conditions Used to Monitor Products of Acid Fusion

Column	Flow rate, mL/min	Isothermal	Programmed	Final
A. Chromosorb 101, 60/80 mesh,[a] 6 ft × 1/8 in. o.d. glass tubing	30-40	6-8 min at 90 °C	12 °C/min to 170-180 °C	0-6 min
B. Chromosorb 105, 60/80 mesh,[a] 6 ft × 1/8 in. o.d. glass tubing	30-40	6-8 min at 90 °C	12 °C/min to 170-180 °C	0-6 min
C. FFAP 10% on 60/80 mesh,[b] Anakron AbS, 3 ft × 1/8 in. o.d. stainless steel	60	3-4 min at 90 °C	16-24 °C/min to 200 °C	5 min

[a] Injector 200 °C, manifold 200 °C, hot wire detector 250 °C, current 175 mA, helium carrier gas. [b] Injector 250 °C, manifold 250 °C, hot wire detector 250 °C, current 175 mA, helium carrier gas.

was constructed out of glass instead of stainless steel in an effort to decrease adsorption. The overall length of the glass trap-loop was 8-10 inches. The horizontal inlet and outlet sections were about 1 inch long and were constructed from 3.1-mm o.d. by 1.5-mm i.d. Pyrex glass tubing. The downward and upward legs of the loop were about 3-4 inches long and were constructed from 5-mm o.d. by 3.5-mm i.d. Pyrex glass tubing. The larger internal diameter of the loop section was necessary to prevent the volatile reaction products from plugging the trap-loop. The bottom section of the loop was loosely packed with about 30-50 mg of Teflon wool. This was required to prevent aerosol formation. Leak-tight connections were obtained with standard 1/8-inch silicone rubber O-rings and 1/8-inch Swagelok fittings. The glass trap-loop and reaction unit from the oven to the inlet of the trap-loop were silanized with trimethylchlorosilane. The transfer line which connects the reaction unit and trap-loop to the gas chromatograph was previously heated using nichrome wire insulated with asbestos. This method of heating was replaced with a heating tape (Briskeat, Briscoe Co.) which was easier to install and provided a more reproducible temperature control. The temperature was usually maintained at 180-200 °C with a Variac.

Calibration curves were constructed using solutions delivered by microsyringe. The syringe was calibrated by the difference in weight of the syringe filled with water and empty. The volume was calculated from the weight and density of water. This method was found to be convenient and reproducible. The calculated volume of the syringe usually agreed within 1-3% of the syringe reading.

Procedure. Samples from 1 to 10 mg were weighed into tared micro-size platinum boats (Fisher Scientific Co.) using a micro-balance (Mettler Instrument Co.). The platinum boats were then transferred to the glove box where the acid fusion reagent was stored. A glove box was necessary to minimize the adsorption of water by the reagent. The phosphoric acid was ground to a fine powder using a mortar and pestle and enough reagent was added to completely cover the sample and fill the reaction boat. The reaction boats were transported to the reaction unit in a desiccator and then quickly transferred to the storage area of the reaction unit. Samples were reacted at 180-200 °C for 5-8 min followed by an additional 10-15 min at 250-275 °C. The volatile reaction products were concentrated in the trap-loop which was immersed in liquid nitrogen. Upon reaction completion, the sample boat was removed from the oven and the liquid nitrogen Dewar was replaced with a trap-heater. The reaction products were then swept directly into the gas chromatograph by the carrier gas where they were separated and analyzed.

Calibration was accomplished by injecting a standard carboxylic acid solution into an empty platinum boat positioned beneath the rubber septum (B, Figure 1, Ref. 9). The calibration boat was heated for 2 min at 200 °C. The carboxylic acid and water were volatilized and concentrated in the trap-loop prior to gas chromatographic analysis. This allowed the construction of calibration curves under conditions comparable to those of actual samples.

The total flush method of syringe injection was adopted using either a 10-μL or 25-μL Hamilton syringe. Sample weight was usually adjusted to release 800 to 1000 μg of the C_2–C_4 carboxylic acids. When using the 10-μL syringe, a 5-μL injection of a 160 μg/μL–200 μg/μL carboxylic acid solution was made into the calibration boat with a 2-μL distilled water flush. With the 25-μL syringe, a 15-μL injection of a 53 μg/μL–67 μg/μL solution was made into the calibration boat with a 5-μL distilled water flush. The 25-μL syringe was preferred since the size of the water peak more closely matched that produced by the reagent. It was also easier to calibrate and make volume readings with the 25-μL syringe. Samples like cellulose acetate propionate which released two carboxylic acids required standard solutions containing both acids. Calibration curves could also be constructed using the anhydrous sodium salts of the C_2–C_4 carboxylic acids. The salts were weighed into tared platinum boats and covered with phosphoric acid. They were then reacted under identical conditions of time and temperature as actual sample boats. In a similar fashion, compounds previously analyzed by acid fusion can be used as standards for calibration. These methods of calibration were more time-consuming compared to calibration by standard solution injection and were rarely used.

Table II. Reagent Study

Reagent	Acetic acid, % recovery poly(vinyl acetate)	Butyric acid, % recovery cholesteryl *n*-butyrate
Sodium bisulfate monohydrate	59.3% ± 19%	···
p-Toluenesulfonic acid monohydrate	···	103.0%
Phosphoric acid	98.0%	99.9%
Phosphorous acid	97.8%	···
Benzenephosphonic acid	···	92.7%

RESULTS AND DISCUSSION

Reagent Selection. Sodium bisulfate monohydrate was initially investigated as a possible acid fusion reagent. The compound has a low melting point (58 °C) and is a fairly strong acid. The thermal stability of sodium bisulfate was examined by Paulik et al. using TGA, DTA, and DTC (*11*). They reported a number of thermal reactions and phase transitions over the temperature range of interest. The compound first melts and loses water of crystallization in two steps forming the hemihydrate and finally the anhydrous sodium bisulfate. The anhydrous salt melts at 180 °C and decomposes into sodium pyrosulfate by splitting out water of composition between two bisulfate groups. This reaction is critical because, although it provides a source of water for hydrolysis, it converts the reagent into a nonacidic compound which is no longer capable of sustaining the hydrolysis. Sodium bisulfate monohydrate produced only qualitative results. Table II shows a low recovery of acetic acid from poly(vinyl acetate) with a large relative standard deviation.

p-Toluenesulfonic acid monohydrate was investigated as a substitute for sodium bisulfate. The compound is a strong monoprotic acid with a melting point of 104-106 °C. Thermal gravimetric analysis indicated that thermal decomposition commenced at about 200 °C with almost complete volatilization of the reagent. Gas chromatographic analysis showed two products, water and toluene. A peak corresponding to

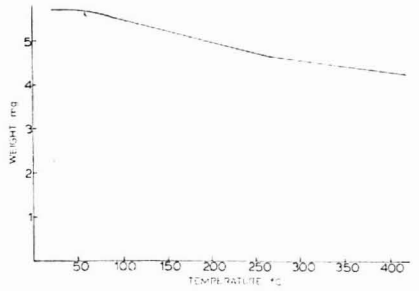

Figure 1. TGA of solid phosphoric acid. Atmosphere: N_2 at 30 mL/min. Heating rate: 10 °C/min

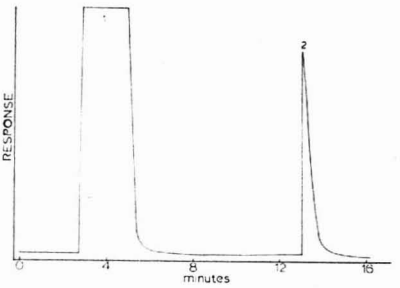

Figure 2. Gas chromatogram of cholesteryl acetate after acid fusion (Column A, Table I). Peak 1, water; 2, acetic acid

sulfur dioxide, a decomposition product of the sulfonic acid group, was not observed (*12*). The sulfur dioxide peak may have been masked by the large water peak. Under actual experimental conditions, the reagent releases approximately 75 to 100 mg of toluene and 15 to 20 mg of water which overloads the chromatographic column. The large toluene peak overlaps the acetic and propionic acid peaks on both Chromosorb 101 and 105 making it impossible to analyze samples containing either acid on these columns. Quantitative hydrolysis and recovery of butyric acid were, however, achieved with cholesteryl butyrate (Table II). Further work was abandoned because of the thermal instability of the reagent.

Crystalline phosphoric acid proved to be an ideal acid fusion reagent. It is a fairly strong acid which melts at 42 °C. The thermogram of solid phosphoric acid illustrated in Figure 1 shows an almost constant weight loss from 60 to 425 °C. This was interpreted as a continuous loss of water. Gas chromatographic analysis confirmed that only water was released from phosphoric acid. The reagent condenses with itself by the elimination of water when heated, forming pyrophosphoric acid and higher condensed species. This reaction is analogous to the condensation of sodium bisulfate to form pyrosulfate. The condensation serves as a needed source of water for hydrolysis; however, unlike sodium bisulfate, the acidic character of the reagent is preserved. Solid phosphoric acid was able to quantitatively hydrolyze and liberate acetic and butyric acid from poly(vinyl acetate) and cholesteryl butyrate as shown in Table II. Phosphoric acid was used in all subsequent quantitative work. The only difficulty with the reagent was its hygroscopicity which necessitated the use of a glove box.

Phosphorous acid and benzenephosphonic acid were briefly examined as possible substitutes for phosphoric acid. Both reagents have acid strength similar to phosphoric acid and can be used without requiring a glove box. Both compounds gave quantitative results as shown in Table II. Benzenephosphonic acid thermally decomposes like *p*-toluenesulfonic acid releasing large quantities of benzene and water. Work was discontinued with phosphorous acid because it releases poisonous phosphine gas when heated above 200 °C (*13*). Phosphorous acid could be considered as a substitute for solid phosphoric acid provided adequate steps were taken to completely trap out the phosphine gas.

Quantitative Analysis. The cholesteryl esters were used in conducting the initial quantitative investigation. The cholesteryl esters were selected because they were sufficiently nonvolatile and were obtainable in high purity, making a check determination of their acid content unnecessary. A typical chromatogram of the reaction products released during acid fusion of cholesteryl acetate is shown in Figure 2. The chromatogram should show two peaks. A large water peak, from 10–20 μL, released by the acid fusion reagent and a carboxylic acid peak liberated by hydrolysis from the ester. The hydroxy and in many cases the polyhydroxy compound resulting from the hydrolysis of the ester are generally nonvolatile and, therefore, not detected. The results in Table III show conversion within 3% of the theoretically expected value and proved results of sufficient precision and accuracy can be achieved following sample reaction and gas chromatographic separation.

Table III. Analysis of Cholesteryl Esters by Acid Fusion Gas Chromatography

Compound	Reaction product	Theoretical recovery, %	Rel std dev
Cholesteryl acetate	Acetic acid	102.8 (3)[a]	0.8
Cholesteryl propionate	Propionic acid	100.9 (5)	0.7
Cholesteryl *n*-butyrate	*n*-Butyric acid	99.9 (4)	1.7
Ethynodiol diacetate	Acetic acid	100.5 (4)	4.0

[a] Number in parentheses indicates the number of determinations.

It is possible to shorten the 30–35 min required for a complete determination, 15–20 min for sample reaction and 15 min for chromatographic separation, by overlapping analyses. A sample reaction can be initiated after the elution of the water peak from the previous sample boat. The delay ensures that the contents of the trap have been completely volatilized and also allows sufficient time for the detector to stabilize after switching from the trap heater to the liquid nitrogen Dewar.

The carbohydrate esters are chemically similar to the cellulose esters and were used as model compounds to examine the possibility of analyzing these commercially important polymers by acid fusion gas chromatography. Table IV compares the results obtained by acid fusion with the theoretical carboxylic acid content. The organic acid content of the nonreducing carbohydrate esters was also checked by saponification (*14*). The chromatogram of the reaction products from sucrose octaacetate following acid fusion is presented in Figure 3. All of the acetylated carbohydrates produced similar chromatograms. In addition to the expected water and acetic acid peaks, Figure 3 contains a number of minor peaks presumably caused by the decomposition of the sucrose moiety. This was confirmed by running a reaction boat containing sucrose and phosphoric acid. Figure 4 shows five decomposition peaks from the sucrose blank. The peaks were identified as carbon dioxide, formic, acetic, and propionic acids. Peak number four was not identified. The carbon dioxide, formic and propionic acids from the decomposition of the sucrose moiety in sucrose octaacetate are clearly visible

Table IV. Analysis of Carbohydrate Esters by Acid Fusion Reaction Gas Chromatography

Compound	Reaction product	Weight percent + standard deviation		
		Acid fusion	Check method	Theoretical
α-D-Cellobiose octaacetate	Acetic acid	73.1 ± 0.7 (5)[a]	···	70.79
α-D-Glucose pentaacetate	Acetic acid	78.4 ± 1.4 (4)	···	76.92
β-D-Ribofuranose 1,2,3,5-tetraacetate	Acetic acid	76.3 ± 1.2 (4)	···	75.47
1-Thio-D-glucose pentaacetate	Acetic acid	71.5 ± 0.8 (4)	···	73.93
β-D-Galactose pentaacetate	Acetic acid	76.3 ± 1.9 (6)	···	76.92
Sucrose octaacetate	Acetic acid	71.9 ± 0.9 (6)	70.43 ± 0.36 (3)	70.79
Sucrose diacetate hexaisobutyrate	Acetic acid	14.5 ± 0.2 (5)	···	14.18
	Isobutyric acid	59.1 ± 1.1 (5)	···	62.42
	Apparent acetic acid	54.8 ± 0.6 (5)	56.8 ± 0.9 (3)	···
Sorbitol hexaacetate	Acetic acid	81.7 ± 1.2 (6)	83.17 ± 0.80 (3)	82.94
Methyl-α-D-galactopyranoside 2,3,4,6-tetraacetate	Acetic acid	65.1 ± 0.5 (4)	66.9 ± 0.1 (3)	66.29
β-D-Ribofuranose 1-acetate-2,3,5-tribenzoate	Benzoic acid	74.9 ± 0.2 (4)	···	72.62
Sucrose benzoate	Benzoic acid	78.3 ± 1.8 (5)	···	80.46

[a] Number in parentheses indicates the number of determinations.

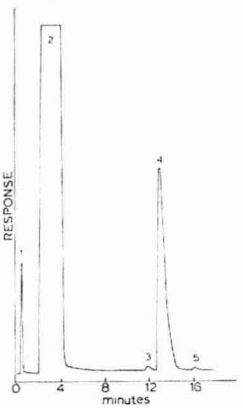

Figure 3. Gas chromatogram of sucrose octaacetate after acid fusion (Column A, Table I), attenuation × 64. Peak 1, carbon dioxide; 2, water; 3, formic acid; 4, acetic acid; 5, propionic acid

Figure 4. Gas chromatogram of sucrose after acid fusion (Column A, Table I), attenuation × 16. Peak 1, carbon dioxide; 2, water; 3, formic acid; 4, unknown; 5, acetic acid; 6, propionic acid

in Figure 3. The small unknown peak and acetic acid peak produced by the decomposition of the sucrose moiety are masked by the large acetic peak liberated by hydrolysis. Results are thus higher by the amount of acetic acid and unknown component produced by decomposition. Correction can be accomplished by running as a blank the respective parent carbohydrate.

The production of volatile acids as decomposition products is a common occurrence in the analysis of carbohydrate esters (*15–17*). As an example, fructose had an acetic acid content of 16% under acidic hydrolysis in sulfuric acid (*17*). Sucrose had an acetic acid content of 3% by acid fusion, however, the results for sucrose octaacetate were high by just 1.5% since the compound is only 50% by weight sucrose. Results in Table IV were corrected for decomposition by running a blank on the parent carbohydrates.

The results in Table IV for sucrose benzoate and β-D-ribofuranose-1-acetate 2,3,5-tribenzoate indicate that acid fusion can be successfully extended to samples containing aromatic monocarboyxlic acids. Gas chromatographic separation of the reaction products was carried out using the FFAP column. Somewhat more drastic conditions were required to achieve complete hydrolysis and to volatilize the higher boiling reaction product. Samples were reacted at 200 °C for 5 min followed by an additional 15–20 min at 300–325 °C. Calibration was achieved by weighing analytical reagent grade benzoic acid into tared platinum boats. Sample and calibration boats were reacted under the same experimental conditions. A typical chromatogram of the reaction products from β-D-ribofuranose-1-acetate 2,3,5-tribenzoate is shown in Figure 5. Although decomposition of the carbohydrate moiety was observed, a correction was unnecessary since the parent carbohydrate degrades without production of benzoic acid. The acetate content of β-D-ribofuranose-1-acetate 2,3,5-tribenzoate was not determined because of insufficient resolution of the acid hydrolyzed acetic acid from the C_1–C_3 decomposition acids. No attempt was made to determine the acetate content on either the Chromosorb 101 or 105 columns. Sucrose benzoate had an elemental carbon content of 68.62% and a 4.65% hydrogen content. The elemental composition indicated a 7.18 degree of substitution which corresponds to a 80.46% combined benzoic acid content. This is in general agreement with the benzoic acid content determined by acid fusion.

The results from the acid fusion analysis of the cellulose esters and poly(vinyl esters) are summarized in Table V. The

Table V. Analysis of Cellulose Esters and Poly(vinyl esters) by Acid Fusion Gas Chromatography

Polymer	Reaction product	Weight percent + standard deviation	
		Acid fusion	Check method
Cellulose acetate	Acetic acid	54.9 ± 0.3 (4)[a]	55.88 ± 0.21 (3)
Cellulose triacetate	Acetic acid	62.2 ± 0.9 (6)	61.96 ± 0.32 (5)
Cellulose acetate propionate	Acetic acid	42.0 ± 0.2 (5)	---
	Propionic acid	18.3 ± 0.1 (5)	---
	Apparent acetic acid	56.8 ± 0.3 (5)	56.65 ± 0.51 (3)
Cellulose acetate butyrate	Acetic acid	42.7 ± 0.4 (5)	---
	Butyric acid	21.7 ± 0.1 (5)	---
	Apparent acetic acid	57.5 ± 0.4 (5)	56.82 ± 0.15 (4)
Cellulose acetate Hydrogen phthalate	Acetic acid	29.3 ± 0.7 (6)	---
	Phthalic acid[b]	46.2 ± 2.9 (6)	---
	Apparent acetic acid	62.6 ± 2.1 (6)	62.13 ± 0.56 (4)
Poly(vinyl acetate)[c]	Acetic acid	69.7 ± 1.4 (5)	68.46 ± 0.09 (3)
Poly(vinyl acetate)[c,d]	Acetic acid	70.2 ± 0.4 (4)	68.46 ± 0.09 (3)
Poly(vinyl acetate)[e]	Acetic acid	69.9 ± 1.3 (6)	69.5 ± 0.7 (3)
Poly(vinyl propionate)[e]	Acetic acid	0.72 ± 0.06 (6)	---
	Propionic acid	73.3 ± 0.9 (6)	---
	Apparent propionic acid	74.2 ± 0.9 (6)	74.5 ± 0.10 (3)

[a] Number in parentheses indicates the number of determinations. [b] Independently determined. [c] Commercial sample. [d] Calibration curve constructed using sodium acetate. [e] Prepared from 99–100% hydrolyzed poly(vinyl alcohol).

Figure 5. Gas chromatogram of β-D-ribofuranose-1-acetate 2,3,5-tribenzoate after acid fusion (Column C, Table I). Peak 1, carbon dioxide; 2, unknown; 3, water; 4, C_1–C_3 acids; 5, benzoic acid

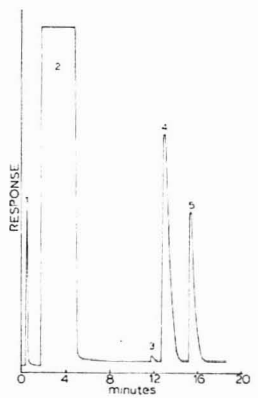

Figure 6. Gas chromatogram of cellulose acetate propionate after acid fushion (Column A, Table I). Peak 1, carbon dioxide; 2, water; 3, formic acid; 4, acetic acid; 5, propionic acid

cellulose esters behaved in the same manner as the carbohydrate esters. The volatile acids derived from the degradation of the cellulose backbone were corrected with a cellulose blank. The accuracy of the acid fusion results was checked by saponification (*16*). It was necessary to express saponification results as percent apparent acetic acid for the mixed esters. The acid fusion results were expressed both as the individual carboxylic acid content and as apparent acetic acid content which allows a direct comparison of the results. By acid fusion, it was possible to determine only the acetic acid content of cellulose acetate hydrogen phthalate. Phthalic acid is nonvolatile and not amenable to gas chromatographic determination under the existing experimental conditions. An independent determination was carried out for the phthalic acid content and combined with the acetic acid value from acid fusion to obtain the apparent acetic acid (*18, 19*). The reaction products released from cellulose acetate propionate are shown in Figure 6. The water, acetic acid, and propionic acid peaks are well resolved. Two decomposition peaks are also shown in the chromatogram.

The acid fusion determination of the poly(vinyl esters) were also checked and compared favorably with the acid content obtained by saponification (*14*). The ability to use sodium acetate for calibration was demonstrated with poly(vinyl acetate). Poly(vinyl propionate), besides liberating the expected propionic acid, had an acetic acid content of 0.72%. The acetic acid was derived from residual acetate groups in the 99–100% hydrolyzed poly(vinyl alcohol) used in the preparation. The analysis of poly(vinyl propionate) demonstrates the ability of acid fusion to determine mixed esters of widely varying composition with good precision and accuracy. No decomposition products were observed from the poly(vinyl esters).

The acid fusion analysis of two vinyl acetate copolymers can be found in Table VI. The vinyl acetate content of poly(ethylene-vinyl acetate) was calculated from the elemental

Table VI. Analysis of Poly(vinyl acetate) Copolymers by Acid Fusion Gas Chromatography

Polymer	Percent combined vinyl acetate ± standard deviation, % weight: Acid fusion	Check method	Vinyl pyrrolidone
Poly(ethylene-vinyl acetate), 18% vinyl acetate	16.8 ± 0.4 (6)[a]	16.84[b]	
Poly(ethylene-vinyl acetate), 18% vinyl acetate	16.5 ± 0.2 (5)[c]	16.84	
Poly(*n*-vinyl pyrrolidone-vinyl acetate) 60/40	41.2 ± 0.7 (4)		58.15[d]

[a] Number in parentheses indicates the number of determinations. [b] Calculated from elemental oxygen analysis. [c] Calibration curve constructed using sodium acetate. [d] Calculated from elemental nitrogen analysis.

Table VII. Analysis of Residual Acetate Groups in Poly(vinyl alcohols) by Acid Fusion Gas Chromatography

Polymer	Percent hydrolyzed ± standard deviation: Acid fusion	Check method	Manufacturer's value
Poly(vinyl alcohol)	73.5 ± 0.3 (5)[a]	72.98 ± 0.31 (3)	75
Poly(vinyl alcohol)	87.6 ± 0.6 (5)	88.13 ± 0.23 (3)	88
Poly(vinyl alcohol)	96.2 ± 0.2 (4)	···	96
Poly(vinyl alcohol)	98.6 ± 0.1 (5)	···	99-100

[a] Number in parentheses indicates the number of determinations.

oxygen analysis. Sodium acetate was again employed as an alternate method of calibration in the analysis of poly(ethylene-vinyl acetate) and the resulting vinyl acetate value agreed favorably with the value determined using the syringe calibration method. The vinyl pyrrolidone content of poly(vinyl pyrrolidone-vinyl acetate) was determined from the elemental nitrogen analysis. The vinyl acetate and vinyl pyrrolidone content are in good agreement. Water and acetic acid were the only observed reaction products from both copolymers.

Poly(vinyl alcohol) is prepared commercially from poly(vinyl acetate) by an acid or base catalyzed saponification reaction. The polymer usually contains residual acetate groups, the number of which is regulated by the reaction conditions. Four poly(vinyl alcohol) samples were analyzed by acid fusion reaction gas chromatography. Saponification was used as a check method for the 75% and 88% hydrolyzed poly(vinyl alcohol) samples. The results in Table VII from the acid fusion of all four poly(vinyl alcohol) samples are in agreement with results obtained by saponification and the degree of hydrolysis stated by the manufacturer. The chromatograms from all four polymers contained only the expected water and acetic acid peak.

LITERATURE CITED

(1) M. Wandel and H. Tengler, *Gummi, Asbest, Kunstst.*, **19**, 141 (1966).
(2) G. Esposito and M. Swann, *J. Paint Technol.*, **43**, 60 (1971).
(3) O. Aydin, B. Kaczmar, and R. Schulz, *Angew. Makromol. Chem.*, **33**, 153 (1973).
(4) W. R. Sorenson and T. W. Campbell, "Preparative Methods of Polymer Chemistry", 2nd ed., Interscience, New York, N.Y., 1968, pp 241-242.
(5) D. M. Ottenstein and D. A. Bantley, *J. Chromatogr. Sci.*, **9**, 673 (1972).
(6) D. A. Geddes and M. N. Gilmour, *J. Chromatogr. Sci.*, **8**, 394 (1970).
(7) R. J. Leibrand and L. L. Dunhom, *Res./Dev.*, **24** (9), 32 (1973).
(8) S. Siggia, L. R. Whitlock, and J. C. Tao, *Anal. Chem.*, **41**, 1387 (1969).
(9) S. P. Frankoski and S. Siggia, *Anal. Chem.*, **44**, 507 (1972).
(10) D. Schlueter, Ph.D. Thesis, University of Massachusetts, Amherst, Mass., 1976.
(11) J. Paulik, F. Paulik, and L. Erdey, *Anal. Chim. Acta*, **34**, 419 (1966).
(12) S. Siggia and L. R. Whitlock, *Anal. Chem.*, **42**, 1719 (1970).
(13) L. Hackspill and J. Weiss, *Chem. Ind.*, 453 (March 1932).
(14) S. Siggia, "Quantitative Organic Analysis via Functional Groups", 3rd ed., Wiley, New York, N.Y., 1963, p 139.
(15) T. F. Murrya, Jr., C. J. Stauch, and H. LeB. Gray, *Ind. Eng. Chem., Anal. Ed.*, **3**, 269 (1931).
(16) L. B. Genung and R. C. Mallatt, *Ind. Eng. Chem., Anal. Ed.*, **13**, 369 (1941).
(17) A. S. Inglis, *Mikrochim. Acta*, **2**, 228 (1957).
(18) R. Williams, Ph.D. Thesis, University of Massachusetts, Amherst, Mass., 1976.
(19) C. Malm, L. B. Genung, and W. Kuchmy, *Anal. Chem.*, **25**, 245 (1953).

RECEIVED for review February 16, 1977. Accepted June 29, 1977. Work supported by the National Science Foundation, Grant No. GP-37493X and CHE76-07378.

Analysis of Polysiloxanes by Alkali Fusion Reaction Gas Chromatography

David D. Schlueter[1] and Sidney Siggia*

Department of Chemistry, University of Massachusetts, Amherst, Massachusetts 01003

The technique of alkali fusion reaction gas chromatography has been applied to the determination of alkyl and aryl groups in polysiloxanes. The method involves the quantitative cleavage of all organic substituents bonded to silicon, producing the corresponding hydrocarbons. Reactions are driven to completion, with no apparent decomposition, in less than 10 minutes by fusing the sample with potassium hydroxide in an inert atmosphere. After concentration of the volatile products, they are separated and determined by gas chromatography. Sample losses are minimized by performing the total analysis in a single piece of apparatus. Fluids, gum rubbers, and resins are handled with equal ease. The percent relative standard deviation of the method is 1.0%; the average deviation between experimental and theoretical or check method results is 0.5% absolute.

Polysiloxanes, also referred to as silicones or polyorganosiloxanes, are commercially important because of unique properties resulting from their dual organic–inorganic composition. The analytical chemistry of this class of polymers has been reviewed in a recent monograph by Smith (*1*). Spectrometric techniques, such as IR and NMR, are powerful tools for the qualitative and quantitative analysis of many functional groups in the intact polymer. Alternatively, these organic substituents can be cleaved from the polymer to produce simple compounds that can be determined by chemical or instrumental techniques.

Alkyl and aryl substituents are readily detected by the above approaches, but quantitative analyses of these groups may be difficult with existing methodology. Instrumental techniques such as NMR (*2, 3*), IR (*4–13*), and UV (*14–17*) spectrometry are useful for analyzing methyl and/or phenyl groups in silicone polymers, but they are generally unable to differentiate isomers or homologues. Chemical cleavage coupled with a separation technique is a more selective approach. Several reaction-based methods have been reported for the quantitative determination of alkyl and aryl groups bonded to silicon and are included in Table I. The limited scope of these methods has led to the present study.

This paper describes the application of alkali fusion reaction gas chromatography to the quantitative analysis of a variety of alkyl and aryl groups in polysiloxane fluids, gums, and resins. Fusion of the polymer with a powdered potassium hydroxide reagent converts these substituents into the corresponding hydrocarbons, which are trapped and then analyzed by gas chromatography (GC). Application of this technique to other reactive functional groups bonded to silicon was also investigated briefly.

EXPERIMENTAL

Fusion Reagent. The alkali fusion reagent is a prefused mixture of potassium hydroxide (J. T. Baker, Analytical reagent grade) and 0.5% sodium acetate. The procedure for its preparation has been described in detail elsewhere (*30*). Typically, the mixture melts around 110 °C. and contains 13–14% water. When preparing this reagent, it is important to avoid excessive heating. If too much water is lost, the molten reaction mass may solidify before the hydrolysis reaction is complete. On the other hand, too much water will make the reagent sticky and difficult to handle. Additionally, it is possible to plug the cold trap if large amounts of water are released. To prevent adsorption of moisture from the atmosphere, the powdered reagent is stored in a small desiccator within a nitrogen-filled glove bag.

Samples. The polysiloxane samples were obtained from Dow Corning Corporation (DC), General Electric Company (GE), Union Carbide Corporation (UC), and gas chromatography supply houses. The source of each sample is indicated in the tables of results. In most cases, samples were analyzed as received. Resin solutions were dried under vacuum before being sampled.

Standards. The hydrocarbon calibration standards were purchased from commercial suppliers. The purity of each was checked by programmed temperature GC on matched 6-foot by $^1/_8$-inch o.d. stainless steel columns packed with 50–80 mesh Porapak Q (Waters Associates, Milford, Mass. 01757). If necessary, the compounds were purified by conventional practices. *m*-Carborane (Ventron Corporation, Alfa Products, Beverly, Mass. 01315) was particularly impure, but vacuum sublimation at room temperature produced a suitable standard.

Apparatus. The total analysis (reaction, trapping, separation, and quantitation) is performed in a single piece of apparatus. Figure 1 is a diagram of the reaction and trapping sections. The reaction portion consists of a pyrolysis tube, combustion furnace assembly, and a mounting frame taken from a commercial unit (Perkin-Elmer Pyrolysis Accessory 154-0825, Norwalk, Conn. 06856). Modifications made to the tube include the addition of a septum inlet (E) directly behind the reaction furnace (F) and the elongation of storage areas (A) and (B) for greater sample capacity. Samples, standards, and reagent are contained in miniature platinum boats (10 mm × 4 mm × 4 mm, Fisher Scientific Co., Pittsburgh, Pa. 15219) and are magnetically manipulated within the confines of the glass tubing with metal cylinders (J) and a hoe-shaped retriever (K). The combustion furnace assembly (F) monitors and controls the temperature within the reaction zone (C).

A loop-shaped piece of 316 grade stainless steel tubing (G) (0.125-inch o.d., 0.093-inch i.d.), connected between the outlet of the reaction furnace and a special low dead-volume GC injector assembly (H) (Perkin-Elmer Part No. 009-0276), serves as a trap for efficiently concentrating most volatile reaction products. All of the transfer tubing from the reaction zone to the injection port, except the lower section of the loop, is heated to 300 °C by a clam-shell type combustion furnace (I) clamped around the tubing. The exposed piece of tubing, which is loosely packed with quartz wool, is cooled in a liquid nitrogen-filled Dewar flask when concentrating the evolved products and heated with a 400 °C nichrome wire heater (*30*) when "injecting" the products into the gas chromatograph. Helium carrier gas flows (60 mL/min) through the reaction unit and cold trap before entering the chromatographic column. Additional details and a photograph of the assembled apparatus are given in Ref. 31.

The products are separated on matched 6-foot by $^1/_8$-inch o.d. stainless steel columns packed with 50–80 mesh Porapak Q. A Perkin-Elmer Model 990 Gas Chromatograph, equipped with dual thermal conductivity detectors and a linear column temperature programmer, was used. The column temperature was maintained at 90 °C during the reaction period. Upon injection of the products, time zero in the chromatograms, the temperature was

[1] Present address, Biochemicals Department, E. I. du Pont de Nemours & Co., Inc., Wilmington, Del. 19898.

Table I. Reaction Methods for the Quantitative Determination of Organic Substituents Bonded to Silicon

Group determined	Reagent	Reaction conditions	Product	Analysis	Ref.
Phenyl	60% aqueous KOH in DMSO	2 h at 120 °C	Benzene	GC	18
Phenyl	Bromine in glacial acetic acid	Boiling solution	Bromobenzene	Titration of excess bromine	19
Ethyl and phenyl	Phosphorous pentoxide and water	30–580 °C over 45 min	Ethane and benzene	GC-FID	20
Methyl and ethyl	Powdered potassium hydroxide	2 h at 250–270 °C	Methane and ethane	Gas buret	21
Methyl	Sulfuric acid	20 min at 280–300 °C	Methane	Gas buret	22, 23
Phenyl	Ethylbromide in the presence of aluminum chloride	. . .	Hexaethylbenzene	Gravimetric	24
Vinyl	Phosphorous pentoxide and water	80–600 °C over 40 min	Ethylene	GC-FID	25
Vinyl	Phosphorous pentoxide and water	Ambient to 500 °C over 45 min	Ethylene	GC-FID	26
Vinyl	90% Sulfuric acid	75–250 °C at 10 °C/min and 1 h at 250 °C	Ethylene	GC-TC	27
Vinyl	Sodium hydroxide pellets	300 ° C for 15 min	Ethylene	Colorimetric	28
Vinyl	Potassium hydroxide pellets	Heat with Meker burner	Ethylene	GC-FID	29

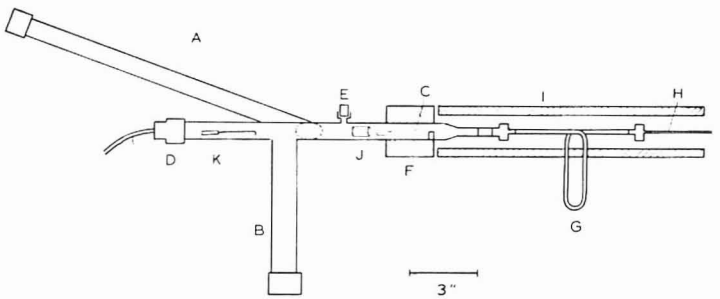

Figure 1. Diagram of the reaction and trapping unit used for alkali fusion reaction GC. The mounting rack and electrical control units are not shown. A, storage area for unreacted samples; B, storage area for reacted samples; C, quartz reaction zone; D, carrier gas inlet; E, side arm with rubber septum; F, variable temperature furnace; G, trap loop; H, injector assembly into gas chromatograph; I, combustion furnace surrounding transfer tubing; J, metal cylinder behind platinum sample boat; K, magnetic retriever

programmed from 90 to 260 °C at 8 °C per minute. Peak areas were measured with a Vidar AutoLab 6300 Digital Integrator (Spectra-Physics, Santa Clara, Calif. 95051). The detector signal was displayed on a Varian G-2500 Recorder (Palo Alto, Calif. 94303).

Procedure. One to five milligrams (±1 μg) of powdered sample or standard is weighed into the tared platinum micro-boats. The boats are then filled with the powdered caustic reagent in the nitrogen-purged glove bag and quickly loaded into the storage arm of the reaction tube (Figure 1, A) with a metal cylinder (J) behind each. When making quantitative analyses, the first sample reacted in a series of runs is used to condition the apparatus. Boats are usually loaded at the end of a work day, thus permitting entrapped air to be purged from the system overnight. When samples are loaded in the morning, the tube is purged for 1 h before turning on the thermal conductivity detector current.

Once a stable baseline is obtained, the liquid nitrogen-filled Dewar flask (−196 °C) is positioned around the unheated section of the trap. The first metal cylinder is magnetically moved forward, pushing the boat in front of it into the heated reaction zone (C). The cylinder is removed to storage area (B). The optimum reaction temperature profile for a fusion reaction will depend on the reactivity of the samples. In this study, the furnace temperature was programmed from 100 to 300 °C over a period of 10 min. As the reaction occurs, the volatile reaction products and water, liberated from the molten mixture, are carried by the flowing helium carrier gas and concentrated in the trap. At the end of the reaction period, i.e., 10 min, the boat is withdrawn from the furnace with the magnetic retriever (K) and deposited with its cylinder in (B). After adjusting the furnace control to its initial temperature setting, the trapped compounds are revolatilized and directed into the gas chromatograph by replacing the Dewar flask with the heater (400 °C). When the separation and integration are completed and the initial conditions reestablished, the procedure is repeated for each sample and standard.

After completion of a series of reactions, the spent boats and metal cylinders are removed from the storage area. Boats are cleaned by soaking in dilute hydrochloric acid, washing with warm water, and heating in the flame of a Meker burner. The inner surfaces of the reaction tube are periodically cleaned with a moistened swab to remove any reagent that may have spilled or splattered from the boats.

Calibration. Calibration curves are prepared for each compound produced. Products which are gases under normal conditions, are injected with a calibrated gas-tight syringe through the septum inlet of the reaction tube. Ambient temperature and pressure corrections are necessary to determine the actual amounts of gas injected. Standard solutions of liquid or solid reaction products are injected by syringe into an empty boat. These products are volatilized by pushing the boat into the heated reaction zone. Solid products having low vapor pressures at room temperature are weighed directly into platinum boats, covered

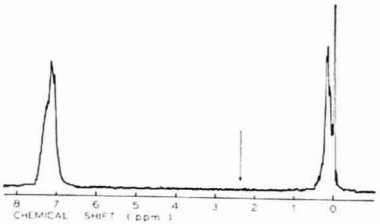

Figure 2. Proton NMR spectrum of DC 710 polymethylphenylsiloxane in carbon tetrachloride. Methyl proton resonance occurs at ~0 ppm while phenyl proton resonance occurs downfield at ~7 ppm. The arrow indicates the location of the dimethylsulfoxide internal standard singlet

with reagent, and stored with the samples.

The preferred approach is to use secondary standards, i.e., well-characterized compounds or polymers that quantitatively react with the reagent to give the desired product. For example, when only methane is determined, GE Viscasil 60 000, a high molecular weight polydimethylsiloxane, is used. DC 704, a polymethylphenylsiloxane, is used as the secondary standard when both methane and benzene are determined.

In all cases, the standards are trapped and chromatographed in exactly the same manner as the reaction products. The best straight line calibration curves are determined by a least-squares regression curve-fitting computer program.

NMR Check Method. A proton nuclear magnetic resonance (NMR) method was developed to determine the methyl and phenyl content of polymethylphenylsiloxanes. Polymer 0.2–0.4 g is weighed, to the nearest 0.1 mg, into a tared sample bottle. Approximately 0.1 g of dimethylsulfoxide (Aldrich Chemical Co., Inc.) internal standard is added and the bottle reweighed. After addition of 1.0 mL of carbon tetrachloride (Aldrich), the vial is tightly capped and shaken. The proton spectrum from −1 to +9 ppm was obtained on a Perkin-Elmer Model R-12A, 60-MHz NMR spectrometer. Figure 2 is a typical spectrum of a silicone containing both methyl and phenyl substituents. The total peak area for each type of proton is obtained by scanning the appropriate resonance regions of the spectrum and summing the integrator output with a Heath DVM. Ten to twenty area determinations were made for each type of proton. The weight percent of each proton type is calculated from the equation:

$$\text{Weight Percent}_h = \left(\frac{100 N_i M_h}{N_h M_i}\right)\left(\frac{A_h}{A_i}\right)\left(\frac{W_i}{W_s}\right)$$

where A is the average integrated area, W is the weight, N is the number of absorbing protons, and M is the formula weight of the internal standard (subscript i), the hydrocarbon group (subscript h), and the sample (subscript s). In the case of methyl groups, this equation simplifies to the following:

$$\text{Weight Percent Methyl} = 38.49\left(\frac{A_{\text{Methyl}}}{A_{\text{DMSO}}}\right)\left(\frac{W_{\text{DMSO}}}{W_{\text{Sample}}}\right)$$

Similarly, the phenyl content is calculated from the equation:

$$\text{Weight Percent Phenyl} = 118.4\left(\frac{A_{\text{Phenyl}}}{A_{\text{DMSO}}}\right)\left(\frac{W_{\text{DMSO}}}{W_{\text{Sample}}}\right)$$

RESULTS AND DISCUSSION

A number of compounds have been suggested for cleaving monovalent organic substituents attached to silicon (*32–39*). The use of potassium hydroxide was investigated. Initial recovery studies at different isothermal reaction temperatures showed that theoretical amounts of methane and benzene could be obtained from polydimethylsiloxanes and polydiphenylsiloxanes. However, reaction times were long at the lower temperatures and splattering of the molten mixture occurred if the reaction zone was too hot. By placing the boat into the oven, initially at 100 °C, and setting the furnace controller for a final temperature of 300 °C, a reproducible temperature–time profile was generated within the reaction zone. Under these reaction conditions, all methyl and phenyl groups were cleaved in 5 min. As a general practice, the boat was left in the reaction zone for 10 min. This temperature programming procedure proved to be suitable for all the samples studied.

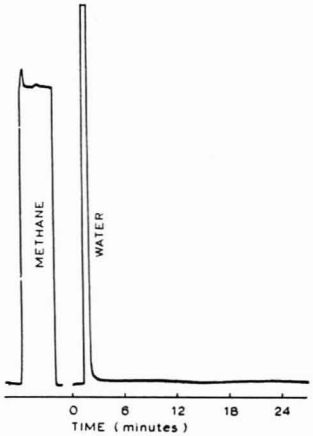

Figure 3. Gas chromatogram of the methane produced from the alkali fusion of GE Viscasil 60 000 polydimethylsiloxane. The water is liberated from the reagent during the reaction

Improvements were made in the trapping section. A 0.093-inch i.d. piece of $^1/_8$-inch tubing provided better heat transfer and was less prone to plug than the more commonly available 0.085-inch i.d. tubing. Aerosol formation and possible blowthrough of the product is avoided by loosely packing the tubing with quartz wool. This was found to be a much more stable packing material than the previously used silanized glass wool, which degrades with time.

Methane (bp −164 °C) is one of the few compounds not retained and concentrated in the cooled loop. This gas, when produced or injected through the pyrolysis unit septum, selectively passes through the trap at a fixed rate resulting in a rectangular shaped "peak". This is illustrated in Figure 3, the gas chromatogram obtained from the fusion of GE Viscasil 60 000. The recorder trace preceding time zero is typical of the detector response due to methane.

Accurate methane peak area measurement was accomplished by adjusting the integrator sensitivity controls. After the integration was initiated, the noise and filtering dials were set at their most insensitive levels. This does not interfere with the integrating process but does prevent the instrument from prematurely turning off. The inability to trap methane is an advantage. Quantitation of the product during the reaction results in a more rapid analysis, signals the end of the reaction, and simplifies any remaining chromatography.

Calibration curves were prepared daily for each product being determined. Over a period of six months, the percent relative standard deviation of the slope of the methane curve was 2.2%. The slope of the benzene calibration curve varied by 1.9% relative over a two-month interval. Analysis of peak area data revealed that the initial sample or standard reacted on any given day gave recoveries that were a few percent lower than expected. For this reason, the first boat was used solely to condition the apparatus.

Table II. Analysis of Polydimethylsiloxanes by Alkali Fusion Reaction Gas Chromatography

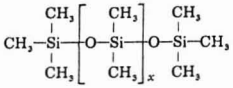

Sample	x[a]	Methyl content, wt %: Alkali fusion[b]	Methyl content, wt %: Theory	% Recovery of theoretical methane
GE SF96-20	4	39.74 ± 0.30	45.86	86.7
GE SF96-50	45	40.74 ± 0.16	41.26	98.7
GE SF96-100	85	40.75 ± 0.06	40.93	99.6
DC 200-100cs	85	41.15 ± 0.35	40.93	100.5
GE SF96-1000	340	40.50 ± 0.28	40.65	99.6
DC 200-12 500 cs	850	40.74 ± 0.49	40.59	100.4
GE Viscasil 60 000	1240	40.55 ± 0.24	40.58	99.9
GE SE-30	...	40.47 ± 0.24	40.55	99.8
GE SE-33	...	39.93 ± 0.42	*c*	...
DC Silastic 430	...	39.75 ± 0.30	*c*	...
GE SE-31	...	38.14 ± 0.33	*c*	...

[a] Average number of dimethylsiloxane repeat units based upon manufacturers' data. [b] The standard deviation is based upon five or more determinations. [c] Sample also contained a low percentage of vinyl groups. See Table VI.

Methyl substituted polysiloxanes are probably the most important class of commercial silicon-containing polymers (*40*). Their physical properties can be modified by controlling the degree of polymerization, branching, and/or cross-linking. Under very basic conditions, one methane molecule is produced for each methyl group present (*21*). A series of polydimethylsiloxanes was analyzed by alkali fusion reaction GC. Table II summarizes the results of this study. Methane gas was used to prepare the calibration curve for GE Viscasil 60 000. This polymer was then used as a secondary standard for preparing subsequent curves. The precision of these determinations varied from 0.2 to 0.8% relative. Theoretical weight percent values were calculated using manufacturers' average molecular weight data and the assumption that the polymers were linear and chain-terminated with trimethylsilyl groups. With the exception of the lowest molecular weight sample, the recovery of methane was within 0.5% absolute of theory. The low value obtained from the GE SF96-20 sample may be due to vaporization of low molecular weight oligomers before reaction.

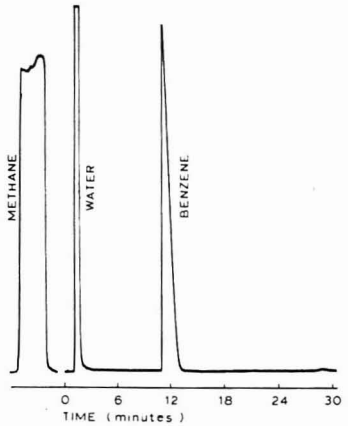

Figure 4. Gas chromatogram of the methane and benzene produced from the alkali fusion of DC 704 polymethylphenylsiloxane

Polymethylphenylsiloxanes are also of commercial importance (*40*). A gas chromatogram of the reaction products obtained from DC 704, a polymethylphenylsiloxane, is shown in Figure 4. Methane and benzene are the only volatile reaction products observed; the water is liberated from the reagent. Calibration curves were initially prepared using benzene and GE Viscasil 60 000 as standards. A sample of DC 704 was reacted 33 times over a period of several days. The percent relative standard deviation of each product was 0.8%, and the weight percent values correlated well with the NMR results. For these reasons, DC 704 was used as the secondary standard when both methyl and phenyl groups were determined. Table III compares the weight percent values determined by both reaction GC and NMR. Agreement between these two different approaches was excellent, well within the expected accuracy of the NMR method. The gum and resin samples could not be dissolved in the carbon tetrachloride–dimethyl sulfoxide mixture and, thus, could not be determined by NMR. Solubility is no problem with the fusion approach.

Table III. Analysis of Polymethylphenylsiloxanes by Alkali Fusion Reaction Gas Chromatography and NMR

Sample	Methyl content, wt %: Alkali fusion[a]	Methyl content, wt %: NMR	Phenyl content, wt %: Alkali fusion[a]	Phenyl content, wt %: NMR
DC 510	35.9 ± 0.1	35.2 ± 2.2	9.96 ± 0.07	9.37 ± 1.16
GE SF-1153	35.8 ± 0.3	34.5 ± 0.8	6.99 ± 0.23	7.02 ± 0.18
GE SE-54[b]	34.5 ± 0.3	...	11.4 ± 0.05	...
GE SE-52	33.4 ± 0.4	...	11.7 ± 0.04	...
OV-3	32.2 ± 0.4	31.0 ± 0.8	17.2 ± 0.2	17.3 ± 1.5
DC 550	21.0 ± 0.2	21.0 ± 0.4	42.1 ± 0.3	41.1 ± 0.8
GE SF-1154	21.0 ± 0.2	20.8 ± 1.8	41.5 ± 0.2	41.3 ± 4.1
DC 556	27.4 ± 0.5	27.5 ± 0.3	28.6 ± 0.1	27.9 ± 0.9
DC 710	14.8 ± 0.1	15.4 ± 0.4	53.2 ± 0.4	54.3 ± 1.0
OV-17	13.8 ± 0.2	14.1 ± 0.7	55.4 ± 0.3	55.4 ± 2.4
DC 704	12.7 ± 0.1	12.6 ± 0.1	66.2 ± 0.5	66.0 ± 0.9
DC 806A	8.68 ± 0.06	...	47.4 ± 0.3	...
DC 840	8.40 ± 0.09	...	47.4 ± 0.3	...
OV-25	5.83 ± 0.09	6.30 ± 0.21	68.6 ± 0.3	70.0 ± 1.1
Polydiphenylsiloxane	0	...	80.7 ± 0.5	*c*

[a] The standard deviation is based upon five or more determinations. [b] Sample also contains a low percentage of vinyl groups. [c] The sample could have between 77.8 and 86.6% by weight phenyl dependent upon the molecular weight distribution.

Table IV. Analysis of Alkyl and Aryl Substituted Polysiloxanes by Alkali Fusion Reaction Gas Chromatography

Sample	Volatile alkali fusion products	Weight percent[a]	Percent theoretical recovery[b]
GE SF-1080	Methane	10.1 ± 0.1	100.8
	Hexane	24.7 ± 0.6	
	Cumene	37.7 ± 0.2	
GE SF-1091	Methane	9.96 ± 0.11	103.4
	Octane	66.0 ± 0.1	
GE SF-1147	Methane	11.0 ± 0.2	95.9[c]
	Decane	59.4 ± 0.9	
DC 203	Methane	7.77 ± 0.06	95.7[d]
	Cumene	13.3 ± 0.1	
	Dodecane	53.8 ± 1.8	
UC L-42	Methane	24.2 ± 0.1	99.8
	Ethylbenzene	33.3 ± 0.8	

[a] The standard deviation is based upon five or more determinations. [b] Refer to the text for the assumptions made in calculating this number. [c] Two small unknown peaks were present in the reaction gas chromatogram. [d] An unidentified peak was present in the reaction gas chromatogram.

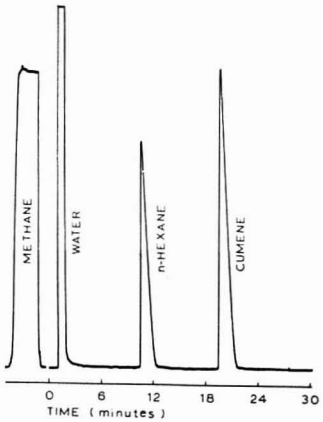

Figure 5. Gas chromatogram of the methane, *n*-hexane, and cumene produced from the alkali fusion of GE SF-1080

Alkyl and aryl groups other than methyl and phenyl may be present in silicones. Several such samples were obtained, but the identity of these substituents was not known. Thus, before a quantitative analysis could be performed, the volatile reaction products were trapped from the gas chromatographic column and their mass spectra obtained. The combined mass spectral and GC retention data permitted identification of these compounds. Figure 5 is the gas chromatogram of the three volatile fusion products produced from GE SF-1080.

The quantitative results obtained from these samples are compiled in Table IV. The appropriate aliphatic and aromatic hydrocarbons were used as standards. In the absence of a suitable check method, it was impossible to determine the accuracy of these values. The consistency of the results, however, can be determined by the simple mass balance recovery equation given below:

$$\text{Recovery} = \sum_{i=1}^{n} P_i + \frac{44.09}{2} \sum_{i=1}^{n} \frac{P_i}{F_i}$$

where P is the weight percent and F is the formula weight of each organic substituent, i. The first term in this equation represents the total weight percent contribution of all the pendant organic groups in the polymer as determined by the alkali fusion technique. The second term represents the corresponding siloxane content; 44.09 is the formula weight of the siloxane repeat unit and the factor 2 is based on the fact that, in fluid-type silicones, there is, on the average, 1 mol of siloxane for every 2 mol of substituent. If quantitative cleavage and recovery of each organic group is achieved, the sum of these weight percent values should approach 100%. Lower values will result if any step in the analysis is not quantitative, the substituents do not produce a volatile product, and/or the polymer is branched or cross-linked. Recovery numbers calculated from the equation are included in Table IV. GE SF-1080 and GE SF-1147 recoveries were expected to be a little low because of small amounts (<1%) of an antioxidant (Ethyl Corporation's Antioxidant 702) that is chemically bonded to the polymer. This particular antioxidant is a phenolic compound and produces the nonvolatile phenolate salt upon alkali fusion. The presence of impurity peaks in the chromatograms obtained from DC 203 and GE SF-1147 also account for the low values. The fact that these

Table V. Analysis of Polysiloxane Copolymers and Formulations

Copolymer	Volatile alkali fusion products	Weight percent: Alkali fusion	Weight percent: Check method
DC 470A	Methane	5.73 ± 0.12 (5)[a]	4.87[c]
DC 472	Methane	11.0 ± 0.3 (11)	11.0 ± 0.3[b]
			15.4[c]
DC 473	Methane	6.99 ± 0.08 (5)	...
Dexsil 300 GC	Methane	23.8 ± 0.4 (6)	24.7[c]
	m-Carborane	38.1 ± 0.7 (6)	39.0[c]
Formulation			
DC Stopcock grease	Methane	35.2 ± 0.2 (6)	...
DC High vacuum grease	Methane	35.5 ± 0.2 (6)	...
Ascolube (silicone) stopcock grease and joint seal	Methane	35.5 ± 0.1 (6)	...
Analabs high temperature red septum	Methane	21.7 ± 0.1 (2)	...
	Benzene	1.88 ± 0.01 (2)	
Analabs RS series high temperature white septum	Methane	25.7 ± 0.3 (2)	...
	Benzene	1.76 ± 0.04 (2)	...
Applied Science high temperature blue septum	Methane	25.8 ± 0.2 (2)	...
	Benzene	8.13 ± 0.03 (2)	...

[a] The number in parentheses is the number of determinations. [b] NMR value using benzene as the internal standard. [c] Approximate values calculated from suppliers' information bulletin.

Table VI. Analysis of Other Organofunctional Groups in Polysiloxanes by Alkali Fusion Reaction Gas Chromatography

Sample	Volatile alkali fusion product determined	Weight percent[a]
DC Silastic 430	Ethylene	0.117 ± 0.005
GE SE-54	Ethylene	0.146 ± 0.010
GE SE-33	Ethylene	0.171 ± 0.010
GE SE-31	Ethylene	0.179 ± 0.009
Versilube F-50[b]	Methane	34.6 ± 0.7

[a] The standard deviation is based upon five or more determinations. [b] No chlorobenzene peak was noted in the gas chromatogram.

recovery values were, in all cases, within 5% of the theoretical model, strongly suggests that a wide variety of alkyl and aryl groups can be accurately determined.

Polydimethylsiloxanes copolymerized with polyoxyethylene, polyethylene, and/or polyoxypropylene were analyzed for methyl content (Table V). Although polyoxyalkalenes react with the reagent, all of their volatile reaction products were retained by the trap and, thus, did not interfere with the methyl determination. The Dexsil GC phases investigated are copolymers in which the siloxane blocks are joined through *m*-carborane linkages. Quite unexpectedly, the *m*-carborane produced in the fusion reaction was sufficiently volatile to be chromatographed and determined (Table V).

Several formulations containing silicones were subjected to alkali fusion. The fact that no extraneous peaks were observed in the chromatograms indicates that the fillers were nonvolatile and did not react or decompose to form volatile products. The qualitative and quantitative results are included in Table V. The three grease samples produced essentially the same weight percent methane, whereas the gas chromatographic septa contained different ratios of methyl and phenyl groups. The other ingredients of the formulations do not appear to hinder the fusion reaction; thus, a preliminary separation of the polysiloxane is unnecessary.

Vinyl groups (0.1–2.0%) are incorporated into polysiloxanes to facilitate cross-linking (*40*). Reaction gas chromatography is the most sensitive and selective method presently available for their determination (*25–29*). Published procedures are included in Table I. Although satisfactory results were reported, our reagent and apparatus offer some additional advantages. The fusion reaction with potassium hydroxide proceeds more rapidly under less drastic conditions than the methods employing acidic reagents (*24–26*). The continuous flow design eliminates secondary reactions, such as the conversion of ethylene to ethane, which are a problem with static systems (*27*). In addition, since all of the volatile product, rather than a small fraction, is chromatographed, greater sensitivity is possible. Table VI lists the vinyl contents we found using our apparatus. The standard deviation at the 0.1 to 0.2 wt % level was between 4 and 7% relative. Ethylene gas was used to prepare the calibration curves.

Chlorination of phenyl groups in polymethylphenylsiloxanes increases their lubricating action (*40*). Alkali fusion of Versilube F-50, a polymer containing chlorophenyl substituents, gave a reaction gas chromatogram similar to that of Figure 3; no chlorinated benzene products were observed. Apparently the reaction conditions were drastic enough to cause replacement of the chloro group; the aromatic material remains in the boat as the nonvolatile potassium phenolate salt (*41*, *42*).

CONCLUSIONS

Although this study was directed at the determination of alkyl and aryl groups in polysiloxanes, it should also be applicable to alkoxy groups. Hanson and Smith (*29*) have demonstrated quantitative cleavage and recovery of the corresponding alcohols using a similar potassium hydroxide reagent. The poor precision (±20% relative) and accuracy (–10% relative) appear to be due to their inefficient water trap. The proven efficiency of our liquid nitrogen bath for retaining alcohols (*30*) should improve the accuracy and precision significantly.

ACKNOWLEDGMENT

The authors thank the following persons for supplying silicone samples: A. M. Quinn of the Dow Corning Corporation, N. G. Holdstock of the General Electric Company, and J. E. Pikula of the Union Carbide Corporation.

LITERATURE CITED

(1) A. L. Smith, Ed., "Analysis of Silicons", John Wiley & Sons, New York, N.Y., 1974.
(2) T. Kubota and T. Takamura, *Bull. Chem. Soc. Jpn.*, **33**, 70–73 (1960).
(3) I. K. O'Neill, M. A. Pringuer, and H. J. Prosser, *J. Pharm. Pharmacol.*, **27**, 222–225 (1975).
(4) K. Kuratani and M. Nakamura, *J. Chem. Soc. Jpn., Pure Chem. Sect.*, **73**, 576–578 (1952).
(5) W. Fishl and I. G. Young, *Appl. Spectrosc.*, **10**, 213–215 (1956).
(6) G. D. Grant and A. L. Smith, *Anal. Chem.*, **30**, 1016 (1958).
(7) T. Uriu, S. Tanaka, and T. Wada, *J. Chem. Soc. Jpn., Ind. Chem. Sect.*, **62**, 1577–1580 (1959).
(8) T. Uriu, S. Tanaka, and H. Yamamoto, *J. Chem. Soc. Jpn., Ind. Chem. Sect.*, **62**, 1581–1583 (1959).
(9) J. H. Lady, G. M. Bower, R. E. Adams, and F. P. Byrne, *Anal. Chem*, **31**, 1100 (1959).
(10) E. R. Shull, *Anal. Chem.*, **32**, 1627 (1960).
(11) H. Yamamoto, *J. Chem. Soc. Jpn., Ind. Chem. Sect.*, **64**, 1464–1466 (1961); *Chem. Abstr.*, **57**, 2854f (1962).
(12) A. Snowacka-Wokroj and T. Biernacka, *Chem. Anal. (Warsaw)*, **9**, 303–314 (1964).
(13) T. Biernacka, and A. Snowacka-Wokroj, *Chem. Anal. (Warsaw)*, **10**, 1233–1245 (1965).
(14) A. P. Kreshkov, Y. Y. Mikhailenko and I. P. Smirenkina, *Zh. Fiz. Khim.*, **32**, 834–837 (1958).
(15) T. Uriu and T. Hakamada, *J. Chem. Soc. Jpn., Ind. Chem. Sect.*, **62** 1421–1428 (1959).
(16) V. S. Fikhtengol'ts and R. V. Zolotareva, *Chem. Abstr.*, **57**, 13943c (1962).
(17) L. A. Efremova and K. K. Popov, *Zavod. Lab.*, **29**, 708 (1963); *Chem. Abstr.*, **59** 8124f (1963).
(18) R. D. Parker, Dow Corning Corporation, Barry, Wales, unpublished procedure.
(19) G. Fritz and H. Burdt, *Z. Anorg. Allg. Chem.*, **317**, 35–40 (1962); *Chem. Abstr.*, **57**, 1443g (1962).
(20) V. M. Krasikova, A. N. Kaganova, and V. D. Lobkov, *J. Anal. Chem. USSR (Engl. Transl.)*, **26**, 1458–1461 (1971).
(21) M. G. Voronkov and V. T. Shemyatenkova, *Bull. Acad. Sci. USSR, Div. Chem. Sci.*, **1961**, 178; *Chem. Abstr.*, **55**, 16285b (1961).
(22) J. Franc and K. Placek, *Collect. Czech. Chem. Commun.*, **38**, 513–515 (1973).
(23) J. Franc, *Chem. Abstr.*, **82**, 67923q (1975).
(24) A. P. Kreshkov, V. T. Shemyatenkova, S. V. Syavtsillo, and N. A. Palamarchuk, *J. Anal. Chem. USSR (Engl. Transl.)*, **15**, 727–730 (1960).
(25) G. W. Heylmun, R. L. Bujalski, and H. B. Bradley, *J. Gas* Chromatogr., **2**, 300–301 (1964).
(26) V. M. Krasikova and A. N. Kaganova, *J. Anal. Chem. USSR (Engl. Transl.)*, **25**, 1212–1215 (1970).
(27) E. R. Bissell and D. B. Fields, *J. Chromatogr. Sci.*, **10**, 164–167 (1972).
(28) J. Franc and K. Placek, *Mikrochim. Acta, II*, (1), 31–36 (1975).
(29) C. L. Hanson and R. C. Smith, *Anal. Chem.*, **44**, 1571–1574 (1972).
(30) S. P. Frankoski and S. Siggia, *Anal. Chem.*, **44**, 507–511 (1972).
(31) D. D. Schlueter, Ph.D. Dissertation, University of Massachusetts, Amherst, Mass., 1976.
(32) C. A. Burkhard and F. J. Norton, *Anal Chem.*, **21**, 304 (1949).
(33) H. Gilman and F. J. Marshall, *J. Am. Chem. Soc.*, **71**, 2066–2069 (1949).
(34) V. Chvalovsky and V. Bazant, *Collect. Czech. Chem. Commun.*, **16**, 580–589 (1951).
(35) J. Franc and J. Dvoracek, *J. Chromatogr.*, **14**, 340–347 (1964).
(36) W. H. Grieve and K. F. Sporek, Winter Meeting, American Chemical Society, Phoenix, Ariz., January 17–21, 1966, paper No. 43.
(37) J. Franc and J. Pour, *Anal. Chim. Acta*, **48**, 129–137 (1969).
(38) J. Franc and K. Placek, *J. Chromatogr.*, **48**, 295–309 (1970).
(39) J. Franc and K. Placek, *J. Chromatogr.*, **67**, 37–48 (1972).
(40) W. Noll, Ed., "Chemistry and Technology of Silicones", Academic Press, New York, N.Y., 1968.
(41) S. J. Lederman and N. Poffenberger, "Encyclopedia of Chemical Technology", Kirk and Othmer, Ed., Interscience, New York, N.Y., Vol. 15, 2nd ed., 1968, p 153.
(42) H. Heaney, *Chem. Rev.*, **62**, 81 (1962).

RECEIVED for review February 11, 1977. Accepted September 19, 1977. This work was supported by the National Science Foundation, Grant Number GP-37493x. Preliminary results of this study were presented at the 168th American Chemical Society Meeting, Atlantic City, N.J., September 13, 1974.

Determination of Imides, Aromatic Polyimides, Polyamides, and Poly(Amide–Imides) by Alkali Fusion Reaction Gas Chromatography

David D. Schlueter[1] and Sidney Siggia*

Department of Chemistry, University of Massachusetts, Amherst, Massachusetts 01003

The technique of alkali fusion reaction gas chromatography has been applied to the analysis of imide monomers and aromatic polyimides, polyamides, and poly(amide–imides). Samples are hydrolyzed with a molten potassium hydroxide reagent at elevated temperatures in a flowing, inert atmosphere. Volatile reaction products are concentrated in a cold trap before separation by gas chromatography. The identity of the amine and/or diamine products aids in the characterization of the monomer or polymer; the amount of each compound generated is used as the basis for quantitative analysis. The average percent relative standard deviation of the method is ±1.0%.

The imide functional group

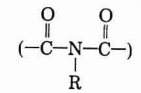

occurs in acylated amides and ureas, in cyclic secondary amides of dicarboxylic acids, and in several heterocyclic systems. The hydrogen atom in unsubstituted imides is weakly acidic and can be titrated with base. Conductometric titrations have been performed in water (*1*) and aqueous ammonia solutions (*2*) using lithium hydroxide as the titrant. Nonaqueous titrations, using sodium or potassium methoxide, have been performed in benzene–methanol (*3*), *n*-butylamine (*3*), ethylenediamine (*4, 5*), and dimethylformamide (*6, 7*); end points were detected visually or potentiometrically. The more weakly acidic imides have also been successfully determined by potentiometric (*8–11*), derivative potentiometric (*12*), derivative spectrophotometric (*12*), and coulometric (*13*) titrations using quaternary ammonium hydroxides as titrants. Other titration methods are based on the reactivity of the imide hydrogen with various reagents. Diacetamide, for example, was titrated at 94 °C in liquid acetamide using sodium acetamide as the titrant (*14*). Succinimide can be titrated with hypobromite; the excess hypobromite present after the end point is determined colorimetrically at 350 nm (*15*). Indirect procedures for the determination of saccharin (*16*) and sodium saccharin (*17*) are based on the formation of their insoluble silver and mercury salts and titration of the excess Ag(I) and Hg(II) with thiocyanate.

Unsubstituted imides, like other compounds containing active hydrogen atoms, have been determined by reacting the sample with methyl magnesium iodide (*18*) or lithium aluminum hydride (*19*) and measuring the methane or hydrogen generated. Siggia and Stahl (*20*) quantitatively reduced amides with lithium aluminum hydride and, after steam distillation, titrated the amine with standardized acid. Although succinimide was the only imide analyzed by this procedure, it should be applicable to others that produce volatile amines upon reduction. Phthalimide has been determined polarographically by electrochemical reduction (*21, 22*).

Several colorimetric methods (*23–27*) are based upon the reaction of imides with hydroxylamine and treatment of the hydroxamic acid with ferric chloride to produce the highly colored ferric hydroxamate. Aryl and substituted aryl glutarimides react with formaldehyde and concentrated sulfuric acid to form compounds that have been determined by fluorescence spectrophotometry (*28*). Many imides can be separated and determined by high performance liquid chromatography (*29*), thin-layer chromatography (*30, 31*), or gas chromatography (*31, 32*).

Polyimides are a class of thermally stable copolymers usually prepared from dianhydrides and diamines or diisocyanates; they are used in the formulation of films, coatings, and binders and in the fabrication of parts for high temperature applications. Aromatic polyamides and poly(amide–imides) also possess superior thermal properties. Surprisingly few methods have been reported for the analysis of these polymers. One of the main reasons for this is their poor solubility in most common solvents.

Carboxy end groups in poly-*m*-phenyleneisophthalamide were titrated potentiometrically in dimethylformamide using a nonaqueous potassium hydroxide solution (*33*). Two indirect titration procedures have been described for the determination of amino end groups in aromatic polyamides. One method involves the reaction of the amine with salicylaldehyde to form the Schiff base. After precipitation of the polymer, the excess, unreacted aldehyde is titrated with potassium hydroxide (*33*). Amino groups have also been acetylated with acetic anhydride in dimethylacetamide. Diethylamine was added, and the excess amine was titrated potentiometrically (*34*). The sequence distribution of an aromatic polyamide terpolymer prepared under various reaction conditions was determined by nuclear magnetic resonance spectrometry (*35*). Infrared spectroscopy (*36, 37*) and mass spectrometry (*38*) have been used to estimate the degree of conversion of polyimides, i.e., the extent of polyamic acid ring closure.

Gomoryova (*39*) hydrolyzed amide and imide linkages with hydrochloric acid and identified the diamines using paper or thin-layer chromatography. The diamine portion of polyamides has also been determined by fusing the sample with an alkali reagent and separating the products by thin-layer chromatography (*40*). Acidification of the melt allowed the separation and identification of the diacid components. Polyimides have been decomposed with hydrazine hydrate and the diamine products identified by gas chromatography (*41*). Polyamides and poly(amide–imides) required a prehydrolysis step. The di-, tri-, or tetracarboxylic acid segments were determined by reaction of the polymer with a 10% aqueous solution of tetramethylammonium hydroxide, pyrolysis of the resulting salt, and identification of the volatile methyl ester by gas chromatography (*41*). Kalinina and Doroshina (*42*) have reviewed the qualitative and quantitative

[1] Present address, Biochemicals Department, E. I. du Pont de Nemours & Co., Inc., Wilmington, Del. 19898.

methods for the analysis of polyamides and polyimides.

This paper reports the application of alkali fusion reaction gas chromatography to the qualitative and quantitative analysis of imide monomers and aromatic polyimides, poly(amide–imides), and polyamides. In this procedure the sample is fused with a potassium hydroxide reagent at elevated temperatures. The amine or diamine formed in the reaction is trapped and then analyzed by gas chromatography. Identification of the volatile product(s) provides valuable compositional information about the sample; the amount of each compound produced serves as the basis for quantitative analysis. The acid portion of the polymer remains in the reaction mixture as the nonvolatile potassium salt.

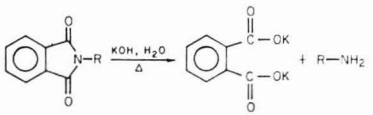

The application of this technique to nylon polymers made from aliphatic difunctional monomers has been previously reported (*43*).

EXPERIMENTAL

Fusion Reagent. The preparation and storage of the alkali fusion reagent have been described in detail elsewhere (*44, 45*).

Samples. *N*-Benzylsuccinimide was synthesized from succinimide, benzyl chloride, and potassium hydroxide according to the procedure described by Werner (*46*). The other imide monomers were purchased from chemical supply houses. When necessary, they were purified by either recrystallization or vacuum sublimation. The polymer samples were supplied by the Plastics Department of E. I. du Pont de Nemours & Co., Inc., the Amoco Chemicals Corporation, and the Polymer Science Department at the University of Massachusetts. Molded polymers were ground into a powder using a file. Metal chips were removed from the sample with a magnet.

Standards. Anhydrous ammonia (Matheson Gas Products) was used as received. Benzylamine hydrochloride was prepared from freshly distilled benzylamine (Eastman No. 579), washed with acetone and dried under vacuum. *m*-Phenylenediamine (Aldrich No. P2395-4), 2,4-toluenediamine (Eastman No. P4580), and 4,4′-methylenedianiline (Aldrich No. 13,245-4) were purified by vacuum sublimation and stored in a light-tight vacuum desiccator.

Apparatus. Detailed descriptions of the fusion reaction gas chromatographic apparatus have been given elsewhere (*45, 47*). Matched 6-foot by $^1/_4$-inch o.d. stainless steel columns packed with 60/80 mesh Chromosorb 103 (Johns-Manville) were used to separate the amine reaction products. Diamines were chromatographed on 4-foot by $^1/_8$-inch o.d. stainless steel columns packed with 10% FFAP on 60/70 mesh Anakrom ABS. Peak areas were measured with a Vidar AutoLab 6300 Digital Integrator (Spectra-Physics). Chromatograms were displayed on a Varian Model G-2500 Recorder. A Du Pont Model 950 Thermogravimetric Analyzer was used to determine the water content and thermal stability of the polymer samples. Elemental nitrogen determinations were made on a Perkin-Elmer Model 240 Elemental Analyzer.

Procedure. A generalized description of the procedure can be found in references 45 and 47.

Calibration. Calibration curves were prepared daily for each compound determined. Anhydrous ammonia was injected with a calibrated 1000-μL gas-tight syringe through the septum inlet of the reaction tube. Ambient temperature and pressure corrections were made to determine the actual amount of gas injected. Benzylamine was generated from reaction of the hydrochloride salt with potassium hydroxide. The diamine standards were weighed into boats, covered with caustic reagent, and volatilized by moving the boat into the heated furnace. In each case, the standard compounds were trapped and chromatographed in the same manner as the volatile reaction products. The best straight line calibration curves were determined by a least-squares regression curve-fitting computer program.

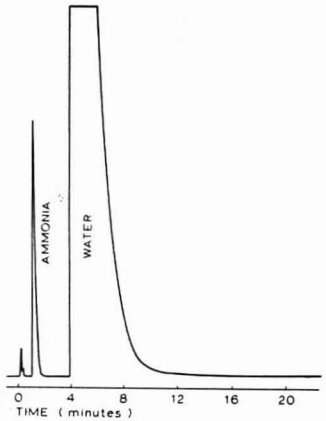

Figure 1. Alkali fusion reaction gas chromatogram produced from sodium saccharin. The column temperature was programmed from 80 to 250 °C at 12°/min

Table I. Analysis of Monomeric Imides by Alkali Fusion Reaction Gas Chromatography[a]

Compound	Reaction product determined	Mol % theoretical recovery	Rel std dev[b]
Diacetamide	Ammonia	98.4	1.0
Succinimide	Ammonia	99.0	1.5
		99.5[c]	0.5
Phthalimide	Ammonia	99.4	1.0
		99.6	1.1
1,8-Naphthalimide	Ammonia	None detected	
Saccharin	Ammonia	98.0[d]	0.9
		99.6[e]	1.1
Sodium saccharin	Ammonia	99.3	1.0
Pyromellitic diimide	Ammonia	98.1	0.9
N-Benzylsuccinimide	Benzylamine	100.9	1.0

[a] Except as noted, samples were reacted isothermally at 250 °C for 30 min. [b] Based on five or more determinations. [c] Sample was heated from 38 to 220 °C over a period of 20 min. [d] Sample was purified by recrystallization from water. [e] Sample was purified by vacuum sublimation.

RESULTS AND DISCUSSION

Monomer Analysis. The alkali fusion hydrolysis of most imide monomers proceeded very smoothly at 250 °C; the reaction mass showed no signs of sample decomposition. Chromosorb 103, a cross-linked polystyrene porous polymer, proved to be a useful chromatographic support for separating the amine products. The low back pressure and ability of the column to handle the comparatively large amounts of water made it compatible with the fusion unit. Reaction gas chromatograms of the monomers generally contained two peaks: water, liberated from the reagent, and the primary amine reaction product. Figure 1 is the reaction gas chromatogram obtained from sodium saccharin. The two small peaks at the beginning of the chromatogram appeared when silanized glass wool was used as the trap packing; when quartz wool was used, these deflections disappeared.

Table I summarizes the results obtained from several representative compounds. The theoretical recovery values

Table II. Structure, Water Content, and Decomposition Temperature of the Polymers Studied

Designation	Structure of repeat unit	Wt % water	Decomposition temperature, °C
PI-1	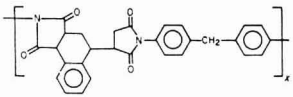	6.5	385
PI-2	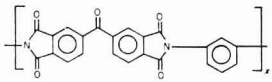	2.2	410
PI-3	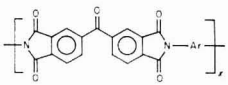 Ar = and 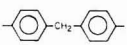	3.4	410
PI-4	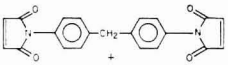 + 4,4'-Methylenedianiline	0.6	310
PA-1	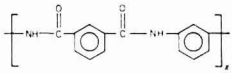	5.8	315
PA-2	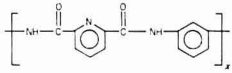	9.7	330
PAI-1	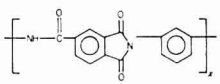	6.2	340
PAI-2	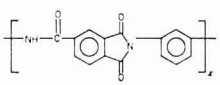	12.6	395
PAI-3	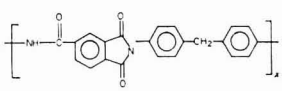	8.9	340

were calculated on the assumption that one molecule of amine is produced from each imide group in the compound and one molecule of diamine is produced from every two imide groups. In most cases, quantitative hydrolysis and recovery of the amine were observed at 250 °C. The average percent relative standard deviation was 1.0%. 1,8-Naphthylimide was especially resistant to hydrolysis; no ammonia was produced at 250 °C. At higher temperatures, some reaction occurred.

Reaction conditions (30 minutes at)	Percent of theoretical ammonia recovered
300 °C.	2
390 °C.	36
450 °C.	57

N-Benzylsuccinimide and sample PI-4 (Table II) were the only two substituted imides studied. The fact that no ammonia was produced from *N*-benzylsuccinimide proves that unreacted succinimide was efficiently removed in the recrystallization procedure. Sample PI-4, as indicated in Table II, is a mixture of a substituted imide and unreacted diamine. The results of its analysis are included with those of the polymers.

The imide functional group also occurs in many heterocyclic systems such as pyrimidines, purines, uracils, hydantoins, and barbituric acids. Alkali fusion of these samples was not investigated in great detail. Uracil was the only compound studied quantitatively. When it was reacted at 400 °C for 25

Table III. Analysis of Polyimides, Polyamides, and Poly(amide-imides) by Alkali Fusion Reaction Gas Chromatography

Sample	Diamine produced	Mol % of Theoretical[a] ± RSD[b] 5 min at 380 °C	30 min from 100 to 390 °C
PI-1	4,4′-Methylenedianiline	98.3 ± 0.8	97.5 ± 0.9
PI-2	*m*-Phenylenediamine	89.1 ± 0.7	
		91.2 ± 0.9	91.0 ± 0.8
		91.6 ± 1.3	91.0 ± 0.7
PI-3	2,4-Toluenediamine	73.1 ± 0.2 } 97.8 ± 0.5	73.2 ± 1.0 } 99.1 ± 1.2
	4,4′-Methylenedianiline	24.8 ± 0.3 }	25.9 ± 0.2 }
PA-1	*m*-Phenylenediamine	100.7 ± 0.6	97.0 ± 1.7
			97.7 ± 1.7
			97.9 ± 1.0
			99.6 ± 2.6
PA-2	*m*-Phenylenediamine	95.9 ± 0.6	92.9 ± 1.0
		96.4 ± 1.5	93.3 ± 0.6
PAI-1	*m*-Phenylenediamine	93.5 ± 0.9	93.1 ± 0.7
			95.3 ± 0.5
PAI-2	*m*-Phenylenediamine	93.5 ± 1.1	97.4 ± 0.9
		94.1 ± 0.6	
		95.1 ± 1.2	
PAI-3	4,4′-Methylenedianiline	98.0 ± 1.1	98.8 ± 1.1

[a] These recovery values are based on the structures shown in Table II, which assume that one mole of diamine is produced for each mole of repeat unit. [b] The relative standard deviation is based on five or more determinations.

Table IV. Comparison of the Nitrogen Content Determined by Alkali Fusion Reaction Gas Chromatography and Elemental Analysis

Sample	Weight percent nitrogen in the polymer ± standard deviation: Alkali fusion reaction gas chromatography — Diamine contribution	Ammonia contribution	Total	Elemental analysis
PI-1	5.96 ± 0.05	0.16 ± 0.01	6.12 ± 0.06	5.90[a]
				5.87[b]; 5.95 ± 0.11[c]
PI-2	6.44 ± 0.06	0.99 ± 0.08	7.43 ± 0.14	7.27[a]; 7.30[b]
PI-3	4.85 ± 0.01	0.44 ± 0.07	6.70 ± 0.09	6.78[a]
	1.41 ± 0.01			6.79[b]; 6.90 ± 0.11[c]
PI-4	8.70 ± 0.15	0.13 ± 0.02	8.83 ± 0.17	9.00 ± 0.06[c]
PA-1	11.84 ± 0.07	0.75 ± 0.16	12.59 ± 0.23	12.33[b]; 12.65 ± 0.06[c]
PA-2	11.26 ± 0.10	1.40 ± 0.04	12.66 ± 0.14	-
PAI-1	9.91 ± 0.09	1.05 ± 0.08	10.96 ± 0.17	10.83[a]; 10.65[b]
PAI-2	9.99 ± 0.10	0.60 ± 0.04	10.59 ± 0.14	10.80[a]
				10.55[b]; 10.71 ± 0.03[c]
PAI-3	7.75 ± 0.09	0.23 ± 0.04	7.98 ± 0.13	8.23 ± 0.03[c]

[a] Dumas combustion analysis on a Perkin-Elmer Model 240 Elemental Analyzer (Olin Research Center, New Haven, Conn. 06504). [b] Micro-Kjeldahl analysis (Olin Research Center). [c] Macro-Kjeldahl analysis (West Experimental Station, Feed, Seed, and Fertilizer Division, University of Massachusetts, Amherst, Mass. 01002).

min, theoretical amounts of ammonia (98.5 ± 3.0%) were produced; at lower temperatures, incomplete recovery was obtained.

Polymer Analysis. Table II summarizes the chemical structures and sample designations of the polymers studied. The weight percent of adsorbed water and the decomposition temperature, both determined by thermogravimetric analysis, are also included. The water content was needed to calculate the dry weight of polymer in each sample. It was not possible to simply dry and weigh the polymers, because they tended to readsorb moisture from the atmosphere too rapidly. Table III summarizes the diamine recoveries obtained with isothermal (5 min at 380 °C) and programmed (100 to 390 °C over 30 min) reaction temperatures. These numbers represent the mole percent of theoretical diamine based on the dry weight of sample and the idealized linear polymer repeat units depicted in Table II. Recoveries were, in all cases, between 90 and 101% of theory. The amount of diamine recovered from a polymer reacted isothermally, was within ±3% of the amount produced by the programmed temperature approach. Average percent relative standard deviations were similar in both cases (±0.9% vs. 1.1%).

Table V. Analysis of Polymer Mixtures by Alkali Fusion Reaction Gas Chromatography

Polymer mixture	Micromoles of *m*-phenylenediamine: Taken[a]	Found	Recovery, %
PI-2	2.24 } 11.50	11.36	98.8
PAI-2	9.26 }		
PA-1	7.23 } 14.66	14.71	100.3
PA-2	7.43 }		
PAI-1	4.99 } 12.66	12.58	99.4
PI-2	7.67 }		
PAI-1	5.28 } 12.37	12.48	100.9
PAI-2	7.09 }		
PA-1	5.51		
PAI-2	5.81 } 14.21	14.33	100.8
PI-2	2.89		
PA-2	8.79		
PAI-1	3.25 } 14.80	14.98	101.2
PA-1	2.76		

[a] These values were calculated from the weight of polymer taken and were corrected for the weight of adsorbed water (Table II) and the average experimental recovery (Table III).

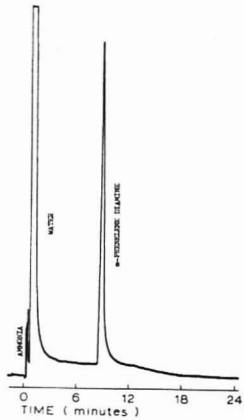

Figure 2. Alkali fusion reaction gas chromatogram produced from poly(amide–imide) PAI-2. The column temperature was programmed from 100 to 250 °C at 12°/min

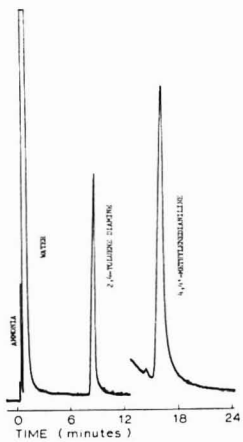

Figure 3. Alkali fusion reaction gas chromatogram produced from the polyimide terpolymer PI-3. The column temperature was programmed from 100 to 250 °C at 12°/min

Figure 2 is the reaction gas chromatogram obtained from poly(amide–imide), PAI-2. Only one diamine was produced. The chromatogram in Figure 3, obtained from the fusion reaction of the polyimide terpolymer PI-3, contains peaks for each diamine. The quantitative analysis of both products revealed that the weight ratio of 2,4-toluenediamine to 4,4′-methylenedianiline in the polymer was 2 to 1.

In an attempt to correlate the alkali fusion recoveries (expressed as weight percent nitrogen) with elemental nitrogen analyses of the polymers, it was noted that the elemental values were higher. Analysis of the fusion residue indicated that no detectable amounts of nitrogen were present. This led to the discovery that ammonia was also produced from the samples. When the nitrogen contribution from ammonia was added to that of the diamine, the total was in good agreement with the elemental value. These results are summarized in Table IV.

Polymer mixtures, as well as pure materials, can be analyzed by alkali fusion reaction gas chromatography. Table V lists the results obtained from the analysis of mixtures of polymers. The amount of *m*-phenylenediamine produced was, in all cases, within 1.2% relative of the theoretical value.

ACKNOWLEDGMENT

The authors thank J. Mitchell, Jr., and E. R. Lovejoy (E. I. du Pont de Nemours & Co., Inc.), O. Vogl and R. A. Gaudiana (University of Massachusetts Polymer Science Department), and E. Vitands (Amoco Chemicals Corporation) for supplying the polymer samples. We are also grateful to P. Korpita and J. Lockman (University of Massachusetts West Experimental Station) and R. C. Rittner (Olin Research Center) for performing the elemental analyses.

LITERATURE CITED

(1) G. R. Jamieson, *J. Appl. Chem.*, **9**, 209 (1959).
(2) F. Gaslini and L. Z. Nahum, *Anal. Chem.*, **31**, 989 (1959).
(3) J. S. Fritz and N. M. Lisicki, *Anal. Chem.*, **23**, 589 (1951).
(4) J. S. Fritz, *Anal. Chem.*, **24**, 674 (1952).
(5) E. F. Hillenbrand, Jr., and C. A. Pentz, "Organic Analysis", Vol. 3, J. Mitchell, Jr., I. M. Kolthoff, E. S. Proskauer, and A. Weissberger, Ed., Interscience, New York, N.Y., 1956, p 193.
(6) M. K. Maurmeyer, M. Margosis, and T. S. Ma, *Mikrochim. Acta*, **1959**, 177.
(7) J. S. Fritz, "Acid-Base Titrations in Nonaqueous Solvents", G. Frederick Smith Chemical Co., Columbus, Ohio, 1952.
(8) R. H. Cundiff and P. C. Markunas, *Anal. Chem.*, **28**, 792 (1956).
(9) J. S. Fritz and S. S. Yamamura, *Anal. Chem.*, **29**, 1079 (1957).
(10) B. H. Beggs and R. D. Spencer, *Anal. Chem.*, **34**, 1590 (1962).
(11) L. W. Marple and J. S. Fritz, *Anal. Chem.*, **35**, 1431 (1963).
(12) H. V. Malmstadt and D. A. Vassallo, *Anal. Chem.*, **31**, 862 (1959).
(13) J. S. Fritz and F. E. Gainer, *Talanta*, **15**, 939 (1968).
(14) G. Jander and G. Winkler, *J. Inorg. Nucl. Chem.*, **9**, 32 (1959).
(15) W. R. Post and C. A. Reynolds, *Anal. Chem.*, **36**, 781 (1964).
(16) P. M. Parikh and S. P. Mukherji, *Analyst (London)*, **85**, 25 (1960).
(17) M. J. Schulte, *Pharm. Weekbl.*, **77**, 1281 (1940); *Chem. Abstr.*, **36**, 7235[9] (1942).
(18) M. Jurecek, *Chem. Listy*, **40**, 239 (1946); *Chem. Abstr.*, **44**, 9220f (1950).
(19) F. A. Hochstein, *J. Am. Chem. Soc.*, **71**, 305 (1949).
(20) S. Siggia and C. R. Stahl, *Anal. Chem.*, **27**, 550 (1955).
(21) E. S. Levin and Z. I. Fodiman, *Chem. Prum.*, **13**, 18 (1963); *Chem. Abstr.*, **58**, 2850e (1963).
(22) V. A. Devyatnin and I. A. Solunina, *Zavod. Lab.*, **32**, (1966); *Chem. Abstr.*, **80**, 43535h (1967).
(23) J. B. Polya and P. L. Tardew, *Zavod. Lab.*, **23**, 1036 (1951).
(24) F. Bergmann, *Anal. Chem.*, **24**, 1367 (1952).
(25) H. Sheppard, B. S. D'Asaro, and A. J. Plummer, *J. Am. Pharm. Assoc., Sci. Ed.*, **45**, 681 (1956).
(26) A. A. Forist and S. Theal, *Anal. Chem.*, **31**, 1042 (1959).
(27) V. Fishman-Goldenberg and P. E. Spoerri, *Anal. Chem.*, **31**, 1735 (1959).
(28) R. P. Haycock, P. B. Sheth, and W. J. Mader, *J. Am. Pharm. Assoc., Sci. Ed.*, **49**, 673 (1960).
(29) D. D. Schlueter, E. I. du Pont de Nemours & Co., Inc., Wilmington, Del., unpublished results.
(30) S. D. Killilea and P. O'Carra, *J. Chromatogr.*, **54**, 284 (1971).
(31) J. H. Pomerantz and R. Ross, *J. Assoc. Off. Agric. Chem.*, **51**, 1058 (1968).
(32) J. Hrivnak, Z. Stota, and J. Kalamar, *J. Chromatogr.*, **29**, 224 (1967); *Chem. Abstr.*, **80**, 96645w (1967).
(33) A. P. Kreshkov, L. N. Shvetsova, and E. A. Emelin, *Sov. Plast. (Engl. Transl.)*, **1968** (10), 53; *Chem. Abstr.*, **70**, 20345q (1969).
(34) E. A. Emelin, V. M. Savinov, and L. B. Sokolov, *J. Anal. Chem. USSR (Engl. Transl.)*, **28**, 1188 (1973); *Chem. Abstr.*, **79**, 146956u (1973).
(35) P. A. Curnuck and M. E. B. Jones, *Br. Polym. J.*, **5**, 21 (1973); *Chem. Abstr.*, **79**, 92629u (1973).
(36) R. J. McGowan, *Anal. Chem.*, **41**, 2074 (1969); **42**, 942 (1970).
(37) N. P. Kulikova, M. V. Shablygin, and L. E. Utevskii, *Khim. Volokna*, **1973** (3), 24; *Chem. Abstr.*, **79**, 92637v (1973).
(38) A. S. Teleshova, E. N. Teleshov, and A. N. Pravednikov, *Vysokomol. Soedin., Ser. A.* **13**, 2309 (1971); *Chem. Abstr.*, **76**, 46644k (1972).
(39) A. Gomoryova, *Chem. Abstr.*, **83**, 59692u (1975).
(40) E. Stahl and L. S. Oey, *Kunststoffe*, **64**, 657 (1974); *Chem. Abstr.*, **82**, 112514v (1975).
(41) O. Mlejnek and L. Cveckova, *J. Chromatogr.*, **94**, 135 (1974).
(42) L. S. Kalinina and L. I. Doroshina, *Chem. Abstr.*, **79**, 54100g (1973).
(43) S. P. Frankoski and S. Siggia, *Anal. Chem.*, **44**, 2078 (1972).
(44) S. P. Frankoski and S. Siggia, *Anal. Chem.*, **44**, 507 (1972).
(45) D. D. Schlueter, Ph.D. Dissertation, University of Massachusetts, Amherst, Mass., 1976.
(46) E. A. Werner, *J. Chem. Soc.*, **55**, 627 (1889).
(47) D. D. Schlueter and S. Siggia, *Anal. Chem.*, **49**, preceding paper in this issue.

RECEIVED for review February 11, 1977. Accepted September 19, 1977. This work was supported by National Science Foundation Grants GP-28054 and GP-37493X. Results of this study were presented at the 168th National Meeting, American Chemical Society, in Atlantic City, N.J., September 13, 1974.

Determination of Metapramine in Plasma by Gas Chromatography with Nitrogen-Selective and Electron-Capture Detection

Alain R. Viala,* Jean-Paul Cano, and Alain G. Durand

Laboratoire de Toxicologie Générale et Biotoxicologie, Faculté de Pharmacie, 27 Boulevard Jean Moulin, 13005 Marseille, France

Theo Erlenmaier

Hewlett-Packard GmbH, Böblingen, West Germany

Roger M. Garreau

Hewlett-Packard France, Lyon, France

Metapramine is determined in plasma by gas chromatography with desipramine as an internal standard, a nitrogen–phosphorus selective detector (N-P D) for the detection of the underivatized compounds and an electron capture detector (ECD) for the *N*-heptafluorobutyric derivatives. The detection limits are respectively 15 ng/mL and 35 ng/mL plasma and the quantitative repeatabilities acceptable (relative standard deviation 3.85% and 6.64%). The N-P D method is the more rapid, the more sensitive, and the more reproducible. However, the ECD method is the more selective with regard to the possible metabolites of metapramine. The two methods are complementary and may be used for pharmacokinetic investigations as well as for toxicological purposes.

A sustained program of investigations involving the tricyclic drugs (*1–5*) had focused attention on metapramine ("19560 RP"), which is 5-methyl-10-methylamino-10,11-dihydrodibenzo[*b, f*]azepine. This psychoactive agent differs from imipramine derivatives in that its molecule contains only one methyl group on the nitrogen atom to the central ring in addition to a methylamino group on carbon 10 (Figure 1). Experimental studies have demonstrated that pharmacologically as well as biochemically, by its action on cerebral amine metabolism, this compound produces a central activity pattern which is different from that of other available psychoactive agents (*6*). It is administered in tablets as the fumarate and in solution for injection as the chlorohydrate.

Metapramine, like the other tricyclic compounds, has two characteristics which profoundly affect its study with regard to pharmacokinetics and analytical toxicology. Its distribution through the human body is very rapid, so that only low concentrations are found in blood serum samples. In addition, it undergoes considerable metabolism in the liver, so that it is present in urine samples only in low concentrations and heavily masked by metabolites. The high sensitivity of gas chromatography, plus its specificity to the appropriate compounds, led to its adoption for this study, using blood serum as the preferred samples.

A number of gas chromatographic procedures have been proposed for the determination of antidepressants in plasma; the most recent tend to utilize nitrogen-selective detectors (*7–10*), but none of these involves metapramine. In this paper, a procedure for metapramine is described which utilizes both a detector which is selective to nitrogen-containing molecules, and which requires no derivatization, and an electron-capture detector which demands a derivatization. The respective advantages of these two detection methods are discussed.

EXPERIMENTAL

Apparatus and Operating Conditions. Two Hewlett-Packard Model 5710 Gas Chromatographs were used. One was equipped with a recently introduced nitrogen-specific detector (Model 18789A "Dual N-P FID") and a glass column, 1.5 m long, 2 mm i.d., packed with 3% of OV-1/OV-17 mixture ($^1/_4$–$^3/_4$) on Gas Chrom Q, 100/120 mesh. Temperatures were regulated at: column 230 °C, injection port 200 °C, detector 300 °C. Gas flow rates were: nitrogen carrier gas 30 mL/min; hydrogen 5.8 mL/min; air 50 mL/min.

The second chromatograph was equipped with a ^{63}Ni electron-capture detector (Model 18724 "EC") and a glass column, 1.2 m long, 4 mm i.d., with the same packing as described above. Temperatures were regulated at: column 220 °C; injection port 250 °C; detector 300 °C. The carrier gas (10% methane in argon) flow rate was 25 mL/min.

The columns were conditioned for at least 48 h at 270 °C before use. If they had not previously been in continuous use, they were treated before an analysis by several injections of a plasma blank extract with metapramine and internal standard, derivatized or not (depending on the detector type), to ensure maximal performance. These precautionary measures would be essential.

Reagents. All solvents and reagents (ethyl ether, cyclohexane, 0.1 N hydrochloric acid, 1.0 N sodium hydroxide) were analytical grade. All aqueous solutions were prepared with bi-distilled water. Ethanol was purified by distillation from potassium hydroxide and zinc. The buffer solution, pH 9.8 was prepared by adding 34.9 mL of 0.1 N sodium hydroxide to 65.1 mL of a solution containing 12.37 g boric acid and 100 mL of 1.0 N sodium hydroxide per liter. The purity of the internal standard desipramine chlorohydrate was checked by thin-layer chromatography on silica gel, using ether–acetone–diethylamine (90:10:1) or benzene–acetone (100:20) treated with 10 mL of a 5% ammonia solution (*1, 4, 5*) as developing solvent. A diluted solution of iodoplatinate was used as locating reagent. The heptafluorobutyric anhydride "Puriss. p.a." (obtained from Fluka AG, Buchs SG, Switzerland) was required as the derivatizing agent for the ECD analysis, and was kept in sealed vials to prevent the ingress of water from the atmosphere.

Standard Solutions. The stock solution of metapramine chlorohydrate in ethanol contained 0.1 mg of metapramine base per mL. By diluting it successively in the same solvent, standard solutions with concentrations between 25 ng and 200 ng per 100 μL were produced. The stock solution of the internal standard, desipramine chlorohydrate in ethanol, contained 0.1 mg of desipramine base per mL and was diluted with the same solvent to obtain a standard solution of 400 ng per 100 μL. It was found that both solutions remained stable for several weeks when stored in a refrigerator.

Glassware. After rinsing in distilled water, all glassware was soaked for 4 h in a hot solution of 3% "RBS 25 Biodegradable"

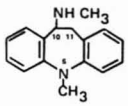

METAPRAMINE
("19560 RP")

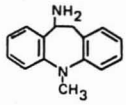

COMPOUND A
("19148 RP")

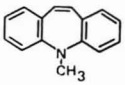

COMPOUND B
("26443 RP")

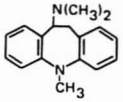

COMPOUND D
("19422 RP")

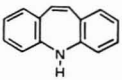

COMPOUND G
("9989 RP")

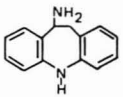

COMPOUND H
("19749 RP")

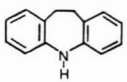

COMPOUND I
("23669 RP")

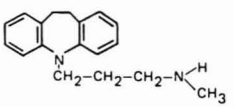

DESIPRAMINE
(Internal standard)

Figure 1. Metapramine, possible metabolites, and desipramine

(obtained from T.C.S., 59130 Lambersart, France). After rinsing again in distilled water, it was left overnight in a dichromato-sulfuric mixture. It was finally rinsed in distilled water and ethanol, and dried at 110 °C.

Procedure. A known quantity of the internal standard solution (containing 400 ng desipramine) was inserted in a centrifuge tube, fitted with a glass stopper. The solvent was allowed to vaporize completely, then 1 to 3 mL of plasma sample was added. After vibrating for 15 s, 2 mL of buffer pH 9.8 was added. An extraction of this aqueous solution was performed by adding 3 mL of diethyl ether, mechanically shaking for 10 min and centrifuging to separate the two phases. The ether phase was removed and the extraction procedures repeated with another 3 mL of diethyl ether. The two ether extracts were combined and concentrated to a volume of about 1 mL. Then 3 mL of 0.1 N hydrochloric acid were added and this mixture shaken for 10 min, and centrifuged. The aqueous phase was neutralized with 1 N sodium hydroxide and 1 mL of buffer pH 9.8 added. Then the solution was again extracted twice with 3 mL diethyl ether as described above. The two ether phases were combined, and the solution evaporated to dryness under vacuum in a nitrogen atmosphere. Finally the residue was dissolved in 100 μL of ethanol.

Between 1 and 2 μL of this solution was injected into the gas chromatograph equipped with the nitrogen-specific detector. The ratio of the peak areas E/E_1 (E = metapramine, E_1 = internal standard) was calculated and referred to a calibration curve (actually a straight line). This calibration had been obtained by performing identical analyses of plasma standard samples to which known quantities of metapramine and a constant quantity of internal standard had been added.

Table I. Retention Times (Minutes) of Metapramine, Desipramine, and Possible Metabolites of Metapramine in Different Detection Modes

	N-P D detection	ECD detection
Metapramine	4.40	
A	4.40	
B	2.67	
D	3.87	
G	3.20	
H	5.47	
I	5.33	
Desipramine	8.67	
Heptafluorobutyric derivatives of:		
Metapramine		3.80
A		2.90
G		1.50
H		3.20
I		4.67
Desipramine		9.80
Compounds B and D: no derivatives are formed		

After the analysis of the sample on the N-detector instrument, the ethanolic solution was evaporated to dryness and the residue dissolved in 100 μL cyclohexane and 1 μL heptafluorobutyric anhydride. Vibration for 30 s was followed by heating to 122 °C for 1 min in the closed tube. The sample was then evaporated to dryness under vacuum in a nitrogen atmosphere. The residue was dissolved in 100 μL cyclohexane.

Between 1 and 3 μL of this solution was injected into the gas chromatograph equipped with the electron-capture detector. The ratio of the peak areas E/E_1 (E = derivative of metapramine, E_1 = derivative of internal standard) was calculated and referred to a calibration curve (again a straight line), which was defined by performing identical analyses of plasma reference samples to which known quantities of metapramine and a constant quantity (around 400 ng) of internal standard had been added.

To increase the reliability of the results, the calibration curves for both detector systems were checked for each series of samples. This was done by performing the complete analysis procedure with two different standard plasma samples containing exactly known quantities of metapramine (e.g., 75 and 125 ng) together with 400 ng internal standard. Each analysis on plasma samples and each injection into the chromatographs was repeated at least twice.

RESULTS

Internal Standard. Several compatible compounds which could be used as an internal standard were studied. The compounds A, G, H, I, and desipramine provoked particular interest (Figure 1). The realization that some of the tested compounds might eventually interfere with peaks of metapramine metabolites, led to the definite conclusion that desipramine was the best choice. The chromatographic separations of the unmodified compounds and of their *N*-heptafluorobutyric derivatives were all shown to be satisfactory (Figure 2 and Table I).

Derivatizing Technique. Several derivatization techniques had been tested to form derivatives of metapramine with a high response for the electron-capture detector. *N*-Heptafluorobutyric imidazole and heptafluorobutyric anhydride were tested under varying operational conditions—temperatures, periods of heating, solvents, etc.

The best results, with respect to sensitivity and reproducibility were produced by a reaction with heptafluorobutyric anhydride at 122 °C for 1 min, as already described under Procedure.

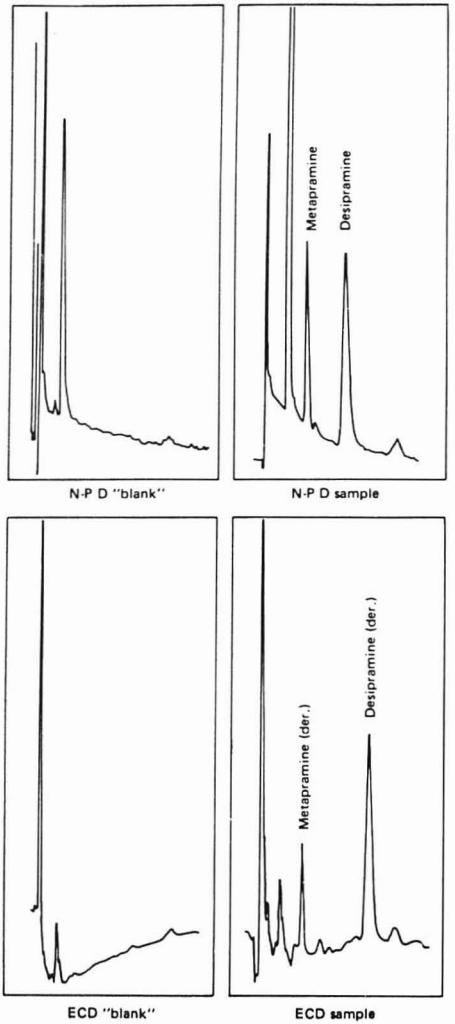

Figure 2. Chromatograms obtained from the plasma extract of a patient who received metapramine fumarate in tablets

The linearity of responses provided proof of good derivatization, subsequently confirmed by thin-layer chromatography. The reaction conditions for the formation of *N*-heptafluorobutyric derivatives applied also to compounds A, G, H and I (Figure 1 and Table I).

Extraction Procedure. The tests on standard plasma samples led to the conclusion that diethyl ether (6 mL in two fractions of 3 mL each) at pH 9.8 ensured a complete extraction of metapramine and desipramine—as well as of the compounds A, B, D, G, H, and I. Additionally, their purification by re-extraction into 0.1 N hydrochloric acid was carried out without measurable loss.

Sensitivity, Reproducibility, and Accuracy. The limits of sensitivity for the quantitative determination of metapramine by the two detection systems were established after the extraction of 2 mL of plasma, solution of the residue in 100 μL solvent, and injection of 1.0 to 1.5 μL. These limits had been found for 15 ng/mL plasma with the N-P D (attenuation $S = 4$) and 35 ng/mL plasma (attenuation $S = 3$) after derivatization. These limits could, if needed, be lowered substantially by increasing the volume of the plasma sample, reducing the amount of solvent added to the residue, and increasing the injected quantity.

Table II. Recovery of Metapramine Added to Human Plasma

Metapramine added, ng/mL	Metapramine found ng/mL	Recovery, %	Rel std dev., %[a]
	N-P D Detection		
48	47.8	99.5	7.9
72	71.8	99.7	2.7
96	96.3	100.3	3.2
126	126.7	100.5	2.5
168	167.8	99.8	3.3
189	189.0	100.0	2.7
252	252.2	100.1	4.7
			Average: 3.85
	ECD Detection		
48	48.0	100.0	8.3
72	71.4	99.1	5.0
96	96.0	100.0	9.3
126	126.0	100.0	4.9
168	167.8	99.8	5.8
189	188.5	99.7	4.5
252	250.8	99.5	8.7
			Average: 6.64

[a] Seven determinations.

The calibration curves for the two analyses were established under the analytical conditions already described using plasma samples which contained a constant quantity of internal standard (500 ng) and increasing quantities of metapramine (from 48 to 252 ng)—made by dilution from the two stock solutions containing 48 and 126 μg/mL, respectively. The determinations were repeated 7 times for each quantity. The accuracy of the results obtained is presented in Table II. Relative standard deviations of the results for concentrations of metapramine in the range 48–252 ng/mL were found to be 2.5–7.9% and 4.5–9.3%, respectively, by N-P D and ECD detection. The deviation was then smaller for the N-P D than for the ECD (which required derivatization).

Specificity. The chromatographic analysis of the plasma "blanks" showed that no compound extracted under the conditions described had interfered with the metapramine, its possible metabolites, and the internal standard desipramine, derivatized or not. Concerning the analysis of plasmas taken from patients under treatment with metapramine, the double detection (N-P D and ECD) procedure allowed the accuracy of determination of the drug concentration to be increased and also the reliability of results (Figure 2 and Table I). It also revealed the nature and quantity of metabolites of the metapramine which were present in the sample.

The specificity of this procedure was demonstrated by the table of the retention times for the different compounds studied (Table I). Any doubts relating to interferences between compound A and metapramine and between compounds I and H, which could remain after the N-P D procedure, were eliminated after EC detection of the derivatized products.

Applications. The procedure was evolved to establish the plasmatic kinetics of metapramine in human subjects. An example is given in Figure 3, where the curve related to a patient who had received oral administration of 150 mg of

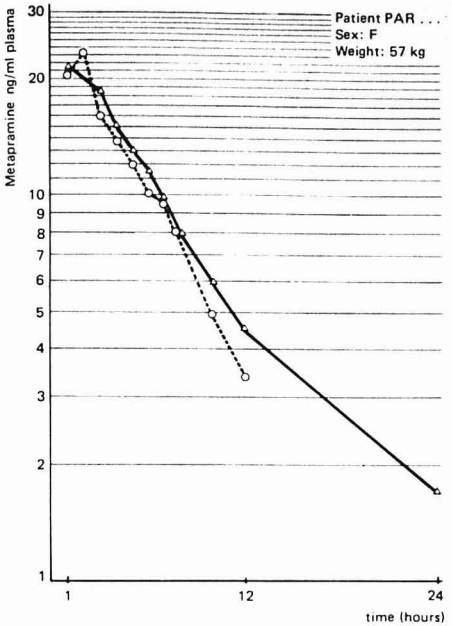

Figure 3. Plasma levels of metapramine after oral administration of a single dose of 150 mg (as fumarate). (Δ—Δ—Δ) N-P D detection. (O--O--O) ECD detection of heptafluorobutyryl derivatives

metapramine fumarate in tablet form. The plasma concentrations were determined not only for single doses but also after repeated dosages of the drug and also after intravenous injection of metapramine chlorohydrate. The urinary excretion was also investigated and the results will be published at a later date. It is important to point out that in plasma the half-life of the compound is 5 to 6 h, that a large disproportion exists between the administered dose and the unchanged drug content in the plasma, and that the biotransformations of the metapramine are fast and intensive.

DISCUSSION

A comparison of the two chromatographic detection methods clearly showed that the N-P D method was faster and easier because the disadvantages of derivatization were avoided. This method also provided excellent reproducibility and was considerably more sensitive than the ECD method which required derivatization. In this particular application however, its selectivity could cause some inconvenience because there was unfortunate mergence of chromatographic peaks from compound A and metapramine on the one hand and from compounds I and H on the other. Where single doses of metapramine were concerned, this caused no problem because compound A did not appear at all in the human plasma and compounds I and H appeared only several hours after administration and then only in negligible quantities compared with the metapramine. Consequently the N-P D method of detection was perfectly applicable for the establishment of the plasmatic kinetics of unchanged metapramine after single doses of the drug. After repeated doses it was no longer possible, at the beginning of the second day, to assure the absence of measurable quantities of compound A, formed by metabolism of metapramine.

The ECD method was slower and more demanding as indicated by the "derivatizing technique" described earlier. The sensitivity was lower than that achieved by the N-P D. On the other hand, in this particular application, the specificity of the method was better because no interference between the main metabolites was observed, including compound A.

This method therefore allowed the results of the kinetic studies of metapramine to be refined and it provided better recognition of the metabolites which could accompany the unchanged compound in the plasma. Simultaneous quantitative determinations of both the unchanged drug and its main metabolites could even be considered. The two detection methods therefore were complementary to each other in this work.

Thus the analytical procedure described is available for pharmacokinetic and bioavailability studies involving metapramine, also for its therapeutic control. It can also be used for diagnostic or prognostic purposes in possible cases of accidental or deliberate poisoning.

ACKNOWLEDGMENT

Suzanne Monjanel has provided invaluable assistance with the mathematical calculations involved.

LITERATURE CITED

(1) A. Viala, F. Gouezo, and C. Gola, *J. Chromatogr.*, **45**, 94 (1969).
(2) A. Viala, J. P. Cano, F. Gouezo, C. Gola, and A. Angeletti, *Sci. Med.*, **2**, 409 (1971).
(3) A. Viala, J. P. Cano, C. Gola, and F. Gouezo, *J. Chromatogr.*, **59**, 297 (1971).
(4) A. Viala, C. Gola, J. P. Cano, and F. Gouezo, *Ann. Pharm. Fr.*, **30**, 445 (1972).
(5) C. Gola, Etudes toxicologiques sur les médicaments antidépressurs dérivés de l'imipramine, Pharm. Thesis, Marseilles, 1971.
(6) Specia Laboratories, Paris, personal communication.
(7) L. A. Gifford, P. Turner, and C. M. B. Pare, *J. Chromatogr.*, **105**, 107 (1975).
(8) A. Jorgensen, *Acta Pharmacol. Toxicol.*, **36**, 79 (1975).
(9) J. Vasiliades and K. C. Bush, *Anal. Chem.*, **48**, 1708 (1976).
(10) D. N. Bailey and R. I. Jatlow, *Clin. Chem. (Winston-Salem, N.C.)*, **22**, 777, 1697 (1976).

RECEIVED for review July 11, 1977. Accepted September 20, 1977. Specia Laboratories of Paris have provided considerable support of this work, and also provided us with the required reference compounds.

Critical Evaluation of the Copper(II) Solubilization Method for the Determination of the Complexation Capacity of Natural Waters

P. G. C. Campbell,* Marc Bisson, Robert Gagné,[1] and André Tessier

Université du Québec, INRS-Eau, C.P. 7500, Ste-Foy, Québec, Canada G1V 4C7

Thermodynamic calculations indicate that for realistic ligand concentrations ($\leq 10^{-6}$ M), the copper(II) solubilization method is insensitive to most monomeric biogenic ligands and underestimates the true complexation capacity of natural waters. Experimental results show that the conditions required by the copper(II) solubilization method favor the removal of dissolved organic carbon by coprecipitation. In the absence of a final ultrafiltration step, the method is subject to interference by colloidal Cu(II)-humic species; a peptization mechanism, involving a stabilizing adsorptive interaction between colloidal Cu(II) hydroxide and the humic materials, is proposed to explain this interference.

The chemical speciation of trace metals in the aquatic environment has a determining influence on their transport, reactions, and biological availability (*1–5*). Of primary importance in determining the speciation of a given trace metal in solution are the nature and concentration of the various ligands present. Provided that the "available" ligand concentration, $[L]_A$, is greater than the total trace metal concentration, $[M]_T$, the degree of complexation will be independent of the metal concentration and will depend only on the concentration of the individual ligands and the magnitude of the appropriate stability constants (*6*).

Inorganic ligands of importance in determining trace metal speciation are relatively few in number (*1, 7*) and their concentrations are readily determined. In contrast, many organic compounds of potential complexing ability are known to occur in natural waters, for example: amino acids, proteins, monosaccharides, polysaccharides, porphyrins, hydroxamic acids, fulvic acids, humic acids (*8–10*). In recognition of the difficulties inherent in identifying and quantifying all the organic ligands present in a given water sample, several workers have developed the "complexation capacity" concept (*11–15*). As the term implies, complexation capacity is a measure of the ability of a water sample to complex or mask the trace metals present. Acceptance of the complexation capacity concept implies that for a given metal it is possible to group together the various ligands present and represent their behavior by means of certain "average" properties.

Several experimental procedures, varying greatly in manipulative complexity, have been proposed for measuring the complexation capacity of natural waters. These can be grouped into chemical methods (*11–14*), based on such physicochemical techniques as solubility determinations and complexometric titrations, and biological methods (*4, 15*). In this paper we present a critical evaluation of the copper(II) solubilization method proposed by Manahan and co-workers (*11, 16,* 17), and compare the results obtained with this technique to those obtained with a reverse colorimetric method.

[1] Present address, Ministère des Richesses naturelles, Service de la Qualité des eaux, Complexe Scientifique, Ste-Foy, Québec, Canada G1P 3W8.

EXPERIMENTAL

General Analytical Procedures. Stock solutions were prepared using reagent-grade chemicals and deionized water (Millipore Milli-Q3 RO/Milli-Q2 system). Dissolved organic carbon was determined with a Beckman Total Organic Carbon Analyzer (Model 915A). Ammonia and total reduced nitrogen determinations were performed colorimetrically (*18*) on a Technicon AutoAnalyzer (Model AA-II), and dissolved organic nitrogen was obtained by difference. Iron analyses were also performed on a Technicon AutoAnalyzer: after digestion of the sample with thioglycolic acid and reduction, iron(II) reacts with 2,4,6-tri(2′-pyridyl)-5-triazine to form a colored complex (*19*).

Copper was determined by atomic absorption spectrophotometry (Varian Techtron Model AA-5). Conventional techniques, involving direct aspiration of the aqueous sample into an air–acetylene flame, were used for complexation capacity measurements. Determination of copper concentrations in filtered river water required preconcentration; a chelation-extraction step involving ammonium pyrrolodine dithiocarbamate and methyl isobutyl ketone was employed (*20*).

Complexation Capacity, Principles. The experimental procedure introduced by Kunkel and Manahan (*11*) for the determination of complexation capacity is based on the solubilization of copper(II) by complexing agents at alkaline pH values. Under the experimental conditions defined by Kunkel and Manahan, the solubility of inorganic Cu(II) reaches a minimum of approximately 2.4×10^{-7} M (15 μg Cu L^{-1}) in the pH range 10–11. In a natural water sample, any increase in copper concentration above this value is attributed to solubilization or complexation involving species other than hydroxo or carbonato ligands.

For comparison purposes, complexation capacity values were also obtained with a copper(II) titration procedure and a reverse colorimetric method. The copper titration procedure involves the measurement of electrochemically labile copper by differential pulse anodic stripping voltammetry after a number of ionic copper spikes have been allowed to equilibrate with the available ligands in the water sample (*13*). The colorimetric method, essentially identical to that used to determine nitrilotriacetic acid (NTA) in aqueous solution (*21*), is based on the complexation of zinc(II) with zincon (2-carboxy-2′-hydroxy-5′-sulfoformazylbenzene). The procedure involves treatment of the water sample with a cation-exchange resin followed by addition of the zinc–zincon reagent (molar ratio 1:13, buffered to pH 9.2). The extent of zinc binding to natural ligands present in the sample is calculated from the reduction at equilibrium in zinc–zincon complexation (*21, 22*).

Complexation Capacity, Copper Solubilization Method. The experimental procedure described by Kunkel and Manahan (*11*) was carried out in triplicate. To each of three 50-mL portions of the filtered water sample was added 5 mL of 5×10^{-2} M $CuSO_4$, followed by sufficient 5×10^{-2} M Na_2CO_3 to raise the pH to a stable value in the range 9.9–10.1. The samples were heated in a hot water bath (ca. 100 °C) for 1 h. To avoid a significant decrease in pH during this treatment, with a concomitant increase in the solubility of inorganic Cu(II), a carbon dioxide-free atmosphere was maintained in the sample flasks by circulating prehumidified nitrogen over the samples during both the heating and cooling steps. Once cooled to room temperature, the contents of each reaction flask were quantitatively transferred to a volumetric flask and diluted to 100 mL with deionized water (pH 10, Na_2CO_3). After thorough mixing, this suspension was filtered through a 0.45-μm membrane filter. To avoid copper contamination of the filtrate, the membrane employed for this filtration

Table I. Complexation Capacity of River Water as Measured by the Copper(II) Solubilization Method

River	Station	No. of samples	Complexation capacity (μmol Cu L^{-1}) Mean	Range
Yamaska	Y-1	6	1.3	0.4–3.2
	Y-2	5	2.7	0.4–4.8
	Y-3	4	1.0	0.6–1.7
	Y-4	5	0.7	0.4–1.0
	Y-5	6	4.1	1.9–9.6
	Y-6	6	0.7	<0.3[a]–1.5
Saint-Francois	SF-1	6	1.5	0.6–3.0
	SF-2	6	1.9	0.9–3.2
	SF-3	4	1.8	0.9–2.8
	SF-4	3	0.4	0.3–0.5
	SF-5	4	0.6	<0.3[a]–1.2
	SF-6	6	4.0	1.9–7.1
	SF-7	5	6.9	2.0–18.7

[a] For the calculation of the mean complexation capacity, values below the detection limit were assigned an arbitrary value of 0.15 μmol L^{-1}.

(Millipore HAWP 04700) was soaked for 2 h in dilute nitric acid (3% v/v), rinsed thoroughly with deionized water, and soaked briefly in alkali (5×10^{-2} M Na_2CO_3) before use. Each filtrate was then acidified to pH <2 with nitric acid (BDH Chemicals, Aristar grade) and analyzed for copper by atomic absorption spectrophotometry. Blank determinations were carried out with three 50-mL portions of deionized water in the place of the natural water sample and the complexation capacity of the original sample, expressed in μmol Cu L^{-1}, was obtained by difference.

Complexation Capacity, Zinc–Zincon Method. Colorimetric complexation capacity determinations were performed with a Technicon AutoAnalyzer (Model AA-II) according to the procedure described by the U.S. Environmental Protection Agency (*23*). Solutions of trisodium nitrilotriacetate (Na_3NTA) in the concentration range 0.2–3.6 μM were used for calibration purposes. The detection limit, defined as twice the background variation recorded when blank samples were analyzed, was 0.07 μM.

Complexation Capacity, Copper(II) Titration Method. The procedure described by Chau and co-workers (*13*) was followed without modification. Differential pulse anodic stripping voltammetry was carried out with a Princeton Applied Research polarograph (Model 174) operating in the differential pulse mode. Voltammograms were recorded with a Houston Instruments Omnigraphic recorder (Model 2000).

Sampling. Water samples were collected periodically from February to November 1975 at thirteen sampling stations maintained on the Yamaska and Saint-Francois Rivers (Quebec, Canada). The samples were filtered through glass fiber filters (Whatman, GF/C, 1.2-μm nominal pore size) that had previously been combusted at 550 °C for 8 h, and the filtrates were subjected to the various analytical procedures described above (see Figure 1).

RESULTS AND DISCUSSION

Precision. Using the copper solubilization method to determine the complexation capacity of prepared EDTA solutions (1 and 10 μM), we obtained reproducible results (relative standard deviation 4–5%); with subsamples drawn from a river water sample, the relative standard deviation was somewhat higher, normally in the range 10–20%. Blank determinations, carried out with deionized water in the place of natural water samples, consistently gave complexation capacity values in the range 0.25–0.5 μM (ca. 15–30 μg Cu L^{-1}). These levels are in reasonable agreement with the calculated solubility of inorganic Cu(II) under the experimental conditions. The detection limit, defined as $2t\sqrt{2}\,\sigma_B/\sqrt{n}$, was about 0.3 μM, where t = "Student" t statistic for $P = 0.05$; σ_B = standard deviation of the blank value in a particular experiment; $n = 3$, the number of replicate determinations (*24*).

Application to River Water Samples. Seasonal samples, collected at various sampling points on the Yamaska and Saint-Francois Rivers during the period from February to November 1975, were analyzed according to the procedure outlined in Figure 1. Average complexation capacity (CC) values, as determined by the copper solubilization method, ranged from 0.4 to 6.9 μM at the different sampling points (Table I). Kunkel and Manahan (*11*) have reported considerably higher values for surface waters in Missouri (15–23 μM), whereas Elder and co-workers (*25*) found levels of less than 1 μM for Lake Tahoe water. Average complexation capacity values at sampling stations located downstream from large lakes (i.e., stations Y-6; SF-4, 5) are generally low. Water quality at certain other stations is significantly influenced by the discharge of industrial effluents (station SF-6, pulp and paper mill; SF-7, copper, lead, and zinc ore processing plant); or municipal sewage (station Y-5); complexation capacity values at these points are consistently higher than those encountered elsewhere in the study area.

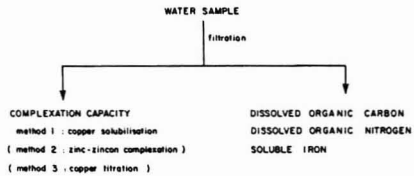

Figure 1. Flow diagram of the analytical procedure. Analyses indicated in parentheses were not performed routinely

In an attempt to explain the observed temporal variation in complexation capacity and the appreciable spatial differences, an investigation of possible relations between complexation capacity and certain other water quality parameters was undertaken. The following parameters were considered: dissolved organic carbon (DOC), dissolved organic nitrogen, soluble iron, soluble copper, and stream flow. The available data were considered on a monthly basis, allowing inter-station comparisons for each sampling date, and for the entire sampling period; only in the case of DOC was a significant correlation with complexation capacity obtained (Figure 2). A positive correlation can be observed between complexation capacity and DOC for the rivers studied if the statistical population considered is limited to a single monthly sampling (e.g., April or November 1975). Over an extended period, i.e., on pooling the data for all months, the correlation is no longer significant.

Thermodynamic Calculations. The observation that the copper solubilization method gives measurable CC values, together with the demonstration of a significant though

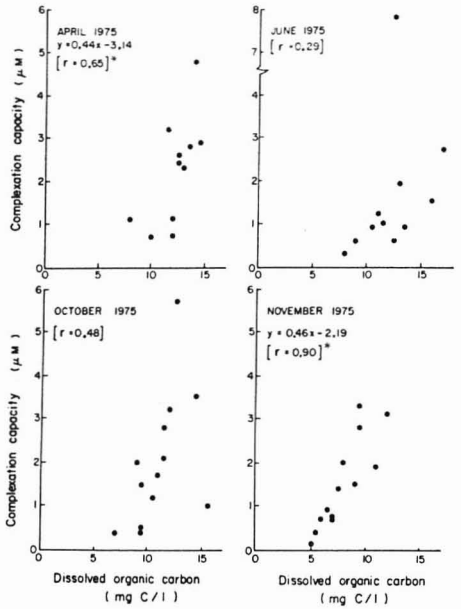

Figure 2. Relation between dissolved organic carbon and complexation capacity. Significant correlation coefficients ($P = 0.05$) are denoted by an asterisk (*)

transitory correlation with DOC levels, raises an obvious question as to the nature of the (organic) ligands responsible for this complexation capacity. It has been shown experimentally that strong synthetic chelating agents, such as NTA and EDTA, are quantitatively determined by the copper solubilization method (*11*, *16*). However, the sensitivity of the method to biogenic ligands likely to be present in river water is unknown. To verify this point, a number of representative monomeric ligands were selected (aspartic acid, glycine, lysine, salicyclic acid, citric acid) and their "solubilization" potential was calculated. Thermodynamic equilibrium was assumed and the relevant constants were obtained from the literature (*6*, *26*).

The theoretical complexation capacity for a particular ligand, L, can be expressed as follows:

$$CC = [Cu^{2+}] \sum_{j=1}^{n} \beta_j [L]^j \qquad (1)$$

where β_j is the stability constant for the complex $Cu(L)_j$. Note that for clarity possible charges on the ligands and metal complexes have been neglected. This calculation was performed for each model ligand under the following defined experimental conditions: excess Cu(II); total ligand concentration, $[L]_T = 10^{-6}$ M or 10^{-5} M. The choice of ligand concentration was based on reported levels of free biogenic monomers in surface waters (*8*, *9*, *27*); 10^{-5} M would seem a reasonable upper limit for the concentrations of such compounds in river water. Complexation capacity values were calculated in this manner at intervals of 0.5 pH unit over the pH range 2 to 14.

Typical results are shown in Figure 3 for three representative amino acids (neutral, acidic, basic) as well as for citric acid and salicyclic acid. In the absence of the necessary thermodynamic data for fulvic acid itself, we chose salicylic

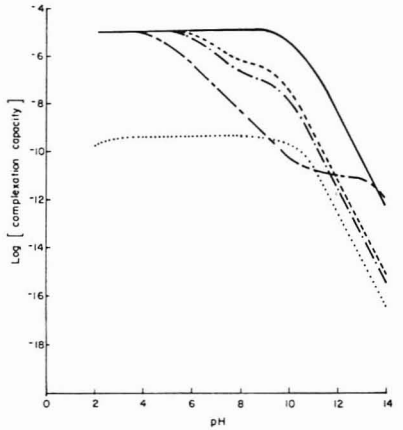

Figure 3. Theoretical complexation capacity of citric acid (—), aspartic acid (- - - -), glycine (— · —), salicylic acid (·····), and lysine (— · · —) as a function of pH. Ligand concentration = 10^{-5} M

acid as a model for the complexation sites in the fulvic acid molecule. Though some precedent exists for this approximation (*1*, *28*), it should be treated with caution. Complexation capacity values at pH 10 vary from $10^{-5.45}$ to $10^{-10.3}$ M; with the exception of citric acid, these levels are far below the detection limit defined earlier (3×10^{-7} M). It follows that monomeric biogenic ligands, similar in nature and solubilization potential to those studied here, will *not* be detected by the copper solubilization technique.

Figure 3 also shows that under the defined conditions of the calculation the complexation capacity at pH 10 is markedly lower than that which would be expected at a natural pH value closer to 7. For $[L]_T = 10^{-5}$ M the CC (pH 7):CC (pH 10) ratio varies from 2 to 850 for the five ligands studied. Note that as this effect depends upon the acid–base properties of the ligand, and the ligand concentration, the same trend would not necessarily be observed for all ligands. Nevertheless, these calculations clearly demonstrate the potential sensitivity of the complexation capacity to pH changes in the critical pH range 7–10.

Polymeric Biogenic Ligands. As the thermodynamic calculations indicated that most monomeric biogenic ligands, if present at realistic concentrations ($\leq 10^{-5}$ M), would not be detected by the copper solubilization technique, we tested several polymeric ligands of natural origin. Two water soluble proteins were selected, casein and gelatin. In addition two samples of humic material were studied: the first sample, designated "humic acid" for the present purposes, was obtained commercially (Aldrich Chemical Co.); the second, termed "fulvic acid", was isolated by ultrafiltration (Diaflo membranes) and lyophilization of a highly colored natural water sample collected from an acidic soft-water swamp on the Laurentian Shield. Aqueous solutions of these substances were prepared and analyzed by the standard copper solubilization procedure. The polymer concentrations chosen were similar to those likely to be found in natural waters (*8*, *9*).

Of the four polymeric ligands studied, only the humic and fulvic acid samples maintained appreciable quantities of Cu(II) in "solution" under the conditions of the experiment (Table II).. At first glance the DOC:CC ratios suggest a great solubilization potential for the humic materials; assuming an organic carbon content of 40% for the fulvic acid (Dr. S. A. Visser, personal communication) and ~50% for the humic

Table II. Complexation Capacity of Biogenic Macromolecules as Determined by the Copper(II) Solubilization Method

Polymer	Concentration (mg C L^{-1})	Complexation capacity (μmol Cu L^{-1})	DOC/CC[a]
Humic acid	6.0	15	32
Fulvic acid	4.0	13	25
Gelatin	0.4	<0.3	...
Casein	0.7	<0.3	...

[a] Ratio of dissolved organic carbon to complexation capacity, each being expressed in μmol L^{-1}.

Table III. Effect of Ultrafiltration on the Apparent Complexation Capacity of Humic Acid[a]

	Filtrate (0.45 μm)	Ultrafiltrate (0.018 μm)
Complexation capacity (μmol Cu L^{-1})	15 ± 3[b]	0.6 ± 0.06[b]
Relative turbidity	64 ± 20[b]	<1

[a] Humic acid concentration 6 mg C L^{-1}. [b] Standard deviation (N = 3).

acid, the apparent equivalent weights would be 750 and 740, respectively. However, an ultrafiltration experiment, designed to verify the physical dimensions of the "soluble" copper species passing through the standard 0.45-μm membrane filter after treatment of the water sample, revealed otherwise.

A solution of humic acid (6 mg C L^{-1}) was subjected to the standard copper solubilization procedure and the final filtrate was divided into two equal portions. An aliquot of the first portion was introduced without acidification into a spectrofluorometer cell, and the relative turbidity was determined by nephelometry; the remainder of this portion was acidified and analyzed for copper by atomic absorption. The second portion was subjected to ultrafiltration in a stirred cell (Amicon Corporation, Model 402) fitted with a Diaflo XM 300 ultramembrane (0.018-μm nominal pore size). The relative turbidity and copper concentration in the ultrafiltrate were then determined as described above. The results of this experiment (Table III) indicate that the major portion (~ 96%) of the copper in the initial (0.45-μm) filtrate is *colloidal* in nature rather than truly soluble. Nephelometric measurements support this conclusion, the turbidity measured in the initial filtrate being completely eliminated by ultrafiltration. In control experiments, it was shown that in the absence of copper(II) the humic acid passed freely through the ultrafilter. Similarly, in the absence of humic acid no appreciable colloidal copper was found in the initial filtrate. The apparently high complexation capacity of the humic acid would thus appear to be an artifact of the experimental procedure; the concentration of soluble complexed copper is in fact almost negligible compared to the amount of colloidal copper present. This suggests that the principal role of the humic acid is not to form soluble copper(II) complexes, but rather to allow colloidal copper(II) to persist in the treated sample, presumably by stabilizing colloidal cupric hydroxide. Shapiro (*29*) has proposed such an interaction, or peptization, to explain the ability of natural organic acids to prevent the precipitation of iron(III) and copper(II) in the pH range 5–11. He found that in the presence of yellow organic acids isolated from lake water, both iron and copper passed through membrane filters of 0.45- and 0.22-μm nominal pore size, but were largely retained on a filter of 0.10-μm pore diameter. A peptization mechanism implies an adsorptive interaction between a colloidal particle and the surfactive humic materials, resulting in the stabilization of the colloid (*30*).

Table IV. Effect of Ultrafiltration on the Apparent Complexation Capacity of River Water

Sample		Complexation capacity[a]	
River	Station	Filtrate (0.45 μm)	Ultrafiltrate (0.018 μm)
Yamaska	Y-1	1.5 ± 0.1	0.3 ± 0.1
	Y-2	3.1 ± 0.1	0.8 ± 0.1
	Y-6	0.7 ± 0.1	0.5 ± 0.2
Saint-Francois	SF-1	2.1 ± 0.3	0.3 ± 0.1
	SF-5	<0.3	<0.3
	SF-7	3.3 ± 0.1	1.0 ± 0.3

[a] Complexation capacity determined in triplicate and expressed as μmol Cu L^{-1} ± standard deviation.

A similar ultrafiltration procedure was subsequently applied to representative river water samples (Table IV). In four of the six samples tested, ultrafiltration significantly reduced the concentration of copper(II) present in the original filtrate; in these cases reductions of the apparent complexation capacity ranged from 70 to 86%, suggesting the presence of appreciable quantities of humic material. Samples Y-6 and SF-5, on which ultrafiltration had little or no effect, were collected downstream from large lakes. Water quality at these sampling points is largely determined by the characteristics of the epilimnetic waters upstream. It would thus be anticipated (*31*, *32*) that the proportion of allochthonous organic material (including humic acids) would be lower at these points than at the other sampling stations located in the more fluvial portions of the watershed. This hypothesis would explain both the consistently low complexation capacity values obtained for samples collected at these points (cf. Table I) and the absence of any appreciable colloidal copper(II) in the 0.45-μm filtrate.

Coprecipitation of Dissolved Organic Carbon. The observation of a significant interaction between colloidal copper(II) and dissolved organic matter in natural water samples raises the possibility that some DOC is lost during the copper solubilization procedure by association with the particulate phase. The copper solubilization technique was applied to six river water samples, and DOC concentrations were determined before and after the analysis. Significant losses (30–50%) were noted for all but one sample, the exception being a sample collected downstream from a lake (site SF-5, see above).

Entrapment of dissolved organic matter by coprecipitation with iron and copper hydroxides has been observed by several workers. Jeffrey and Hood (*33*) suggested this technique as a means of concentrating dissolved organic matter from seawater. Using iron(III) at pH 7.6–10, they obtained yields of 79–95% for labeled (^{14}C) dissolved organic matter of algal origin but undetermined nature. Chapman and Rae (*34*) reported somewhat lower yields (48–73%) for ^{14}C-labeled amino acids, using excess copper at pH 9. In other words, the experimental conditions required by the copper solubilization method also favor the removal of dissolved organic matter by coprecipitation. In the present context such losses would seem to compromise the use of this method to determine the complexation capacity of natural waters as a significant fraction of the very material being measured is at least partially lost during the analysis. Indeed, it has been suggested (*34*) that those organic solutes possessing a metal complexing capacity should be preferentially removed by coprecipitation.

Comparison of Complexation Capacity Values Obtained by Different Methods. Using river water samples collected on two successive months, we carried out complexation capacity determinations in parallel with two dif-

Table V. Comparison of Complexation Capacity Values Obtained by the Copper(II) Solubilization and Zinc(II)-Zincon Methods

Sample		Complexation capacity (μmol L^{-1})			
		October 1975		November 1975	
River	Station	Copper(II) solubilization method	Zinc–zincon method	Copper(II) solubilization method	Zinc–zincon method
Yamaska	Y-1	1.0	0.22	1.5	0.15
	Y-2	3.5	0.07	3.1	0.11
	Y-3	1.9	0.11	0.7	0.22
	Y-4	0.4	0.07	0.7	0.30
	Y-5	2.1	0.15	1.9	0.60
	Y-6	1.5	0.07	0.7	<0.07
Saint-Francois	SF-1	1.2	0.11	2.1	0.15
	SF-2	3.2	0.07	1.4	0.15
	SF-3	2.8	0.11	0.9	0.07
	SF-4	0.4	<0.07	0.4	0.07
	SF-5	0.5	0.07	<0.3	0.18
	SF-6	5.7	0.11	2.8	0.07
	SF-7	2.0	0.07	3.3	<0.07

Table VI. Comparison of Complexation Capacity Values Obtained by Different Methods

Sample		Complexation capacity (μmol L^{-1})			
		Copper(II) solubilization method		Copper(II) titration method	Zinc(II)–zincon method
River	Station	Filtrate (0.45 μm)	Ultrafiltrate (0.018 μm)		
Yamaska	Y-1	1.5	0.31	0.74	0.15
Saint-Francois	SF-1	2.1	0.29	0.72	0.15

ferent analytical techniques: the copper(II) solubilization method, and the zinc–zincon colorimetric method. Though designed for the determination of NTA, this latter technique is inherently nonselective. Provided that thermodynamic equilibrium is rapidly established, the zinc–zincon method will respond indiscriminately to other ligands present having conditional stability constants towards zinc(II) comparable to or greater than that of the Zn–NTA complex (*21*, *22*). With a single exception, the complexation capacity values obtained by the copper solubilization technique were higher than those obtained by the colorimetric method (Table V). For the 22 samples in which the complexation capacity was greater than the detection limit, the CC (Cu):CC (Zn) ratio varied from 2 to 52, the average value over the two-month period being ca. 19 (relative standard deviation 85%). As suggested by the variability of this ratio, no consistent relation could be found between the complexation capacity values yielded by these two techniques. Even after ultrafiltration, higher CC values were obtained using the copper solubilization method than with the zinc–zincon procedure. Clearly the two techniques respond differently when applied to natural waters; this different response can be attributed, at least in part, to the well established differences in stability of zinc and copper complexes (*35*) and to the insensitivity of the zinc–zincon technique to humic materials.

On two occasions additional complexation capacity measurements were performed according to the copper(II) titration procedure suggested by Chau (*13*). This method gave intermediate results falling between the values derived from the copper(II) solubilization technique (0.45-μm filtration) and those obtained by the zinc–zincon method (Table VI). Though no general conclusion can be drawn from only two samples, the comparative results obtained are remarkably similar. Note, however, that the copper(II) titration method has recently been shown to be subject to kinetic artifacts (*36*) and to interference from surfactive materials (*37*, *38*).

CONCLUSIONS

Several experimental methods have been proposed for measuring the complexation capacity of natural waters (*11–15*). The copper(II) solubilization technique has as advantages its conceptual and experimental simplicity, coupled with acceptable analytical sensitivity. However, weighed against these points are several disadvantages: (1) the required use of an alkaline reaction medium (pH 10) very different from the original sample; (2) the inherent insensitivity of the method to a variety of monomeric biogenic ligands; (3) the dual response of the method, in the absence of an ultrafiltration step, to both complexed and peptized copper(II); (4) the appreciable loss of dissolved organic matter by coprecipitation with copper(II) hydroxide. These considerations seriously compromise the determination of the complexation capacity of natural waters by the copper solubilization method. For determining the concentration of strong ligands in such waters, or for evaluating the complexation capacity of media suspected to contain high ligand concentrations (e.g. waste water), it may still prove to be a useful technique *provided* that an ultrafiltration step is incorporated into the experimental procedure to eliminate the interference by colloidal Cu(II)–humic species.

ACKNOWLEDGMENT

The authors thank H. Casey and F. H. Dawson for helpful comments and discussion, and S. A. Visser for having furnished the fulvic acid sample. The able technical assistance of M. Geoffroy and G. Trudel is gratefully acknowledged.

LITERATURE CITED

(1) W. Stumm and P. A. Brauner, "Chemical Oceanography", 2nd ed., J. P. Riley and G. Skirrow, Ed., Academic Press, New York, N.Y., 1975, Vol. 1, Chap. 3, pp 173–239.
(2) R. T. Barber, "Trace Metals and Metal-Organic Interactions in Natural Waters", P. C. Singer, Ed., Ann Arbor Science Publishers, Ann Arbor, Mich., 1973, Chap. 11, pp 321–338.
(3) J. Shapiro, *Verh. Int. Ver. Limnol.*, **17**, 456–466 (1969).

(4) A. G. Lewis, P. H. Whitfield, and A. Ramnarine, *Mar. Biol.*, **17**, 215–221 (1972).
(5) V. M. Brown, T. L. Shaw, and D. G. Shurben, *Water Res.*, **8**, 797–803 (1974).
(6) W. Stumm and J. J. Morgan, "Aquatic Chemistry, an Introduction Emphasizing Chemical Equilibria in Natural Waters", Wiley-Interscience, New York, N.Y., 1970, Chap. 6, pp 238–299.
(7) F. Morel, R. E. McDuff, and J. J. Morgan, "Trace Metals and Metal-Organic Interactions in Natural Waters", P. C. Singer, Ed., Ann Arbor Science Publishers, Ann Arbor, Mich., 1973, Chap. 6, pp 157–200.
(8) B. T. Croll, *Water Treat. Exam.*, **21**, 213–238 (1972).
(9) P. A. Cranwell, *Environ. Chem.*, **1**, 22–54 (1975).
(10) A. E. Martell, *Pure Appl. Chem.*, **44**, 81–113 (1975).
(11) R. Kunkel and S. E. Manahan, *Anal. Chem.*, **45**, 1465–1468 (1973).
(12) M. S. Shuman and G. P. Woodward, *Anal. Chem.*, **45**, 2032–2035 (1973).
(13) Y. K. Chau, R. Gächter, and K. Lum-Shue-Chan, *J. Fish. Res. Board Can.*, **31**, 1515–1519 (1974).
(14) S. Ramamoorthy and D. J. Kushner, *J. Fish. Res. Board. Can.*, **32**, 1755–1766 (1975).
(15) E. W. Davey, M. J. Morgan, and S. J. Erickson, *Limnol. Oceanogr.*, **18**, 993–997 (1973).
(16) S. E. Manahan and M. J. Smith, *Water Sewage Works*, **120**, 102–106 (1973).
(17) D. R. Jones IV and S. E. Manahan, *Anal Chem.*, **49**, 10–12 (1977).
(18) J. Reardon, J. A. Foreman, and R. L. Searcy, *Clin. Chim. Acta.*, **14**, 403–405 (1966).
(19) P. F. Collins, H. Diehl, and D. F. Smith, *Anal. Chem.*, **31**, 1862–1867 (1959).
(20) R. R. Brooks, B. J. Presley, and I. R. Kaplan, *Talanta*, **14**, 809–816 (1967).
(21) J. E. Thompson and J. R. Duthie, *J. Water Pollut. Control Fed.*, **40**, 306–319 (1968).
(22) G. F. Longman, M. J. Stiff, and D. K. Gardiner, *Water Res.*, **5**, 1171–1175 (1971).
(23) "Methods for Chemical Analysis of Waters and Wastes", U.S. Environmental Protection Agency, Cincinnati, Ohio, 1974.
(24) J. D. Ingle, *J. Chem. Educ.*, **51**, 100–105 (1974).
(25) J. F. Elder, K. E. Osborn, and C. R. Goldman, *Water Res.*, **10**, 783–787 (1976).
(26) L. G. Sillen and A. E. Martell, "Stability Constants of Metal Ion Complexes", Special Publication No. 17, The Chemical Society, London, 1964; Supplement No. 1, Special Publication No. 25, 1971.
(27) C. C. Crawford, J. E. Hobbie, and K. L. Webb, *Ecology*, **55**, 551–563 (1974).
(28) D. S. Gamble and M. Schnitzer, "Trace Metals and Metal–Organic Interactions in Natural Waters", P. C. Singer, Ed., Ann Arbor Science Publishers, Ann Arbor, Mich., 1973, Chap. 9, pp 265–302.
(29) J. Shapiro, *J. Am. Water Works Assoc.*, **56**, 1062–1082 (1964).
(30) P. McFadyen and E. Matijević, *J. Inorg. Nucl. Chem.*, **35**, 1883–1893 (1973).
(31) G. E. Hutchinson, "A Treatise on Limnology", Vol. 1, "Geography, Physics and Chemistry", J. Wiley and Sons, New York, N.Y., 1957, Chap. 17, pp 878–902.
(32) H. B. N. Hynes, "Eutrophication: Causes, Consequences, Correctives", National Academy of Science, Washington, D.C., 1969, pp 188–196.
(33) L. M. Jeffrey and D. W. Hood, *J. Mar. Res.*, **17**, 247–271 (1958).
(34) G. Chapman and A. C. Rae, *Nature (London)*, **214**, 627–628 (1967).
(35) H. Irving and R. J. P. Williams, *J. Chem. Soc.*, 3192–3210 (1953).
(36) K. W. Hanck and J. W. Dillard, *Anal. Chim. Acta*, **89**, 329–338 (1977).
(37) P. L. Brezonik, P. A. Brauner, and W. Stumm, *Water Res.*, **10**, 605–612 (1976).
(38) P. G. C. Campbell, N. Kinsey, and A. Tessier, unpublished work, University of Quebec, 1976.

RECEIVED for review April 11, 1977. Accepted September 20, 1977. This research was supported by the Quebec Department of Natural Resources, Water Quality Branch, and by the National Research Council of Canada.

CORRESPONDENCE

Molecular Weight and Association of Coal-Derived Asphaltenes

Sir: Molecular weight measurements on petroleum asphaltenes have been carried out by a variety of techniques, and the results used to form hypotheses about the state of association of these molecules in solution and their macrostructures (*1*). Very little similar research has been published on coal-derived asphaltenes. The association of these species and their derivatives has been reported in the literature in terms of hydrogen-bonded complexes which can be separated into acidic and basic components (*2*). Nuclear magnetic resonance studies of hydrogen bonding between coal asphaltene fractions and the OH proton of *o*-phenylphenol, or the nitrogen electron donors pyridine (*3*) and quinoline (*4*) have been described. We now wish to report on the preliminary results obtained by studying Vapor Pressure Osmometry (VPO) molecular weights of coal-derived asphaltenes, and coal-derived asphaltene derivatives as a function of concentration in the solvents benzene and tetrahydrofuran.

EXPERIMENTAL

Coal-derived asphaltenes were separated by solvent fractionation (*5*, *6*) from coal liquids produced in five major demonstration liquefaction processes: Synthoil, HRI H-Coal, FMC COED, Catalytic Inc. SRC, and PAMCO SRC.

A Mechrolab Model 301A Vapor Pressure Osmometer was used to determine molecular weights with benzil employed as a standard. In normal runs, 6–8 concentrations over the range 4–36 g/L were employed in the solvents benzene or tetrahydrofuran for extrapolation to infinite dilution. A plot of the data for a sample of Synthoil asphaltene is shown in Figure 1. Computer-assisted least-squares analysis was carried out for the linear portions of each curve. The resulting lines, with accompanying standard deviations of the slopes and intercepts of the lines along with correlation coefficients, are presented in Tables I and II for the coal-derived asphaltenes, and products derived from Synthoil asphaltene by silylation and chromatographic fractionation on silica gel. Trimethyl silyl ethers of asphaltenes were synthesized by refluxing the asphaltene with excess 1,1,1,3,3,3-hexamethyldisilazane (HMDS) in dry tetrahydrofuran, and the number of trimethylsilyl groups introduced was determined by silicon analysis (*7*). Under the conditions used to silylate the asphaltenes, nitrogen-containing functional groups in coal have been reported not to react to form derivatives (*7*). We found no evidence for NH silylation by examining the asphaltenes before and after silylation with infrared spectroscopy in dilute carbon disulfide solutions (*8*).

RESULTS AND DISCUSSION

The results shown in Figure 1 and Tables I and II indicate that association of coal-derived asphaltenes takes place in both benzene and tetrahydrofuran over the concentration range of 4–36 g/L. All of the asphaltenes afford positive linear correlations between concentration and molecular weight. Correlation coefficients are reasonably significant. (The correlation coefficients of 15 of the 19 least-squares equations presented in this paper are ≥ 0.95 which indicates that the simplifying assumption that molecular weights vs. concentration may be reasonably approximated as linear in dilute solution, is valid.) The slopes of the linear correlation lines are greater in benzene than in THF, but the molecular weight values obtained by extrapolating the plots to infinite dilution are in very good agreement. This suggests that association is more significant in the less polar solvent benzene, but that coal-derived asphaltene dissociation tends to go to completion in either solvent at infinite dilution.

Table I. Molecular Weight of Asphaltenes vs. Concentration[a] in Benzene and THF

Asphaltene	Solvent	Least-squares equation	Corr. coeff.	Av. MW at zero concn	Dev., %
Synthoil	THF[b]	MW = 2.85 ± 0.96 C + 568 ± 17.5	0.83		
		MW = 2.42 ± 0.10 C + 562 ± 2.2	0.99	561	1.0
	Benzene	MW = 11.1 ± 0.60 C + 552 ± 10.4	0.995		
HRI H-Coal	THF	MW = 3.02 ± 0.36 C + 471 ± 6.0	0.95	492	4.3
	Benzene	MW = 6.27 ± 0.30 C + 513 ± 7.6	0.99		
FMC-COED	THF	MW = 0.16 ± 0.10 C + 382 ± 1.9	0.89	375	1.9
	Benzene	MW = 5.61 ± 0.26 C + 368 ± 4.5	0.99		
Cat. Inc. SRC	THF	MW = 1.11 ± 0.38 C + 486 ± 7.6	0.77	483	0.5
	Benzene	MW = 4.74 ± 0.58 C + 481 ± 12.1	0.95		
PAMCO SRC	THF	MW = 1.83 ± 0.16 C + 502 ± 3.3	0.96	533	5.6
	Benzene	MW = 7.26 ± 0.51 C + 563 ± 10.1	0.98		

[a] Concentration, g/L. [b] Results from two asphaltene samples prepared independently.

Table II. Molecular Weight of Synthoil Asphaltene Products vs. Concentration[a] in Benzene and THF

	VPO solvent	Least-squares equation	Corr. coeff.	Av. MW at zero concn	Dev, %
Starting asphaltene	THF[b]	MW = 2.42 ± 0.10 C + 562 ± 2.2	0.99		
		MW = 2.85 ± 0.96 C + 568 ± 17.5	0.83	561	1.0
	Benzene	MW = 11.1 ± 0.60 C + 552 ± 10.4	0.995		
Silylated asphaltene	THF	MW = 1.35 ± 0.13 C + 639 ± 2.5	0.97		
	Benzene	MW = 4.93 ± 0.95 C + 600 ± 21.9	0.87	620	3.1
Benzene eluted asphaltene from silica gel (45)[c]	THF	MW = 2.03 ± 0.09 C + 521 ± 1.8	0.99	534	2.3
	Benzene	MW = 3.71 ± 0.27 C + 546 ± 6.5	0.97		
Et_2O eluted asphaltene from silica gel (37)[c]	THF	MW = 2.68 ± 0.30 C + 512 ± 7.6	0.95	521	1.5
	Benzene	MW = 8.0 ± 0.20 C + 531 ± 4.9	0.997		
THF eluted asphaltene from silica gel (benzene soluble) (9)[c]	THF	MW = 1.16 ± 0.09 C + 472 ± 3.0	0.98	472	—
THF eluted asphaltene from silica gel (benzene insoluble) (9)[c]	THF	MW = 6.84 ± 0.70 C + 869 ± 21	0.98	869	—

[a] Concentration, g/L. [b] Results from two asphaltene samples prepared independently. [c] Percent recovered from solvent elution chromatography.

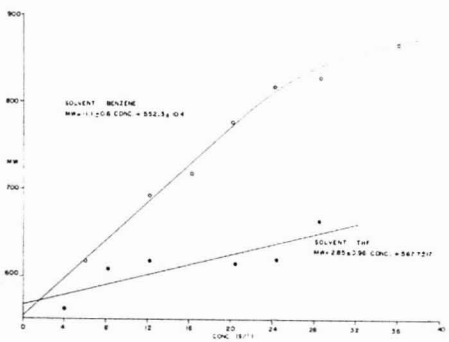

Figure 1. VPO molecular weights vs. concentration of Synthoil asphaltene in benzene and THF

The results are significant because the majority of molecular weight data for coal liquefaction products, and coal-derived asphaltenes are reported for VPO molecular weights measured in benzene at finite concentrations. Such values, in many cases, represent the number average molecular weights of associated species, not the molecular weight of the true dissociated monomeric species.

The molecular weights of Synthoil asphaltene products vs. concentration in benzene and THF are shown in Table II. The slopes of the equations are lower in THF than in benzene, as were the slopes of the other asphaltene equations. The value found for the silylated asphaltene, 620, is in good agreement with a calculated value of 605 for a Synthoil asphaltene which has 48% of its oxygen silylated. Solvent elution chromatography with silica gel has been scaled up, and a third minor fraction has been obtained, by elution with tetrahydrofuran, in addition to the two major fractions previously reported by elution with benzene and diethyl ether (*5*, *6*). The third fraction was found to be only ≈50% soluble in benzene. The benzene insoluble portion had a molecular weight of 869 which explains why the benzene and diethyl ether fractions previously reported (*5*) could have MW value less than the starting asphaltene. Assuming complete dissociation at infinite dilution, the arithmetically combined molecular weights of the separated components afford a calculated molecular weight of 541 for the starting asphaltene. This value is in excellent agreement with the value of 561 measured directly from the whole asphaltene.

If one considers the slope of the MW vs. concentration curve as a measure of association, then it is instructive to consider

Table III. Slope of Molecular Weight vs. Concentration

Asphaltene	Slope
Starting	11.1
48% O silylated	4.9
Benzene eluted from silica gel	3.7
Et_2O eluted from silica gel	8.0

how association would be expected to vary among the different asphaltene products. Since the slopes and association are greater in benzene, we will consider only that series (Table III). We feel that these preliminary results tend to support the hydrogen bonding donor–acceptor (*5, 6*) model of coal-derived asphaltene association (*2–4*) more than the charge transfer complexation model previously suggested to explain association in petroleum asphaltene (*10–12*). Actually, the donor–acceptor concept is a much more universal and broad principle (*9*).

The reasoning for this is as follows: silylation eliminates phenolic OH functions and would be expected to reduce H-bonding; the benzene eluted fraction from silica gel is known to have a reduced basic nitrogen concentration (*5, 6*) which would also reduce the hydrogen-bonding possibilities; the Et_2O eluted fraction, which contains the major portion of both the basic nitrogen and oxygen, still contains some phenolic OH (*5, 8*), and therefore would be expected to show the smallest decrease in associative properties relative to starting asphaltene.

In conclusion, the extrapolated molecular weights, at zero concentration, for coal-derived asphaltenes and their derivatives are found to be almost identical in the solvents benzene and tetrahydrofuran. The average deviation found is 2.5% for eight such asphaltenes in benzene and tetrahydrofuran. This implies that coal-derived asphaltenes approach complete dissociation as their concentrations approach infinite dilution in both benzene and tetrahydrofuran in contrast to petroleum-derived asphaltenes which are apparently not dissociated in either benzene (*13*), or tetrahydrofuran (*1*) over the ranges 2–7 wt % and 1.2–2.4 wt %, respectively. For the former case, with Athabasca asphaltenes, a solvent of higher polarity, such as pyridine, was required to cause significant variation in the observed molecular weights as a function of concentration.

ACKNOWLEDGMENT

The authors thank the FMC Corporation, Hydrocarbon Research, Inc., Catalytic Inc., PAMCO, and the Pittsburgh Energy Research Center of ERDA for generously supplying samples of their coal liquid products.

LITERATURE CITED

(1) J. R. Dickie and T. F. Yen, *Anal. Chem.*, **39**, 1847 (1967).
(2) H. N. Sternberg, R. Raymond, and F. K. Schweighardt, *Science*, **188**, 49 (1975).
(3) F. K. Schweighardt, R. A. Friedel, and H. L. Retcofsky, *Appl. Spectrosc.*, **30**, 291 (1976).
(4) S. R. Taylor, L. G. Galya, B. J. Brown, and N. C. Li, *Spectrosc. Lett.*, **9**, 733 (1976).
(5) I. Schwager and T. F. Yen, *Am. Chem. Soc., Div. Fuel Chem., Prepr.*, **21** (5), 199 (1976).
(6) I. Schwager and T. F. Yen, in "Liquid Fuels from Coal", R. T. Ellington, Ed., Academic Press, New York, N.Y., 1977, pp 233–248.
(7) S. Friedman, L. Zahn, M. Kaufman, and I. Wender, *Fuel*, **40**, 38 (1961).
(8) I. Schwager, P. A. Farmanian, and T. F. Yen, *Am. Chem. Soc., Div. Pet. Chem., Prepr.*, **22** (2), 677 (1977).
(9) T. F. Yen, in "Workshop on Coal Chemistry Preprint", Stanford Research Institute, 1976, pp 144–164.
(10) G. A. Sill and T. F. Yen, *Fuel*, **48**, 61 (1969).
(11) T. F. Yen, *Fuel*, **52**, 93 (1973).
(12) T. F. Yen and D. K. Young, *Carbon*, **11**, 33 (1973).
(13) S. E. Moschopedis, J. F. Fryer, and J. G. Speight, *Fuel*, **55**, 227 (1976).

I. Schwager
W. C. Lee
T. F. Yen*

University of Southern California
Chemical Engineering Department
University Park
Los Angeles, California 90007

RECEIVED for review July 18, 1977. Accepted September 12, 1977. This research was supported by the United States Energy Research and Development Administration under contract No. E(49-18)-2031.

Interference of 1-Chloro-2-propanol in the Determination of Bis(chloromethyl) Ether in Air by Gas Chromatography–Mass Spectrometry

Sir: Selected ion monitoring (SIM) is frequently used for the determination of bis(chloromethyl) ether (BCME), a highly toxic and carcinogenic compound (*1–4*). The retention time of BCME on a GC column and the strongest mass fragments at m/e = 79, 81, 49, and 51 produced under electron-impact (EI) conditions are used (*5–7*). In this correspondence it will be shown that under these circumstances and using a high resolution glass capillary column with the commonly applied GC phase SE-30, the presence of BCME is not unambiguously established.

Recently we investigated the headspace above soil contaminated with degradation products of burned polyurethane foam used for thermal isolation. The air was sampled with Tenax GC. The compounds trapped were desorbed by heat and subsequently separated on a high-resolution SE-30 glass capillary column. Figure 1 shows the resulting gas chromatogram. Identification of the compounds was carried out on a Varian MAT 112 GC/MS/DS combination using direct coupling of the capillary column and continuous repetitive measurement of mass spectra. Figure 2 shows the EI mass spectrum at the top of GC peak 1. Besides the base peak at m/e = 45 and lower mass fragments, the spectrum contained fragments at m/e = 79/81 and 49/51 of which the intensity ratio corresponded with the ratio in a reference spectrum of BCME. Under the gas chromatographic conditions used, the retention time of GC peak 1 was identical with that of BCME, so it seemed likely that BCME was present in the headspace. However, in that case m/e = 45 and some lower mass fragments, which are absent in the reference spectrum of BCME, must be attributed to another compound eluting at the same time as BCME from the column.

A more satisfactory explanation can be found if it is as-

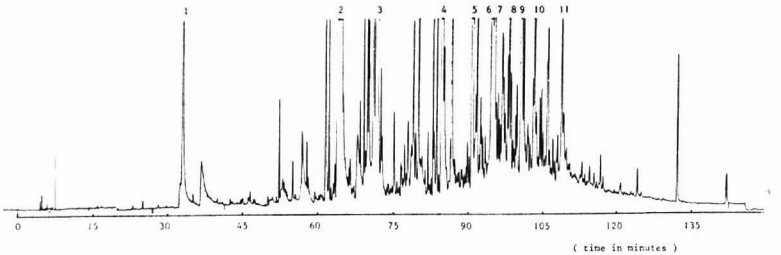

Figure 1. Gas chromatogram of the air sample. Column, 60 m × 0.25 mm i.d. glass capillary column coated with SE-30; temp. program, 0–200 °C with 2 °C/min; carrier gas, helium, 0.8 kg/cm^2. Identified compounds: (1) 1-chloro-2-propanol; (2) aniline; (3) *O*-toluidine; (4) quinoline; (5,6,7) methylquinolines; (8) ethylquinoline; (9) dimethylquinoline; (10) anthracene; (11) phenanthrene

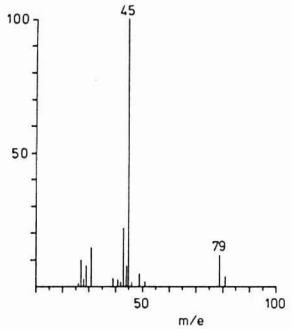

Figure 2. Electron impact mass spectrum of compound 1

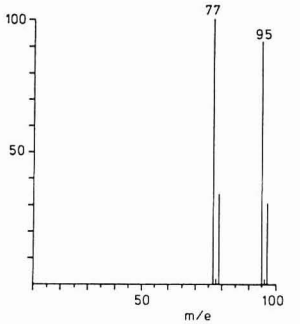

Figure 3. Isobutane chemical ionization mass spectrum of compound 1

sumed that the compound under investigation is 1-chloro-2-propanol. Indeed, the spectrum of GC peak 1 corresponded roughly with a reference spectrum of 1-chloro-2-propanol.

Figure 3 shows the isobutane chemical-ionization mass spectrum of GC peak 1. The spectrum contained fragments at m/e = 95/97 corresponding with the $(M + H)^+$ ion of 1-chloro-2-propanol and at m/e = 77/79 corresponding with the loss of water, a characteristic fragment of isobutane CI mass spectra of secondary alcohols (*8*). Based on these CI results, GC peak 1 was definitely identified as 1-chloro-2-propanol. This compound gives the same retention time on a SE-30 column and produces mass fragments at m/e = 79/81 and 49/51 in the same intensity ratio as BCME. Therefore, 1-chloro-2-propanol could be mistaken as BCME by using SIM on a SE-30 column and again it is demonstrated that, even using sophisticated methods for the determination of a specific compound, this still may yield false results.

ACKNOWLEDGMENT

A. C. Lakwijk (Centraal Laboratorium TNO) is gratefully acknowledged for recording the mass spectra.

LITERATURE CITED

(1) B. L. van Duuren, B. M. Goldschmidt, L. Langseth, G. Mercado, and A. Sinak, *Arch. Environ. Health*, **16**, 472 (1968).
(2) B. L. van Duuren, A. Sinak, B. M. Goldschmidt, C. Katz, and S. Melchionne, *J. Natl. Cancer Inst.*, **43**, 481 (1969).
(3) K. J. Leong, H. N. Mac Farland, and W. H. Reese, Jr., *Arch. Environ. Health*, **22**, 663 (1971).
(4) S. Laskin, M. Kuscher, R. T. Drew, V. P. Capiello, and N. Nelson, *Arch. Environ. Health*, **23**, 135 (1971).
(5) L. A. Shadoff, G. I. Kallos, and J. S. Woods, *Anal. Chem.*, **45**, 2341 (1973).
(6) K. P. Evans, A. Mathias, N. Mellor, R. Sillvester, and A. E. Willams, *Anal. Chem.*, **47**, 821 (1975).
(7) L. S. Frankel and R. F. Black, *Anal. Chem.*, **48**, 732 (1976).
(8) B. L. Jelus, R. K. Murray, Jr., and B. Munson, *J. Am. Chem. Soc.*, **97**, 2362 (1975).

Frans L. Schulting*
Eric R. J. Wils

Chemical Laboratory TNO
Rijswijk (ZH)
The Netherlands

RECEIVED for review July 18, 1977. Accepted September 28, 1977.

Exchange of Comments: Repetitive Determination of Isonicotinic Acid Hydrazide in Flow-Through Systems by Series Reactions

Sir: We read with interest the recent paper by Dutt and Mottola (*1*) where a procedure is proposed for the repetitive analysis of isonicotinic hydrazide. The procedure is reported to be rapid, highly selective, and particularly applicable where an automated procedure is indicated. We wish to comment on that aspect of the report which concerns the application to pharmaceutical dosage forms. The authors employed the USP XVIII method (*2*) which involves an iodometric titration procedure. This method was found to be inapplicable for dosage forms containing reducing sugars as excipients. As a result of a comparative study of four commonly used assay procedures (*3*), the nitrite titration was adopted in USP XIX (*4*) which has been *official* since July 1, 1975. The nitrite method does not suffer from the drawbacks noted for the iodometric method.

The authors appear to be confused about compendial specifications. In the last sentence of their paper they state "The content of isoniazid found per tablet was, however, consistently lower than the minimum 98.0% stipulated by the USP XVIII." While the potency statement for the drug entity, Isoniazid USP, is "not less than 98.0 percent····"; "Isoniazid Tablets contain not less than 93.0 percent and not more than 107.0 percent of the labeled amount of $C_6H_7N_3O$." The authors apparently conducted single tablet assays, whereas the *official* procedure calls for samples obtained from a powder mass representative of not less than 20 tablets. Furthermore, the monograph includes a *Content Uniformity* specification (*4*). This is a test for homogeneity based on the individual tablet analysis of 10 tablets. The specification is met if the content of each of the 10 tablets falls within the limits of 85.0 percent and 115.0 percent of the average of the potency limits specified in the monograph. Under certain conditions it is even possible for the specification to be met if a single tablet falls within the range of 75.0 percent and 125.0 percent of the average of the potency limits specified in the monograph.

LITERATURE CITED

(1) V. V. S. Eswara Dutt and H. A. Mottola, *Anal. Chem.*, **49**, 776 (1977).
(2) "The United States Pharmacopeia", 18th rev., Mack Publishing Co., Easton, Pa., 1970 p 349.
(3) M. I. Blake, D. Bode, and H. J. Rhodes, *J. Pharm. Sci.*, **63**, 1303 (1974).
(4) "The United States Pharmacopeia", 19th rev, Mack Publishing Co., Easton, Pa., 1975, pp 273, 648.

J. F. Fitzloff

Department of Medicinal Chemistry

M. I. Blake*

Department of Pharmacy
University of Illinois at the Medical Center
Chicago, Illinois 60612

RECEIVED for review May 20, 1977. Accepted August 29, 1977.

Sir: Two distinctive elements can be identified in Fitzloff and Blake's note. They: 1) point out that in the XIX Edition of the USP the nitrite method has been adopted for isoniazid determination, and, 2) make reference to a misquote in the last paragraph of our paper (*1*).

We concede that at the time of performing the work reported in our paper, we had access to the XVIII Edition of USP, but the XIX Edition was not yet in our library. We did, however, indicate in the introduction (reference 17 in our paper) that Blake et al. (2) compared four widely used standard methods and recommended the nitrite method on the basis of recoveries obtained in the presence of glucose, sucrose, lactose (this corresponds to reference 3 in their comments). It shall be pointed out that for the particular case of tablets, the iodometric procedure seems to give satisfactory results for comparison since interfering sugars, if present, do not cause serious problems as might be the case with samples normally containing higher amounts of sugar, such as syrups. Blake et al. (2) provided results pointing in this direction (Table in p 1304 there) and went further concluding that (p 1305) "Consistent results were obtained for the analysis of the tablet dosage form by the four methods."

In their comments on our limited application to tablets, Fitzloff and Blake disclosed a misquote in the last paragraph of our paper (*1*). Their comments on compendial specifications are well taken and we apologize to the readers for failing to correct this on time. We reported results for three tablets but collected data for more tablets and in most instances (9 out of 10) the percent content was lower than 93.0. With respect to this, and as indicated earlier (*1*), in our method the presence of common diluents, such as sugars, starch, citric and oxalic acid, exert no interference even if present in a thousandfold excess with respect to isoniazid.

We hope these comments clarify the matter and reiterate our belief that the determination proposed by us is simpler, faster, and more easily adapted to automation than other reported methods, particularly if compared with the nitrite titration as it is specified in XIX USP (*3*).

LITERATURE CITED

(1) V. V. S. Eswara Dutt and H. A. Mottola, *Anal. Chem.*, **49**, 776 (1977).
(2) M. I. Blake, D. Bode, and H. J. Rhodes, *J. Pharm. Sci.*, **63**, 1303 (1974).
(3) "The United States Pharmacopeia," 19th rev., Mack Publishing Co., Easton, Pa., 1975.

V. V. S. Eswara Dutt

Department of Health and Human Ecology
California State College
San Bernardino, California 92407

Horacio A. Mottola*

Department of Chemistry
Oklahoma State University
Stillwater, Oklahoma 74074

RECEIVED for review July 8, 1977. Accepted August 29, 1977.

AIDS FOR ANALYTICAL CHEMISTS

Analyzer for Determining Fuel Vaporization Pressure Curves of Gasoline and Gasoline–Alcohol Fuels

John H. Baudino, Frank J. Chloupek, and Arthur W. Crowley*

Atlantic Richfield Company, Harvey Technical Center, Harvey, Illinois 60426

Volatility characteristics of gasolines have been related to engine performance as detailed in a review by G. H. Unzelman and E. S. Forster of Ethyl Corporation (*1*). The typical volatility characteristics of fuels RVP, T° (V/L 20) and 10, 50 and 90% evaporated temperatures are measured by ASTM Methods D-323, D-2533, and D-86 or D-216, respectively. These fuel properties, which are used as production specifications, are all measured under equilibrium conditions or as a function of changing temperature and are method dependent.

This paper describes the development of an analyzer for determining a nonequilibrium volatility characteristic of fuels. The characteristic is the pressure increase with time resulting from the vaporization of a fuel. The property is measured while vaporizing a fuel sample under conditions of constant volume, temperature, and initial reduced pressure. This characteristic should be more representative of fuel performance than one measured under equilibrium conditions because fuel vaporization does not reach equilibrium in the intake system of an engine (*2*).

The analyzer and method have been named the Fuel Vaporization Pressure Analyzer (FVP Analyzer) and Fuel Vaporization Pressure Test (FVP Test), respectively. The output of the analyzer is the fuel vaporization pressure curve, a pressure vs. time curve, which is unique for each fuel. The fuel is injected with a snap sample injector into a vaporization chamber and the pressure of vaporization is recorded on a calibrated strip-chart recorder. Only a small quantity of fuel (40–80 μL) is required for the measurement. The use of a snap sample injector, described in the paper, makes it possible to introduce a known quantity of fuel into the analyzer while having a minimum effect on the vaporization pressure results. The test conditions of the vaporization chamber can be varied to provide the capability of determining vaporization pressure curves of fuels over a wide range of conditions.

In addition to the analyzer design, this paper covers the results of experiments which show the effects of sample size, initial pressure, and temperature on the fuel vaporization pressure curves. The precision of the test method is demonstrated by repeatability experiment results using isooctane and Indolene clear gasoline. Also reported are the vaporization pressure curves of fuels containing alcohol. These fuels have been difficult to characterize by the usual test methods (*3–5*).

In general, using this analyzer and method, fuels can be characterized by their vaporization pressure curves rapidly with good precision. The potential of predicting a fuel's performance from its vaporization pressure curve has been demonstrated using gasoline and gasoline–alcohol fuels (*4*). Experiments are in progress to further demonstrate the applications of the FVP Test results and will be the subject of a future paper.

EXPERIMENTAL

Apparatus. The Fuel Vaporization Pressure Analyzer consists of a nominal 1-L spherical glass vaporization chamber, diagramed in Figure 1, equipped with two pressure transducers (Validyne DP-15), a sheathed thermocouple, a nominal 500-mL reference pressure reservoir, and a fixed-volume snap sample injector. The sample injector is positioned so that vaporization takes place in the center of the sphere. A catch pan is positioned immediately below the end of the sample injector rod to retain all of the fuel in the center of the chamber.

The snap sample injector is detailed in Figure 2. It is a modification of the type previously offered by Precision Sampling Corporation for injection of smaller size samples (*6*). A calibrated circular groove in the injector rod holds a known volume of sample when the rod is withdrawn into a Teflon sleeve. In this position, the sleeve seals the sample until injection, and the sample injector can be dried, heated, or placed in a vacuum without loss of sample. This type of injector was chosen so that the small fuel samples could be accurately injected with a minimum effect on the vaporization pressures caused by the injection.

The chamber and other items shown in Figure 1 are mounted in a constant temperature box and attached to a standard vacuum system for evacuating and adjusting the test pressure. This system consists of a vacuum pump, manometer, 0.0 to 20.0 mm Hg range Dubrovin vacuum gauge, and cylinder of dry, hydrocarbon-free air. The transducers are connected to demodulators (Validyne CD-15) calibrated to different sensitivities and the output signals are recorded on a variable chart speed, two-channel recorder (Hewlett-Packard Model 7100B with Model 17501A multiple span modules). Temperatures are recorded on a multipoint recorder. The chamber temperature and initial pressure can be adjusted within the ranges of −18.0 to +38.0 ± 0.03 °C and 0.1 mm Hg to atmospheric pressure, respectively. The precision of these test pressure measurements is ±0.02 from 0.1 to 20.0 mm Hg and ±0.5 mm Hg from 20 mm Hg to atmospheric pressure. The two valves located at the bottom of the chamber are Fischer & Porter Co. Quick Opening Threaded Glass Valves with Teflon stems and a 4-mm base size.

Reagents. The analyses of the Indolene clear gasoline and other test fuels are given in Table I.

Procedure. A 100-mL sample of fuel to be tested is conditioned to a constant temperature (4.0 to 24.0 ± 0.02 °C) in a sealed bottle using a constant temperature bath. A volume of the fuel is then sampled with the snap sample injector, taking precautions to ensure that no air is taken in with the sample. The injector is positioned and secured in the center of the vaporization chamber while maintaining the chamber at the test temperature under a slight positive pressure with dry air. The system is evacuated to 0.1 mm Hg, pressurized back to atmospheric pressure and evacuated to 0.1 mm Hg again to purge the chamber of any hydrocarbons remaining from the previous run. The pressure is then adjusted to the desired test pressure. After the system is equilibrated at the test temperature and pressure (about 10 min), valves 1 and 2 shown in Figure 1 are closed.

The differential pressure is set at zero and observed to ensure no leaks and complete equilibration of the system before injection of the fuel sample. The recorder is started (2.54 cm/s) and the sample is injected into the vaporization chamber. As the fuel vaporizes, the increasing pressure is detected by the pressure transducers and the different sensitivity outputs are recorded continuously on the strip-chart recorder. The outputs are set to give full scale readings of 6.33 ± 0.007 and 19.00 ± 0.02 mm Hg to cover the vaporization pressure ranges of most fuel samples.

Table I. Analyses of Test Fuels

Fuel	Indolene Clear	A	B	C	D	E	EA	F	FA	G	GA
Alcohol, vol %	0	0	0	0	0	0	5	0	5	0	5
RVP, psi[a]	10.2	11.0	13.2	14.4	9.9	9.4	13.0	9.2	11.9	13.8	16.7
T ° F (V/L 20)[b]	132	124	110	112	140	...	...	...	...	...	...
Distillation (D 86), °F											
% Evaporated											
IBP	89	99	81	...	100	97	95	92	95	87	85
10	128	120	103	90	137	137	116	123	109	102	94
20	154	136	114	155	183	185	147	142	116	112	101
30	181	158	127	205	214	208	204	158	145	125	108
40	205	181	142	216	229	227	225	179	171	141	129
50	225	205	164	219	239	237	236	207	198	163	157
60	243	230	189	224	250	244	245	233	223	197	191
70	264	259	215	228	270	257	258	269	261	227	224
80	291	301	229	234	326	286	286	322	316	245	245
90	327	343	254	247	398	353	356	351	345	277	276
EP	408	420	375	379	488	469	460	439	432	405	402

[a] Modified to use no water for fuels containing alcohol. [b] Modified to use mercury for fuels containing alcohol.

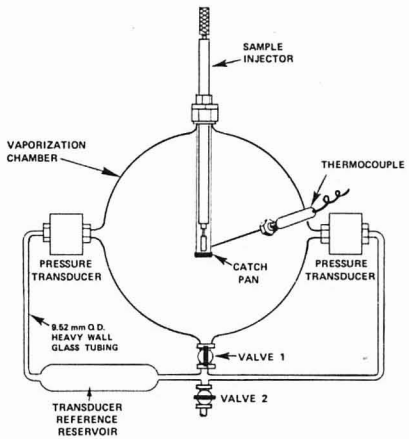

Figure 1. Schematic drawing of fuel vaporization pressure apparatus

When the pressure approaches a constant value, the recorders are turned off, valve 1 is opened to equalize the pressure between the chamber and reference reservoir and then valve 2 is opened. The system is pressurized to a slight positive pressure and the sample injector is removed and made ready for the next sample.

Calibration. The responses of the transducers are set at the desired sensitivities by pressurizing the system with air to the desired full scale pressure and adjusting the output of the demodulators to full scale. The analyzer is zeroed before each run and the calibration is checked daily or when necessary. The check is made by measuring the vaporization pressure of a span liquid under total vaporization conditions (0.1 mm Hg and 24 °C). The normal span liquid is isooctane. To check the span at lower temperatures, *n*-pentane is used.

The snap sample injector volumes are calibrated using isooctane vaporization pressures obtained at 0.1 mm Hg pressure and 24 °C and then back-calculating the liquid volume injected using the ideal gas equation. The volumes of the sample injectors used for this study were determined to be 76.7, 58.1, and 38.8 ± 0.2 μL.

Since each injector rod occupies a certain volume, which results in a pressure increase when the sample is injected, a correction in the pressure readings is necessary. The pressure correction for this volume is determined by injecting an empty sample injector, with the sample space at the same pressure as in the chamber, into the chamber and measuring the increased pressure under test conditions. In addition, the vaporization pressure data reported in this paper are corrected to a standard chamber volume of 1.00 L.

Table II. Repeatability Data

	PVP, mm Hg						TVP,
Time, s	0.50	1.0	3.0	6.0	12.0	30.0	mm Hg
	Indolene clear						
Run No.							
1	1.02	1.49	2.34	2.94	3.58	4.61	10.14
2	0.91	1.37	2.19	2.75	3.40	4.46	10.04
3	0.99	1.45	2.25	2.81	3.43	4.45	10.08
4	0.89	1.31	2.21	2.80	3.41	4.42	10.06
5	0.85	1.33	2.20	2.83	3.50	4.55	10.06
6	0.90	1.35	2.16	2.74	3.38	4.44	10.16
Av	0.93	1.38	2.23	2.81	3.45	4.49	10.09
Std dev	0.06	0.07	0.06	0.07	0.08	0.08	0.05
Range	0.17	0.18	0.18	0.20	0.20	0.19	0.12
	Isooctane						
Run No.							
1	0.10	0.17	0.45	0.86	1.32	1.74	9.00
2	0.07	0.14	0.42	0.80	1.25	1.73	9.02
3	0.08	0.15	0.43	0.81	1.27	1.78	9.04
4	0.10	0.17	0.44	0.83	1.28	1.74	9.00
5	0.10	0.16	0.43	0.82	1.29	1.84	9.02
6	0.09	0.16	0.44	0.83	1.29	1.83	9.00
7	0.10	0.16	0.44	0.84	1.32	1.86	9.02
Av	0.09	0.16	0.44	0.83	1.29	1.79	9.01
Std dev	0.01	0.01	0.01	0.02	0.03	0.05	0.02
Range	0.03	0.03	0.03	0.06	0.07	0.11	0.04

RESULTS AND DISCUSSION

The vaporization pressure curves of isooctane and Indolene clear fuel in Figure 3 were determined with the FVP Analyzer. A 76.7-μL sample was vaporized at 24 °C and an initial reduced pressure of 660 mm Hg. These curves show the pressure rise with vaporization for 30 s, but data were recorded until all the fuel vaporized or a constant pressure was approached. Vaporization of the sample occurs at the center of the chamber. The pressure increase in the chamber was found to be uniform, as indicated by identical responses by the two transducers. Under these test conditions, the total vaporization pressure of some fuel samples is approached within 10 min. However, with the initial conditions of 24 °C and 0.1 mm Hg pressure, most samples approach total vaporization within 5 to 6 s. Results obtained at 0.1 mm Hg reduced pressure will be referred to as total vaporization pressures (TVP's) and those at higher pressures as partial vaporization pressures (PVP's).

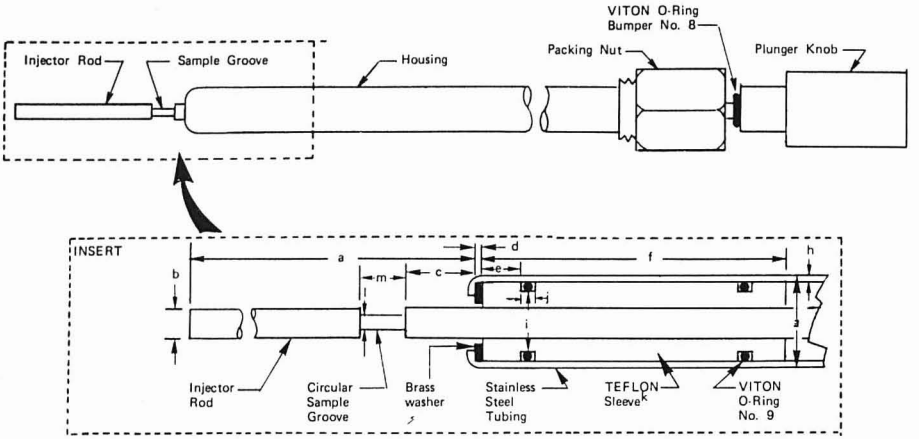

Figure 2. Schematic drawing of snap sample injector. Cut-away schematic drawing of packing to hold fuel sample is shown in insert. a = 41.3 ± 0.5 mm, b = 4.648 ± 0.013 mm, c = 6.35 ± 0.02 mm, d = 1.24 ± 0.38 mm, e = 6.0 ± 0.5 mm, f = 50.8 ± 0.5 mm, g = 9.52 ± 0.10 mm, h = 0.51 + 0.02, −0.04 mm, i = 5.97 ± 0.02 mm, j = 2.007 ± 0.025 mm, k = 4.648 ± 0.025 mm i.d., 8.560 + 0.000, −0.051 mm od, l = 2.381 ± 0.013 mm, m = as required for sample size

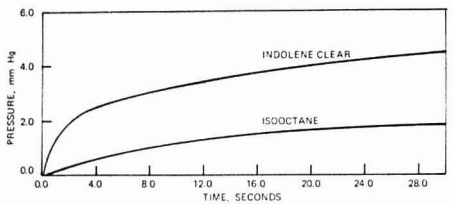

Figure 3. Vaporization pressure curves

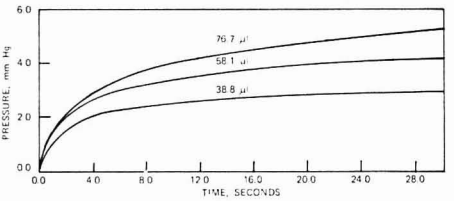

Figure 4. Effect of sample size on FVP curves with Fuel A

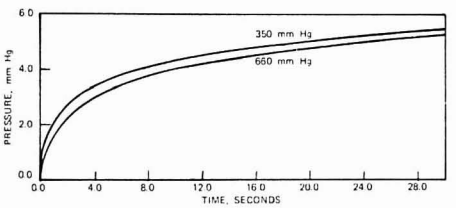

Figure 5. Effect of initial pressure on FVP curves with Fuel A

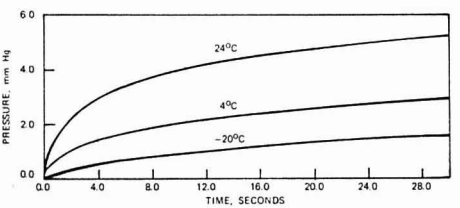

Figure 6. Effect of temperature on FVP curves with Fuel A

The repeatability of the test method is very good under both of the above conditions. Repeatability data using Indolene clear and isooctane are given in Table II. The PVP data were obtained using 76.7-μL samples at 24 °C and 660 mm Hg initial pressure. The maximum pressure ranges with Indolene clear and isooctane are 0.2 and 0.1 mm Hg, respectively. As expected, the data using the pure material, isooctane, is more repeatable. Also given in Table II are the TVP results for Indolene clear and isooctane. These tests were made using 76.7-μL samples at 24 °C and 0.1 mm Hg initial pressure. These data indicate that TVP's can also be measured with good precision.

Effect of Variables. All measurements are made at the same chamber volume of 1 L but the sample size, initial pressure, and temperature can be varied to determine a fuel's vaporization pressure curve under different test conditions. The effects of these variables on vaporization curves were evaluated using a typical full boiling range gasoline, Fuel A.

The effect of sample size on the vaporization curve was determined at 24 °C and an initial reduced pressure of 660 mm Hg. Three different sample injectors were used to inject 76.7, 58.1, and 38.8 μL. The Figure 4 curves show the greatest effect of sample size to be on the initial vaporization pressures, i.e., within about the first 24 s. The effect then decreases with time until the vaporization pressure increases are directly proportional to the increase in sample size.

The effect of initial pressure was determined using a 76.7-μL sample at 24 °C and two initial reduced pressures of 660 and 350 mm Hg. The maximum effect, as shown in Figure 5, occurs after 2 s of vaporization. The effect then decreases and becomes insignificant as vaporization nears completion.

The effect of temperature on the vaporization pressure curve is shown in Figure 6. The three vaporization pressure

Table III. Partial and Total Vaporization Pressure Data on Test Fuels

Fuel	Time, s	PVP, mm Hg 0.50	0.75	1.0	3.0	6.0	12.0	30.0	60.0	120	240	360	600	900	TVP, mm Hg
A		1.0	1.3	1.5	2.6	3.4	4.2	5.3	6.1	6.9	7.6	8.1	8.5	8.7	9.4
B		1.3	1.9	2.1	3.6	4.5	5.5	7.0	8.0	8.0	9.5	9.9	10.1	10.2	10.6
C		1.4	1.6	1.8	2.6	3.1	3.7	4.4	5.3	6.2	7.5	8.3	9.1	9.8	10.6
D		0.8	1.0	1.1	1.6	2.0	2.4	3.1	3.6	4.5	5.5	6.1	6.7	7.0	7.9
E		0.7	0.9	1.0	1.6	2.0	2.4	3.2	3.9	4.8	5.8	6.1	...	...	8.4
EA		1.0	1.4	1.6	2.5	3.1	3.6	4.4	5.1	6.0	7.0	7.6	...	...	9.5
F		0.9	1.2	1.5	2.8	3.7	4.4	5.4	6.1	6.8	7.4	7.8	...	...	9.1
FA		1.1	1.5	1.8	3.1	4.0	4.9	6.2	7.1	7.9	8.5	8.8	...	...	10.1
G		1.0	1.9	2.2	3.6	4.6	5.5	6.9	7.8	8.6	9.3	9.6	...	...	10.6
GA		1.8	2.4	2.8	4.4	5.5	6.5	8.0	8.8	9.6	10.3	10.6	...	...	11.6

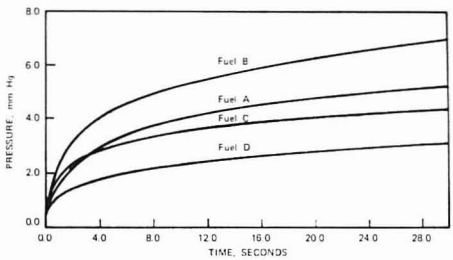

Figure 7. FVP curves of typical fuels

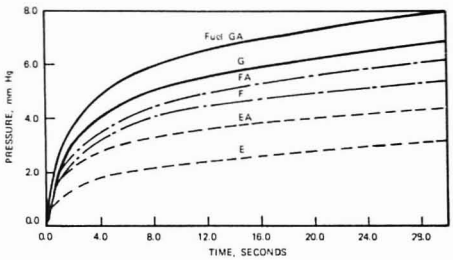

Figure 8. FVP curves of fuels with and without alcohol

curves of Fuel A were determined using a 76.7-μL sample at an initial reduced pressure of 660 mm Hg. The fuel sample was vaporized at 24, 4, and −20 °C. The rate of vaporization is shown to change with temperature and the effect is nonlinear.

FVP Curves of Typical Fuels. The differences between the vaporization pressure curves of fuels are demonstrated using fuels covering the distillation range of most gasolines produced, Fuels A through D. The vaporization pressure curves of these fuels were recorded for 15 min using a 76.7-μL sample at 24 °C and an initial reduced pressure of 660 mm Hg. Partial vaporization pressure (PVP) readings taken along the curves are listed in Table III, and the first thirty-second section of the vaporization pressure curves are shown in Figure 7. As shown by these curves, each fuel has a characteristic curve which is dependent on the composition of the fuel.

The total vaporization pressures (TVP's) of these fuels are also listed in Table III. The TVP's were determined using 76.7-μL samples at 24 °C and an initial reduced pressure of 0.1 mm Hg. At these conditions, the fuels approach total vaporization within 5 to 6 s with the possible exception of Fuel D, the highest boiling range fuel. The TVP of a fuel can then be used along with the PVP at any time to calculate the percent vaporized.

Alcohol–Gasoline Fuels. The usual volatility characterization tests, D-86 distillation, RVP, and T° (V/L 20), all require modifications or additional data interpretation to be applied to alcohol–gasoline fuels. The RVP test must be run dry and the calculation modified to measure fuels of this nature (7). The T° (V/L 20) test uses glycerin, but when alcohol is present in the fuel, mercury must be used (7). Normal interpretation of the distillation data will lead to erroneous driveability conclusions due to the "alcohol plateau" (4).

To determine the potential of the FVP test for characterizing fuels containing alcohol, three base gasolines were formulated to represent low, medium, and high volatility gasolines, Fuels E, F, and G, respectively. To each of these fuels five volume percent alcohol (4:1 volume ratio of methanol to *tert*-butanol) was added to give Fuels EA, FA, and GA.

The fuel vaporization pressure readings from the curves measured using the fuels with and without alcohol are listed in Table III along with the TVP data on these fuels. The curves were determined using 76.7-μL samples at 24 °C and an initial pressure of 660 mm Hg. Figure 8 shows thirty-second sections of the vaporization pressure curves of the low, medium, and high volatility fuels. The effect of adding five percent of the alcohol mixture to the three gasolines, also given in the Figure, is shown to be variable and may be composition dependent. However, the effect on the TVP is independent of the base gasoline, with a constant 1 mm Hg pressure increase for the five percent added alcohol as shown in Table III.

ACKNOWLEDGMENT

The authors thank J. A. Glover, R. P. Page, D. C. Tong, J. G. Vlasic, and A. G. Widen for their valuable contributions to this study.

LITERATURE CITED

(1) G. H. Unzelman and E. S. Forster, *Pet. Refiner*, **39**, 109 (1960).
(2) E. F. Obert, "Internal Combustion Engines and Air Pollution", Intext Educational Publishers, New York and London, 1973, p 253.
(3) E. E. Wigg and R. S. Lunt, SAE Paper No. 741008 (1974).
(4) A. W. Crowley et al, SAE Paper No. 750419 (1975).
(5) S. J. W. Pleeth, "ALCOHOL—A fuel for Internal Combustion Engines",Chapman & Hall Ltd., London, 1949, pp 211–213.
(6) Catalog PS-72, Precision Sampling Corporation.
(7) P. P. Lifland, Mobil Research and Development Corporation, Paulsboro, N.J., personal communication, October 4, 1974.

RECEIVED for review May 12, 1977. Accepted August 29, 1977. This research was conducted under contract of the Inter-Industry Emission Control Program-2 (IIEC-2) as Atlantic Richfield Program I of Project V (Alternate Fuels).

Modified Microwave-Induced Plasma Discharge Chamber

Andrew T. Zander,[1] Rod K. Williams, and Gary M. Hieftje*

Department of Chemistry, Indiana University, Bloomington, Indiana 47401

Microwave-induced plasmas (MIP's) in argon or helium possess a number of advantages for use as excitation sources in atomic emission spectrometry (*1, 2*). These plasmas have high excitation temperatures so that a great number of elements, including the halogens and many nonmetals, can be determined at high sensitivity in the UV and visible regions. The power required for stable operation of an MIP is relatively low, generally below 200 W. Also, atmospheric-pressure argon or helium plasmas consume much less support gas than other types of plasmas, and have minimal requirements for cooling. Because of their low operating power, these plasmas often produce unusually low background molecular spectra, further enhancing their utility.

An MIP is formed in a discharge tube placed in a cavity to which microwave power is transmitted via a coaxial cable or waveguide. The most frequently used resonant cavities for operation at 2450 MHz are the $^1/_4$-wave Evenson cavity and the $^3/_4$-wave Broida cavity (*3*). The plasma can be viewed either radially or axially.

By far, the most extensive use of MIP's as emission sources has been as detectors for gas chromatographic systems (*4–11*). The GC carrier gas can be argon or helium and the generally used flow rates are compatible with stable MIP operation. In such an application, the MIP has been employed to excite elements such as C, H, N, P, B, O, and the halogens, providing highly selective and sensitive detection and determination.

The major limitation to using the MIP as an emission source in present configurations revolves around injection of aerosol samples into the plasma. The low power ordinarily utilized does not afford a high enough plasma energy density to evaporate and atomize aqueous droplets. Also, the stability of the plasma is degraded when even a relatively small amount of sample material is injected. These problems have not proved to be insurmountable, but they have hindered extensive use of MIP's in optical emission analysis.

The problems associated with aerosol sample injection into MIP's have been alleviated in two ways. In the first approach, an aerosol desolvation system (*12*) is placed between the nebulizer and the plasma to evaporate and remove the solvent from the gas stream before the sample reaches the plasma (*13, 14*). Although this method offers high nebulization efficiency, the MIP is still required to atomize the analyte from the resulting dry aerosol particles.

Alternatively, the liquid sample can be both desolvated and atomized prior to its introduction into the MIP (*15–18*). The low current, low power microarc atomizer described by Layman and Hieftje (*15*) serves this purpose; analyte atoms are generated efficiently by cathodic sputtering of the sample applied to a tungsten filament external to the MIP. However, in the original configuration (*15*), the microarc was interfaced to the plasma chamber in such a way that the MIP extinguished when solvent was evaporated into it. Evaporation rates of approximately 6 μL/m were used. To overcome this limitation, provision for automatic reignition of the plasma with a high voltage spark was made. Fricke, Rose, and Caruso (*16, 17*) have taken advantage of the high atomization efficiencies of carbon cup and tantalum-ribbon electrothermal atomizers to release analyte atoms for injection into an MIP. In this application, the plasma was kept from being extinguished by carefully controlling the solvent evaporation rate to less than 1.7 μL/min, thereby also lengthening the analysis time. Recently, Kirkbright (*18*) described a new commercial MIP system which utilizes a Ta-ribbon atomizer. In this system, solvent vapor is vented away from the MIP, enabling continuous operation of the plasma without increasing analysis time. However, this venting requires careful control of the gas flows to ensure stable plasma operation.

In the present study, a new method was developed for operating an MIP on a continuous basis, and in conjunction with an external desolvation and atomization system. With this method, the MIP is not extinguished during solvent evaporation, drying time of the applied sample is not extended, and extra venting of the evaporate is not necessary. In the new approach, a portion of the MIP is kept operating by partially isolating it from the rest of the plasma within the plasma chamber. This auxiliary or "pilot" plasma is bypassed during sample or solvent injection and is therefore not affected by such events. Of course, during solvent evaporation, the primary excitation plasma is extinguished; however, the microwave cavity is thermally stabilized during this period by the existence of the auxiliary plasma. Following desolvation, the "pilot" plasma automatically reignites the primary discharge. In addition to the convenience it provides, the auxiliary plasma eliminates the necessity of retuning the cavity.

EXPERIMENTAL

The atmospheric pressure argon MIP was powered by a 100-W microwave generator (Model HV-15A, Scintillonics, Inc., Fort Collins, Colo.) which was stabilized by a 500-W Sola constant voltage power transformer. The 2450-MHz output is conducted via a $^3/_8$-in. coaxial cable (Type RG-9, Belden Corp., Richmond, Ind.) to a $^3/_4$-wave Broida cavity, fitted with a double-stub tuner (Model 306A, PRD Electronics, Westbury, Long Island, N.Y.) for impedance matching.

The plasma exists near the tuning-stub end of the cavity inside a 6-mm i.d. quartz chamber. As shown in Figure 1, sample vapor is introduced into the plasma at a point approximately halfway between the plasma ends. During emission measurements, the plasma is viewed axially. Into one end of the plasma chamber, a smaller quartz tube (4-mm i.d.) was inserted. Within this inner sleeve were positioned two tightly fitting carbon washers (4-mm o.d., 2-mm i.d., 2 mm long) made from spectrographic-grade graphite rod (National Carbon Co., Union Carbide Corp.); the carbon washers are spaced approximately 1 cm apart and enclose approximately $^1/_3$ of the MIP region.

Primary argon flow to the MIP at approximately 375 mL/min is from the external sample atomization apparatus located in a direction perpendicular to the plasma chamber. An auxiliary argon flow, of about 75 mL/min, enters the chamber axially from the direction of the pilot plasma and enables a stable plasma to exist between the carbon washers. The primary MIP passes through the carbon washer at its one end; this results in stable positioning of the plasma in the center of the chamber.

The sample introduction system was based on a microarc atomizer (*15*); however, the microarc housing and electrode configuration were modified somewhat for improved operational and mechanical stability. This modified configuration will be described in a later communication; of course, any sample introduction system can be used which desolvates and atomizes the sample external to the MIP.

In operation, the MIP is ignited within the cavity by means of a Tesla coil. The presence of the carbon washers does not adversely affect the ignition or the tunability of the cavity, and aids in reducing plasma wander. Aqueous samples are applied

[1] Present address, Department of Chemistry, Cleveland State University, Cleveland, Ohio 44115.

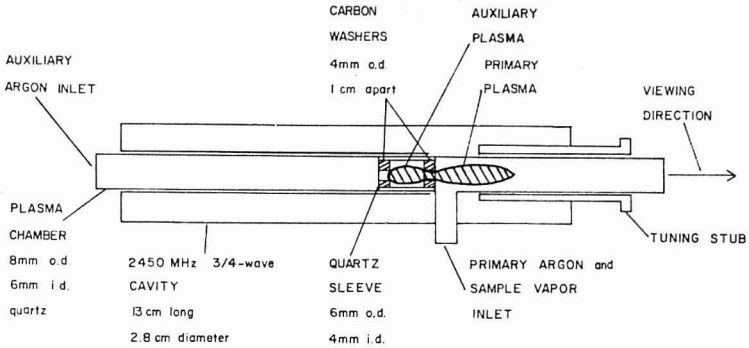

Figure 1. $^3/_4$-wave resonant cavity with modified plasma chamber

with a syringe in microliter amounts to the microarc filament. The sample is then dried, at a rate between 2 to 6 μL/min, by heating the filament with a constant current between 1 and 2 A. During drying, the evaporated solvent is carried through the plasma chamber by the primary argon flow; depending upon the rate of solvent evaporation, the primary MIP will either be weakened or extinguished. However, the auxiliary plasma is unaffected by the passage of solvent vapor and continues to operate, keeping the chamber thermally stabilized. After removal of all solvent vapor from the cell, the primary MIP is reignited by the pilot plasma and rapidly stabilizes. The microarc is then struck to atomize the sample and send it into the discharge.

The flow rates for the primary and auxiliary inlets, 375 mL/min and 75 mL/min, respectively, were chosen to optimize sample transport to the MIP and reduce the effects of the presence of the carbon washers within the plasma chamber, while minimizing auxiliary plasma instability. Excessively high primary flow rates were found to produce a primary plasma which bent around the sample inlet port; too low a flow rate leads to an easily extinguished MIP.

The auxiliary flow rate is also critical. Below approximately 50 mL/min, the auxiliary flow produces a plasma which rotates at high speed around the edges of the carbon washer placed at the argon inlet end of the plasma. This rotation adds a high frequency fluctuation to the background signal level. Coincident with rotation, the auxiliary plasma appears bluish green in color, indicative of emission from carbon (C_2) in the plasma. Above 50 mL/min, the auxiliary plasma remains centered and stationary and appears identical in color and configuration to the primary MIP.

RESULTS AND DISCUSSION

Portions of the argon MIP spectrum were scanned to determine the effect of the graphite washers on the spectral character of the plasma. The C I line at 2478.6 Å was easily observable as were most other lines, at very low intensity, of the Swan system ($A^3\pi_g - X^3\pi_u$) of the emission spectrum of C_2. There was no evidence of the weaker C_2 systems, or any of the C_3 spectrum. These spectral features could all be decreased to negligible levels, except for the C I 2478.6-Å line, by appropriate adjustment of the auxiliary argon flow. The use of the plasma for C detection is thus restricted. The carbon pieces never become hot enough to glow and no evidence of increased continuum background emission was noted.

The excitation temperature of the MIP with and without the carbon washers in place was determined by measuring the relative radiances of argon lines having known wavelengths, energies, and transition probabilities (*19*). Table I lists the argon lines used. The plasma was viewed axially using a quartz lens to focus an unmagnified image of the plasma on the entrance slit of the monochromator. The temperature of the

Table I. Argon Lines Used for Excitation Temperature Estimation (*20*)

λ(A)	E_k, cm^{-1}	g_i	g_k	A_{ki}, 10^8 s^{-1}
4333.56	118469	3	5	0.0060
4300.10	116999	3	5	0.00394
4272.17	117151	3	3	0.0084
4266.29	117184	3	5	0.00333
4259.36	118871	3	1	0.0415
4200.67	116943	5	7	0.0103
4198.32	117563	3	1	0.0276
4190.71	116999	5	5	0.00254
4181.88	118460	1	3	0.0058
4164.18	117151	5	3	0.00295
4158.59	117184	5	5	0.0145
4044.42	118469	3	5	0.00346
3948.98	118460	5	3	1.5 x 10^{-4}

Table II. Detection Limit[a] Comparison between Unmodified and Modified MIP's

Element	Wavelength, nm	Unmodified MIP[b] detection limit, pg	Modified MIP detection limit, pg
Ca	422.7	10.0	3.2
Cu	324.7	1.6	7.4
Pb	283.3	3.8	3.8

[a] Detection limit taken at S/N = 2. [b] Taken from Ref. 15.

MIP with the graphite-contained auxiliary plasma was determined to be approximately 4300 K while the temperature of the unmodified MIP in the same cavity was 5100 K. Although the difference in excitation temperature is significant, the lower temperature of the auxiliary-plasma-aided MIP is still within the range of excitation temperatures routinely encountered with MIP's (2), and is not expected to adversely affect the capability of the MIP for excitation.

The signal levels obtained with the auxiliary-plasma-aided MIP were equivalent to those produced by the unmodified MIP. However, reproducibility of the signals was substantially improved, 3% RSD compared to 15–25% (*15*), probably because the unmodified MIP requires reignition by a spark after solvent evaporation. Because reignition employs as one electrode the grounded microarc sample filament, the analyte which was earlier dried on the filament might be lost or disrupted somewhat during reignition.

Table II lists representative detection limits obtained with the unmodified and modified MIP; as expected, no appreciable difference exists between the different sets.

CONCLUSIONS

Modification of the plasma chamber for an MIP by causing an auxiliary plasma to exist between two carbon washers within the plasma chamber affords a simple and efficient means of interfacing MIP's and external sample atomization systems.

The auxiliary plasma does not eliminate drift of the MIP spectral background when sample vapor is carried into the chamber; even the smallest amount of solvent vapor causes such changes. However, drift severity is reduced in that the MIP is never totally extinguished.

LITERATURE CITED

(1) S. Greenfield, H. McD. McGreachin, and P. B. Smith, *Talanta*, **22**, 553 (1973).
(2) R. K. Skogerboe and G. N. Coleman, *Anal. Chem.*, **48**, 611A (1976).
(3) F. C. Fehsenfeld, K. M. Evenson, and H. P. Broida, *Rev. Sci. Instrum.*, **36**, 294 (1965).
(4) A. J. McCormack, S. C. Tong, and W. D. Cooke, *Anal. Chem.*, **37**, 1470 (1965).
(5) C. A. Bache and D. J. Lisk, *Anal. Chem.*, **39**, 786 (1967).
(6) R. M. Dagnall, S. J. Pratt, T. S. West, and D. R. Deans, *Talanta*, **16**, 797 (1969).
(7) R. M. Dagnall, S. J. Pratt, T. S. West, and D. R. Deans, *Talanta*, **17**, 1009 (1970).
(8) C. A. Bache and D. J. Lisk, *Anal. Chem.*, **43**, 950 (1971).
(9) W. E. Grossman, J. Eng, and Y. C. Tong, *Anal. Chim. Acta*, **60**, 447 (1972).
(10) H. Kawaguchi, T. Sakamota, and A. Mizuike, *Talanta*, **20**, 321 (1973).
(11) Y. Talmi and D. T. Bostick, *Anal. Chem.*, **47**, 2145 (1975).
(12) C. Veillon and M. Margoshes, *Spectrochim. Acta, Part B*, **23**, 553 (1973).
(13) F. Lichte and R. K. Skogerboe, *Anal. Chem.*, **45**, 399 (1973).
(14) R. K. Skogerboe and G. N. Coleman, *Appl. Spectrosc.*, **30**, 504 (1976).
(15) L. R. Layman and G. M. Hieftje, *Anal. Chem.*, **47**, 194 (1975).
(16) F. Fricke, O. Rose, and J. A. Caruso, *Anal. Chem.*, **47**, 2018 (1975).
(17) F. Fricke, O. Rose, and J. A. Caruso, *Talanta*, **23**, 317 (1976).
(18) G. Kirkbright, Paper No. 454, Pittsburgh Conference on Analytical Chemistry and Applied Spectroscopy, Cleveland, Ohio, March 1977.
(19) H. R. Griem, "Plasma Spectroscopy", McGraw-Hill, New York, N.Y., 1964.
(20) W. L. Wiese, M. W. Smith, and B. M. Miles, "Atomic Transition Probabilities", National Bureau of Standards Publication 22, Vol. II, U.S. Department of Commerce, October 1969.

RECEIVED for review June 3, 1977. Accepted August 24, 1977. This work was supported in part by the Office of Naval Research and by the National Science Foundation.

Monitoring and Identification of Nonvolatile Organic Deposits in Used Catalysts

Jacob Shen* and J. L. O'Kane

The Standard Oil Company (Ohio), 4440 Warrensville Center Road, Warrensville Heights, Ohio 44128

Pyrolysis gas chromatography has been much used in the characterization of nonvolatile materials such as polymers (*1*, *2*), solid samples from natural resources (*3-5*), samples of biological interest (*6-8*), etc. The coupling of a pyrolysis device to other analytical instruments such as a combined GC/MS system has made possible on-line identification of pyrolyzates, and thus added another useful dimension to the technique. Literature reports on the use of pyrolysis for catalyst analysis, however, have been few. This paper describes the use of a combined Pyrolysis GC/MS/Computer system for the determination of nonvolatile organic deposits in used catalysts.

Nonvolatile organics deposited in the catalyst may reduce the effective surface area of the latter. They may also upset the calculation of carbon balance which is usually based on the gas chromatographic analysis of reactor effluents. A fast, convenient, and sensitive method to monitor and identify the nonvolatile organics deposited in used catalyst is therefore desirable. The information obtained can be invaluable in regenerating the used catalyst.

EXPERIMENTAL

The basic configuration of the combined CDS 100/Varian 1200/Finnigan 3000/System 150 pyrolysis GC/MS/Computer system has been described previously (*9*). A CDS 100 pyrolyzer with a coil probe was used for pyrolysis. Typically 10 ~30 mg of a used catalyst was ground and placed in between two glass wool plugs in a small quartz tube which could be placed in the middle of a coil probe. The coil probe was then inserted into a heated chamber connected to the analytical column through a heated switching valve. Pyrolysis was subsequently carried out at 800 °C for 10 s. The pyrolyzates were swept into the column and separated and identified by the combined GC/MS/computer system.

The GC column used was a glass one (10 feet × $^1/_8$ foot) packed with Carbowax 20M supported by Gas Chrom Q 80/100 mesh. The oven temperature was programmed from room temperature to 180 °C at 6 °C/min. The helium flow rate used was 20 mL/min.

RESULTS AND DISCUSSION

Figure 1 shows the computer reconstructed pyrogram of a used catalyst recovered from a hydrocarbon reactor. A good amount of CO_2 and water are observed. Benzene is also identified as a major pyrolyzate. In addition, a small amount of phenol is also present in the pyrogram.

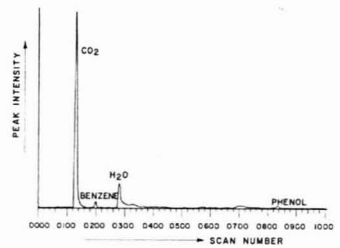

Figure 1. Pyrogram (800 °C/10 s) of a used catalyst recovered from a hydrocarbon reactor

Prior to its pyrolysis, the used catalyst sample has been heated in the heated chamber at 200 °C for 20 min. No organic volatiles, however, have been observed in this heating period. This further indicates that benzene and other pyrolyzates are not trapped organics in the used catalyst, but are actually thermodegradative products of some relatively nonvolatile materials deposited in the catalyst.

When a new catalyst sample is pyrolyzed under identical conditions, none of these organic pyrolyzates has been observed, indicating that catalyst itself is not the source for organic compounds observed. The presence of organic deposits in the used catalysts has been further confirmed by total organic carbon (TOC) analysis showing about 1% (wt %) of total organic carbon.

The observation of phenol is interesting. Since pyrolysis of the catalyst sample took place 20 min after it was put into the heated chamber, pyrolysis actually took place in a helium atmosphere. Hence, phenol must not be a thermal oxidation product and should be a pyrolyzate directly derived from an oxygen-containing nonvolatile deposit in the catalyst. It therefore indicates that oxidation of the hydrocarbon feed

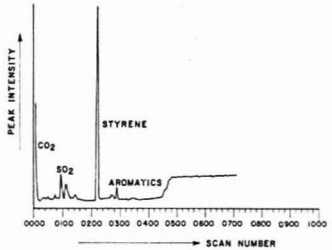

Figure 2. Pyrogram (800 °C/10 s) of a used catalyst from an unsaturated hydrocarbon reactor

apparently has taken place leading to the formation of some oxygen-containing oligomers which may have subsequently deposited in the catalyst.

The results obtained thus can be useful in providing information pertaining to the reaction mechanisms that might have taken place under the catalytic conditions used. The results can also provide useful information for the regeneration of the used catalyst.

Figure 2 shows the pyrogram of another used catalyst recovered from a C_4 olefin reactor. Styrene was observed as the single major pyrolyzate in this case. A small amount of other aromatic fragments was also observed.

It is well known that predominantly styrene monomer is recovered in the pyrolysis of polystyrene. The observation of styrene as the single major pyrolyzate in the pyrogram of a used catalyst thus indicates polystyrene may have been deposited in the catalyst during the reaction. Styrene monomer must have resulted from dimerization of the original feed.

In our experience, a small amount of sample (~10 mg) has been generally adequate for this type of analysis. The catalyst recovered from the reactor can be directly used for analysis without any pretreatment or extraction. Valuable information pertaining to the chemical characteristics of the nonvolatile organic deposits can be obtained in less than an hour from the time a catalyst sample is taken from the reactor.

LITERATURE CITED

(1) T. A. Gough and C. E. R. Jones, *Chromatographia*, **8**, 696 (1975).
(2) C. E. R. Jones and G. E. J. Reynolds, *Br. Polym. J.*, **1**, 197 (1969).
(3) R. L. Hanson, N. E. Vanderborgh, and D. G. Brookins, *Anal. Chem.*, **49**, 390 (1977).
(4) R. P. Suggate, *N.Z. J. Sci.*, **15**, 601 (1972).
(5) J. Romovacek and J. Kubat, *Anal. Chem.*, **40**, 1119 (1968).
(6) H. L. C. Meuzelaar, P. G. Kistemaker, and M. A. Posthumus, *Biomed. Mass Spectrom.*, **1**, 312 (1974).
(7) W. B. Stavinoha and S. T. Weintraub, *Anal. Chem.*, **46**, 757 (1974).
(8) J. P. Anhalt and C. Fenselau, *Anal. Chem.*, **47**, 219 (1975).
(9) J. Shen, *Anal. Chem.*, **49**, 886 (1977).

RECEIVED for review July 25, 1977. Accepted September 5, 1977. Permission for Publication by the Standard Oil Company (Ohio) is gratefully acknowledged by the authors.

Removal of Europium Shift Reagents from Nuclear Magnetic Resonance Samples

Gary P. Juneau[1]

Department of Chemistry, Louisiana State University, Baton Rouge, Louisiana 70803

The addition of tris-(1,1,1,2,2,3,3-heptafluoro-7,7-dimethyloctane-4,6-dionato)europium(III), $Eu(fod)_3$, to organic substrates containing complex-forming functional groups, e.g., –OH, $–NH_2$, etc., generally results in downfield displacements of NMR signals (*1*, *2*). These lanthanide induced shifts are sometimes useful in separating overlapping signals and obtaining information concerning intermolecular distances. Approximately 15 mg of the substrate is usually required to obtain acceptable spectra using continuous wave NMR spectrometers, and in many instances where only a small quantity of a sample is available, it is quite desirable to recover the sample after completion of the shift reagent experiment.

Bisbenzylisoquinoline alkaloids and sesquiterpene lactones have been successfully separated from $Eu(fod)_3$ by this method. Reagent grade chloroform and methanol were used in the procedure. The $Eu(fod)_3$ was supplied by Aldrich Chemical Co. and the silica gel by Brinkman Instruments, Inc.

Active silica gel, 50–200 mesh, suitable for column chromatography, is swelled with chloroform and poured into a 1 cm × 10 cm column. The solution containing the mixture of the sample plus the shift reagent is carefully poured into the top. The column is then eluted with 25 mL of chloroform followed by 15 mL of 20% methanol in chloroform, and 3-mL fractions are collected. $Eu(fod)_3$ is eluted in the first two or three fractions and can be found by its bright red-orange fluorescence under short-wave ultraviolet light. The substrate can be located in the methanol–chloroform fractions by fluorescence or by evaporation. After the procedure is completed, no evidence of the shift reagent can be found in the NMR spectrum of the purified substrate.

While this technique permits easy recovery of valuable organic samples for other experiments, it is difficult to ensure the purity and quality of the shift reagent removed. The europium complex should not be re-used because it may be partially hydrolyzed or contaminated with traces of associated nucleophiles such as alcohols, water, etc., from the solvents.

[1]Present address, Mississippi State Chemistry Laboratory, Mississippi State, Starkville, Miss. 39759.

ACKNOWLEDGMENT

The author acknowledges George Newkome for his helpful advice.

LITERATURE CITED

(1) A. Cockerill, G. Davies, R. Harden, and D. Rackham, *Chem. Rev.*, **73**, 553 (1973).
(2) B. C. Mayo, *Chem. Soc. Rev.*, **2** (1), 49 (1973).

RECEIVED for review May 16, 1977. Accepted September 9, 1977. This work was supported by the Chemistry Department of Louisiana State University at Baton Rouge.

Borohydride-Flame Determination of Arsenic in Phosphoric Acid

Irving May* and L. Paul Greenland

U.S. Geological Survey, Reston, Virginia 22092

The requirement for the arsenic content of ACS grade of phosphoric acid is limited to not more than 1 ppm As (*1*). The ACS test method is a photometric silver diethyldithiocarbamate procedure. Difficulties with the test have been reported (*2*) because of interference by larger concentrations of antimony frequently present in phosphoric acid. We undertook to test an alternative procedure for determining arsenic in phosphoric acid which would avoid the antimony interference. This was accomplished with a procedure for evolving arsenic using sodium borohydride and determining the arsenic by atomic absorption spectrophotometry using the nitrogen–hydrogen flame. This procedure is a variation of procedures used by others (*3*, *4*) and also in this laboratory for geochemical samples. The work presented here is the first application of a borohydride-atomic absorption method to the determination of arsenic in phosphoric acid. This procedure is more rapid than the silver diethyldithiocarbamate procedure currently used in the ACS test method (*1*).

EXPERIMENTAL

Atomic Absorption Instrument. A Varian Model 1200 was used for this study. The peak-reading mode was employed without background correction. The optimum instrument settings are: Wavelength, 197.2 nm; spectral band pass, 1 nm; current, 7 mA; H_2-7 (approximately 11 L/min); N_2-6 (approximately 10 L/min); burner height, set for maximum sensitivity.

Hydride Generating Apparatus. The reaction flask (Figure 1) consists of a two-necked 100-mL flask connected to a distillation trap and then to a gas inlet adapter. The outlet tube of the adapter is connected to the burner inlet with a short length of Tygon tubing.

Reagents. Sodium borohydride, freshly prepared 5% aqueous solution. Dissolve 2 pellets of sodium hydroxide per 100 mL. Potassium iodide, 10% aqueous solution. Hydrochloric acid, 6N. Standard solution: Dissolve sufficient As_2O_3 in a NaOH solution to give a 1000 ppm As solution. Just before use, dilute 2.0 mL of the standard to 100 mL with 6 N HCl to prepare a standard solution.

Procedure. Pipet 1.0 mL (1.67 g) of a phosphoric acid sample or 0.01–0.06 mL of the standard solution into the reaction flask. Add 20 mL of 6 N hydrochloric acid and swirl the contents of the flask to ensure complete mixing. Add 0.5 mL of the iodide solution and mix. Insert the glass distillation trap and join the assembly with the gas inlet unit. Fill a plastic-tripped plunger-type pipet such as an Oxford pipet with 5 mL of the sodium borohydride solution. Insert the pipet into the 10/30 joint of the reaction flask so as to make a gas-tight seal. Observe absorbance readings using the "A" damping control until the readings stabilize at a minimum value. Set the zero, depress the "peak" and "read" buttons. Deliver the borohydride solution by rapidly depressing the plunger (vigorous evolution of hydrogen produces thorough mixing). Record the peak readings. Repeat for each of the standard solutions. Plot the absorbances vs. the weights of As taken for the standards. Determine the As contents of the sample taken from the curve.

RESULTS AND DISCUSSION

The 197.2-nm line was selected because of its adequate sensitivity but greater freedom from noise compared to the more sensitive 193.7-nm line. The hydride evolution apparatus used here was assembled from standard glassware. An advantage of this generator is the reduction of spray entering the burner compared with other generators. Results comparable to ours should be obtainable with other hydride generating apparatus and with other instruments.

There is a significant difference in sensitivity with most hydride methods between As(III) and As(V), 40% greater for

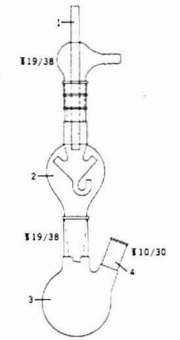

Figure 1. Hydride Generating Apparatus. (1) Nitrogen inlet. (2) Spray trap. (3) 100-mL generating flask. (4) Side-arm inlet for pipet

Table I. Standard Addition Data

As, ppm	Absorbance		
0	0.012	0.010	0.010[a]
0.2	0.065	0.055	0.059[a]
0.4	0.117	0.103	0.083[a]
0.8	0.191	0.197	0.193[a]
1.2	0.236	0.269	0.254[a]

[a] Added as As(V).

Table II. Test of ACS Reagent Grade Phosphoric Acids

Sample		As found, ppm	Recovery of 1 ppm spike, %
Mfr. 1	lot 1	<0.1	99
	lot 2	<0.1	95
	lot 3	<0.1	99
Mfr. 2	lot 1	<0.1	106
	lot 2	<0.1	102

As(III) by our procedure. This difference was demonstrated by Siemer and Koteel (*5*) to be due to the slower reduction of As(V). They overcame this problem by freezing the arsine evolved, then regenerating the arsine for the atomic absorption determination. We reduce any As(V) which may be present to As(III) with potassium iodide prior to the borohydride reduction step. Tests with an arsenic tracer (^{76}As) showed that under the conditions of the determination, 6.0% of the arsenic is not evolved. The efficacy of the iodide reduction was confirmed with a standard addition technique in which phosphoric acid was spiked with both As(III) and As(V). Absorbances of the two As species (Table I) are indistinguishable. The intercept of the standard addition curve yields less than 0.06 ppm As in this phosphoric acid.

Antimony interference is negligible, if it exists at all. Readings obtained for antimony indicate a factor of about 400 in favor of arsenic. It is conceivable that this could be due to traces of arsenic in our antimony salt.

To test our procedure in actual practise, five batches of ACS grade phosphoric acid from two manufacturers were tested. All samples were found to contain less than 0.1 ppm As. The five samples were spiked to contain 1 ppm As and re-analyzed. These results (Table II) confirm the absence of interference

from 1 mL phosphoric acid when diluted with 20 mL of 6 N HCl.

Our data indicate that the sensitivity and precision of this procedure are quite adequate for the ACS test requirement.

LITERATURE CITED

(1) "Reagent Chemicals", American Chemical Society Committee on Analytical Reagents, 5th ed., American Chemical Society, Washington, D.C., 1974.
(2) Private Communications, Members of the ACS Committee on Analytical Reagents.
(3) K. C. Thompson and D. R. Thomerson, *Analyst (London)*, **99**, 595 (1974).
(4) J. A. Fiorino, J. W. Jones, and S. G. Capar, *Anal. Chem.*, **48**, 120 (1976).
(5) D. D. Siemer and P. Koteel, *Anal. Chem.*, **49**, 1096 (1977).

RECEIVED for review June 13, 1977. Accepted September 14, 1977.

Calibration Procedure to Minimize Errors in Continuous Analysis by Ion Selective Electrodes

Lorenzo Liberti* and Antonio Pinto

Istituto di Ricerca Sulle Acque-Consiglio Nazionale delle Ricerche, via De Blasio 5, Zona Industriale, 70122 Bari, Italy

The response time, i.e., the time lag required for ion selective electrodes to assume their new equilibrium potential when subjected to a rapid change in activity of the primary ion, in some cases represents the most critical limitation to application of ion potentiometry to continuous analysis(*1*).

This report describes a simple procedure to minimize errors related to the use of ion selective electrodes in continuous monitoring. The electrode response after a selected time is compared with a calibration curve obtained contacting the electrodes with standard solutions for the same time. One is thus able to continuously monitor quickly changing concentrations, provided the appropriate calibration curve is used.

This "dynamic" calibration procedure has been satisfactorily used to study the kinetics of the exchange reaction between Na_2SO_4 solutions and anion resins in chloride form.

EXPERIMENTAL

In the rate measurements about 10 mg of chloride resin were brought in contact with 0.8 L of a Na_2SO_4 solution in a thermostated vessel. Stirring speed and Na_2SO_4 concentration ranged between 2000–4000 rpm and 1×10^{-3}–1.8 N respectively. The chloride release was followed by a Cl-Select-ion and a Lazaran reference electrode, using an Expandomatic SS-2 potentiometer (all from Beckman Instruments Inc.), and the mV variations were recorded by a Philips PM 8010 double channel recorder. The 100% of exchange was usually reached in a matter of minutes.

For each resin, a calibration curve was prepared according to the following procedure. By the aid of an automatic buret (Autoburette ABU 12 from Radiometer, Copenhagen), known amounts of a NaCl solution were continuously added to an Na_2SO_4 solution, using the same experimental conditions (stirring speed, temperature, etc.) as in the related exchange kinetic experiments, and the potential variations recorded. NaCl concentration and feed rate were so adjusted that an over-all amount of Cl^- corresponding to 100% exchange with that resin was added in real time (i.e., the time required for the exchange reaction to be over). By comparison with such dynamic calibration curves, the potential vs. time curves in kinetic runs were converted into concentration vs. time plots.

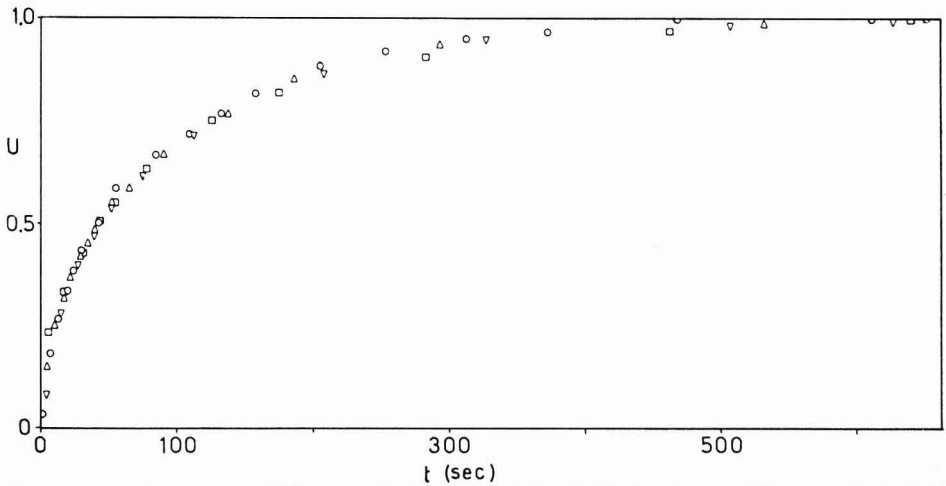

Figure 1. Degree of exchange for Cl^-/SO_4^{2-} exchange kinetics on anion resin Kastel A 105. (Actual variation of Cl^- concentration from 42.6×10^{-3} mequiv/L at time 0 to about 45.6×10^{-3} mequiv/L at equilibrium; 6×10^{-3} N Na_2SO_4) (different symbols are used to identify repeated experiments)

RESULTS AND DISCUSSION

In ordinary exchange runs, very small amounts of resins were used, so that final Cl^- concentrations in solution up to 5×10^{-3} mequiv/L were reached. With the fastest resins, the exchange reaction was completed after about 200 s; hence, an average buildup of about 2.5×10^{-5} mequiv/L s^{-1} of chloride was to be continuously monitored. With system response times experimentally ranging from about 3 to 30 s, depending mainly on Na_2SO_4 concentration, conventional calibration techniques based on equilibrium potentials were not useful in this situation.

Experimental potential vs. time plots were then referred to dynamic calibration curves prepared with Cl^- feed rate $\leq 2.5 \times 10^{-5}$ mequiv/L s^{-1}. The ratio of electrode response time to Cl^- feed rate ranged accordingly between 1×10^3 and 1.2×10^5 L s^2/mequiv. The results of some typical rate measurements made with this procedure are shown in Figure 1, where the degree of exchange ($U = [Cl^-]_t/[Cl^-]_\infty$) with time over a quadruplicate set of runs is reported. As can be seen, good reproducibility is obtained, with a standard deviation lower than ±5%. Furthermore, by allowing the same limited time for potential measurements in the kinetic runs and in the related calibration curves, the precision of the method was assured (actual Cl^- concentrations, obtained by this technique, differed less than ±7% from values calculated on the basis of weight and full exchange capacity of the resin). The proposed procedure is expected to work also in similar applications of continuous ion-selective potentiometry, provided that a sufficiently high ratio ($\geq 10^3$ L s^2/mequiv) between electrode response time and primary ion feed rate is allowed.

LITERATURE CITED

(1) B. Fleet, T. H. Ryan, and M. J. D. Brand, *Anal. Chem.*, **46**, 12 (1974).

RECEIVED for review March 4, 1977. Accepted July 18, 1977.

Demountable Temperature Jump Cell

John R. Sutter*

Chemistry Department, Howard University, Washington, D.C. 20059

Richard M. Reich

American Instrument Company, Silver Spring, Maryland 20910

In general, Temperature Jump Cells are designed with permanently mounted cylindrical or conical quartz rods to guide monochromatic light through the solution onto the detector. This arrangement, however, presents certain limitations for any given cell. Depending on the reaction being investigated, one might need a cell with: long path length in order to use very dilute solutions or compensate for a low absorptivity; minimum heated volume to conserve a precious reactant or to compensate for a small reaction ΔH; a geometry designed to study the fastest reactions (minimize $^1/_2$ RC) or to maintain the temperature after perturbation for the longest possible time in order to study a slower reaction.

We have been experimenting with the cell design shown in Figure 1. The center, transparent, sample compartment is the important feature of the cell. This section is milled from Lucite and the optical surfaces are polished. It is sandwiched between the two Kel-F halves forming the body of the cell and holding the electrodes. The four bolts holding the cell together are not shown in Figure 1. The center section shown has a 1.0-cm by 1.0-cm hole and a thickness of 0.2 cm. The lower electrode mounts flush whereas the upper one is recessed 0.1 cm from the Lucite plate. This recess increases the heated volume to 0.3 mL. The cell has a 1.0-cm light path, and a conductivity cell constant, d/A, of 0.3 cm^{-1}.

Also of importance is the improvement in light gathering ability of this cell. The 1.0- by 0.2-cm cross-section yields a 0.2-cm area which is to be compared to a 0.3-cm diameter circular rod functioning as the cell window. The rod offers only 0.07 cm^2 of window. This represents a maximum increase of 2.8 in available light, producing a corresponding increase in S/N.

The Temperature-Jump apparatus used with the cell has been described previously (*1*). The cell of Figure 1 was tested in the manner outlined there. A block diagram of the cell is also contained there.

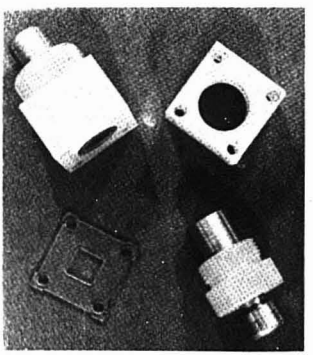

Figure 1. Temperature Jump Cell

A heating time constant of 300 ns is easily obtained. The temperature of the heated solution will persist, with no noticable sag, for about 3 s after perturbation. After this time, the observed absorbance will drift slowly and exponentially (30–45 s) back to the absorbance corresponding to that at the thermostat temperature.

Various sample spacers have been tried, e.g. a. 0.5- by 0.5-cm hole with 0.3-cm thickness will give twice the jump height compared to the cell just described, at a sacrifice in path length

and light gathered. This cell has a conductivity cell constant of 1.6 compared to the cell constant of 0.3 noted for the first cell. This means that for a given salt concentration, the resistance of one cell is 5.3 times larger than the other, and thus the heating time constant is slower by the same amount. Center sections should be chosen with this in mind.

The obvious limitations of the cell are that solvents that attack Lucite cannot be used and that wavelengths in the UV can not be reached with plastic windows.

ACKNOWLEDGMENT

The authors thank Paolo Priarone for the cell construction.

LITERATURE CITED

(1) R. M. Reich and J. R. Sutter, *Anal. Chem.*, **49**, 1081 (1977).

RECEIVED for review May 31, 1977. Accepted September 8, 1977.

Low Volume Reference Electrode for Electrochemical Detection and Fraction Collection in High Performance Liquid Chromatography

Curt R. Freed* and Paul A. Asmus

University of Colorado Medical Center, Division of Clinical Pharmacology: C237, 4200 East Ninth Avenue, Denver, Colorado 80262

High performance liquid chromatography with electrochemical detection (LCEC) has been shown to provide selective and sensitive analysis of easily oxidized organic compounds and was recently reviewed (*1*). The utility of this method for the analysis of catecholamines has been demonstrated (*2*, *3*). We have used modifications of this technology to study brain catecholamine metabolism and have needed to measure both the concentration of trace metabolites and specific activity of a tritium label on dopamine and norepinephrine. Using a commercially available electrochemical detection system (Bio-analytical Systems, West Lafayette, Ind.), we could successfully measure the concentration of catecholamines in rat brain tissue. Because of the large volume of the reference electrode compartment in the standard electrochemical system, however, we could not collect fractions for radioactivity measurements without mixing of adjacent chromatographic bands.

We have developed a modification of the commercial detector which allows both monitoring of the chromatogram and collection of fractions. A simple low volume silver tube with a silver chloride coating is placed in the outflow stream of the electrochemical detection block and serves as a silver–silver chloride reference electrode. Current through the mobile phase is maintained by placing a short length of stainless steel tubing (auxiliary electrode) in the flowing stream. Fractions are collected directly from the steel tubing.

Our present chromatographic system employs an ion-exchange column with acetate/citrate mobile phase and a mobile phase flow rate of 1 mL/min with peak widths of 3.5 and 5.0 mL for norepinephrine and dopamine, respectively. Since the total volume of the reference and auxiliary electrodes is 30 μL, no mixing of chromatographic peaks occurs. The signal-to-noise ratio and sensitivity are the same as the commercial electrode. Because the silver chloride coat of the reference electrode is in the outflow stream, the coating must be reapplied every few days by the electrolytic technique noted below. It should be noted that the arrangment prescribed here will only be useful for trace analysis work where the current is small (typically nanoamperes) and no significant ohmic losses occur.

EXPERIMENTAL

A silver tube was formed from 1 cm × 2 cm × 0.005 inch silver foil (MC & B, Norwood, Ohio) by rolling around a 1-mm o.d. paper clip. The overlap was filled by silver soldering and the resulting tube cleaned with brief exposure to 6 N HNO_3 followed by 0.1 N HCl. Silver chloride was formed on the surface by connecting the silver tube to the positive terminal of a 9-V battery. A platinum electrode was attached to the negative terminal and both electrodes were immersed and current was passed in 0.1 N HCl for 30 s. Figure 1 shows a schematic diagram comparing the two electrode systems. The silver–silver chloride electrode is connected to the outlet of the carbon paste electrode with a short piece of Teflon tubing and fittings. The stainless steel auxiliary electrode is connected to the reference electrode with a short piece of polyethylene tubing. Electrical connections are conveniently made with alligator clips.

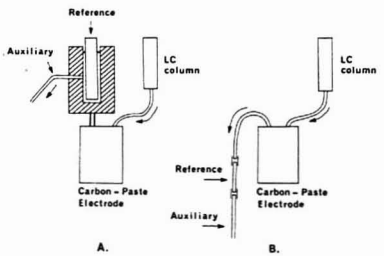

Figure 1. (A) Standard electrochemical detector system. (B) Modified low dead volume reference electrode system with silver–silver chloride tube as reference electrode and stainless steel auxiliary electrode

LITERATURE CITED

(1) P. T. Kissinger, *Anal. Chem.*, **49**, 447A (1977).
(2) C. Refshauge, P. T. Kissinger, R. Dreiling, L. Blank, R. Freeman, and R. Adams, *Life Sci.*, **14**, 311 (1974).
(3) R. Keller, A. Oke, I. Mefford, and R. N. Adams, *Life Sci.*, **19**, 995 (1976).

RECEIVED for review July 11, 1977. Accepted September 9, 1977.

CORRECTION

Steady-State Kinetic Treatment of the Emission from Reduced Pressure Microwave Induced Discharges in Helium

In this article by F. W. Lampe, T. H. Risby, and F. A. Serravallo, *Anal. Chem.*, **49**, 560 (1977), the following changes should be made:

Equation 10:

$$\langle \epsilon \rangle = \pi^2 \nu^2 \lambda^2 m \left(\sqrt{1 + \frac{e^2 E_0{}^2 M \times 10^{14}}{4\pi^4 \nu^4 \lambda^2 m^3}} - 1 \right)$$

$$\frac{e^2 E_0{}^2 M \times 10^{14}}{4\pi^4 \nu^4 \lambda^2 m^3} \leqslant 0.1$$

Equation 11:

$$\langle \epsilon \rangle \approx \frac{e^2 E_0{}^2 M \times 10^{14}}{8\pi^2 \nu^2 m^2} \text{ ergs}$$

Table 1: Electric field (E°) = 18.0 V/cm at 1 Torr Helium

These changes are necessary as a result of a typographical error which was carried through from Equation 10.

CORRECTION

Removal of Water in the Distillation of Hydrocarbon Mixtures

In this article by T. H. Gouw, *Anal. Chem.*, **49**, 1887 (1977), Figure 1 is incorrect. The correct figure is shown here.

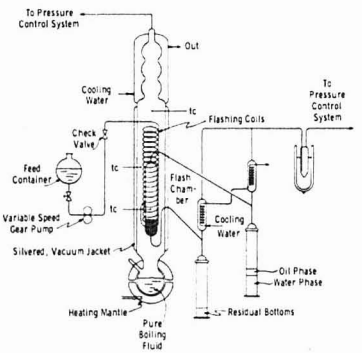

ANALYTICAL CHEMISTRY

VOLUME 49, 1977

Editor, HERBERT A. LAITINEN

EDITORIAL HEADQUARTERS

1155 Sixteenth St., N.W.
Washington, D.C. 20036

Managing Editor: JOSEPHINE M. PETRUZZI

Associate Editor: ANDREW A. HUSOVSKY

Assistant Editors: BARBARA CASSATT, NANCY J. ODDENINO, AND DEBORAH C. STEWART

Editorial Assistant (LabGuide): JOANNE MULLICAN

EDITORIAL DEPARTMENT

20th and Northampton Streets
Easton, Pa. 18042

Head: CHARLES R. BERTSCH
Associate Editor: ELIZABETH R. RUFE

ADVISORY BOARD

DONALD H. ANDERSON, RICHARD P. BUCK, VELMER FASSEL, DAVID FIRESTONE, ROBERT A. HOFSTADER, MARJORIE G. HORNING, PHILIP F. KANE, BARRY L. KARGER, J. JACK KIRKLAND, LYNN L. LEWIS, HARRY B. MARK, JR., WALTER C. MCCRONE, HARRY L. PARDUE, EUGENE A. SAWICKI, W. D. SHULTS

AMERICAN CHEMICAL SOCIETY BOOKS AND JOURNALS DIVISION

Director: D. H. MICHAEL BOWEN

Published by the American Chemical Society, 1155 Sixteenth St., N.W., Washington, D.C. 20036

January	1–192	1A–98A
February	193–352	99A–264A
March	353–528	265A–370A
April	529–688	371A–460A
May	689–896	461A–574A
June	897–1088	575A–668A
July	1089–1280	669A–758A
August	1281–1472	759A–842A
September	1473–1648	843A–964A
October	1649–1888	965A–1080A
November	1889–2128	1081A–1192A
December	2129–2420	1193A–1282A

Annual Reviews (April) 1R–286R

AUTHOR INDEX

Note: In this Author Index, titles of papers are listed after the name of each author of the paper. Multiple authorship is not indicated. Complete authorship may be ascertained by consulting the original paper.

Abe, H. On-line digitization system for a grating infrared spectrophotometer. 1875

Achenbach, M. Quantitative comparison of combined gas chromatographic/mass spectrometric profiles of complex mixtures. 1623

Adam, W. Determination of polymer-supported carbodiimides. 676

Adams, J. M. Quantitative analysis of aluminosilicates and other solids by x-ray photoelectron spectroscopy. 2001

Adams, M. J. Determination of absolute fluorescence quantum efficiency of quinine bisulfate in aqueous medium by optoacoustic spectrometry. 1850

Adams, R. N. Liquid chromatographic determination of picomole quantities of aromatic amine carcinogens. 683

Aikens, D. A. Composition differences in commercial polyethylene bottles and their relation to the stability of stored part-per-billion mercury(II) solutions. 668

Albe, W. R. On-column reaction gas chromatography for determination of chloromethyl methyl ether at one part-per-billion level in ambient air. 1817

Albe, W. R. Determination of anions in boiler blow-down water with ion chromatography. 1176

Alder, J. F. Determination of mercury by atomic absorption spectrometry with graphite tube atomization. 336

Aldous, K. M. Determination of organic carbon by thermal volatilization plasma emission spectrometry. 1235

Aldous, K. M. Design and evaluation of a fiber optic fluorometric flow cell. 2051

Alexander, V. Determination of carotenoid concentrations in marine phytoplankton by resonance Raman spectrometry. 695

Algie, S. H. Empirical approximations to equations based on the error function. 186

Alkemade, C. T. J. Comments on fluorescence excitation profiles in flame. 2111

Allemand, C. D. Modified inductively coupled plasma arrangement for easy ignition and low gas consumption. 1450

Allen, B. J. Quantitative hydrolysis-gas chromatographic methods for the determination of selected acids and glycols in polyesters. 741

Allen, P. V. Determination of ethylene oxide in gas sterilants by Fourier transform infrared spectrometry. 1602

Allwine, K. J. Minicomputer data processing system for air monitoring studies. 357a

Almond, H. R. Jr. Pharmaceuticals and related drugs. 110r

Alonso, J. A. Multiple ion detection system with miniscan facilities and expanded mass range for magnetic sector mass spectrometers. 543

Altree-Williams, S. Quantitative x-ray diffractometry on milligram samples prepared on silver filters. 429

Amato, D. V. Short excitation wavelength fluorometric detection in high-pressure liquid chromatography of indole peptide, naphthyl, and phenol compounds. 1836

Ammons, J. M. Separation and determination of nanogram amounts of inorganic arsenic and methylarsenic compounds. 621

Anbar, M. Glass lined field ionization sources. 2121

Anbar, M. Isotopic assay of nanomole amounts of nitrogen-15 labeled amino acids by collision-induced dissociation mass spectrometry. 1832

Anderle, D. Separation of trioses and tetroses as trimethylsilyl oximes by gas chromatography. 137

Anders, O. U. Representative sampling and proper use of reference materials. 33a

Anderson, D. H. Fourier Transform infrared analysis below the one-nanogram level. 2275

Anderson, P. J. Quantitative comparison of combined gas chromatographic/mass spectrometric profiles of complex mixtures. 1623

Ando, M. E. Sub-part-per-trillion detection of polycyclic aromatic hydrocarbons by laser induced molecular fluorescence. 955

Ando, T. Ligand-exchange gas chromatographic separation of pyridine bases. 1179

Andreae, M. O. Determination of arsenic species in natural waters. 820

Andrew, J. Determination of porphyrins at low concentration using porphinatocopper(II) phosphorescence. 1482

Andrews, J. E. Qualitative analysis of thin gallium nitride films with secondary ion mass spectrometry. 1536

Anese, C. P. Low capacity codes for mass spectra based on statistical moments. 1456

Anson, F. C. Digital device for precise determination of drop times at dropping mercury electrodes. 1270

Anson, F. C. Cyclic and differential pulse voltammetric behavior of reactants confined to the electrode surface. 1589

Anthony, D. H. J. Immiscible solvent extraction scheme for biodegradation testing of polyethoxylate nonionic surfactants. 398

Archer, V. S. Differential pulse polarographic determination of nitrate and nitrite. 479

Arguello, M. D. Ion-exchange separation and determination of calcium and magnesium. 1595

Armstrong, N. R. X-ray photoelectron/Auger electron spectroscopic studies of tin and indium metal foils and oxides. 1228

Arnac, M. Voltammetric and chronopotentiometric studies of the quinone and hydroquinone system in anhydrous formic acid. 806

Arpino, P. Gas-solid and gas-liquid chromatography using porous layer open tube columns made with graphitized thermal carbon black. 768

Arpino, P. Separation of acids from asphalts. 1222

Artigas, F. Multiple ion detection system with miniscan facilities and expanded mass range for magnetic sector mass spectrometers. 543

Arvanitis, S. Mechanism of neutral carrier mediated ion transport through ion-selective bulk membranes. 1567

Asmus, P. A. Low volume reference electrode for electrochemical detection and fraction collection in high performance liquid chromatography. 2379

Ataman, O. Y. Determination of ammonia in aqueous solutions by infrared spectrometry following preconcentration on zeolite. 1331

Atsuya, I. Interelement effects and a possible excitation mechanism in a low-pressure microwave induced helium plasma. 266

Atsuya, I. Enhancement of emission by potassium chloride in the low-pressure microwave-induced plasma emission spectrometer. 1489

Aue, W. A. A high-speed, high-purity extraction apparatus. 1465

Baca, P. Determination of trace levels of nitrates by an extraction-photometric method. 2249

Baillart, J. Multiple ion detection system with miniscan facilities and expanded mass range for magnetic sector mass spectrometers. 543

Baiocchi, F. A. Precision in thermodynamic properties of solution determined by gas-liquid chromatography. 1029

Bajo, S. Liquid-liquid extraction of cadmium with diethyldithiocarbamic acid. 158

Bajo, S. Liquid-liquid extraction of gold with nickel bis(diethyldithiocarbamate) and its application to activation analysis 1771

Baker, J. E. Evaluation of the local thermal equilibrium model for quantitative secondary ion mass spectrometric analysis (correction). 896

Baker, J. K. Identification and chemical classification of drugs based on the relative response of a nitrogen selective detector and a flame ionization detector in gas chromatographic analysis. 906

Bakker, S. Sealed stainless cell for differential scanning calorimetry on volatile systems. 522

Bancroft, G. M. Calibration studies for quantitative x-ray photoelectron spectroscopy of ions. 1044

Bandi, W. R. Differential thermal analysis-evolved gas analysis for the determination of carbide and nitride phases in steel. 649

Bankston, D. C. Atomic emission spectrometer/spectrograph for the determination of barium in microamounts of diatom ash. 1017

Bard, A. J. Simple sample cell for examination of solids and liquids by photoacoustic spectroscopy. 697

Bard, A. J. Photothermal spectroscopy. 2057

Barford, R. A. Determination of sulfobetaine amphoteric surfactants by reverse phase high performance liquid chromatography. 2228

Barnes, B. K. Determination of trace transition elements in solids by proton induced x-ray emission analysis. 432

Barnes, R. M. Modified inductively coupled plasma arrangement for easy ignition and low gas consumption. 1450

Barnhart, J. W. Simplified gas chromatographic method for the determination of chlorpheniramine in serum. 1085

Barr, E. W. Combined thin-layer chromatography/flameless atomic absorption method for the identification of inorganic ions and organometallic complexes. 189

Barr, E. W. Recent developments in thin-layer chromatography. 83a

Barry, E. F. Determination of trace transition elements in solids by proton induced x-ray emission analysis. 432

Bartholomew, J. C. Surface studies of mammalian cells grown in culture by x-ray photoelectron spectroscopy. 1290

Bates, R. G. Determination of hydrogen ion concentrations in seawater from 5 to 40°C: standard potentials at salinities from 20 to 45‰. 29

Bates, R. G. Activity coefficients and osmotic coefficients in aqueous solutions of choline chloride at 25°C. 209

Bates, R. G. Acid-base properties of tris(hydroxymethyl)aminomethane (Tris) buffers in sea water from 5 to 40°C. 867

Batistoni, D. A. Spectroscopic element detector for gas chromatography. 2215

Batley, G. E. Determination of heavy metals in sea water by atomic absorption spectrometry after electrodeposition on pyrolytic graphite-coated tubes. 2031

Battaglia, S. Experimentally measured mass absorption coefficients in quantitative x-ray diffraction analysis. 1168

Baudino, J. H. Analyzer for determining fuel vaporization pressure curves of gasoline and gasoline-alcohol fuels. 2368

Baxter, T. Leachability of neutron irradiated fly ash. 1994

Bean, J. R. Unheated external column and inlet modification of a gas chromatograph for phosphine determinations. 1468
Beardsley, J. D. Petroleum. Fuels, gaseous and liquid. 235r
Bearse, R. C. Proton induced x-ray emission analysis of L-cells grown in vitro. 2203
Beasley, T. H. Determination and characterization of gallotannin by high performance liquid chromatography. 238
Becker, J. W. Determination of composition and molecular weight of polyester urethanes by high resolution proton magnetic resonance spectrometry. 722
Beckman, A. O. History of spectrophotometry at Beckman Instruments, Inc. 280a
Beezer, A. E. Bioassay of nystatin bulk material by flow microcalorimetry. 34
Beezer, A. E. Bioassay of antifungal antibiotics by flow microcalorimetry. 1781
Bekassy, S. Gas-solid and gas-liquid chromatography using porous layer open tube columns made with graphitized thermal carbon black. 768
Bell, A. D. Determination and characterization of gallotannin by high performance liquid chromatography. 238
Bennett, H. D. Analytical chemists at the launch pad. 322a
Benson, P. A. Field-ionization relative sensitivities for analysis of coal-derived liquids determined as a function of ion-source temperature and binary-mixture composition. 1847
Bentley, G. E. Preparation of electrodeless discharge lamps for elements forming gaseous covalent hydrides. 551
Berger, P. S. Dynamically refreshable computer display controller with vertical line generator for mass spectrometry applications. 1462
Berti, M. Determination of selenium in blood serum by proton-induced x-ray emission. 1313
Betty, K. R. 1024-Point transient recorder. 342
Betty, K. R. Frequency response plots for Savitzky-Golay filter functions. 351
Bicknell, R. Determination of ethyl and methyl parathion in runoff water with high performance liquid chromatography 1551
Birke, R. L. Determination of sulfide and thiols in the presence of vitamin B_{12a} by pulse polarography. 1380
Birks, J. W. Direct measurement of activation energies: an alternative formulation of the kinetics problem. 1074
Birks, L. S. Predicting absolute sensitivity and limit of detection for x-ray analysis of pollution samples. 1505
Bishop, E. Metal rod and wire electrode holders. 1880
Bishop, E. Auxiliary compartment for coulometric titration. 1885
Bisson, M. Critical evaluation of the copper(II) solubilization method for the determination of the complexation capacity of natural waters. 2358
Blaedel, W. J. Calculator program yielding confidence limits for least squares straight line regression analysis (correction). 523
Blaedel, W. J. Study of the steady-state current at tubular electrodes in the micromolar concentration region. 1563
Blaedel, W. J. Study of anodic stripping voltammetry with collection at tubular electrodes. 49
Blaha, J. Solution of general equilibrium systems by the system equation. 1660
Blair, W. R. Chemical and physical considerations in the use of atomic absorption detectors coupled with a gas chromatograph for determination of trace organometallic gases. 378
Blaisdell, B. E. Automatic computer construction, maintenance, and use of specialized joint libraries of mass spectra and retention indices from gas chromatography-mass spectrometry systems. 180
Blake, M. I. Repetitive determination of isonicotinic acid hydrazide in flow-through systems by series reactions. Comments. 2367
Blank, C. L. Determination of serotonin and dopamine in mouse brain tissue by high performance liquid chromatography with electrochemical detection. 354
Bloom, H. Sampling of metal air particulates for analysis by furnace atomic absorption spectrometry. 346
Blount, H. N. Small volume, high performance cell for nonaqueous spectroelectrochemistry. 1646
Blum, K. Determination of primidone by electron-capture gas chromatography. 903
Bodini, M. E. Voltammetric determination of nitrate ion at parts-per-billion levels. 485
Boese, S. W. Differential pulse polarographic determination of nitrate and nitrite. 479
Bond, A. M. Fundamental and second harmonic alternating current cyclic voltammetric theory and experimental results for simple electrode reactions involving solution-soluble redox couples (correction). 896
Bond, A. M. High speed synchronous data generation and sampler system: application to on-line fast Fourier transform faradaic admittance measurements. 1797
Bond, A. M. On-line fast Fourier transform faradaic admittance measurements: real-time deconvolution of heterogeneous charge transfer kinetic effects for thermodynamic and analytical measurements. 1805
Bond, R. E. Thin-layer differential pulse voltammetry. 1792
Bontempelli, G. Cathodic behavior of trans-dicyanobis(diethylphenylphosphine)nickel complex. 1005
Boocock, G. B. A stable free radical reagent and solid phase suitable for a nitric oxide dosimeter. 1672
Boon, J. J. Solvent-free and splitless injection method for open tubular columns. 1881
Bordun, M. Thin-layer chromatographic determination of hydrazine in aqueous and alcoholic media. 161
Boslett, J. A. Jr. Determination of parts per billion levels of electrodeposited metals by energy dispersive x-ray fluorescence spectrometry. 1734
Boss, C. B. Calculation of the velocity of a desolvating aerosol droplet in an analytical flame. 2112
Botz, F. K. Chemical ionization mass spectrometry of salts and thermally labile organics with field desorption emitters as solids probes. 1160
Boulton, R. B. Simultaneous analysis of light elements using prompt nuclear reaction gamma rays. 1297
Boutilier, G. D. Comparison of image devices vs. photomultiplier detectors in atomic and molecular luminescence spectrometry via signal-to-noise ratio calculations. 1048
Boutilier, G. D. Pulsed vs. continuous wave atomic fluorescence spectrometry. 1076
Bouyoucos, S. A. Determination of ammonia and methylamines in aqueous solutions by ion chromatography. 401
Bower, N. W. Precision of flame atomic absorption measurements of arsenic, cadmium, calcium, copper, iron, magnesium, molybdenum, sodium, and zinc. 574
Bowers, L. D. Analytical aspects of immobilized enzyme columns. 1929
Bowie, L. J. Automated systems for radioimmunoassay. 1183a
Bowman, L. M. Jr. Exclusion chromatography in dense gases: an approach to viscosity optimization. 243
Bradley, M. P. T. Petroleum. Hydrocarbons. 249r
Braman, R. S. Separation and determination of nanogram amounts of inorganic arsenic and methylarsenic compounds. 621
Branigan, P. D. Atomic absorption spectrometric determination of sub-part-per-million quantities of tin in extracts and biological materials with a graphite furnace. 1090
Braun, T. Literature growth and decay: an activation analysis resume. 682a
Breadmore, S. E. Determination of americium and curium in biological samples by extraction and liquid scintillation counting. 1268
Breitenbach, L. P. Fourier transform infrared spectrometric determination of gaseous performic acid. 1346
Brent, D. A. Cleaning of mass spectrometer ion sources by electropolishing. 674
Bresseleers, C. M. Chelex-100 ion-exchange filter membranes for preconcentration in x-ray fluorescence spectrometric analysis of water. 1326
Bricker, J. L. Separation and determination of nanogram amounts of inorganic arsenic and methylarsenic compounds. 621
Bright, D. S. Miniature helical stirrer. 191
Brilmyer, G. H. Photothermal spectroscopy. 2057
Brinckman, F. E. Chemical and physical considerations in the use of atomic absorption detectors coupled with a gas chromatograph for determination of trace organometallic gases. 378
Brindle, M. P. Modification of pulse polarograph for rapid scanning and its use with stationary electrodes. 1459
Brits, R. J. N. Determination of uranium in natural water by preconcentration on anion-exchange resin and delayed-neutron counting. 67
Brittain, H. G. Spectrophotometric microdetermination of alkaline earth and lanthanide elements with hydroxy naphthol blue and ethylenediaminetetraacetic acid. 969
Brockman, D. Dry ashing of animal tissues for atomic absorption spectrometric determination of zinc, copper, cadmium, lead, iron, manganese, magnesium and calcium. 1644
Broderius, S. J. Direct determination and calculation of aqueous hydrogen sulfide. 424
Brookins, D. G. Characterization of coal by laser pyrolysis gas chromatography. 390
Brooks, E. E. Thin-layer differential pulse voltammetry. 1792
Brost, D. F. Determination of optimum compromise flame conditions in simultaneous multielement flame spectrometry. 2280
Brown, A. P. Cyclic and differential pulse voltammetric behavior of reactants confined to the electrode surface. 1589
Brown, A. R. Evaluation of polyurethane foam for sampling of pesticides, polychlorinated biphenyls and polychlorinated naphthalenes, in ambient air. 1668
Brown, H. R. Comparison of inorganic interferences in atomic absorption spectrometric determination of arsenic and selenium. 1417
Brown, J. R. Calibration studies for quantitative x-ray photoelectron spectroscopy of ions. 1044
Brown, K. F. Evaluation of a cesium positive ion source for secondary ion mass spectrometry. 2023
Brown, P. R. Identification of nucleosides and bases in serum and plasma samples by reverse-phase high performance liquid chromatography. 2237
Bruckenstein, S. Phase-selective fundamental and second harmonic alternating current voltammetry of bismuth(III) and lead(II) at a continuously mercury-coated rotating platinum disk electrode. 1789
Brunner, T. R. Classification of binary carbon-13 nuclear magnetic resonance spectra. 2136
Bryant, M. F. Microprocessor-controlled, scanning dye laser for spectrometric analytical systems. 1702
Buchanan, M. V. Positional and geometric characterization of olefinic double bonds by fluorine magnetic resonance spectrometry. 2146
Buck, R. P. Field effect potentiometric sensors. 2315
Buffle, J. Measurement of complexation properties of humic and fulvic acids in natural waters with lead and copper ion-selective electrodes. 216
Bujdoso, E. Literature growth and decay: an activation analysis resume. 682a
Burg, W. R. Air pollution. 1r
Burgard, D. R. Factor analysis of the mass spectra of oligodeoxyribonucleotides. 1444
Burgasser, A. J. Determination of sulfur in organic molecules by spectrophotometric titration. 1987
Burrows, K. C. Modification of pulse polarograph for rapid scanning and its use with stationary electrodes. 1459

Bursey, M. M. Acetylation as a chemical ionization technique in medium-pressure chemical ionization mass spectrometry. 1071
Burt, J. A. Modulation photolysis as an alternative to flash photolysis. 1130
Bury, R. Redox thermodynamics and electron transfer reactivity of heme by enthalpimetry and voltammetry. 1573
Busch, K. W. Determination of optimum compromise flame conditions in simultaneous multielement flame spectrometry. 2280
Buser, H. R. Determination of 2,3,7,8-tetrachlorodibenzo-p-dioxin in environmental samples by high-resolution gas chromatography and low-resolution mass spectrometry. 918
Buso, G. Determination of selenium in blood serum by proton-induced x-ray emission. 1313
Butaeva, I. L. Gas chromatographic determination of trace amounts of sulfur compounds in industrial effluents. 128
Butler, E. A. Air buoyancy equations for single-pan balances. 2126
Buttrill, S. E. Jr. New drift-tube source for use in chemical ionization mass spectrometry. 1497
Cade, R. Determination of ammonia in biological solutions by second-derivative spectrometry. 83
Calkins, R. C. Nonferrous metallurgy-light metals: aluminum, beryllium, titanium, and magnesium. 72r
Callis, J. B. Analysis of multicomponent fluorescence data. 564
Callis, J. B. Rapid scanning fluorescence spectroscopy. 747a
Campana, J. E. Negative ion chemical ionization mass spectrometry of volatile metal chelates. 1501
Campbell, I. M. Software package to collect and process radiogas chromatographic data. 1726
Campbell, P. G. C. Critical evaluation of the copper(II) solubilization method for the determination of the complexation capacity of natural waters. 2358
Canelli, E. Determination of organic carbon by thermal volatilization plasma emission spectrometry. 1235
Cano, J. P. Determination of metapramine in plasma by gas chromatography with nitrogen-selective and electron-capture detection. 2354
Cantwell, F. F. Potentiometric titration of acids in the presence of a nonionic resin. 1256
Cappelloni, M. N. Determination of trace acetylene in oxygen with a portable acetylene analyzer. 1218
Cappon, C. J. Gas-chromatographic determination of inorganic mercury and organomercurials in biological materials. 365
Cardone, M. J. Photographic techniques for fluorescent spots on thin-layer chromatographic plates. 1640
Carmack, G. Effect of pressure on electrical conduction in ion exchange resins. 767
Carmack, G. D. Assay of phenobarbital with an ion-selective electrode. 1577
Caroli, S. Reference materials for ultraviolet spectrophotometry. 711
Carr, P. W. Fourier analysis of the transient response of potentiometric enzyme electrodes. 799
Carr, P. W. Analytical aspects of immobilized enzyme columns. 1929
Carr, T. W. Negative ions in plasma chromatography-mass spectrometry. 828
Carreira, L. A. Micro sampling and the use of a flow cell for coherent anti-Stokes Raman spectrometry. 959
Casalini, C. Titration of thioethers. 1002
Castagnola, A. Monoionic liquid membrane potential in non-isothermal systems. 212
Cesana, A. Gamma-ray activity determination in large volume samples with a germanium-lithium detector. 1156
Cesarano, G. Titration of thioethers. 1002
Chakrabarti, C. L. Evaluation of pyrolytic-graphite-coated tubes for graphite furnace atomic absorption spectrometry. 90
Chakrabarti, C. L. Studies on the mechanism of atom formation in graphite furnace atomic absorption spectrometry (correction). 192
Chakrabarti, C. L. Mechanism of atom loss in graphite furnace atomic absorption spectrometry. 1100
Chakrabarti, C. L. Studies on the mechanism of atom formation in graphite furnace atomic absorption spectrometry (correction). 1647
Chakrabarti, C. L. Atomization from a platform in graphite furnace atomic absorption spectrometry. 2018
Chambers, J. Q. Voltammetry and potentiometry of tetrathiafulvalene halides. 802
Chambers, W. F. Calculator program yielding confidence limits for least squares straight line. Comment. 884
Chan, J.-L. Iodine-amine charge-transfer complexes as spectrophotometric detectants in high pressure liquid chromatography. 2080
Chang, D. Critical experimental parameters in gas chromatographic-mass spectrometric analysis of oligopeptide hydrolysates at the picomole level. 1241
Chang, S.-K. Determination of nitrite ion using differential pulse polarography. 2272
Chantooni, M. K. Jr. Acid-base equilibriums of some acids in propylene carbonate. 503
Chasteen, N. D. Determination of molybdenum in seawater by electron paramagnetic resonance spectrometry. 461
Chatigny, M. A. Potential hazard associated with removal of needles from septa in injection ports of a gas chromatograph. 670
Chen, H.-F. Representation-space transformation for the display of multivariate chemical information. 1357
Cheng, C. N. Determination of the D and L isomers of some protein amino acids present in soils. 2
Cheng, F. S. Amperometric measurement of enzyme reactions with an oxygen electrode using air oxidation of reduced nicotinamide adenine dinucleotide. 1785
Chesler, S. N. Chemically-bonded aminoisalane stationary phase for the high-performance liquid chromatographic separation of polynuclear aromatic compounds. 2306
Chester, T. L. Analytical capabilities of the selectively modulated interferometric dispersive spectrometer. 113
Chester, T. L. Throughput advantage and disadvantage in analytical ultraviolet-visible spectrometry by considerations of signal and noise spectral bandpasses. 119
Chian, E. S. K. Gas stripping, sorption, and thermal desorption procedures for preconcentrating volatile polar water-soluble organics from water samples for analysis by gas chromatography. 1023
Chloupek, F. J. Analyzer for determining fuel vaporization pressure curves of gasoline and gasoline-alcohol fuels. 2368
Choppin, G. Precision titration mini-calorimeter. 1878
Choudhury, H. Dry ashing of animal tissues for atomic absorption spectrometric determination of zinc, copper, cadmium, lead, iron, manganese, magnesium and calcium. 1644
Chow, C. D. Analysis of high polymers. 159r
Chow, F. K. Separation of aromatic amine isomers by high pressure liquid chromatography with a copper(II)-bonded phase. 1756
Chowdhry, B. Z. Bioassay of antifungal antibiotics by flow microcalorimetry. 1781
Chretien, J. R. Topological analysis of gas-liquid chromatographic behavior of alkenes. 747
Christian, G. D. Analysis of multicomponent fluorescence data. 564
Christian, G. D. Rapid scanning fluorescence spectroscopy. 747a
Christian, G. D. Quantitative analyses of multicomponent fluorescence data by the methods of least squares and non-negative least sum of errors. 2155
Christian, G. D. Amperometric measurement of enzyme reactions with an oxygen electrode using air oxidation of reduced nicotinamide adenine dinucleotide. 1785
Christie, J. H. Square wave voltammetry at the dropping mercury electrode: theory. 1899
Christie, J. H. Square wave voltammetry at the dropping mercury electrode: experimental. 1904
Chu, C.-H. Separation of organic acids on amberlite XAD copolymers by reversed phase high pressure liquid chromatography. 860
Chu, C.-H. Amberlite XAD copolymers in reversed phase gravity flow and high pressure liquid chromatography. 757
Ciccarelli, M. F. QUAN - a computer program for quantitative x-ray fluorescence analysis. 345
Clark, B. R. Preparative-scale liquid chromatographic fractionation of crude oils derived from coal and shale. 1766
Clark, C. R. Gas and high pressure liquid chromatographic properties of some 4-nitrobenzamides of amphetamines and related arylalkylamines. 912
Clark, C. R. Iodine-amine charge-transfer complexes as spectrophotometric detectants in high pressure liquid chromatography. 2080
Clay, D. A. Determination of total sulfur in gasoline by gas chromatography with a flame photometric detector. 126
Clayton, J. W. Jr. Determination of pK_a values of acid components in atmospheric condensates by linearization of segmented titration curves. 1429
Clem, T. R. Automated electrodic potentiometry system. 1908
Clementz, D. M. Radiometric determination of alkyl aromatic sulfonates in crude oils. 1148
Cobler, J. G. Analysis of high polymers. 159r
Cochran, R. L. Selective spectral-line modulation technique for high sensitivity continuum-source atomic absorption spectrometry (correction). 685
Cochran, R. L. Spectral and noise characteristics of a 300-watt Eimac arc lamp. 2040
Cochran, R. L. Selective spectral-line modulation technique for high sensitivity continuum-source atomic absorption spectrometry. 98
Cochran, R. N. Statistically weighted principal component analysis of rapid scanning wavelength kinetics experiments. 846
Cohen, Y. Shipboard measurement of dissolved nitrous oxide in sea water by electron capture gas chromatography. 1238
Colaruotolo, J. F. Determination of chlorine, bromine, phosphorus, and sulfur in organic molecules by ion chromatography. 884
Colaruotolo, J. F. Determination of sulfur in organic molecules by spectrophotometric titration. 1987
Colautti, P. Determination of selenium in blood serum by proton-induced x-ray emission. 1313
Coleman, W. M. Preparative gel permeation chromatographic separation of solvent refined coal. 533
Colwell, L. Analysis of explosives by high performance liquid chromatography and chemical ionization mass spectrometry. 1039
Connors, K. A. Graphical interpolation method for the kinetic analysis of three-component mixtures. 1650
Cook, R. L. Solid state programmable switching device for semiautomated multichannel gas analyses with nondispersive infrared spectrometers. 893
Cook, T. E. Design and evaluation of a vidicon based derivative spectrometer. 871
Cooks, R. G. Identification of barbiturates by chemical ionization and mass-analyzed ion kinetic energy spectrometry. 435
Cooney, R. P. Comparison of multichannel SIT image vidicon and photomultiplier sequential linear scanning systems for the measurement of steady-state and transient fluorescence of molecules in solution. 939
Cooney, R. P. Comparison of image devices vs. photomultiplier detectors in atomic and molecular luminescence spectrometry via signal-to-noise ratio calculations. 1048
Cooney, R. P. Instrumental effects on limits of detection in gas phase fluorescence detection of gas chromatographic effluents. 1057
Copeland, T. R. Categorization of papers by trace metal content using atomic absorption spectrometric and pattern recognition techniques. 2285

Corain, B. Cathodic behavior of trans-di=cyanobis(diethylphenylphosphine)nickel complex. 1005
Couper, J. R. Petroleum. Asphalt. 240r
Cournoyer, R. Fourier Transform infrared analysis below the one-nanogram level. 2275
Covington, A. K. Buffer solutions for test=ing glass electrode performance in aque=ous solutions over the pH range 0–14 at 25° C. 1363
Cowen, J. P. Coprecipitation and electrode=position of polonium from sea water. 494
Cox, J. A. Donnan dialysis enrichment of cations. 1272
Crainiceanu, A. Gas chromatographic column for separation of organochlorine insecticide residues. 2123
Crawford, E. F. Clipped free induction decay signal analysis. 508
Cronin, S. E. Determination of the D and L isomers of some protein amino acids present in soils. 2
Crosmun, R. Signal flicker noise and noise power spectra. Reply to comments. 340
Crouch, S. R. Transducer for measurement of flow rates in stopped-flow mixing systems (correction). 352
Crouch, S. R. Spectrophotometric and kinetics investigation of the Berthelot reaction for the determination of ammo=nia. 464
Crow, F. W. Determination of molecular compositions on a quadrupole mass spectrometer by pulsed positive ion negative ion chemical ionization mass spectrometry. 1884
Crowe, H. R. Determination of the compo=sition of mixtures of sodium chromite and chromic oxide by electron spin reso=nance spectrometry. 962
Crowe, H. R. Effect of cavity loading on analytical electron spin resonance spec=trometry. 1353
Crowley, A. W. Analyzer for determining fuel vaporization pressure curves of gasoline and gasoline–alcohol fuels. 2368
Csanyi, L. J. Variable-time kinetic deter=mination of 2-propanol and other alco=hols by means of mutual induction in oxidations by chromium(VI). 980
Culberson, C. H. Determination of hydro=gen ion concentrations in seawater from 5 to 40°C: standard potentials at salinities from 20 to 45‰. 29
Culberson, C. H. Acid-base properties of tris(hydroxymethyl)aminomethane (Tris) buffers in sea water from 5 to 40°C. 867
Cunningham, K. M. Investigation of detec=tion limits for solutes dissolved in water measured by laser Raman spectrometry. 70
Curran, D. J. Determination of catechola=mines by thin-layer linear sweep voltam=metry. 1205
Curtis, D. B. Determination of sulfur in environmental materials by thermal neutron capture prompt gamma-ray spectrometry. 1741
Cushman, D. R. Petroleum. Wax. , 276r
Dale, A. D. Determination of mefruside and its metabolites in urine by high performance liquid chromatography. 1311
D'Alonzo, R. P. Determination of micromo=lar quantities of primary amides by flame emission spectrometry. 262
Dalrymple-Alford, P. Peak shapes in semidifferential electroanalysis. 1390
D'Amato, N. A. Simultaneous determina=tion of cocaine and benzoylecgonine in urine by gas–liquid chromatography. 1974
Daniewski, M. M. A high-speed, high-pur=ity extraction apparatus. 1465
Dannenberg, J. J. Propylene incorporation in 1-butene copolymers by carbon-13 nuclear magnetic resonance spectrome=try. 1405
Darling, C. M. Iodine–amine charge-trans=fer complexes as spectrophotometric detectants in high pressure liquid chro=matography. 2080
Daves, G. D. Critical experimental parame=ters in gas chromatographic–mass spec=trometric analysis of oligopeptide hydro=lysates at the picomole level. 1241
Davidson, E. R. Analysis of multicompo=nent fluorescence data. 564
Davidson, E. R. Quantitative analyses of multicomponent fluorescence data by the methods of least squares and non-ne=gative least sum of errors. 2155
Davidson, I. E. Direct determination of thioamide drugs in biological fluids by cathodic stripping voltammetry. 1195
Davis, B. Crown ether catalyzed derivatiza=tion of carboxylic acids and phenols with pentafluorobenzyl bromide for electron capture gas chromatography. 832
Davis, D. G. Surface electrochemistry of iron porphyrins and iron on tin oxide electrodes. 194
Davis, D. W. Filter attenuation corrections for the x-ray fluorescence analysis of atmospheric aerosols. 1990
Dayringer, H. E. Comparison of various K-nearest neighbor voting schemes with the self-training interpretive and retriev=al system for identifying molecular sub=structures from mass spectral data. 1720
DeAngelis, T. P. Mercury–gold minigrid optically transparent thin-layer elec=trode. 602
DeAngelis, T. P. Carbon and mercury–car=bon optically transparent electrodes. 1395
DeAngelis, T. P. Thin-layer differential pulse voltammetry. 1792
Deardorff, E. R. Performance of a nitrogen dioxide permeation device. 1823
De Galan, L. Supply and removal of sample vapor in graphite thermal atomizers. 2176
De Haseth, J. A. Reconstruction of gas chromatograms from interferometric gas chromatography/infrared spectrometry data. 1977
DeLap, R. A. Liquid chromatographic determination of residual acrylamide monomer in aqueous and nonaqueous dispersed phase polymeric systems. 154
De Leeuw, J. W. Solvent-free and splitless injection method for open tubular co=lumns. 1881
Denton, M. B. High solids sample introduc=tion for flame atomic absorption analysis 1413
Denton, M. B. Performance of the Super Modified Simplex. 1422
DePace, A. C. Quantitative determination of benzoylecgonine and cocaine in human biofluids by gas–liquid chromatography. 1965
DePalma, R. A. Application of pattern recognition techniques to the interpreta=tion of severely overlapped voltammetric data: studies with experimental data. 1376
Desiderio, D. M. Gas chromatography–=mass spectrometry study of acetylaceto=nyl dipeptide methyl esters. 287
Des Marais, D. J. Tube cracker for opening glass-sealed ampoules under vacuum (correction). 192
Dessy, R. E. Computer networking: a rational approach to lab automation. 1100a
DeWalle, F. B. Gas stripping, sorption, and thermal desorption procedures for preconcentrating volatile polar water–so=luble organics from water samples for analysis by gas chromatography. 1023
Dickinson, R. B. Jr. Low-temperature fluorescence spectrometric determination of polycyclic aromatic hydrocarbons by matrix isolation. 701
Dillard, J. W. Determination of the com=plexing capacity of natural water by cobalt(III) complexation. 404
Dillard, J. W. Digital simulation of differ=ential pulse polarography with incremen=tal time change. 1246
Dinnin, J. I. Inorganic and geological ma=terials. 34r
DiNunzio, J. E. Donnan dialysis enrich=ment of cations. 1272
Doerfler, D. L. Software package to collect and process radiogas chromatographic data. 1726
Dolan, J. W. Chlorine-selective detection for liquid chromatography with a Coulson electrolytic conductivity detector. 326
Donahey, S. A. Software package to collect and process radiogas chromatographic data. 1726
D'Orazio, P. Protein response of silver sulfide crystal membrane electrodes. 41
D'Orazio, P. Ion electrode measurements of complement and antibody levels using marker-loaded sheep red blood cell ghosts. 2083
Dorn, H. C. Preparative gel permeation chromatographic separation of solvent refined coal. 533
Dorsey, G. F. Determination of the epoxide equivalent weight of glycidyl ethers by proton magnetic resonance spectrometry 1144
Dorsey, J. G. Determination of the epoxide equivalent weight of glycidyl ethers by proton magnetic resonance spectrometry 1144
Doub, W. H. Jr. Digital microcoulometric measurements of cadmium anodic strip=ping at the micrometer hanging mercury drop electrode. 199
Doughty, D. A. Determination of water in oil emulsions by a microwave resonance procedure. 690
Dresbach, D. Determination of ethyl and methyl parathion in runoff water with high performance liquid chromatography 1551
Dromey, R. G. Inverted file structure for molecular formula and homologous series searching of large data bases. 1982
Drushel, H. V. Determination of nitrogen in petroleum fractions by combustion with chemiluminescent detection of nitric oxide. 932
D'Silva, A. P. Determination of uranium in ores by an x-ray excited optical lu=minescence technique. 638
Dubois, J. E. Topological analysis of gas–li=quid chromatographic behavior of alk=enes. , 747
Dudley, K. H. Colorimetric hydroxyla=mine–iron(III) methods for studies of the enzymic hydrolyses of cyclic imides and of amic acids. 292
Duenges, W. 4-Bromomethyl-7-methoxy=coumarin as a new fluorescence label for fatty acids. 442
Duer, W. C. Effect of chloride ion and ionic strength on the response of a cop=per(II) ion-selective electrode. 877
Duewer, D. L. Relating molecular structure to metal chelate stability and reagent selectivity: abstract factor analysis of the chelate formation equilibriums for some diaminetetracarboxylic acids. 1940
Duhamel, A. P. Qualitative analysis of thin gallium nitride films with secondary ion mass spectrometry. 1536
Dulson, W. Extension of the low tempera=ture range of a microprocessor-controlled gas chromatograph. 1279
Durand, A. G. Determination of metapra=mine in plasma by gas chromatography with nitrogen-selective and electron-cap=ture detection. 2354
Dutcher, J. S. Determination of the N-=hydroxy and phenolic metabolites of drugs derived from acetanilide by O-al=kylation and selected ion monitoring. 1843
Dutt, V. V. S. E. Kinetics of oxalate attack on ferrozine–iron(II) complex and regen=eration of ligand in determination of iron(II). 319
Dutt, V. V. S. E. Repetitive determination of isonicotinic acid hydrazide in flow-=through systems by series reactions. 776
Dutt, V. V. S. E. Repetitive determination of isonicotinic acid hydrazide in flow-=through systems by series reactions. Reply to comment. 2367
Duty, R. C. Isomer distribution and identi=fication for the chlorination reaction of acetylated 3-, 4-, 5-, and 6-chloro-2-me=thylanilines by gas–liquid chromatogra=phy. 743
East, G. A. Metal rod and wire electrode holders. 1880
East, G. A. Auxiliary compartment for coulometric titration. 1885
Eaton, G. R. Electron paramagnetic reso=nance sample cell for lossy samples. 1277
Eaton, S. S. Electron paramagnetic reso=nance sample cell for lossy samples. 1277
Eatough, D. J. Determination of nitrite by direct injection enthalpimetry. 1779
Eckschlager, K. Information theory as applied to chemical analysis. 1265
Eddy, R. S. Determination of chlorine, bromine, phosphorus, and sulfur in or=ganic molecules by ion chromatography. 884
Edmonds, J. W. Particle size effects in the determination of respirable α-quartz by x-ray diffraction. 2196

Edwards, W. B. III. Deuterium nuclear magnetic resonance spectra from milli= gram quantities of isotopically enriched compounds (correction). 1280
Edwards, W. B. III. Deuterium nuclear magnetic resonance spectra from milli= gram quantities of isotopically enriched compounds. 674
Efstathiou, C. E. Kinetics of the periodate reaction with some vicinal glycols studied with a perchlorate ion selective electrode as a periodate ion sensor. 410
Efstathiou, C. E. Kinetic study of the periodate–α–amino alcohol reactions with a perchlorate ion selective electrode: catalytic effect and determination of manganese. 414
Eisentraut, K. J. Determination of titanium in aircraft lubricating oils by atomic absorption spectrophotometry. 454
Eliezer, I. Sample-loss mechanism in a constant-temperature graphite furnace. 2008
Elliz, J. H. Gas and high pressure liquid chromatographic properties of some 4-nitrobenzamides of amphetamines and related arylalkylamines. 912
Elsea, G. M. Quantitative hydrolysis–gas chromatographic methods for the deter= mination of selected acids and glycols in polyesters. 741
Elwood, T. A. Purification of polyphenyl ethers by vacuum distillation. 1886
Emilsson, T. Teflon powders for near in= frared spectra of hydrides. 1458
Engler, E. M. Voltammetry and potentiom= etry of tetrathiafulvalene halides. 802
Enke, C. G. Analog storage register for fast transient recording. 19
Enke, C. G. Transducer for measurement of flow rates in stopped-flow mixing systems (correction). 352
Enomoto, J. Determination of 4,4'-alkyl- and alkoxy-disubstituted azoxybenzenes by isocratic reverse phase high perfor= mance liquid chromatography. 1963
Ensor, D. Precision titration mini-calorim= eter. 1878
Epstein, M. S. Waveform effects in wavel= ength modulation spectrometry. 458
Erdmann, D. E. Water analysis. 139r
Erdtmann, G. Determination of 13 ele= ments with atomic numbers between 12 and 47 by 14-MeV helium-3 activation analysis. 1510
Erlenmaier, T. Determination of metapra= mine in plasma by gas chromatography with nitrogen–selective and electron-cap= ture detection. 2354
Erlich, R. H. Pharmaceuticals and related drugs. 110r
Erni, F. Dynamic slurry-packing technique for liquid chromatography columns. 1958
Esposito, G. G. Determination of phosgene in air by gas chromatography and in= frared spectrophotometry. 1774
Evans, C. A. Jr. Evaluation of the local thermal equilibrium model for quantita= tive secondary ion mass spectrometric analysis (correction). 896
Evans, C. A. Jr. Determination of the surface predominance of toxic elements in airborne particles by ion microprobe mass spectrometry and Auger electron spectrometry. 1514
Evans, C. A. Jr. Evaluation of a cesium primary ion source on an ion microprobe mass spectrometer. 1399
Evans, J. F. Radiofrequency oxygen plasma treatment of pyrolytic graphite electrode surfaces. 1632
Evans, S. Quantitative analysis of alumino= silicates and other solids by x-ray pho= toelectron spectroscopy. 2001
Evenson, M. A. Clinical chemistry. 16r
Evett, I. W. Prediction of peak wavelengths and intensities in synchronously excited fluorescence emission spectra. 1710
Ewan, G. T. Simultaneous analysis of light elements using prompt nuclear reaction gamma rays. 1297
Fabiani, C. Monoionic liquid membrane potential in non-isothermal systems. 212
Farwell, S. O. Minicomputer data process= ing system for air monitoring studies. 357a
Fasching, J. L. Deceptive "correct" separa= tion by the linear learning machine. 2114
Fassel, V. A. Multielement detection limits and sample nebulization efficiencies of an improved ultrasonic nebulizer and a conventional pneumatic nebulizer in inductively coupled plasma–atomic emis= sion spectrometry. 632
Fassel, V. A. Determination of uranium in ores by an x-ray excited optical lumines= cence technique. 638
Fassett, J. D. Quantitation of secondary ion mass spectrometric images by micro= photodensitometry and digital image processing. 2322
Faulkner, L. R. Normal pulse voltammetry in electrochemically poised systems. 489
Faulkner, L. R. Chemical characterization via fluorescence spectral files and data compression by Fourier transformation. 2069
Feldman, C. Determination of traces of arsenic in siliceous materials. 825
Feldman, C. Spectroscopic element detector for gas chromatography. 2215
Felkel, H. L. Jr. Design and evaluation of a random access vidicon–echelle spectrom= eter and application to multielement determinations by atomic absorption spectrometry. 1112
Felker, P. Microdetermination of nitrogen in seed protein extracts with the salicy= late–dichloroisocyanurate color reaction. 1080
Fenselau, C. The mass spectrometer as a gas chromatograph detector. 563a
Ferguson, A. M. Defocused metastable scanning with a mass spectrometer and laboratory data system. 174
Fernando, Q. Determination of pK_a values of acid components in atmospheric con= densates by linearization of segmented titration curves. 1429
Fernando, Q. Rate of extraction of copper from aqueous solution. 1636
Ferra, M. I. A. Buffer solutions for testing glass electrode performance in aqueous solutions over the pH range 0–14 at 25° C. 1363
Fick, N. H. Petroleum. Lubricants, oils and greases. 238r
Figura, P. Characterization of the calcium form of Chelex-100 for trace metal stu= dies. 1950
Fike, R. R. Determination of catechola= mines by thin-layer linear sweep voltam= metry. 1205
Finston, H. L. Extraction of mercury by dithizone and stability of the extracted complex. 983
Fisch, M. H. Propylene incorporation in 1-butene copolymers by carbon-13 nu= clear magnetic resonance spectrometry. 1405
Fisher, N. S. Atomic emission spectrome= ter/spectrograph for the determination of barium in microamounts of diatom ash. 1017
Fisher, R. L. Determination of sub-micro= gram per cubic meter levels of N-nitroso= dimethylamine in air. 1821
Fishman, M. Automated atomic absorption spectrometric determination of total arsenic in water and streambed materi= als. 1599
Fishman, M. J. Water analysis. 139r
Fishman, V. A. Simple sample cell for examination of solids and liquids by photoacoustic spectroscopy. 697
Fitch, W. L. Quantitative comparison of combined gas chromatographic/mass spectrometric profiles of complex mix= tures. 1623
Fitzgerald, J. M. Precision of quantitative electron spin resonance using copper(II) bound to ion-exchange resins. 250
Fitzgerald, J. M. Parameters influencing the electron spin resonance signal inten= sity of metal ion complex-exchanged resins. 1840
Fitzloff, J. F. Repetitive determination of isonicotinic acid hydrazide in flow-= through systems by series reactions. Comments. 2367
Fitzpatrick, F. A. Oximes for high perfor= mance liquid and electron capture gas chromatography of prostaglandins and thromboxanes. 1032
Flavian, S. Unrecognized systematic errors in quantitative analysis by gas–liquid chromatography. 2222
Flynn, N. W. Glass lined field ionization sources. 2121
Folkers, K. Critical experimental parame= ters in gas chromatographic–mass spec= trometric analysis of oligopeptide hydro= lysates at the picomole level. 1241
Folsom, T. R. Coprecipitation and electro= deposition of polonium from sea water. 494
Foltz, A. K. Food. 194r
Ford, A. Ultrasonic absorption spectra of vanadium benzohydroxamic acid in 1-bu= tanol. 881
Ford, P. T. Determination of hydrogen content of fuel by low resolution proton nuclear magnetic resonance spectrome= try. 594
Foreback, C. C. Separation and determina= tion of nanogram amounts of inorganic arsenic and methylarsenic compounds. 621
Forrest, J. Silver-110 microgram sulfate analysis for the short time resolution of ambient levels of sulfur aerosol. 1579
Fowler, W. K. Background fluorescence spectra observed in atomic fluorescence spectrometry with a continuum source. 944
Fraisse, D. Glass lined field ionization sources. 2121
Frank, H. Gas chromatography–mass spec= trometry study of acetylacetonyl dipep= tide methyl esters. 287
Fraser, J. M. Petroleum. Introduction. , 273r
Frazer, J. W. Integrating analog-to-digital converter displaying high signal fidelity and noise immunity. 1869
Frazer, J. W. Equivalence-point determi= nations for automated potentiometric titrations with ion-selective electrodes. 1250
Frederick, L. G. Determination of trace acetylene in oxygen with a portable acetylene analyzer. 1218
Freed, C. R. Low volume reference elec= trode for electrochemical detection and fraction collection in high performance liquid chromatography. 2379
Freed, D. J. In situ generation of standards for gas chromatographic analysis. 139
Freed, D. J. Generation of nitrosamines for gas chromatographic analysis via direct injection. 1544
Freel, J. Petroleum. Catalysts. 243r
Freeman, D. H. Particle porosimetry by inverse gel permeation chromatography. 1183
Freeman, D. H. Corrosion of stainless steel by organic solvent mixtures. 1637
Frei, R. W. Dynamic slurry–packing techni= que for liquid chromatography columns. 1958
Freiser, H. Effect of pressure on electrical conduction in ion exchange resins. 767
Freiser, H. Assay of phenobarbital with an ion-selective electrode. 1577
Freiser, H. Relating molecular structure to metal chelate stability and reagent selec= tivity: abstract factor analysis of the chelate formation equilibriums for some diaminetetracarboxylic acids. 1940
Freiser, H. Determination of trace levels of nitrates by an extraction-photometric method. 2249
Freudenthal, J. Pulse-counting techniques in organic mass spectrometry. 2205
Frick, W. Critical experimental parameters in gas chromatographic–mass spectrome= tric analysis of oligopeptide hydrolysates at the picomole level. 1241
Friswell, N. J. Determination of hydrogen content of fuel by low resolution proton nuclear magnetic resonance spectrome= try. 594
Fritz, J. S. Preparation and analytical applications of a propylenediaminetetraa= cetic acid resin. 418
Fritz, J. S. Ion-exchange separation and determination of calcium and magnesi= um. 1595
Froehlich, P. M. Enhancement of the fluorescence intensity of derivatives of amino acids in mixed solvent systems. 1606
Fry, R. C. High solids sample introduction for flame atomic absorption analysis. 1413
Fuerst, R. G. Performance of a nitrogen dioxide permeation device. 1823
Fujii, T. Trace determination of vinyl chloride in water by direct aqueous injec= tion gas chromatography–mass spectro= metry. 1985
Fujimura, K. Ligand-exchange gas chro= matographic separation of pyridine bas= es. 1179
Fujinaga, T. Acid–base equilibriums of some acids in propylene carbonate. 503

Fujioka, Y. Separation and determination of copper(II) and iron(II) as their monothiothenoyltrifluoroacetone complexes with pyridine by extraction spectrophotometry and reversed-phase thin-layer chromatography. 2241
Fujishima, A. Photothermal spectroscopy. 2057
Fujiwara, K. Subnanogram fluorine determination by aluminum monofluoride molecular absorption spectrometry. 2035
Funduc, I. Gas chromatographic column for separation of organochlorine insecticide residues. 2123
Fung, K. W. Determination of iron(III) with a copper selective electrode. 497
Fung, Y. S. Determination of iron(III) with a copper selective electrode. 497
Funk, E. W. Determination of vanadium in Athabasca bitumen and other heavy hydrocarbons by visible spectrometry. 972
Furnas, T. C. Determination of parts per billion levels of electrodeposited metals by energy dispersive x-ray fluorescence spectrometry. 1734
Furr, A. K. Determination of fluorine by neutron activation analysis. 1507
Furuta, N. Multielement analysis by continuum source atomic absorption spectrometry with the aid of analog data treatment. 1263
Fuwa, K. Multielement analysis by continuum source atomic absorption spectrometry with the aid of analog data treatment. 1263
Fuwa, K. Subnanogram fluorine determination by aluminum monofluoride molecular absorption spectrometry. 2035
Fyfe, W. S. Calibration studies for quantitative x-ray photoelectron spectroscopy of ions. 1044
Gaddy, R. H. Autoradiography of californium-252 wire neutron sources. 517
Gagne, R. Critical evaluation of the copper(II) solubilization method for the determination of the complexation capacity of natural waters. 2358
Gallaway, W. S. History of spectrophotometry at Beckman Instruments, Inc. 280a
Galwey, R. K. Current follower stabilization in potentiostats. 677
Games, L. M. Composition, treatment efficiency, and environmental significance of dye manufacturing plant effluents. 1433
Garden, J. S. Multiple-curve procedure for improving precision with calibration-curve-based analyses. 1655
Garfinkel, D. Progress curve algorithm for calculating enzyme activities from kinetic assay spectrophotometric measurements. 1716
Garreau, R. M. Determination of metapramine in plasma by gas chromatography with nitrogen-selective and electron-capture detection. 2354
Garrett, R. B. Energy dispersive x-ray fluorescence spectrometry for determination of twenty-six trace and two major elements in geochemical specimens. 62
Garrett, R. B. Determination of forty elements in geochemical samples and coal fly ash by x-ray fluorescence spectrometry. 1012
Gaylor, V. F. Phase-selective cathodic stripping voltammetry for determination of water-soluble mercaptans. 1386
Gearhart, H. L. Solid state programmable switching device for semiautomated multichannel gas analyses with nondispersive infrared spectrometers. 893
Gehrke, C. W. Fertilizers. 186r
Gelpi, E. Multiple ion detection system with miniscan facilities and expanded mass range for magnetic sector mass spectrometers. 543
Genna, J. L. Modified inductively coupled plasma arrangement for easy ignition and low gas consumption. 1450
Gerstein, B. C. Pulsed nuclear magnetic resonance spectrometry for nondestructive determination of hydrogen in coal. 75
Getty, R. H. Precolumn synthesis of trimethylsilyl derivatives of aqueous phosphate for gas chromatographic analysis. 1086
Giam, C. S. Characterization of lignites by pyrolysis-gas chromatography. 1540
Giam, P. Y. Characterization of lignites by pyrolysis-gas chromatography. 1540
Giauque, R. D. Energy dispersive x-ray fluorescence spectrometry for determination of twenty-six trace and two major elements in geochemical specimens. 62
Giauque, R. D. Determination of forty elements in geochemical samples and coal fly ash by x-ray fluorescence spectrometry. 1012
Giddings, J. C. Theoretical and experimental characterization of field-flow fractionation (correction). 523
Giddings, J. C. Exclusion chromatography in dense gases: an approach to viscosity optimization. 243
Giddings, J. C. Peak shifts and distortion due to solute relaxation in flow field-flow fractionation. 659
Giddings, J. C. Peak broadening factors in thermal field-flow fractionation. 1750
Giessen, B. C. Categorization of papers by trace metal content using atomic absorption spectrometric and pattern recognition techniques. 2285
Gilath, I. Breakdown of alkaline complex cyanide by ion-exchange. 516
Gilbertson, G. Essential oils and related products. 83r
Gilpin, R. K. Pharmaceuticals and related drugs. 110r
Gladney, E. S. Determination of sulfur in environmental materials by thermal neutron capture prompt gamma-ray spectrometry. 1741
Glass, E. D. Effect of modulation wave form on the utility of emission background corrections obtained with an oscillating refractor plate. 1121
Glotfelty, E. Field air sampling of pesticide vapors with polyurethane foam. 7
Gochman, N. Automated systems for radioimmunoassay. 1183a
Goda, L. Y. Energy dispersive x-ray fluorescence spectrometry for determination of twenty-six trace and two major elements in geochemical specimens. 62
Goda, L. Y. Determination of forty elements in geochemical samples and coal fly ash by x-ray fluorescence spectrometry. 1012
Godse, D. D. Analysis of acidic monoamine metabolites by gas chromatography-mass spectrometry. 915
Gold, A. Stoichiometry of nitrogen dioxide determination in triethanolamine trapping solution. 1448
Goldberg, I. B. Determination of the composition of mixtures of sodium chromite and chromic oxide by electron spin resonance spectrometry. 962
Goldberg, I. B. Effect of cavity loading on analytical electron spin resonance spectrometry. 1353
Goldberg, M. C. Investigation of detection limits for solutes dissolved in water measured by laser Raman spectrometry. 70
Gomez, E. Determination of vanadium in Athabasca bitumen and other heavy hydrocarbons by visible spectrometry. 972
Gonnord, M. F. Gas-solid and gas-liquid chromatography using porous layer open tube columns made with graphitized thermal carbon black. 768
Goode, S. R. Computerized curve-fitting to determine the equivalence point in spectrophotometric titrations. 1408
Goodwin, T. E. Characterization of lignites by pyrolysis-gas chromatography. 1540
Goss, L. P. Micro sampling and the use of a flow cell for coherent anti-Stokes Raman spectrometry. 959
Goto, M. Peak shapes in semidifferential electroanalysis. 1390
Gouw, T. H. Removal of water in the distillation of hydrocarbon mixtures. 1887, 2380
Graham, J. A. Evidence for solute-brush interactions on nonpolar chemically bonded stationary phases in gas chromatography. 133
Gramberg, L. G. Pulse-counting techniques in organic mass spectrometry. 2205
Grasselli, J. G. Teaching analytical chemistry: real world needs. 182a
Gray, D. N. Immobilized enzymes in analytical chemistry. 1069a
Gray, R. C. Simple sample cell for examination of solids and liquids by photoacoustic spectroscopy. 697
Green, D. C. Voltammetry and potentiometry of tetrathiafulvalene halides. 802
Green, L. A. Determination of the epoxide equivalent weight of glycidyl ethers by proton magnetic resonance spectrometry 1144
Greenland, L. P. Borohydride-flame determination of arsenic in phosphoric acid. 2376
Greenwood, G. J. Field-ionization relative sensitivities for analysis of coal-derived liquids determined as a function of ion-source temperature and binary-mixture composition. 1847
Gregoire, D. C. Atomization from a platform in graphite furnace atomic absorption spectrometry. 2018
Gregory, R. P. IV. Multichannel pipet for parallel aliquoting of samples and reagents into centrifugal analyzer minidiscs. 1608
Greizerstein, H. B. Simultaneous determination of chlordiazepoxide and its N-demethyl metabolite in 50-μL blood samples by high pressure liquid chromatography. 2235
Greter, F. L. Measurement of complexation properties of humic and fulvic acids in natural waters with lead and copper ion-selective electrodes. 216
Griffin, R. G. High resolution NMR in solids. 951a
Grushka, E. Separation of aromatic amine isomers by high pressure liquid chromatography with a copper(II)-bonded phase. 1756
Grushka, E. Chemically bonded stationary phases in chromatography. 1004a
Guenther, E. Essential oils and related products. 83r
Guerin, M. R. Preparative-scale liquid chromatographic fractionation of crude oils derived from coal and shale. 1766
Guerra, R. E. Particle size effects in the determination of respirable α-quartz by x-ray diffraction. 2196
Guilbault, G. G. Urease coupled ammonia electrode for urea determination in blood serum. 795
Guilbault, G. G. Applications of the piezoelectric crystal detector in analytical chemistry. 1890
Guiochon, G. Gas-solid and gas-liquid chromatography using porous layer open tube columns made with graphitized thermal carbon black. 768
Guiochon, G. Separation of acids from asphalts. 1222
Gunn, A. M. Determination of phosphorus in milk powders by optical emission spectrometry with a high frequency inductively-coupled argon plasma source 1492
Gurney, M. Determination of total fluoride in soil and vegetation using an alkali fusion-selective ion electrode technique. 53
Gustafson, F. J. Spectroscopic system for the study of fluorescent lanthanide probe ions in solids. 1474
Gustafson, F. J. Ultra-trace method for lanthanide ion determination by selective laser excitation. 1680
Guthrie, J. L. Determination of 2,4- and 2,6-diaminotoluene in flexible urethane foams. 1676
Gwyn, S. A. Defocused metastable scanning with a mass spectrometer and laboratory data system. 174
Haaland, D. M. Internal-reference solid-electrolyte oxygen sensor. 1813
Haas, W. J. Jr. Multielement detection limits and sample nebulization efficiencies of an improved ultrasonic nebulizer and a conventional pneumatic nebulizer in inductively coupled plasma-atomic emission spectrometry. 632
Hackleman, D. E. Field effect potentiometric sensors. 2315
Hadjiioannou, T. P. Kinetics of the periodate reaction with some vicinal glycols studied with a perchlorate ion selective electrode as a periodate ion sensor. 410
Hadjiioannou, T. P. Kinetic study of the periodate-α-amino alcohol reactions with a perchlorate ion selective electrode: catalytic effect and determination of manganese. 414
Hadzi, D. Combined retrieval system for infrared, mass, and carbon-13 nuclear magnetic resonance spectra. 2141
Haegele, K. D. Gas chromatography-mass spectrometry study of acetylacetonyl dipeptide methyl esters. 287
Haegele, K. D. Determination of phenylethylmalonamide by electron-capture gas chromatography. 1969

Haerdi, W. Measurement of complexation properties of humic and fulvic acids in natural waters with lead and copper ion-selective electrodes. 216
Haines, W. E. Petroleum. Nonmetal elements and compounds. 256r
Hall, M. E. Spectrophotometric determination of acrylonitrile. 2277
Ham, G. J. Determination of americium and curium in biological samples by extraction and liquid scintillation counting. 1268
Hamilton, H. E. Determination of primidone by electron-capture gas chromatography. 903
Hamilton, H. E. Determination of phenylethylmalonamide by electron-capture gas chromatography. 1969
Hanai, T. Chromatography of chlorinated biphenyls on an ion-exchange resin. 764
Hanai, T. Liquid chromatography of chlorinated biphenyls on pyrolytically-deposited carbon. 1954
Hanck, K. W. Determination of the complexing capacity of natural water by cobalt(III) complexation. 404
Hanley, P. R. Evaluation of a cesium primary ion source on an ion microprobe mass spectrometer. 1399
Hanna, D. A. Analytical aspects of immobilized enzyme columns. 1929
Hannaford, P. Determination of boron isotope ratios by atomic absorption spectrometry. 1852
Hannaker, P. Multielement trace analysis of geological materials with solvent extraction and flame atomic absorption spectrometry. 1485
Hansen, E. H. Pumping pressure and reagent consumption in flow injection analysis. Comments. 1858
Hansen, L. D. Determination of nitrite by direct injection enthalpimetry. 1779
Hanson, G. Determination of molybdenum in seawater by electron paramagnetic resonance spectrometry. 461
Hanson, R. H. Precolumn synthesis of trimethylsilyl derivatives of aqueous phosphate for gas chromatographic analysis. 1086
Hanson, R. L. Characterization of coal by laser pyrolysis gas chromatography. 390
Haraguchi, H. Multielement analysis by continuum source atomic absorption spectrometry with the aid of analog data treatment. 1263
Hargis, L. G. Spectrophotometric and stopped-flow reaction-rate study of the formation of 10-molybdo-2-vanadophosphoric acid. 779
Harless, R. L. Analysis of technical chlordane by gas chromatography/mass spectrometry. 734
Harnly, J. M. Improvements in the measurements of characteristic concentrations in continuum source atomic absorption spectrometry. 665
Harnly, J. M. Background correction for the analysis of high-solids samples by graphite furnace atomic absorption. 2187
Harrington, G. W. Determination of nitrite ion using differential pulse polarography 2272
Harris, C. M. Digital analysis of electronic absorption spectra. 864a
Harris, H. Analysis of explosives by high performance liquid chromatography and chemical ionization mass spectrometry. 1039
Hashizume, T. Ligand interference preventive buffer in determination of copper(II) by a cupric ion selective electrode. 1868
Hass, J. R. Acetylation as a chemical ionization technique in medium-pressure chemical ionization mass spectrometry. 1071
Hassan, S. S. M. Microdetermination of m-dinitro compounds with cyanide and silver electrodes. 45
Hatch, F. Techniques in gas chromatography/chemical ionization mass spectrometry. 169
Hatch, F. Reactant ion monitoring for selective detection in gas chromatography/chemical ionization mass spectrometry. 731
Hattman, E. A. Solid and gaseous fuels. 176r
Hattori, M. Acid–base equilibriums of some acids in propylene carbonate. 503
Hawkridge, F. M. Small volume, high performance cell for nonaqueous spectroelectrochemistry. 1646
Hayes, J. M. Tube cracker for opening glass-sealed ampoules under vacuum (correction). 192
Hayes, J. M. High precision pulse counting: limitations and optimal conditions. 306
Hebert, A. J. Portable field water sample filtration unit. 672
Hefner, R. D. Solid state programmable switching device for semiautomated multichannel gas analyses with nondispersive infrared spectrometers. 893
Heiden, R. W. Composition differences in commercial polyethylene bottles and their relation to the stability of stored part-per-billion mercury(II) solutions. 668
Heineman, W. R. Mercury–gold minigrid optically transparent thin-layer electrode. 602
Heineman, W. R. Carbon and mercury–carbon optically transparent electrodes. 1305
Heineman, W. R. Thin-layer differential pulse voltammetry. 1792
Heller, C. A. Detection of trinitrotoluene in water by fluorescent ion-exchange resins. 2251
Hendler, R. W. Automated electrodic potentiometry system. 1908
Hendler, R. W. Automated electrodic potentiometry of potassium ferricyanide and respiratory components. 1914
Henslee, W. W. Particle size effects in the determination of respirable α-quartz by x-ray diffraction. 2196
Hercules, D. M. Analytical study of chemiluminescence from the vitamin B_{12}–luminol system. 446
Hertz, H. S. Chemically-bonded aminosilane stationary phase for the high-performance liquid chromatographic separation of polynuclear aromatic compounds. 2306
Heydanek, M. G. Jr. Tracing the origin of off-flavors in a breakfast cereal. 901a
Hickman, D. A. Determination of mercury by atomic absorption spectrometry with graphite tube atomization. 336
Hieftje, G. M. Selective spectral-line modulation technique for high sensitivity continuum-source atomic absorption spectrometry (correction). 685
Hieftje, G. M. Integrating analog-to-digital converter displaying high signal fidelity and noise immunity. 1869
Hieftje, G. M. Physical characterization of the helium–oxygen–acetylene flame as an atom cell for atomic spectrometry. 2013
Hieftje, G. M. Spectral and noise characteristics of a 300-watt Eimac arc lamp. 2040
Hieftje, G. M. Calculation of the velocity of a desolvating aerosol droplet in an analytical flame. 2112
Hieftje, G. M. Selective spectral-line modulation technique for high sensitivity continuum-source atomic absorption spectrometry. 98
Hieftje, G. M. Modified microwave-induced plasma discharge chamber. 2372
Highfield, J. G. Determination of absolute fluorescence quantum efficiency of quinine bisulfate in aqueous medium by optoacoustic spectrometry. 1850
Hilcoat, B. L. Determination of 6-mercaptopurine in plasma by mass spectrometry. 725
Hillenbrand, D. F. Positional and geometric characterization of olefinic double bonds by fluorine magnetic resonance spectrometry. 2146
Hilpert, L. R. Chemically-bonded aminosilane stationary phase for the high-performance liquid chromatographic separation of polynuclear aromatic compounds. 2306
Hinderberger, E. J. Effect of modulation wave form on the utility of emission background corrections obtained with an oscillating refractor plate. 1121
Hines, W. J. Determination of hydrogen sulfide, carbonyl sulfide, carbon disulfide, and sulfur dioxide in gases and hydrocarbon streams by gas chromatography/flame photometric detection. 123
Hinton, E. R. Matrix isolation Fourier transform infrared spectrometry of polycyclic aromatic hydrocarbons. 86
Hirsch, R. F. Analysis of variance in analytical chemistry. 691a
Hirsch, R. F. Ion-exchangers for gas–solid chromatography. 1549
Hirt, W. E. Interference of nitrate in the determination of formaldehyde by the chromotropic acid method. 1865
Hites, R. A. Composition, treatment efficiency, and environmental significance of dye manufacturing plant effluents. 1433
Hlavay, J. Applications of the piezoelectric crystal detector in analytical chemistry. 1890
Hodge, V. F. Coprecipitation and electrodeposition of polonium from sea water. 494
Hoffman, N. E. Reversed phase high performance liquid chromatographic separations of nucleotides in the presence of solvophobic ions. 2231
Hoffmann, D. Redox potential and quinone content of cigarette smoke. 1924
Holfeld, H. S. Portable gas chromatograph for the acetylene reduction assay for nitrogenase. 1275
Holland, J. F. Correction of right-angle fluorescence measurements for the absorption of excitation radiation. 706
Holland, J. F. Electron impact ionization mass spectrometry using field desorption activated emitters as solid sample probes. 1164
Holler, F. J. Transducer for measurement of flow rates in stopped-flow mixing systems (correction). 352
Holmes, W. F. Dynamically refreshable computer display controller with vertical line generator for mass spectrometry applications. 1462
Holt, B. D. Preparation of carbon dioxide from sulfates, sulfur dioxide, air, and water for determination of oxygen isotope ratio. 1664
Holton, F. Determination of trace transition elements in solids by proton induced x-ray emission analysis. 432
Honda, R. Solvent effect on the liquid–liquid distribution of monothiothenoyltrifluoroacetone and its metal chelates of copper(II), cobalt(II), and zinc(II). 2246
Honjo, T. Separation and determination of copper(II) and iron(II) as their monothiothenoyltrifluoroacetone complexes with pyridine by extraction spectrophotometry and reversed-phase thin-layer chromatography. 2241
Honjo, T. Solvent effect on the liquid–liquid distribution of monothiothenoyltrifluoroacetone and its metal chelates of copper(II), cobalt(II), and zinc(II). 2246
Horikawa, T. T. Compositional analyses of methyl methacrylate–methacrylic acid copolymers by carbon-13 nuclear magnetic resonance spectrometry. 77
Horlick, G. 1024-Point transient recorder. 342
Horlick, G. Frequency response plots for Savitzky–Golay filter functions. 351
Horlick, G. Atomic spectrochemical measurements with a Fourier transform spectrometer. 1446
Horne, F. H. Statistically weighted principal component analysis of rapid scanning wavelength kinetics experiments. 846
Horvath, C. Liquid chromatography of ionogenic substances with nonpolar stationary phases. 142
Horvath, C. Enhancement of retention by ion-pair formation in liquid chromatography with nonpolar stationary phases. 2295
Hoshika, Y. Gas chromatographic determination of lower aliphatic primary amines as their fluorine-containing Schiff bases. 541
Hoskins, L. C. Determination of carotenoid concentrations in marine phytoplankton by resonance Raman spectrometry. 695
Hougen, F. W. Column packer for gas chromatography. 684
Hougen, F. W. Simple microreactor for subtractive gas chromatography. 1078
Hough, M. Determination of aromaticities of coal derivatives by nuclear magnetic resonance spectrometry and the Brown–Ladner equation. 585
Howald, R. A. Sample-loss mechanism in a constant-temperature graphite furnace. 2008
Howald, R. A. Elimination of chloride interferences with mercuric ions in the determination of nitrates by the phenoldisulfonic acid method. 857
Howell, N. G. Evaluation of silicon vidicon detector sensitivity for atomic spectrometry applications. 106

Hu, J. C-A. Pyrolysis gas chromatography analysis of rubbers and other high polymers. 537

Hubbard, A. T. Quantitative elemental analysis of substituted hydrocarbon monolayers on platinum by Auger electron spectroscopy with electrochemical calibration. 2330

Hughes, E. E. Performance of a nitrogen dioxide permeation device. 1823

Hughes, M. C. Modification of pulse polarograph for rapid scanning and its use with stationary electrodes. 1459

Hughes, T. C. Multielement trace analysis of geological materials with solvent extraction and flame atomic absorption spectrometry. 1485

Hume, D. N. Determination of nitrilotriacetate in environmental water by gas chromatography of the trimethylsilyl ester. 374

Hunt, D. F. Chemical ionization mass spectrometry of salts and thermally labile organics with field desorption emitters as solids probes. 1160

Hunt, D. F. Determination of molecular compositions on a quadrupole mass spectrometer by pulsed positive ion negative ion chemical ionization mass spectrometry. 1884

Hunt, R. D. Determination of ammonia in biological solutions by second-derivative spectrometry. 83

Hunt, R. W. Jr. Spectrophotometric and stopped-flow reaction-rate study of the formation of 10-molybdo-2-vanadophosphoric acid. 779

Hurst, R. W. Carbon and mercury-carbon optically transparent electrodes. 1395

Hurtubise, R. J. Comparison of experimental and theoretical calibration curves in solid-surface fluorescence analysis. 2160

Hurtubise, R. J. Room-temperature phosphorescence of compounds adsorbed on sodium acetate. 2164

Hurtubise, R. J. Separation of hydroaromatics and polycyclic aromatic hydrocarbons and determination of tetralin and naphthalene in coal-derived solvents. 2253

Hurwitz, J. K. Ferrous metallurgy. 54r

Husser, E. R. Liquid chromatographic determination of residual acrylamide monomer in aqueous and nonaqueous dispersed phase polymeric systems. 154

Iatridis, B. Determination of germanium in oxides, ores, and alloys by chlorination and gas chromatography. 909

Ikeda, M. Colorimetric determination of hippuric acid in urine and liver homogenate. 1494

Imamura, T. Determination of 4,4'-alkyl- and alkoxy-disubstituted azoxybenzenes by isocratic reverse phase high performance liquid chromatography. 1963

Imasaka, T. Detection limit of fluorescein as determined by fluorometry with an esculin laser source. 667

Ingle, J. D. Jr. Signal flicker noise and noise power spectra. Comments. 339

Ingle, J. D. Jr. Precision of flame atomic absorption measurements of arsenic, cadmium, calcium, copper, iron, magnesium, molybdenum, sodium, and zinc. 574

Ingle, J. D. Jr. Fluorometric reaction rate method for determination of silver. 1066

Ingle, J. D. Jr. Design and operation of a fluorometric reaction rate instrument. 1060

Inshakov, M. D. Gas chromatographic determination of trace amounts of sulfur compounds in industrial effluents. 128

Isenhour, T. L. Comparison of various K-nearest neighbor voting schemes with the self-training interpretive and retrieval system for identifying molecular substructures from mass spectral data. 1720

Isenhour, T. L. Reconstruction of gas chromatograms from interferometric gas chromatography/infrared spectrometry data. 1977

Ishibashi, N. Detection limit of fluorescein as determined by fluorometry with an esculin laser source. 667

Ishibashi, N. Ligand interference preventive buffer in determination of copper(II) by a cupric ion selective electrode. 1868

Ishizuka, T. Laser-vaporized atomic absorption spectrometry of solid samples. 1339

Issaq, H. J. Combined thin-layer chromatography/flameless atomic absorption method for the identification of inorganic ions and organometallic complexes. 189

Issaq, H. J. Recent developments in thin-layer chromatography. 83a

Itoh, H. Separation and determination of copper(II) and iron(II) as their monothiothenoyltrifluoroacetone complexes with pyridine by extraction spectrophotometry and reversed-phase thin-layer chromatography. 2241

Iverson, D. G. Calculator program yielding confidence limits for least squares straight line regression analysis (correction). 523

Iverson, D. G. Study of the steady-state current at tubular electrodes in the micromolar concentration region. 1563

Izutsu, K. Acid-base equilibriums of some acids in propylene carbonate. 503

Jackson, K. W. Design and evaluation of a fiber optic fluorometric flow cell. 2051

Jackson, M. D. Evaluation of polyurethane foam for sampling of pesticides, polychlorinated biphenyls and polychlorinated naphthalenes, in ambient air. 1668

Jacobs, G. Redox potential and quinone content of cigarette smoke. 1924

Jadamec, J. R. Optical multichannel analyzer for characterization of fluorescent liquid chromatographic petroleum fractions. 1316

Jagoutz, E. Application of the fundamental parameter method for the determination of major and minor elements in fused geological samples with x-ray fluorescence spectrometry. 717

Jakovljevic, I. M. Lead or thallium salts as external heavy atoms for room temperature quantitative phosphorescence. 2048

James, G. W. Parts-per-million determinations of uranium and thorium in geologic samples by x-ray spectrometry. 967

James, W. D. Leachability of neutron irradiated fly ash. 1994

Janghorbani, M. Leachability of neutron irradiated fly ash. 1994

Janicki, C. A. Pharmaceuticals and related drugs. 110r

Jensen, S. Residue analysis of sediment and sewage sludge for organochlorines in the presence of elemental sulfur. 316

Jezorek, J. R. Use of molecular sieves to dry nonaqueous solutions of transition metal salts. 1874

Johansson, M. Determination of intact oxazepam by electron capture gas chromatography after an extractive alkylation reaction. 1545

Johnson, B. M. An improved fabrication technique for alkali flame ionization detector salt tips (correction). 192

Johnson, D. C. Electrocatalysis of the reduction of iron(III) by halides adsorbed at platinum electrodes in perchloric acid solutions. 1918

Johnson, D. E. Compositional analyses of methyl methacrylate-methacrylic acid copolymers by carbon-13 nuclear magnetic resonance spectrometry. 77

Johnson, D. L. Separation and determination of nanogram amounts of inorganic arsenic and methylarsenic compounds. 621

Johnson, D. W. Rapid scanning fluorescence spectroscopy. 747a

Johnson, J. D. Simplified gas chromatographic method for the determination of chlorpheniramine in serum. 1085

Johnson, J. M. Design, construction, and applications of a galactose selective electrode. 789

Jones, A. R. Preparative-scale liquid chromatographic fractionation of crude oils derived from coal and shale. 1766

Jones, D. R. IV. Elimination of copper-carbonate complex interference in chelating agent analysis by copper solubilization. 10

Jones, P. W. In situ decomposition product isolated from Tenax GC while sampling stack gases. 512

Jordan, J. Redox thermodynamics and electron transfer reactivity of heme by enthalpimetry and voltammetry. 1573

Jozefowicz, M. L. Determination of L-hydroxyproline in meat protein by quantitative carbon-13 Fourier transform nuclear magnetic resonance spectrometry. 1140

Juneau, G. P. Removal of europium shift reagents from nuclear magnetic resonance samples. 2375

Jungers, R. H. Determination of total sulfur in gasoline by gas chromatography with a flame photometric detector. 126

Jupille, T. Consistent terminology for efficiency in high performance thin-layer chromatography. 1867

Jurney, E. T. Determination of sulfur in environmental materials by thermal neutron capture prompt gamma-ray spectrometry. 1741

Justice, J. B. Jr. Comparison of various K-nearest neighbor voting schemes with the self-training interpretive and retrieval system for identifying molecular substructures from mass spectral data. 1720

Jyo, A. Ligand interference preventive buffer in determination of copper(II) by a cupric ion selective electrode. 1868

Kabasakalian, P. Determination of gentamicin complex components in fermentation broth by in-situ fluorimetric measurements of 4-chloro-7-nitrobenzo-2-oxa-1,3-diazole derivatives. 953

Kadlec, R. Software package to collect and process radiogas chromatographic data. 1726

Kadone, H. Detection limit of fluorescein as determined by fluorometry with an esculin laser source. 667

Kaiman, B. D. An improved fabrication technique for alkali flame ionization detector salt tips (correction). 192

Kaiser, D. G. Oximes for high performance liquid and electron capture gas chromatography of prostaglandins and thromboxanes. 1032

Kalliney, S. Determination of gentamicin complex components in fermentation broth by in-situ fluorimetric measurements of 4-chloro-7-nitrobenzo-2-oxa-1,3-diazole derivatives. 953

Kallos, G. J. On-column reaction gas chromatography for determination of chloromethyl methyl ether at one part-per-billion level in ambient air. 1817

Kalyanaraman, S. Solvent extraction separation of scandium with 4-methyl-3-penten-2-one as its thiocyanate complex. 1192

Kambara, H. Determination of impurities in gases by atmospheric pressure ionization mass spectrometry. 270

Kanazawa, K. K. Current follower stabilization in potentiostats. 677

Kane, P. F. Surface characterization. 221r

Kang, H. K. Acid interference in the determination of arsenic by atomic absorption spectrometry. 1829

Kanomata, I. Determination of impurities in gases by atmospheric pressure ionization mass spectrometry. 270

Kanzaki, N. Phase-selective fundamental and second harmonic alternating current voltammetry of bismuth(III) and lead(II) at a continuously mercury-coated rotating platinum disk electrode. 1789

Kanzaki, Y. Phase-selective fundamental and second harmonic alternating current voltammetry of bismuth(III) and lead(II) at a continuously mercury-coated rotating platinum disk electrode. 1789

Kapetanovic, I. M. Determination of the N-hydroxy and phenolic metabolites of drugs derived from acetanilide by O-alkylation and selected ion monitoring. 1843

Karasek, F. W. Plasma chromatography of phosphorus esters. 1746

Karger, B. L. Analysis of explosives by high performance liquid chromatography and chemical ionization mass spectrometry. 1039

Kasai, Y. Automated determination of carboxylic acids by anion-exchange chromatography with specific color reaction. 655

Katayama, M. Atomic absorption spectrophotometry based on the polarization characteristics of the Zeeman effect. 1106

Kaufman, F. B. Voltammetry and potentiometry of tetrathiafulvalene halides. 802

Kaushik, R. C. Synthesis and ion-exchange properties of crystalline stannic vanadophosphate. 165

Kawaguchi, H. Interelement effects and a possible excitation mechanism in a low-pressure microwave induced helium plasma. 266

Kawaguchi, H. Enhancement of emission by potassium chloride in the low-pressure microwave-induced plasma emission spectrometer. 1489
Kawai, M. Determination of 6-mercaptopurine in plasma by mass spectrometry. 725
Kawai, T. Amalgam electrode designed for precise electromotive force measurements. 190
Kaye, W. History of spectrophotometry at Beckman Instruments, Inc. 280a
Keliher, P. N. Correction for interferences of spectral origin with continuum source, echelle wavelength modulated atomic absorption spectrometry. 838
Keller, H. P. Dynamic slurry-packing technique for liquid chromatography columns. 1958
Keller, K. P. Quantitative hydrolysis-gas chromatographic methods for the determination of selected acids and glycols in polyesters. 741
Keller, R. W. Liquid chromatographic determination of picomole quantities of aromatic amine carcinogens. 683
Kelly, P. M. Correction of right-angle fluorescence measurements for the absorption of excitation radiation. 706
Kemmerer, R. R. Matrix isolation Fourier transform infrared spectrometry of polycyclic aromatic hydrocarbons. 86
Kenan, W. R. Jr. Field effect potentiometric sensors. 2315
Keyes, M. H. Immobilized enzymes in analytical chemistry. 1069a
Kho, B. T. Short excitation wavelength fluorometric detection in high-pressure liquid chromatography of indole peptide, naphthyl, and phenol compounds. 1836
Khoo, K. H. Determination of hydrogen ion concentrations in seawater from 5 to 40°C: standard potentials at salinities from 20 to 45‰. 29
Khopkar, S. M. Solvent extraction separation of scandium with 4-methyl-3-penten-2-one as its thiocyanate complex. 1192
Kiba, T. Separation and determination of copper(II) and iron(II) as their monothiothenoyltrifluoroacetone complexes with pyridine by extraction spectrophotometry and reversed-phase thin-layer chromatography. 2241
Kiba, T. Solvent effect on the liquid-liquid distribution of monothiothenoyltrifluoroacetone and its metal chelates of copper(II), cobalt(II), and zinc(II). 2246
Kihara, S. Voltammetric determination of ultratraces of albumin, cysteine and cystine at the hanging mercury drop electrode. 2108
Kikta, E. J. Jr. Chemically bonded stationary phases in chromatography. 1004a
Kim, J. H. Gas stripping, sorption, and thermal desorption procedures for preconcentrating volatile polar water-soluble organics from water samples for analysis by gas chromatography. 1023
Kim, K-Y. Diode array spectrometer for the simultaneous determination of hemoglobins in whole blood. 555
Kim, S. H. Plasma chromatography of phosphorus esters. 1746
Kinder, H. D. Quantitative hydrolysis-gas chromatographic methods for the determination of selected acids and glycols in polyesters. 741
Kipling, B. Ionic diffusion and selectivity of a cation exchange membrane in nonaqueous solvents. 629
Kira, S. Colorimetric determination of hippuric acid in urine and liver homogenate. 1494
Kirchner, S. J. Rate of extraction of copper from aqueous solution. 1636
Kirkbright, G. F. Determination of phosphorus in milk powders by optical emission spectrometry with a high frequency inductively-coupled argon plasma source 1492
Kirkbright, G. F. Determination of absolute fluorescence quantum efficiency of quinine bisulfate in aqueous medium by optoacoustic spectrometry. 1850
Kissinger, P. T. Determination of tetrahydroisoquinoline alkaloids in biological materials with high performance liquid chromatography. 530
Kissinger, P. T. Amperometric and coulometric detectors for high-performance liquid chromatography. 447a
Kissinger, P. T. Reverse-phase ion-pair partition chromatography. Comments. 883
Kissinger, P. T. Determination of catecholamines in urine by reverse-phase liquid chromatography with electrochemical detection. 2109
Kitos, P. A. Proton induced x-ray emission analysis of L-cells grown in vitro. 2203
Klazema, B. Sealed stainless cell for differential scanning calorimetry on volatile systems. 522
Kmetec, E. Design, construction, and applications of a galactose selective electrode. 789
Knight, H. G. Determination of fluorine by neutron activation analysis. 1507
Koenig, R. T. Essential oils and related products. 83r
Kogan, M. J. Quantitative determination of benzoylecgonine and cocaine in human biofluids by gas-liquid chromatography. 1965
Koirtyohann, S. R. Effect of modulation wave form on the utility of emission background corrections obtained with an oscillating refractor plate. 1121
Koizumi, H. Atomic absorption spectrophotometry based on the polarization characteristics of the Zeeman effect. 1106
Kolling, O. W. Measurement of solvent polarity by nuclear magnetic resonance and electron spin resonance spectral probes. 591
Kolthoff, I. M. Acid-base equilibriums of some acids in propylene carbonate. 503
Kolthoff, I. M. Voltammetric determination of ultratraces of albumin, cysteine and cystine at the hanging mercury drop electrode. 2108
Kolthoff, I. M. Analytical chemistry in the USA in the first quarter of this century. 480a
Kometani, T. Y. Flameless atomic absorption spectrometric determination of ultratrace elements in silicon tetrachloride. 2289
Konigstein, J. Separation of trioses and tetroses as trimethylsilyl oximes by gas chromatography. 137
Koteel, P. Comparison of methods of hydride generation atomic absorption spectrometric arsenic and selenium determination. 1096
Kounaves, S. P. Anodic stripping peak currents: electrolysis potential relations for reversible systems. 56
Kovacik, V. Separation of trioses and tetroses as trimethylsilyl oximes by gas chromatography. 137
Kowalski, B. R. Intrinsic dimensionality of smell. 596
Kozeniauskas, R. Determination of nitrite ion using differential pulse polarography 2272
Krapf, G. Differential thermal analysis-evolved gas analysis for the determination of carbide and nitride phases in steel. 649
Kressin, I. K. Electrodeposition of plutonium and americium for high resolution α spectrometry. 842
Krishen, A. Gel permeation chromatography of low molecular weight materials with high efficiency columns (correction) 1647
Krishen, A. Gel permeation chromatography of low molecular weight materials with high efficiency columns. 898
Krishnamurty, K. V. Tris(pyrrolidine dithiocarbamato)cobalt(III) chelate matrix for trace metal preconcentration from aqueous solution by coprecipitation 222
Krol, G. J. Short excitation wavelength fluorometric detection in high-pressure liquid chromatography of indole peptide, naphthyl, and phenol compounds. 1836
Krottinger, D. L. Reaction-rate method for the determination of hydrocortisone. 1586
Krstulovic, A. M. Identification of nucleosides and bases in serum and plasma samples by reverse-phase high performance liquid chromatography. 2237
Krug, E. L. R. Interference of nitrate in the determination of formaldehyde by the chromotropic acid method. 1865
Krug, F. J. Pumping pressure and reagent consumption in flow injection analysis. Comments. 1858
Kruger, T. L. Identification of barbiturates by chemical ionization and mass-analyzed ion kinetic energy spectrometry. 435
Ku, A. Y. Corrosion of stainless steel by organic solvent mixtures. 1637
Kuehl, D. W. Identification of trace contaminants in environmental samples by selected ion summation analysis of gas chromatographic-mass spectral data. 521
Kullberg, L. Precision titration mini-calorimeter. 1878
Kuo, P. P. K. Gas stripping, sorption, and thermal desorption procedures for preconcentrating volatile polar water-soluble organics from water samples for analysis by gas chromatography. 1023
Kuwana, T. X-ray photoelectron/Auger electron spectroscopic studies of tin and indium metal foils and oxides. 1228
Kuwana, T. Double wavelength spectrophotometry with a rapid scanning instrument. 1348
Kuwana, T. Radiofrequency oxygen plasma treatment of pyrolytic graphite electrode surfaces. 1632
Kuznetsova, L. M. Gas chromatographic determination of trace amounts of sulfur compounds in industrial effluents. 128
Laba, J. P. A high-speed, high-purity extraction apparatus. 1465
Laguitton, D. Simultaneous determination of composition and mass thickness of thin films by quantitative x-ray fluorescence analysis. 1152
Lahmann, W. Opto-acoustic trace analysis in liquids with the frequency-modulated beam of an argon ion laser. 549
Laitinen, H. A. Peer Review. Should the Author be Anonymous (editorial). 1
Laitinen, H. A. Automated Identification of Microbes (editorial). 193
Laitinen, H. A. Global Environmental Monitoring (editorial). 353
Laitinen, H. A. Single Atom Detection (editorial). 529
Laitinen, H. A. Centennial History of Analytical Chemistry (editorial). 689
Laitinen, H. A. Microprocessors Come of Age (editorial). 897
Laitinen, H. A. Should NSF Support Industrial Research (editorial). 1089
Laitinen, H. A. Letters to the Editor (editorial). 1281
Laitinen, H. A. International Participation in Scientific Meetings (editorial). 1473
Laitinen, H. A. The Editorial Process (editorial). 1649
Laitinen, H. A. The Analytical Division Fellowship Program (editorial). 2129
Lamb, W. J. Sheet resistivity measurements of chemically modified electrodes by four-point probe method. 1639
Lambert, N. W. Petroleum. Physical properties. 246r
Lambrecht, R. W. An improved fabrication technique for alkali flame ionization detector salt tips (correction). 192
Lampe, F. W. Steady-state kinetic treatment of the emission from reduced pressure microwave induced discharges in helium. 560 , 2380
Landis, J. B. Kinetic study of the cyanogen bromide-pyridine reaction applied to thiocyanate determinations in serum. 785
Langford, C. H. Studies on the mechanism of atom formation in graphite furnace atomic absorption spectrometry (correction). 192
Langford, C. H. Studies on the mechanism of atom formation in graphite furnace atomic absorption spectrometry (correction). 1647
Larrabee, G. B. Surface characterization. 221r
Larsen, J. G. High speed synchronous data generation and sampler system: application to on-line fast Fourier transform faradaic admittance measurements. 1797
Larsen, R. D. Clipped free induction decay signal analysis. 508
LaRue, T. A. Portable gas chromatograph for the acetylene reduction assay for nitrogenase. 1275
Lasoski, B. A. Determination of sub-microgram per cubic meter levels of N-nitrosodimethylamine in air. 1821
Last, T. A. Analog storage register for fast transient recording. 19
Latham, D. R. Petroleum. Nonmetal elements and compounds. 256r
Latshaw, D. R. Determination of trace acetylene in oxygen with a portable acetylene analyzer. 1218

Laurence, D. F. Trace chloride determination by rate controlled coulometric titration. 1557

Lavallee, D. K. Evaluation of tetraphenylporphinatozinc(II) as a stable standard for porphyrin determinations by fluorescence spectrometry. 1453

Lavallee, D. K. Determination of porphyrins at low concentration using porphinatocopper(II) phosphorescence. 1482

Lawson, G. Weak peak enhancement by selective ion trapping in a quadrupole ion storage source. 1619

Lawton, W. H. Digital analysis of electronic absorption spectra. 864a

Layman, L. R. Integrating analog-to-digital converter displaying high signal fidelity and noise immunity. 1869

Layton, S. F. Field desorption and electron impact mass spectra of ionic dyes. 922

Lee, W. C. Molecular weight and association of coal-derived asphaltenes. 2363

Leggett, D. C. Determination of 2,4,6-trinitrotoluene in water by conversion to nitrate. 880

Leggett, D. J. Numerical analysis of multicomponent spectra. 276

Lehman, J. P. Gas chromatography/mass spectrometry interface simplified and quantified. 518

Lehmann, W. D. Determination of alkali elements by field desorption mass spectrometry. 1744

Lemyk, B. Determination of free and total potential haloforms in drinking water. 814

Lennox, J. C. Voltage controlled oscillator for signal-proportional data acquisition rates. 681

Leoni, L. Experimentally measured mass absorption coefficients in quantitative x-ray diffraction analysis. 1168

Lewis, R. G. Analysis of technical chlordane by gas chromatography/mass spectrometry. 734

Lewis, R. G. Evaluation of polyurethane foam for sampling of pesticides, polychlorinated biphenyls and polychlorinated naphthalenes, in ambient air. 1668

Lewis, R. K. Evaluation of a cesium primary ion source on an ion microprobe mass spectrometer. 1399

Leyden, D. E. Voltage controlled oscillator for signal-proportional data acquisition rates. 681

Li, K-P. Dynamics of the desolvating droplet in a laminar flame. 2086

Liao, J. C. Reversed phase high performance liquid chromatographic separations of nucleotides in the presence of solvophobic ions. 2231

Liberti, L. Calibration procedure to minimize errors in continuous analysis by ion selective electrodes. 2377

Lichte, F. E. Effect of modulation wave form on the utility of emission background corrections obtained with an oscillating refractor plate. 1121

Light, T. S. Null-point control of acidity with a differential pH electrode system. 1009

Lillian, D. Determination of phosgene in air by gas chromatography and infrared spectrophotometry. 1774

Lin, A. W. C. X-ray photoelectron/Auger electron spectroscopic studies of tin and indium metal foils and oxides. 1228

Lin, C-H. Representation-space transformation for the display of multivariate chemical information. 1357

Linder, H. R. Dynamic slurry-packing technique for liquid chromatography columns. 1958

Lindstrom, F. Mechanism of reduction of cadmium by aminoiminomethanesulfinic acid in alkaline media. 26

Lindstrom, R. M. Selection and cleaning of plastic containers for storage of trace element samples. 2264

Linfield, W. M. Determination of sulfobetaine amphoteric surfactants by reverse phase high performance liquid chromatography. 2228

Linton, R. W. Determination of the surface predominance of toxic elements in airborne particles by ion microprobe mass spectrometry and Auger electron spectrometry. 1514

Litman, R. Determination of trace transition elements in solids by proton induced x-ray emission analysis. 432

Litman, R. Extraction of mercury by dithizone and stability of the extracted complex. 983

Little, C. J. Determination of mefruside and its metabolites in urine by high performance liquid chromatography. 1311

Littlejohn, M. A. Qualitative analysis of thin gallium nitride films with secondary ion mass spectrometry. 1536

Lloyd, J. B. F. Prediction of peak wavelengths and intensities in synchronously excited fluorescence emission spectra. 1710

Lo, J. M. Preconcentration of mercury, gold, and copper in sea water with lead diethyldithiocarbamate for neutron activation analysis. 1146

London, J. W. Progress curve algorithm for calculating enzyme activities from kinetic assay spectrophotometric measurements. 1716

Lopez, M. Ionic diffusion and selectivity of a cation exchange membrane in nonaqueous solvents. 629

Lord, D. A. Determination of trace metals in fresh water mussels by atomic absorption spectrometry with direct solid sample injection. 257

Loveland, J. W. Petroleum. Analytical and process instrumentation. 262r

Lowe, R. M. Determination of boron isotope ratios by atomic absorption spectrometry. 1852

Lowry, J. D. Multichannel pipet for parallel aliquoting of samples and reagents into centrifugal analyzer minidiscs. 1608

Lowry, S. R. Comparison of various K-nearest neighbor voting schemes with the self-training interpretive and retrieval system for identifying molecular substructures from mass spectral data. 1720

Loyd, R. J. High speed synchronous data generation and sampler system: application to on-line fast Fourier transform faradaic admittance measurements. 1797

Ludewig, H. J. Opto-acoustic trace analysis in liquids with the frequency-modulated beam of an argon ion laser. 549

LueYen, E. Analytical possibilities of phase resolved phosphorimetry. 1262

Lundgren, J. L. Analytical studies and applications of ferroin type chromogens immobilized by adsorption on a styrene-divinylbenzene copolymer. 974

Lurio, A. Detection sensitivities for thick specimens in proton and electron induced x-ray spectrometry. 1737

Lyerla, J. R. Jr. Compositional analyses of methyl methacrylate-methacrylic acid copolymers by carbon-13 nuclear magnetic resonance spectrometry. 77

Lyon, W. S. Literature growth and decay: an activation analysis resume. 682a

Lytle, F. E. Two-photon excited molecular fluorescence in optically dense media. 2054

Macaskill, J. B. Activity coefficients and osmotic coefficients in aqueous solutions of choline chloride at 25°C. 209

McBride, R. R. Detection of trinitrotoluene in water by fluorescent ion-exchange resins. 2251

McCloskey, J. A. Calculations of isotopic distribution in molecules extensively labeled with heavy isotopes. 281

McCracken, M. S. Reaction-rate method for the determination of hydrocortisone. 1586

McCreery, R. L. Thin-layer electrochemical technique for monitoring electrogenerated reactive intermediates. 206

McCrone, W. C. How to buy a microscope. 659a

McCue, M. Qualitative and quantitative determination of suspected components in mixtures by target transformation factor analysis of their mass spectra. 284

McDonald, D. C. Use of internal standards for atomic absorption spectrometric analyses of samples atomized by sputtering. 1336

McDowell, A. E. Performance of a silicon target vidicon tube as a multiwavelength detector for liquid chromatography. 1171

McDuffie, B. Characterization of the calcium form of Chelex-100 for trace metal studies. 1950

McEwen, C. N. Field desorption and electron impact mass spectra of ionic dyes. 922

McGandy, E. L. Software package to collect and process radiogas chromatographic data. 1726

McGill, J. E. Mechanism of reduction of cadmium by aminoiminomethanesulfinic acid in alkaline media. 26

McGill, J. R. Intrinsic dimensionality of smell. 596

McIntyre, N. S. X-ray photoelectron spectroscopic studies of iron oxides. 1521

McKeag, R. G. Column packer for gas chromatography. 684

McKeag, R. G. Simple microreactor for subtractive gas chromatography. 1078

McKinney, R. W. Determination of 2,4- and 2,6-diaminotoluene in flexible urethane foams. 1676

McKinstry, W. E. Solid and gaseous fuels. 176r

Macksey, J. A. Nonferrous metallurgy-light metals: aluminum, beryllium, titanium, and magnesium. 72r

McLafferty, F. W. Performance prediction and evaluation of systems for computer identification of spectra. 1441

McLafferty, F. W. Comparison of various K-nearest neighbor voting schemes with the self-training interpretive and retrieval system for identifying molecular substructures from mass spectral data. 1720

McLafferty, F. W. Computer assignment of elemental compositions of mass spectral peaks from isotopic abundances. 1723

McLaren, J. W. Determination of trace metals in fresh water mussels by atomic absorption spectrometry with direct solid sample injection. 257

MacMurdo, K. W. Autoradiography of californium-252 wire neutron sources. 517

McNelis, E. Kinetics of the periodate reaction with some vicinal glycols studied with a perchlorate ion selective electrode as a periodate ion sensor. 410

McQuaker, N. R. Determination of total fluoride in soil and vegetation using an alkali fusion-selective ion electrode technique. 53

McReynolds, J. H. Glass lined field ionization sources. 2121

McReynolds, J. H. Isotopic assay of nanomole amounts of nitrogen-15 labeled amino acids by collision-induced dissociation mass spectrometry. 1832

Maddox, W. L. Analysis of cigarette smoke by Fourier transform infrared spectrometry. 331

Magatti, A. W. Determination of gentamicin complex components in fermentation broth by in-situ fluorimetric measurements of 4-chloro-7-nitrobenzo-2-oxa-1,3-diazole derivatives. 953

Maggio, M. S. Digital analysis of electronic absorption spectra. 864a

Magini, M. Monoionic liquid membrane potential in non-isothermal systems. 212

Magno, F. Cathodic behavior of trans-di(cyanobis(diethylphenylphosphine)nickel complex. 1005

Magnusson, P. Determination of intact oxazepam by electron capture gas chromatography after an extractive alkylation reaction. 1545

Maguire, J. H. Colorimetric hydroxylamine-iron(III) methods for studies of the enzymic hydrolyses of cyclic imides and of amic acids. 292

Mahan, K. I. Mercury retention in untreated water samples at the part-per-billion level. 662

Mahan, S. E. Mercury retention in untreated water samples at the part-per-billion level. 662

Mahle, N. H. Automated cleanup of herbicides by adsorption chromatography for the determination of 2,3,7,8-tetrachloro-dibenzo-p-dioxin. 386

Maker, P. D. Fourier transform infrared spectrometric determination of gaseous performic acid. 1346

Malinowski, E. R. Qualitative and quantitative determination of suspected components in mixtures by target transformation factor analysis of their mass spectra 284

Malinowski, E. R. Theory of error in factor analysis. 606

Malinowski, E. R. Determination of the number of factors and the experimental error in a data matrix. 612

Mallard, C. S. Portable gas chromatograph for the acetylene reduction assay for nitrogenase. 1275
Mallard, T. M. Portable gas chromatograph for the acetylene reduction assay for nitrogenase. 1275
Malloy, B. Determination of optimum compromise flame conditions in simultaneous multielement flame spectrometry. 2280
Malloy, T. B. Jr. Micro sampling and the use of a flow cell for coherent anti-Stokes Raman spectrometry. 959
Malmstadt, H. V. Reaction-rate method for the determination of hydrocortisone. 1586
Malmstadt, H. V. Multichannel pipet for parallel aliquoting of samples and reagents into centrifugal analyzer minidiscs. 1608
Malmstadt, H. V. Microprocessor-controlled, scanning dye laser for spectrometric analytical systems. 1702
Mamantov, G. Matrix isolation Fourier transform infrared spectrometry of polycyclic aromatic hydrocarbons. 86
Mamantov, G. Analysis of cigarette smoke by Fourier transform infrared spectrometry. 331
Mamantov, G. Low-temperature fluorescence spectrometric determination of polycyclic aromatic hydrocarbons by matrix isolation. 701
Mamantov, G. Optically transparent vitreous carbon electrode. 1470
Manahan, S. E. Elimination of copper-carbonate complex interference in chelating agent analysis by copper solubilization. 10
Manes, M. Flow method for determination of desorption isotherms and pore size distribution. 991
Manly, C. F. Use of molecular sieves to dry nonaqueous solutions of transition metals. 1874
Mannan, C. A. Short excitation wavelength fluorometric detection in high-pressure liquid chromatography of indole peptide, naphthyl, and phenol compounds. 1836
Mareci, T. H. Quantitative analysis of mixtures by carbon-13 nuclear magnetic resonance spectrometry. 2130
Margerum, D. W. Simultaneous kinetic analysis of multicomponent mixtures. 2090
Margerum, D. W. Simultaneous kinetic and spectral analysis with a vidicon rapid-scanning stopped-flow spectrometer. 2098
Margeson, J. H. Performance of a nitrogen dioxide permeation device. 1823
Margoshes, M. Pumping pressure and reagent consumption in continuous flow analysis with unsegmented reaction streams. 17
Margoshes, M. Pumping pressure and reagent consumption in flow injection analysis. Reply to comments. 1861
Marinkovic, M. Sample-loss mechanism in a constant-temperature graphite furnace. 2008
Mark, H. B. Jr. Determination of ammonia in aqueous solutions by infrared spectrometry following preconcentration on zeolite. 1331
Mark, H. B. Jr. Spectrophotometric determination of vitamin K compounds. 1343
Mark, H. B. Jr. Carbon and mercury-carbon optically transparent electrodes. 1395
Marsel, J. Combined retrieval system for infrared, mass, and carbon-13 nuclear magnetic resonance spectra. 2141
Marshall, R. A. G. Cumulative sum charts for monitoring of radioactivity background counts. 2193
Marten, T. R. Determination of mefruside and its metabolites in urine by high performance liquid chromatography. 1311
Mascellani, G. Titration of thioethers. 1002
Mascini, M. Urease coupled ammonia electrode for urea determination in blood serum. 795
Matalon, R. Automated cleanup of herbicides by adsorption chromatography for the determination of 2,3,7,8-tetrachlorodibenzo-p-dioxin. 386
Maters, W. L. Solvent-free and splitless injection method for open tubular columns. 1881
Mathiason, D. R. Separation method for coal-derived solids and heavy liquids. 1225
Matousek, J. P. Determination of heavy metals in sea water by atomic absorption spectrometry after electrodeposition on pyrolytic graphite-coated tubes. 2031
Mattson, C. S. Multivariate statistical approach to the fingerprinting of oils by infrared spectrometry. 297
Mattson, C. S. Classification of petroleum pollutants by linear discriminant function analysis of infrared spectral patterns. 500
Mattson, J. S. Multivariate statistical approach to the fingerprinting of oils by infrared spectrometry. 297
Mattson, J. S. Design and applications of an on-line minicomputer system for dispersive infrared spectrophotometry. 470
Mattson, J. S. Classification of petroleum pollutants by linear discriminant function analysis of infrared spectral patterns. 500
Mattson, J. S. Carbon and mercury-carbon optically transparent electrodes. 1395
May, I. Borohydride-flame determination of arsenic in phosphoric acid. 2376
May, W. E. Chemically-bonded aminosilane stationary phase for the high-performance liquid chromatographic separation of polynuclear aromatic compounds. 2306
Meehan, E. J. Principles of nephelometric titrations and application to titration of dilute solutions of bromide. 2268
Mefford, I. Liquid chromatographic determination of picomole quantities of aromatic amine carcinogens. 683
Megargle, R. G. Determination of parts per billion levels of electrodeposited metals by energy dispersive x-ray fluorescence spectrometry. 1734
Melander, W. Liquid chromatography of ionogenic substances with nonpolar stationary phases. 142
Melander, W. Enhancement of retention by ion-pair formation in liquid chromatography with nonpolar stationary phases. 2295
Meloan, C. E. Ultrasonic absorption spectra of vanadium benzohydroxamic acid in 1-butanol. 881
Melville, R. S. Future trends in clinical chemistry. 594a
Menden, E. E. Dry ashing of animal tissues for atomic absorption spectrometric determination of zinc, copper, cadmium, lead, iron, manganese, magnesium and calcium. 1644
Meresz, O. Determination of free and total potential haloforms in drinking water. 814
Metzler, D. E. Digital analysis of electronic absorption spectra. 864a
Meyer, E. F. Precision in thermodynamic properties of solution determined by gas-liquid chromatography. 1029
Meyer, M. L. Mercury-gold minigrid optically transparent thin-layer electrode. 602
Michael, S. S. Determination of arsenic in sulfide samples containing antimony by atomic absorption spectrometry. 451
Midgley, D. Criterion for judging the acceptability of analytical methods. 510
Midgley, D. The interpretation of non-ideal calibrations of ion-selective electrodes. 1211
Milano, M. J. Diode array spectrometer for the simultaneous determination of hemoglobins in whole blood. 555
Milazzo, G. Reference materials for ultraviolet spectrophotometry. 711
Millard, M. M. Surface studies of mammalian cells grown in culture by x-ray photoelectron spectroscopy. 1290
Miller, A. G. Laser Raman spectrometric determination of oxy anions in nuclear waste materials. 2044
Miller, M. P. Spectroscopic system for the study of fluorescent lanthanide probe ions in solids. 1474
Miller, T. C. Chemical characterization via fluorescence spectral files and data compression by Fourier transformation. 2069
Millero, F. J. Effect of chloride ion and ionic strength on the response of a copper(II) ion-selective electrode. 877
Mills, W. N. Multiple-curve procedure for improving precision with calibration-curve-based analyses. 1655
Missen, A. W. Detection of 3,3'-spirobiphthalide from the oxidation of amitriptyline. 1864
Mitchell, D. G. Determination of organic carbon by thermal volatilization plasma emission spectrometry. 1235
Mitchell, D. G. Multiple-curve procedure for improving precision with calibration-curve-based analyses. 1655
Mittler, A. Determination of trace transition elements in solids by proton induced x-ray emission analysis. 432
Miyakura, T. Determination of 4,4'-alkyl- and alkoxy-disubstituted azoxybenzenes by isocratic reverse phase high performance liquid chromatography. 1963
Miyashita, Y. On-line digitization system for a grating infrared spectrophotometer 1875
Mohammad, M. Application of the line shape of linear scan and cyclic voltammograms for the determination of the rate constant and reversible $E_{1/2}$ for a chemical reaction preceded by a reversible charge transfer. 60
Mohan, M. S. Activity coefficients and osmotic coefficients in aqueous solutions of choline chloride at 25°C. 209
Mohr, R. H. Preparation of high alloy aluminum spectroscopic reference materials by compacting alloy powder. 679
Mollica, J. A. Thin-layer chromatographic determination of hydrazine in aqueous and alcoholic media. 161
Molnar, I. Liquid chromatography of ionogenic substances with nonpolar stationary phases. 142
Molnar, I. Enhancement of retention by ion-pair formation in liquid chromatography with nonpolar stationary phases. 2295
Molnar, P. Enhancement of retention by ion-pair formation in liquid chromatography with nonpolar stationary phases. 2295
Moody, J. R. Selection and cleaning of plastic containers for storage of trace element samples. 2264
Moore, W. M. Phase-selective cathodic stripping voltammetry for determination of water-soluble mercaptans. 1386
Moorhead, E. D. Digital microcoulometric measurements of cadmium anodic stripping at the micrometer hanging mercury drop electrode. 199
Morf, W. E. Mechanism of neutral carrier mediated ion transport through ion-selective bulk membranes. 1567
Morf, W. E. Calculation of liquid-junction potentials and membrane potentials on the basis of the Planck theory. 810
Morgan, A. E. Test of a quantitative approach to secondary ion mass spectrometry on glass and silicate standards. 927
Morris, J. L. Jr. Normal pulse voltammetry in electrochemically poised systems. 489
Morris, M. C. Rubber. 133r
Morrison, G. H. Evaluation of silicon vidicon detector sensitivity for atomic spectrometry applications. 106
Morrison, G. H. Sampling error in ion microprobe analysis. 1529
Morrison, G. H. Quantitation of secondary ion mass spectrometric images by microphotodensitometry and digital image processing. 2322
Mosback, H. Pumping pressure and reagent consumption in flow injection analysis. Comments. 1858
Moschini, G. Determination of selenium in blood serum by proton-induced x-ray emission. 1313
Mottola, H. A. Kinetics of oxalate attack on ferrozine-iron(II) complex and regeneration of ligand in determination of iron(II). 319
Mottola, H. A. Repetitive determination of isonicotinic acid hydrazide in flow-through systems by series reactions. 1706
Mottola, H. A. Nonmembrane amperometric sensor for dissolved oxygen in flow-through systems. 2118
Mottola, H. A. Repetitive determination of isonicotinic acid hydrazide in flow-through systems by series reactions. Reply to comments. 2367
Moyer, E. Pharmaceuticals and related drugs. 110r
Moyers, E. M. Preparation and analytical applications of a propylenediaminetetraacetic acid resin. 418

Mubarak, A. Elimination of chloride interferences with mercuric ions in the determination of nitrates by the phenoldisulfonic acid method. 857
Mueller, J. A high-speed, high-purity extraction apparatus. 1465
Mujsce, A. M. In situ generation of standards for gas chromatographic analysis. 139
Mujsce, A. M. Generation of nitrosamines for gas chromatographic analysis via direct injection. 1544
Mule, S. J. Quantitative determination of benzoylecgonine and cocaine in human biofluids by gas–liquid chromatography. 1965
Mun, I. K. Computer assignment of elemental compositions of mass spectral peaks from isotopic abundances. 1723
Munk, M. E. Computer-assisted interpretation of carbon-13 nuclear magnetic resonance spectra applied to structure elucidation of natural products. 2075
Munson, B. Techniques in gas chromatography/chemical ionization mass spectrometry. 169
Munson, B. Reactant ion monitoring for selective detection in gas chromatography/chemical ionization mass spectrometry. 731
Munson, B. Chemical ionization mass spectrometry: ten years later. 772a
Murata, T. Qualitative and quantitative chemical ionization mass spectrometry of triglycerides. 728
Murata, T. Analysis of triglycerides by gas chromatography/chemical ionization mass spectrometry. 2209
Murphy, L. D. Enhancement of the fluorescence intensity of derivatives of amino acids in mixed solvent systems. 1606
Murphy, P. J. Determination of mercury in silver or silver nitrate by atomic absorption spectrometry. 255
Murray, R. W. Surface electrochemistry of iron porphyrins and iron on tin oxide electrodes. 194
Myers, M. N. Theoretical and experimental characterization of field-flow fractionation (correction). 523
Myers, M. N. Exclusion chromatography in dense gases: an approach to viscosity optimization. 243
Myers, M. N. Peak shifts and distortion due to solute relaxation in flow field-flow fractionation. 659
Myers, M. N. Peak broadening factors in thermal field-flow fractionation. 1750
Nadeau, J. S. A stable free radical reagent and solid phase suitable for a nitric oxide dosimeter. 1672
Natusch, D. F. S. Theoretical assessment of precision in dual wavelength spectrophotometric measurement. 2170
Navratil, J. D. Open-pore polyurethane columns for collection and preconcentration of polynuclear aromatic hydrocarbons from water. 2260
Naworal, J. D. Software package to collect and process radiogas chromatographic data. 1726
Neher, M. B. In situ decomposition product isolated from Tenax GC while sampling stack gases. 512
Nelms, L. H. Personal vinyl chloride monitoring device with permeation technique for sampling. 994
Newell, R. D. Bioassay of nystatin bulk material by flow microcalorimetry. 34
Newell, R. D. Bioassay of antifungal antibiotics by flow microcalorimetry. 1781
Newman, L. Silver-110 microgram sulfate analysis for the short time resolution of ambient levels of sulfur aerosol. 1579
Nichols, A. C. Iodine-amine charge-transfer complexes as spectrophotometric detectants in high pressure liquid chromatography. 2080
Nicholson, A. A. Determination of free and total potential haloforms in drinking water. 814
Nielson, K. K. Matrix corrections for energy dispersive x-ray fluorescence analysis of environmental samples with coherent/incoherent scattered x-rays. 641
Nieman, T. A. Determination of trace concentrations of cobalt(II) and other metals by the chemiluminescent oxidation of gallic acid. 1322
Nieman, T. A. Laboratory real time clock featuring computer, experiment, and manual interaction. 1466
Niki, H. Fourier transform infrared spectrometric determination of gaseous perform ic acid. 1346
Nixon, W. B. Acetylation as a chemical ionization technique in medium-pressure chemical ionization mass spectrometry. 1071
Noller, B. N. Sampling of metal air particulates for analysis by furnace atomic absorption spectrometry. 346
Norelius, J. T. Evaluation of tetraphenylporphinatozinc(II) as a stable standard for porphyrin determinations by fluorescence spectrometry. 1453
Norvell, V. E. Optically transparent vitreous carbon electrode. 1470
Nowak, R. J. Spectrophotometric determination of vitamin K compounds. 1343
Nulton, C. P. Software package to collect and process radiogas chromatographic data. 1726
O'Connell, A. W. Analysis of coconut oil–diethanolamine condensates by gas chromatography. 835
O'Connor, J. M. Thin-layer chromatographic determination of hydrazine in aqueous and alcoholic media. 161
O'Dea, W. A. Apparatus for preparing nitrogen from ammonium chloride for nitrogen-15 determinations. 514
Ogata, M. Colorimetric determination of hippuric acid in urine and liver homogenate. 1494
Ogawa, T. Detection limit of fluorescein as determined by fluorometry with an esculin laser source. 667
Oglesby, G. B. Effect of chloride ion and ionic strength on the response of a copper(II) ion-selective electrode. 877
O'Halloran, R. J. Fundamental and second harmonic alternating current cyclic voltammetric theory and experimental results for simple electrode reactions involving solution-soluble redox couples (correction). 896
O'Haver, T. C. Waveform effects in wavelength modulation spectrometry. 458
O'Haver, T. C. Improvements in the measurements of characteristic concentrations in continuum source atomic absorption spectrometry. 665
O'Haver, T. C. Correction for interferences of spectral origin with continuum source, echelle wavelength modulated atomic absorption spectrometry. 838
O'Haver, T. C. Background correction for the analysis of high-solids samples by graphite furnace atomic absorption. 2187
Ohmori, S. Colorimetric determination of hippuric acid in urine and liver homogenate. 1494
Ohtaki, H. Amalgam electrode designed for precise electromotive force measurements. 190
Oikawa, K. On-line digitization system for a grating infrared spectrophotometer. 1810
O'Kane, J. L. Monitoring and identification of nonvolatile organic deposits in used catalysts. 2374
O'Keeffe, A. E. Advances in assembling permeation tubes. 1278
O'Laughlin, J. W. Differential pulse polarographic determination of nitrate and nitrite. 479
Oldham, K. B. Peak shapes in semidifferential electroanalysis. 1390
Olsen, R. R. Palladium and titanium thin films as probes for determination of hydrogen in helium. 853
Olson, K. R. Loss of carbon-14 and mercury-203 labeled methylmercury from various solutions. 23
Olson, K. W. Multielement detection limits and sample nebulization efficiencies of an improved ultrasonic nebulizer and a conventional pneumatic nebulizer in inductively coupled plasma-atomic emission spectrometry. 632
Omenetto, N. Pulsed vs. continuous wave atomic fluorescence spectrometry. 1076
O'Neill, I. K. Determination of L-hydroxyproline in meat protein by quantitative carbon-13 Fourier transform nuclear magnetic resonance spectrometry. 1140
O'Neill, I. K. Determination of 2-aminoethyl dihydrogen phosphate by phospho rus-31 Fourier transform nuclear magnetic resonance spectrometry. 588
Ophaug, R. H. Determination of fluorine in blood plasma. 38
Opheim, L. N. Determination of phosphorus in milk powders by optical emission spectrometry with a high frequency inductively-coupled argon plasma source 1492
Ord, D. A. Determination of mefruside and its metabolites in urine by high performance liquid chromatography. 1311
Osteryoung, J. G. Determination of some thiourea-containing pesticides by pulse voltammetric methods of analysis. 2310
Osteryoung, R. A. Digital simulation of differential pulse polarography with incremental time change. 1246
Osteryoung, R. A. Square wave voltammetry at the dropping mercury electrode: theory. 1899
Osteryoung, R. A. Square wave voltammetry at the dropping mercury electrode: experimental. 1904
Oteiza, R. M. Reaction-rate method for the determination of hydrocortisone. 1586
Ozawa, Y. Automated determination of carboxylic acids by anion-exchange chromatography with specific color reaction. 655
Padmanabhan, G. R. Thin-layer chromatographic determination of hydrazine in aqueous and alcoholic media. 161
Palermo, P. J. Gas chromatographic determination of β-hydroxyethylhydrazine in the presence of its synthesis by-products. 2213
Palme, C. Application of the fundamental parameter method for the determination of major and minor elements in fused geological samples with x-ray fluorescence spectrometry. 717
Palumbo-Doretti, M. Reference materials for ultraviolet spectrophotometry. 711
Pannell, L. K. Defocused metastable scanning with a mass spectrometer and laboratory data system. 174
Pardue, H. L. Kinetic study of the cyanogen bromide–pyridine reaction applied to thiocyanate determinations in serum. 785
Pardue, H. L. Design and evaluation of a vidicon based derivative spectrometer. 871
Pardue, H. L. Design and evaluation of a random access vidicon–echelle spectrometer and application to multielement determinations by atomic absorption spectrometry. 1112
Pardue, H. L. Performance of a silicon target vidicon tube as a multiwavelength detector for liquid chromatography. 1171
Parissakis, G. Determination of germanium in oxides, ores, and alloys by chlorination and gas chromatography. 909
Parkinson, T. F. Determination of fluorine by neutron activation analysis. 1507
Parris, G. E. Chemical and physical considerations in the use of atomic absorption detectors coupled with a gas chromatograph for determination of trace organometallic gases. 378
Parris, N. Determination of sulfobetaine amphoteric surfactants by reverse phase high performance liquid chromatography 2228
Parrish, J. R. Macroporous resins as supports for a chelating liquid ion-exchanger in extraction chromatography. 1189
Parrish, W. Simultaneous determination of composition and mass thickness of thin films by quantitative x-ray fluorescence analysis. 1152
Parsons, M. L. Preparation of electrodeless discharge lamps for elements forming gaseous covalent hydrides. 551
Paschal, D. C. Determination of ethyl and methyl parathion in runoff water with high performance liquid chromatography 1551
Pasteur, G. A. Quantitative determination of stabilizers in tetraethylene glycol dimethacrylate by high-pressure liquid chromatography. 363
Patel, A. H. Detection of tetrahydrocannabinol in blood and serum using a fluorescent derivative and thin-layer chromatography. 163
Patel, D. D. Detection of tetrahydrocannabinol in blood and serum using a fluorescent derivative and thin-layer chromatography. 163
Patriarche, G. J. Spectrophotometric determination of vitamin K compounds. 1343

Patton, C. J. Spectrophotometric and kinetics investigation of the Berthelot reaction for the determination of ammonia. 464
Pauls, R. E. Band broadening studies using parameters for an exponentially modified Gaussian. 625
Pearson, C. D. Determination of hydrogen sulfide, carbonyl sulfide, carbon disulfide, and sulfur dioxide in gases and hydrocarbon streams by gas chromatography/flame photometric detection. 123
Pearson, K. H. Determination of parts per billion levels of electrodeposited metals by energy dispersive x-ray fluorescence spectrometry. 1734
Pearson, R. M. Spectrophotometric determination of cobalt complexed with the p-nitrophenylhydrazone of diacetylmonoxime and ethylenediamine. 580
Pederson, L. A. Compositional analyses of methyl methacrylate–methacrylic acid copolymers by carbon-13 nuclear magnetic resonance spectrometry. 77
Peele, G. L. Cleaning of mass spectrometer ion sources by electropolishing. 674
Pecsok, P. J. Digital device for precise determination of drop times at dropping mercury electrodes. 1270
Pemberton, J. E. Small volume, high performance cell for nonaqueous spectroelectrochemistry. 1646
Pembleton, R. G. Pulsed nuclear magnetic resonance spectrometry for nondestructive determination of hydrogen in coal. 75
Penca, M. Combined retrieval system for infrared, mass, and carbon-13 nuclear magnetic resonance spectra. 2141
Pennings, A. J. Sealed stainless cell for differential scanning calorimetry on volatile systems. 522
Perone, S. P. Application of pattern recognition techniques to the interpretation of severely overlapped voltammetric data: theoretical studies. 1369
Perone, S. P. Application of pattern recognition techniques to the interpretation of severely overlapped voltammetric data: studies with experimental data. 1376
Perone, S. P. Factor analysis of the mass spectra of oligodeoxyribonucleotides. 1444
Perry, J. A. Microprocessor-controlled, scanning dye laser for spectrometric analytical systems. 1702
Pesek, J. J. Evidence for solute–brush interactions on nonpolar chemically bonded stationary phases in gas chromatography. 133
Petering, H. G. Dry ashing of animal tissues for atomic absorption spectrometric determination of zinc, copper, cadmium, lead, iron, manganese, magnesium and calcium. 1644
Petersen, B. A. Analysis of explosives by high performance liquid chromatography and chemical ionization mass spectrometry. 1039
Petersen, B. A. Analysis of thyroid hormones as their heptafluorobutyryl methyl ester derivatives by gas chromatography – mass spectrometry. 1304
Petri, H. Determination of 13 elements with atomic numbers between 12 and 47 by 14-MeV helium-3 activation analysis. 1510
Phillips, C. S. G. Ion-exchangers for gas–solid chromatography. 1549
Pickering, R. E. Short excitation wavelength fluorometric detection in high-pressure liquid chromatography of indole peptide, naphthyl, and phenol compounds. 1836
Pierce, F. D. Comparison of inorganic interferences in atomic absorption spectrometric determination of arsenic and selenium. 1417
Pietrzyk, D. J. Amberlite XAD copolymers in reversed phase gravity flow and high pressure liquid chromatography. 757
Pietrzyk, D. J. Separation of organic acids on amberlite XAD copolymers by reversed phase high pressure liquid chromatography. 860
Pinto, A. Calibration procedure to minimize errors in continuous analysis by ion selective electrodes. 2377
Pitner, T. P. Deuterium nuclear magnetic resonance spectra from milligram quantities of isotopically enriched compounds (correction). 1280
Pitner, T. P. Deuterium nuclear magnetic resonance spectra from milligram quantities of isotopically enriched compounds. 674
Place, A. R. Application of N,N-dimethylformamide to atomic absorption spectrophotometry of organometallic compounds. 2122
Podolak, G. E. Determination of phosgene in air by gas chromatography and infrared spectrophotometry. 1774
Poe, D. P. Removal of iron, copper, cadmium, cobalt, and nickel from sodium hydroxide by precipitation and extraction with phenyl-2-pyridyl ketoxime. 889
Poinescu, I. C. Particle porosimetry by inverse gel permeation chromatography. 1183
Poldoski, J. E. Computer-assisted furnace atomic absorption spectrometric analysis 891
Pollock, G. E. Determination of the D and L isomers of some protein amino acids present in soils. 2
Porter, L. K. Apparatus for preparing nitrogen from ammonium chloride for nitrogen-15 determinations. 514
Preiss, B. Direct transfer of thin-layer chromatographic fractions into vials. 671
Prescott, S. R. Negative ion chemical ionization mass spectrometry of volatile metal chelates. 1501
Preston, J. M. Plasma chromatography of phosphorus esters. 1746
Price, D. R. Liquid chromatographic determination of residual acrylamide monomer in aqueous and nonaqueous dispersed phase polymer systems. 154
Price, P. C. New drift-tube source for use in chemical ionization mass spectrometry. 1497
Pringuer, M. A. Determination of 2-amino ethyl dihydrogen phosphate by phosphorus-31 Fourier transform nuclear magnetic resonance spectrometry. 588
Propst, R. C. Cathodic pulse stripping analysis of iodine at the parts-per-billion level. 1199
Prosser, H. J. Determination of L-hydroxyproline in meat protein by quantitative carbon-13 Fourier transform nuclear magnetic resonance spectrometry. 1140
Prudencio, M. Multiple ion detection system with miniscan facilities and expanded mass range for magnetic sector mass spectrometers. 543
Puon, S. Potentiometric titration of acids in the presence of a nonionic resin. 1256
Qureshi, M. Synthesis and ion-exchange properties of crystalline stannic vanadophosphate. 165
Rabenstein, D. L. Mercury-based electrochemical detector for liquid chromatography for the detection of glutathione and other sulfur-containing compounds. 1036
Ramette, R. W. Determination of hydrogen ion concentrations in seawater from 5 to 40°C: standard potentials at salinities from 20 to 45%. 29
Ramette, R. W. Acid-base properties of tris(hydroxymethyl)aminomethane (Tris) buffers in sea water from 5 to 40°C. 867
Ramljak, Z. Separation of acids from asphalts. 1222
Ramstad, T. Automated cleanup of herbicides by adsorption chromatography for the determination of 2,3,7,8-tetrachlorodibenzo-p-dioxin. 386
Ratzlaff, K. L. Theoretical assessment of precision in dual wavelength spectrophotometric measurement. 2170
Rebec, M. Kinetic study of the cyanogen bromide–pyridine reaction applied to thiocyanate determinations in serum. 785
Rechnitz, G. A. Protein response of silver sulfide crystal membrane electrodes. 41
Rechnitz, G. A. Ion electrode measurements of complement and antibody levels using marker-loaded sheep red blood cell ghosts. 2083
Reddy, M. M. Tris(pyrrolidine dithiocarbamato)cobalt(III) chelate matrix for trace metal preconcentration from aqueous solution by coprecipitation. 222
Redfield, H. L. Preparation of high alloy aluminum spectroscopic reference materials by compacting alloy powder. 679
Reeves, R. L. Digital analysis of electronic absorption spectra. 864a
Reich, R. M. Capacitor discharge temperature-jump apparatus with nanosecond capabilities. 1081
Reich, R. M. A demountable temperature jump cell. 2378
Reid, P. I. Quantitative analysis of aluminosilicates and other solids by x-ray photoelectron spectroscopy. 2001
Reilley, C. N. Uniqueness of carbon-13 nuclear magnetic resonance spectra of acyclic saturated hydrocarbons. 1134
Reilly, D. A. Determination of hydrogen cyanide in combustion gases by a four-channel continuous analyzer. 322
Reiner, D. Removal of iron, copper, cadmium, cobalt, and nickel from sodium hydroxide by precipitation and extraction with phenyl-2-pyridyl ketoxime. 889
Reiser, R. W. Determination of sub-microgram per cubic meter levels of N-nitrosodimethylamine in air. 1821
Reiszner, K. D. Personal vinyl chloride monitoring device with permeation technique for sampling. 994
Renberg, L. Residue analysis of sediment and sewage sludge for organochlorines in the presence of elemental sulfur. 316
Resnick, E. W. Electrocatalysis of the reduction of iron(III) by halides adsorbed at platinum electrodes in perchloric acid solutions. 1918
Resnick, R. B. Quantitative determination of benzoylecgonine and cocaine in human biofluids by gas–liquid chromatography. 1965
Retcofsky, H. L. Determination of aromaticities of coal derivatives by nuclear magnetic resonance spectrometry and the Brown–Ladner equation. 585
Reuter, W. Detection sensitivities for thick specimens in proton and electron induced x-ray spectrometry. 1737
Reutergardh, L. Residue analysis of sediment and sewage sludge for organochlorines in the presence of elemental sulfur. 316
Rexroad, P. R. Fertilizers. 186r
Reynolds, R. L. Filter attenuation corrections for the x-ray fluorescence analysis of atmospheric aerosols. 1990
Richards, J. A. Low capacity codes for mass spectra based on statistical moments. 1456
Richardson, J. H. Sub-part-per-trillion detection of polycyclic aromatic hydrocarbons by laser induced molecular fluorescence. 955
Richmond, I. J. Determination of hydrogen content of fuel by low resolution proton nuclear magnetic resonance spectrometry. 594
Richter, B. E. Determination of nitrite by direct injection enthalpimetry. 1779
Ridder, G. M. Simultaneous kinetic analysis of multicomponent mixtures. 2096
Ridder, G. M. Simultaneous kinetic and spectral analysis with a vidicon rapid-scanning stopped-flow spectrometer. 2098
Rigdon, L. P. Equivalence-point determinations for automated potentiometric titrations with ion-selective electrodes. 1250
Riggin, R. M. Determination of tetrahydroisoquinoline alkaloids in biological materials with high performance liquid chromatography. 530
Riggin, R. M. Determination of catecholamines in urine by reverse-phase liquid chromatography with electrochemical detection. 2109
Rindfleisch, T. C. Quantitative comparison of combined gas chromatographic/mass spectrometric profiles of complex mixtures. 1623
Rinehart, E. A. Analytical microwave spectrometry. 249a
Rion, K. F. Characterization of lignites by pyrolysis–gas chromatography. 1540
Risby, T. H. Steady-state kinetic treatment of the emission from reduced pressure microwave induced discharges in helium. 560
Risby, T. H. Negative ion chemical ionization mass spectrometry of volatile metal chelates. 1501, 2380
Ritter, G. L. Dimensionality and the number of features in "learning machine" classification methods. 2116
Roberts, R. F. Stabilizing the manganese tetramethylenedithiocarbamate/methyl isobutyl ketone extract. 1862

Robertson, W. M. Determination of the composition of mixtures of sodium chromite and chromic oxide by electron spin resonance spectrometry. 962
Rogers, C. H. Determination of total sulfur in gasoline by gas chromatography with a flame photometric detector. 126
Rogers, L. B. Band broadening studies using parameters for an exponentially modified Gaussian. 625
Rogers, L. B. Micro sampling and the use of a flow cell for coherent anti-Stokes Raman spectrometry. 959
Ronning, M. A. Detection of trinitrotoluene in water by fluorescent ion-exchange resins. 2251
Rook, H. L. Performance of a nitrogen dioxide permeation device. 1823
Rosenfeld, J. M. Determination of 6-mercaptopurine in plasma by mass spectrometry. 725
Rosie, D. M. Identification of nucleosides and bases in serum and plasma samples by reverse-phase high performance liquid chromatography. 2237
Rosin, D. Chromatographic measurement of submicromolar strong complexing capacity in phytoplankton media. 226
Roth, J. R. Quantitation of secondary ion mass spectrometric images by microphotodensitometry and digital image processing. 2322
Rothman, L. D. Voltage controlled oscillator for signal-proportional data acquisition rates. 681
Routh, M. W. Performance of the Super Modified Simplex. 1422
Rulon, P. W. Photographic techniques for fluorescent spots on thin-layer chromatographic plates. 1640
Ruo, T. C. S. Determination of tetraethyllead in gasolines by high performance liquid chromatography. 1761
Rus, V. Gas chromatographic column for separation of organochlorine insecticide residues. 2123
Rutenberg, A. C. Determination of the epoxide equivalent weight of glycidyl ethers by proton magnetic resonance spectrometry. 1144
Ruzic, I. Fundamental and second harmonic alternating current cyclic voltammetric theory and experimental results for simple electrode reactions involving solution-soluble redox couples (correction). 896
Ruzicka, J. Pumping pressure and reagent consumption in flow injection analysis. Comments. 1658
Saba, C. S. Determination of titanium in aircraft lubricating oils by atomic absorption spectrophotometry. 454
Saetre, R. Mercury-based electrochemical detector for liquid chromatography for the detection of glutathione and other sulfur-containing compounds. 1036
Saltzman, B. E. Air pollution. 1r
Sandmann, J. Determination of tryptophan in plasma with a spectrofluorometer system. 950
Saner, W. A. Optical multichannel analyzer for characterization of fluorescent liquid chromatographic petroleum fractions. 1316
Sansone, E. B. Potential hazard associated with removal of needles from septa in injection ports of a gas chromatograph. 670
Santhanam, K. S. V. Photothermal spectroscopy. 2057
Santini, R. E. Design and evaluation of a vidicon based derivative spectrometer. 871
Sasa, S. Determination of serotonin and dopamine in mouse brain tissue by high performance liquid chromatography with electrochemical detection. 354
Sasaki, S. On-line digitization system for a grating infrared spectrophotometer. 1875
Sastri, C. S. Determination of 13 elements with atomic numbers between 12 and 47 by 14-MeV helium-3 activation analysis. 1510
Sattler, P. F. Colorimetric determination of niobium in sodium metal with thiocyanate. 80
Saturday, K. A. Physical characterization of the helium-oxygen-acetylene flame as an atom cell for atomic spectrometry. 2013
Savage, C. M. Fourier transform infrared spectrometric determination of gaseous performic acid. 1346
Sawyer, D. T. Voltammetric determination of nitrate ion at parts-per-billion levels. 485
Schabron, J. F. Separation of hydroaromatics and polycyclic aromatic hydrocarbons and determination of tetralin and naphthalene in coal-derived solvents. 2253
Scheppele, S. E. Field-ionization relative sensitivities for analysis of coal-derived liquids determined as a function of ion-source temperature and binary-mixture composition. 1847
Schick, J. W. Petroleum. Wax. , 276r
Schieffer, G. W. Study of anodic stripping voltammetry with collection at tubular electrodes. 49
Schifreen, R. S. Analytical aspects of immobilized enzyme columns. 1929
Schiller, J. E. Separation method for coal-derived solids and heavy liquids. 1225
Schiller, J. E. Preparation and low-voltage mass spectrometry sensitivities of methylated polynuclear aromatic hydrocarbons 1260
Schiller, J. E. Nitrogen compounds in coal derived liquids. 2292
Schilling, J. G. Determination of bromine in silicate rocks by epithermal neutron activation analysis. 1998
Schilt, A. A. Analytical studies and applications of ferroin type chromogens immobilized by adsorption on a styrene-divinylbenzene copolymer. 974
Schlueter, D. D. Determination of imides, aromatic polyimides, polyamides, and poly(amide-imides) by alkali fusion reaction gas chromatography. 2349
Schlueter, D. D. Analysis of polysiloxanes by alkali fusion reaction gas chromatography. 2343
Schmeltz, I. Redox potential and quinone content of cigarette smoke. 1924
Schmitter, J. M. Separation of acids from asphalts. 1222
Schoeffel, J. A. Quantitative elemental analysis of substituted hydrocarbon monolayers on platinum by Auger electron spectroscopy with electrochemical calibration. 2330
Schoeller, D. A. High precision pulse counting: limitations and optimal conditions. 306
Schouteten, C. J. H. Sealed stainless cell for differential scanning calorimetry on volatile systems. 522
Schreinlechner, I. E. Colorimetric determination of niobium in sodium metal with thiocyanate. 80
Schulten, H. R. Determination of alkali elements by field desorption mass spectrometry. 1744
Schulting, F. L. Interference of 1-chloro-2-propanol in the determination of bis(chloromethyl) ether in air by gas chromatography-mass spectrometry. 2365
Schultz, H. Solid and gaseous fuels. 176r
Schumaker, R. R. Voltammetry and potentiometry of tetrathiafulvalene halides. 802
Schwager, I. Molecular weight and association of coal-derived asphaltenes. 2363
Schwall, R. J. High speed synchronous data generation and sampler system: application to on-line fast Fourier transform faradaic admittance measurements. 1797
Schwall, R. J. On-line fast Fourier transform faradaic admittance measurements: real-time deconvolution of heterogeneous charge transfer kinetic effects for thermodynamic and analytical measurements. 1805
Schwartz, L. M. Nonlinear calibration. 2062
Schweighardt, F. K. Determination of aromaticities of coal derivatives by nuclear magnetic resonance spectrometry and the Brown-Ladner equation. 585
Schwertner, H. A. Determination of primidone by electron-capture gas chromatography. 903
Schwertner, H. A. Determination of phenylethylmalonamide by electron-capture gas chromatography. 1969
Scibona, G. Monoionic liquid membrane potential in non-isothermal systems. 212
Scilla, G. J. Sampling error in ion microprobe analysis. 1529
Scoggins, M. W. Spectrophotometric determination of ethylene glycol in motor oil. 582
Scott, B. A. Voltammetry and potentiometry of tetrathiafulvalene halides. 802
Scott, K. N. Quantitative analysis of mixtures by carbon-13 nuclear magnetic resonance spectrometry. 2130
Scuppa, B. Monoionic liquid membrane potential in non-isothermal systems. 212
Seiber, J. N. Chlorine-selective detection for liquid chromatography with a Coulson electrolytic conductivity detector. 326
Seim, H. J. Spectrophotometric determination of cobalt complexed with the p-nitrophenylhydrazone of diacetylmonoxime and ethylenediamine. 580
Seim, H. J. Nonferrous metallurgy-light metals: aluminum, beryllium, titanium, and magnesium. 72r
Selig, W. Equivalence-point determinations for automated potentiometric titrations with ion-selective electrodes. 1250
Selucky, M. L. Determination of tetraethyllead in gasolines by high performance liquid chromatography. 1761
Semonian, B. P. Flow method for determination of desorption isotherms and pore size distribution. 991
Sepaniak, M. J. Laser two-photon excited fluorescence detection for high pressure liquid chromatography. 1554
Serravallo, F. A. Steady-state kinetic treatment of the emission from reduced pressure microwave induced discharges in helium. 560
Seymour, M. D. Determination of pK_a values of acid components in atmospheric condensates by linearization of segmented titration curves. 1429
Shabanowitz, J. Chemical ionization mass spectrometry of salts and thermally labile organics with field desorption emitters as solids probes. 1160
Shabanowitz, J. Determination of molecular compositions on a quadrupole mass spectrometer by pulsed positive ion negative ion chemical ionization mass spectrometry. 1884
Shaikh, A. U. Determination of sub-microgram per liter quantities of arsenic in water by arsine generation followed by graphite furnace atomic absorption spectrometry. 1093
Sharma, S. P. Oxide films on sputtered tin-nickel alloy exposed to pure oxygen and air. 987
Shatkay, A. Unrecognized systematic errors in quantitative analysis by gas-liquid chromatography. 2222
Shaw, L. M. Progress curve algorithm for calculating enzyme activities from kinetic assay spectrophotometric measurements. 1716
Shearer, J. C. Fourier Transform infrared analysis below the one-nanogram level. 2275
Sheehan, T. L. Analytical study of chemiluminescence from the vitamin B_{12}-lumichrome system. 446
Shelley, C. A. Computer-assisted interpretation of carbon-13 nuclear magnetic resonance spectra applied to structure elucidation of natural products. 2075
Shen, J. In-situ sampling system for thermal volatilization analysis of nonvolatile materials by gas chromatography-mass spectrometry. 886
Shen, J. Monitoring and identification of nonvolatile organic deposits in used catalysts. 2374
Shiau, L.-J. Determination of mercury in edible oils by combustion and atomic absorption spectrophotometry. 1641
Shimek, E. L. Jr. Determination of primidone by electron-capture gas chromatography. 903
Shimek, E. L. Jr. Determination of phenylethylmalonamide by electron-capture gas chromatography. 1969
Shiono, S. Determination of 4,4'-alkyl- and alkoxy-disubstituted azoxybenzenes by isocratic reverse phase high performance liquid chromatography. 1963
Shrauger, N. K. Minicomputer data processing system for air monitoring studies 357a
Siegfried, R. Determination of acid POH groups of hydrolysis-susceptible esters of phosphorous acid. 1584
Siemer, D. D. Comparison of methods of hydride generation atomic absorption spectrometric arsenic and selenium determination. 1096

Sievers, R. E. Open-pore polyurethane columns for collection and preconcentration of polynuclear aromatic hydrocarbons from water. 2260
Siggia, S. Determination of micromolar quantities of primary amides by flame emission spectrometry. 262
Siggia, S. Determination of imides, aromatic polyimides, polyamides, and poly(amide-imides) by alkali fusion reaction gas chromatography. 2349
Siggia, S. Determination of carboxylic esters by acid fusion reaction gas chromatography. 2337
Siggia, S. Analysis of polysiloxanes by alkali fusion reaction gas chromatography. 2343
Sill, C. W. Determination of thorium and uranium in ores and mill tailings by alpha spectrometry (correction). 1648
Sill, C. W. Radiochemical determination of lead-210 in uranium ores and air dusts. 302
Sill, C. W. Determination of thorium and uranium isotopes in ores and mill tailings by alpha spectrometry. 618
Silver, H. F. Separation of hydroaromatics and polycyclic aromatic hydrocarbons and determination of tetralin and naphthalene in coal-derived solvents. 2253
Simon, P. J. Categorization of papers by trace metal content using atomic absorption spectrometric and pattern recognition techniques. 2285
Simon, W. Mechanism of neutral carrier mediated ion transport through ion-selective bulk membranes. 1567
Simons, D. S. Evaluation of the local thermal equilibrium model for quantitative secondary ion mass spectrometric analysis (correction). 896
Singer, L. Determination of fluorine in blood plasma. 38
Singley, K. F. Determination of sulfur in organic molecules by spectrophotometric titration. 1987
Sinnamon, J. T. Integrating analog-to-digital converter displaying high signal fidelity and noise immunity. 1869
Sirota, G. R. Determination of tetraalkyllead compounds in biological materials. 823
Sloman, K. G. Food. 194r
Smit, M. C. B. Determination of uranium in natural water by preconcentration on anion-exchange resin and delayed-neutron counting. 67
Smith, B. W. Pulsed vs. continuous wave atomic fluorescence spectrometry. 1076
Smith, D. E. Fundamental and second harmonic alternating current cyclic voltammetric theory and experimental results for simple electrode reactions involving solution-soluble redox couples (correction). 896
Smith, D. E. High speed synchronous data generation and sampler system: application to on-line fast Fourier transform faradaic admittance measurements. 1797
Smith, D. E. On-line fast Fourier transform faradaic admittance measurements: real-time deconvolution of heterogeneous charge transfer kinetic effects for thermodynamic and analytical measurements. 1805
Smith, D. H. Quantitative comparison of combined gas chromatographic/mass spectrometric profiles of complex mixtures. 1623
Smith, J. C. Gas-chromatographic determination of inorganic mercury and organomercurials in biological materials. 365
Smith, L. K. Peak broadening factors in thermal field-flow fractionation. 1750
Smith, L. L. Jr. Direct determination and calculation of aqueous hydrogen sulfide. 424
Smith, R. M. Design and evaluation of a fiber optic fluorometric flow cell. 2051
Smith, S. G. Characterization of lignites by pyrolysis-gas chromatography. 1540
Smyth, M. R. Determination of some thiourea-containing pesticides by pulse voltammetric methods of analysis. 2310
Smyth, W. F. Direct determination of thioamide drugs in biological fluids by cathodic stripping voltammetry. 1195
Snelling, C. R. Jr. Computer-assisted interpretation of carbon-13 nuclear magnetic resonance spectra applied to structure elucidation of natural products 2075
Solc, A. Separation of acids from asphalts. 1222
Solomon, R. A. On-column reaction gas chromatography for determination of chloromethyl methyl ether at one part-per-billion level in ambient air. 1817
Soltero-Rigau, E. Identification of barbiturates by chemical ionization and mass-analyzed ion kinetic energy spectrometry. 435
Soltmann, B. Electron impact ionization mass spectrometry using field desorption activated emitters as solid sample probes. 1164
Songco, D. Automated electrodic potentiometry system. 1908
Sonnenschein, A. Short excitation wavelength fluorometric detection in high-pressure liquid chromatography of indole peptide, naphthyl, and phenol compounds. 1836
Sovocool, G. W. Analysis of technical chlordane by gas chromatography/mass spectrometry. 734
Spencer, F. W. Classification of petroleum pollutants by linear discriminant function analysis of infrared spectral patterns. 500
Spencer, M. J. Multivariate statistical approach to the fingerprinting of oils by infrared spectrometry. 297
Spewar, M. J. Classification of petroleum pollutants by linear discriminant function analysis of infrared spectral patterns. 500
Spencer, R. Automated atomic absorption spectrometric determination of total arsenic in water and streambed materials. 1599
Sperry, R. R. Glass lined field ionization sources. 2121
Srinivasan, V. S. Palladium and titanium thin films as probes for determination of hydrogen in helium. 853
Srinivasan, V. S. Teflon powders for near infrared spectra of hydrides. 1458
Srinivasan, V. S. Sheet resistivity measurements of chemically modified electrodes by four-point probe method. 1639
Stafford, G. C. Determination of molecular compositions on a quadrupole mass spectrometer by pulsed positive ion negative ion chemical ionization mass spectrometry. 1884
Stancer, H. C. Analysis of acidic monoamine metabolites by gas chromatography-mass spectrometry. 915
Starks, S. A. Multivariate statistical approach to the fingerprinting of oils by infrared spectrometry. 297
Statham, P. J. Deconvolution and background subtraction by least-squares fitting with prefiltering of spectra. 2149
Stehl, R. H. Liquid chromatographic determination of residual acrylamide monomer in aqueous and nonaqueous dispersed phase polymeric systems. 154
Stein, J. D. Evaluation of a cesium positive ion source for secondary ion mass spectrometry. 2023
Steinberg, M. Differential thermal analysis and reaction kinetics for nth-order reaction. 998
Steinhart, H. Determination of tryptophan in plasma with a spectrofluorometer system. 950
Sternson, L. A. Liquid chromatographic determination of picomole quantities of aromatic amine carcinogens. 683
Stevens, J. W. Jr. Spectrophotometric determination of acrylonitrile. 2277
Stevens, T. S. Determination of anions in boiler blow-down water with ion chromatography. 1176
Stewart, K. K. Depulsing system for positive displacement pumps. 2125
Stieg, S. Determination of trace concentrations of cobalt(II) and other metals by the chemiluminescent oxidation of gallic acid. 1322
Stievano, B. M. Determination of selenium in blood serum by proton-induced x-ray emission. 1313
Stolzberg, R. J. Chromatographic measurement of submicromolar strong complexing capacity in phytoplankton media. 226
Stolzberg, R. J. Determination of nitrilotriacetate in environmental water by gas chromatography of the trimethylsilyl ester. 374
Stone, H. M. Detection of 3,3'-spirobiphthalide from the oxidation of amitriptyline. 1864
Stone, J. Precolumn synthesis of trimethylsilyl derivatives of aqueous phosphate for gas chromatographic analysis. 1086
Storms, H. A. Evaluation of a cesium positive ion source for secondary ion mass spectrometry. 2023
Stradling, G. N. Determination of americium and curium in biological samples by extraction and liquid scintillation counting. 1268
Straub, W. A. Ferrous metallurgy. 54r
Strausz, O. P. Determination of tetraethyllead in gasolines by high performance liquid chromatography. 1761
Stromberg, S. Determination of tranexamic acid in biological material by electron capture gas chromatography after direct derivatization in an aqueous medium. 369
Stromberg, S. Determination of intact oxazepam by electron capture gas chromatography after an extractive alkylation reaction. 1545
Strong, J. M. Determination of the N-hydroxy and phenolic metabolites of drugs derived from acetanilide by O-alkylation and selected ion monitoring. 1843
Stroupe, R. C. Low-temperature fluorescence spectrometric determination of polycyclic aromatic hydrocarbons by matrix isolation. 701
Stuart, J. D. Micro sampling and the use of a flow cell for coherent anti-Stokes Raman spectrometry. 959
Sturgeon, R. E. Evaluation of pyrolytic-graphite-coated tubes for graphite furnace atomic absorption spectrometry. 90
Sturgeon, R. E. Studies on the mechanism of atom formation in graphite furnace atomic absorption spectrometry (correction). 192
Sturgeon, R. E. Mechanism of atom loss in graphite furnace atomic absorption spectrometry. 1100
Sturgeon, R. E. Studies on the mechanism of atom formation in graphite furnace atomic absorption spectrometry (correction). 1647
Suffet, I. H. Design and optimization of a Teflon Helix Continuous Liquid-Liquid Extraction Apparatus and its application for the analysis of organophosphate pesticides in water. 231
Sunahara, H. Laser-vaporized atomic absorption spectrometry of solid samples 1339
Surprenant, H. L. Uniqueness of carbon-13 nuclear magnetic resonance spectra of acyclic saturated hydrocarbons. 1134
Sutter, J. R. Capacitor discharge temperature-jump apparatus with nanosecond capabilities. 1081
Sutter, J. R. A demountable temperature jump cell. 2378
Swartz, J. L. Null-point control of acidity with a differential pH electrode system. 1009
Swartz, P. A. Performance of the Super Modified Simplex. 1422
Sweeley, C. C. Electron impact ionization mass spectrometry using field desorption activated emitters as solid sample probes. 1164
Sweeney, R. A. Fertilizers. 186r
Swofford, H. S. Jr. New drift-tube source for use in chemical ionization mass spectrometry. 1497
Szabo, A. Determination of molybdenum in seawater by electron paramagnetic resonance spectrometry. 461
Szentrimay, R. Double wavelength spectrophotometry with a rapid scanning instrument. 1348
Taguchi, V. Y. Determination of 6-mercaptopurine in plasma by mass spectrometry. 725
Takahashi, S. Qualitative and quantitative chemical ionization mass spectrometry of triglycerides. 728
Takeuchi, T. Vertical furnace-type sampling device for pyrolysis gas chromatography. 348
Tallant, D. R. Spectroscopic system for the study of fluorescent lanthanide probe ions in solids. 1474
Tallman, D. E. Determination of sub-microgram per liter quantities of arsenic in water by arsine generation followed by

graphite furnace atomic absorption spectrometry. 1093
Talmi, Y. Optical multichannel analyzer for characterization of fluorescent liquid chromatographic petroleum fractions. 1316
Talmi, Y. Signal flicker noise and noise power spectra. Reply to comments. 340
Tamura, Z. Automated determination of carboxylic acids by anion-exchange chromatography with specific color reaction. 655
Tanimura, T. Automated determination of carboxylic acids by anion-exchange chromatography with specific color reaction. 655
Tannenbaum, S. R. An unknown salivary morpholine metabolite. 715a
Tattershall, B. W. Identification of components of mixtures by retrospective computer subtraction of gas-phase infrared spectra. 772
Taylor, J. W. Positional and geometric characterization of olefinic double bonds by fluorine magnetic resonance spectrometry. 2146
Taylor, L. T. Preparative gel permeation chromatographic separation of solvent refined coal. 533
Taylor, P. J. Design, construction, and applications of a galactose selective electrode. 789
Taylor, S. K. Field desorption and electron impact mass spectra of ionic dyes. 922
Teague, J. D. Gas and high pressure liquid chromatographic properties of some 4-nitrobenzamides of amphetamines and related arylalkylamines. 912
Teets, R. E. Correction of right-angle fluorescence measurements for the absorption of excitation radiation. 706
Terrani, M. Gamma-ray activity determination in large volume samples with a germanium-lithium detector. 1156
Terrell, R. E. Petroleum. Metals in oils. 255r
Tessier, A. Critical evaluation of the copper(II) solubilization method for the determination of the complexation capacity of natural waters. 2358
Thoma, A. P. Mechanism of neutral carrier mediated ion transport through ion-selective bulk membranes. 1567
Thomas, J. H. III. Oxide films on sputtered tin-nickel alloy exposed to pure oxygen and air. 987
Thomas, J. M. Quantitative analysis of aluminosilicates and other solids by x-ray photoelectron spectroscopy. 2001
Thomas, Q. V. Application of pattern recognition techniques to the interpretation of severely overlapped voltammetric data: theoretical studies. 1369
Thomas, Q. V. Application of pattern recognition techniques to the interpretation of severely overlapped voltammetric data: studies with experimental data. 1376
Thornburg, W. Pesticide residues. 98r
Tiffany, B. Autoradiography of californium-252 wire neutron sources. 517
Timnick, A. Correction of right-angle fluorescence measurements for the absorption of excitation radiation. 706
Tindall, G. W. Effect of matrix composition on line intensity in the determination of light elements in organic compounds by x-ray fluorescence spectrometry. 1403
Tishbee, A. Needle guide for liquid or gas syringe. 1267
Tobin, R. S. Immiscible solvent extraction scheme for biodegradation testing of polyethoxylate nonionic surfactants. 398
Todd, J. F. J. Weak peak enhancement by selective ion trapping in a quadrupole ion storage source. 1619
Tokousbalides, P. Low-temperature fluorescence spectrometric determination of polycyclic aromatic hydrocarbons by matrix isolation. 701
Tolk, N. H. In situ spectrochemical analysis of solid surfaces by ion beam sputtering. 16a
Tosk, J. Redox potential and quinone content of cigarette smoke. 1924
Towns, R. L. R. Determination of parts per billion levels of electrodeposited metals by energy dispersive x-ray fluorescence spectrometry. 1734
Trachman, H. L. Atomic absorption spectrometric determination of sub-part-per-million quantities of tin in extracts and biological materials with a graphite furnace. 1090
Tregnaghi, C. Determination of selenium in blood serum by proton-induced x-ray emission. 1313
Trestianu, S. Gas chromatographic column for separation of organochlorine insecticide residues. 2123
Trusell, F. C. Petroleum. Crude oils. 231r
Tsai, W.-C. Determination of mercury in edible oils by combustion and atomic absorption spectrophotometry. 1641
Tsang, W. Instrument for the generation of reactive gases. 13
Tsong, I. S. T. In situ spectrochemical analysis of solid surfaces by ion beam sputtering. 16a
Tsou, G. C. Filter attenuation corrections for the x-ray fluorescence analysis of atmospheric aerosols. 1990
Tsuge, S. Vertical furnace-type sampling device for pyrolysis gas chromatography. 348
Tsunoda, K. Subnanogram fluorine determination by aluminum monofluoride molecular absorption spectrometry. 2035
Tsurumi, M. Amalgam electrode designed for precise electromotive force measurements. 190
Tuan, V.-D. Instrument for the facilitation of room temperature phosphorimetry with continuous filter paper device. 1126
Tucker, R. G. Gel permeation chromatography of low molecular weight materials with high efficiency columns (correction) 1647
Tucker, R. G. Gel permeation chromatography of low molecular weight materials with high efficiency columns. 898
Tuggle, R. M. Determination of phosgene in air by gas chromatography and infrared spectrophotometry. 1774
Turkelson, V. T. Determination of anions in boiler blow-down water with ion chromatography. 1176
Turner, B. C. Field air sampling of pesticide vapors with polyurethane foam. 7
Turner, J. A. Digital simulation of differential pulse polarography with incremental time change. 1246
Turner, J. A. Square wave voltammetry at the dropping mercury electrode: theory. 1899
Turner, J. A. Square wave voltammetry at the dropping mercury electrode: experimental. 1904
Tyberg, A. J. Atomic absorption spectrometric determination of sub-part-per-million quantities of tin in extracts and biological materials with a graphite furnace. 1090
Tyrrell, H. J. V. Bioassay of nystatin bulk material by flow microcalorimetry. 34
Tyrrell, H. J. V. Bioassay of antifungal antibiotics by flow microcalorimetry. 1781
Ulrich, W. F. History of spectrophotometry at Beckman Instruments, Inc. 280a
Unni, C. K. Determination of bromine in silicate rocks by epithermal neutron activation analysis. 1998
Uthe, J. F. Determination of tetraalkyllead compounds in biological materials. 823
Uwamino, Y. Laser-vaporized atomic absorption spectrometry of solid samples. 1339
Valentine, J. L. Acid interference in the determination of arsenic by atomic absorption spectrometry. 1829
Vallee, B. L. Interelement effects and a possible excitation mechanism in a low-pressure microwave induced helium plasma. 266
Vallee, B. L. Enhancement of emission by potassium chloride in the low-pressure microwave-induced plasma emission spectrometer. 1489
Vandenbelt, J. M. Standards in analytical instrumentation. 386a
Van den Broek, W. M. G. T. Supply and removal of sample vapor in graphite thermal atomizers. 2176
Vanderborgh, N. E. Characterization of coal by laser pyrolysis gas chromatography. 390
Vanderborght, B. M. Enrichment of trace metals in water by adsorption on activated carbon. 311
Vanderborght, B. M. Chelex-100 ion-exchange filter membranes for preconcentration in x-ray fluorescence spectrometric analysis of water. 1326
Van der Meent, D. Solvent-free and split-less injection method for open tubular columns. 1881
Vanderwielen, A. J. Determination of ethylene oxide in gas sterilants by Fourier transform infrared spectrometry. 1602
Van Grieken, R. E. Enrichment of trace metals in water by adsorption on activated carbon. 311
Van Grieken, R. E. Chelex-100 ion-exchange filter membranes for preconcentration in x-ray fluorescence spectrometric analysis of water. 1326
Veazey, R. L. Laboratory real time clock featuring computer, experiment, and manual interaction. 1466
Veillon, C. Enhancement of emission by potassium chloride in the low-pressure microwave-induced plasma emission spectrometer. 1489
Venkataraghavan, R. Comparison of various K-nearest neighbor voting schemes with the self-training interpretive and retrieval system for identifying molecular substructures from mass spectral data. 1720
Venkataraghavan, R. Computer assignment of elemental compositions of mass spectral peaks from isotopic abundances. 1723
Venza-Raczka, M. Software package to collect and process radiogas chromatographic data. 1726
Verboom, G. Voltammetric and chronopotentiometric studies of the quinone and hydroquinone system in anhydrous formic acid. 806
Verebey, K. G. Quantitative determination of benzoylecgonine and cocaine in human biofluids by gas-liquid chromatography. 1965
Veres, S. Variable-time kinetic determination of 2-propanol and other alcohols by means of mutual induction in oxidations by chromium(VI). 980
Vessman, J. Determination of tranexamic acid in biological material by electron capture gas chromatography after direct derivatization in an aqueous medium. 369
Vessman, J. Determination of intact oxazepam by electron capture gas chromatography after an extractive alkylation reaction. 1545
Viala, A. R. Determination of metapramine in plasma by gas chromatography with nitrogen-selective and electron-capture detection. 2354
Vidal Madjar, C. Gas-solid and gas-liquid chromatography using porous layer open tube columns made with graphitized thermal carbon black. 768
Vinson, J. A. Detection of tetrahydrocannabinol in blood and serum using a fluorescent derivative and thin-layer chromatography. 163
Violante, N. Reference materials for ultraviolet spectrophotometry. 711
Vire, J. C. Spectrophotometric determination of vitamin K compounds. 1343
Vitenberg, A. G. Gas chromatographic determination of trace amounts of sulfur compounds in industrial effluents. 128
Viviani-Nauer, A. Mechanism of neutral carrier mediated ion transport through ion-selective bulk membranes. 1567
Vo Dinh Tuan Comparison of multichannel SIT image vidicon and photomultiplier sequential linear scanning systems for the measurement of steady-state and transient fluorescence of molecules in solution. 939
Von Minden, D. L. Simultaneous determination of cocaine and benzoylecgonine in urine by gas-liquid chromatography. 1974
Von Wandruszka, R. M. A. Room-temperature phosphorescence of compounds adsorbed on sodium acetate. 2164
Vouros, P. Analysis of explosives by high performance liquid chromatography and chemical ionization mass spectrometry. 1039
Vouros, P. Analysis of thyroid hormones as their heptafluorobutyryl methyl ester derivatives by gas chromatography - mass spectrometry. 1304
Vukovic, M. Square wave voltammetry at the dropping mercury electrode: experimental. 1904
Wadelin, C. W. Rubber. 133r

Wagner, C. D. Factors affecting quantitative determinations by x-ray photoelectron spectroscopy. 1282
Wagner, C. D. Factors affecting quantitative determinations by x-ray photoelectron spectroscopy (correction). 2128
Wagoner, W. S. Preparation of high alloy aluminum spectroscopic reference materials by compacting alloy powder. 679
Wakabayashi, I. Ultrasonic absorption spectra of vanadium benzohydroxamic acid in 1-butanol. 881
Walden, G. Comparison of multichannel SIT image vidicon and photomultiplier sequential linear scanning systems for the measurement of steady-state and transient fluorescence of molecules in solution. 939
Walden, G. L. Instrument for the facilitation of room temperature phosphorimetry with continuous filter paper device. 1126
Walker, J. A. Instrument for the generation of reactive gases. 13
Wallace, J. B. Determination of trace acetylene in oxygen with a portable acetylene analyzer. 1218
Wallace, J. E. Determination of primidone by electron-capture gas chromatography 903
Wallace, J. E. Determination of phenylethylmalonamide by electron-capture gas chromatography. 1969
Walters, M. J. Quantitative analysis of aluminosilicates and other solids by x-ray photoelectron spectroscopy. 2001
Walton, H. F. Chromatography of chlorinated biphenyls on an ion-exchange resin. 764
Walton, H. F. Liquid chromatography of chlorinated biphenyls on pyrolytically-deposited carbon. 1954
Walton, H. F. Open-pore polyurethane columns for collection and preconcentration of polynuclear aromatic hydrocarbons from water. 2260
Warner, I. M. Analysis of multicomponent fluorescence data. 564
Warner, I. M. Quantitative analyses of multicomponent fluorescence data by the methods of least squares and non-negative least sum of errors. 2155
Warren, D. C. Precision of quantitative electron spin resonance using copper(II) bound to ion-exchange resins. 250
Warren, D. C. Parameters influencing the electron spin resonance signal intensity of metal ion complex-exchanged resins. 1840
Warsh, J. J. Analysis of acidic monoamine metabolites by gas chromatography-mass spectrometry. 915
Watson, B. Immobilized enzymes in analytical chemistry. 1069a
Watson, C. A. Near infrared reflectance spectrophotometric analysis of agricultural products. 835a
Weeks, S. J. Pulsed vs. continuous wave atomic fluorescence spectrometry. 1076
Wehry, E. L. Matrix isolation Fourier transform infrared spectrometry of polycyclic aromatic hydrocarbons. 86
Wehry, E. L. Low-temperature fluorescence spectrometric determination of polycyclic aromatic hydrocarbons by matrix isolation. 701
Wei, J. C. Preconcentration of mercury, gold, and copper in sea water with lead diethyldithiocarbamate for neutron activation analysis. 1146
Weiner, E. R. Investigation of detection limits for solutes dissolved in water measured by laser Raman spectrometry. 70
Weisel, C. P. Deceptive "correct" separation by the linear learning machine. 2114
Welling, H. Opto-acoustic trace analysis in liquids with the frequency-modulated beam of an argon ion laser. 549
Wells, M. M. Gas and high pressure liquid chromatographic properties of some 4-nitrobenzamides of amphetamines and related arylalkylamines. 912
Werner, H. W. Test of a quantitative approach to secondary ion mass spectrometry on glass and silicate standards. 927
West, P. W. Personal vinyl chloride monitoring device with permeation technique for sampling. 994
Westberg, H. H. Minicomputer data processing system for air monitoring studies 357a
Wheeler, R. C. Determination of trace metals in fresh water mussels by atomic absorption spectrometry with direct solid sample injection. 257
Whidby, J. F. Deuterium nuclear magnetic resonance spectra from milligram quantities of isotopically enriched compounds (correction). 1280
Whidby, J. F. Deuterium nuclear magnetic resonance spectra from milligram quantities of isotopically enriched compounds. 674
White, C. N. Petroleum. Analytical and process instrumentation. 262r
White, C. W. In situ spectrochemical analysis of solid surfaces by ion beam sputtering. 16a
White, D. C. Determination of low levels of sulfur in organics by combustion microcoulometry. 1615
White, R. E. Unheated external column and inlet modification of a gas chromatograph for phosphine determinations. 1468
White, W. W. Determination of mercury in silver or silver nitrate by atomic absorption spectrometry. 255
Whitney, R. W. Solid state programmable switching device for semiautomated multichannel gas analyses with nondispersive infrared spectrometers. 893
Wiebers, J. L. Factor analysis of the mass spectra of oligodeoxyribonucleotides. 1444
Wijchers, T. Comments on fluorescence excitation profiles in flame. 2111
Wilkins, C. L. Classification of binary carbon-13 nuclear magnetic resonance spectra. 2136
Williams, D. T. Determination of ammonia in biological solutions by second-derivative spectrometry. 83
Williams, E. T. Extraction of mercury by dithizone and stability of the extracted complex. 983
Williams, P. Evaluation of a cesium primary ion source on an ion microprobe mass spectrometer. 1399
Williams, P. Determination of the surface predominance of toxic elements in airborne particles by ion microprobe mass spectrometry and Auger electron spectrometry. 1514
Williams, R. J. Determination of carboxylic esters by acid fusion reaction gas chromatography. 2337
Williams, R. K. Modified microwave-induced plasma discharge chamber. 2372
Willis, C. P. Radiochemical determination of lead-210 in uranium ores and air dusts. 302
Wils, E. R. J. Interference of 1-chloro-2-propanol in the determination of bis(chloromethyl) ether in air by gas chromatography-mass spectrometry. 2365
Wilson, N. K. Analysis of technical chlordane by gas chromatography/mass spectrometry. 734
Wilson, R. L. Fluorometric reaction rate method for determination of silver. 1066
Wilson, R. L. Design and operation of a fluorometric reaction rate instrument. 1060
Wimberly, F. Software package to collect and process radiogas chromatographic data. 1726
Winefordner, J. D. Analytical capabilities of the selectively modulated interferometric dispersive spectrometer. 113
Winefordner, J. D. Throughput advantage and disadvantage in analytical ultraviolet-visible spectrometry by considerations of signal and noise spectral bandpasses. 119
Winefordner, J. D. Comparison of multichannel SIT image vidicon and photomultiplier sequential linear scanning systems for the measurement of steady-state and transient fluorescence of molecules in solution. 939
Winefordner, J. D. Background fluorescence spectra observed in atomic fluorescence spectrometry with a continuum source. 944
Winefordner, J. D. Comparison of image devices vs. photomultiplier detectors in atomic and molecular luminescence spectrometry via signal-to-noise ratio calculations. 1048
Winefordner, J. D. Instrumental effects on limits of detection in gas phase fluorescence detection of gas chromatographic effluents. 1057
Winefordner, J. D. Pulsed vs. continuous wave atomic fluorescence spectrometry. 1076
Winefordner, J. D. Instrument for the facilitation of room temperature phosphorimetry with continuous filter paper device. 1126
Winefordner, J. D. Analytical possibilities of phase resolved phosphorimetry. 1262
Winward, M. R. Air buoyancy equations for single-pan balances. 2126
Wirth, M. J. Two-photon excited molecular fluorescence in optically dense media. 2054
Wise, S. A. Chemically-bonded aminosilane stationary phase for the high-performance liquid chromatographic separation of polynuclear aromatic compounds. 2306
Wishnok, J. S. An unknown salivary morpholine metabolite. 715a
Wittick, J. J. Separation of five major alkaloids in gum opium and quantitation of morphine, codeine, and thebaine by isocratic reverse phase high performance liquid chromatography. 359
Wojtowicz, C. Simultaneous determination of chlordiazepoxide and its N-demethyl metabolite in 50-μL blood samples by high pressure liquid chromatography. 2235
Wolff, C. M. Nonmembrane amperometric sensor for dissolved oxygen in flow-through systems. 2118
Wolochow, H. Potential hazard associated with removal of needles from septa in injection ports of a gas chromatograph. 670
Woodriff, R. Elimination of chloride interferences with mercuric ions in the determination of nitrates by the phenoldisulfonic acid method. 857
Woodriff, R. Sample-loss mechanism in a constant-temperature graphite furnace. 2008
Woodruff, H. B. Computer-assisted interpretation of carbon-13 nuclear magnetic resonance spectra applied to structure elucidation of natural products. 2075
Woodruff, H. B. Dimensionality and the number of features in "learning machine" classification methods. 2116
Woolley, E. M. Air buoyancy equations for single-pan balances. 2126
Wooton, D. L. Preparative gel permeation chromatographic separation of solvent refined coal. 533
Wright, G. J. Defocused metastable scanning with a mass spectrometer and laboratory data system. 174
Wright, J. C. Trace analysis of nonfluorescent ions by selective laser excitation of lanthanide ions. 1690
Wright, J. C. Spectroscopic system for the study of fluorescent lanthanide probe ions in solids. 1474
Wright, J. C. Ultra-trace method for lanthanide ion determination by selective laser excitation. 1680
Wu, C. Design and optimization of a Teflon Helix Continuous Liquid-Liquid Extraction Apparatus and its application for the analysis of organophosphate pesticides in water. 231
Wu, C. Y. Separation of five major alkaloids in gum opium and quantitation of morphine, codeine, and thebaine by isocratic reverse phase high performance liquid chromatography. 359
Wuepper, J. L. Cross section of analytical problem solving in the home appliance industry. 1032a
Wynalda, M. A. Oximes for high performance liquid and electron capture gas chromatography of prostaglandins and thromboxanes. 1032
Wyttenbach, A. Liquid-liquid extraction of cadmium with diethyldithiocarbamic acid. 158
Wyttenbach, A. Liquid-liquid extraction of gold with nickel bis(diethyldithiocarbamate) and its application to activation analysis. 1771
Yacynych, A. M. Carbon and mercury-carbon optically transparent electrodes. 1395
Yamaguchi, S. Principles of nephelometric titrations and application to titration of dilute solutions of bromide. 2268
Yamamoto, H. Calculations of isotopic distribution in molecules extensively labeled with heavy isotopes. 281

Yang, F. J. Theoretical and experimental characterization of field-flow fractionation (correction). 523
Yang, F. J. Peak shifts and distortion due to solute relaxation in flow field-flow fractionation. 659
Yang, R. T. Differential thermal analysis and reaction kinetics for nth-order reaction. 998
Yany, F. Determination of polymer-supported carbodiimides. 676
Yasuda, K. Atomic absorption spectrophotometry based on the polarization characteristics of the Zeeman effect. 1106
Yates, D. A. Effect of modulation wave form on the utility of emission background corrections obtained with an oscillating refractor plate. 1121
Yau, W. W. Characterizing skewed chromatographic band broadening. 395
Yeager, F. W. Determination of composition and molecular weight of polyester urethanes by high resolution proton magnetic resonance spectrometry. 722
Yeager, H. L. Ionic diffusion and selectivity of a cation exchange membrane in nonaqueous solvents. 629
Yeager, W. J. Quantitative comparison of combined gas chromatographic/mass spectrometric profiles of complex mixtures. 1623
Yeh, S. J. Preconcentration of mercury, gold, and copper in sea water with lead diethyldithiocarbamate for neutron activation analysis. 1146
Yen, T. F. Molecular weight and association of coal-derived asphaltenes. 2363
Yeransian, J. A. Food. 194r
Yeung, E. S. Laser two-photon excited fluorescence detection for high pressure liquid chromatography. 1554
Yim, K. W. K. Chemical characterization via fluorescence spectral files and data compression by Fourier transformation. 2069
Yllo, M. S. Liquid chromatographic determination of picomole quantities of aromatic amine carcinogens. 683
Young, G. G. Portable field water sample filtration unit. 672
Youssefi, M. Determination of sulfide and thiols in the presence of vitamin B_{12a} by pulse polarography. 1380
Yuen, W. K. Atomic spectrochemical measurements with a Fourier transform spectrometer. 1446
Zaborsky, L. M. II. Determination of polyester prepolymer oligomers by high performance liquid chromatography. 1166
Zafonte, L. Filter attenuation corrections for the x-ray fluorescence analysis of atmospheric aerosols. 1990
Zander, A. T. Waveform effects in wavelength modulation spectrometry. 458
Zander, A. T. Improvements in the measurements of characteristic concentrations in continuum source atomic absorption spectrometry. 665
Zander, A. T. Correction for interferences of spectral origin with continuum source, echelle wavelength modulated atomic absorption spectrometry. 838
Zander, A. T. Modified microwave-induced plasma discharge chamber. 2372
Zdeb, M. Multiple-curve procedure for improving precision with calibration-curve-based analyses. 1655
Zehr, R. D. Analysis of technical chlordane by gas chromatography/mass spectrometry. 734
Zetaruk, D. G. X-ray photoelectron spectroscopic studies of iron oxides. 1521
Zetlmeisl, M. J. Trace chloride determination by rate controlled coulometric titration. 1557
Ziegler, H. W. Determination and characterization of gallotannin by high performance liquid chromatography. 238
Zirino, A. Anodic stripping peak currents: electrolysis potential relations for reversible systems. 56
Zombola, R. R. Proton induced x-ray emission analysis of L-cells grown in vitro. 2203
Zupan, J. Combined retrieval system for infrared, mass, and carbon-13 nuclear magnetic resonance spectra. 2141

KEYWORD INDEX

AA Methods Manual (book review) 244a
Absorption coeff x ray diffraction 1168
Absorption spectra digital analysis review 864a
Absorption spectroscopy factor analysis 612
Absorptivity molar detn spectra evaluation 276
Acceptability analytical method criterion 510
Accuracy in Trace Analysis (book review) 244a
Acetaldehyde generator 13
Acetanilide deriv detn 1843
Acetate detn laser Raman 70
Acetate sodium adsorbed sample phosphorescence 2164
Acetone corrosion stainless steel 1637
Acetone thiothenoyltrifluoro reagent copper iron 2241
Acetonitrile transition metal perchlorate dehydrating 1874
Acetylacetonyl dipeptide methyl ester 287
Acetylated chloromethylaniline chlorination chromatog analysis 743
Acetylation ionization mass spectrometry 1071
Acetylene detn oxygen portable app 1218
Acetylene helium oxygen flame 2013
Acetylene phosphine removal atomic fluorescence 944
Acid arom detn NMR 2130
Acid arsenic detn atomic absorption 1829
Acid derivatization gas chromatog 832
Acid dissocn propylene carbonate solvent 503
Acid fusion reaction gas chromatog 2337
Acid glycol analysis polyester 741
Acid group detn phosphorous acid 1584
Acid org liq chromatog 860
Acid potentiometric titration 1429
Acid potentiometric titrn nonionic resin 1256
Acid sepn asphalt 1222
Acidity detn phosphorous acid ester 1584
Acrolein generator 13
Acrolein std generation oxidn 139
Acrylamide monomer detn polymer 154
Acrylonitrile spectrophotometric detn 2277
Acrylonitrile std generation thermolysis 139
Actinide scintillation counting 1268
Activation analysis literature periodical 682a
Activation analysis sampling ref material 33a
Activation epithermal neutron bromine detn 1998
Activation helium 3 analysis 1510
Activation neutron fluorine detn 1507
Activation proton light element detn 1297
Activity aq choline chloride 209
Activity cupric ion 877
Activity ion potentiometric sensor 2315
Activtion energy detn gas reaction 1074
Admittance faradaic analysis thermodn 1805
Admittance faradaic fast Fourier transform 1797
Adsorbed halide electrocatalyst iron 1918
Adsorbed sample sodium acetate phosphorescence 2164
Adsorbed sample voltammetry 1589
Adsorbent ferroin deriv polymer immobilized 974
Adsorbent flue gas Tenax GC 512
Adsorption chromatog chlorodibenzodioxin 386
Adsorption chromatog herbicide 386
Adsorption malthene acid extn 1222
Advances in Chromatography, Vol. 14 (book review) 242a
Advances in Chromatography, Vol. 15 (book review) 650a
Advances in Infrared and Raman Spectroscopy, Vol. 2 (book review) 242a
Advances in Mass Spectrometry in Biochemistry and Medicine, Vol. II (book review) 650a
Advances in X-Ray Analysis, Vol. 20 (book review) 940a
Aerosol atm analysis correction 1990
Aerosol sulfate detn air 1579
Aerosol velocity analytical flame 2112
Air anal permeation tube 1278
Air carrier gas plasma chromatog 828
Air dust analysis lead 210 302
Air pollutant detn review 1r
Air pollution sulfate detn 1990
Air Pollution. 3rd Ed. Vol. III, Measuring, Monitoring and Surveillance of Air Pollution (book review) 648a
Air sampling pesticide foam 7
Airborne particulate analysis nitrate 485
Alc amino periodate reaction kinetics 414
Alc detn catalytic 980
Alc gasoline fuel volatility 2368
Alc subtractive gas chromatog 1078
Alcoholism tetrahydroisoquinoline alkaloid 530
Aldehyde subtractive gas chromatog 1078
Aldehydes. Photometric Analysis, Vol. 4 (book review) , 652a
Algorithm chem information graph display 1357
Algorithm chromatog band broadening 395
Algorithm enzyme detn 1716
Algorithm mass spectra assignmnet 1723
Aliph amine gas chromatog 541
Aliquoting parallel multichannel pipet 1608
Alk earth cation selective electrode 1567
Alk earth detn photometry 969
Alkali flame detector fabrication 192
Alkali fusion gas chromatog 2349 2343
Alkali metal cation selective electrode 1567
Alkali metal detn mass spectroscopy 1744
Alkaloid detn gum opium 359
Alkaloid tetrahydroisoquinoline chromatog 530
Alkane NMR computer 1134
Alkene detn NMR fluorine 19 2146
Alkene gas chromatog topol analysis 747
Alkoxyazoxybenzene detn liq chromatog 1963
Alkylazoxybenzene detn liq chromatog 1963
Alloy aluminum std prepn 679
Alloy analysis atomic absorption 1336
Alloy analysis germanium chromatog 909
Alloy analysis laser atomic absorption 1339
Alloy film analysis x ray 1152
Alloy nonferrous analysis manganese 414
Alloy x ray analysis 345
Allylacetic acid analysis Auger spectroscopy 2330
Allylamine monolayer analysis Auger spectroscopy 2330
Alpha quartz respirable detn air 2196
Alpha spectrometry detn thorium uranium ores 1648
Alpha spectrometry thorium urnanium isotope 618
Aluminate detn radioactive waste 2044
Aluminosilicate analysis photoelectron spectroscopy 2001
Aluminum alloy std prepn 679
Aluminum analysis review 72r
Aluminum detn proton activation 1297
Aluminum fluoride mol absorption spectrometry 2035
Aluminum receiver copper Donnan dialysis 1272
Aluminum sepn iron extn chromatog 1189
Amalgam electrode emf detn 190
Amberlite immobilized ferroin deriv 974
Amberlite liq chromatog acid 860
Amberlite XAD chromatog packing 757
Amberlite XAD support extn chromatog 1189
Americium electrodeposition high resoln spectrometry 842
Americium scintillation counting 1268
Amic acid enzymic hydrolysis 292
Amide primary detn flame spectrometry 262
Amine aliph gas chromatog 541
Amine arom carcinogen liq chromatog 683
Amine arom isomer chromatog 1756
Amine detection liq chromatog 2080
Amine detn water chromatog 401
Amine drug chromatog nitrobenzamide deriv 912
Amino acid chromatog spectrometry 1241
Amino acid deriv fluorescence enhancement 1606
Amino acid isomer detn soil 2
Amino acid liq chromatog 860
Amino acid nitrogen 15 spectrometry 1832
Amino alc periodate reaction kinetics 414
Aminobenzaldehyde reagent hydrazine detn 161
Aminoethyl phosphate detn P NMR 588
Aminohippuric acid phosphorescence detn 2164
Aminoiminomethanesulfinic acid redn cadmium 26
Aminopropyltrimethyoxysilane copper bonded phase chromatog 1756
Aminosilane bonded phase liq chromatog 2306
Aminotoluene detn polyurethane foam 1676
Amitriptyline oxidn spirobiphthalide detn 1864
Ammonia detn Berthelot reaction 464
Ammonia detn blood 83
Ammonia detn preconcn zeolite IR 1331
Ammonia detn water chromatog 401
Ammonia gradient elution gas chromatog 1179
Ammonium chloride conversion nitrogen app 514
Ammonium tetramethyldithiocarbamate water analysis 1862
Amperometric detector liq chromatog review 447a
Amperometry catecholamine 2109
Amperometry electrode detn oxygen 2118
Amphetamine chromatog nitrobenzamide deriv 912
Amphoteric surfactant liq chromatog 2228
Ampoules glass sealed tube cracker vacuum 192
Anal analog storage register recording 19
Anal coconut oil diethanolamide 835
Anal data 2116
Analog data treatment atomic absorption 1263
Analog digital converter computer 1869
Analog storage register recording anal 19
Analysis acetanilide drug metabolite 1843
Analysis air mass spectrometry 270
Analysis characterization rubber review 133r
Analysis chem education industry 182a
Analysis chem US history 480a
Analysis coal gaseous fuel review 176r
Analysis data aquisition recorder 342
Analysis faradaic admittance 1805
Analysis ferrous metallurgy review 54r
Analysis fly ash surface 1514
Analysis glycol acid polyester 741
Analysis hydrocarbon petroleum review 249r
Analysis information theory statistics 1265
Analysis inorg geol material review 34r
Analysis launch pad 322a
Analysis light metal review 72r
Analysis non-Nnernstian response 1211
Analysis of Petroleum for Trace Metals (book review) 238a
Analysis of Rocket Propellants (book review) , 738a
Analysis petroleum review 231r 262r
Analysis piezoelec crystal detector review 1890
Analysis precision calibration curve 1655
Analysis regression calculator program 523
Analysis review polymer 159r
Analysis variance 691a
Analysis water review 139r
Analysis x ray fluorescence correction 1990
Analytical Biochemistry of Insects (book review) 738a
Analytical chem home appliance industry 1032a

Analytical Chemistry. 2nd Ed. (book review) 826a
Analytical flame aerosol velocity 2112
Analytical method acceptability criterion 510
Analytical Methods for Use in Geochemical Exploration (book review) 348a
Analytical Pyrolysis (book review) , 936a
Analytical reagent sodium hydroxide purifn 889
Analyzer fuel vaporization pressure 2368
Analyzer spectrofluorometry optical petroleum 1316
Aniline chloro isomer distribution 743
Animal tissue ashing element detn 1644
Anion exchanger conduction mechanism 767
Anionic dye mass spectra 922
Annual Book ASTM Standards, 1976 Pt 30 Soap, Engine Coolants, Polishes, Halogenated Organic Solvents, Activated Carbon, Industrial Chem (book review) 244a
Annual Book ASTM Standards, 1976 Pt. 41 Statistical Methods, Space Simulation, Particle Size Measurement, Detn. of Nonmetallic Materials (book review) 244a
Annual Book of ASTM Standards, 1976, Pt. 42 or Spectroscopy, Microscopy, Chromatography and Resinography (book review) 350a
Annual Book of ASTM Standards, 1977, Pt. 29 on Paint-Fatty Oils and Acids, Solvents; Miscellaneous; Aromatic Hydrocarbons; Naval Stores (book review) 738a
Annual Reports on Analytical Atomic Spectroscopy, Vol. 5 (book review) 738a
Annual Reports on NMR Spectroscopy, Vol. 6B (book review) 74a
Anodic stripping cadmium detn 199
Anodic stripping thin layer 1792
Anodic stripping voltammetry cadmium 56
Anodic stripping voltammetry tubular electrode 49
Anova analytical chem 691a
Anthracene detection fluorescence 955
Anthracene detection vidicon 939
Antibiotic antifungal assay calorimetry 1781
Antibody complement assay ion electrode 2083
Antiferromagnetic paramagnetic transition chromium compd 962
Antimony detn paper classification 2285
Antimony electrodeless discharge lamp 551
Antimony present arsenic detn sulfide 451
Antioxidant gel permeation chromatog 898
Antioxidant phenol dimethacrylate analysis 363
AntiStokes coherent Raman spectrometry cell 959
App atomic absorption spectrometer background correction 2187
App Hb detn blood 555
App sampling filtering water 672
Appliance industry analytical chem 1032a
Applied Spectroscopy Reviews, Vol. 11 (book review) , 242a
Arc lamp spectral noise 2040
Arenesulfonate radiometry crude oil 1148
Argon laser opticoacoustic analysis 549
Arom acid detn NMR 2130
Arom amine carcinogen liq chromatog 683
Arom amine isomer chromatog 1756
Arom hydrocarbon coal fluorometry 701
Arom hydrocarbon detn coal liquefaction 2253
Arom hydrocarbon polycyclic detection 955
Arom hydrocarbon polycyclic detn 701
Arom hydrocarbon polynuclear methylation 1260
Arom polycyclic hydrocarbon IR analysis 86
Arom polynuclear liq chromatog 2306
Aromaticity coal NMR 585
Arsenate detn natural water 820
Arsenic detn atomic absorption 1096
Arsenic detn atomic absorption acid 1829
Arsenic detn atomic absorption interference 1417
Arsenic detn phosphoric acid 2376
Arsenic detn siliceous material 825
Arsenic detn sulfide antimony present 451
Arsenic detn water atomic absorption 1599
Arsenic detn water spectrometry 1093
Arsenic flame atomic absorption 574
Arsenic methylarsenic sepn detn 621
Arsenite detn natural water 820
Arsine detn natural water 820
Ash analysis arsenic 825
Ash fly analysis x ray 1012
Ash fly surface element 1514
Ash sulfur detn 1741
Ashing animal tissue element detn 1644
Asphalt acid sepn 1222
Asphalt review 240r
Asphaltene acid extn adsorption 1222
Asphaltene coal mol wt assocn 2363
Assocn asphaltene coal 2363
Atlas of Carbon-13 NMR Data (book review) 348a
Atlas of Thermoanalytical Curves, Vols. 1-5 (book review) 936a
Atm aerosol analysis correction 1990
Atm sulfate control 1664
Atmospheric Chemistry (book review) 545a
Atom formation graphite furnace mechanism 192
Atom formation mechanism graphite furnace 1647
Atom loss graphite furnace atomization 1100
Atomic absorption analysis internal std 1336
Atomic absorption arsenic detn 451 2376
Atomic absorption arsenic detn acid 1829
Atomic absorption arsenic selenium interference 1417
Atomic absorption boron isotope detn 1852
Atomic absorption detn arsenic water 1599
Atomic absorption DMF solvent 2122
Atomic absorption flameless mercury detn 336
Atomic absorption flameless tin detn 1090
Atomic absorption geol analysis 1485
Atomic absorption graphite furnace 2176
Atomic absorption hydride generation 1096
Atomic absorption mercury 1641
Atomic absorption mercury detn silver 255
Atomic absorption nebulizer 1413
Atomic absorption optical modulator flame 98
Atomic absorption platform graphite furnace 2018
Atomic absorption silicon chloride analysis 2289
Atomic absorption spectrometer background correction app 2187
Atomic absorption spectrometer vidicon echelle 1112
Atomic absorption spectrometer Zeeman effect 1106
Atomic absorption spectrometry atom loss 1100
Atomic absorption spectrometry continuum source 665 685 1263
Atomic absorption spectrometry graphite furnace 90
Atomic absorption spectrometry interference correction 838
Atomic absorption spectrometry laser vaporized 1339
Atomic absorption spectrometry seawater 2031
Atomic absorption spectrophotometry computer 891
Atomic absorption spectrophotometry flame precision 574
Atomic absorption spectrophotometry titanium 454
Atomic absorption thin layer chromatog 189
Atomic absorption tissue ashing 1644
Atomic emission analysis background correction 1121
Atomic emission spectrometry nebulizer 632
Atomic fluorescence electrodeless discharge lamp 551
Atomic fluorescence interference background fluorescence 944
Atomic fluorescence spectrometry 1076
Atomic spectrometry flame 2013
Atomic spectrometry microprocessor laser 1702
Atomization graphite platform 2018
Atomization sputtering atomic absorption analysis 1336
Atomizer atomic absorption spectrometry 1413
Atomizer graphite sample supply removal 2176
Auger spectroscopy indium tin foil 1228
Auger spectroscopy substituted hydrocarbon monolayer 2330
Automated electrode potentiometry redox reaction 1908 1914
Automated potentiometric titrn equivalence point 1250
Automated radioimmunoassay system 1183a
Automated unsegmented flow app 1861
Automation lab computer networking 1100a
Autoradiog californium 252 wire 517
Azoxybenzene isocratic reverse phase chromatog 1963
Background correction atomic absorption 838
Background correction atomic absorption spctrometer 1106
Background correction radiation counter 2193
Background correction wavelength modulation 1121
Background fluorescence interference atomic fluorescence 944
Background helium oxygen acetylene flame 2013
Balance single pan buoyancy 2126
Band broadening chromatog peak 625
Barbiturate identification mass spectrometry 435
Barium calcite surface ESCA calibration 1044
Barium detn diatom 1017
Barium hypobromite reagent amide detn 262
Barrier film plastic analysis tin 1090
Base nucleoside chromatog 2237
Base pyridine ligand exchange chromatog 1179
Benchmark Papers in Analytical Chemistry, Vol. 2: Thermal Analysis (book review) 350a
Benzaldehyde dimethylamino reagent hydrazine detn 161
Benzene asphaltene assocn 2363
Benzene detection fluorescence 955
Benzene heptane mass spectroscopy 1847
Benzenesulfonic acid ionization propylene carbonate 503
Benzohydroxamato vanadium ultrasonic spectrometer 881
Benzoic acid ionization propylene carbonate 503
Benzoic acid liq chromatog 860
Benzophenone detection phosphorimetry 1262
Benzoquinone electrochem redn semiquinone 806
Benzotetrathiafulvalene voltammetry acetonitrile bromide 802
Benzoylecgonine cocaine detn gas chromatog 1965
Benzoylecgonine cocaine detn urine 1974
Benzylamine liq chromatog detection 2080
Berthelot reaction ammonia detn 464
Beryllium analysis review 72r
Beryllium chloride analysis copper iron 2241
Betaine sulfo surfactant chromatog 2228
Bibliography of Liquid Column Chromatography 1971-1973 and Survey of Applications (book review) 738a
Bibliography on Atomic Energy Levels and Spectra, July 1971 through June 1975 (book review) 832a
Biodegrdn nonionic surfactant analysis 398
Biol analysis cesium 1744
Biol analysis differential pulse voltammetry 1792
Biol analysis fluorine 2035
Biol analysis gold 1771
Biol analysis light element 1297
Biol material arsenic detn acid 1829
Biol tissue analysis tin 1090
Biolog material surface review 221r
Biphenyl bromo detection phosphorimetry 1262
Biphenyl chloro deriv chromatog 764
Biphenyl chloro liq chromatog 1954
Bismuth detn voltammetry 1789
Bitumen vanadium detn visible spectra 972
Block Copolymers: Overview and Critical Survey (book review) 550a
Blood ammonia detn 83
Blood analysis anodic stripping voltammetry 1792
Blood analysis ion beam sputtering 16a
Blood chlordiazepoxide detn chromatog 2235
Blood cocaine benzoylecgonine detn 1965
Blood detn tetrahydrocannabinol 163
Blood galactose detn 789
Blood Hb detn app 555
Blood oxazepam detn 1545
Blood plasma mercaptopurine detn 725
Blood plasma metapramine detn 2354
Blood serum chlorpheniramine detn 1085
Blood serum phenylethylmalonamide detn 1969
Blood serum primidone 903
Body fluid tranexamate detn 369
Boiler blowdown water analysis 1176
Bonded copper phase liq chromatog 1756

Bonded phase aminosilane liq chromatog 2306
Bonded phase reaction solute chromatog 133
Borohydride redn arsenic atomic absorption 2376
Boron detn proton activation 1297
Boron isotope detn atomic absorption 1852
Bottle polyethylene mercury sample stability 668
Brain dopamine serotonin detn 354
Brain hormone amino acid 1241
Brain tetrahydroisoquinoline alkaloid 530
Brass analysis laser atomic absorption 1339
Bromide dil soln nephelometric titrn 2268
Bromide electrocatalysis iron redn 1918
Bromide oxidn interference nitrate detn 2249
Bromide reagent mercury silver sepn 255
Bromide silver potentiometric sensor 2315
Bromine compd mass spectra assignment 1723
Bromine detn org ion chromatog 884
Bromine detn silicate rock 1998
Bromobiphenyl detection phosphorimetry 1262
Bromomethylmethoxycoumarin fatty acid 442
Buffer ligand interference preventive 1868
Buffer testing glass electrode 1363
Buffer trishydroxymethylaminomethane seawater 867
Buoyancy balance single pan 2126
Butene propylene polymer analysis 1405
Cadmium atomization graphite platform 2018
Cadmium coated graphite electrode voltammetry 485
Cadmium detn anodic stripping 199
Cadmium detn chemiluminescence 1322
Cadmium detn paper classification 2285
Cadmium detn transition metal present 2090
Cadmium electrolysis potential water 56
Cadmium emf amalgam electrode 190
Cadmium extn diethyldithiocarbamic acid 158
Cadmium flame atomic absorption 574
Cadmium preconcn chelate water analysis 222
Cadmium redn aminoiminomethanesulfinic acid 26
Cadmium removal sodium hydroxide 889
Cadmium x ray sensitivity 1505
Calcite surface ESCA calibration 1044
Calcium flame atomic absorption 574
Calcium fluoride copptn lanthanide detn 1680
Calcium magnesium sepn detn 1595
Calculator program confidence limit polemic 884
Calculator program regression analysis 523
Calibration curve analysis precision 1655
Calibration curve solid surface fluorometry 2160
Calibration ion selective electrode 2377
Calibration nonideal ion selective electrode 1211
Calibration nonlinear confidence limit analysis 2062
Calibration permeation nitrogen dioxide 1823
Calibration quant ESCA 1044
Californium 252 wire autoradiog 517
Calorimeter soln titrn design 1878
Calorimetry antifungal antibiotic assay 1781
Calorimetry differential scanning cell 522
Capacitor discharge temp jump kinetics 1081
Carbide detn steel DTA 649
Carbide formation graphite furnace 2008
Carbodiimide polymer supported detn 676
Carbohydrate ester gas chromatog 2337
Carbohydrate NMR carbon computer 2075
Carbon black graphitized gas chromatog 768
Carbon detection gallium nitride 1536
Carbon detector gas chromatog 2215
Carbon detn substituted hydrocarbon monolayer 2330
Carbon dioxide detn mass spectrometry 270
Carbon dioxide oxygen isotope measurement 1664
Carbon disulfide chromatog flame photometry 123
Carbon electrode vitreous 1470
Carbon NMR data base 2136
Carbon optically transparent electrode 1395
Carbon org detn plasma spectrometry 1235
Carbon tetrachloride corrosion stainless steel 1637
Carbon 13 NMR acrylic polymer 77
Carbon 13 NMR alkane 1134
Carbon 13 NMR polyolefin 1405
Carbon 13 NMR quant analysis 2130
Carbonate detn laser Raman 70
Carbonate detn radioactive waste 2044
Carbonyl sulfide chromatog flame photometry 123
Carboxylic acid automatic detn chromatog 655
Carboxylic acid derivatization chromatog 832
Carboxylic ester gas chromatog 2337
Carboxymethylaminopropane resin ion exchanger 418
Carcinogen arom amine liq chromatog 683
Carcinogen bischloromethyl ether detn air 2365
Carcinogen nitrosamine gas chromatog 1544
Carotene detn opticoacoustic 549
Carotenoid detn phytoplankton 695
Carrier gas negative ion identification 828
Catalyst analysis org deposit 2374
Catalyst crown ether derivatization acid 832
Catalyst petroleum review 243r
Catalyst surface characterization review 221r
Catalyst thiocyanate nitrite detn 2272
Catalytic isopropyl alc detn 980
Catalytic manganese detn 414
Catecholamine detn kinetic photometric 2090
Catecholamine urine chromatog 2109
Catecholamine voltammetry thin layer cell 1205
Categorization compd data 2114
Cathodic pulse stripping iodine detn 1199
Cathodic stripping voltammetry mercaptan detn 1386
Cathodic stripping voltammetry thioamide drug 1195
Cation enrichment Donnan dialysis 1272
Cation exchange membrane ion diffusion 629
Cation exchanger gas chromatog support 1549
Cation exchanger tin vanadophosphate 165
Cation selective electrode choline 209
Cation selective membrane electrode 1567
Cationic dye mass spectra 922
Cavity loading effect ESR analysis 1353
Cell calorimetry differential scanning 522
Cell L trace element detn 2203
Cell spectrophotometer temp jump 2378
Cell thin layer micrometer voltammetry 1205
Cell thin layer voltammetry 1792
Cellulose ester gas chromatog 2337
Cement sulfur detn 1741
Centrifugal analyzer minidisk sample aliquoting 1608
Cephalosporin detn oxidn titrn 1002
Ceramic glass spectro electrochem microcell 1646
Ceramic surface characterization review 221r
Cereal packaging resin flavor 901a
Cereal spectrochem review 835a
Cesium detn mass spectroscopy 1744
Cesium iodide diffusion cation exchanger 629
Cesium ion source mass spectrometer 1399
Cesium ion source mass spectrometry 2023
Chalcopyrite analysis copper iron 2241
Characteristic concn continuum source 665
Characterization analysis rubber review 133r
Characterization of Metal and Polymer Surfaces. Vol. 1, Metal Surfaces (book review) , 830a
Characterization of Metal and Polymer Surfaces, Vol. 2, Polymer Surfaces (book review) , 830a
Characterization structure fluorescence computer 2069
Charcoal sampling vinyl chloride 994
Charge transfer chem reaction 60
Charge transfer complex iodine amine 2080
Charge transfer faradaic admittance 1805
Chelate detn wastewater carbonate 10
Chelate mass spectroscopy neg ion 1501
Chelate preconcn lead detn water 222
Chelate stability mol structure ligand 1940
Chelating metal propylenediaminetetraace tate resin 418
Chelation enrichment water trace metal 311
Chelation humic fulvic acid water 216
Chelex trace metal river water 1950
Chem analysis education industry 182a
Chem analysis US history 480a
Chem bonded phase chromatog review 1004a
Chem clin method review 594a
Chem clin review 16r
Chem information graph display algorithm 1357
Chem ionization field desorption spectrometry 1160
Chem ionization mass spectrometry 1497
Chem ionization mass spectrometry review 772a
Chem ionization mass spectroscopy chelate 1501
Chem ionization mass spectroscopy chromatog 169 731
Chem reaction kinetics detn 60
Chemical Derivatization in Liquid Chromatography (book review) 645a
Chemiluminescence luminol vitamin B12 detn 446
Chemiluminescence nitrogen detn petroleum 932
Chemiluminescence trace metal detn 1322
Chemisorbed porphyrin tin dioxide 194
Chemisorption: An Experimental Approach (book review) , 828a
Chlordane gas chromatog mass spectrometry 734
Chlordiazepoxide detn blood chromatog 2235
Chloride choline aq activity 209
Chloride copper selective electrode 877
Chloride detn boiler blowdown water 1176
Chloride detn coulometric titrn 1557
Chloride electrocatalysis iron redn 1918
Chloride interference nitrate detn 857
Chloride potassium emission spectra 1489
Chlorination acetylated chloromethylaniline chromatog analysis 743
Chlorination germanium gas chromatog 909
Chlorine compd mass spectra assignment 1723
Chlorine detn org ion chromatog 884
Chlorine detn substituted hydrocarbon monolayer 2330
Chlorine interference fluorine detn 1507
Chloro biphenyl liq chromatog 1954
Chlorobiphenyl chromatog 764
Chlorodibenzodioxin adsorption chromatog 386
Chloromethyl ether detn chloropropanol 2365
Chloromethyl methyl ether detn air 1817
Chloromethylaniline acetylated chlorination chromatog analysis 743
Chloronitrobenzooxadiazole fluorometry gentamicin 953
Chloropicric acid ionization propylene carbonate 503
Chlorotrifluoroethylene monolayer analysis Auger spectroscopy 2330
Chlorpheniramine detn blood serum 1085
Cholesterol detn NMR 2130
Cholesteryl ester gas chromatog 2337
Choline cation selective electrode 209
Chromate detn radioactive waste 2044
Chromatog adsorption chlorodibenzodioxin 386
Chromatog adsorption herbicide 386
Chromatog amphetamine nitrobenzamide deriv 912
Chromatog analysis chlorination acetylated chloromethylaniline 743
Chromatog arom amine isomer 1756
Chromatog band broadening skewed 395
Chromatog biphenyl chloro deriv 764
Chromatog carboxylic acid automatic detn 655
Chromatog catecholamine urine 2109
Chromatog chem ionization mass spectroscopy 169 731
Chromatog chlordiazepoxide detn blood 2235
Chromatog coal oil tar 1225
Chromatog copper iron detn 2241
Chromatog detn amine water 401
Chromatog dopamine serotonin 354
Chromatog electrochem detector 1036
Chromatog ethyl lead gasoline 1761
Chromatog exclusion solvent dense gas 243
Chromatog extn support macroporous resin 1189
Chromatog flame photometry hydrogen sulfide 123
Chromatog fluorescence monitor 1836
Chromatog fluorescent petroleum analyzer 1316
Chromatog gallotannin 238
Chromatog gas acetanilide deriv 1843
Chromatog gas acid phenol derivatization 832
Chromatog gas aliph amine 541

Chromatog gas alkene topol analysis 747
Chromatog gas carboxylic ester 2337
Chromatog gas carcinogen nitrosamine 1544
Chromatog gas chlordane 734
Chromatog gas cocaine benzoylecgonine 1974
Chromatog gas cocaine benzoylecgonine detn 1965
Chromatog gas column packer 684
Chromatog gas detn chlorpheniramine 1085
Chromatog gas dipeptide ester 257
Chromatog gas drug forensic 906
Chromatog gas effluent fluorescence detection 1057
Chromatog gas factor analysis 612
Chromatog gas germanium detn 909
Chromatog gas glow discharge detector 2215
Chromatog gas hydrolysis polyester 741
Chromatog gas hydroxyethylhydrazine detn 2213
Chromatog gas leak 670
Chromatog gas mass spectrometry pollutant 521
Chromatog gas mass spectroscopy chelate 1501
Chromatog gas mercury organomercurial 365
Chromatog gas monoamine metabolite 915
Chromatog gas nitrogenase detn 1275
Chromatog gas nonionic surfactant 835
Chromatog gas organochlorine pesticide 2123
Chromatog gas organochlorine pesticide sludge 316
Chromatog gas organometal detn 378
Chromatog gas oxazepam deriv 1545
Chromatog gas peak dead vol 625
Chromatog gas phosphate silyl deriv 1086
Chromatog gas phosphine 1468
Chromatog gas polyimide polyamide 2349
Chromatog gas pyrolysis furnace 348
Chromatog gas pyrolysis polymer 537
Chromatog gas radioassay program RADGLC 1726
Chromatog gas sample injection splitless 1881
Chromatog gas siloxane analysis 2343
Chromatog gas subtractive microreactor 1078
Chromatog gas sulfonated polymer support 1549
Chromatog gas systematic error 2222
Chromatog gas triose tetrose 137
Chromatog gas vinyl chloride detn 1985
Chromatog gas volatile polymer 886
Chromatog gasoline detn sulfur 126
Chromatog gel high efficiency column 898
Chromatog gel particle porosimetry 1183
Chromatog gel permeation coal liq 533
Chromatog high performance 359
Chromatog high performance thin layer 1867
Chromatog high pressure detector 1836
Chromatog ion org elemental analysis 884
Chromatog ionic compd 142
Chromatog ligand exchange pyridine base 1179
Chromatog liq acrylamide 154
Chromatog liq amine detection 2080
Chromatog liq arom amine carcinogen 683
Chromatog liq azoxybenzene 1963
Chromatog liq chloro biphenyl 1954
Chromatog liq column packing 1958
Chromatog liq computer interrogation app 681
Chromatog liq detector Raman spectrometry 959
Chromatog liq detector ref electrode 2379
Chromatog liq electrochem detector review 447a
Chromatog liq laser fluorometer detector 1554
Chromatog liq mass spectroscopy explosive 1039
Chromatog liq mefruside metabolite 1311
Chromatog liq org acid 860
Chromatog liq organochlorine pesticide 326
Chromatog liq polynuclear arom 2306
Chromatog liq polyterephthalate oligomer 1166
Chromatog liq silicon vidicon tube 1171
Chromatog liq sulfobetaine surfactant 2228
Chromatog liq syncrude 1766
Chromatog liq vidicon detector 939
Chromatog mass spectrometry computer program 180
Chromatog mass spectrometry glyceride 2209
Chromatog mass spectroscopy pulse counting 2205
Chromatog mol wt materials gel permeation 1647
Chromatog nucleoside base 2237
Chromatog nucleotide high performance 2231
Chromatog packing Amberlite XAD 757
Chromatog parathion water 1551
Chromatog phase chem bonded review 1004a
Chromatog plasma negative ion identification 828
Chromatog primidone detn 903
Chromatog prostaglandin thromboxane oxime 1032
Chromatog pump depulsing system 2125
Chromatog pyrolysis coal characterization 390
Chromatog pyrolysis gas catalyst deposit 2374
Chromatog pyrolysis gas lignite 1540
Chromatog reverse phase ion pair 883
Chromatog solute reaction bonded phase 133
Chromatog spectrometry amino acid 1241
Chromatog spectrometry hormone thyroid 1303
Chromatog syringe needle guide 1267
Chromatog tetrahydroisoquinoline alkaloid 530
Chromatog thermal field flow 1750
Chromatog thin layer atomic absorption 189
Chromatog thin layer color photog 1640
Chromatog thin layer fluorescence densitometry 2160
Chromatog thin layer fraction collector 671
Chromatog thin layer hydrazine detn 161
Chromatog thin layer review 83a
Chromatogram comparison library data 1623
Chromatogram reconstruction computerized review 563a
Chromatogram reconstruction IR interferogram 1977
Chromatograph gas mass spectrometer interface 518
Chromatograph gas microprocessor controlled 1279
Chromatographic Methods in Gas Analysis (book review) 652a
Chromatographic Science Series, Vol. 7: Fundamentals of Integrated GC–MS (book review) , 350a
Chromatography of Steroids (book review) 645a
Chromic oxide detn sodium chromite 962
Chromite sodium detn chromic oxide 962
Chromium detn alloy powder 1336
Chromium detn paper classification 2285
Chromium detn silicon chloride 2289
Chromium diketonate chromatog mass sepctroscopy 1501
Chromium enrichment chelation water analysis 311
Chromium oxidn alc detn 980
Chromopate formaldehyde detn nitrate interference 1865
Chroomatog. retention ion pair 2295
Cigaret smoke analysis IR 331
Cigaret smoke redox quinone 1924
Cinoxacin detn phosphorimetry 2048
Cleaning plastic container sample storage 2264
Clin analysis continuous unsegmented flow polemic 1861
Clin chem method review 594a
Clin chem review 16r
Clinical Chemistry (book review) 347a
Clipped free induction decay NMR 508
Clock computer 1466
Coal analysis review 176r
Coal aromaticity NMR 585
Coal asphaltene mol wt assocn 2363
Coal characterization pyrolysis chromatog 390
Coal fluorometry arom hydrocarbon 701
Coal fly ash analysis 1012
Coal hydrogen detn NMR 75
Coal liq analysis arom 701
Coal liq gel permeation chromatog 533
Coal liq mass spectrometry std 1260
Coal liq mass spectroscopy 1847
Coal liq nitrogen compd 2292
Coal liquefaction solvent chromatog 2253
Coal oil liq chromatog 1766
Coal oil tar chromatog 1225
Coal sulfur detn 1741
Cobalt atomic absorption DMF solvent 2122
Cobalt detn chemiluminescence 1322
Cobalt detn paper classification 2285
Cobalt detn seawater spectrometry 2031
Cobalt detn silicon chloride 2289
Cobalt detn spectrophotometry 580
Cobalt diketonate thio extn 2246
Cobalt enrichment chelation water analysis 311
Cobalt perchlorate acetonitrile soln dewatering 1874
Cobalt removal sodium hydroxide 889
Cobaltic ion complexation natural water 404
Cocaine benzoylecgonine detn gas chromatog 1965
Cocaine benzoylecgonine detn urine 1974
Coconut oil diethanolamide anal 835
Code mass spectra statistical moment 1456
Codeine detn gum opium 359
Coherent antiStokes Raman spectrometry cell 959
Collector fraction thin layer chromatog 671
Colloquium Spectroscopicum Internationale. XVIII (book review) 936a
Color photog thin layer chromatog 1640
Colorimetric and Fluorimetric Analysis of Steroids (book review) 830a
Colorimetry enzymic hydrolysis 292
Colorimetry hippurate 1494
Coiorimetry hydrogen sulfide water 424
Colorimetry nitrogen protein 1080
Column high efficiency gel chromatog 898
Column packer gas chromatog 684
Column packing liq chromatog 1958
Combustion analysis petroleum luminescence 932
Combustion gas hydrogen cyanide detn 322
Compaction powder alloy std prepn 679
Compd data categorization 2114
Compilation of ASTM Standards on Precision and Accuracy for Various Applications (book review) 938a
Complement antibody assay ion electrode 2083
Complex atomic absorption DMF solvent 2122
Complex cyanide detn ion exchange 516
Complexation capacity natural water 2358
Complexation natural water cobaltic ion 404
Complexation phytoplankton seawater copper 226
Complexing agent interference copper detn 1868
Complexometric detn vitamin K compd 1343
Compn anal polyurethane NMR 722
Component analysis kinetics detn 846
Comprehensive Analytical Chemistry, Vol. VI (book review) 940a
Comprehensive Analytical Chemistry, Vol. VIII (book review) 652a
Compromise flame condition multielement analysis 2280
Compton scattered radiation silver 1168
Computer air monitoring 357a
Computer alkane NMR 1134
Computer analog digital converter 1869
Computer application alloy film analysis 1152
Computer application atomic absorption analysis 1112
Computer application desorption isotherm 991
Computer application faradaic admittance 1797 1805
Computer application IR analysis 500
Computer application kinetic analysis multicomponent 2090
Computer application lanthanide ion fluorometry 1474
Computer application mass spectroscopy 2322
Computer assignment elemental compn 1723
Computer atomic absorption spectrophotometry 891
Computer chromatog mass spectroscopy chelate 1501
Computer clock 1466
Computer controlled laser spectrochem analysis 1702
Computer display mass spectrometry 1462
Computer fluorescence structure characterization 2069
Computer identification spectra 1441
Computer information retrieval mol structure 1720
Computer information retrieval spectra 2141
Computer IR spectrometer 470
Computer networking lab automation 1100a
Computer NMR natural product structure 2075
Computer program mass spectrometry chromatog 180

Computer program radio gas chromatog 1726
Computer program x ray analysis 345
Computer subtraction IR spectra 772
Computer voltage controlled oscillator 681
Computerized curve fitting spectrophotome= tric titrn 1408
Computers in Polymer Sciences (book re= view) 832a
Concn characteristic continuum source 665
Cond elec benzotetrathiafulvalene halide 802
Condensation product gel permeation chro= matog 898
Conduction mechanism anion exchanger 767
Conductometric titrn nonaq phosphorous acid 1584
Conductometry hydrogen detn helium 853
Confidence limit analysis nonlinear calibra= tion 2062
Confidence limit calculator program polemic 884
Conformation protein electrode 41
Connective tissue detn meat 1140
Contamination Control in Trace Element Analysis (book review) 439a
Continuous analysis ion selective electrode 2377
Continuous flow analysis 1858
Continuous flow analysis pulseless pump 2125
Continuous flow analysis unsegmented stream 17
Continuous unsegmented flow clin analysis polemic 1861
Continuous wave atomic fluorescence spec= trometry 1076
Continuum source atomic absorption spec= trometry 665 685 838 1263
Continuum source atomic fluorescence back= ground 944
Controlled rate coulometer chloride 1557
Converter analog digital computer 1869
Coolant nuclear analysis hydrogen 853
Coolant spacecraft analysis 322a
Copolymer Amberlite XAD chromatog pack= ing 757
Copper analysis ion beam sputtering 16a
Copper atomic absorption DMF solvent 2122
Copper atomization graphite platform 2018
Copper bonded phase liq chromatog 1756
Copper chelation humic fulvic acid 216
Copper coated graphite electrode voltamme= try 485
Copper detn alloy powder 1336
Copper detn ESR 250
Copper detn extn photometry chromatog 2241
Copper detn ion selective electrode 1868
Copper detn paper classification 2285
Copper detn silicon chloride 2289
Copper detn transition metal present 2090
Copper detn x ray fluorescence 1734
Copper diketonate extn 2246
Copper enrichement seawater 1146
Copper enrichment Donnan dialysis 1272
Copper extn kinetics fast detn 1636
Copper flame atomic absorption 574
Copper perchlorate acetonitrile soln dewater= ing 1874
Copper phytoplankton complexation seawa= ter 226
Copper preconcn chelate water analysis 222
Copper removal sodium hydroxide 889
Copper selective electrode chloride 877
Copper selective electrode iron detn 497
Copper sepn nickel extn chromatog 1189
Copper solubilization natural water complex= ation 2358
Copper zinc intermetallic stripping voltam= metry 1792
Copptn polonium seawater 494
Correction background atomic absorption spctrometer 1106
Correction interference atomic absorption spectrometry 838
Correction right angle fluorescence 706
Correction x ray analysis 717
Corrosion product stainless steel identifica= tion 322a
Corrosion stainless steel org solvent 1637
Coulometer controlled rate chloride 1557
Coulometric detector liq chromatog review 447a
Coulometric titrn app double compartment 1885
Coulometric titrn chloride detn 1557
Coulometry anodic stripping cadmium 199
Coulometry gas chromatog wastewater 128
Coulometry stripping electrode holder 1880
Coulson conductivity detector organochlorine 326
Coumarin deriv fatty acid label 442
Counter radiation background correction 2193
Counting pulse high precision 306
Criterion acceptability analytical method 510
Crown ether catalyst derivatization acid 832
Crude oil arenesulfonate radiometry 1148
Cryogenic gas chromatograph 1279
Crystal piezoelec detector analysis review 1890
Crystal violet reagent nitrate detn 2249
Cupric ion activity 877
Curium scintillation counting 1268
Current tubular electrode voltammetry ferri= cyanide 1563
Curve fitting spectrophotometric titrn com= puterized 1408
Cyanide complex detn ion exchange 516
Cyanide hydrogen detn combustion gas 322
Cyanide reagent dinitro compd detn 45
Cyano complex ion exchange 516
Cyano ethyl nickel electrochem redn 1005
Cyanogen bromide pyridine reaction 785
Cyanomorpholine morpholine nitrosation saliva 715a
Cyclic imide enzymic hydrolysis 292
Cyclic voltammetric theory 896
Cyclic voltammetry electrode bound reactant 1589
Cyclic voltammetry glass ceramic cell 1646
Dansyl amino acid deriv fluorescence 1606
Data acquisition voltage controlled oscillator 681
Data anal 2116
Data analysis multicomponent fluorescence matrix 564
Data aquisition analysis recorder 342
Data base carbon NMR 2136
Data comparison chromatog mass spectrosco= py 1623
Data compd categorization 2114
Data matrix factor detn error 612
Data processing air monitoring 357a
Data redn multicomponent fluorescence 2155
Daughter ion scanning mass spectrometer 174
Dead vol gas chromatog peak 625
Deadtime counting uncertainty 306
Deconvolution spectral peak 2149
Dehydrating transition metal salt nonaq 1874
Dehydrogenase detn NADH peroxidase 1785
Delay time ion selective electrode 2377
Dense gas solvent exclusion chromatog 243
Densitometry fluorescence thin layer chro= matog 2160
Densitometry image quantitation mass spec= troscopy 2322
Deoxyribonucleotide oligo mass spectra 1414
Deposition stripping iodide film 1199
Depth profile analysis mass spectrometer 1399
Depulsing system pos displacement pump 2125
Derivatization acid phenol gas chromatog 832
Derivatization phosphate precolumn chroma= tog 1086
Design soln titrn calorimeter 1878
Desolvating aerosol droplet velocity flame 2112
Desolvating droplet dynamics laminar Flame 2086
Desorption isotherm detn flow method 991
Desorption thermal org compd water 1023
Detection chromatog reactant ion monitoring 731
Detection limit fluorescence gas chromatog 1057
Detection limit fluorometry laser source 667
Detection limit multicomponent atomic emission 632
Detector analysis piezoelec crystal review 1890
Detector chemiluminescence nitric oxide 932
Detector electrochem liq chromatog review 447a
Detector flame gas chromatog 126
Detector glow discharge gas chromatog 2215
Detector liq chromatog ref electrode 2379
Detector luminescence spectrometry 1048
Detector multiwavelength liq chromatog 1171
Detector Raman spectrometry liq chromatog 959
Detector vidicon flame emission spectrometry 106
Detector vidicon liq chromatog 939
Detn chem reaction kinetics 60
Detn drop time polarog 1270
Detn statistical weighting 846
Detn thorium uranium ores alpha spectrome= try 1648
Detns x ray photoelectron spectroscopy 2128
Deuterated sample NMR holder 674
Deuterium NMR compds 1280
Diacetylmonoxime nitrophenylhydrazone reagent cobalt 580
Dialysis Donnan cation enrichment 1272
Diatom barium detn 1017
Dibenzodioxin tetrachloro detn environment 918
Dichromate potassium ref UV spectrometry 711
Dictionary of Chromatography (book review) 71a
Dielec property water oil emulsion 690
Diesel fuel pollutant identification 500
Diethanolamide coconut oil anal 835
Diethyldithiocarbamate lead sewater extn 1146
Diethyldithiocarbamate nickel extn gold 1771
Diethyldithiocarbamic acid cadmium extn 158
Diethylene glycol content polyester 741
Diethylether corrosion stainless steel 1637
Differential pulse polarog nitrite detn 2272
Differential pulse polarog simulation 1246
Differential pulse voltammetry adsorbed sample 1589
Differential pulse voltammetry thin layer 1792
Diffraction x ray absorption coeff 1168
Diffraction x ray silver filter 429
Diffusion const quinone hydroquinone 806
Diffusion ion cation exchange membrane 629
Diffusion mechanism graphite furnace 2008
Diffusion pump fluid distn 1886
Digital analog converter computer 1869
Digital analysis absorption spectra review 864a
Digital app drop time 1270
Digital image processing mass spectroscopy 2322
Digital microcoulometric measurement anod= ic stripping 199
Digital simulation pulse polarog 1246
Digitization spectrophotometer IR 1875
Diketonate chromium chromatog mass sepct= roscopy 1501
Dil soln nephelometric titrn 2268
Diluent effect thiothenoyltrifluoroacetonate extn 2246
Dimethylamine reaction nitrogen oxide 1821
Dinitro compd detn 45
Dioxin tetrachlorodibenzo detn environment 918
Dipeptide acetylacetonyl methyl ester 287
Dipeptide liq chromatog 860
Diphenylquinone formation Tenax GC 512
Discharge chamber microwave induced plas= ma 2372
Discharge helium light emission 560
Discharge lamp electrodeless gaseous hydride 551
Dispersive spectrometer selectively modulat= ed interferometer 113
Display computer mass spectrometry 1462
Dissocn kinetics Zincon metal complex 2090
Distn hydrocarbon water removal 1887
Disulfide voltammetry 2108
Dithiocarbamate nickel extn gold 1771
Dithizone reagent mercury extn 983
Divinylbenzene styrene immobilized ferroin deriv 974
DMF solvent atomic absorption 2122
Donnan dialysis cation enrichment 1272
Dopamine brain chromatog 354
Double bond position alkene detn 2146
Dowex pressure elec cond 767
Drift tube ion source 1497
Drinking water haloform detn 814
Drop time detn polarog 1270
Droplet desolvating dynamics laminar Flame 2086
Dropping mercury electrode voltammetry 1904
Drug activity factor analysis 612
Drug analysis differential pulse voltammetry 1792

Drug gas chromatog forensic 906
Dry milk phosphorus detn 1492
DTA carbide nitride detn steel 649
DTA reaction kinetics detn 998
Dual wavelength spectrophotometry precision 2170
Dust air analysis lead 210 302
Dye adsorption silylated electrode 1639
Dye manuf wastewater treatment 1433
Dynamic slurry packing chromatog column 1958
Dynamics desolvating droplet laminar Flame 2086
Easy ignition inductively coupled plasma 1450
Echelle vidicon atomic absorption spectrometer 1112
Echelle wavelength modulated atomic absorption 838
Editorial Analytical Division Fellowship Program 2129
Editorial Automated Identification Microbes 193
Editorial Centennial History Analytical Chemistry 689
Editorial Editorial Process 1649
Editorial Global Environmental Monitoring 353
Editorial Letters to the Editor 1281
Editorial Microprocessors Come Age 897
Editorial NSF Support Industrial Research 1089
Editorial Peer Review. Author Anonymous 1
Editorial Scientific Meetings International Participation 1473
Editorial Single Atom Detection 529
EDTA chelate formation const 1940
EDTA detn wastewater carbonate 10
EDTA reagent alk earth lanthanide 969
Education analysis chem industry 182a
Efficiency nebulizer atomic emission spectrometry 632
Elec cond benzotetrathiafulvalene halide 802
Elec cond pressure Dowex 767
Elec potential liq junction 810
Electroanalysis semidifferential peak shape 1390
Electroanalytical Chemistry (book review) a, 74a
Electroanalytical Chemistry, Vol. 10 (book review) , 650a
Electroanalytical Chemistry, Vol. 9 (book review) 350a
Electrocatalysis halide iron redn 1918
Electrochem detector chromatog 1036
Electrochem detector liq chromatog review 447a
Electrochem iron porphyrin stannic oxide 194
Electrochem redn benzoquinone semiquinone 806
Electrochem redn nickel ethyl cyano 1005
Electrochem spectro glass ceramic microcell 1646
Electrochem thin layer cell 1205
Electrochemical Stripping Analysis (book review) 823a
Electrochemical Studies of Biological Systems (book review) 648a
Electrochemistry of Biological Molecules (book review) 1055a
Electrode amalgam emf detn 190
Electrode bound reactant voltammetry 1589
Electrode cation selective choline 209
Electrode cation selective membrane 1567
Electrode copper selective 1868
Electrode copper selective chloride 877
Electrode copper selective iron detn 497
Electrode detn amperometry oxygen 2118
Electrode detn fluorine 38
Electrode detn galactose 789
Electrode detn protein 41
Electrode detn urea 795
Electrode dropping mercury voltammetry 1904
Electrode enzyme Fourier analysis 799
Electrode glass testing buffer 1363
Electrode graphite metal coated voltammetry 485
Electrode holder stripping coulometry 1880
Electrode ion antibody complement assay 2083
Electrode ion selective calibration 2377
Electrode ion selective nonideal calibration 1211
Electrode ion selective phenobarbital detn 1577
Electrode liq nonisothermal potential membrane 212
Electrode mercury drop stripping coulometry 199
Electrode mercury dropping voltammetry 1899
Electrode optically transparent 1395
Electrode optically transparent hydrolysis kinetics 206
Electrode oxygen contg functional group 1632
Electrode perchlorate glycol oxidn 410
Electrode perchlorate selective periodate kinetics 414
Electrode potentiometry automated redox reaction 1908 1914
Electrode reaction faradaic admittance 1805
Electrode reaction quinone hydroquinone 806
Electrode reactions solution soluble redox couples 896
Electrode ref liq chromatog detector 2379
Electrode rotating mercury coated platinum 1789
Electrode silver dinitro compd detn 45
Electrode stationary pulse polarograph 1459
Electrode tin oxide resistivity 1639
Electrode transparent gold mercury 602
Electrode tubular anodic stripping voltammetry 49
Electrode tubular current ferricyanide voltammetry 1563
Electrode vitreous carbon 1470
Electrodeless discharge lamp gaseous hydride 551
Electrodeposition polonium seawater 494
Electrodeposition preconcn x ray analysis 1734
Electrodeposition transuranium element spectrometry 842
Electrolysis potential cadmium water 56
Electrolyte chromatog 142
Electron capture gas chromatog 832
Electron impact ionization mass spectroscopy 1164
Electron induced x ray analysis 1737
Electron spectroscopy indium tin foil 1228
Electrooxidn tetrathiafulvalene acetonitrile bromide 802
Element detn animal tissue ashing 1644
Element fluorometry math 641
Element fly ash surface 1514
Element surface transformed fibroblast 1290
Elemental analysis substituted hydrocarbon monolayer 2330
Elemental org analysis ion chromatog 884
Emf detn amalgam electrode 190
Emission background correction wavelength modulation 1121
Emission flame spectrometry vidicon detector 106
Emission light helium discharge 560
Emission spectra fluorescence forensic 1710
Emission spectra potassium chloride 1489
Emission spectrometry phosphorus 1492
Emulsion oil water detn 690
Encyclopedia of Electrochemistry of the Elements, Vol. VII (book review) 439a
Encyclopedia of Electrochemistry of the Elements, Vol. X (book review) 550a
Energy dispersive x ray analysis 1734
Energy dispersive x ray fluorescence 62
Enrichment cation Donnan dialysis 1272
Enrichment sample ion source 518
Environment analysis cesium 1744
Environment gas chromatog low temp 1279
Environment pollutant arsenic detn 621
Environment pollutant detn 521
Environment tetrachlorodibenzodioxin detn 918
Environmental material sulfur detn 1741
Environmental Monitoring (book review) 439a
Environmental pollutant analysis ammonia 1331
Environmental Pollutants: Selected Analytical Methods (book review) 236a
Environmental Toxicity of Aquatic Radionuclides (book review) 74a
Enzyme detn algorithm 1716
Enzyme electrode Fourier analysis 799
Enzyme immobilization analysis review 1069a
Enzyme immobilized flow analyzer 1929
Enzymic detn urea 795
Enzymic hydrolysis colorimetry 292
EPA Manual of Chemical Methods for Pesticides and Devices (book review) 238a
Epinephrine detn catecholamine present 2090
Epithermal neutron activation bromine detn 1998
Epoxy resin equiv wt 1144
EPR sample cell lossy material 1277
Equation isotope distribution 281
Equil evaluation ion mass spectrometric analysis 896
Equil system calcn simulation equation 1660
Equivalence point automated potentiometric titrn 1250
Equivalence point photometric titrn 1408
Erbium detn selective laser excitation 1680
Error analytical chem 691a
Error detn data matrix 612
Error dual wavelength spectrophotometry 2170
Error function empirical approxn 186
Error function potentiometric titrn 1250
Error ion selective electrode 2377
Error sampling ion microprobe analysis 1529
Error sodium glass electrode 1363
Error systematic gas chromatog 2222
Error theory factor analysis 606
ESCA quant analysis 1282
ESCA quant calibration 1044
Escherichia respiration membrane potentiometry 1914
Esculin laser source fluormetry 667
ESR analysis cavity loading effect 1353
ESR chromite chromic oxide detn 962
ESR quant analysis 250
ESR solvent polarity 591
ESR surface review 221r
ESR transition metal exchange resin 1840
Essential oil analysis review 83r
Ester carboxylic gas chromatog 2337
Ester kinetic analysis 1650
Ester methyl acetylacetonyl dipeptide 287
Ester phosphorous acid acidity detn 1584
Ester phosphorus detn air 1746
Etching oxygen plasma graphite 1632
Ethane detn oxygen mass spectrometry 270
Ether crown catalyst derivatization acid 832
Ether polyphenyl purifn 1886
Ethoxylate biodegrdn analysis extn 398
Ethyl cyano nickel electrochem redn 1005
Ethyl lead chromatog gasoline 1761
Ethyldithiocarbamate tellurium chromatog atomic absorption 189
Ethylene glycol detn lubricating oil 582
Ethylene monolayer analysis Auger spectroscopy 2330
Ethylene oxide detn gas sterilant 1602
Ethylenediamine reagent cobalt detn 580
Europium ion probe excitation fluorometry 1690
Europium NMR shift sepn 2375
Evolved gas analysis steel phase 649
Exchange resin transition metal ESR 1840
Excitation mechanism plasma spectrochem analysis 266
Excitation sodium fluorescence 2111
Excitation two photon fluorescence 2054
Exclusion chromatog solvent dense gas 243
Explosive mass spectroscopy liq chromatog 1039
Exponentially modified Gaussian chromatog peak 625
Ext plastic analysis tin 1090
External heavy atom phosphorimetry 2048
Extn app reboiling 1465
Extn chromatog support macroporous resin 1189
Extn copper iron detn 2241
Extn geol analysis 1485
Extn gold detn 1771
Extn kinetics copper fast detn 1636
Extn mercury dithizone reagent 983
Extn nitrate detn 2249
Extn scandium detn 1192
Extn silver detn zinc spelter 1066
Extn sodium hydroxide purifn 889
Extn thiothenoyltrifluoroacetonate diluent effect 2246
Fabrication alkali flame detector 192
Factor analysis error theory 606
Factor analysis mass spectra 284
Factor analysis mass spectra nucleoside 1444
Factor detn data matrix 612
Faradaic admittance analysis thermodn 1805
Faradaic admittance fast Fourier transform 1797
Fast Fourier transform faradaic admittance 1797 1805
Fat mass spectrometry 728
Fatty acid flurescence label 442
Feces actinide detn 1268
Ferricyanide voltammetry tubular electrode current 1563

Ferroin chromogen polymer immobilized 974
Ferrous metallurgy analysis review 54r
Ferrozine ligand regeneration iron detn 319
Fertilizer analysis review 186r
Fiber optic flow cell fluorometer 2051
Fibroblast transformed surface element 1290
Field desorption mass spectroscopy alkali 1744
Field effect potentiometric sensor 2315
Field flow fractionation characterization 523
Field flow fractionation solute relaxation 659
Field ionization mass spectroscopy 1847
Field ionization source glass lined 2121
Film alloy analysis x ray 1152
Film gallium nitride analysis 1536
Filter air sampling metal particle 346
Filter attenuation x ray fluorescence 1990
Filter function frequency response plot 351
Filter silver x ray diffraction 429
Filtering sampling app water 672
Fire polyurethane foam cyanide detn 322
Fish contaminant detn 521
Fish tetraalkyllead detn atomic absorption 823
Fission product cadmium extn 158
Flame analytical aerosol velocity 2112
Flame atomic absorption spectrophotometry precision 574
Flame condition compromise multielement analysis 2280
Flame detector gas chromatog 126
Flame emission spectrometry vidicon detector 106
Flame helium oxygen acetylene 2013
Flame laminar dynamics desolvating droplet 2086
Flame optical modulator atomic absorption 98
Flame photometry chromatog hydrogen sulfide 123
Flame retardant polystyrene analysis 886
Flame spectrometry primary amide detn 262
Flameless atomic absorption sample loss 2008
Flameless Atomic Absorption Analysis: An Update (book review) 442a
Flameless atomic absorption mercury detn 336
Flameless atomic absorption tin detn 1090
Flavor resin cereal packaging 901a
Flow cell fiber optic fluorometer 2051
Flow cell micro Raman spectrometry 959
Flow injection analysis 1858
Flow method desorption isotherm detn 991
Flue gas adsorbent Tenax GC 512
Flue gas nitrite detn 1779
Fluoranthene detection fluorescence 955
Fluorescamine amino acid deriv fluorescence 1606
Fluorescein detn fluorometry laser source 667
Fluorescence and Phosphorescence Spectroscopy: Physicochemical Principles and Practice (book review) 931a
Fluorescence atomic spectrometry microprocessor laser 1702
Fluorescence background interference atomic fluorescence 948
Fluorescence computer structure characterization 2069
Fluorescence data analysis matrix 564
Fluorescence detection gas chromatog effluent 1057
Fluorescence detector vidicon 939
Fluorescence emission spectra forensic 1710
Fluorescence enhancement amino acid deriv 1606
Fluorescence monitor chromatog 1836
Fluorescence polycyclic arom hydrocarbon detection 955
Fluorescence quantum optoacoustic spectrometry 1850
Fluorescence right angle correction 706
Fluorescence sodium excitation 2111
Fluorescence spectrometry arom hydrocarbon 701
Fluorescence spectrometry atomic 1076
Fluorescence spectroscopy rapid scanning 747a
Fluorescence two photon excitation 2054
Fluorescence x ray alloy film 1152
Fluorescence x ray analysis 1734
Fluorescence x ray analysis computer 345
Fluorescence x ray analysis correction 1990
Fluorescence x ray analysis geol 717
Fluorescence x ray analysis multielement 1012
Fluorescence x ray geochem analysis 62
Fluorescence x ray matrix correction 641
Fluorescence x ray matrix effect 1403
Fluorescent petroleum analyzer chromatog 1316
Fluorescent resin TNT detection water 2251
Fluorescent spot chromatog color photog 1640
Fluoride calcium copptn lanthanide detn 1680
Fluoride detn soil vegetation 53
Fluorimetric detn diaminotoluene polyurethane 1676
Fluorine detn mol absorption spectrometry 2035
Fluorine detn neutron activation 1507
Fluorine detn plasma 38
Fluorine detn proton activation 1297
Fluorine detn substituted hydrocarbon monolayer 2330
Fluorine 19 NMR alkene detn 2146
Fluormetry esculin laser source 667
Fluoro Schiff base amine chromatog 541
Fluorobenzaldehyde derivatization amine chromatog 541
Fluorobenzyl deriv acid phenol chromatog 832
Fluoroethane compressed chromatog solvent 243
Fluorometer fiber optic flow cell 2051
Fluorometer lanthanide ion probe excitation 1474
Fluorometer laser detector liq chromatog 1554
Fluorometer reaction rate 1060
Fluorometer tryptophan detn 950
Fluorometry arom hydrocarbon coal 701
Fluorometry gentamicin chloronitrobenzoxadiazole 953
Fluorometry lanthanide ion probe excitation 1474
Fluorometry laser nonfluorescent ion detn 1690
Fluorometry laser trace lanthanide detn 1680
Fluorometry multicomponent mixt anal 2155
Fluorometry multicomponent system analysis 564
Fluorometry porphyrin detn phenylporphinatozinc std 1453
Fluorometry silver detn 1066
Fluorometry solid surface calibration curve 2160
Flurescence label fatty acid 442
Fly ash analysis arsenic 825
Fly ash analysis x ray 1012
Fly ash leachability neutron irradiated 1994
Fly ash nitrite detn 1779
Fly ash surface element 1514
Foam polyurethane aminotoluene detn 1676
Foam polyurethane combustion cyanide detn 322
Foam polyurethane pesticide air 1668
Foam polyurethane pesticide sampling 7
Food analysis review 194r
Forensic cocaine benzoylecgonine detn 1965
Forensic drug gas chromatog 906
Forensic explosive residue analysis 1039
Forensic fluorescence emission spectra 1710
Forensic science metal 2285
Formaldehyde detn chromotropate nitrate interference 1865
Formaldehyde generator 13
Formation const EDTA chelate 1940
Formic acid quinone hydroquinone 806
Formula mol information system 1982
Fourier analysis enzyme electrode 799
Fourier fast transform faradaic admittance 1797
Fourier transform faradaic admittance 1805
Fourier transform IR analysis microscopy 2275
Fourier transform IR ethylene oxide 1602
Fourier transform IR performic acid 1346
Fourier transform matrix isolation IR 86
Fourier transform NMR 508
Fourier transform spectrometer 1446
Fraction collection liq chromatog electrode 2379
Fraction collector thin layer chromatog 671
Fractionation field flow solute relaxation 659
Fractionation thermal field flow 1750
Fragmentography mass vinyl chloride detn 1985
Free induction decay clipped NMR 508
Frequency modulated argon laser 549
Frequency response plot filter function 351
Fuel gaseous analysis review 176r
Fuel hydrocarbon review 235r
Fuel oil nitrogen compd coal 2292
Fuel oil pollutant identification 500
Fuel vaporization pressure analyzer 2368
Fulvic acid chelation water 216
Functional group NMR 1134
Fundamental parameter x ray analysis 717
Fundamentals of Clinical Chemistry (book review) 545a
Fundamentals of Integrated GC–MS, Pt. III: The Integrated GC–MS Analytical System (Chromatographic Science Series, Vol. 7) (book review) 738a
Fungicide activity microcalorimetry 1781
Furnace graphite atomic absorption 2176
Furnace graphite atomic absorption spectrometry 90
Furnace graphite sample loss mechanism 2008
Furnace vertical pyrolyzer chromatog 348
Fused geol sample analysis 717
Galactose detn blood 789
Gallic acid reagent metal detn 1322
Gallium nitride analysis mass spectroscopy 1536
Gallotannin chromatog 238
Gamma activity detn potassium 1156
Gamma prompt spectrometry proton activation 1297
Gamma spectrometry sulfur detn air 1741
Gas analysis chromatog flame photometry 123
Gas analysis IR spectra subtraction 772
Gas analysis IR spectrometer 893
Gas chromatog acetanilide deriv 1843
Gas chromatog acid phenol derivatization 832
Gas chromatog aliph amine 541
Gas chromatog alkene topol analysis 747
Gas chromatog amino acid 1241
Gas chromatog carboxylic ester 2337
Gas chromatog carcinogen nitrosamine 1544
Gas chromatog chlordane 734
Gas chromatog cocaine benzoylecgonine 1974
Gas chromatog cocaine benzoylecgonine detn 1965
Gas chromatog column packer 684
Gas chromatog computer program 180
Gas chromatog coulometry wastewater 128
Gas chromatog detn chlorpheniramine 1085
Gas chromatog dipeptide ester 287
Gas chromatog drug forensic 906
Gas chromatog effluent fluorescence detection 1057
Gas chromatog factor analysis 612
Gas chromatog flame detector 126
Gas chromatog germanium detn 909
Gas chromatog glow discharge detector 2215
Gas chromatog graphitized carbon black 768
Gas chromatog hydrolysis polyester 741
Gas chromatog hydroxyethylhydrazine detn 2213
Gas chromatog isomer chloromethylaniline 743
Gas chromatog leak 670
Gas chromatog ligand exchange 1179
Gas chromatog mass spectrometry pollutant 521
Gas chromatog mass spectroscopy 169 731 2205
Gas chromatog mass spectroscopy chelate 1501
Gas chromatog mercury organomercurial 365
Gas chromatog monoamine metabolite 915
Gas chromatog nitrogenase detn 1275
Gas chromatog nonionic surfactant 835
Gas chromatog NTA detn water 374
Gas chromatog org compd water 1023
Gas chromatog organochlorine pesticide 2123
Gas chromatog organochlorine pesticide sludge 316
Gas chromatog organometal detn 378
Gas chromatog oxazepam deriv 1545
Gas chromatog peak dead vol 625
Gas chromatog phosgene air 1774
Gas chromatog phosphate silyl deriv 1086
Gas chromatog phosphine 1468
Gas chromatog polyimide polyamide 2349
Gas chromatog pyrolysis catalyst deposit 2374
Gas chromatog pyrolysis furnace 348
Gas chromatog pyrolysis laser 390
Gas chromatog pyrolysis lignite 1540
Gas chromatog pyrolysis polymer 537
Gas chromatog radioassay program RADGLC 1726

Gas chromatog sample injection splitless 1881
Gas chromatog siloxane analysis 2343
Gas chromatog stationary phase reaction 133
Gas chromatog subtractive microreactor 1078
Gas chromatog sulfonated polymer support 1549
Gas chromatog syringe needle guide 1267
Gas chromatog systematic error 2222
Gas chromatog thermodn precision 1029
Gas chromatog triose tetrose 137
Gas chromatog vinyl chloride detn 1985
Gas chromatog volatile polymer 886
Gas chromatogram comparison library data 1623
Gas chromatogram reconstruction IR interfe= rogram 1977
Gas chromatograph detector mass spectrom= eter review 563a
Gas chromatograph mass spectrometer inter= face 518
Gas chromatograph microprocessor controlled 1279
Gas Chromatography in Food Analysis (book review) 545a
Gas dense solvent exclusion chromatog 243
Gas reaction activtion,energy detn 1074
Gas reactive generator 13
Gas sterilant analysis ethylene oxide 1602
Gas stripping org compd water 1023
Gaseous hydride electrodeless discharge lamp 551
Gasoline ethyl lead chromatog 1761
Gasoline sulfur detn chromatog 126
Gasoline volatility vaporization pressure 2368
Gaussian exponentially modified chromatog peak 625
Gel chromatog high efficiency column 898
Gel chromatog particle porosimetry 1183
Gel permeation chromatog coal liq 533
Gel permeation chromatog mol wt materials 1647
Generator reactive gas 13
Gentamicin fluorometry chloronitrobenzoox= adiazole 953
Geochem analysis x ray fluorescence 62 1012
Geol analysis extn atomic absorption 1485
Geol analysis light element 1297
Geol analysis thorium uranium 967
Geol material analysis review 34r
Geol material cadmium extn 158
Geol x ray fluorescence analysis 717
Geometry alkene detn NMR 2146
Germanium detn gas chromatog 909
Germanium electrodeless discharge lamp 551
Glass analysis ion beam sputtering 16a
Glass analysis mass spectrometry 927
Glass ceramic spectro electrochem microcell 1646
Glass electrode testing buffer 1363
Glass lined field ionization source 2121
Glow discharge detector gas chromatog 2215
Glyceride chromatog mass spectrometry 2209
Glyceride mass spectrometry 728
Glycol acid analysis polyester 741
Glycol oxidn periodate monitroing 410
Glycolate detn boiler blowdown water 1176
Gold detn extn neutron activation 1771
Gold enrichement seawater 1146
Gold mercury transparent electrode 602
Gradient elution ammonia gas chromatog 1179
Gran plot error function titrn 1250
Graph display chem information algorithm 1357
Graphical interpolation kinetic analysis 1650
Graphite atomizer sample supply removal 2176
Graphite coated tubes spectrometry 90
Graphite electrode metal coated voltammetry 485
Graphite furnace atom loss 1100
Graphite furnace mechanism atom formation 192
Graphite furnace platform atomic absorption 2018
Graphite furnace sample loss mechanism 2008
Graphite oxygen plasma etching 1632
Graphite tube atomization mercury detn 336
Graphitized carbon black gas chromatog 768
Grass tetrachlorodibenzodioxin detn 918
Gravity flow chromatog Amberlite XAD 757
Grease lubricant review 238r
Gum opium alkaloid detn 359
Half wave potential detn 60
Halide benzotetrathiafulvalene elec cond 802
Halide electrocatalysis iron redn 1918
Halide surface characterization review 221r
Haloform detn drinking water 814
Halogen detector gas chromatog 2215
Handbook of Enzymatic Methods of Analysis (book review) 735a
Handbook of Radioimmunoassay (book review) 736a
Hanging mercury drop electrode 199
Hazards in the Chemical Laboratory. 2nd Ed (book review) 830a
Hb detn blood app 555
Heat reaction detn app 1878
Helium discharge light emission 560
Helium nuclear coolant analysis hydrogen 853
Helium oxygen acetylene flame 2013
Helium plasma microwave induced excitation 266
Helium 3 activation analysis 1510
Helix stirrer 191
Heme redox reaction thermodn 1573
Hemolysis immune detn ion electrode 2083
Heptane benzene mass spectroscopy 1847
Herbicide adsorption chromatog 386
Hetaeron ion pair chromatog retention 2295
Heteroarom nitrogen coal liquefaction 2292
High performance chromatog opium alkaloid 359
High performance liq chromatog 2306
High performance liq chromatog azoxybenz= ene 1963
High performance liq chromatog electrode 2379
High performance liq chromatog review 447a
High pressure chromatog Amberlite XAD 757
High pressure chromatog detector 1836
High pressure liq chromatog 860
High pressure liq chromatog amine 1756 2080
High pressure liq chromatog detector 1554
High Resolution NMR Spectroscopy in Solids (book review) , 648a
Hippurate colorimetry 1494
Hippuric acid amino phosphorescence detn 2164
History analysis chem US 480a
History spectrophotometer manuf 280a
Holder electrode stripping coulometry 1880
Home appliance industry analytical chem 1032a
Hormone amino acid brain 1241
Hormone thyroid chromatog spectrometry 1304
Humic acid chelation water 216
Hydrazine detn thin layer chromatog 161
Hydrazine hydroxyethyl detn gas chromatog 2213
Hydride gaseous electrodeless discharge lamp 551
Hydride generation atomic absorption 1096
Hydride IR Teflon pellet 1458
Hydrocarbon acyclic satd NMR 1134
Hydrocarbon aliph liq chromatog 2306
Hydrocarbon analysis chromatog flame pho= tometry 123
Hydrocarbon analysis petroleum review 249r
Hydrocarbon arom polycyclic detn 701
Hydrocarbon arom polynuclear methylation 1260
Hydrocarbon distn water removal 1887
Hydrocarbon fuel review 235r
Hydrocarbon polycyclic arom detection 955
Hydrocarbon polycyclic arom IR analysis 86
Hydrocarbon removal water 2260
Hydrocarbon substituted monolayer elemen= tal analysis 2330
Hydrocarbon vanadium visible spectroscopy 972
Hydrochloric acid stabilization mercury detn 336
Hydrocortisone detn reaction rate 1586
Hydrogen cyanide detn combustion gas 322
Hydrogen detection gallium nitride 1536
Hydrogen detn coal NMR 75
Hydrogen detn helium 853
Hydrogen detn jet fuel NMR 594
Hydrogen ion detn seawater 29
Hydrogen peroxide stabilization mercury detn 336
Hydrogen sulfide chromatog flame photome= try 123
Hydrogen sulfide detn water 424
Hydrolysis enzymic colorimetry 292
Hydrolysis gas chromatog polyester 741
Hydrolysis kinetics optically transparent electrode 206
Hydroquinone inhibitor dimethacrylate analysis 363
Hydroquinone quinone formic acid 806
Hydroxide sodium analytical reagent purifn 889
Hydroxy naphthol blue reagent phototmetry 969
Hydroxyethylhydrazine detn gas chromatog 2213
Hydroxyindoleacetate detn 915
Hydroxyindoleacetic acid phosphorescence detn 2164
Hydroxyl group detn phosphorous acid 1584
Hydroxylamine enzymic hydrolysis 292
Hydroxyphenylalanine detn catecholamine present 2090
Hydroxyproline detn meat 1140
Hydroxyquinoline chelation metal water analysis 311
Hydroxytrytophan phosphorescence detn 2164
Hypobromite barium reagent amide detn 262
Identification computer spectra 1441
Ilosvay soln storage life 1218
Imidazolinyloxy oxide nitric oxide detn 1672
Imide fusion gas chromatog 2349
Imine quinone hydrolysis kinetics 206
Iminomethanesulfinic acid redn cadmium 26
Immobilization enzyme analysis review 1069a
Immobilized ferroin chromogen 974
Immune hemolysis detn ion electrode 2083
Impact electron ionization mass spectroscopy 1164
Indium emf amalgam electrode 190
Indium foil oxide ESCA Auger 1228
Indoleacetic acid hydroxy phosphorescence detn 2164
Induction chromium oxidn alc detn 980
Induction decay clipped free NMR 508
Inductively coupled plasma atomic emission 632
Inductively coupled plasma source spectro= metry 1450
Industry chem analysis education 182a
Industry home appliance analytical chem 1032a
Information chem graph display algorithm 1357
Information retrieval computer spectra 2141
Information retrieval mol structure computer 1720
Information system mol formula 1982
Information theory analysis statistics 1265
Infrared and Raman Spectroscopy, Pt. B (book review) , 940a
Infrared Methods in Air Analysis (part num= ber 993-9236) (book review) 442a
Injection sample gas chromatog splitless 1881
Inorg analysis review 34r
Insecticide detn air 1746
Instrumentation analytical std review 386a
Instrumentation petroleum review 262r
Interelement effect spectrochem analysis 266
Interface gas chromatograph mass spectrom= eter 518
Interference atomic absorption arsenic sele= nium 1417
Interference chloride nitrate detn 857
Interference correction atomic absorption spectrometry 838
Interference ligand preventive buffer 1868
Interference mol fluorescence atomic fluores= cence 944
Interferogram IR gas chromatogram recon= struction 1977
Interferometer selectively modulated disper= sive spectrometer 113
Intermetallic copper zinc stripping voltam= metry 1792
Internal ref oxygen sensor 1813
Internal std atomic absorption analysis 1336
Interpolation graphical kinetic analysis 1650
Interrogation app computer liq chromatog 681
Introduction Proton Nuclear Magnetic Reso= nance Spectroscopy (book review) 235a

Iodide electrocatalysis iron redn 1918
Iodide film deposition stripping 1199
Iodine amine charge transfer complex 2080
Iodine detn cathodic pulse stripping 1199
Ion beam sputtering surface analysis 16a
Ion chromatog org elemental analysis 884
Ion Cyclotron Resonance Spectrometry (book review) 1055a
Ion diffusion cation exchange membrane 629
Ion electrode antibody complement assay 2083
Ion exchange calcium magnesium sepn 1595
Ion exchange chromatog support 1189
Ion exchange cobalt detn 580
Ion exchange cyanide complex detn 516
Ion exchange resin trinitrotoluene detection 2251
Ion exchanger conduction mechanism 767
Ion exchanger copper ESR 250
Ion exchanger propylenediaminetetraacetate resin 418
Ion exclusion chromatog acrylamide 154
Ion mass spectrometric analysis equil evaluation 896
Ion microprobe analysis sampling error 1529
Ion pair chroomatog. retention 2295
Ion pair reverse phase chromatog 883
Ion reactant monitoring chromatog detection 731
Ion selective electrode calibration 2377
Ion selective electrode copper detn 1868
Ion selective electrode copper extn 1636
Ion selective electrode nonideal calibration 1211
Ion selective electrode periodate kinetics 414
Ion selective electrode phenobarbital detn 1577
Ion selective electrode potetiometric titrn 1250
Ion selective field effect transistor 2315
Ion source cesium mass spectrometer 1399
Ion source cesium mass spectrometry 2023
Ion source cleaning mass spectrometer 674
Ion source mass spectrometry 1497
Ion source sample enrichment 518
Ion storage mass spectroscopy 1619
Ionic dye mass spectra 922
Ionization acetylation mass spectrometry 1071
Ionization chem mass spectrometry 1497
Ionization chem mass spectrometry review 772a
Ionization const detn spectra evaluation 276
Ionization electron impact mass spectroscopy 1164
Ionization mass spectroscopy chromatog 731
Ionization source glass lined 2121
IR ammonia detn 1331
IR analysis Fourier transform microscopy 2275
IR detn phosgene air 1774
IR Fourier transform ethylene oxide 1602
IR hydride Teflon pellet 1458
IR interferogram gas chromatogram reconstruction 1977
IR matrix isolation Fourier transform 86
IR oil spill fingerprinting 297
IR performic acid detn 1346
IR petroleum pollutant identification 500
IR spectra computer subtraction 772
IR spectrometer computer 470
IR spectrometer switching device 893
IR spectrophotometer digitization 1875
Iron atomic absorption DMF solvent 2122
Iron detn alloy powder 1336
Iron detn copper selective electrode 497
Iron detn extn photometry chromatog 2241
Iron detn ferrozine ligand regeneration 319
Iron detn paper classification 2285
Iron detn silicon chloride 2289
Iron flame atomic absorption 574
Iron oxide analysis gold 1771
Iron oxide photoelectron 1521
Iron porphyrin electrochem stannic oxide 194
Iron preconcn chelate water analysis 222
Iron redn halide electrocatalysis 1918
Iron removal sodium hydroxide 889
Iron sepn aluminum extn chromatog 1189
Irrigation water analysis nitrate 485
Isocratic reverse phase chromatog azoxybenzene 1963
Isomer arom amine chromatog 1756
Isomer chloromethylaniline gas chromatog 743
Isoniazid microdetn repetitive 776
Isonicotinic hydrazide detn polemic 2367
Isooctane vaporization pressure curve 2368
Isopropyl alc detn catalytic 980
Isopropyl ether corrosion stainless steel 1637
Isotope analysis nitrogen app 514
Isotope boron detn atomic absorption 1852
Isotope diln mass spectroscopy source 2121
Isotope distribution equation 281
Isotopic abundance mass spectra assignment 1723
Jet fuel hydrogen detn NMR 594
Jump cell temp spectrophotometer 2378
Ketone subtractive gas chromatog 1078
Ketoxime phenylpyridyl extn metal 889
Kinetic analysis multicomponent mixt 2090
Kinetic analysis ternary mixt 1650
Kinetic const quinone hydroquinone 806
Kinetic fluorometry silver detn 1066
Kinetic photometric multicomponent anal spectrometer 2098
Kinetics Berthelot reaction ammonia detn 464
Kinetics charge transfer faradaic admittance 1805
Kinetics chem reaction detn 60
Kinetics detn temp jump app 1081
Kinetics detn thermal analysis 998
Kinetics hydrolysis optically transparent electrode 206
Kinetics oxalate attack ferrozineiron 319
Kinetics periodate amino alc reaction 414
Kovats index topol analysis 747
Kraft mill wastewater sulfur compd 128
L cell trace element detn 2203
Lab automation computer networking 1100a
Laboratory Instruments: Global Market Survey (book review) 75a
Laminar Flame dynamics desolvating droplet 2086
Laminarity helium oxygen acetylene flame 2013
Lamp arc spectral noise 2040
Lamp electrodeless discharge gaseous hydride 551
Lanthanide detn photometry 969
Lanthanide detn selective laser excitation 1680
Lanthanide ion probe excitation fluorometry 1690
Lanthanide ion probe fluorometry app 1474
Lanthanum 138 gamma activity 1156
Laser argon opticoacoustic analysis 549
Laser excitation selective lanthanide detn 1680
Laser fluorometry nonfluorescent ion detn 1690
Laser induced fluorescence polycyclic arom 955
Laser pyrolysis gas chromatog 390
Laser Raman analysis solute 70
Laser Raman spectrometry oxyanion 2044
Laser scanning dye spectrometric analysis 1702
Laser source esculin fluormetry 667
Laser source fluorometer lanthanide excitation 1474
Laser two photon excitation detector 1554
Laser vaporized atomic absorption spectrometry 1339
Launch pad analysis 322a
Leachability fly ash neutron irradiated 1994
Lead anodic stripping detn 49
Lead calcite surface ESCA calibration 1044
Lead chelation humic fulvic acid 216
Lead contamination air sampling 346
Lead detn biol voltammetry 1792
Lead detn chemiluminescence 1322
Lead detn paper classification 2285
Lead detn seawater spectrometry 2031
Lead detn voltammetry 1789
Lead detn water preconcn chelate 222
Lead diethyldithiocarbamate sewater extn 1189
Lead emf amalgam electrode 190
Lead enrichment chelation water analysis 311
Lead ethyl chromatog gasoline 1761
Lead external heavy atom phosphorimetry 2048
Lead tetraalkyl detn fish 823
Lead 210 detn ore air 302
Leaf necrosis home appliance industry 1032a
Leaf sulfur detn 1741
Least square curve precision analysis 1655
Least square fluorescence data redn 2155
Least squares confidence limit polemic 884
Library mass spectra retention index 180
Ligand exchange gas chromatog 1179
Ligand interference preventive buffer 1868
Ligand mol structure chelate stability 1940
Ligand regeneration iron detn 319
Light element detn org compd 1403
Light element detn proton activation 1297
Light emission helium discharge 560
Light metal analysis review 72r
Light polarization background correction spectrometer 1106
Lignite pyrolysis gas chromatog 1540
Linear programming fluorescence data redn 2155
Liq chromatog Amberlite XAD 757
Liq chromatog amine 1756
Liq chromatog amine detection 2080
Liq chromatog azoxybenzene 1963
Liq chromatog chloro biphenyl 1954
Liq chromatog column packing 1958
Liq chromatog computer interrogation app 681
Liq chromatog detector Raman spectrometry 959
Liq chromatog detector ref electrode 2379
Liq chromatog electrochem detector review 447a
Liq chromatog laser fluorometer detector 1554
Liq chromatog mefruside metabolite 1311
Liq chromatog org acid 860
Liq chromatog organochlorine pesticide 326
Liq chromatog polynuclear arom 2306
Liq chromatog silicon vidicon tube 1171
Liq chromatog syncrude 1766
Liq chromatog syringe needle guide 1267
Liq chromatog vidicon detector 939
Liq electrode membrane potential nonisothermal 212
Liq extn organophosphate pesticide 231
Liq extn pesticide organophosphate 231
Liq junction elec potential 810
Liq trace analysis opticoacoustic 549
Liquefaction coal asphaltene osmometry 2363
Liquefaction coal nitrogen heteroarom 2292
Liquefaction coal solvent chromatog 2253
Liquid Chromatography of Polymers and Related Materials (book review) 1058a
Liquid Scintillation Counting, Vol. 4 (book review) 738a
Liquid Scintillation: Science and Technology (book review) 240a
Literature activation analysis 682a
Lithium detn proton activation 1297
Liver cadmium extn diethyldithiocarbamate 158
Liver hippurate detn 1494
Liver sulfur detn 1741
Loading effect ESR analysis 1353
Loarzepam detn blood 1545
Loss sample mechanism graphite furnace 2008
Lossy material EPR sample cell 1277
Low gas consumption plasma source 1450
Low mol wt gel chromatog 898
Lubricant oil grease review 238r
Lubricating oil ethylene glycol detn 582
Lubricating oil pollutant identification 500
Lubricating oil titanium detn 454
Luminescence combustion analysis petroleum 932
Luminescence spectrometry detector 1048
Luminescence uranium detn ore 638
Luminol chemiluminescence vitamin B12 detn 446
Macroporous resin support extn chromatog 1189
Magnesium analysis review 72r
Magnesium calcium sepn detn 1595
Magnesium detn paper classification 2285
Magnesium detn proton activation 1297
Magnesium flame atomic absorption 574
Malthene acid extn adsorption 1222
Manganese atomic absorption DMF solvent 2122
Manganese detn catalytic 414
Manganese detn chemiluminescence 1322
Manganese detn paper classification 2285
Manganese detn silicon chloride 2289
Manganese detn water ext stability 1862
Manganese preconcn chelate water analysis 222
Manuscript requirements 686
Mass absorption x ray diffraction 1168
Mass filter mass spectroscopy 1619
Mass fragmentography vinyl chloride detn 1985
Mass ion energy spectra barbiturate 435
Mass spectra comparison library data 1623
Mass spectra factor analysis 284
Mass spectra ionic dye 922
Mass spectra oligodeoxyribonucleotide 1444
Mass spectra silyl oxime sugar 137

Mass spectra statistical moment code 1456
Mass spectrometer cesium ion source 1399
Mass spectrometer daughter ion scanning 174
Mass spectrometer gas chromatograph detector review 563a
Mass spectrometer gas chromatograph interface 518
Mass spectrometer ion source cleaning 674
Mass spectrometer multiple ion detection 543
Mass spectrometer quadrupole mol compn 1884
Mass spectrometry acetanilide deriv 1843
Mass spectrometry acetylation ionization 1071
Mass spectrometry air analysis 270
Mass spectrometry amino acid 1241
Mass spectrometry cesium ion source 2023
Mass spectrometry chem ionization review 772a
Mass spectrometry chlordane 734
Mass spectrometry chromatog computer program 180
Mass spectrometry chromatog glyceride 2209
Mass spectrometry computer display 1462
Mass spectrometry dipeptide ester 287
Mass spectrometry field desorption 1160
Mass spectrometry gas chromatog pollutant 521
Mass spectrometry ion source 1497
Mass spectrometry methylated arom 1260
Mass spectrometry monoamine metabolite 915
Mass spectrometry negative ion identification 828
Mass spectrometry secondary ion quant 927
Mass spectrometry triglyceride 728
Mass spectrometry vinyl chloride detn 1985
Mass spectroscopy alkali metal detn 1744
Mass spectroscopy chelate neg ion 1501
Mass spectroscopy chem ionization chromatog 169 731
Mass spectroscopy chromatog catalyst deposit 2374
Mass spectroscopy computer elemental compn 1723
Mass spectroscopy electron impact ionization 1164
Mass spectroscopy factor analysis 612
Mass spectroscopy field ionization 1847
Mass spectroscopy field ionization source 2121
Mass spectroscopy gallium nitride analysis 1536
Mass spectroscopy liq chromatog explosive 1039
Mass spectroscopy peak enhancement 1619
Mass spectroscopy pulse counting 2205
Mass spectroscopy secondary ion quantitation 2322
Math element fluorometry 641
Matrix effect x ray fluorescence 1403
Matrix isolation fluorescence spectroscopy 701
Matrix isolation Fourier transform IR 86
Matrix multicomponent fluorescence data analysis 564
Meat analysis nitrite polarog 2272
Meat hydroxyproline detn 1140
Mechanism atom formation graphite furnace 192
Mechanism conduction anion exchanger 767
Mechanism sample loss graphite furnace 2008
Mefruside metabolite detn urine 1311
Membrane cation exchange ion diffusion 629
Membrane electrode cation selective 1567
Membrane Electrodes (book review) 347a
Membrane potential 810
Membrane potential nonisothermal liq electrode 212
Membrane trace metal concn 1326
Mercaptan detn cathodic stripping voltammetry 1386
Mercaptan wastewater detn 128
Mercapto group detn 1036
Mercaptopurine detn blood plasma 725
Merck Index: An Encyclopedia of Chemicals and Drugs (book review) 240a
Mercurous iodide deposition stripping analysis 1199
Mercury carbon optically transparent electrode 1395
Mercury coated platinum electrode rotating 1789
Mercury detn atomic absorption flameless 336
Mercury detn biol material 365
Mercury detn oil 1641
Mercury detn silver atomic absorption 255
Mercury detn transition metal present 2090
Mercury drop electrode stripping coulometry 199
Mercury drop time detn 1270
Mercury dropping electrode voltammetry 1899 1904
Mercury enrichment chelation water analysis 311
Mercury enrichment seawater 1146
Mercury extn dithizone reagent 983
Mercury gold transparent electrode 602
Mercury loss sample water 662
Mercury preconcn chelate water analysis 222
Mercury removal chloride interference nitrate 857
Mercury sample stability polyethylene bottle 668
Metal atomic absorption DMF solvent 2122
Metal atomic absorption spectrometry 257
Metal chelate chromatog mas spectroscopy chelate 1501
Metal complex gas chromatog support 1549
Metal detector gas chromatog 2215
Metal detn gas chromatog 378
Metal detn water enrichment 311
Metal ion chelation propylenediaminetetraacetate 418
Metal particle air sampling 346
Metal petroleum review 255r
Metal surface characterization review 221r
Metal trace concn membrane 1326
Metal trace detn chemiluminescence 1322
Metallurgy ferrous analysis review 54r
Metallurgy nonferrous analysis review 72r
Metapramine detn blood plasma 2354
Methacrylate copolymer compn NMR 77
Methacrylate tetraoxyethylene stabilizer chromatog 363
Methacrylic acid copolymer compn NMR 77
Methane detn oxygen mass spectrometry 270
Methanesulfinic acid aminoimino redn cadmium 26
Methanesulfonic acid ionization propylene carbonate 503
Methionine gentamicin methylation 953
Methods for Emission Spectrochemical Analysis. 1977 Supplement (book review) 936a
Methods for Emission Spectrochemical Analysis, 1977 Supplement (book review) 1058a
Methyl ester acetylacetonyl dipeptide 287
Methylamine detn water chromatog 401
Methylarsenic arsenic sepn detn 621
Methylarsinic acid detn natural water 820
Methylarsonic acid acid natural water 820
Methylated arom mass spectrometry 1260
Methylation polynuclear arom hydrocarbon 1260
Methylmercury loss volatilization water 23
Methylpentenone extn scandium detn 1192
Methylsilyl deriv phosphate chromatog 1084
Methylsilyl oxime deriv sugar chromatog 137
Micro flow cell Raman spectrometry 959
Microcalorimetry nystatin detn 34
Microcell glass ceramic spectro electrochem 1646
Microcoulometric measurement anodic stripping 199
Microdetn repetitive isoniazid 776
Microdetn vinyl chloride water 1985
Micrometer hanging mercury drop electrode 199
Microphotodensitometry image quantitation mass spectroscopy 2322
Microprobe ion analysis sampling error 1529
Microprobe mass spectrometer ion source 1399
Microprocessor controlled gas chromatograph 1279
Microprocessor controlled laser spectrometric analysis 1702
Microreactor subtractive gas chromatog 1078
Microsample analysis Fourier transform IR 2275
Microscope purchase review 659a
Microscopy Fourier transform IR analysis 2275
Microscopy surface review 221r
Microtechniques for the Clinical Laboratory: Concepts and Applications (book review) 439a
Microwave induced helium discharge 560
Microwave induced helium plasma excitation 266
Microwave induced plasma discharge chamber 2372
Microwave resonance water detn 690
Microwave spectrometry analysis review 249a
Milk dry phosphorus detn 1492
Mineral surface characterization review 221r
Minicomputer in the Laboratory: with examples using the PDP-11 (book review) 932a
Minidisk centrifugal analyzer sample aliquoting 1608
Minor Miracle: An Informal History of the National Science Foundation (book review) 75a
Mirror rotating phosphorimeter automated 1126
Mitochondria spectra 1348
Mixture analysis mass spectroscopy quant 284
Modern Fluorescence Spectroscopy, Vols. I and II (book review) 735a
Modulated selectively interferometer dispersive spectrometer 113
Modulation photolysis 1130
Modulation wavelength emission background correction 1121
Modulator optical flame atomic absorption 98
Mol absorption spectrometry fluorine detn 2035
Mol fluorescence interference atomic fluorescence 944
Mol formula information system 1982
Mol sieve dewatering nonaq soln 1874
Mol structure information retrieval computer 1720
Mol structure ligand chelate stability 1940
Mol wt asphaltene coal 2363
Mol wt materials gel permeation chromatog 1647
Mol wt polyurethane detn 722
Molar absorptivity detn spectra evaluation 276
Molecular Spectroscopy (book review) , 832a
Molybdate vanadate reaction phosphate 779
Molybdenum atomic absorption detn 451
Molybdenum atomization graphite platform 2018
Molybdenum detn saline water 461
Molybdenum flame atomic absorption 574
Molybdovanadophosphoric acid formation 779
Monitoring air data processing 357a
Monoamine metabolite detn 915
Monochromator x ray fluorescence analysis 1734
Monolayer substituted hydrocarbon elemental analysis 2330
Morphine detn gum opium 359
Morpholine nitrosation saliva cyanomorpholine 715a
Morpholinecarbodithioate nickel identification spacecraft coolant 322a
Multichannel analyzer petroleum optical 1316
Multichannel pipet parallel aliquoting 1608
Multicomponent analysis fluorescence spectroscopy 747a
Multicomponent analysis mass spectroscopy source 2121
Multicomponent detection limit atomic emission 632
Multicomponent kinetic photometric anal spectrometer 2098
Multicomponent mixt anal fluorometry 2155
Multicomponent mixt kinetic analysis 2090
Multicomponent spectra numerical analysis 276
Multielement analysis compromise flame condition 2280
Multielement analysis x ray fluorescence 1012
Multielement atomic absorption detn 1263
Multielement atomic absorption spectrometry 1112
Multielement trace analysis geol 1485
Multiple curve precision improvement analysis 1655
Multiple ion detection mass spectrometer 543
Multiplicity stationary electrode polarog curve 1369 1376
Multiwavelength detector liq chromatog 1171

Mussel trace metal detn 257
NADH dehydrogenase detn peroxidase 1785
Naphthalene detection fluorescence 955
Naphthalene detn coal liquefaction 2253
Natural gas sulfur detn 1615
Natural product structure NMR computer 2075
Natural water complexation capacity 2358
Natural water complexation cobaltic ion 404
Natural water uranium detn 67
Nebulizer atomic absorption 1413
Nebulizer atomic emission spectrometry 632
Necrosis leaf home appliance industry 1032a
Needle guide chromatog syringe 1267
Neg ion mass spectroscopy chelate 1501
Negative ion chromatog mass spectrometry 828
Neon discharge lamp boron detn 1852
Neopolarogram deriv semidifferential elec= troanalysis 1390
Nephelometric titrn dil bromide soln 2268
Neutron activation analysis sewater 1146
Neutron activation epithermal bromine detn 1998
Neutron activation fluorine detn 1507
Neutron activation gold detn 1771
Neutron counting uranium detn 67
Neutron irradiated fly ash leachability 1994
New Products 524a
Newburger's Manual of Cosmetic Analysis, 2nd Ed (book review) 1058a
Nickel atomic absorption DMF solvent 2122
Nickel detn alloy powder 1336
Nickel detn seawater spectrometry 2031
Nickel detn silicon chloride 2289
Nickel detn x ray fluorescence 1734
Nickel diethyldithiocarbamate extn gold 1771
Nickel enrichment chelation water analysis 311
Nickel ethyl cyano electrochem redn 1005
Nickel morpholinecarbodithioate identifica= tion spacecraft coolant 322a
Nickel perchlorate acetonitrile soln dewater= ing 1874
Nickel preconcn chelate water analysis 222
Nickel removal sodium hydroxide 889
Nickel sepn copper extn chromatog 1189
Nickel tin sputtered oxidn 987
Nicotinic acid ref UV spectrometry 711
Niobium detn sodium 80
Nitrate detn chloride interference 857
Nitrate detn extn photometry 2249
Nitrate detn laser Raman 70
Nitrate detn radioactive waste 2044
Nitrate detn voltammetry 485
Nitrate detn water polarog 479
Nitrate interference formaldehyde detn chromotropate 1865
Nitrate silver analysis mercury 255
Nitric oxide chemiluminescence detector 932
Nitric oxide detn nitrogen mass spectrometry 270
Nitride detn steel DTA 649
Nitride gallium analysis mass spectroscopy 1536
Nitrite detn air particulate 1779
Nitrite detn differential pulse polarog 2272
Nitrite detn radioactive waste 2044
Nitrite detn water polarog 479
Nitro compd detn 45
Nitrobenzamide deriv amphetamine chroma= tog 912
Nitrogen carrier gas plasma chromatog 828
Nitrogen compd coal liq 2292
Nitrogen detection gallium nitride 1536
Nitrogen detn petroleum chemiluminescence 932
Nitrogen detn protein seed 1080
Nitrogen detn substituted hydrocarbon monolayer 2330
Nitrogen detn wastewater TNT 880
Nitrogen dioxide permeation calibration 1823
Nitrogen dioxide triethanolamine stoichiom= etry 1448
Nitrogen isotope analysis app 514
Nitrogen oxide reaction dimethylamine 1821
Nitrogen 15 amino acid spectrometry 1832
Nitrogenase detn gas chromatog 1275
Nitrophenylhydrazone diacetylmonoxime reagent cobalt 580
Nitrosamine carcinogen gas chromatog 1544
Nitrosation morpholine saliva 715a
Nitrosodimethylamine detn air 1821
Nitrous oxide detn seawater 1238
NMR alkane computer 1134
NMR carbon 13 acrylic polymer 77
NMR carbon 13 polyolefin 1405
NMR carbon 13 quant analysis 2130
NMR clipped free induction decay 508
NMR coal aromaticity 585
NMR computer natural product structure 2075
NMR data base carbon 2136
NMR detn epoxy equiv 1144
NMR deuterium compds 1280
NMR factor analysis 612
NMR fluorine 19 alkene detn 2146
NMR holder deuterated sample 674
NMR hydrogen detn coal 75
NMR hydrogen detn jet fuel 594
NMR hydroxyproline 1140
NMR P aminoethyl phosphate detn 588
NMR polyester urethane compn 722
NMR shift europium sepn 2375
NMR solid review 951a
NMR solvent polarity 591
NMR surface review 221r
NMR: Basic Principles and Progress, Vol. 12 (book review) 550a
NMR: Basic Principles and Progress, Vol. 13, Introductory Essays (book review) 441a
Noise dual wavelength spectrophotometry 2170
Noise signal flicker spectrometry polemic 339 340
Noise spectral bandpass spectrometry 119
Nomenclature thin layer chromatog 1867
Nonaq conductometric titrn phosphorous acid 1584
Nonaq soln water removal 1874
Nonferrous alloy analysis manganese 414
Nonferrous metallurgy analysis review 72r
Nonfluorescent ion detn laser fluorometry 1690
Nonideal calibration ion selective electrode 1211
Nonionic resin potentiometric titrn acid 1256
Nonionic surfactant biodegrdn analysis 398
Nonionic surfactant gas chromatog 835
Nonisothermal liq electrode membrane po= tential 212
Nonlinear calibration confidence limit analy= sis 2062
Nonmetal analysis petroleum review 256r
Norepinephrine detn catecholamine present 2090
NTA detn wastewater carbonate 10
NTA detn water gas chromatog 374
Nuclear coolant analysis hydrogen 853
Nucleoside base chromatog 2237
Nucleoside chromatog high performance 2231
Nucleoside NMR carbon computer 2075
Nucleotide chromatog high performance 2231
Nucleotide oligodeoxyribo mass spectra 1444
Null point pH control 1009
Numerical analysis multicomponent spectra 276
Nystatin detn microcalorimetry 34
Odorant structure olfaction relation 596
Oil coal chromatog 1225
Oil crude arenesulfonate radiometry 1148
Oil emulsion water detn 690
Oil essential analysis review 83r
Oil identification Fourier transform IR 2275
Oil lubricant review 238r
Oil mercury detn 1641
Oil spill fingerprinting IR 297
Oilseed spectrochem review 835a
Olfaction odorant structure relation 596
Oligodeoxyribonucleotide mass spectra 1444
Oligomer gel permeation chromatog 898
Oligomer terephthalate detn chromatog 1166
Open tubular column chromatog 768
Open tubular column gas chromatog 1881
Opium alkaloid 359
Opium gum alkaloid detn 359
Optical analyzer spectrofluorometry petrole= um 1316
Optical modulator flame atomic absorption 98
Optical transparent electrode 602
Optically transparent electrode 1395 1470
Optically transparent electrode hydrolysis kinetics 206
Opticoacoustic trace analysis liq 549
Optimization analysis super modified simplex 1422
Optimization viscosity exclusion chromatog 243
Optoacoustic spectrometry quantum fluores= cence 1850
Ore analysis germanium chromatog 909
Ore analysis thorium uranium isotope 618
Ore analysis uranium 638
Ore uranium analysis lead 210 302
Org acid liq chromatog 860
Org carbon detn plasma spectrometry 1235
Org compd analysis fluorine 2035
Org compd cation selective electrode 1567
Org compd mass spectrometry 1160
Org compd water anal 1023
Org solvent stainless steel corrosion 1637
Org sulfur detn spectrophotometric titrn 1987
Organic Structural Analysis (book review) 74a
Organochlorine pesticide gas chromatog 2123
Organochlorine pesticide liq chromatog 326
Organochlorine pesticide sludge gas chroma= tog 316
Organomercurial detn biol material 365
Organometal detn gas chromatog 378
Organometallic analysis chromatog atomic absorption 189
Organometallic atomic absorption DMF solvent 2122
Organophosphate pesticide liq extn 231
Oscillating refractor plate wavelength modu= lation 1121
Oscillator voltage controlled data acquisition 681
Osmometry vapor pressure asphaltene 2363
Osmotic coeff aq choline chloride 209
Overlapped voltammetry data pattern recog= nition 1369 1376
Oxadiazole high pressure liq chromatog 1554
Oxalate attack ferrozineiron kinetics 319
Oxalic acid reagent carbodiimide 676
Oxazepam detn blood 1545
Oxide analysis germanium chromatog 909
Oxide chromic detn sodium chromite 962
Oxide ethylene detn gas sterilant 1602
Oxide indium tin ESCA Auger 1228
Oxide iron photoelectron 1521
Oxide nitric chemiluminescence detector 932
Oxide surface characterization review 221r
Oxide tin electrode resistivity 1639
Oxidn bromide interference nitrate detn 2249
Oxidn electrochem tetrathiafulvalene brom= ide 802
Oxidn gallic acid chemiluminescence 1322
Oxidn glycol monitroing periodate 410
Oxidn sputtered tin nickel 987
Oxidn titrn thioether drug 1002
Oxime methylsilyl deriv sugar chromatog 137
Oxime prostaglandin thromboxane chroma= tog 1032
Oxinesulfonic acid reagent silver detn 1066
Oxyanion detn radioactive waste 2044
Oxyarsine detn natural water 820
Oxygen amperometry electrode detn 2118
Oxygen analysis acetylene 1218
Oxygen detection gallium nitride 1536
Oxygen detn nitrogen mass spectrometry 270
Oxygen detn substituted hydrocarbon mono= layer 2330
Oxygen helium acetylene flame 2013
Oxygen isotope measurement 1664
Oxygen modification graphite electrode 1632
Oxygen sensor internal ref 1813
Oyster analysis anodic strippping voltamme= try 1792
Oyster cadmium extn diethyldithiocarbamate 158
Packaging cereal resin flavor 901a
Packer column gas chromatog 684
Packing column liq chromatog 1958
Palladium thin film hydrogen detn 853
Paraffin wax review , 276r
Paramagnetic antiferromagnetic transition chromium compd 962
Parathion water chromatog 1551
Particle metal air sampling 346
Particle porosimetry gel chromatog 1183
Particle size respirable quartz detn 2196
Particulate airborne analysis nitrate 485
Particulate nitrite detn air 1779
Pattern recognition data 2116
Pattern recognition overlapped voltammetry data 1369 1376
Peak distortion field flow fractionation 659
Peak enhancement mass spectroscopy 1619

Peak shape semidifferential electroanalysis 1390
Peak spectral deconvolution 2149
Pellet Teflon IR hydride 1458
Pentenone methyl extn scandium detn 1192
Peptide amino acid detn 1241
Perchlorate electrode glycol oxidn 410
Perchlorate selective electrode periodate kinetics 414
Performic acid gaseous detn 1346
Periodate amino alc reaction kinetics 414
Periodate oxidn glycol monitroing 410
Periodical activation analysis 682a
Permeation calibration nitrogen dioxide 1823
Permeation tube air anal 1278
Peroxidase NADH dehydrogenase detn 1785
Peroxide stabilization mercury detn 336
Persulfate reagent silver detn 1066
Pesticide detn air 1668
Pesticide organochlorine gas chromatog 2123
Pesticide organochlorine liq chromatog 326
Pesticide organochlorine sludge gas chromatog 316
Pesticide organophosphate liq extn 231
Pesticide residue review 98r
Pesticide sampling polyurethane foam 7
Pesticide thiourea pulse voltammery 2310
Petroleum analysis instrumentation review 262r
Petroleum analysis review 231r
Petroleum catalyst review 243r
Petroleum hydrocarbon analysis review 249r
Petroleum metal review 255r
Petroleum nitrogen detn chemiluminescence 932
Petroleum nonmetal analysis review 256r
Petroleum phys property review 246r
Petroleum pollutant classification IR 500
Petroleum review , 273r
Petroleum sulfonate detn radiometry 1148
Petroleum sulfur detn 1615
PH control null point 1009
PH detn glass electrode 1363
Pharmaceutical analysis review 110r
Phase resolved phosphorimetry analytical 1262
Phase selective cathodic stripping voltammetry 1386
Phase selective voltammetry 1789
Phase steel evolved gas analysis 649
Phenanthroline ligand regeneration 319
Phenobarbital detn ion selective electrode 1577
Phenol antioxidant dimethacrylate analysis 363
Phenol derivatization gas chromatog 832
Phenol high pressure liq chromatog 860
Phenoldisulfonic acid reagent nitrate detn 857
Phenoxyacetic acid liq chromatog 860
Phenyl phosphine ethyl cyano nickel 1005
Phenylacetic acid detn NMR 2130
Phenylamine reagent nitrite detn polarog 2272
Phenylethylmalonamide detn blood serum 1969
Phenylporphinatozinc std porphyrin detn fluorometry 1453
Phenylpropionic acid detn NMR 2130
Phenylpyridyl ketoxime extn metal 889
Phenyltetramethylimidazolinyloxy oxide reagent 1672
Phosgene detn air IR 1774
Phosphate analysis molybdate vanadate reaction 779
Phosphate detn boiler blowdown water 1176
Phosphate detn laser fluorometry 1690
Phosphate detn laser Raman 70
Phosphate detn radioactive waste 2044
Phosphate gas chromatog silyl deriv 1086
Phosphine gas chromatog 1468
Phosphine phenyl ethyl cyano nickel 1005
Phosphine removal acetylene atomic fluorescence 944
Phosphorescence analysis room temp 2164
Phosphoric acid analysis arsenic 2376
Phosphorimeter automated rotating mirror 1126
Phosphorimetry external heavy atom 2048
Phosphorimetry phase resolved analytical 1262
Phosphorimetry porphyrin 1482
Phosphorus detector gas chromatog 2215
Phosphorus detn dry milk 1492
Phosphorus detn org ion chromatog 884
Phosphorus ester detn air 1746
Photoacoustic spectrometer 697
Photochromism modulation photolysis 1130
Photoelectron iron oxide 1521
Photoelectron spectroscopy aluminosilicate analysis 2001
Photoelectron spectroscopy detns x ray 2128
Photoelectron spectroscopy indium tin foil 1228
Photoelectron spectroscopy x ray calibration 1044
Photoelectron x ray spectroscopy quant 1282
Photog image quantitation mass spectroscopy 2322
Photoionization cross section 2001
Photolysis modulation 1130
Photometric kinetic multicomponent anal spectrometer 2098
Photometry alk earth lanthanide detn 969
Photometry Berthelot reaction ammonia detn 464
Photometry copper iron detn 2241
Photometry flame simultaneous multielement 2280
Photometry niobium detn 80
Photometry nitrate detn 2249
Photometry scandium detn 1192
Photomultiplier sequential linear scanning detector 939
Photon two excitation detector chromatog 1554
Photothermal spectroscopy 2057
Phthalaldehyde amino acid deriv fluorescence 1606
Phys property petroleum review 246r
Phytoplankton carotenoid detn 695
Phytoplankton complexation seawater copper 226
Picric acid ionization propylene carbonate 503
Piezoelec crystal detector analysis review 1890
Pipet multichannel parallel aliquoting 1608
Pittsburgh conference 115a
Pittsburgh conference: exposition 165a
Plant analysis cobalt 580
Plasma chromatog negative ion identification 828
Plasma discharge chamber microwave induced 2372
Plasma excitation mechanism spectrochem analysis 266
Plasma fluorine detn 38
Plasma inductively coupled atomic emission 632
Plasma inductively coupled source spectrometry 1450
Plasma mercaptopurine detn 725
Plasma nucleoside base detn 2237
Plasma oxygen etching graphite 1632
Plasma spectrometry carbon org detn 1235
Plasma tryptophan detn 950
Plastic barrier film analysis tin 1090
Plastic container sample storage cleaning 2264
Plasticizer gel permeation chromatog 898
Plate oscillating refractor wavelength modulation 1121
Platelet aggregation prostaglandin thromboxane 1032
Platform graphite furnace atomic absorption 2018
Plating problem home appliance industry 1032a
Platinum adsorbed halide electrocatalyst 1918
Platinum electrode voltammetry 1789
Platinum substrate monolayer analysis 2330
Plutonium electrodeposition high resoln spectrometry 842
Pneumatic nebulizer atomic emission spectrometry 632
Poised system pulse voltammetry 489
Polarity solvent ESR NMR 591
Polarization light background correction spectrometer 1106
Polarog detn nitrate nitrite water 479
Polarog differential pulse simulation 1246
Polarog drop time detn 1270
Polarog nitrite detn 2272
Polarog stationary electrode curve multiplicity 1369 1376
Polarog sulfide thiol vitamin B12a 1380
Polarog thiourea pesticide 2310
Polarograph pulse rapid scanning 1459
Polarographic Oxygen Sensors (book review) 823a
Pollutant detn air review 1r
Pollutant environmental analysis ammonia 1331
Pollutant gas chromatog mass spectrometry 521
Pollutant petroleum identification IR 500
Pollutant x ray sensitivity 1505
Pollution air sulfate detn 1990
Polonium detn seawater 494
Polyamide polyimide gas chromatog 2349
Polycyclic arom hydrocarbon detection 955
Polycyclic arom hydrocarbon detn 701
Polycyclic arom hydrocarbon IR analysis 86
Polyester glycol acid analysis 741
Polyester urethane compn NMR 722
Polyethylene bottle mercury sample stability 668
Polyimide polyamide gas chromatog 2349
Polymer dense gas exclusion chromatog 243
Polymer fingerprint home appliance industry 1032a
Polymer identification Fourier transform IR 2275
Polymer immobilized ferroin chromogen 974
Polymer pyrolysis gas chromatog 537
Polymer resoln pyrolysis chromatog 348
Polymer supported carbodiimide detn 676
Polymer surface characterization review 221r
Polymer thermal volatilization analysis 886
Polymn inhibitor hydroquinone chromatog 363
Polynuclear arom hydrocarbon methylation 1260
Polynuclear arom liq chromatog 2306
Polyphenyl ether purifn 1886
Polypropylene bottle mercury sample stability 668
Polystyrene dense gas exclusion chromatog 243
Polystyrene flame retardant analysis 886
Polystyrene macroporous support extn chromatog 1189
Polyterephthalate oligomer liq chromatog 1166
Polyurethane compn anal NMR 722
Polyurethane foam aminotoluene detn 1676
Polyurethane foam combustion cyanide detn 322
Polyurethane foam pesticide air 1668
Polyurethane foam pesticide sampling 7
Polyurethane pyrene removal water 2260
Polyvinylpyrrolidone dense gas exclusion chromatog 243
Porosimetry particle gel chromatog 1183
Porous layer open tubular column 768
Porphinatozinc std porphyrin detn fluorometry 1453
Porphyrin detn fluorometry phenylporphinatozinc std 1453
Porphyrin iron electrochem stannic oxide 194
Porphyrin phosphorescence detn 1482
Portable app acetylene detn oxygen 1218
Pos displacement pump depulsing system 2125
Potassium chloride emission spectra 1489
Potassium dichromate ref UV spectrometry 711
Potassium gamma activity detn 1156
Potential elec liq junction 810
Potential electrolysis cadmium water 56
Potential half wave detn 60
Potential membrane nonisothermal liq electrode 212
Potential potentiometric sensor 2315
Potentiometric sensor field effect 2315
Potentiometric titration acid 1429
Potentiometric titrn acid nonionic resin 1256
Potentiometric titrn automated equivalence point 1250
Potentiometry direct ion selective electrode 2377
Potentiometry electrode automated redox reaction 1908 1914
Potentiometry electrode response 799
Potentiostat current follower stabilization 677
Powder analysis atomic absorption 1336
Powder compaction alloy std prepn 679
Pptn sodium hydroxide purifn 889
Practical High Performance Liquid Chromatography (book review) 71a
Precision calibration curve analysis 1655
Precision dual wavelength spectrophotometry 2170
Precision flame atomic absorption spectrophotometry 574
Precision pulse counting 306
Precolumn phosphate derivatization chromatog 1086
Preconcn chelate lead detn water 222
Preconcn zeolite ammonia detn 1331

Pressure elec cond Dowex 767
Pressure pumping continuous flow analysis 17
Pressure pumping flow injection analysis 1858
Pressure vaporization fuel analyzer 2368
Primary amide detn flame spectrometry 262
Primidone detn chromatog 903
Principal component analysis kinetics detn 846
Principles of Moessbauer Spectroscopy (book review) 347a
Proceedings of the First European Symposium on Thermal Analysis (book review) 348a
Proceedings of the Second International Symposium on Clinical Enzymology (book review) 441a
Prompt gamma spectrometry proton activation 1297
Propylene butene polymer analysis 1405
Propylene carbonate solvent acid dissocn 503
Propylenediaminetetraacetate resin ion exchanger 418
Prostaglandin oxime chromatog 1032
Protein electrode detn 41
Protein nitrogen detn seed 1080
Protein voltammetry 2108
Proton activation light element detn 1297
Proton induced x ray analysis 1737
Pryidine reagent copper iron detn 2241
Pt. 31 of 1977 Annual Book of ASTM Standards on Water (book review) , 938a
Pulse counting high precision 306
Pulse counting org mass spectroscopy 2205
Pulse differential polarog simulation 1246
Pulse rapid scanning polarograph 1459
Pulse stripping cathodic iodine detn 1199
Pulse voltammetry differential thin layer 1792
Pulse voltammetry electrode bound reactant 1589
Pulse voltammetry poised system 489
Pulsed atomic fluorescence spectrometry 1076
Pump pos displacement depulsing system 2125
Pumping pressure continuous flow analysis 17
Pumping pressure flow injection analysis 1858
Purity assay chromatog atomic absorption 189
Pyrene detection fluorescence 955
Pyrene removal water polyurethane 2260
Pyridine base ligand exchange chromatog 1179
Pyridine cyanogen bromide reaction 785
Pyridyldiphenyltriazine polymer immobilized chromogen 974
Pyrolysis chromatog coal characterization 390
Pyrolysis gas chromatog catalyst deposit 2374
Pyrolysis gas chromatog furnace 348
Pyrolysis gas chromatog lignite 1540
Pyrolysis gas chromatog polymer 537
Pyrolytic graphite coated tubes spectrometry 90
Pyrolyzer vertical furnace chromatog 348
Pyrrolidine thiocarbamatocobalt chelate water 222
Quadrupole mass spectrometer mol compn 1884
Quadrupole Mass Spectrometry and Its Applications (book review) 645a
QUAN computer program analysis 345
Quant x ray photoelectron spectroscopy 1282
Quantitation photog image mass spectroscopy 2322
Quantitative Mass Spectrometry in Life Sciences (book review) 736a
Quantum fluorescence optoacoustic spectrometry 1850
Quartz alpha respirable detn air 2196
Quartz oscillator wavelength modulation 1121
Quaternary ammonium electrode membrane potential 212
Quinone cigaret smoke redox 1924
Quinonе hydroquinone formic acid 806
Quinone imine hydrolysis kinetics 206
Radiation counter background correction 2193
Radio and Microwave Spectroscopy (book review) 235a
Radioactive fraction collection chromatog plate 671
Radioactive waste oxyanion detn 2044
Radioassay gas chromatog program RADGLC 1726
Radioimmunoassay automated system 1183a
Radiometric lead 210 detn 302
Radiometry sulfonate detn petroleum 1148
Rain potentiometric titration 1429
Raman laser analysis solute 70
Raman laser spectrometry oxyanion 2044
Raman spectrometry micro flow cell 959
Raman spectroscopy carotenoid 695
Random access atomic absorption system 1112
Rapid scan vidicon spectrometer 871
Rapid scanning fluorescence spectroscopy 747a
Rapid scanning pulse polarograph 1459
Rapid scanning vidicon spectrometer 2098
Rate const detn voltammetry 60
Rate data acquisition signal proportional 681
Rate reaction fluorometer 1060
Reactant ion monitoring chromatog detection 731
Reaction gas chromatog acid fusion 2337
Reaction rate detn hydrocortisone 1586
Reaction rate fluorometer 1060
Reactive gas generator 13
Reactor activation energy detn 1074
Reactor subtractive gas chromatog 1078
Reagent Chemicals, 5th Ed. Supplement No. 1 524
Reagent consumption continuous flow analysis 17
Reagent consumption flow injection analysis 1858
Recorder data aquisition analysis 342
Recording analog storage register anal 19
Redn cadmium aminoiminomethanesulfinic acid 26
Redn electrochem benzoquinone semiquinone 806
Redn electrochem nickel ethyl cyano 1005
Redn iron halide electrocatalysis 1918
Redox chem reaction kinetics 60
Redox cigaret smoke quinone 1924
Redox heme reaction thermodn 1573
Redox reaction automated electrode potentiometry 1908 1914
Ref electrode liq chromatog detector 2379
Ref material activation analysis 33a
Ref material aluminum alloy 679
Ref material UV spectrophotometry 711
Reflectance spectrochem review 835a
Refractor plate oscillating wavelength modulation 1121
Regeneration ligand iron detn 319
Register analog storage recording anal 19
Relaxation Kinetics (book review) + 548a
Removal sample graphite atomizer 2176
Residue Reviews, Vol. 64 (book review) 550a
Resin flavor cereal packaging 901a
Resin fluorescent TNT detection water 2251
Resin macroporous support extn chromatog 1189
Resistivity tin oxide electrode 1639
Resistor failure home appliance industry 1032a
Respirable alpha quartz detn air 2196
Response parameter multielement flame photometry 2280
Retention index mass spectra library 180
Reverse phase isocratic chromatog azoxybenzene 1963
Reversed phase liq chromatog 860
Review absorption spectra digital analysis 864a
Review air pollution 1r
Review amperometric coulometric detector chromatog 447a
Review analysis characterization rubber 133r
Review analysis polymer 159r
Review asphalt 240r
Review chem bonded phase chromatog 1004a
Review chem ionization mass spectrometry 772a
Review clin chem 16r
Review clin chem method 594a
Review coal fuel gaseous analysis 176r
Review enzyme immobilization analysis 1069a
Review essential oil analysis 83r
Review ferrous metallurgy analysis 54r
Review fertilizer analysis 186r
Review food analysis 194r
Review hydrocarbon fuel 235r
Review inorg geol material analysis 34r
Review light metal analysis 72r
Review lubricant oil grease 238r
Review mass spectrometer gas chromatograph detector 563a
Review microscope purchase 659a
Review microwave spectrometry analysis 249a
Review NMR solid 951a
Review of Literature. X-Ray Diffraction, 7th Ed (book review) 736a
Review of Literature. X-Ray Fluorescence Spectrometry, 7th Ed (book review) 736a
Review paraffin wax , 276r
Review pesticide residue 98r
Review petroleum , 273r
Review petroleum analysis 231r
Review petroleum analysis instrumentation 262r
Review petroleum catalyst 243r
Review petroleum hydrocarbon analysis 249r
Review petroleum metal 255r
Review petroleum nonmetal analysis 256r
Review petroleum phys property 246r
Review pharmaceutical analysis 110r
Review piezoelec crystal detector analysis 1890
Review spectrochem analysis food 835a
Review std analytical instrumentation 386a
Review surface characterization technique 221r
Review thin layer chromatog 83a
Review water analysis 139r
Riboflavin detection vidicon 939
Right angle fluorescence correction 706
River water trace metal Chelex 1950
Rock analysis arsenic 825
Rock analysis gold 1771
Rock analysis thorium uranium 967
Rock analysis x ray fluorescence 717
Rock silicate analysis bromine 1998
Rotating mercury coated platinum electrode 1789
Rotating mirror phosphorimeter automated 1126
Rubber pyrolysis gas chromatog 537
Rubber silicone gas chromatog 2343
Salicylic acid ionization propylene carbonate 503
Saline water molybdenum detn 461
Saliva analysis nitrite polarog 2272
Saliva morpholine nitrosation cyanomorpholine 715a
Salt mass spectrometry 1160
Sample aliquoting centrifugal analyzer minidisk 1608
Sample cell lossy material EPR 1277
Sample enrichment ion source 518
Sample injection gas chromatog splitless 1881
Sample loss mechanism graphite furnace 2008
Sample storage plastic container cleaning 2264
Sample supply removal graphite atomizer 2176
Sample water mercury loss 662
Sampling activation analysis 33a
Sampling error ion microprobe analysis 1529
Sampling filtering app water 672
Sampling metal particle air 346
Sampling pesticide polyurethane foam 7
Sampling vinyl chloride charcoal 994
Savitzky Golay filter function 351
Scandium detn extn photometry 1192
Scanning differential calorimetry cell 522
Scanning dye laser spectrometric analysis 1702
Scanning fluorescence spectroscopy 747a
Scanning mass spectrometer daughter ion 174
Schiff base amine gas chromatog 541
Scintillation counting actinide 1268
Seawater analysis transition metal 974
Seawater atomic absorption spectrometry 2031
Seawater hydrogen ion detn 29
Seawater nitrous oxide detn 1238
Seawater phytoplankton complexation capacity 226
Seawater polonium detn 494
Seawater trishydroxymethylaminomethane buffer 867
Second harmonic voltammetry 1789
Secondary ion mass spectrometry 2023
Secondary ion mass spectrometry quant 927
Secondary ion mass spectroscopy 1536
Secondary ion mass spectroscopy quantitation 2322
Seed protein nitrogen detn 1080

Selected Annual Reviews of the Analytical Sciences, Vol. 4 (book review) 832a
Selective laser excitation lanthanide detn 1680
Selectively modulated interferometer dispersive spectrometer 113
Selenium detn atomic absorption 1096
Selenium detn atomic absorption interference 1417
Selenium detn opticoacoustic 549
Selenium detn serum 1313
Selenium electrodeless discharge lamp 551
Selenium org compd gas chromatog 378
Semiconductor surface characterization review 221r
Semidifferential electroanalysis peak shape 1390
Semiquinone electrochem redn benzoquinone 806
Sensitivity optimization chromatog mass spectrometry 518
Sensitivity pollutant x ray 1505
Sensitivity x ray analysis 1737
Sensor potentiometric field effect 2315
Sepn europium NMR shift 2375
Serotonin brain chromatog 354
Serum albumin voltammetry 2108
Serum blood chlorpheniramine detn 1085
Serum blood phenylethylmalonamide detn 1969
Serum nucleoside base detn 2237
Serum primidone 903
Serum selenium detn 1313
Serum thiocyanate detn 785
Serum urea detn 795
Sewater extn lead diethyldithiocarbamate 1146
Shale oil liq chromatog 1766
Sheet resistivity silylated electrode 1639
Signal flicker noise spectrometry polemic 339 340
Signal proportional data acquisition rate 681
Silane copper bonded phase chromatog 1756
Silica analysis ion beam sputtering 16a
Silica respirable particle size detn 2196
Silica silicon potentiometric sensor 2315
Silicate analysis mass spectrometry 927
Silicate rock analysis bromine 1998
Siliceous material analysis arsenic 825
Silicon chloride analysis atomic absorption 2289
Silicon intensified target vidicon detector 939
Silicon intensified vidicon detector spectrometry 106
Silicon silica potentiometric sensor 2315
Silicon vidicon tube liq chromatog 1171
Silicone rubber gas chromatog 2343
Siloxane analysis gas chromatog 2343
Silver analysis mercury 255
Silver bromide potentiometric sensor 2315
Silver Compton scattered radiation 1168
Silver detn chemiluminescence 1322
Silver detn kinetic fluorometry 1066
Silver electrode dinitro compd detn 45
Silver electrode liq chromatog detector 2379
Silver filter x ray diffraction 429
Silver sulfide cupric selective electrode 877
Silyl deriv phosphate gas chromatog 1086
Silyl oxime deriv sugar chromatog 137
Silylated electrode sheet resistivity 1639
Simplex super modified optimization analysis 1422
Simulation differential pulse polarog 1246
Simulation equation equil system calcn 1660
Simultaneous multielement flame photometry 2280
Slag analysis arsenic 825
Sludge organochlorine pesticide gas chromatog 316
Slurry packing dynamic chromatog column 1958
Smoke analysis IR spectrometry 331
Smoke cigaret redox quinone 1924
Sodium acetate adsorbed sample phosphorescence 2164
Sodium analysis niobium 80
Sodium chromite detn chromic oxide 962
Sodium detn proton activation 1297
Sodium error glass electrode 1363
Sodium flame atomic absorption 574
Sodium fluorescence excitation 2111
Sodium hydroxide analytical reagent purifn 889
Sodium iodide diffusion cation exchanger 629
Soil amino acid isomer detn 2
Soil fluoride detn 53
Soil tetrachlorodibenzodioxin detn 918
Solid electrolyte oxygen sensor 1813
Solid laser atomization atomic absorption 1339
Solid NMR review 951a
Solid surface fluorometry calibration curve 2160
Solute analysis laser Raman 70
Solute reaction bonded phase chromatog 133
Solute relaxation field flow fractionation 659
Solvent analysis cesium 1744
Solvent chromatog coal liquefaction 2253
Solvent dense gas exclusion chromatog 243
Solvent DMF atomic absorption 2122
Solvent effect diffusion cation exchanger 629
Solvent free injection gas chromatog 1881
Solvent polarity ESR NMR 591
Soly tetrathiafulvalene radical bromide 802
Sorption org compd water 1023
Source continuum atomic absorption spectrometry 665
Source flicker dual wavelength spectrophotometry 2170
Soybean analysis anodic stripping voltammetry 1792
Spacecraft material analysis 322a
Spectra absorption digital analysis review 864a
Spectra computer identification 1441
Spectra fluorescence emission forensic 1710
Spectra information retrieval computer 2141
Spectra IR computer subtraction 772
Spectra mitochondria 1348
Spectra multicomponent numerical analysis 276
Spectral noise arc lamp 2040
Spectral overlap correction atomic absorption 838
Spectral peak deconvolution 2149
Spectro electrochem glass ceramic microcell 1646
Spectrochem anal plasma discharge chamber 2372
Spectrochem analysis computer 2141
Spectrochem analysis food review 835a
Spectrochem analysis interelement effect 266
Spectrochem analysis solid surface 16a
Spectrochem analysis super modified simplex 1422
Spectrochem digital analysis review 864a
Spectrofluorometry optical analyzer petroleum 1316
Spectrometer atomic absorption background correction app 2187
Spectrometer atomic absorption vidicon echelle 1112
Spectrometer atomic absorption Zeeman effect 1106
Spectrometer diode array Hb 555
Spectrometer Fourier transform 1446
Spectrometer IR computer 470
Spectrometer IR switching device 893
Spectrometer mass interface gas chromatograph 518
Spectrometer photoacoustic 697
Spectrometer selectively modulated interferometer dispersive 113
Spectrometer stopped flow rapid scanning 2098
Spectrometer tryptophan detn 950
Spectrometer ultrasonic vanadium benzohydroxamato 881
Spectrometer vidicon rapid scan 871
Spectrometric analysis microprocessor controlled laser 1702
Spectrometric detn vitamin K compd 1343
Spectrometry amino acid nitrogen 15 1832
Spectrometry ammonia 83
Spectrometry arsenic detn water 1093
Spectrometry atom formation atomic absorption 1647
Spectrometry atomic absorption atom loss 1100
Spectrometry atomic absorption atomizer 1413
Spectrometry atomic absorption continuum source 665 1263
Spectrometry atomic absorption interference correction 838
Spectrometry atomic absorption metal 257
Spectrometry atomic emission nebulizer 632
Spectrometry atomic fluorescence 1076
Spectrometry barium 1017
Spectrometry chromatog amino acid 1241
Spectrometry chromatog hormone thyroid 1304
Spectrometry digital analysis review 864a
Spectrometry electrodeposition transuranium element 842
Spectrometry emission phosphorus 1492
Spectrometry flame emission vidicon detector 106
Spectrometry fluorescence arom hydrocarbon 701
Spectrometry formaldehyde chromotropate 1865
Spectrometry inductively coupled plasma source 1450
Spectrometry IR polycyclic hydrocarbon 86
Spectrometry luminescence detector 1048
Spectrometry mass analysis air 270
Spectrometry mass chlordane 734
Spectrometry mass chromatog glyceride 2209
Spectrometry mass dipeptide ester 287
Spectrometry mass field desorption 1160
Spectrometry mass gas chromatog pollutant 521
Spectrometry mass monoamine metabolite 915
Spectrometry mass triglyceride 728
Spectrometry mass vinyl chloride detn 1985
Spectrometry microwave analysis review 249a
Spectrometry nomenclature 687
Spectrometry nucleoside base 2237
Spectrometry optoacoustic quantum fluorescence 1850
Spectrometry plasma carbon org detn 1235
Spectrometry pyrolytic graphite coated tubes 90
Spectrometry signal flicker noise polemic 339 340
Spectrometry UV visible slit width 119
Spectrometry wavelength modulation waveform 458
Spectrophotometer IR digitization 1875
Spectrophotometer manuf history 280a
Spectrophotometer scanning double wavelength 1348
Spectrophotometer temp jump cell 2378
Spectrophotometric amine detection liq chromatog 2080
Spectrophotometric detn acrylonitrile 2277
Spectrophotometric titrn computerized curve fitting 1408
Spectrophotometric titrn sulfur detn org 1987
Spectrophotometry atomic absorption computer 891
Spectrophotometry cobalt detn 580
Spectrophotometry dual wavelength precision 2170
Spectrophotometry flame atomic absorption precision 574
Spectrophotometry numerical analysis spectra 276
Spectrophotometry std review 386a
Spectrophotometry UV std ref material 711
Spectroscopic detector gas chromatog 2215
Spectroscopic std aluminum alloy 679
Spectroscopy absorption factor analysis 612
Spectroscopy mass field ionization 1847
Spectroscopy photothermal 2057
Spectroscopy Raman carotenoid 695
Spectroscopy rapid scanning fluorescence 747a
Spectroscopy surface review 221r
Spectroscopy x ray photoelectron quant 1282
Spelter zinc analysis silver 1066
Spirobiphthalide detn amitriptyline oxidn 1864
Splitless injection gas chromatog 1881
Sputtering atomization atomic absorption analysis 1336
Sputtering ion beam surface analysis 16a
Sq wave voltammetry theory 1899
Square wave voltammetry mercury electrode 1904
Stability const detn spectra evaluation 276
Stability ext manganese detn water 1862
Stability mercury dithizone complex 983
Stability mercury sample polyethylene bottle 668
Stainless steel corrosion org solvent 1637
Stainless steel corrosion product identification 322a
Stannic oxide electrochem iron porphyrin 194
Stationary electrode polarog curve multiplicity 1369 1376
Stationary electrode pulse polarograph 1459
Stationary phase aminosilane liq chromatog 2306
Stationary phase chem bonded review 1004a

Stationary phase copper bonded chromatog 1756
Stationary phase reaction solute chromatog 133
Statistical moment code mass spectra 1456
Statistical weighting kinetics detn 846
Statistics information theory analysis 1265
Statistics nonlinear calibration analysis 2062
Std aluminum alloy prepn 679
Std analytical instrumentation review 386a
Std indium tin surface analysis 1228
Std internal atomic absorption analysis 1336
Std mass spectrometry coal liq 1260
Std phenylporphinatozinc porphyrin detn fluorometry 1453
Std ref material UV spectrophotometry 711
Std vinyl chloride generation 139
Steel analysis carbide nitride DTA 649
Steel analysis laser atomic absorption 1339
Steel stainless corrosion product identification 322a
Sterilant gas analysis ethylene oxide 1602
Steroid detn carbon 13 NMR 2130
Steroid NMR carbon computer 2075
Stirrer helix 191
Stoichiometry triethanolamine nitrogen dioxide 1448
Stopped flow rapid scanning spectrometer 2098
Storage life Ilosvay soln 1218
Storage sample plastic container cleaning 2264
Straight line confidence limit polemic 884
Stripping anodic cadmium detn 199
Stripping cathodic pulse iodine detn 1199
Stripping coulometry electrode holder 1880
Stripping voltammetry copper zinc intermetallic 1792
Stripping voltammetry tubular electrode 49
Structure characterization fluorescence computer 2069
Structure mol information retrieval computer 1720
Styrene divinylbenzene immobilized ferroin deriv 974
Subtraction IR spectra computer 772
Subtractive gas chromatog microreactor 1078
Sugar chromatog methylsilyl oxime deriv 137
Sulfa liq chromatog 860
Sulfate aerosol detn air 1579
Sulfate air pollution detn 1990
Sulfate atm control 1664
Sulfate detn boiler blowdown water 1176
Sulfate detn laser Raman 70
Sulfate detn radioactive waste 2044
Sulfhydryl group detn 1036
Sulfide analysis arsenic 451
Sulfide hydrogen chromatog flame photometry 123
Sulfide polarog vitamin B12a 1380
Sulfide silver cupric selective electrode 877
Sulfide wastewater detn 128
Sulfite detn boiler blowdown water 1176
Sulfobetaine surfactant liq chromatog 2228
Sulfonate detn petroleum radiometry 1148
Sulfonated polymer support gas chromatog 1549
Sulfonic acid liq chromatog 860
Sulfur compd kraft mill wastewater 128
Sulfur detector gas chromatog 2215
Sulfur detn environmental material 1741
Sulfur detn gasoline chromatog 126
Sulfur detn org ion chromatog 884
Sulfur detn org spectrophotometric titrn 1987
Sulfur detn petroleum 1615
Sulfur detn substituted hydrocarbon monolayer 2330
Sulfur dioxide chromatog flame photometry 123
Sulfur sample binder analysis 1012
Supply sample graphite atomizer 2176
Support extn chromatog macroporous resin 1189
Surface analysis indium tin std 1228
Surface analysis quant ESCA 1044
Surface area detn phosphorescence 2164
Surface characterization technique review 221r
Surface fluorometry calibration curve 2160
Surface spectrochem analysis 16a
Surfactant nonionic biodegrdn analysis 398
Surfactant sulfobetaine liq chromatog 2228
Switching device IR spectrometer 893
Syncrude liq chromatog 1766
Syringe needle guide chromatog 1267
Systematic error gas chromatog 2222
Tabulation of Infrared Spectral Data (book review) 936a
Tailing analysis thorium uranium isotope 618
Tar coal chromatog 1225
Target transformation factor analysis 284
Teflon pellet IR hydride 1458
Tektite analysis ion beam sputtering 16a
Tellurium diethyldithiocarbamate chromatog atomic absorption 189
Temp helium oxygen acetylene flame 2013
Temp jump app kinetics detn 1081
Temp jump cell spectrophotometer 2378
Tenax GC diphenylquinone formation 512
Terephthalate oligomer detn chromatog 1166
Ternary mixt kinetic analysis 1650
Testing glass electrode buffer 1363
Tetrahydrocannabinol blood detn 163
Tetrahydrofuran corrosion stainless steel 1637
Tetrahydroisoquinoline alkaloid chromatog 530
Tetralin detn coal liquefaction 2253
Tetraoxyethylene dimethacrylate stabilizer chromatog 363
Tetraselenafulvalene voltammetry acetonitrile bromide 802
Tetrathiafulvalene voltammetry acetonitrile bromide 802
Tetrose gas chromatog 137
Thallium external heavy atom phosphorimetry 2048
Thebaine detn gum opium 359
Theoretical experimental characterization 523
Thermal analysis kinetics detn 998
Thermal Analysis of Minerals (book review) 931a
Thermal desorption org compd water 1023
Thermal field flow fractionation 1750
Thermal volatilization analysis polymer 886
Thermodn faradaic admittance 1805
Thermodn gas chromatog precision 1029
Thermodn heme redox reaction 1573
THF asphaltene assocn 2363
Thick sample x ray analysis 1737
Thickness detn alloy film 1152
Thin film alloy analysis 1152
Thin layer chromatog atomic absorption 189
Thin layer chromatog color photog 1640
Thin layer chromatog copper iron 2241
Thin layer chromatog fluorescence densitometry 2160
Thin layer chromatog fraction collector 671
Thin layer chromatog high performance 1867
Thin layer chromatog hydrazine detn 161
Thin layer chromatog review 83a
Thin layer differential pulse voltammetry 1792
Thin layer micrometer cell voltammetry 1205
Thioamide drug cathodic stripping voltammetry 1195
Thiobisbenzothiazole identification spacecraft coolant 322a
Thiocarbamatocobalt pyrrolidine chelate water 222
Thiocyanate catalyst nitrite detn 2272
Thiocyanate detn serum 785
Thiocyanate reagent niobium detn 80
Thioether drug oxidn titrn 1002
Thiol polarog vitamin B12a 1380
Thiol voltammetry 2108
Thiophene monolayer analysis Auger spectroscopy 2330
Thiothenoyltrifluoroacetonate extn diluent effect 2246
Thiothenoyltrifluoroacetone reagent copper iron detn 2241
Thiourea dioxide redn cadmium 26
Thiourea pesticide pulse voltammery 2310
Thorium detn x ray 967
Thorium isotope detn ore 618
Thromboxane oxime chromatog 1032
Thyroid hormone chromatog spectrometry 1304
Time drop detn polarog 1270
Time resoln phosphorimeter 1126
Tin analysis gold 1771
Tin detn biol tissue plastic 1090
Tin dioxide chemisorbed porphyrin 194
Tin foil oxide ESCA Auger 1228
Tin nickel sputtered oxidn 987
Tin oxide electrode resistivity 1639
Tin vanadophosphate cation exchanger 165
Tissue actinide detn 1268
Tissue analysis tin 1090
Titanium analysis review 72r
Titanium detn lubricating oil 454
Titanium thin film hydrogen detn 853
Titration potentiometric acid 1429
Titrn automated potentiometric equivalence point 1250
Titrn coulometric app double compartment 1885
Titrn nephelometric dil bromide soln 2268
Titrn oxidn thioether drug 1002
Titrn potentiometric acid nonionic resin 1256
Titrn soln calorimeter design 1878
Titrn spectrophotometric computerized curve fitting 1408
TLC: High Performance Thin-Layer Chromatography (book review) 735a
TNT detection water fluorescent resin 2251
TNT detn wastewater 880
Topics in Chemical Instrumentation. II (book review) 648a
Topol analysis gas chromatog alkene 747
Toxicol drug gas chromatog 906
Toxicology Annual, Vol. 2 (book review) 832a
Trace analysis helium 3 activation 1510
Trace analysis liq opticoacoustic 549
Trace analysis sampling 33a
Trace analysis square wave voltammetry 1904
Trace element detn 432
Trace element detn geochem 62
Trace element detn geol material 1485
Trace element detn L cell 2203
Trace element detn silicon chloride 2289
Trace element sample storage 2264
Trace element spectrometry nebulizer 1413
Trace ion detn fluorometry 1474
Trace lanthanide detn laser fluorometry 1680
Trace metal Chelex river water 1950
Trace metal concn membrane 1326
Trace metal detn chemiluminescence 1322
Trace metal detn water enrichment 311
Trace metal mussel detn 257
Trace nonfluorescent ion detn fluorometry 1690
Tranexamate detn body fluid 369
Transducer measurement flow rate 352
Transform Fourier spectrometer 1446
Transformed fibroblast element surface 1290
Transistor ion selective field effect 2315
Transition metal detn atomic absorption 90
Transition metal detn immobilized ferroin deriv 974
Transition metal exchange resin ESR 1840
Transition metal salt nonaq dehydrating 1874
Transparent optically electrode 1395
Transuranium element electrodeposition spectrometry 842
Triethanolamine stoichiometry nitrogen dioxide 1448
Triglyceride mass spectrometry 728
Trimethylarsine detn natural water 820
Trinitrotoluene detn wastewater 880
Triose gas chromatog 137
Trishydroxymethylaminomethane buffer seawater 867
Tritium Measurement Techniques: National Council on Radiation Protection and Measurements Report No. 47 (book review) 75a
Tryptophan detn plasma 950
Tryptophan hydroxy phosphorescence detn 2164
Tube cracker glass sealed ampoules vacuum 192
Tube permeation air anal 1278
Tubular electrode anodic stripping voltammetry 49
Two photon excitation fluorescence 2054
Ultrasonic nebulizer atomic emission spectrometry 632
Ultrasonic spectrometer vanadium benzohydroxamato 881
Ultratrace element detn silicon chloride 2289
Unsegmented stream continuous flow analysis 17
Uranium detn natural water 67
Uranium detn ore luminescence 638
Uranium detn x ray 967
Uranium isotope detn ore 618
Uranium ore analysis lead 210 302
Uranium ores alpha spectrometry detn thorium 1648
Urea detn serum 795
Urease reactor optimization 1929
Urethane polymer pyrene removal water 2260
Urine actinide detn 1268
Urine catecholamine chromatog 2109
Urine cocaine benzoylecgonine detn 1965 1974

Urine hippurate detn 1494
Urine mefruside metabolite detn 1311
Urine tetrahydroisoquinoline alkaloid 530
UV spectrophotometry std ref material 711
UV visible spectrometer performance 113
UV visible spectrometry slit width 119
Valinomycin cation selective electrode 1567
Vanadate analysis reaction molybdate phosphate 779
Vanadium atomization graphite platform 2018
Vanadium benzohydroxamato ultrasonic spectrometer 881
Vanadium detn bitumen visible spectra 972
Vanadophosphate tin cation exchanger 165
Vanillylmandelate detn 915
Vapor pressure detn gasoline 2368
Vapor pressure osmometry asphaltene 2363
Vaporization pressure fuel analyzer 2368
Variance analysis 691a
Vegetation fluoride detn 53
Velocity aerosol analytical flame 2112
Vertical furnace pyrolyzer chromatog 348
Vidicon detector flame emission spectrometry 106
Vidicon detector liq chromatog 939
Vidicon echelle atomic absorption spectrometer 1112
Vidicon rapid scan spectrometer 871
Vidicon rapid scanning spectrometer 2098
Vidicon tube silicon liq chromatog 1171
Vinyl chloride microdetn water 1985
Vinyl chloride sampling charcoal 994
Vinyl chloride std generation 139
Vinyl ester gas chromatog 2337
Viscosity optimization exclusion chromatog 243
Visible spectra vanadium detn bitumen 972
Vitamin B12 detn luminol chemiluminescence 446
Vitamin B12a sulfide thiol detn 1380
Vitamin K compd detn spectrometric 1343
Vitreous carbon electrode 1470
Volatility vaporization pressure gasoline 2368
Volatilization methylmercury loss water 23
Volatilization thermal analysis polymer 886
Voltage controlled oscillator data acquisition 681
Voltammery thiourea pesticide 2310
Voltammetry anodic stripping cadmium 56
Voltammetry anodic stripping tubular electrode 49
Voltammetry catecholamine thin layer cell 1205
Voltammetry cathodic stripping mercaptan detn 1386
Voltammetry cathodic stripping thioamide drug 1195
Voltammetry cyclic glass ceramic cell 1646
Voltammetry data overlapped pattern recognition 1369 1376
Voltammetry ferricyanide tubular electrode current 1563
Voltammetry mercury dropping electrode 1899
Voltammetry nitrate detn 485
Voltammetry platinum electrode 1789
Voltammetry protein 2108
Voltammetry pulse poised system 489
Voltammetry semidifferential electroanalysis 1390
Voltammetry sq wave theory 1899
Voltammetry square wave mercury electrode 1904
Voltammetry thin layer differential pulse 1792
Voltammetry thin layer micrometer cell 1205
Warfare agent detn air 1746
Water anal org compd 1023
Water analysis 891
Water analysis review 139r
Water chromatog parathion 1551
Water detn hydroxyethylhydrazine gas chromatog 2213
Water detn nitrogen mass spectrometry 270
Water detn oil emulsion 690
Water hydrogen sulfide detn 424
Water irrigation analysis nitrate 485
Water manganese detn ext stability 1862
Water removal hydrocarbon distn 1887
Water removal nonaq soln 1874
Water vinyl chloride microdetn 1985
Wave sq voltammetry theory 1899
Waveform wavelength modulation spectrometry 458
Wavelength modulated echelle atomic absorption 838
Wavelength modulation emission background correction 1121
Wavelength modulation spectrometry waveform 458
Wax paraffin review , 276r
Wine carboxylic acid detn 655
Wire californium 252 autoradiog 517
Workshop on the Analytical Needs of the Future as Applied to Coal Liquefaction (book review) 441a
X ray analysis computer program 345
X ray analysis electrodeposition preconcn 1734
X ray analysis thick sample 1737
X ray analysis trace element 2203
X ray diffraction absorption coeff 1168
X ray diffraction silver filter 429
X ray emission selenium 1313
X ray emission trace element 432
X ray excited optical luminescence 638
X ray fluorescence alloy film 1152
X ray fluorescence analysis correction 1990
X ray fluorescence analysis geol 717
X ray fluorescence analysis multielement 1012
X ray fluorescence geochem analysis 62
X ray fluorescence matrix correction 641
X ray fluorescence matrix effect 1403
X ray photoelectron spectroscopy 1228
X ray photoelectron spectroscopy aluminosilicate 2001
X ray photoelectron spectroscopy calibration 1044
X ray photoelectron spectroscopy quant 1282
X ray pollutant sensitivity 1505
X ray thorium uranium detn 967
X-Ray Fluorescence Analysis of Environmental Samples (book review) + 550a
Zeeman effect atomic absorption spectrometer 1106
Zeolite preconcn ammonia detn 1331
Zinc atomization graphite platform 2018
Zinc copper intermetallic stripping voltammetry 1792
Zinc detn silicon chloride 2289
Zinc detn transition metal present 2090
Zinc detn x ray fluorescence 1734
Zinc diketonate thio extn 2246
Zinc enrichment chelation water analysis 311
Zinc flame atomic absorption 574
Zinc preconcn chelate water analysis 222
Zinc spelter analysis silver 1066
Zinc tetraphenylporphin std fluorometry 1453
Zincon reagent transition metal 2090

"A"-PAGE INDEX

The Analytical Approach

Analytical chemists at the launch pad. Helein D. Bennett. 322A
Cross section of analytical problem solving in the home appliance industry. J. L. Wuepper. 1032A
Tracing the origin of off-flavors in a breakfast cereal. Menard G. Heydanek, Jr. 901A
An unknown salivary morpholine metabolite. John S. Wishnok and Steven R. Tannenbaum. 715A

Books (see Keyword Index)

Editors' Column

ANALYTICAL CHEMISTRY—A new approach. 557A
ANALYTICAL CHEMISTRY's advisory board meeting. 833A
Analytical chemistry goes to Mars. 655A
Analytical chemists and TOSCA. 247A
Asbestos: definition and measurement. 1063A
Historical notes. 1253A
Implementation of TSCA. 1177A
New journals; *LabGuide*. 79A
NSF peer review. 945A
Pittsburgh conference. 445A
Scientific journals. 741A
SI units. 1253A
Too many meetings? 353A

Instrumentation

Amperometric and coulometric detectors for high-performance liquid chromatography. Peter T. Kissinger. 447A
Analytical microwave spectrometry. Edgar A. Rinehart. 249A
Automated systems for radioimmunoassay. Nathan Gochman and Lemuel J. Bowie. 1181A
Factors affecting atomization and measurement in graphite furnace atomic absorption spectrometry. R. E. Sturgeon. 1255A
High resolution NMR in solids. R. G. Griffin. 951A
How to buy a microscope. Walter C. McCrone. 659A
Immobilized enzymes in analytical chemistry. D. N. Gray, M. H. Keyes, and B. Watson. 1067A
The mass spectrometer as a gas chromatograph detector. Catherine Fenselau. 563A
Minicomputer data processing system for air monitoring studies. S. O. Farwell, H. H. Westberg, K. J. Allwine, and N. K. Shrauger. 357A
Near infrared reflectance spectrophotometric analysis of agricultural products. C. A. Watson. 835A
Rapid scanning fluorescence spectroscopy. D. W. Johnson, J. B. Callis, and G. D. Christian. 747A
Recent developments in thin-layer chromatography. Haleem J. Issaq and Edward W. Barr. 83A
Zeeman effect-based background correction in atomic absorption spectrometery. Steven D. Brown. 1269A

Report

Analysis of variance in analytical chemistry. Roland F. Hirsch. 691A
ANALYTICAL CHEMISTRY's authors: publication practices. Josephine M. Petruzzi. 1217A
Analytical chemistry in the USA in the first quarter of this century. I. M. Kolthoff. 480A
Chemical ionization mass spectrometry: ten years later. Burnaby Munson. 772A
Chemically bonded stationary phases in chromatography. Eli Grushka and Edward J. Kitka, Jr. 1004A
Computer networking: a rational approach to lab automation. Raymond E. Dessy. 1100A
Digital analysis of electronic absorption spectra. David E. Metzler, Carol M. Harris, Richard L. Reeves, W. H. Lawton, and Mary S. Maggio. 864A
Future trends in clinical chemistry. Robert S. Melville. 594A
History of spectrophotometers at Beckman Instruments, Inc. A. O. Beckman, W. S. Gallaway, W. Kaye, and W. F. Ulrich. 280A
In situ spectrochemical analysis of solid surfaces by ion beam sputtering. N. H. Tolk, I. S. T. Tsong, and C. W. White, 16A
Literature growth and decay: an activation analysis résumé. T. Braun, W. S. Lyon, and E. Bujdosó. 682A
Metals in bioenvironmental systems. G. B. Morgan and E. W. Bretthauer. 1210A
Representative sampling and proper use of reference materials. Oswald U. Anders. 33A
Standards in analytical instrumentation. J. M. Vandenbelt. 386A
Teaching analytical chemistry: real world needs. Jeanette G. Grasselli. 182A

Author Index

Anderson, D. H. 2275
Asmus, P. A. 2379

Baca, P. 2249
Barford, R. A. 2228
Batistoni, D. A. 2215
Baudino, J. H. 2368
Bearse, R. C. 2203
Bisson, M. 2358
Blake, M. I. 2367
Brost, D. F. 2280
Brown, P. R. 2237
Brunner, T. R. 2136
Buchanan, M. V. 2146
Buck, R. P. 2315
Busch, K. W. 2280

Campbell, P. G. C. 2358
Cano, J-P. 2354
Chang, S-K. 2272
Chesler, S. N. 2306
Chloupek, F. J. 2368
Christian, G. D. 2155
Copeland, T. R. 2285
Cournoyer, R. 2275
Crowley, A. W. 2368

Davidson, E. R. 2155
de Galan, L. 2176
Durand, A. G. 2354

Edmonds, J. W. 2196
Erlenmaier, T. 2354
Eswara Dutt, V. V. S. 2367

Fassett, J. D. 2322
Feldman, C. 2215
Fitzloff, J. F. 2367
Flavian, S. 2222
Freed, C. R. 2379
Freiser, H. 2249
Freudenthal, J. 2205
Fujioka, Y. 2241

Gagné, R. 2358
Garreau, R. M. 2354
Giessen, B. C. 2285
Gramberg, L. G. 2205
Greenland, L. P. 2376
Greizerstein, H. B. 2235
Guerra, R. E. 2196

Hackleman, D. E. 2315
Hadži, D. 2141
Hall, M. E. 2277
Harnly, J. M. 2187
Harrington, G. W. 2272
Heller, C. A. 2251
Henslee, W. W. 2196
Hertz, H. S. 2306
Hieftje, G. M. 2372
Hillenbrand, D. F. 2146
Hilpert, L. R. 2306
Hoffman, N. E. 2231
Honda, R. 2246
Honjo, T. 2241, 2246
Horvath, C. 2295
Hubbard, A. T. 2330
Hurtubise, R. J. 2160, 2164, 2253

Itoh, H. 2241

Juneau, G. P. 2375

Kiba, T. 2241, 2246
Kitos, P. A. 2203
Kometani, T. Y. 2289
Kozeniauskas, R. 2272
Krstulovic, A. M. 2237

Lee, W. C. 2363
Liao, J. C. 2231
Liberti, L. 2377
Lindstrom, R. M. 2264
Linfield, W. M. 2228

McBride, R. R. 2251
Malloy, B. 2280
Mareci, T. H. 2130
Marsel, J. 2141
Marshall, R. A. G. 2193
May, I. 2376
May, W. E. 2306
Meehan, E. J. 2268
Melander, W. 2295
Molnar, I. 2295
Molnar, P. 2295
Moody, J. R. 2264
Morrison, G. H. 2322
Mottola, H. A. 2367
Murata, T. 2209

Natusch, D. F. S. 2170
Navratil, J. D. 2260

O'Haver, T. C. 2187
O'Kane, J. L. 2374
Osteryoung, J. G. 2310

Palermo, P. J. 2213
Parris, N. 2228
Penca, M. 2141
Pinto, A. 2377

Ratzlaff, K. L. 2170
Reich, R. M. 2378
Ronning, M. A. 2251
Rosie, D. M. 2237
Roth, J. R. 2322

Schabron, J. F. 2253
Schiller, J. E. 2292
Schlueter, D. D. 2343, 2349
Schoeffel, J. A. 2330
Schulting, F. L. 2365
Schwager, I. 2363
Scott, K. N. 2130
Shatkay, A. 2222
Shearer, J. C. 2275
Shen, J. 2374
Sievers, R. E. 2260
Siggia, S. 2337, 2343, 2349
Silver, H. F. 2253
Simon, P. J. 2285
Smyth, M. R. 2310
Statham, P. J. 2149
Stevens, J. W., Jr. 2277
Sutter, J. R. 2378

Taylor, J. W. 2146
Tessier, A. 2358

van den Broek, W. M. G. T. 2176
Viala, A. R. 2354
von Wandruszka, R. M. A. 2164

Walton, H. F. 2260
Warner, I. M. 2155
Wilkins, C. L. 2136
Williams, R. J. 2337
Williams, R. K. 2372
Wils, E. R. J. 2365
Wise, S. A. 2306
Wojtowicz, C. 2235

Yamaguchi, S. 2268
Yen, T. F. 2363

Zander, A. T. 2372
Zombola, R. R. 2203
Zupan, J. 2141

Future Articles

Determination of Industrial Dyes in Water by Laser Excited Resonance Raman Spectroscopy
L. Van Haverbeke, P. F. Lynch, and C. W. Brown

Use of Muonic X-rays for Nondestructive Analysis of Bulk Samples for Low-Z Constituents
J. J. Reidy, R. L. Hutson, H. Daniel, and K. Springer

High Performance Liquid Chromatographic Determination of Unreacted Acrylamide in Emulsion or Aqueous Homopolymers or Emulsion Copolymers
F. J. Ludwig and M. F. Besand

Feedback Excitation Nuclear Magnetic Resonance Spectrometry and Its Application to Simultaneous Temperature Measurement
D. W. Vidrine and P. E. Peterson

Influence of Some Matrix Elements on the Determination of Copper and Manganese by Furnace Atomic Absorption Spectrometry
J. Smeyers-Verbeke, Y. Michotte, and D. L. Massart

Sterically Crowded Trialkylsilyl Derivatives for Chromatography and Mass Spectrometry of Biologically-Important Compounds
M. A. Quilliam and J. B. Westmore

Test for Racemization in Model Peptide Synthesis by Direct Chromatographic Separation of Diastereomers of the Tetrapeptide Leucylalanylglycylvaline
S. B. H. Kent, A. R. Mitchell, G. Barany, and R. B. Merrifield

SARTORIUS DOES IT AGAIN!

Introducing new microprocessor-equipped electronic balances with new capabilities, new add-on data keyboards, and new low (from $1,295) prices.

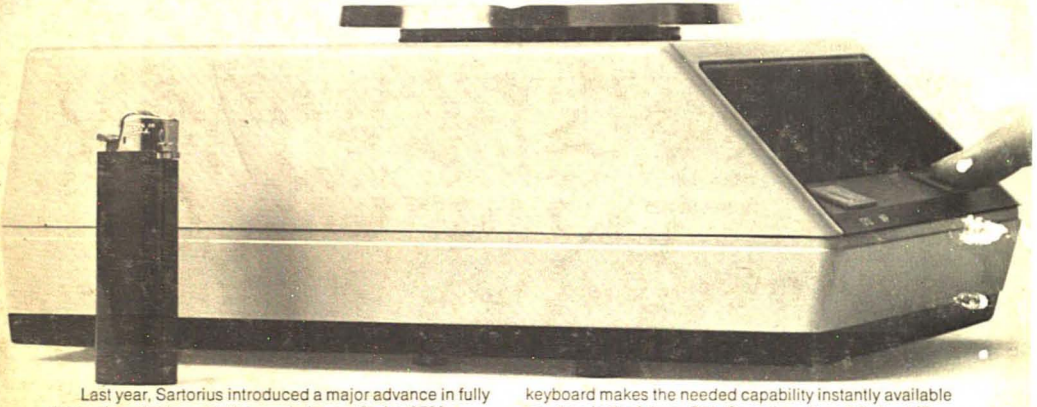

Last year, Sartorius introduced a major advance in fully electronic weighing with the revolutionary Series 3700 Balances.

This year, Sartorius does it again with its new MP models. These extremely versatile electronic top-loading balances utilize Texas Instruments microprocessors to vastly expand data handling and processing capabilities.

With optional plug-in keyboards that can be added anytime, MP models can be used to convert weight data, select programs, recall information and even calculate results.

Some typical applications for these balances include: instantaneous conversion from metric to non-metric calibration (weighings in pounds, ounces, carats, grains, pennyweights, etc.), parts counting, mean weight determination, percentage weighing, and variable integration time for more precise animal weighings.

MP models also provide complete weighings in 1-2 seconds, instant electronic taring, automatic overload protection, a built-in vibration filter, data storage memory, and are available with BCD and analog outputs.

Can you afford to buy a new balance without these capabilities?

When you choose a Sartorious MP model, you have selected a balance that will be quite as advanced tomorrow as it is today. Even if you do not need all its capabilities now, the purchase of the appropriate plug-in keyboard makes the needed capability instantly available any time in the future. Only Sartorius offers this flexibility.

For all their advanced technology, Sartorius MP models, priced as low as $1,295 are significantly less expensive than many other electronic balances without such features. For literature, write: Sartorius Balances Division, Brinkmann Instruments, Inc., Cantiague Road, Westbury, N.Y. 11590.

sartorius

CIRCLE 21 ON READER SERVICE CARD

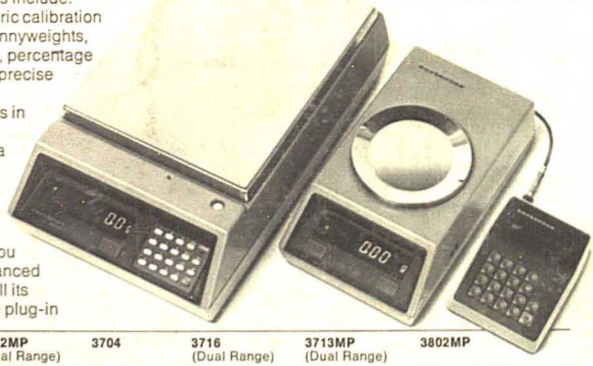

MODEL (Partial Listing)	1205MP	1202MP	1212MP (Dual Range)	3704	3716 (Dual Range)	3713MP (Dual Range)	3802MP
Weighing Range	0-160g	0-300g	0-30g 0-300g	0-1200g	0-120g 0-1200g	0-300g 0-3000g	0-6000g
Readability	0.001g	0.01g	0.001g 0.01g	0.01g	0.01g 0.1g	0.01g 0.1g	0.1g
Price	$2295.	$1295.	$1650.	$2195.	$1995.	$2495.	$3225.

31 JUL 2521